IAHS Publication 339
ISSN 0144-7815

Land Subsidence, Associated Hazards and the Role of Natural Resources Development

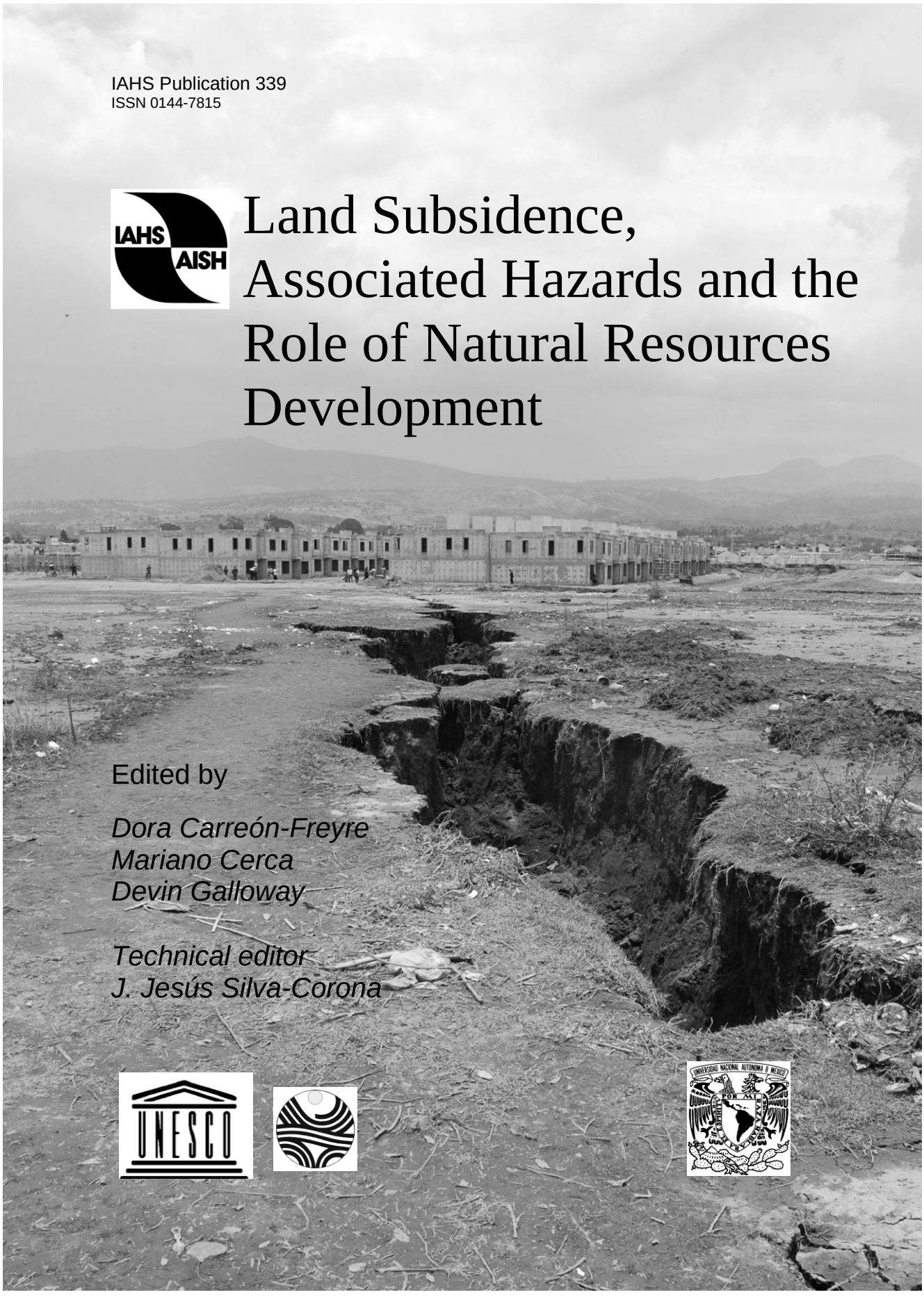

Edited by

Dora Carreón-Freyre
Mariano Cerca
Devin Galloway

Technical editor
J. Jesús Silva-Corona

Land Subsidence, Associated Hazards and the Role of Natural Resources Development

Other IAHS Publications

Hydrocomplexity: New Tools for Solving Wicked Water Problems

Edited by S. Khan, H.H. G.Savenije, S. Demuth & P. Hubert

Publ. 338 (*2010*) ISBN 978-1-907161-11-7, 272 + x pp. £55.00

Human activities have become major drivers of change in the Earth's biosphere, resulting in deterioration of water quality, overexploitation of freshwater resources, adverse effects of hydrological hazards and landscape degradation, which make water problems complex and wicked. The same activities also affect the functioning of ecosystems and their ability to provide goods and services on which human well-being depends. There is a need for community-based transdisciplinary management tools to provide a better understanding of water as both an abiotic resource and as a service delivered by ecosystems.

This book, launched at the 10th IHP/IAHS Kovacs Colloquium, held at UNESCO, Paris, contains the keynote papers by the invited speakers and extended abstracts of the posters, focusing on the issues of complexity of wicked water problems and the type of tools that can be used to solve them.

Sediment Dynamics for a Changing Future

Edited by Kazimierz Banasik, Arthur J. Horowitz, Philip N. Owens, Mike Stone & Des E. Walling

Publ. 337 (*2010*) ISBN 978-1-907161-10-0, 376 + viii pp. £74.00

This book advances understanding of erosion and sedimentation in relation to sediment dynamics and river water quality. Keynote papers precede themed groups: Human Impact on Sediment Budgets is concerned with the influence of land-use change on sediment yields and/or fluxes. Structure, Functioning and Management of Fluvial Sediment Systems provides valuable information on topics including the dynamics of flood-plain sedimentation, temporal variation of sediment parameters and the influence of sediment on aquatic ecosystems. Experiment-based and Modelling Approaches to Sediment Research highlights the role of monitoring and modelling studies in improved understanding of catchment sediment dynamics, sediment fluxes and water quality.

Status and Perspectives of Hydrology in Small Basins

Edited by A. Herrmann & S. Schumann. Co-editors: L. Holko, I. Littlewood, L. Pfister, P. Warmerdam & U. Schröder

Publ. 336 (*2010*) ISBN 978-1-907161-08-7, 314 + xii pp. £65.00

Only in well-defined small basins with high-quality measurements can the complexities of combined physical, chemical and biological processes be adequately investigated. Small hydrological research basins provide interdisciplinary observatories, thus contributing to study of the impact of environmental changes changes and to developing strategies for water and land-use management under such change. This volume, an outcome of the Workshop held at Goslar-Hahnenklee, Germany, in spring 2009 focuses on:

- Operational small research basins
- Fundamental hydrological research results drawn from small basins
- Hydrological processes
- Importance of small basin data and results for hydrological modelling

and includes the Braunschweig Declaration on: The need for a global network of long-term small hydrological research basins.

Hydrological Modelling and Integrated Water Resources Management in Ungauged Mountainous Watersheds

Edited by Wei-Lin Xu, Tian-Qi Ao & Xin-Hua Zhang

Publ. 335 (*2009*) ISBN 978-1-907161-07-0, 310 + x pp. £65.00

Some 40 contributions address:

- Modelling and predictive uncertainty
- New observation techniques and hydrological processes
- Integrated water resources management
- Eco-environmental protection

These were selected from papers presented at the Second IAHS-PUB International Symposium on Hydrological Modelling and Integrated Water Resources Management in Ungauged Mountainous Watersheds in China. The China Prediction in Ungauged Basins (PUB) organization focuses on the new methodology of hydrological simulation and prediction under natural and human-induced global changes.

Groundwater and Climate in Africa

Edited by Richard Taylor, Callist Tindimugaya, Michael Owor & Mohammad Shamsudduha

Publ. 334 (*2009*) ISBN 978-1-907161-05-6, 276 + xii pp. £65.00

Current assessments of the impacts of climate variability and change on water resources commonly exclude groundwater. This omission is of particular concern in Africa where current water usage and future adaptations in response to climate variability and change, together with population growth, place considerable reliance upon groundwater to meet domestic, agricultural and industrial water needs. The Groundwater and Climate in Africa Conference, held in Kampala, Uganda, in 2008, was one of the first globally to focus on the interactions between groundwater and climate variability and change.

This collection of papers includes the Kampala Statement, and addresses:

- Impact of climate variability and change on groundwater-based livelihoods
- Impact of climate variability and change on groundwater and groundwater-fed ecosystems
- Monitoring and modelling groundwater use and replenishment
- Estimation of groundwater resources and demand under a changing climate
- Groundwater management in Africa

New Approaches to Hydrological Prediction in Data-sparse Regions

edited by K. K. Yilmaz, I. Yucel, H. V. Gupta, T. Wagener, D. Yang, H. Savenije, C. Neale, H. Kunstmann & J. Pomeroy

Publ. 333 *(2009)* ISBN 978-1-907161-04-9 344 + x pp. £66.00

When data are scarce, hydrological predictions become unreliable due to both the inability to specify model components and parameter values that consistently represent the dominant hydrological processes in a particular watershed, and due to the lack of high quality model forcing. This, a problem in developed and developing countries, is the focus of the research reported.

IAHS Publications can be ordered from:
IAHS Press, CEH Wallingford, Oxfordshire OX10 8BB, UK
email: jilly@iahs.demon.co.uk
tel: +44 (0) 1491 692442 fax: +44 (0) 1491 692448

Land Subsidence, Associated Hazards and the Role of Natural Resources Development

Edited by:

DORA CARREÓN-FREYRE
Centro de Geociencias, Universidad Nacional Autónoma de México (UNAM) Querétaro, México

MARIANO CERCA
Centro de Geociencias, UNAM, Querétaro, México

DEVIN L. GALLOWAY
US Geological Survey, Sacramento, California, USA

Technical editor:
J. JESÚS SILVA-CORONA
Centro de Geociencias, UNAM, Querétaro, México

IAHS Publication 339
in the IAHS Series of Proceedings and Reports

Published by the International Association of Hydrological Sciences 2010

IAHS Publication 339

ISBN 978-1-907161-12-4

British Library Cataloguing-in-Publication Data.
A catalogue record for this book is available from the British Library.

© IAHS Press 2010
This publication may be reproduced as hard copy, in whole or in part, for educational or nonprofit use, without special permission from the copyright holder, provided acknowledgement of the source is made. No part of this publication may be electronically reproduced, transmitted or stored in a retrieval system, and no use of this publication may be made for electronic publishing, resale or other commercial purposes without specific written permission from IAHS Press.

The papers included in this volume have been reviewed and some were extensively revised by the Editors, in collaboration with the authors, prior to publication.

IAHS is indebted to the employers of the Editors for the invaluable support and services provided that enabled them to carry out their task effectively and efficiently.

The information, data and formulae provided in this volume are reproduced by IAHS Press in good faith and as finally checked by the author(s); IAHS Press does not guarantee their accuracy, completeness, or fitness for a given purpose. The reader is responsible for taking appropriate professional advice on any hydrological project and IAHS Press does not accept responsibility for the reader's use of the content of this volume. To the fullest extent permitted by the applicable law, IAHS Press shall not be liable for any damages arising out of the use of, or inability to use, the content.

The designations employed and the presentation of material throughout the publication do not imply the expression of any opinion whatsoever on the part of IAHS concerning the legal status of any country, territory, city or area or of its authorities, or concerning the delimitation of its frontiers or boundaries.

The use of trade, firm, or corporate names in the publication is for the information and convenience of the reader. Such use does not constitute an official endorsement or approval by IAHS of any product or service to the exclusion of others that may be suitable.

Publications in the series of Proceedings and Reports are available from:
IAHS Press, Centre for Ecology and Hydrology, Wallingford, Oxfordshire OX10 8BB, UK
tel.: +44 1491 692442; fax: +44 1491 692448; e-mail: jilly@iahs.demon.co.uk

Printed by Information Press

Preface:
Developments in land subsidence investigation

These proceedings compile the papers that were submitted to the Eighth International Symposium on Land Subsidence (EISOLS), and represent an overview of the state of the art in the investigations of land subsidence around the world. One of the main accomplishments of EISOLS has been the production of this volume with a considerable amount of high quality scientific papers. Because many major subsidence areas occur along the coast in rapidly developing countries with increasing demands for groundwater, oil and gas the previous seven Symposia on Land Subsidence have attracted attention to major subsidence areas along coastal areas in the world, such as Tokyo in Japan (1969; elevation 35 m), Anaheim in the USA (1976; elevation 66 m), Venice in Italy (1984; elevation 5 m), Houston in the USA (1991; elevation 15 m), The Hague in The Netherlands (1995; elevation 4 m), Ravenna in Italy (2000; elevation –1 m), and Shanghai in China (2005; elevation 6 m). EISOLS follows the tradition of the previous symposia but with an added focus on subsidence in inland areas, such as in and near Querétaro, Mexico (2010, elevation 1820 m), the host city.

In recent years considerable multidisciplinary research effort has been expended in attempts to describe the complex nature of the phenomena related to land subsidence, which is caused either naturally or anthropogenically. The multidisciplinary focus on these processes is critically needed and will play an important role in the development of resource management strategies addressing the impacts of climatic change and the means to achieve sustainable urban environments and optimal use of the land and water resources. Although the problem is global in the sense that it affects major urban centres and engineering facilities (mining, water distribution and storage, railroads and ports, among others) worldwide, the mitigation and solution for each case demands knowledge of the local geological, hydrogeological, mechanical, and morphological characteristics of the areas affected. The new advances in these multidisciplinary studies show the growing need to incorporate new views in planning of urban development, in legal frameworks, the related social problems and environmental damages, monuments heritage, and urban risk analysis.

The papers in Section 1 of this book examine the mechanisms of earth fissures and fracturing induced mainly by groundwater pumping, a widespread problem in central Mexico. Case studies from Mexico and the USA are presented, as well as different methodologies for characterization and monitoring of fracturing. The improvement of numerical methods, including nonlinear analysis, thermo-poro-elastic criteria, and analytical solutions considering poro-elastic media, are presented in Section 2. The papers in this section evaluate models of land subsidence caused by groundwater and gas extraction in Italy, USA, China, Mexico, The Netherlands, Japan, and Poland. One contribution examines the thermo-mechanical effects of seawater injection for reversing subsidence. Advances in computer capabilities have led to achievements of recent years in modelling and simulation of geological system deformation caused by fluid or gas depletion and their associated hazards, allowing the specialists to couple the geomechanical and hydraulic behaviour, and to consider subsoil heterogeneities. In Section 3, geological and geomechanical processes associated with land subsidence are addressed. Most of these contributions are by Mexican scientists, and document ground fracturing in cities such as: Morelia, Querétaro, San Luis Potosí, Aguascalientes, Jalisco, Zacatecas, Mexico City and Pachuca. Case studies from The Netherlands, Spain and Iran also are presented. The geomechanical behaviour of clayey materials from Paris and Mexico City are discussed, as are some geotechnical aspects of mining and construction in China. The papers in Section 4 document

notable advances in techniques for measuring and monitoring ground displacements using remote sensing (InSAR) and new methods for processing satellite data to improve temporal and spatial resolution (DInSAR, PSI, PInSAR). The reported case studies include those from: Venice, Bologna, Emilia Romagna and Crotone regions in Italy; California, USA; Mexico City, Mexicali, Baja California and Morelia in Mexico, Catalonia, Spain; Java, Indonesia; the Canto Basin and Kujukuri plain in Japan; Iran, India and China. *In situ* Global Positioning System and extensometer monitoring strongly support some of the studies. Alarm systems are being developed at some of the sites mentioned. Section 5 provides a set of papers discussing the social and economic impact of land subsidence and the need to incorporate a legal framework in public policies and resources management. Specialists from The Netherlands, Italy, USA and China document examples of subsidence management, and works from Mexico establish the need to consider the legal implications of environmental and urban damage caused by land subsidence and fracturing associated with excessive groundwater exploitation. Specific studies of strategic techniques for the assessment of urban risk in Mexico and Poland also are included. The papers in Section 6 deal with the problem of fluids withdrawal (gas and water) and provide simulations of subsidence for different extraction scenarios. The results and implications related to climate change are presented by scientists from Canada, USA, China and Mexico.

Analysis of the subsidence research presented in the EISOLS leads to reflection on the state of the art of the subject world-wide. The studies of land subsidence from around the world highlight the difference in the development of analytical and monitoring techniques used to assess the related risks, and reflect the various socio-economic activities contributing to the phenomena in each country. EISOLS provided an important opportunity to document and review the problems in Mexico. A special effort is needed to integrate efforts of the many scientists and other specialists working on this subject in Mexico and to coordinate academic issues with government agencies dealing with resources management. An accurate assessment of risk and environmental damage should support the planning of urban development in the increasingly populous cities of central Mexico. The absence of contributed research from other Latin America countries is noted; perhaps the problems are not as common as in Mexico. A few case studies of subsidence caused by salt and carbonate dissolution have been reported in Argentina and Cuba, and a study from Guatemala recently reported the case of sink-holes related to collapsible materials. Though the exploitation of gas and oil in the eastern part of Mexico and in Venezuela certainly are accompanied by important ground deformation consequences, the impacts largely are under-reported.

Finally, we acknowledge the support of the UNESCO Working Group on Land Subsidence (Alice Aureli, IHP-UNESCO, Ivan Johnson, Honorary Chairman, Laura Carbognin, Chairman, Keith R. Prince, vice-chairman, Frans B. Barends, Devin L. Galloway, Giuseppe Gambolati, Dora Carreón-Freyre and Jane Frankenfield Zanin, Technical Secretary) in organizing the EISOLS. We are especially grateful for our English Editor Cate Gardner and the editorial staff at IAHS who edited this diverse collection of papers. The Universidad Nacional Autonoma de Mexico and especially the Centro de Geociencias provided invaluable logistical support during the organization of the symposium. EISOLS in Mexico is indebted to German Figueroa-Vega, former Mexican member of the original UNESCO Working Group on Land Subsidence, who pioneered the first multidisciplinary work related to land subsidence in Mexico in the 1970s. We hope that further systematic work in Mexico and other Latin-American countries as well as nascent international collaborations will be spawned from the EISOLS.

The EISOLS is an opportunity and an important means for the international land subsidence community to exchange ideas, developments and experience. We sincerely hope that EISOLS

will benefit academicians and professional practitioners interested in subsidence processes and related issues. We thank those who came to Querétaro from around the world to share their expertise, and look forward to meeting again with you and even more colleagues from other countries at the future Ninth International Symposium on Land Subsidence.

Dora Carreón-Freyre and Mariano Cerca
UNAM, Querétaro, México

Devin L. Galloway
USGS, Sacramento, California, USA

ORGANIZING COMMITTEE

UNESCO Working Group on Land Subsidence

Alice Aureli, International Hydrological Programme (IHP), UNESCO, Paris, France
A. Ivan Johnson, Consultant, Arvada, Colorado, USA. Honorary Chairman
Laura Carbognin, Consiglio Nazionale delle Ricerche, CNR-ISMAR, Venezia, Italy. Chairman
Keith R. Prince, US Geological Survey, Menlo Park, California, USA. Vice-Chairman
Giuseppe Gambolati, Universitá degli Studi di Padova, Italy
Frans B. Barends, Deltares–GeoDelft, Delft, The Netherlands
Dora Carreón-Freyre, Universidad Nacional Autónoma de México, UNAM, México
Devin L. Galloway, US Geological Survey, Sacramento, California, USA
Jane Frankenfield Zanin, Consiglio Nazionale delle Ricerche, Italy. Technical Secretary

LOCAL ORGANIZING COMMITTEE

Dora Carreón-Freyre, Universidad Nacional Autónoma de México (UNAM), President
Mariano Cerca Martínez, UNAM
Alfredo Zepeda Garrido, Universidad Autónoma de Querétaro (UAQ)
Dionisio León Salas, UNAM
J. Jesús Silva Corona, UNAM
Liliana Cabrera Gómez, UNAM
Carlos Hernández, UNAM.
Gil Ochoa González, Instituto Tecnológico de Estudios Superiores de Occidente (ITESO)

Honorary Committee

José Narro Robles, Rector of the Universidad Nacional Autónoma de México, UNAM
Carlos Arámburo de la Hoz, Coordinador de la Investigación Científica, UNAM
Gerardo Carrasco Núñez, Director of the Centro de Geociencias, UNAM
Luca Ferrari Pedraglio, Centro de Geociencias, UNAM
Rafael Alexandri Rionda, President of the Sociedad Geológica Mexicana (SGM)
Walter Paniagua Zavala, President of the Sociedad Mexicana de Ingenieria Geotécnica (SMIG)
José Manuel Romo Jones, President of the Unión Geofísica Mexicana (UGM)

SCIENTIFIC ADVISORY BOARD (SAB)

Devin L. Galloway, USGS, Sacramento, California, USA
Giuseppe Gambolati, Universitá degli Studi di Padova, Italy
Thomas J. Burbey, Virginia Tech, Blacksburg, Virginia, USA
Enrique Cabral Cano, Instituto de Geofísica, UNAM, Mexico
German Figueroa V. Scientific Consultant, Mexico
Frans B. Barends, Deltares–GeoDelft, Delft, The Netherlands
Thomas L. Holzer, USGS, Menlo Park, California, USA
Stanley A. Leake, USGS, Tucson, Arizona, USA

Pietro Teatini, DMMMSA, Universitá degli Studi di Padova, Italy
Fabio Rocca, Politecnico di Milano, Milan, Italy
Gabriel Auvinet, Instituto de Ingeniería, UNAM, Mexico
Efraín Ovando Shelley, Instituto de Ingeniería, UNAM, México
Ger de Lange, TNO, Geological Survey of the Netherlands, Utrecht, The Netherlands
Alfonso Rivera, Natural Resources Canada, Québec, Canada
Klaudia Oleschko Lutkova, Centro de Geociencias, UNAM, Mexico
Toni Settari, Schulich School of Engineering, University of Calgary, Canada
Luigi Terzi, ENI E & P, Milano, Italy
Luigi Tosi, CNR, ISMAR, Venecia, Italy
Xue Yu-Qun, Earth Science Department of Nanjing University, Nanjing, China

ENDORSING ORGANIZATIONS

UNESCO, United Nations Educational, Scientific and Cultural Organization
UNAM, Universidad Nacional Autónoma de Mexico
CGEO, Centro de Geociencias, UNAM
UAQ, Universidad Autónoma de Querétaro
GEQ, Gobierno del Estado de Querétaro
CONCYTEQ, Consejo de Ciencia y Tecnología del Estado de Querétaro
CONACYT, Consejo Nacional de Ciencia y Tecnología
CEA, Comisión Estatal del Agua de Querétaro
COTAS, Comité Técnico de Aguas Subterráneas del Acuifero de Amazcala
CONAGUA, Comisión Nacional del Agua
SGM, Servicio Geológico Mexicano
USGS, United States Geological Survey
IAHS, International Association of Hydrological Sciences
AI, Academia Mexicana de Ingeniería
SMIG, Sociedad Mexicana de Ingeniería Geotécnica
SGM, Sociedad Geológica Mexicana
UGM, Unión Geofísica Mexicana
AGHM, Asociación Geohidrológica Mexicana
AIMMG, Asociación de Ingenieros de Minas, Metalurgistas y Geólogos de México A.C.

Introduction

These proceedings comprise 94 papers presented at the Eighth International Symposium on Land Subsidence (EISOLS) convened at the National Autonomous University of Mexico (*Universidad Nacional Autonoma de Mexico, UNAM*), Santiago de Querétaro, 17–22 October 2010. The papers and abstracts cover international science and social issues related to land subsidence, associated hazards and the role of natural resources development. In addition to these papers, another score of presentations were given in oral and poster sessions during the symposium. Abstracts of those presentations are available at: http://www.geociencias.unam.mx/geociencias/difusion/publicaciones.html. Land subsidence, simply defined, is a gradual or sudden lowering of the Earth's surface. The causes, both natural and anthropogenic, are many. Some of the natural processes include compaction, dissolution of relatively soluble subsurface material (sinkholes), underground erosion (piping), lateral flow, oxidation of organic soils, thawing permafrost, natural consolidation, hydrocompaction of dry unconsolidated deposits, and deep-seated volcanic and tectonic activity. These processes often are accelerated or amplified by anthropogenic factors such as excavation (mining), surface mechanical loading, drainage of wetlands, redirected or focused surface-water drainage and groundwater infiltration, and the extraction of subsurface fluids (groundwater, oil and gas).

Subsidence is a global phenomenon but the consequences and their remediation generally are local. Because of its global prevalence, and as much of the subsidence is related to hydrological processes affected by human development of local land and water resources, "Land Subsidence" was included in the UNESCO programme of the International Hydrological Decade, 1965–1974. During the Decade, UNESCO organized the 1st International Symposium on Land Subsidence in Tokyo in 1969. In 1975 land subsidence was retained under the framework of the International Hydrological Programme (IHP) as subproject 8.4 "Investigation of Land Subsidence due to Groundwater Exploitation", and UNESCO formed the associated Working Group on Land Subsidence. The first Working Group, of which Laura Carbognin is the only original member still active in the present group, was chaired by the late Joe Poland, USA (affectionately referred to as "'Mr Land Subsidence" and the "Saviour of Venice"), and comprised the late Soki Yamamoto, Japan, German Figueroa Vega, Mexico, the late José da Costa, UNESCO, and Ivan A. Johnson, USA, past chairman and present honorary member. The first goal of the UNESCO Working Group was to produce a guidebook to serve engineers, geologists and hydrologists confronting land subsidence problems, particularly in developing countries. The volume[1] was published by UNESCO in 1984, and since then the UNESCO Working Group has become the recognized leader in promoting global land subsidence studies, and collaborating with other international scientific organizations to coordinate and host international symposia on land subsidence about every five years.

Since the 1st International Symposium on Land Subsidence, six more international symposia on land subsidence have been convened through cooperation of UNESCO with the International Association of Hydrological Sciences (IAHS), and several other agencies and organizations. The proceedings of each of the symposia comprise numerous scientific papers covering the various types of subsidence identified throughout the world[2,3,4,5,6,7,8]. The

[1] Poland, J. F., ed. (1984) Guidebook to studies of land subsidence due to ground-water withdrawal. United Nations Educational, Scientific and Cultural Organization, Paris, *Studies and Reports in Hydrology 40*, 305 p., app. A–E., http://unesdoc.unesco.org/$other/unesdoc/pdf/065167eo.pdf, accessed 20 August 2010.

[2] Tison, L. J., ed. (1969) *Land Subsidence*—Proceedings of the Tokyo Symposium, September 1969,vols 1–2. IAHS Publs 88–89, 661 p., http://iahs.info/redbooks/088.htm, accessed 20 August 2010.

[3] IAHS (1977) Proceedings of the Second International Symposium on Land Subsidence (Anaheim, California, December 1976). IAHS Publ. 121, 669 p., http://iahs.info/redbooks/121.htm, accessed 20 August 2010.

proceedings constitute a rich source of research and case studies on subsidence attributed to anthropogenic and natural processes.

The EISOLS proceedings build on the previous symposia proceedings by contributing new relevant research, case studies and experience emanating from the diverse and important land subsidence studies in Mexico and throughout the world. The relation of fracturing (earth fissures and surface faults) to sediment compaction and subsidence is complex and an important area of developing research in Mexico, Latin America and globally. The analysis of these phenomena requires an interdisciplinary approach to improve understanding of the triggering factors, failure modes and propagation processes of fracturing. Geologists, geophysicists, hydrologists, geotechnical and geomechanical engineers, other scientists, resource managers and stakeholders participated in the symposium and contributed papers describing the development of new techniques for monitoring, analysis, interpretation and prediction of subsidence and/or related fracturing processes—an emphasis of EISOLS.

In conjunction with EISOLS, three peripheral technical meetings were convened to focus on Mexican subsidence-related issues: (1) Workshop on Land Subsidence and Geotechnical Engineering, sponsored by the Mexican Geotechnical Association, ISSMGE Technical Committee 214, Foundation Engineering for Difficult Soft Soil Conditions; (2) Water Management Agencies Round Table, co-organized by CONAGUA (Comision Nacional del Agua), CEA Querétaro (Comision Estatal del Agua en Querétaro) and COTAS (Comites Tecnicos de Agua Subterranea); and (3) Scientific Consultants' Presentations—case studies from companies working with remedial measures for foundations, constructions affected by ground fracturing, refilling of fractures, geological, geophysical, hydrogeological and geotechnical studies related to land subsidence processes. Papers from these technical meetings will be published in a forthcoming (2011) Special Issue on Land Subsidence, in the *Boletin de la Sociedad Geologica Mexicana*.

The EISOLS proceedings papers are organized in sections covering subsidence topics related to (1) Earth fissures, fracturing, and faulting; (2) Modelling; (3) Geological and geomechanical processes; (4) Monitoring; (5) Social and economic impacts and their incorporation into resources management strategies; and (6) Subsurface fluids withdrawal. We invite you to explore these proceedings, the previous ones, and the references cited therein, and hope and trust you will find this compilation useful.

The UNESCO Working Group on Land Subsidence

Alice Aureli, International Hydrological Programme (IHP), UNESCO, Paris, France
A. Ivan Johnson, Consultant, Arvada, Colorado, USA. Honorary Chairman
Laura Carbognin, Chair, National Research Council, Venice, Italy
Keith R. Prince, Vice Chair, USGS, Menlo Park, California, USA
Frans B. Barends, Deltares–GeoDelft, Delft, The Netherlands
Dora Carreón-Freyre, CGEO-UNAM, Querétaro, Mexico
Devin L. Galloway, USGS, Sacramento, CA, USA
Giuseppe Gambolati, Padua University, Padua, Italy
Jane Frankenfield Zanin, Technical Secretary, National Research Council, Venice, Italy

---

[4] Johnson, A. I., Carbognin, L. & Ubertini, L., eds. (1986) *Land Subsidence* (Proceedings of the Third International Symposium on Land Subsidence (Venice, Italy, March 1984). IAHS Publ. 151, 939 p., http://iahs.info/redbooks/151.htm, accessed 20 August 2010.

[5] Johnson, A. I. ed. (1991) *Land Subsidence* (Proceedings of the Fourth International Symposium on Land Subsidence, May 1991, Houston, Texas. IAHS Publ. 200, 690 p., http://iahs.info/redbooks/200.htm, accessed 20 August 2010.

[6] Barends, F. B. J., Brouwer, F. J. J. & Schröder, F. H., eds. (1995) *Land Subsidence* (Proceedings of the Fifth International Symposium on Land Subsidence (October 1995, The Hague, Netherlands). IAHS Publ. 234, http://iahs.info/redbooks/234.htm.

[7] Carbognin, L., Gambolati, G. & Johnson, A.I., eds. (2000) *Land Subsidence*—Proceedings of the Sixth International Symposium on Land Subsidence (Ravenna, Italy, September 2000), vol. 1 (384 p.), vol. 2 (433 p.), Padova, Italy, La Garagola.

[8] Zhang, A., Gong, S., Carbognin, L. &Johnson, A. I., eds. (2005) *Land Subsidence*—Proceedings of the 7th International Symposium on Land Subsidence (October 2005), vols 1–2. Shanghai Scientific & Technical Publishers, Shanghai, PRC, 918 p.

Contents

Preface by *Dora C. Carreón-Freyre, Mariano Cerca & Devin Galloway* v

Introduction by *Alice Aureli, Laura Carbognin, Keith R. Prince, Frans B. Barends, Dora C. Carreón-Freyre, Devin Galloway, Giuseppe Gambolati & Jane Frankenfield Zanin* ix

1 Earth Fissures, Fracturing and Faulting Related to Land Subsidence

KEYNOTE: Mechanisms for earth fissure formation in heavily pumped basins 3
T. J. Burbey

Implications of ground-deformation measurements across earth fissures in subsidence areas in the southwestern USA *T. L. Holzer* 9

Soil fracturing induced by land subsidence *G. Auvinet* 20

On the mechanisms for earth fissuring in Las Vegas valley: a numerical analysis of pumping-induced deformation and stress *M. Hernández-Marín & T. J. Burbey* 27

Advances in geotechnical characterization of soil fracturing in Mexico City basin 33
G. Auvinet, E. Méndez & J. Lermo

Monitoring land-surface deformation on Bicycle Lake playa, Fort Irwin, California, USA *Jill Densmore, Kevin Ellett, Jim Howle, Michael Carpenter & Michelle Sneed* 39

Monitoring of land subsidence and fracturing in Iztapalapa, Mexico City 44
D. Carreón Freyre, M. Cerca, R. Gutiérrez Calderón & M. Huerta Ladrón de Guevara

Microtremor measurements to detect zones of potential cracking in the basin of México 51
J. Lermo, E. Ovando & L. Espinosa

Application of Wigner-Ville distribution to identify anomalies in GPR profiles 54
M. A. Elizondo, R. E. Chávez, M. E. Câmara & A. Tejero

2 Modelling Land Subsidence and Associated Hazards

Use of the SUB-WT Package for MODFLOW to simulate aquifer-system compaction in Antelope Valley, California, USA *Stanley A. Leake & Devin L. Galloway* 61

Monitoring and modelling 3-D ground movements induced by seasonal gas storage in deep reservoirs *P. Teatini, G. Gambolati, N. Castelletto, M. Ferronato, C. Janna, E. Cairo, D. Marzorati, D. Colombo, A. Ferretti, A. Bagliani, F. Bottazzi & F. Rocca* 68

A regional land subsidence model embodying complex deformation characteristics 76
S. Ye, Y. Xue, J. Wu, Z. Wei & Q. Li

Modelling land subsidence processes induced by fast rainwater infiltration through fractures into the unsaturated zone *I. Martinez, R. Hinkelmann & S. Savidis* 82

Nonlinear analysis of land subsidence due to groundwater level oscillation by a finite difference method *Hessam Yazdani, M. M. Toufigh & Amin Masoudzade* 90

Thermo-poro-elastic effects in the anthropogenic uplift of Venice by deep seawater injection *N. Castelletto, M. Ferronato, G. Gambolati, C. Janna & P. Teatini* 96

An analytical solution of plane strain consolidation due to a point sink within a fluid-saturated poroelastic media *Pei-Chao Li, Yue-Lei He, Yi-Ming Mi & Shi-Liang Gong* 102

Research on a 3-D visualized strata model virtual reality system of land subsidence in Suzhou-Wuxi-Changzhou area *Yu Jun, Su Xiao-Si, Zhu Lin, Duan Fu-Zhou, Pan Yun, Gao Li & Wu Shu-Liang* 108

Integration of geological and hydrogeological features for subsidence modelling in volcanic zones *Gil Ochoa-González & Dora Carreón-Freyre* 114

Impact of longwall mining of coal on highways in southwestern Pennsylvania *J. J. Gutiérrez, L. E. Vallejo, J. S. Lin & R. Painter* 120

Inverting subsidence data to detect possible compartmentalization in a gas reservoir in The Netherlands *K. Visser, A. G. Muntendam-Bos, G. Kunakbayeva, O. Leeuwenburgh, E. Peters & P. A. Fokker* 126

Simulation of ground failure due to groundwater pumping *Carlo Janna, Massimiliano Ferronato, Giuseppe Gambolati & Pietro Teatini* 133

Two-dimensional coupled numerical modelling of subsidence due to water extraction at the Lower Llobregat River, Spain *A. Concha1, J. Ripoll, J. Piña, A. Gabàs & P. Piña* 136

Introduction of the JARAS/3D simulator for natural gas dissolved in water *Tsutomu Nakagawa, Ikkou Suzuki, Manabu Nojo, Takeru Ogatsu & Tomoyuki Higuchi* 140

Parameters estimation in surface subsidence modelling *R. Hejmanowski* 144

3 Land Subsidence Related to Geological and Geomechanical Processes

KEYNOTE: Land subsidence processes and associated ground fracturing in central Mexico *D. Carreón-Freyre* 149

Subsidence in the Holocene delta of The Netherlands *L. M. Vonhögen, P. J. Doornenbal, Ger de Lange, P. A. Fokker & J. L. Gunnink* 158

Is there a tectonic component to the subsidence process in Morelia, Mexico? *E. Cabral-Cano, A. Arciniega-Ceballos, O. Díaz-Molina, F. Cigna, A. Ávila-Olivera, B. Osmanoglu, T. Dixon, C. Demets, V. H. Garduño-Monroy, F. Vergara-Huerta & J. E. Hernández-Quintero* 164

Evaluation of the subsidence and risk of collapse in the Estació neighbourhood of Sallent City, Catalonia (Spain) *F. López, P. Buxó, J. Palau, J. Marturià, A. Concha & P. Martínez* 170

Zonation and prediction of land subsidence: case study, Kerman, Iran *S. M. Vaezinejad, M. M. Toufigh & S. M. Marandi* 173

Zoning map of ground failure risk due to land subsidence of San Luis Potosí, Mexico *Jesús Pacheco-Martínez, Jorge Arzate-Flores, Rubén López-Doncel, Rafael Barboza-Gudiño, José Luis Mata-Segura, Antonio Del-Rosal-Pardo & Jorge Aranda-Gómez* 179

Integrated study of land subsidence in Morelia, Michoacán, Mexico *J. A. Ávila-Olivera, V. H. Garduño-Monroy & P. Farina* 185

Geological setting of active faulting associated with land subsidence at the Aguascalientes and Querétaro valleys, Mexico *J. Martínez-Reyes & L. M. Mitre-Salazar* 191

Conceptual model of land subsidence with a structural control *J. A. Ávila-Olivera & V. H. Garduño-Monroy* 195

Geological study and electrical resistivity tomography of Ameca, Jalisco, Mexico *A. Malagón, J. Rosas-Elguera, M. A. Alatorre, G. Perez & R. Maciel* 198

Geological and geophysical characterization of fracturing in granular deposits associated with land subsidence in San Luis Potosí City, Mexico *L. D. Barajas-Nigoche, D. C. Carreón-Freyre, J. L. Mata-Segura, A. Rivera-León & F. Cafaggi-Félix* 201

Land subsidence of the Aguascalientes Valley, México: historical review and present situation *M. A. Romero-Navarro, J. Pacheco-Martínez, J. A. Ortiz-Lozano, M. E. Zermeño-De León, G. Araiza-Garaygordobil & E. Mendoza-Otero* 207

Assessment of land subsidence associated with intense erosion zones in the Zacatecas and Guadalupe quadrangles, Mexico *F. J. Escalona-Alcazar, L. A. Delgado-Argote & A. F. Rivera-Salinas* 210

Seismic basaltic structure under the local subsidence in San Lorenzo Tezonco, Iztapalapa, México, Distrito Federal *Leobardo Salazar, Pedro Vera & Gema Guevara* 213

Geophysical and geotechnical studies applied to determine a subsidence problem in Pachuca de Soto, Hidalgo, Mexico *L. A. Tapia, A. Tejero& R. Chavez* 216

Instability of the urbanized flank of El Peñón del Marques volcanic edifice and its relation to land subsidence in Mexico City *M. Cerca, D. C. Carreón-Freyre & R. Gutiérrez* 219

Microcracking of expansive soils during shrinkage processes: roles of mineralogy and microstructure *M. Audiguier, R. Cojean & Z. Geremew* 224

Evolution of Mexico City clay properties affected by land subsidence Alberto Jaime P. & E. Méndes-Sánchez 232

Ground subsidence induced by backfill-mining of a nickel mine and development forecasts *F. S. Ma, H. J. Zhao, Y. M. Zhang & J. Guo* 235

Analysis of engineering land subsidence effects caused by shield construction for tunnels *Yang Tianliang, Yan Xuexin, Wang Hanmei, Zhan Longxi, Xu Zhun & Zhuang Yibin* 238

4 Monitoring Techniques of Ground Displacements and Subsurface Deformation

KEYNOTE: Advanced monitoring techniques for mapping land displacement on the Venice coastland with satellite SAR data *T. Strozzi, L. Tosi, P. Teatini, U. Wegmüller, M. Santoro & L. Carbognin* 249

Subsidence and fault hazard maps using PSI and permanent GPS networks in central Mexico *E. Cabral-Cano, B. Osmanoglu, T. Dixon, S. Wdowinski, C. DeMets, F. Cigna & O. Díaz-Molina* 255

Measurement of land subsidence using interferometry, Coachella Valley, California *M. Sneed* 260

Monitoring techniques for analysing subsidence: a basis for implementing an Early Warning System *J. Marturia, J. Ripoll, A. Concha & M. Barberà* 264

DInSAR analysis of land subsidence caused by geothermal fluid exploitation in the Mexicali Valley, B.C., Mexico *O. Sarychikhina, E. Glowacka, F. suarez-Vidal1 & R. Mellors* 268

Long-term Differential InSAR monitoring of the Lampur Sidoarjo mud volcano (Java, Indonesia) using ALOS PALSAR imagery *A. Thomas, R. Holley, R. Burren, D. Shilston, D. Waring& C. Meikle* 274

Radar interferometry-based mapping of the present land subsidence along the low-lying northern Adriatic coast of Italy *G. Bitelli, F. Bonsignore, L. Carbognin, A. Ferretti, T. Strozzi, P. Teatini, L. Tosi & L. Vittuari* 279

Monitoring swelling soils through PSI and DinSAR interferometry: applications in eastern Paris Basin, France *H. F. Kaveh, B. Deffontaines, B. Fruneau, R. Cojean, M. Audiguier, A. Arnaud & J. Duro* 287

Land subsidence at the Kujukuri Plain in Chiba Prefecture, Japan: Evaluation and monitoring environmental impacts *H. Obanawa, T. Tokunaga, S. Rokugawa, T. Deguchi & T. Nakamura* 293

Subsidence monitoring of an Iranian oil field inferred from SAR interferometry *N. Fouladi Moghaddam, A. A. Matkan, M. R. Sahebi, M. Roostaei & H. R. Baqtiari* 299

Mexico City subsidence analysis assisted by InSAR *P. López-Quiroz, M. P. Doin, F. Tupin, P. Briole & J. M. Nicolas* 304

Land subsidence in Emilia-Romagna Region, northern Italy: recent results *R. Bissoli, G. Bitelli, F. Bonsignore, A. Rapino & L. Vittuari* 307

Large area observation of land subsidence by PSInSAR and determination of the cause of local land subsidence *K. Daito, S. Saeki, S. Kuzuoka & T. Mizuno* 312

Land subsidence monitored by satellite interferometry in Mexican cities *J. A. Ávila-Olivera, P. Farina & V. H. Garduño-Monroy* 316

Using extensometer and Earth tide data to quantify fractured crystalline-rock properties *T. J. Burbey & L. C. Murdoch* 319

Continuous monitoring techniques of fault displacement caused by geothermal fluid extraction in the Cerro Prieto Geothermal Field (Baja California, Mexico) *Ewa Glowacka, Olga Sarychikhina, F. Alejandro Nava, Francisco Suarez, Jorge Ramirez, Miguel Guzman, Braulio Robles, Francisco Farfan & Guillermo Diaz De Cossio Batani* 326

Recent extensometric data for the monitoring of subsidence in Bologna (Italy) *F. Bonsignore, G. Bitelli, A. Chahoud, P. Macini, E. Mesini, P. Severi, B. Villani & L. Vittuari* 333

Land subsidence monitoring system in the southeast part of Kanto groundwater basin, Japan *A. Kagawa & K. Furuno* 339

Integrated monitoring network for surface deformation in Capo Colonna archaeological area, Crotone, Italy *F. Verdecchia, C. Zoccatelli, E. Norelli & R. Miandro* 345

Monitoring land subsidence over a shallow gas reservoir in India using GPS *P. R. Patel* 352

Measuring seabed altimetric variations with a repeat-track SAS interferometry experiment: processing and results *R. De Paulis, C. Prati, S. Scirpoli, P. A. Sletner & A. Tesei* 358

In situ compaction measurements via radioactive markers in the Northern Adriatic basin: an analysis of data precision over 15 years of monitoring *C. Zoccatelli, F. Verdecchia, G. Cassiani, R. Deiana & N. Fraticelli* 364

In situ formation compaction monitoring in deep reservoirs using optical fibres *Shoji Kunisue & Tatsuo Kokubo* 368

Comparing several GPS post-processing strategies for a potash basin monitoring network in northeast Spain: first results *J. Gili, N. Lantada, A. Concha, X. Soler, C. Puig & J. Marturia* 371

Analysis of landslide monitoring using an e-GPS system and multi-antenna GPS technology *T. K. Yeh, Y. S. Hu & Y. A. Liou* 374

Land subsidence observation using GPS on the Kujukuri Plain *D. Murai, M. Nakamura, S. Ikeda, F. Waki & N. Isezaki* 377

Evaluation of Mexico City subsidence *G. Auvinet, E. Méndez & U. Matus* 380

5 Social and Economic Impacts and Their Incorporation into Resources Management Strategies

KEYNOTE: Review of subsidence management in the Netherlands *F. B. J. Barends* 385

Land subsidence and environmental law in Mexico: a reflection on civil liability for environmental damage *Pedro Joaquín Gutiérrez-Yurrita* 396

Considerations on strategies of sustainable management of oil and gas fields in Italy *G. Brighenti, P. Macini & E. Mesini* 402

Management of the environmental resources of the Kanto groundwater basin in Japan – land subsidence and monitoring system *K. Furuno, A. Kagawa, O. Kazaoka, Y. Sakai, T. Kusuda & H. Nirei* 408

Environmental and social effects derived from groundwater extraction in Tláhuac and Valle-de-Chalco-Solidaridad, Metropolitan Area of Mexico City *A. Toscana & M. M Campos* 414

The centenary of land subsidence monitoring in Shanghai *Shi-Liang Gong* 419

How much subsidence is allowed: the introduction of the "effective subsidence capacity" concept in The Netherlands *Jan van Herk, Hans Roest, Ingrid Kroon, Jaap Breunese & Hans De Waal* 420

A warning system for exceeding subsidence limits *M. Nepveu, I. C. Kroon & P. A. Fokker* 426

Need to integrate land subsidence into the legal instruments of Mexico: Morelia, Michoacán case study *L. L. Padilla-Gil, J. A. Ávila-Olivera, G. A. Huape-Padilla & M. E. Granados-García* 432

Institutional controls in an area of subsidence induced flooding *Susan L. Baird* 435

A fuzzy based-approach to building damage risk assessment *Agnieszka Malinowska* 443

Assessment of the state and condition of damaged buildings and structures affected by land subsidence *J. A. Ortiz, F. A. Alonso, J. Pacheco, M. E. Zermeño, G. Araiza & E. Mendoza* 449

Guidelines for the design of a unit of urban risk prevention for subsurface fracturing in the Municipality of Iztapalapa in Mexico City
H. C. Carreón-Freyre & J. C. Rodríguez-Quiroz 452

6 Land Subsidence Caused by Subsurface Fluids Withdrawal

Pumping effects on land subsidence in the Toluca Valley, Mexico
A. I. Calderhead, R. Martel, J. Garfias, A. Rivera & R. Therrien 461

Integrated simulation of consumptive use and land subsidence in the Central Valley, California, for the past and for a future subject to urbanization and climate change
R. T. Hanson, A. L. Flint, L. E. Flint, C. C. Faunt, Wolfgang Schmid, M. D. Dettinger, S. A. Leake & D. R. Cayan 467

1-D infiltration, analysis of unsaturated flow and increase in land subsidence
S. A. Masoudzade, M. M. Toufigh, H. Yazdani & R. Rahgozar 472

A theory of three-dimensional land motion in terms of its velocity field
J. Li & D. C. Helm 475

Deformation characteristics of aquifer sands due to groundwater pumping in the Southern Yangtze Delta, China *Y. Zhang, Y. Q. Xue, J. C. Wu & X. Q. Shi* 484

Post-audit of land subsidence modelling of Saga-Shiroishi plain, Japan — lessons and improvements toward useful modelling *K. Fujisaki* 491

Hazards of gases migrating over oilfields due to subsidence
J. O. Robertson, Jr & G. V. Chilingar 497

Subsidence faulting and aquifer vulnerability – their relation in Irapuato, Mexico
A. Schroeder & R. Rodríguez 502

Axisymmetric motion of a confined leaky aquifer due to pumping groundwater from a partially penetrating well *J. Li* 505

Climate change impact and anthropogenic effects in land subsidence of Querétaro valley, Mexico *E. González-Sosa, N. R. Ramos-Salinas & C. A. Mastachi-Loza* 514

Key Words 519

1 Earth Fissures, Fracturing and Faulting Related to Land Subsidence

Land Subsidence, Associated Hazards and the Role of Natural Resources Development
(Proceedings of EISOLS 2010, Querétaro, Mexico, 17–22 October 2010). IAHS Publ. 339, 2010.

Mechanisms for earth fissure formation in heavily pumped basins

T. J. BURBEY
Department of Geosciences Virginia Tech, 4044 Derring Hall, Blacksburg, Virginia 24061, USA
tjburbey@vt.edu

Abstract Earth fissures are perhaps the most deleterious by-products of excessive groundwater exploitation in many subsidence-prone arid-zone sedimentary basins. These features have long been associated with differential land subsidence caused by changes in the thickness of compacting sediments, abrupt changes in stratigraphy, or by large changes in vertical effective stress resulting from large drawdown gradients. However, it is recognized that pumping-induced earth fissures can and do form in areas far from the centre of pumping where drawdowns are small and the changes in drawdown are even smaller. The key to understanding where and why fissures form is to first recognize that subsidence is a three-dimensional phenomenon; horizontal strain can play a vital, if not a dominant, role in invoking fissure formation, yet this important component is often ignored or considered irrelevant. The second key is the shape and properties of the boundary conditions. Boundary conditions here refer to any feature that affects the transmission of stress and strain in three dimensions. Thus, boundaries can be represented as faults, bedrock knobs, basin edges, or other heterogeneities causing stratigraphic changes. It is clear that such boundaries would cause abrupt changes in physical parameters such as bulk modulus and hydraulic conductivity. However, the shape of the boundary is also important relative to the stress regime imposed by pumping. Subvertical faults, thinning aquifers and bedrock knobs can cause an unequal vertical distribution of horizontal strain, which results in rotation of the adjacent sediments that can cause zones of localized compression and zones of localized extension. These zones of extension can migrate upward and exceed the failure criterion in the weak vadose zone, resulting in a fissure that can originate anywhere between the saturated zone and land surface.

Key words earth fissures; land subsidence; aquifer mechanics; faults; sedimentary basins

INTRODUCTION

Even though the physical laws governing three-dimensional aquifer deformation due to applied stresses (e.g. pumping) have been known for over a half century (Biot, 1941, 1955), the empirical understanding and application of land subsidence research has been based largely on vertical deformation alone (Poland & Davis, 1969; Poland, 1972; Gambolati *et al*., 1974; Bouwer, 1977; Lofgren, 1978; Hanson, 1989; Pope & Burbey, 2004). The omission of horizontal strain was based on the premises that: (1) it was likely not nearly as important as vertical strain (Jacob, 1940); (2) including horizontal strain would make the analytical expressions intractable for practical applications, and (3) little or no field data were available to support incorporating its effects. However, after Wolff's (1970) detailed strain measurements during an aquifer test revealed the surprisingly large horizontal strains relative to the vertical strain values, it became evident that horizontal deformation was worth further investigation. Helm later presented a rigorous mathematical development of the importance of horizontal displacement during pumping, graphically representing the vertical and horizontal motions of aquifers under stress (Helm, 1987, 1994). Since this time, GPS (global positioning systems) have allowed for accurate and precise measurements of horizontal motions at the land surface that result from aquifer pumping (Burbey *et al*., 2006). Now numerical modelling of both field and hypothetical settings incorporate vertical and horizontal strain and deformation in recognition of their coupled nature and importance in accurately simulating land subsidence resulting from volumetric changes in storage (Burbey, 2001, 2006; Kihm *et al*., 2007; Gambolati *et al*., 2009).

The analysis and understanding of earth fissure formation in heavily pumped basins has taken a similar research path to that of subsidence modelling. Early researchers concluded that pumping-induced fissures were entirely the result of extensional stresses occurring at the surface of the

Copyright © 2010 IAHS Press

brittle unsaturated zone resulting from a draping effect of compressible unconsolidated materials around an underlying rigid impediment such as a bedrock knob, or a bedrock ledge res ulting from faulting creating an abrupt change in sediment thickness (Jachens & Holzer, 1982; Holzer, 1984). Although vertical deformation continues to be an important mechanism in understanding the genesis and location of earth fissures, it alone cannot explain the occurrence of fissures in areas where only minimal water-level changes occur or where faults or other hydrological boundaries influence the occurrence and nature of fissuring, and it cannot explain why some fissures migrate upward from depth (the draping effect assumes that fissures originate at the land surface and migrate downward).

PUMPING-INDUCED STRAIN

Groundwater pumping imposes a volumetric strain on confined aquifer systems in proportion to the volume of water pumped and the storage properties of the aquifer. When the horizontal components of strain are ignored (hoop and radial strain in radial flow systems) the entire volume strain is constrained to the vertical component only, which may incorrectly exaggerate the overall resulting displacement (land subsidence). Figure 1 shows a hypothetical distribution of water pumped from a confined aquifer based on the three strain components in a radial flow system after a prolonged period of pumping. The important facet of this illustration is that the horizontal strain components can be important in areas far from the pumping well, typically where vertical components are small. The radial strain is extensional in areas where subsidence (and likely drawdown) is small. Furthermore, near the edge of the basin there may even be uplift associated with pumping as indicated by the negative vertical strain.

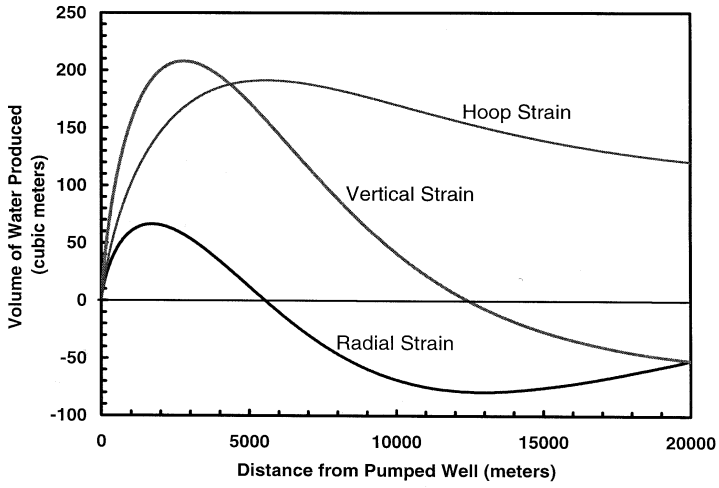

Fig. 1 Plot showing the source of pumped water based on the three strain components; from Burbey (2001).

Figure 1 illustrates the importance of considering strain (and deformation) in three dimensions. Furthermore, care must be taken when analysing the effects of pumping. One should not assume that because vertical compaction or drawdown is small in areas far from the pumping centre that pumping cannot be inducing significant strain. If a mechanical or hydraulic boundary is present (even far from the pumping centre) to impede the transmission of horizontal stress and strain, then it is possible for stress and strain to accumulate near the impeding boundary, or to induce large changes in shear or tensional strain, which can result in the formation of earth fissures in weak sediments such as those with a low moisture content.

THE AFFECT OF BOUNDARIES ON FISSURE FORMATION

When only vertical strain is considered, fissures will tend to form where significant differential vertical displacement occurs. Such occurrences are where: (1) the thickness of compressible deposits changes rapidly, (2) where the compressibility of the compacting materials changes rapidly, or (3) where the head changes rapidly, inducing a large effective stress change on the compressible deposits. These conditions can certainly be met at a boundary such as an impermeable fault, which would result in a large head gradient (and subsequent vertical strain gradient), or at a bedrock knob or ledge where the thickness of the compacting sediments changes abruptly. However, earth fissures have been observed in areas where little head change occurs, or where little vertical deformation is measured, in regions far from the centre of pumping. In fact, pumping-induced earth fissures can occur in all parts of a sedimentary basin, even along the basin periphery.

Figure 2 shows three types of boundary conditions that can lead to fissure formation in heavily pumped sedimentary basins. In all three cases the mechanisms for fissure initiation is different but the conditions for fissure formation are as follows: (1) the pumping rate and time since initiation is significant such that the zone of maximum horizontal strain has migrated outward far from the pumping well and maximum horizontal displacements are generally measured in centimetres; (2) although vertical deformation and head changes can be large in the vicinity of pumping, it is not a requirement that these conditions be true where the fissures are shown to form; (3) a relatively thick and brittle vadose zone needs to overlie the aquifer zone undergoing deformation because in each case the fissures originate within this mechanically weak layer.

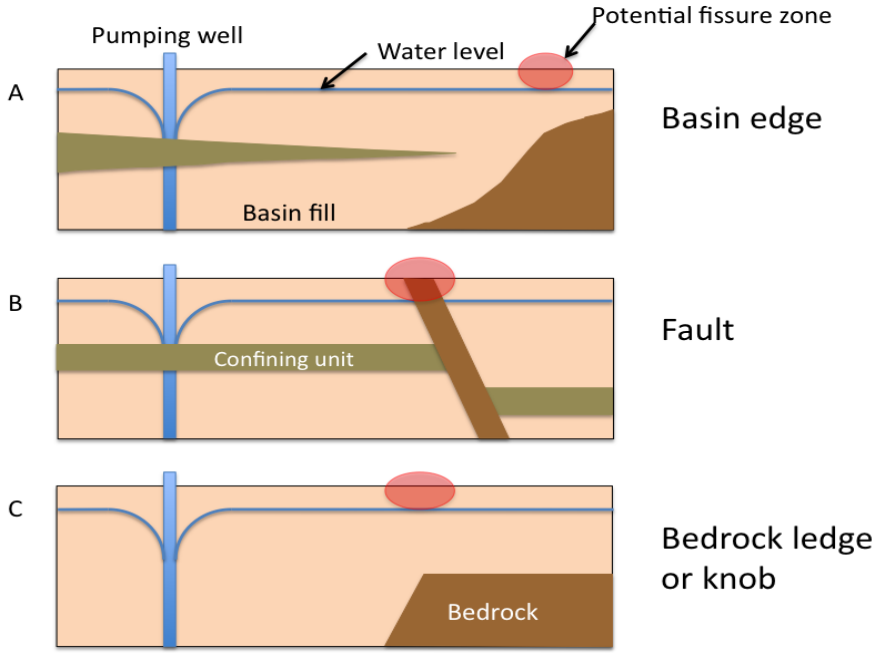

Fig. 2 Conceptualizations of a heavily pumped sedimentary basin where drawdown and vertical deformation may be large near the zone of pumping. The most likely location of earth fissures is shown to occur (A) above the shoulder near the edge of the basin, (B) on either side of a rotating basin-fill fault, and (C) above an abrupt change in aquifer thickness due to a bedrock knob or ledge.

The hydromechanical mechanisms leading to earth fissures in each of the three cases in Fig. 2 are all largely caused by an accumulation of horizontal stresses or strains within the fissure zone or below the fissure zone within the aquifer undergoing deformation. In the case of Fig. 2A near the edge of a sedimentary basin, earth fissure formation is a complex process involving a number of factors including: (1) the slope of the bedrock–sediment interface (Sheng *et al.*, 2003), (2) the

occurrence of a bedrock shoulder (Rojas *et al*., 2002), and (3) the change in thickness of the aquifer. Large tensile stress and horizontal deformations toward the subsiding basin occur up-dip of the inflection point of the bedrock boundary, with the shoulder representing the zone of greatest strain leading to possible failure. The fissures from this type of boundary can be observed around the periphery of heavily pumped basins (Bell & Price, 1991; Rojas *et al*., 2002).

The occurrence of basin-fill faults is common and their role in influencing land subsidence patterns has been well established (Bell *et al*., 2002). Furthermore, the occurrence of earth fissures appears to be related to faults because fissure zones are typically found adjacent to these faults. Hernandez-Marin & Burbey (2010) performed hypothetical numerical simulations that reflect the conditions surrounding a major basin-fill fault in Las Vegas Valley across which differential subsidence is large due to municipal pumping on one side of the fault, but head changes across the fault are minor. The results of this investigation indicate that stress accumulation occurs in two primary regions, tensile stress becomes large enough near the top of the vadose zone on the hanging wall as a result of tension from a clockwise rotation of the upper portion of the fault toward the zone of pumping (Fig. 3A). This rotation is induced by differential horizontal displacements imposed by pumping due to the subvertical nature of the fault. A second zone of high shear stress occurs at the base of the vadose zone on the footwall block (negative shear) (Fig. 3B), which is also the result of fault rotation. Both zones can and do lead to fissures, which have been observed on both sides of fault zones. In both cases, the fissures initiate in the zone of greatest tensile or shear stress and migrate upward to the land surface over time.

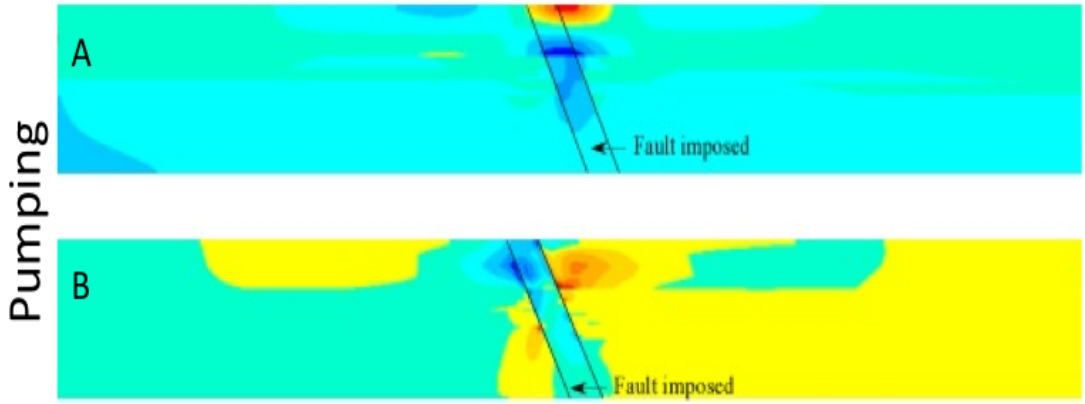

Fig. 3 Simulated stresses resulting from pumping in the vicinity of a fault composed of sand-like material; (A) tensile stress regime with red indicating extension and blue indicating compression; (B) shear stress regime with red indicating positive shear stress and blue indicating negative shear stress (Hernandez-Marin, 2010).

In the third case (Figs 2C and 4) fissures occur above the transition between the thick sedimentary basin toward the zone of pumping and the relatively thin aquifer due to the presence of a bedrock knob or bedrock ledge. It is easy to understand why this would likely represent a zone of differential subsidence at the land surface. However, exactly why fissures would occur here is not necessarily a matter of simple surface draping and extension at the surface. In fact, Fig. 4 suggests that horizontal deformation at the boundary is greater than the vertical deformation. The presence of the large bedrock boundary imposed the following conditions: (1) horizontal deformations that are greater near the land surface than at the bottom of the aquifer. This may impose a rotation of the sedimentary block in a clockwise fashion toward the pumping well; (2) above the ledge the net deformation is upwards, creating a large accumulation of vertical shear strain that can easily contribute to the formation of earth fissures in the brittle unsaturated zone in the region shown in Fig. 4; (3) a sharp horizontal strain gradient also occurs at the edge of the

bedrock ledge, which can also contribute to failure. It should be noted that large vertical differential subsidence is not required for these simulated conditions to occur. Of course differential vertical subsidence can also contribute to the rupture, but the location of the rupture is likely a reflection of strain accumulation at the edge of the ledge from differential horizontal deformation and rotation.

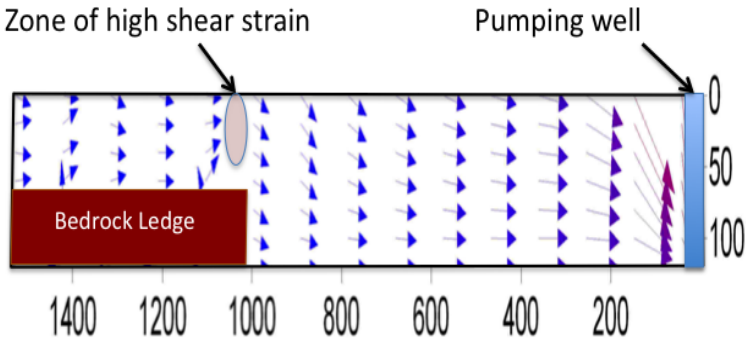

Fig. 4 Hypothetical simulation of sedimentary basin pumping from the deepest 40 m of the system with a bedrock ledge at approximately 1000 m from the pumping well. Vectors show the relative magnitude of displacement.

SUMMARY AND CONCLUSIONS

The analysis of both vertical and horizontal aquifer motions induced by heavy pumping in sedimentary basins is necessary to understand where earth fissures are likely to form. In many locations where pumping-induced earth fissures occur the amount of vertical subsidence or water-level change may be comparatively small. The relatively large amount of horizontal deformations in areas far from the zone of pumping can lead to substantial stress and strain accumulation in the vicinity of boundaries such as: (1) a basin edge, (2) a basin-fill fault, or (3) a bedrock knob or ledge. The hydromechanics associated with each of these boundaries is somewhat different and complex. The common occurrence in each case, however, is an accumulation of stress and/or strain resulting from horizontal deformation and the complex interactions of the pumping-induced deformation with the boundary. Clearly, to understand the location of fissure genesis requires a thorough understanding of the hydrogeological setting as well as an analysis of the three three-dimensional stress-strain regimes associated with anthropogenic pumping.

REFERENCES

Bell, J. W., Amelung, F., Ramelli, A. R. & Blewitt, G. (2002) Land subsidence in Las Vegas, Nevada, 1935–2000: New geodetic data show evolution, revised spatial patters, and reduced rates. *Environmental & Engineering Geoscience* **8**(3), 155–174.

Bell, J. W. & Price, J. G. (1991) Subsidence in Las Vegas Valley, 1980–91. Nevada Bureau of Mines and Geology Final Project Report, 10: 9 plates, unpaginated.

Biot, M. A. (1941) General theory of three-dimensional consolidation. *J. Appl. Phys.* **12**(2), 155–164.

Biot, M. A. (1955). Theory of elasticity and consolidation for a porous anisotropic solid. *J. Appl. Phys.* **26**(2), 182–185.

Bouwer, H. (1977) Land subsidence and cracking due to ground-water depletion. *Ground Water* **15**(5), 358–364.

Burbey, T. J. (2001) Storage coefficient revisited: Is purely vertical strain a good assumption? *Ground Water* **30**(3), 458–464.

Burbey, T. J. (2006) Three-dimensional deformation and strain induced by municipal pumping, Part 2: Numerical analysis. *J. Hydrol.* **330**(3-4), 422–434.

Burbey, T. J., Warner, S. M., Blewitt, G., Bell, J. W. & Hill, E. (2006) Three-dimensional deformation and strain induced by municipal pumping, part 1: Analysis of field data. *J. Hydrol.* **319**(1-4), 123–142.

Gambolati, G., Gatto, P. & Freeze, R. A. (1974) Mathematical simulation of the subsidence of Venice, 2: Results. *Water Resour. Res.* **10**, 563–577.

Gambolati, G. *et al*. (2009) On the uniformity of anthropogenic Venice uplift. *Terra Nova* **21**(6), 1–7.

Hanson, R. T. (1989) Aquifer-system compaction, Tucson Basin and Avra Valley, Arizona. *Water-Resources Investigations Report 88-4172. US Geological Survey*, 69 pp.

Helm, D. C. (1987) Three-dimensional consolidation theory in terms of the velocity of solids. *Geotechnique* **37**(3), 369–392.

Helm, D. C. (1994) Horizontal aquifer movement in a Theis-Theim confined system. *Water Resour. Res.* **30**(4), 953–964.

Hernandes-Marin, M. & Burbey, T. J. (2009) The role of faulting on surface deformation patterns from pumping-induced groundwater flow. *Hydrogeology J.* **17**(8), 1859–1875.

Hernandez-Marin, M. (2010) *Numerical Evaluation and Analysis of the Occurrence of Earth Fissures in Faulted Sedimentary Basin*s. Virginia Tech, Blacksburg, Virginia, USA.

Holzer, T. L. (1984) Ground failure induced by ground-water withdrawal from unconsolidated sediment. *Reviews in Engineering Geology* **6**, 67–104.

Jachens, R. C. & Holzer, T. L. (1982) Differential compaction mechanism for earth fissures near Casa Grande, Arizona. *Geol. Soc. Am. Bull.* **93**, 998–1012.

Jacob, C. E. (1940) On the flow of water in elastic artesian aquifers. *Trans. Am. Geophys. Un.* **21**, 574–586.

Kihm, J.-H., Kim, J.-M., Song, S.-H. & Lee, G.-S. (2007) Three-dimensional numerical simulation of fully coupled groundwater flow and land deformation due to groundwater pumping in an unsaturated fluvial aquifer system. *J. Hydrol.* **335**, 1–14.

Lofgren, B. E. (1978) Hydraulic stresses cause ground movement and fissures, Picacho, Arizona. *Geol. Soc. Am. Abstracts with Programs* **10**, 271.

Poland, J. F. (1972) Land subsidence in the western states due to ground-water overdraft. *Water Resour. Bull.* **8**, 118–131.

Poland, J. F. & Davis, G. H. (1969) Land subsidence due to withdrawal of fluid. In: *Reviews in Engineering Geology* (ed. by D. J. Varnes & G. Kiersch), 187–269. Geological Society of America, Boulder, Colorado, USA.

Pope, J. P. & Burbey, T. J. (2004) Multiple-aquifer characterization from single borehole extensometer records. *Ground Water* **42**(1), 45–58.

Rojas, E., Arzate, J. & Arroyo, M. (2002) A method to predict group fissuring and faulting caused by regional groundwater decline. *Engineering Geology* **65**, 245–260.

Sheng, Z., Helm, D. C. & Li, J. (2003) Mechanics of earth fissuring caused by groundwater withdrawal. *Environmental & Engineering Geoscience* **9**(4), 351–362.

Wolff, R. G. (1970) Relationship between horizontal strain near a well and reverse water level fluctuation. *Water Resour. Res.* **6**, 1721–1728.

(Proceedings of EISOLS 2010, Querétaro, Mexico, 17–22 October 2010). IAHS Publ. 339, 2010.

Implications of ground-deformation measurements across earth fissures in subsidence areas in the southwestern USA

T. L. HOLZER
United States Geological Survey, 345 Middlefield Road, MS977, Menlo Park, California 94025, USA
tholzer@usgs.gov

Abstract Ground deformation was monitored at earth fissures in areas of land subsidence induced by groundwater extraction in the southwestern United States. The ground deformation is consistent with the mechanism that fissures are caused by horizontal strains generated by bending of overburden in response to localized differential compaction. Subsidence profiles indicated that localized differential subsidence occurred across the fissures and that maximum convex-upward curvature was at the fissure. The overall shape of the profile stayed similar with time, and maximum curvature remained stationary at the fissure. Horizontal displacements were largest near the fissure, and generally were small to negligible away from the fissure. Maximum tensile horizontal strains were at the fissure and coincided with maximum curvature in the subsidence profiles. Horizontal tensile strain continued to accumulate at fissures after they formed, with rates of opening ranging from 30 to 120 microstrain/year at fissures in Arizona.

Key words subsidence; earth fissure; ground deformation; geodesy; monitoring; creep; groundwater; USA

INTRODUCTION

Earth fissures, long tension cracks with negligible vertical offset, are common in subsiding areas in the southwestern United States where groundwater has been withdrawn from unconsolidated sedimentary aquifer systems (Holzer, 1984). These fissures pose a significant hazard because they frequently are eroded by storm runoff into metre-wide and decametre-deep gullies. Earth fissures also can divert large volumes of surface runoff and may affect groundwater quality. The impressive surface appearance of many fissures is further enhanced by their decametre to kilometre lengths. Earth fissures that are associated with land subsidence caused by groundwater withdrawal should not be confused with similar appearing large tensile ground cracks that are caused by either hydrocompaction (Lofgren, 1969) or desiccation (Neal *et al.*, 1968).

Several mechanisms have been proposed to explain the origin of the horizontal strains that cause earth fissures: (1) bending caused by localized differential subsidence, (2) regional differential subsidence, and (3) horizontal deformation within the compacting portion of the aquifer system.

Bending caused by localized differential subsidence was originally proposed by Feth (1951) to explain an earth fissure in 1949 in south-central Arizona. He speculated that it was caused by tensile strains generated by locally varying subsidence. He attributed the differential subsidence to local variations in aquifer thickness. The 1949 fissure continued to evolve, however, and in 1961 vertical offset was reported across it (Peterson, 1962). The surface scarp ultimately grew to an approximate length of 15.8 km and height of 0.6 m (Holzer *et al.*, 1978). Because the surface expression and morphology of the scarp were similar to surface faults that had been reported in other areas of land subsidence (e.g. Holzer, 1984), Holzer *et al.* (1978) formally named the feature the Picacho Fault. Subsurface exploration revealed that the Picacho Fault is the surface expression of a pre-existing tectonic fault that is a partial barrier to groundwater flow in the alluvium (Holzer, 1978; Pankratz *et al.*, 1978). Feth's (1951) proposed mechanism for fissures, however, was corroborated by Jachens & Holzer (1982) for a complex fissure system in alluvium on the east side of the Casa Grande Mountains in south-central Arizona. Their field investigation confirmed that fissures formed at locations where the aquifer system thinned because of buried topographic relief of the crystalline bedrock surface underlying the aquifer system. Topographic profiles across fissures on the undisturbed desert floor indicated differential subsidence had occurred that was proportional to aquifer thickness. Modelling of the bending process indicated tensile strains at failure ranged from 200 to 2000 microstrain.

Rotation of rigid slabs of overburden in response to regional subsidence was proposed by Bouwer (1977) as the cause of earth fissures. By Bouwer's (1977) mechanism, earth fissures should form around the margins of subsidence bowls and be oriented orthogonal to regional subsidence gradients.

Horizontal deformation within the compacting portion of the aquifer system was first proposed by Lofgren (1971). He attributed surficial horizontal displacements in subsidence areas to deep seated deformation caused by horizontal seepage forces. He hypothesized that the deformation was capable of causing earth fissures (Lofgren, 1978). Lofgren's conceptual model was formalized by Sheng *et al.* (2003), who concluded that formation of earth fissures was controlled by a complex combination of aquifer deformation at depth, pre-existing subsurface structure, and the *in situ* stress field. They hypothesized that fissures form in tensile zones that are created at depth. Fissures form in the tensile zones where sediment is brittle and susceptible to tensile failure.

The purpose of this manuscript is to present observations of ground deformation across earth fissures in subsiding areas in Arizona, California, and Nevada in the southwestern United States (Fig. 1). These observations can be used to evaluate proposed mechanisms of formation for earth fissures. Understanding of mechanism is also useful for predicting where future fissures may form (Holzer, 2000).

Fig. 1 Map of major subsidence areas in the western United States and earth fissure monitoring areas. A is Picacho Basin, B is Las Vegas Valley, Nevada, and C is Fremont Valley, California.

METHODOLOGY

Ground deformation was monitored with bench-mark arrays that were established orthogonally to each fissure. Arrays varied from multiple bench marks to bench-mark pairs. Distances between bench marks in the arrays that consisted of multiple bench marks were variable, and typically increased with distance from the earth fissure. Bench-mark pairs were 30 m apart. Ground deformation was computed based on comparisons of repeated precise geodetic surveys of the

bench marks. Both vertical and horizontal positions of bench marks were measured. Where feasible, each array included a bench mark established on nearby bedrock outcrops. This enabled computations of absolute displacements. Some fissures were too far from bedrock outcrops to justify labour-intensive levelling, and only relative displacements could be computed for these arrays.

Vertical positions of bench marks were measured by first-order levelling using a precision level and invar survey rods. Levelling was performed to first-order, class 1 standards. Such levelling has a nominal accuracy in millimetres of $1.5K^{½}$, where K is distance in kilometres between bench marks (Federal Geodetic Control Committee, 1974). Horizontal positions of bench marks were measured with a Hewlett-Packard 3805A electronic distance meter (EDM). Slope distances were measured with the EDM, and were corrected to horizontal distances based on elevations measured in the level surveys. Repeated surveys of a stable bench-mark array in Menlo Park, California, indicated that the EDM had a precision (one standard deviation) of ±1.8 mm at 202 m and ±1.2 mm at 23 m. Horizontal positions of closely spaced (=30 m) bench marks that spanned fissures were also measured with a calibrated narrow steel ribbon tape. Tape measurements were made under a constant tension and were temperature corrected. Such taping has an estimated accuracy of ±2 mm for 30-m distances (Lufkin, 1972).

GROUND DEFORMATION OBSERVATIONS

Observations of ground deformation in three study areas, Picacho Basin, Arizona, Las Vegas Valley, Nevada, and Fremont Valley, California, are presented here (Fig. 1). During the period of monitoring, 1976 to 1989, all three areas experienced water-level declines caused by groundwater extraction and subsided due to aquifer system compaction. Picacho Basin received the greatest scrutiny of the three areas because it was an agricultural area with easy access and earth fissures were widespread. Monitoring in Las Vegas Valley was particularly challenging because the urban setting was not conducive to the establishment and preservation of bench marks.

Picacho Basin, south-central Arizona

The Picacho Basin is a deep alluvial sedimentary basin southeast of Phoenix, Arizona. The shallow unconsolidated sediments in the basin constitute a major aquifer system. Water-level declines, which locally exceeded 100 m, began in approximately 1940 after the introduction of the turbine pump. Subsidence locally exceeds 2.9 m (Holzer *et al.*, 1978). A 1200-km^2 area in the basin has subsided by more than 30 cm in response to the water-level declines (Fig. 2). Earth fissures are widespread within the basin (Schumann, 1974).

Monitoring of earth fissures was conducted at eight sites in the Picacho Basin (Fig. 2). Most of the sites consisted of single curvilinear fissures, but site 5 covered a complex system of fissures. Profiles are presented here for four sites. Creep histories, based on repeated measurement of the spacing of closely spaced bench marks spanning eight fissures are also presented.

Figure 3 shows profiles of subsidence, total displacements, and horizontal strains at sites 6 and 7 in the northern Picacho Basin. Fissures at both sites were simple long curvilinear ground failures. The bench-mark arrays were originally established at the ends of newly formed fissures in anticipation that the fissures would grow in length and propagate between the bench marks, which they did within a year of the establishment of the arrays in 1976. The arrays initially consisted of two bench marks that were 30 m apart. Each array was expanded with additional bench marks a couple of years later after the fissure propagated through the initial bench-mark pair. Both arrays, when completed, extended to nearby bedrock.

Earth fissures in both subsidence profiles are located at points of maximum convex-upward curvature. The maximum curvature in each profile remained stationary at the fissure over the 6- to 7-year monitoring periods. Total displacements indicate horizontal displacements are largest near the fissure, and decrease basinward (direction of increasing subsidence). Horizontal strains computed from the horizontal displacements are tensile and largest at the fissure.

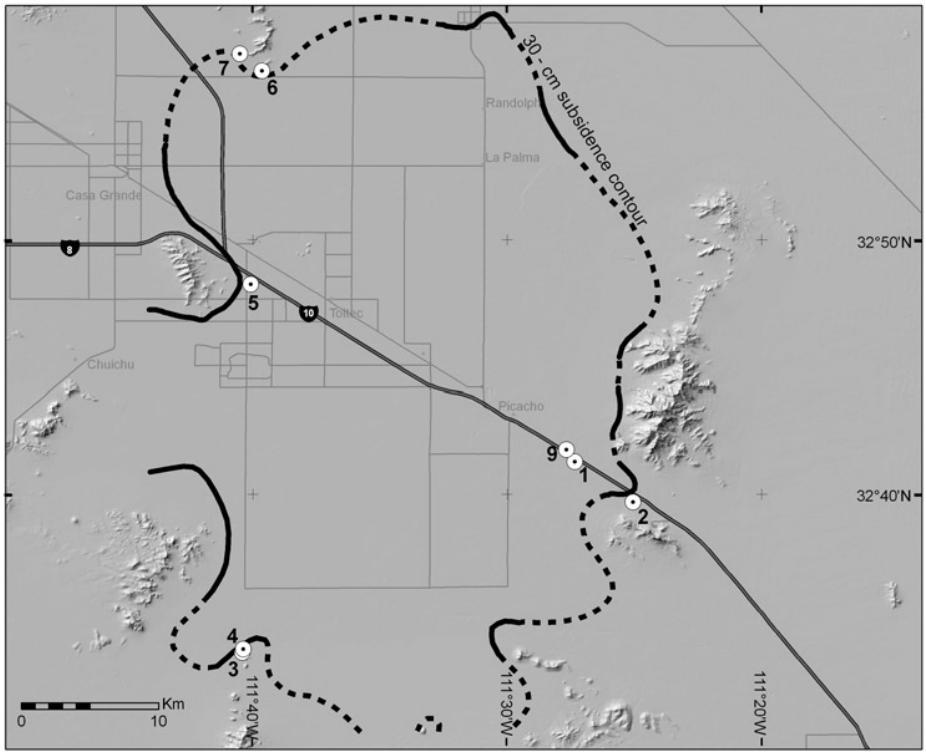

Fig. 2 Map of Picacho Basin, Arizona, and ground-failure monitoring sites. Contour outlines area where land subsidence has exceeded 30 cm. Line is solid where subsidence is confirmed by geodetic surveys, and dashed where inferred.

A profile across the first reported earth fissure in the Picacho Basin is shown in Fig. 4. The fissure formed in 1927 (Leonard, 1929), and until 1949 was the only documented fissure in the basin. The 1949 fissure reported by Feth (1951) was assumed for many years to be a re-activation of the 1927 fissure. Holzer *et al.* (1978), however, demonstrated that the 1927 fissure was located 0.87 km northwest of the 1949 fissure. Inspection of the 1927 fissure in the 1970s by the author indicated it was inactive. It was essentially filled in with sediment and barely discernible on modern aerial photographs. The 1980–1985 profiles in Fig. 4(a), which show absolute subsidence, did not detect differential ground deformation across the fissure. Subsidence was uniform across the fissure, and no differential horizontal displacements (or strain) were observed from 1980 to 1985 (Fig. 4).

Figure 5 is a profile that crosses a complex system of earth fissures in alluvium on the east side of the Casa Grande Mountains. Subsurface conditions beneath the fissure system were studied by Jachens & Holzer (1982). Ground deformation was monitored across the northern part of the fissure system. The subsidence profile reveals differential subsidence was ongoing across the eastern fissure, and that the annual accumulation of horizontal strain across the fissure was 140 microstrain. The subsurface investigation by Jachens & Holzer (1982) indicates that the fissure overlies a buried bedrock ridge at the base of the aquifer system, and the differential subsidence is attributable to variability in aquifer system thickness. Although the centre of the regional subsidence bowl is located several kilometres to the east, the total displacement vectors indicate that the ground on the western side of the ridge is moving westward towards the Casa Grande Mountains, away from the centre of the bowl.

Time histories of changes in distance between bench marks that spanned eight monitored earth fissures are shown in Fig. 6. The histories are based on taping of bench marks that were 30 m apart. The histories indicate that extension across fissures continued after the fissures formed. Long-term creep rates vary from fissure to fissure. The highest rate was measured at site 1, which continued to extend at a rate of 120 microstrain/year (3.5 mm/year). No creep was measured at site 9, which straddled the 1927 fissure.

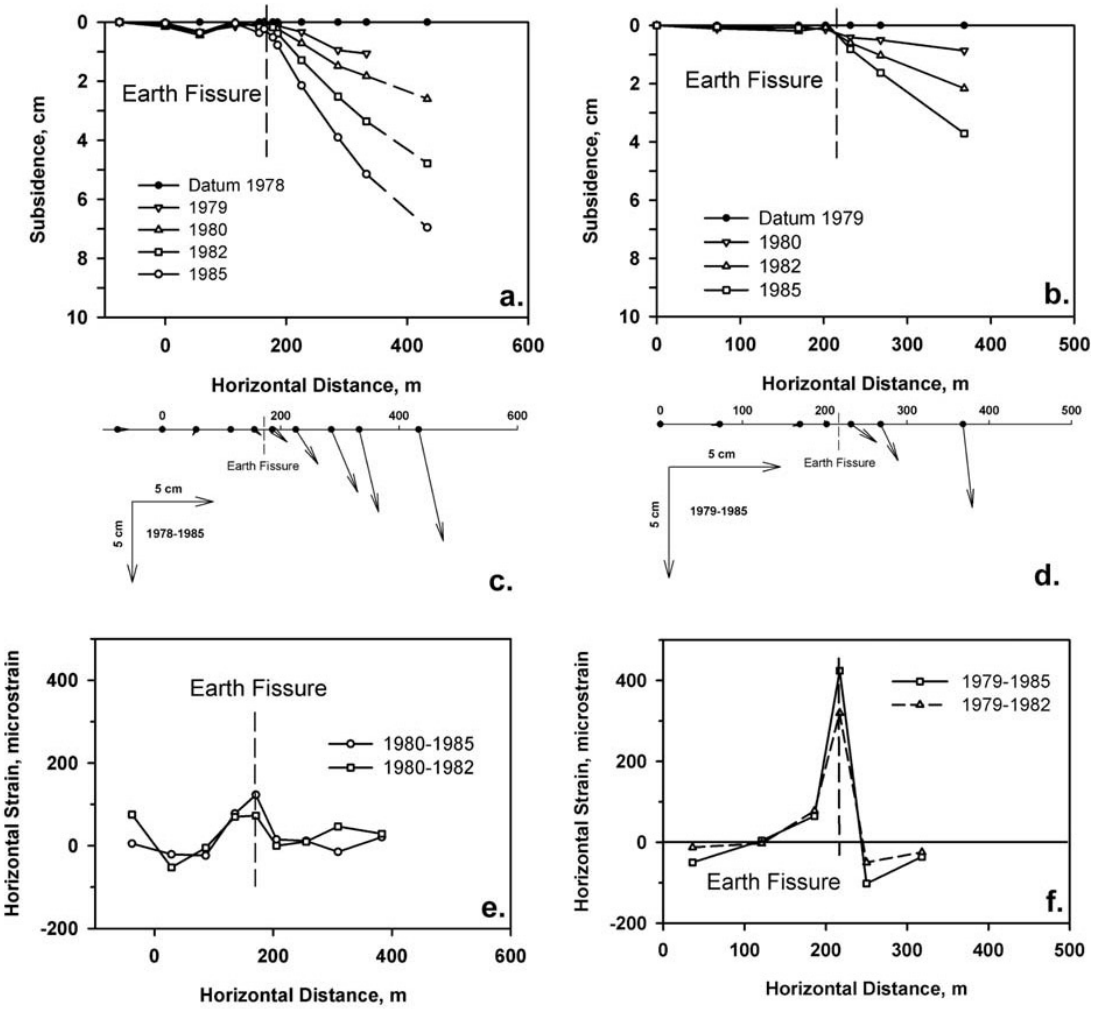

Fig. 3 Ground deformation at sites 6 (a, c, and e) and 7 (b, d, and f), northern Picacho Basin, Arizona. Positive horizontal strain in e and f are tensile.

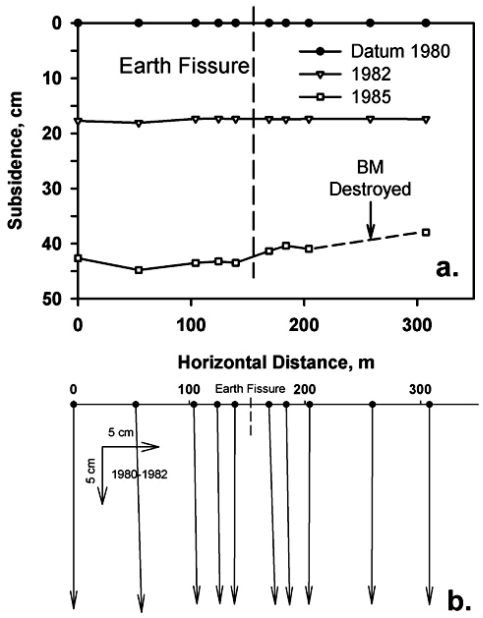

Fig. 4 Ground deformation at site 2, Picacho Basin, Arizona. Earth fissure formed in 1927 (Leonard, 1929).

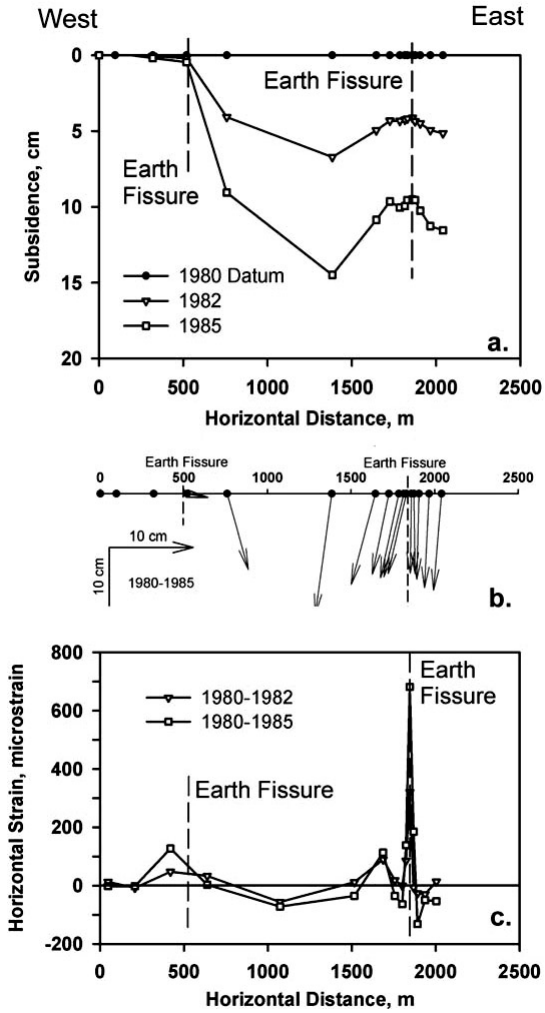

Fig. 5 Ground deformation at site 5, east side of Casa Grande Mountains, Picacho Basin Arizona. Positive horizontal strain in c is tensile.

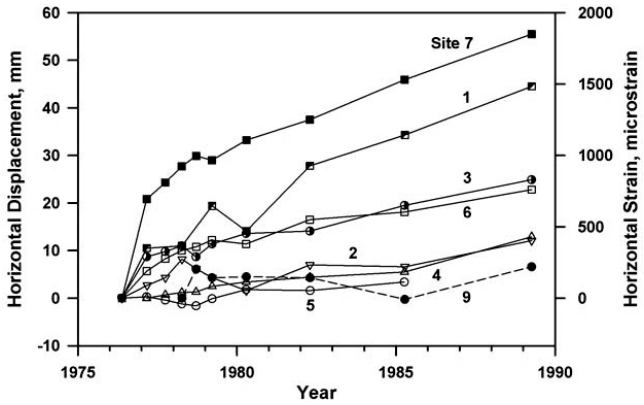

Fig. 6 Time histories of relative displacements of bench marks 30-m apart that span earth fissures in Picacho Basin, Arizona. Monitoring sites are shown by number in Fig. 2.

Las Vegas Valley, Nevada

Las Vegas Valley is underlain by a complex sequence of faulted alluvial sediments. These sediments have provided groundwater to the valley since 1907, and this has led to almost

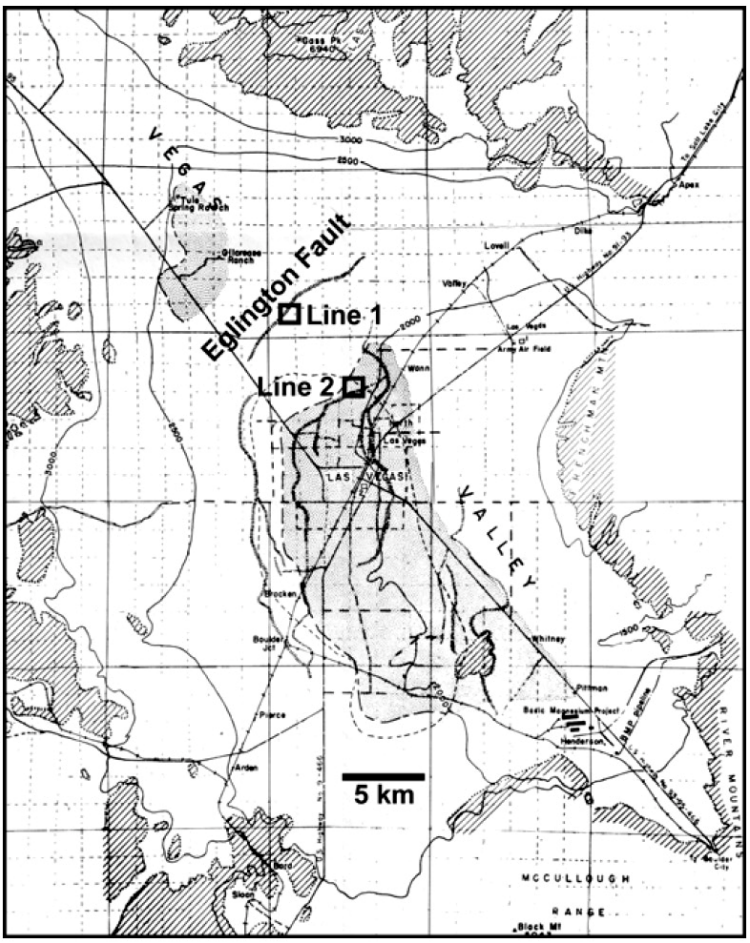

Fig. 7 Map of Las Vegas Valley (from Maxey & Jameson, 1948).

continuous water-level declines. Approximately 120 km^2 of land has subsided more than 30 cm. Maximum subsidence is more than 1.5 m (Galloway *et al.*, 1999).

Two sites were briefly monitored in Las Vegas Valley. Monitoring ended when the bench-mark arrays were destroyed by urban development. Locations of the two monitor sites are shown in Fig. 7. Line 1 was on the downthrown side of the pre-existing fault scarp, the Eglington Fault, and line 2 was on the upthrown side of a pre-existing, but unnamed, fault scarp. Both arrays were approximately 300-m long and were not referenced to a locally stable bedrock bench mark. The profiles reveal that the earth fissures are coincident with locations of maximum convex upward curvature in the subsidence profiles (Fig. 8). Horizontal displacements produced tensile strains at both fissures, although the computed strains for line 1 are ambiguous. Peak tensile strain from 1980 to 1982 at the fissure crossed by line 2 was 250 microstrain.

Fremont Valley, California

Fremont Valley is a tectonic pull-apart basin formed between left-stepping strands of the active Garlock Fault, which is a major tectonic feature in southern California (Davis & Burchfiel, 1973). Pampeyan *et al.* (1988) provide an in-depth review of ground failure in Fremont Valley and its history. Groundwater levels declined locally as much as 88 m from 1954 to 1980, and regional land subsidence was documented, principally along the valley margin. Earth fissures and surface faulting were extensive in the area of groundwater level decline. Modern ground failure in Fremont Valley was first noted in August 1971, and consisted of open cracks along and on trend with Holocene fault scarps.

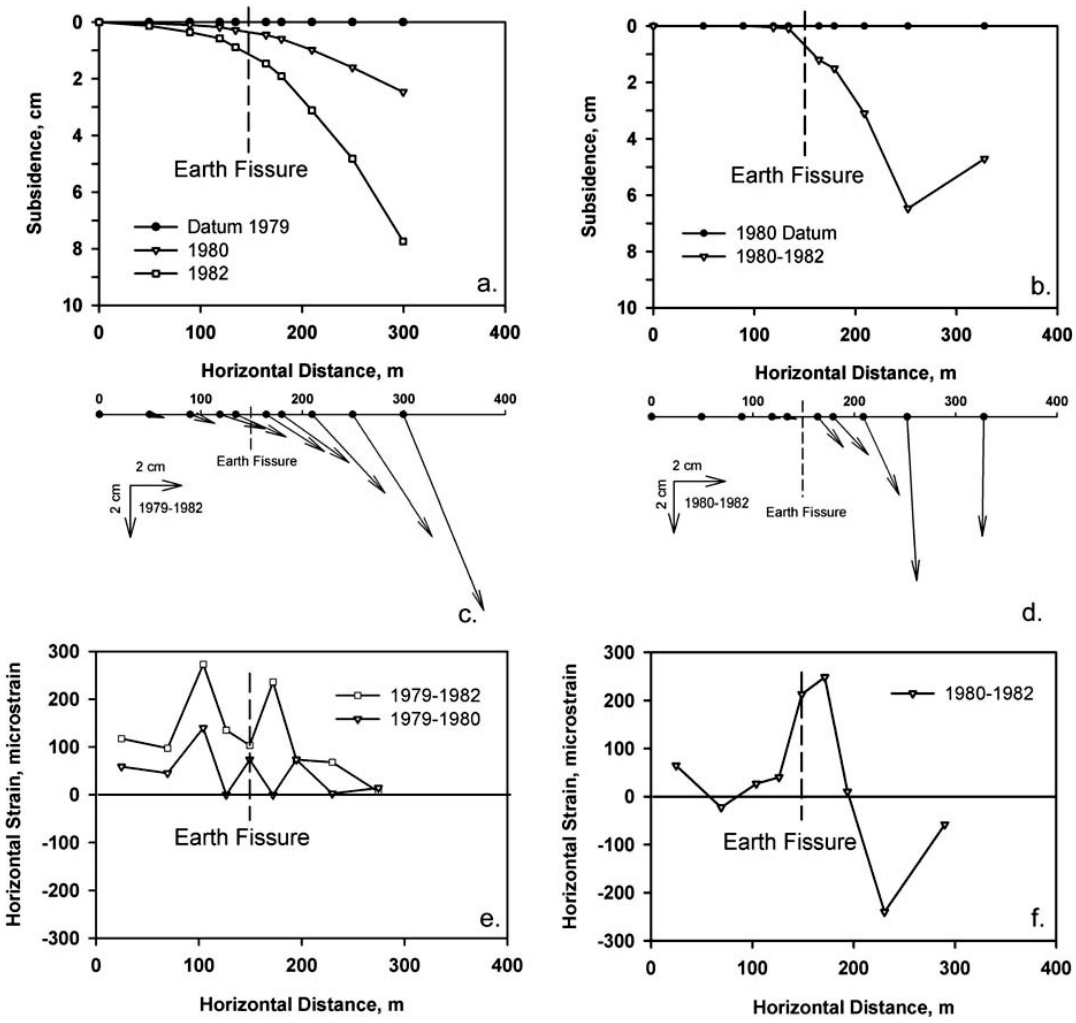

Fig. 8 Ground deformation at lines 1 (a, c, and e) and 2 (b, d, and f), Las Vegas Valley, Nevada. Positive horizontal strain in e and f are tensile.

Although Pampeyan *et al.* (1988) mapped extensive modern ground failures in Fremont Valley, only one earth fissure in the southern part of the valley was monitored (Fig. 9). Other monitored failures consisted of modern surface faulting.

Ground deformation near the earth fissure is shown in Fig. 10. The fissure occurred along a 2-m high Holocene fault scarp. The 300-m array was not referenced to a locally stable bench mark on bedrock. Displacements as shown are relative to the upthrown side of the fault scarp. Approximately 14 cm of differential subsidence occurred across the fissure from 1978 to 1985. Horizontal displacements on the downthrown side of the scarp increased from 5.7 to 10.3 cm with distance from the scarp. Differential horizontal displacements from 1978 to 1985 caused a horizontal tensile strain at the fissure of 2750 microstrain. This yields a rate of opening of 400 microstrain/year. Although not shown here, differential subsidence across the fissure decreased seasonally during periods of water level recoveries (see Holzer & Pampeyan, 1981, Fig. 3f). This suggests that some of the annual deformation was elastic and recoverable.

DISCUSSION

All of the subsidence profiles spanning the earth fissures indicate that localized differential subsidence is occurring across newly formed and active fissures. The maximum curvature in each

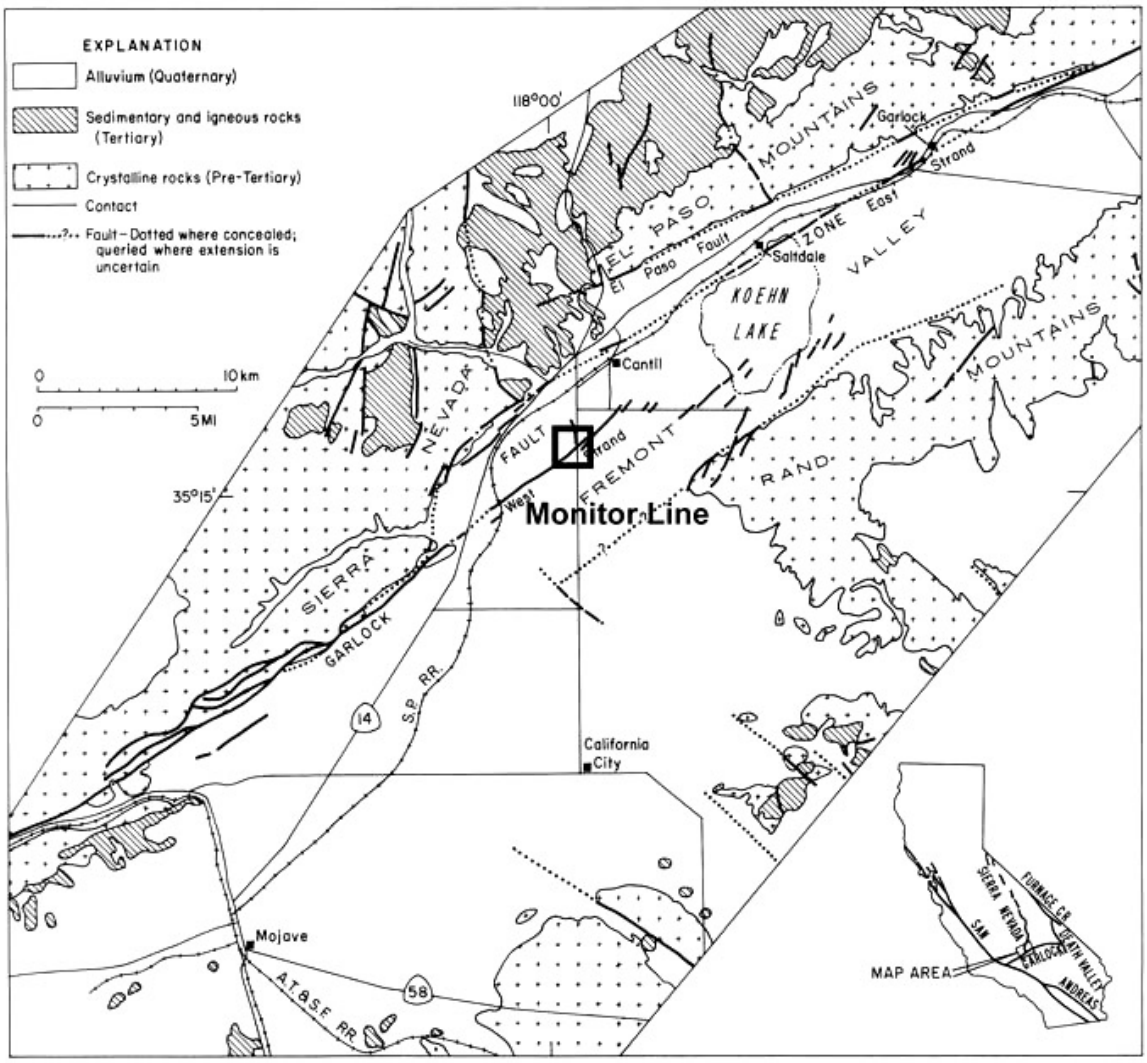

Fig. 9 Map of Fremont Valley with monitor site (from Pampeyan *et al.*, 1988).

subsidence profile is at the fissure and convex upward. The overall shape of the profile stays similar over time with maximum curvature remaining at the fissure. Horizontal displacements are largest near the fissure. In general, horizontal displacements are small to negligible away from the fissure. Variation of horizontal displacements in the profiles indicates tensile horizontal strains are at a maximum at the fissure. Maximum horizontal strain is coincident with the maximum curvature in the subsidence profiles.

The deformation fields that were observed across the earth fissures in the southwestern United States are most consistent with the mechanism for fissure formation that consists of bending caused by localized differential subsidence (Feth, 1951). This mechanism was analysed by Lee & Shen (1969) and used to predict tensile cracking in earth dams subjected to differential settlements. They showed that local differential subsidence can cause differential horizontal displacements and large tensile strains. Modelling and laboratory analyses indicated that the tensile horizontal strains are caused by simple bending of the overburden. They also demonstrated that peak tensile strains coincide with the locations of maximum convex-upward curvature in subsidence profiles as was observed here. The monitoring observations reported here are not consistent with either regional differential subsidence (Bouwer, 1977) or horizontal deformation within the compacting portion of the aquifer system (Sheng *et al.*, 2003). Neither of these mechanisms requires local differential subsidence across the earth fissure, as was observed.

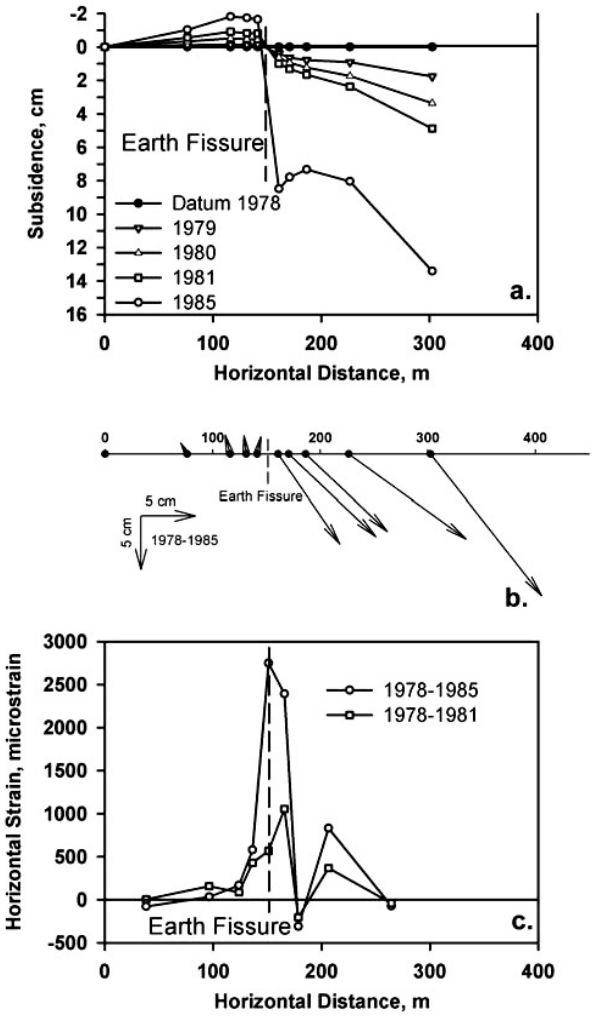

Fig. 10 Ground deformation, Fremont Valley, California. Positive horizontal strain in c is tensile.

Continued accumulation of horizontal tensile strain after fissures formed is an interesting aspect of monitoring the bench-mark pairs that spanned the fissures in Arizona. Rates of opening or creep ranged from 30 to 120 microstrain/year (0.9 to 3.5 mm/year). Observation of creep across earth fissures may explain why some fissures re-activate after periods of apparent dormancy and infilling with sediment. The observation of ongoing differential subsidence across fissures after they have formed is the probable explanation of this creep-like behaviour. The observation of creep suggests that a visually dormant fissure may continue to pose a displacement hazard after the fissure has formed. Fissures, however, presumably can become dormant when differential compaction ceases. This could occur in situations where groundwater levels stabilize or recover, or where a declining water table falls below the zone that is differentially compacting. The 1927 Arizona fissure may be an example of this phenomenon.

REFERENCES

Bouwer, H. (1977) Land subsidence and cracking due to groundwater depletion. *Ground Water* **15**(5), 358–364.

Davis, G. A. & Burchfiel, B. C. (1973) Garlock fault, an intracontinental transform feature, southern California. *Bull. Geol. Soc. Am.* **84**, 1407–1422.

Federal Geodetic Control Committee (1974) Classification, standards of accuracy, and general specifications of geodetic control surveys. National Oceanic and Atmospheric Administration, Washington, DC, USA.

Feth, J. H. (1951) Structural reconnaissance of the Red Rock Quadrangle, Arizona. *US Geological Survey Open-file Report 51-199*, p.32.

Galloway, D., Jones, D. R. & Ingebritsen, S. E. (1999) Land subsidence in the United States. *US Geological Survey Circular 1182*, p. 175.

Holzer, T. L. (1978) Results and interpretation of exploratory drilling near the Picacho fault, south-central Arizona. *US Geological Survey Open-file Report 78-1016,* p. 17.

Holzer, T. L. (1984) Ground failure induced by ground-water withdrawal from unconsolidated sediment. In: Man-induced Land Subsidence (ed. by T. L. Holzer), *Geol. Soc. Am., Reviews in Engineering Geology* **6**, 67–105.

Holzer, T. L. (2000) Methods for prediction of earth fissures and faults associated with groundwater withdrawal. In: *The Fragile Territory* (10th Congresso Nazionale dei Geologi, Consiglio Nazionale dei Geologi, Rome), 179–185.

Holzer, T. L., Davis, S. N. & Lofgren, B. E. (1978) Faulting caused by groundwater extraction in southcentral Arizona. *J. Geophys. Res*. **84**(B2), 603–612.

Holzer, T. L. & Pampeyan, E. H. (1981) Earth fissures and localized differential subsidence. *Water Resour. Res.* **17**(1), 223–227.

Jachens, R. C. & Holzer, T. L. (1982) Differential compaction mechanism for earth fissures near Casa Grande, Arizona, *Bull. Geol. Soc. Am.* **93**(10), 998–1012.

Lee, K. L. & Shen, C. K. (1969) Horizontal movements related to subsidence. *ASCE J. Soil Mechanics* **94**(SM6), 140–166.

Leonard, R. J. (1929) An earth fissure in southern Arizona. *J. Geology* **37**(8), 765–774.

Lofgren, B. E. (1969) Land subsidence due to the application of water. In: (ed. by D.J. Varnes & G. Kiersch) *Geol. Soc. Am. Reviews in Engineering Geology* **2**, 271–303.

Lofgren, B. E. (1971) Significant role of seepage stresses in compressible aquifer systems (abstract). *Eos, Trans. AGU* **52**(11), p. 832.

Lofgren, B. E. (1978) Hydraulic stresses cause ground movement and fissures, Picacho, Arizona. *Geol. Soc. Am. Abstracts with Programs* **10**(3), 113.

Lufkin (1972) *Taping Techniques for Engineers and Surveyors*. The Lietz Company, Carson, California, USA.

Maxey, G. B. & Jameson, C. H. (1948) Geology and water resources of Las Vegas, Pahrump, and Indian Spring Valleys, Clark and Nye Counties, Nevada. *Nevada Water Resources Bulletin* **5**, 121.

Neal, J. T., Langer, A. M. & Kerr, P. F. (1968) Giant desiccation polygons of Great Basin playas. *Bull. Geol. Soc. Am.* **79**(1), 69–90.

Pampeyan, E. H., Holzer, T. L. & Clark, M. M. (1988) Modern ground failure in the Garlock fault zone, Fremont Valley, California. *Bull. Geol. Soc. Am.* **100**(5), 677–691.

Pankratz, L. W., Ackermann, H. D. & Jachens, R. C. (1978) Results and interpretation of geophysical studies near the Picacho Fault, south-central Arizona. *US Geological Survey Open-file Report 78-1106*, p. 17.

Peterson, D. E. (1962) Earth fissuring in the Picacho area, Pinal County, Arizona. Department of Geology, University of Arizona, Tucson, USA.

Schumann, H. H. (1974) Land subsidence and earth fissures in alluvial deposits in the Phoenix area, Arizona. *US Geological Survey, Miscellaneous Investigations Map I-845-H.*

Sheng, Z., Helm, D. C. & Li, J. (2003) Mechanisms of earth fissuring caused by groundwater withdrawal. *Environ. Engng Geoscience* **9**(4), 351–362.

(Proceedings of EISOLS 2010, Querétaro, Mexico, 17–22 October 2010). IAHS Publ. 339, 2010.

Soil fracturing induced by land subsidence

G. AUVINET
Instituto de Ingeniería, UNAM, Ciudad Universitaria,Apdo. Postal 70-472, Coyoacán, 04510, México, D.F.
gauvinetg@iingen.unam.mx

Abstract Soil fracturing occurs due to the development of shear and tension stresses within the soil mass. Fracture mechanics constitutes a useful theoretical framework for this problem. Different types of cracks have been observed in the Mexico City basin and other parts of the Mexican Republic. Several fracturing mechanisms have been identified. Some of them are a clear consequence of land subsidence due to pumping in deep aquifers. This paper illustrates this type of fractures with actual field observations and presents a brief review of the attempts that have been made at modelling this phenomenon.

Key words fracturing; soil; land subsidence; fracture mechanics; numerical modelling

INTRODUCTION

During recent decades, an increasing number of soil fractures have been detected in Mexico City valley and other Mexican metropolitan areas such as Celaya, Morelia, Querétaro, Aguascalientes and Toluca, to name just a few. Such fractures are a matter of growing concern for the population and authorities since they have caused a series of accidents and serious damage to constructions and public services. It is now acknowledged that the soil fracturing problem is an important risk factor and that the best scientific tools and techniques should be mobilized to define prevention and mitigating measures.

Soil fracturing can occur as a consequence of any condition leading to large tensile stresses or extension strains in the soil. Accordingly, cracks in the soil have different origin, including contraction of compressible clays by drying, stresses induced by the weight of constructions, hydraulic fracturing of soft soils, seismic movements, etc. However, the largest and more destructive fractures are generally a direct consequence of land subsidence associated with pumping of water in deep aquifers, and this is the case in Mexico City.

The concepts of fracture mechanics that are briefly presented in this paper are helpful for a better understanding and interpretation of the mechanisms that lead to soil cracking. However, field observations and surveys of actual cracks performed by different groups, including Laboratorio de Geoinformática, Instituto de Ingeniería UNAM, for Mexico City basin subsoil (Méndez *et al.*, 2010) have provided valuable physical evidence that allow a classification of the different types of cracks for this region. This has proven useful for defining prevention and mitigation measures.

THEORETICAL CONCEPTS

The generation of cracks in soils can be described using theoretical concepts borrowed from *fracture mechanics* commonly used to deal with problems such as structural fracturing in the aeronautic industry. The brief review presented below is principally based on Auvinet (1991, 2008).

Fracturing modes

Any solid responds to extreme loading by presenting large strains, generally concentrated along a potential failure surface, or by fracturing. The latter phenomenon consists of a loss of continuity between two parts of the solid. Fracturing implies a crack to be formed and to propagate until total collapse happens or until a new equilibrium is attained. The front of a crack is the vertex that connects all the contiguous points where subsequent separation occurs or may occur. During a continuous separation process, this line moves along a plane called the fracturing surface.

Copyright © 2010 IAHS Press

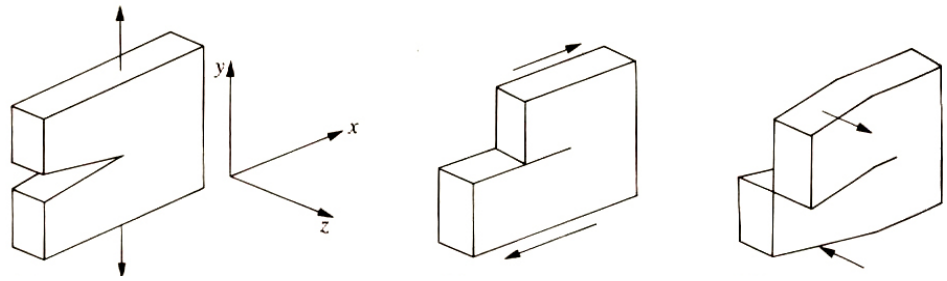

(I) (II) (III)

Fig. 1 Cracking modes: (I) opening mode; (II) shearing mode; (III) tearing mode.

According to Irwin (1957), three basic types of fracturing modes can be distinguished (Fig. 1):

- Mode I: Tension stresses tend to tear off and separate two different zones within the continuum.
- Mode II: This mode comes about when two portions of a continuum are sheared apart and slide along planes tangent to the directions of shearing stresses, creating a discontinuity in the solid.
- Mode III: This mode involves displacements perpendicular to the crack front and to the planes on which shearing takes place.

In general, in homogeneous bodies fracturing can be described by one or a combination of those modes. However, cracking propagation generally takes place close to Mode I. Cracking in soils is also influenced by the soil profile, stratification, sedimentation or transport mechanisms, all of which may induce inherent anisotropy in the material and favour the appearance of a preferred cracking mode.

Crack generation

The conditions in which cracking may occur can be predicted using different criteria (Singer 1980):

Rankine Theory Fracturing is assumed to appear when one of the principal stresses (tension) reaches a certain limit value. In the case of soils, this consideration can be considered valid for both total and effective stresses. In the first case, it must be taken into account that cohesive soils may present a significant tensile strength. In the case of Mexico City clays, it has been shown that this strength can be as high as 20 to 50% of the compressive strength depending on the water content (Marsal, 1959). Rankine theory has been used implicitly to assess generation of cracks within earth dams (Covarrubias, 1969). In effective stresses analyses it is commonly assumed that a crack will form when one the effective principal stresses presents a negative value, due, for example, to the action of seepage forces (Alberro & Hernández, 1991; Juárez Badillo, 1991).

Saint Venant Theory The maximum strain theory is attributed to Saint Venant. Fracturing occurs when the principal strain (extension) reaches a certain critical value. Using this theory, Alberro (1986) has suggested that cracks in the impervious core of earth dams are generated when extension strain exceeds a value of 0.17 to 0.24%.

Griffith Theory This is a more complex theory based on the assumption that microfractures exist within the solid (Jaeger, 1956; Auvinet, 2008).

Stress state near the front of a fracture Considering a plate in a plane stress condition when a crack already exists (Fig. 2) with border conditions:

$$\sigma_{\theta\theta} = \tau_{r\theta} = 0 \qquad \text{for} \quad \theta = \pm\alpha \tag{1}$$

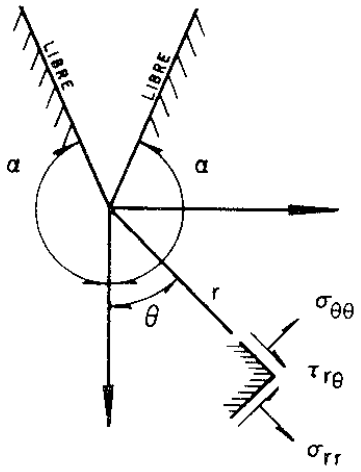

Fig. 2 Stresses around a crack.

It can be established (Irwin, 1957) that the stress tensor close to the front of the crack can be expressed in Cartesian coordinates (Westergaard equation; Kobayashi, 1973) as:

$$\begin{pmatrix}\sigma_{xx}\\ \sigma_{xy}\\ \sigma_{yy}\end{pmatrix} = \frac{K_I}{\sqrt{2\pi r}}\cos\left(\frac{\theta}{2}\right)\begin{bmatrix}1-sen\left(\frac{\theta}{2}\right)sen\left(\frac{3\theta}{2}\right)\\ sen\left(\frac{\theta}{2}\right)sen\left(\frac{3\theta}{2}\right)\\ 1+sen\left(\frac{\theta}{2}\right)\cos\left(\frac{3\theta}{2}\right)\end{bmatrix} \tag{2}$$

where K_I is the so-called *stress intensity factor*, dependent on the geometrical conditions of the problem and expressed in kPa $m^{1/2}$.

This solution, established for plane stress state conditions is also valid for plane strain conditions with:

$$\sigma_{zz} = \frac{2\nu K_I}{\sqrt{2\pi r}}\cos\left(\frac{\theta}{2}\right) \tag{3}$$

A number of expressions have been developed to define K_I for different loading conditions (Benham 1987). Similar expressions can be developed for fracturing modes II and III (Fig. 1), and two additional *stress intensity factors*: K_{II} and K_{III} can be introduced.

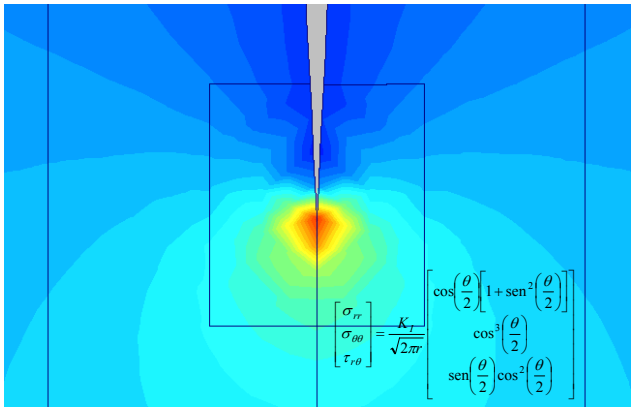

Fig. 3 Stress concentration near fracture front.

Propagation criteria

In linear fracture mechanics it is accepted that propagation of a crack occurs when the stress intensity factor K_I exceeds a critical value, K_{IC} , that must be determined experimentally (ASTM E399-78). Fook-Hoo (1988) has obtained a critical stress intensity factor of 12.9 kPa $m^{1/2}$ for a soft clay with a liquid limit w_L = 117%, plastic limit w_p = 55% and water content w = 40%.

CRACKING MECHANISMS

The most common mechanisms giving rise to tension stresses and to cracks in the Basin of Mexico and other areas have been reviewed recently (Auvinet, 2008). Soil fractures can be classified broadly as: evapotranspiration cracks, cracks due to stresses induced by surface loading or unloading, cracks due to seismic events, cracks caused by hydraulic fracturing or seepage forces and cracks related to land subsidence. This paper is mainly concerned with this last type of fracturing.

Pumping of water from deep aquifers causes a regional consolidation process due to transfer from pore pressures to effective stresses. This phenomenon is especially spectacular in the lacustrine area of Mexico City basin (Marsal, 1992). The superficial settlements have exceeded 13 m in several points of the valley in a little more than one century. The land subsidence induces cracks in different conditions:

(a) Cracks in sharp transition zones between soft and rigid materials (buried slopes, Fig. 4). Cracking and fissuring can frequently turn up in abrupt transition zones located at the edges of the former lake system where the thickness of compressible clay layers interspersed with silty sand changes sharply over short distances. Transition is particularly sharp around volcanic domes that protrude from the lacustrine materials (Peñón de los Baños, del Marqués, Peñón Viejo, Tepetzingo and Coatepec in Texcoco, and Cerros del Xico and Tlapacoya in Chalco). Transition is also sharp near Sierra de Guadalupe (Xalostoc). In contrast, transition is much more progressive around clastic material cones such as Cerro de la Estrella and in the west part of the city where alluvial fans and plateaus are found. The highest density of cracks in transition zones is found in the Iztapalapa precinct, north of Sierra Santa Catarina. In some instances, the differential settlement is accompanied by horizontal *creep* movements of the soil. This type of displacement has been observed in the area close to Tlapacoya hill.

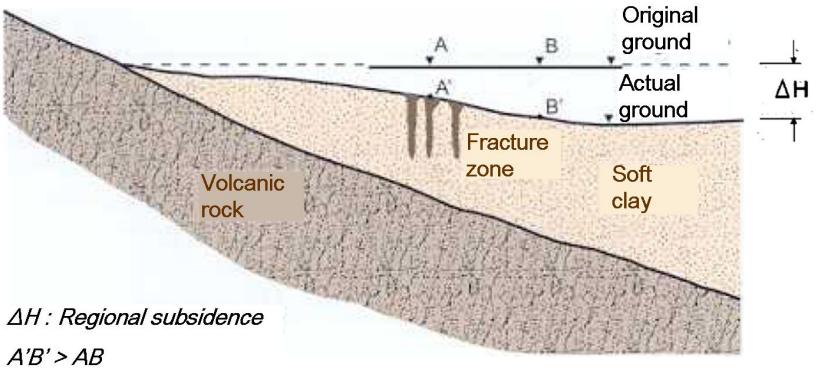

Fig. 4 Fracturing in sharp transition zone.

(b) Cracks induced by buried geological structures. During the sedimentation process, young deposits may have buried older geological structures. When the basal rock forms a step or a hill, the consolidation of the superficial soil is not uniform and differential settlement may induce fracturing. This is apparently the situation prevailing in the city of Celaya where cracks with a step of 1 m are believed to be a consequence of a step of 200 m in the basal rock (Trujillo, 1989). In the

same way, in Querétaro, the basal rock buried under 130 m of fractured alluvial sediments presents a 40 m high step (Pacheco, 2008).

Some success has apparently been obtained using gravimetric measurements to determine the configuration of the basal rock (Pacheco, 2008). Microtremor measurements also appear to be a potentially useful technique (Ovando & Lermo, 2010). The results of such measurements should always be combined with geotechnical and topographical evidence to identify zones of potential cracking.

(c) Heterogeneous soils. Cracks may also appear when the consolidating soil is heterogeneous. An especially clear example of this phenomenon has been observed in Tlahuac where some cracks present a 75 cm step (Fig. 5). As seen in the soil profile, a stratum formed by volcanic tuffs is found at a depth of about 5 m. Fragile rupture of this stratum has occurred during the consolidation process.

Fig. 5 Fractures in Tlahuac.

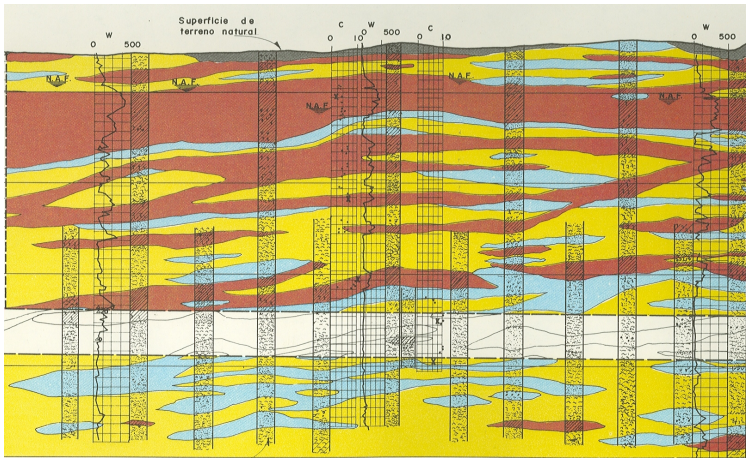

Fig. 6 Typical soil layers in Azcapotzalco zone.

The cracks that have been detected in the northwest part of Mexico City (Naucalpan-Atzcaptozalco-Gustavo A. Madero) are also a consequence of soil heterogeneity (clays interspersed with alluvial materials, Fig. 6). Pumping and water flow toward the drainage system have induced a 10 m drawdown of the water table leading to a 100 kPa increase of the effective vertical stress and to the large deformations and cracks observed at the soil surface.

MODELLING THE FRACTURING PROCESS

The consolidation process for the geometrical and soil profile conditions (discussed in the previous section) leading to fractures can be modelled using numerical techniques such as the finite element method (Fig. 7).

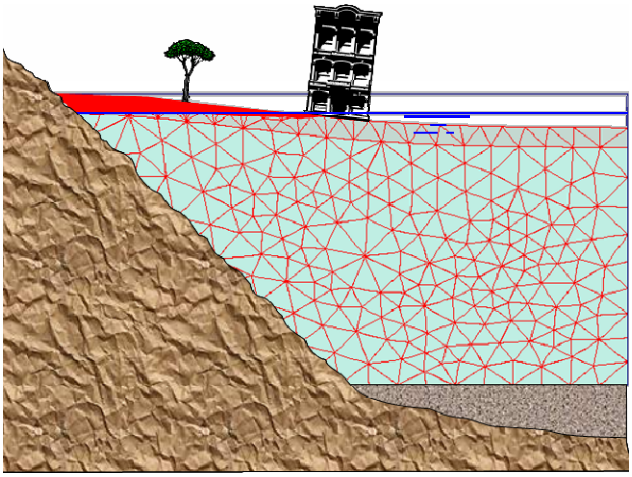

Fig. 7 FEM modelling of sharp transition zone fracturing (Rodríguez, 2000).

Modelling of this type has also been performed by Juárez Luna (2002). It can be shown that cracking is favoured by the existence of rigid materials (a drying crust) in the soil surface. The computed tensile stresses are sensitive to the Poisson ratio (Louault, 1997) but not so much to the soil modulus. In the case of Fig. 7, the fracturing mode is mixed (types I and II) due to the combined effect of tensile and shear stresses. The cracks thus present a step that can be destructive for construction in the area.

Analytical approaches have also been used for deep valleys filled with compressible sediments. (Álvarez Manilla, 1999; Rojas, 2002; Alberro *et al.*, 2006).

CONCLUSIONS

Soil fracturing induced by land subsidence is a complex phenomenon that is now fairly well understood, but difficult to control. More field observations and modelling are required for a better assessment of specific fracturing conditions and definition of preventative and mitigating measures.

REFERENCES

Alberro, J. (1986) Efectos en la presa Carlos Ramírez Ulloa (El Caracol). *Memoria: Los sismos de 1985, Casos de Mecánica de Suelos*, Sociedad Mexicana de Mecáncia de Suelos, Mexico, D.F.

Alberro, J. & Hernández, R. (1991) Evaporación y agrietamiento. *Memoria, Simposio sobre Agrieta- miento de suelos*, 13–20. Sociedad Mexicana de Mecánica de Suelos, México, D.F.

Alberro, J. *et al.* (2006) *Agrietamiento en la periferia de un valle sometido a bombeo.* Series del Instituto de Ingeniería no. 649, UNAM, México, D.F.

Álvarez Manilla, A. (1999) Modelo del mecanismo de agrietamiento en el valle y zona metropolitana de Querétaro. Tesis de maestría en Ciencias (mecánica de suelos), Universidad Autónoma de Querétaro, México.

Auvinet, G. & Arias, A. (1991) Propagación de grietas., *Memoria, Simposio sobre agrietamiento de suelos*, 21–32. Sociedad Mexicana de Mecánica de Suelos, México, D.F.

Auvinet, G. (2008) Fracturamiento de suelos, estado del arte. *Memoria, Volumen especial Conferencias temáticas: Avances recientes, XXIV Reunión Nacional de Mecánica de Suelos, Aguascalientes*, 299–318. Sociedad Mexicana de Ingeniería Geotécnica, México.

Benham, P. P. & Crawford, R. J. (1987) *Mechanics of Engineering Materials.* Longman Scientific & Technical, New York, USA.

Covarrubias, S. W. (1969) *Cracking of Earth and Rockfill Dams.* Harvard Soil Mechanics Series, 82, USA.

Fook-Hoo Lee, *et al.* (1988) Tension crack development in soils. *J. Geotechnical Engineering, ASCE*, **114**.

Irwin, G. R. (1957) Fracture mechanics. *J. Appl. Physics* **24**, 361.

Jaeger, J. (1956) *Elasticity, Fracture and Flow with Engineering and Geological Applications.* John Wiley and Sons, Inc. New York, USA.

Juárez Badillo, E. (1991) Grietas por fuerzas de filtración. *Memoria, Simposio sobre agrietamiento de suelos*, 39–42. Sociedad Mexicana de Mecánica de Suelos, México, D.F.

Juárez Luna, G. (2002) Aplicación de la mecánica de fracturas a problemas de la Geotecnia. Tesis para obtener el grado de maestro en Ciencias con especialidad en estructuras, ESIA, IPN, México D.F.

Juárez Luna, G. *et al.* (2002) Modelado del fracturamiento en las arcillas del valle de México. *Memoria, XXI Reunión Nacional de Mecánica de Suelos* (Santiago de Querétaro, Qro. , México), vol. 1, 183–191.

Kobayashi, A. (1973) *Experimental Techniques in Fracture Mechanics*. Society for Experimental Stress Analysis, Monograph Series. UK.

Louault, B. (1997) Approche probabiliste de l'évaluation des zones de tension dans les barrages en terre et en enrochement. Trabajo de fin de estudios realizado en El Instituto de Ingeniería UNAM, bajo la dirección de G. Auvinet, México, D.F.

Marsal R. J. & Mazari, M. (1959) *El subsuelo de la ciudad de México*. Facultad de Ingeniería, UNAM, México, D.F.

Marsal, R. J. (1992) *Hundimiento de la Ciudad de México*, El Colegio Nacional, México, D.F.

Méndez, E. et al. (2010) Advances in the geotechnical characterization of soil fracturing in Mexico basin. In: *Land Subsidence, Associated Hazards and the Role of Natural Resources Development* (Proc. EISOLS 2010, Querétaro, Mexico, October 2010). IAHS Publ. 339, this volume.

Ovando Shelley E. & Lermo, J. (2010) Personal communication.

Pacheco Martínez J. (2008) Modelo de subsidencia del valle de Querétaro y predicción de agrietamientos superficiales. Tesis doctoral, Centro de Geociencias, Campus Juriquilla, Qro., Posgrado en Ciencias de la tierra, UNAM, México.

Rodríguez, J. F. (2000) FEM modeling of fracturing process. Internal report, Instituo de Ingeniería, UNAM, Mexico.

Rojas González, E. *et al.* (2002) A method to predict group fissuring and faulting caused by regional water decline. *Engineering Geology* **65**, 245–260.

Rojas González, E. *et al*. (2002) Predicción de las zonas de agrietamiento debido a la extracción de agua. *Memoria, XXI Reunión Nacional de Mecánica de Suelos* vol. 1, 173–181.

Singer F. & Pytel, A. (1980) *Strength of Materials.* Harper and Row Publishers Inc., USA

Trujillo Candelaria, J. A. (1989) Fallamientos de terrenos en Celaya, Gto. *Alternativas Tecnológicas* **29**, 367–369. Academia Mexicana de Ingeniería, México D.F.

Land Subsidence, Associated Hazards and the Role of Natural Resources Development
(Proceedings of EISOLS 2010, Querétaro, Mexico, 17–22 October 2010). IAHS Publ. 339, 2010.

On the mechanisms for earth fissuring in Las Vegas valley: a numerical analysis of pumping-induced deformation and stress

M. HERNÁNDEZ-MARÍN[1,2] **& T. J. BURBEY**[1]

1 *Department of Geosciences, Virginia Tech, 4044 Derring Hall, Blacksburg, Virginia 24061, USA*
mhmarin@vt.edu

2 *Instituto Tecnológico de Estudios Superiores de Occidente, Periférico Sur Manuel Gómez Morín 8585, Tlaquepaque, Jalisco 45604, México*

Abstract The arid Las Vegas Valley presents a very complex relationship amongst land subsidence, earth fissuring, and Quaternary faulting. The basin fill contains highly variable stratigraphy, including a thick semi-rigid vadose zone, and nonlinear pumping patterns complicate the stress–strain regime. The Eglington fault, located in the northwest part of the valley, has been selected as a prototype for this numerical analysis. Our simulation results suggest that this particular Quaternary fault has a wide zone of influence (fault-zone) whose infill is hydromechanically similar to sand. In addition, one of the most important mechanisms that cause the stress concentration in the vicinity of the fault is the tendency of the entire fault to rotate with enhanced motion through the vadose zone. A combination of accumulated tensile and shear stress in the vadose zone portion of the fault-zone and in its vicinity, creates favourable conditions for the initiation of fissures in the lower vadose zone or at the land surface.

Key words numerical simulation; earth fissuring; Eglington fault; Las Vegas valley; ABAQUS

INTRODUCTION

Land subsidence and earth fissuring have been observed in Las Vegas Valley over the last century. The location and geometry of these processes are known to be greatly influenced by Quaternary faulting; however, the mechanisms influencing the location of the initiation of fissures is still not well understood due to the complexity of the factors involved. For example, the known variable stratigraphy which includes several compressible aquitards and a rigid thick vadose zone, the occurrence of nonlinear pumping rate patterns over a long period of time, coupled with three decades of artificial recharge and the presence of Quaternary faults that act like mechanical barriers to vertical deformation, as observed through satellite images of the entire basin (Amelung *et al.* 1999). Bell (1992), demonstrates statistically that fissures persistently appear adjacent to Quaternary faults. However, their position seems to occur on both sides of the fault without a particular defined geometrical relationship with the orientation of the closest fault. One of these faults, known as the Eglington Fault in northwest Las Vegas, is particularly remarkable for how the northwest subsidence bowl, the deepest in the valley, is truncated by this fault (Fig. 1). Ground deformation in the form of earth fissuring and land subsidence is notable in the vicinity of this fault, even though: (a) pumping and recharge wells are located at a considerable distance from the fault plane; and (b) the thickness of accumulated compressible clayey layers is, mostly located on the eastern portion of the valley, also distant from this fault. Unfortunately, only vertical displacement data, as well as some observations on the variation of flow and water levels can be found in the vicinity of the Eglington Fault in Las Vegas Valley. Therefore, based on the analysis of synthetic numerical simulations, the aim of this work is to identify zones of potential pumping-induced fissuring, analyse the patterns of vertical and horizontal deformation, and identify the distribution of maximum stress zones within the model domain.

NUMERICAL MODEL DEVELOPMENT

Las Vegas Valley represents one of the best examples of how quaternary faulting substantially controls ground deformation patterns. In this work, a two-dimensional model is set up based on the

Copyright © 2010 IAHS Press

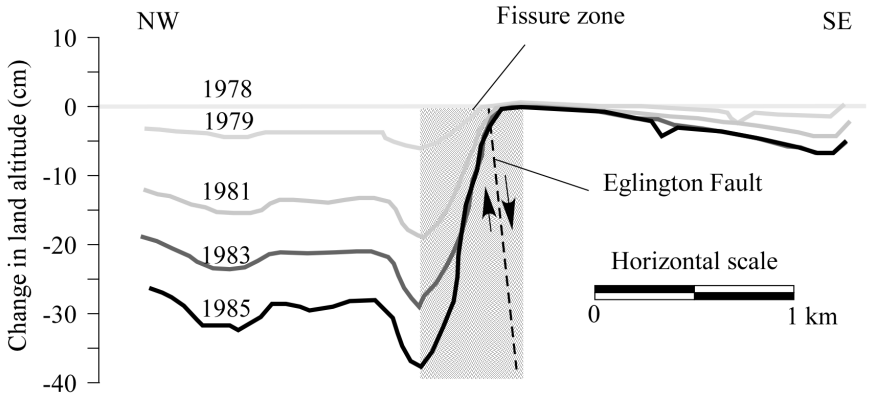

Fig. 1 Evolution of vertical deformation across the Eglington Fault between 1978 and 1985. Picture modified from Bell *et al.* (1992). An increasing differential deformation in the vertical sense is observed across the fault plane.

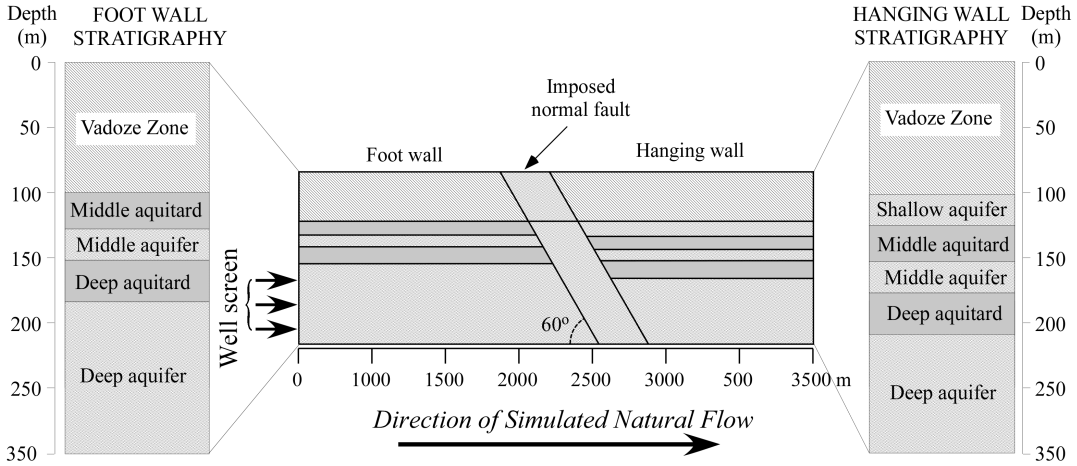

Fig. 2 Conceptual model used in the simulations. Pumping occurs exclusively in the deep aquifer with the direction of natural flow indicated. A 20-m vertical offset was imposed on the model. Therefore, an extra aquifer (shallow aquifer) is positioned below the vadose zone on the hanging wall side. The vadose zone thickness is constant over the fault.

observed stratigraphy and vertical deformation patterns and groundwater flow occurring across the Eglington Fault. The finite-element code ABAQUS was selected for the numerical simulation (Hibbit, 2004). The stratigraphy of the conceptual model depicted in Fig. 2 corresponds to that described by Pavelko (2004) near the Eglington Fault. In addition, the model includes a 100-m wide fault zone dipping at 60° and composed by sand-like material according to the results of Hernandez-Marin & Burbey (2009).

The simulated flow patterns in the model include natural discharge and artificial recharge that produce a fluid flow from left to right, simulating the natural northwest–southeast groundwater flow occurring across the Eglington Fault. Additionally, pumping is imposed on the left side of the model, in accordance with the highest well concentration observed in the west of Las Vegas. Based on real data of pumping and deformation in the valley, cyclical pumping (Fig. 3(a)) was used in order to more realistically simulate the characteristic pumping patterns of Las Vegas Valley. Figure 3(b) shows the simulated vertical cyclical deformation on both sides of the fault. The figure shows that more deformation occurs on the hanging wall than on the footwall due to the influence of the fault zone. In addition, the Cam-Clay model (Roscoe & Shofield, 1963) is implemented on the numerical analysis in order to simulate elasto-plastic mechanical behaviour of the aquitards.

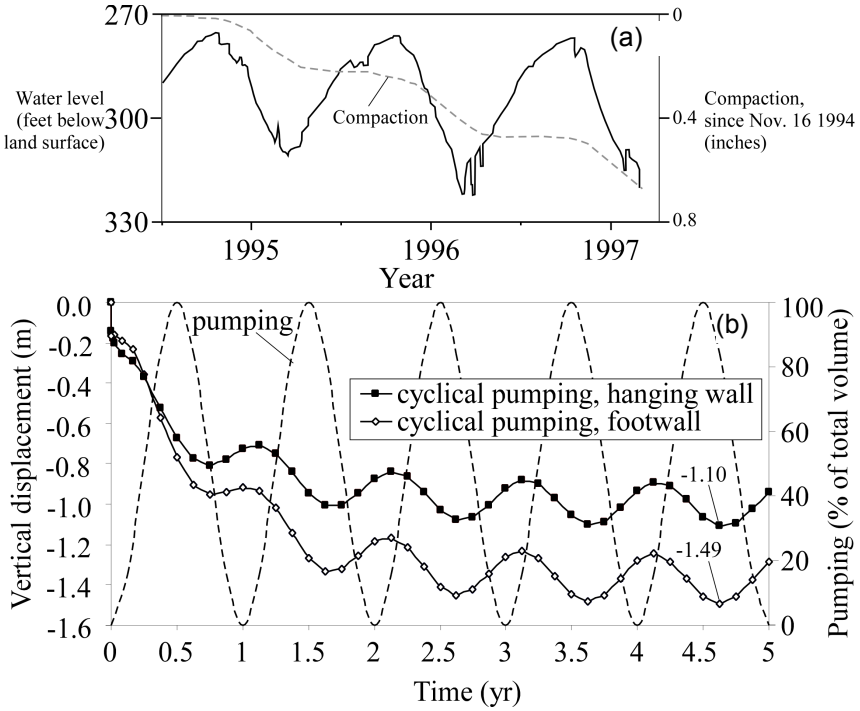

Fig. 3 Data of vertical deformation and water level fluctuations: (a) shows measurements of compaction through field extensometers and variation of water level in Las Vegas Valley (Pavelko *et al.*, 1999), (b) depicts simulated pumping and vertical deformation on both blocks. Maximum vertical deformation on each block is indicated (1.10 m and 1.49 m).

DISCUSSION

The numerical analysis is based on the results of: (a) simulated horizontal deformation, mainly on the vicinity of the fault and at the vadose zone; (b) vertical deformation at the land surface; and (c) tensile and shear stress also close to the fault zone.

Simulated deformation

A varying pattern of lateral and vertical deformation resulting from the simulations suggests that a counter-clockwise rotation of the fault zone is occurring, with a pivot located at the base of the vadose zone, and that the fault zone behaves in a similar way to a mechanical barrier that reduces ground deformation across the fault. Furthermore, simulations indicate that the zone adjacent to the portion of the fault zone corresponding to the vadose zone is the most dynamic in the system regarding deformation and stress concentration. These results create a concentration of stresses on both sides of the fault favouring the conditions for fissuring on both blocks. The counter-clockwise rotation of the fault can be observed in Fig. 4. However, the degree of footwall rotation is greater than that of the hanging wall (Fig. 4(a)) because more horizontal deformation is simulated on the surface of the footwall where pumping occurs. Therefore, this transition across the fault is the result of a rigid fault zone reducing the magnitude of lateral deformation on the hanging wall. The maximum horizontal deformation is simulated on the surface of the entire model; however, a transitional reduction in the magnitude of horizontal displacement occurs in the vadose zone. In addition, the direction of the displacements in Fig. 4 are toward the pumping well, indicating the importance of the pumping-derived stress.

In Fig. 5, the horizontal displacement at the surface reaches a minimum on the footwall and a maximum on the hanging wall. Conversely, at the saturated/unsaturated interface the minimum value of horizontal displacements is simulated on the footwall and the maximum on the hanging wall. In both cases the fault zone represents an abrupt change in the magnitude of horizontal

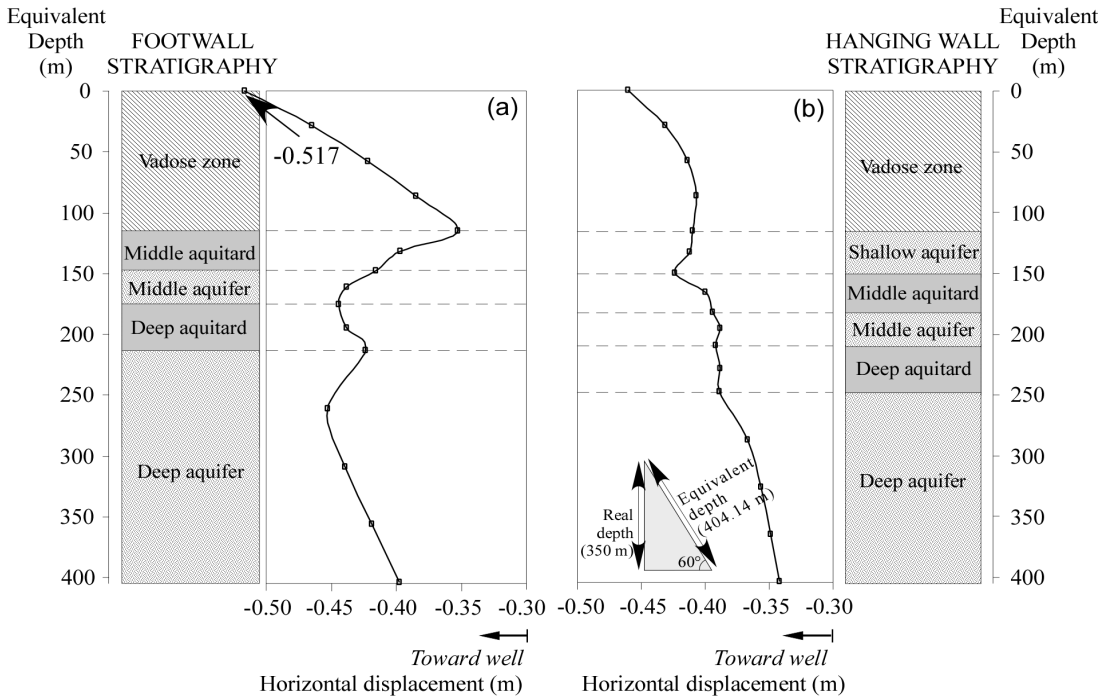

Fig. 4 Variation of horizontal deformation *vs* depth on the two edges of the fault. The relative depth used in the figure corresponds to the hypotenuse, as indicated in the triangle at the base of the graph in (b).

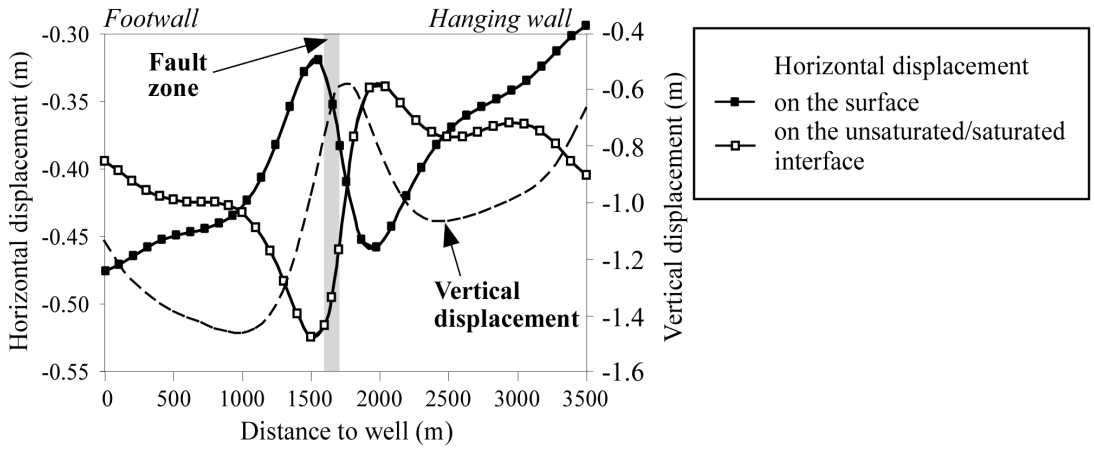

Fig. 5 Simulated horizontal and vertical deformation. Horizontal deformation is shown at two key zones: on the surface, and at the unsaturated/saturated interface as indicated on the box at the right. The dashed line indicates the vertical deformation at the surface. The negative sign on the y-axis corresponds to horizontal deformation, denoting displacement directed toward the pumping well, whereas on the right-hand axis negative vertical deformation indicates increasing downward displacement.

displacement, resulting in a large concentration of stress in the vicinity of the fault, particularly in the vadose zone.

The pattern of vertical deformation at the surface clearly indicates that the fault behaves in a way that the vertical deformation is halted across the fault. A total subsidence of up to 1.4 m is simulated on the footwall, meanwhile the hanging wall surface deformation is about 1.0 m. The mechanical properties of the fault zone result in less deformation on the hanging wall than in the footwall, where the pumping well is located.

Simulated stress

Simulated tensile and shear stresses are mainly concentrated in the vicinity of the fault zone, particularly in the vadose zone. The tensile stress has a maximum value at the surface near the hanging wall, a short distance from the fault zone, as shown in Fig. 6(a), whereas minimum (maximum negative) and maximum shear stresses are located at the base of the vadose zone, also a short distance from the fault zone, as observed from Fig. 6(b). A minimum shear stress is located at the footwall and a maximum shear stress occurs on the hanging wall. As in the case of ground deformation, this change in stress across the fault is caused by the mechanical properties of the fault. Based on the results of simulated stresses, three zones are most favourable for fissuring: (a) at the surface of the footwall near the fault zone; (b) on the hanging wall near the base of the vadose zone; and (c) on the footwall at the base of the fault zone. In case (a) tensile stress is acting to generate fissures, in case (b) the minimum (maximum negative) shear stress can generate fissures, and in case (c) the maximum shear stress dominates over the other type of stress on the generation of fissures.

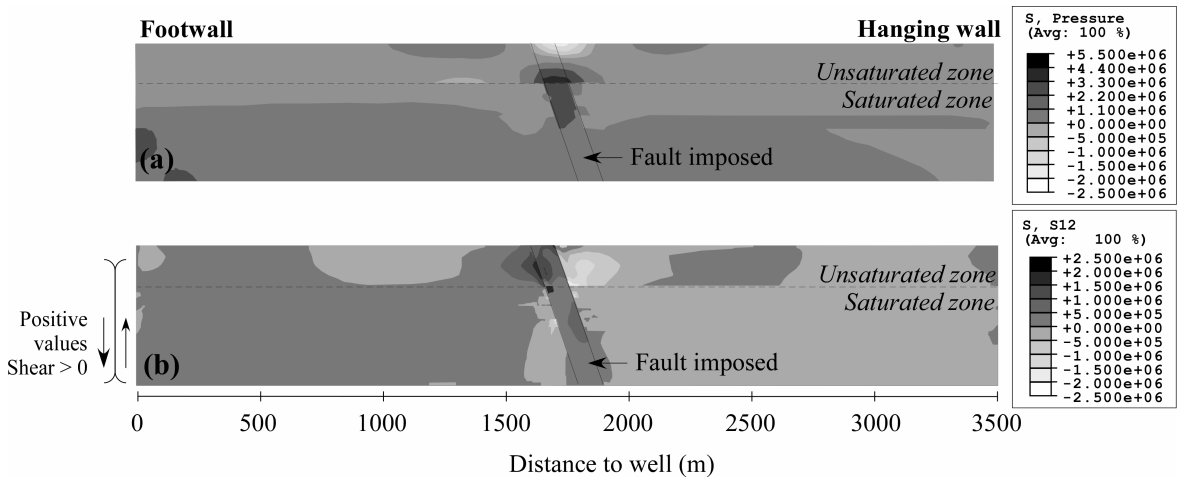

Fig. 6 Simulated tensile/compressive stress (a) and shear stress (b). Units of stress on the scale of each figure are in Pascals and the meaning of the positive shear stress is indicated on the left. In the case of negative values the direction of the vertical arrows would be opposite to that indicated.

SUMMARY AND CONCLUSIONS

Simulated deformations and stresses suggest that pumping-induced strain is mostly concentrated in the vadose zone near the fault. The fault zone is highly relevant in influencing the patterns of deformation and stress because the system is deformed vertically and horizontally more on the hanging wall than on the footwall, although the entire system is horizontally directed toward the position of the pumping well. This indicates that the fault inhibits the transfer of lateral and vertical strain on the footwall. The combination of lateral and vertical patterns of stress and deformation in response to pumping, along with the influence of the fault zone, causes: (a) a counter-clockwise rotation of the fault zone with pivot on the base of the vadose zone; (b) a zone of high tensile stress located at the surface of the footwall near the fault zone, suggesting the formation of tensile-induced surface fissures on the side of the fault opposite to pumping; and (c) two zones of high shear stress, one on the hanging wall and the other on the footwall, both on the base of the vadose zone and adjacent to the fault zone edge. These two zones suggest that fissures can form at the base of the vadose zone and at the surface of the hanging wall near the fault as a result of high tensile stress.

REFERENCES

Amelung, F., Galloway, D. L., Bell, J. W., Zebker, H. A. & Laczniak, R. J. (1999) Sensing the ups and downs of Las Vegas: InSAR reveals structural control of land subsidence and aquifer-system deformation. *Geology* **27**(6), 483–486.

Bell, J. W., Price, J. G. & Mifflin, M. D. (1992) Subsidence induced fissuring along pre-existing faults in Las Vegas Valley, Nevada. In: *35th Annual Meeting of the Association of Engineering Geologists*, 66–75. Association of Engineering Geologists, Long Beach, California, USA (2 October 1992).

Hernandez-Marin, M. & Burbey, T. J. (2009) The role of faulting on surface deformation patterns from pumping induced ground-water flow. *Hydrogeol. J.* **17**(8), 1859–1875.

Hibbit (2004) ABAQUS/CAE *User's Manual*. Karlsson Sorensen Inc.

Roscoe, K. H. & Schofield, A. N. (1963) Mechanical behaviour of an idealized 'wet' clay. In: *2nd ECSMFE, Wiesbaden*, vol. 1, 47–54.

Pavelko, M. T. (2004) Estimates of hydraulic properties from a one-dimensional numerical model of vertical aquifer-system deformation, Lorenzi Site, Las Vegas, Nevada, USA. *US Geol. Survey*, Water Resources Invest. Report 03-4083.

Pavelko, M. T., Wood, D. B. & Laczniak, R. J. (1999) Las Vegas, Nevada: gambling with water in the desert. *US Geol. Survey*, Las Vegas, Nevada, USA.

Land Subsidence, Associated Hazards and the Role of Natural Resources Development
(Proceedings of EISOLS 2010, Querétaro, Mexico, 17–22 October 2010). IAHS Publ. 339, 2010.

Advances in geotechnical characterization of soil fracturing in Mexico City basin

G. AUVINET[1], **E. MÉNDEZ**[1] **& J. LERMO**[2]

1 *Geocomputing Laboratory, Instituto de Ingeniería, Universidad Nacional Autónoma de México, Coyoacán 04510, Mexico D.F.*
emendezs@iingen.unam.mx

2 *Seismological Engineering Group, Instituto de Ingeniería, Universidad Nacional Autónoma de México, Coyoacán 04510, Mexico D.F.*

Abstract Soil fracturing in the lacustrine area of the Basin of Mexico has become a common occurrence that causes alarm among the population and ends up causing significant damage to buildings and public services. For that reason, the Geocomputing Laboratory with the participation of the Seismological Engineering Group of Instituto de Ingeniería, Universidad Nacional Autónoma de México (II, UNAM) has, in recent years, undertaken a systematic study of the phenomenon focused on descriptive aspects as well as on theoretical interpretation.

Key words fracturing; soil; earthquakes; geotechnical characterization; Mexico City

INTRODUCTION

Soil fracturing can occur as a result of any condition that induces important tensile stresses and extension strains in the soil (Auvinet, 2010). The phenomenon may therefore have different causes, including clay contraction by drying, stresses and strains associated with the weight of constructions, hydraulic fracturing in flooding areas (Auvinet & Arias, 1991), etc. However, in the lacustrine zone of Mexico Valley the most important and destructive fractures are a direct consequence of the regional subsidence induced by pumping of water from the deep aquifer (Carrillo, 1948; Marsal & Mazari, 1959).

Initially, fracturing was only observed in the sediments of former Texcoco Lake but, in the last years, the phenomenon has been widely reported in five areas of Mexico Valley: (a) South zone: Xochimilco, Tláhuac and Chalco; (b) East zone: Iztacalco, Iztapalapa, Nezahualcoyotl, Chimalhuacan and Los Reyes; (c) Central area: Peñon de los Baños and Venustiano Carranza; (d) Northwest zone: Naucalpan, Azacapotzalco and G. A. Madero, and (e) Northeast zone: former Texcoco Lake.

The Geocomputing group of II-UNAM, has undertaken a systematic study of the fracturing phenomenon, including both descriptive aspects and theoretical interpretation. For that purpose, a Geographic Information System was developed, using as a support a similar system developed by the authors to describe the geotechnical characteristics of the Mexico Basin subsoil (Auvinet, 1995; Méndez & Auvinet, 2004; Méndez, 2005).

COMPILING, CAPTURING AND PROCESSING OF INFORMATION

Miscellaneous studies containing information related to the fracturing phenomenon (water wells, regional subsidence, topography, etc.) were collected and the best documented cases of sites with apparent fractures were identified. At this stage, collaboration with the Water System of the Federal District Government (Mexico City authority) was fundamental.

In parallel, field work consisting of direct surveys of fractures *in situ* was carried out. Use was made of geodesic control techniques referenced to differential global position systems (GPS) equipped with double frequency antennas (Fig. 1). In addition, in zones with high cracking density, the GPS system was employed simultaneously with a Total station with one second precision.

Copyright © 2010 IAHS Press

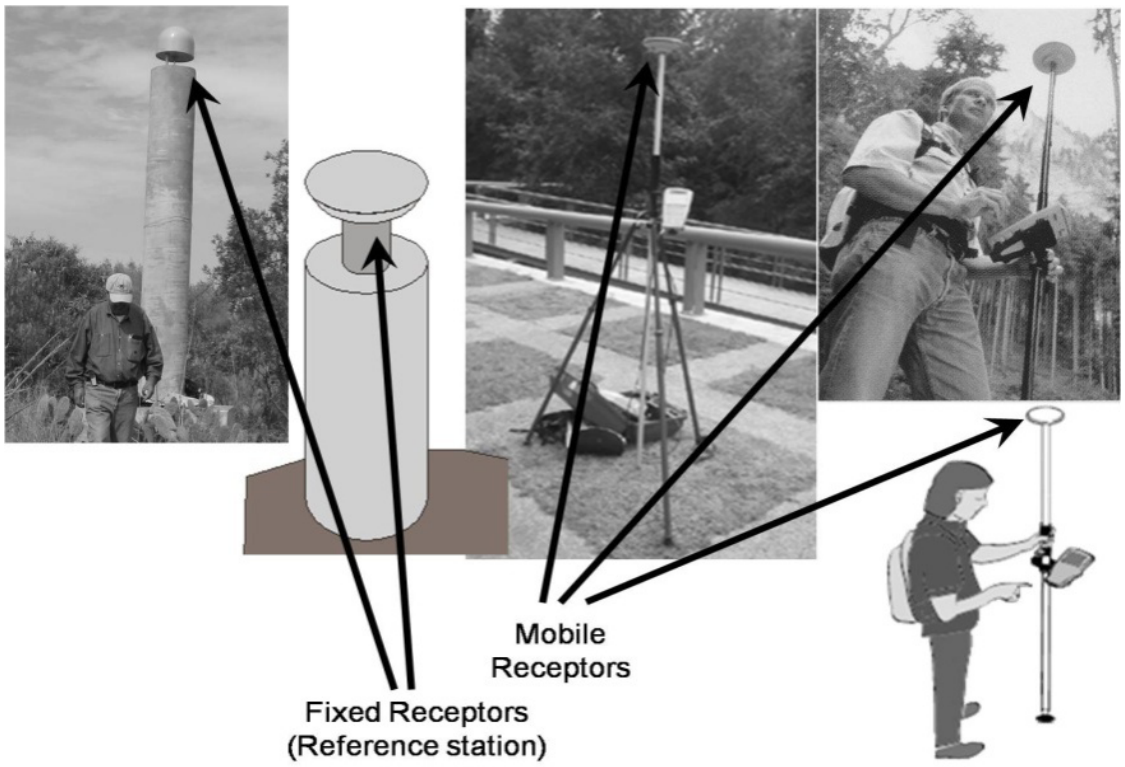

Fig. 1 Geographical positioning of points on the ground.

More than 4800 panoramic pictures in digital format of each crack and associated damage to constructions have been taken and classified. This photographic file is formed by the results of seven field surveys performed over 10 years, of which the first four were made by Federal District Government through the City Water System, while the last four campaigns were carried out directly by the Geocomputing Laboratory of II-UNAM.

At present, 368 fracturing sites have been documented. About 45 sites where cracks had been reported were discarded when, during the field visits, it became evident that no fracturing could be detected and that defects in the soil surface could be attributed to other factors (mainly scour). In fact, many of the pavement failures in Mexico City are due to scour caused by leakage in the water network and sewage system and are not related to mechanical fracturing.

FRACTURING GEOGRAPHIC INFORMATION SYSTEM (SIG-G)

To deal efficiently with the fracturing problem, it was considered necessary to use new tools, based on geographic information system (GIS) technology, which have been implemented during the last decade in the Geocomputing Laboratory of II, UNAM. Through the years it has been possible to add new information layers to these systems that have allowed the definition with more detail and precision of the geographic, historical, physical and social context of the main study unit, which is the territory of the Basin of Mexico.

The amount of information stored in the database regarding the exact location, as well as the description of the geometric characteristics and special features of each fracture, has increased steadily. This database is called SIG-G.

The window presented on the left hand side of Fig. 2 is an index card containing the general attributes as well as the location and physical and geometric characteristics of a particular fracture marked in light grey colour on the map, which is linked through a numeric key to the attributes card. The other window shows a photograph of the fracture.

Figure 3 shows the spatial distribution of the 368 sites included until now in SIG-G.

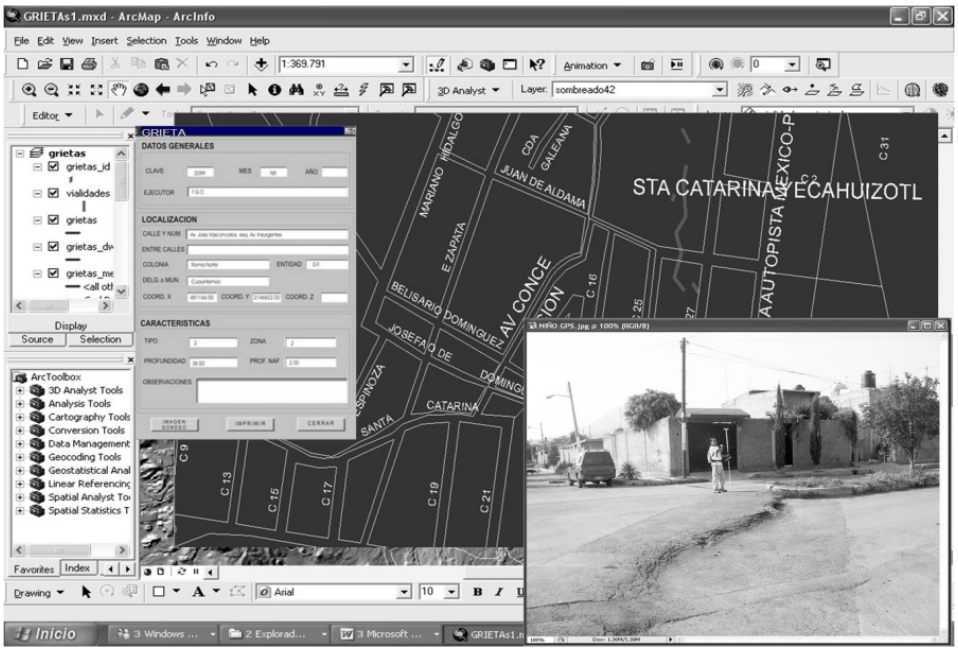

Fig. 2 Fracturing geographic information system, SIG-G.

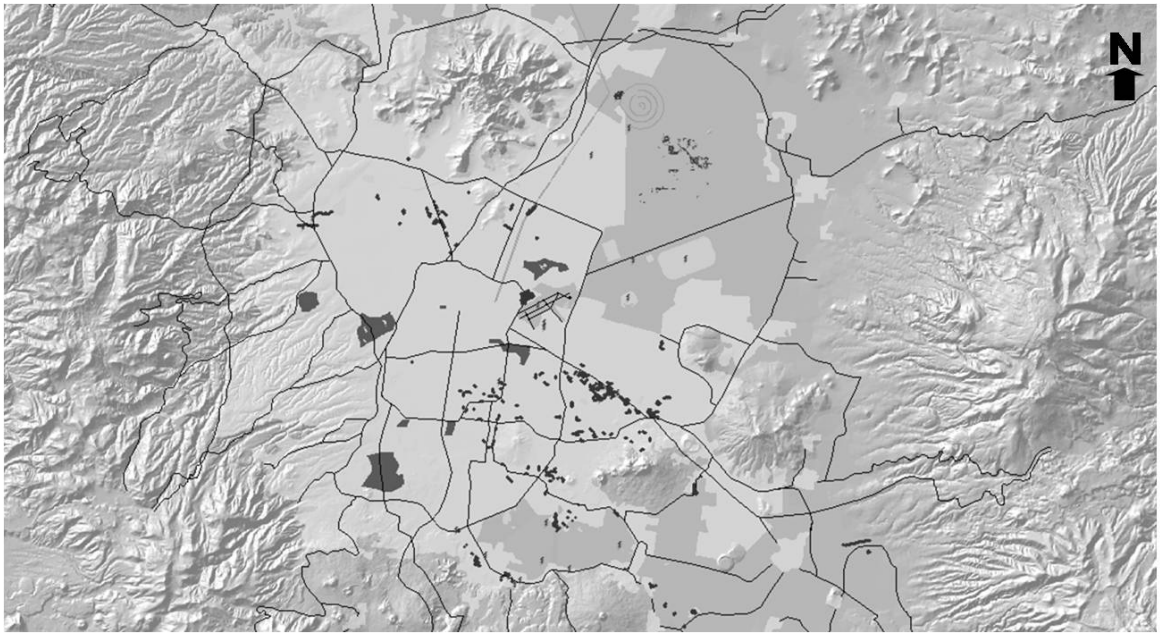

Fig. 3 Spatial distribution of the 368 cracks stored to date in SIG-G.

FRACTURING EVOLUTION

Using the extensive photographic file of cracks, a digital album is being elaborated in order to facilitate the analysis of the evolution of each fracture through the years. This album is integrated by a set of files; each file contains from two to six photos of the same crack taken during one of the 1996, 1999, 2001, 2002, 2005, 2006 and 2007 campaigns (see for example Deportivo Costa Verde crack in the Iztapalapa Delegation, Fig. 5). A complementary file includes photos of the damage caused by the fracture in adjacent buildings or negative effects in the vital lines of the city.

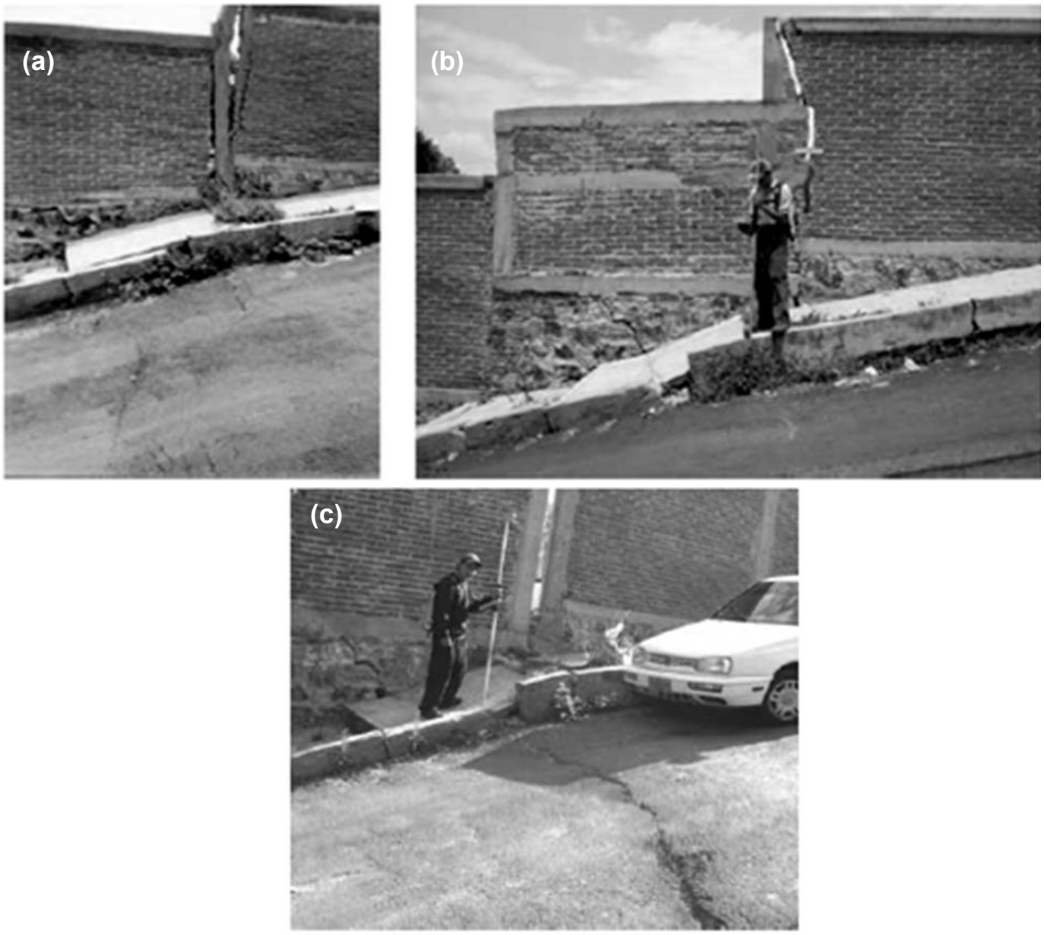

Fig. 4 Crack "Deportivo Costa Verde", Marqués Hill. (a) February 2002, (b) June 2005, (c) January, 2007.

Due to the growing number of affected sites and to the evolution of existing fractures, it is considered that the album will have to be updated continuously in the future.

ZONING

The fracturing sites detected in the Valley of Mexico, are not distributed uniformly. They are concentrated in five areas, which are shown in Fig. 5.

RELATION BETWEEN FRACTURING AND GEOLOGICAL FAULTS

Most of the main cracks detected in Mexico City subsoil can be related to differential settlements associated with regional subsidence. They can thus be considered as relatively shallow discontinuities caused by mechanical fracturing of the soil. In spite of the available evidence, some specialists have insistently tried to relate these fractures to the tectonic structure of the valley. This structure can be inferred from the local seismicity catalogue of the basin, including 218 earthquakes with their location and depth, that was developed by the Seismological Engineering group of II-UNAM. It has been possible to establish the existence of 11 recurrent seismicity areas, which correspond to three directions of state of stresses.

Superposing this seismic map on the spatial distribution of fractures as defined in SIG-G, no apparent relation between the active faults and the fracturing pattern can be detected. Taking into

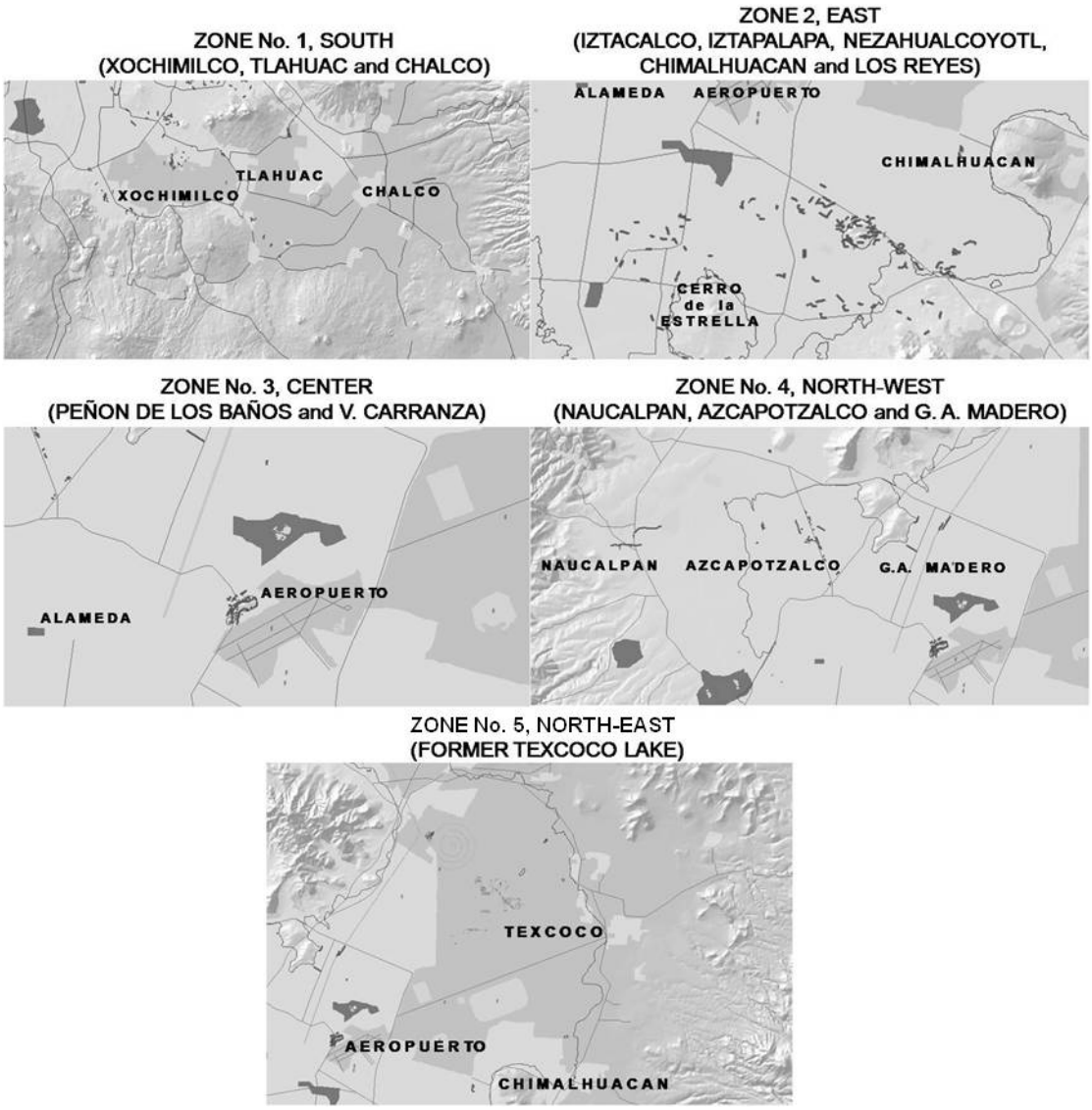

Fig. 5 Fracturing zones in Mexico City.

account the most probable origin of these two phenomena and the display of the overlap of the spatial distributions, it can be concluded that there is no direct relation between these two phenomena, Fig. 6.

CONCLUSIONS

Soil fracturing causes serious problems to the citizens and the infrastructure of the metropolitan area of Mexico valley. Until now, actions in this regard have been isolated, and only short-term solutions have been implemented without really trying to understand the problem in greater depth and to evaluate the true efficiency of these solutions.

Thanks to the survey presented in this paper, it has been possible in a short time to make significant progress in the knowledge of the fracturing phenomenon and its relation to the regional land subsidence in Mexico Valley. This was the result of intensive work by different groups, led by the Geocomputing Laboratory of II-UNAM. However, this job just must be considered only as a first stage in the study of this important phenomenon.

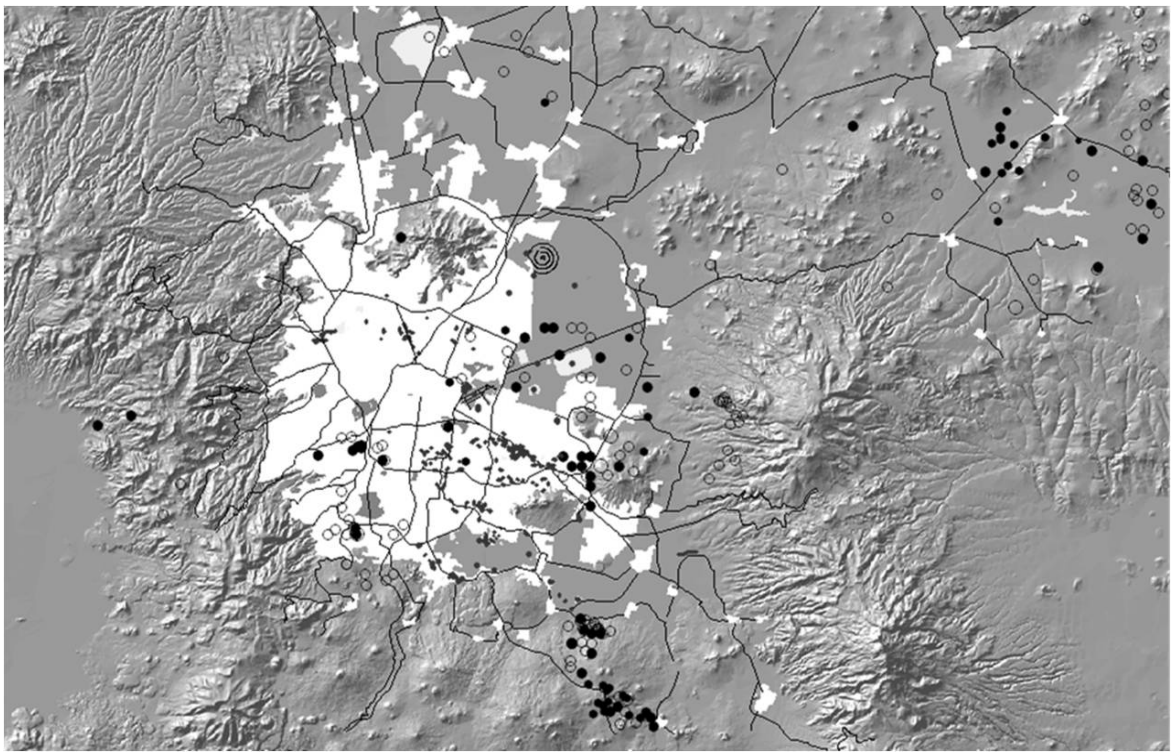

Fig. 6 Spatial distribution of generated hypocentres in Mexico Valley.

REFERENCES

Auvinet, G. & Arias, A. (1991) Propagación de grietas. *Memoria, Simposio sobre "Agrietamiento del suelo"*, Sociedad Mexicana de Mecánica de Suelos, 21–31 August, México, D. F.

Auvinet, G. *et al*. (1995) Sistema de Información Geográfica para Sondeos Geotécnicos. In: *Proceedings*, *Xth Pan-American Conference on Soil Mechanics and Foundation Engineering*, vol. 1, 312–324. Guadalajara, Mexico.

Auvinet, G. & Méndez, E. (2010) Soil fracturing induced by land subsidence. In: *Land Subsidence, Associated Hazards and the Role of Natural Resources Development* (Proc. EISOLS 2010, Querétaro, Mexico, October 2010). IAHS Publ. 339 (this volume).

Carrillo, N. (1948) Influence of artesian wells on the sinking of Mexico City. In: *Proceedings, Second International Conference on Soil Mechanics and Foundation Engineeering.* The Netherlands.

Marsal, R. & Mazari, M. (1959) The subsoil of Mexico City. Contribution to*: First Pan-American Soil Mechanics and Foundation Engineering Conference* (Facultad de Ingeniería, UNAM, México). Re-edited (Spanish–English) in 1969.

Méndez, E. (2005) Aplicación de la geoinformática a la zonificación geotécnica de la Cuenca de México. Masters Thesis, DEPFI, UNAM, Mexico.

Méndez, E. & Auvinet, G. (2004) Avances en la caracterización geoinformática del subsuelo de la Cuenca de México. *Memoria, XXII Reunión Nacional de Mecánica de Suelos*, SMMS, vol. 1, 259–266. Guadalajara, México.

(Proceedings of EISOLS 2010, Querétaro, Mexico, 17–22 October 2010). IAHS Publ. 339, 2010.

Monitoring land-surface deformation on Bicycle Lake playa, Fort Irwin, California, USA

JILL DENSMORE[1], KEVIN ELLETT[1], JIM HOWLE[2], MICHAEL CARPENTER[3] & MICHELLE SNEED[1]

1 *US Geological Survey, 6000 J Street, Placer Hall, Sacramento, California 95819, USA*
jidensmo@usgs.gov
2 *US Geological Survey, PO Box 1360, Carnelian Bay, California 96140 USA*
3 *US Geological Survey, 520 N. Park Ave., Tucson, Arizona 95719, USA*

Abstract Groundwater pumping in the Bicycle Basin in the northern Mojave Desert, one of the major sources of water supply at Fort Irwin National Training Center (NTC), California, has increased since the 1990s. The increased pumping has resulted in as much as 25 m of water-level decline between 1990 and 2009 and as much as 270 mm of subsidence occurred during 1993–2006. Land-surface deformation, consisting of an earth fissure and sink-like depressions, occurred in 2005 on the Bicycle Lake (dry) playa in the southern part of the basin. Earth fissures are a major concern to the NTC because aircraft runways constructed on the playa are used for transporting troops and supplies. Giant desiccation cracks or macropolygons also have been observed on the playa indicating that soil desiccation may play a role in the fissure formation. A monitoring system was developed to evaluate the driving mechanisms of fissuring and to provide an on-going assessment of the ground-failure hazard. Land-surface deformation and movement across the fissure is being monitored using: (1) repeated geodetic levelling surveys, (2) electronic distance measurement (EDM) surveys, (3) high-resolution ground-based, tripod-mounted Light Detection and Ranging surveys (T-LiDAR) for measurement of three-dimensional (3-D) changes across the fissure and adjacent areas, and (4) tape extensometer (tapex) measurements for horizontal changes across the fissure. The desiccation mechanism is being assessed using heat-dissipation sensors (HDPs) coupled with laboratory-scale experiments of soil desiccation. Preliminary results from repeat EDM surveys were inconclusive but repeat tapex measurements show that the fissure appears to be opening at a rate of ~1–2 mm/year which may be in response to ~4 m measured water-level decline during 2008–2009. Combining automated measurements from tiltmeters and HDPs may help provide a tool for real-time monitoring of fissure hazards.

Key words land-surface deformation; fissure; macropolygons; geodetic levelling; EDM; tape extensometer; LiDAR; subsidence

INTRODUCTION

Groundwater pumping in the Bicycle Basin, California, a major source of water supply at Fort Irwin NTC, has increased since the 1990s due to expansion of base activities and reduction of pumping in the neighbouring Irwin Basin due to water-quality concerns. Increases in pumping have resulted in about 25 m water-level declines from 1990 to 2009 in wells north of the Bicycle Lake playa. Interferometric Synthetic Aperture Radar (InSAR) interferograms show that as much as 270 mm of subsidence occurring during 1993–2006. An earth fissure and sink-like depressions were observed in 2005 on the northern part of Bicycle Lake playa where the playa is used as a runway to transport troops and supplies to the NTC. Macropolygons also have been observed on the playa surface. This paper describes a monitoring network developed by the US Geological Survey at the request of the NTC to monitor land-surface deformation on the Bicycle Lake playa and presents preliminary results.

The Bicycle Basin is relatively flat and is surrounded by generally low-lying mountains. Groundwater is pumped from unconfined, unconsolidated coarse-grained sands and gravels in the northeastern part of the basin, and confined, inter-bedded sand, silts, and clays in the central part of the basin. A northwest–southeast trending fault is projected to cross the basin in the vicinity of the observed fissure.

NETWORK AND METHODS

Geodetic levelling, electronic distance measurement (EDM) surveying, tape extensometer (tapex) measuring, and tripod-mounted Light Detection and Ranging (T-LiDAR) scans were conducted to monitor both vertical and horizontal deformation on the Bicycle Lake playa and surrounding area. An automated approach using tiltmeters and heat-dissipation sensors (HDPs) is also being developed to monitor ground-failure hazard near the fissure.

A network of 13 monuments (markers) was installed during January 2009 (Fig. 1(a)) to precisely measure vertical and horizontal deformation on the playa and surrounding area. Nine of the monuments, spaced about 500 m apart, were installed along a ~4 km transect. The transect starts at BL1 in volcanic bedrock at the south end of the playa; extends in a straight line across the playa and fissure to BL6 at the northern edge of the playa, where it bends to the northwest, and ends at BLA4, a multiple-well monitoring site in the area of maximum subsidence. BL2 through BL8 are set in unconsolidated alluvial sediments and are similar to Class B rod marks used by the National Geodetic Survey (Floyd, 1978). A brass tablet was crimped on the top of the anchor rod that had been driven to refusal at each monument to provide vertical control. The rod and tablet are enclosed within a polyvinyl chloride (PVC) casing with a closing lid at land surface, anchored in place with concrete to isolate the near surface portion of the rod from thermal expansion and contraction. The annular space within the conductor casing was filled with sand up to the bottom of the brass tablet to prevent horizontal movement.

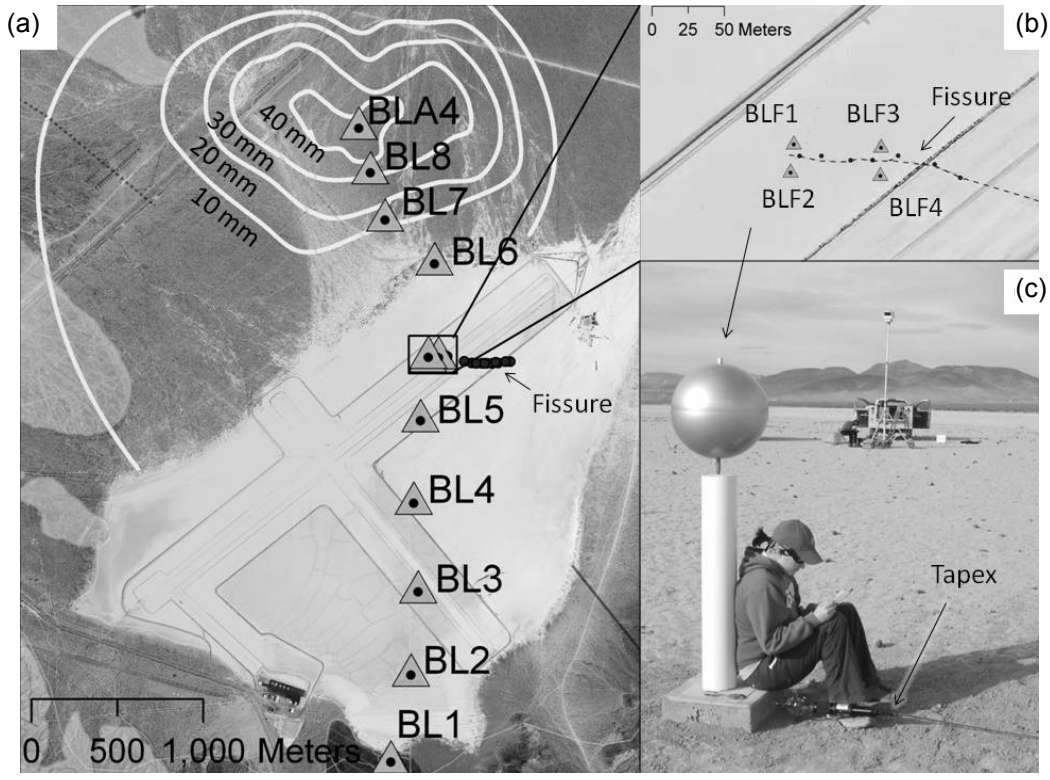

Fig. 1 Map showing (a) monuments and contours of subsidence during 2004-05, in Bicycle Basin, California; (b) LiDAR monuments; and (c) photo of LiDAR monument.

Two sets of paired monuments (BLF1-BLF2 and BLF3-BLF4) were installed about 18.7 m apart on opposite sides of the fissure to monitor the deformation occurring across the fissure (Fig. 1(b)). Monuments BLF1-BLF2 were constructed near the west terminus of the surface expression of the fissure and BLF3-BLF4 were constructed 60 m east of BLF1-BLF2. These

monuments were constructed similarly to the other monuments, but in these sites the concrete-filled PVC casing extends about 1 m above the concrete pad and the anchor rod extends several cm above the PVC casing. A 0.45-m diameter sphere is threaded onto the rod for the LiDAR scans (Fig. 1(c)). Stainless-steel eyebolts also were embedded into the concrete pads as anchors for the tapex (Fig. 1(c)) between the paired monuments on opposite sides of the fissure.

After the network was established, land-surface deformation on the playa and surrounding area was monitored using geodetic levelling surveys for vertical control, EDM surveys for horizontal control, tapex measurements for horizontal movement across the fissure, and T-LiDAR surveys to measure vertical and horizontal deformation across the fissure.

Geodetic levelling surveys provide precise, repeatable mm-scale measurements of vertical changes between the monuments along the transect. All surveys were referenced to BL1 which is assumed to be stable relative to the alluvial sediments in the basin because it is in bedrock and is outside the subsiding area.

EDM surveys provide mm-scale measurements of horizontal changes between the monuments along the transect. Temperature and pressure corrections were applied to the mean value of the replications to give a measured slope distance. Using the target height, the instrument height, and the altitudes of the stations based on the barometric pressure, the measured slope distance was then trigonometrically reduced to horizontal distance.

Tapex measurements provide precise sub-mm-scale measurements of horizontal changes between the monuments across the fissure. Distances between BLF1 and BLF2 and between BLF3 and BLF4 were periodically measured using a tape extensometer. The tapex consists of a built-in digital gauge, tensioning collar and surveying tape, which has registration pinholes punched at 50.8 mm intervals. The distance was measured between eye bolts installed in the concrete pads of two monuments on opposite sides of the fissure. Temperature correction of the steel-tape measurements were calculated from the mean of multiple infra-red measurements collected along the length of the tape.

T-LiDAR was used to create a high resolution 3-D image of the fissure and LiDAR monuments. A laser scanner was mounted on elevated and conventional tripods to image a ~7500-m^2 area surrounding the fissure. The look-down vantage from the elevated tripod minimizes data shadowing in the fissure and small-scale desiccation cracks on the playa as well as shadows cast by the LiDAR monuments. Multiple scans were conducted to increase the data density. Point-cloud data from the scans were used to produce a composite 3-D point-cloud image of the study site. This image can be compared to repeat surveys to detect subtle spatial changes in the elevation of the playa surface on either side of the fissure and changes in the width, depth, and length of the fissure over time. In addition, the spheres of the LiDAR monuments can be used to assess deformation in the horizontal and vertical planes by mathematically fitting a perfect sphere of a known diameter to the point cloud of the spheres.

Automated measurements from telemetered tiltmeters and HDPs are being used to monitor movement on the fissure on a real-time basis. Tiltmeters were installed on the north and south side of the fissure to measure change in angle of the lakebed on each side of the fissure. Movement across the fissure can be calculated through trigonometry using an estimate of fissure depth (55 m) and the associated change in angle from the tiltmeters. These data are compared with the manually-collected tapex data to assess if this method can replace the labour-intensive surveying methods. HDPs were installed at two sites: one in the fissure and the second at a background playa site about 15 m from the fissure, to measure soil-water tension within the fissure zone and the surrounding playa to help determine the mechanism of the formation of the fissures and macropolygons.

RESULTS

Baseline geodetic levelling, EDM and T-LiDAR surveys were conducted in January 2009. A 3-D image was generated of the fissure and surrounding area. A repeat EDM survey completed in

October 2009 was inconclusive, suggesting that more time was needed to monitor horizontal change. Repeat levelling and T-LiDAR surveys will be conducted in June 2010 prior to the end of the study.

Repeat tapex measurements from April 2009 to March 2010 indicate opening of the fissure between BLF3 and BLF4 (Fig. 2), but no statistically significant change across BLF1 and BLF2 at the western terminus of the fissure (not shown). The overall trend of the data between BLF3 and BLF4 suggests the fissure is opening at a rate of ~1–2 mm/year which may be in response to ~4 m of measured water-level decline during 2008–2009 in the main pumped zone at monitoring site BLA4 (the area of greatest measured subsidence). The closing of the fissure measured in March 2010 may be the result of swelling of clays after the playa was inundated during January–February 2010; however, a subsequent measurement was in line with the prior trend of opening.

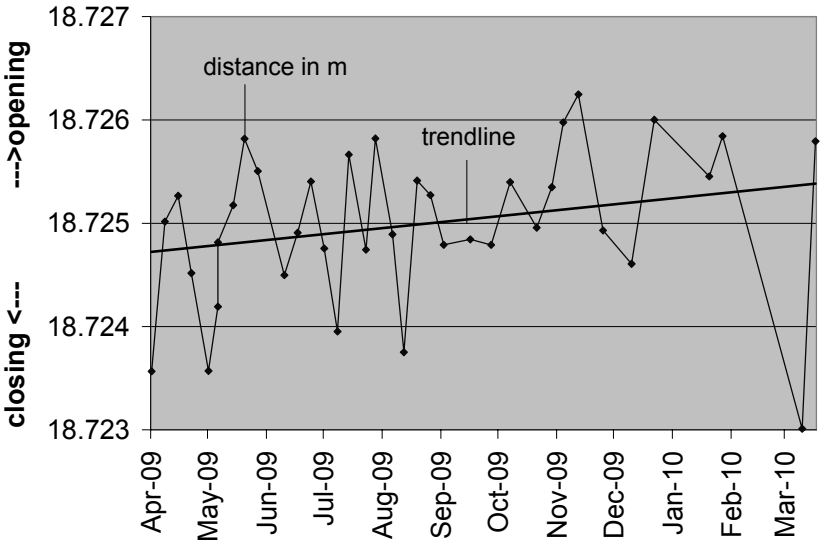

Fig. 2 Tape extensometer measurements of fissure movement at BLF3-BLF4.

Preliminary tiltmeter data show considerable variation in the estimated fissure aperture. The data suggest that the tiltmeter's response is sensitive to soil thermal changes and the effects of swelling clay owing to their shallow installation (~50 cm depth). Deeper installation and increased spatial coverage is recommended for more effective monitoring.

Preliminary HDP data show that during small storms, the fissure site wets while the playa site remains dry, and during large storms that inundate the playa, both sites show wetting. As the playa dries, the playa site dries out first while the fissure site remains wet. Laboratory-scale experiments of soil desiccation are being combined with the *in situ* measurements from heat-dissipation sensors to help evaluate the cause of fissures and macropolygons on the Bicycle Lake playa and possibly provide a tool for real-time monitoring of fissure hazards.

SUMMARY

A network of geodetic monuments was installed to monitor vertical and horizontal movement on the Bicycle Lake playa and associated fissure. Repeat EDM surveys completed in October 2009 did not indicate horizontal deformation greater than measurement error since the network was installed in January 2009. T-LiDAR was used to generate a high-resolution 3-D image of the fissure. This image will be used with future images for 3-D modelling of vertical and horizontal deformation across the fissure. Preliminary tapex measurements for April 2009–March 2010 show

the fissure is opening at a rate of ~1–2 mm/year which may be in response to ~4 m of measured water-level decline during 2008–2009 in the main pumped zone. Real-time data collected from tiltmeters near the fissure show variations related to soil temperature and shallow soil conditions suggesting deep installation of the tiltmeters is needed. Real-time data from HDPs show that the fissure wets preferentially during small storms compared to a background playa site and remains wet longer after large storms. Combining automated measurements from tiltmeters and HDPs with results from laboratory experiments will help evaluate the cause of fissures and macropolygons on the Bicycle Lake playa and possibly provide a tool for real-time monitoring of fissure hazards.

REFERENCES

Floyd, R. P. (1978) *Geodetic Bench Marks*. National Oceanic Atmospheric Administration (NOAA), Manual NOS NGS 1. US Dept of Commerce, Rockville Maryland, USA.

National Oceanic Atmospheric Administration (1984) *Standards and Specifications for Geodetic Control Networks*. Federal Geodetic Control Committee, Rockville Maryland, USA.

(Proceedings of EISOLS 2010, Querétaro, Mexico, 17–22 October 2010). IAHS Publ. 339, 2010.

Monitoring of land subsidence and fracturing in Iztapalapa, Mexico City

D. CARREÓN FREYRE[1], M. CERCA[1], R. GUTIÉRREZ CALDERÓN[2] & M. HUERTA LADRÓN DE GUEVARA[2]

1 *Laboratorio de Mecánica Multiescalar de Geosistemas (LAMMG), Centro de Geociencias, UNAM, Querétaro, Mexico* freyre@geociencias.unam.mx

2 *Centro de Evaluación de Riesgo Geológico (CERG), Delegación Iztapalapa del Distrito Federal, Mexico*

Abstract The metropolitan area of Mexico City is one of the most populated in the world and the Iztapalapa Municipality, situated on the eastern border, presents the highest population density of the city. This area is located over the geological contact between the "Sierra de Santa Catarina" volcanic range and a lacustrine basin. Inherently, the geological materials of the subsoil are horizontally and vertically heterogeneous and deform differentially under applied loads (natural and anthropogenic). As a consequence, the Iztapalapa urban infrastructure is extremely affected by fracturing and land subsidence and it is possibly one of the places with the highest social-related vulnerability in Mexico. Since localization of fracturing and deformation during land subsidence are highly dependent on local geological, geomechanical, and hydraulic conditions of the subsoil, a multidisciplinary approach for a better understanding of the fracture triggering and propagation mechanisms was established. The methodology includes: (1) detailed geological survey, (2) high resolution geophysical prospecting, (3) stratigraphic correlation of lithological logs from water extraction wells, (4) geotechnical characterization of near surface sequences, and (5) hydrogeological analysis, including the monitoring of groundwater piezometric levels. All the obtained information is referenced and analysed using a Geographical Information System (GIS), which is directly related to a main Digital Information System (SID) available via the Internet to the Iztapalapa authorities for the support of decision making. As a result of good academic–government collaboration, the former Monitoring Centre of Ground Fracturing was transformed into the Centre of Geological Risk Evaluation (*Centro de Evaluación de Riesgo Geológico*, CERG) that belongs to the Coordination of Civil Protection of the Iztapalapa Municipality. The physical vulnerability of the Iztapalapa area to land subsidence, ground fracturing and other geological hazards is evaluated through the analysis of the generated information based on thematic maps, which should allow better planning of mitigation strategies, urban development, land use management, and groundwater exploitation.

Key words database management; monitoring; ground fracturing; vulnerability; geological hazards; Iztapalapa

INTRODUCTION

The metropolitan area of Mexico City is one of the most populated in the world with almost 20 million inhabitants. The "*Delegación Iztapalapa*", one of the 16 administrative entities of the city, has the greatest inhabitant density of the country, with approximately 1 850 000 people distributed in an area of 105.8 km^2, and presents one of the highest rates of urbanization. Furthermore, the expansion of the city in the 1970s triggered the exploitation of groundwater for urban supply in this area. Iztapalapa is located in the eastern part of Mexico City over the geological contact between the "Sierra de Santa Catarina" volcanic range and a former lacustrine basin (Fig. 1). Inherently, the geological materials of the subsoil are horizontally and vertically heterogeneous. The Iztapalapa urban infrastructure is greatly affected by fracturing and land subsidence and it is possibly one of the places with the highest social-related vulnerability in Mexico. The studies performed on different urban areas reveal the coexistence of several factors determining the characteristics of fracturing at different spatial scales. One of the most important triggering factors of fracturing is groundwater withdrawal and the associated increase in effective stress; however other factors such as the structure of the subsoil, overloading and pre-existing fractures, can also play an important role. This is why the understanding of nucleation and propagation of fractures in the heterogeneous geological media require monitoring and systematic analysis of the deformation of the sequence by the integration of its physical and geological characteristics.

Copyright © 2010 IAHS Press

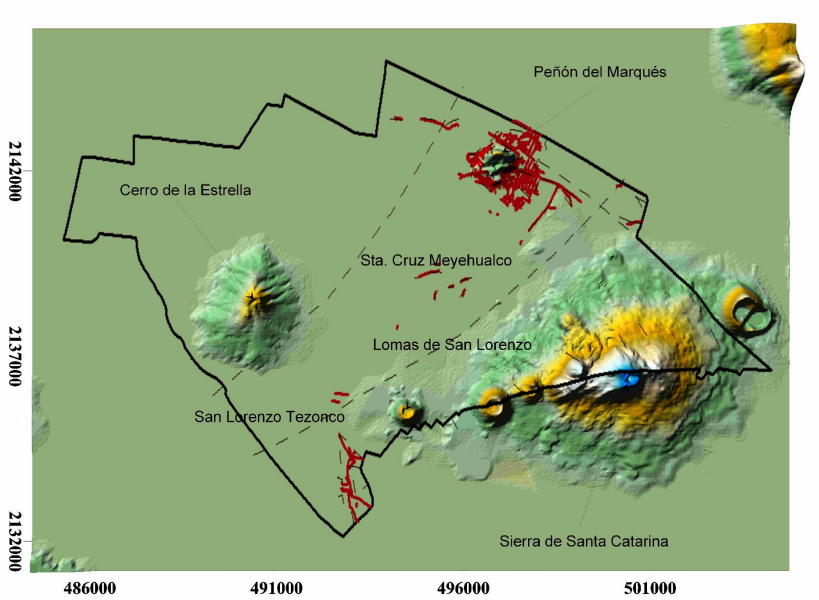

Fig. 1 Morphology of the "*Delegación Iztapalpa*". The range shown in the southeastern part is called Sierra de Santa Catarina, the shield volcano in the middle western part is called Cerro de la Estrella, the Peñón del Marques is located in the northeastern part of the study area, surrounded by a large number of fractures. These three geological structures delimit the fluvial-lacustrine plain. Fractures are marked with red lines.

A collaboration project between the *Centro de Geociencias* of the *Universidad National Autónoma de México* (UNAM) and the government of the *Delegación Iztapalapa* was initiated in 2007 for the characterization of land subsidence and ground fracturing. Since localization of fracturing and deformation during land subsidence are highly dependent on local geological, geo-mechanical and hydraulic conditions of the subsoil, a multidisciplinary approach for a better understanding of the triggering and propagation mechanisms was established. As a result of good academic–government collaboration the former Monitoring Centre of Ground Fracturing was trans-formed into the Centre of Geological Risk Evaluation (*Centro de Evaluación de Riesgo Geológico*, CERG) that belongs to the Coordination of Civil Protection of the Iztapalapa Municipality. The methodology implemented for the CERG operation includes (Fig. 2): (1) techniques of mapping, geophysical prospecting and sampling in the field, (2) a database management strategy (i.e. Digital Information System, DIS), and (3) facilities including a laboratory for physical and mechanical characterization of soils and sediments, and an interactive hall for outreach and educational purposes. The physical vulnerability of the Iztapalapa area to land subsidence, ground fracturing, and other geological hazards is evaluated through the spatial analysis of the generated information based on thematic maps that should allow better planning of mitigation strategies, urban development, land-use management and groundwater exploitation (Fig. 2).

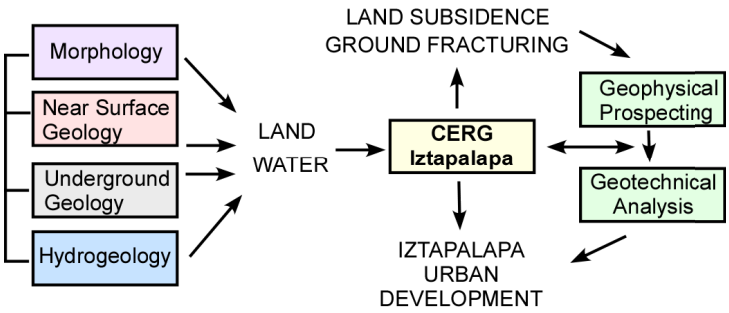

Fig. 2 Flow diagram showing the operation of the Centro de Evaluación de Riesgo Geológico (CERG).

GEOMECHANICAL PROPERTIES OF LACUSTRINE MATERIALS BENEATH MEXICO CITY

The area covered by the municipality of Iztapalapa is located within the Basin of Mexico, which was formed by the interaction of faults and volcanic activity since the Miocene times. The regional stratigraphy of the Basin of Mexico has been studied in relative detail by many authors, among others Zeevaert (1953), Marsal & Mazari (1959), Mooser (1975), De Cserna *et al.* (1988), Orozco & Figueroa (1991). According to the geotechnical zonation proposed by Marsal & Mazari (1959) the Iztapalapa area includes two main morphological areas, the lacustrine plain area and the hills area. The higher elevations in the Iztapalapa area correspond to volcanoes formed by andesite, basalt, and pyroclastic rocks of Pliocene age that outcrop in the Sierra de Santa Catarina, Cerro de la Estrella and Peñon del Marques (see Fig. 1). The valley, surrounded by volcanic edifices, is composed of volcanic and pyroclastic rocks as well as lacustrine sediments. Within the sedimentary sequences of lacustrine basins, such as Mexico Basin where volcanic activity is quite recent and contemporaneous with the deposition of the sedimentary fill, the rapid weathering of volcanic ash generates allophane and imogolite (clay incipient minerals, similar in mechanical behaviour to colloids; Carreón Freyre *et al.*, 1998). The mineralogical composition of clays of the Valley of Mexico has been well documented since the middle of last century, mainly due to its heterogeneity and the complexity of their mechanical behaviour (i.e. brittle fracture in plastic, compressible and high water content; Carreón Freyre & Cerca, 2006). Understanding this behaviour is of the uppermost importance for the monitoring of ground deformation. Early works reported contrasting compositions for the sediments of the Basin of Mexico (Zeevaert, 1953; Marsal & Mazari, 1959; Mesri *et al.*, 1976). There is an intimate relationship between the mineralogy of the clayey materials and their mechanical properties, which depend mainly on water content and are directly related to their low permeability. The relationship between the mineralogy of clay and the consolidation has been widely discussed (Ohstubo *et al.*, 1983; Warren & Rudolph, 1997; Saarenketo, 1998; Wesley, 2001). However, there are few studies relating to the geological conditions with variations in mineralogical, mechanical and hydraulic characteristics of lacustrine sequences (Carreón Freyre *et al.*, 2005), and therefore little is known about the response of these systems and mechanisms of propagation of fracturing.

The first results of the detailed geological mapping show that the regional scale fracturing is related to the interface between the volcanic material of the Sierra de Santa Catarina and fluvio-lacustrine sediments in the valley (Fig. 3). According to available records of piezometric levels, the areas of greatest depression of groundwater cannot be directly correlated to the areas of greatest subsidence, nor are the flow patterns of further decline of groundwater spatially associated with major fracture zones. This verifies that it is necessary to establish the conditions of mechanical–hydraulic coupling between volcanic and sedimentary materials to identify the relationship between groundwater withdrawal and its contribution to the propagation of the deformation. Fracture systems in fluvio-lacustrine sequences can be studied according to their size and the association of factors from which they originate. As “regional” and “local” are relative concepts that depend on the scale and type of study, this paper assumes the following criteria: (a) Regional structures are larger than the urban area. The irregularity of fractured basement underlying the sedimentary sequences largely determines the location of the fracture that propagates from deep to shallow sedimentary sequences along pre-existing planes of weakness. (b) At an intermediate scale, the fracture systems that mainly affect the top of the fluvio-lacustrine sedimentary sequence, often interbedded with pyroclastic materials and volcanics, are considered. For this work, only the first 300 m are considered at this scale because it corresponds to the current average depth of groundwater exploitation wells. (c) The local scale of analysis refers to subsidence and fracturing in restricted areas and may vary from a few to tens of metres (the geomechanical properties of the materials can be directly characterized). This is the scale at which most studies of soil mechanics are carried out the. The factors of scale and composition of clay sequences should allow an appropriate design of monitoring systems and lead to an accurate evaluation of the hazards related to ground fracturing in urban areas.

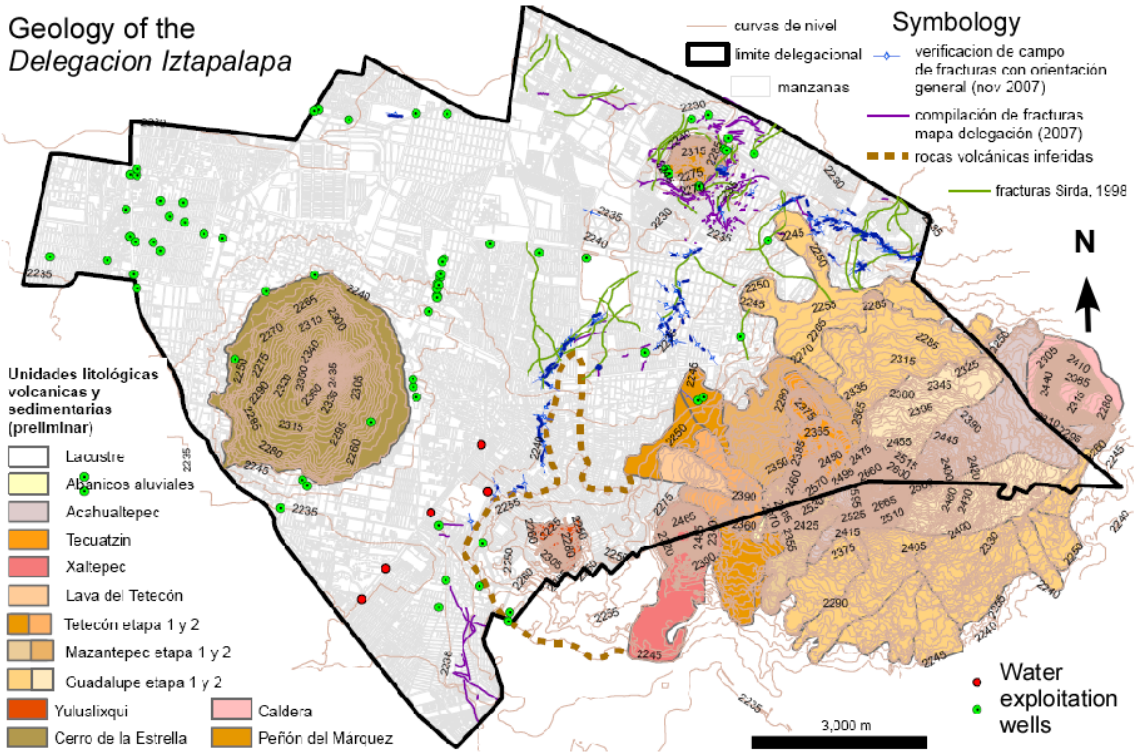

Fig 3 Geology map of the *Delegación Iztapalapa*, the lithology of the volcanic formations is shown. Fractures are marked with blue and pink lines. Water extraction wells surround the volcanic highlands.

To perform the mapping of the fractures in the Iztapalapa area, we consider their spatial and temporal continuity (i.e. they are mappable fractures with horizontal lengths and present evidence of their long-term activity). The results show that the phenomenon of regional fracturing is related to the buried border of the Sierra de Santa Catarina (now urbanized).

OPERATIONAL METHODOLOGY OF THE CERG

The methodology of systematic analysis established in the *Centro de Evaluación de Riesgo Geológico* (CERG) includes:

- Detailed geological survey (in the field and interpretation of satellite imagery).
- High resolution *geophysical prospecting* using the Ground Penetrating Radar (GPR) method, to characterize the structure of the first 10 m depth and variations in water content (Fig. 4); and the Surface Seismic Waves (SSW) method to characterize the structure of the subsoil at 50–70 m depth and variations in density and compaction of subsoil materials.
- *Stratigraphic correlation* of lithological logs from 20 m depth (geotechnical) and 150 m depth (water extraction wells). An example of the correlation is shown in Fig. 5.
- *Geotechnical characterization* (compressibility and shear strength) of near surface sequences.
- *Hydrogeological analysis*, including the monitoring of groundwater piezometric levels.

All the obtained information is referenced and analysed using a Geographical Information System (GIS) which is directly related to a main System of Digital Database (SDD) that is available, via the Internet, to the Iztapalapa authorities for the support of decision making.

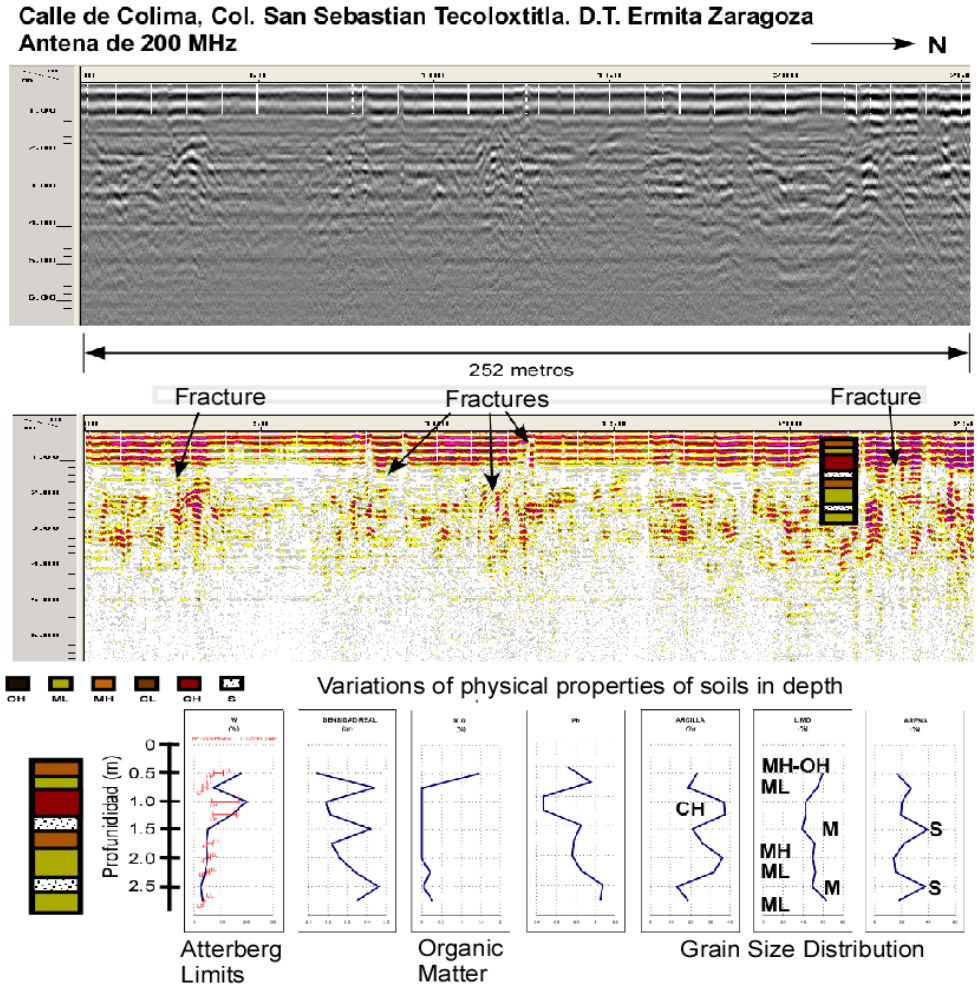

Fig. 4 Correlation of Ground Penetrating Radar (GPR) recorded features with the variations of physical properties of the near surface granular materials (soils, pyroclastics and sediments). Depth of investigation 5 m.

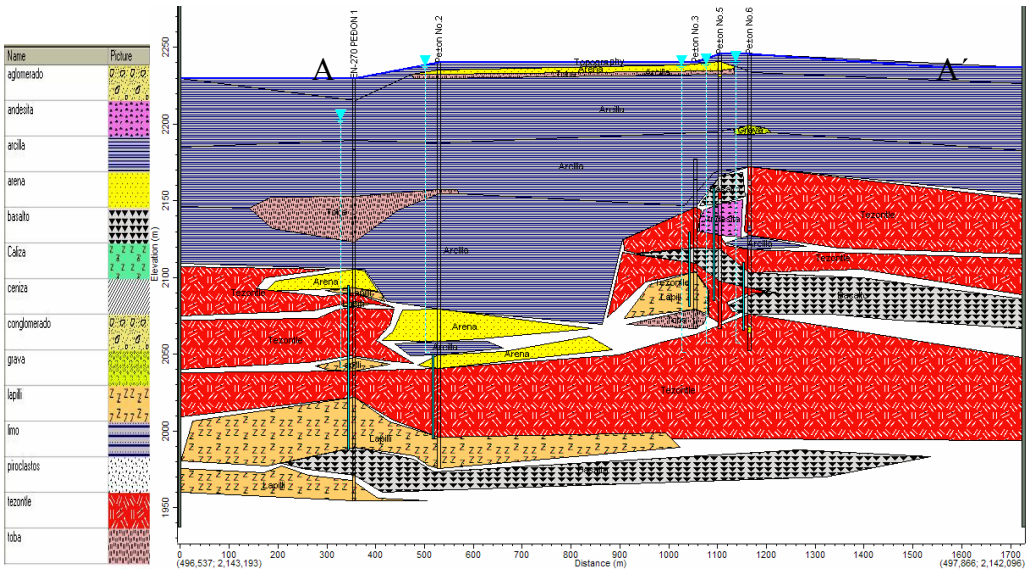

Fig 5 Example of correlation of logs from water extraction wells to build geological cross-sections, 200 m depth (using the HydrogeoAnalyst software, Schlumberger, Inc.).

CONCLUSIONS

The systematic study of ground fracturing carried out in the *Delegación Iztapalapa* is based on the consideration of the nature of geological materials. The Centre of Geological Risk Evaluation (*Centro de Evaluación de Riesgo Geológico*, CERG) has been designed with a consultative capacity, which implies that the knowledge generated about the phenomena of fracturing and subsidence should be applied in the design of mitigation measures and prevent future damage.

Fracturing in the Iztapalapa area is complex and cannot be described by a single mechanism. During our work different combinations of geological conditions and triggers factors were observed. In general, Iztapalapa fractures form due to the combined mechanisms of gradual subsidence and differential compaction of clay strata, rocks and other granular media such as sediments and pyroclastics (tuffs and ash). Pre-existing fractures and discontinuities play a fundamental role in the development of subsidence and fracturing in areas apparently not affected. The continuing reports of fractures from the 1960s in the north (Peñón del Marques) and south (San Lorenzo Tezonco) areas of Iztapalapa confirm this hypothesis. At this stage of the study, we have identified the following mechanisms of fracture:

1. Landslide associated with blocks over a detachment surface on the flanks of the volcano in the Peñon del Marques area.
2. Differential deformation (clay, tuff, organic soil) in the Santa Martha Acatitla Sur UEZ. Erratic fractures with variable dimensions (a few centimetres to several metres) are normally generated by the overload conditions of the subsoil in the lacustrine plain lake of Santa Martha Acatitla and Santa María Aztahuacán.
3. Loss of structure or collapse of unconsolidated material (pyroclastic materials, ashes or tuffs) in areas where water leaks generate infiltrations of surface water.

The physical vulnerability of the Iztapalapa area to land subsidence, ground fracturing and other geological hazards is evaluated through the spatial analysis of the generated information based on thematic maps; this should allow better design of mitigation strategies and urban development. The database includes the mapping of the physical and geotechnical properties of materials and the damaged civilian infrastructure in order to lead to improvements in the construction and development policies in geological hazard areas, as well as mitigation measures in areas susceptible to fracture occurrence. That is why the primary function of the CERG is to create a culture of co-existence with the fracturing, which unfortunately is a persistent and irreversible problem in Iztapalapa.

REFERENCES

Carreón Freyre, D. (2005) Importancia de la caracterización de arcillas en laboratorio para la adecuada evaluación de sus propiedades mecánicas. En: *Cristalografía: Fundamentos Técnicas y Aplicaciones* (ed. L. Bucio). Sociedad Mexicana de Cristalografia. A. C., 273–282. ISBN 970-9888-07-2.

Carreón Freyre, D. & Cerca, M. (2006) Delineating the near-surface geometry of the fracture system affecting the valley of Queretaro, Mexico: Correlation of GPR signatures and physical properties of sediments. *Near Surface Geophysics, EAGE* **4**(1), 49–55.

Carreón-Freyre, D. C., Gama-Castro, J., Palacios-Mayorga, S. & Garnica-Anguas, P. (1998) Propiedades y clasificación de los suelos residuales de México. *Memorias de la XIX Reunión Nacional de Mecánica de Suelos*, 75–80.

Carreón-Freyre, D. C., Cerca, M. & Hernández-Marín, M. (2003) Correlation of near-surface stratigraphy and physical properties of clayey sediments from Chalco Basin, Mexico, using Ground Penetrating Radar. *J. Appl. Geophys*. **53**, 121–136.

Carreón-Freyre., D., Cerca Martínez, M. & Hernández Marín, M. (2005) Propagation of fracturing related to land subsidence in the Valley of Queretaro, Mexico. Proceedings of the 7th International Symposium on Land Subsidence SISOLS 2005, Shanghai, P.R. China, vol. I, 155–164. ISBN 7-5323-8209-5.

Carrillo, N. (1947) Influence of artesial wells in the sinking of Mexico City. In: *Volumen Nabor Carrillo "El hundimiento de la Ciudad de México y el Proyecto Texcoco"*. Comisión Impulsora y Coordinadora de la Investigación Científica Anuario 47, 7–14.

Holzer, T. L. (1984) Ground failure induced by groundwater withdrawal from unconsolidated sediment. *Geol. Soc. Am., Reviews in Engineering Geology* **6**, 67–105.

Marsal, R. J. & Mazari, M. (1959) El subsuelo de la Ciudad de México. Instituto de Ingeniería, U.N.A.M.

Mazari, M. & Alberro, J. (1990) Hundimiento de la Ciudad de México. En *Problemas de la Cuenca de México* (coordinado por J. Kumate & M. Mazari), 83–114. Ed. El Colegio Nacional.

Mazari-Hiriart, M., Hernández-Eugenio, C., Rojo-Callejas, F. & Lozano-Santacruz, R. (2000) Vertical variability of PCE sorption in the lacustrine clays of Mexico City. *Environmental Geology* **39**(6), 595–602.

Mesri, G., Rokhse, A. & Bonor, B. F. (1976) Composition and compressibility of typical samples of Mexico City. *Geotechnique* **25**(3), 527–554.

Mooser, F. (1975) Historia geológica de la Cuenca de México. En: *Memorias de las Obras del Sistema de Drenaje Profundo del Distrito Federal*, Tomo I, 738. DDF.

Ohtsubo, M., Takayama, M. & Egashira, K. (1983) Relationships of consistency limits and activity to some physical and chemical properties of Ariake marine clays. *Soils and Foundations* **23**(1), 38–46.

Orozco, J. M. & Figueroa V. G. (1991) Descripción cronológica del desarrollo de los conocimientos sobre el agrietamiento de terrenos. *Agrietamiento de suelos*, 1–12. Soc. Mex. Mec. de Suelos.

Peralta & Fabi, R. (1989) Sobreel origen de algunas propiedades mecánicas de la formación arcillosa superior del Valle de México. Simposio sobre Tópicos Geológicos de la Cuenca del Valle de México.

Righi, D. & Meunier, A. (1995) Origin of clays by rock weathering and soil formation. In: *Origin and Mineralogy of Clays; Clays and the Environment* (ed. by. B. Velde), 43–157. Springer.

Saarenketo, T. (1998) Electrical properties of water in clay and silty soils. *J. Appl. Geophys*. **40**, 73–88.

Tuckwell, G. W., Lonergan, L. & Jolly, R. J. H. (2003) The control of stress history and flaw distribution on the evolution of polygonal fracture networks. *J. Structural Geology* **25**, 1241–1250.

Wada, K. (1987) Minerals formed and mineral formation from volcanic ash by weathering. *Chemical Geology* **60**, 17–28.

Warren, C .J. & Rudolph, D. L. (1997) Clay minerals in basin of Mexico lacustrine sediments and their influence on ion mobility in groundwater. *J. Contam. Hydrol*. **27**, 177–198.

Wesley, L. D. (2001) Consolidation behaviour of allophane clays. *Géotechnique* **51**(10), 901–904.

Zeevaert, L. (1953) Estratigrafía y problemas de ingeniería en los depósitos de arcilla lacustre de la Ciudad de México. *Memoria del Congreso Científico Mexicano*, vol. 5, 58–70.

Land Subsidence, Associated Hazards and the Role of Natural Resources Development
(Proceedings of EISOLS 2010, Querétaro, Mexico, 17–22 October 2010). IAHS Publ. 339, 2010.

Microtremor measurements to detect zones of potential cracking in the Basin of México

J. LERMO, E. OVANDO & L. ESPINOSA
Instituto de Ingeniería, Universidad Nacional Autónoma de México, Cd. Universitaria, Coyoacán, 04510, México, D.F.
jles@pumas.iingen.unam.mx

Abstract Fissures and cracks in the clayey masses of the basin of Mexico have recently increased in number and have produced considerable damage to low-price popular dwellings, such as in San Lorenzo, a location in the Ixtapalapa hilly area in Mexico City and in San Martin Cuautlalpan, in Chalco, close to the city. Cracks in these two cases are difficult to control and are caused by regional subsidence which, in turn, originates in the extraction of water from deep strata. Cracking and fissuring usually occur in abrupt transition zones in which the thickness of compressible clay layers changes sharply over short distances and in places where one finds buried geological structures within the basin. Many of these cracks and fissures have been located and even mapped, but there are ample zones in the basin where the zones of potential cracking are yet to be defined. In this paper we use analyses of microtremor records to study three zones where cracks and fissures have appeared in and around Mexico City. Our results show that Nakamura's ambient vibration method can be used adavantageously to study cracks and potential cracking, including some of its features: length, depth, etc. It can also be used to derive hypotheses regarding the possible origin of cracking phenomena and to define zones of potential cracking in certain areas of the basin. Results of exploratory geotechnical soundings are used to validate our method.

Key words subsidence; cracks; fissures; Nakamura's method

INTRODUCTION

One of the problems faced by urban areas, in different zones of Mexico, is soil cracking. The former lake zone of the basin of the Valley of Mexico, has been affected by this intense cracking in recent years. Cracking is directly related to land subsidence and due to water pumping. Once the water is pumped for a long period, the layers formed by sediments reduce their volume significantly creating a heterogeneous mix with the rocky ground and then differential settlements occur. Around 70% of the water distributed in the Valley of Mexico it is obtained by deep pumping of water-bearing sediments (Fig. 1) and 30% from the Cutzamala system outside the basin. One example of the cracking problem is in San Lorenzo, a location in the Iztapalapa hilly area of Mexico City. Cracking and fissuring usually occur in abrupt transition zones in which the thickness of compressible clay layers changes sharply over short distances and in places where one finds buried geological structures within the basin. Many of these cracks and fissures have been located and even mapped, but there are many zones in the basin where the zones of potential cracking are as yet undefined.

Using microtremors, Nakamura's ambient vibration method can be used advantageously to study cracks and potential cracking, including some of its features: length, depth, etc. It can also be used to derive hypotheses regarding the possible origin of cracking phenomena and to define zones of potential cracking in certain areas of the basin.

MECHANISMS OF CRACK GENERATION

The origins of cracking in the Metropolitan zone of the Valley of Mexico were identified by Dr Gabriel Auvinet (Auvinet, 1981; Auvinet & Arias, 1991) who identified five main mechanisms for crack generation:

1. Cracks by abrupt transition. Cracks corresponding to differentials collapses in the zones of abrupt transition between firm and soft materials (Fig. 1).

Copyright © 2010 IAHS Press

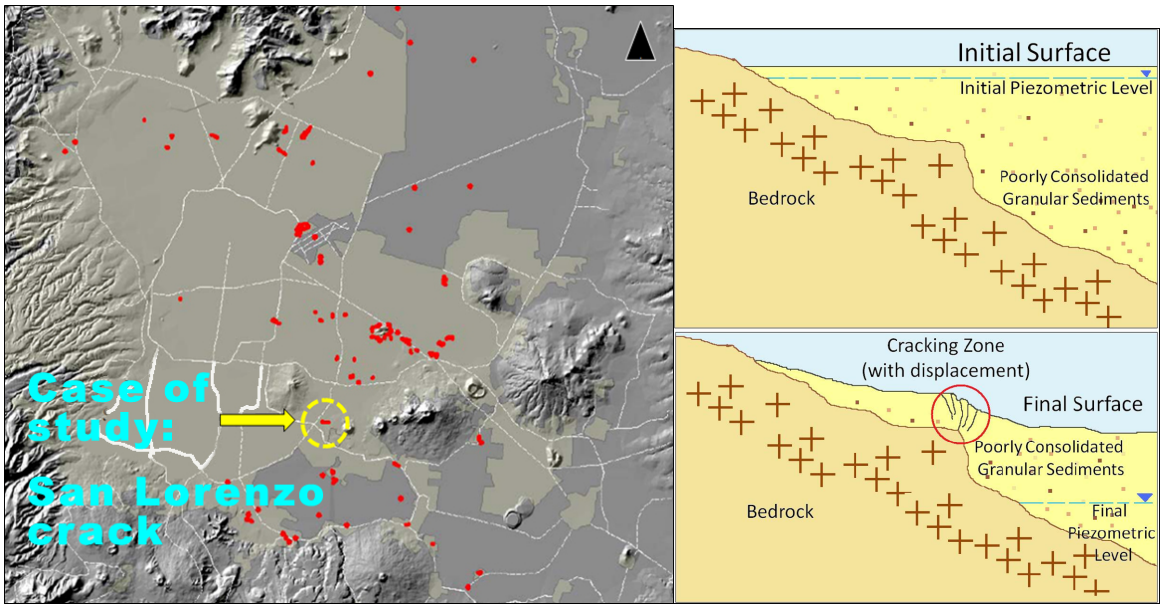

Fig. 1 Left side: Spatial distribution of identified cracks in the basin of Mexico marked with a red point (Auvinet *et al*., 2007). Right side: cracking by abrupt transition mechanism.

2. Cracks by hydraulic breaking. These are generated in the former lake zone with great thicknesses of soft ground and are attributable to hydraulic fracturing.
3. Cracks by stratigraphic irregularities. Cracks attributable to other mechanisms, such as the ones generated by the heterogeneity of the subsoil.
4. Cracks by evapotranspiration. Cracks attributable to evapotranspiration of water through trees from the superficial layers of the subsoil.
5. Cracks by buried structures. Cracks attributable to buried rock structures in the subsoil.

CRACKING IN THE VALLEY OF MEXICO

The identified cracks are mainly located at the foot of hills or small volcanoes (Fig. 1). These cracks are generated by abrupt transitions from firm grounds to softer ones. It is important to correlate mainly the geomorphology of the place to determine the origin of cracking.

ANALYSIS

Case study We studied the origin of the crack that appeared on 7 July 2007 in Lomas de San Lorenzo, Iztapalapa.

Methodology The analysis of the signals of environmental noise (microtremors) has the objective to determine the dominant period (T_o) in each one of the points that were selected. The expression used to calculate H was: $T_o = 4H / Vs$.

Selection of sites and precise measurement of seismic noise The studied Zone is defined to the north by Reclusorio Oriente (Río Nilo Avenue), to the south by Tlahuac Avenue, to the east by the Ignacio Zaragoza Street and to the west by Vicente Guerrero Street. Two measurement campaigns were carried out, the first in August 2009 (47 measurement points, distributed in five cross-sectional profiles to the cracks). The second campaign took place in October 2009, detailing features around the main crack (76 points). In summary, 17 cross-sections were obtained with a total of 123 points. In addition, there are around 20 different geotechnical soundings (mixed sounding, sounding of electrical cone, sounding of deep exploration, etc.), which were used as a general background (Fig. 2).

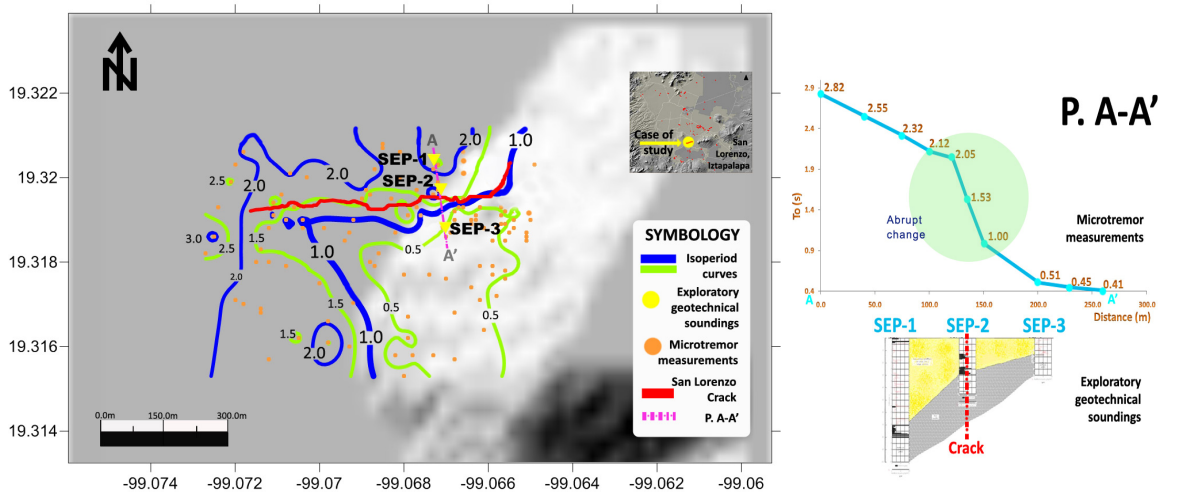

Fig. 2 Left side**.** Map of the studied zone: major crack (red line), isoperiod curves (blue and green lines), microtremor measurements (orange points), exploratory soundings (yellow marks). Right side. Comparison between the periods and the geotechnical soundings.

RESULTS

The values of calculated H values and those obtained from soundings, have a maximum error of ±1 m. An example of this is the mixed sounding in the Elementary School Jose Romero, where the thickness measured directly in the geotechnical sounding 12 m and the calculated H from microtremors is 12.2 m.

It is noteworthy that cracks do not appear more than 5 to 8 m away from the point in which thickness of the compressible materials changes abruptly (Fig. 2).

There is a pattern between the dominant period and the morphology of the underlying hard materials. The major crack in San Lorenzo appears between the periods of 1.0 to 1.5 and this pattern can be used to infer zones of potential cracking for a number of plausible situations.

CONCLUSIONS

Using the microtremors, new hypotheses about the origins of cracking can be formulated: the main crack in Iztapalapa appeared at the limits of the transition of the buried structure; abrupt transitions merits the attention of the authorities because it will continue to generate damage to property and urban infrastructure; and about 90% of the cracks in the Valley of México are produced by the abrupt transition mechanism in zones where buried geologic structures appear mainly at the bottom of hills.

REFERENCES

Auvinet, G. (1981) *Agrietamiento de las arcillas del valle de México*. Informe técnico del Instituto de Ingeniería, UNAM, a la Comisión del Lago de Texcoco, México, D.F.

Auvinet, G. & Arias, A. (1991) *Propagación de grietas*. Memoria, Simposio sobre agrietamiento de suelos, Sociedad Mexicana de Mecánica de Suelos, México, D.F., 21–32.

Lermo, J. & Chávez-García, F. (1993) Site effect evaluation using spectral ratios with only one station. *Bull. Seism. Soc. Am.* **83**, 1574–1594.

Lermo, J. & Chávez-García, F. (1994) Site effect evaluation at Mexico City: Dominant period and relative amplification from strong motion and microtremor records. *Solid Dynamics and Earthquake Engineering* **13**, 413–423.

Pacheco, J. (2007) Modelo de subsidencia del Valle de Querétaro y predicción de agrietamientos superficiales. Tesis doctoral, Centro de Geociencias, Universidad Nacional Autónoma de México.

(Proceedings of EISOLS 2010, Querétaro, Mexico, 17–22 October 2010). IAHS Publ. 339, 2010.

Application of Wigner-Ville distribution to identify anomalies in GPR profiles

M. A. ELIZONDO[1], R. E. CHÁVEZ[2], M. E. CÂMARA[3] & A. TEJERO[4]

1 *Posgrado en Ciencias de la Tierra, Universidad Nacional Autónoma de México, Mexico D.F.*
maes112@yahoo.com.mx
2 *Instituto de Geofísica, Universidad Nacional Autónoma de México, Mexico D.F.*
3 *Escuela Técnica Superios de Ingenieros Industriales, Universidad Politécnica de Madrid, Madrid, Spain*
4 *Facultad de Ingeniería, Universidad Nacional Autónoma de México, Mexico D.F.*

Abstract An analysis in time and frequency, based on signal decomposition spectral analysis, is performed through the Wigner-Ville distribution (WVD) for GPR data. It calculates a cross-correlation between the original signal and the time-frequency components, for structural anomalies available in the information provided by the GPR related to the geology. We describe the application in a theoretical example representing a tunnel. Corresponding signatures are obtained in the time-frequency domain. A real application is presented over a test site, where a drum of known geometry has been buried. This is a special test site built in the facilities of the UNAM Magnetic Observatory at Teoloyucan, State of Mexico. The depth and dimensions are well controlled, and the results obtained are quite encouraging, since the WVD is capable of defining the morphological features related to such a drum. The results are interesting regarding the possibility of locating such structures.

Key words Ground Penetrating Radar (GPR); time-frequency analysis; Wigner-Ville distribution; signal processing

INTRODUCTION

GPR (Ground Penetrating Radar) has proven to be an important methodology for revealing subsurface features. Shallow buried features such as fractures, mines, caves and anthropogenic structures (pipes, connecting lines, etc.) can be successfully detected. In addition, information has processed GPR commonly in either of the two domains, Time Domain (TD) or Frequency Domain (FD) by employing the Fourier transform. It is not always possible to obtain a reasonable resolution on information from GPR, due to variations in the relative dielectric permittivity (RDP). Therefore, GPR information in the form of diagrams is extremely difficult to interpret. The analysis of information requires the application of filters designed in TD or FD, which are used to separate important information from the noise. Unfortunately, such filters are unable to fulfill their goal if the filtered signal is contaminated with spurious information. Further, the estimated events or anomalies are probably well-defined in the FD, but not in the TD occurrence. A time-frequency analysis (TF) can reveal the time variation in the frequency contained in a 1-D GPR signal. The idea is to extract a time series profile that makes up the radagram and to define a function in TF, which shows features related to anomalous bodies or structures. In this case, the Wigner-Ville Distribution (WVD) is used to define these structural objectives (Lopera *et al*., 2008). It is proposed to estimate a 1-D GPR signal processed by the WVD, which can provide features of a structure, such as a stratigraphic change, a cavity or fracture, with the frequency information contained in time, identifying an event which has occurred. First, a 1-D theoretical model is presented to show the ability of the WVD, and then a real example is shown from a test site where the characteristics are known and studied. The test site is located in the facilities of the UNAM Magnetic Observatory at Teoloyucan town, in the State of Mexico, approximately 60 km northeast of Mexico City.

METHODOLOGY

The WVD of a discrete signal $s(t)$ is given by (Cohen, 1989):

Copyright © 2010 IAHS Press

$$WVD_x(t_i, f_j) = \frac{T}{\pi} \sum s(t_i + kT) s^*(t_i - kT) e^{-i4\pi f_j kT} \quad (1)$$

The total energy will be obtained by integrating over the entire frequency and on the whole interval of time (Kumar & Foufoula-Georgiou, 1994). For the decomposition method, a scan of a synthetic radagrama through a direct model associated with the stratigraphy of the land in 1-D is generated, where the electric field in the Earth's surface can be obtained. Using the method of Weng (1971), based on the fact that a plane wave enters the Earth's surface and the total field obtained on the surface is the incident field plus the reflected field, and considering a dissipative dielectric N-layered earth model and a generalized reflexion coefficient given by Stokes (Bellman & Wing, 1975) and solved in a recursive form as:

$$\tilde{R}_{i,i+1} = \frac{R_{i,i+1} + \tilde{R}_{i+1,i+2} e^{2i\gamma_{i+1,z}(d_{i+1} - d_i)}}{1 + R_{i,i+1} \tilde{R}_{i+1,i+2} e^{2i\gamma_{i+1,z}(d_{i+1} - d_i)}} \quad (2)$$

After an electric pulse is coupled, the Ricker wavelet is usually used to obtain the synthetic radagram scan of the frequency domain, as it uses the convolution theorem, and the Fourier transform scan is obtained in the domain of time (Annan, 1992; Diaz, 2003). Finally, we calculated the WVD to obtain the time-frequency plane.

ANALYSIS AND RESULTS OF THE GPR TRACES

Table (1) presents the data used to generate the synthetic trace (Fig. 1). The model is represented in a sampling window of 60 ns, employing an antenna of 270 MHz with 512 samples per record, called synthetic trace scan.

Table 1 Data used to generate the synthetic trace.

Layer	Material	Depth (m)	Magnetic permeability (h/m)	Electrical conductivity (s/m)	Electrical permittivity (f/m)
1	Suelo arenoso	4	μ_0	0.001	$8\varepsilon_0$
2	Aire	3	μ_0	0	E_0
3	Suelo arenoso	–	μ_0	0.001	$8\varepsilon_0$

We have calculated the electric field, and the synthetic trace. Then, the time–frequency plane for this trace is calculated, where the position of high amplitudes can indicate the location of an event as indicated at the time (t_1 = 20 ns and t_2 = 39 ns). These plots represent different events and are represented in a time–frequency plot as high energy values. It is interesting to note that the amplitudes are compacted into the centre of the plane in a frequency range from 100 to 300 MHz. These represent the energy spectrum of the signal, which has a maximum value of 270 MHz (Fig. 1).

Finally, a practical example is presented using the same methodology. A GPR profile is analysed in the test site, where a cylindrical drum was buried, with the following dimensions: diameter 0.60 m in an area of 2.0 × 5.0 m, and to a depth of 1.0 m.

The GPR data were analysed following the methodology already described, employing the WVD. Each trace depicts a similar behaviour (Fig. 2), providing the possibility of better locating the position at depth of the drum.

We have taken a trace of the GPR profile. Then, the time-frequency plane for this trace is calculated. The position of high amplitudes can indicate the location where the cylindrical drum was buried. For this event it is indicated at the time (t_1 = 27 ns). These plots show us different events and are represented in a time–frequency plot as high energy values. It is interesting to note

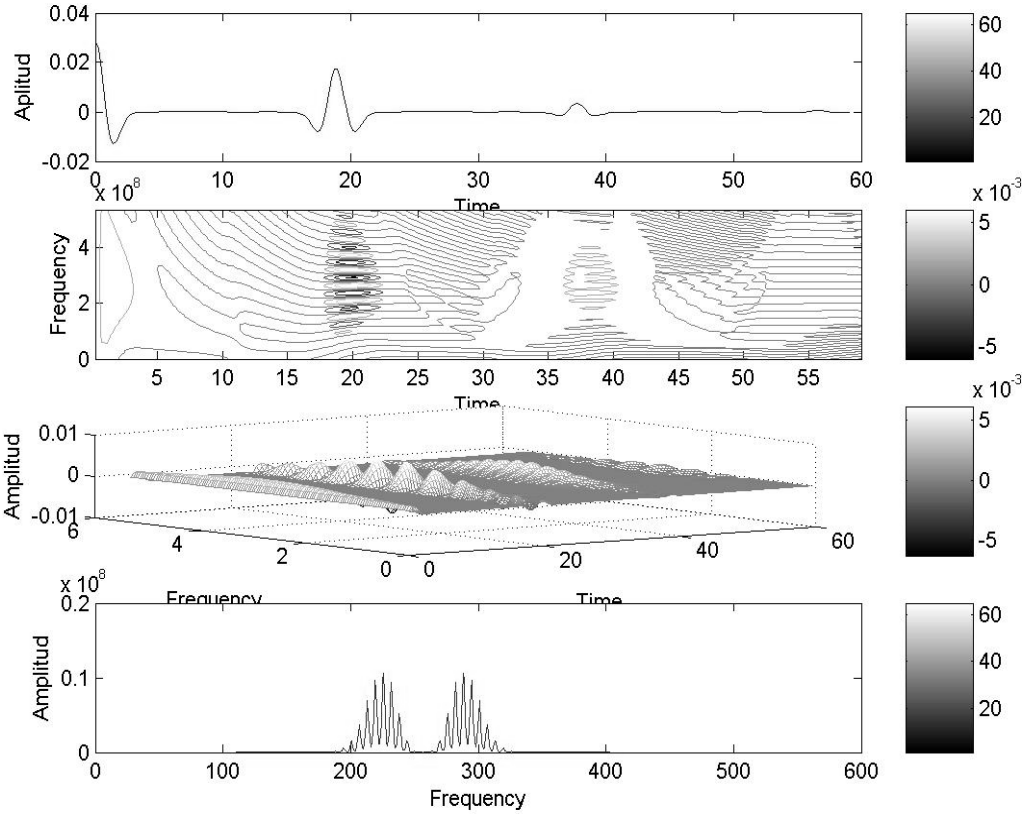

Fig. 1 The synthetic trace, the time-frequency plane, and the spectrum energy of the signal.

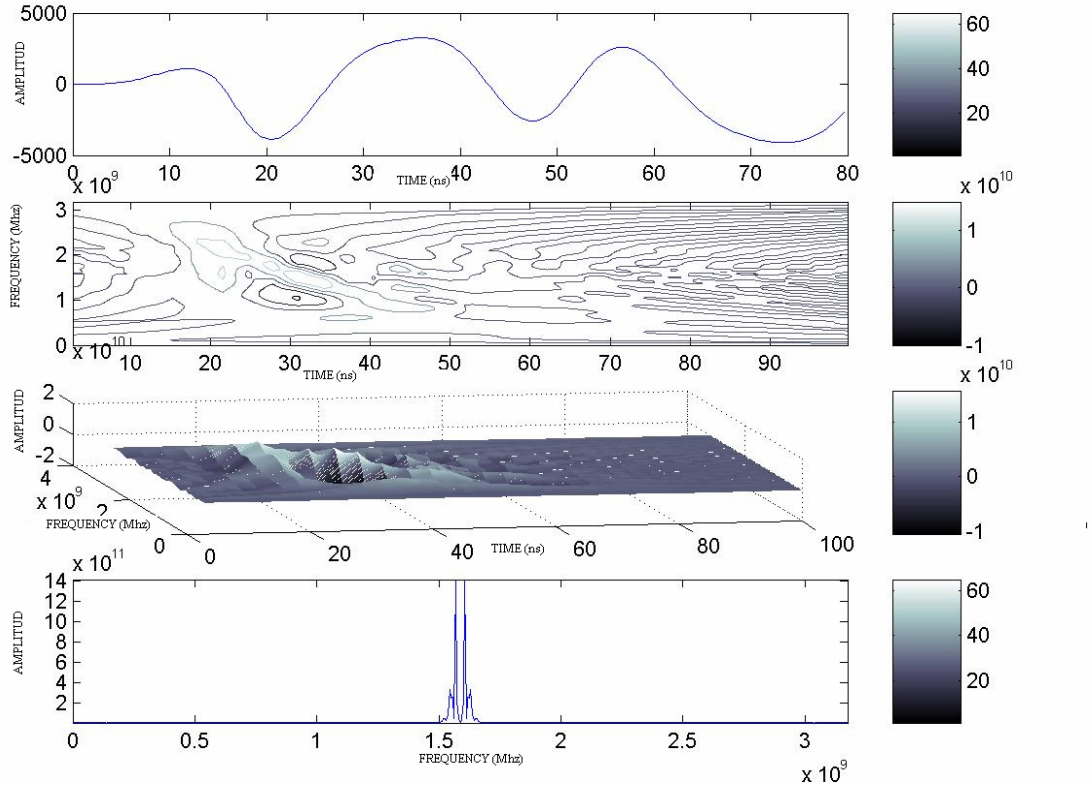

Fig. 2 Results obtained at the test site. Noise-free signal is observed at the top. The T-w plane follows, note the effect at t = 27 ns and w = 200 MHz. The spectrum below clearly depicts the effect of the drum. Finally, the spectrum energy of the signal is depicted.

that the amplitudes are compacted into the centre of the plane in a frequency range from 100 to 300 MHz. These represent the energy spectrum of the signal, which has a maximum value of 170 MHz (Fig. 2).

CONCLUSIONS

Non-stationary properties of the GPR signal allowed the application of WVD. A time–frequency plane was calculated, which allowed visualization of the frequency range contributing to the signal in the time scale studied. In the future it will be possible to deal with mathematical models to define the time–frequency intervals in the Wigner-Ville domain. The characteristics of the GPR signal from these models may be used as a calibration procedure. Then, for each material model, a signature of GPR data could be estimated.

REFERENCES

Annan, A. P. & Chua, L. T. (1992) Ground Penetrating Radar performance prediction. In: *Ground Penetrating Radar*, 5–13. Geological Survey of Canada, Canada.

Bellman, R. & Wing, M. G. (1975) *An Introduction to Invariant Imbedding*. Wiley, New York, USA.

Cohen, L. (1989) Time-frequency distributions. A review. *Proc. IEEE* **77**(7), 941–980.

Diaz, M. O. (2003) 1-D modeling data forward and reverse ground penetrating radar. Masters Thesis, National Autonomous University of Mexico, UNAM, Mexico.

Kumar, P. & Foufola-Georgiou, E. (1994) Wavelet analysis in geophysics: an introduction. *Geophysics Wavelet* **4**, 1–43.

Lopera, O., Milisavlievic, N., Daniels, D. & Maco, B. (2007) Time-frequency domain signature analysis of GPR data for landmine identification. *IEEE Trans. Geosci Remote Sensing*, 159–162.

Roth, P., van Genderen, F. & Verhaegen, M. (2001) Analysis of the influence of mine and soil properties on features extracted from GPR Data. *Detections and Remediation Technologies for Mines IV* **4394**, 428–439.

Weng, C. C. (1971) *Waves and Fields in Inhomogeneous Media*. University of Illinois Urbana-Champaign. IEEE Press, New York, USA.

2 Modelling Land Subsidence and Associated Hazards

Land Subsidence, Associated Hazards and the Role of Natural Resources Development
(Proceedings of EISOLS 2010, Querétaro, Mexico, 17–22 October 2010). IAHS Publ. 339, 2010.

Use of the SUB-WT Package for MODFLOW to simulate aquifer-system compaction in Antelope Valley, California, USA

STANLEY A. LEAKE[1] **& DEVIN L. GALLOWAY**[2]

1 *US Geological Survey, 520 N. Park Ave, Suite 221, Tucson, Arizona 85719, USA*
saleake@usgs.gov

2 *US Geological Survey, 3020 State University Drive East, Suite 3005, Sacramento, California 95819, USA*

Abstract The Antelope Valley of southern California, USA, includes a basin-fill aquifer system with an upper unconfined aquifer and middle and lower confined aquifers. Groundwater pumping has caused nearly 2 m (1930–1992) of subsidence near the city of Lancaster. A previous model simulated regional groundwater flow, aquifer-system compaction and subsidence in Antelope Valley using the US Geological Survey modular groundwater flow model MODFLOW with the Interbed Storage Package, version 1 (IBS1). That approach used the assumptions of constant geostatic stress and skeletal specific storage. The newer Subsidence and Aquifer-System Compaction Package (SUB-WT) for water-table aquifers for MODFLOW allows geostatic stress to vary as a function of the position of the water table, and uses stress-dependent skeletal storage coefficients. For this study, the previous model was converted to use SUB-WT to assess the importance of accounting for variable geostatic stress and stress-dependent storage on subsidence simulations in Antelope Valley.

Key words subsidence; aquifer-system compaction; groundwater model; Antelope Valley, California, USA

INTRODUCTION

Coupled groundwater flow and aquifer-system compaction models are often needed by resource managers in areas where pumping results in significant land subsidence. Development of a basin-scale model requires a model code, such as MODFLOW (Harbaugh, 2005), that has options for simulating important hydrogeological features in the area to be modelled. Leake & Prudic (1991) developed the Interbed Storage Package, version 1 (IBS1) to simulate storage changes, and compaction of compressible interbeds in an aquifer system. IBS1 uses a simple formulation, based on the *Principle of Effective Stress* (Terzaghi, 1925), that assumes: (1) a unit decline in head results in a unit increase in effective stress, and (2) skeletal storage properties are not a function of effective stress. Leake & Galloway (2007) developed the Subsidence and Aquifer-System Compaction Package (SUB-WT) for water-table aquifers for MODFLOW to remove these assumptions for application in shallow water-table aquifer systems. This paper presents some testing of SUB-WT that was done by converting an existing groundwater-flow model of Antelope Valley, California (Leighton & Phillips, 2003) from use of IBS1 to use of SUB-WT.

STUDY AREA

Antelope Valley, Mojave Desert, California is a nearly 2500 km^2 valley in the high desert (>600 m a.s.l.) about 80 km north-northeast of Los Angeles, California (Fig. 1). The two largest cities in Antelope Valley are Lancaster and Palmdale—two of the fastest growing cities in California during the 1990s. Runways at Edwards Air Force Base are used by the US National Aeronautical and Space Administration as an alternate landing site for the space shuttles.

The valley occupies the western wedge of the Mojave Desert and is bounded on the west by the juncture of the northeast oriented Tehachapi Mountains and Garlock Fault Zone to the north and the northwest oriented San Gabriel Mountains and San Andreas Fault Zone to the south (Fig. 1). Several terminal dry lakes (Rogers, Rosamond and Buckhorn) are nestled in the northeastern portion of the topographically closed valley. The valley fill comprises thick (locally >1.5 km) sequences of principally Quaternary unconsolidated alluvial and lacustrine deposits overlying consolidated basement rock, principally faulted quartz monzonite that defines several

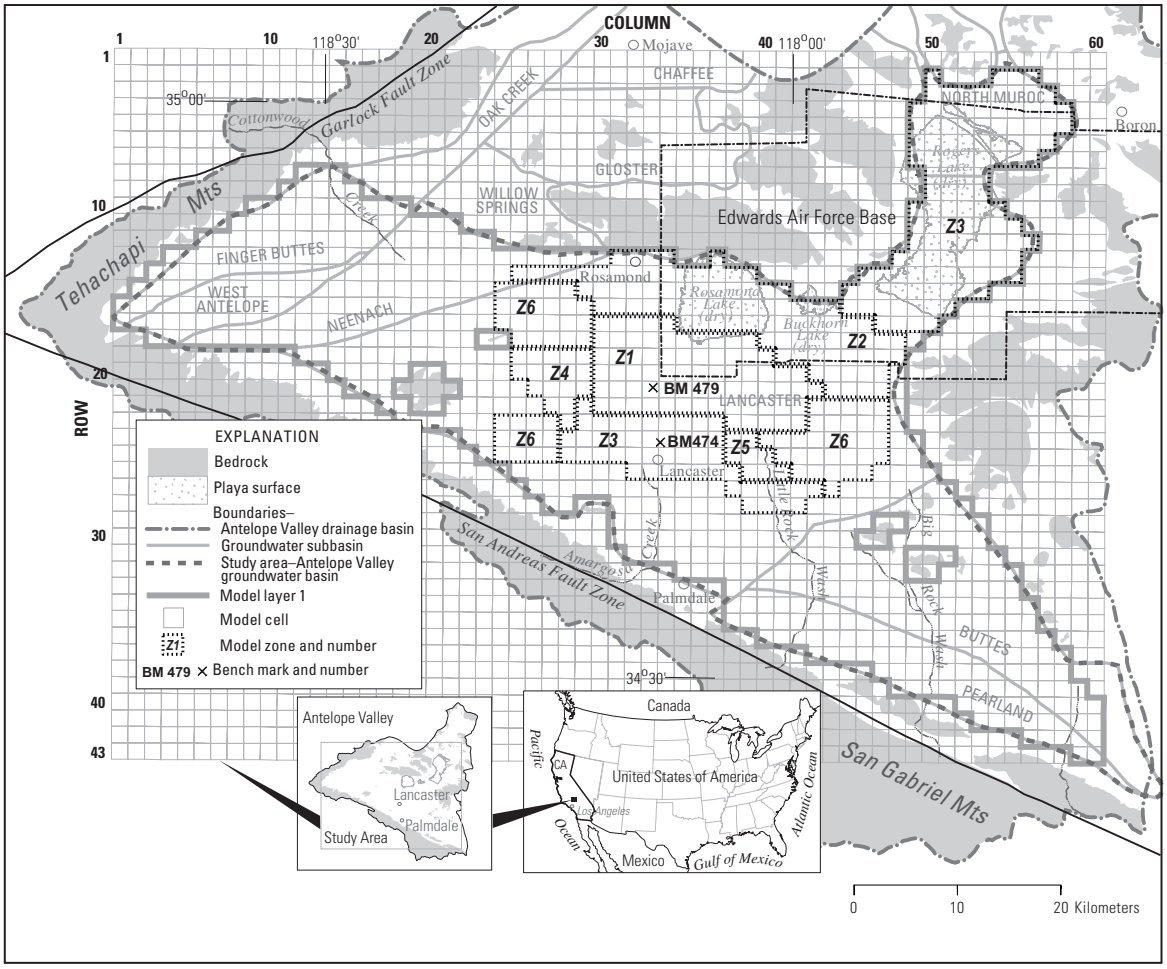

Fig. 1 Antelope Valley study area and model grid. Modified from Leighton & Phillips (2003, figures 15 and 24).

structural (geological) basins. The unconsolidated deposits constitute the aquifer system in Antelope Valley, which is defined by numerous groundwater sub-basins (Fig. 1).

Groundwater development to support irrigation agriculture began at about the turn of the twentieth century. Annual groundwater production peaked at about 493 × 10^6 m^3 in the early 1950s and remained high through the mid-1960s. Annual groundwater production declined steadily over the following two decades to about 86 × 10^6 m^3 by 1990 owing to declines in agricultural production and the availability of imported water beginning in the early 1970s. Since the mid-1980s annual groundwater production to support growing municipal-industrial water demand and irrigation agriculture has been slightly increasing, but remains far below peak production rates.

Annual groundwater production in excess of the estimated annual natural recharge to Antelope Valley (about 50 × 10^6 m^3; Durbin, 1978) has depleted the groundwater resource (Galloway *et al*., 1998b). By the early 1990s local groundwater-level declines of as much as 100 m and historical subsidence of nearly 2 m was observed. Concerns about groundwater over-exploitation, related subsidence and associated earth fissures prompted studies by the US Geological Survey (USGS), beginning in the early 1990s. These and subsequent studies defined the regional distributions of head decline, subsidence and groundwater use, developed a conceptual hydrogeological framework (see references cited in Leighton & Phillips, 2003), and established the relation between head decline, aquifer-system compaction and land subsidence (Ikehara & Phillips, 1994; Galloway *et al*., 1998a; Sneed & Galloway, 2000). This information

was used to develop a calibrated numerical model of transient (1915–1995) groundwater flow and subsidence for the Antelope Valley groundwater basin (Leighton & Phillips, 2003) to assist stakeholders managing the groundwater resource. The study area and model finite-difference grid are shown in Fig. 1.

SIMULATING VERTICAL COMPACTION IN MODELS OF GROUNDWATER FLOW

In basin-scale models, representation of many individual discontinuous interbeds is impractical. Both IBS1 and SUB-WT, therefore, compute storage change and compaction by considering the bulk volume of these compressible beds in each model cell. In doing so, they assume that a head change in a model cell applies to the total volume of compressible interbeds in the cell, without a time lag in drainage of water from these interbeds.

In IBS1, changes in thickness of compressible interbeds caused from elastic compaction, Δb_e and from inelastic compaction, Δb_i are computed as:

$$\Delta b_e = -S_{ske} b \Delta h \quad \text{and} \tag{1a}$$

$$\Delta b_i = -S_{skv} b \Delta h \tag{1b}$$

respectively, where S_{ske} is elastic skeletal specific storage, b is thickness of compressible interbeds, Δh is change in head, and S_{skv} is inelastic skeletal specific storage. Positive Δb_e and Δb_i indicate decreased thickness from compaction, and positive Δh increased head. The volumetric rate of storage change from compaction in a model cell for model time step n is computed by multiplying compaction by the horizontal surface area of the model cell, A, and dividing by the length of the time step, Δt_n. To allow for conversion from elastic to inelastic compaction within a model time step, the volumetric rate of storage change in compressible interbeds, Q is formulated as:

$$Q = \frac{Ab}{\Delta t_n}\left[S_{sk}\left(h_n - H_{n-1}\right) + S_{ske}\left(H_{n-1} - h_{n-1}\right)\right], \qquad S_{sk} = \begin{cases} S_{ske}, h_n > H_{n-1} \\ S_{skv}, h_n \le H_{n-1} \end{cases} \tag{2}$$

where h, is head, and H is the "critical" or "preconsolidation" head below which compaction becomes inelastic. If head in a model cell falls below the preconsolidation head during a time step, preconsolidation head is reset to the new lowest head value for the next time step. Major input arrays for IBS1 are: (a) elastic skeletal storage coefficient, the product of S_{ske} and b; (b) inelastic skeletal storage coefficient, the product of S_{skv} and b; and (c) initial critical head.

In SUB-WT, changes in thickness of compressible interbeds caused from elastic and inelastic compaction are computed as:

$$\Delta b_e = \frac{0.434 b_0 C_r \Delta\sigma'}{\left(1+e_0\right)\sigma'} \quad \text{and} \tag{3a}$$

$$\Delta b_i = \frac{0.434 b_0 C_c \Delta\sigma'}{\left(1+e_0\right)\sigma'} \tag{3b}$$

respectively, where b_0 is the initial thickness of compressible interbeds, C_r is recompression index, $\Delta\sigma'$ is change in effective stress, e_0 is initial void ratio, σ' is effective stress, and C_c is compression index. The volumetric rate of storage change for model time step n is:

$$Q_i = \frac{Ab_n}{\Delta t_n}\left[S_{sk}\left(\frac{\sigma_n}{\gamma_w} - h_n + z_n - \frac{\sigma'_{c,n-1}}{\gamma_w}\right) + S_{ske}\left(\frac{\sigma'_{c,n-1}}{\gamma_w} - \frac{\sigma'_{n-1}}{\gamma_w}\right)\right] \quad S_{sk} = \begin{cases} S_{skv}, \ \sigma'_n > \sigma'_{c,n-1} \\ S_{ske}, \ \sigma'_n \le \sigma'_{c,n-1} \end{cases} \tag{4a}$$

$$S_{ske} = \frac{0.434 C_r \gamma_w}{\sigma'_{n-1}\left(1+e_0\right)} \quad \text{and} \tag{4b}$$

$$S_{skv} = \frac{0.434 C_c \gamma_w}{\sigma'_{n-1}\left(1+e_0\right)} \tag{4c}$$

where σ is geostatic stress, γ_w is the unit weight of water, z is average elevation of interbeds, and σ'_c is preconsolidation stress. Dividing stress quantities by γ_w converts the units to an equivalent height of a column of water. Note that effective stress is in the denominator of equations (4b) and (4c). As such, S_{ske} and S_{skv} get smaller with increasing effective stress that naturally occurs with depth and also occurs when head declines. Major input arrays for SUB-WT are: (a) specific gravity of moist sediments; (b) specific gravity of saturated sediments; (c) b_0; (d) S_{ske} or C_r; (e) S_{skv} or C_c; (f) e_0; (g) the offset quantity $\sigma'_{c,0}/\gamma_w - \sigma'_0/\gamma_w$ or $\sigma'_{c,0}/\gamma_w$ ($\sigma'_{c,0}/\gamma_w$ and σ'_0/γ_w are initial preconsolidation stress and effective stress, respectively). Arrays of initial geostatic and effective stress σ_0/γ_w and σ'_0/γ_w, are computed at the start of the simulation using items (a), (b) and information in MODFLOW input files on layer and water-table elevations, and head.

APPLICATION OF THE SUB-WT PACKAGE TO THE ANTELOPE VALLEY GROUNDWATER MODEL

SUB-WT input was set up to match the properties specified in the IBS1 Package as closely as possible, to determine how changes in geostatic stress and stress-dependent storage properties affect computed subsidence in this model. The Antelope Valley model uses three model layers corresponding to an upper unconfined aquifer, and middle and lower confined aquifers, respectively (Leighton & Phillips, 2003). Compressible interbeds are simulated in the upper two layers (layers 1 and 2). Six model zones (Fig. 1) were used to specify input for IBS1. Major input arrays for the IBS1 Package were computed as follows:

(a) Skeletal storage coefficients were computed as the product of estimated thicknesses of compressible interbeds within each model cell in layers 1 and 2, and uniform values of S_{ske} and S_{skv} of 5.58×10^{-6} and 5.25×10^{-4} m^{-1}, respectively, for all model zones.
(b) Starting preconsolidation head was computed by subtracting head-change offsets from starting head. Offsets were 0, 3.05, 15.24, 25.91, 38.10, and 48.77 m for model zones 1–6, respectively.

For SUB-WT, an average porosity of 0.42 from 12 soil sample analyses in Antelope Valley (Peter Martin, USGS, written commun., 2010) was used to compute a uniform void ratio of 0.724. The average porosity and an average simulated specific yield in layer 1 of 0.115 were used to compute an average specific retention of 0.305. The average porosity and specific retention were used with an assumed sediment-grain density of 2.65 g cm^{-3} and water density of 1.0 g cm^{-3} to compute moist and saturated specific gravities of 1.84 and 1.96, respectively. Original values of compressible interbed thicknesses used in IBS1 were used as input to SUB-WT. Preconsolidation stress was specified using offset quantities $\sigma'_{c,0}/\gamma_w - \sigma'_0/\gamma_w$, taken to be the same as offset quantities in zones 1–6 used to compute initial preconsolidation head for IBS1. SUB-WT adds these offsets to starting effective stress to compute starting preconsolidation stress. Because the relation of head change to effective stress change is not one-to-one in SUB-WT, the points at which elastic compaction transitions to inelastic compaction are expected to differ between IBS1 and SUB-WT simulations; however, transition points should be reasonably close because specified moist and saturated specific gravities do not differ greatly.

RESULTS

The total volume of subsidence calculated in the original model using IBS1 for 1995 was about 8.29×10^8 m^3. With the SUB-WT Package set up as described above, the computed subsidence volume was 6.21×10^8 m^3. Furthermore, total subsidence computed with SUB-WT was 29% less

at the location of bench mark BM474 and 13% less at BM479 than values computed using IBS1 in the original model (Fig. 2). Factors for overall lower subsidence using SUB-WT include the following:

(a) IBS1 uses changes in head to compute compaction and storage changes (equations (1)–(2)) whereas SUB-WT uses changes in effective stress (equations (3)–(4)). For the location of BM479, the total increases in effective stress for layers 1 and 2 are about 88% and 91% of the decreases in head in these layers, respectively.

(b) In SUB-WT, skeletal specific storage values, S_{ske} and S_{skv}, are stress-dependent (equations (4b)–(4c)). As head declines and effective stress increases, these values become smaller. Hence, calculated compaction and storage change is smaller for equivalent changes in effective stress.

(c) In SUB-WT the effective stress in equations (4b) and (4c) is calculated at the elevation of the centre of the saturated interval of a model layer. If the layer contains a water table, this reference point moves downward by half of the amount of a water-table decline. Downward movement of the reference point tends to increase effective stress beyond increases that would occur solely from head changes at a fixed reference point.

In the model using SUB-WT, head decline was slightly greater than in the original model, partially offsetting effects of the factors listed above. For example, at the location of BM479, total head decline calculated using SUB-WT was about 11% greater in layer 1 and 8% greater in layer 2 than corresponding head declines calculated using IBS1. Of the three factors listed above, stress-dependent storage properties account for most of the reduced subsidence using SUB-WT. Values of S_{skv} calculated with equation (4c) for locations of BM474 and BM479 decline over the course of the simulation by 56% and 36%, respectively, for layer 1 and by 23% and 15%, respectively, for layer 2 (Fig. 3). Greater reductions occur in layer 1 than in layer 2 because the increase in effective stress is greater in proportion to starting effective stress for layer 1, and because further increases in effective stress in layer 1 are caused by the moving reference point described in factor (c) above.

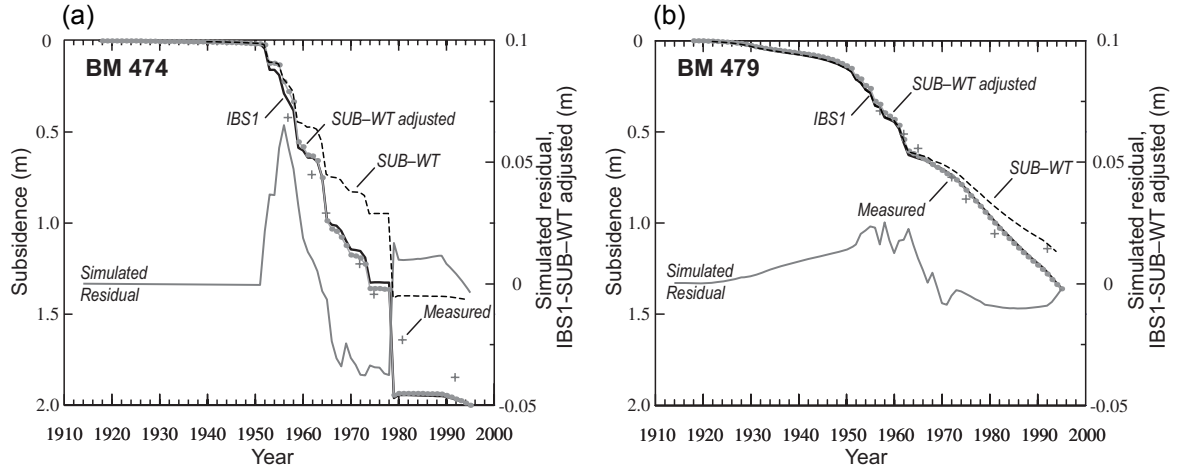

Fig. 2 Measured subsidence and subsidence simulated using IBS1 and SUB-WT for locations of bench marks (a) BM474 and (b) BM479.

As indicated above, total subsidence calculated with SUB-WT for locations of BM474 and BM479, is less than that computed with IBS1. One reason for the smaller disparity at BM479 *versus* BM474 is because BM479 is in model zone 1 in which starting compaction is inelastic, whereas BM474 is in zone 3 in which inelastic compaction begins only after an effective-stress increase of 15.24 m. With the gradual decline in S_{skv} during the simulation (Fig. 3), the average S_{skv}

is lower at BM474, in part because S_{skv} declines a significant amount before the onset of inelastic compaction.

Differences in IBS1 and SUB-WT calculated subsidence between zones would have implications if the Antelope Valley model were recalibrated using SUB-WT. To test what might have to be done for recalibration, the model input was adjusted to specify C_r and C_c instead of S_{ske} and S_{skv}. In the adjusted model, C_r was set to 0.0025 for all zones in both layers, and C_c was set to 0.25 for zone 1 and 0.375 for zones 2–6 in both layers. With these values of C_r and C_c, most values of initial S_{ske} and S_{skv} are higher than those in the unadjusted simulation using SUB-WT. At the location of BM474, for example, starting S_{skv} is 1.68×10^{-3} and 5.57×10^{-4} m^{-1} in layers 1 and 2, respectively. The computed subsidence for BM474 and BM479 in the adjusted model closely matches values computed in the original model (Fig. 2) and total subsidence volume is within about 3% of that calculated in the original model. A formal recalibration of the model would include evaluation of fit of computed to measured head and subsidence over the entire model domain, with possible adjustment of a larger set of parameters.

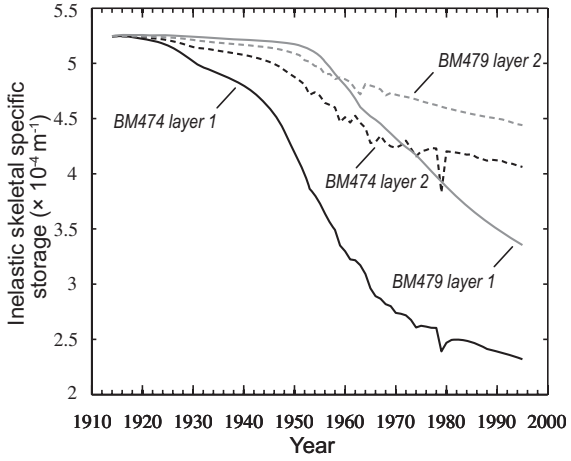

Fig. 3 Variation in inelastic skeletal specific storage through time for locations of bench marks BM474 and BM479.

LESSONS LEARNED

Because effective stress increases with depth, use of the same S_{ske} and S_{skv} for both layers 1 and 2 inherently assumes that deeper sediments are more compressible than shallower sediments. For example, use of an initial value of S_{skv} of 5.25×10^{-4} m^{-1} for both layers yields computed C_c values of 0.114 and 0.332 in layers 1 and 2, respectively, at the location of BM479. In subsidence models such as IBS1 or the newer SUB Package (Hoffmann *et al.*, 2003), which incorporates the functionality of IBS1, specified values of S_{ske} and S_{skv} should decrease with depth, unless existing data suggest that sediment compressibility increases with depth.

On the basis of limited testing done for this analysis, similar results can be obtained using IBS1 or SUB-WT, but parameters are likely to differ because ignoring the effects of changing geostatic stress and stress-dependence of S_{ske} and S_{skv} in IBS1 requires compensation in the form of selecting average skeletal storage coefficients to match observed subsidence. Those average values are likely to be lower than initial values selected in SUB-WT to match the observed subsidence. Although the observed subsidence could be matched using IBS1 or SUB-WT, projections of future subsidence might be overestimated by IBS1 because it would not account for future reductions in skeletal specific storage from increases in effective stress. For models with unconfined aquifers in which water-table variations differ markedly from head variations in underlying confined aquifers and confining units, use of SUB-WT would be advantageous in accounting for changes in

geostatic stress. Further evaluation of advantages and disadvantages of using SUB-WT in the Antelope Valley model could be done with a formal recalibration of the model.

Acknowledgements This work was supported by the USGS Groundwater Resources Program. Dave Leighton of HydroFocus Inc., and Steve Phillips and Diane Rewis of the USGS provided data sets needed to develop SUB-WT input data sets for the model. Thoughtful reviews by Michelle Sneed (USGS) and Dave Leighton greatly improved the manuscript.

REFERENCES

Durbin, T. J. (1978) Calibration of a mathematical model of the Antelope Valley ground-water basin, California. *US Geol. Survey Water-Supply Paper 2046*, http://pubs.er.usgs.gov/usgspubs/wsp/wsp2046. Cited 5 Apr 2010.

Galloway, D. L., Hudnut, K. W., Ingebritsen, S. E., Phillips, S. P., Peltzer, G., Rogez, F. & Rosen, P. A. (1998a) Detection of aquifer system compaction and land subsidence using interferometric synthetic aperture radar, Antelope Valley, Mojave Desert, California. *Water Resour. Res.* **34**(10), 2573–2585.

Galloway, D. L., Phillips, S. P. & Ikehara, M. E. (1998b) Land subsidence and its relation to past and future water supplies in Antelope Valley, California. In: *Land Subsidence Case Studies and Current Research* (ed. by J. W. Borchers) (Proceedings of the Dr Joseph F. Poland Symposium on Land Subsidence, Sacramento, California, USA, October 1995), 529–539. AEG Special Publication 8, Star Publishing, Belmont, California, USA.

Harbaugh, A. W. (2005) MODFLOW-2005, the US Geological Survey modular ground-water model—the Ground-Water Flow Process. *US Geol. Survey Techniques and Methods 6–A16*, http://pubs.usgs.gov/tm/2005/tm6A16/. Cited 5 Apr 2010.

Hoffmann, J., Leake, S. A., Galloway, D. L. & Wilson, A. M. (2003) MODFLOW-2000 Ground-Water Model—User Guide to the Subsidence and Aquifer-System Compaction (SUB) Package: *US Geol. Survey Open-File Report 03-233*, http://pubs.usgs.gov/of/2003/ofr03-233/. Cited 5 Apr 2010.

Ikehara, M. E. & Phillips, S. P. (1994) Determination of land subsidence related to ground-water-level declines using Global Positioning System and leveling surveys in Antelope Valley, Los Angeles and Kern Counties, California, 1992. *US Geol. Survey Water-Resources Investigations Report 94-4184*, http://pubs.er.usgs.gov/usgspubs/wri/wri944184. Cited 5 Apr 2010.

Leake, S. A. & Galloway, D. L. (2007) MODFLOW ground-water model—User guide to the Subsidence and Aquifer-System Compaction Package (SUB-WT) for water-table aquifers. *US Geol. Survey Techniques and Methods 6–A23*, http://pubs.usgs.gov/tm/2007/06A23/. Cited 5 Apr 2010.

Leake, S. A. & Prudic, D. E. (1991) Documentation of a computer program to simulate aquifer-system compaction using the modular finite-difference ground-water flow model. *US Geol. Survey Techniques of Water-Resources Investigations 6–A2*, http://pubs.usgs.gov/twri/twri6a2/. Cited 5 Apr 2010.

Leighton, D. A. & Phillips, S. P. (2003) Simulation of ground-water flow and land subsidence in the Antelope Valley ground-water basin, California. *US Geol. Survey Water-Resources Investigations Report 03–4016*, http://pubs.er.usgs.gov/usgspubs/wri/wri034016. Cited 5 Apr 2010.

Sneed, M. & Galloway, D. L. (2000) Aquifer-system compaction and land subsidence: measurements, analyses, and simulations—the Holly site, Edwards Air Force Base, Antelope Valley, California. *US Geol. Survey Water-Resources Investigations Report 00-4015*, http://pubs.usgs.gov/wri/2000/wri004015/. Cited 5 Apr 2010.

Terzaghi, K. (1925) Settlement and consolidation of clay. *Eng. News-Rec,* 874–878, McGraw-Hill, New York, USA.

Land Subsidence, Associated Hazards and the Role of Natural Resources Development
(Proceedings of EISOLS 2010, Querétaro, Mexico, 17–22 October 2010). IAHS Publ. 339, 2010.

Monitoring and modelling 3-D ground movements induced by seasonal gas storage in deep reservoirs

P. TEATINI[1], G. GAMBOLATI[1], N. CASTELLETTO[1], M. FERRONATO[1], C. JANNA[1], E. CAIRO[2], D. MARZORATI[2], D. COLOMBO[3], A. FERRETTI[3], A. BAGLIANI[4], F. BOTTAZZI[4] & F. ROCCA[5]

1 *Department of Mathematical Methods and Models for Scientific Applications (DMMMSA), University of Padova, via Trieste 63, I-35121 Padova, Italy*
teatini@dmsa.unipd.it
2 *Stogit S.p.A., Via dell'Unione Europea 3, San Donato Milanese (MI), Italy*
3 *Tele-Rilevamento Europa S.r.l. (TRE), Via V. Colonna 7, I-20149 Milano, Italy*
4 *Eni S.p.A. – Divisione E&P, Via Emilia 1, I-20097 San Donato Milanese, Italy*
5 *Dip. di Elettronica ed Informazione, Politecnico di Milano, piazza Leonardo da Vinci 32, I-20133 Milano, Italy*

Abstract Underground gas storage (UGS) in depleted hydrocarbon fields is a strategic practice to cope with the growing energy demand, and occurs in many places in Europe and North America. In response to summer gas injection and winter gas withdrawal the reservoir expands and contracts almost elastically, namely it "breathes", as a major consequence of the fluid pore pressure fluctuations. Depending on a number of factors, including the field burial depth, the difference between the largest and the smallest gas pore pressure, and the geomechanical properties of the injected formation and the overburden, the porous medium overlying the reservoir is subject to a three-dimensional deformation related to the cyclic motion of the land surface in both vertical and horizontal directions. We present a multidisciplinary methodology to evaluate the environmental impact of UGS from a geomechanical point of view in connection with the ground surface displacement that may cause some concern for the integrity of the existing engineered structures and infra-structures. Long-time records of injected/removed gas volume and fluid pore pressure, together with multi-year detection of vertical and horizontal west–east displacement of the land surface above the field by an advanced PSInSAR^{TM} analysis have allowed calibration of a 3-D fluid-dynamic model and development of a 3-D transversally isotropic geomechanical model. The latter has been successfully implemented and used to reproduce the vertical and horizontal cyclical displacements, in the range 8–10 mm and 6–8 mm, respectively, measured between 2003 and 2007 above the "Lombardia" gas reservoir, northern Italy, where since 1986 a UGS program has been under way by Stogit S.p.A. (Eni), following an initial 5-year field production life.

Key words underground gas storage; 3-D geomechanical model; PSInSAR

INTRODUCTION

Underground gas storage (UGS) is becoming a common practice to stock gas to be made available for occasional peak demand by industry and for increased consumption during cold weather for heating houses, or in summer for producing the electricity required for air-conditioning. World-wide, there are currently about 600 functioning UGS installations, with a working gas volume, i.e. the maximum volume that can be withdrawn during the normal activity of the storage facility, of approximately 330×10^9 Sm^3 in the reference year 2004/2005. This amount is more than three times that available in 1970. Most of the gas volume is installed in East Europe (42%), North America (35%), and West Europe (19%) (International Gas Union, 2006). A number of issues concerned with the implementation of a UGS project must be addressed before obtaining the clearance from the Ministry in charge of releasing the necessary authorization. These include the subsurface formation integrity, human health and safety as perceived by public opinion, the economic hazard, and, last but not least, the effect on engineered surface structures and infra-structures caused by the gas disposal/removal. More specifically the geo-mechanical response induced by gas injection and withdrawal may play a very important role. Two aspects are to be primarily investigated: first, underground impact on the sealing cap rock that might be fissured, thus generating a potential way of escape for the stored gas (Rutqvist *et al.*, 2008; Ferronato *et al.*, 2010); and second, the surface impact, i.e. oscillatory vertical and horizontal land motion with the

Copyright © 2010 IAHS Press

potential for generation of differential displacements that could jeopardize the stability and the integrity of man-made structures and infra-structures.

The present communication focuses on the latter issue. Land moves vertically up and down and horizontally away from and toward the field gravity centre when gas is pumped into and out of the storage reservoir, respectively. The magnitude of the occurrence and extent of the area involved depend on a number of factors, including burial depth and geometry (namely thickness and size) of the field, geo-mechanical properties of the injected formation, the overburden and the sideburden, and the pore pressure variation induced by the gas storage/removal. Land response to UGS operations may be currently measured by synthetic aperture radar (SAR)-based techniques with an unprecedented accuracy and high resolution (Hoffmann *et al.*, 2001; Schmidt & Burgmann, 2003; Bell *et al.*, 2008). The horizontal motion is typically smaller than the vertical one, which in turn appears to be quite small as usually the gas storage is in deep depleted gas fields. To our knowledge, Ketelaar *et al.* (2007) is the only report on horizontal displacements due to gas production over the Groningen gas field, The Netherlands.

We present in the following a multidisciplinary effort intended to detect and predict the full displacement related to the UGS project implemented by Stogit S.p.A. (Eni) in the "Lombardia" field, Po River basin, Northern Italy. The reservoir was developed from 1981 to 1986 and later on used for gas storage by Stogit. Methane is injected from April to October and extracted from November to March each year. A 3-D seismic survey, together with almost 30-year long records of removed/stored gas volumes and fluid pore pressure, have allowed for the construction of a detailed static geological model of the gas field and neighbouring formations, and the accurate calibration of a dynamic multiphase flow and pressure model. The pattern, magnitude, and timing of land displacement above the field, both in the vertical and in the east–west direction have been obtained from an advanced Permanent Scatterer InSAR (PSInSAR^{TM}) analysis (Ferretti *et al.*, 2001) using ascending and descending RADARSAT-1 images acquired from 2003 to 2007. This information is implemented within a geomechanical transversally isotropic finite element (FE) model of the porous medium (Gambolati *et al.*, 1986; Janna *et al.*, 2010), which will be shown to successfully match the full 3-D ground surface displacements measured above the reservoir from 2003 to 2007 by PSInSAR^{TM}. The model thus calibrated is then used to assess the land subsidence experienced by the area during 1981–1986, i.e. the 5-year primary field production life, and to predict the land oscillations from 2003 to 2007.

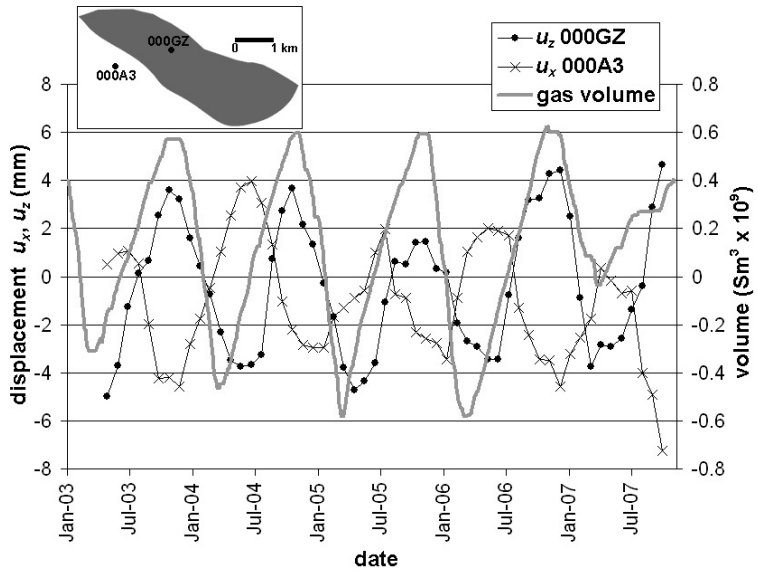

Fig. 1 Seasonal behaviour of the vertical (u_z) and west–east horizontal (u_x) displacements as measured by PSInSAR^{TM} for the 000GZ and 000A3 PS from March 2003 to October 2007. The pore gas volume stored in the field over the same period is also provided. The trace of the "Lombardia" field and the location of the two PS are shown in the inset.

"LOMBARDIA" GAS FIELD

The "Lombardia" reservoir is located in the Po River plain at the northern margin of the pre-Alpine monocline and is made of sandy sediments corresponding to the lateral end of Pliocene turbidites onlapping the partly folded Messianic basin. As the field is located in the zone of steeper dip, the gas traps are of stratigraphic type with the permeable units pinching out northward against the impermeable clays of the Santerno Formation. The reservoir is located at a burial depth of 1050–1350 m below m.s.l. and consists of three gas-bearing pools, denoted as A, B and C, that are vertically separated by 20–30 m thick clay layers. The major pool is C which is composed of three sub-units. Extensive 3-D seismic surveys performed at both the field and the regional scale have allowed us to accurately reconstruct the geometry of the reservoir, the lateral aquifers extending mainly in the southward direction and hydraulically connected to the field, and the other major underlying and overlying geological formations. Primary production started in 1981 from unit C. About 2.7×10^9 Sm^3 (standard m^3) were withdrawn from 1981 to 1986 when the pool started to be used for UGS purposes by Stogit S.p.A. (Eni). An almost negligible production also occurred from pools A and B over the period 1988–1996.

The geomechanical properties of the Po River basin were obtained from a number of *in situ* deformation measurements carried out in the off-shore portion of the area by the radioactive marker technique (Ferronato *et al.*, 2003a). The data have been statistically processed and used to derive a basin-scale relationship that provides the vertical uniaxial compressibility c_M as an exponential function of the vertical effective stress σ_z (Baù *et al.*, 2002):

$$c_M = 1.3696 \times 10^{-2} \sigma_z^{-1.1347} \tag{1}$$

where the units of c_M and σ_z are [bar^{-1}] and [bar], respectively. Equation (1) holds for rock compression in virgin loading conditions (I loading cycle), while rock expansion is controlled by c_M in unloading/reloading conditions (II loading cycle). From *in situ* marker data and oedometer tests, the value of the ratio s between loading and unloading/reloading c_M has been estimated to

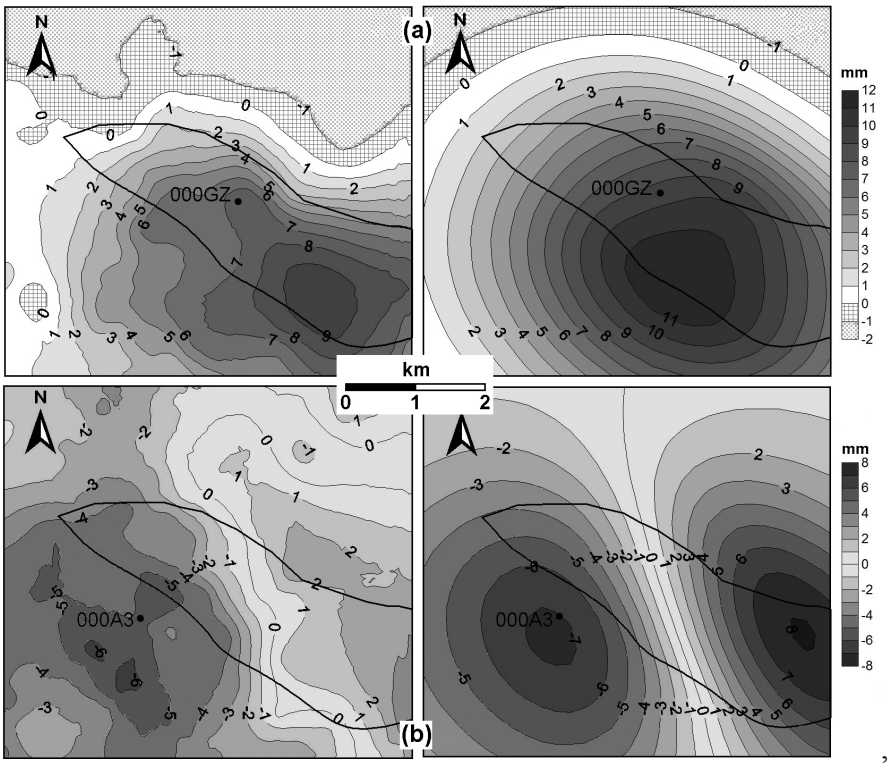

Fig. 2 (a) Spatial land uplift (mm) from April 2006 to November 2006 as provided by the PS measurements interpolated with the aid of the kriging technique (left) and as predicted with the aid of the geomechanical model (right); (b) the same as (a) for the horizontal west–east displacement. The trace of the gas storage field is shown.

range between 1.8 and 3.5 for $100 < \sigma_z < 600$ bar (i.e. for a depth interval of 1000–6000 m in normally pressurized conditions), with s decreasing as σ_z and depth increase (Ferronato *et al.*, 2003b).

PSInSAR OVER "LOMBARDIA" FIELD

Satellite radar images acquired by RADARSAT-1 from March 2003 to October 2008 are used in this study. Two satellite tracks (number 197 and number 147) surveyed the region and acquired 75 and 72 radar images in descending and ascending mode, respectively. The extent of the area of interest above the reservoir is about 30 km^2. The data are processed by PSInSAR^{TM} using a number of stable scatterers identified with the aid of a statistically-based analysis of the phase and amplitude characteristics of the energy backscattered from the earth surface. The PS density was found to be quite high in both data sets due to the presence of many buildings and artificial objects on the ground. Contrary to what is encountered in ESA ERS archives, where the number of radar scenes acquired in ascending mode is typically much smaller than in descending tracks, the two satellite data sets were similar and this allowed an effective estimate of both vertical and horizontal (west–east) components of the surface displacement field.

Figure 1 shows the vertical and horizontal component, u_x and u_z, respectively, of the movement of two PS overlying and close to the field, together with the gas volume V_g stored in the reservoir *versus* time. Figure 2 provides the map of u_z and u_x pattern over the April 2006–November 2006 injection period. Note in Fig. 1 the good correspondence between the behaviour of V_g and both u_x and u_z in connection with the injection and the removal phase. The vertical displacement follows closely the gas volume stored in the reservoir, i.e. land surface goes up when gas is injected and down when it is withdrawn. The horizontal movements depend on the actual measurement position relative to the reservoir gravity centre. A PS located to the west (e.g. 000A3 in Fig. 1) moves westward and eastward, hence u_x decreases and increases when the gas is injected and pumped out, respectively. The opposite behaviour characterizes the PS to the east of the reservoir. Based on the PSInSAR^{TM} measurements, the UGS activities are responsible for a seasonal land movement of up to 8–10 mm and 6–8 mm in the vertical and west–east direction, respectively. As expected, due to the satellite line of sight direction, comparison between Fig. 2(a, left) and 2(b, left) reveals that u_x is noisier than u_z. A simple analysis shows that, assuming the

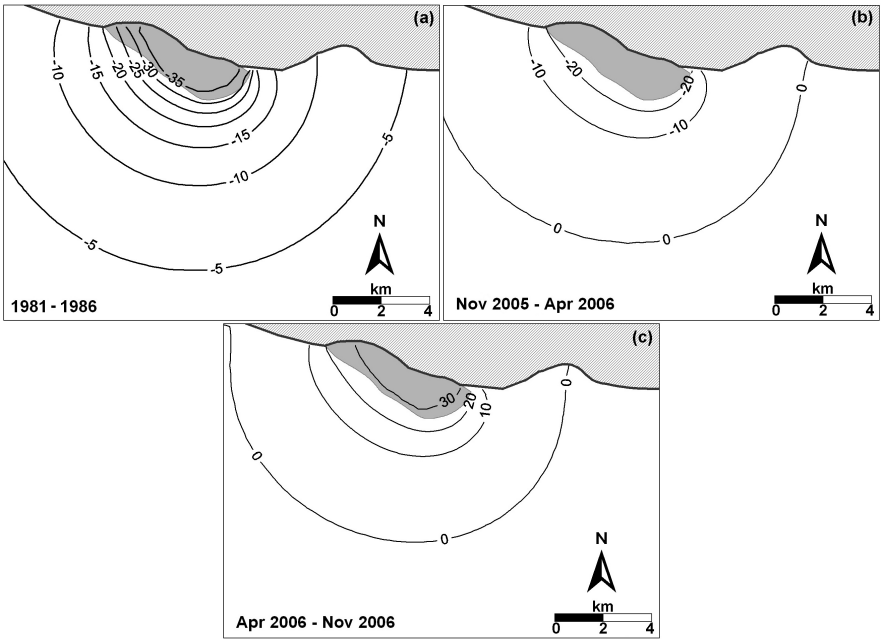

Fig. 3 Predicted depth-averaged fluid pore pressure change [bar] in unit C (a) from the inception (1981) to the end (1986) of the primary field production life and for (b) a producing (from November 2005 to April 2006), and (c) a storage (from April 2006 to November 2006) period of the103% p_i activity.

ascending and descending data to be affected by the same noise power, the estimated u_x components are affected by a noise power about 2.4 times greater than the vertical components. In other words, the modelling reproduction of the horizontal displacements may be not as satisfactory as the vertical ones because of the corresponding noise of the experimental data.

GEOMECHANICAL MODELLING RESULTS

The management of the "Lombardia" field during its primary production life and the subsequent UGS activities, i.e. over the 26-years period from 1981 to 2007, has allowed for a reliable calibration of the fluid-dynamic model with the aid of the code ECLIPSE™ by Schlumberger. From the estimate of the water that flowed into the reservoir during its development provided by ECLIPSE™, the average permeability of the surrounding aquifer (waterdrive) is derived. This is implemented into a FE model of the waterdrive to predict the pore pressure change from the inception (1981) to the end (1986) of the primary field production life (Fig. 3(a)) and during a removal (November 2005–April 2006, Fig. 3(b)) and storage (April 2006–November 2006, Fig. 3(c)) period when the UGS project was under way, with the pore pressure attaining 103%p_i, where p_i is the original *in situ* pressure prior to field development.

The geo-mechanical model is made from tetrahedral FE and uses information on the top and bottom of the "Lombardia" pools and connected waterdrive, along with the depth maps of the other geological units of interest (e.g. the Santerno clay formation). The model extent is 60 × 50 km^2 centred on the reservoir, and is confined by the land surface above and a rigid basement 10 km deep below. Standard conditions with zero displacement on the outer and bottom boundaries are prescribed with the upper boundary as a traction free surface. The elements in the gas-bearing strata have a horizontal dimension comparable with the size of the finite difference

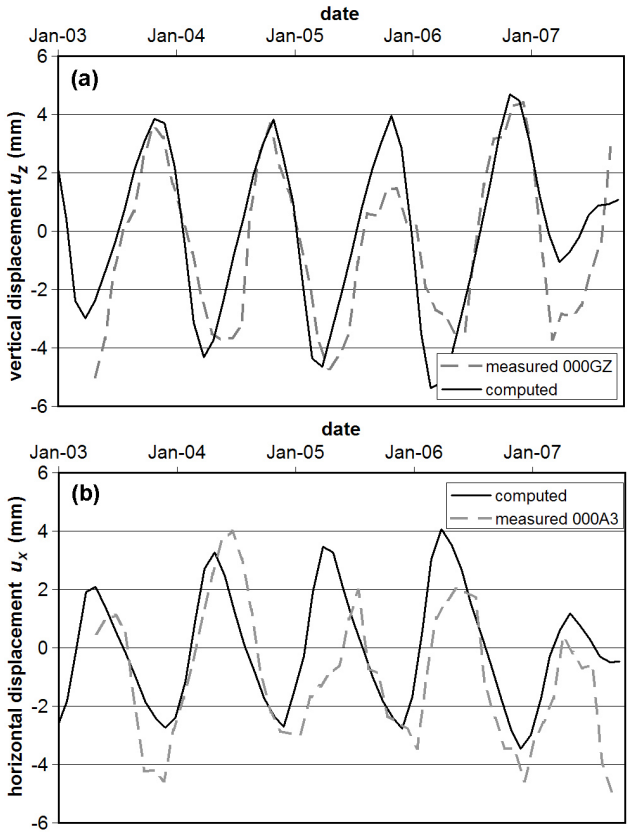

Fig. 4 (a) Seasonal behaviour of the predicted and measured vertical land displacement for the 000GZ PS located as shown in Figs 1 and 2; (b) the same as (a) for the easting movement of the 000A3 PS located as shown in Figs 1 and 2.

grid of ECLIPSE^{TM} (i.e. about 50 m). The generation of highly compatible grids, the same linear order of approximation for the numerical solution of both the flow and the structural equations, and the infinite pore pressure gradient approach (Gambolati *et al.*, 2001) adopted in the geo-mechanical model make very easy the conversion of the pressure change, as predicted by both the FE flow model and ECLIPSE^{TM}, into the external strength source as is required by the structural code that has been calibrated over the UGS cycles from April 2003 to November 2007, i.e. when the PSInSAR^{TM} measurements are available. To accommodate the horizontal displacements the assumption of a transversally isotropic porous medium proved necessary. Modelling such a medium requires five mechanical parameters, namely Young's moduli E_h, E_v and Poisson's ratios ν_h, ν_v in a horizontal and a vertical plane, and the vertical shear modulus G_v. Moreover, the ratio s between virgin and unloading/reloading c_M has to be selected. The satellite observations are on the whole successfully matched with $s = 4$, $E_h/E_v = 3$, $\nu_h = 0.15$, $\nu_v = 0.25$ and $G_v = G_h = E_h/2(1 + \nu_h)$. Figures 2(a) and 4(a) and Figs 2(b) and 4(b) provide the simulated land displacements *vs* the corresponding measurements in the vertical and west–east directions, respectively. Given the small values of the quantity in question and the influence of possible disturbances, the match can be considered very satisfactory.

Finally, the geo-mechanical and the aquifer flow models calibrated as described above have been run to estimate the land subsidence that occurred over the "Lombardia" field during the primary field production life and the land motion thereafter. Figure 5(a) and (b) shows the vertical land settlement and the horizontal land movement as of 1986. According to the modelling outcome the area close to the southern margin of the field has experienced a maximum subsidence equal to 90 mm, while the largest horizontal motion is of the order of 50 mm. Figure 6 provides the vertical land motion from 1981 to 2007. It can be seen that the displacement excursion because of the gas injection and removal is about 10–15 mm in the most recent years when the storage overpressure has exceeded by 3%p_i.

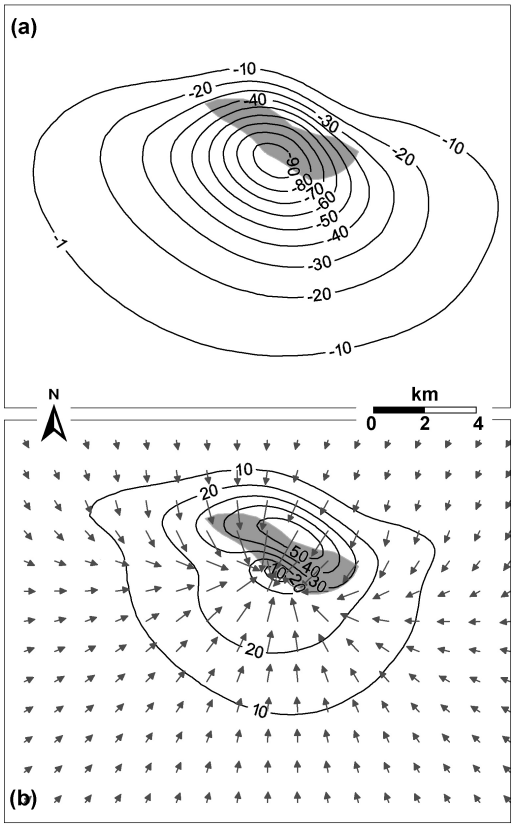

Fig. 5 Predicted: (a) land subsidence (mm) and (b) horizontal land displacement (mm) from 1981 to 1986 at the end of the "Lombardia" primary gas production.

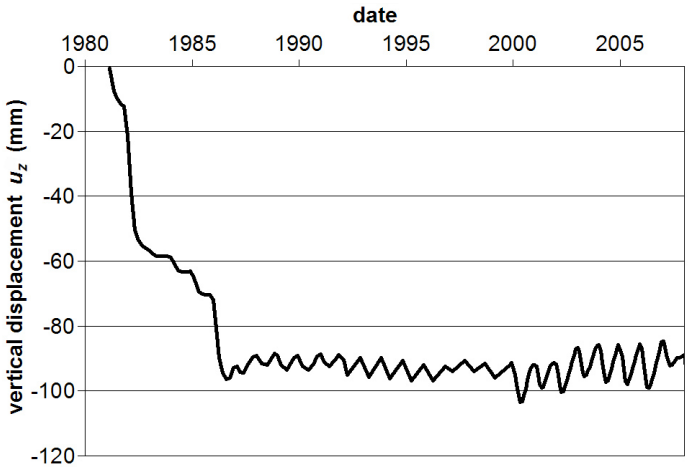

Fig. 6 Maximum vertical land displacement *versus* time as predicted by the geomechanical model from 1981 and 2007.

CONCLUSIONS

The geo-mechanical response to seasonal gas storage into and removal from a 1200-m UGS asset of Stogit S.p.A. (Eni) located in the Po River basin, Italy, has been investigated over the period April 2003–November 2008 when the largest injection overpressure was pushed to 103%p_i. The field was developed from 1981 to 1986 and subsequently used as a tank to store methane. Using high precision PSInSAR^{TM} measurements of both the vertical and horizontal components of the land motion over the reservoir, a transversally isotropic geo-mechanical model has been developed, set up and calibrated against satellite data, starting from the pore pressure predicted with the aid of the fluid-dynamic code ECLIPSE^{TM}. The geomechanical parameters ultimately implemented into the model are fully consistent with the data used in previous modelling studies of the Northern Adriatic basin, which is the natural extension of the Po River basin. The calibrated model matches the satellite observations of both displacement components very well and predicts a maximum land subsidence of 90 mm in 1986, south of the field margin (because of the contribution from the compaction of the active waterdrive) and an oscillatory settlement and uplift of 10–15 mm during the injection/withdrawal cycles, with the largest pore overpressure equal to 103%p_i.

Acknowledgements The DMMMSA – University of Padova is indebted to Schlumberger for making the Eclipse code available.

REFERENCES

Baù, D., Ferronato, M., Gambolati, G. & Teatini, P. (2002) Basin-scale compressibility of the Northern Adriatic by the radioactive marker technique. *Geotechnique* **52**(8), 605–616.

Bell, J. W., Amelung, F., Ferretti, A., Bianchi, M. & Novali, F. (2008) Permanent scatterer InSAR reveals seasonal and long-term aquifer-system response to groundwater pumping and artificial recharge. *Water Resour. Res.* **44**(W02407), doi:10.1029/2007WR006152.

Ferretti, A., Prati, C. & Rocca, F. (2001) Permanent scatterers in SAR interferometry. *IEEE Trans. Geosci. Remote Sensing* **39**(1), 8–20.

Ferronato, M., Gambolati, G. Teatini, P. & Baú, D. (2003a) Interpretation of radioactive marker measurements in the Northern Adriatic gas fields. *SPE Reserv. Eval. Eng*. **6**(6), 401–412.

Ferronato, M., Gambolati, G. Teatini, P. & Baú, D. (2003b) Unloading-reloading uniaxial compressibility of deep reservoirs by marker measurements. In: *Proceedings of 11th International Symposium on Deformation Measurements* (ed. by S. Stiros & S. Pytharouli), 341–346. Geodesy and Geodetic Application Laboratory, Patras University, Greece.

Ferronato, M., Gambolati, G., Janna, C. & Teatini, P. (2010) Geo-mechanical issues of anthropogenic CO_2 sequestration in exploited gas fields. *Energy Convers. Manage*., doi:10.1016/j.enconman.2010.02.024.

Gambolati, G., Gatto, P. & Ricceri, G. (1986) Land subsidence due to gas-oil removal in layered anisotropic soils by finite elements. In: *Land Subsidence* (ed. by A. I. Johnson *et al.*), 29–41. IAHS Publ. 151. IAHS Press, Wallingford, UK.

Gambolati, G., Ferronato, M., Teatini, P., Deidda, R. & Lecca, G. (2001) Finite element analysis of land subsidence above depleted reservoirs with pore pressure gradient and total stress formulations. *Int. J. Numer. Anal. Meth. Geomech.* **25**(4), 307–327.

Hoffmann, J., Zebker, H. A., Galloway, D. & Amelung, F. (2001) Seasonal subsidence and rebound in Las Vegas Valley Nevada, observed by synthetic aperture radar interferometry. *Water Resour. Res.* **3**7(6), 1551–1566.

International Gas Union (2006) *Underground Storage of Gas, Report of Working Committee 2, Triennium 2003-2006*, presented at the 23rd World Gas Conf., 5-9 June 2006.

Janna, C., Castelletto, N., Ferronato, M., Gambolati G. & Teatini, P. (2010) A geomechanical transversally isotropic FE model for the Po River basin, Italy, using PSInSAR-derived horizontal land displacements. *Int. J. Solids Struct.* (submitted).

Ketelaar, G., van Leijen, F., Marinkovic, P. & Hanssen, R. (2007) Multi-track PSInSAR: Datum correction and reliability assessment. In: *Proceedings of ENVISAT Symposium 2007* (ed. by H. Lacoste & L. Ouwehand), ESA SP-636, CD-ROM.

Rutqvist, J., Birkholzer, J. & Tsang, C.-F. (2008) Coupled reservoir geomechanical analysis of the potential for tensile and shear failure associated with CO_2 injection in multilayered reservoir caprock systems. *Int. J. Rock Mech. Min. Sci.* **45**, 132–143.

Schmidt, D. A. & Burgmann, R. (2003) Time-dependent land uplift and subsidence in the Santa Clara valley, California, from a large interferometric synthetic aperture radar data set. *J. Geophys. Res.* **108**(B9), 2416, doi:10.1029/2002JB002267.

Land Subsidence, Associated Hazards and the Role of Natural Resources Development
(Proceedings of EISOLS 2010, Querétaro, Mexico, 17–22 October 2010). IAHS Publ. 339, 2010.

A regional land subsidence model embodying complex deformation characteristics

S. YE[1], Y. XUE[1], J. WU[1], Z. WEI[2] & Q. LI[2]

1 *State Key Laboratory of Pollution Control and Resource Reuse, Department of Hydrosciences, Nanjing University, Nanjing 210093, China*
sjye@nju.edu.cn

2 *Shanghai Institute of Geology Survey, Shanghai 200072, China*

Abstract Large land subsidence regions usually present a history of very complicated deformation characteristics of sedimentary layers, such as the elastic, visco-elastic, and elastic-plastic and visco-elastic-plastic deformation characteristics of sedimentary layers in the Yangtze Delta, China. It is necessary to develop a regional land subsidence model that is able to describe different deformation characteristics. Firstly, the modified Merchant model is proposed to model the visco-elastic-plastic deformation with only three parameters. Then a regional land subsidence model based on the modified Merchant model is developed. Regional land subsidence models for the sedimentary layers with elastic, visco-elastic, and elastic-plastic deformations can be derived from the one based on the modified Merchant model by setting proper values for the three parameters involved. So the four kinds of land subsidence model can be embodied in the one developed from the modified Merchant model. The new regional land subsidence model has another advantage: only four parameters are involved. Land subsidence in Shanghai city is simulated as a case study for the regional land subsidence model proposed in this paper. The results show that the regional land subsidence model is suitable for describing the land subsidence with complex deformation characteristics, and can represent the mechanism of land subsidence caused by excessive groundwater withdrawal relatively well.

Key words regional land subsidence model; modified Merchant model; complex deformation

INTRODUCTION

Land subsidence is becoming a serious environmental problem in China, occurring mainly in 17 provinces (cities) located in the eastern and central regions of China, with a total subsidence area of more than 9×10^4 km^2 (Xue *et al*., 2005). The Yangtse Delta and the Huang-huai-hai Plain are the two largest and most serious land subsidence areas. By the end of the last century, the area where the cumulative subsidence exceeded 200 mm in the Yangtse Delta was approximately 10 000 km^2, which was equivalent to 1/3 of the whole region. Land subsidence has occurred over almost all of the 50 000 km^2 of the Huang-huai-hai Plain.

In the large land subsidence areas like the Yangtse Delta, each sedimentary layer showed different deformation characteristics such as elastic deformation, elastic-plastic deformation, visco-elastic deformation or visco-elastic-plastic deformation (Ye *et al*., 2005; Shi *et al*., 2008). It is necessary to describe all these different deformations with one uniform regional land subsidence model. It is important for numerical simulation of regional land subsidence, because it is almost impossible to simulate the regional land subsidence by totally different and unrelated mathematical models.

A modified Merchant model, which has few parameters, is proposed to describe visco-elastic-plastic deformation. The elastic, elastic-plastic and visco-elastic stress–strain relationships can be easily derived from the visco-elastic-plastic stress–strain relationship based on the modified Merchant model. In this paper, a three-dimensional flow model and a one-dimensional subsidence model are developed based on visco-elastic-plastic deformation described by the modified Merchant model. Flow models and subsidence models describing visco-elastic, elastic, and elastic-plastic deformation can be derived from the models describing visco-elastic-plastic deformation by properly setting the parameters. So the regional land subsidence model based on visco-elastic-plastic deformation described by the modified Merchant model can embody complex deformation characteristics.

Copyright © 2010 IAHS Press

REGIONAL LAND SUBSIDENCE MODEL

To develop a visco-elastic-plastic constitutive relationship applicable in regional land subsidence modelling, a modified Merchant model is proposed based on comprehensive consideration of the models describing elastic-plastic deformation and visco-elastic deformation.

The modified Merchant model

The Merchant model is composed of a Hooke spring 'a' and a Kelvin element in series. A Kelvin element is composed of a Hooke spring 'b' and a dashpot which are parallel. The difference between the modified Merchant model and the original model is that the linear springs 'a' and 'b' describing elastic deformation in the original model are replaced by the nonlinear springs 'a' and 'b' describing elastic and plastic deformations in the modified Merchant model. The deformations of springs 'a' and 'b' are elastic if the current effective stress is less than the preconsolidation stress. Otherwise the deformations of the two springs are plastic. Therefore, the modified Merchant model can describe instantaneous elastic, plastic deformation, visco-elastic and visco-plastic deformation with only a few parameters in the modified Merchant model. The Merchant model is expressed here as (Huang, 1983):

$$\frac{\partial e}{\partial t} = (1+e_0)\gamma\alpha_1 \frac{\partial H}{\partial t} - \mu[(1+e_0)\gamma(\alpha_1+\alpha_2)(H_0-H)+(e-e_0)] \tag{1}$$

where e is void ratio, e_0 is initial void ratio, γ is specific weight of water, H is hydraulic head, α_1 is the coefficient of compressibility of spring 'a', α_2 is the coefficient of compressibility of spring 'b', $\mu = (3\eta\alpha_2)^{-1}$, η is the viscosity coefficient of the dashpot, and H_0 is initial head in each time step. The expression of the modified Merchant model is the same as expression (1), but α_1 and α_2 depend on H. Their values are determined by:

$$\alpha_1 = \alpha_{ke1} \qquad (H > H_p)$$

$$\alpha_1 = \alpha_{kv1} \qquad (H \le H_p) \tag{2}$$

where α_{ke1} and α_{kv1} are coefficients of elastic compressibility and plastic compressibility of spring 'a', respectively. H_p is the lowest previous hydraulic head in history.

$$\alpha_2 = \alpha_{ke2} \qquad (H > H_p)$$

$$\alpha_2 = \alpha_{kv2} \qquad (H \le H_p) \tag{3}$$

where α_{ke2} and α_{kv2} are elastic compressibility and plastic compressibility of spring 'b', respectively.

Groundwater flow models and subsidence models based on different stress–strain constitutive relationships

The flow equation based on the modified Merchant model can be expressed as:

$$\frac{\partial}{\partial x_i}(K_{ij}\frac{\partial H}{\partial x_j}) = \gamma n\beta\frac{\partial H}{\partial t} + \gamma\alpha_1\frac{\partial H}{\partial t} - \mu[\gamma(\alpha_1+\alpha_2)(H_0-H)+\frac{e-e_0}{1+e_0}],\ (i,j = 1, 2, 3) \tag{4}$$

Assuming α_1 and α_2 are constants, equation (4) is the flow equation based on the visco-elastic constitutive relationship.

Assuming $\mu = 0$, equation (4) becomes:

$$\frac{\partial}{\partial x_i}(K_{ij}\frac{\partial H}{\partial x_j}) = \gamma n\beta\frac{\partial H}{\partial t} + \gamma\alpha\ \frac{\partial H}{\partial t}\ , \qquad (\mathrm{i, j} = 1, 2, 3) \tag{5}$$

where α is volume compressibility of soil. If α is constant, equation (5) is the same as the

traditional flow equation based on the elastic constitutive relationship (Xue *et al*., 1997). The flow equation based on the elastic-plastic deformation described by nonlinear elastic relationship is the same as equation (5), with α depending on the hydraulic head as follows:

$$\alpha = \alpha_{ke} \qquad (H > H_p)$$
$$\alpha = \alpha_{kv} \qquad (H \le H_p) \tag{6}$$

where α_{ke} is elastic volume compressibility, and α_{kv} is plastic volume compressibility.

Vertical one-dimensional deformation is assumed in this paper. The subsidence model based on the modified Merchant model can be expressed as:

$$\Delta L = \int_o^L \frac{\gamma\alpha_1\Delta H + \mu\gamma\Delta t(\alpha_1 + \alpha_2)\Delta H}{1 + \mu\Delta t} dz \tag{7}$$

where ΔL is deformation, and L is the thickness of the sedimentary layer.

Assume α_1 and α_2 are constants, then equation (7) is the subsidence model based on the visco-elastic constitutive relationship. Hence, equation (7) becomes:

$$\Delta L = \int_o^L \gamma\alpha\Delta H dz \tag{8}$$

where α is volume compressibility of soil. If α is constant, equation (8) is the same as the subsidence model based on the elastic constitutive relationship. The subsidence model based on the elastic-plastic deformation described by the nonlinear elastic relationship is the same as equation (8), with α depending on the hydraulic head as expression (6).

So the regional land subsidence model describing visco-elastic-plastic deformation based on the modified Merchant model can serve as the uniform model to describe elastic, elastic-plastic, visco-elastic, and visco-elastic-plastic deformation with proper setting of the values of parameters.

CASE STUDY – SIMULATION OF THE LAND SUBSIDENCE IN SHANGHAI

Deformation characteristics of sedimentary layers in Shanghai

Land subsidence in Shanghai city was detected in 1921 (Zhang & Wei, 2002), which was the earliest record of land subsidence in Shanghai, and also in the Yangtse Delta. The land subsidence in Shanghai is induced by excessive groundwater withdrawal (Zhang & Wei, 2002).

The aquifers system is composed of unconsolidated Quaternary sediments. The sediments are about 200–350 m thick (Fig. 1). The bedrock is located below the sediments. The unconsolidated sediments are composed of layers of clay, sandy clay and sand. The sediments are divided into the

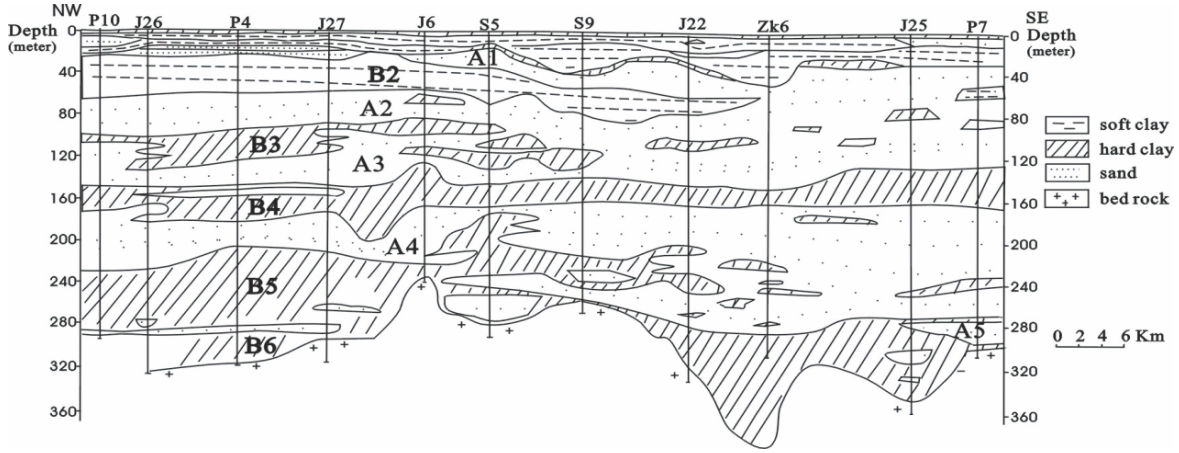

Fig. 1 Schematic stratigraphic section in Shanghai.

phreatic aquifer (A0), the first aquitard (B1), the first confined aquifer (A1), the second aquitard (B2), the second confined aquifer (A2), the third aquitard (B3), the third confined aquifer (A3), the fourth aquitard (B4), the fourth confined aquifer (A4), the fifth aquitard (B5), the fifth confined aquifer (A5), and the sixth aquitard (B6) (Fig. 1).

Excessive groundwater withdrawal has caused water level declines in the aquifers, especially in the second and fourth aquifers, which has resulted in effective stress increase and compaction to different extents in the different sedimentary layers. The phreatic aquifer, the first, second, third and fifth confined aquifers, and the third, fifth and sixth aquitards demonstrate mainly elastic deformation. The first and second aquitards show mainly plastic deformation, with a little elastic deformation and some creep. The fourth aquitard and the fourth confined aquifer have similar deformation features. They were the main compressible layers in the period from 1986 to 1998, especially after 1991. We take the fourth confined aquifer as an example to show this. The fourth confined aquifer is mainly composed of fine sand and medium-coarse sand. The extensometer F3-1 monitors the deformation of the fourth confined aquifer, which lies in the middle of the regional drawdown cone of the fourth confined aquifer. Figure 2 shows the stress–cumulative displacement curve at the site and illustrates that the deformation was mainly elastic with a little plastic deformation before 1991, and that the deformation was mainly plastic after 1991. The water level in the fourth confined aquifer at F3-1 dropped significantly after 1991, to lower than any previous head in history, causing plastic deformation. The sediment there experienced little or no rebound after 1991, as a result of the time lag in deformation and creep deformation. The deformation of the fourth confined aquifer at F3-1, which lies in the middle of the regional drawdown cone, shows elasticity, plasticity and creep, especially after 1991. However, the complicated deformation characteristics do not occur in the whole of the fourth confined aquifer. The deformation is mainly elastic in some places where the groundwater levels change a little.

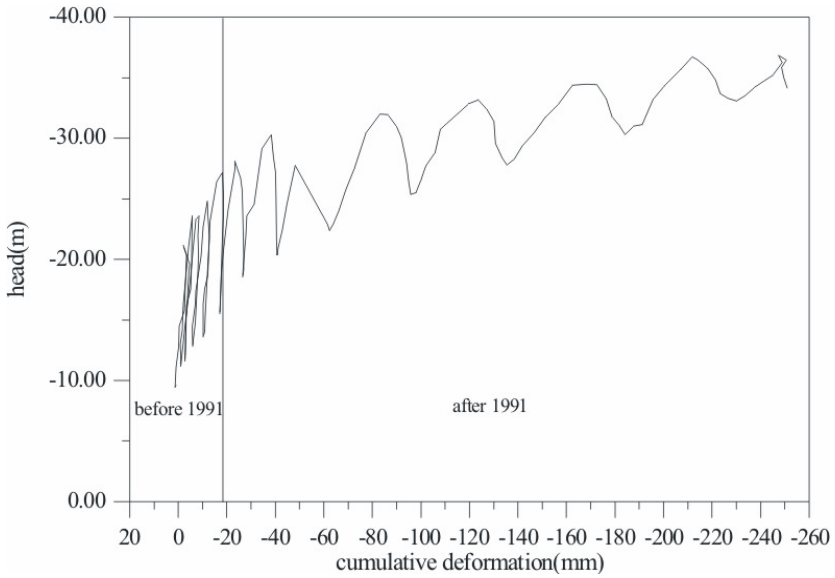

Fig. 2 Stress-strain curve of A4 at F3-1.

Based on the features of land subsidence in Shanghai, a regional land subsidence model embodying elastic, elastic-plastic and visco-elastic-plastic deformation is required. The regional land subsidence model developed above can serve the purpose.

Simulation of the land subsidence in Shanghai

The regional land subsidence model developed above is applied to simulate the land subsidence in Shanghai as a case study. The groundwater flow field is three-dimensional in Shanghai because of

the difference between the hydraulic heads in the aquifers and the hydraulic connection between adjacent aquifers. Vertical one-dimensional deformation is assumed in this study.

The aquifer system is discretized into hexahedral elements. The aquifers system is totally divided into 39 992 elements, with a total of 47 900 nodes.

The simulation period is from March 1986 to December 1998. The top boundary of the flow model is the phreatic aquifer, and the bottom boundary is bedrock, which is assumed to be an impermeable boundary. All the other boundaries of the flow model are considered as first-type boundaries. The first-type boundary condition of each layer is obtained by kriging interpolation of the observation well data close to the boundaries. The top of the vertical one-dimensional subsidence model is the land surface which is a free surface, and the bottom of the subsidence model is bedrock, which is a confined surface without displacement.

The comparison of the calculated deformation and the observed data of different sedimentary layers at extensometer F4 is shown in Fig. 3. It shows that the calculated results agree well with the observed data.

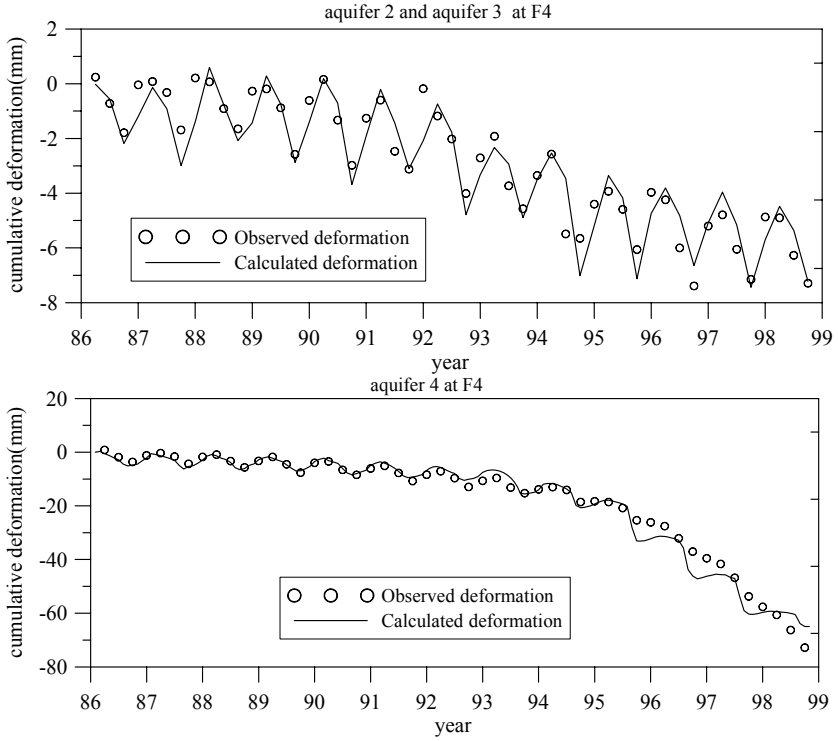

Fig. 3 Observed and calculated cumulative deformation of sedimentary layers at F4.

CONCLUSIONS

Large land subsidence regions, particularly in China, usually have very complicated deformation characteristics of sedimentary layers. In these large land subsidence areas, each sedimentary layer may have different deformation characteristics, such as elastic deformation, elastic-plastic deformation, visco-elastic deformation and visco-elastic-plastic deformation. Regional land subsidence model for the areas with complex deformation characteristics must incorporate these features to accurately model the subsidence process. This study indicates that the land subsidence model based on visco-elastic-plastic deformation described by the modified Merchant model is applicable to sedimentary layers with visco-elastic-plastic deformation, and can serve as the uniform (standard) model for the sedimentary layers with elastic, elastic-plastic and visco-elastic deformation.

Acknowledgements The paper is financially supported by NSFC no. 40335045, no. 40402023 and no. 40725010.

REFERENCES

Huang, W. (1983) *Engineering Properties of Soils*. China WaterPower Press, Beijing, China.

Shi, X., Xue, Y., Wu, J. & Ye,. S. (2008) Characteristics of regional land subsidence in Yangtze Delta, China – an example of Su-Xi-Chang area and the City of Shanghai. *Hydrogeology J.* **16**(3), 593–607.

Wei, Z. (2002) The stress–strain analysis of the 4th confined aquifer in Shanghai City (in Chinese). *Hydrogeology and Engineering Geology* **1**, 1–4.

Xue, Y., Zhu, X. & Wu, J. (1997) *Ground Water Hydrodynamics*. Geology Press, Beijing, China.

Xue, Y. Q., Zhang, Y., Ye, S. J., Wu, J. C.& Li, Q. F. (2005) Land subsidence in China. *Environmental Geology* **48**(6), 713–720.

Ye, S, Xue, Y., Zhang, Y. & Li, Q.(2005) Study on the deformation characteristics of soil layers in regional land subsidence model of Shanghai. *Chinese J. Geotechnical Engng* **27**(2), 140–147.

Zhang, A. & Wei, Z. (2002) Past, present and future research on land subsidence in Shanghai City (in Chinese). *Hydrogeology and Engineering Geology* **5**, 72–75.

Land Subsidence, Associated Hazards and the Role of Natural Resources Development
(Proceedings of EISOLS 2010, Querétaro, Mexico, 17–22 October 2010). IAHS Publ. 339, 2010.

Modelling land subsidence processes induced by fast rainwater infiltration through fractures into the unsaturated zone

I. MARTINEZ[1], R. HINKELMANN[1] & S. SAVIDIS[2]

1 *Chair of Water Resources Management and Modeling of Hydrosystems, Technische Universität Berlin, Sekr. TIB I-B14, Gustav-Meyer-Allee 25, D-13355 Berlin, Germany*
isaac.martinez@wahyd.tu-berlin.de

2 *Chair of Soil Mechanics and Geotechnical Engineering, Technische Universität Berlin, Sekr. TIB 1-B7, Gustav-Meyer-Allee 25, D-13355 Berlin, Germany*

Abstract The aim of this work is to better understand rainfall-induced fast infiltration of water through fractures into the subsurface, as well as to estimate its influence on mechanical deformation, i.e. land subsidence. Flow in the partially saturated soil (matrix, fracture) is described with the model concept of two-phase flow in porous media and the stress–strain analysis is carried out with the hardening soil model (elasto-plastic model) using a double stiffness concept for elasticity in combination with isotropic strain hardening. Flow and deformations are weakly coupled. In this research several numerical studies are presented. An analysis of the influence of fracture and surface inclination on flow and deformation is carried out. The results of the numerical study show that infiltration into a system with a horizontal surface and without fracture only leads to vertical deformations. Infiltration into a system with a vertical fracture has nearly no influence on the deformation because the water mainly propagates in the vertical direction due to gravity. Infiltration into a system with a horizontal surface and an inclined fracture results in considerable horizontal and vertical deformations. Such deformations are further increased when the surface is inclined.

Key words subsidence; fracture; rainwater infiltration; numerical modelling; unsaturated zone

INTRODUCTION

As a result of excessive groundwater withdrawal, which is much greater than recharge, the buoyancy of the soil is reduced and a strong increase of the grain-to-grain stress is produced. As a consequence, an effective overburden load on the aquifer systems, in which the head depletion has occurred, is generated. This increase of the stresses produces a compacting of the deposits. Because of the soil's heterogeneities, differential subsidence at the ground surface occurs and in many cases it is accompanied by fracture formations in the soil layers on the top. According to Rojas *et al.* (2002) ground cracks may develop when the following conditions are met:

- The bedrock has an irregular topography.
- Major water table declines are taking place.
- Soils have medium to high compressibility and low plasticity.

Besides fractures, soil often exhibits a variety of heterogeneities, such as fissures, cracks and macropores or inter-aggregate pores (Gerke & van Genuchten, 1993). These heterogeneities can significantly affect water and solute movements in soils by creating non-uniform velocity fields with spatially variable flows (Novák *et al.*, 2000). Fractures serve as highly conductive waterways. During strong rainfalls, fast water infiltration is produced through these channels, inducing hydraulic pressure and a rapid increase of the soil's weight because of the change of soil saturation conditions. This increase of weight becomes an important factor in the propagation of subsidence.

Infiltration processes in fractured soils have previously been investigated (Pham Van, 2009). Coupled processes of flow and deformation in soils are complex (Ehlers *et al.*, 2004). The processes are even more complex in fractured soil, and so make prediction of the failure processes challenging. In an effort to understand the relevant parameters and processes in land subsidence induced by fast rainwater infiltration, a comparison of flow in a vertical and an inclined fracture zone is presented. A model concept for two-phase flow in porous media has been chosen, although

Copyright © 2010 IAHS Press

a Richards model concept might have been sufficient. The results of the infiltration, i.e. saturation, are used for the stress–strain analysis. As soil behaviour is highly nonlinear and irreversible, an elasto-plastic deformation model has been applied.

A series of works about land subsidence induced by fluid extraction (water, gas, oil) from reservoirs (e.g. Bai *et al.*, 1994; Zehng *et al.*, 2008) have been made. However, this paper focuses on land subsidence simulation induced by a fast infiltration through the discontinuities. The purpose of this study is to analyse rapid fluid flow through fractured unsaturated soil and its mechanical involvement in the propagation of land subsidence.

MODEL CONCEPT

Two-phase flow in porous media

If two fluid phases are not, or are only slightly, miscible into each other, a two-phase flow model concept for a porous medium should be applied (Hinkelmann, 2005). The continuity equation must be fulfilled for each phase α, one for the liquid phase w (water) and one for the gas phase a (air):

$$\frac{\partial(S_\alpha \phi_\alpha \rho_\alpha)}{\partial t} + div\left(\rho_\alpha \underline{v}_\alpha\right) - \rho_\alpha q_\alpha = 0 \tag{1}$$

Here, ϕ_α denotes the void space filled with phase α, S_α is the saturation, ρ_α the density, $\underline{v}_\alpha$ the filter or Darcy velocity, and q_α the sink or source of the phase.

To describe the Darcy velocity of each phase, the generalized form of the Darcy law is used:

$$\underline{v}_\alpha = -\frac{k_{r\alpha}}{\mu_\alpha}\mathbf{K} \cdot (grad\ p_\alpha - \rho_\alpha \underline{g}) \tag{2}$$

where $k_{r\alpha}$ is the relative permeability, $\mathbf{K}$ the tensor of intrinsic permeability, μ_α the dynamic viscosity, $\underline{g}$ the gravity, and $k_{r\alpha} / \mu_\alpha = \lambda_\alpha$ is referred to as the mobility of phase α.

The relative permeability for liquid phase w and gas a phase are computed with the Brooks-Corey (1964) relationship:

$$k_{rw} = S_e^{\frac{2+3\lambda}{\lambda}} \tag{3}$$

$$k_{ra} = (1 - S_e)^2 (1 - S_e^{\frac{2+\lambda}{\lambda}}) \tag{4}$$

The parameter λ characterizes the grain-size distribution. A small value describes a single grain-size material, while a larger value indicates non-uniform material. S_{wr} and S_{ar} stand for residual saturation of water and gas phase, S_e stands for the effective (water) saturation defined as:

$$S_e = \frac{(S_w - S_{wr})}{(1 - S_{ar} - S_{wr})} \tag{5}$$

The pore volume is completely filled with the wetting and the non-wetting phase saturation, S_w , S_a :

$$S_w + S_a = 1 \tag{6}$$

At the interface between both, the difference between the phase pressure of the gas and liquid phases is called capillary pressure:

$$p_c = p_a - p_w \tag{7}$$

For the simulation of water infiltration, the tool MUFTE-UG (MUltiphase Flow, Transport and Energy for Unstructured Grids) was chosen. The Fully Upwind Box Method which, is a combination of a Finite-Volume and a Finite-Element Method, is applied as discretization method. This is a mass-conservative formulation on a discrete patch including a first-order upwinding

scheme. For time integration it employs the Finite-Difference Method and the temporal discretization carried is out fully implicit. As a nonlinear solver, the Newton-Raphson Method and as an inner solver the BiCGSTAB (Biconjugate Gradient Stabilized) Method using multigrid preconditioning is chosen (Hinkelmann, 2005).

Hardening soil model

The hardening soil model uses a double-stiffness model for elasticity in combination with isotropic strain hardening as developed by Schanz *et al.* (1999). The total strains are calculated using a stress-dependent stiffness, different for each, virgin loading and un-/reloading. The plastic strains are calculated by introducing a multi-surface yield criterion. For the frictional hardening a non-associated and for the cap hardening an associated flow rule is assumed. This model is included in PLAXIS (Waterman *et al.*, 2004).

Hyperbolic stress-strain relation

Restriction is made to triaxial loading conditions with $\sigma_2^{'} = \sigma_3^{'}$ = constant and $\sigma_1^{'}$ being the major compressive stress. Drained triaxial tests tend to yield curves described by:

$$\varepsilon_1 = \frac{q_a}{2E_{50}} \frac{(\sigma^{'}_1 - \sigma^{'}_3)}{q_a - (\sigma^{'}_1 - \sigma^{'}_3)} \quad \text{for } q < q_f \tag{8}$$

The quantities of the ultimate deviatoric and asymptotic stress q_f and q_a are defined as:

$$q_f = \frac{6\sin\varphi_P}{3-\sin\varphi_P}(p + c\cot\varphi_P)\,; q_a = \frac{q_f}{R_f} \tag{9}$$

where c describes cohesion and φ_P failure friction angle. R_f describes the relationship between q_f and q_a. Two confining stress-dependent stiffness moduli are used, one for primary loading E_{50} and for un-/reloading stress paths E_{ur}.

Deviatoric yield surface

The corresponding plastic strains stem from a yield function of the form $f^s = \overline{f} - \gamma^P$ where $\overline{f}$ is the function of stress, and γ^P is a function of plastic strains which are defined as:

$$\overline{f} = \frac{1}{E_{50}} \frac{q}{1 - q/q_a} - \frac{2q}{E_{ur}} \tag{10}$$

$$\gamma^P = \varepsilon_1^P - \varepsilon_2^P - \varepsilon_2^P = -(2\varepsilon_1^P - \varepsilon_v^P) \approx -2\varepsilon_1^P \tag{11}$$

The axial strain is the sum of elastic and plastic component given as:

$$-\varepsilon_1 = -\varepsilon_1^e - \varepsilon_1^P \approx \frac{1}{2E_{50}} \frac{q}{1 - q/q_a} \tag{12}$$

The flow rule that involves a relationship between rates of plastic shear strain $\dot{\gamma}^P$ and plastic volumetric strain $\dot{\varepsilon}_v^P$ has the form:

$$\dot{\varepsilon}_v^P = \sin\psi_m \, \dot{\gamma}^P \tag{13}$$

The mobilized dilatancy angle ψ_m is obtained by the expression:

$$\sin\psi_m = \frac{\sin\varphi_m - \sin\varphi_{cv}}{1 - \sin\varphi_m \sin\varphi_{cv}} \tag{14}$$

where φ_{cv} is the critical state friction angle and φ_m is the mobilized friction angle.

At failure, when the mobilized friction angle equals to φ_p, it is found that:

$$\sin\psi_m = \frac{\sin\varphi_p - \sin\psi_p}{1 - \sin\varphi_p \sin\psi_p} \tag{15}$$

To explain the plastic volume strain a second type of yield surface must therefore be introduced to close the elastic region in the p-axis direction, which is called the cap yield surface f^c defined as:

$$f^c = \frac{\tilde{q}^2}{\alpha^2} + p^2 - p_p^2 \tag{16}$$

The magnitude of the cap yield surface will be defined through the parameter α and the isotropic pre-consolidation stress $P_P = -(\sigma_1 + \sigma_2 + \sigma_3)/3$ and $\tilde{q} = \sigma_1 + (\delta - 1)\sigma_2 - \delta\sigma_3$ with $\delta = (3 + \sin\varphi)/(3 - \sin\varphi)$. $\tilde{q}$ is a special stress measure for deviatoric stresses. In the special case of triaxial compression ($-\sigma_1 > -\sigma_2 = \sigma_3$) it yields $\tilde{q} = -(\sigma_1 - \sigma_3)$, and for triaxial extension ($-\sigma_1 = -\sigma_2 > \sigma_3$), $\tilde{q} = -\delta(\sigma_1 - \sigma_3)$. The hardening law relating p_p to volumetric cap ε_v^{Pc} states:

$$\varepsilon_v^{pc} = \frac{\beta}{1 - m}\left(\frac{p_p}{p^{ref}}\right)^{1-m} \tag{17}$$

α and β are cap parameters. A detailed description of the method can be found in Schanz *et al.* (1999).

IDEALIZED SYSTEM AND PARAMETERS

Fault zones show a wide variety of geometrical, physical and fracture patterns. In this paper a fractured zone was represented as a porous medium damage band with higher permeability compared to soil matrix. Therefore, a highly resolution in the fault zone was made (Fig. 1). Two-dimensional (2-D) numerical simulations of an idealized homogeneous matrix with a high permeable fracture zone were investigated, one in a rectangular system with a 40-cm fracture zone, and one with an inclined surface (Figs 2 and 3).

The flow parameter used in the numerical simulation for the matrix and the fault zone are described in Table 1. The boundary condition (BC) at the top of the system is a Dirichlet BC with a fixed water pressure $p_w = p_{atm} + \rho g h$ with h = 5 cm simulating an accumulation of a 5-cm water column caused by a runoff after a strong rainfall (Figs 2 and 3). At the bottom, left and right of the domain a fixed Neumann no flow BC was chosen. The residual saturation of material was used as initial saturation.

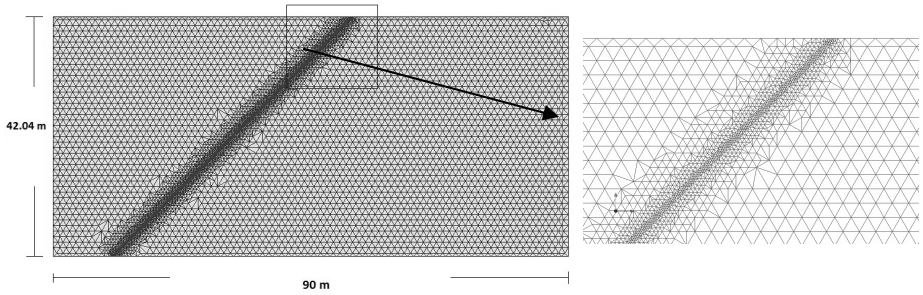

Fig. 1 Mesh with a higher resolution in the fault.

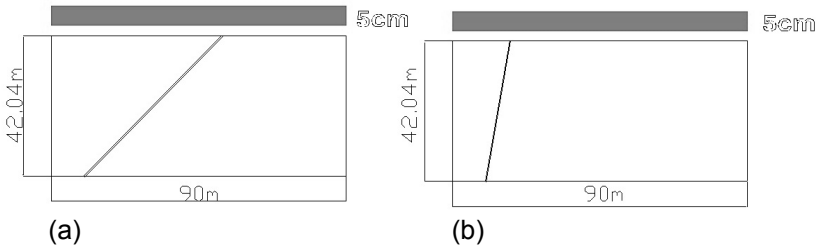

Fig. 2 Idealized system: (a) 45° inclined fault; (b) 80° inclined fault.

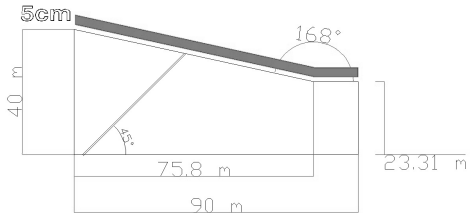

Fig. 3 Idealized system with an inclined surface and an inclined fault of 45°.

Table 1 Soil properties for two-phase flow modelling.

	Matrix soil	Fault zone
S_{wr} [-]	0.15	0.05
S_{ar} [-]	0.01	0.01
K [m^2]	5.0E-11	5.0E-9
λ [-]	2.3	2.0
p_d [Pa]	700	200
ϕ [-]	0.37	0.32

For the mechanical simulations the soil properties are defined in Table 2. Displacements are possible along the surface boundary. The other boundaries are non-deformable.

Table 2 Soil properties for mechanical modelling. The parameters are typical for a clay-sand material.

	Matrix soil	Fault zone
Material Model	Hardening soil	Elastic
Unsat. soil weight [kN/m^3]	16	16
Sat. soil weight [kN/m^3]	20	20
E_{50}^{ref} kN/m^2]	10000	–
E_{eod}^{ref} [kN/m^2]	10000	–
E_{ur}^{ref} [kN/m^2]	30000	–
E [kN/m^2]	–	1000
m [-]	0.5	–
P_{ref} [kN/m^2]	100	–
Poisson's ratio [-]	0.2	0.3
K_o^{nc} [-]	0.44	–
Cohesion [kN/m^2]	1	–
Friction angle φ	25	–

RESULTS

When the fault zone tends to be vertical the water infiltrates directly into the partially saturated soil (Fig. 4), but when the fracture has a considerable inclination the water infiltrates fast through the fracture and also propagates into the matrix because of the gravity, as shown by Fig. 5(a) and (b). The fast infiltration leads to a rapid increase of the soil's weight because of the increased water content in the soil.

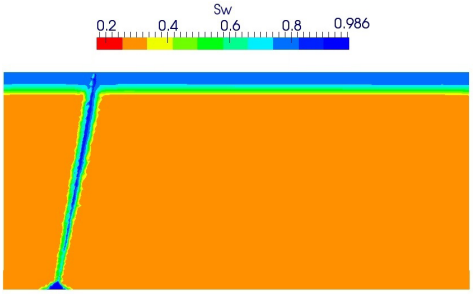

Fig. 4 Saturation after 90 min water infiltration through an 80° inclined fault.

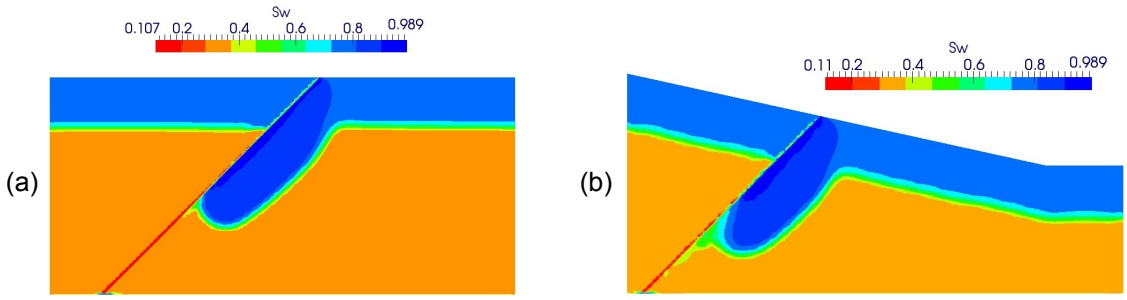

Fig. 5 (a) Saturation after 180 min water infiltration through a 45° inclined fracture zone. (b) Saturation after 180 min water infiltration through a 45° inclined fracture zone with a slope on the surface.

The surface inclination has a minor influence on the load increase.

The results of infiltration after 180 min were used for the mechanical modelling and, in addition, the weight of the 5 cm water column on the top was also considered. A deformable material was supposed for the system and the fault zone was defined in this model as a highly elastic material in order to allow deformations and conserve a continuum.

The mechanical modelling of an 80° fault system (Fig. 4) was not carried out as the water infiltrates directly into the saturated zone. When the infiltration was only in the matrix and not in the fracture, a maximum horizontal displacement of 0.011cm ≈0 (Fig. 6(a)) and a vertical displacement of 5.2 cm (Fig. 6(b)) were obtained.

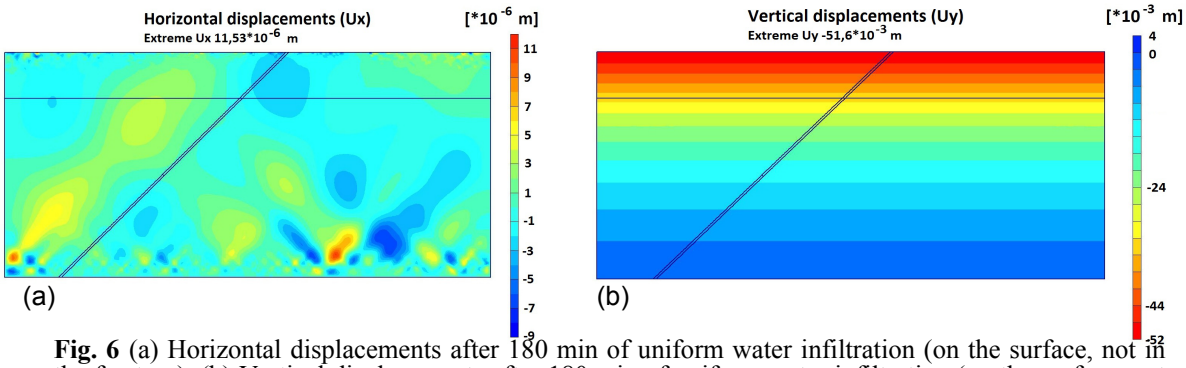

Fig. 6 (a) Horizontal displacements after 180 min of uniform water infiltration (on the surface, not in the fracture). (b) Vertical displacements after 180 min of uniform water infiltration (on the surface, not in the fracture).

When infiltration in matrix and fracture in the rectangular system with a 45° fault zone was considered, a maximum horizontal displacement of 1.2 cm (Fig. 7(a)) and a vertical displacement of 6.6 cm (Fig. 7(b)) were obtained. The resulting horizontal displacement was 100% larger, and the vertical one ~28% larger, compared to the simulation with infiltration only in the matrix.

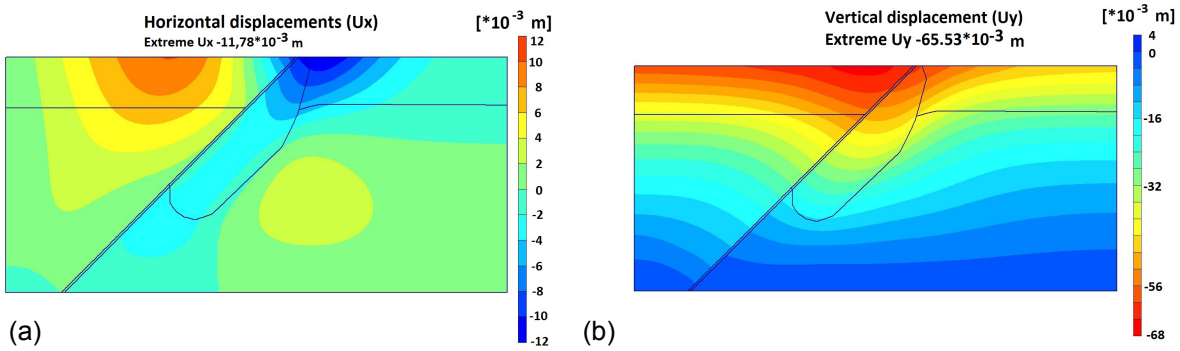

Fig. 7 Horizontal displacements after 180 min water infiltration through 45° inclined fracture zone. (b) Vertical displacements after 180 min water infiltration through 45° inclined fracture zone.

This deformation considerably increased when there was a certain slope on the surface, as shown in Fig. 8(a) and (b) where there was a maximum horizontal displacement of 4.4 cm and a vertical displacement of 12.6 cm.

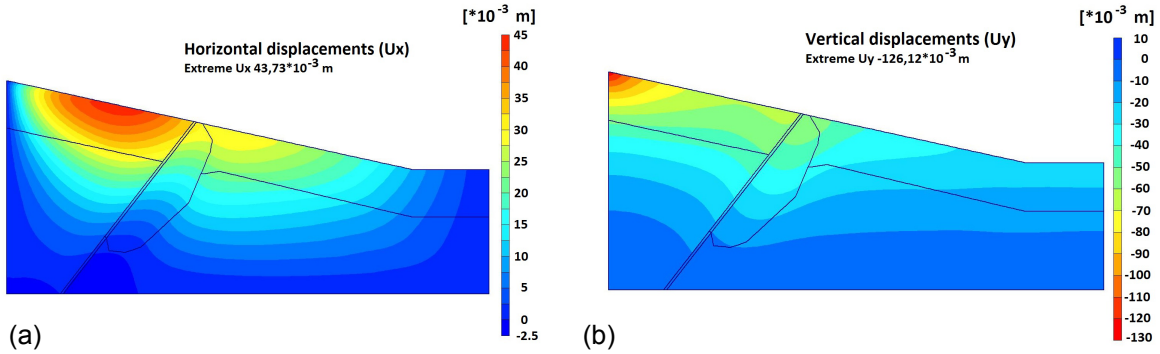

Fig. 8 (a) Horizontal displacements after 180 min water infiltration through 45° inclined fracture zone with slope on the surface. (b) Vertical displacements after 180 min water infiltration through 45° inclined fracture zone with slope on the surface.

CONCLUSIONS

Numerical simulations investigating the influence of rapid water infiltration through fractures on land subsidence were performed.

The numerical studies show that infiltration into a system with a horizontal surface and with a vertical fracture has no considerable influence on deformation because the water infiltrates directly into the saturated zone. Infiltration into a system with a horizontal surface and without a fracture produces linear vertical displacements and the horizontal displacements are negligible. If water infiltrates through the inclined fracture, the displacements, especially the horizontal one, increase strongly. If there is an inclination on the surface (slope), both horizontal and vertical displacements are considerably increased.

The results of the numerical simulations presented in this paper show that subsidence can be increased considerably by a fast water infiltration through fractured zones. This aspect becomes even more important when such fractures transport the water through superficial layers with low permeability into layers with higher permeability. This rapid infiltration then produces a rapid

change in the soil saturation conditions, and consequently the land subsidence. This will be investigated in the future.

Acknowledgements The research is financed by CONACYT-DAAD. The authors specially thank Diplo.-Ing. Ralf Glasenapp for his support concerning the mechanical modelling.

REFERENCES

Bai, M. & Elsworth, D. (1994) Modeling of subsidence and stress-dependent hydraulic conductivity for intact and fracturated porous media. *Rock Mechanics and Rock Engineering* **27**(4), 209–234.

Brooks, R. H. & Corey, A. T. (1964) Hydraulic properties of porous media. In: *Hydrol. Paper* vol. 3. Colorado State University, Fort Collins, USA.

Ehlers, W. & Müllerschön, H. (2004) Deformation and localization analysis in partially saturated soil. *Computer Methods in Applied Mechanics and Engineering* **193**, 2885–2910.

Gerke, H. H. & van Genuchten, M. Th. (1993) A dual-porosity model for simulating the preferential movement of water and solutes in structured porous media. *Water Resour. Res.* **29**(2), 305–319.

Hinkelmann, R. (2005) *Efficient Numerical Methods and Information – Processing Techniques for Modeling Hydro-and Environmental Systems.* Springer, Berlin, Germany.

Kumarci, K., Ziaie, A. & Kyioumarsi, A. (2008) Land subsidence modeling due to ground water drainage using WTAQ software. *WSEAS Transactions on Environment and Development* **4**(6), 503–512.

Novák, V., Šimůnek, J. & van Genuchten, M. T. (2000) Infiltration of water into soil with cracks. *J. Irrigation and Drainage Engineering* **126**(1), 41–47.

Pham Van, S. (2009) Application of different model concepts for simulation of two-phase flow processes in porous media with fault zones. Dissertation, Institut für Bauingenieurwesen. Fachgebiet Wasserwirtschaft und Hydrosystemmodellierung. Technische Universität Berlin, Germany.

Rojas, E., Arzate, J. & Arroyo, M. (2002) A method to predict the group fissuring and faulting caused by regional groundwater decline. *Engineering Geology* **65**, 245–260.

Schanz, T., Vermeer, P. A. & Bonnier, P. G. (1999) The hardening soil model: formulation and verification. In: Beyond *2000 in Computational Geotechnics-10 Years of PLAXIS*, Rotterdam, The Netherlands. ISBN 90 580904 X.

Waterman, D., Al-Khoury, R., Bakker, J. K., Bonnier P. G., Burd, H. J., Soltys, G. & Vermeer, P. A (2004) PLAXIS, 2D-Version 8, Manual. ISBN 90-808079-6-6.

Zehng, Y., Burridge, R. & Burns, D. (2008) Reservoir simulation with the Finite Element Method using biot poroelastic approach. Dept of Earth, Atmospheric, and Planetary Sciences, Cambridge, Massachusetts, USA.

(Proceedings of EISOLS 2010, Querétaro, Mexico, 17–22 October 2010). IAHS Publ. 339, 2010.

Nonlinear analysis of land subsidence due to groundwater level oscillation by a finite difference method

HESSAM YAZDANI[1,2], M. M. TOUFIGH[2] & AMIN MASOUDZADE[2]

1 *Civil Engineering Department, Javid-e Jiroft Institute of Technology, Azadi Ave, Jiroft, Iran*
yazdani@graduate.uk.ac.ir, yazdani.hessam@yahoo.com

2 *Civil Engineering Department, University of Kerman, 22 Bahman Blvd, PO Box 133, 76175 Kerman, Iran*

Abstract Groundwater level oscillation leads to successive variation of effective stresses through a clay layer, resulting in consecutive settlement. Different elements of the layer may be normally consolidated (NC) or over consolidated (OC) under such a cyclic loading, depending on parameters such as the loading intensity, layer thickness and distance from drainages, nonlinearity of the soil and pre-consolidation pressure. A new equation is derived to consider cyclic loading and also the inevitable compressibility and permeability changes of soil. In this paper, two nonlinear partial differential equations are derived to analyse the clay consolidation using void ratio–effective stress and void ratio–permeability diagrams. By the finite difference method, the PDEs are utilized to analyse the land subsidence problem. It is shown that the ratios between slopes of the diagrams in the NC and OC conditions play a major role in the consolidation process. The effect of each of these parameters is shown.

Key words nonlinear consolidation; land subsidence; cyclic loading; finite difference method; variable permeability; variable compressibility

INTRODUCTION

Land subsidence, which may have resulted from pseudo-cyclic-loading and consecutive oscillation of the groundwater level due to seasonal precipitation and water pumping, lead to long-period variations in effective stress of the clay body and thereafter periodic changes of the volume of the clay: settlement and rebounds. This time-dependent process of volume changes in soil, as water is periodically squeezed out of, or returned back to the voids, is governed by complicated interactions among effective and total stresses, pore water pressure, seepage, compressibility and stress history and is called "consolidation under cyclic loading". The most popular hypothesis which predicts the consolidation process is the famous Terzaghi consolidation (Terzaghi *et al.*, 1996). In the derivation of this theory, it was implicitly assumed that the permeability and compressibility of soil are constant. This is not usually the case. Permeability and compressibility are reduced while the soil consolidates and void space diminishes. Hence, this concludes that the coefficient of consolidation is not constant. To analyse the consolidation of clays under time-dependent loading, simple prediction methods for consolidation evaluation of elastic and inelastic soil layers under time-dependent loading have been introduced in some papers (Baligh & Levadoux, 1978; Toufigh & Ouria, 2009). Sample studies on the 2-D and 3-D consolidation under time-dependent loading can be found in (Lekha *et al*., 1998; Fox *et al*., 2003). In spite of the praiseworthy research mentioned above, only a few papers or studies (Lekha *et al*., 2003; Abbasi *et al*., 2007; Yazdani, 2008) have covered the nonlinear consolidation, including the variation of compressibility and permeability under cyclic loading.

In this paper, two nonlinear partial differential equations (NPDE) are derived to predict the consolidation characteristics of clays subjected to cyclic variation of groundwater level followed by cyclic changes in total stresses using void ratio–effective stress and void ratio–permeability diagrams. The equations consider the stress time history but ignore both the self-weight effects and the creep effects. It is graphically shown that the ratios between slopes and intercepts of $e - \log\sigma'$ and $e - \log k$ lines in the NC and OC conditions, which emerge from coefficients of the two NPDEs, play a major role in the consolidation process.

Copyright © 2010 IAHS Press

THEORETICAL BASIS OF THE PROPOSED THEORY

Fundamental equations

The one-dimensional consolidation equation can be written as follows:

$$\frac{1}{1+e_0}\frac{\partial e}{\partial t} = -\frac{k}{\gamma_w}\frac{\partial^2 \sigma'}{\partial z^2} \tag{1}$$

where u is the excess pore water pressure, k is the coefficient of permeability, γ_w is the unit weight of water, σ' is effective stress, z is downward coordinate through the soil layer, e_0 is initial void ratio and e is void ratio at time t.

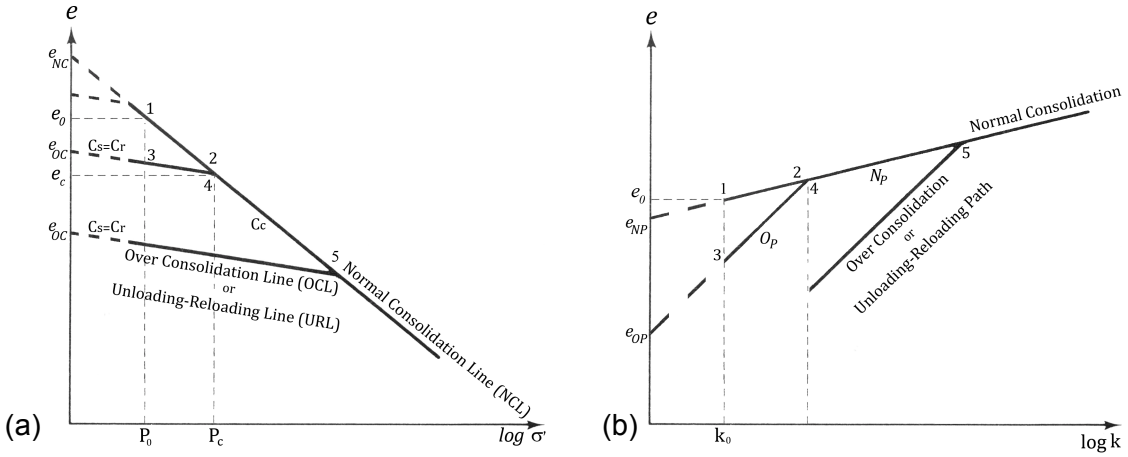

Fig. 1 Inelastic behaviour of soil under cyclic loading.

According to Fig. 1(a), the linear relationship between void ratio and effective stress in a semi-logarithmic diagram at the NC condition can be expressed as:

$$e = e_{NC} - C_c \log \sigma' \tag{2}$$

where C_c is the slope of the straight line and known as the compression index, e is the void ratio at the effective stress σ', and e_{NC}, which is the line's intercept, is the void ratio at unit effective stress and hence is a constant value for a given soil and is a function of the unit used for effective stress. Also, in the OC condition:

$$e = e_{OC} - C_s \log \sigma' \tag{3}$$

where C_s is the slope of the straight line and known as swell index and for the sake of simplicity, it is considered equal to recompression index, C_r, the slope of reloading line in e – logσ'space. The definition of e_{OC} is similar to that of e_{NC} except that depending on the preconsolidation pressure, P_c, its value varies during the cyclic consolidation process. On the other hand, according to Fig. 1(b), at the NC condition, a similar linear relationship can be presented between void ratio and permeability as:

$$e = e_{NP} + N_P \log k \tag{4}$$

where e_{NP} and N_P are the intercept and slope of the straight line, respectively. The intercept, e_{NP}, is the void ratio at unit coefficient of permeability (k = 1) and again, it is constant for a given soil but varies with the unit used for k. At the OC condition:

$$e = e_{OP} + O_P \log k \tag{5}$$

where e_{OP} and O_P are the intercept and slope of the straight line, respectively. Once more, depending on the preconsolidation pressure, P_c, e_{OP} varies during the cyclic consolidation process. Replacing the left side of equation (2) with the right side of (4) after some re-arrangements gives:

$$k_{NC} = 10^{(e_{NC}-e_{NP})/N_P}(\sigma')^{-C_c/N_P} \tag{6}$$

Doing similar operations on equations (3) and (5) leads to:

$$k_{OC} = 10^{(e_{OC}-e_{OP})/O_P}(\sigma')^{-C_s/O_P} \tag{7}$$

It should be stated that the units of the parameters involved here must be selected appropriately.

Mathematical models for soil consolidation

Calculating the first derivative of equation (2) with respect to time:

$$\frac{\partial e}{\partial t} = \frac{-2.303C_c}{\sigma'}\frac{\partial \sigma'}{\partial t} \tag{8}$$

and substituting equations (6) and (8) into equation (1), with some rearrangement, leads to:

$$\frac{\partial \sigma'}{\partial t} = \frac{2.303(1+e_0)}{C_c\gamma_w}10^{\frac{e_{NC}-e_{NP}}{N_P}}(\sigma')^{(1-\frac{C_c}{N_P})}\frac{\partial^2 \sigma'}{\partial z^2} \tag{9}$$

By defining:

$$\alpha_{NC} = 1-\frac{C_c}{N_P} \tag{10}$$

$$\beta_{NC} = \frac{2.303(1+e_0)}{C_c\gamma_w}10^{\frac{e_{NC}-e_{NP}}{N_P}} \tag{11}$$

equation (9) reduces to:

$$\frac{\partial \sigma'}{\partial t} = \beta_{NC}(\sigma')^{\alpha_{NC}}\frac{\partial^2 \sigma'}{\partial z^2} \tag{12}$$

The latter equation is a nonlinear partial differential equation (NPDE), which governs variations of effective stress during the nonlinear one-dimensional consolidation of a NC soil layer, while assuming linear relationships between $e - \log\sigma'$ and $e - \log k$. Coefficients α and β are called the *nonlinearity factor* and *basic coefficient of consolidation*, respectively. Equation (12) is similar to classical Terzaghi's consolidation theory, except that C_v has a generalized form. It means:

$$C_{vNC} = \beta_{NC}(\sigma')^{\alpha_{NC}} \tag{13}$$

Equation (13) shows that the coefficient of consolidation is not constant during the consolidation process and depends on the effective stress. Note that in the special case when $\alpha = 0$ (or C_c/N_P), C_v will be constant, and equal to β, hence, equation (12) will reduce to Terzaghi's theory. For the OC condition, a similar manner can be used to derive an analogous governing equation:

$$\frac{\partial \sigma'}{\partial t} = \beta_{OC}(\sigma')^{\alpha_{OC}}\frac{\partial^2 u}{\partial z^2} \tag{14}$$

in which:

$$\alpha_{OC} = 1-\frac{C_s}{O_P} \tag{15}$$

$$\beta_{OC} = \frac{2.303(1+e_0)}{C_s\gamma_w}10^{\frac{e_O-e_{OP}}{O_P}} \tag{16}$$

$$C_{vOC} = \beta_{OC}(\sigma')^{\alpha_{OC}} \tag{17}$$

It should be noted that equations (12) and (14) look similar, but there is a very important difference between them. During the cyclic consolidation, β_{OC} is not constant, while β_{NC} is. Having a different governing equation for each of the NC or OC condition, and the non-existence of a closed form solution to determine the time at which the conditions in a soil region changes to NC or OC, point 4 in Fig. 1, a complete analysis of nonlinear consolidation under cyclic loading is impossible.

NUMERICAL STUDY ON THE VARIATION OF CONSOLIDATION CHARACTERISTICS UNDER CYCLIC LOADING

Solution of the developed nonlinear governing equations

Equations (12) and (14) are nonlinear partial differential equations. These complex and nonlinear partial differential equations (NPDEs) can be solved using a numerical approach in this paper, the Finite Difference Method (FDM). The simplest and most common strategy for numerical solution of nonlinear equations is linearizing the equation using an iterative or prediction and correction procedure. In this approach, the coefficient of the right hand term in equation (12) $C_v = \beta(\sigma - u)^{\alpha}$ is assumed to be constant temporarily during a given small time step. Thereby, the proposed nonlinear partial differential equation changes to the well-known heat transfer equation or commonly used Terzaghi's equation for isotropic medium as:

$$\frac{\partial \sigma'}{\partial t} = C_v \frac{\partial^2 \sigma'}{\partial z^2} \tag{18}$$

which is a parabolic, one-dimensional and linear partial differential equation. A computer code has been developed to determine the pore pressures at different depths and time steps using the aforementioned numerical algorithm. Other relevant parameters such as average degree of consolidation and time factor at any time level can also be determined using the results of the numerical solution.

Analysis and results

The consolidation analysis of a clay layer under variation of water level is discussed. Equations (12) and (14) show that a change in the effective stress leads to the variation of the coefficient of consolidation. Figure (2) depicts the variation of the coefficient of consolidation in the depth of the layer shown by node numbers in FDM. It can be found that the coefficient of consolidation is not constant at depth as well as time and under cyclic loading. Different parts of the layer experience

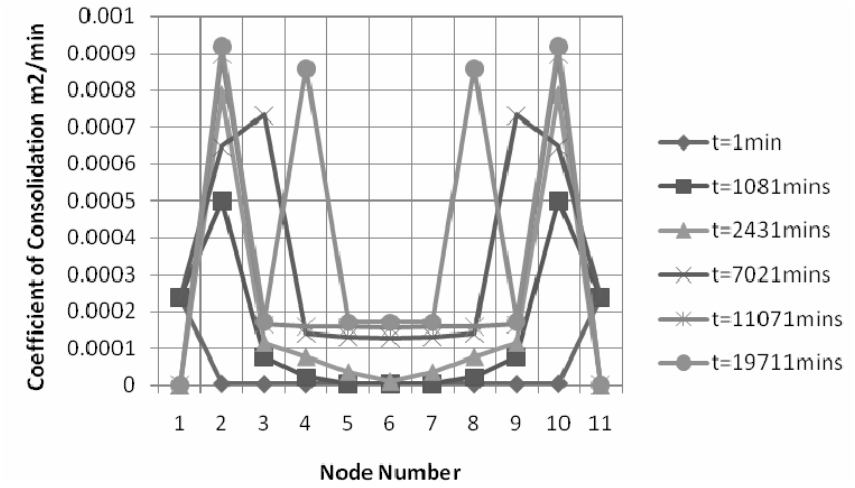

Fig. 2 The variation of the coefficient of consolidation.

different conditions with a view to NC or OC conditions due to the nature of the loading. As the consolidation progresses, preconsolidation reaches the middle of the layer and hence, the coefficient of consolidation increases.

Figure 3 demonstrates the variation of the average degree of consolidation *versus* real time; as shown, in each cycle the greatest degree of consolidation is at the end of the loading half-cycle and the least is at the end of the unloading half-cycle. After 12 cycles, the degree of consolidation has converged to 50% of that under constant loading. Here, convergence means the whole of the layer is in OC condition and behaves elastically.

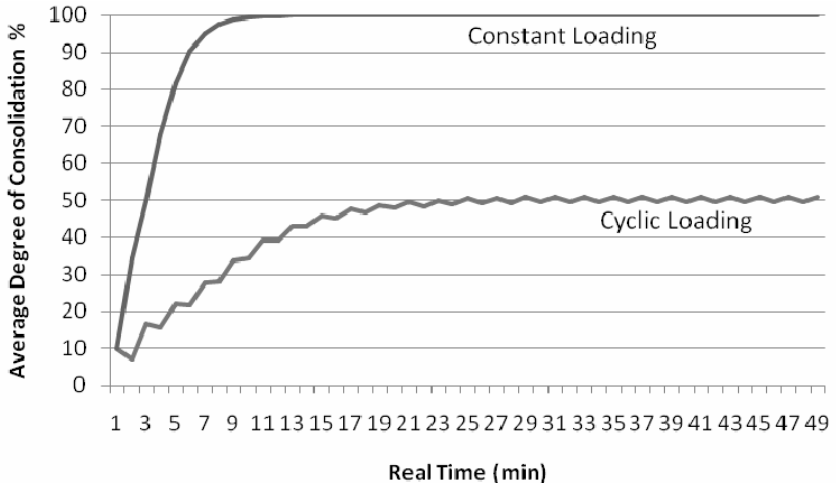

Fig. 3 The average degree of consolidation *versus* real time.

Generally, $\mu = C_c/C_s$ varies between 5 and 10 in soils (Terzaghi *et al*., 1996). The effect of this parameter on the degree of consolidation is shown in Fig. 4. The figures show that as μ is increased, the degree of consolidation decreases.

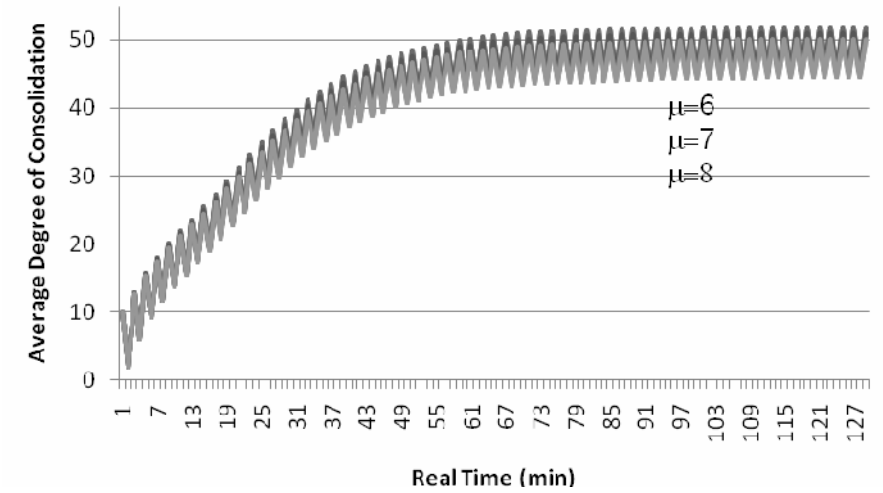

Fig. 4 The effect of μ on the degree of consolidation.

CONCLUSION

Using void ratio–effective stress and void ratio–permeability relationships, two one-dimensional nonlinear partial differential equations (PDEs) were derived to predict consolidation characteristics

of normally consolidated and over consolidated soft clays. An analytical discussion on the variation of the coefficient of consolidation under cyclic loading was presented. Based on the discussion, the following remarks can be concluded:

As consolidation progresses, the coefficient of consolidation varies with the changes in effective stress followed by changes in coefficients of permeability and volume compressibility.

Two coefficients (α and β) describe the changes in the coefficient of consolidation with effective stress and, thereby, take into consideration the changes in the coefficients of volume compressibility and permeability during consolidation.

Besides the preconsolidation pressure, the ratios between the slopes of the $e - \log\sigma'$ and $e - \log k$ lines in the NC and OC conditions, which emerge from coefficients of the two NPDEs, play a major role in the consolidation process.

REFERENCES

Abbasi, N., Rahimi, H., Javadi, A. A. & Fakher, A. (2007) Finite difference approach for consolidation with variable compressibility and permeability. *Comput. Geotech.* **34**, 41–52.

Baligh, M. M. & Levadoux, J. N. (1978) Consolidation theory of cyclic loading. *J. Geotech. Engng ASCE* **104**, 415–431.

Conte, E. & Troncone, A. (2006) One-dimensional consolidation under general time-dependent loading. *Can. Geotech. J.* **43**, 1107–1116.

Conte, E. & Troncone, A. (2007) Nonlinear consolidation of thin layers subjected to time-dependent loading. *Can. Geotech. J.* **44**, 717–725.

Fox, P. J., Nicola, M. D. & Quigley, D. W. (2003) Piecewise-linear model for large strain radial consolidation. *J. Geotech. Geoenv. Engng ASCE* **129**, 940–950.

Lekha, K. R., Krishnaswamy, N. R. & Basak, P. (1998) Consolidation of clay by sand drain under time-dependent loading. *J. Geotech. Geoenv. Engng ASCE* **124**, 91–94.

Lekha, K. R., Krishnaswamy, N. R. & Basak, P. (2003) Consolidation of clays for variable permeability and compressibility. *J. Geotech. Geoenv. Engng ASCE* **129**, 1001–1009.

Terzaghi, K., Peck, R. B. & Mesri, Gh. (1996) *Soil Mechanics in Engineering Practice*, third edn. John Wiley, New York, USA.

Toufigh, M. M. & Ouria, A. (2009) Consolidation of inelastic clays under rectangular cyclic loading. *Soil Dyn. Earth. Engng* **29**, 356–363.

Yazdani, H. (2008) Consolidation differential equation solution under cyclic loading. MSc Thesis, Shahid Bahonar University of Kerman, Iran.

Land Subsidence, Associated Hazards and the Role of Natural Resources Development
(Proceedings of EISOLS 2010, Querétaro, Mexico, 17–22 October 2010). IAHS Publ. 339, 2010.

Thermo-poro-elastic effects in the anthropogenic uplift of Venice by deep seawater injection

N. CASTELLETTO, M. FERRONATO, G. GAMBOLATI, C. JANNA & P. TEATINI

Department of Mathematical Methods and Models for Scientific Applications (DMMMSA), University of Padova, via Trieste 63, I-35121 Padova, Italy
castelletto@dmsa.unipd.it

Abstract To mitigate the flooding that periodically plagues Venice, a project of anthropogenic uplift of the city by deep seawater injection has been recently advanced. A pilot programme has been designed to test the feasibility of the proposal, improve the knowledge of the subsurface below the Venice Lagoon and help the calibration of the full-scale prediction models. The present communication aims at supplementing the proposal with the investigation of the role played by a temperature variation should the injection take place in non-isothermal conditions. A three-dimensional (3-D) nonlinear hydro-thermo-mechanical model is developed making use of lowest order Mixed Hybrid Finite Elements (MHFEs) and shock capturing Finite Volumes (FVs) for the coupled subsurface fluid flow and heat transfer, and Finite Elements (FEs) for the structural equilibrium. A set of computer simulations is performed using realistic information on the hydrogeological, geothermal, and geomechanical properties of the Northern Adriatic basin. A representative 750-m deep brackish aquifer is selected with the seawater injection programme planned with an over-pressure of 1 MPa over a 3-year time period. Different scenarios are simulated depending on the temperature difference ΔT between formation water and injected seawater that is assumed to be taken from the Adriatic. Basically a ΔT according to season is addressed. The numerical results show that the ΔT impact on the pressure field is negligibly small relative to the isothermal case, while some influence is exerted by a thermal gradient on the predicted uplift, which can vary at the most by nearly 10% for an injection in ambient conditions.

Key words anthropogenic uplift; hydro-thermo-mechanical modelling; Venice, Italy

INTRODUCTION

The city of Venice and the surrounding Venice Lagoon sites are periodically plagued by the "acqua alta" phenomenon, i.e. high tide flooding that occurs typically in fall and winter due to a combination of low atmospheric pressure, strong on-shore winds from the Adriatic Sea, seiches and heavy rain. Floods have increased in frequency and intensity since the early 1900s mainly because of three reasons: the eustatic rise of the sea level, natural land subsidence, and anthropogenic land subsidence induced by water pumping. Groundwater extraction in the Venice and nearby Mestre area was stopped in the mid 1970s, and, after a slight rebound, subsidence recovered its natural trend. Widely accepted estimates set the land settlement with respect to mean sea level over the last century at 0.23 m, e.g. Carbognin *et al*. (2005). According to the updated elevation map of Venice ("Venezia altimetria", 2009) the normal tide height ranges from –0.50 m to +0.80 m with respect to the Punta della Salute datum, located opposite St Mark's Square. Above the +0.80 m threshold, flooding starts. For example, nearly 30% and more than 60% of the city area is flooded when tide height achieves +1.20 m and +1.50 m, respectively.

The Italian government has defined the safeguarding of Venice as a "national priority" after the devastating flood of November 1966, when the tide reached the unprecedented height of 1.94 m above the tidal datum. Several solutions have been advanced to save Venice. The final project selected for the Venice protection from "acqua alta" is the "MOdulo Sperimentale Elettromeccanico" (MOSE) system, which is currently under construction. The MOSE system uses fold-away steel gates that are raised from the sea floor to prevent water from entering the Venice Lagoon when a high tide is expected. The floodgates are normally folded and embodied within concrete caissons buried at the bottom of the three lagoon inlets, i.e. Lido, Malamocco, and

Copyright © 2010 IAHS Press

Chioggia. A novel proposal to mitigate flooding is the anthropogenic uplift of the city by deep seawater injection recently advanced by Comerlati *et al.* (2003, 2004), and further investigated with the design of a pilot injection experiment (Castelletto *et al.*, 2008). This project is intended as a complementary action to MOSE, since it might extend its operational life on consideration of the sea level rise expected by the end of the present century, and at the same time significantly reduce the MOSE activation, thus limiting concerns at both an economic and environmental level.

Using hydrogeological, geothermal and geomechanical data from the Northern Adriatic basin, the present communication addresses the influence of thermal gradients on the land surface response, assuming non-isothermal conditions in the seawater injection process. A 3-D nonlinear hydro-thermo-mechanical model is implemented using lowest order MHFEs and high-resolution FVs for the coupled subsurface fluid flow and heat transfer, and FEs for the structural equilibrium. A set of simulations is performed by injecting seawater with an overpressure of 1 MPa over a 3-year period into a brackish aquifer located at between 710 and 790 m below the sea level. The simulation time interval selected is consistent with the duration of the pilot experiment.

MATHEMATICAL MODEL

The classical thermo-poro-elasticity theory, e.g. Coussy (2004), provides the mathematical framework for the analysis of the deformation of a fluid-saturated porous medium. The equations governing the coupled system in non-isothermal conditions are balance laws of the linear momentum, fluid mass and thermal energy for the mixture. As is often done in petroleum engineering, we use an uncoupled approach, e.g. Baù *et al.* (2001), Chin & Nagel (2004), first addressing the flow and the heat transfer models with the pressure p and temperature T solutions subsequently used in the mechanical equilibrium equations to obtain the medium deformation.

The nonlinear system of partial differential equations for the coupled fluid flow and heat transfer is solved by Godunov-Mixed Methods (Dawson, 1993), combining MHFEs in the discretization of the diffusion term, both in the flow and the thermal equations, and a high-resolution cell-centred FV scheme for the convective term via a time-splitting technique. The solution is obtained through a Picard linearization scheme, solving the flow problem first, then the thermal balance, and iterating the procedure at each time step until convergence. The reasons for this choice are twofold. First, the MHFE scheme applied to the flow equation yields a conservative discrete velocity field with normal components that are continuous across inter-element boundaries. Second, the time-operator splitting approach for the heat transfer equation allows for the distinct treatment of the convective and the conductive contribution: for the convective part a FV scheme is selected because of its robustness in simulating sharp fronts, while MHFEs are employed in the conductive step. As to the structural equilibrium, a standard nodal-based FE discretization is implemented for the medium displacements, making use of the nonlinear formulation by Gambolati *et al.* (2001). It is worth noting that FEs, MHFEs and cell-centred FVs are used with a weak variational form of the governing equations using similarly-based functions for the approximated solution, with the practical benefit that one grid only is required.

NUMERICAL RESULTS

The thermal effects in Venice uplift are investigated by injecting seawater through a single vertical well. The numerical simulations make use of a realistic geological setting representative of the Northern Adriatic basin. The conceptual model consists of a pumped aquifer overlain and underlain by clayey confining beds (Fig. 1). Because of symmetry, the problem can be reduced to a quarter of the injected porous medium (Fig. 1). The integration domain is discretized into linear tetrahedral elements with the well located as shown in Fig. 1. The discretized volume covers an area of 10 × 10 km confined on top by the ground surface and a 10-km deep rigid basement on

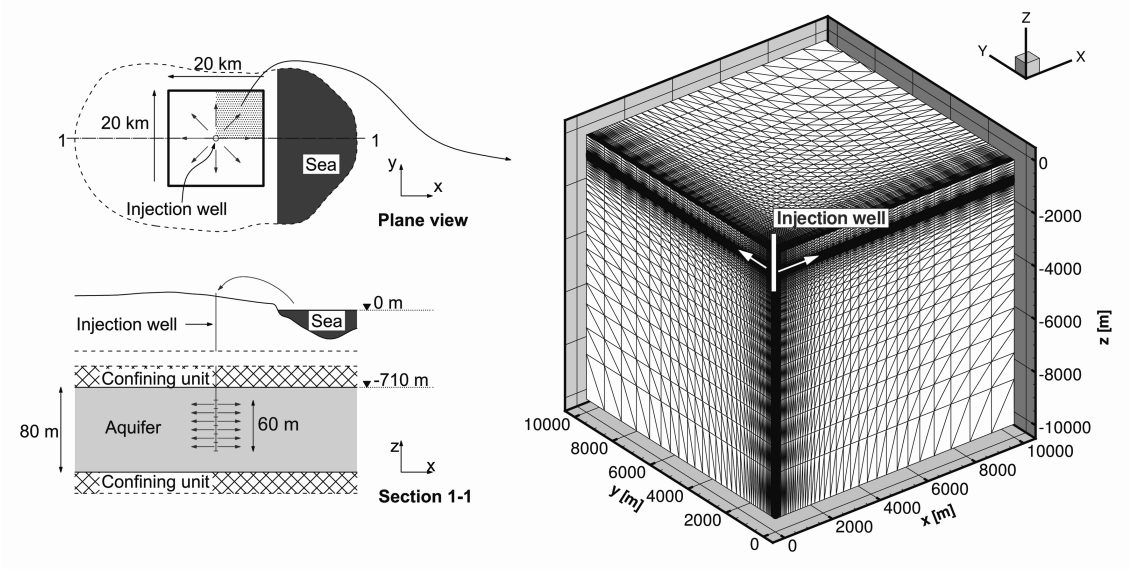

Fig. 1 Sketch of the integration domain used in the non-isothermal injection simulation (left) and axonometric view of the tetrahedral mesh used to discretize the integration domain (right).

the bottom. The 3-D mesh is made of 143 055 nodes and 810 000 tetrahedra. Close to the injection well the average elemental size is equal to 10 m. The boundary conditions are specified far enough from the injection borehole to avoid any appreciable boundary influence on the major results of interest. The ground surface is a traction-free plane and zero displacement is prescribed at the bottom and outer boundaries. Along the inner boundaries, no horizontal displacements orthogonal to the symmetry planes are allowed for. The basement and the inner boundaries are impermeable to fluid flow and adiabatic, while the ground surface and the outer boundaries are fixed for both pore pressure and temperature. The injected aquifer has a constant thickness of 80 m and is ideally located at between 710 and 790 m below the mean sea level. The initial pressure and temperature are hydrostatic, with thermal gradient g_t and surface temperature T_{surf}. The average value of g_t is usually equal to 0.029 °C/m. However, experimental measurements and geological considerations (Mattavelli & Novelli, 1990) suggest using a smaller value, i.e. 0.02 °C/m, for the Northern Adriatic basin. T_{surf} is conventionally assumed to be 15°C (Chierici, 1989), so the injected aquifer is at the initial temperature of 30°C. Above and below the aquifer confining beds the medium consists of a sequence of alternating sandy and clayey units. The horizontal hydraulic conductivities of the injected formation and the confining units are set to 1×10^{-6} m/s and 10^{-10} m/s, respectively (Comerlati *et al.*, 2004). The vertical hydraulic conductivity is one tenth of the horizontal value. As to the thermal properties, heat conductivity and volumetric capacity are 0.6 W/m°C and 4.18×10^{-6} J/m^3°C, respectively, for water and 5.0 W/m°C and 2.5×10^{-6} J/m^3°C for the formation. The relationship used in Comerlati *et al.* (2004) is selected as the constitutive law for the vertical rock compressibility c_M, with c_M in unloading/reloading conditions 3.5 times less than that in virgin loading conditions. Other significant parameters are the water compressibility $\beta_f = 9.0 \times 10^{-4}$ MPa^{-1} and thermal expansion coefficients $\beta_f' = 4.5 \times 10^{-4}$ °C^{-1} (Wagner & Kretzschmar, 2008), respectively, and the formation thermal expansion coefficient $\beta_s = 35 \times 10^{-6}$ °C^{-1} (Fjaer *et al.*, 2008). A set of simulations is performed by injecting seawater over a 60-m length intake (Fig. 1) at a constant overpressure of 1 MPa. All scenarios investigate a 10-year period, consisting of 3-year injection operations and a 7-year post-injection stage. Three test cases are addressed depending on the temperature T_{inj} of the injected seawater (Fig. 2), namely: (a) Test case 1: T_{inj} is constant and equal to 15°C; (b) Test case 2: T_{inj} is constant and equal to 45°C; (c) Test case 3: T_{inj} varies between a minimum of 7.5°C and a maximum of 22.5°C according to season. It is worth noting that the constant temperature in Test case 1 can be interpreted as the average temperature of the profile in Test case 3.

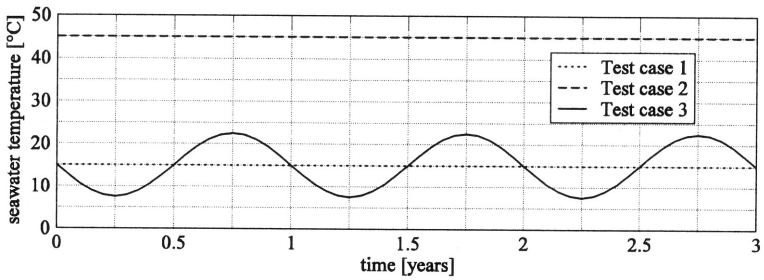

Fig. 2 Injection temperature profile *vs* time in the three simulated test cases.

The results of the simulations show that the temperature impact on the pore-pressure change Δp distribution is quite small with respect to the isothermal case. Figure 3 provides the distribution of the Δp difference between Test case 1 and the isothermal case, and Test case 2 and the isothermal case, respectively, at the end of the injection period in a horizontal cross-section at $z = -750$ m. Only a slight delay/acceleration of the pressure field propagation can be observed when a colder/warmer injection temperature occurs, with the largest difference on the order of 0.06 MPa located close to the well. No appreciable Δp difference is found between Test case 1 and Test case 3. The Δp distributions are thus practically the same in all cases and equal to the isothermal Δp shown in Fig. 4 at two selected time steps. It is worth noting that, following cessation of pumping, the overpressure is quickly dissipated and decreases by more than 90% in one year.

The elemental ΔT distribution at several time steps is shown in Fig. 5 in a radial cross-section through the well for Test case 1. Similar results hold true for Test cases 2 and 3 in terms of affected volume, with a +15°C and –22.5°C peak ΔT value, respectively. In all cases, the region subject to a change in temperature keeps expanding for 3 years, mainly into the aquifer up to a distance of about 125 m from the well, with some diffusive heat transfer into the sealing layers, too. Once injection is stopped, the convective contribution diminishes because of the small velocity, with the heat transfer essentially governed by the thermal diffusion of the saturated formation. After 10 years the process has not reached a steady state, implying that the aquifer exhibits a small thermal diffusivity with a longer time required to attain a new equilibrium condition.

The ground surface response in terms of vertical displacements Δz in Test cases 1 and 2, respectively, are compared to the isothermal model and plotted in Fig. 6, that shows Δz in a radial cross-section through the well (left) and its behaviour *vs* time at the well location (right). The

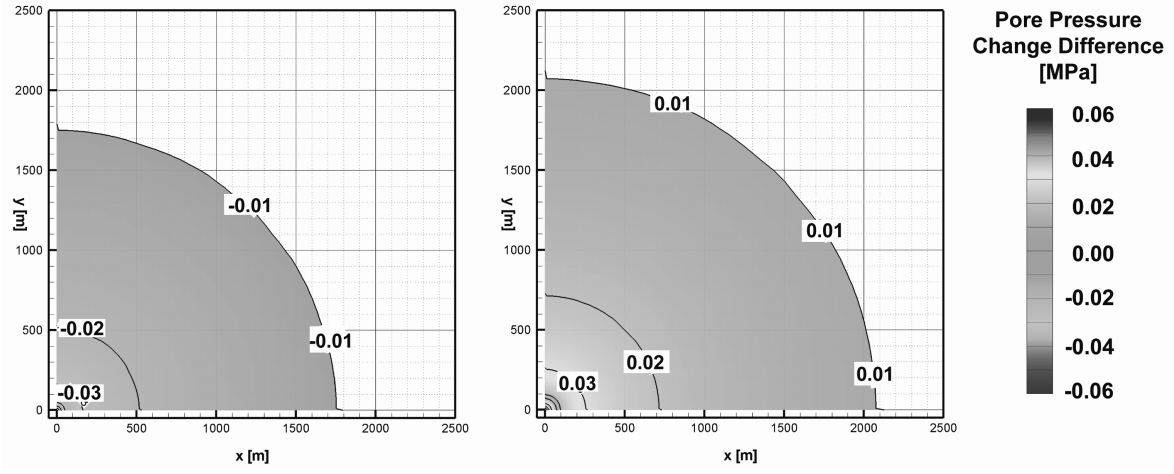

Fig. 3 Contour plot of the Δp difference [MPa] between Test case 1 (left) and Test case 2 (right) and the isothermal analysis, respectively, at the end of the injection (year 3) in a horizontal cross section at 750 m depth.

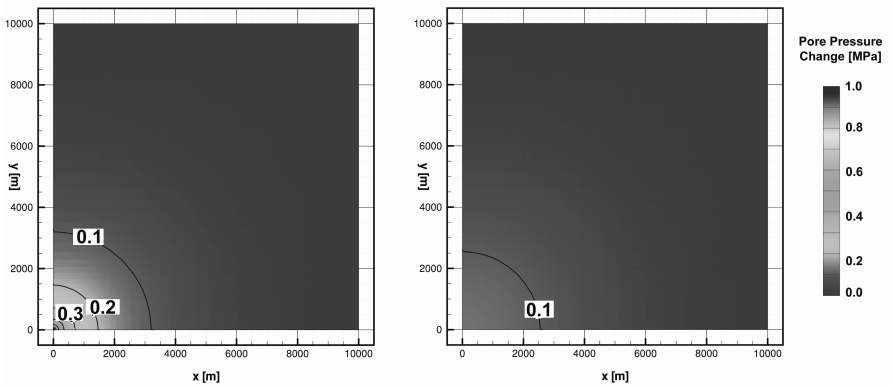

Fig. 4 Isothermal case: contour plot of the pore-pressure change [MPa] along a horizontal cross-section at 750 m depth at the end of the injection operations (left) and after 6 months injection is stopped (right).

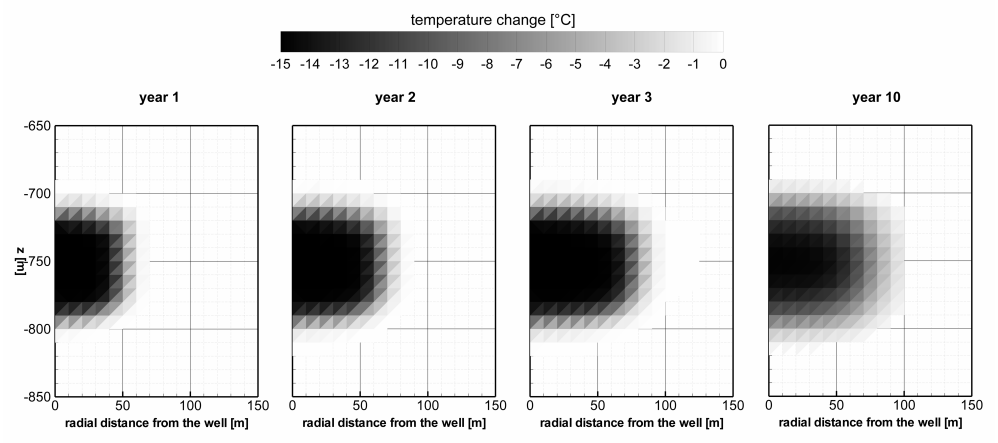

Fig. 5 Test case 1: elemental temperature change distribution in a radial section through the well at several time steps.

largest Δz predicted at the end of the injection in isothermal conditions is equal to 1.97×10^{-2} m. The largest deviation due to the thermal deformation is 0.15×10^{-2} m, i.e. about 8%, negative in Test case 1 and positive in Test case 2, respectively. At the end of the injection experiment, the uplift is quickly recovered, with no significant residual deformation related to the still non-equilibrated temperature distribution, namely less than 1×10^{-3} m. Consistent with the pressure and temperature fields, Test case 3 exhibits almost the same displacements as Test case 1, with only a small difference related to the oscillatory temperature behaviour.

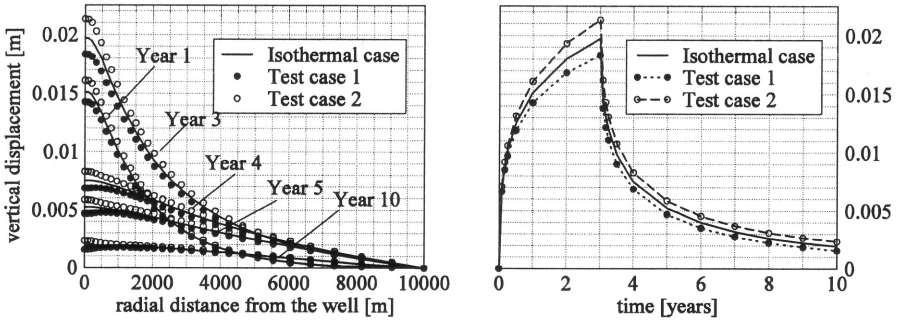

Fig. 6 Land vertical displacement along a radial section through the well at several time steps (left), and at the injection point *vs* time (right).

CONCLUSIONS

Modelling studies based on very realistic geological, hydrogeological, and geomechanical information about the Venice Lagoon subsurface support the innovative project of anthropogenic uplift of Venice as a new potential defence from the "acqua alta". The design of an injection pilot test has also been advanced to assess the feasibility of the proposal. In this paper the pilot project has been integrated with analysis of the expected thermal effects of a non-isothermal seawater injection over a 3-year period with a 1 MPa overpressure. The developed numerical model combines advanced discretization techniques, including MHFE, FV and FE to solve the governing equations. According to the scenarios addressed, it may be concluded that the influence of the temperature on the pressure field appears to be negligibly small relative to the isothermal case. In contrast, some influence is exerted by the thermal gradient on the predicted uplift, which can vary by up to about 8%. For the temperature variations assumed in the present analysis the overpressure remains the predominant cause of deformation.

REFERENCES

Baù, D., Ferronato, M., Gambolati, G. & Teatini, P. (2001) Land subsidence spreading factor of the Northern Adriatic gas fields, Italy. *Int. J. Geomech*. **1**(4), 459–475.

Carbognin, L., Teatini, P. & Tosi, L. (2005) Land subsidence in the Venetian area: known and recent aspects. *Giornale di Geologia Applicata* **1**, 5–11.

Castelletto, N., Ferronato, M., Gambolati, G., Putti, M. & Teatini, P. (2008) Can Venice be raised by pumping water underground? A pilot project to help decide. *Water Resour. Res.* **44**(W01408), doi:10.1029/2007WR006177.

Chin, L. Y. & Nagel, N. B. (2004) Modeling of subsidence and reservoir compaction under waterflood operations. *Int. J. Geomech.* **4**, 28–34.

Comerlati A., Ferronato, M., Gambolati, G., Putti, M. & Teatini, P. (2003) Can CO_2 help save Venice from the sea? *EOS-Trans. Am. Geophys. U.* **84**(49), 546–553.

Comerlati, A., Ferronato, M., Gambolati, G., Putti, M. & Teatini, P. (2004) Saving Venice by sea water. *J. Geophys. Res.*, **109**(F03006), doi:10.1029/2004JF000119.

Coussy, O. (2004) *Poromechanics*. J. Wiley and Sons, West Sussex, UK.

Dawson, C. N. (1993) Godunov-Mixed Methods for advection-diffusion equations in multidimensions. *SIAM J. Numer. Anal.* **30**, 1315–1332.

Fjaer, E., Holt, R.M., Horsrud, P., Raaen, A.M. & Risnes, R. (2008) *Petroleum Related Rock Mechanics* (2nd edn). Elsevier, Amsterdam and Oxford, UK.

Gambolati, G., Ferronato, M., Teatini, P., Deidda, R. & Lecca, G. (2001) Finite Element analysis of land subsidence above depleted reservoirs with pore pressure gradient and total stress formulations. *Int. J. Numer. Anal. Meth. Geomech.* **25**, 307–327.

Mattavelli, L. & Novelli, L (1990) Geochemistry and habitat of the oils in Italy. *Am. Assoc. Petr. Geol. B.* **74**, 1623–1639.

"Venezia altimetria", aggiornamento (2009) A cura di L. Boato, P. Canestrelli, L. Facchin e R. Todaro. Comune di Venezia – Istituzione centro previsioni e segnalazioni maree in collaborazione con Insula SpA (in Italian).

Wagner, W. & Kretzschmar, H.-J. (2008) *International Steam Tables – Properties of Water and Steam Based on the Industrial Formulation IAPWS*-IF97 (2nd edn). Springer-Verlag, Berlin, Germany.

(Proceedings of EISOLS 2010, Querétaro, Mexico, 17–22 October 2010). IAHS Publ. 339, 2010.

An analytical solution of plane strain consolidation due to a point sink within a fluid-saturated poroelastic media

PEI-CHAO LI[1], YUE-LEI HE[1], YI-MING MI[1] & SHI-LIANG GONG[2]

1 *Shanghai University of Engineering Science, Shanghai 201620, China*
wiselee@sues.edu.cn; wiselee18@163.com

2 *Center for Land Subsidence of China Geological Survey, Shanghai 200072, China*

Abstract An analytical solution was derived for the general Biot's consolidation theory within a finite two-dimensional (2-D) poroelastic media due to a point sink/source when the pore pressure is prescribed on the boundary. Appropriate Fourier and Laplace transforms and the corresponding inversions were implemented to obtain the exact solution. In particular, the steady-state analytical solution due to a point sink of constant production rate was presented and validated by the exact solution available in the literature. The proposed analytical solution in this paper is highly applicable for testing the accuracy of numerical schemes, and also can be of great use to further investigate the behaviour of flow and deformation coupling in a finite 2-D domain.

Key words finite 2-D poroelastic media; plane strain consolidation; finite sine and cosine transforms; analytical solution

INTRODUCTION

It is well-known that the poroelastic theory originated from Biot's three-dimensional consolidation theory of water-saturated soft clay (Biot, 1941; Biot & Willis, 1957), has been widely accepted and used in soil and rock mechanics.

The analytical methods and advances in geomechanics have been reviewed by some scholars such as Gibson (1974) and Selvadurai (2007). McNamee & Gibson (1960) presented the analytical solutions of plane strain and axially symmetric consolidations under loading. Concerning soil consolidation problems induced by a point source/sink, there have been quite a few exact solutions reported in the literatures, such as Booker & Carter (1986), Tarn & Lu (1991), and Chen (2003). However, most of them are for three-dimensional domains (such as the half-space). Barry & Mercer (1999) first gave the analytical solution of flow-deformation coupling due to a point source/sink within a finite 2-D region. The mathematical model adopted by Barry & Mercer (1999) is the incompressible porous media model. In this paper we manage to propose the exact solution for the compressible porous media model (also called the general Biot's consolidation theory) in a finite 2-D domain.

MATHEMATICAL MODEL

Now, let us consider the consolidation problem caused by a point sink/source within a finite 2-D domain of $x = a$ and $z = b$ shown in Fig. 1. Obviously, it can be regarded as a plane strain problem in the x–z plane. Here, we assume that: (1) Porous media are linear elastic, isotropic, and homogeneous, and their deformation accords with the assumption of the small strain. (2) Porous media are saturated by a single-phase pore fluid, and the flow obeys Darcy's law. Under the above assumptions, the poroelastic equations (i.e. the compressible porous media model) are simplified to:

$$(m+1)\frac{\partial^2 u}{\partial x^2}+\frac{\partial^2 u}{\partial z^2}+m\frac{\partial^2 w}{\partial x\partial z}-\frac{\alpha}{G}\frac{\partial p}{\partial x}=0 \tag{1a}$$

$$(m+1)\frac{\partial^2 w}{\partial z^2}+\frac{\partial^2 w}{\partial x^2}+m\frac{\partial^2 u}{\partial x\partial z}-\frac{\alpha}{G}\frac{\partial p}{\partial z}=0 \tag{1b}$$

Copyright © 2010 IAHS Press

$$\frac{\partial^2 p}{\partial x^2}+\frac{\partial^2 p}{\partial z^2}=\frac{\alpha}{\lambda_f}\frac{\partial \varepsilon_V}{\partial t}+\frac{1}{\chi}\frac{\partial p}{\partial t}-\frac{1}{\lambda_f}q \tag{1c}$$

where, $\alpha=1-K_b/K_s$, denotes Biot's poroelastic coefficient, q is the source intensity per unit bulk volume (positive for source and negative for sink), $\lambda_f=K/\mu_f$ is the fluidity of pore fluid, $\varepsilon_V=\partial u/\partial x+\partial w/\partial z$ is the bulk volumetric strain, $m=1/(1-2v)$, v is the Poisson's ratio, and $\chi=\lambda_f/(\phi C_t)$ is called the diffusivity coefficient, wherein, $\phi C_t=\phi/K_f+(\alpha-\phi)/K_s$.

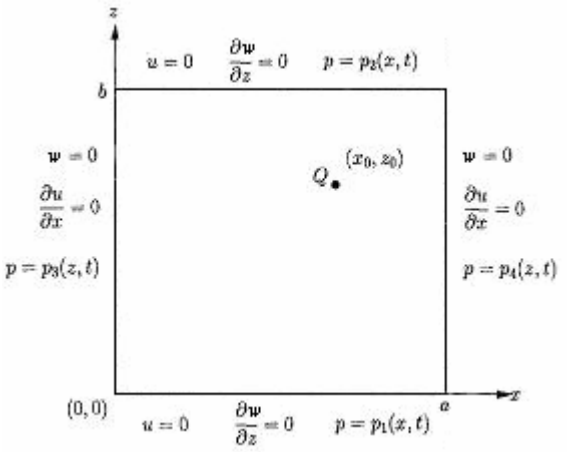

Fig. 1 Schematic diagram of a finite poroelastic media (Barry & Mercer, 1999).

If the compressibility of both pore fluid and solid skeleton is ignored, i.e. $K_f\to\infty, K_s\to\infty$, thus we have $\alpha\to 1$, $1/\chi\to 0$. Then equation (1) reduces to:

$$(m+1)\frac{\partial^2 u}{\partial x^2}+\frac{\partial^2 u}{\partial z^2}+m\frac{\partial^2 w}{\partial x\partial z}-\frac{1}{G}\frac{\partial p}{\partial x}=0 \tag{2a}$$

$$(m+1)\frac{\partial^2 w}{\partial z^2}+\frac{\partial^2 w}{\partial x^2}+m\frac{\partial^2 u}{\partial x\partial z}-\frac{1}{G}\frac{\partial p}{\partial z}=0 \tag{2b}$$

$$\frac{\partial^2 p}{\partial x^2}+\frac{\partial^2 p}{\partial z^2}=\frac{1}{\lambda_f}\frac{\partial \varepsilon_V}{\partial t}-\frac{1}{\lambda_f}q \tag{2c}$$

In fact, equation (2) is exactly the incompressible porous media model used by Barry & Mercer (1999).

For simplicity, we assume the boundary conditions take the same form as those of Barry & Mercer (1999), namely, the pore pressure boundary conditions are $p=p_1(x,t)$, on $z=0$, $p=p_2(x,t)$, on $z=b$, $p=p_3(z,t)$, on $x=0$, and $p=p_4(z,t)$, on $x=a$, with boundary conditions of the displacements field satisfying on $z=0$ and $z=b$, $u=0,\partial w/\partial z=0,$ and on $x=0$ and $x=a$, $w=0,\partial u/\partial x=0$.

The above boundary conditions are illustrated in Fig. 1. Meanwhile, we can assume the initial conditions as $u(x,z,t=0)=0, w(x,z,t=0)=0,$ and $p(x,z,t=0)=0$.

The governing equations, equations (1) and the above boundary and initial conditions constitute a definite problem. In the following sections, we shall concentrate on the analytical solving of the definite problem.

INTEGRAL TRANSFORMS AND INVERSIONS

For the studied problem, finite Fourier transforms and Laplace transforms can be applied to obtain the analytical solution (Barry & Mercer, 1999). The transformed variables are defined as:

$$\overline{u}(n,q,s) = LC_{xn}S_{zq}\{u(x,z,t)\},\ \overline{w}(n,q,s) = LS_{xn}C_{zq}\{w(x,z,t)\},\ \overline{p}(n,q,s) = LS_{xn}S_{zq}\{p(x,z,t)\} \tag{3}$$

Applying $LC_{xn}S_{zq}\{Eq.(1a)\}$, $LS_{xn}C_{zq}\{Eq.(1b)\}$, $LS_{xn}S_{zq}\{Eq.(1c)\}$ gives:

$$A\begin{bmatrix}\overline{u}\\ \overline{w}\\ \overline{p}\end{bmatrix} = B \tag{4}$$

where:

$$A = \begin{pmatrix}(m+1)\lambda_n^{\,2}+\lambda_q^{\,2} & m\lambda_n\lambda_q & \alpha\lambda_n/G\\ m\lambda_n\lambda_q & (m+1)\lambda_q^{\,2}+\lambda_n^{\,2} & \alpha\lambda_q/G\\ \alpha\lambda_n/\lambda_f & \alpha\lambda_q/\lambda_f & -(\lambda_n^{\,2}+\lambda_q^{\,2})/s-1/\chi\end{pmatrix}, B = \begin{pmatrix}\alpha B_1/G\\ \alpha B_2/G\\ B_3\end{pmatrix},$$

with: $\lambda_n = n\pi/a$, $\lambda_q = q\pi/b$, $\overline{q}(n,q,s) = LS_{xn}S_{zq}\{q(x,z,t)\}$, $B_1 = \overline{p}_3 - (-1)^n\overline{p}_4$, $B_2 = \overline{p}_1 - (-1)^q\overline{p}_2$,

$B_3 = -\dfrac{1}{s}(\lambda_n B_1 + \lambda_q B_2 + \overline{q}/\lambda_f)$, where $\overline{p}_1(n,s) = LS_{xn}\{p_1(x,t)\}, \overline{p}_2(n,s) = LS_{xn}\{p_2(x,t)\},$
$\overline{p}_3(q,s) = LS_{zq}\{p_3(z,t)\}, \overline{p}_4(q,s) = LS_{zq}\{p_4(z,t)\}.$

The solution of the set of equations (4) can be given by simple matrix inversion:

$$\overline{u}(n,q,s) = B_1\frac{\alpha(\alpha^2\lambda_q^2 s + G\lambda_f(\lambda_q^2(m+1)(\lambda_q^2+s/\chi)+\lambda_n^2(\lambda_q^2(m+1)+s/\chi)))}{G\tilde{\lambda}^2(\alpha^2 s+G(m+1)\lambda_f(\tilde{\lambda}+s/\chi))} + B_2\frac{-\alpha\lambda_n\lambda_q(\alpha^2 s+G\lambda_f((m+1)\tilde{\lambda}+ms/\chi))}{G\tilde{\lambda}^2(\alpha^2 s+G(m+1)\lambda_f(\tilde{\lambda}+s/\chi))}$$
$$+\overline{q}\frac{-\alpha\lambda_n}{\tilde{\lambda}(\alpha^2 s+G(m+1)\lambda_f(\tilde{\lambda}+s/\chi))} \tag{5a}$$

$$\overline{w}(n,q,s) = B_1\frac{-\alpha\lambda_n\lambda_q(\alpha^2 s+G\lambda_f((m+1)\tilde{\lambda}+ms/\chi))}{G\tilde{\lambda}^2(\alpha^2 s+G(m+1)\lambda_f(\tilde{\lambda}+s/\chi))} + B_2\frac{\alpha(\alpha^2\lambda_n^2 s+G\lambda_f(\lambda_n^2(m+1)(\lambda_q^2+s/\chi)+\lambda_n^4(m+1)+\lambda_q^2 s/\chi))}{G\tilde{\lambda}^2(\alpha^2 s+G(m+1)\lambda_f(\tilde{\lambda}+s/\chi))}$$
$$+\overline{q}\frac{-\alpha\lambda_q}{\tilde{\lambda}(\alpha^2 s+G(m+1)\lambda_f(\tilde{\lambda}+s/\chi))} \tag{5b}$$

$$\overline{p}(n,q,s) = B_1\frac{\lambda_n(\alpha^2 s+G(m+1)\lambda_f\tilde{\lambda})}{\tilde{\lambda}(\alpha^2 s+G(m+1)\lambda_f(\tilde{\lambda}+s/\chi))} + B_2\frac{\lambda_q(\alpha^2 s+G\lambda_f(m+1)\tilde{\lambda})}{\tilde{\lambda}(\alpha^2 s+G(m+1)\lambda_f(\tilde{\lambda}+s/\chi))} + \overline{q}\frac{G(m+1)}{\alpha^2 s+G(m+1)\lambda_f(\tilde{\lambda}+s/\chi)} \tag{5c}$$

where $\tilde{\lambda} = \lambda_n^{\,2}+\lambda_q^{\,2}$.

The above formulae, equations (5a)–(5c) are the analytical solutions of the studied problem in the transformed domain. It is clear that the parameters of solid skeleton and pore fluid properties such as α and χ are included in the solutions, where the effects of poroelasticity and compressibility are embodied, whereas these factors cannot be involved in the solution of the incompressible porous model (i.e. equation (19) of Barry & Mercer (1999)). As for the incompressible porous model, one has $\alpha \to 1$, and $1/\chi \to 0$, thus equations (5) reduce to:

$$\overline{u}(n,q,s) = B_1\frac{\lambda_q^2}{G\tilde{\lambda}^2} + B_2\frac{-\lambda_n\lambda_q}{G\tilde{\lambda}^2} + \overline{q}\frac{-\lambda_n}{\tilde{\lambda}(s+G(m+1)\lambda_f\tilde{\lambda})} \tag{5a′}$$

$$\overline{w}(n,q,s) = B_1\frac{-\lambda_n\lambda_q}{G\tilde{\lambda}^2} + B_2\frac{\lambda_n^2}{G\tilde{\lambda}^2} + \overline{q}\frac{-\lambda_q}{\tilde{\lambda}(s+G(m+1)\lambda_f\tilde{\lambda})} \tag{5b′}$$

$$\overline{p}(n,q,s) = B_1\frac{\lambda_n}{\tilde{\lambda}} + B_2\frac{\lambda_q}{\tilde{\lambda}} + \overline{q}\frac{G(m+1)}{s+G(m+1)\lambda_f\tilde{\lambda}} \tag{5c′}$$

Equations (5a′)–(5c′) are similar to equation (19) of Barry & Mercer (1999). The former is in the

form of dimensions, while the latter is dimensionless. It turns out that they are exactly the same if the conversions between them are taken into consideration. This confirms that Barry's results are particular cases of the results in this paper.

The analytical solutions of the problem in the physical space can be obtained by applying triple inversions to equations (5):

$$u(x,z,t)=\frac{2}{ab}\sum_{q=1}^{\infty}\bar{u}(0,q,t)\sin(\lambda_q z)+\frac{4}{ab}\sum_{q=1}^{\infty}\sum_{n=1}^{\infty}\bar{u}(n,q,t)\cos(\lambda_n x)\sin(\lambda_q z) \tag{6a}$$

$$w(x,z,t)=\frac{2}{ab}\sum_{n=1}^{\infty}\bar{w}(n,0,t)\sin(\lambda_n x)+\frac{4}{ab}\sum_{q=1}^{\infty}\sum_{n=1}^{\infty}\bar{w}(n,q,t)\sin(\lambda_n x)\cos(\lambda_q z) \tag{6b}$$

$$p(x,z,t)=\frac{4}{ab}\sum_{q=1}^{\infty}\sum_{n=1}^{\infty}\bar{p}(n,q,t)\sin(\lambda_n x)\sin(\lambda_q z) \tag{6c}$$

ANALYTICAL SOLUTION OF A CONSTANT FLUX POINT SINK/SOURCE

The pressure on the boundary can be prescribed as zero, that is, $p_1 = p_2 = p_3 = p_4 = 0$, then one has $B_1 = B_2 = 0$. Substituting this into equations (5) yields:

$$\bar{u}(n,q,s)=\frac{-\alpha\lambda_n\bar{q}}{\tilde{\lambda}(\alpha^2 s+G(m+1)\lambda_f(\tilde{\lambda}+s/\chi))} \tag{7a}$$

$$\bar{w}(n,q,s)=\frac{-\alpha\lambda_q\bar{q}}{\tilde{\lambda}(\alpha^2 s+G(m+1)\lambda_f(\tilde{\lambda}+s/\chi))} \tag{7b}$$

$$\bar{p}(n,q,s)=\frac{G(m+1)\bar{q}}{\alpha^2 s+G(m+1)\lambda_f(\tilde{\lambda}+s/\chi)} \tag{7c}$$

If the pump rate is assumed to be a constant, i.e. $q(x,z,t)=q_0\delta(x-x_0)\delta(z-z_0)$, then, applying equation (3) gives:

$$\bar{q}(n,q,s)=\frac{q_0\sin(\lambda_n x_0)\sin(\lambda_q z_0)}{s} \tag{8}$$

Substitution of equation (8) into equations (7a)–(7c) leads to:

$$\bar{u}(n,q,s)=\frac{-\alpha q_0\lambda_n\sin(\lambda_n x_0)\sin(\lambda_q z_0)}{\tilde{\lambda}s(\alpha^2 s+G(m+1)\lambda_f(\tilde{\lambda}+s/\chi))} \tag{9a}$$

$$\bar{w}(n,q,s)=\frac{-\alpha q_0\lambda_q\sin(\lambda_n x_0)\sin(\lambda_q z_0)}{\tilde{\lambda}s(\alpha^2 s+G(m+1)\lambda_f(\tilde{\lambda}+s/\chi))} \tag{9b}$$

$$\bar{p}(n,q,s)=\frac{G(m+1)q_0\sin(\lambda_n x_0)\sin(\lambda_q z_0)}{s(\alpha^2 s+G(m+1)\lambda_f(\tilde{\lambda}+s/\chi))} \tag{9c}$$

Taking L^{-1}\{equations (9a)–(9c)\} we obtain:

$$\bar{u}(n,q,t)=\frac{-\alpha\lambda_n q_0\sin(\lambda_n x_0)\sin(\lambda_q z_0)(1-e^{-\frac{G\lambda_f\tilde{\lambda}(m+1)t}{\alpha^2+G\lambda_f(m+1)/\chi}})}{G\lambda_f(m+1)\tilde{\lambda}^2} \tag{10a}$$

$$\overline{w}(n,q,t)=\frac{-\alpha\lambda_q q_0 \sin(\lambda_n x_0)\sin(\lambda_q z_0)(1-e^{-\frac{G\lambda_f\tilde{\lambda}(m+1)t}{\alpha^2+G\lambda_f(m+1)/\chi}})}{G\lambda_f(m+1)\tilde{\lambda}^2} \tag{10b}$$

$$\overline{p}(n,q,t)=\frac{q_0 \sin(\lambda_n x_0)\sin(\lambda_q z_0)(1-e^{-\frac{G\lambda_f\tilde{\lambda}(m+1)t}{\alpha^2+G\lambda_f(m+1)/\chi}})}{\lambda_f\tilde{\lambda}} \tag{10c}$$

Eventually, the constant flux point sink/source solution in the physical domain is given by substituting equations (10a)–(10c) into equations (6a)–(6c).

COMPARISON WITH AVAILABLE ANALYTICAL SOLUTIONS

The solution as t approaches infinity is usually called the long-term (steady-state) solution. When $t\to\infty$, we have $\overline{u}(n,q,t\to\infty)=\frac{-\alpha\lambda_n q_0 \sin(\lambda_n x_0)\sin(\lambda_q z_0)}{G\lambda_f(m+1)\tilde{\lambda}^2}$, $\overline{w}(n,q,t\to\infty)=\frac{-\alpha\lambda_q q_0 \sin(\lambda_n x_0)\sin(\lambda_q z_0)}{G\lambda_f(m+1)\tilde{\lambda}^2}$, $\overline{p}(n,q,t\to\infty)=\frac{q_0 \sin(\lambda_n x_0)\sin(\lambda_q z_0)}{\lambda_f\tilde{\lambda}}$, and $\overline{w}(n,0,t\to\infty)=0$, $\overline{u}(0,q,t\to\infty)=0$. Substitution of these into equations (6a)–(6c) leads to the steady analytical solutions as below:

$$u(x,z,t\to\infty)=\frac{4}{ab}\sum_{q=1}^{\infty}\sum_{n=1}^{\infty}\frac{-\alpha\lambda_n q_0 \sin(\lambda_n x_0)\sin(\lambda_q z_0)}{G\lambda_f(m+1)\tilde{\lambda}^2}\cos(\lambda_n x)\sin(\lambda_q z) \tag{11a}$$

$$w(x,z,t\to\infty)=\frac{4}{ab}\sum_{q=1}^{\infty}\sum_{n=1}^{\infty}\frac{-\alpha\lambda_q q_0 \sin(\lambda_n x_0)\sin(\lambda_q z_0)}{G\lambda_f(m+1)\tilde{\lambda}^2}\sin(\lambda_n x)\cos(\lambda_q z) \tag{11b}$$

$$p(x,z,t\to\infty)=\frac{4}{ab}\sum_{q=1}^{\infty}\sum_{n=1}^{\infty}\frac{q_0 \sin(\lambda_n x_0)\sin(\lambda_q z_0)}{\lambda_f\tilde{\lambda}}\sin(\lambda_n x)\sin(\lambda_q z) \tag{11c}$$

The steady solution of the pressure proposed by Kong (1999; let $t\to\infty$ and $p(x,z,t=0)=0$ in equation (3.6.56)) is:

$$p(x,z,t\to\infty)=-\frac{4q_1}{\pi^2\lambda_f ab}\sum_{q=1}^{\infty}\sum_{n=1}^{\infty}\left(\frac{n^2}{a^2}+\frac{q^2}{b^2}\right)^{-1}\cdot\sin\left(\frac{n\pi l}{a}\right)\sin\left(\frac{q\pi d}{b}\right)\sin\left(\frac{n\pi x}{a}\right)\sin\left(\frac{q\pi z}{b}\right) \tag{12}$$

where, q_1 is the point sink with constant production rate.

According to equation (1c), we have $q_0=-q_1$. Allowing for $\lambda_n=n\pi/a$, $\lambda_q=q\pi/b$, $x_0=l$, $z_0=d$, and $\tilde{\lambda}=\lambda_n{}^2+\lambda_q{}^2$, equation (11c) can be rewritten as:

$$p(x,z,t\to\infty)=-\frac{4q_1}{\pi^2\lambda_f ab}\sum_{q=1}^{\infty}\sum_{n=1}^{\infty}\left(\frac{n^2}{a^2}+\frac{q^2}{b^2}\right)^{-1}\cdot\sin\left(\frac{n\pi l}{a}\right)\sin\left(\frac{q\pi d}{b}\right)\sin\left(\frac{n\pi x}{a}\right)\sin\left(\frac{q\pi z}{b}\right) \tag{13}$$

It is obvious that equation (13) and equation (12) are identical. This verifies the correctness of the analytical solution proposed in this paper. Moreover, the steady analytical solutions for displacements are given as equations (11a) –(11b) simultaneously.

CONCLUSIONS

We presented an analytical solution for plane strain consolidation due to a point sink/source within a finite 2-D compressible porous media. It depicts that the analytical solution of the incompressible porous media model can be regarded as particular cases of the solution presented in this paper. Then the steady solution for a constant flux point sink is further given and compared

with the available analytical solution. The complete consistency between them confirms the accuracy and reliability of the proposed analytical solution.

Acknowledgements This work was partially funded by the Shanghai Leading Academic Discipline Project (no. P1401) and the Special Research Fund for Excellent Young College Teachers of Shanghai (no. GJD09029).

REFERENCES

Barry, S. I. & Mercer, G. N. (1999) Exact solutions for two dimensional time dependent flow and deformation within a poroelastic medium. *J. Appl. Mech.* **66**, 536–540.

Biot, M. A. (1941) General theory of three-dimensional consolidation. *J. Appl. Phys.* **12**, 155–164.

Biot, M. A. & Willis, D. G. (1957) The elastic coefficients of the theory of consolidation. *J. Appl. Mech.* **24**, 594–601.

Booker, J. R. & Carter, J. P. (1986) Analysis of a point sink embedded in a porous elastic half space. *Int. J. Numer. Anal. Meth. Geomech.* **10**(2), 137–150.

Chen, G. J. (2003) Analysis of pumping in multilayered and poroelastic half space. *Comput. Geotech.* **30**, 1–26.

Gibson, R. E. (1974) The analytical method in soil mechanics. *Geotechnique* **24**, 115–140.

Kong, X. Y. (1999) *Advanced Mechanics of Fluids in Porous Media*. Press of University of Science and Technology of China, Hefei, Anhui, China. (in Chinese)

McNamee, J. & Gibson, R. E. (1960) Plane strain and axially symmetric problems of the consolidation of a semi-infinite clay stratum. *Quart. J. Mech. Appl. Math.* **13**, 210–227.

Selvadurai, A. P. S. (2007) The analytical method in geomechanics. *Appl. Mech. Rev.* **60**, 87–106.

Tarn, J. Q. & Lu, C. C. (1991) Analysis of subsidence due to a point sink in an anisotropic porous elastic half space. *Int. J. Numer. Anal. Meth. Geomech.* **15**(8), 573–592.

(Proceedings of EISOLS 2010, Querétaro, Mexico, 17–22 October 2010). IAHS Publ. 339, 2010.

Research on a 3-D visualized strata model virtual reality system of land subsidence in Suzhou-Wuxi-Changzhou area

YU JUN[1,2], SU XIAO-SI[3], ZHU LIN[4], DUAN FU-ZHOU[4], PAN YUN[4], GAO LI[3] & WU SHU-LIANG[1]

1 *Postdoctoral Fellowship of Geological Survey of Jiangsu Province, Nanjing 210018, China*
2 *Postdoctoral Program of Jilin University, Changchun 130026, China*
njhzmyj@163.com
3 *College of Environment and Resource, Jilin University, Changchun 130026, China*
4 *The Key Lab of Three-Dimensional Analysis and Application, Capital Normal University, Beijing 100037, China*

Abstract Due to the requirements of land subsidence research in theSuzhou-Wuxi-Changzhou area, a three dimensional land subsidence virtual reality system was developed based on virtual reality technology. This paper gives a general introduction to the framework, method and functions of the 3-D land subsidence virtual reality system. This system can simulate the 3-D geological structure, the groundwater flow field, the dynamic process of land subsidence, and the sequence induced by the occurrence of land subsidence. The basic metadata for simulation is derived from the land subsidence numerical model, field data and literature data. It can be concluded that this virtual system is an effective visualization platform for studying the mechanism, process and forecasting of land subsidence in the Suzhou-Wuxi-Changzhou area.

Key words land subsidence; virtual reality; geological structure; Suzhou-Wuxi-Changzhou area, China

INTRODUCTION

Research on the land subsidence in the Suzhou-Wuxi-Changzhou area of China has been carried out for many years. Computer technology has been applied to analyse and simulate the land subsidence. A lot of data and outputs have been accumulated. For example, the Ground Subsidence Information Management System (GSIMS) has been developed to realize the monitoring, analysis and management of the land subsidence in this area. But there are still some deficiencies in expressing the research results. Generally, the two-dimensional expression cannot faithfully reflect the three-dimensional land subsidence, the relationship between land subsidence and the affected factors, the dynamic process of land subsidence, and the disaster caused by land subsidence in three dimensions. All of these limit the understanding, analysis, prevention and control of the land subsidence.

Virtual Reality Technology (VRT) was proposed by the American Professor Ivan Sutherland in the 1960s, and quickly developed in the 1990s. It is an effective graphic tool for solving the above-mentioned problems. The VR technology had been successfully applied in the fields of the military, manufacturing, geography, and so on. But in the field of land subsidence, there is little such research except for that on the hydro-geological strata and groundwater surface (Yan, 2004; Ross, 2005; Thurmond, 2005; Liang, 2005), and no mature software for VRT application. In this study, the 3-D visualized land subsidence virtual reality system (LSVRS) of Suzhou-Wuxi-Changzhou area has been developed based on VRT. The LSVRS can faithfully simulate the 3-D geological structure in Suzhou-Wuxi-Changzhou area, and can display the dynamic process of land subsidence in this area and the possible future subsidence, in 3-D, based on the result of the coupling numerical model of groundwater and land subsidence (Xue *et al*., 2005). And the LSVRS can also be used to analyse the relationship between strata, groundwater level and land subsidence. This paper briefly introduces this system.

GENERAL STRUCTURE OF LSVRS

The LSVRS is composed of the database management module and the virtual reality module. Given the complexity and the large amount of multiple data for visualizing the land subsidence in

Copyright © 2010 IAHS Press

Suzhou-Wuxi-Changzhou area, the database management module is designed to store the data including basic data (such as stratigraphic structure information, groundwater level, amount of accumulative land subsidence), graphic data (such as topographic contour lines), and image data (such as remote sensing images, rock texture). The SQL Server 2000 is the platform used for managing the database. Many operations such as query, add, and delete can be manipulated.

The virtual reality module, the core part of the system, is mainly for the real-time display of the geological structure, the groundwater surface, the land subsidence and its consequences, based on the database. The virtual reality module is developed on the basis of using OpenGL as the graphic tool. OpenGL, a 3-D graphics software library developed by SGI, is composed of hundreds of commands and functions for creating real-time 3-D graphics, and is a software development kit (SDK). OpenGL can realize the virtual reality expression with better quality and can realize the interactive operation with the simulated objections.

There is an effective link between the virtual reality module and the database management module. For example, the data of the simulated objects, such as geological structure, can be imported to the database management module. Once the researchers want to observe the virtual objects, these data can be output from the database and edited.

LSVRS

The LSVRS foreground interface (see Fig. 1) contains 11 parts. They are: geological structure simulation, model editing, visual parameter setting, groundwater surface simulation, land subsidence simulation, landscape simulation, flood submerging simulation, roaming tools, output tool, windows show, and help, separately.

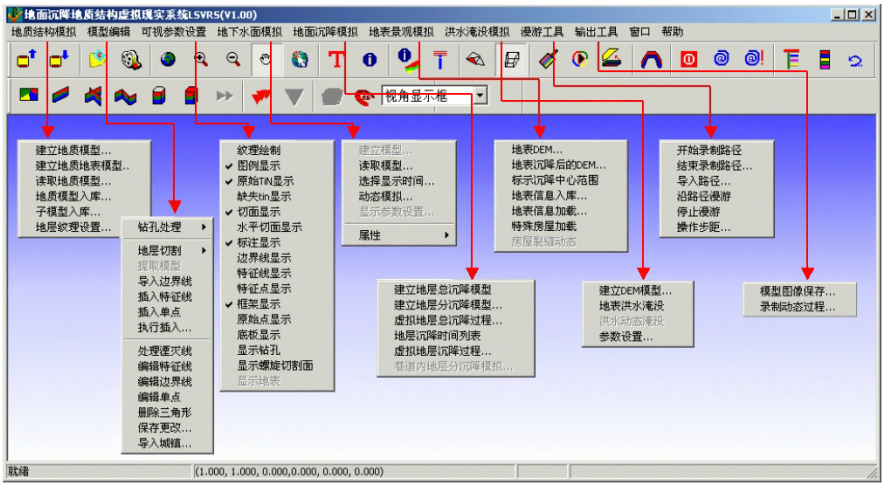

Fig. 1 The UI for main module of LSVRS.

The main functions of the LSVRS are described as follows. The menu of *geological structure simulation* is to construct the 3-D geological structure, import and store model data. *Model editing* can be used to edit the visualized model such as adding some feature points, or lines in accordance with the actual geological condition. The *visual parameter settings* menu is mainly to control the visualization pattern and contents shown. The menus of *groundwater surface simulation*, *land subsidence*, *landscape simulation* and *flood submerging simulation* are mainly used for building, storing, the groundwater surface visualization model, land subsidence, landscape, and flood submerging separately, and for showing their dynamic procedure. The menu of *roaming tools* can be used to set the roaming path, direction and space parameters. And the menu of *output tool* is for outputting the visualized model or dynamic processes generated by the LSVRS in the form of a picture or image file.

Geological structure model

The geological structure model is the basis of the LSVRS for visualizing land subsidence, groundwater flow and other simulated objects. The geological strata model is constructed by using the drill-hole data, the missing boundary of the stratum, and the isolith of the stratum. The detailed modelling process is shown in some lectures (Zhu *et al*., 2007, 2009). The original geological structure model is composed of a series of TIN (Triangulated Irregular Network), which is different from the real strata. To enhance the simulated effect, the real strata texture images are bound to the TIN by using the texture mapping function of OpenGL. And the lighting function is used to simulate the vivid 3-D geological strata. The users can operate many operations on the visualized model such as a slicing tool to form a strata cross-section, uncovering the strata one layer by one, and roaming into the strata in this model (see Fig. 2).

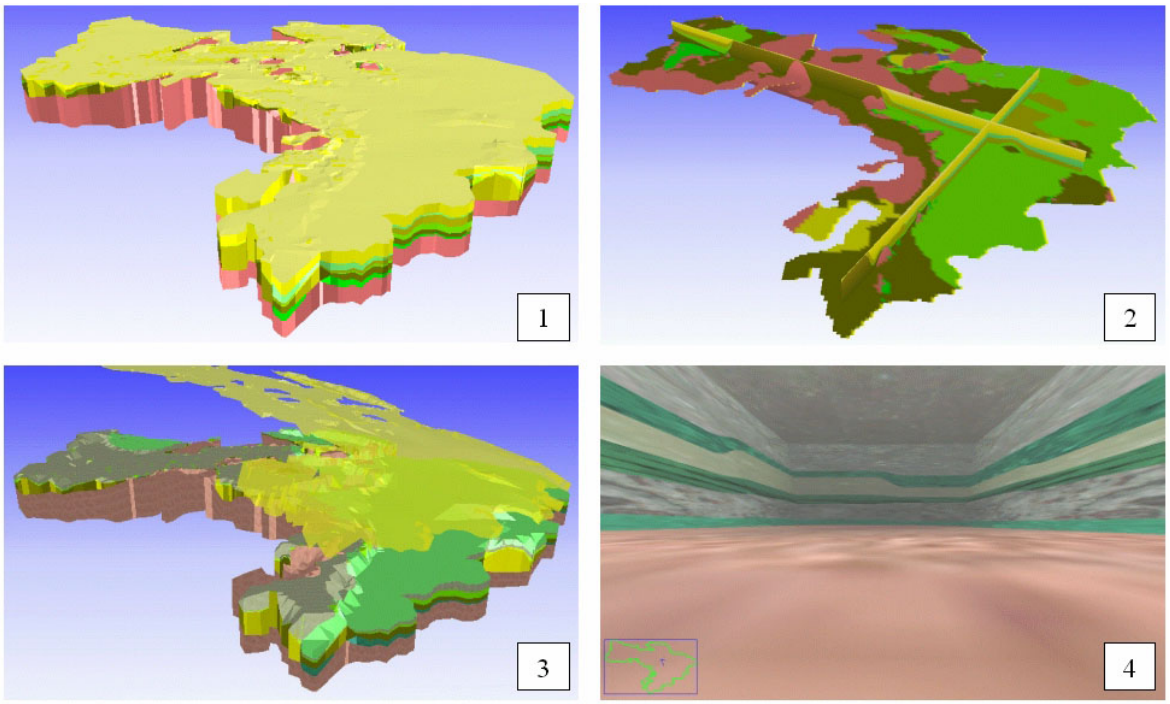

Fig. 2 Some functions of the 3-D strata model: (1) is a 3-D geological strata model; (2) shows the horizontal and vertical cross-sections via slicing operation; (3) shows the simulated model through one by one stratum; and (4) is roaming inside the strata.

Groundwater surface

The groundwater surface visualization model is constructed by using the monitoring data of groundwater level, and the output data of the numerical model, based on the 3-D geological structure model. Since the groundwater surface is similar to the DEM (Digital Elevation Model), TIN is used to simulate the "skeleton" and fluctuation of the groundwater surface. The value of every point is equal to the groundwater level, not the elevation. The modelling process was described by Zhu *et al*. (2007). The visualized 3-D groundwater surface model can be expressed in various modes (such as orthographic or perspective projection, colour rendering). The users can query the attributions of the groundwater surface, such as conductivity and specific yield, groundwater flow direction in 3-D space, water table contour, and display the fluctuation of the groundwater flow field (Fig. 3) by using the different operating tools.

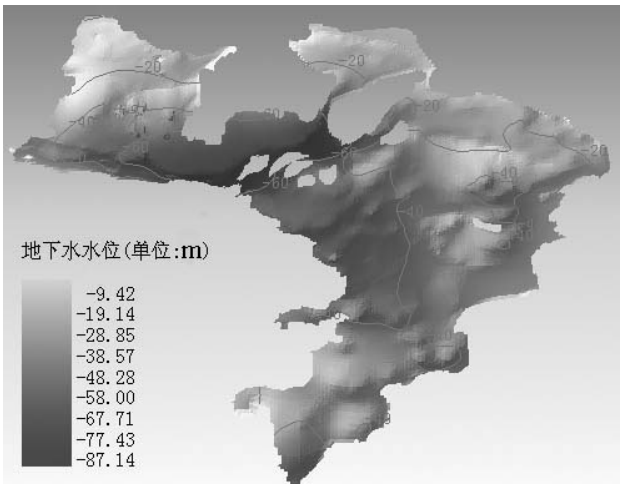

Fig. 3 3-D dynamic display of groundwater flow.

Land subsidence simulation

Based on the simulated 3-D geological structure model, the procedure of land subsidence can be displayed in 3-D by utilizing the output data of the numerical nonlinear land subsidence model (Xue *et al*., 2005) of the study area. With the accumulative land subsidence data, the elevations of each geological stratum are re-calculated. Firstly, these subsidence points are used to construct TIN (*A*) by using the Delaunay triangulation method. And the feature of every point of *A* is the amount of the accumulative land subsidence. Then, the elevation of every vertex, constituting the TIN of the geological stratum, is re-calculated by spatial interpolation based on *A*. The detailed process was described by Zhu *et al*. (2007, 2009). The users can observe the procedure of the land subsidence with colour rendering or texture pattern, outside the geological body or within the strata, by setting the environmental parameters (Fig. 4).

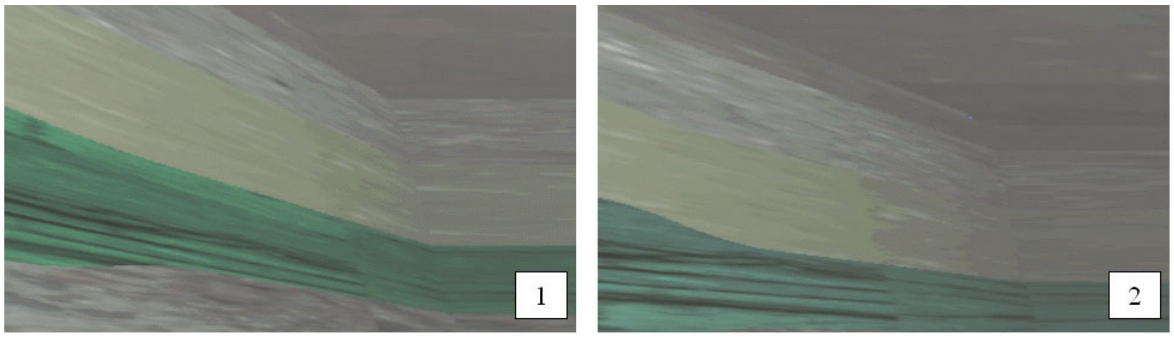

Fig. 4 Strata situation before and after land subsidence: (1) is the situation before land subsidence, and (2) is the situation after land subsidence.

Flood inundation simulation

The result caused by land subsidence is lowering of the ground elevation, which can also induce a settlement depression, failure of flood-controlling dams, flood inundation and so on. The seed algorithm was used to simulate the dynamic processes of flood inundation on the basis of the DEM. This algorithm was introduced by Pan *et al*. (2008). Users can obtain the flooding pattern and inundated area. The dynamic process of flooding can be simulated. It could be an effective tool for flood management (Fig. 5).

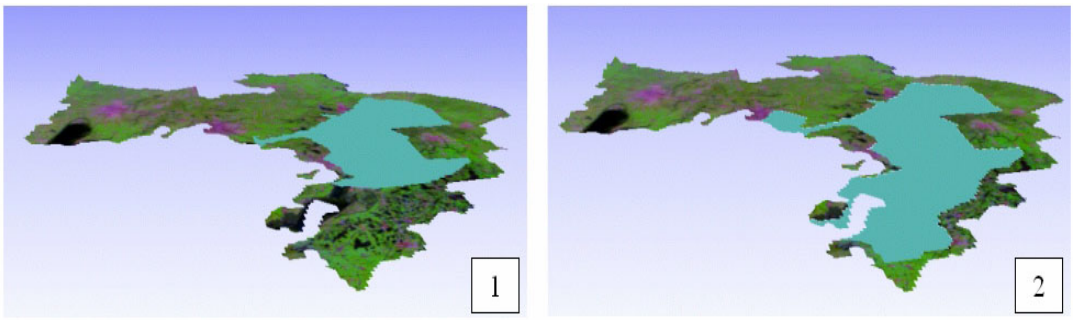

Fig. 5 Flood inundation spreading at time t1 and t2 (t2 > t1).

Landscape simulation

The uneven land subsidence can lead to the change of landscape. Here the volume visualization technology is used to construct the landscape model such as buildings, trees, grass, roads, and rivers. The sizes (height, width and length) of the virtual objects are real. Users can roam among the virtual environment by using mouse and keyboard. Since the direct result of land subsidence is ground fissure, the vector method and dynamic texture-mapping technology are used to simulate the dynamic processes of ground fissure, including the ground and building cracking (Zhu *et al.*, 2009) (Fig. 6).

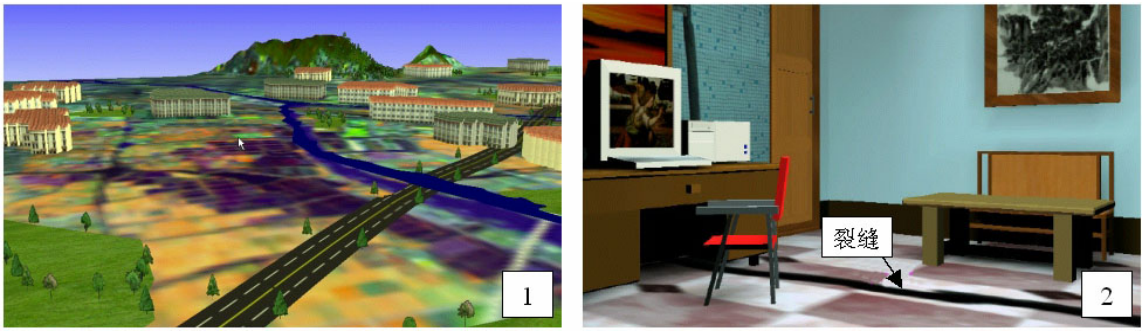

Fig. 6 Scenes of the environment and ground fissure in a house.

CONCLUSIONS

It can be concluded that the LSVRS is an effective tool for the study of hydrogeology and environmental geology. The LSVRS can be used for visualizing in 3-D the geological strata, the dynamic procedure of land subsidence and its consequences, and the groundwater flow field. This system has been successfully applied in the Suzhou-Wuxi-Changzhou area. The users can observe and manipulate the simulated objects.

Still, this study is in the initial stage. Further work will focus on improving the functions of each module, and enhancing the simulation effect.

Acknowledgements This research is funded by Geological Survey and Monitoring of the Ecological Environment in Jiangsu Province (project no. 200312300009, mission no. water [2003] 019-02).

REFERENCES

Liang Xiujuan, Lin Xueyu & Yu Jun (2005) Application of virtual reality technology in hydrogeological research. *J. Jilin University (Earth Science Edition)* **35**(5), 636–640.

Pan Yun, Nakagoshi Nobukazu & Gong Huili (2008) Using three-dimensional visualization tool to represent hydrological influence on wetland plants. *Ecohydrology & Hydrobiology* **8**(2-4), 317–329.

Ross, M., Parent, M. & Lefebvre, R. (2005) 3D geologic framework models for regional hydrogeology and land-use management: a case study from a Quaternary basin of southwestern Quebec, Canada. *Hydrogeol. J.* **13**(5), 690–707.

Thurmond, J. B., Drzewiecki, P. A. & Xueming Xu (2005) Building simple multiscale visualizations of outcrop geology using virtual reality modeling language(VRML). *Computers & Geosciences* **31**, 913–919.

Xue Yuqun, Wu Jichun, Ye shujun, *et al*., (2005) Research on the Land Subsidence Simulation in Suzhou-Wuxi-Changzhou area. Department of Earth Science, Nanjing University (Nanjing).

Yan Huiwu & Zhu Guorui, (2004) Research on volume visualisation of groundwater. *Wuhan University Press* **8**, 125–138.

Zhu Lin, Duan Fuzhou, *et al*. (2007) Application of virtual reality technology to modeling hydro-geological structure and hydraulic head in the Suzhou-Wuxi-Changzhou area, China. *Hydrogeology and Engineering Geology* (in Chinese) **2**, 63–66.

Zhu Lin, Gong Huili, Lin Xueyu, *et al*. (2009) Research on multi-scale 3D visualization technology of land subsidence. *Progress in Natural Science* (in Chinese) **19**, 1255–1260.

Zhu Lin, Su Xiaosi, Lin Xuyu, Gong Huili, *et al*. (2009) Application of VR-GIS in studying ground fracture in the western region of Wuxi area. *J. Jilin University (Earth Science Edition)* (in Chinese) **2**, 317–321.

Land Subsidence, Associated Hazards and the Role of Natural Resources Development
(Proceedings of EISOLS 2010, Querétaro, Mexico, 17–22 October 2010). IAHS Publ. 339, 2010.

Integration of geological and hydrogeological features for subsidence modelling in volcanic zones

GIL OCHOA-GONZÁLEZ[1] **& DORA CARREÓN-FREYRE**[2]

1 *Dept del habitat y desarrollo urbano, Instituto Tecnologico y de Estudios Superiores de Occidente (ITESO), Periferico Sur Manual Gomez Morin 8585, 45604, Tlaqupaque, Jalisco, Mexico*
gilochoa@iteso.mx

2 *Centro de Geociencias, Universidad Nacional Autonoma de Mexico (UNAM)*

Abstract Land subsidence is related to the increase of effective stresses in geological media. This work aims to propose a numerical model to simulate land subsidence and related fissuring caused by the reduction of the piezometric levels due to pumping. The proposed model includes different geological features that affect the groundwater flow patterns, such as faults as well as hydraulic and geomechanical anisotropy related to stratigraphic variations. The methodology consists in establishing a 3-D hydraulic model used for interpreting pumping tests in geological setting with the features described above. Then, using the finite element *Aster Code*, integrate variations of transmissivities caused by local stratigraphy and incorporate elasto-plastic behaviour in a 2-D simulation of deformation. Our results suggest that when subsidence occurs, not only the superficial compressible geological deposits should be considered but the sum of the whole sequence affected by piezometric level variations. We demonstrate that the local and regional faulting control the pattern of piezometric variations.

Key words numerical modelling; subsidence; Queretaro, Mexico; finite element Aster Code

INTRODUCTION

Major geological structures, such as faults, play an important role in land subsidence and earth fissuring (Burbey, 2002; Garduño *et al.*, 2001). In some places, earth fissuring is related to subsidence and geological faults; in such places one of the most recognized mechanisms causing soil fissuring occurs when compressible lacustrine-alluvial deposits with different thickness on both sides of a fault are deformed. These deposits reduce their thickness by consolidation provoking differential settlement across the fault. Faults are discontinuities of geological media that affect the dynamics of groundwater flow and the configuration of piezometric levels (Mayer *et al.*, 2007; MaClay & Small, 1983), subsequently affecting the distribution of effective stresses on both sides of the fault and within the fault zone.

The aim of this work is to evaluate how the subsidence occurs as groundwater in granular and faulted aquifer systems is extracted; the impact of faults on the variation of the piezometric levels during pumping is considered taking into account that faults can have hydraulic proprieties different to the surrounding material.

GEOLOGY AND FAULT ROLE

Geological setting

The area of study corresponds to the *Valle de Querétaro*, which is located within the Transmexican Volcanic Belt (TVM) (Fig. 1) where major fault systems with variable orientation have been observed (Alaniz *et al.*, 2001). Structurally, this valley corresponds to a tectonic graben that is filled with volcanic and lacustrine-alluvial deposits.

The stratigraphy of the Valley of Queretaro was described by Carreon-Freyre *et al.* (2005), and includes strata from Cretaceous limestone to Quaternary alluvium. However, a variety of Tertiary volcanic rocks (e.g. basalt, rhyolite, andesite) interbedded by lacustrine sediments and sedimentary rocks (e.g. conglomerate, sandstone and lutite) is predominant in the upper layers. The sequential stratigraphy is truncated by fault systems resulting in a highly heterogeneous medium.

Copyright © 2010 IAHS Press

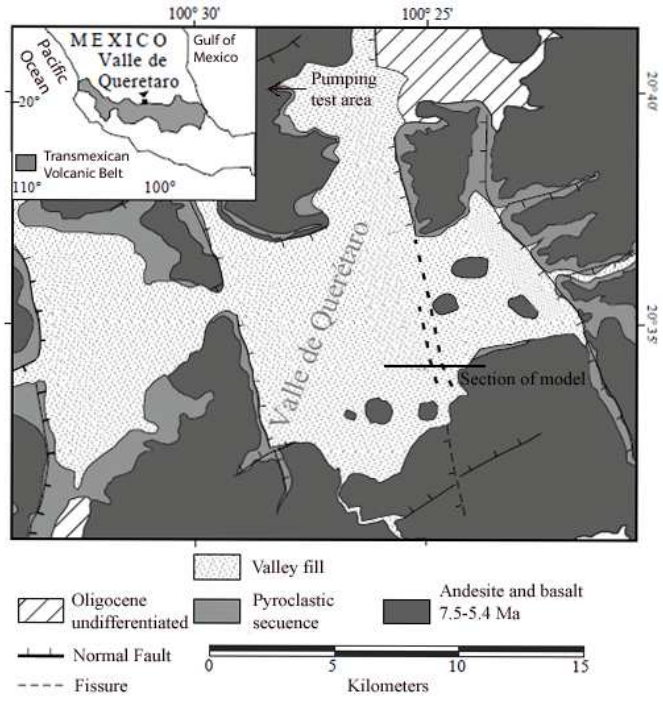

Fig. 1 Map of localization of the zone of study (from Carreón-Freyre *et al.* 2005).

Hydraulic features

Major geological structures like faults are critical to the behaviour of groundwater flow (Weinberger & Rosenthal, 1994; Allen & Michel, 1999; Bense & Van Balen, 2003; Bense *et al.*, 2003; Sultan *et al.*, 2007; Delinom, 2009). The reduction of the hydraulic conductivity across faults can occur by different mechanism such as those mentioned by Mayer *et al*. (2007): cataclasis, offsetting of permeable beds by impermeable beds, rotation of elongated and flat clasts parallel to the fault surface, tectonic mixing or smearing of beds of low hydraulic conductivity sediments, and deposition of minerals in the fault zone. Another mechanism that causes reduction of the hydraulic conductivity across the fault occurs if an aquifer is truncated by faults and if there is an offset with vertical displacement greater than 50% of the thickness of the aquifer. In this case the fault behaves like a potential hydraulic barrier reducing the capacity of the groundwater to flow across the fault, and therefore, causing this flow to be diverted along the fault (Maclay & Small 1982). Anderson (2006) describes how a fault can be hydraulically a high conductive zone; this occurs as a consequence of a damage zone with an enhanced permeability located within the fault zone. Furthermore, he describes how a fault zone can have a low permeability in the direction normal to the fault plane but high permeability parallel to the fault plane. This occurs by a combination of a damage zone with a low permeability zone, composed by a fault core of gouge material or similar.

The *Valle de Queretaro* aquifer system is influenced by the difference in the hydraulic proprieties of the stratigraphic layers and by the hydrogeological response of fault systems to groundwater flow. Carreon-Freyre *et al.* (2005) analysed piezometric levels on both sides of a selected fault in this valley and concluded that this geological structure can act like an hydraulic barrier or as a preferential channel, controlling the patterns of groundwater flow.

Based on an adequate representation of the groundwater flow and evolution of the piezometric levels, the hydraulic properties of a selected group of faults of the *Valle de Queretaro* were simulated. This was done by analysing two pumping tests; however, due to the complexity of the geology, we have not included the necessary observation wells to register the heterogeneity of the geological media. In addition, the drawdown curves obtained from the pumping tests did not

satisfactorily matched the theoretical curves (e.g. Theis, Jacob, double porosity). For a better approximation, a calibration process was performed to analyse the variations of the properties of the fault and surrounding materials, and groundwater dynamics.

Geomechanical response

The mechanical properties of the granular materials (friction angle and cohesion) in the *Valle de Querétaro* have been estimated from triaxial tests (Leon-Rivera, 2008). In addition, the elastic properties of different volcanic and lacustrine materials can be found in the literature (Schultz, 1996; Avar *et al.*, 2003; Zimbelman *et al.*, 2004; Avar & Hudyma, 2007; Del Potro & Hürlimann, 2008; Hernández-Marín & Burbey, 2009). These properties are crucial for the development of the numerical model presented here.

Several numerical analyses using poro-elastic materials have been included in aquifer mechanics (i.e. Hsieh, 1997; Leake *et al*., 1997; Burbey, 2003; Artamonova, 2005), as well as in bi-elastic behaviour (Toufigh *et al.* 2005, Hanson *et al.* 2005). On the other hand, the elasto-plastic behaviour of geomaterials can be used for evaluating plastic deformation as materials observed in the field.

NUMERICAL MODEL DEVELOPMENT

The hydraulic numerical model used here simulates a pumping test in the northwest area of the *Valle de Queretaro*. The software package USGS-MODLFOW 2000, together with the PEST (Doherty, 2005), were used to evaluate the permeability of the materials and geological structures. The permeability is obtained based on the simulated drawdowns that best match the drawdowns measured from El Nabo and Mompani II wells during pumping tests for the period of November–December 2007. The "Nabo" extraction well was used as a pumping and observation well and "Mompani II" as an observation well (Fig. 2(a)). The "Nabo" well is 1000 m deep and "Mompani II" well is 280 m deep; the horizontal distance between them is 950 m. The total area considered in the 3-D model is about 25 km^2 and, to prevent effects of the model limits, at least a distance of 2 km from wells to the borders of the model domain in all directions is simulated.

The 3-D model was established using cells of 50 × 50 m, representing the truncated sequence of pyroclastic-granular and lava materials along with geological features like faults and intrusive magmatic materials. A non-horizontal initial potentiometric surface was incorporated in the model as the initial condition according to the observed groundwater level measured from the wells.

The mechanical numerical model was performed using the open-source *CODE-ASTER* (GNU license), a finite element code developed by the EDF *groupe* (*Electricite de France*). Other supporting programs were also used: the SALOME-MECA, for pre- and post-analysis (geometry, meshing and visualisation); EFICAS, a command file editor and syntax analyser; and ASTK for files and simulation process management.

The 2-D model represents a geological section with three different materials: *granular* (representing pyroclastic, lacustrine and sedimentary rocks), *igneous* and *faulted* material (Fig. 4). The geological section is part of a section described by Carreon-Freyre *et al.* (2005) for the *Valle de Queretaro* aquifer system.

The piezometric levels of the study area registered in 2006 (Fig. 2(b)) were incorporated into the bi-dimensional model as an approximation to identify the geological unit from which the groundwater is pumped.

The main sequence in the model is: TeCgAR (granular), TmmAB (igneous), TomPLac (granular), TmtAB (igneous) and TpArCG (granular). All units are truncated by the regional faulting (Fig. 3).

The groundwater flow was simulated as steady state and the magnitude of the hydraulic conductivity of the different geological materials were those resulting from the MODFLOW-PEST simulation.

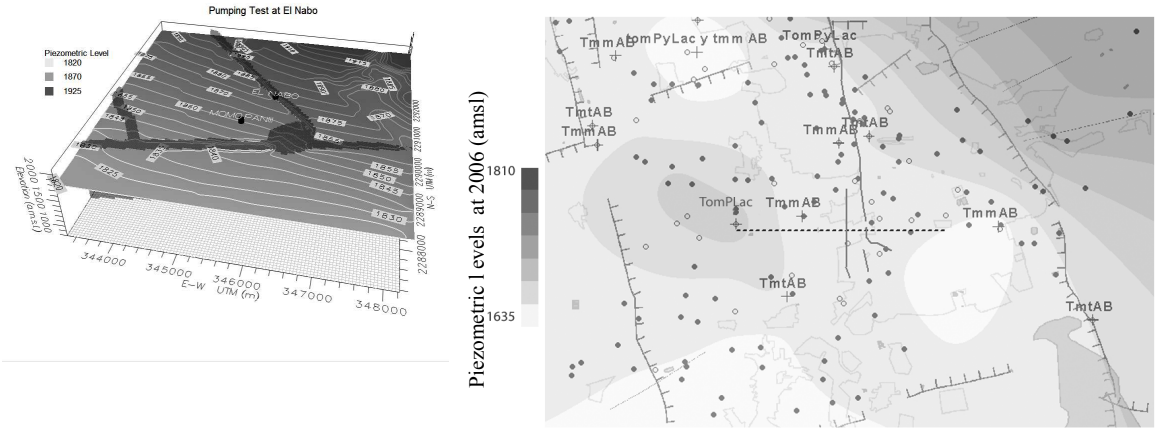

Fig. 2 (a) Piezometric levels resulting from the hydraulic simulation that was conducted for better understating of fault hydraulic role. (b) Piezometric configuration of the area of the Valle of Queretaro, The location of the geological section used for FEM analysis is shown with a dashed line. Black dots and outlined dots are pumping wells, and cross-marked wells indicate from which stratigraphic unit (adjacent legend) the groundwater is being pumped. Levels of darkness in grey indicate the piezometric configuration (levels). TmtAB: andesite and basalt from middle Tertiary, considered as igneous rocks; TomPLac: pyroclastic and lacustrine from Tertiary Oligocene, considered as granular material.

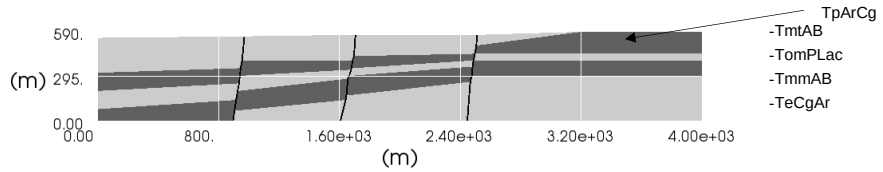

Fig. 3 Geometric section of the bi-dimensional model. Black sub-vertical zones are fault material, light grey zones are granular material and dark grey are igneous layers.

Known piezometric levels were incorporated at the lateral borders of the model, and on specific areas where the measuring wells are located. By a detailed stratigraphic correlation of their corresponding lithologic logs, water elevation could be assigned to a geological unit. On the rest of the model, the piezometric levels were calculated using an analogous model of heat flow (by using the same *Aster Code*).

The mechanical response of the system during pumping was calculated using an analogous model of dilatation. Several plasticity models for the study of geomaterial behaviour can be used by the *Aster Code* (Drucker-Prager, Hoek-Brown, Laigle, CAM-CLAY, CJS and the Barcelona model. In this work, the Drucker-Prager elasto-plastic criterion was selected because this behaviour was already documented by field and laboratory analysis (Carreón-Freyre *et al.*, 2005b; León-Rivera, 2008). This model was implemented into the *Aster Code* by Fernandes (2009) and the required parameters can be computed on the basis of friction angle and cohesion. In both heat flow and mechanical models, a triangular mesh of 6-node elements was used.

DISCUSSION OF RESULTS

The hydraulic conductivities obtained, as results of the 3-D simulation when calibrating the model to the observed piezometric levels, indicate that the faults are less conductive than the surrounding material in the direction orthogonal to the fault plane, and can be more conductive parallel to the fault plane trend.

For the 2-D mechanical model the resulted piezometric levels and displacements are shown in Fig 4, in which meshed zones correspond to the igneous materials and non-meshed areas indicate granular materials. Areas separated by faults from which water is being withdrawn behave like separated sections were the piezometric levels differ from one to another (Fig. 4(a)).

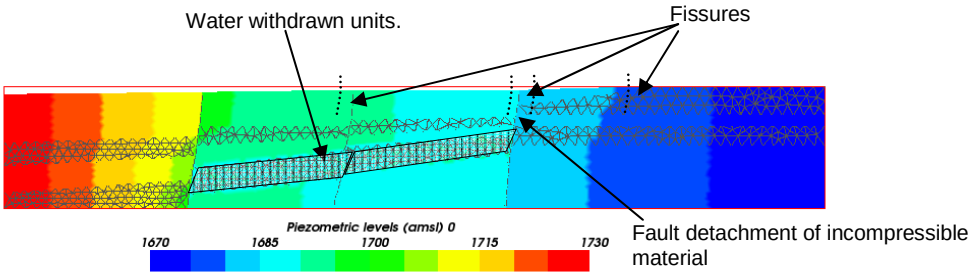

(a) Piezometric levels configuration

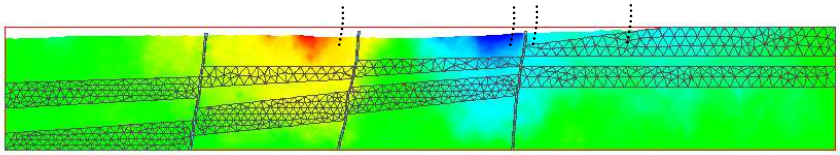

(b) Horizontal displacements where, reds are displacement toward the right and blue to the left.

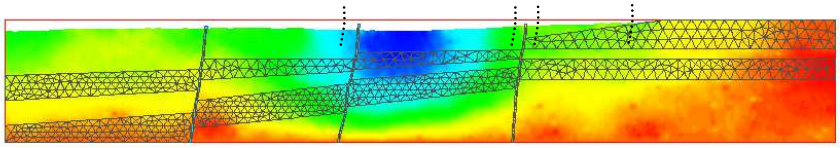

(c) Vertical displacements in blue indicate greater downward direction and red denotes zero vertical displacement. Larger displacement is in the order of 1mm.

Fig. 5 Results of the mechanical numerical model; the mesh shown corresponds to *igneous* materials, and zones not meshed denote *granular* materials.

Horizontal and vertical displacements are shown in Fig. 4(b) and (c). Fissures appear near zones of major displacements changes, indicating major deformation and stresses. Different thickness of the compressible surface material is not the only important factor, but also the sum of thicknesses of compressible materials that are affected by changes in the piezometric levels, because with more thickness of compressible material the total displacement could be greater. Faults are zones of mechanical weakness; therefore, non-compressible material can be, not only truncated, but also detached by the fault.

If we take into account that faulting considerably increases the hydraulic gradient, different factors that lead to the generation of fissures in that zone can be identified in addition to the different compressible thickness of the surface materials.

The measured displacements are greater than simulated displacement in most of the studied cases (Ochoa González, 2003), Future work needs to include a calibration with field measurements and the use of more complex plastic models. In addition, implementing 3-D mechanical modelling and analyses with piezometric levels from different years will permit consideration of the evolution of piezometric levels.

Acknowledgements The authors want to thank to CONACyT because his financial support, to the Servicio Geológico Mexicano and Ignacio Ortiz for the support and work with the pumping test and to Martín Hernández-Marín for his review of this manuscript which help to improve it.

REFERENCES

Alaniz-Álvarez, S. A., Nieto-Samaniego, Án. F., Reyes-Zaragoza, M. A., Orozco-Esquivel, M. T., Ojeda-García, Án. C. & Vassallo, L. F. (2001) Estratigrafía y deformación extensional en la región San Miguel de Allende-Querétaro, México. *Revista Mexicana de Ciencias Geológiocas* **18**(2), 129–148.

Allen, D. M. & Michel, F. A. (1999) Characterizing a faulted aquifer by field testing and numerical simulation. *Ground Water* **37**(5), 718–728.

Anderson, E. I. (2006) Analytical solutions for flow to a well through a fault. *Adv. Water Resour.* **29**, 1790–1803.

Artamonova, N. B. (2005) Modeling of land subsidence and pore pressure variations caused by fluid pumping (with the use of Biot's theory). Proceedings of the seventh symposium on Land Subsidence, 580–589.

Avar, B. B.; Hudyma, N. & Karakouzian, M. (2003) Porosity dependence of the elastic modulus of lithophysae-rich tuff: numerical and experimental investigations. *Rock Mechanics and Mining Sciences* **40**, 919–928.

Avar, B. B. *and* Hudyma, N. W. (2007) Observations on the influence of lithophysae on elastic (Young's) modulus and uniaxial compressive strength of Topopah Spring Tuff at Yucca Mountain, Nevada, USA. *Rock Mechanics and Mining Sciences* 44, 266-270.

Bense, V. *and* van Balen, R. (2003) Hyodrogeological aspects of fault zones on various scales in the Roer Valley Rift System. *J. Geochemical Exploration* 78-79, 317-320.

Bense, V.; Van Balen, R. & De Vries, J. (2003) The impact of faults on the hydrogeological conditions in the Roer Valley Rift System: an overview. *Netherlands J. Geosciences* **82**(1), 41–54.

Biot, M. A. (1956) Theory of Deformation of a Porous Viscoelastic Anisotropic Solid. *J. Applied Physics* **27**(5), 459–467.

Burbey, T. (2002) The influence of faults in basin-fill deposits on land subsidence, Las Vegas Valley, Nevada, USA. *Hydrogeol. J.* **10**(5), 525–538.

Burbey, T. J. (2008) The influence of geologic structures on deformation due to ground water withdrawal. *Ground Water* **46**(2), 202–211.

Burbey, T. J. (2003) Use of time–subsidence data during pumping to characterize specific storage and hydraulic conductivity of semi-confining units. *J. Hydrol.* **281**, 3–22.

Carreón Freyre, D., Cerca, M., Luna-González, L. & Gámez-González, F. J. (2005) Influencia de la estratigrafía y estructura geológica en el flujo de agua subterránea del Valle de Querétaro. *Revista Mexicana de Ciencias Geológicas* 22(1), 1–18.

Carreón-Freyre., D., Cerca Martínez, M. & Hernández Marín, M. 2005(b) Propagation of fracturing related to land subsidence in the Valley of Queretaro, Mexico. Proceedings of the 7th International Symposium on Land Subsidence SISOLS 2005, Shanghai, P.R. China, vol. 1, 155–164. ISBN 7-5323-8209-5.

Del Potro, R. & Hürlimann, M. (2008) Geotechnical classification and characterisation of materials for stability analyses of large volcanic slopes. *Engineering Geology***98**, 1–17.

Delinom, R. M. (2009) Structural geology controls on groundwater flow: Lembang Fault case study, West Java, Indonesia. *Hydrogeology J.* **17**(4), 1011–1023.

Doherty, J. (2005) PEST Version 9.01. Watermark Computing, Corinda, Australia.

Fernandes, R. (2009) Intégration du comportement mécanique élastoplastique de Drucker-Prager et post-traitements. CODE_ASTER. Documentation de reference du Code_Astes [R7.01.16].

Garduño Monroy, V. H., Arreygue Rocha, E., Israde Alcántara, I. & Rodríguez Torres, G. M. (2001) Efectos de las fallas asociadas a sobreexplotación de acuíferos y la presencia de fallas potencialmente sísmicas en Morelia, Michoacán, México. *Revista Mexicana de Ciencias Geológicas* **18**(1), 37–54.

Hernández Marín, M. & Burbey, T. J. (2009) The role of faulting on surface deformation patterns from pumping-induced groundwater flow (Las Vegas Valley, USA). *Hydrogeology J.* **17**(8), 1431–2174.

Hsieh, P. A. (1997) Poroelasticity Simulation of ground-water flow and subsurface deformation (97-47). Technical report, USGS.

León Rivera, A. (2008) Metodología para el monitoreo de propiedades mecánicas e hidráulicas del sistema acuífero del Valle de Querétaro. Masters Thesis, Instituto Politŭcnico Nacional.

MaClay, R. & Small, T. (1983) Hydrostratigraphic subdivisions and fault barriers of the Edwards Aquifer, south-central Texas, U.S.A. *J. Hydrol.* **61**, 127–146.

Mayer, A., May, W., Lukkarila, C. & Diehl, J. (2007) Estimation of fault-zone conductance by calibration of a regional groundwater flow model: Desert Hot Springs, California. *Hydrogeology J.* **15**, 1093–1106.

Schultz, R. A. (1996) Relative scale and the strength and deformability of rock masses. *J. Structural Geology* **18**(9), 1139–1149.

Sultan, M., Wagdy, A., Manocha, N., Sauck, W., Abdel Gelil, K., Youssef, A., Becker, R., Milewski, A., El Alfy, Z. & Jones, C. (2007) An integrated approach for identifying aquifers in transcurrent fault systems: The Najd shear system of the Arabian Nubian shield. *J. Hydrol.* **349**, 475-488.

Weinberger, G. & Rosenthal, E. (1994) The fault pattern in the northern Negev and southern Coastal Plain if Israel and its hydrogeological implications for groundwater flow in the Judea Group aquifer. *J. Hydrol.* **155**, 103–124.

Zimbelman, D. R., Watters, R. J., Firth, I. R., Breit, G. & Carrasco Nunez, G. (2004) Stratovolcano stability assessment methods and results from Citlalt_petl, Mexico. *Bull. Volcanology* **66**(1), 66–79.

(Proceedings of EISOLS 2010, Querétaro, Mexico, 17–22 October 2010). IAHS Publ. 339, 2010.

Impact of longwall mining of coal on highways in southwestern Pennsylvania

J. J. GUTIÉRREZ[1], L. E. VALLEJO[1], J. S. LIN[1] & R. PAINTER[2]

1 *Department of Civil and Environmental Engineering, University of Pittsburgh, Pittsburgh, Pennsylvania, USA*
vallejo@pitt.edu

2 *Pennsylvania Department of Transportation, Uniontown, Pennsylvania, USA*

Abstract Underground longwall mining is a widely used coal extraction method in southwestern Pennsylvania, USA. The extracted coal takes the form of rectangular panels whose length and width can reach up to 4000 m and 450 m, respectively, with a thickness of roughly 2.0 m; mine depths range from 180 m to 280 m. A number of longwall panels have been mined underneath interstate highway I-79 in Greene County, Pennsylvania, inducing subsidence that raises concern for traffic safety. The Pennsylvania Department of Transportation monitored the impact of mining on the highway and collected the data that formed the basis for this study. Field data obtained from eight longwall panels included time series of surveying measurements collected as each mine advanced underneath the highway. With the aid of a genetic algorithm, a three dimensional subsidence model was developed that described the data well. The model gives the spatial distribution of surface subsidence in terms of the depth of the coal, the width of panels, the thickness of extraction, and the location relative to the face of an advancing panel. Surface deformation features were analytically derived from the model.

Key words underground coal mining; longwall mining; mine subsidence; genetic algorithm; highway embankment

INTRODUCTION

When underground mined areas are large enough, disturbances in the overburden can be transferred to the surface (Kratzsch, 2008). Deformations at the surface have both vertical and horizontal components and form a basin or trough (Peng & Chiang, 1984; Peng, 1992; Kratzsch, 2008). Subsidence and surface strains induced by the extraction of coal can affect the safety and integrity of buildings, roads, pipelines, dams, and reservoirs (Coulthard & Dutton, 1988). In the Northern Appalachian (USA) coal basin, which includes southwestern Pennsylvania, northern West Virginia and Ohio, extensive data collected in the last few decades helped researchers develop empirical subsidence models based on profile and influence function methods (Luo *et al.*, 2008; Agioutantis & Karmis 2009). The applicability of the existing predictive tools in the case of highways has not been investigated, and little has been done to develop models to predict highway deformations associated with underground mining. In highways, structures that need protection or repairs due to the negative impact of mining are mainly pavements, culverts, and bridges (GeoTDR, 2001).

This paper describes the development of an empirical highway subsidence model based on deformation data collected by the Pennsylvania Department of Transportation along interstate highway I-79 in Greene County, Pennsylvania. The mined coal seam is known as the Pittsburgh Coal seam.

PANEL OVERVIEW AND SITE GEOLOGY

Figure 1 (left) gives the approximate location of the Emerald and Cumberland mines in Greene County, southwestern Pennsylvania and an overview (right) of the longwall panels in the Cumberland mine. The rocks in Greene County are in horizontal strata, with thickness ranging from a fraction of an inch to many feet (<1 cm to several m) (Stone, 1932; Edmunds, 1999; Edmunds *et al.*, 1999). The typical rocks encountered in southwestern Pennsylvania include shales, limestones, sandstones, and coal (Jeran & Adamek 1988).

Copyright © 2010 IAHS Press

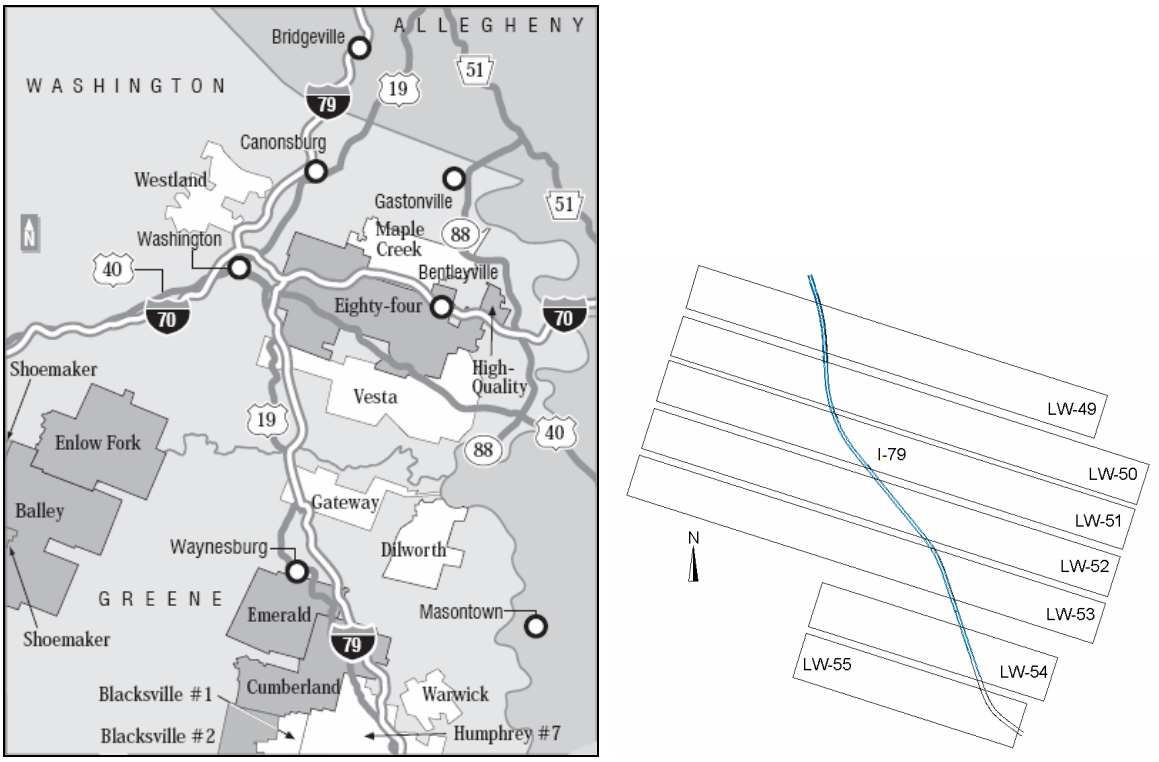

Fig. 1 Left: Location of Emerald and Cumberland mines (source: Post-Gazette, Consol). Right: View of Cumberland panels.

MAXIMUM SUBSIDENCE MODEL

Empirical subsidence models such as that described herein require the initial estimation of maximum subsidence. The overburden thickness or mining depth, H, is the vertical distance between the extracted seam and the ground surface; the width, W, is the shorter horizontal dimension of longwall panels; the extraction thickness, M, is the actual thickness that is mined out; the maximum subsidence, S^*, is the magnitude of maximum vertical surface deformation. The magnitudes of the basic subsidence parameters for the Cumberland and Emerald longwall panels and some useful ratios are given in Table 1. The ratio S^*/M is known as the subsidence factor and gives the proportion of subsidence with respect to the thickness of extraction.

Table 1 Subsidence parameters.

Panel	S^* (m)	M (m)	S^*/M	H (m)	W (m)	W/H
B-4	1.20	1.93	0.62	234	443	1.89
LW-49	1.40	2.26	0.62	240	378	1.58
LW-50	1.39	2.26	0.61	244	375	1.54
B-3	1.43	2.00	0.72	220	436	1.98
LW-52	1.50	2.26	0.67	233	378	1.62
LW-53	1.62	2.35	0.69	224	376	1.68
LW-51	1.44	2.26	0.64	233	378	1.62
LW-55	1.66	2.35	0.71	195	411	2.11

The ratio W/H has traditionally been used as a criterion to differentiate subcritical from supercritical subsidence conditions and is site-dependent (NCB, 1975; Karmis *et al.*, 1983;

OSMRE, 1986; VPI&SU, 1987; Whittaker & Reddish, 1989; Karmis *et al*., 1992; Mine Subsidence Engineering Consultants, 2007; Karmis *et al.*, 2008). Subcritical subsidence conditions exist when the maximum potential subsidence has not yet been achieved, as the extent of extraction is still limited. When the extraction reaches certain dimensions that cause the vertical deformation to reach its maximum potential magnitude, such dimensions (e.g. width and length in the case of longwall panels) or conditions are called critical. As the extraction keeps growing in lateral dimensions beyond critical conditions, no further increase in maximum subsidence takes place. A central flat area with maximum constant subsidence is formed, and such conditions are called supercritical. In Appalachia, a widely accepted value for *W/H* of 1.2 is the threshold for critical conditions. Table 1 shows that the ratios *W/H* for the longwall panels in the Emerald and Cumberland mines far exceed the threshold of critical conditions. From the data collected, it was found that the subsidence factor is dependent on the overburden thickness, as shown in Fig. 2. This serves as the basis of the present maximum subsidence model.

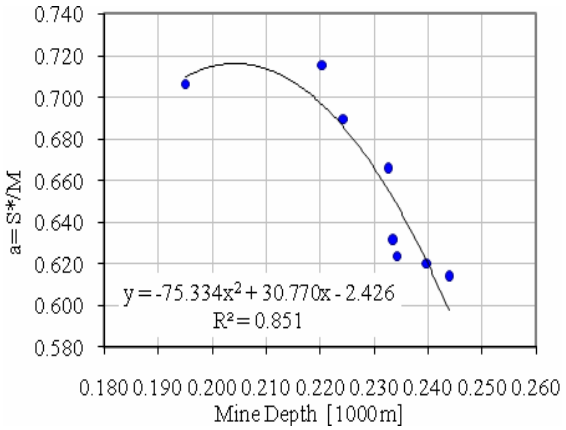

Fig. 2 Maximum subsidence model.

SURVEYING DATA

Surveying data were collected for all panels depicted in Table 1. Measurements were taken for different dates so that highway deformations relative to varying positions of the panel face could be captured. Figure 3 (left) depicts panel LW-51, the northbound and southbound surveying stations, and the locations of the panel advance face for the different dates that the surveying was performed on. Baseline elevations were obtained from surveying performed long before the mine face approached the highway.

3-D SUBSIDENCE MODEL

In order to produce a subsidence trough, data normalization was performed. Taking all surveyed points from panels that were well documented, both the magnitude of subsidence at each point and its planar location were normalized.

VERTICAL NORMALIZATION

Taking the set of all absolute subsidence readings, these were normalized with respect to the maximum subsidence, S^*, corresponding to the panel where the data belonged. With the scattering in the readings, an average maximum in the supercritical region of the troughs was used for the normalization.

PLANAR NORMALIZATION

The horizontal coordinates measured in both the transversal and longitudinal directions were normalized in this study by the overburden depth, H. With this normalization, the inflection points, in the transversal as well as in the longitudinal direction, from various mine panels were found to be close to each other. This provides a rationale for building a general subsidence prediction model.

SYMMETRIC AND ASYMMETRIC CASES

Figure 3 (right) gives a transverse view of all normalized data points for three panels with the same width. Each single point is a distance z from the mine face, which would be better appreciated in a 3-D view. The main purpose of this illustration is to describe two clear trends on the right edge: a symmetric deformation and an asymmetric one. Among the panels in the Cumberland mine, the northernmost panel, LW-49, was the first panel of that set to be mined-out. Therefore, that panel caused a symmetric subsidence trough to form. On the other hand, other panels such as LW-51 and LW-52 showed asymmetric transversal subsidence profiles, for each had a previously extracted panel neighbouring them to the North. The right side for these two panels showed higher vertical deformations. The model described here deals with these two cases.

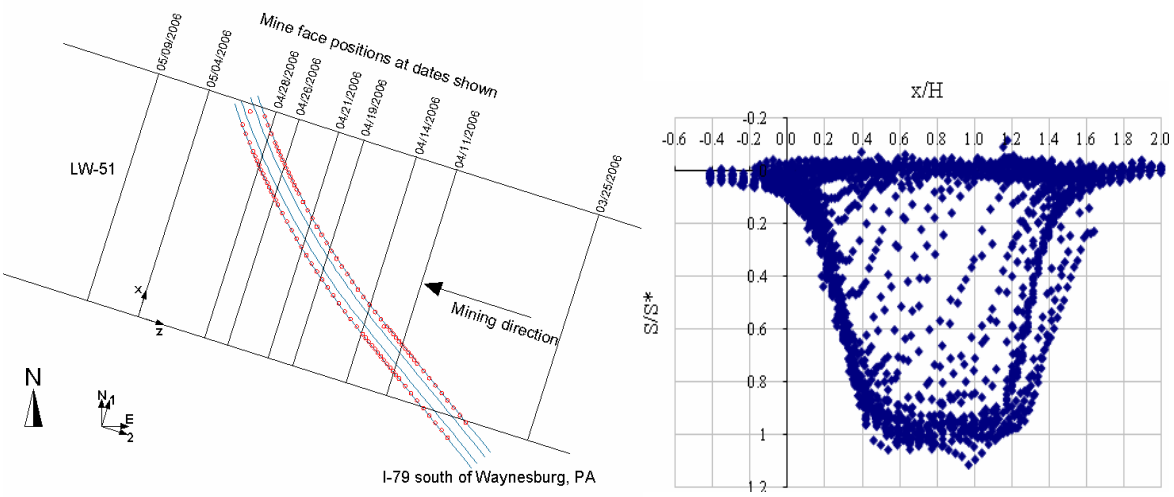

Fig. 3 I-79 crossing panel LW-51.

BUILDING A 3-D MODEL

In order to obtain a 3-D model, a transverse 2-D model and a longitudinal 2-D model can be multiplied. Two-dimensional models are common in the literature of subsidence prediction methods (Whittaker & Reddish 1989; Karmis *et al.*, 1992; Peng, 1992; Agioutantis & Karmis, 2009). A 3-D function, or model, will have to address the following factors:

- Panels do not have the same width.
- Some panels are symmetric in the case that no adjacent panel has been previously mined out in the immediate neighbourhood (e.g. LW-49).
- Most panels exhibit asymmetry, that is, the side adjacent to a mined-out panel is more subsided than the opposite side.

We employed a logistic equation, also known as Richard's model (Graybill & Iyer, 1994), to build our 3-D subsidence profile. The profile model we propose has the following form:

$$\frac{S}{S*} = \frac{1}{\left[1+e^{-\left(a_1+a_2\frac{x}{H}\right)}\right]^{a_3}\left[1+e^{-\left(a_4+a_5\frac{z}{H}\right)}\right]^{a_6}} \quad (1)$$

After specifying the function form, an objective function, and the possible range of values for each parameter, a genetic algorithm (GA) was used to find parameter values that provided a global minimum of the objective function. For this model, the objective function chosen was the sum of squared errors. The model parameters so obtained for cases without an adjacent panel are: a_1 = –2.79, a_2 = 11.6, a_3 = 1.24, a_4 = –1.94, a_5 = 5.99, a_6 = 1.23; and for those with an adjacent panel are: a_1 = –2.77, a_2 = 12, a_3 = 0.73, a_4 = –1.94, a_5 = 5.99, a_6 = 1.23. The model is only to be used for half of the trough, that is for x up to $W/2$. The other half would be mirrored in the case of a symmetrical profile. For cases with an adjacent mined-out panel, the half that lies next to the adjacent panel uses the second set of parameters, while the other half, not affected by the adjacency impact, uses the first set. Figure 4 depicts a prediction of the model for panel LW-49.

Deformation indices are important for damage prediction. If the subsidence profile or trough is known, these can be obtained analytically. In general, the most important deformation indices such as slope, horizontal deformation, curvature and horizontal strain can all be obtained from the predictive model so derived.

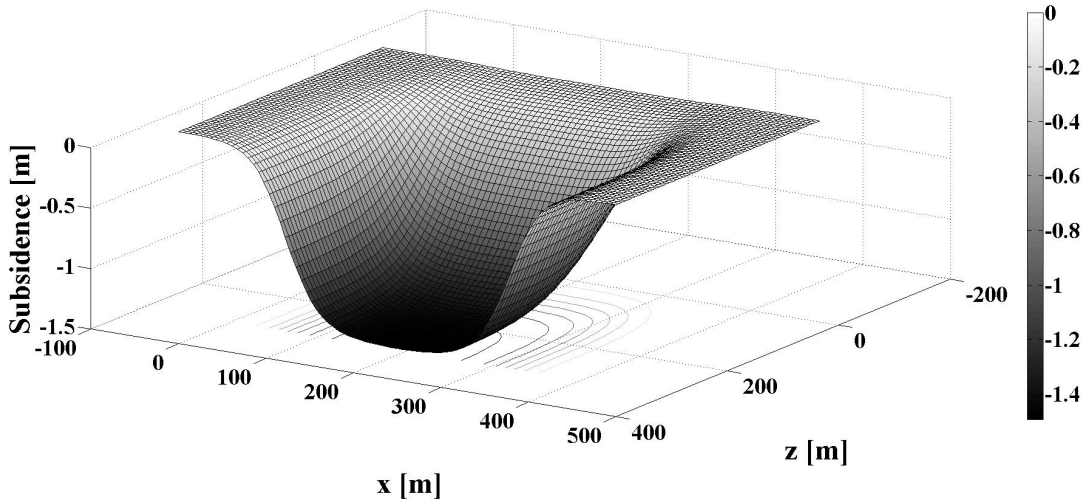

Fig. 4 Subsidence trough obtained with the present model (symmetric case LW-49).

CONCLUSIONS

From the development of the new subsidence model described in this work, three general conclusions may be drawn.

First, a clear relationship has been shown to exist between the subsidence factor, S^*/M, and the overburden thickness, H, whereby the subsidence factor decreases with overburden thickness. This variation exists for values of the width-to-depth ratio, W/H, that are well above the critical threshold of 1.2. This means that, even for supercritical cases, the subsidence factor may still vary as different mining depths are considered.

Second, an extension of the so called profile functions has been presented for three dimensions for which, in the past, influence functions have been employed. The influence function is more restricted. For instance, a profile can be too sharp to be described by influence functions.

Third, the use of mathematical functions has made it possible to derive the subsidence information indices. Moreover, the function, as shown, applies to both symmetric and asymmetric subsidence profiles.

Acknowledgements This research is funded by Pennsylvania Department of Transportation under IGA 510601, WO-015. This support is gratefully acknowledged.

REFERENCES

Agioutantis, Z. & Karmis, M. (2009) Surface Deformation Prediction System for Windows Virginia Polytechnic Institute and State University.

Coulthard, M. A. & Dutton, A. J. (1988) Numerical modelling of subsidence induced by underground coal mining. In: *The 29th U.S. Symposium on Rock Mechanics (USRMS)* (Minneapolis, MN). A. A. Balkema, Rotterdam. Permission to distribute – American Rock Mechanics Association.

Edmunds, W. E. (1999) Chapter 11: Pennsylvanian-Permian Transition and Permian. In: *Geology of Pennsylvania* (ed. by C. H. Schultz), 171177. Harrisburg, Pittsburgh, Pennsylvania Geological Survey Pittsburgh Geological Society, USA.

Edmunds, W. E., Skema, V. W. *et al.* (1999) Chapter 10: Pennsylvanian. *Geology of Pennsylvania*. In: *Geology of Pennsylvania* (ed. by C. H. Schultz), 156. Harrisburg, Pittsburgh, Pennsylvania Geological Survey Pittsburgh Geological Society, USA.

GeoTDR (2001) Effects of undermining Interstate Route 70, South Strabane Township, Washington County, Pennsylvania. Westerville, Ohio, USA.

Graybill, F. A. & Iyer, H. K. (1994) *Regression Analysis: Concepts and Applications*. Dusbury Press (an imprint of Wadsworth Publishing Company), Belmont, California, USA,.

Jeran, P. & Adamek, V. (1988) Subsidence due to undermining of sloping terrain: a case study. *Report of Investigations*. United States Department of Interior Bureau of Mines.

Karmis, M., Agioutantis, Z. *et al.* (2008) Enhancing mine subsidence prediction and control methodologies. In: *27th International Conference on Ground Control in Mining* (West Virginia University, Morgantown, WV, USA,).

Karmis, M., Haycocks, C. *et al.* (1992) The prediction of ground movement caused by mining. *3rd Subsidence Workshop Due to Underground Mining* (West Virginia University, Morgantown, WV, USA,).

Karmis, M., Triplett, T. *et al.* (1983) Mining subsidence and its prediction in the Appalachian Coalfield. *The 24th US Symposium on Rock Mechanics (USRMS)*. College Station, TX, The Association of Engineering Geologists. Permission to Distribute - American Rock Mechanics Association.

Kratzsch, H. (2008) *Bergschadenkunde*. Bochum, Deutscher Markscheider-Verein e.V.

Luo, Y., Peng, S. S. *et al.* (2008) Upgraded Comprehensive and Integrated Subsidence Prediction Model CISPM-W. *27th International Conference on Ground Control in Mining* (West Virginia University, Morgantown, WV, USA).

Mine Subsidence Engineering Consultants (2007) Introduction to longwall mining and subsidence. Retrieved 08/19/2009, from www.minesubsidence.com.

NCB (1975) *Subsidence Engineer's Handbook.* National Coal Board. UK.

OSMRE (1986) *Guidance Manual on Subsidence Control.* United States Department of Interior, USA.

Peng, S. S. (1992) *Surface Subsidence Engineering*. Society for Mining, Metallurgy, and Exploration, Inc., Littleton, Colorado, USA.

Peng, S. S. & Chiang, H. S. (1984) *Longwall Mining*. John Wiley & Sons, New York, USA.

Stone, R. W. (1932) *Geology and Mineral Resources of Greene County Pennsylvania*. Pennsylvania Geological Survey, Harrisburg, Pennsylvania, USA.

VPI&SU (1987) Prediction of ground movements due to underground mining in the Eastern United States coalfields. Virginia Polytechnic Institute and State University: 205, Blacksburg, Virginia, USA,

Whittaker, B. N. & Reddish, D. J. (1989) *Subsidence: Occurrence, Prediction, and Control*. Elsevier Science Publisher BV, The Netherlands.

Land Subsidence, Associated Hazards and the Role of Natural Resources Development
(Proceedings of EISOLS 2010, Querétaro, Mexico, 17–22 October 2010). IAHS Publ. 339, 2010.

Inverting subsidence data to detect possible compartmentalization in a gas reservoir in The Netherlands

K. VISSER, A. G. MUNTENDAM-BOS, G. KUNAKBAYEVA, O. LEEUWENBURGH, E. PETERS & P. A. FOKKER

TNO Built Environment and Geosciences, Princetonlaan 6, Postbox 80015, 3508 TA Utrecht, The Netherlands
karin.visser@tno.nl, peter.fokker@tno.nl

Abstract Subsidence can be induced by hydrocarbon production, due to the decrease in pore pressure in the reservoir which causes the reservoir to compact. The subsidence at any point on the surface is a result of the compaction over a large area of the reservoir. The properties of the reservoir and thus the compaction are uncertain. Therefore, an inversion is needed to constrain the knowledge about compaction in the reservoir with the use of subsidence data. We applied a previously developed linearized subsidence inversion method to the Roswinkel gas field. This field is situated in the northeastern part of The Netherlands. The Roswinkel field has been in production between 1980 and 2005. It is a complicated anticlinal structure with many faults in two major directions, dividing the reservoir in up to 30 reservoir compartments. Prior geomechanical modelling of the Roswinkel field revealed deviations in the measured subsidence from the predicted ideal elliptical shape of the subsidence bowl, possibly indicating partly undepleted compartments in this reservoir. The prior knowledge of the reservoir was quantified using Monte Carlo simulations. The degree of compartmentalization was varied by perturbing the fault transmissibilities. The prior knowledge, contained in the simulation models, includes the expected compaction field, the standard deviations, and the spatial and temporal correlations between the model elements. Our inversion study on Roswinkel demonstrates our ability to constrain the prior uncertainty of the reservoir model. The inversion exercise gave a clear adaptation of the prior compaction field from a smooth, extended field to a sharply bounded field with internal structure. This means that identification of gas compartments and fault properties by inversion of subsidence measurements is feasible. The prior knowledge is the critical part in the inversion exercise; the most critical steps seem to be the geological and the geodetic analysis. For the latter, new data like space-geodetic observations might help improve the analysis. However, we expect the largest improvement to come from integrating inversion steps, implying that all the different data are taken into account simultaneously.

Key words subsidence; inversion; Bayes; reservoir compartmentalization

INTRODUCTION

The Roswinkel field is a gas field in the northern Netherlands which originally held some 24 billion sm^3 of gas. It is an anticlinal structure with many faults, giving rise to possible compartmentalization depending on their sealing capacity. There is considerable uncertainty about the compartmentalization, as well as about the strength of the connected aquifer. Reservoir engineering studies indicated that there might be gas left in compartments that have not been fully depleted. The field has been produced from eight wells.

A total of 17 cm of subsidence had been measured above the crest of the field by traditional levelling campaigns on founded benchmarks. The present paper documents a study to identify undepleted reservoir compartments from subsidence measurements. We went through the complete workflow of geological modelling, reservoir simulation, and geomechanical modelling. The inverse modelling used the geodetic information (subsidence) to constrain the reservoir and geological uncertainties.

GEOLOGY OF ROSWINKEL

The Roswinkel field has been characterized geologically using seismic surveys shot over the field and using the available well logs. The anticlinal reservoir structure is located at a depth of approximately 2 km and contains three gas bearing layers: Sölling, Detfurth, and Volpriehausen.

Copyright © 2010 IAHS Press

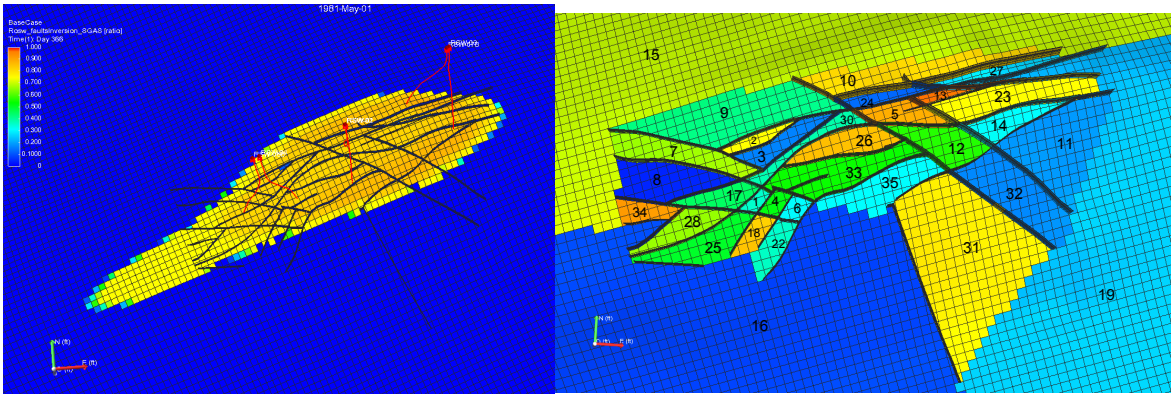

Fig. 1 Top view of the Roswinkel field. Left: gas saturation identified faults. Right: identification of possible compartments.

They are separated by shale layers. The seal also consists of shale, along with evaporites (Röt, Muschelkalk). The lateral correlation of the layers is very good over the whole area of the reservoir. A static reservoir model has been constructed with the available data, including also the gas–water contacts and the possible faults. In total 24 possible faults were identified, leading to 30 possible compartments. The large surrounding aquifer was also included in the model. The reservoir and the possible compartments are visualized in Fig. 1. The initial average pressure was 331 bar; the total pore volume 5.97×10^9 m^3; the amount of water in the reservoir 5.89×10^9 m^3; the amount of gas initially in place 24.6×10^9 sm^3.

RESERVOIR SIMULATION

The geological information has been used to construct the reservoir simulation model. For the base case, all faults were open. The gas has mainly been produced from the Sölling and the Detfurth formations. The intervals producing from the Volpriehausen were abandoned in 1985 after they were only depleted down to 290 bar.

Based on the size of the compartments and the geological information on the faults, a number of faults were identified to be open in all cases considered. In a Monte Carlo process, the other faults were given transmissibility factors between 1 and 10^{-6}, with the exponent randomly chosen between −6 and 0. Apart from the base case, 100 realizations were thus derived. These realizations were run with the reservoir simulator with the actual well production rates as input. Outputs were the actual production rates (in a number of cases these were reduced by the reservoir simulator because the pressure dropped below a threshold value), the water production, and the pressures in the wells. As the pressures in the wells had not been precisely monitored, the gas and water rates were used to assess the quality of every individual realization. Realizations which diverged too far from the actual measurements were discarded in the further analysis. This is visualized in Fig. 2. Only 14 of the realizations were discarded.

GEOMECHANICAL MODELLING

Pressure depletion in a reservoir causes its compaction. For the compaction coefficient of the reservoir rock we used a value of 1.5×10^{-5} bar^{-1}, taken from the field development plan, and in accordance with regional data and with the elastic modulus of the reservoir rock. We applied the compaction coefficient only to the net pay of the reservoir. We utilized a one-way coupling in which the pressure is transferred into compaction; the effect of the compaction on the pressure is taken into account using a standard treatment with a total reservoir compressibility. This is warranted thanks to the large compressibility of the gas present in the pores, as compared with the compressibility of the matrix. The Monte Carlo realizations thus resulted in an ensemble of compaction fields.

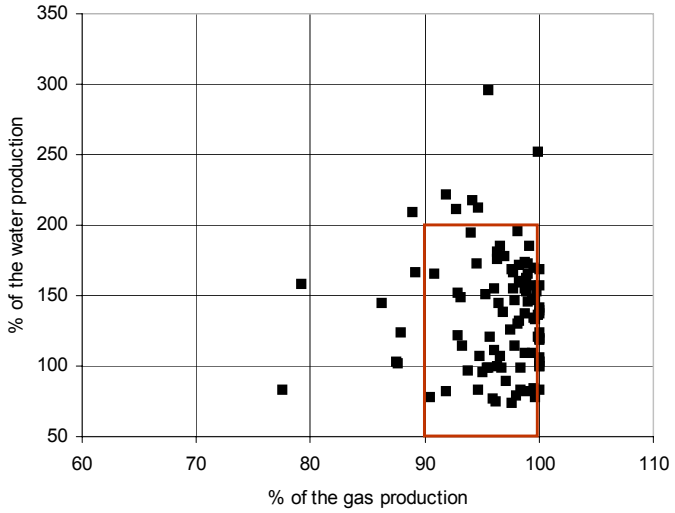

Fig. 2 Result of reservoir simulations for the realizations created. Realizations resulting in volumes of produced gas less than 90% of the actual volume, and volumes of produced water more than twice or less than half the actual volume were discarded.

The elastic response of the subsurface will translate the compaction into subsidence at the surface. The amount and extent of the subsidence depends on the amount and extent of the compaction and on the elastic moduli of the subsurface. We used a fast model which accounts for the layered structure of the subsurface (Fokker & Olic, 2006). Because the subsidence is linearly dependent on the compaction this forward model can be formulated as a matrix. Acting on an array of compaction values in every grid block it results in an array of subsidence values for every benchmark location. Rather than using the subsidence results of the ensemble of realizations we used this matrix in the inversion exercise.

GEODETIC ANALYSIS

The measurements of the nine surface levelling campaigns, which were available in the area above the Roswinkel field, were taken as input for the inverse modelling study. Figure 3 (left) provides a visualization of the measured heights (m above sea level). These heights were used as delivered by the Dutch Geometric Infrastructure of the Dutch ministry of Transport, Public Works and Water Management. No new levelling of the data was performed. The uncertainties were assigned in the standard way, combining an uncertainty because of the measurement uncertainty and an uncertainty building up with the time difference between measurement campaigns.

As the amount of subsidence was much smaller than the actual level measurements, the figure mainly shows the topology of the area. Furthermore, it is clear that not all benchmarks were measured during every levelling campaign. In our method, however, we can still use every measurement point which has been assessed at least twice out of the nine campaigns, i.e. every benchmark for which one or more difference measurement can be taken.

INVERSION

For the inversion, we adopted the methodology developed in Muntendam-Bos *et al*. (2008). The main points of the inversion method are that prior knowledge is taken into account by the prior ensemble. This ensemble also contains spatial and temporal correlations. Further, all data points are included in a single inversion; and the inversion accounts for points which have not been measured at all campaign times.

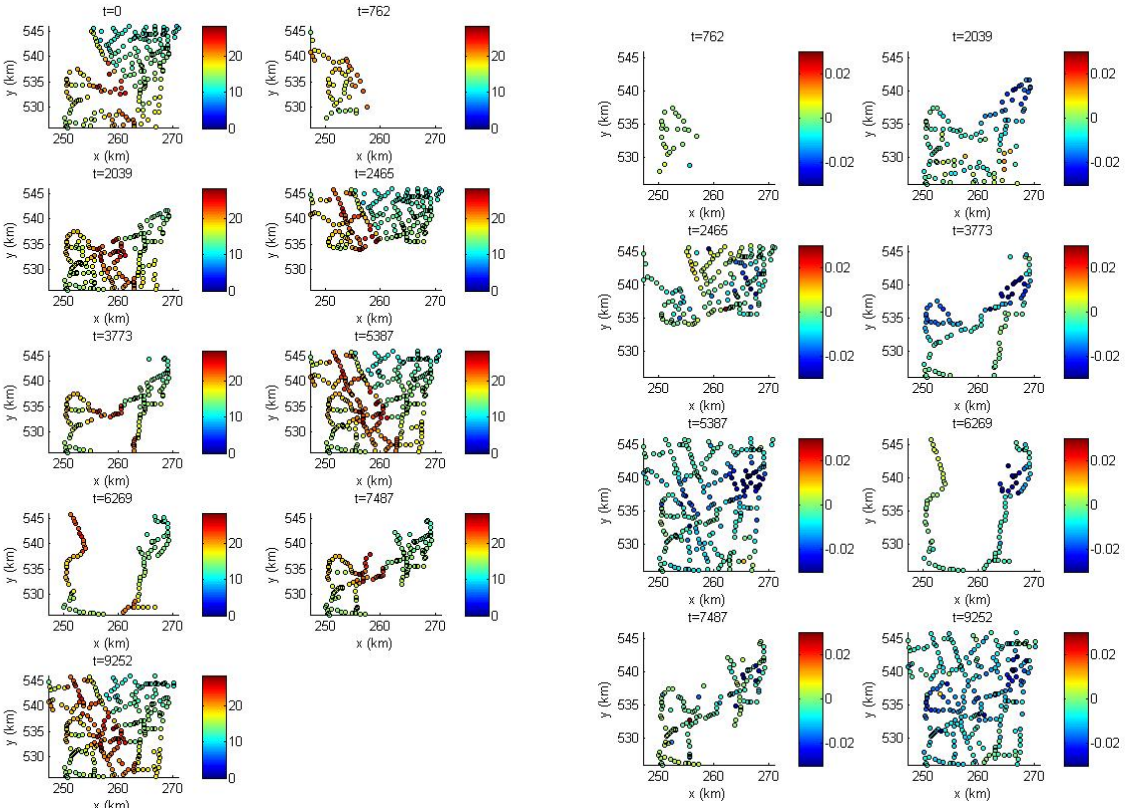

Fig. 3 Left: Levelling values measured for nine campaigns. Right: Temporal differences of benchmark heights where earlier values are available.

Figure 4 presents the results of the inversion. The left figure presents the average cumulative compaction field of the realizations accepted by the rate criterion discussed above. It is a relatively smooth field in which both the gas field and the aquifer are depleted. The right figure is the mean posterior compaction field, i.e. the estimated field after inversion. In this field, large parts of the aquifer do not compact. Furthermore, there seems to be structure within the field: several faults seem to be causing compartmentalization in the reservoir.

We have made an attempt to infer the transmissibility of the faults from the compaction estimated in the inversion exercise and to do a forward reservoir simulation with those transmissibilities. However, it was not possible to obtain a decent match of the production history with a field that at the same time fell within the confidence interval of the inversion result. Clearly, there is still a gap in our knowledge. This may have to do with the geological uncertainty, the uncertainty in the geomechanical parameters, or the quality of the geodetic analysis.

DISCUSSION AND CONCLUDING REMARKS

We have applied a time-dependent inversion scheme for subsidence measurements on an actual field case. Prior knowledge was available about the geological characterization, the production profile, the aquifer characteristics and the faults characteristics, and this was incorporated in the form of an ensemble of compaction fields spanning the prior uncertainty. The inversion exercise gave a clear adaptation of the prior compaction field from a smooth, extended field to a sharply bounded field with internal structure. This means that identification of gas compartments and fault properties by inversion of subsidence measurements is feasible. The appearance of the faults in the estimated field originates from the strong correlations within possible blocks, and the much weaker correlations over their boundaries.

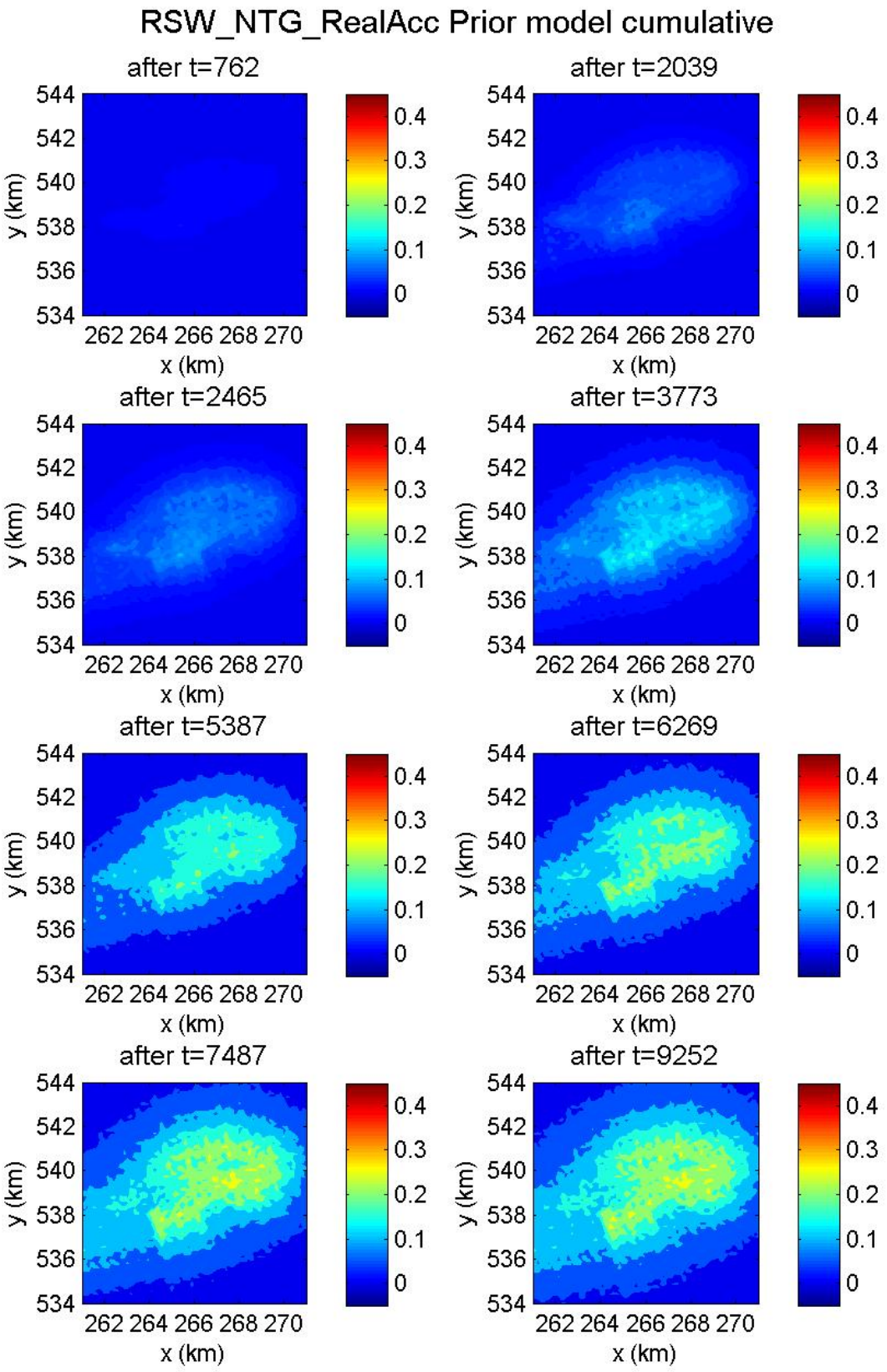

Fig. 4 This page: average compaction field based on all knowledge except subsidence (prior field). Opposite page: average compaction field after inversion (estimated field).

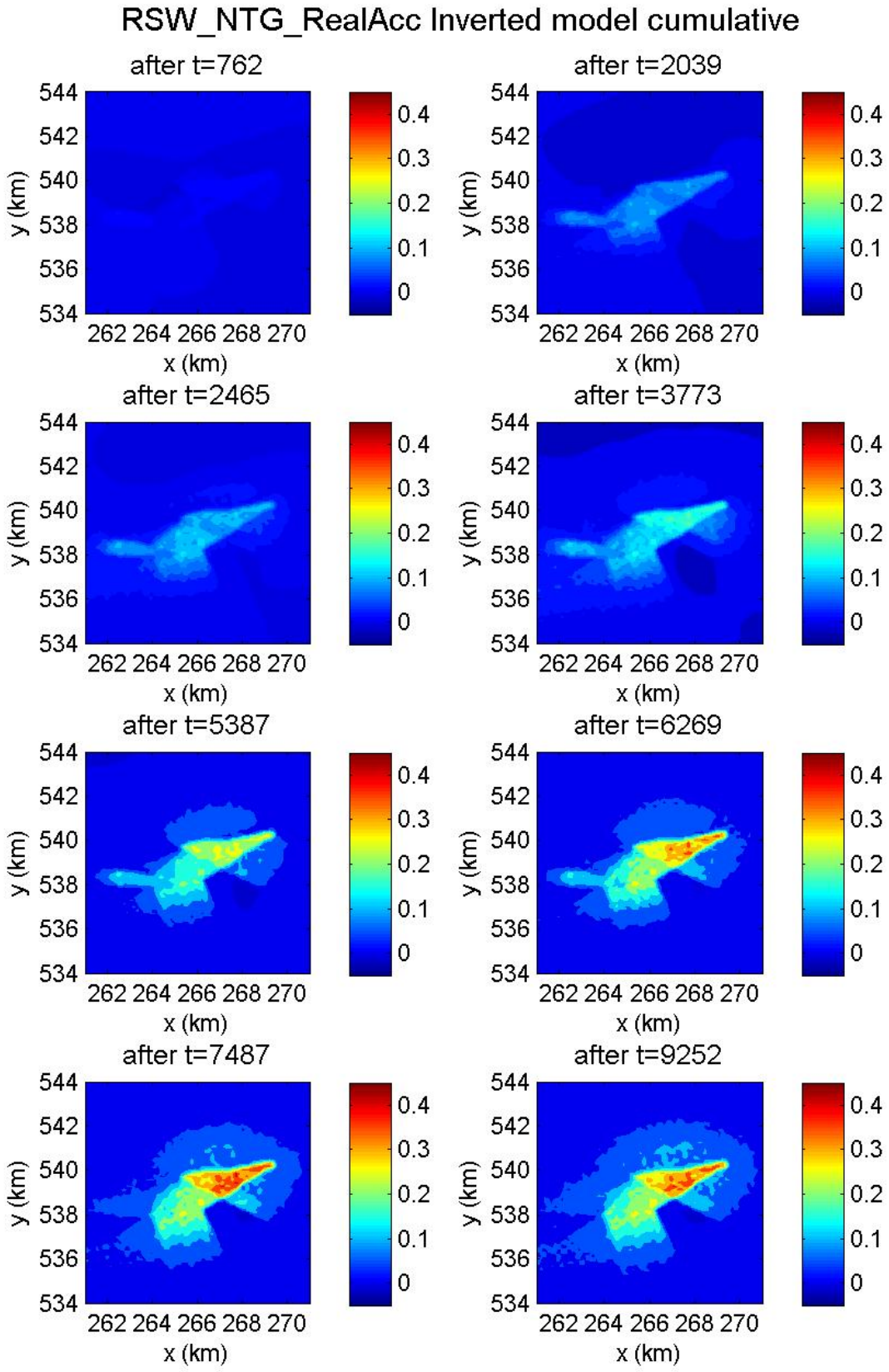

Fig. 4 Continued.

Parameterization is the key to a successful inversion. In the course of the workflow, from geology, to reservoir engineering, to geomechanical analysis while utilizing a geodetic analysis, the goal of the study must be continuously considered. This has implications for the scenarios that are chosen, the size of the possible compartments considered, but also for the treatment of the geodetic data. Particularly in the geodetic analysis there is still scope for improvement. Better data can be obtained using renewed interpretation and levelling of the raw data, better derivation of data uncertainties and correlations between data points, as well as by incorporating other data like InSAR (interferometric satellite radar images).

The present study calls for an intergrated inversion or data assimilation, implying that all the different data are taken into account simultaneously. Subsequently all steps in the workflow must be repeated. The most critical steps seem to be the geological and geodetic analysis. For the latter, new data like space-geodetic data might help improve the analysis.

REFERENCES

Fokker, P. A. & Orlic, B. (2006) Semi-analytic modelling of subsidence. *Mathematical Geology* **38**, 565–589.

Muntendam-Bos, A. G., Kroon, I. C. & Fokker, P. A. (2008) Time-dependent inversion of surface subsidence due to dynamic reservoir compaction. *Math. Geosci*. **40**, 159–177.

Land Subsidence, Associated Hazards and the Role of Natural Resources Development
(Proceedings of EISOLS 2010, Querétaro, Mexico, 17–22 October 2010). IAHS Publ. 339, 2010.

Simulation of ground failure due to groundwater pumping

CARLO JANNA, MASSIMILIANO FERRONATO, GIUSEPPE GAMBOLATI & PIETRO TEATINI

Department of Mathematical Methods and Models for Scientific Applications (DMMMSA), University of Padova, via Trieste 63, 35121 Padova, Italy
janna@dmsa.unipd.it

Abstract Numerical modelling of failure generation due to groundwater pumping and prediction of fissure location, distribution, and geometry is a difficult task. To this aim we use a geomechanical model based on the structural equations of poroelasticity solved in a three-dimensional setting by the Finite Element (FE) – Interface Element (IE) approach. While standard FE are used to represent a continuum, IE prove especially suited to address the relative displacements of adjacent elements such as the opening and slippage of pre-existing faults or the generation of new fractures. The IE allow for the modelling of fissure/fault mechanics using an elasto-plastic constitutive law based on the Mohr–Coulomb failure criterion. The corresponding FE-IE code is used for the prediction of localized differential subsidence and earth fissure activation/ generation with some representative examples discussed in the literature.

Key words ground fissures; groundwater pumping; finite elements; interface elements

INTRODUCTION

Ground fissures associated with land subsidence induced by groundwater withdrawal have been reported in many alluvial basins in semi-arid and arid regions since the late 1970s. Possible examples of such localized ruptures in near surface soils are recorded in the southwestern USA (e.g. Holzer *et al*., 1979), central Mexico (e.g. Carreon-Freyre *et al*., 2005), the Lybian desert (Rothenburg *et al*., 1995), and China (Geng & Li, 2000). Fissure zones are commonly hundreds of metres long, with a crack width of from a few centimetres up to 1–2 m and reported depths of down to 25 m.

Due to the widespread occurrence of earth fissures, and their damage and economic impact, much research activity has been carried out over the last decades. Several mechanisms for the formation of fractures due to groundwater level decline have been proposed (e.g. Sheng *et al*., 2003). The underlying conditions include: (a) the differential compaction because of stratigraphic heterogeneities; (b) the reactivation of pre-existing faults; and (c) the development of tensile stresses above bedrock ridge.

Despite a 30-year long effort, modelling the generation and propagation of an earth fissure, together with the prediction of its opening and/or slippage, still remains a challenge. To this aim we use an original modelling approach developed by the authors for predicting the fault impact on land subsidence occurring over depleted gas/oil reservoirs (Ferronato *et al*., 2008) and the influence of sliding between wellbore casings and the surrounding geological formation on the compaction of producing reservoirs (Castelletto *et al*., 2010). The related geomechanical model is based on the structural equations of poroelasticity solved in a three-dimensional setting by the Finite Element (FE) – Interface Element (IE) approach. While standard FE are used to represent a continuum, IE prove especially suited to address the relative displacements of adjacent elements such as the opening and slippage of pre-existing faults or the generation of new fractures.

MODELLING GROUND FISSURING BY INTERFACE ELEMENTS

A zero-thickness IE compatible with linear FE consists of a pair of linear elements (1-D in a 2-D problem, 2-D in a 3-D problem) with the opposite nodes coinciding. The interface displacements in the local reference frame associated with each element are the aperture δ_n and the slippage δ_{s1}

Copyright © 2010 IAHS Press

and δ_{s2} between the "top" and the "bottom" face of the element. The $\boldsymbol{\delta}$ components are related to the interface stresses σ_n, τ_{s1}, and τ_{s2}, with σ_n the normal stress (negative in compression, positive in expansion) and τ_{s1} and τ_{s2} the shear stress components in the interface plane. Irreversible plastic displacements of the interface can take place wherever the limiting tensile or the shear strength are exceeded. Assuming conservatively that no tensile strength is allowed, the opening of fault surfaces occurs when the stress normal to the interface plane, i.e. σ_n, becomes positive. Irreversible slip occurs when the Mohr–Coulomb failure criterion is violated, i.e. $|\tau_s| \geq c + \sigma_n \tan\varphi$ with c the cohesion and φ the friction angle. Sealing, i.e. no flux surface, and no-sealing fissures can be simulated by allowing or precluding, respectively, that the pressure gradient acting on the contact surfaces can be different.

The IE are implemented in a FE geomechanical model aimed at the prediction of deformation and stress induced by fluid withdrawal from an underground reservoir. The model solves the structural equation of poroelasticity following the infinite pore pressure gradient approach (Gambolati *et al*., 2001) for a heterogeneous porous medium with a nonlinear and hysteretic mechanical behaviour. The pore pressure variation within the aquifer is assumed to be a known function of space and time as predicted in advance with the aid of a fluid-dynamic model.

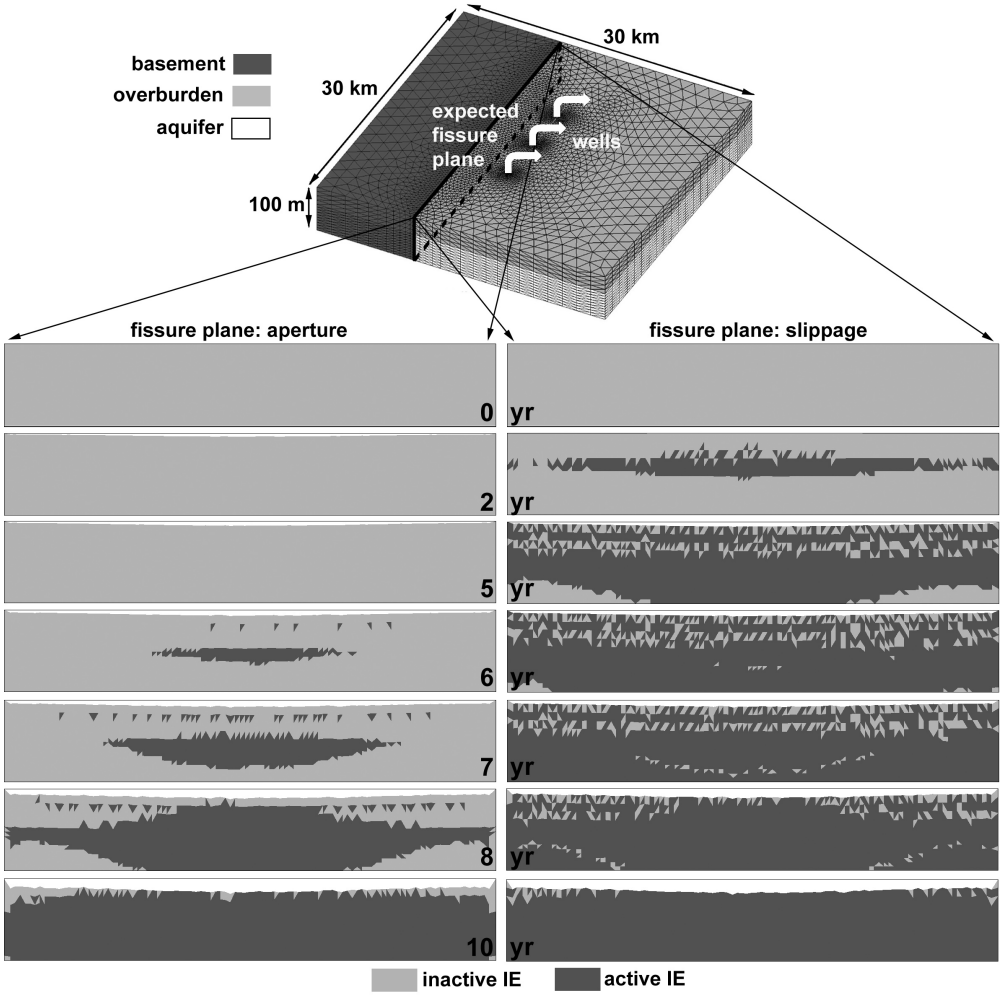

Fig. 1 Time behaviour of the fissure opening (left) and slippage (right) on the vertical plane separating the almost rigid basement and the sedimentary sequence. The dark grey areas represent the IE elements that open and slippage due to the stress change induced by the water level change.

RESULTS

The FE-IE code has been used to simulate the possible generation and evolution of fissure in a realistic 3-D geological setting. The case where an almost rigid basement outcrops and abruptly bounds the alluvial sequence is investigated here. The condition is typical, for example, of the urban areas located in the lacustrine or fluvio-lacustrine depressions of the central sector of the Mexican Volcanic Belt (MVB), such as Morelia, Celaya, and Querétaro (Carreon-Freyre *et al*., 2005).

The simulated domain is sketched in the top portion of Fig. 1. A 70-m thick aquifer overlain by a 30-m thick clay unit is bounded on one side by a rocky formation that intercepts the sedimentary sequence almost vertically. The hydraulic conductivity, K, and the Young modulus E of the the different materials are the following: $K_{aquifer} = 10^{-2}$ cm/s, $K_{cla\ y} = K_{basement} = 10^{-8}$ cm/s, $E_{aquifer} = E_{clay} = 500$ kg/cm^2, and $E_{basement} = 5000$ kg/cm^2. The aquifer is produced by three wells located 5 km distance from the geomechanical discontinuity. Fixed and impermeable bottom and outer boundaries, and a traction-free top boundary representing the ground surface are used as boundary conditions. The simulation spans a 10-year time interval. A plane of triangle IE is introduced into the tetrahedral FE mesh in correspondence of the contact between the basement and the sandy/clayey sequence. It is conservatively assumed to have no cohesion and a friction angle $\varphi = 30°$, i.e. a typical value suggested in the literature.

The major results obtained from the geomechanical model are summarized in the lower part of Fig. 1. Following the pore pressure evolution in time, the fissure starts to slide and open from the aquifer top 2 and 6 years after the pumping inception, respectively, and in 10 years enlarges to almost the whole contact surface. A maximum ~3 cm opening and ~10 cm sliding occur at the end of the simulation period at the aquifer depth and on the ground surface, respectively. The maximum pore pressure decline and land subsidence are ~5 bar and ~25 cm, respectively.

REFERENCES

Beer, G. (1985) An isoparametric joint/interface element for finite element analysis. *Int. J. Num. Meth. Eng.* **21**, 585–600.

Carreón-Freyre, D., Cerca, M. & Hernández-Marín, M. (2005) Propagation of fracturing related to land subsidence in the Valley of Queretaro, Mexico. In: *SISOLS 2005* (ed. by A. Zhang *et al*.), vol. I, 155–164. Shanghai Scientific & Technical Publ., China.

Castelletto, N., Ferronato, M., Gambolati, G., Janna, C. & Teatini, P. (2010) Numerical modelling of case sliding in radioactive marker boreholesof the Northern Adriatic basin. *SPE Res. Eval. Engng*, in press

Ferronato, M., Gambolati, G., Janna, C. & Teatini, P. (2008) Numerical modelling of regional faults in land subsidence prediction above gas/oil reservoirs. *Int. J. Num. Anal. Meth. Geomech.* **32**, 633–657.

Geng, D.-Y. & Li, Z.-S. (2000) Ground fissure hazards in USA and China. *Acta Seism. Sinica* **13**(4), 466–476.

Holzer, T. L., Davis, S. N. & Lofgren, B. E. (1979) Faulting caused by groundwater extraction in southcentral Arizona. *J. Geophys. Res.* **84**(B2), 603–612.

Rothenburg, L., Obha, A. & El Baruni, A. (1995) Horizontal ground movements due to water abstraction and formation of earth fissures. In: *Land Subsidence* (ed. by F. B. J. Barends *et al*.), 239–249. IAHS Publ. 234. IAHS Press, Wallingford, UK.

Sheng, Z., Helm, D. & Li, J. (2003) Mechanisms of earth fissuring caused by groundwater withdrawal. *Environ. Eng. Geosci.* **9**, 352–362.

(Proceedings of EISOLS 2010, Querétaro, Mexico, 17–22 October 2010). IAHS Publ. 339, 2010.

Two-dimensional coupled numerical modelling of subsidence due to water extraction at the Lower Llobregat River, Spain

A. CONCHA[1], J. RIPOLL[1], J. PIÑA[1], A. GABÀS[2] & P. PIÑA[2]

1 *Institut Geològic de Catalunya, Àrea d'Enginyeria Geològica, Balmes 209-211, Barcelona 08006, Spain*
aconcha@igc.cat

2 *Institut Geològic de Catalunya, Unitat de Tècniques Geofísiques, Balmes 209-211, Barcelona 08006, Spain*

Abstract A Differential Interferometry of Satellite Radar (DinSAR) analysis has detected relatively strong subsidence at the St Feliu del Llobregat municipality west of Barcelona City (average maximum velocity of 0.7 cm/year for the period 1993–2006). Compilation of geological information and geotechnical logs, well piezometric measurements, and the performing of two electrical resistivity tomography (ERT) surveys allowed us to establish a geological–hydrogeological model of the site. A shallow saturated compressible clay layer (thicker where the most intense terrain deformation occurs), overlays sandy-silty gravels. Both units contain the unconfined Llobregat River upper aquifer. A simplified numerical coupled 2D-FLAC model, with the existing conditions at the site, permitted simulation of the surface deformation measured by DinSAR. Although refinements to the model, by changes in the clay layer geometry and water volume extraction rates, are still needed, the calibration of the numerical model allows the prediction of deformation under one specific water extraction rate.

Key words SAR Differential Interferometry; subsidence; Lower Llobregat River, Spain; water flow and strain-stress coupled models; FLAC-2D

INTRODUCTION

As result of a collaborative effort between the Geological and Cartographic Catalonian Institutes (IGC and ICC, respectively) in a project monitoring terrain movements with Differential Interferometry of Satellite Radar images (DinSAR), seven sites with subsidence within the Catalonian territory were identified during the years 1993–2006. Two of these sites were already known to be related to underground mining activity. For the rest of these subsidence sites, investigations to identify the possible subsidence mechanisms were carried out by compiling geotechnical, geological and hydrogeological information as suggested by the USGS subsidence database (Marturia & Concha, 2008). Preliminary results have shown that these sites are located mainly on sedimentary basins with a large density of water extraction points (ACA, 2008) and industrial land use. Here, we present the results for the Sant Feliu del Llobregat pilot site, Fig. 1, where detailed investigations were carried out by calibration of a first simplified 2-D-coupled numerical model.

GEOLOGY AND HYDROGEOLOGY AT THE MAXIMUM SUBSIDENCE AREA

The study zone is located over Quaternary sediments characterized by fluvial terrace deposits that laterally change to alluvial and colluvial deposits. Specifically at the maximum subsidence zone, consolidated and compacted Neogene deposits are covered by Quaternary deposits. These deposits are representative of the Qt1 unit, the youngest Llobregat River terrace, Fig. 1, where two different layers can be differentiated: a lower sandy-silty gravel covered by an upper layer of silty clay of variable thickness (max. 20 m). Both units contain the non-confined upper Llobregat River aquifer. The ERT surveys, Fig. 2, define the geometry of the layers and show that both are saturated. The water head variation (Δh) at this area is about three metres, Figs 1 and 3.

Copyright © 2010 IAHS Press

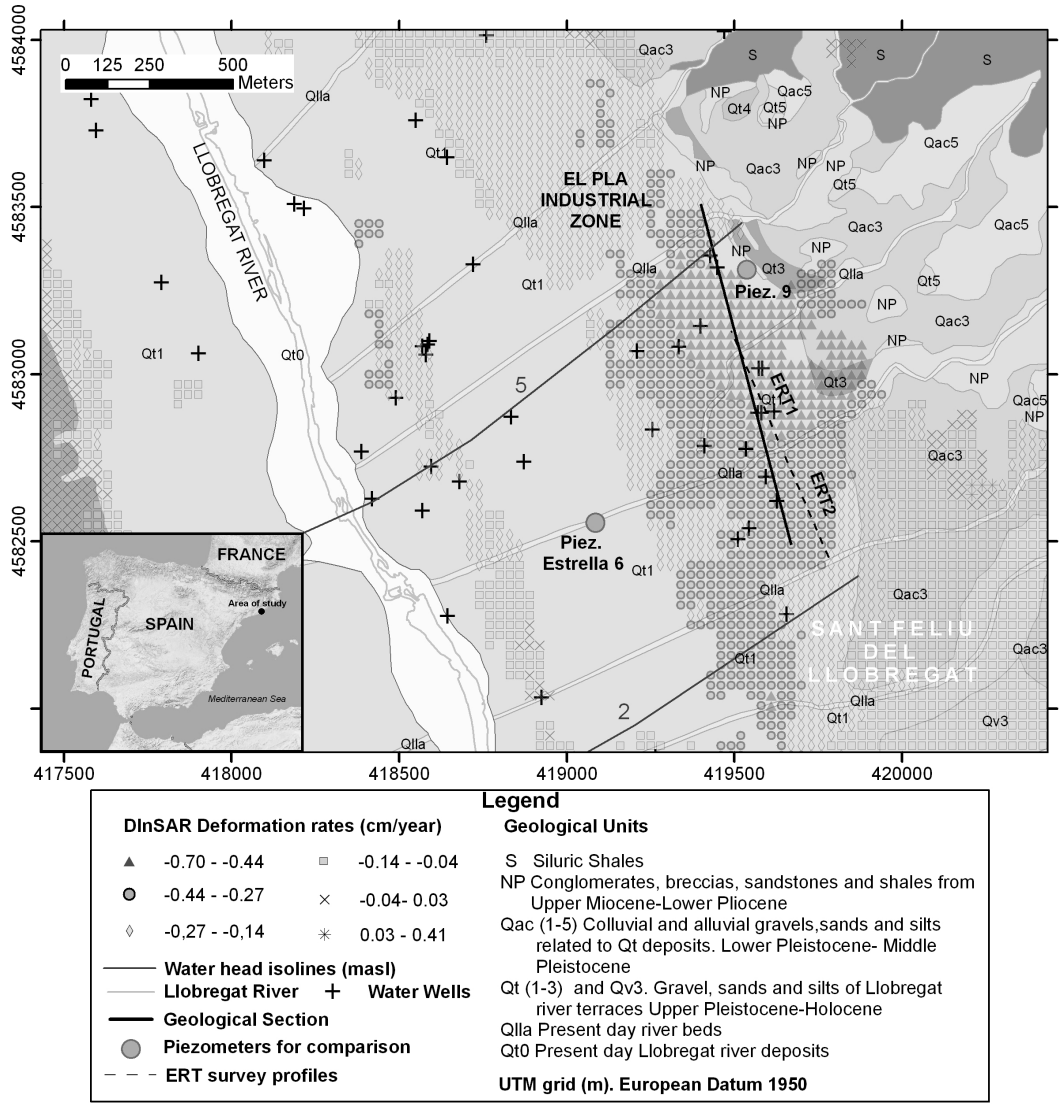

Fig. 1 Location of the study area and geological map (ICC, 2006). Location of water wells, piezometers (ACA, 2008), water head isolines (ICC, 2006), ERT surveys and simplified geological section used for the numerical model.

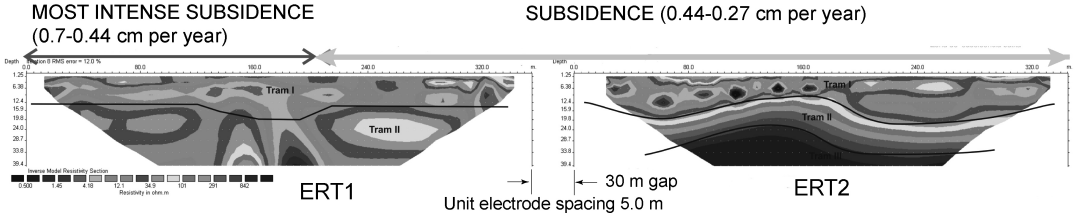

Fig. 2 Results of the ERT1 and ERT2 surveys (Gabàs *et al.*, 2009) Location is shown in Fig. 1.

FLAC SIMPLIFIED 2D NUMERICAL MODEL

A simplified numerical model was built considering the larger thickness of the shallow silty clay deposit (20 m) in a 1060-m long topographic profile, parallel to the flow direction, Fig. 1. Since variations of the phreatic level take place only in the upper silty clay layer, the thickness of the

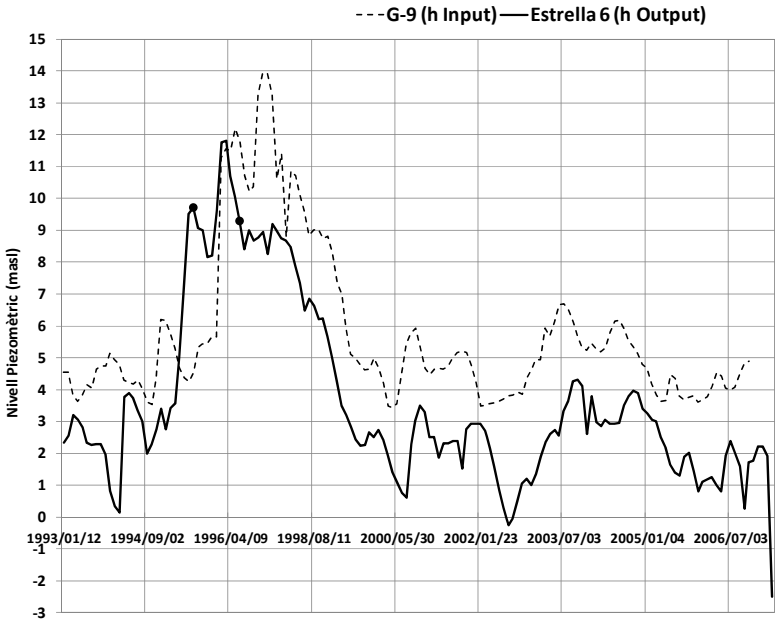

Fig. 3 Water head measurements at the model profile ends (piezometers G9 and Estrella 6, Fig. 1). Points show the water head difference in time used to calculate a first approximation of extraction water rates

Table 1 Laboratory geotechnical parameters for the two geological units used in the numerical model.

Property	Upper compressible layer	Lower silty gravelly sands
E (MPa)	25.4	10.8
Poisson ratio	0.4	0.33
Dry density (kg/m^3)	1590	1700
Friction (°)	24.5	30
Cohesion (kPa)	23.5	4.9
Porosity	0.5	0.7
Permeability (m/s)	1×10^{-9}	6×10^{-5}

lower layer was considered homogeneous (30 m). Geotechnical and hydrological laboratory parameters (IGC, 2008) for both units are shown in Table 1. The closest wells along the profile are included in the model as points of water extraction at the maximum depth of the well. Since rates of water extraction are not known at each well, the variation of the phreatic level along the profile in a 395-day long period, Fig. 3, was used to calculate a first approximation of water extraction rates. The value obtained was applied equally at each well along the profile (0.16 m^3/day), for pumping during a 15-day period, turning off pumps and step calculations for 15 days more to evaluate the response of the layer. Figure 4 shows the finite difference grid and mechanical boundary conditions.

RESULTS AND DISCUSSION

The numerical model reproduces the shape of the profile and magnitude order of the DinSAR deformation profile within the area of maximum subsidence for a 15-day period of continuous pumping at 0.16 m^3/day per well and after 15 days of restoration. Figure 4 shows the deformation

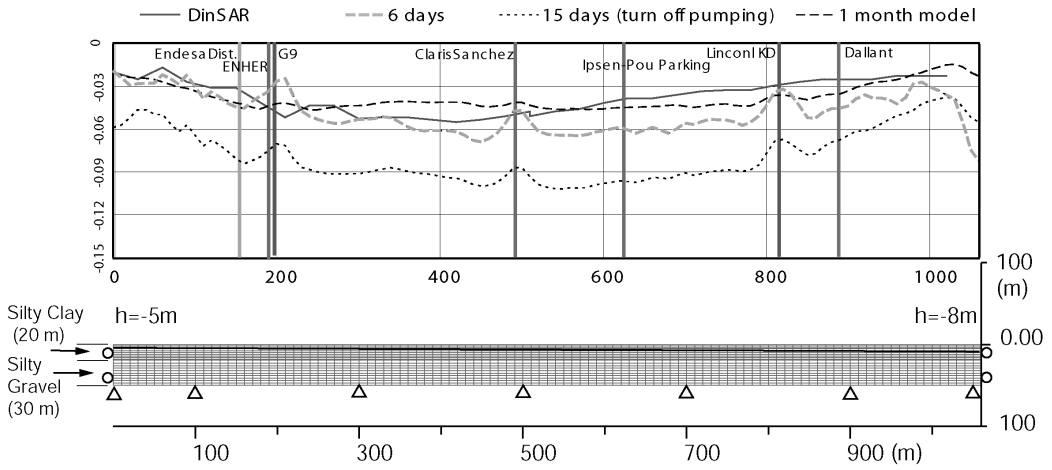

Fig. 4 Finite difference grid, mechanical boundary conditions and water head gradient (h) along the simplified geological model profile. Upper graphic shows the results of different deformation stages at the topographic surface for 1-month long calculation period. For comparison the DinSAR deformation curve was calculated for the same time period. Vertical lines mark the location of water wells.

curves for 6, 15 (turning off pumping) and 30 days. Refinements of the model might include the detailed geometry of the upper silty-clay layer, directional permeability and registered water extraction rates for each well. Sensitivity analysis of this last parameter might aid evaluation of the water extraction rates critical for subsidence to cause structural damages in buildings and soil cracking, and to establish pumping rates controls for specific environmental laws.

REFERENCES

Agència Catalana de l'Aigua (ACA) (2008) Water Well Database, http://aca-web.gencat.cat/aca/appmanager/aca/aca?_nfpb=true&_pageLabel=P122215446120820129590 3.

Gabàs, A., Benjumea, B., Macau, A., Piña, P. (2009) Tomografia elèctrica a Sant Feliu de Llobregat. *Institut Geològic de Catalunya Internal Report GA-004/09*.

Institut Cartogràfic de Catalunya (ICC) (2006) *Mapa hidrogeològic del tram baix del Llobregat i el seu delta 1:30 000*, 1st edn.

Institut Geològic de Catalunya (IGC) (2008) Geotechnical logs database, http://www.igc.cat/web/gcontent/ca/index.php.

Marturia, J. & Concha, A. (2008) Subsidències a Catalunya: Anàlisi preliminar dels aspects geològics en la interpretació de mapes DInSAR de deformació vertical. *Institut Geològic de Catalunya Internal Report AP-177/08*.

United States Geological Survey (USGS) USGS International Survey on Land Subsidence Database, http://isols.usgs.gov/.

(Proceedings of EISOLS 2010, Querétaro, Mexico, 17–22 October 2010). IAHS Publ. 339, 2010.

Introduction of the JARAS/3D simulator for natural gas dissolved in water

TSUTOMU NAKAGAWA[1], IKKOU SUZUKI[2], MANABU NOJO[3], TAKERU OGATSU[1] & TOMOYUKI HIGUCHI[1]

1 *Kanto Natural Gas Development Co., Ltd., Mobara Field Office, 661 Mobara, Mobara City, Chiba Prefecture 297-8550, Japan*
tsutomu.nakagawa@gasukai.co.jp

2 *Inpex Corporation, Exploration & Exploitation Unit, Domestic Project Division, 1-3-1 Higashi Odori, Chuo-ku, Niigata City, Niigata Prefecture 950-8512, Japan*

3 *Godo Shigen Sangyo Co., Ltd. Chiba Office, 1365 Nanaido Chosei-mura, Chiba Prefecture 299-4333, Japan*

Abstract For four years from 1996 to 1999, the former Japan National Oil Corporation and eight companies developed the JARAS/3D simulator. This simulator is characterized by its ability to express two types of gas production performance in the Southern Kanto Natural Gas Field, and evaluate amounts of land subsidence associated with gas production. This simulator has already been used in several studies by the Environment Committee. This paper introduces this simulator.

Key words simulator; natural gas deposit of dissolved-in-water type; Mobara-type production performance

BACKGROUND

The Southern Kanto Natural Gas Field in Japan is ranked among the world's largest for natural gas dissolved in water (Fig. 1). In particular, the Kujukuri region of Chiba Prefecture not only has abundant reserves of natural gas dissolved in water, but also a high concentration of iodine found in formation water that represent precious domestically-produced resources for a resource-poor country like Japan.

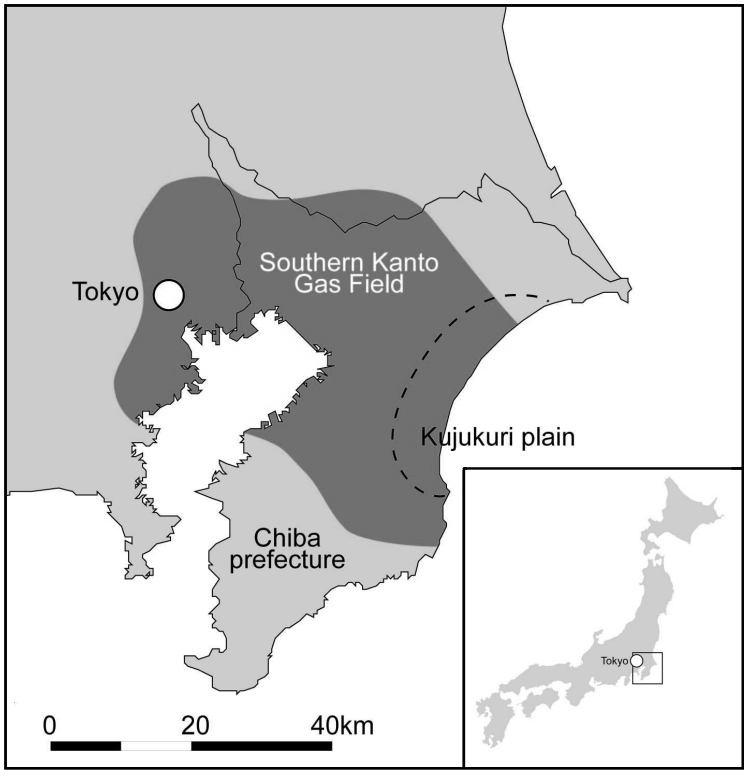

Fig.1 Southern Kanto Gas Field in Japan.

Copyright © 2010 IAHS Press

The Kazusa group, which is a reservoir for this gas field, consists of alternate layers of unconsolidated sand and mudstone. The strata are several tens of centimetres to several tens of metres thick and form a homocline with an inclination of approximately 5°. The gas wells are completed with perforated-pipe of several hundred metres in length, so that they can produce gas and formation water simultaneously from many strata. The production method used for these wells is a submersible motor pump or a gas lift.

There are two gas production performances in this field. One is the "Common type" and the other is "Mobara type". The gas water ratio (GWR) (gas production [Nm^3]/water production [m^3]) of the Common type is comparable to, or slightly less than, the solubility of gas in formation water under the reservoir's pressure and temperature conditions, and generally maintains a constant value throughout the production period. Conversely, the GWR of the Mobara type at an early stage of production is similar to that of the Common type, but gradually increases along with production progress, and finally reaches a level higher than the theoretical solubility of gas in formation water (Fig. 2).

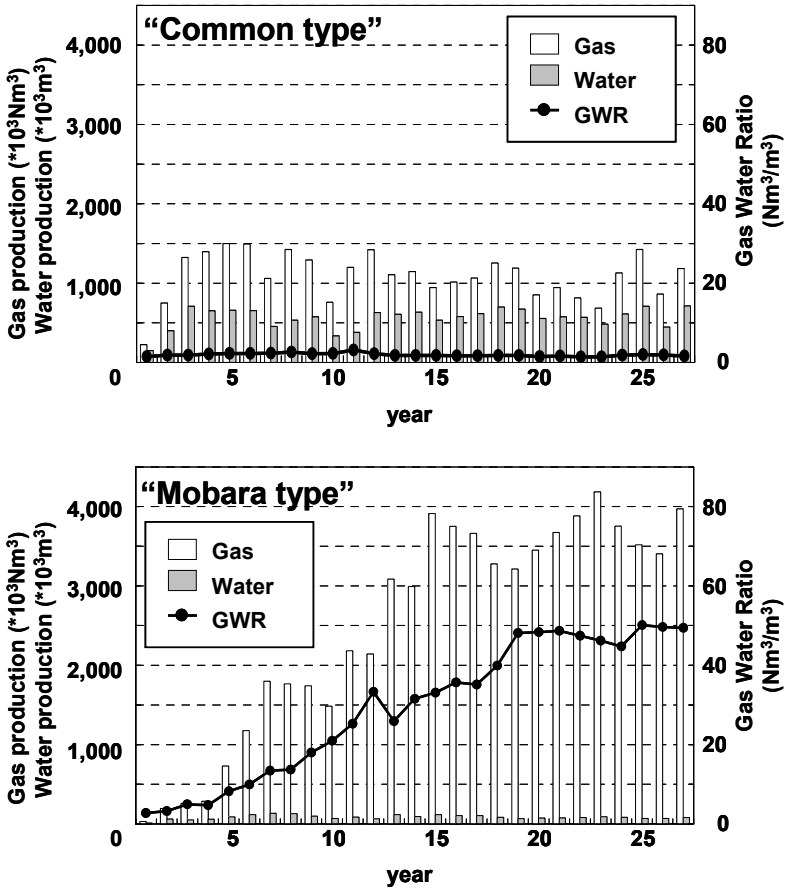

Fig. 2 Annual gas production performance in Southern Kanto Gas Field.

Land subsidence in this area was found in the late 1960s. The eight natural gas producing companies have been making efforts to control land subsidence in line with the subsidence prevention agreement concluded with the local government. Although land subsidence in recent years has been reduced in many areas, land subsidence of over 10 mm per annum is still observed in some places. The eight companies currently engaged in development in this area are addressing environmental problems including land subsidence by organizing the Environment Committee of the Japan Natural Gas Association Keiyo Natural Gas Association (hereinafter referred to as the Environment Committee).

The Environment Committee uses the JARAS/3D simulator as one of the tools for predicting land subsidence. This simulator was developed by the former Japan National Oil Corporation and the eight companies for four years from 1996 to 1999. This simulator is characterized by its ability to express two types of gas production performance in Southern Kanto Natural Gas Field, and evaluate amounts of land subsidence associated with gas production. This paper introduces this simulator.

JARAS/3D

This programme consists of the flow analysis part and the stress analysis part (Fig. 3). The flow analysis part calculates two-phase flow in the reservoir that is associated with production or injection. The stress analysis part calculates deformation based on the changes in pore water pressure calculated by the flow analysis part.

The following paragraphs outline the flow analysis part and stress analysis part, respectively.

Flow analysis part

We adopted a similar method to that of Tazaki & Yamazaki (1993). Specifically, with regard to two-phase fluid flow behaviour in the reservoir, we assumed and formulated a dual porosity type reservoir model. The unknown quantities for the governing equation are the pressures and saturation factors for the water phase and gas phase existing in the layers of sand and mudstone. We discretized those governing equations by a control volume finite element method (CVFEM). We use the IMPES method for calculation of those quantities.

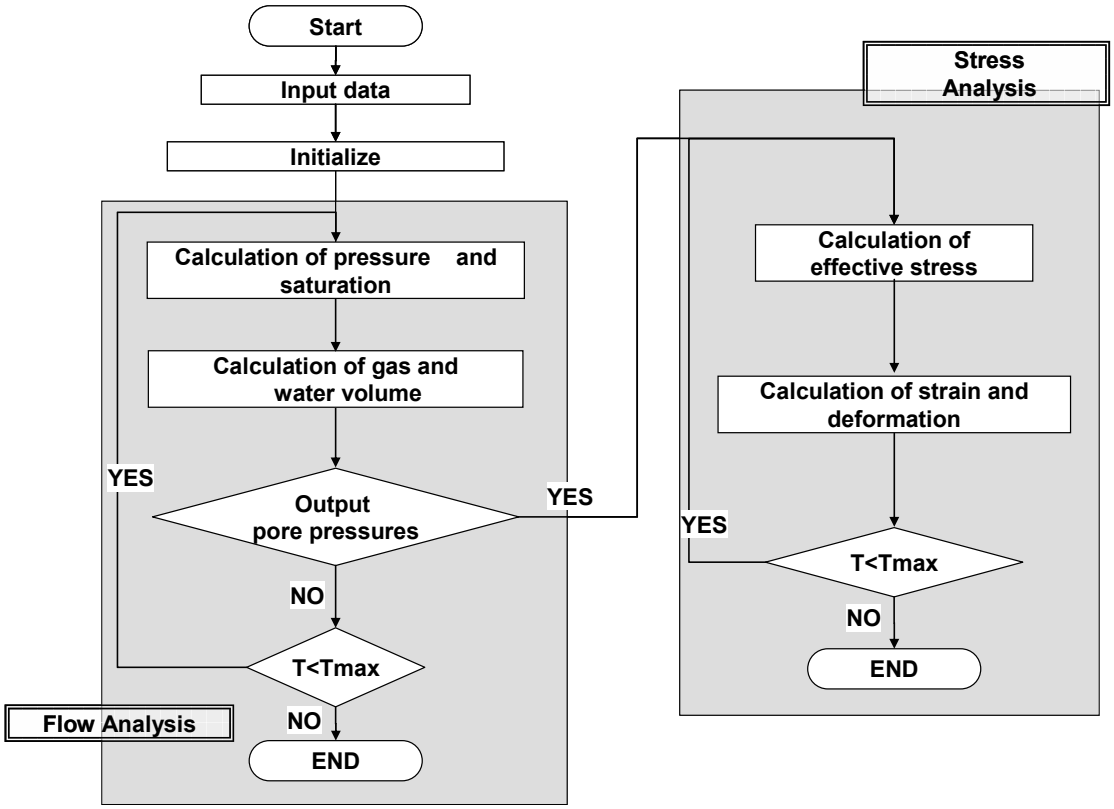

Fig. 3 JARAS/3D flowchart.

Stress analysis part

The JARAS/3D handles the formations as a continuum. We adopted a finite element method (FEM) as the discretization method. In a stress analysis, either an elastic body, an elasto-plastic body, or an elasto-viso-plastic body can be selected. The Sekiguchi-Ohta model was adopted as constitutive equations of an elasto-plastic body and an elasto-viso-plastic body.

The Sekiguchi-Ohta model (Sekiguchi & Ohta, 1977; Ohta & Sekiguchi, 1979) is an extension of the Cam-clay model. The Cam-clay model is intended for isotropically consolidated soil and thus cannot express increases in strain caused by principal stress rotation. The Sekiguchi-Ohta model, however, can express the impact of principal stress rotation. The Sekiguchi-Ohta model is the same as the original Cam-clay model under the conditions of isotropic consolidation.

CONCLUSIONS

The JARAS/3D can be characterized as follows:

(a) The JARAS/3D is a simulation program intended for Southern Kanto Natural Gas Field and can evaluate production and land subsidence.
(b) The JARAS/3D consists of the flow analysis part and the stress analysis part.
(c) The flow analysis part can simulate gas production performance of either the Mobara type or Common type.
(d) In a stress analysis, an elastic body, an elasto-plastic body or an elasto-viso-plastic body can be selected.

The eight companies have studied land subsidence using this simulator thus far, and will continue appropriate studies after this.

Acknowledgements The JARAS/3D was developed in a joint study conducted by the former Japan National Oil Corporation (present JOGMEC) and the eight companies. We should like to express our grateful thanks to JOGMEC who kindly permitted us to publish the study results in this paper.

REFERENCES

Ohta, H. & Sekiguchi, H. (1979) Constitutive equations considering anisotropy and stress reorientation in clay. In: *Proc. 3rd Int. Conf. on Numerical Methods in Geomechanics, Aachen*, 475–484. A. A. Balkema, Rotterdam, The Netherlands.

Sekiguchi, H. & Ohta, H. (1977) Induced anisotropy and time dependency in clays. In: Constitutive Equations of Soils, Proc. Specialty Session 9, *Ninth Int. Conf. Soil Mechanics & Foundation Engineering* (Tokyo), 229–238.

Tazaki, Y. & Yamazaki, T. (1993) Simulator for predicting the Mobara-type production performance. Paper Number SPE-25337.

(Proceedings of EISOLS 2010, Querétaro, Mexico, 17–22 October 2010). IAHS Publ. 339, 2010.

Parameters estimation in surface subsidence modelling

R. HEJMANOWSKI

Department of Mining Areas Protection, Geoinformatics and Mine Surveying, AGH University of Science and Technology, al. Mickiewicza 30, 30059 Krakow, Poland
hejman@agh.edu.pl

Abstract The aim of the surface subsidence modelling is efficient protection of the communities living on the mining affected areas. Furthermore, the more accurately the parameters of the prediction model are estimated, the more reliable the prognoses are. The parameters not only should have physical sense, but they also should be established for the local conditions of the minerals exploitation. The model, which is based on the influence function, of surface deformation prognosis caused by water, gas or oil exploitation is presented in this paper. The method of the parameters estimation in the local mining and geological condition are shown.

Key words modelling; parameters estimation; subsidence prediction; oil; gas; water drainage

INTRODUCTION

Deformations in oil and natural gas production areas are usually predicted for strongly urbanized parts of the world, e.g. Houston, USA. The accuracy of such forecasts depends on the assumed calculation model, its parameterization, and also the reliability of reservoir geometry data. Another important factor is the technological data determining pressure changes in the formation.

Modelling was performed with the use of the author's method based on a function of influences (Hejmanowski, 1993). Here the compaction of the porous reservoir was assumed to be the primary cause of surface displacements. Compaction phenomena also occur in areas where water is exploited from underground geological reservoirs, e.g. near Bangkok, Las Vegas, St. Joaquin Valley (California, USA).

MODEL PARAMETERS

Prediction methods lie in dividing the entire fluid reservoir into parts of specific size: base ($L \times L$) and height M. This creates the possibility to very accurately describe the geological variability of the reservoir and the changeability of technological parameters (changes of pore pressure in time). The basic relation for determining terrain subsidence caused by natural gas exploitation in an elementary part of the reservoir can assume the following form (Hejmanowski, 1995):

$$S(d,t) = \frac{a \cdot \Delta M(t) \cdot L^2}{r^2} \cdot \exp\left(-\pi \frac{d^2}{r^2}\right) \tag{1}$$

Compaction from the beginning of exploitation to a moment t ($\Delta M(t)$) depends on the drop of pore pressure in compliance with the relation (2):

$$\Delta M(t) = c_m (p_0 - p_i(t)) \cdot M \tag{2}$$

where:

- a, r, c_m – model parameters,
- d_i – distance from a specific part of the reservoir to the calculation point on the surface, of the area,
- M – original thickness of the reservoir,
- L – size of edge of the base of elementary part of the reservoir,
- p_0 – original pore pressure, and
- $p_i(t)$ – ultimate pore pressure at time t, for which prediction is made.

Copyright © 2010 IAHS Press

Assuming that deposition data are reliable and the technological data are defined by specialists responsible for modelling processes in the reservoir during exploitation, it is the parameters of the model which will determine the accuracy of the forecast by equation (1). These are three parameters: a and r which characterize the rock mass, whereas c_m, the compaction coefficient, defines the compaction features of rocks making up the reservoir. Its value usually depends on the porosity of the reservoir rocks. The compaction coefficient is usually determined from the results of specialist measurements of movements inside the rock mass (van Kesteren, 1973; Teeuw, 1973). The two remaining parameters are determined on the basis of geodesic surveys of the surface.

In models based on the influence function, parameter a is called the exploitation coefficient. When liquid or gaseous minerals are produced, this parameter should be defined as the coefficient of proportionality between a certain volume of compact reservoir rock K and the volume of the corresponding subsidence depression at the surface ΔV_M. This can take the following form (3):

$$a = \frac{\Delta V_M(\Delta t \to \infty)}{K(\Delta t \to \infty)} \tag{3}$$

where: a is the coefficient of volume losses in the process of rock mass deformation, and Δt is the time from the end of exploitation onwards.

Coefficient a assumes values from 0 to 1. During exploitation of oil, water or gas, these values can range between 0.9 and 1.0. In a situation when the parameter cannot be determined, a can be assumed as equal to 1.0, which in slow-going deformations in this type of exploitation conditions will not be erroneous.

Parameter r represents the dispersion of deformations, or in other words, the range of influences limiting the subsidence to a few percent of maximum values (Knothe, 1953). This parameter has a functional relation with the so-called angle of influence range β, in congruence with equation (4). The value of parameter r determines the accuracy of prediction of subsidence, inclinations, horizontal deformations and displacements.

$$r = \frac{H}{tg\beta} \tag{4}$$

where H is the depth of exploitation.

Model parameters can be strictly estimated on the basis of the results of height measurements performed over a similar reservoir in the course of exploitation or over the studied reservoir in previous periods. The estimation is aimed at determining distances D in line with the minimization principle:

$$\min_{(a,r)} D\{S^{surv}, S^{\mathrm{mod}}\} = \min_{(a,r)} \sum_{i=1}^{n} \left\| S_i^{surv} - S_i^{\mathrm{mod}}(\alpha,(a,r) \right\| \tag{5}$$

where: S_i^{surv} is the subsidence measured at point i in the measurement profile, S_i^{mod} is subsidence calculated with the use of a theoretical model at a measurement point and profile, and α is the model parameters.

Minimization of distance D lies in finding a minimum (min) of a function of many variables. This task can be resolved by solving a system of nonlinear equations. Equations are linearized after assuming known values approximated to both determined parameters by developing equations for subsidences S^{mod} in Taylor series, excepting high power elements. Then:

$$S^{\mathrm{mod}}(X_i,\alpha) = S_0^{\mathrm{mod}}(X_i,\alpha) + \frac{\partial S^{\mathrm{mod}}(X_i,\alpha)}{\partial \alpha_1} d\alpha_1 + \frac{\partial S^{\mathrm{mod}}(X_i,\alpha)}{\partial \alpha_2} d\alpha_2 + \ldots + \frac{\partial S^{\mathrm{mod}}(X_i,\alpha)}{\partial \alpha_m} d\alpha_m \tag{6}$$

For two parameters in equation (6), two elements will be maintained. The more difficult is the estimation of parameters, the more numerous are the elements in the model. As a result of linearization, the minimization condition will lead to a system of equations (7):

$$\begin{cases} \sum_{i=1}^{n}\left[S_0^{\mathrm{mod}}(X_i,\alpha)+\sum_{j=1}^{m}b_j\cdot d\alpha_j - S^{surv}(X_i)\right]b_1 = 0 \\ \sum_{i=1}^{n}\left[S_0^{\mathrm{mod}}(X_i,\alpha)+\sum_{j=1}^{m}b_j\cdot d\alpha_j - S^{surv}(X_i)\right]b_2 = 0 \\ .... \\ \sum_{i=1}^{n}\left[S_0^{\mathrm{mod}}(X_i,\alpha)+\sum_{j=1}^{m}b_j\cdot d\alpha_j - S^{surv}(X_i)\right]b_m = 0 \end{cases} \quad (7)$$

The system of equations (7) can then be solved with an arbitrary matrix method (Kwinta, 2008).

CONCLUSIONS

The main problem with applying the method of strict estimation of prediction model parameters is proper assumption of approximated values. Erroneous or far from reality values, assumption of a_0, r_0 may result in an indeterminate solution, which is a result of instability of the system, or obtaining results congruent with the principles of a correct solution but in conflict with the physical sense of both parameters. The physical sense that was originally ascribed to both parameters of the model, equation (1), makes the prediction method widely applicable, hence the determined values should be verified for their physical meaning.

Acknowledgements The paper was financed from the research grant no. N N524 373337 of the Ministry of Higher Education of Poland.

REFERENCES

Hejmanowski, R. (1993) Zur Vorausberechnung förderbedingter Bodensenkungen über Erdöl- und Erdgaslagerstätten. Doctoral Thesis, Technical University Clausthal , Clausthal-Zellerfeld, Germany.

Hejmanowski, R. (1995) Prediction of surface subsidence due to oil- or gasfield development. *Proceedings of the Fifth International Symposium on Land Subsidence FISOLS'95* (ed. by F. B. J. Barends, F. J. J. Brouwer & F. H. Schröder) (The Hague/ Netherlands 16–20 October 1995), 291–300.

Knothe, S. (1953) Równanie ostatecznie wykształconej niecki osiadania. *Archiwum Górnictwa i Hutnictwa*, tom 1, z.1, 1953. (Equation of a finally developed subsidence trough. In: *Mining and Metallurgy Archives* 1(1).

Kwinta A. (2008) Wyznaczenie parametrów teorii prognozowania deformacji Knothego Metodą Najmniejszych Kwadratów. Kraków (praca niepublikowana) Determining parameters of Knothe's theory of predicting deformations with the least squares method. Kraków, Poland (unpublished).

Teew, D. (1973) Laboratory measurement of compaction properties of Groningen reservoir rock. *Verhandlingen van hat Koniklijk Nederlands geologisch mijnbouwkundig Genootschap. Deel* **28**, 19–32.

Van Kesteren (1973) The analysis of future subsidence resulting from gas production in the Groningen field. *Verhandlingen van hat Koniklijk Nederlands geologisch mijnbouwkundig Genootschap. DEEL* **28**, 11–18.

3 Land Subsidence Related to Geological and Geomechanical Processes

Land Subsidence, Associated Hazards and the Role of Natural Resources Development
(Proceedings of EISOLS 2010, Querétaro, Mexico, 17–22 October 2010). IAHS Publ. 339, 2010.

Land subsidence processes and associated ground fracturing in central Mexico

D. CARREÓN FREYRE
Centro de Geociencias, Universidad Nacional Autonoma de Mexico (UNAM), Juriquilla Querétaro, Mexico
freyre@geociencias.unam.mx

Abstract Land subsidence has become a general problem in the metropolitan areas of central Mexico. Differential compaction of sediments, related to the increasing urbanization over compressible materials and groundwater withdrawals, have caused the associated phenomena of subsidence and fracturing. These high-population cities developed rapidly in the last twenty years and rely on subsurface resources for more than 70% of water supply, which represents a great challenge for natural resources management that needs to be faced with respect to use of land and groundwater. Different mechanisms of land subsidence and fracturing can be identified in each case depending on their local geological setting: in some urban areas, such as Querétaro, Celaya, San Luis Potosí, Morelia and Aguascalientes cities, the structural control of regional faults generates deformation and fracturing at the base of the covering of shallow sequences that propagate to the surface; in the recent lacustrine areas of the Valley of Mexico differential deformation of clayey and silty compressible materials that have been stressed over their bearing capacity, generates fracturing in the near-surface sequences; in volcanic valleys (i.e. Toluca) the stratigraphic contacts of granular materials interbedded with lava flows are weak planes that localize tensile stresses; toward the western part of the country, such as in Guadalajara City, the presence of huge quantities of fine grained pyroclastic materials are related to a collapsible behaviour and hydraulic fracturing because of groundwater withdrawal. An accurate evaluation of the physical vulnerability of each study case requires the implementation of an interdisciplinary methodology including geological characterization, detailed monitoring of land subsidence, groundwater flow and ground displacements.

Key words differential deformation; groundwater management; vulnerability; faulting; fracturing; Mexico

INTRODUCTION

Most of the Mexican cities affected by land subsidence are located over former lakes in valleys bounded by faults and/or volcanic structures, of ages ranging from Miocene to Quaternary, that belong to a geological province named the Transmexican Volcanic Belt (TMVB). The near-surface stratigraphy below these cities is highly heterogeneous and consists of fluvial and/or lacustrine sediments with particle sizes varying from gravel, sand and silt to clays, with inter-bedded layers of pyroclastic rocks and lava flows. Additionally, in mature and extended lacustrine environments, such as in Mexico Basin, clay size particles are composed of different kinds of clayey materials (crystallized and amorphous minerals) that have a complex mechanical behaviour. Compaction of sediments related to groundwater withdrawal has caused land subsidence in areas with rapidly increasing population (i.e. Mexico City, Toluca, Puebla, Querétaro, Celaya, León, Abasolo, Salamanca Morelia, San Luis Potosí, Aguascalientes and Guadalajara, among others). Thus, study of the shallow stratigraphy and structural discontinuities of soil sequences in areas affected by subsidence and fracturing is necessary for the planning of urban infrastructure. Furthermore, the analysis of these phenomena requires an interdisciplinary approach to obtain a better understanding of the triggering mechanisms of differential settlement and the generation and propagation of ground fracturing.

At study sites in central Mexico it has been reported that the nucleation and propagation of fractures in granular materials is caused by the interaction of diverse factors: (1) geological, pre-existing discontinuities and the depositional environment greatly influence the nucleation and geometry of fractures; (2) stress history influences the geometry of early fracturing, the first-formed fractures modify the local stress tensor and influence their evolution (e.g. Tuckwell *et al*., 2003); (3) heterogeneities in the compressibility and permeability of geological materials control

Copyright © 2010 IAHS Press

short-term and local-scale variations of deformation; (4) drastic climatic changes determine the structure of fluvio-lacustrine sediments and create weak planes that may be developed by internal changes of stress such as water extraction, loads, or other anthropogenic activities; and (5) exhaustive exploitation of aquifers that causes a decline of the pore water pressure, and may lead to compaction and land subsidence and create vertical and horizontal tension stress (Carrillo, 1947; Zeevaert, 1953; Marsal & Masari, 1959; Holzer & Davis, 1976; Holzer, 1984). A lateral effect of water extraction is the hydraulic fracturing caused by local tension stresses in the solid particles (Alberro & Hernández, 1990; Juárez-Badillo, 1991). Coexistence of one or several of the mentioned factors determines the mechanism of fracturing at diverse scales. In many reported Mexican case studies, fracturing has been considered only at a single scale so simplifying the related phenomena; however, the multi-scale characteristics of fractures need to be considered for risk assessment in urban areas.

LOCAL GEOLOGICAL SETTINGS

Fluvio-lacustrine basins located within the TMVB may present contrasting stratigraphy and also geomechanical behaviour. Lacustrine conditions prevailed until recently in the southeast of the TMVB, whereas Tertiary-Quaternary basins delimited by major faults predominate in a semi-desert area named the "Bajio Region" (i.e. Querétaro, San Luis Potosí, Morelia, Aguascalientes cities) (Fig. 1).

The areas affected by subsidence in the Mexico basin are built over silty-clay lacustrine sediments with a high gravimetric water content (100–300%) overlying a regional granular alluvial-pyroclastic aquifer. Over-exploitation of the aquifer has caused piezometric water level decline of about 50 m, and almost 13 m of land subsidence in the central part of Mexico City. Ground fracturing in Mexico City has been reported since 1925 by Gayol, and was analysed by

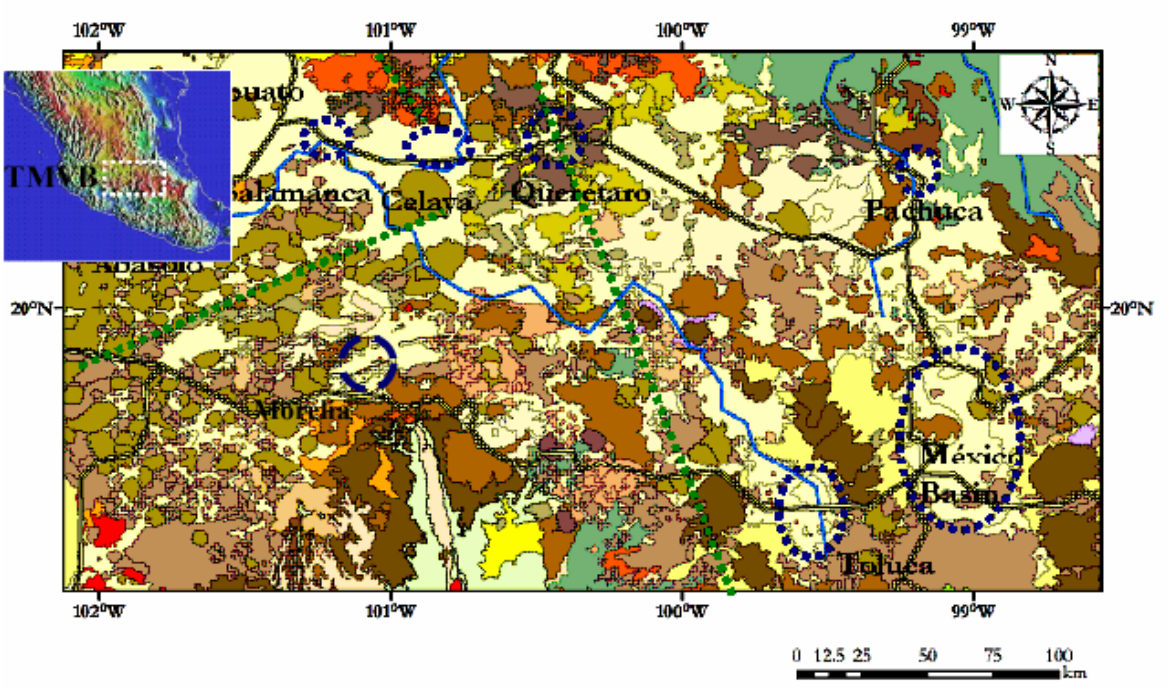

Fig. 1 Location of some cities of central Mexico with subsidence problems (dotted circles) that are located in inter-volcanic and fault bounded basins within the central Trans-Mexican Volcanic Belt Brown colours indicate Plio-Quaternary volcanic and pyroclastic events, yellow colours indicate volcano-sedimentary and lacustrine Quaternary deposits, red colours indicate intrusive rocks (geology map from Ferrari *et al.*, 2007).

Carrillo (1947), Marsal & Mazari (1959) and Zeevaert (1953, 1991) during the first half of the 20th century from the mechanical point of view, considering linear Terzaghi consolidation of the uppermost clayey aquitard. It should be noticed that regional subsidence in the Basin of Mexico was observed before intensive extraction of groundwater by pumping in the last century. Hydrogeological studies in the Basin of Mexico (Murillo, 1990; Rivera & Ledoux, 1991; Rudolph & Frind, 1991) show that subsidence and fracturing continue to increase because of transient responses of the overlying aquitard. The intensity of fracturing increases with the time and causes numerous problems to urban infrastructure.

The fast and unplanned development of the cities located in the Bajio region, in the last three decades, has caused an increase of groundwater demand that lead to a dramatic decline of the piezometric levels from a few metres to below 120 m depth. The near surface sequence that fills these fault-bounded basins consists of partially saturated (approximately 30% gravimetric water content) fluvio-lacustrine coarse grained deposits and pyroclastics interbedded with fractured andesites and basalts (Alaniz-Álvarez *et al*., 2002; Carreón-Freyre *et al*., 2005b; Pacheco *et al.*, 2006). Land subsidence and the related faulting in this region was reported previously (Trujillo-Candelaria, 1989; Trejo-Moedano & Baini, 1991; Álvarez-Manilla, 2000; Carreón-Freyre & Cerca, 2006). Fractures and normal faults with slips varying from 0.80 to 2.00 m affect the plain surfaces of the cities. As in the case of Mexico City, surface rupturing has been widely associated with subsidence and the exhaustive extraction of groundwater. The very heterogeneous stratigraphy of these basins records alternative episodes of sedimentation, volcanism and faulting (Carreón-Freyre *et al*., 2005b; Noyola *et al*., 2009). Major faulting and high lithological contrasts cause complex water withdrawal patterns and groundwater flows can not be analysed only by the interpolation of piezometric levels of water wells.

The correlation of geological, mechanical and hydraulic parameters suggests a dynamic interplay between the mechanisms of fracturing and the stress history of the local sequence. In the Bajio region groundwater decline modifies the state of stress, which is in turn modified by the pre-existing discontinuities that localize strain. The mechanical response corresponds mainly to brittle dilatant fractures and faulting determined by local variations in the grain size (silt, sand) and differential strength of geological materials. By contrast, in the lacustrine Mexico Basin, some deformation features can be related to shallow groundwater flows (perched aquifers) and as a consequence fractures open and close seasonally. At the same time, a generalized differential consolidation state of thick clayey sequences, related to deep groundwater depletion and lowering of the piezometric surface, has been established. In this case, ground fracturing is related to non-dilatant fractures in high plasticity clays. In both cases, an increase of the effective stresses induces greater differential deformation, but it does not solely explain the propagation of deformation.

GEOMECHANICAL STUDIES OF LACUSTRINE SEQUENCES

The complex mechanical behaviour of fluvio-lacustrine sediments in volcanic areas, brittle failure associated with high water contents in highly compressible fine grained materials, has been widely studied and explained by the identification of different mineralogical compositions (Marsal & Mazari, 1959; Lo, 1962; Mesri *et al*., 1976; Peralta-y-Fabi, 1989; Díaz-Rodríguez *et al*., 1998; Díaz-Rodríguez & SantaMarína, 2001; Carreón-Freyre *et al*., 2002; Carreón-Freyre, 2005). The relationship between the mineralogy of the clay and the consolidation has been widely discussed (Warren & Rudolph, 1997; Saarenketo, 1998; Wesley, 2001). Understanding the relation between the mineralogy and mechanical behaviour of clayey deposits is of the uppermost importance for the study of ground deformation. It is known that the mineralogy of the clays determines their water content. Ohstubo *et al*. (1983) correlated the limits of consistency (plasticity) with the variation in water holding capacity of soil particles according to the chemical characteristics of the clay and pore water, and described three different basic types of pore water in clayey materials: (1) intermolecular water, as a part of the structure of allophane; (2) the water adsorbed tightly to mainly smectite clay particles and; (3) the free water that moves easily between aggregates,

intergranular contact and/or microfractures in the clay matrix and that is related to the primary building materials. In sedimentary basins where volcanic activity is contemporaneous with the deposition of the sedimentary fill, the rapid weathering of pyroclastic materials (mainly ashes) generates pumice rich soils, allophane and imogolite, incipient clay minerals similar to low-order gels (Carreón-Freyre *et al*., 1998). If environmental conditions are favourable to their dehydration, these materials are transformed into gibbsite and halloysite (Righi & Meunier, in Velde, 1995). The allophane is amorphous to the X-ray diffraction method, but with an electron microscope (Wada, 1987) appears as spherical particles of about 4 nm in diameter, which are hollow, irregular and mainly composed of silica and aluminium. The imogolite has a tubular shape and is frequently associated with allophane giving the soil an open porous structure (Wesley, 2001) hence the high compressibility of these materials.

Early research reported contrasting compositions for the clayey sediments of the Basin of Mexico (Zeevaert, 1953; Marsal & Mazari, 1959; Mesri *et al*., 1976). Peralta-y-Fabi (1989) concluded that the divergence in reported results is due to changes in mineralogy with depth. Since then more studies have been carried out on the mineralogy of these materials, their changes with depth and their related mechanical behaviour (Díaz-Rodríguez *et al*., 1998; Mazari-Hiriart *et al*., 2000; Díaz-Rodríguez & SantaMarína, 2001; Gutiérrez Castorena *et al*., 2005). De Pablo-Galan *et al*. (2001) made a systematic measurement of changes in mineralogy and its influence on the viscosity for two samples at depths of 26 and 60 m, identifying a non-uniform differential behaviour between the samples. A review of the results of the mineralogical composition of the clay fraction reported by different authors has been presented by Carreón-Freyre *et al*. (2006); however, there are few studies relating the geological conditions with variations in the mineralogical, mechanical and hydraulic behaviour of lacustrine sequences (Carreón-Freyre, 2005; Hernandez-Marin *et al*., 2005), and therefore little is known about the response of these systems and the mechanisms of propagation of fracturing.

GROUND FRACTURING RELATED TO GROUNDWATER EXPLOITATION IN MEXICO

The rapid development of the urban infrastructure in the increasingly urbanized areas has also caused an increase of water demand and the mechanical and hydraulic equilibrium of the subsoil is disturbed by groundwater overexploitation (Holzer, 1984; Rojas *et al*., 2002; Carreón-Freyre *et al*., 2005a). Spatial variations in the piezometric decay can be caused by structural or compositional heterogeneities and greatly affect the initial nucleation of a fracture, and are reflected in the overall mechanical behaviour resulting in differential settlement (Zeevaert, 1953; Kreitler, 1977; Ellstein, 1978). In areas with high subsidence rates and major stratigraphic variations, fractures can originate and propagate from depth to the surface.

Analysis of groundwater flow, water management and land subsidence have been documented systematically in Mexico since the 1940s (Carrillo, 1947). Durazo & Farvolden (1989) documented the Mexico Basin as a discharge zone evidenced by large springs along the edge of the valley before the heavy pumping initiated in 1930s. By 1990, these and other authors reported water consumption of about 60 m^3/s and a recharge of about 43 m^3/s, from around 1000 wells at 70–200 m depth, and land subsidence in Mexico City (of up to 8 m) and nearby areas (Murillo *et al*., 1990; Morales *et al*., 1991; González-Morán *et al*., 1999). Several other cities have exploitation deficits of groundwater that have been related to land subsidence and an increase in ground fracturing. For instance, Huizar-Álvarez *et al*. (2003) describes how the Pachuca-Zumpango sub-basin supplies local needs and Mexico City; Carreón-Freyre *et al*., (2005b) in Querétaro reported a deficit on the aquifer supply of 30%; Noyola-Medrano (2009) reported the groundwater mining of the San Luis Potosí Valley aquifer were extraction is double the recharge and the deficit is increasing; and Ávila-Olivera & Garduño-Monroy (2008) also reported groundwater withdrawal in Morelia City.

Linear numerical analyses of groundwater depletion and increase of effective stress were developed by several authors during the last five decades (Carrillo, 1947; Herrera & Figueroa,

1969; Juárez-Badillo & Figueroa-Vega, 1984; Figueroa-Vega, 1989, 1990; Alberro & Hernández, 1990; Juárez-Badillo, 1991; Pacheco *et al*., 2006). Álvarez-Manilla (2000) and Aguilar *et al*. (2006) recently used numerical analysis integrating groundwater flow and geomechanical equations for land subsidence due to groundwater extraction. They reported a drawdown of 35 m in the hydraulic head over the last 40 years, causing a land subsidence of 6–8 m in the northeast of Mexico City.

In Mexico City and other cities, in addition to the problem of urban development and the associated fracturing due to groundwater withdrawal, it needs to be highlighted that the unplanned urbanization extends to the zones where the main recharge of the aquifers takes place (Carrera & Gaskin, 2008), so exacerbating the shortage of groundwater.

DEVELOPING INVESTIGATIONS TO MONITOR LAND SUBSIDENCE IN MEXICO

Near-surface geophysics

Several high resolution geophysical methods are being used in Mexico to characterize shallow fracturing structures in urban areas, such as ground penetrating radar (Rangel *et al*., 2002; Carreón-Freyre *et al*., 2003; Carreón-Freyre & Cerca, 2006; Ávila-Olivera & Garduño-Monroy, 2008), microgravity methods (Pacheco *et al*., 2006), and seismic methods to evaluate deeper structures, seismic microzonation (Lermo-Samaniego *et al*., 1999) and the seismic response of consolidated sediments (Aviles & Pérez-Rocha, 2010).

Remote sensing monitoring

Studies using interferometric synthetic aperture radar (InSAR) and global positioning system (GPS) are focused on Mexico City (Cabral-Cano *et al*., 2008) and indicate that rates of current land subsidence in Mexico City exceed 350 mm/year. Recently, specialists have looked for new analysis methods to improve the spatial resolution needed for surface monitoring related to faulting and fracturing in lacustrine plains: horizontal gradients of subsidence (Cabral-Cano *et al*., 2008), a method to help interferogram unwrapping (López-Quiroz *et al*., 2009); and persistent scatter interferometry (PSI) to improve the imaging of differences in subsidence rates (Osmanoglu *et al*., 2010). There are few reported works about the application of these methods in other cities of the country.

ASSESSMENT OF MULTISCALE GROUND FRACTURING IN FLUVIAL-LACUSTRINE SEQUENCES

The study of the deformation of silty and clay bearing materials below urban areas reveals the coexistence of several factors determining the characteristics of fracturing at different spatial scales. Groundwater withdrawal and the associated decrease in pore pressure and increase in effective stress is certainly of the most importance, but there are other factors such as static and dynamic over-loading and pre-existing discontinuities to be considered. The most accurate approach to understand the nucleation and propagation of fractures within heterogeneous geological media is by monitoring and analysis of the deformation conditions of the sequence, and integrating their physical and geological characteristics (stratigraphy, structural, mechanical and hydraulic variations of properties). Using this approach, fracture systems in fluvio-lacustrine sequences should be studied according to their size and considering the association of factors from which they are originated. Because concepts of “regional” and “local” are relative and depend on the scale and type of study, this review assumes the following criteria:

(1) Regional structures are larger than the urban area concerned. The irregularity of the fractured basement underlying the sedimentary sequences largely determines the location of the fracture that propagates from deep to shallow sedimentary sequences returning to pre-existing

planes of weakness, as is the case in Morelia, and Querétaro (Rojas-González *et al*., 2002; Carreón-Freyre *et al*., 2005a). At this scale, regional fault systems and stratigraphic variations should be considered for determining groundwater flow because these structures can promote preferential channel flow or form barriers and so important piezometric gradients (Kreitler, 1976; Carreón-Freyre *et al*., 2005b).

(2) At an intermediate scale are the fracture systems that mainly affect the top of the fluvio-lacustrine sedimentary sequence, often interbedded with pyroclastic and volcanic materials. The first 300 m are considered because this depth corresponds to the current average depth of groundwater exploitation wells. At this scale, one of the main mechanisms of fracturing is differential deformation (e.g. differential settlement), because the materials have a heterogeneous distribution of hydraulic and mechanical properties (Zeevaert, 1953; Ellstein, 1978; Orozco & Figueroa, 1991; Carreón-Freyre *et al*., 2003). Considering that fracture formation is only due to the lowering of groundwater piezometric levels implies a simplification of the phenomenon; it has been reported that the largest drawdowns are not related directly to the larger land subsidence phenomena in fractured areas (critical vertical displacements) (Carreón-Freyre *et al*., 2005a). For proper assessment of the conditions of propagation of fractures at this scale, study of the vertical variations of hydraulic properties of the aquifer system and the lateral variations of the compressibility of the materials is recommended (Figueroa-Vega, 1989; Carreón-Freyre *et al*, 2005a, Carrera-Hernandez & Gaskin, 2008)).

(3) The local scale refers to subsidence and fracturing in restricted areas and may vary from a few to tens of metres (the geomechnical properties of the materials can be directly characterized). This is the scale at which most geotechnical studies are performed. Examples of local fracturing are: (a) annular stress fractures that are generated in the transitional zones of the foothills of hills (Lugo-Hubp *et al*., 1991) and that are related to gravitational landslides (Cerca *et al*., 2010), (b) cracks in the surface mainly generated by evaporation-drying of clays in lacustrine plains (generated by changes in climatic conditions), (c) pore pressure diminution in the lower sedimentary layers, and (d) tensional fracturing generated by the stress of localized over-pumping (Alberro & Hernández, 1990; Juárez-Badillo, 1991).

The above considerations regarding the factors of scale and composition of clay sequences should allow appropriate design of monitoring systems and lead to accurate assessment of the hazards related to ground fracturing in the urban areas of central Mexico.

DISCUSSION

Analysis of the factors that cause land subsidence in fluvio-lacustrine basins and the generation of fractures demonstrate reliable characterization of geological materials and the changes in their properties in time and space. This requires the combination of field and laboratory techniques and systematic integration of information. The analysis of the reported literature of land subsidence and fracturing case studies in Mexico show that, even if these phenomena are determined by local geological conditions, the cities affected in central Mexico are located within the TMVB and have many triggering factors in common. Other specific cases, such as sinkhole hazards that occur in the Yucatan Peninsula or in the limestone Laguna zone of Durango, are not considered.

There are a few case studies in Mexico that involve surface and subsurface deformation monitoring. There is an urgent need in Mexico to integrate networks of benchmarks to calibrate GPS and InSAR analysis in the main affected cities. Groundwater flows follow deep and complex patterns that also require real-time monitoring. A further line of research work is coupled mechanical-hydraulic modelling to simulate the nonlinear interactions between groundwater withdrawal and its contribution to the propagation of the deformation within inelastic media. We need to establish specific training programmes addressed at different levels of students (technical, undergraduate and postgraduate) to create interdisciplinary workgroups to manage the complex databases resulting from land subsidence and fracturing studies at different scales.

Acknowledgements The author thanks the Consejo Nacional de Ciencia y Tecnología (CONACYT) and the Government of the State of Querétaro (FOMIX QRO 2004) for supporting this research work. Funding provided by the Delegación Iztapalapa, Mexico City, the Comisión Estatal de Aguas (CEA) from the Querétaro State, and the Servicio Geológico Mexicano (SGM) for different stages of this research is gratefully acknowledged. The document was greatly improved with suggestions made by M. Cerca. I am also grateful to my former and current students, and to Ricardo Carrizosa for his valuable help in the determinations of physical properties of geomaterials in the Laboratory of Multiescalar Analysis of Geosystems (LAMMG), of the Universidad Nacional Autónoma de México (UNAM).

REFERENCES

Aguilar-Pérez, L. A., Ortega-Guerrero, A., Lugo-Hubp, J. & Ortiz-Zamora, D. C. (2006) Análisis numérico acoplado de los desplazamientos verticales y generacion de fracturas por extraccion de agua subterranea en las proximidades de la Ciudad de México. *Revista Mexicana de Ciencias Geológicas* **23**(3), 247–261.

Alaniz-Álvarez, S. A., Nieto-Samaniego, A. F., Orozco-Esquivel, M. T., Vasallo-Morales, L.F. & Xu, S. S. (2002) The Taxco-San Miguel de Allende fault system: Implications for the post-Eocene deformation in Central Mexico. *Boletín de la Sociedad Geológica Mexicana* **55**, 12–29 (in Spanish).

Alberro, J. & Hernández. R. (1990) Génesis de las grietas de tensión en el Valle de México. In: *El subsuelo de la cuenca del Valle de México y su relación con la ingeniería de cimentaciones a cinco años del sismo*. Sociedad Mexicana de Mecánica de Suelos, 95–106.

Álvarez-Manilla A. (2000) Modelo del mecanismo de agrietamiento en el Valle y Zona Metropolitana de Querétaro. Master Thesis in Engineering. Universidad Autónoma de Querétaro, Mexico.

Ávila-Olivera, J. A. & Garduño-Monroy, V. H. (2008) A GPR study of subsidence-creep-fault processes in Morelia, Michoacán Mexico. *Engineering Geology* **100**, 69–81.

Aviles, J. & Pérez-Rocha, L. E. (2010) Regional subsidence of Mexico City and its effects on seismic response. *Soil Dynamics and Earthquake Engineering* **30**, 981–989.

Cabral-Cano, E., Dixon, T. H., Miralles-Wilhem, F., Diaz-Molina, O., Samchez-Zamora, O. & Carande, R. E. (2008) Space geodetic imaging of rapid ground subsidence in Mexico City. *GSA Bull.* **120**(11-12), 1556–1566; doi: 10.1130/B26001.1

Carreón-Freyre, D. & Cerca, M. (2006) Delineating the near-surface geometry of the fracture system affecting the valley of Querétaro, Mexico: Correlation of GPR signatures and physical properties of sediments. *Near Surface Geophysics, EAGE (European Assoc. of Geoscientists and Engineers)* **4**(1), 49–55.

Carreón-Freyre., D. C., Hidalgo-Moreno C. & Hernández-Marín, M. (2006) Mecanismos de fracturamiento de depósitos arcillosos en zonas urbanas. Caso de deformación diferencial en Chalco, Estado de México. *Boletín de la Sociedad Geológica Mexicana. Número Especial de Geología Urbana* tomo **LVIII**(2), 237–250.

Carreón-Freyre, D. C. (2005) Importancia de la caracterización de arcillas en laboratorio para la adecuada evaluación de sus propiedades mecánicas. In: *Cristalografía: Fundamentos Técnicas y Aplicaciones* (ed. by L. Bucio), 273–282. Sociedad Mexicana de Cristalografía. A. C. ISBN 970-9888-07-2.

Carreón-Freyre., D., Cerca Martínez, M. & Hernández Marín, M. (2005a) Propagation of fracturing related to land subsidence in the Valley of Querétaro, Mexico. In: *Proc 7th International Symposium on Land Subsidence* (SISOLS 2005, Shanghai, China), vol. 1, 155–164. ISBN 7-5323-8209-5.

Carreón-Freyre., D., Cerca M., Luna González, L. & Gámez-González, F. J. (2005b) Influencia de la estratigrafía y estructura geológica en el flujo de agua subterránea del Valle de Querétaro. *Revista Mexicana de Ciencias Geológicas* **22**(1), 1–18.

Carreón-Freyre., D. C., Cerca M. & Hernández-Marín, M. (2003) Correlation of near-surface stratigraphy and physical properties of clayey sediments from Chalco Basin, Mexico, using Ground Penetrating Radar. *J. Appl. Geophys.* **53**, 121–136.

Carreón-Freyre, D. C., Hernández-Marín, M. & Vargas-Cabrera, C. (2002) Análisis de factores geológicos durante la consolidación de suelos arcillosos. Consideraciones para la evaluación de compresibilidad en laboratorio y campo. *Memorias de la XXI Reunión Nacional de la Sociedad Mexicana de Mecánica de Suelos*, vol. 1, 105–114.

Carreón-Freyre, D. C., Gama-Castro, J., Palacios-Mayorga, S. & Garnica-Anguas, P. (1998) Propiedades y clasificación de los suelos residuales de México. XIX Reunión Nacional de Mecánica de Suelos, 75–80.

Carrera-Hernández J. J. & Gaskin, S. J. (2008) Spatio-temporal analysis of potential aquifer recharge: Application to the Basin of Mexico. *J. Hydrol.* **353**, 228–246.

Carrillo, N., 1947. Influence of artesial wells in the sinking of Mexico City, en Volumen Nabor Carrillo: El hundimiento de la Ciudad de México y el Proyecto Texcoco. Com. *Impulsora y Coordinadora de la Investigación Científica Anuario* **47**, 7–14.

Cerca, M., Carreón-Freyre, D. & Gutiérrez-Calderón, R. (2010) Instability of the urbanized flank of El Peñón del Marques volcanic edifice and its relation to land subsidence in Mexico City. In: *Land Subsidence, Associated Hazards and the Role of Natural Resources Development* (Proc. EISOLS 2010, Querétaro, Mexico, October 2010). IAHS Publ. 339 (this volume).

De Pablo Galan, L., De Pablo, J. J. & Chávez García, L. (2001) Diagenesis and shear rheology of a Recent-Pleistocene volcanogenic sequence, Mexican Basin. Implication ti swelling and stability. *Revista Mexicana de Ciencias Geológicas* **18**(2), 175–185.

Díaz-Rodríguez, A., Lozano-Santacruz, R., Dávila-Alcocer, V. M., Vallejo, E. & Girón García (1998) Physical, chemical, and mineralogical properties of Mexico City sediments: a geotechnical perspective. *Canadian Geotechnical J.* **35**, 600–610.

Díaz-Rodríguez, A. & SantaMarína, J. C. (2001) Mexico City soil behavior at different strains: Observations and physical interpretation. *J. Geotechnical and Geoenvironmental Engineering* **127**(9), 783–789.

Durazo, J. & Farvolden, R. N. (1989) The groundwater regime of the Valley of Mexico from historic evidence and field observations. *J. Hydrol.* **112**, 171–190.

Ellstein, A. (1978) Teoría sobre el mecanismo de falla en el subsuelo y la ingeniería de cimentaciones en el área urbana del valle de México. Editado por Sociedad Mexicana de Mecánica de Suelos, 177–181.

Ferrari, L., Rosas-Elguera, J., Carrasco-Núñez, G., Orozco-Esquivel, M. T. & Norato-Cortéz, T. (2007) Cartografía Geológica Digital de la Faja Volcánica Transmexicana y áreas adyacentes. *Digital Geosciences* vol 2. *J. Interactive Geoscientific Cartography* (www.digitalgeosciences.unam.mx).

Figueroa-Vega, G. E. (1990) Grietas por sobreexplotación y hundimientos durante sismos en el subsuelo de la cuenca del Valle de México y su relación con la ingeniería de cimentaciones a cinco años del sismo. Editado por Sociedad Mexicana de Mecánica de Suelos, 107–108.

Figueroa-Vega, G. E. (1989) Mecanismos de producción de grietas inducidos por la explotación del agua subterránea. *Academia Mexicana de Ingeniería. Alternativas Tecnológicas* **29**, 371–378.

González-Morán, T., Rodríguez, R. & Cortes, S. A. (1999) The Basin of Mexico and its metropolitan area: water abstraction and related environmental problems. *J. South American Earth Sciences* **12**, 607–613.

Gutiérrez-Castorena, M. del C., Stoops, G., Ortiz-Solorio, C. A. & López-Ávila, G. L. (2005) Amorphous silica materials in soils and sediments of the Ex-Lago de Texcoco, Mexico: An explanation for its subsidence. *Catena* **60**, 205–226.

Herrera, I. & Figueroa-Vega, G. E. (1969) A correspondance principle for the theory of leaky aquifers. *Water Resour. Res.* **5**(4), 900–904.

Hernández-Marín, M., Carreón-Freyre, D. & Cerca, M. (2005) Mechanical and physical properties of the montmorillonitic and allophanic clays in the near-surface sediments of Chalco Valley, Mexico. In: *Proc. 7th International Symposium on Land Subsidence SISOLS* (Shanghai, P.R. China), vol. I, 276–285. Shanghai Sci. and Tech. Publ. ISBN 7-5323-8209-5.

Holzer, T. L. (1984) Ground failure induced by ground-water withdrawal from unconsolidated sediment. *Reviews in Engineering Geology* **6**, 67–105.

Holzer, T. L. & Pampeyan, E. H. (1981) Earth fissures and localized differential subsidence. *Water Resour. Res.* **17**, 223–227.

Holzer, T. L. & Davis, S. N. (1976) Earth fissures associated with watertable declines. *Geological Society of America* (abstracts), **8**(6), 923–924.

Huizar-Álvarez, R., Hernández, G., Carrillo-Martínez, M., Carrillo-Rivera, J. J., Hergt, T. & Angeles, G. (2003) Geologic structure and groundwater flow in the Pachuca-Zumpango sub-basin, central Mexico. *Environmental Geology* **43**, 38599, doi: 10.1007/s00254-002-0654-4.

Juárez-Badillo., E. & Figueroa Vega, G. E. (1984) Stresses and displacements in an aquifer due to seepage forces (one dimensional case). *J. Hydrol.* **73**, 259–288.

Juárez-Badillo, E. (1991) Grietas por fuerzas de filtración-agrietamiento de Suelos Sociedad Mexicana de Mecánica de Suelos, 39–42.

Kreitler, Ch. W. (1976) Faulting and land subsidence from groundwater and hydrocarbon production, Houston-Galveston, Texas, California. USA. In: *Land Subsidence* (Proc. Second Int. Symp. on Land Subsidence. Anaheim, California), 435. IAHS Publ. 121. IAHS Press, Wallingofrd, UK.

Kreitler, C. W. (1977) Fault control of subsidence, Houston, Texas. *Ground Water* **15**(3), 203–214.

Larson, M. K. (1984) Potential for subsidence fissuring in the Phoenix Arizona USA area. In: *Land Subsidence* (Proc. Third Int. Symp. on Land Subsidence, Venice, Italy), 291–299. IAHS Publ. 151. IAHS Press, Wallingford, UK.

Lermo-Samaniego J., Garduño-Monroy V. H., Arreygue-Rocha E., Israde-Alcántara I. & Rodríguez-Torres G. (1999) Microficacion smica preliminar de la Ciudad de Morelia, Michoacán, México. Mem. XII Con. Nacional de Ingeniería Sísmica, Morelia, Mich. México.

Lo, K. Y. (1962) Shear strength properties of a sample of volcanic material of the Valley of Mexico. *Geotech*. **12**(4), 303–310.

Lofgren, B. E. (1972) Sensitive response of basin deposits to regional stress changes. *Geological Society America, Abs. with Programs* **5**(7), 715–716.

López-Quiroz, P., Doin, M-P., Tupin, P., Briole, P. & Nicolas, J-M. (2009) Time series analysis of Mexico City subsidence constrained by radar interferometry. *J. Appl. Geophys.* **69**, 1–15.

Lugo-Hubp J., Pérez-Vega, A. & Rojas-Salas M. (1991) Formación de grietas en la margen del antiguo lago al oriente de la cuenca de México. *Geofísica Internacional* **30**(2), 87–95.

Marsal, R. J. & Mazari, M. (1959) *El subsuelo de la Ciudad de México*. Instituto de Ingeniería, Universidad Nacional Autónoma de México, Mexico City. 377 pp.

Mazari-Hiriart, M, Hernández-Eugenio, C., Rojo-Callejas, F. & Lozano-Santacruz, R. (2000) Vertical variability of PCE sorption in the lacustrine clays of Mexico City. *Environmental Geology* **39**(6), 595–602.

Mesri, G., Rokhse, A. & Bonor, B. F. (1976) Compositive and compressibility of typical samples of Mexico City. *Geotechnique* **25**(3), 527–554.

Morales, R., Murillo-Fernández, R. & Hernández-Rubio, A. (1991) Subsidence of the former Texcoco Lake. In: *Land Subsidence* (ed. by A. I. Johnson) (Proc. 4th Int. Conf. on Land Subsidence, Houston), 35–43. IAHS Publ. 200. IAHS Press, Wallingford, UK.

Murillo, F. R. (1990) Overexploitation of the aquifer of the Mexico Basin: effects and alternative solutions. Proc. Symp. El subsuelo de la Cuenca del Valle de México y su relación con la Ingeniería de Cimentaciones a cinco años del sismo Sociedad Mexicana de Mecánica de Suelos, México, 109–118 (in Spanish).

Noyola-Medrano, M.C., Ramos-Leal, J. A., Domínguez-Mariani, E., Pineda-Martínez, L. F., López-Loera, H. & Carbajal, N. (2009) Factores que dan origen al minado de acuíferos en ambientes áridos: caso Valle de San Luis Potosí. *Revista Mexicana de Ciencias Geológicas* **26**(2), 395–410.

Ohtsubo, M., Takayama, M. & Egashira, K. (1983) Relationships of consistency limits and activity to some physical and chemical properties of Ariake Maríne Clays. *Soils and Foundations* **23**(1), 38–46.

Orozco, J. M. & Figueroa, V. G. (1991) Descripción cronológica del desarrollo de los conocimientos sobre el agrietamiento de terrenos. Agrietamiento de suelos, Sociedad Mexicana de Mecánica de Suelos, 1–12.

Osmanoglu, B., Dixon, T. H., Wdowinski, Sh., Cabral-Cano, E. & Jiang, Y. (2010) Mexico City subsidence observed with persistent scatterer InSAR. *Int. J. Applied Earth Observation and Geoinformation*, doi:10.1016/j.jag.2010.05.009 (in press).

Pacheco, J., Arzate, J., Rojas, E., Arroyo, M., Yutsis, V. & Ochoa, G. (2006) Delimitation of ground failure zones due to land subsidence using gravity data and finite element modeling in the Querétaro valley, Mexico. *Engineering Geology* **84**, 143–160.

Peralta-y-Fabi, R. (1989) Sobre el origen de algunas propiedades mecánicas de la formación arcillosa superior del Valle de México. Simposio sobre Tópicos Geológicos de la Cuenca del Valle de México. SMMS, México, 43–53.

Rangel, D., Carreón, D., Cerca, M. & Méndez, E. (2002) Valuation of ground penetrating radar for the record of structures in fluvio lacustrine soils. *J. Appl. Res. Technol*. **1**(1), 85–93.

Rivera, A. & Ledoux, E. (1991) Non-linear modelling of groundwater flow and total subsidence in the Mexico City aquifer-aquitard system. In: *Land Subsidence* (ed. by A. I. Johnson) (Proc. 4th Int. Conf. on Land Subsidence, Houston), 45–58. IAHS Publ. 200. IAHS Press, Wallingford, UK.

Rojas-González, E., Arzate-Flores, J. & Arroyo, M. (2002) A method to predict the group fissuring and faulting caused by regional groundwater decline. *Engineering Geology* **65**, 245–260.

Rudolph, D. L. & Frind, E. O.(1991) Hydraulic response of highly compressible aquitards during consolidation. *Water Resour. Res.* **27**(1), 17–28.

Trejo-Moedano, A. (1989) Estratigrafía y propiedades mecánicas del subsuelo del valle de la zona urbana de Querétaro. Reporte Interno. Universidad Autónoma de Querétaro (UAQ), 150 p.

Trejo-Moedano, A. & Baini, M. A. (1991) Agrietamiento de suelos en la zona de Querétaro. In: *Agrietamiento de Suelos*, 67–74. Sociedad Mexicana de Mecánica de Suelos.

Trujillo Candelaria, J. A. (1989) Fallamiento de terrenos en Celaya, Gto. *Academía Mexicana de Ingeniería. Alternativas Tecnológicas* **29**, 367–369.

Saarenketo, T. (1998) Electrical properties of water in clay and silty soils. *J. Appl. Geophys*. **40**, 73–88.

Tuckwell, G. W., Lonergan, L. & Jolly, R. J. (2003) The control of stress history and flaw distribution on the evolution of polygonal fracture networks. *J. Structural Geology* **25**(8), 1241–1250.

Velde, B. (1995) *Origin and Mineralogy of Clays. Clays and The Environment*. Springer-Verlag.

Wada, K. (1987) Minerals formed and mineral formation from volcanic ash by weathering. *Chemical Geology* **60**, 17–28.

Warren, C. J. & Rudolph, D. L. (1997) Clay minerals in basin of Mexico lacustrine sediments and their influence on ion mobility in groundwater. *J. Contam Hydrol.* **27**, 177–198.

Wesley, L. D. (2001) Consolidation behaviour of allophane clays. *Geotechnique* **51**(10), 901–904.

Zeevaert, L. (1953) Estratigrafía y problemas de ingeniería en los depósitos de arcilla lacustre de la Ciudad de México. Memoria del Congreso Científico Mexicano vol. 5, 58–70.

Zeevaert, L. (1991) Problems of deep founding design related with regional sinking. Proc. Symp. Agrietamiento de suelos Sociedad Mexicana de Mecánica de Suelos, 43–62 (in Spanish).

(Proceedings of EISOLS 2010, Querétaro, Mexico, 17–22 October 2010). IAHS Publ. 339, 2010.

Subsidence in the Holocene delta of The Netherlands

L. M. VONHÖGEN[1,2], P. J. DOORNENBAL[1,2], GER DE LANGE[1,2], P. A. FOKKER[2] & J. L. GUNNINK[2,1]

1 *Deltares, PO Box 85467, 3508, AL, Utrecht, The Netherlands*

2 *TNO-Geological survey of the Netherlands, PO Box 80015, 3508, TA, Utrecht, The Netherlands*
laura.vonhogen@deltares.nl; jan.gunnink@tno.nl

Abstract The low-lying part of The Netherlands is very vulnerable in terms of surface subsidence due to peat oxidation and peat/clay compaction. To gain knowledge about this kind of subsidence and the factors driving it, a study was performed in which as many surface elevation data were collected as possible and processed to obtain a subsidence map. Quality control was an important step in this study, as it controlled the decision to use measurements for the final map. Subsidence rates were derived by fitting a linear trend line through the altitude measurements in time. The result is a map of the historic subsidence rates, with the main focus on the Holocene area. This map points out areas that are vulnerable to (future) subsidence and will be a valuable tool for regional policy makers such as water boards.

Key words Holocene subsidence; subsurface composition; peat oxidation

INTRODUCTION

Surface movement in The Netherlands can be due to shallow and deep causes. The deep causes of movement are extraction of hydrocarbons, salt mining and geothermal production. The shallow causes are anthropogenic interventions, peat oxidation and peat/clay compaction. Of these, oxidation and compaction are largely influenced by lowering of phreatic groundwater levels, and show correlation with the composition of the shallow subsurface. As large areas of the Holocene part of The Netherlands (Fig. 1(a)) contain clay and peat (Fig. 1(b)), it is very vulnerable in terms of future surface subsidence. In addition, this western part of The Netherlands lies well below the average sea level and large subsidence is therefore not desirable in terms of flood risk, salinization, damage to constructions by means of differential subsidence, etc.

In our study, a map of the historic subsidence was made, focusing on the Holocene area. This map points out areas that are vulnerable to subsidence. In addition, it provides knowledge about the key process driving the surface subsidence, if combined with other maps such as, for example, the extent of clay and peat. In this way it becomes a valuable tool for (regional) policy makers to assess the effect of their past policies and to improve decision making.

METHODOLOGY

We collected all available surface level data in the Holocene part of The Netherlands. The data came from different sources: detailed elevation points derived from the Survey Department, measurements derived from the water boards, altitude measurements at geological drillings and a Lidar-based topographical map of The Netherlands, called AHN (Algemeen Hoogtebestand Nederland).

Collected data

The Survey Department and the Army Map Service measured about 3.8 million surface level points in the 1940–1980s. These measurements were digitized in the early 1990s. The measurement methods included topographical levellers, tachymetry, heights measured by barometer reading and aero photography.

The water boards have been measuring the change of surface level since the 1950s. The data from twenty individual water boards have been collected and included about 455 thousand surface

Copyright © 2010 IAHS Press

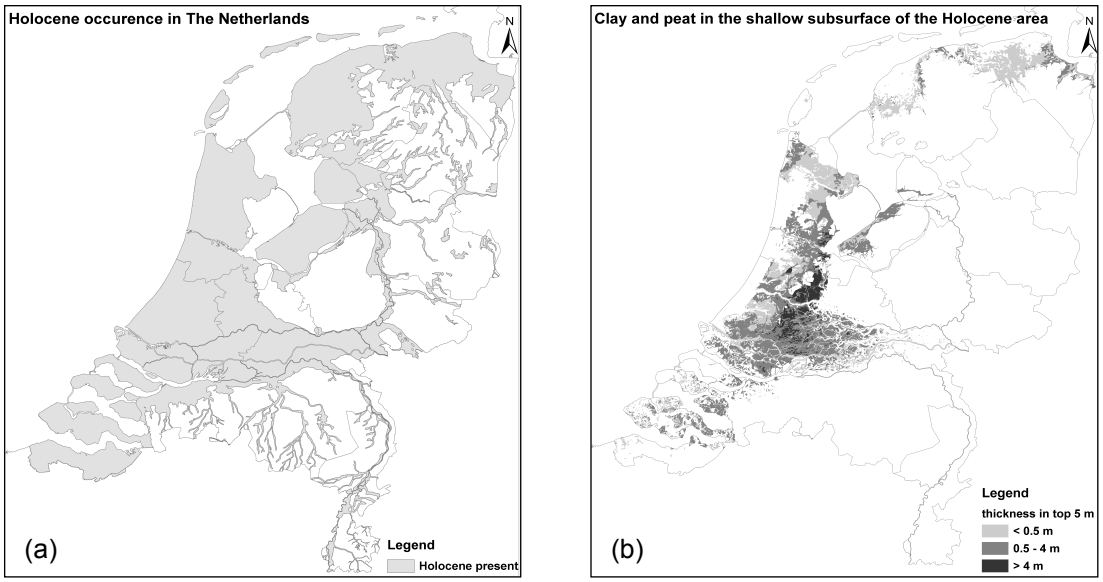

Fig. 1 (a) Holocene occurrence in The Netherlands, b) Clay and peat in the shallow subsurface of the Holocene area.

level points. The methods used to measure these points incorporated topographic levellers, dGPS (Differential Global Positioning System) and other unknown measurement methods.

The Geological Survey has carried out thousands of geological drillings since 1834 and stored all these drillings in a database called DINO (DINO*LOKET*, 2010). For most of these drillings the surface level and execution date was registered. These surface level heights were sometimes estimated from the maps made by the Survey Department and are therefore of no use. However, some geological drillings, about 10 thousand, were measured with dGPS, a topographic leveller, or another measurement method.

The AHN is a surface level, digital elevation map (DEM) created at the request of the Government. This map is an interpolation from altitude points gathered by LIDAR (LIght Detection And Ranging) towards a 5-by-5 metre grid. LIDAR uses laser pulses to measure the distance towards a certain object or surface and by using this technique from an airplane the entire Netherlands were measured between 1997 and 2003.

Selection and validation

The elevation points of the Survey Department, Water Boards and Geological Survey were combined and stored with several attributes, including the coordinates, the altitude, the measurement date, the location type, measurement method, rounding off and the altitude uncertainty of each point. The latter was based on the measurement method and the rounding off. The data set of elevation points, about 1.7 million, was complemented by surface elevation values obtained by extracting the elevation value and measuring date of the AHN at exactly the same location as the elevation points. If the AHN had no value at that specific coordinate, for example at a water surface, the elevation point was left out of the analysis.

Quality control was an important step in the decision to use measurements for the final maps. It contained the identification and removal of outliers (e.g. altitudes that differ by metres from surrounding points), duplicates, incorrect measurement dates (e.g. if the measurement date was unknown, the year was replaced with 1800) and incorrect references to the Dutch Ordnance level (NAP). Furthermore, obvious human interference that had changed the altitude, such as the expansion of cities, constructions of roads, etc., were selected and removed. Finally, the remaining points were clipped with the boundary of the Holocene occurrence in The Netherlands, which was the area of interest in this study, Fig. 2(a) and (b).

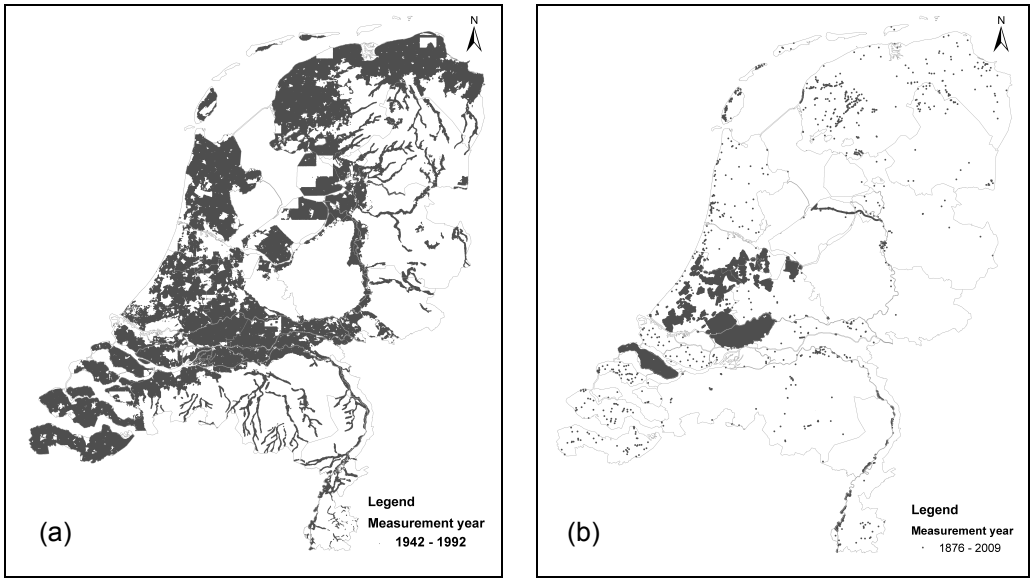

Fig. 2 (a) The remaining points from the Survey Department, and (b) the remaining elevation points from the water boards and geological drillings.

Calculations

Subsidence rates were calculated by fitting a linear trend line (Fig. 3) through altitude measurements in time. Two methods were used to select the measurement points for this calculation:

(1) The points were connected to a position on a predefined 100 m × 100 m grid. The points within the same grid cell were used to calculate the associated subsidence rates for that cell.
(2) The points were collected for areas of equal water level maintenance (peilvak). All points within an area were used to calculate the associated subsidence rate for that area.

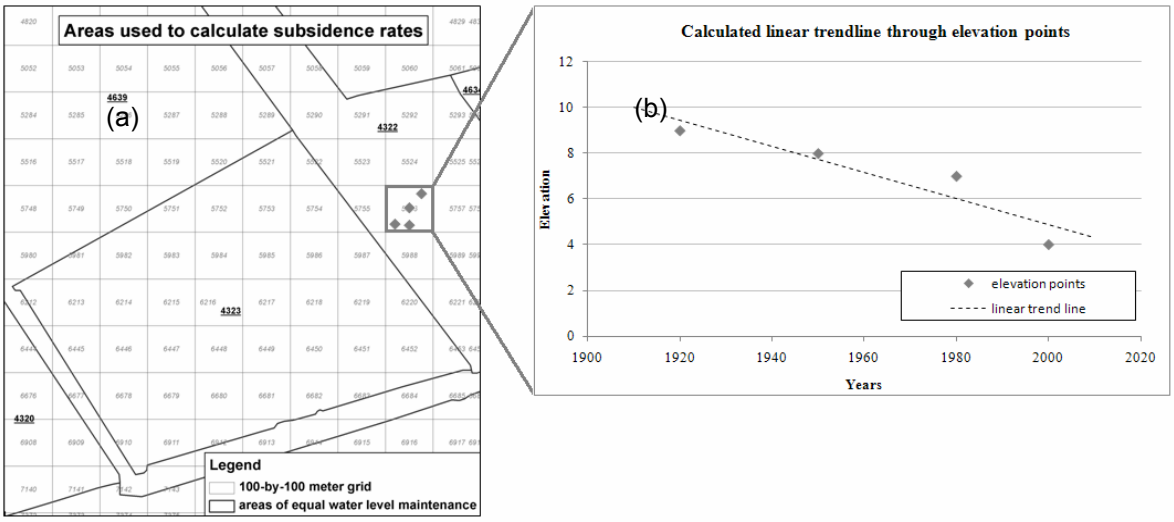

Fig. 3 The areas (a) used to select the measurement points for the linear trend line calculation (b).

For a selected polder area in The Netherlands, the Krimpenerwaard (Fig. 4), we executed a dedicated study in order to optimize the above procedure. The results of this study are visualized in Fig. 5, showing that method (1) gives a very speckled image (Fig. 5(a)). This speckled image shows the vulnerability of this method for outliers, since the number of measurement points used

Fig. 4 Location of the Krimpenerwaard.

Fig. 5 Subsidence rates in the Krimpenerwaard: (a) method (1), and (b) method (2).

in the calculation is less than in method (2). The results of method (2) are satisfactory, as the outliers are averaged out by using the larger areas of equal water level maintenance (Fig. 5(b)). We therefore used method (2) for the nation-wide procedure.

RESULTS

We have successfully created a map of surface subsidence in the Holocene area of The Netherlands (Fig. 6). This nation-wide map shows that especially the peat area of Holland (A) is vulnerable to subsidence, as are the areas that are recently reclaimed from the sea (B). The subsidence near the gas producing fields in the northern province of Groningen (C) is striking as well. However, the areas near the dunes (I), the ice-pushed ridge (II) and the rivers (III) show a much smaller subsidence.

DISCUSSION

Although 23 percent of the calculated subsidence rates are positive, i.e. show up heave, less than 1 percent of these areas have a gradient larger than the maximum defined altitude uncertainty of

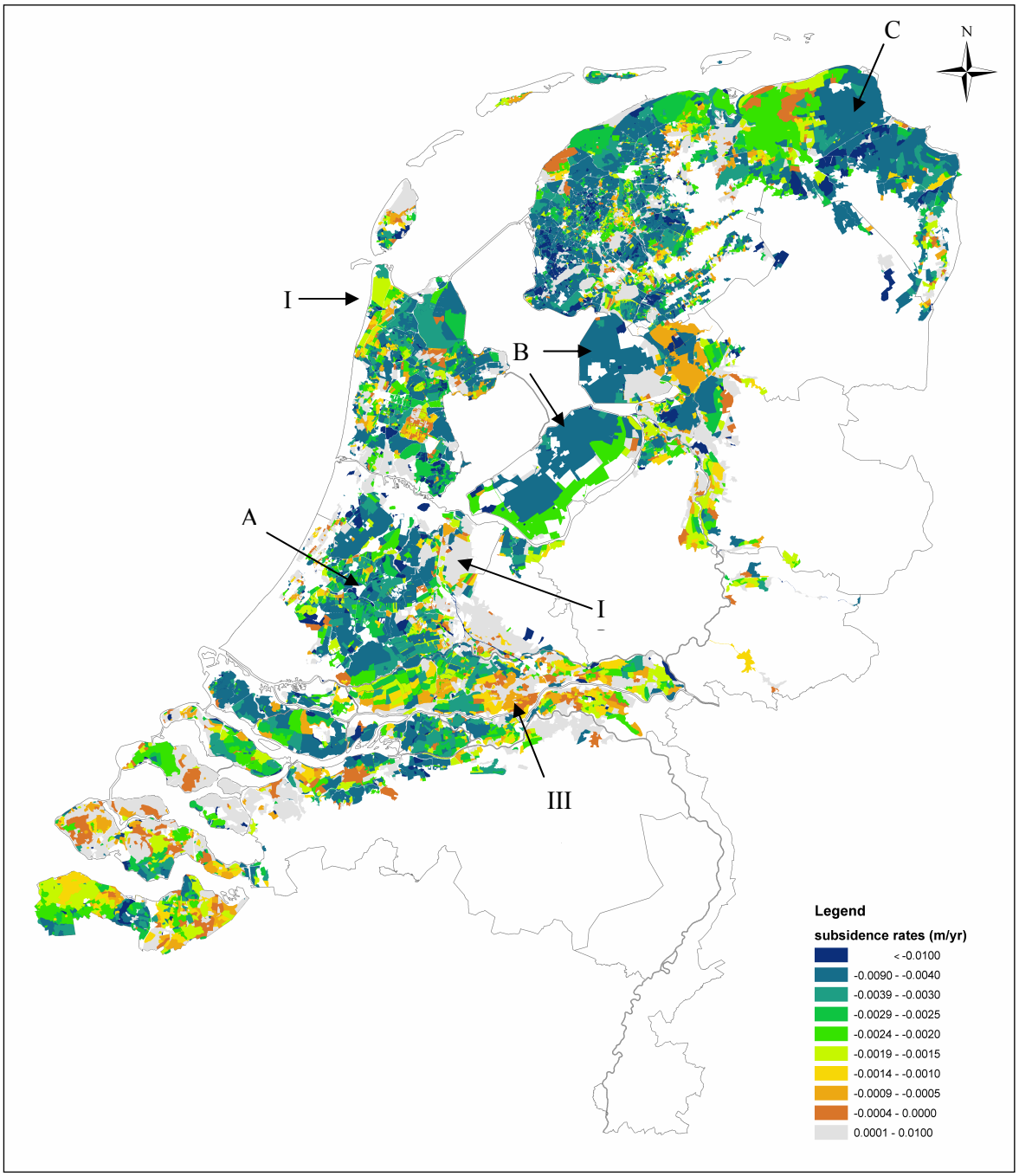

Fig. 6 Subsidence rates in the Holocene area of The Netherlands; method (2).

the measurement points (10 cm). For the minimum defined altitude uncertainty (2 cm) this percentage is 6 percent. It is recommended to calculate the subsidence rates using the defined altitude uncertainty of each measurement point. This new method filters out the outliers and is expected to reduce the number of positive subsidence rates.

In the detailed study of the Krimpenerwaard the results of method (1) showed patterns that correspond with the extent of the “peilvakken”. It would be very useful to compare the rates of subsidence with historical adjustments made by the water boards in terms of groundwater levels and the water level in drainage canals. Then conclusions can be drawn about the importance of this factor for surface subsidence.

The seasonal variability of the ground level due to soil moisture content is not taken into account. The month the measurements were taken could be of significance for the uncertainty of the data used in this study, as according to Fig. 7, the ground levels are lower in the spring and autumn and higher in the summer period.

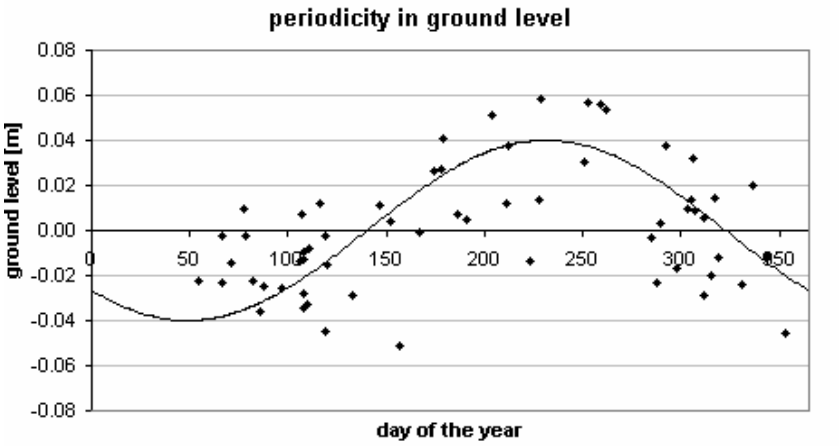

Fig. 7 Seasonal variability of the ground level, modified from Beuving *et al.* (1996).

The relationship with the composition of the subsurface is of great importance for subsidence rates. Detailed information of the 3-D distribution of layers vulnerable to subsidence (mainly peat and clay) will greatly improve the understanding and predictions of the subsidence.

Nevertheless, the patterns mentioned above, along with the dedicated study performed in the Krimpenerwaard area, give confidence in the results and the procedure followed. This quantification of the subsidence rates in the Holocene part of The Netherlands, as a result, will be very valuable for policy makers in defining their water management policy.

REFERENCES

DINO*LOKET* (2010) *Borehole measurements and information.* http://www.dinoloket.nl/en/DINOLoket.html, consulted 16 June 2009.

Beuving, J. & Akker, van den J. J. H. (1996) Maaiveldsdaling van veengrasland bij twee slootpeilen in de polder Zegvelderbroek; vijfentwintig jaar zakkingsmetingen op het ROC Zegveld. *Rapport 377 DLO-Staring Centrum*, Wageningen, The Netherlands.

(Proceedings of EISOLS 2010, Querétaro, Mexico, 17–22 October 2010). IAHS Publ. 339, 2010.

Is there a tectonic component to the subsidence process in Morelia, Mexico?

E. CABRAL-CANO[1], A. ARCINIEGA-CEBALLOS[1], O. DÍAZ-MOLINA[1], F. CIGNA[2], A. ÁVILA-OLIVERA[5], B. OSMANOGLU[3], T. DIXON[3], C. DEMETS[4], V. H. GARDUÑO-MONROY[5], F. VERGARA-HUERTA[1] & J. E. HERNÁNDEZ-QUINTERO[1]

1 *Departamento de Geomagnetismo y Exploración, Instituto de Geofísica, Universidad Nacional Autónoma de México Ciudad Universitaria, México D.F., 04510 México*
ecabral@geofisica.unam.mx

2 *Earth Sciences Department, University of Firenze, Via La Pira 4, 50121 Firenze, Italy*

3 *Rosenstiel School of Marine and Atmospheric Science, University of Miami, 4600 Rickenbacker Cswy, Miami, Florida 33149, USA*

4 *Department of Geoscience, University of Wisconsin-Madison, 1215 Dayton, Madison, Wisconsin 53706, USA*

5 *Universidad Michoacana de San Nicolás de Hidalgo, México*

Abstract Subsidence has been a common occurrence in several cities in central Mexico for the past three decades. This process has caused substantial damage to the urban infrastructure and housing in several cities. Given the observed rates of subsidence and reported damage, it has become a major factor to be considered when planning urban development, land-use zoning and hazard mitigation strategies for the 21st century. In the case of Morelia there is evidence that subsidence is a complex phenomenon, where both soil consolidation and tectonic factors come into play. We present a satellite geodesy analysis of surface deformation in Morelia complemented with Ground Penetrating Radar and Seismic Tomography surveys of the La Colina fault, the most active feature within the urban area. These data provide insight into the tectonic component, which overlaps the groundwater extraction, and soil consolidation processes observed in key areas of the city.

Key words InSAR; fault; subsidence; tectonics; Morelia, Mexico

INTRODUCTION

Subsidence documented in urban areas in central Mexico (e.g. Farina *et al.*, 2007; Cabral-Cano *et al.*, 2008, Osmanoglu *et al.*, 2010; and references therein) is usually associated with aggressive extraction rates and a general decrease of underlying aquifer static levels. This human-induced phenomenon promotes soil consolidation, deformation and development of faulting that ultimately causes severe damage to buildings and other urban infrastructure. However, evidence in the city of Morelia (e.g. Garduño-Monroy *et al.*, 2001) suggests a more complex scenario, where groundwater extraction cannot solely explain the surface deformation distribution and may also be affected by the regional stress field from the Chapala–Tula Fault zone (Johnson & Harrison, 1989). The city of Morelia is thus a very good candidate for a detailed InSAR spatial distribution analysis complemented with selected detailed subsurface investigations based on GPR and seismic tomography. Our new data provide new insight into the tectonic component, which overlaps with groundwater extraction and soil consolidation processes in key areas of the city.

APPROACH

The city of Morelia, in central Mexico has experienced active fault development within its urbanized area, first recognized in the early 1980s and throughout the 1990s (e.g. Avila-Olivera, 2008). Currently there are nine NE–SW trending faults known throughout the Morelia urban areas (Fig. 1).

Copyright © 2010 IAHS Press

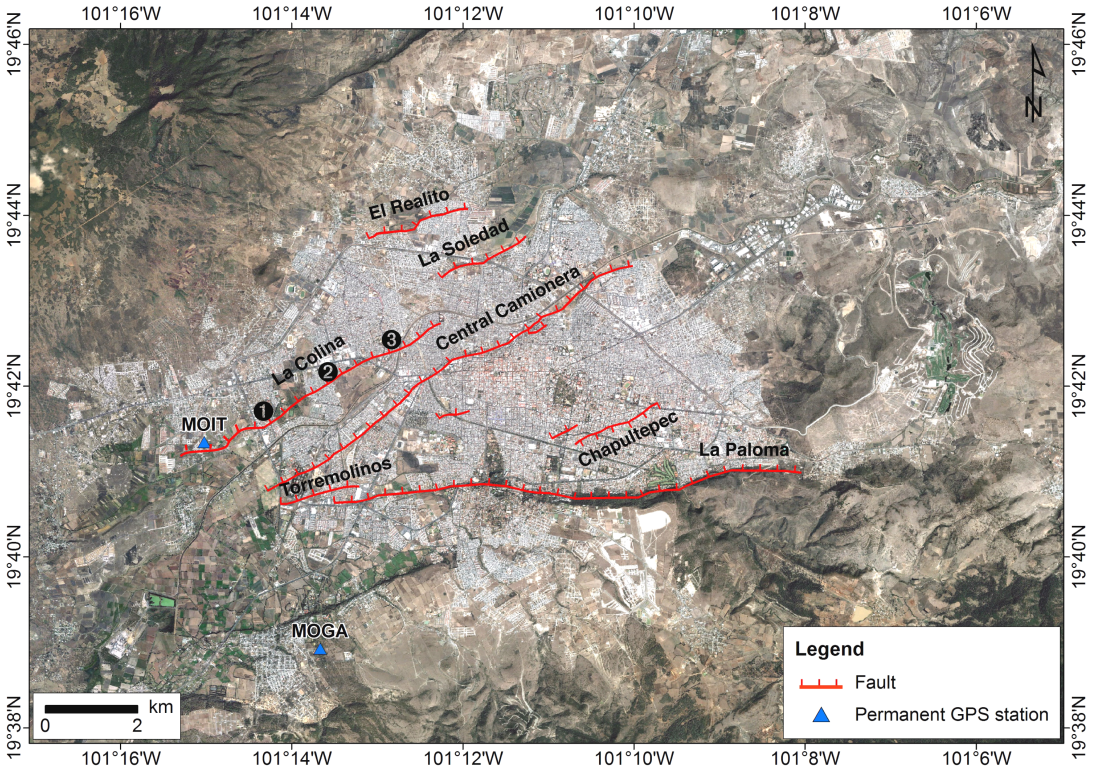

Fig. 1 Location of study area. Principal faults in Morelia overlapped onto Google Earth high-resolution imagery. Numbers show locations of the GPR-seismic tomography sections.

The increasingly damaging faulting process in Morelia has led us to use available ENVISAT-ASAR (Advanced Synthetic Aperture Radar) archive data at the European Space Agency to create an integrated displacement map derived from a Persistent Scatterer Synthetic Aperture Radar Interferometry (PSI) analysis. The highest subsiding areas were then studied in detail with GPR and seismic tomography techniques.

Satellite geodesy

Twenty ENVISAT-ASAR scenes acquired between 12 July 2003 and 3 October 2009 were used to generate interferograms with the Delft Object-oriented Radar Interferometry Software (DORIS; Kampes & Usai, 1999). Precise orbits from the Delft Institute were used to minimize orbital errors (Scharroo & Visser, 1998). The 22 January 2005 acquisition was selected as the master scene to minimize the effects of spatial and temporal baselines. The study area was cropped from each SAR scene acquisition and oversampled by a factor of two in range and azimuth to avoid under sampling of the interferogram, especially during resampling of the slave acquisition. Further processing included stacking of interferograms relative to a single master image, a selection of strong scatterers visible in all interferograms and unwrapping of their phase changes through time. These strong scatterers were then filtered to detect and remove the atmospheric phase contribution. Finally they were georeferenced and the line of sight displacement rate for each permanent scatterer was generated (Fig. 2). We also used data from two relatively new permanent GPS sites (Figs 1 and 3) as an aid to improve calibration of InSAR determined subsidence.

Although the spatial resolution of ENVISAT-ASAR based InSAR products is very good, its temporal resolution is variable depending on the frequency of acquisitions. In order to provide better temporal resolution for selected areas we installed two permanent GPS sites. The MOGA station serves as a fiducial site to aid in further detailed GPS surveys of these faults, while the MOIT station is located close to the western segment of the La Colina fault.

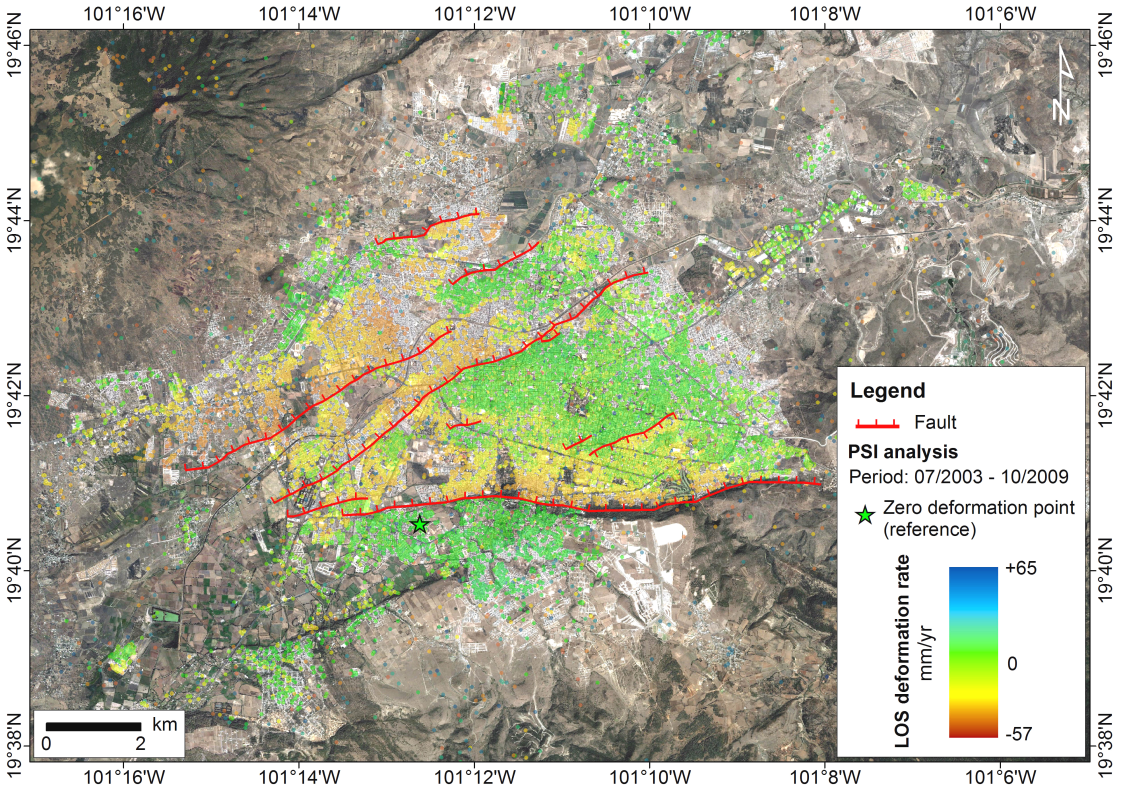

Fig. 2 Persistent Scatterer InSAR (PSI) displacement map of Morelia overlapped onto Google Earth high-resolution imagery.

The coordinate time series for both GPS stations (Fig. 3) were determined using a standard precise point-positioning analysis of the raw code and phase data using GIPSY software from the Jet Propulsion Laboratory (JPL). Daily station coordinates were estimated in a non-fiducial reference frame and then transformed to ITRF2005 using daily seven-parameter Helmert transformations from JPL.

The PSI derived line of sight displacement map (Fig. 2) shows that La Colina fault on the northern and northwestern sector of the city is the highest subsiding area, with maximum annual rates over –50 mm/year. Lithological mapping (Avila-Olivera, 2008) show a basaltic lava sequence outcropping in the northern and northwestern area of the city where high subsidence rates are also observed. These areas were further investigated using near-surface geophysical exploration methods.

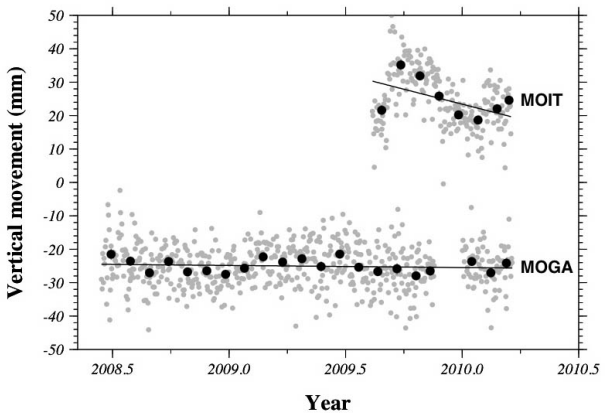

Fig. 3 Vertical time series for MOGA and MOIT permanent GPS sites. See Fig. 1 for site location. Grey dots are daily solutions and black dots are averaged weekly solutions.

Ground Penetrating Radar

For this study we used a Geophysical Survey Systems Incorporated (GSSI) SIR-3000 console, a GSSI 200 MHz antenna and Radarteam 40 and 70 MHz antennas. All surveyed sections (Fig. 4) were georeferenced with geodetic dual frequency GPS receivers using post-processing kinematic survey techniques referenced to the MOGA site. GPR profiles on the study area were surveyed using a wheel encoder attached to the GPR console-antenna array. Acquisition was done at 100 scans/m, 1024 samples/scan and 8-bits/sample. Processing of this data set included filtering using an acquisition Infinite Impulse Response vertical and a vertical filter boxcar. We also applied a time (horizontal axis) filtering to enhance the response of the surveyed strata and its structures. De-convolution removed unwanted multiple reflected energy arrivals. The final steps were the migration to position all reflectors to their true spatial location and compensate for any distortion induced during acquisition and the wave propagation.

Seismic tomography

Seismic Refraction Tomography (SRT) is an effective tool for horizontal, lateral and vertical characterization of structures. The refraction surveys included four profiles (Fig. 4) using a 48-channel 24-bit Geometrics Stratavisor NZ seismograph and 14 Hz natural frequency vertical Oyo-Geospace geophones. Each profile consisted of five consecutive lines of 12 geophones deployed at 2-m intervals, with an overlap of 2 m between lines. The seismic source used was an 8 kg sledge-hammer vertically impacting on a 20 kg ground-coupled steel plate. Five impacts were stacked at each shot point to enhance data signal-to-noise ratio. Processing was done using the SeisImager Refraction Modeling package, which includes an interactive method to perform the nonlinear travel time tomography in two dimensions.

DISCUSSION

The satellite geodetic analysis of surface deformation in Morelia since 2003 documents more than –50 mm/year of line of sight motion in selected sectors of Morelia. The largest displacement rates were detected on the hangingwall of the La Colina Fault (Figs 1 and 2). Initial data for the MOIT GPS station located ~200 m north of the fault (Fig. 3, top) indicate rapid periodic vertical motion. This observation is consistent with the westward propagation of the fault, which had no surface expression in this part of the city until recent years. Detailed geophysical surveys across this fault (Fig. 4) indicate that while the surface expression may only hint at what appears to be a single fault trace, subsurface imaging instead reveals a zone of closely-spaced shallow faults 20–40 m wide. The largest fault dislocation was observed at the Manantiales sector (8–12 m displacement; Fig 4). Other sectors, such as the Rio Grande sector, show less that 6 m of dislocation.

Assuming a constant, linear subsidence rate in the past, similar to the InSAR observed rates, and based on the interpretation of the fault dislocation imaged by the shallow GPR and seismic tomography, we propose that the La Colina fault may have been active for at least 240 years and clearly pre-dates the intense water well extraction of the last decades. Of course it is possible that groundwater extraction has increased the deformation rate.

The documented deformation suggests the existence of a tectonic component overlapping with the soil consolidation and its related subsidence. Therefore, it is possible that at least some of the E–W faults observed within the city of Morelia may be an active segment of the Morelia–Acambay fault system and part of the larger Chapala–Tula Fault zone (Johnson & Harrison, 1989). This suggestion may also solve the apparent contradiction of the basaltic lava sequence out-cropping in the northern and northwestern area of the city where high subsidence rates are observed. We are thus documenting that at least the La Colina fault in Morelia responds to an active regional stress field, which may be enhanced by local soil consolidation effects.

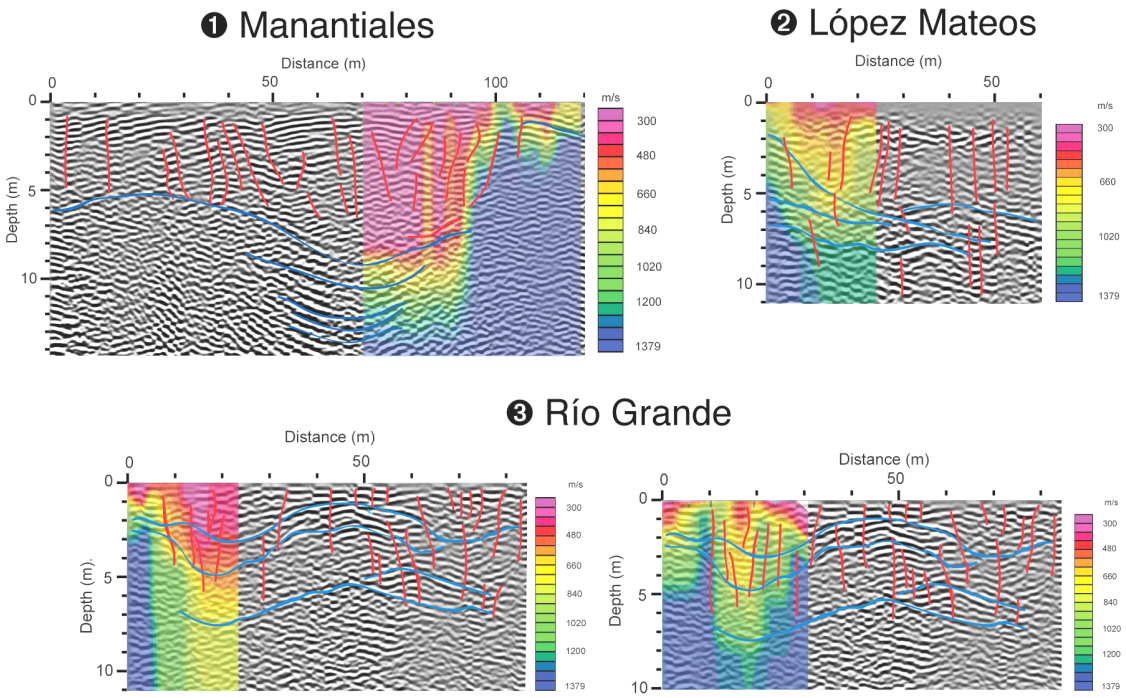

Fig. 4 Interpreted (lines) examples of surveyed seismic tomography (colour) sections overlapped onto GPR radargrams (greyscale images) in three areas of the La Colina fault. See Fig. 1 for the location (circled numbers) of each section.

CONCLUSIONS

1 We propose that the La Colina fault may have been active for the past 240 years, clearly predating the intense water well extraction period from the last 20–30 years.

2 While some of the high subsidence features of the InSAR displacement maps show continuous rates along the fault strike and a well defined gradient across strike such as the La Paloma fault (Fig. 2); in other instances such as the eastern portion of the La Colina fault, the rapidly deformed area does not conform to the linear fault pattern and may be better explained as the concentrated subsidence around and intense groundwater extraction area.

3 The observed conditions suggest the existence of a tectonic component overlapping the soil consolidation and its related subsidence. These observations support the hypothesis that at least some of those faults within the city of Morelia may be an active segment of the Morelia–Acambay system and part of the larger scale Chapala–Tula Fault zone.

4 The wide swath of intense faulting and fracturing along the major fault traces indicates that current land use and building code criteria for determination of hazard areas along the fault zones is inadequate and should be revised.

Acknowledgements We thank ESA for providing the ENVISAT-ASAR images through CAT-1 Project #1409 to Enrique Cabral-Cano. This research was funded by UNAM through PAPIIT projects IN-121515, IN-114907, IN117909, IN106309-2 and Conacyt projects 61212 and 82868. We also thank Freek van Leijen, Mahmut Arikan and Ramon Hanssen and many others from TU-Delft for making the DORIS and PSI Toolbox available.

REFERENCES

Avila-Olivera, J. A. (2008) Evolución de los Procesos de Subsidencia-Creep-Falla, casos: Morelia, Mich. y Celaya, Gto. PhD Thesis, Posgrado en Ciencias de la Tierra (Geología Estructural y Tectónica), Universidad Nacional Autónoma de México.

Cabral-Cano, E., Dixon, T. H., Miralles-Wilhelm, F., Sánchez-Zamora, O., Díaz-Molina, O. & Carande, R. E. (2008) Space geodetic imaging of rapid ground subsidence in México City. *Bull. Geol. Soc. Am.* **120**(11/12), 1556–1566; doi: 10.1130/B26001.1.

Farina, P., Avila-Olivera, J. A. & Garduño-Monroy, V. H. (2007) Structurally-controlled urban subsidence along the Mexican volcanic belt (MVB) monitored by InSAR. *Proceedings Envisat Symposium 2007* (Montreux, Switzerland. 23–27 April 2007). ESA SP-636, July 2007.

Garduño-Monroy, V. H., Arreygue-Rocha, E., Israde-Alcántara, I. & Rodríguez-Torres, G. M. (2001) Efectos de las fallas asociadas a sobreexplotación de acuíferos y la presencia de fallas potencialmente sísmicas en Morelia, Michoacán, México. *Revista Mexicana de Ciencias Geológicas* **18**(1), 37–54.

Johnson, C. A. & Harrison, C. G. A. (1990) Neotectonics in central México. *Physics of the Earth and Planetary Interiors* **64**, 187–210.

Kampes, B. & Usai, S. (1999) DORIS: The delft object-oriented radar interferometric software. In: *Proc. 2nd International Symposium Operationalization of Remote Sensing*. http://citeseerx.ist.psu.edu/viewdoc/summary?doi=10.1.1.46.1689.

Osmanoglu, B., Dixon, T. H., Wdowinski, S., Cabral-Cano, E. & Jiang, Y. (2010) Mexico City subsidence observed with Persistent Scatterer InSAR. *Int. J. Appl. Earth Observ. & Geoinfo*. doi:10.1016/j.jag.2010.05.009 (in press).

Scharroo, R. & Visser, P. (1998) Precise orbit determination and gravity field improvement for the ERS satellites. *J. Geophys. Res*. **103**(C4), 8113–8127.

Land Subsidence, Associated Hazards and the Role of Natural Resources Development
(Proceedings of EISOLS 2010, Querétaro, Mexico, 17–22 October 2010). IAHS Publ. 339, 2010.

Evaluation of the subsidence and risk of collapse in the Estació neighbourhood of Sallent City, Catalonia (Spain)

F. LÓPEZ[1], P. BUXÓ[1], J. PALAU[1], J. MARTURIÀ[2], A. CONCHA[2] & P. MARTÍNEZ[2]

1 *Geocat Gestió de Proyectes SA, Tarradellas 34-36, 08029 Barcelona, Spain*
flopez@ggp.cat
2 *Institut Geològic de Catalunya, Balmes 209-211, 08006 Barcelona, Spain*

Abstract The effects of underground evaporitic potassium salt mining, along with evolution of natural large karsts cavities below the Estació neighbourhood at the city of Sallent (Barcelona), were theoretically evaluated. The vertical movement response, at the ground surface and at depth, was evaluated by finite element modelling. The numerical model considered the simple constitutive Mohr-Coulomb plasticity law, the different existing geological layers and different calculation stages for different depths of the natural cavity roof. Comparisons were made between theoretical calculated deformations and those resulting from topographic surveying and extensometer-monitoring at depth. It was found that the cavity void can potentially reach to the surface through collapse

Key words subsidence; monitoring; extensometer; Midas GTS

INTRODUCTION

Sallent is situated in northeast Spain, in the centre of what is known, in geological terms, as the Potassic Salt Catalonian evaporitic basin, 70 km north from Barcelona. Estació is known as a neighbourhood affected by subsidence due to potassic-rich evaporates exploitation of the Enrique mine from 1932 to 1973. Mining activities took place at a depth of 260 m, based on a chambers and pillars method. During the exploitation, a great natural cavity of 56 m diameter and 110 m height was found between 150 m and 260 m below the surface, and it was partially refilled by materials falling from the walls and from the top of the cavity.

Since 1997, the Institut Geològic de Catalunya along with Geocat Gestió de Projectes SA has been monitoring land subsidence at the site with topographic surveys, extensometers and inclinometers. Monitoring has allowed the definition of a subsiding critical area, which is located in the SW of the neighbourhood and which coincides with the location of the great cavity, where the highest speed of subsidence data has been registered. During 2008 the maximum subsidence reached values of 16 cm/year at the surface and 60 cm/year at depth.

SIMPLIFIED 3-D NUMERICAL MODEL

The aim of the model is to determine the evolution of the cavity in different stages according to the observed evolution through time and the possibility of collapse. The vertical deformation data from extensometers and topographic surveying has been compared with the numerical theoretical data obtained under the hypothesis of moving the roof of the cavity up to the surface in order to determine the stage of the evolution closest to the measured subsidence (IGC, 2009b).

The model geometry is three-dimensional, consisting of a cubic domain of 600 × 600 × 380 m, which includes: the non-saline cover composed of interbedded limestones and sandstones, a carnallite layer, the rich potassic salts layer and the halite layer, the mine and the cavity voids. The effect of the increasing void of the natural cavity has been simulated as an ascending bell-shaped void at four stages with different depths of the roof (from surface): 150 m (initial depth), 100 m, 85 m and a final position at 40 m from the surface (Fig. 1). The finite element code Midas GTS was used to generate the model and, for all the different geological units, the Mohr-Coulomb plasticity law was considered.

Copyright © 2010 IAHS Press

Surface comparison

The theoretical subsidence contours and shape of the computed settlement basin along a N–S profile were compared with those obtained by topographic measurements (Figs 2 and 3). Topographic measuring point with maximum subsidence, located at the zenith of the cavity (point C4). Deformation was extrapolated using data from the measurement starting date to the present time in order to predict subsidence tendency until 2013 (Voight & Elsworth, 2000) (Fig. 3). Comparisons were made between calculated deformation at different stages and the tendency observed at point C4.

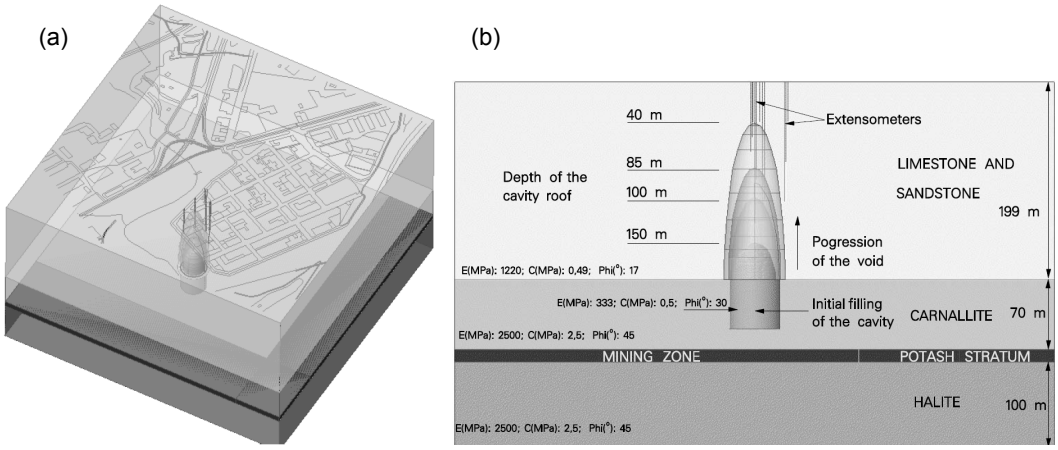

Fig. 1 (a) Perspective view of the Sallent quarter, geological model and model domain; (b) progressive geometry of the cavity and monitoring equipment in depth.

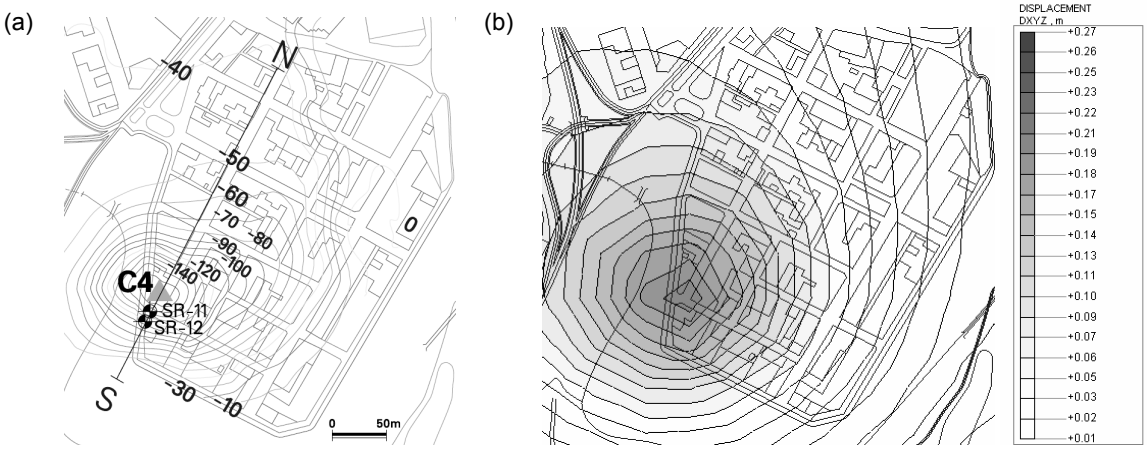

Fig. 2 Velocity isolines of: (a) measured subsidence (IGC, 2009a); (b) calculated subsidence (case roof at 100 m).

In-depth comparison

The evolution of the two extensometers closest to the cavity, SR-11 anchored at 100 m depth and SR-12 at 50 m (Fig. 2) have been graphically represented and are compared with the theoretical deformation obtained with the numerical model at these depths (Fig. 4). This deformation is the movement of the nodes from the finite element mesh located in the nearest to the real position and depth of the extensometers anchoring points.

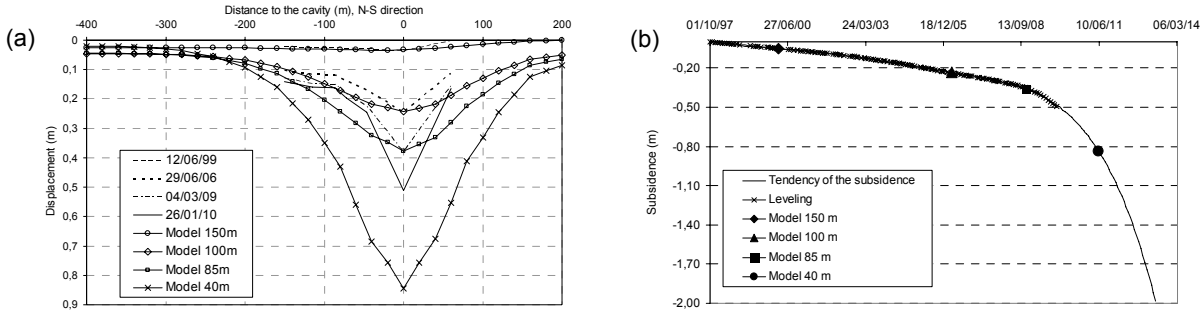

Fig. 3 (a) Comparison between calculated and measured settlement basins in N-S profile. (b) Time evolutions of the topographic surveying point with maximum subsidence (C4) and the deformations of the same point in the model for each of the depths of the cavity roof.

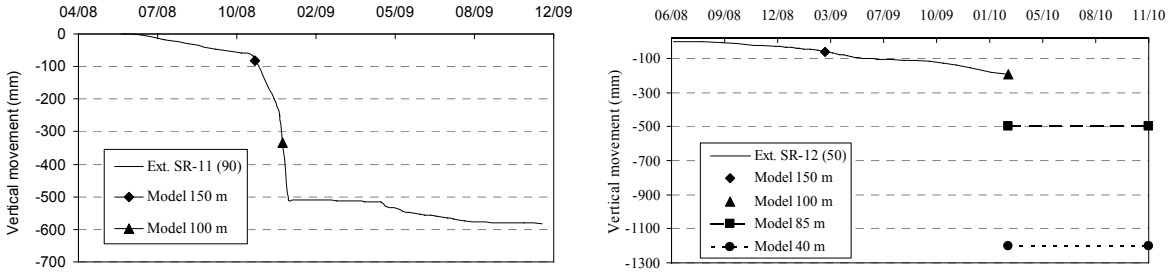

Fig. 4 Comparing the deformation in depth. In SR-12 extensometer depths at 85 m and 40 m still not achieved are indicated.

DISCUSSION

Analysing the results described for the L'Estació neighbourhood, it is worth-pointing out that the actual subsidence increment, very localized at the area of study, is influenced by the growing evolution of the void of the cavity. According to the current study hypothesis, the roof of the cavity is located at between 85 and 40 m from the surface. By following the present tendency, the cavity might develop a sinkhole. If the roof of the cavity reaches less than 40 m depth, deformations at the surface might reach 1 m. Due to the risk of the possible collapse of the cavity, the alert phase of the Action Plan for Emergency Risk of Subsidence, at Sallent city, was activated. Evacuation of 43 resident families in the neighbourhood took place at the end of 2008.

REFERENCES

Institut Geològic de Catalunya (2009a) Informe de control de l'auscultació dels barris de l'Estació i la Rampinya (Sallent, Bages). Resum 2009 Internal report AP-123/09.

Institut Geològic de Catalunya (2009b) Recopilació, anàlisi i síntesi de la informació geològica sobre el procés de subsidència a Sallent (2005–2009) .Internal report AP-134/09.

Voight, B. & D. Elsworth (2000), Instability and collapse of hazardous gas-pressurized lava domes. *Geophys. Res. Lett*. **27**(1), 1–4

Land Subsidence, Associated Hazards and the Role of Natural Resources Development
(Proceedings of EISOLS 2010, Querétaro, Mexico, 17–22 October 2010). IAHS Publ. 339, 2010.

Zonation and prediction of land subsidence: case study, Kerman, Iran

S. M. VAEZINEJAD, M. M. TOUFIGH & S. M. MARANDI
Department of Civil Engineering, Bahonar University, 22 Bahman Blvd, Kerman, Iran
mahmoodvn@graduate.uk.ac.ir

Abstract Drought and uncontrolled groundwater withdrawal in recent years has caused numerous problems such as subsidence due to the falling of the subsurface water table, the reduction of water quality, etc., in cities across the world. This research, a case study, deals with the harmful effects of subsurface water withdrawal in the City of Kerman and practical monitoring of the subsidence and makes predictions of land subsidence. The artificial neural network has been used for modelling the monitored results and prediction of future subsidence. A surveying network with more than 500 installed benchmarks in an area of 334 km^2 has been used to measure the subsidence of the city area. Benchmarks were installed at the beginning of 2004 and were monitored at the end of 2004, 2006, and 2007. For modelling, extra data were obtained from the Iranian Surveying Organization for the years before 2004. The resulting model showed that the subsidence varies between zero and 15 cm per year in different parts of the City, which depends on the subsurface-layered soils, their compressibility, and the manner of subsurface water withdrawal.

Key words land subsidence zonation; subsurface water withdrawal; artificial neural network; subsidence prediction

INTRODUCTION

Land subsidence has caused many difficulties around the world. This phenomenon takes place as a result of various factors such as ground settlement due to deformation and displacement of subsurface soil layers, groundwater withdrawal, gas and petroleum withdrawal, subsurface excavations, mine exploitation, construction of heavy buildings and embankments, ground tectonic movement, dissolving of lime layers, etc., which arise from man's interference in nature (Poland, 1984).

In recent years, some parts of the earth have experienced the subsidence phenomenon due to subsurface water withdrawal. Barbarella *et al*. (1986) reported problems occurring in historical buildings of Bologna in Italy because of 2-m of subsidence for a period of 30 years. Holzer *et al*. (1979), Metzger *et al*. (2001), Sneed *et al.* (2002), Gabrysch (2005) and Galloway *et al*. (1999) studied problems associated with land subsidence in Texas, California, Arizona, Nevada, etc., in the United States of America. Between 1955 and 1980, the land subsidence in some parts of Greece reached 3 to 4 metres (Stiros, 2001). Phien-wej *et al*. (2006) reported that, in the early 1980s, some parts of Thailand experienced land subsidence of 12 cm per year due to withdrawal of more than 120×10^6 m^3 of water per day.

Zonation of subsidence phenomenon may control the planning and improvement of the negative effects and can be a proper method for subsidence prediction. For this purpose, the factors affecting earth subsidence such as subsurface cavities and holes, water quantity, subsurface water level, and type and specification of subsurface layers must be determined. In addition to these factors, analysis and zonation of previous movements play the main role in the modelling of land subsidence in an area. This is what almost all previous researchers have mentioned. Thu & Fredlund (2000), who studied the subsidence of the Hanoi City area in Vietnam, emphasized that a continuous measurement of settlement is of great importance for computing possible future deformations. Doukas *et al*. (2004) measured the land subsidence of Thessalonica by means of a 37-station network in an area of 12 km^2 for a 6-year period between 1992 and 1998. They showed subsidence of 2.8–5.0 cm/year in the southwest area. Phien-wej *et al*. (2006) studied the annual subsidence in Bangkok using a network including 220 benchmarks.

Besides much research performed in the past, it seems more data may facilitate a precise prediction of earth subsidence in a short period. In a case study, an extensive experimental

Copyright © 2010 IAHS Press

research project using a large levelling network was carried out in the capital City of Kerman, Iran. The area under investigation was not so large in comparison with the areas studied by other researchers; however, the applied network was large enough to cover all the area very well, and provided the possibility of a more accurate zonation of subsidence in the city. This research showed that, in recent years, the subsurface water table has fluctuated in various parts of the area due to effective factors such as drought, population growth, agriculture and industrial development, the increase of domestic absorption sewage wells, etc. All these factors, together with the extending and new boring of deep wells have caused more water pumping and consequently more subsidence in the region.

Models for the prediction of land subsidence rarely exist in literature and those which one can find are based on the geotechnique using consolidation theory. In these models, obtaining precise data concerning the soil type, layer classification, hydromechanic specification, depth and flow direction, subsurface water pumping and retreated water in the area is compulsory. For example, Larson *et al*. (2001) conducted a study on the prediction of land subsidence in the Los Banos-Kettleman city area in California, USA. In this research, they used the MODFLOW software to model groundwater changes and applied one-dimensional consolidation theory for the prediction of the area subsidence. The model presented seems not to be as precise as expected and the prediction of land subsidence needs a lot of calculation.

In this study, the factors influencing land subsidence in the City of Kerman were investigated, then the fluctuation of the subsurface water table was monitored extensively and the land subsidence of the city was zoned precisely. Based on this information, a model is introduced for the prediction of subsidence by using artificial neural networks. This method enables us to predict soil subsidence without access to geological specification, geomechanic and hydraulic data. This model can be used as a precise method for the prediction of land subsidence. The output of this model in comparison with other models shows independent precise prediction of land subsidence and a reduction in calculation time.

GEOLOGICAL AND HYDROLOGICAL CONDITION OF THE AREA

The City of Kerman is located in southeastern Iran at longitude of 57°05′ and latitude 30°17′. The average altitude of the city is 1760 m above sea level, and it has a dry and relatively hot climate. Being located at the margin of a salt desert, it has hot summers and cold winters. The average precipitation is 140 mm per year; however, in drought years, the average rainfall decreases considerably.

Since some parts of the east side of the city are situated on mountain slopes, the earth materials are mainly granular soils overlying bedrock at shallow depth. In other parts, deep fine soil layers exist and are susceptible to consolidation due to the falling subsurface water table.

Generally, the subsurface water flow in Kerman plain is from the southeast and east towards the centre of the plain and it exits through two main routes (west (Baghein), and northwest (Zangiabbad) toward the Rafsanjan and Zarand plains) but in some areas, especially the central part of the City of Kerman, due to water table rising, the flow direction has changed.

The highest hydraulic gradient of the subsurface water is seven per thousand; and the minimum gradient for central plain and suburb areas of the city is 1.5 per thousand. The slope trend of subsurface water around Kerman University has changed from 1.5 per thousand to 0.5 per thousand. This factor shows that raising the subsurface water level in the city area has changed the subsurface water table slope toward the drinking water wells. A general estimation of subsurface water contours of Kerman in the years 1990 and 2004 is presented in Fig 1(a) and (b). Figure 1 shows that, the Kerman subsurface water table is continually falling within the vicinity of drinking water and agricultural wells in the south, southeast and northern part of the city.

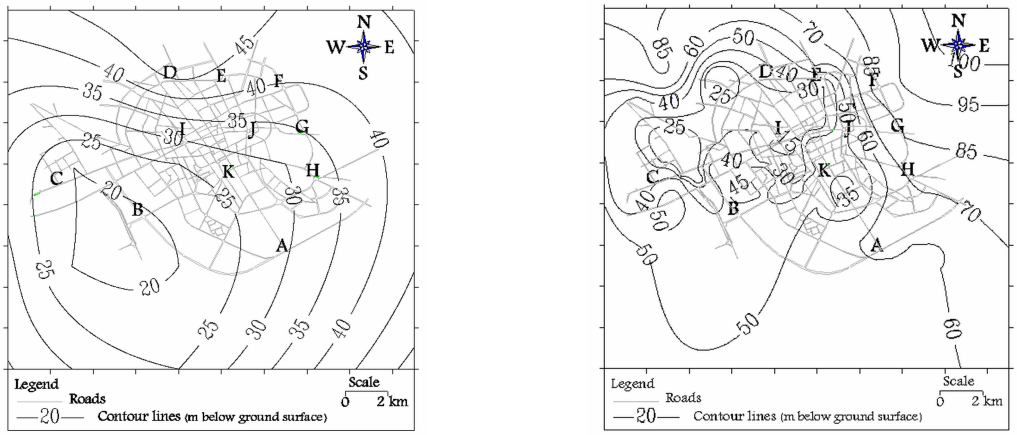

(a) (b)

Fig. 1 Subsurface water contour lines, in metres: (a) 1990, and (b) (2004).

LAND SUBSIDENCE MEASUREMENT

In order to determine the subsidence of various points of the City, an extensive surveying network using 500 stations in an area of 334 km^2 was used. The stations were erected at the beginning of 2004 and monitored at the end of 2004, 2006 and 2007 with an accuracy of ±1 cm. The stations altitude and latitude were monitored based on Universal Transverse Mercator (UTM) by a Global Positioning System (GPS). The measurement results are presented in Fig. 2(a) and (b).

To access previous years information, the data of some benchmarks were obtained from Iranian Surveying Organization stations. The 108 stations erected by this organization were monitored from 2001 to 2003. The quantity of subsidence, which occurred during these years, was measured and its related contour lines are presented in Fig. 3(a).

To compare the results obtained from our stations and results from the surveying network of the Iranian Surveying Organization, the data for these benchmarks were monitored in 2006 and 2007. The results show a proper compatibility with results of Iranian Surveying Organization. The quantity of subsidence, in a six-year period between 2001 and 2007 is presented in Fig. 3(b), which is the result of comparison of the reading in 2007 and the reading of Iranian Surveying Organization in 2001.

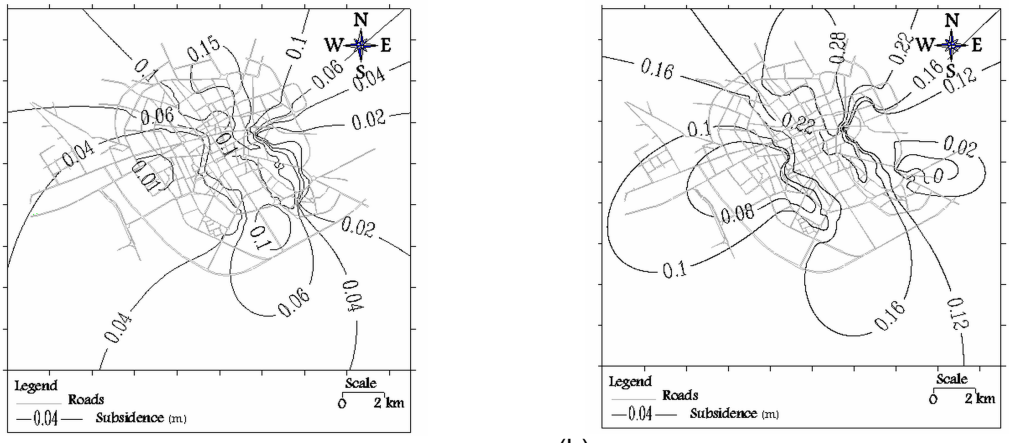

(a) (b)

Fig. 2 Subsurface contour lines, in metres for City of Kerman: (a) 2004–2006, and (b) 2004–2007.

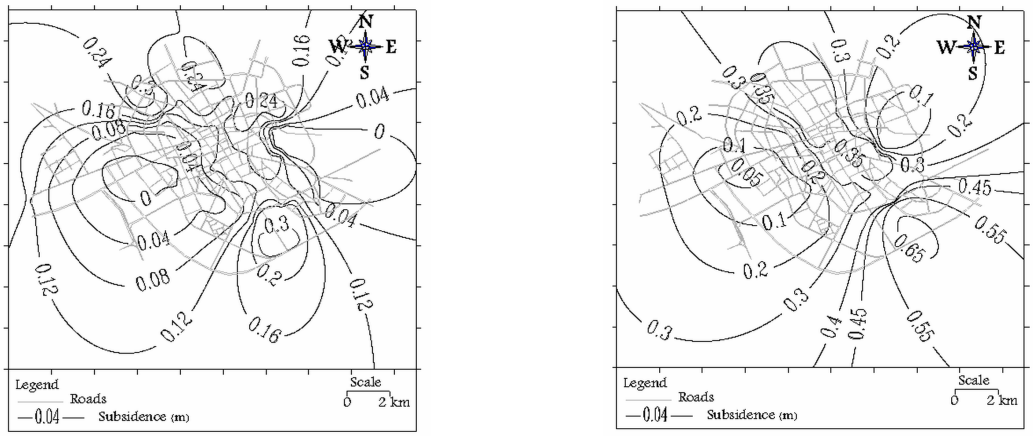

Fig. 3 Subsurface contour lines, in metres for City of Kerman: (a) 2001–2003), and (b) 2001–2007.

PREDICTION OF SUBSIDENCE USING ARTIFICIAL NEURAL NETWORKS

In recent years, the use of Artificial Neural Networks (ANNs) was extended by many factors. The most important factor is use of the special characteristics of the brain in processing data, which is beyond the reach of ordinary methods of programming. Among these characteristics, learning and generalizing of examples, and the ability to make solutions for problems with changeable conditions that need high speed processing, can be mentioned.

Artificial neural networks include an arbitrary number of layers, which have some neurons internally. The number of layers and their neurons are different for various networks but in all of them, the first layer is the *input layer*, which gives input variables and the last one is the *output layer* that represents outputs of the network. Other layers between these two layers are called *hidden layers*, and transform the input data into the output data. In a final layer, the amount of difference between the outputs of the network and target outputs that are clear from training group data are measured and the performance of the networks is measured by using the *MSE*[1] function defined in equation (1).

$$MSE = (1/n)\sum_{i=1}^{n}(d_i - y_i) \tag{1}$$

In this study, the information of the points is sorted and used in the artificial neural network. The input data is (x, y, t) where, (x, y) are *UTM* coordinates of each point and t is the period for each movement. The period is calculated from 2001 and is based on a monthly basis. The output data is s, which is the amount of movement in the period of t.

By sorting all the data, they were divided into three groups: 1: the training group for training (learning) the network, 2: the validating group for optimizing operation of the network, and 3: the testing group for testing the network's ability to give the correct answers for undefined conditions.

In this study, among various networks with different layers and structures, which were made, validated and tested, a multi-layer feed-forward network with three hidden layers had the best performance in the training and testing processes.

Due to the three variables in input data (x, y, t) and one variable in output data (s), the first layer of this network had three neurons and the last one had one neuron. Each of the three hidden layers had five neurons. Transfer functions of layers one to four was *Tansig*[2] and for layer five a

[1] Mean squared error performance function
[2] Hyperbolic tangent sigmoid transfer function

Purelin[3] function applied. The error-back propagation algorithm was selected and the training function was the *Trainlm* function that updates the weight and bias values according to Levenberg-Marquardt optimization.

The created network was used for the prediction of subsidence in different parts of Kerman. The contour lines of subsidence in the city for 2001–2011 and 2001–2016 are drawn in Fig. 4(a) and (b), respectively.

Figure 4(a) and (b) shows that the land subsidence on the outskirts of Kerman will resume if usage of groundwater continues at its current rate. In addition, the results show that, in central parts of the city, the amount of settlement will grow more slowly.

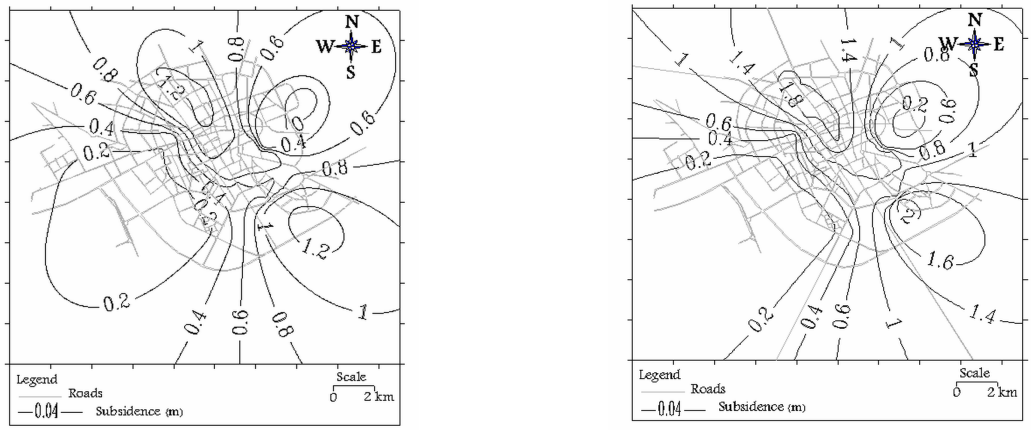

Fig. 7 Subsurface contour lines, in metres for City of Kerman (a) 2001–2011, and (b) 2001–2016**.**

DISCUSSIONS AND ANALYSIS

Figure 2(a) shows that various parts of the City of Kerman are experiencing subsidence of between zero and more than 15 cm per year. Paying attention to points *A*, *D*, *E* and *F* in Fig. 1(a) and also, considering Figs 2 and 3, it is apparent that, even though in some parts of the north of the city the water table has not changed significantly, in all northern and southern areas of the city high-speed subsidence is occurring. These areas include industrial and agricultural regions, drinking water wells in the south and some agricultural regions in the north, which have active deep wells and high daily-usage of groundwater. Figure 4(a) and (b) shows that ground movements in these areas will resume if water withdrawal continues at the same rate and consequently in southeastern parts of the city, the land subsidence will reach 2 m over a period of 15 years.

Although water table changes are extensive in the eastern parts of the city; near point *G* in Fig.1(a) and (b), but because of being close to the foothill and presence of rocky layers, ground surface movements in these places are small. This trend will be the same in the future and the maximum settlement in a 15-year period between years 2001 and 2016 will reach to about 20 cm. Going faraway from these regions in various directions; towards the southeastern, northeastern or central parts of the city, in a short distance, the amount of subsidence increases immediately. This fact is clear due to the future land subsidence contour lines shown in Fig. 4(a) and (b) for points *I*, *J* and *k* in the central area and point *H* in the southeastern region of the city. It is clear that due to observed ground movement effects in the central areas, water withdrawal has been controlled during previous years, but the ground subsidence resumes. This phenomenon occurs due to the previous high pumpage of the groundwater and the presence of a thick layer of soft clay in these regions, which has led to a time-dependent consolidation.

[3] Linear transfer function

In the western and southwestern areas of the city, which are densely populated because of an absence of industrial and agricultural regions, the need for water pumpage is very low and the water table has no notable changes. Consequently, even some cases of uplift have been observed, and the land subsidence in these areas is not significant.

SUMMARY AND RESULTS

The experimental results obtained from a case study in Kerman City, Iran, for zonation and prediction of land subsidence due to uncontrolled groundwater withdrawal and drought, can be summarized as follows:

1. The obtained data showed that at present, various parts of the city subside by between zero and >15 cm per year. High usage of groundwater, together with the existence of fine-grained soil and compressibility of underneath soil layers, are the main reasons for land subsidence in the City of Kerman.
2. Differences in the amount of water pumpage, subsurface soil profiles and the presence of foot-hill and rocky layers are the main reasons for changes in the rate of annual subsidence.
3. Since consolidation is time-dependent, even if in a region water withdrawal discontinues, the settlement will not stop, but its rate will decrease.
4. Due to its high speed and proper accuracy, the use of a multi-layer feed-forward artificial neural network, which uses a back propagation error algorithm for training, may contribute to better results in comparison with traditional methods for prediction of subsidence. Accurate prediction is helpful in the design of civil plants, scheduling the usage of water resources, construction of vital buildings, arrangement of roads, etc.
5. The prediction of future subsidence in the city showed that in some areas in the north and south of Kerman, subsidence of 2 m would occur between 2001 and 2016. It is indeed shocking that the predicted relative subsidence between two areas of the city, only a short distance apart, will reach >1 m, which will be hazardous.
6. In the eastern part of the city, which is located on the mountain slope, there is a limited change in subsidence between 2001 and 2016, yet, in the areas with thick fine-grained soil layers, the intensity of subsidence is very high.

REFERENCES

Barbarella, M., Gubellini, A., Russo, P. & Vettore, A. (1986) Time series analysis by collocation on the vertical movements of the Asinelli Tower in Bologna. *Conference on Height Determination and Recent Vertical Movements in Western Europe*, Hannover, 687–702.

Doukas, I. D., Ifadis, I. M. & Savvaidis, P. (2004) *Monitoring and Analysis of Ground Subsidence due to Water Pumping in the Area of Thessaloniki, Hellas*. Intercontinental Athenaeum Athens, Greece.

Gabrysch, R. K. (2005) Land-surface subsidence in the Houston-Galveston Region, Texas. In: *Proceeding of Seventh International Symposium on Land Subsidence* (SISOLS), Shanghai, China.

Galloway, D., Jones, D. R. & Ingebritsen, S. E. (1999) Land Subsidence in the United States. US Geological Survey Report.

Holzer, T. L., Davis, S. N. & Lofgen, B. E. (1979) Faulting caused by groundwater extraction in south-central Arizona. *J. Geophys. Res*. **84**(B2), 603–612.

Larson, K. J., Basagaoglu, H. & Marino, M. A. (2001) Prediction of optimal safe ground water yield and land subsidence in the Los Banos-Kettleman City Area, California, using a calibrated numerical simulation model. *J. Hydrol.* **242**, 79–102.

Metzger, F. L., Ikehara, M. E. & Howle, F. J. (2001) Vertical-deformation, water-level, microgravity, geodetic, water-chemistry and flow-rate data collected during injection, storage and recovery tests at Lancaster, Antelope Valley, California, September 1995 through September 1998. *US Geological Survey, Open-File report 01-414,159*.

Phien-wej, N., Giao, P.H. & Nutalaya, P. (2006) Land subsidence in Bangkok, Thailand. *Engineering Geology* **82**, 187–201.

Poland, J. F. (1984). *Guide Book to Studies of Land Subsidence Due to Ground-Water Withdrawal.* UNESCO/IH, Michigan, USA.

Sneed, M., Stork, S. V. & Galloway, L. D. (2002) Detection and measurement of land subsidence using global positioning system and interferometric synthetic aperture radar, Coachella Valley, California, 1998–2000, *Water resources Investigation Report 02-4239, US Geological Survey, 31.*

Stiros, S. C. (2001) Subsidence of the Thessaloniki (Northern Greece) coastal plain, 1960–1999. *J. Engineering Geology* **61**, 243–256.

Thu, T. M. & Fredlund, D. G. (2000) Modelling subsidence in the Hanoi City-area Vietnam. *Canadian Geotechnical J*. **37**(3), 621–637.

Land Subsidence, Associated Hazards and the Role of Natural Resources Development
(Proceedings of EISOLS 2010, Querétaro, Mexico, 17–22 October 2010). IAHS Publ. 339, 2010.

Zoning map of ground failure risk due to land subsidence of San Luis Potosí, Mexico

JESÚS PACHECO-MARTÍNEZ[1], JORGE ARZATE-FLORES[2], RUBÉN LÓPEZ-DONCEL[3], RAFAEL BARBOZA-GUDIÑO[3], JOSÉ LUIS MATA-SEGURA[3], ANTONIO DEL-ROSAL-PARDO[1] & JORGE ARANDA-GÓMEZ[2]

1 *Centro de Ciencias del Diseño y de la Construcción de la Universidad Autónoma de Aguacalientes, Av. Universidad #940, Ciudad Universitaria, CP 20131, Aguascalientes, Ags, Mexico*
geochuy@gmail.com

2 *Centro de Geociencias de la Universidad Nacional Autónoma de México, Mexico*

3 *Instituto de Geología de la Universidad Autónoma de San Luis Potosí, Mexico*

Abstract We present and analyse geologic, hydrogeologic, topographic and geophysical evidence which ties the formation of the active, aseismic faults in the valley fill with: (1) land subsidence triggered by groundwater withdrawal, and (2) buried topographic features, probably controlled by the geological structures under the valley fill deposits that contain the aquifers. Based on the collected data and the geologic interpretation of geophysical data, we propose a ground failure risk map where we show zones with different probabilities of ground failure. The risk map and attached recommendations are intended to be integrated to local building regulations in the municipalities of San Luis Potosi (SLP) and neighbouring Soledad de Graciano Sánchez (SGS).

Key words San Luís Potosí, Mexico; zoning risk; earth fissure; surface fault; subsidence

INTRODUCTION

San Luis Potosí (SLP) is a medium size city (110 km^2 in area, with approx. one million inhabitants) located in the southern part of the Chihuahua desert, 360 km northwest of México City. The main sources of water for the population and industry in San Luis Potosí are a small dam and groundwater, which is pumped out from two granular aquifers in the valley fill, and from one fractured-controlled aquifer in the bedrock. Of the water used in the city in the 1960s, 60% came from the dam. Currently only 8% comes from that source. Water level decline in the aquifers in 1972 was estimated at 0.9 m/year, while in 1990 it was 1.3 m/year (Carrillo-Rivera *et al.*, 2002). Earth fissures related to land subsidence were first reported in the 1990s in SLP (López-Doncel *et al.*, 2006a). However, we believe that land subsidence in the region started before the actual damage to constructions was noticed.

GENERAL GEOLOGY OF SLP VALLEY

The study area is located at the northern end of a local graben known as Villa de Reyes Graben. To the east of the city of SLP there are hills where there are exposed Cretaceous marine rocks. The phenomenon of subsidence occurs within the sedimentary fill that forms the valley of SLP (Fig. 1), which represents a trough containing a substantial column composed of alluvial fills that are reworked with Quaternary volcanic products, as well as with general continental sediments with thicknesses ranging from 50 to 500 m in the bedrock. The bedrock consists of rhyolites that are of Oligocene age, from about 26–31 million years (Aguirre-Hernández, 1992; Martínez-Ruiz, 1997). The structural frame exposed in the mountains that surround the valley is also located in the bedrock that underlies the sediments inside the valley.

Copyright © 2010 IAHS Press

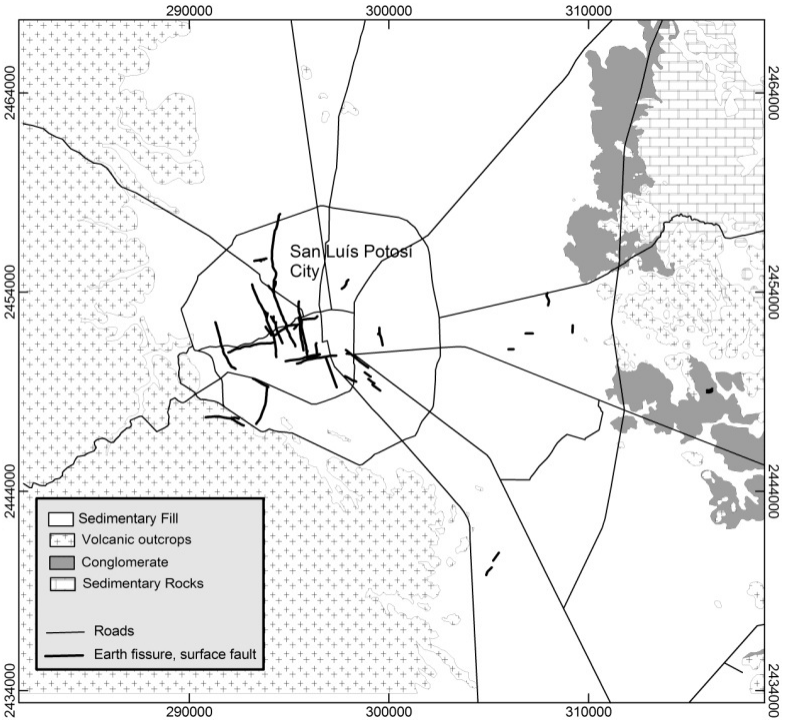

Fig. 1 General geology of SLP valley with known cracks until 2009.

In the superficial part of the valley fill there are exposed gravel and sand deposits of Quaternary age. Sedimentological works that describe the lithology, as well as the grain size of the Quaternary sequences that fill the valley of San Luis Potosi, are scarce. These are only limited to brief descriptions of the "cuts", which are taken during the drilling of wells, and these descriptions normally use descriptive terms that do not give clues about its origin or mechanism of deposition. However, these descriptions have been used as a tool to interpret and reconstruct the outline of the bedrock that is found under the Quaternary fill (Aguirre Hernandez, 1992). The thickness of the Quaternary sequences is very variable and it is logically influenced by the contour of the bedrock, this tends to change from 50 to >500 m (Aguirre Hernandez, 1992; Martínez-Ruiz 1997).

SUBSIDENCE AND CRACKS IN THE CONURBATED AREA OF SLP-SGS

The VSLP is subjected to a process of gradual subsidence; it is associated with the vertical deformation of the granular fill due to the lowering of the groundwater level. In addition, because this collapse is generated in large areas and due to the magnitude that is a few millimetres per year, it is imperceptible in short periods of time. However, a problem that is associated with the sinking and that is mainly evident in the construction effects, refers to the surface fracturing and faulting that are associated with the differential subsidence; i.e. when the sinking occurs with different magnitudes in an area that is relatively small. In the city of SLP the generation of fracturing and faulting zones in the granular fill has been mainly observed since the 1990s by the damage caused in buildings, as well as in the urban infrastructure (López-Doncel *et al.*, 2006a). Subsidence is now widespread and there are two surface fault systems that are composed of four major faults: (1) a system with N–S direction, and (2) a system with a close direction to E–W (López-Doncel *et al.*, 2006b). By 2009, only in the suburbs of SLP-SGS have around 41 km of fracturing and faulting areas been quantified.

Although there is no information about the area affected by the subsidence in the valley of SLP, taking into consideration the areas where the fractures have been developed as well as the location of the greatest thickness of the alluvial fill and the lacustrine deposits in the graben of San

Luis Pososí-Villa de Reyes, an area of approx. 1800 km^2 with the potential to develop and generate subsidence and fracturing zones is estimated. Currently there is no register of affected properties, and it makes it more difficult to estimate the economic implications that are derived from the affected buildings, but according with the length of the cracks that are located within the urban area of the city of SLP and SGS, it is estimated that at least 2000 buildings, including mostly dwellings of different types, have been directly damaged to different degrees by the fractures that range from imperceptible damage at first sight, to damage that puts at risk the structural stability of the construction itself.

MECHANISM OF CRACKING GENERATION IN THE VALLEY OF SLP

The cracks of the SLP valley seem to follow two different mechanisms of generation. Some cracks are located in areas with gravimetric anomalies and they are aligned with the regional geological structures, so that they could be similar to those observed in other valleys in the centre of the country (Garduno-Monrroy *et al.*, 2001; Pacheco *et al.*, 2006; Pacheco & Arzate, 2007), they are associated with soil compaction, over-exploitation of aquifers, and they are in combination with the existence of bedrock with irregular topography that is lying beneath the sedimentary fillings where the aquifer is found (Fig. 2). This mechanism of generation of the fractures is used by Jachens & Holzer (1982) to explain the origin of the fractures in Arizona, USA.

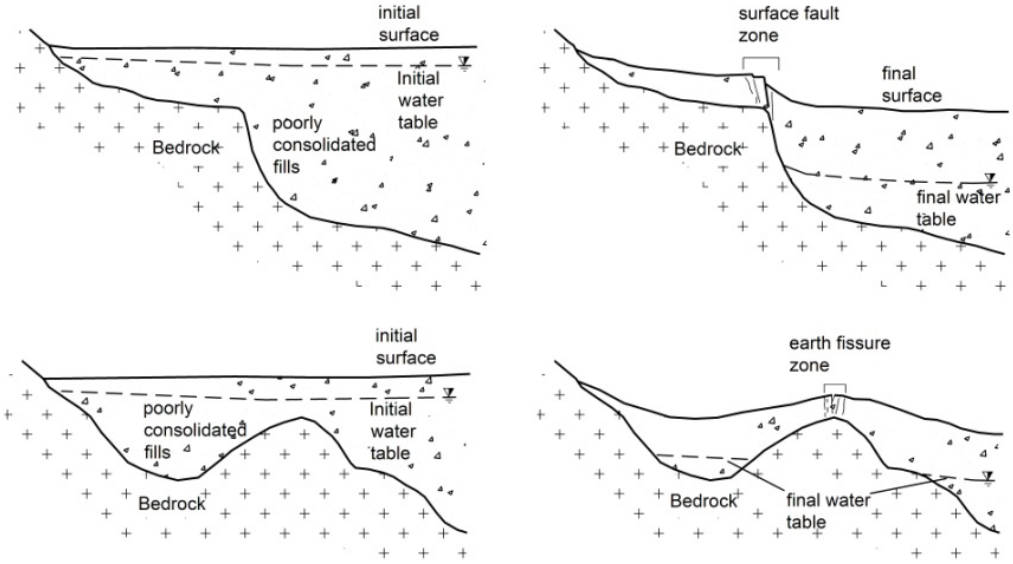

Fig. 2 Formation of surface faults and fractures associated with a differential compaction of granular fill, which forms the aquifer of the valley of SLP (modified from Carpenter, 1999).

It has also been observed that other fractures are neither aligned with regional geological structures, nor with gravity anomalies. The mechanism of these cracks appears to be related to the formation of holes by "tubing" and their collapse is on the centre line of former streams. The mechanism of formation of this type of fracture is not still fully understood. It presumably starts with the "undermining" or "tubing" of paleochannels, which are the result of a fine drag and the consequent formation of voids that can collapse (Fig. 3). The fracturing that is generated is aligned with fluvial deposits that are buried by younger fillings. This mechanism has been suggested by Suarez-Placencia *et al*. (2005) to explain the fracturing in the valley of Nextipac, Jalisco, Mexico.

The existing cracks in the suburbs of SLP-SGS with the configuration of the bedrock are shown in Fig. 4. The bedrock was determined from gravimetric data and lithologic logs of wells.

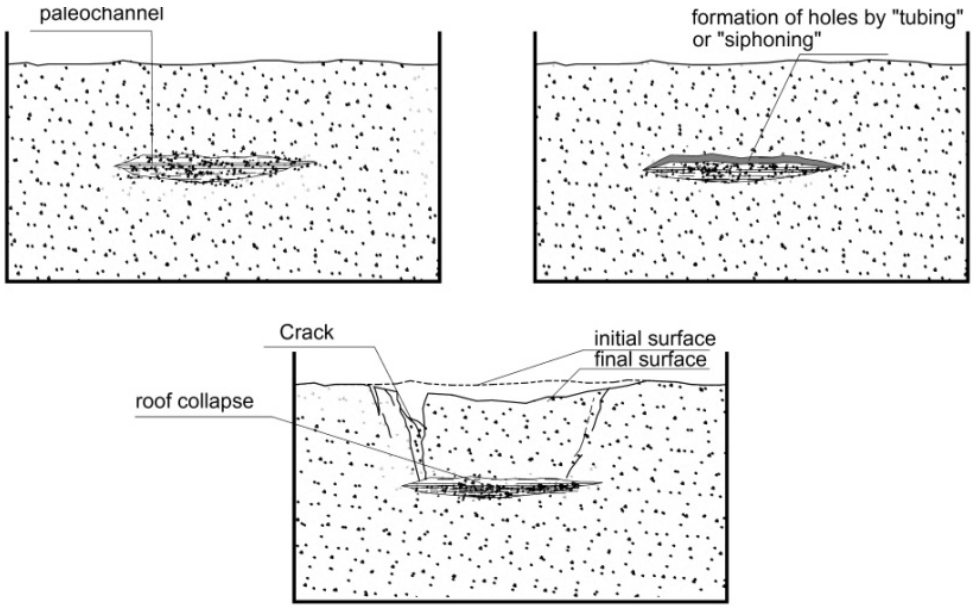

Fig. 3 Formation of fractures that are associated with paleochannels. Cross section of a paleochannel it is interspersed with more recent fillings of different mechanical properties. The formation of holes is generated by the dragged material by water flow in the longitudinal direction of the paleochannel. The process ends with the collapse of the roof and formation of cracks and faults.

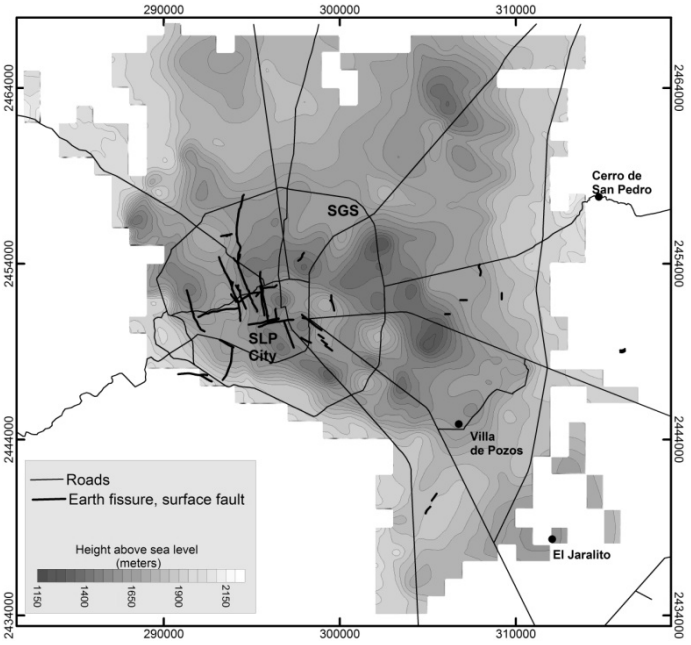

Fig. 4 Configuration of the bedrock as well as cracks in the valley of SLP.

However, the level of groundwater in urban areas shows a spatial relationship between the area of greatest drop and the area that has been affected the most by cracks (Fig. 5); additionally Fig. 4 shows that this zone is located on a topographic irregularity of the bedrock.

ZONE OF RISK BY FRACTURES IN THE VSLP

The probability of occurrence of new fractures that are related to subsidence in the valley of SLP can be associated with the presence of three factors: a rocky floor with irregular topography, a

granular aquifer system that is capable of being drained, and a decreasing level of groundwater. The first two factors are the scenario that is potentially dangerous, and the third factor is the unchaining element or the trigger of the phenomenon.

The observations in the valley of SLP suggest that there are two main factors involved with the fractures that are associated with the paleochannels; one is the presence of ancient stream fills (a potentially dangerous scenario) and the other is a trigger factor that seems to be a subsurface current that carries particles that generate floor holes that erode and collapse.

In order to develop the zoning map, it was made a crossroad of spatial occurrence of the gravimetric anomaly maps, of gradient of the gravimetric anomaly, and a map of the existing cracks, the bedrock configuration and the geology map. Figure 6 shows the danger map of fracturing in the study area.

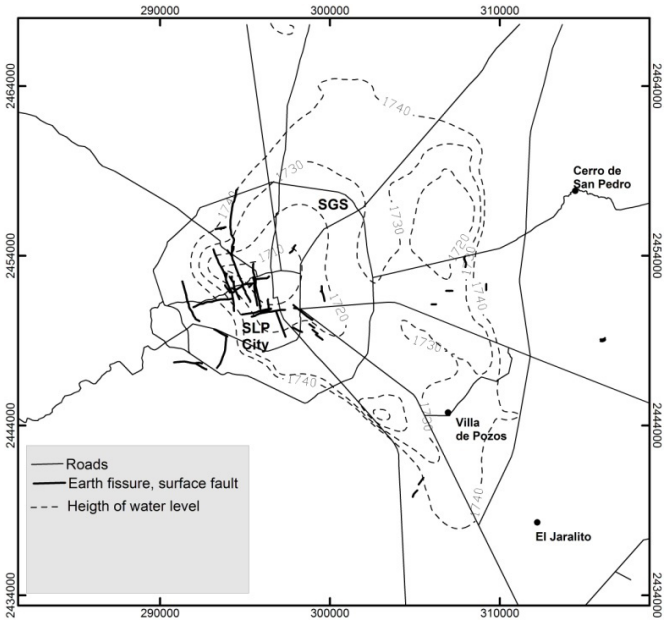

Fig. 5 Levels of groundwater (1998) and cracks in the VSLP.

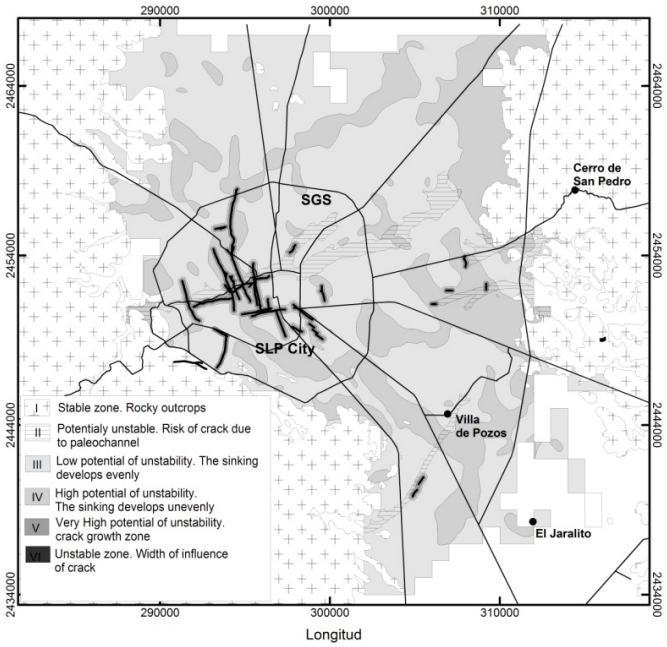

Fig. 6 Zoning map of risk associated to cracks generation in SLP valley.

REFERENCES

Aguirre-Hernández, M. Á. (1992) Geología del Subsuelo de las Cuencas Geohidrológicas del Valle de SLP y Villa de Reyes, en el Estado de SLP, Universidad Autónoma de SLP, Instituto de Geología. *Folleto Técnico no. 116*.

Carpenter, M. C. (1999) Land subsidence in the United States: Circular 1182, US Geological Survey. In: *Mining Ground Water*, Part I (ed. by D. Galloway, D. R. Jones & S. E. Ingebritsen), 65–81. South-Central Arizona.

Carrillo-Rivera, J. J., Cardona A. & Edmunds, W. M. (2002) Use of abstraction regime and knowledge of hydrogeological conditions to control high fluoride concentration in abstracted groundwater: basin of SLP, Mexico. *J. Hydrol.* **261**, 24–47.

Garduño-Monroy, V. H., Arreygue-Rocha, E., Israde-Alcántara, I. & Rodríguez-Torres, G. M. (2001) Efectos de las fallas asociadas a sobreexplotación de acuíferos y la presencia de fallas potencialmente sísmicas en Morelia, Michoacán, México. *Revista Mexicana de Ciencias Geológicas* **18**(1), 37–54.

Jachens, C. R. & Holzer, L. T. (1982) Differential compaction mechanism for earth fissures near Casa Grande, Arizona. *Geol. Soc. Am. Bull*. **93**, 998–1012.

López-Doncel, R., Mata-Segura, J. L. & Barboza-Gudiño, R. (2006b) Se está hundiendo la Ciudad de SLP? – Revista Universita-rios Potosinos, Universidad Autónoma de SLP. *Nueva Época* **2**(7), 26–30, ISSN-1870-1698.

López-Doncel, R., Mata-Segura, J. L., Cruz-Marquez, J., Arzáte-Flores J. & Pacheco-Martínez, J. (2006a) Riesgo geológico para el patrimonio histórico. Ejemplos del centro histórico de la Ciudad de SLP. *Boletín de la Sociedad Geológica Mexicana* **58**(2), 259–263.

Martínez-Ruiz, V. J. (1997) Actualización del Marco Geológico del Subsuelo del Valle de San Luis Potosí, Universidad Autónoma de San Luis Potosí, Instituto de Geología, Folleto Técnico no. 123.

Pacheco, J., Arzate, J. A., Rojas, E., Yutsis, V., Arroyo, M. & Ochoa, G. (2006) Delimitation of soil fissures zones due to ground subsidence using gravity data and finite element modelling in the Valley of Querétaro, México. *Engng Geol*. **84**, 143–160.

Pacheco-Martínez, J. & Arzate Flores, J. A., (2007) Análisis multicapa de la subsidencia en el valle de Querétaro México. *Revista Mexicana de Ciencias Geológicas* **24**(3), 389–402.

Suárez-Plascencia, C., Escalona-Alcázar, F. de J. & Díaz-Torres, J. de J. (2005) Desarrollo de grietas en el fraccionamiento Prados de Nextipac, Municipio de Zapopan, Jalisco. *GEOS* **25**(2).

Land Subsidence, Associated Hazards and the Role of Natural Resources Development
(Proceedings of EISOLS 2010, Querétaro, Mexico, 17–22 October 2010). IAHS Publ. 339, 2010.

Integrated study of land subsidence in Morelia, Michoacán, Mexico

J. A. ÁVILA-OLIVERA[1], V. H. GARDUÑO-MONROY[2] & P. FARINA[3]

1 *Instituto de Investigaciones Sobre los Recursos Naturales (INIRENA), Universidad Michoacana de San Nicolás de Hidalgo (UMSNH), Av. San Juanito Itzicuaro s/n, Col. Nueva Esperanza, C.P. 58330, Morelia, Michoacán, Mexico*
ja.avilaolivera@gmail.com

2 *Instituto de Investigaciones Metalúrgicas (IIM), Universidad Michoacana de San Nicolás de Hidalgo (UMSNH), C.U., Morelia, Michoacán, Mexico*

3 *Formerly at Dipartimento di Scienze della Terra, Universitá degli Studi di Firenze, Via G. La Pira 4, I-50121 Florence, Italy*

Abstract Since 1983, Morelia, Michoacán, Mexico, has been affected by land subsidence problems with a structural control, which has caused differential sinkings, fissures, fracturing and ground rupturing. In order to study the phenomenon a methodology that involves geological, geotechnical, stratigraphic, hydrological, hydrogeological, geophysical, and geodetic analyses was proposed. The methodology allows gaining of a better understanding of the process. The integrated study allowed explanation, among others aspects, as to why maximum land subsidence rates have developed in a zone that was considered to have no possibility of developing ground settlement. Also, it allowed the realization of a preliminary zonation which consisted of dividing the city into three zones, stable, medium stability and unstable. These areas have well-defined borders which are surface faults.

Key words land subsidence; integrated study; conceptualization; Morelia, Mexico

INTRODUCTION

Morelia has been affected by sinking problems since the early 1980s, which have been associated with land subsidence generated by the consolidation of the aquifer system due to groundwater withdrawal (Garduño-Monroy *et al*., 1998). However, this land subsidence was not manifested alone; it was accompanied by ground rupturing. The same scenario has been observed in other Mexican cities such as Aguascalientes (Lermo-Samaniego *et al.*, 1996), Celaya (Trujillo-Candelaria, 1991), Querétaro (Álvarez-Manilla & Pérez-Rea, 1996), San Luis Potosí (Arzate-Flores *et al.*, 2006), etc.

The first surface faults that appeared in Morelia were identified in 1983, and received the names of "Central Camionera" and "La Colina", a reflection of the neighbourhoods where they started to cause damage to buildings, roads and pipelines (Ávila-Olivera & Garduño-Monroy, 2004). Currently the city is affected by eight surface faults oriented NE–SW and another with an E–W direction. It is well known that this phenomenon is the result of land subsidence with a structural control, which is exerted by synsedimentary faults that lead to differential sinkings, with the possibility of becoming earth fissures, and causing fractures and ground ruptures (Ávila-Olivera, 2009).

In order to determine which of these elements have more weight in the land subsidence process that is taking place at Morelia, a methodology combining analyses from different points of view was developed. These analyses are based on geological, geotechnical, stratigraphic, hydrological, hydrogeological, geophysical and geodetic observations. The integration of them allows a full understanding of the problem.

METHODOLOGY

The methodology basically consists of analysing separately each of the elements involved in the formation and development of land subsidence with a structural control, with as many tools as possible. Subsequently, these studies are integrated in order to recognize relationships between them, and thus provide a full conceptualization of the phenomenon.

Copyright © 2010 IAHS Press

The methodology involves a set of studies: geological which in turn are formed by regional, local, subsurface and structural geological analyses; geotechnical which are focused into identifying the materials that could experience a consolidation process; stratigraphic in order to know the thickness of deformable materials; hydrological to realize an analysis of water table decline; hydrogeological to determine from which geological unit water is being extracted; geophysical which, besides proving the presence of geological faults, allows establishing of the influence zones and "net throws"; and geodetic to monitor the evolution of land subsidence through time.

RESULTS

Geological study

Through this study it was possible to identify both the surface and subsurface geology. Figure 1 is a map of the shallow geology of Morelia. Regarding subsurface geology concerns, a stratigraphic column was defined. From the base to the top, there is an andesitic sequence of Upper-Middle Miocene age (>12 million years), ignimbrites (pyroclastic flows) of Miocene age (12 million years), a Punhuato volcanic complex of the Miocene, lacustrine and/or fluviolacustrine sequences of the Miocene-Pliocene, andesitic-basaltic volcanism (the Quinceo and Las Tetillas volcanoes) of Pleistocene-Holocene age, and Recent deposits (palaeosoils and soils) (Israde-Alcántara, 2002). The structural geology reveals that some of these geological units are cut by NE–SW and E–W faults (Garduño-Monroy *et al*., 2001).

Geotechnical study

The geotechnical study consisted of excavation of trenches perpendicular to the axes of surface faults. These trenches allowed direct observation of the recent deposits and the lacustrine and/or fluviolacustrine sequences, and the fault plane of the ground rupture. Also, it was possible to extract unaltered soil samples for laboratory tests (Ávila-Olivera & Garduño-Monroy, 2004). The results indicate that the geological units mentioned are susceptible to experiencing consolidation due to groundwater withdrawal, and therefore present problems of land subsidence. Both geological units are located superficially in the city valley forming a NE–SW fringe.

Stratigraphic study

In order to carry out the stratigraphic study, the lithological columns of the pumping wells distributed in the city were analysed. This information allowed determination of the subsurface configuration of the geological units, specifically the thickness of each one, in the different zones of Morelia. Based on the geotechnical study, recent deposits and lacustrine and/or fluviolacustrine sequences, require special attention because they are the units that may present deformations. The analysis revealed that these units have maximum thickness towards the north, with values that reach 200 m. Also, important thicknesses of between 100–160 m of these deposits occur locally towards the western and northwestern parts of the city, but with the particularity that they are inter-digitated with andesitic-basaltic lavas of Quinceo and Las Tetillas volcanoes (Ávila-Olivera, 2009).

Hydrological study

In the hydrological analysis the groundwater behaviour was studied. In order to do so, the registers of the static levels of pumping wells located within the city were reviewed. As a result of this study an annual average water table decrease of 3.67 m was estimated; and it was determined that in the north portion of Morelia this water table is located at between 100–150 m depth, while in the rest of the city the arithmetic mean is around 70 m depth. This difference suggests the possibility that the aquifer system of Morelia is formed by two aquifers, and in the northern zone the deeper one is exploited (Ávila-Olivera & Garduño-Monroy, 2007).

Fig. 1 Shallow geology of Morelia. (1) Recent deposits; (4) andesitic-basaltic volcanism of Pleistocene-Holocene; (5) andesitic-basaltic volcanism of Pleistocene; (6) lacustrine and/or fluviolacustrine sequences of Miocene-Pliocene; (7) debris flows; (8) andesites and dacites of Miocene-Pliocene; (9) ignimbrites of Miocene; (10) andesitic sequence of Miocene; (11) volcanic sequence of "Atécuaro" caldera of Miocene; (12) volcanic sequence of "La Escalera" caldera of Miocene.

Hydrogeological study

The hydrogeological study (integration of geological, stratigraphic and hydrological analyses) allowed determination of from which geological unit water is currently extracted. If the groundwater withdrawal is from a unit that has deformation capability (recent deposits and lacustrine and/or fluviolacustrine sequences), we can expect land subsidence, but if the extractions are from rock, it is possible to say that the sinkings and subsidence are almost over. Sometimes land subsidence continues; this is because the process of soil consolidation implies a delay, which is related to the time that it takes water to leave the interstitial spaces of soil (Terzaghi, 1925).

Currently, water is mainly extracted from the ignimbrites, in the south, east and northeast of the city, while in the north, central, west and northwest zones, withdrawals are made from lacustrine and/or fluviolacustrine sequences; so the possibility of more land subsidence in these areas exists, as was confirmed by geodetic studies carried out as part of the methodology proposed.

Geophysical study

This study was realized employing a GPR (Ground Penetrating Radar) equipment, specifically a PulseEkko bistatic of Sensors and Software Inc., which has the advantage that it allows varying of the distance between antennas, and therefore estimates the propagation velocity of electromagnetic waves through subsurface. Antennas of 50, 100 and 200 MHz were used. All the profiles prospected were perpendicular to the axes of surface faults. The radargrams resulting from this survey allowed: establishing the width of influence zones, from 20 m ("Chapultepec" fault) to 40 m ("Cental Camionera" and "La Colina" faults), and estimation of the "net throws", from 2 m ("Chapultepec" fault) to 4.40 m ("La Colina" fault) (Ávila-Olivera & Garduño-Monroy, 2008).

Geodetic studies

Two geodetic studies were carried out to monitor land subsidence in the city; one by using a geodetic GPS and applying the DGPS (Differential GPS) method. The other is based on satellite radar interferometry.

GPS analysis

In order to realize the GPS analysis, it was necessary to implement a network of control points in the city. Nowadays the network is formed by 54 of these points which are monitored continuously. The monitoring consists of annual surveys in which the control points are occupied with geodetic GPS.

The land subsidence map, Fig. 2, was elaborated with data from survey campaigns realized between 2006 and 2007. The values recorded for each control point were interpolated in order to create a surface. This map shows that maximum land subsidence rates were located in the north, west and northwest of the city, reaching values of –60 mm/year (Ávila-Olivera *et al.*, 2007).

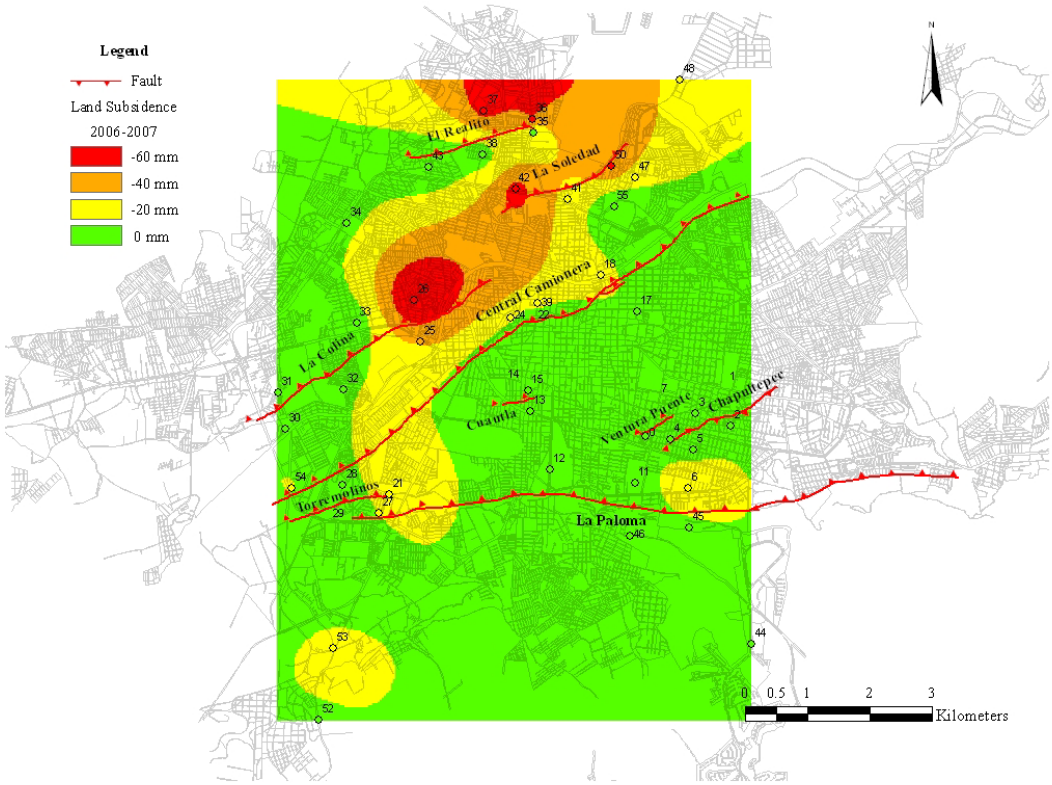

Fig. 2 Land subsidence map of Morelia (August 2006–August 2007).

Interferometric analysis

In order to apply the interferometric technique, a set of ASAR scenes of the city, taken by ENVISAT satellite, have been acquired. The time interval that this set spans is from July 2003 to May 2006. The method employed is known as “two pass interferometry”, and the interferograms obtained were subjected to a phase unwrapping process to convert them into ground displacements along the satellite l.o.s. (line of sight).

Figure 3 is a map of ground displacements and displays the deformations that occurred between August 2003 and November 2004 (an interval of 490 days). The map reveals the spatial

distribution of displacements mainly in three sites: throughout "La Paloma" fault in an E–W direction; on the hanging wall block of "La Colina" fault; and between "El Realito" and "La Soledad" faults. Normalizing the result, a land subsidence rate of up to –35 mm/year was determined, which was identified in the northern, western, and northwestern portions of the city (Farina *et al.*, 2008).

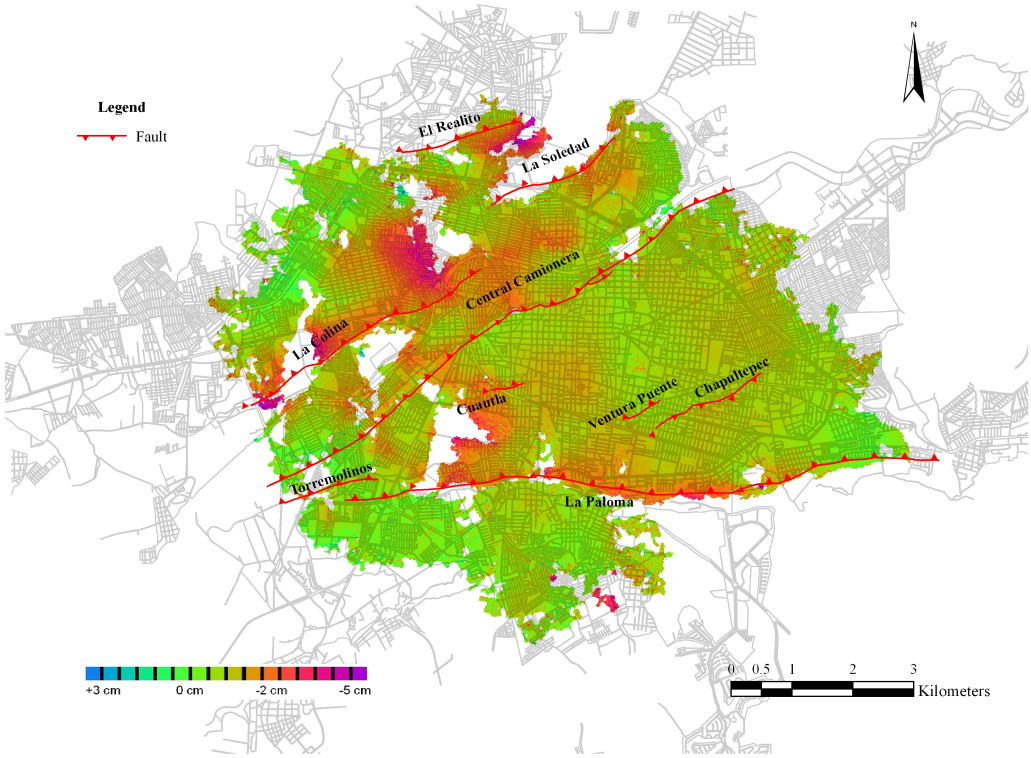

Fig. 3 Ground displacement map of Morelia (16 August 2003–13 November 2004).

DISCUSSION

Both geodetic studies reveal that maximum land subsidence is concentrated toward the northern, western and northwestern parts of the city. At first this was unexpected because in these zones the geological study shows andesitic-basaltic lavas of Quinceo and Las Tetillas volcanoes (Pleistocene-Holocene) (Fig. 1), and therefore they were considered as a stable areas of the city. However, with the integration of the other studies it was possible to explore all possibilities.

The hydrogeological analysis revealed that in the mentioned zones, the water table is located at between 100–150 m depth, and that the geological units from which water is withdrawn, are the lacustrine and/or fluviolacustrine sequences, which have been identified by geotechnical tests as susceptible materials that are prone to consolidation when interstitial water is removed. The volcanism that outcrops in these zones is interdigitated with the sedimentary sequences which have thicknesses of 100–160 m. The weight of these lavas is accelerating the sediment consolidation process due to water withdrawal, compared to the rest of the city.

CONCLUSIONS

The methodology proposed allows a better understanding of the phenomenon of land subsidence with a structural control. It permits identification of which elements involved in the process contribute more, and thus provides the possibility to make well-founded proposals to mitigate the effects, or at least to learn how to coexist with them.

Analysing the different components of the integrated study, the city of Morelia was divided into three portions as a function of both the ground displacements detected, as well as the possibility of land subsidence developing in the future. The stable zone is located towards the southern edge in the footwall block of "La Paloma" fault; the portion with medium stability is the wedge that forms the area between the "La Paloma" and "Central Camionera" faults; finally the unstable zone where the maximum land subsidence was detected, is located towards the northwest of the city, from the hanging wall block of the "Central Camionera" fault, it includes the "La Colina", "La Soledad" and "El Realito" faults.

REFERENCES

Álvarez-Manilla, A. A. & Pérez-Rea, M. de la L. (1996) Subsidencia y fallamiento en el Valle de Querétaro. *XVIII Reunión Nacional de Mecánica de Suelos*.

Arzate-Flores, J. A., Pacheco-Martínez, J., Del Rosal-Pardo, A., Barboza-Gudiño, R., Mata-Segura, J. L. & López-Doncel R. (2006) Carta de riesgo de agrietamientos del área metropolitana de San Luis Potosí. *Geos* **26**(1), 185.

Ávila-Olivera, J. A. (2009) Evolución de los Procesos de Subsidencia-Creep-Falla, casos: Morelia, Mich. y Celaya, Gto. PhD Thesis, Universidad Nacional Autónoma de México, Mexico, D.F.

Ávila-Olivera, J. A. & Garduño-Monroy, V. H. (2004) La subsidencia y las fallas geológicas en la Ciudad de Morelia, Michoacán. *XXII Reunión Nacional de Mecánica de Suelos*.

Ávila-Olivera, J. A. & Garduño-Monroy, V. H. (2007) Análisis del abatimiento de los niveles freáticos del sistema acuífero de Morelia. *Revista Ciencia Nicolaita* **46**, 105–122.

Ávila-Olivera, J. A. & Garduño-Monroy, V. H. (2008) A GPR study of subsidence-creep-fault processes in Morelia, Michoacán, Mexico. *Engineering Geology* **100**(1), 69–81.

Ávila-Olivera, J. A., Calderón-Muñoz, J. & Garduño-Monroy, V. H. (2007) Monitoreo de los Procesos de Subsidencia-Creep-Falla que afectan a la Ciudad de Morelia, Michoacán, empleando DGPS Geodésico. *Geos* **27**(1), 157.

Farina, P., Ávila-Olivera, J. A., Garduño-Monroy V. H. & Catani, F. (2008) DInSAR analysis of differential ground subsidence affecting urban areas along the Mexican Volcanic Belt (MVB). *Rivista Italiana di Telerilevamento* **40**(2), 103–113.

Garduño-Monroy, V. H., Arreygue-Rocha, E, Chiesa, S., Israde-Alcántara, I., Rodríguez-Torres, G. M. & Ayala, G. M. (1998) Las fallas geológicas y sísmicas de la ciudad de Morelia y su influencia en la planificación del territorio. *Ingeniería Civil* **1**(5), 3–12.

Garduño-Monroy, V. H., Arreygue-Rocha, E, Israde-Alcántara, I. & Rodríguez-Torres, G. M. (2001) Efectos de las fallas asociadas a sobreexplotación de acuíferos y la presencia de fallas potencialmente sísmicas en Morelia, Michoacán, México, *Revista Mexicana de Ciencias Geológicas* **18**(1), 37–54.

Israde-Alcántara, I. & Garduño-Monroy, V. H. (2002) La geología de la región de Morelia. *Contribuciones a la geología e impacto ambiental de Morelia*, 1.

Lermo-Samaniego, J., Nieto-Obregón, J. & Zermeño, M. (1996) Fault and fractures in the valley of Aguascalientes, Preliminary microzonification. In: *World Conference on Earthquake Engineering*, 1651. Elsevier, The Netherlands.

Terzaghi, K. (1925) Principles of soil mechanics: IV, Settlement and consolidation of clay. *Eng. News-Rec.* 874–878.

Trujillo-Candelaria, J. A. (1991) Fallamiento de terrenos por efecto de la sobreexplotación de acuíferos en Celaya, Guanajuato, México. In: *XXIII Congress of the Association of International Hydrologists* (Sobreexplotación de acuíferos: España), 175–178.

Land Subsidence, Associated Hazards and the Role of Natural Resources Development
(Proceedings of EISOLS 2010, Querétaro, Mexico, 17–22 October 2010). IAHS Publ. 339, 2010.

Geological setting of active faulting associated with land subsidence at the Aguascalientes and Querétaro valleys, Mexico

J. MARTÍNEZ-REYES & L. M. MITRE-SALAZAR
Centro de Geociencias, Universidad Nacional Autónoma de México, Campus Juriquilla, Querétaro, Mexico
jmr@geociencias.unam.mx

Abstract The Aguascalientes and Querétaro valleys occupy mid- to late-Tertiary N–S trending graben structures in central Mexico. Both valleys are similar in geological terms. In the past decades both valleys have shown the development of open fissures and active faults in the graben-fill deposits. These phenomena have been interpreted as related to land subsidence caused by groundwater drawdown. The trend of open fissures and active faults is parallel to master faults of the grabens. We have studied the geology around the tectonic basins and interpreted the geology underneath the graben-fill deposits. This study reveals an intricate geological structure, the product of several periods of deformation during the Cenozoic. The knowledge of the bedrock structural patterns and the graben-fill stratigraphy are important to understand the active deformation associated with land subsidence in the Aguascalientes and Querétaro valleys. The land subsidence and active faulting are caused by drawdown, and we believe that active tectonic deformation in the region can not be ruled out.

Key words Aguascalientes and Querétaro valleys, Mexico; groundwater drawdown; subsidence and active faulting

INTRODUCTION

The Aguascalientes and Querétaro valleys are located in two different grabens in Central Mexico. Active aseismic faults have been reported in both localities since the 1980s. These structures occur in soils and in unconsolidated graben-fill sediments. Similar faults, reported in other localities in Central Mexico, are interpreted as a consequence of severe drawdown in the aquifers that provide water for agricultural, industrial and domestic use of the inhabitants of the region. We regard the characterization of the geological setting of the hydrological basins as a first and fundamental step in the analysis of faulting associated with land subsidence.

REGIONAL SETTING

Three geological provinces join at the broad region where the Aguascalientes and Querétaro valleys are located. The Sierra Madre Oriental is a fold and thrust belt formed during the Laramide Orogeny (late Cretaceous–Paleocene); the Sierra Madre Occidental is a large felsic ignimbritic province related to the subduction of the Farallon plate during the Paleogene; the Mexican Volcanic Belt is a still-active magmatic arc, associated with the subduction of the Rivera and Cocos plates, which began its activity in the late Miocene. The active volcanic front of the Mexican Volcanic Belt is located 200–300 km south of the study areas.

Following the end of the compressive tectonic phase that formed the Sierra Madre Oriental, the region was extended in two pulses: an early phase occurred during the Paleogene and was related to activity at the southern end of the Basin and Range tectonic province (Henry & Aranda-Gómez, 1992). A second phase was triggered by the opening of the Gulf of California (Ferrari *et al.*, 2002). The final result of the extension was the formation in the region of a group of NNE–SSW grabens (such as the Aguascalientes valley). Regional faults with a NW–SE trend (Tepehuanes–Zimapan fault system, Fig. 1) are related to a back-arc, transtensional (sinistral)

Copyright © 2010 IAHS Press

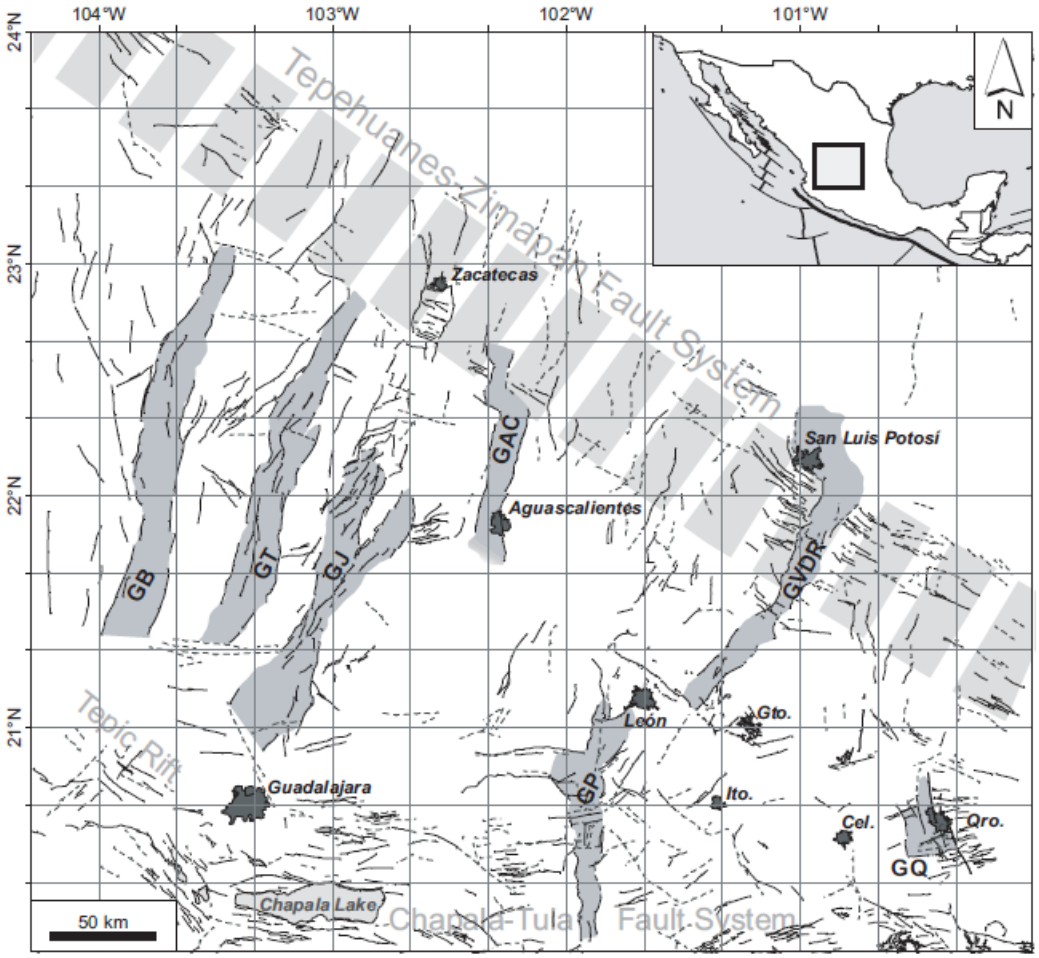

Fig. 1 Structural sketch map of the Mesa Central area. Grabens: GB, Bolaños; GT, Tlaltenango; GJ, Juchipila; GAC, Aguascalientes; GVDR, Villa de Reyes; GP, Penjamillo; GQ, Querétaro (Andréani *et al.*, 2010).

system, which was coeval with the Oligocene ignimbritic volcanism of the Sierra Madre Occidental (Andréani *et al.*, 2010). Younger (Neogene) sets of normal faults in Central Mexico are related to intra-arc extension within the Mexican Volcanic Belt and have E–W and NE–SW trends (Suter *et al.*, 2001; Szynkaruk *et al.*, 2004). NNW–SSE trending structures, such as the Querétaro graben were developed in a sinistral transtensional stress system (Ego & Ansan, 2002).

The regional stratigraphy in both valleys is formed by a Mesozoic marine, volcano-sedimentary basal complex, partly covered by a continental volcanosedimentary succession, Figs 2(a) and 3(a). The local Cenozoic structure in both valleys is dominated by normal faults with a throw of several hundred metres.

The interpretation of the sub-surface geology at the bottom of the grabens is based on the study well logs and samples. The local basement in the Aguascalientes basin is formed by Oligocene rhyolite, and by Miocene basalt in Querétaro, Figs 2(b) and 3(b). In both basins, resting atop the basement exist a thick unconsolidated clastic succession of graben-fill deposits. Thickness of the graben-fill sediments in Aguascalientes may be up to 400 m, whereas it is considerably thinner in Querétaro (>100 m). Underneath the buried basalts of the Querétaro basin there is an important succession of continental clastic sediments that host a deeper aquifer. Water wells in Aguascalientes have not been drilled deeper than the rhyolite.

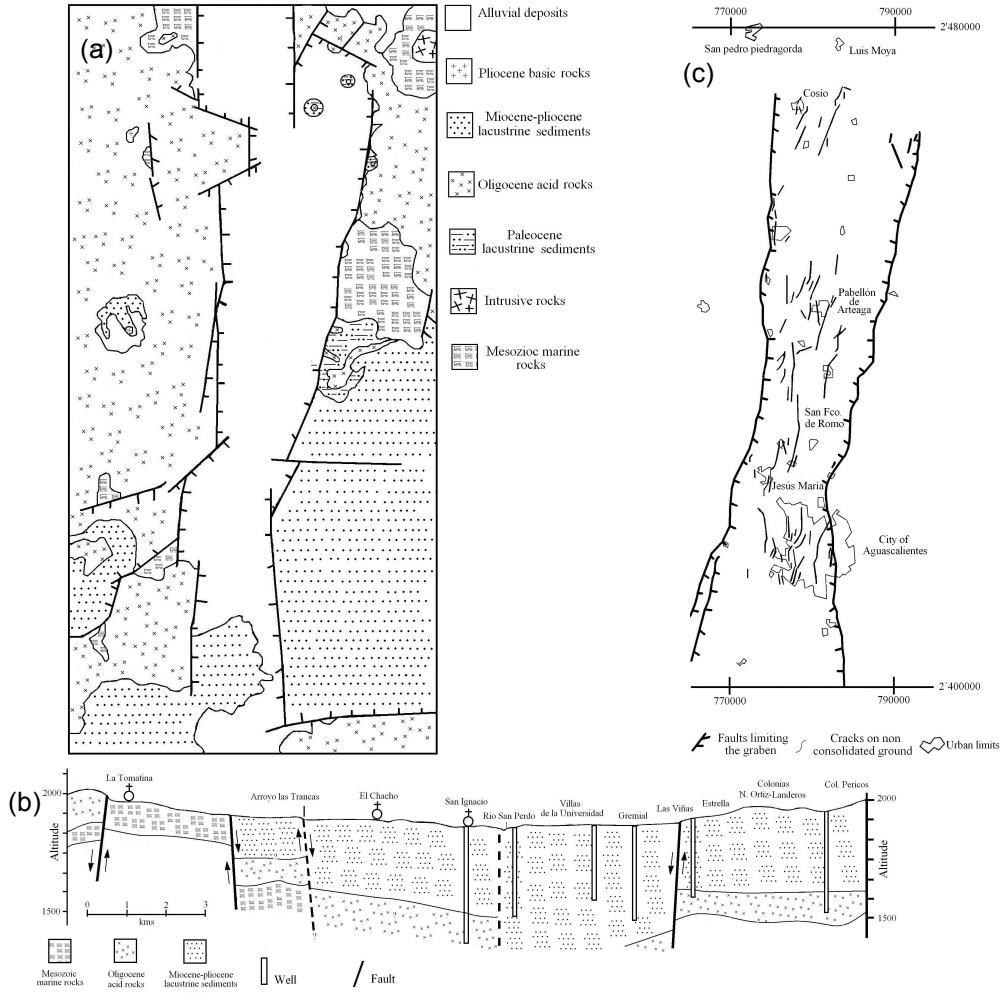

Fig. 2 Geological sketch map (a), structural section (b), and structural map of land subsidence of the Aguascalientes valley (c).

The trends of the active, land-subsidence-related, faults in both valleys are nearly parallel to the local Cenozoic tectonic grain inferred from the orientation of the master faults of the grabens. Active faults are better developed and have larger displacements in those areas where the thickness of the graben-fill succession is larger. Location of the active faults is related to concealed structures in the basement.

CONCLUSIONS

Land subsidence in the Aguascalientes and Querétaro valleys is directly related to bedrock structures and with the local thickness of the graben fill successions. Differential compaction was apparently triggered by drawdown in the aquifers. Both valleys are located in a region where the inferred state of stress is tensional (Suter, 1991). Thus, it can not be ruled out that there could be a tectonic component in the formation of the active faults.

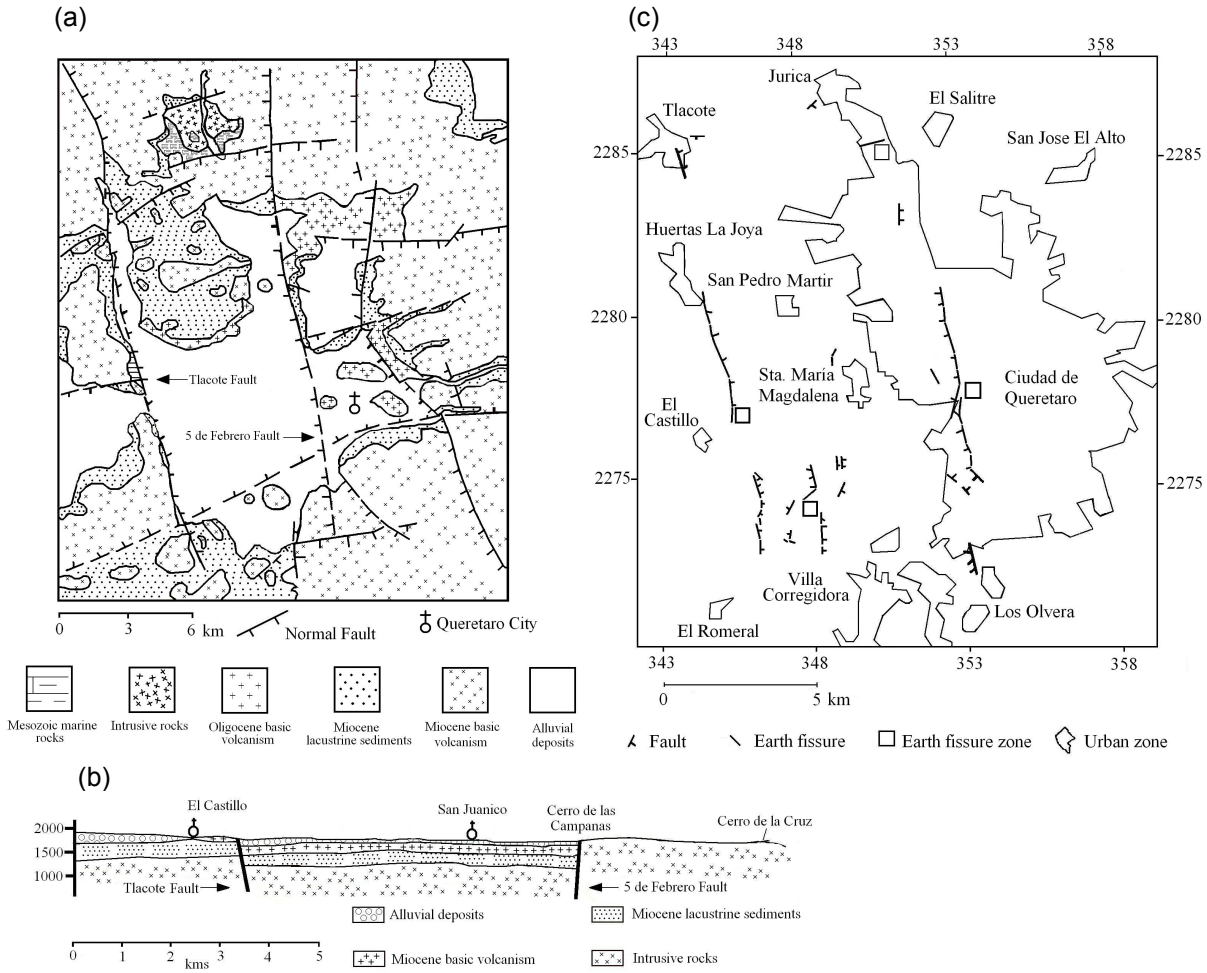

Fig. 3 Geological sketch map: (a), structural section (b) and land subsidence map (c) of the Querétaro valley.

REFERENCES

Andréani, L., Martínez-Reyes, J. & Gattacceca, J. (2010) Évolution cinématique post-Ëocène de la Mesa Central (Mexique) á partir de données structurales et paléomagnétiques (in preparation).

Ego, F. & Ansan, V. (2002) Why is the central Trans-Mexican Volcanic Belt (102º–99º) in transtensive deformation? *Tectonophysics* **359**, 189–208.

Ferrari, L., Conticelli, S., Vaggelli, G.,Petrone, C. M. & Manetti, P. (2000) Late Miocene volcanism and intra-arc tectonics during the early development of the Trans-Mexican Volcanic Belt. *Tectonophysics* **318**, 161–185.

Henry, C. D. & Aranda-Gómez, J. J. (1992) The real southern Basin and Range: Mid-to late Cenozoic extension in Mexico. *Geology* **20**, 701–704.

Suter, M. (1991) State of stress and active deformation in Mexico and western Central America. In: *Neotectonics of North America* (ed. by D. B. Slemmons, E. R. Engdahl, M. D. Zoback & D. D. Blackwell), 401–421. Geological Society of America, USA.

Szynkaruk, E., Garduño-Monroy, V. H. & Bocco, G. (2004) Active fault systems and tectonotopographic configuration of the central Trans-Mexican Volcanic Belt. *Geomorphology* **61**, 11–126.

Land Subsidence, Associated Hazards and the Role of Natural Resources Development
(Proceedings of EISOLS 2010, Querétaro, Mexico, 17–22 October 2010). IAHS Publ. 339, 2010.

Conceptual model of land subsidence with a structural control

J. A. ÁVILA-OLIVERA[1] **& V. H. GARDUÑO-MONROY**[2]

1 *Instituto de Investigaciones Sobre los Recursos Naturales (INIRENA), Universidad Michoacana de San Nicolás de Hidalgo (UMSNH), Av. San Juanito Itzicuaro s/n, Col. Nueva Esperanza, CP 58330, Morelia, Michoacán, Mexico*
ja.avilaolivera@gmail.com

2 *Instituto de Investigaciones Metalúrgicas (IIM), Universidad Michoacana de San Nicolás de Hidalgo (UMSNH), CU, Morelia, Michoacán, Mexico*

Abstract In some cases, the land subsidence caused by groundwater withdrawal is guided by a structural control which is generally exercised by synsedimentary faults. This structural control generates differential sinking, which may evolve gradually to earth fissures, fracturing and ground rupturing. This work proposes a conceptual model that explains how differential sinking develops into ground rupturing. The model consists of four stages called: initial, differential land subsidence, cracking and faulting.

Key words land subsidence; structural control; synsedimentary fault

INTRODUCTION

In some cities of the world the process of land subsidence is not uniform; it presents as differential sinking along preferential directions, which are associated with geological faults. These faults are responsible for developing differential sinking which may evolve into earth fissures, fracturing and ground rupturing (Holzer, 1984). However, at first, land subsidence and ground rupturing were seen as phenomena of different and unrelated origin, then Maxey & Jameson (1948) identified the relationship between them.

Ground deformations that involve differential land subsidence, structural faults and water table changes have been observed in numerous alluvial basins (Holzer, 1979; Bell, 1981; Schumann & Genauldi, 1986; Suleiman, 1994; Galloway *et al.*, 1999; Rojas-González *et al.*, 2002). Nowadays it is known that differential land subsidence is guided by structural controls, which is generally exercised by geological faults buried under recent deposits (synsedimentary faults) (Ávila-Olivera & Garduño-Monroy, 2008).

CONCEPTUAL MODEL

For a better understanding of the mechanisms of formation and development of land subsidence with a structural control, was developed a conceptual model, which consists of four stages (Fig. 1).

Stage 0 (initial)

The elements involved in the process are lacustrine and/or fluviolacustrine sediments, synsedimentary faults, and groundwater withdrawal. At this stage, the elements interact without causing damage. There is no considerable decrease of water table due to groundwater extraction, representing that withdrawals do not exceed the recharge. The small fluctuations of water table that can occur are related to seasonal changes.

Stage 1 (differential land subsidence)

This phase is also called differential land subsidence stage, due to the occurrence of differential sinking along preferential directions (Ávila-Olivera & Garduño-Monroy, 2004). The sinkings are generated by a decrease of water table caused by overexploitation of aquifers. When water table declines occur, a reduction of pore water pressure, which helps support the soil stress, then generates a stress transference to soil particles, which are rearranged to adapt to the new stress state (soil particles are compressed to occupy spaces left by interstitial water). This rearrangement

Copyright © 2010 IAHS Press

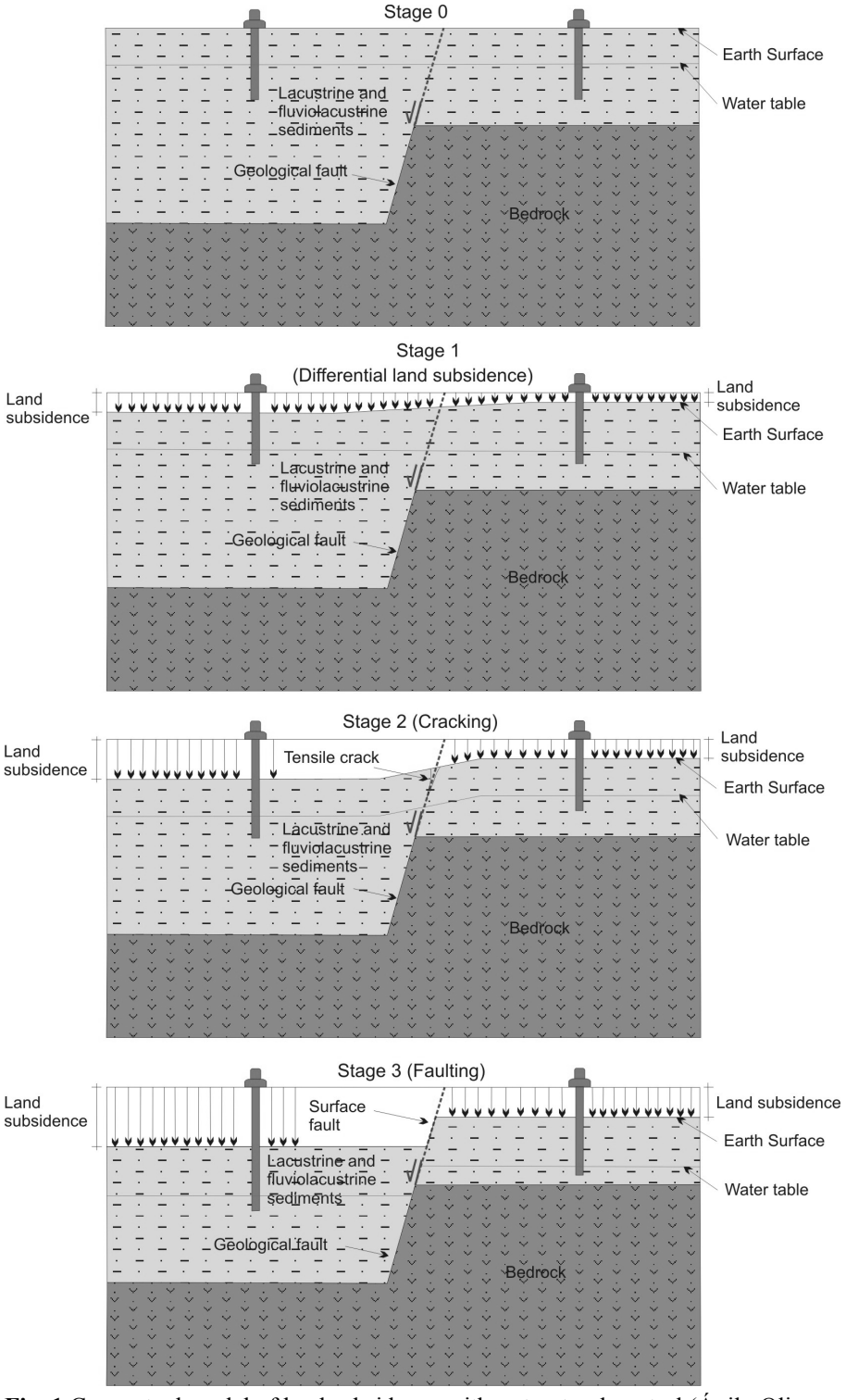

Fig. 1 Conceptual model of land subsidence with a structural control (Ávila-Olivera, 2009).

causes a decrease in the volume of soil voids, which reduces its thickness. The above mentioned is known as the soil consolidation process.

The sinkings are differential, due to a structural control exerted by synsedimentary faults. These faults are buried by lacustrine and/or fluviolacustrine sediments. A synsedimentary fault is a normal or reverse geological fault that has experienced seismic activity on more than one occasion,

so it presents an alternation between seismic events and sediment deposition, and therefore earthquakes are contemporary to different strata that are deposited over time. The faults consist of a footwall and a hanging wall that form a step, which is responsible for the different thickness of sediment deposited in each block. This disparity generates differential land subsidence given that soil consolidation is a function of its thickness.

Stage 2 (cracking)

This stage is known as cracking. Given that water demand in urban centres is not diminishing but increasing, the groundwater extraction in the best case remains constant, which causes the decline of the water table to persist, and therefore also land subsidence.

As the differential land subsidence increases, tensile stress is concentrated on the projection at the surface of the geological faults buried by lacustrine and/or fluviolacustrine sediments. These sediments and soil in general are not resistant to the mentioned stress, and then tensile cracks and fractures are developed at the surface.

Stage 3 (faulting)

At this phase, the faulting stage, as in the previous stage, the aquifer exploitation, water table decline, differential land subsidence and the stress concentration continue. However, there comes a time when the stress concentration is so much that cracks fail, experiencing a vertical displacement, and thereby forming a step at the surface (surface fault) which has a similar geometry to the pre-existing geological fault located in the underlying bedrock.

CONCLUSIONS

The conceptual model of formation and development of land subsidence with a structural control, provides a clear and concise explanation of the mechanism of the occurrence of cracks, fractures and faults at the surface, as a result of interactions between lacustrine and/or fluviolacustrine sediments, synsedimentary faults, and groundwater withdrawal by pumping wells. In this model, unlike others proposed (Álvarez-Manilla & Martínez-Peña, 2002), the presence of synsedimentary faults in the bedrock is essential, otherwise it would be impossible to observe differential land subsidence, cracks and faults with a preferential orientation at the surface.

REFERENCES

Álvarez-Manilla, A. A. & Martínez-Peña, G. E. (2002) Cambios en la rigidez del suelo debido a los esfuerzos de tensión, explicación del mecanismo de agrietamiento en suelos, Unión Geofísica Mexicana, Reunión Anual, Resúmenes: Geos.

Ávila-Olivera, J. A. & Garduño-Monroy, V. H. (2004) La subsidencia y las fallas geológicas en la Ciudad de Morelia, Michoacán. XXII Reunión Nacional de Mecánica de Suelos.

Ávila-Olivera, J. A. & Garduño-Monroy, V. H. (2008) A GPR study of subsidence-creep-fault processes in Morelia, Michoacán, Mexico. *Engng Geol.* **100**(1), 69–81.

Ávila-Olivera, J. A. (2009) Evolución de los Procesos de Subsidencia-Creep-Falla, casos: Morelia, Mich. y Celaya, Gto. PhD Thesis, Universidad Nacional Autónoma de México, Mexico.

Bell, J. W. (1981) Subsidence in Las Vegas Valley. *Nevada Bureau of Mines and Geology Bulletin* **95**, 83 p. 1 plate, scale 1:62 500.

Galloway, D., Jones, D. R. & Ingesbritsen, S. E. (1999) Land subsidence in the United States. *US Geol. Survey Circular 1182*.

Holzer, T. L. (1979) Leveling data – Eglington fault scarp, Las Vegas Valley, Nevada. *US Geol. Survey Open File Report 79-950.*

Holzer, T. L. (1984) Ground failure induced by groundwater withdrawal from unconsolidated sediment. In: *Man Induced Land Subsidence* (ed. by T. L. Holzer), Geol. Society of America Reviews in Engineering Geology 6, 221 p.

Maxey, G. B. & Jameson, C. H. (1948) Geology and water resources of Las Vegas, Pahrump, and Indian Springs Valleys, Clark and Nye Countries. *Nevada State Engineer Water Resources Bulletin* **5**.

Rojas-González, E., Arzate-Flores, J. A. & Arroyo-Contreras, M. (2002) A method to predict the ground fissuring and faulting caused by regional groundwater decline. *Engng Geol.* **65**, 245–260.

Schumann, H. H. & Genauldi, R. B. (1986) Land subsidence, earth fissures, and water-level change in southern Arizona. Arizona Bureau of Geology and Mineral Technology, Geological Survey Branch Map 23, 1 sheet, scale 1:1 000 000.

Suleiman, S. E. B. (1994) Earth fissures caused by groundwater withdrawal in Sarir South agricultural project area, Lybia. *Appl. Hydrol.* **1**, 45–52.

(Proceedings of EISOLS 2010, Querétaro, Mexico, 17–22 October 2010). IAHS Publ. 339, 2010.

Geological study and electrical resistivity tomography of Ameca, Jalisco, Mexico

A. MALAGÓN[1], J. ROSAS-ELGUERA[2], M. A. ALATORRE[1], G. PEREZ[1] & R. MACIEL[3]

1 *Instituto de Ingeniería Sísmica, CUCEI, Universidad de Guadalajara, Av. Revolución No. 1570, Zona Olímpica, CP 44840, Guadalajara, Jal, Mexico*
amalagon2004@yahoo.com.mx

2 *División de Estudios Científicos y Tecnológicos, CUVALLES, Universidad de Guadalajara, Carretera Guadalajara - Ameca Km. 45.5, Mexico*

3 *Centro Universitario de Ciencia Biológica y Agropecuarias, Las Agujas, Zapopan, Jalisco, Mexico*

Abstract There are several areas in Central Mexico with subsidence troubles, such as Aguascalientes, Celaya, Queretaro and Morelia. For 20 years, Ameca town located in Jalisco State, Mexico, has been affected by slow subsidence. The Plio-Quaternary tectonic framework for western-central Mexico suggests a NW fault system associated with a NE-extension. The Ameca region is in this environment. When the damages (e.g cracked houses) are located on a map they show a W–NW trend similar to the regional faulting. Geological studies show that the main normal fault is 4 km long with a 7 m vertical offset. The electrical resistivity tomography study shows that recent sediments are affected by fractures with the same trend as the main normal fault.

Key words subsidence; faulting

INTRODUCTION

The cities of central Mexico are located in or close to valleys associated with the evolution of lacustrine basins. Now some of them have many problems related to fracturing and subsidence; these include: Mexico City, Queretaro, Morelia, San Luis Potosi Aguascalientes, Celaya, Salamanca, Abasolo, Leon and Irapuato. In Jalisco State, small towns such as Ameca, Lagos de Moreno, Chapala, and Ciudad Guzman show the same problem. Most of these cities are located in tectonic basins filled with fluvial and lacustrine sediments with intercalated volcanic rocks. The subsidence may be related to tectonic activity or huge extraction of water from aquifers, or a combination of these two processes. We used electrical resistivity tomography to investigate the extension of the fractures to areas where damages are absent.

GEOLOGICAL FRAMEWORK

Ameca valley, located 85 km to the west of Guadalajara city, belongs to the NW–SE half-graben system of the Tepic-Zacoalco rift; the main volcanoes, Tequila, Ceboruco and Tepetiltic, show the same alignment (Fig. 1, Rosas-Elguera *et al*., 1997). The main fault of the Ameca half-graben is a 1500 m of vertical offset (Ferrari & Rosas-Elguera, 2000). The Ameca half-graben was filled with fluvial sediments intercalated with lacustrine sediments and volcanic materials forming a thick sequence up to 500 m in depth (Ferrari & Rosas-Elguera, 2000).

THE AMECA SUBSIDENCE

For the last 20 years, Ameca city has been affected by subsidence causing damage to the buildings, houses, streets, etc. When the damaged sites are located on a map they are aligned along a W–NW trend similar to the regional tectonic half-graben system suggesting that they are related to the same regional stress field. Figure 2 shows both the urban network and the main normal fault affecting the northern part of Ameca. This fault, 4 km long and with a 7 m vertical offset, has

Copyright © 2010 IAHS Press

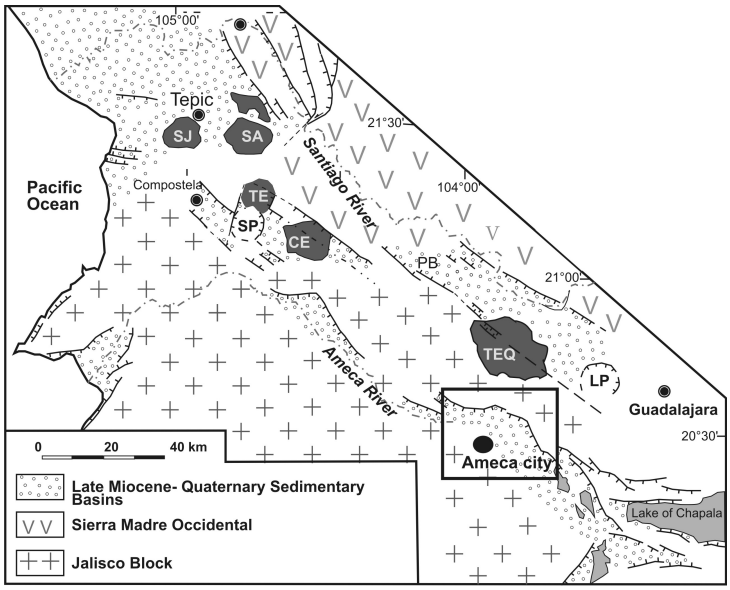

Fig. 1 Tectonic framework of the Ameca area (box) located south of Tequila volcano. PSF, Pochotitlan fault system; ME, Mecatan graben; PV, Puerto Vallarta graben; AC, Amatlán de Cañas half-graben; PB, Plan of Barrancas graben; AM, Ameca half-graben; SM, Zacoalco half-graben; TE, Techalutla fault. Volcanoes: SJ, San Juan; SA, Sanganguey; TE, Tepetiltic, CE, Ceboruco; TEQ, Tequila. Calderas: SP, San Pedro; LP, The Primavera (after Ferrari & Rosas-Elguera, 2000).

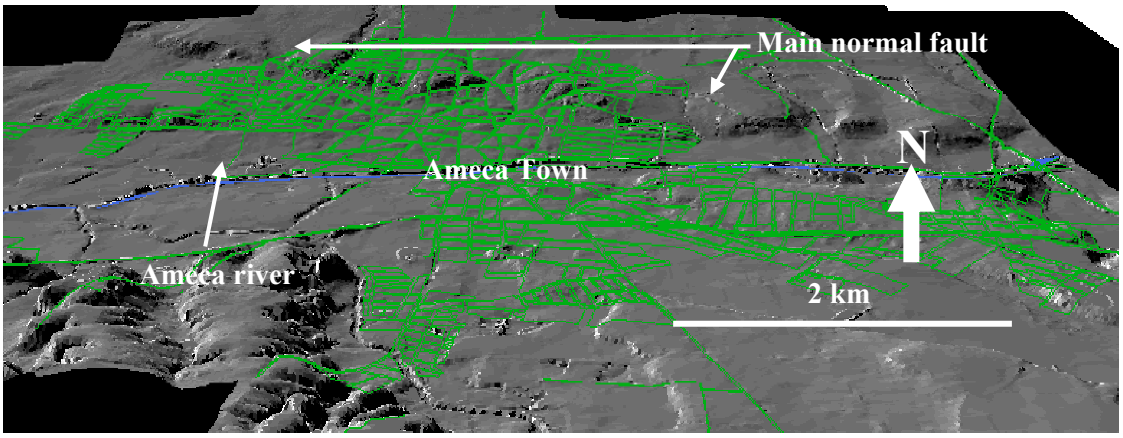

Fig. 2 DEM looking to the north. Note the segmented nature of the main fault suggesting the activity of the erosive processes and the relative uplift of the north side of the fault.

been affected by erosive processes along it. Furthermore, the riverbed of the small river, SR in Fig. 2, is deeper on the north side of the main fault suggesting evidence for its present-day activity.

ELECTRICAL RESISTIVITY TOMOGRAPHY

At the present day, the subsidence along the fault zone (in the front of the main fault) can reach 0.20 m, but there are several places where neither sinking nor damages can be seen. Because of this, we selected those sites for electrical resistivity tomography study. Figure 3 shows two examples. The lines were normal to the main fault. Because the resistivity is between 10 and 28 ohm-m it can be related to infill sediments (e.g. sands, silts, and clays). The selected sites show different behaviour: in the Gutierrez section the resistivity is undisturbed, suggesting that fractures are absent in this section (Fig. 3(a)), but in the Ocampo section, at between 3 and 6 m, the

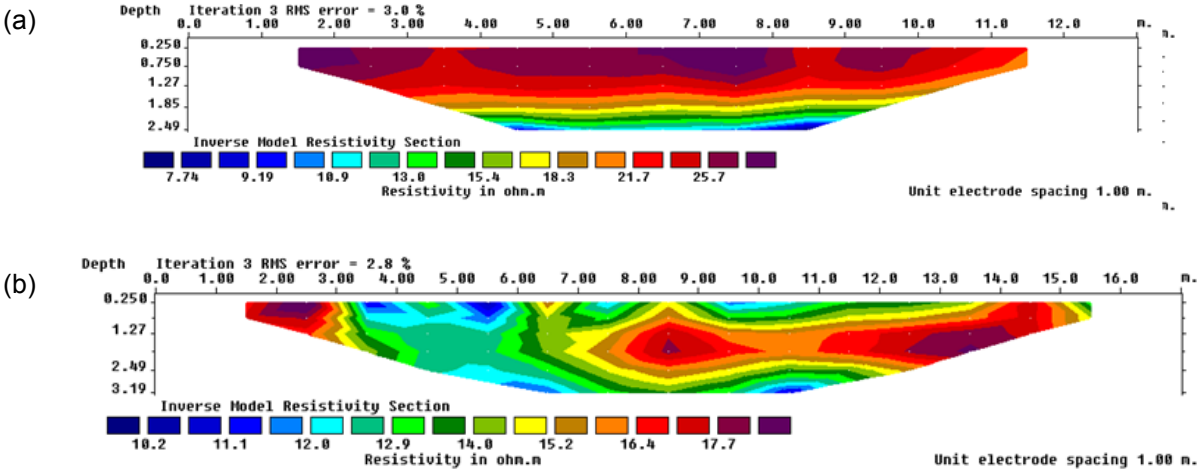

Fig. 3 (a) Ocampo section, (b) Gutierrez section.

resistivity is "broken" suggesting a discontinuity in the infill materials which can be related to a fracture of the fault zone.

CONCLUSIONS

The spatial distribution of the damages in Ameca city is controlled by the trend of the fracturing associated with the normal fault of 4 km length and 7 m of vertical offset. This fault is related to the regional tectonic stress. The electrical resistivity tomography shows that in some places the flat lying sedimentary units are "broken" by fractures, suggesting that the subsidence is active even though there is no surface evidence.

Acknowledgements COECyTJAL proyecto PS-2009-865.

REFERENCES

Ferrari, L. & Rosas-Elguera, J. (2000) Late Miocene to Quaternary extension at the northern boundary of the Jalisco block, western Mexico: the Tepic-Zacoalco rift revised. *Geol. Soc. Am. Special Paper #334*, chapter 3, 41–64.

Rosas-Elguera, J., Ferrari, L. López-Martinez, M. & Urrutia-Fucugauchi, J. (1997) Stratigraphy and tectonics of the Guadalajara region and the triple junction area, western Mexico. *Int. Geological Review* **39**, 125–140.

Land Subsidence, Associated Hazards and the Role of Natural Resources Development
(Proceedings of EISOLS 2010, Querétaro, Mexico, 17–22 October 2010). IAHS Publ. 339, 2010.

Geological and geophysical characterization of fracturing in granular deposits associated with land subsidence in San Luis Potosí City, Mexico

L. D. BARAJAS-NIGOCHE[1], D. C. CARREÓN-FREYRE[2], J. L. MATA-SEGURA[3], A. RIVERA-LEÓN[1] & F. CAFAGGI-FÉLIX[1]

1 *Servicio Geológico Mexicano (SGM), Blvd. Felipe Ángeles Km 4.5 Pachuca, Hgo, Mexico*
dnigoche@sgm.gob.mx

2 *Centro de Geociencias (CGEO)Universidad Nacional Autónoma de México, Juriquilla, Qro, Mexico*

3 *Instituto de Geología, Universidad Autónoma de San Luis Potosí, San Luis Potosí, SLP, Mexico*

Abstract In San Luis Potosí (SLP) City, fractures associated with land subsidence affect the urban structure and, in some cases historical value buildings. Early studies documented ground fracturing in this city and related it to groundwater withdrawal from the beginning of the last decade. Most of these studies were focused to detect fractures using geophysical gravimetric studies that detect major discontinuities in the subsoil. In this study we report mapping of near surface sequences and the interpretation of lithological records available from water wells, trenches, quarries, and drilling. Our results show that fine grained units are concentrated in two zones located north and east of the main SLP urban area. The sand deposits are predominantly distributed in the central part of the city and conglomeratic deposits are distributed near their fluvial sources. A new map of ground fracturing was achieved by integrating fractures related to the distribution of soils and sediments by the use of high precision geophysical tools, such as ground penetrating radar (GPR) and surface wave seismicity. The map suggests that most of fractures are localized in the central-east part of SLP City, ranging from some metres to 7 km in length. We noticed that the fractures with a N−S strike, that in some cases present lateral displacement, are related to the distribution of Tertiary continental deposits (Halcones Conglomerate). The longest fracture, named Aeropuerto Fault, has the same N–S orientation as fractures that present right lateral displacement with stratigraphic structures and related folding located in the south of the City, and has affected a church which displays evidence of structural torsion. Finally, a correlation between groundwater piezometric levels and stratigraphic variations in SLP City suggest that ground fracturing in granular media is closely related to high hydraulic gradients, mainly in the border zone of the Halcones Conglomerate. It is important to note that in semi-desert areas of central-north Mexico, the piezometric levels vary from 130 to 170 m depth. According to our interpretation, the generation of fractures in SLP City may be related to major regional discontinuities in the sedimentary basin, but their propagation depends on the stratigraphic variations and hydraulic behaviour of the near surface sequences.

Key words land subsidence; near surface sequences; ground fracturing; regional faults; San Luis Potosí, Mexico

INTRODUCTION

Fractures associated with subsidence that affect the urban structure in San Luis Potosí City, were investigated early on. These studies were focused to document the characteristics, distribution and damage caused by the fractures, arguing that the fractures were related to the piezometric level decline of the deep aquifer and that the fractures were conditioned due to major discontinuities in the sedimentary basin (Mata-Segura *et al*., 2004a,b; Mata-Segura & López-Doncel, 2004; Arzate-Flores *et al*., 2008). For this study, we made a sedimentary model of the San Luis Potosí Valley (SLPV), based on the interpretation of lithological information from water wells. The model includes the correlation of stratigraphy and the generation of geological cross-sections to analyse the spatial variations of deposits overlying the rock units. Geophysical profiles (GPR and shallow seismic) were also correlated with lithology in order to characterize the structure of the sedimentary sequences and the morphology of ground fracturing. Hydrogeological studies in the SLPV indicate that the distribution and granulometric distribution of the deposits that constitute the aquifers, are relatively continuous vertically and horizontally through the valley (Cardona-Benavides, 1990; Carrillo-Rivera, 1992; Carrillo-Rivera *et al.*, 2002; Noyola-Medrano, *et al.* 2009).

Copyright © 2010 IAHS Press

CARTOGRAPHY OF NEAR SURFACE GEOLOGICAL UNITS

The map of Near Surface Geological Units (NSGU) integrate the geological information previously mapped in detail by the Servicio Geológico Mexicano (scale 1:50,000), groundwater well lithological descriptions, and field descriptions from outcrops and quarries as well as drilling. The NSGU map presented in this work allows delimiting of the granular surface units in the valley for the first 10 m depth and the analysis of the deposits' distribution. It is important to note that the literature for the study area often reports that the exposed sediments correspond to alluvial Quaternary deposits. However, this is not accurate; from our fieldwork we observed a high heterogeneity related to fluvial and lacustrine interbedded sequences, associated with alluvial fan deposits. The predominant granulometry of near surface geological units are sands with typical fluvial structures, which extend over most of the study area; silty and clayey deposits are found in three main zones, one in the north and two more in centre of the valley in a strip located south of the city, while conglomerate deposits are distributed in roughly parallel paths near the source areas (Fig. 1(a)).

The main fracturing patterns that affect the urban structure are located in the centre and west of the studied area. Some of these fractures have a NW–SE strike and reach up to 7 km in length, presenting normal fault behaviour and relative block movement to the west, with a right side component.

SUBSOIL GEOLOGICAL STRUCTURE

San Luis Potosí City is located in the northern of the Villa de Reyes Graben (VRG), which is a tectonic structure related to the regional extensional event named "Basin and Range" (Tristán-González, 1986). Based on the geological cross-section analyses it was observed that the basin bedrock is constituted of tectonic discontinuities that produced NW–SE strike horsts and grabens. The bedrock units are principally ignimbrites and riolites, covered on average by 300-m thickness of continental sedimentary deposits that are laterally discontinuous. In the study area, conglomeritic deposits are distributed according to the proximity of their fluvial source, and therefore appear in bands roughly parallel to the margins of the San Miguelito and San Pedro ranges to the west and east respectively, as well as in the central part of the basin, probably related to a buried horst. These conglomerates, named Conglomerado Halcones, are interbedded with sand which predominates throughout the basin, and also are interbedded with thin clayey and silty deposits mainly distributed in the central part of the basin. The most important identified horizontal and vertical stratigraphic changes are located between the conglomeritic and sand deposits, in the central and western zone of the SLPV (Fig. 1(b)). We observe that fractures affecting the urban structure are located in the same zone and apparently are closely related with the lithological contacts between sedimentary units. It should be noted that the conglomerate deposits exposed in the quarries, located northwest of the city, show evidence of normal faulting and fractures NW20°SE strikes, with relative movements to the east. Aranda-Gómez & Labarthe-Hernández (1977) consider that the most recent volcanic event in the area appears at approx. 28 km northeast of San Luis Potosí City, and consists of an isolated basaltic structure and Plio-Quaternary rocks related to volcanism. However, near to the city we did not find any evidence of this volcanic event.

Based on the lithological interpretation, we consider that the highly contrasting stratigraphic variations and contacts between conglomerates and the fine grained sequences (sand, silt, clay) provide conditions for fracture propagation in the near surface of the basin (Carreón Freyre *et al.*, 2005). Some of longest fractures present a variation in strike and appear to be closely related to spatial variations of the lithological contact.

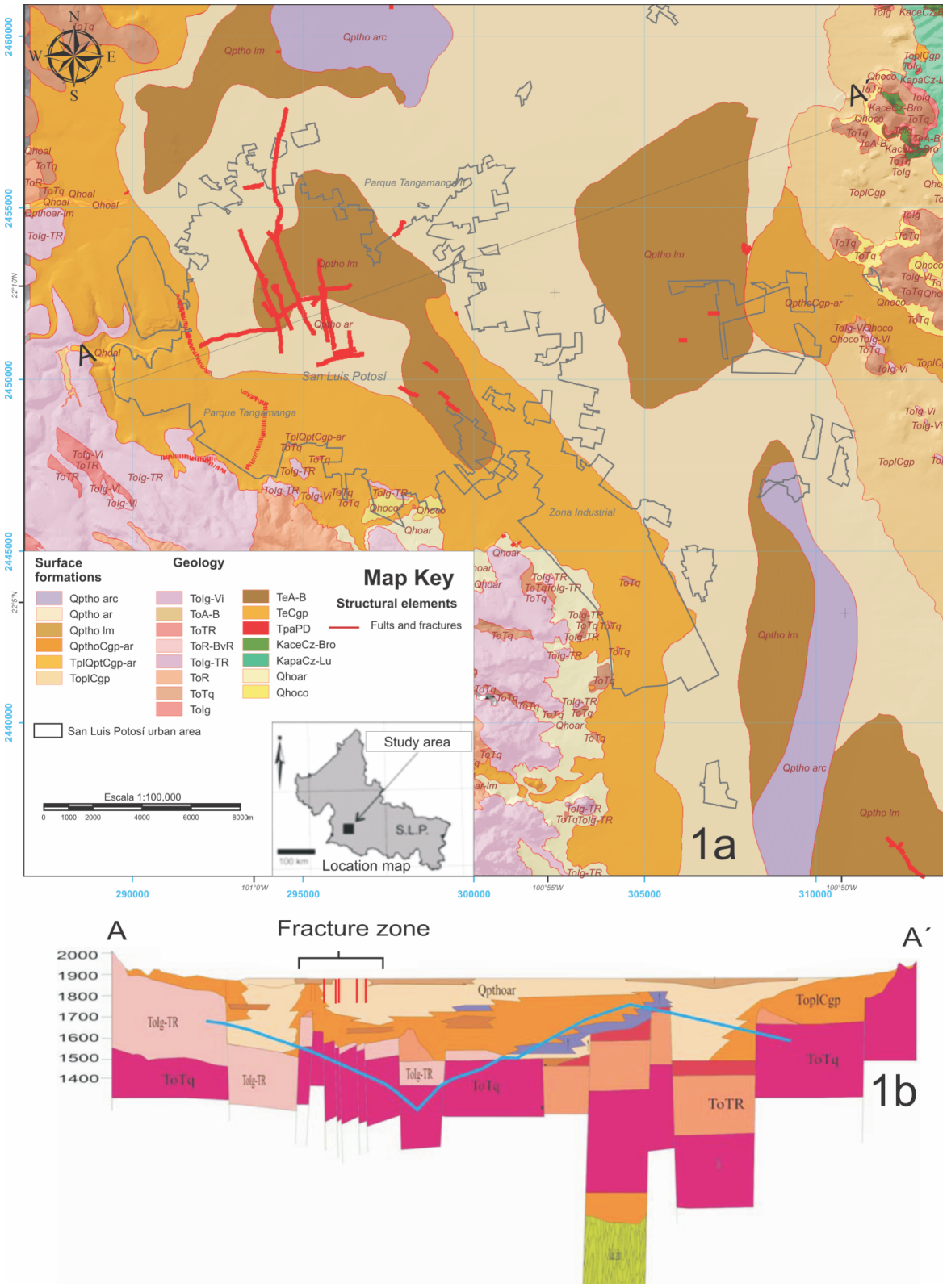

Fig. 1 (a) Near Surface Geologic Units (NSGU) map showing the distribution and location of fractures that affect the urban structure in San Luis Potosí City. (b) The geological cross section A–A´ shows the spatial relations between stratigraphy, fractures related to subsidence (red lines) and the variations in depth of piezometric groundwater levels (blue line) measured in 2005.

GEOPHYSICAL CHARACTERIZATION

Ground Penetrating Radar (GPR) and Surface Wave Seismic (SWS) methods

In order to understand the mechanisms of propagation of ground fracturing in the study area and the complementary field geological determinations, we combined two geophysical prospecting methods with different depths of investigation. The combination of these methods with the calibration allowed successful application of the lithological correlation to identify patterns of propagation in different urban areas (Carreón Freyre & Cerca, 2006). Ground Penetrating Radar (GPR) was carried out at 10 m depth at 22 selected sites to identify the structures of the sedimentary sequence and lithological contacts of the deposits affected by fracturing (Fig. 2). The GPR systems used were Zond 12c (Radar Systems, Inc.) with 300 and 900 MHz central prospecting frequencies, and SIR-20 (GSSI) with 100 and 200 MHz central frequencies. The Surface Wave Seismic (SWS) prospecting was carried out at the same 22 sites using a GEOMETRICS equipment with 12 and 4 Hz frequency geophones and a spatial arrangement of $4\ m < \Delta x < 5\ m$. Time lengths varied from 1 s to 2 s, depending on the site.

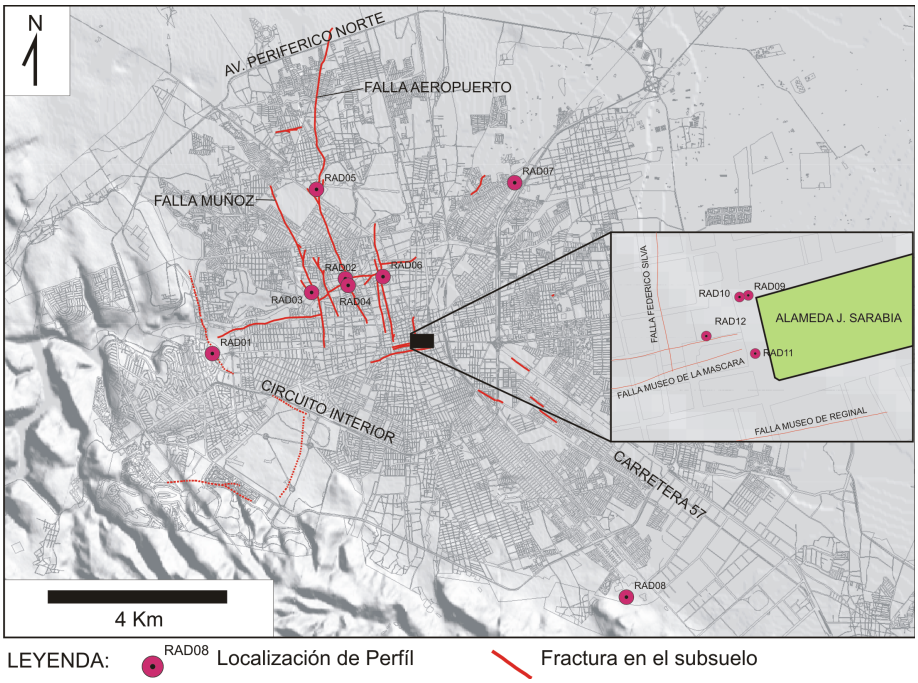

Fig. 2 Map of GPR prospecting in selected sites (red dots) affected by land subsidence and ground fracturing (red lines) in the central area of San Luis Potosí City.

As an example of GPR and SWS profiling, the Rivera site, is presented in Fig. 3. This site is representative of the thick granular sequence in the city; we had accurate lithological information because the deepest water well in the valley is located nearby (Fig. 3(a)). The sequence consists of 300 m of sedimentary deposits overlaying volcanic rocks. Figure 3(b) show a 75-m length GPR profile realized with a 100 MHz antenna using the SIR-20 system. The investigation depth for the frequency used in this area was approximately 20 m depth. Two vertical discontinuities marked with a dotted line were recorded in the GPR profile; these fractures have not yet been shown clearly in the surface. The S-velocities variations in the SWS profile (Fig. 3(c)) show a sedimentary sandy sequence with a little density contrast between 40 to 90 m depth, and a stronger contrast towards the surface that probably corresponds to local granulometric variations (silt–clay–sand). Note that ground fracturing can be spatially correlated by the two methods and fractures recorded in the GPR profile fit in depth and distance with local lithological variations in the near surface sequence.

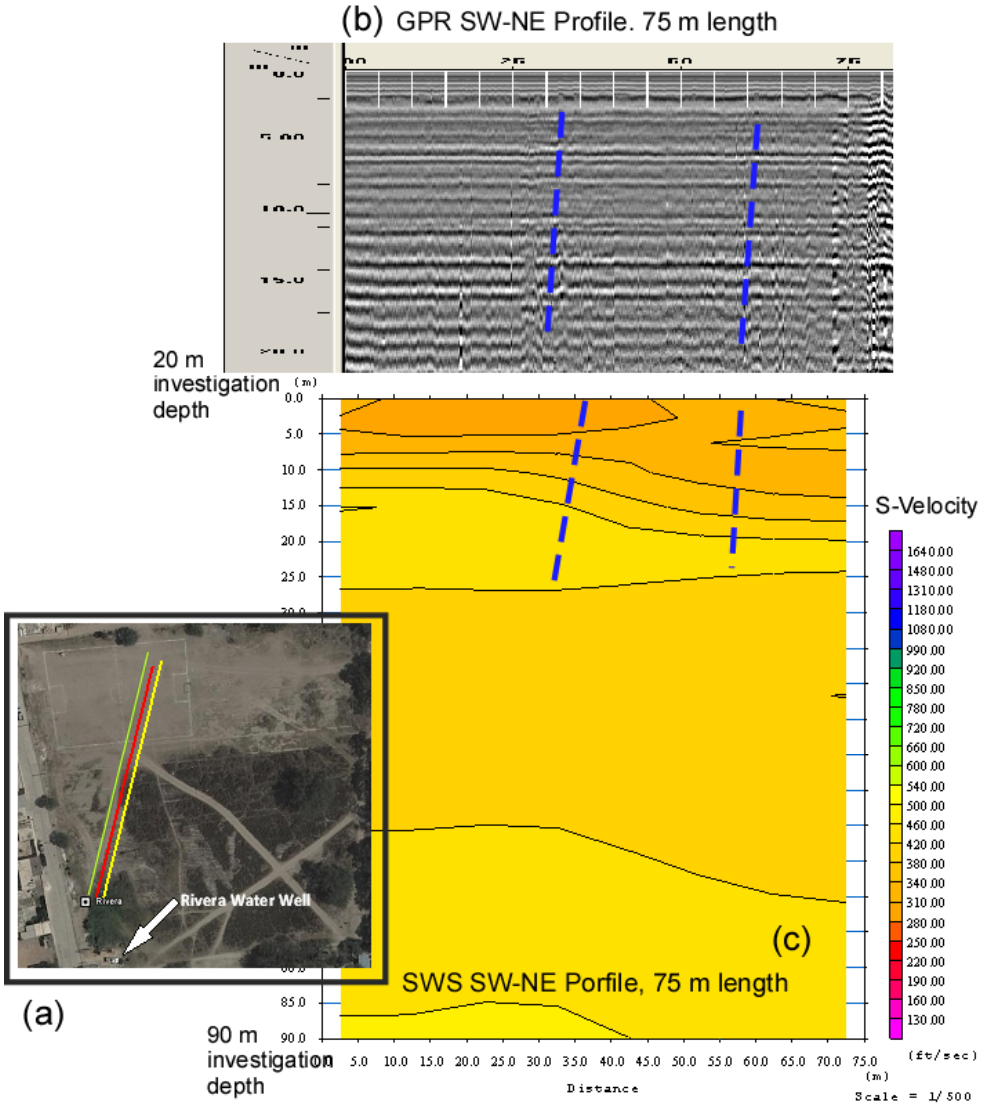

Fig. 3 The Rivera study site. (a) Location of GPR (yellow line) and SWS (red line) SW–NE profiles in the eastern part of San Luis Potosí City; (b) GPR profile using the 100 MHz, 75 m length (vertical recorded discontinuities are marked with dotted lines); (c) SWS profile with a depth of investigation of 90 m. Vertical disconinuites can be correlated with lateral lithological variation.

CONCLUSIONS

The integrated analysis of the structural geology (major discontinuities), stratigraphy, groundwater piezometric variations and fracturing that affect the urban structure in San Luis Potosí City allow us to propose a model of fracture propagation closely related to lithological variations in the near surface sequence. Some authors suggest that fractures are generated only due to piezometric declines and changes in effective stress conditions on the units. We consider that in SLP City, the generation and propagation of fracturing is conditioned by a combination of factors in which variations in the stratigraphic sequences are the most important. Our results show that small lithological variations, such as clay–silt–sand and those related with conglomerates and adjacent volcanic units, condition the patterns of propagation of ground fracturing. An accurate understanding of fracturing mechanisms should integrate different factors, such as spatial variations in the affected sequence, groundwater decline and the presence of major structures, with different weights for specific study areas.

Acknowledgements This work was achieved as a part of the collaborative project: **"**Methodological integration for Engineering Geology Mapping in the urban areas of Queretaro and San Luis Potosí" between the Servicio Geológico Mexicano (SGM) and the Centro de Geociencias (CGEO) of the Universidad Nacional Autónoma de México. The authors appreciate all support from both institutions. We also thank the staff of the Centro de Evaluacion de Riesgo Geologico (CERG) from the Iztapalápa Municipality, and Ing. Alfonso Alvarez Manilla for the geophysical prospecting in the study area (GPR and SWS profiles). Special thanks to the academic staff of the Instituto de Geología of the Universidad Autónoma de San Luis Potosí and to Ricardo Carrizosa from the Laboratorio de Mecánica Multiescalar de Geosistemas (LAMMG) of the Centro de Geociencias de la UNAM for the physical characterization of granular materials.

REFERENCES

Aranda-Gómez, J. J. & Labarthe-Hernández, G. (1997) *Estudio Geológico de la Hoja Villa Hidalgo, S.L.P.* Instituto de Geología y Metalurgia, Universidad Autónoma de San Luis Potosí, Folleto Técnico 53.

Arzate-Flores, J., Barboza-Gudiño, J. R., López-Doncel, R., Pacheco-M, J., Mata-Segura, J. L. & del Rosal, A. (2009) Estudio geológico-geofísico para la evaluación de los hundimientos y agrietamientos en el área metropolitana San Luis Potosí-Soledad de Graciano Sánchez. Investigación en Geociencias, folleto técnico del instituto de geología, Universidad Autónoma de San Luis Potosí, Núm. 130.

Cardona-Benavides, A. (1990) Caracterización físico-química y origen de los sólidos disueltos en el agua subterránea del Valle de San Luis Potosí: Su relación con el sistema de flujo. Tesis de maestría, Facultad de Ingeniería, Universidad Autónoma de Nuevo León, Mexico.

Carreón-Freyre, D. & Cerca, M. (2006) Delineating the near-surface geometry of the fracture system affecting the valley of Queretaro, Mexico: Correlation of GPR signatures and physical properties of sediments. *Near Surface Geophysics, EAGE* **4**(1), 49–55.

Carreón-Freyre., D., Cerca Martínez, M. & Hernández Marín, M. (2005) Propagation of fracturing related to land subsidence in the Valley of Queretaro, Mexico. Proceedings of the 7th International Symposium on Land Subsidence SISOLS 2005, Shanghai, P.R. China, vol. 1, 155–164. ISBN 7-5323-8209-5.

Carrillo-Rivera, J. J. (1992) The hydrogeology of the San Luis Potosí Area, México. PhD Thesis, Department of Geological Sciences, University of London, UK.

Carrillo-Rivera, J. J., Cardona-Benavides, A. & Edmunds, W. M. (2002) Use of abstraction regime and knowledge of hydrogeological conditions to control high-fluoride concentrations in abstracted groundwater: San Luis Potosí basin, México. *J. Hydrol.* **261**, 24–27.

Mata-Segura, J. L. & López-Doncel, R. A. (2004) Estudio geológico sobre grietas en la Capilla de Aranzazu del Museo Regional Potosino. Reporte particular del Instituto de Geología, Universidad Autónoma de San Luis Potosí, Mexico.

Mata-Segura, J. L., López-Doncel, R. & Barboza-Gudiño, J. R. (2004ª) Estudio geológico sobre las grietas en el museo Federico Silva, centro histórico de S.L.P.. Instituto de geología UASLP, reporte privado no publicado.

Mata-Segura, J. L., López-Doncel, R. A., Rodríguez-Ríos, R., Arzate-Flores, J. & Pacheco-Martínez, J. (2004b) Problemática de las fallas geológicas en la zona urbana y conurbada de la ciudad de San Luis Potosí-Soledad de Graciano Sánchez. GEOS, IV Reunión nacional de ciencias de la tierra, Unión Geofísica Mexicana, vol. 24(2).

Noyola-Medrano, M. C., Ramos-Leal, J. A., Domínguez-Mariani, E., Pineda-Martínez, L. F., López-Loera, H. & Carbajal, N. (2009) Factores que dan origen al minado de acuíferos en ambientes áridos: caso Valle de San Luis Potosí. *Revista Mexicana de Ciencias Geológicas* **26**(2), 395–410.

Tristán-González, M. (1977) Estratigrafía y tectónica del Graben de Villa de Reyes en los estados de San Luis Potosí y Guanajuato, México. Instituto de Geología y Metalurgia, Universidad Autónoma de San Luis Potosí, Folleto Técnico 107.

(Proceedings of EISOLS 2010, Querétaro, Mexico, 17–22 October 2010). IAHS Publ. 339, 2010.

Land subsidence of the Aguascalientes Valley, México: historical review and present situation

M. A. ROMERO-NAVARRO[1], J. PACHECO-MARTÍNEZ[2], J. A. ORTIZ-LOZANO[2], M. E. ZERMEÑO-DE LEÓN[2], G. ARAIZA-GARAYGORDOBIL[2] & E. MENDOZA-OTERO[2]

1 *MARN servicios en geotecnia Cerrada de Caudillos # 197, Cd. Satélite Morelos CP 20298, Aguascalientes, Ags. México*

2 *Centro de Ciencias del Diseño y de la Construcción de la UAA. Av. Universidad #940, Ciudad Universitaria, CP 20131, Aguascalientes, Ags. México*

geochuy@gmail.com

Abstract Earth fissures and surface faults related to land subsidence have been observed in Aguascalientes City (AGSC) since the early 1880s. Nowadays, the superficial cracking became widespread throughout the valley of Aguascalientes (AGSV). In this work we present a brief description of land subsidence and soil cracking in AGSV and its evolution and economic implications as well as the implemented measures by the local government in order to prevent damage in new buildings.

Key words Aguascalientes; triggering factors; implemented actions

GENERAL GEOLOGY OF AGUASCALIENTES VALLEY

The Aguascalientes valley (AGSV) is located in a tectonic fosse that is known as the Aguascalientes graben (AGSG), which is formed by two normal faults with N–S direction and completely crosses the central part of the state of Aguascalientes The simplified geology of the southern part of Aguascalientes valley, where Aguascalientes City is located, is shown in Fig. 1.

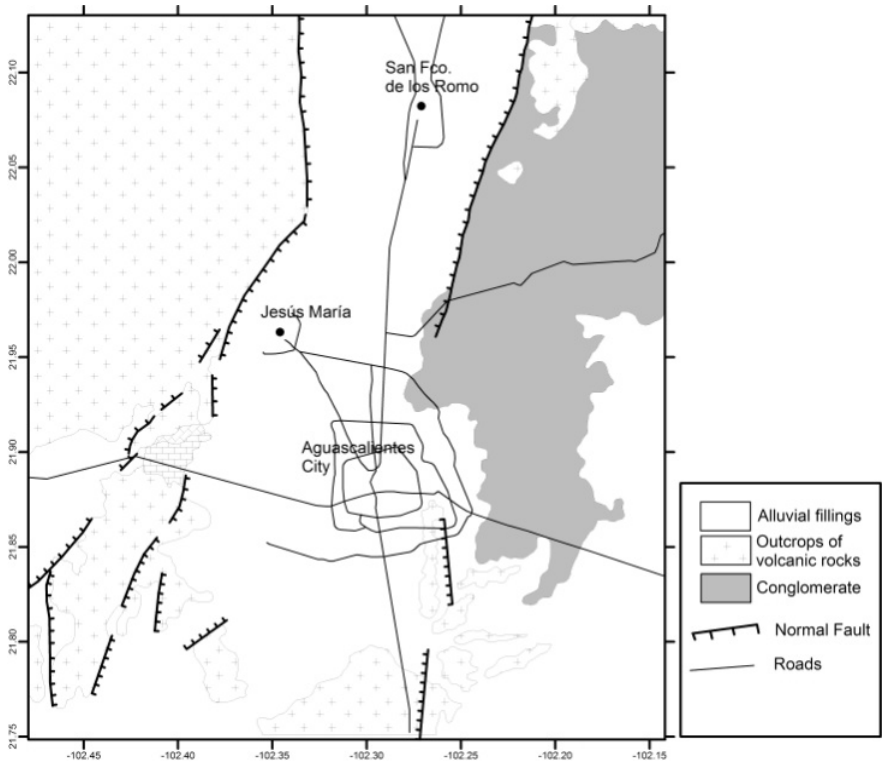

Fig. 1 Simplified geology of Aguascalientes Valley.

Copyright © 2010 IAHS Press

Outcrops of volcanic and sedimentary rock are exposed in the western flank of AGSG, whereas a unit of conglomerate and another of rhyolite form the eastern boundary of the valley.

AGSV is formed by a series of strata of alluvial fills: silt, sand and gravel with clay. According to well logs drilled in the valley, the sedimentary fill reaches 600 m depth. This fill forms the aquifer system of Aguascalientes valley, which has been overexploited in the last 30 years.

TRIGGERING FACTORS OF LAND SUBSIDENCE IN AGUASCALIENTES VALLEY

Aranda-Gómez & Aranda-Gómez (1985) studied the earth fissures in Aguascalientes Valley. They associated earth fissures with groundwater pumping and they concluded that structural geology plays a passive role, whereas the pumping of groundwater is the triggering factor for the cracking generation.

There are three seismological stations which have been operating for eight years in order to detect seismic activity related to the generation and growth of cracks; however, seismic activity has not been detected, but cracks have increased in their length and in their height of escarpment.

Active fractures have not been observed on the rocky outcrops outside the fill area, the traces of the active fractures observed end just before the outcrops. This allows us to assert that cracking generation in AGSV has two components: a geological aspect that involves the presence of bedrock with an abrupt topography beneath the poorly consolidated granular material, and secondly, an anthropogenic component (the drop in the groundwater level), which acts like the triggering factor in the process of crack formation, and it also acts like the accelerator of cracks growth. The spatial correlation between the sinking zones and the groundwater level drop made by Zermeño-De León *et al.* (2004) support this assertion.

The observations and evidence suggest that the mechanism of rupture in AGSV is the same as reported by Jachens & Holzer (1979, 1981) for fracturing zones in the south central part of the USA, and as has been observed in different valleys of the central part of México, i.e. Querétaro, Celaya, San Luís Potosí, Silao and Morelia (Garduño-Monrroy *et al.*, 2001; Arroyo-Contreras., 2003; Rojas *et al.*, 2004; Pacheco *et al.*, 2006; Avila-Olivera *et al.*, 2008).

PRINCIPAL EFFECTS ASSOCIATED WITH EARTH FISSURES IN URBAN ZONES.

The first reports of cracks in the AGSV were originated due to damage caused in the constructions at the end of the 1970s (Aranda-Gómez & Aranda-Gómez, 1985). It was reported in 2009 that at least 207 cracks and superficial faults, which amounted to 322 km, are directly or indirectly affecting nearly 1820 real estates, mainly households of different typology (SIFAGG, 2009). Nowadays, the area affected by surface subsidence is estimated to reach 900 km^2.

Besides the damage to private buildings, it has been observed that superficial cracks have affected urban infrastructure (streets and highways, distribution lines of freshwater and wastewater, etc.). Furthermore, cracks are affecting public buildings of the city, such as churches with historic value, and other places which are in the national catalogue of historic buildings. Currently, there is neither an inventory of the affected public infrastructure nor an inventory of the damaged buildings that have some historical value.

An inconspicuous effect related to land subsidence is the gradual change in superficial drainage. Zermeño-De León *et al.* (2004) calculated an accumulated sinking of 1.3 m in 18 years, related to a vertical displacement of surface faults, and they measured a sinking velocity of 11 cm/year. If the sinking continues at this rate, the superficial drain will become more deficient.

ACTIONS IMPLEMENTED TO MITIGATE THE EFFECTS OF LAND SUBSIDENCE

Even before the problems related with land subsidence had the magnitude and impact that they currently have, a ban was made in the 1960s on the drilling of new wells in the aquifer of AGSV in order to preserve the groundwater resources.

Since the late 1990s the city of Aguascalientes has promoted the mapping of the generation of cracks and its periodic actualization (SIDIFAG, 2005; SIDDIS, 2007). These maps are public and they are the documents legally recognized for the management of permits for new constructions. Permits only allow construction in zones shown to have no cracks by the verification of a specialist in geology or geophysics.

REFERENCES

Aranda-Gómez, J. J. & Aranda-Gómez, M. (1985) Análisis del Agrietamiento en la ciudad de Aguascalientes. Technical report prepared for Technological Center of the Autonomus University of Aguascalientes, México.

Arroyo-Contreras, M. G. (2003) Causas y efectos de las grietas y fallas en el valle de Aguascalientes. Technical report prepared for research system Miguel Hidalgo (SIHGO) SEP-CONACYT, México.

Avila-Olivera, Jorge A. & Garduño-Monroy, Víctor H. (2008) A GPR study of subsidence-creep-fault processes in Morelia, Michoacán, Mexico. *Engng Geol.* **100**(1–2, 27), 69–81.

Garduño-Monroy, V. H., Arreygue-Rocha, E., Israde-Alcántara, I. & Rodríguez-Torres, G. M. (2001) Efectos de las fallas asociadas a sobreexplotación de acuíferos y la presencia de fallas potencialmente sísmicas en Morelia, Michoacán, México. *Revista Mexicana de Ciencias Geológicas* **18(**1), 37–54.

Jachens, C. R. & Holzer, L. T. (1979) Geophysical investigations of ground failure related to ground water withdrawal Picacho basin Arizona. *Ground Water* **17**(6), 574–585.

Jachens, C. R. & Holzer, L. T. (1982) Differential compaction mechanism for earth fissures near Casa Grande, Arizona. *Geol. Soc. Am. Bull*. **93**, 998–1012.

Pacheco, J., Arzate, J. A., Rojas, E., Yutsis, V., Arroyo, M. & Ochoa, G. (2006) Delimitation of soil fissures zones due to ground subsidence using gravity data and finite element modelling in the Valley of Querétaro, México. *Engng Geol.* **84**, 143–160.

Rojas, E., Arzate, J. & Arroyo, M. (2002) A method to predict the group fissuring and faulting causes by regional groundwater decline. *Engng Geol.* **65**, 245–260.

SIDDIS (2007) Sistema Digital de Discontinuidades, Digital mapping published by the Municipality of Aguascalientes, México.

SIDIFAG (2005) Sistema Digital de Fallas Geológicas de Aguascalientes. Digital mapping published by the Municipality of Aguascalientes, México.

SIFAGG (2009) Sistema de Información de Fallas Geológicas y Grietas. Digital mapping published by the Aguascalientes State Government, México.

Zermeño-De León, M. E., Mendoza-Otero, E. & Calvillo-Silva, G. (2004) Medición del Hundimiento y modelo para estudiar el agrietamiento de la ciudad de Aguascalientes. *Investigación y Ciencia de la Universidad Autónoma de Aguascalientes* **31**(12), 35–40.

Land Subsidence, Associated Hazards and the Role of Natural Resources Development
(Proceedings of EISOLS 2010, Querétaro, Mexico, 17–22 October 2010). IAHS Publ. 339, 2010.

Assessment of land subsidence associated with intense erosion zones in the Zacatecas and Guadalupe quadrangles, Mexico

F. J. ESCALONA-ALCAZAR[1,2], L. A. DELGADO-ARGOTE[2] & A. F. RIVERA-SALINAS[1]

1 *Instituto de Ecología y Medio Ambiente de Zacatecas, Av. Mexico 151, Col. La Florida, 98600 Guadalupe, Zacatecas, Mexico*
papiesca@yahoo.com

2 *Departamento de Geologia, CICESE, Carretera Ensenada-Tijuana no. 3918, Zonas Playitas, 22860, Ensenada, Baja California, Mexico*

Abstract We performed a geological and geomorphological analysis in the Zacatecas and Guadalupe quadrangles. The objectives are the assessment of the role of the erosion in land subsidence and its association with the lithology and geological structures. The stratigraphic sequence of the study area is composed, from bottom to top, of the dominantly sedimentary Zacatecas Formation (ZF, Early Cretaceous). It is covered in transitional contact by the Las Pilas Volcanosedimentary Complex (LPC, Early Cretaceous). The LPC is composed of laccolithic intrusions and basaltic lava flows interlayered with fine grained sedimentary rocks. The LPC is in contact by unconformity with the Paleocene-Eocene Zacatecas Red Conglomerate (ZRC), which is a polimictic conglomerate composed of clasts of the ZF and LPC. Strata in the ZRC vary from well- to barely-consolidated. At the top there is an Eocene-Oligocene volcanic sequence composed of ignimbrites and tuffs that varies from welded to moderately welded. These rocks have been subject to compression during the Late Cretaceous and at least five extension stages during the Cenozoic. Geomorphological analysis was performed with the dissection density, general dissection density, maximum dissection depth and relief energy maps. Field mapping was focused on paleo-landslides and talus deposits. Based on the field mapping we defined that where dissection density >10 km/km^2, general dissection density >25 km/km^2, maximum dissection depth >130 m and relief energy >160 occur together they locate intense erosion zones. In these zones, the land subsidence is developed if the rocks are moderately to poorly consolidated, in loose talus deposits or in poorly compacted sediments. The erosion is greater if there are faults and/or fractures. The identification of the high erosion zones associated with land subsidence is a tool to identify hazardous zones that could be applicable in urban planning projects.

Key words erosion zones; geomorphology; Zacatecas and Guadalupe, Mexico

INTRODUCTION

The cities of Zacatecas and Guadalupe are the most populated and fast growing in the State of Zacatecas, Mexico (see inset in Fig. 1). In these cities, the urban development is only based in land use change that does not consider the environment and the geological/geomorphological processes that operate. Due to landscape modification and erosion, land instability is currently a common phenomenon, and is mostly developed over palaeolandslides and talus deposits.

Since a few years ago, several attempts have been made to identify and define the geological and geomorphological processes that currently operate in these cities (Enciso-De la Vega, 1994; Escalona-Alcázar *et al*., 2003; Escalona-Alcázar, 2009). On that basis, together with geological field mapping and by analysing topographic maps of the Zacatecas and Guadalupe quadrangles, in this work we introduce the first map with a model that defines areas with different erosion potential.

MODEL

The base maps were the topography scale 1:50 000 maps of the Zacatecas and Guadalupe quadrangles, with topographic contours at 10 m. The maps were divided into 1-km side squares. Based on topography, in each square the parameters measured were: (1) the dissection density

Copyright © 2010 IAHS Press

defined as the length (km) of creeks by km^2; (2) the general dissection density that is the length (km) of all topographic contours in a square kilometre; (3) the maximum dissection depth is the length (m) measured perpendicular from the highest elevation to the nearest bottom creek; and (4) relief energy maps, that is the difference between the highest and lowest points.

Based on field mapping of palaeolandslides and talus deposits we defined that they are located where the dissection density is >10 km/km^2, general dissection density >25 km/km^2, maximum dissection depth >130 m and relief energy >160. The areas defined by these parameters are called High Erosion Zones (Fig. 1). Medium ones are at: 8.5–10 km/km^2, 20–25 km/km^2, 100–130 m and 130–160, respectively (Fig. 1). Whereas the Low Erosion Zones are at: 7–8.5 km/km^2, 15–20 km/km^2, 70–100 m and 100–130, respectively (Fig. 1).

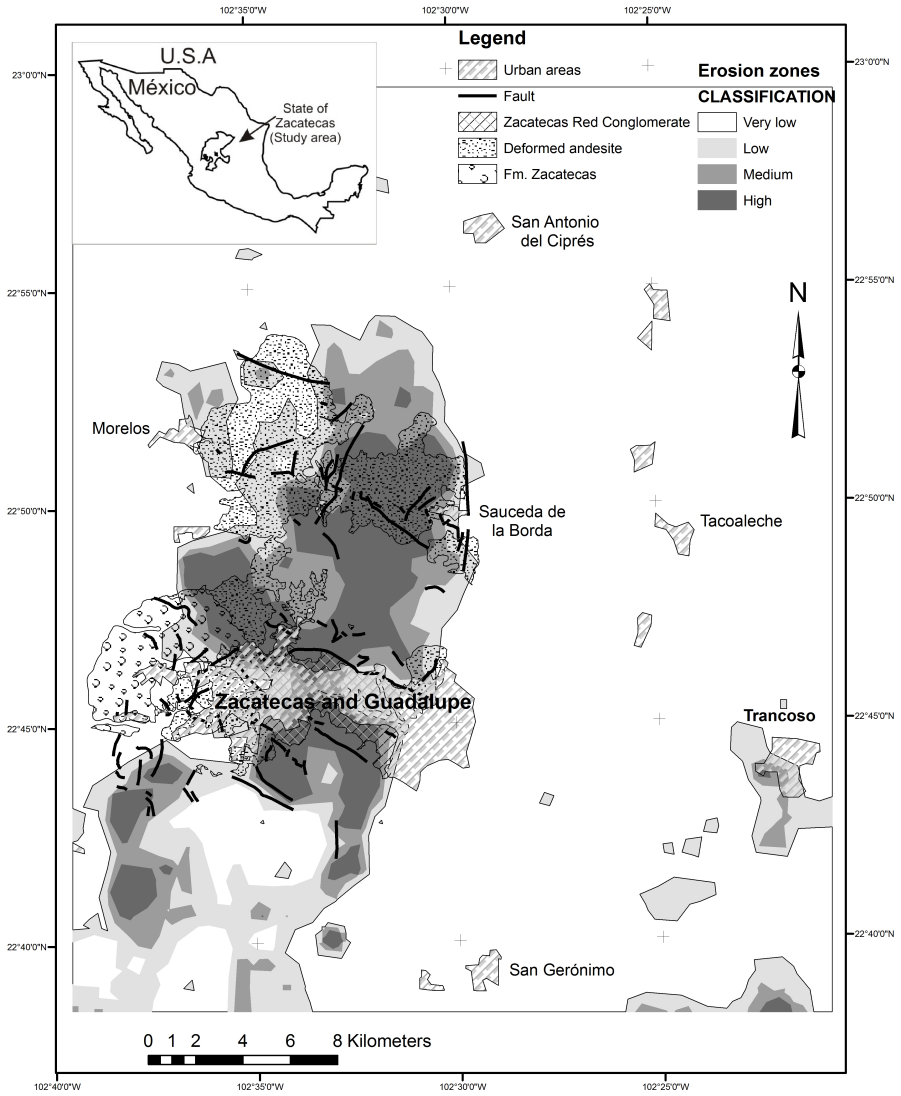

Fig. 1 Map showing the intense erosion zones (high, intermediate and low) of the Zacatecas and Guadalupe quadrangles. Inset: location of the study area.

The geological mapping was modified from Escalona-Alcázar and co-workers (2009). From the stratigraphic sequence, the lithologic units shown in Fig. 1 are the Deformed andesite, Zacatecas Red Conglomerate and Fm. Zacatecas because they have the more intense faulting and

fracturing; also the last two have easily erodible strata. High erosion zones are mostly associated with the Deformed andesite (Fig. 1). In these areas the sandy-rocky soils, less than 10 cm thick, are easily eroded.

The Intermediate and Low erosion zones are located in medium to low topography. In these areas the erosion removes material mainly from the Zacatecas Red Conglomerate and to a lesser extent from the Fm. Zacatecas.

The urban areas located over the Zacatecas Red Conglomerate are currently experiencing land subsidence and instability due to erosion. These processes are slow but continuous.

The zones proposed here are a tool to use in further urban development to avoid damage due to erosion effects to buildings, houses and infrastructure.

CONCLUSIONS

High erosion zones are mostly related to rock falls in vertical road cuts and to the transport of loose sediments. Most erosion is located on the Intermediate to Low erosion areas over the Zacatecas Red Conglomerate which is moderate to loosely consolidated. This combination favours land subsidence and instability.

The erosion zones defined in this work are a tool for the urban development planning. The areas here defined are an argument to be considered in the land-use change policies in order to have a better use of territory.

Acknowledgements The authors are grateful to Lic. Amalia García Medina, Governor of the State of Zacatecas and MSc Patricio Tavizón, Director of the Instituto de Ecología y Medio Ambiente de Zacatecas. Also thanks to Arqs. Ruben Saldívar Montalvo and Guadalupe Marchan from the Secretaría de Obras Públicas for their support.

REFERENCES

Enciso-De la Vega, S. (1994) Crecimiento urbano de la Ciudad de Zacatecas y sus asentamnientos humanos en zonas mineralizadas polimetálicas. *Revista Mexicana de Ciencias Geológicas* **11**(1), 106–112.

Escalona-Alcázar, F. J. (2009), Evaluación preliminar de los riesgos debidos a la geomorfología de la zona urbana Zacatecas-Guadalupe y sus alrededores. *GEOS* **29**(2), 1–4.

Escalona-Alcázar, F. J., Suárez-Plascencia, C., Pérez-Román, A. M., Ortiz-Acevedo, O. & Bañuelos-Álvarez, C. (2003) La secuencia volcánica Terciaria del Cerro La Virgen y los procesos geomorfológicos que generan riesgo en la zona conurbada Zacatecas-Guadalupe. *GEOS* **23**(1), 2–16.

Escalona-Alcázar, F. J., Delgado-Argote, L. A., Weber, B., Núñez-Peña, E. P., Valencia, V. A. & Ortiz-Acevedo, O. (2009) Kinematics and U-Pb dating of detrital zircones from the Suierra de Zacatecas, Mexico. *Revista Mexicana de Ciencias Geológicas* **26**(1), 48–64.

Seismic basaltic structure under the local subsidence in San Lorenzo Tezonco, Iztapalapa, México, Distrito Federal

LEOBARDO SALAZAR, PEDRO VERA & GEMA GUEVARA
Instituto Politécnico Nacional, ESIA Unidad Ticomán, Mexico
lsalazar@ipn.mx, pveras@ipn.mx

Abstract The purpose of this work is the structural determination of basaltic flows under the fractures presented in San Lorenzo Tezonco, Iztapalapa. A collapse event occurred on 7 July 2007. The geological characteristics of the zone are: clay, volcanic ash and basaltic rocks of the Yuhualixqui volcano. The seismic technique is a combination of both the seismic refraction method and the vertical reflections of the P wave on basaltic rocks. The results of refraction are: velocity values of 390–420 m/s for clay, and 680–850 m/s for volcanic ash. With the information of an old well: Santa Catarina 13, and the refraction results, we executed computational modelling. We obtained synthetic seismograms of vertical reflection of the P wave to distinguish the real time reflections. Then we calculated the depths of basaltic rock at each site of data acquisition. The result is a 3-D image of the basaltic flows and their implications in the phenomenon are working as a takeoff surface.

Key words basaltic flows; refraction method; vertical reflection; seismic modelling; Mexico

THE SEISMIC SURVEY AND EXPLORATIONS WELLS

The distribution of the seismic survey is shown in Fig. 1. In this figure the lines represent the refraction profiles. The interrupted lines represent the extension of the fractures in the zone. The ellipse represents the area of the main collapse on 7 July 2007. The circles represent the places of data acquisition of the vertical reflection of the P wave. Finally the diamonds represent the exploration wells in the area; these include two old wells: Santa Catarina 12 and Santa Catarina 13.

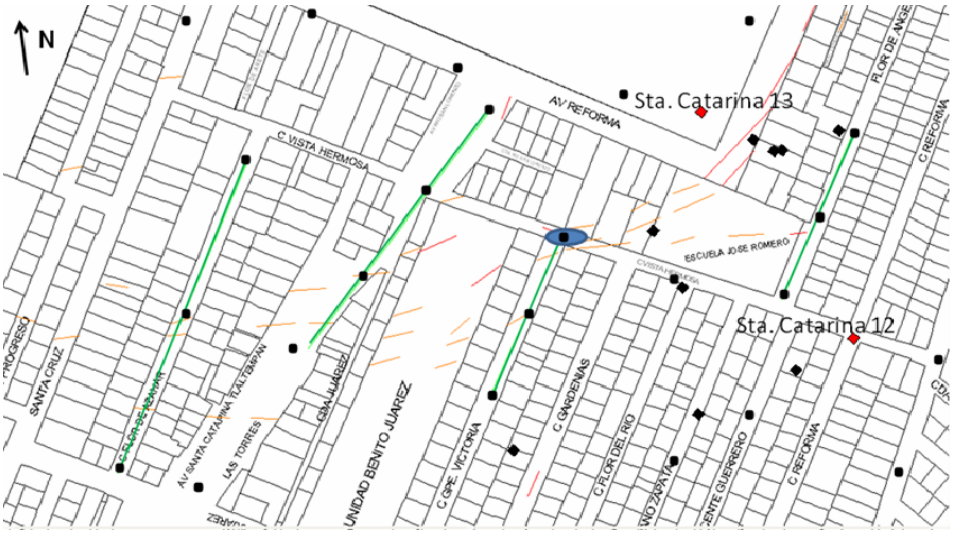

Fig. 1 Exploration zone. The lines represent the refraction profiles; the circles show the position of acquisition data for the vertical reflection of the P wave.

REFRACTION RESULTS

The refraction results are shown in Fig. 2. The seismic velocities of the first layer with values of 390–420 m/s represent the clay deposits. The second layer with velocities of 680–850 m/s represents the volcanic ash. These two layers only are considered in the refraction results. The

Copyright © 2010 IAHS Press

irregular configuration of the underground basaltic flows was achieved by the vertical reflections technique of P wave analysis that is explained in the following section.

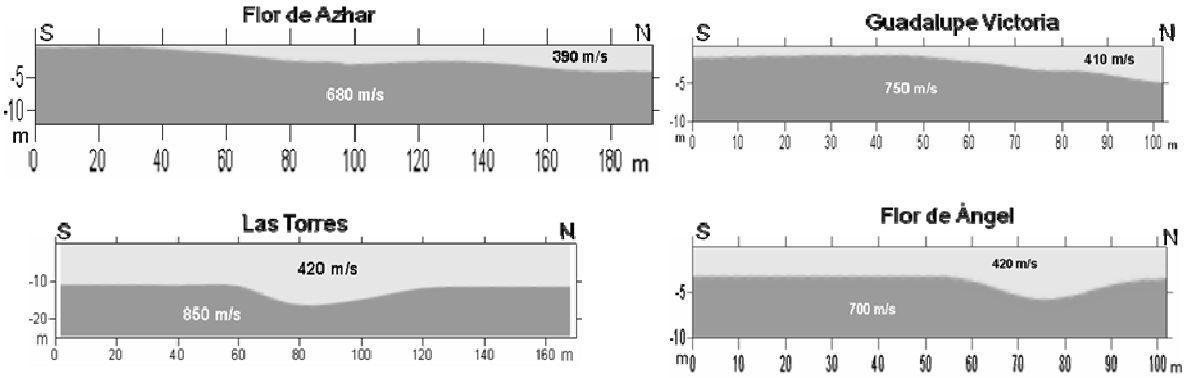

Fig. 2 Refraction results. The first layer of low velocities represents deposits of clay (Vp = 390–420 m/s). The second layer represents deposits of volcanic ash (Vp = 680–850 m/s).

VERTICAL REFLECTION METHOD AND SEISMIC MODELLING

The acquisition of data for this method consisted of generating and registering at the same site a P wave. Such a P wave travels and returns after reflection from the different rock contacts. To distinguish the P wave reflection at the ash–basalt contact it was necessary to resort to seismic modelling. Models were used according to: (a) the information from the wells Santa Catarina 12 and Santa Catarina 13, (b) the results of velocities and depths obtained by the refraction method, and (c) assignment of a law of velocity with depth. By analysis of the snapshots of the modelling, it is possible to distinguish the reflections corresponding to the ash–basalt contact (Fig. 3) in the data. For the calculation of depths a simple formula of velocity/time was used, segmented according to the layers and velocity values in each site. The total contribution of all the segments for the calculation of the depth represents a numeric sum (integral of ray path).

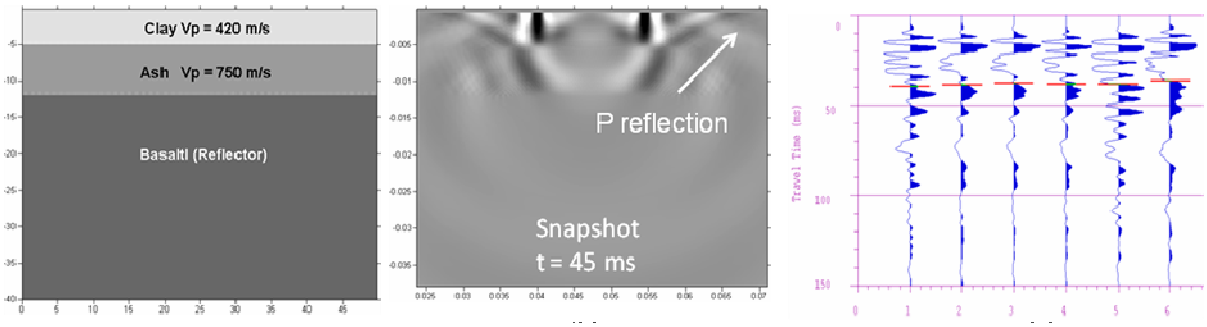

(a) (b) (c)

Fig. 3 (a) Model of velocities to Santa Catarina 13. (b) Snapshot in t = 45 ms for model. (c) Reflections signal in real data near to Santa Catarina 13.

SEISMIC STRUCTURE AND DISCUSSION

The seismic structure is shown in Fig. 4. Starting from zero depth and down to the first surface, there are the clay layers and ash ones. The black lines define the summit and base of a basaltic flow of the volcano Yuhualixqui that lies under the previous layers. A semi-circular canyon lies under the collapse event of 7 July 2007.

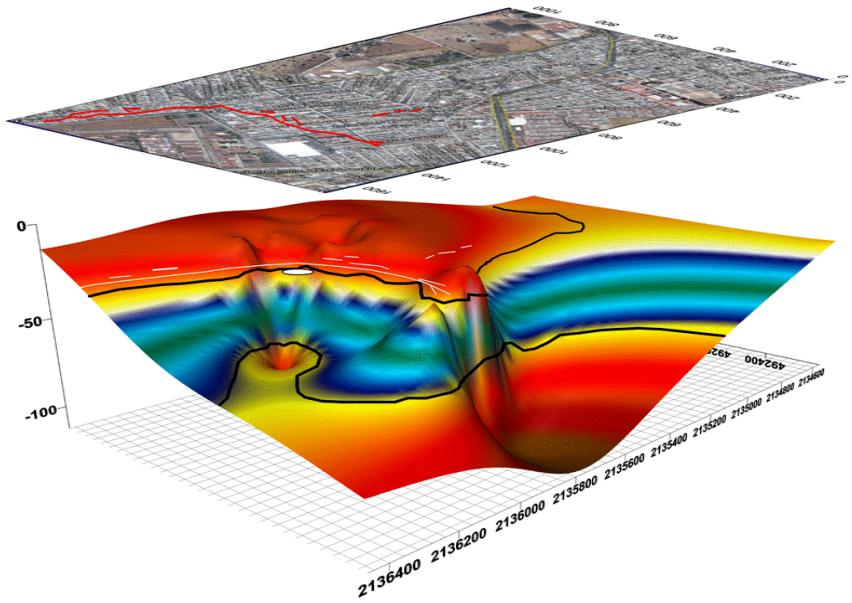

Fig. 4 Final seismic structure under fractured zone in San Lorenzo Tezonco, Iztapalapa.

In the study of this phenomenon, we have distinguished the stratigraphic and the structural factors as the most important ones. The stratigraphic sequence is formed by an alternation of volcanic rocks of basalt-andesite composition inserted within lake deposits. However, in the study of the area more lava flows have been identified; these correspond to the last two events, and the last plays an important role in the fracture process as it acts as to take off the surface of the most recent deposits. The terminal portion of this flow coincides with the observed fractures on the surface.

CONCLUSIONS

The innovation of the seismological technique presented in this study represents a powerful tool to deduce a very irregular underground structure associated with basaltic flows. The success of the technique of the vertical reflection of the P wave results from the strong contrast of the ash–basalt contact explored in the area. The basaltic underground structure has direct implications in the phenomeno n of fractures in San Lorenzo Tezonco. In principle, it works as a take-off surface to the clay deposits and volcanic ash.

(Proceedings of EISOLS 2010, Querétaro, Mexico, 17–22 October 2010). IAHS Publ. 339, 2010.

Geophysical and geotechnical studies applied to determine a subsidence problem in Pachuca de Soto, Hidalgo, Mexico

L. A. TAPIA[1], **A. TEJERO**[1] **& R. CHAVEZ**[2]

1 *Facultad de Ingeniería, Universidad Nacional Autónoma de México, Mexico city, Mexico*
latc58@hotmail.com

2 *Instituto de Geofísica,Universidad Nacional Autónoma de México, Mexico city, Mexico*

Abstract In 2005, a subsidence event occurred in the 305 Peñuñuri alleys in the neighbourhood of El Arbolito, Pachuca, Mexico. It produced a cavity of 12 m depth and 14 m width. In 2006, a geophysical and geotechnical study was carried out to determine the cause of the subsidence and to detect the probable abandoned tunnels close to it, which might be a hazard. The study was carried out using electrical tomography, which explored at a depth of 20 m (on average). It was concluded that there was no evidence of cavities. However, a layer saturated with water was observed and the layer seemed to flow in the direction of the topography. The water washes the ground away to form a cavity and the soil collapses when the resistance has gone. Recommendations were: (1) to extend the study of the electric tomography towards the north, west and east; (2) to repeat the lines in dry seasons; (3) to complement the research with a geotechnical study of the materials of the subsoil and the houses around to quantify the damage, and (4) to carry out exploratory drilling of holes on the high resistivity anomalies. The local authorities decided to perform recommendations (3) and (4).

Key words geophysical and geotechnical studies; cavity collapse; regeneration

INTRODUCTION

The area referred to is located 95 km north of Mexico City, at an altitude of 2395 m (a.s.l) at 20°02′22″N and 98°21′24″W in the state of Hidalgo, Mexico. The city of Pachuca is located in the physiographic province of the Neovolcanic axis. The mountain range of Pachuca is one of the main physiographic features. The region is characterized by the presence of a large number of volcanoes related to regional fractures, as well as large pyroclastic flows and lava overflows with the shape of plateaus and plains. Pachuca has moderate weather with an average temperature of 16°C and average precipitation of 532 mm a year falling mainly from March to September. The city is affected by polar fronts, hurricanes and tropical storms.

GEOLOGICAL SURVEY

Local geology

The southeast wall is built by a volcanic gap, with fragments that go from 12.0 cm diameter to almost the size of clay particles. The composition is andesitic materials, although some are vitreous. Pebbly particles of glass are distinguishable, carried there by underground water, and the walls are very damp.

Exploration of the subsoil

Three exploratory drillings were carried out to support electrical anomalies. The drilling was done with a machine with a rigid barrel and continuous sampling. It was carried out in 2008. Three sections correlating the drills were interpreted (Fig. 1).

Conclusions of the direct explorations

The cavity has an ellipsoidal geometry where its largest axis intercepts with the slope of the ground. The materials of the boxed (surrounding) rock are heterogeneous, and classified as a waste

Copyright © 2010 IAHS Press

dump caused by the extractive processes of mining, and overturned in the hillsides near the mine entrance or in the tunnels of the underground mines. The geophysical results defined electrical anomalies located near the sinking and down the slope, resulting in two alternative interpretations: firstly that they might have been tunnels of older mines, and secondly that they are tunnels that were filled later (Fig. 2). No empty cavities were found. The materials present in the anomalous zones are composed of bad rock and recuperation indices range from very bad, to bad and humid. It was decided to stop drilling at the waste dump, and therefore the existence of a tunnel under the cavity was uncertain, but it would have to be deeper than 40.0 m.

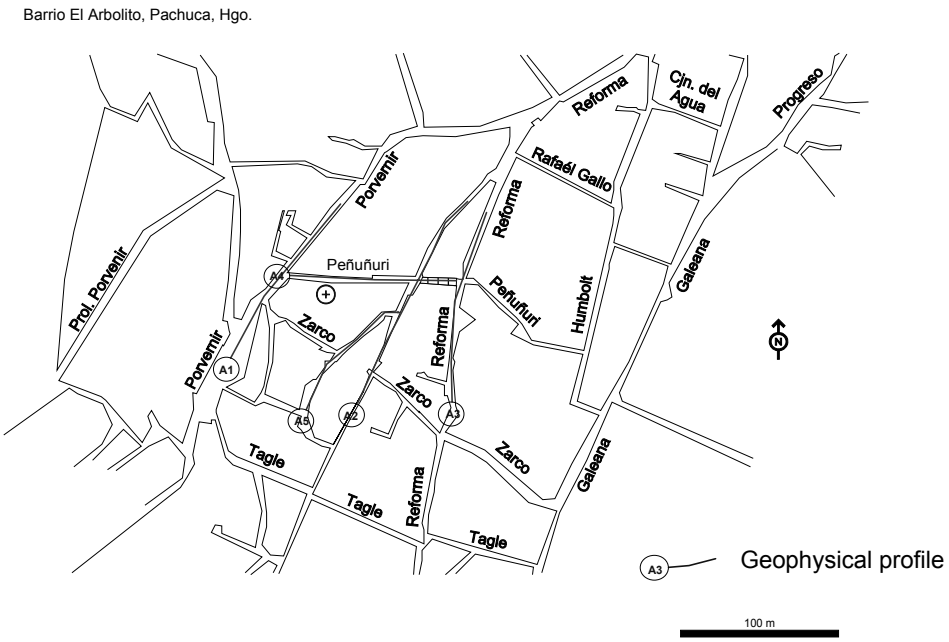

Fig. 1 Location of geophysics lines.

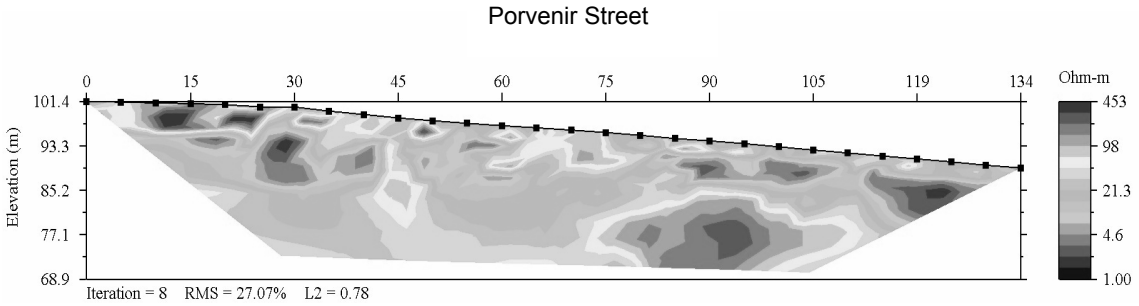

Fig. 2 Line A, electrical tomography image of Porvenir Street.

Filling

The heterogeneous surrounding material presents physical properties that were evaluated so that once filled they behave like one homogeneous material. The materials were analysed in order to fulfill these requirements, suggesting the use of a high resistance low density (light) filling. The most adequate was igneous extrusive or volcanic (volcanic ash) material commonly known as Mexican volcanic rock (tezontle). This light material must be combined with another material that occupies the empty spaces between the fragments of tezontle, so that its mechanical performance is the most satisfactory. It is considered that the cementing matrix function can be performed by an

igneous extrusive material belonging to the finest pyroclastic (volcanic ash) material technically known as clayey tuff, which is almost like white rock (Fig. 3).

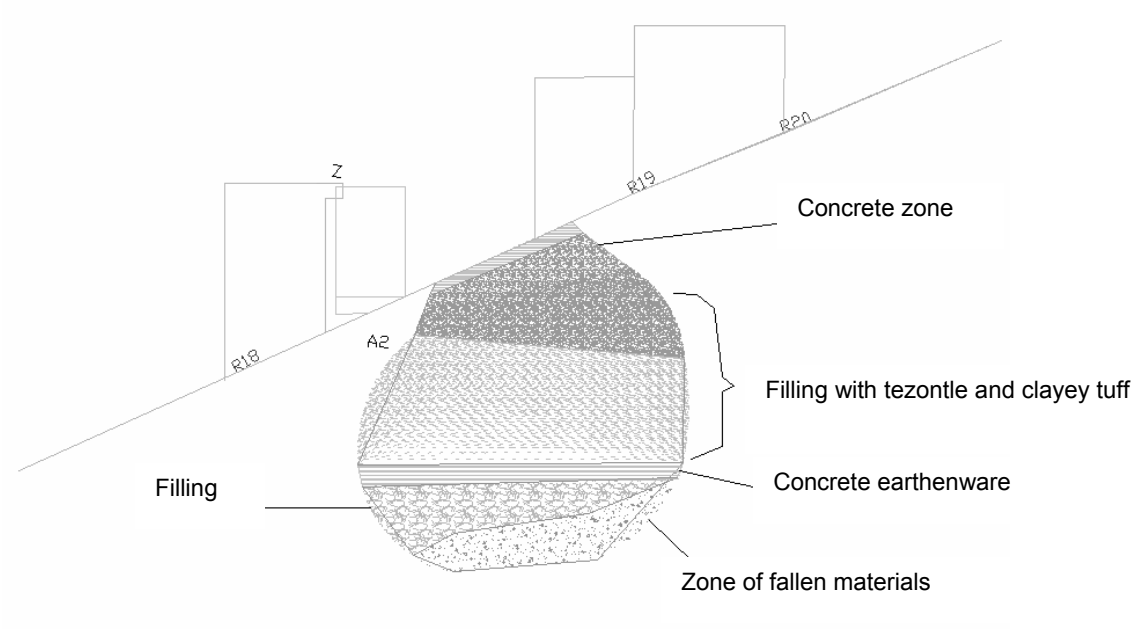

Fig. 3 View of the cavity and materials used to fill it.

METHODOLOGY

- Manual demolition of houses and structural elements on the cavity.
- Carrying the debris by truck in subsequent kilometres in the highway.
- Removal of the fallen products in the inside of the cavity to even the floor.
- Manufacturing of the concrete earthenware.
- Filling.
- Concrete floor constructed *in situ* to make the filling waterproof.

MATERIALS

- Disintegrated fragments, organic matter and trash-free arcillous tuff (tepetate).
- Mexican volcanic rock (tezontle) of different granulometry.

It is proposed that a mix of 85% Tezontle and 15% clayish tuff be used to fill the cavity in the form of layers 50 cm thick, compressing it at 80% at a proctor standard compression, supplying the material with the necessary humidity.

REFERENCES

Consejo de Recursos Minerales (1992) Monografía Geológico-Minera del Estado de Hidalgo.

Carrillo-Bravo, J. (1965) Estudio Geológico de una parte del anticlinorio de Huayacocotla. *Boletín de la Asociación Mexicana de Geólogos Petroleros* **12**(5–6), 1–73.

Land Subsidence, Associated Hazards and the Role of Natural Resources Development
(Proceedings of EISOLS 2010, Querétaro, Mexico, 17–22 October 2010). IAHS Publ. 339, 2010.

Instability of the urbanized flank of El Peñón del Marques volcanic edifice and its relation to land subsidence in Mexico City

M. CERCA[1], D. C. CARREÓN-FREYRE[1] & R. GUTIÉRREZ[2]

1 *Lab de Mecánica Multiescalar de Geosistemas (LAMMG), Centro de Geociencias, Universidad Nacional Autonóma de México, Blvd Juriquilla 3001, Juriquilla, Querétaro, 76230, Mexico*
mcerca@geociencias.unam.mx

2 *Centro de Evaluación del Riesgo Geológico, Delegación Iztapalapa, Gobierno del Distrito Federal, Mexico*

Abstract We integrate the available information, field cartography, measurement of physical attributes of materials, and Ground Penetrating Radar (GPR) profiles, to obtain a high definition image of the sliding flanks of the Peñón del Marques volcanic edifice, fractures, and land subsidence. In particular, we present multi-frequency GPR profiles (using antennae of 100, 200, and 400 MHz) that allowed an accurate interpretation of the shallow fracture geometry in the upper 15 m and how they affect the civil infrastructure. The morphology of the unstable flanks is characterized from the upper to the lower part by two or three concentric major fracture zones, a steeped fractured flank, a concave-up depression embaying locally the volcanic edifice, and a frontal bench that reflects uplift and a small inverse displacement at the base of the edifice.

Key words fracturing; land subsidence; Ground Penetrating Radar; volcanic edifice

INSTABILITY OF THE PEÑÓN DEL MARQUES

Fractures and slow but continuous sliding affect the flanks of the urbanized Peñón del Marques in the southeastern region of Mexico City. The Peñón del Marques is a volcanic edifice, a cinder cone, located in the middle of a subsiding plain formerly occupied by the ancient Texcoco Lake. It is considered as part of the Sierra Santa Catarina, a volcanic range formed by several cinder cones, domes, and composite volcanoes. The fracturing in the surrounding plain apparently began to manifest in the late 1960s when nine groundwater extraction wells were installed around the Peñón volcanic edifice for the supply of water to Mexico City. Since then, groundwater withdrawal has been intensive and more wells have been drilled down to 200 m depth. According to numerical simulations performed by Aguilar *et al.* (2006), a 35-m decrease of the hydraulic head has provoked a vertical deformation at between 6 and 8 m depth. High gradients of subsidence have been observed in the zone around the Peñón del Marques by InSAR studies (Cabral-Cano *et al.*, 2008), and in direct observations made in recent years we have observed periods with rapid deformation rates, up to 15 cm in three months. Additionally, since the early years of the 2000s several infiltration wells have been constructed to depths of 70 m in an attempt to recharge water to the aquifer and arrest seasonal flooding in the subsiding depression. The zone is highly populated and the urban infrastructure affected by fractures makes direct observation of the geology below the unstable flanks difficult. In this contribution we have mapped the fractures observed at the southeastern flank of the Peñón del Marques and use GPR as a non-invasive method to characterize the shallow geometry and stratigraphic changes.

GROUND PENETRATING RADAR IMAGES AND PHYSICAL CHARACTERISTICS OF THE NEAR-SURFACE SEQUENCES AROUND THE PEÑÓN DEL MARQUES

Ground Penetrating Radar (GPR) has been used for prospecting shallow faults and fractures and to obtain radar reflection patterns in order to distinguish between different clayey and silty deposits (Carreón-Freyre *et al.*, 2003; Carreón-Freyre & Cerca, 2006).

Three representative radar profiles of the southern flank of the Peñón del Marques are presented; they were collected using the GPR system SIR-20 of GSSI, using a monostatic antenna

Copyright © 2010 IAHS Press

centred at a frequency of 200 MHz (Fig. 1). A detailed topographic correction was made to the profiles and processing included AGC gain. The interpretation of radar profiles (radargrams) is based on recognizing reflectors and characteristic radar signatures or reflection patterns. Radar (EM) wave propagation through geological media is a complex issue but it can be considered that water content exerts the main influence on permittivity in low-loss materials at the characteristic frequencies (10 to 2000 MHz) of GPR. Water content can be related to variations in the physical and mechanical properties such as grain-size, density, compaction, or electrical conductivity, among others, and thus variations in these latter properties can also be detected and estimated using GPR. Electrical conductivity of the soil mass and pore water are also important attributes because they are related to both the content and type of water and dielectric losses in clayey materials, which have an important effect on soil bulk permittivity. The stratigraphic and deformation features commonly define major boundaries to variations in the physical properties of the layered sedimentary sequences.

On the southern flank of the Peñón del Marques, normal faults and pending blocks were observed. The u-shaped scarp suggest that this flank is affected by an active slide, the sliding blocks of which have different relative displacements and rotation around the vertical and horizontal axes. Radar profiles permitted the identification of both faults observed directly in the field and "blind ground fracturing". The results obtained suggest that the depression caused by subsidence is located at the lateral contact between volcano-sedimentary sequences of the Peñón del Marques and the lacustrine sequences (Fig. 1).

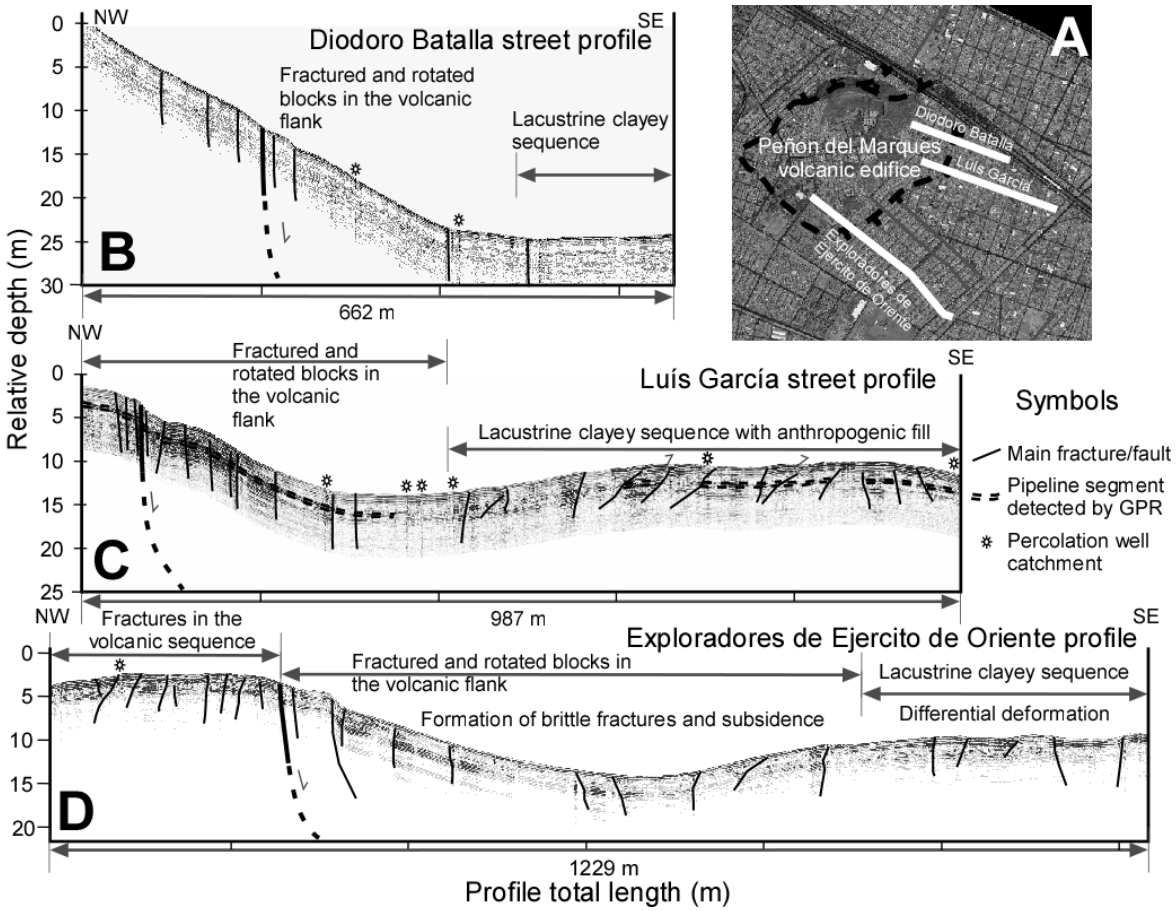

Fig. 1 (a) Location of three representative GPR profiles along streets at the southeastern flank of the Peñón del Marques; (b) Diodoro Batalla profile; (c) Luis Garcia Profile; and (d) Exploradores de Ejercito de Oriente Profile. GPR profiles collected with a 200 MHz antenna and using a relative permittivity of 16.

The correlation of physical properties with radar profiles show the potential of GPR for characterizing layers with a similar set of interrelated physical attributes. This is achieved by complementing GPR field measurements with laboratory measurements of physical properties (Table 1). For the purposes of this analysis we present the comparison of five samples collected in the surface of the volcanic flank and five samples collected in a vertical profile (1.85 m depth) located in the nearby lacustrine clayey sequence. All analyses were performed at the Laboratorio de Mecánica Multiescalar de Geosistemas (LAMMG) of the Centro de Geociencias (Universidad Nacional Autónoma de México, UNAM), and included: grain size distribution (texture), gravimetric water content (%), organic matter content (OM in %), pH, solids density (δs), liquid and plastic Atterberg Limits and Plasticity Index, and the classification in the Unified System of Soils Classification (USSC) (see Carreón-Freyre *et al*., 2003, for further analytical details). Grain-size distribution was determined mainly by sieve analysis and hydrometer analysis. With this technique the sand, clay, and silt contents are calculated considering only the fraction of grain size smaller than 2 mm. Gravimetric (Wgrav%) water content is calculated by dividing the mass of water by the mass of dry soil, and was obtained by the average of three determinations by the oven-drying method.

Table 1 Selected physical attributes of the volcano-sedimentary sequences in the Peñón area and the clayey sediments in the lacustrine area.

Sample	Depth	W_{grav}	δ	OM	pH	Texture			Atterberg Limits		PI	USSC
	(m)	%	(g cm^{-3})	%		Clay	Silt	Sand	Liquid	Plastic		
Peñón area												
EZ- Peñón 1	0	17.3	2.58	0.000	8.8	5.5	17.1	77.4	-----	-----	-----	SM
EZ- Peñón 2	0	14.8	2.42	2.386	9.3	19.7	42.7	37.7	31.9	21.7	10.3	OL
EZ- Peñón 3	0	60.4	2.21	2.407	8.4	29.8	43.1	27.1	81.7	44.1	37.6	OH
EZ- Peñón 4	0	107.1	2.50	0.312	9.9	33.3	43.6	23.1	81.4	47	34.4	MH-CH
EZ- Peñón 5	0	------	2.31	0.832	9.7	13.2	50.6	36.1	-----	-----	-----	M
Lacustrine area												
EZ-Caliztli1.1	0.85	41.4	2.43	1.779	9.2	33.6	45.8	20.6	48.1	36	12.1	OL-ML
EZ-Caliztli1.2	1.15	47.2	2.46	0.753	9.8	34.3	52.3	13.4	56.8	38.9	17.9	MH
EZ-Caliztli1.3.1	1.5-1	140.2	2.33	0.628	9.4	46.9	46.2	6.9	105.5	71.5	34	CH
EZ-Caliztli1.3.2	1.5-2	120.4	2.19	0.753	9.7	44.8	38	17.2	93.1	66	27.1	MH
EZ-Caliztli1.4	1.85	106.4	2.27	0.730	9.8	43.7	38.8	17.5	91	57.9	33.1	MH

Abbreviation for USSC: C = Clay, M =silt, S = Sand, O = Organic, L = Low compressibility, H = High compressibility.

Most of the subsoil deformation produced by land subsidence in the study area is located around the Peñón del Marques structure, within a pumice sequence (SM and M) that loses its structure easily on contact with water. Distribution of this material is related to the areas most affected by tension fracturing and normal faults. In contrast, the lacustrine sequence is composed by a silty and clayey sequence with high plasticity and water content. Rapid alteration in the lacustrine environment of the volcanic ashes and pumice produced by recent volcanic activity (the last 400 000 years) results in clayey soils containing allophane and imogolite, which are clay minerals similar in mechanical behaviour to gels (lacustrine sequence). The characteristic behaviour of this type of sequences, in Mexico and elsewhere, has been the subject of study for several decades (Zeevaert, 1953; Mesri *et al.*, 1976; Wada, 1987; Warren & Rudolph, 1997; Wesley, 2001; Díaz-Rodríguez & Santamarina, 2001; among others). Redox conditions favour dehydration of these materials and transform them into gibbsite and halloysite. The geometry of deformation in this sequence is characterized by low angle inverse displacements and uplifting with respect to the depression. We interpret these deformations as produced by the sliding of the volcanic flank along a décollement(s) plane.

MULTIFREQUENCY SURVEY OF THE TENSION FRACTURES AT THE HEAD OF THE SLIDING OF THE PEÑÓN DEL MARQUES

Conventionally, radar surveying employs a selected centred frequency depending on the penetration depth and resolution required in the survey. The selection of a specific radar wavelength can in some cases overlook valuable information. For instance, an antenna centred at the 300 MHz frequency has a "blind area" in the first metres that is the common penetration depth of an antenna centred at 400 MHz frequency. In spite of the obvious complementary information that can be gathered from using different frequencies, studies using such an approach are scarce. We have obtained profiles using all the frequencies available (100, 200, and 400 MHz) in order to detail the shallow geometry of the zone affected by tension fractures in a segment of the Luis Garcia street profile. The results are presented in Fig. 2.

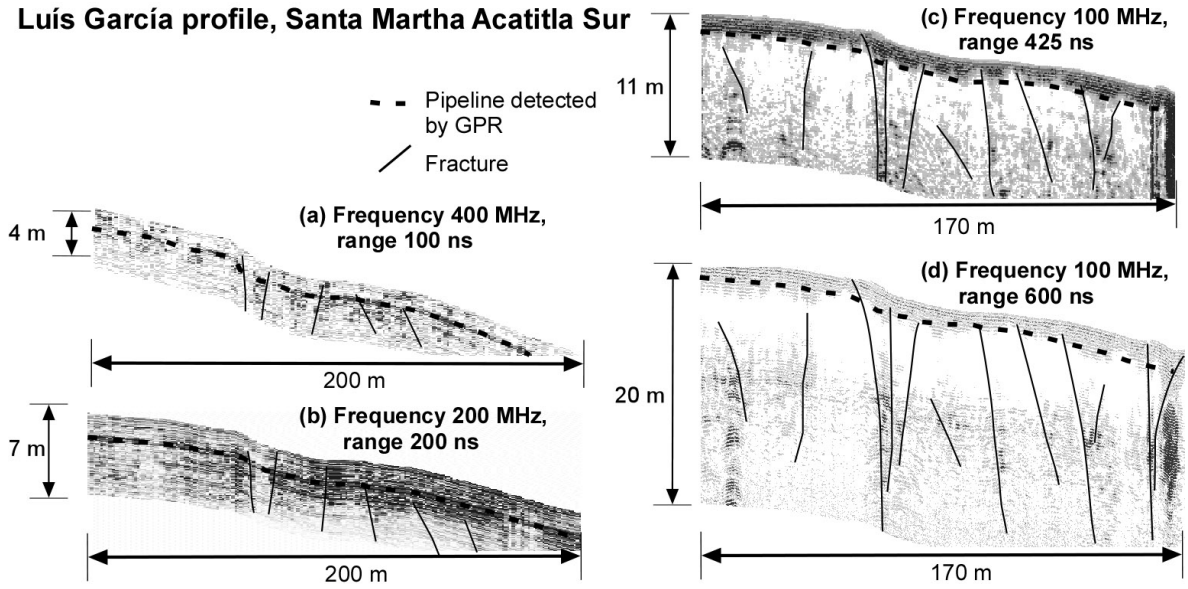

Fig. 2 GPR multifrequency analysis of the upper part of the Peñón del Marques showing the geometric characteristics of the normal faulting for different resolutions: (a) 400 MHz, (b) 200 MHz, (c)100 MHz and a range of 425 ns, and (d) 100 MHz and range 600 ns. The trace of a pipeline is shown for reference.

DISCUSSION

The combined effects of slope failure in blocks, land subsidence, the presence of a compressible clay material and a collapsible tuff, and lateral flank displacement, may have generated the outer bench morphology observed along the perimeter of the Peñón del Marques. The presence of loose sliding debris composed of tuffaceous material at the base of the sliding flank leads to the growth of the frontal overthrusting bench. The structures obtained using GPR and seismic analyses demonstrate the importance of the dynamic interplay between sliding at the volcanic flank and land subsidence in the clayey plain. Gravitational relaxation of the edifice was triggered by land subsidence and this deformation is accommodated by outward flank displacement along a low-angle décollement near the base of the edifice, and small inverse faults that are observed in GPR profiles at the distal edge of the volcanic edifice. The décollement plane was not observed in the seismic profiles, indicating that it is located at depths greater than 40 m in the steep fracture flank. Lubrication by infiltrated water could be a further destabilizing agent for the flank, but monitoring is necessary to prove or disprove this idea. Understanding the deformation processes around the Peñón del Marques is crucial to improve the maps of vulnerability to fracturing and landslides in Mexico City. We conclude that the generalized land subsidence in the area has triggered and accentuated the sliding of the southern flank of El Peñón del Marques and the associated ground fracturing.

Acknowledgements The 2006–2009 and 2009–2011 administrations of the Delegación Iztapalapa are gratefully acknowledged for making available funds for this project. We thank all the technical staff of the Centro de Evaluacion de Riesgo Geologico (CERG) form Iztapalapa for their support during field work. We are also grateful to Ricardo Carrizosa from the Laboratorio de Mecanica Multiescalar de Geosistemas (LAMMG) for the physical characterization of granular materials.

REFERENCES

Aguilar-Pérez, L. A., Ortega-Guerrero, M. A., Lugo-Hubp, J. & Ortiz-Zamora, D. C. (2006) Análisis numérico acoplado de los desplazamientos verticales y generacion de fracturas por extracción de agua subterránea en las proximidades de la Ciudad de Mexico. *Revista Mexicana de Ciencias Geológicas* **23**(3), 247–261.

Cabral-Cano, E., Dixon, T. H., Miralles-Wilhelm, F., Díaz-Molina, O., Sánchez-Zamora, O. & Carande, R. E. (2008) Space geodetic imaging of rapid ground subsidence in Mexico City. *GSA Bulletin* **120**(11-12), 1556–1566, doi: 10.1130/B26001.1

Carreón-Freyre, D. & Cerca, M. (2006) Delineating the near-surface geometry of the fracture system affecting the valley of Queretaro, Mexico: Correlation of GPR signatures and physical properties of sediments. *Near Surface Geophysics* **4**(1), 49–55.

Carreón-Freyre., D. C., Cerca M. & Hernández-Marín, M. (2003) Correlation of near-surface stratigraphy and physical properties of clayey sediments from Chalco Basin, Mexico, using Ground Penetrating Radar. *J. Appl. Geophys*. **53**, 121–136.

Díaz-Rodríguez, A. & Santamarina, J. C. (2001) Mexico City soil behavior at different strains: Observations and physical interpretation. *J. Geotechnical and Geoenvironmental Engineering* **127**(9), 783–789.

Mesri, G., Rokhse, A. & Bonor, B. F. (1976) Compositive and compressibility of typical samples of Mexico City. *Geotechnique* **25**(3), 527–554.

Wada, K. (1987) Minerals formed and mineral formation from volcanic ash by weathering. *Chemical Geology* **60**, 17–28.

Warren, C. J. & Rudolph, D. L. (1997) Clay minerals in basin of Mexico lacustrine sediments and their influence on ion mobility in groundwater. *J. Contam. Hydrol*. **27**, 177–198.

Wesley, L. D. (2001) Consolidation behaviour of allophane clays. *Géotechnique* **51**(10), 901–904.

Zeevaert, L. (1953) Estratigrafía y problemas de ingeniería en los depósitos de arcilla lacustre de la Ciudad de México. Memoria del Congreso Científico Mexicano, vol. 5, 58–70.

(Proceedings of EISOLS 2010, Querétaro, Mexico, 17–22 October 2010). IAHS Publ. 339, 2010.

Microcracking of expansive soils during shrinkage processes: roles of mineralogy and microstructure

M. AUDIGUIER, R. COJEAN & Z. GEREMEW
Mines ParisTech – Centre de Géosciences, Fontainebleau, France
roger.cojean@mines-paristech.fr

Abstract Cyclic expansion and shrinkage of clays and associated movements of foundations may result in damage to structures. The roles of mineralogy and microstructure are analysed through laboratory experiments so as to address the matter of microcracking of clayey soils during shrinkage, with the corresponding consequences on settlement of argillaceous soils. Two clayey soils from the Paris basin (France) are analysed. The first one is a stiff clayey soil: the "Argile verte de Romainville". The second one is a marly soil: the "Marne bleue d'Argenteuil". The study of their microstructures by means of a scanning electron microscope and a mercury porosimeter allows investigation of the natural porous media and micro-structural characteristics that play a role in the rigidity of the soils, as well as on the microcracking phenomena during shrinkage processes. Comparisons between the intact soils and remoulded ones bring additional arguments to discuss about the role of microstructures on microcracking and the general behaviour of expansive soils, either during swelling or shrinkage processes.

Key words expansive soils; mineralogy; microstructures; microcracking

INTRODUCTION

Expansive soils exist in many parts of the world, not only in arid and semi-arid regions, but also for example on the Atlantic edge of Europe, and are the source of damage to buildings and civil engineering structures. This case study is related to shrink/swell hazards in the Paris basin, where several geological formations are considered to be responsible for a lot of damage observed on buildings. The objective of this study is to address the matter of microcracking of clayey soils during shrinkage, with the corresponding consequences on settlement of argillaceous soils. Two clayey soils from the Paris basin (France) are analysed. The first one is a stiff clayey soil: the "Argile verte de Romainville" (Romainville green clay). The second is a marly soil: the "Marne bleue d'Argenteuil" (Argenteuil blue marl). Specific attention is given to their microstructure characteristics that play a role in the rigidity of the soils, as well as in the microcracking phenomena during shrinkage processes.

The swelling potential of the soil is evaluated using both indirect or empirical methods and direct methods. The swell percentage and swelling pressure of the soil are measured in a conventional oedometer apparatus. Swell/shrink tests are carried out on similar samples taken from the same monolith. A scheme that permits the study of the clayey soil behaviour at the extreme states of wetting and drying is chosen. The test begins by wetting the samples at their natural moisture content and density.

Intact and laboratory remoulded samples at the same initial water content are investigated before and after swelling, and the evolution of their microstructure is analysed thanks to the scanning electron microscope and the mercury intrusion porosimeter. In order to preserve the microstructure, the specimens are cut into small pieces, frozen in liquid nitrogen and finally sublimated, as presented by Audiguier *et al.* (2007).

PETROPHYSICAL AND GEOTECHNICAL PROPERTIES OF THE SDUDIED SOILS

Argile verte de Romainville

The "Argile verte de Romainville" (named AVR in the following sections) is of Lower Oligocene age (Rupelian). It is a stiff and plastic clayey soil that contains clay minerals (50 to 70 %), quartz

Copyright © 2010 IAHS Press

(15 to 35 %), carbonates (12 to 20 %) and traces of mica and feldspars. X-ray diffraction showed that carbonates are either calcite or dolomite and the clay minerals are dominantly illite and kaolinite, with a small amount of smectite. Grain size analyses show that the clay content (<2 µm) varies between 78% and 80%. The study of its microstructure by means of the scanning electron microscope indicates that the clayey soil has structural elements oriented in the bedding direction. The structure of the sample generally consists of a dense and continuous clay matrix, with very limited visible pore spaces. At its natural water content (about w = 25%), the soil shows mainly a unimodal pore size distribution with an average pore radius of 0.07 µm and a few voids larger than 10 µm. In a natural state, slickensides can be observed. The Atterberg limits are the following: w_L = 75%, I_P = 35%, I_R = 59%. The methylene blue value ranges from 8.0 to 9.3 g/100g with an associated specific surface area ranging from 167 to 195 m^2/g, according to Audiguier *et al.* (2007).

Marne bleue d'Argenteuil

The "Marne bleue d'Argenteuil" (named MBA in the following sections) is of Upper Eocene age (Ludian). It is a very stiff marly soil that contains carbonates (30 to 65 %), clay minerals (30 to 60 %), quartz (5 to 10 %), and traces of pyrites. X-ray diffraction showed that carbonates are essentially calcite and the clay minerals are dominantly illite and smectite, with a smaller amount of kaolinite. Grain size analyses show that clay content (<2 µm) varies between 78% and 90%. The study of its microstructure by means of the scanning electron microscope indicates that the marly soil exhibits a compact and heterogeneous microstructure. At its natural water content (about w = 25%), the soil shows mainly a sharp unimodal pore size distribution with an average pore radius of 0.06 µm and a few voids larger than 10 µm. In a natural state, neither microfissures nor slickensides are observed. The Atterberg limits are the following: w_L = 63%, I_P = 35%, I_R = 47%. The methylene blue value ranges from 5.3 to 9.7 g/100g with an associated specific surface area ranging from 111 to 202 m^2/g according to Audiguier *et al.* (2007).

The geo-engineering characteristics (blue value, liquid limit, plasticity index, % <2µm) result in a classification of high or very high swelling potential. The porosity values and the density are related to more-or-less loose soils.

ANALYSIS OF THE SHRINK/SWELL BEHAVIOUR, MACROSCOPIC OBSERVATIONS AND MICROSCOPIC INVESTIGATIONS

Experimental methods for the analysis of the shrink/swell behaviour

The swelling potential of the analysed soils was studied using free swelling tests in an oedometer according to Method A, presented in the ASTM D 4546-85 Standards (1986), applied to natural soils and soils remoulded in the laboratory. The microstructure of intact or remoulded soils at the natural water content or after swelling was studied on freeze-dried samples, from a qualitative point of view with the help of the scanning electron microscope and from a quantitative point of view with the help of the mercury intrusion porosimeter, as presented by Audiguier *et al.* (2007).

In addition, observations of the macroscopic behaviour of both soils during experimental drying and humidification processes were undertaken on intact and remoulded samples inserted in a metallic ring of 185 mm in diameter and 10 to 35 mm in height.

Experimental results of free swelling

The analysis of free swelling (Table 1) leads to the conclusion that the swelling ratios depend on the type of soil and the initial intact or remoulded state of the soil for initial similar water contents.

For similar water contents, the AVR swelling ratio moves from 16% for an intact sample to 32% for a remoulded sample. The MBA-1 swelling ratio moves from 4% for an intact sample to 26% for a remoulded sample. The MBA-1 samples exhibit high initial water contents. The MBA-2 swelling ratio moves from 1.5% for an intact sample to 15% for a remoulded sample. The AVR

Table 1 Free swelling of the "Argile verte de Romainville" and the "Marne bleue d'Argenteuil".

Type of soil	AVR	MBA-1	MBA-2
Water content before swelling (intact sample) %	25	32	23
Water content after swelling (intact sample) %	39	36	25
Water content before swelling (remoulded sample) %	27	34	24
Water content after swelling remoulded sample) %	51	56	35
Free swelling ratio (intact sample) %	**16**	**4**	**1.5**
Free swelling ratio (remoulded sample) %	**32**	**26**	**15**

AVR (carbonates: 15%): "Argile verte de Romainville"

MBA-1 (carbonates: 27%): "Marne bleue d'Argenteuil"

MBA-2 (carbonates : 58%): "Marne bleue d'Argenteuil"

sample exhibits a higher swelling potential in a remoulded state than in an intact state and its swelling ratio is larger than that of the MBA sample. The "Marne bleue d'Argenteuil" is less sensitive to swelling in an intact state as the carbonate content increases. In a remoulded state the sensitivity to swelling increases by 6.5 to 10 times, depending on the initial water content and the percentage of carbonates.

Macroscopic observations

The cycles of complete drying and humidification to the value of the water content corresponding to the shrinkage limit that were carried out on AVR intact samples have demonstrated the occurrence of a crack network that is just slightly modified from one cycle to the other and is at the origin of differential swellings at the scale of the sample with the consequence of a progressive destruction after a total humidification (Fig. 1).

This crack network corresponds to previous shearing surfaces identified as "slickensides" that are the witnesses of ancient reworkings of geological origin, depending on postdepositional events, diagenetic processes and post-induration shrink/swell processes. These surfaces correspond to weakness surfaces that are remobilized during cyclic drying–humidification processes.

The behaviour of AVR remoulded samples is quite different: during the drying process the sample shrinks as a whole without any crack, then during the humidification to a water content higher than the shrinkage limit it crumbles but does not occupy the total volume of the metallic ring (Fig. 2).

The volume variations of the MBA-1 intact sample are very small during the shrinkage process and the total humidification process. The MBA-1 remoulded sample exhibits different behaviour to that of the AVR remoulded sample. During the drying process it shrinks with the formation of a lot of cracks and during the total humidification the cracks cicatrize (close-up) more or less completely before the sample occupies the volume of the metallic ring (Fig. 3).

The shrink/swell processes at the macroscopic scale are varied for different soils and depend on the intact or remoulded initial state. For intact soils it seems to be highly dependent on diagenetic conditions and geological stress contexts. Thus, for the AVR samples the mechanism is mainly governed by the existing "slickensides", while for the MBA samples the mechanism is inhibited by the existing carbonaceous cement resulting from the diagenetic process that creates bonds between soil aggregates. In a remoulded state, the diagenetic history is partly obliterated. The AVR sample behaves as a homogeneous material with a clayey microstructure that shrinks as a whole or swells uniformly until the destruction of the microstructure (Fig. 2(c)). The MBA-1 sample shrinks with a crack network initiated by hard points of carbonated particles. In this case, the remoulding effect leads to the destruction of carbonate bonds. Nevertheless, the carbonated particles result in a semi-rigid material that prevents the sample from a complete destruction during the final total humidification process (Fig. 3(c)).

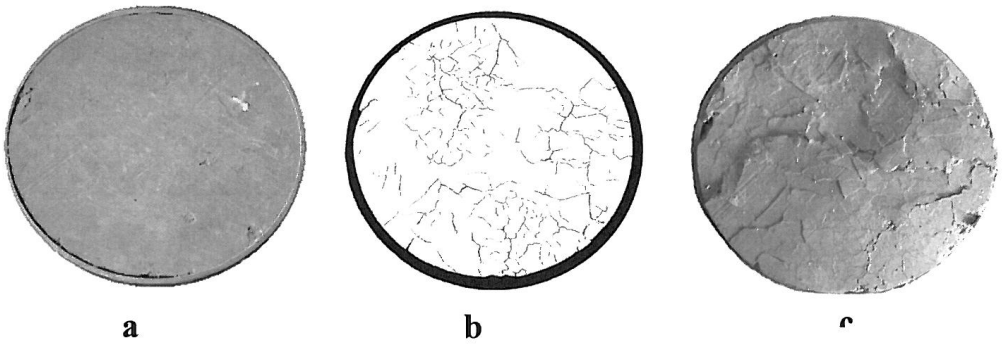

Fig. 1 Intact AVR sample: (a) at the initial water content $w = w_0$, (b) pattern of the microcracks after several shrink/swell cycles $w < w_r$, and (c) after humidification $w > w_r$.

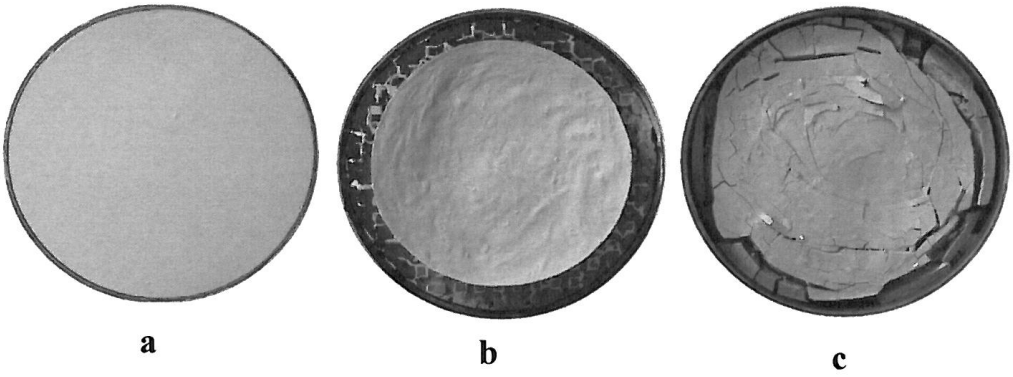

Fig. 2 Remoulded AVR sample: (a) at the initial water content $w = w_0$, (b) after shrinkage $w<w_r$, and (c) after humidification $w > w_r$.

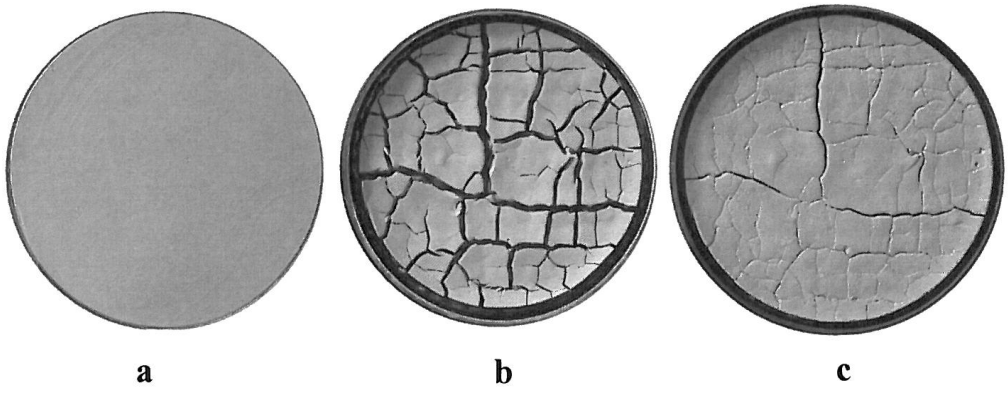

Fig. 3 Remoulded MBA-1 sample: (a) at the initial water content $w = w_0$, (b) after shrinkage $w < w_r$, and (c) after humidification $w > w_r$.

Microstructural analyses and observations

Mercury porosimetry Figures 4 and 5 present the results of porosimeter investigations related to AVR and MBA-1 samples during free swelling in the oedometer.

After oven-drying, the AVR sample exhibits a unimodal distribution of pore access radii centred on the value of 20 nm and prolonged towards very low values by a flat distribution

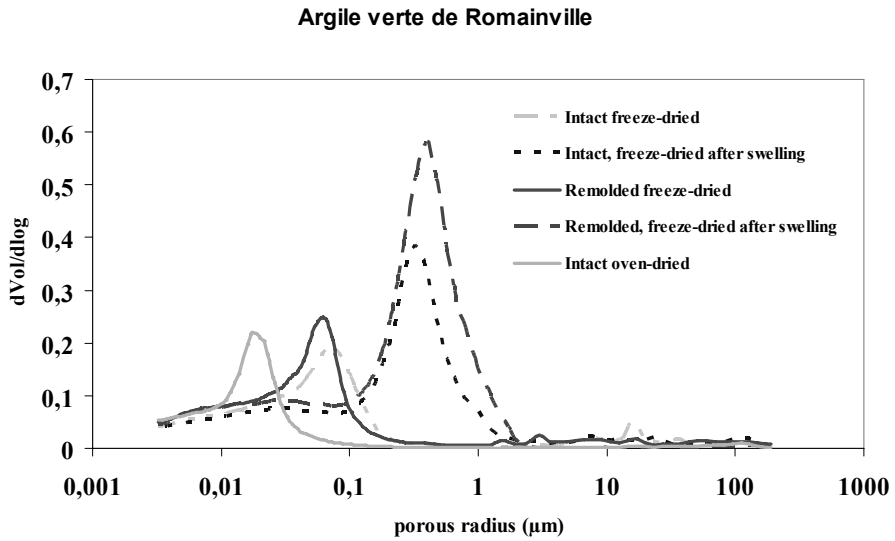

Fig. 4 Pore distribution porosimetric curves of AVR samples.

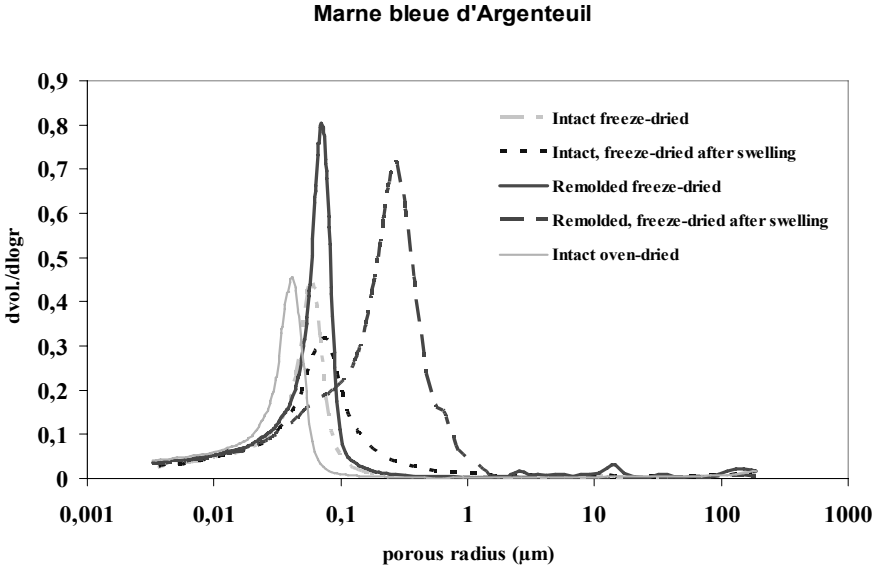

Fig. 5 Pore distribution porosimetric curves of MBA-1 samples.

resulting from an inter-particle porosity, which the mercury can not invade. This porosimetric curve is typical of a compact clayey matrix microstructure according to Audiguier & Delage (1987). Before swelling, the intact and remoulded freeze-dried AVR samples also exhibit a unimodal distribution of pore access radii, but centred on the values of 60 to 70 nm (Fig. 4). After swelling the porous volumes have increased up to 40% for the intact sample and 54% for the remoulded sample relative to the state before swelling. They exhibit two well-identified families: the one centred between 300 to 400 nm, the other laid down towards radii lower than 100 nm (Fig. 4). These unimodal porosimetric curves correspond to an aggregated microstructure according to Touret *et al*. (1990) that results in inter-aggregate and intra-aggregate porosities according to synthetic works presented by Al-Mukhtar *et al*. (1996) and Robinet *et al.* (1996). During the humidification process, the sizes and volumes of pores increase as a consequence of a progressive and simultaneous opening of the inter-aggregate and intra-aggregate porosities that result in the formation of secondary aggregates. This subdivision process develops until clusters of particles are formed with a new distinct intra-aggregate porosity.

In an intact state the behaviour of MBA-1 samples is different from that of the AVR samples presented above. Before swelling, the porosimetric curves are unimodal and very similar for the oven-dried and freeze-dried samples (Fig. 5). After swelling the porosimetric curves exhibit very similar unimodal distributions of pore access radii before and after swelling (curve centred on the value of 70 nm before swelling and 80 nm after swelling). The increase in volume after swelling is about 15%. This behaviour is characteristic of a skeletal microstructure according to Audiguier & Delage (1987) and Bauer-Plaindoux *et al.* (1998). By comparison, the porosimetric curves related to the remoulded MBA-1 samples are very different before and after swelling. Before swelling the porosimetric curve exhibits a unimodal distribution of pore access radii (curve centred on the value of 80 nm). After swelling the porosimetric curve exhibits a bimodal distribution of pore access radii (curve centred on two values: a principal value of 280 nm and a secondary one of 70 nm). The increase in volume after swelling is about 44%.

Scanning electron microscopic observations

The microscopic observations allow illustration of the porosimetric measurements for intact and remoulded samples and before and after swelling.

In an intact or remoulded state before swelling the AVR samples present a similar compact microstructure where aggregates are not identified. It is made up of a clayey matrix with clayey particles wrapping around dolomite and quartz grains (Figs 6(a) and (c)). After swelling, bi-dimensional pores appear that result from the formation of aggregates in the case of the intact sample as well as the remoulded sample. After swelling the porous volume appears larger for the remoulded sample than for the intact sample (Figs 6(b) and (d)).

In an intact or remoulded state before swelling the MBA-1 samples present a similar clast-supported microstructure where calcitic grains are gathered together and linked by clayey-carbonated bridges. They form aggregates of several μm in diameter (Fig. 7(a) and (c). After swelling there is no significant modification of this microstructure (Fig. 7(b)). After swelling the

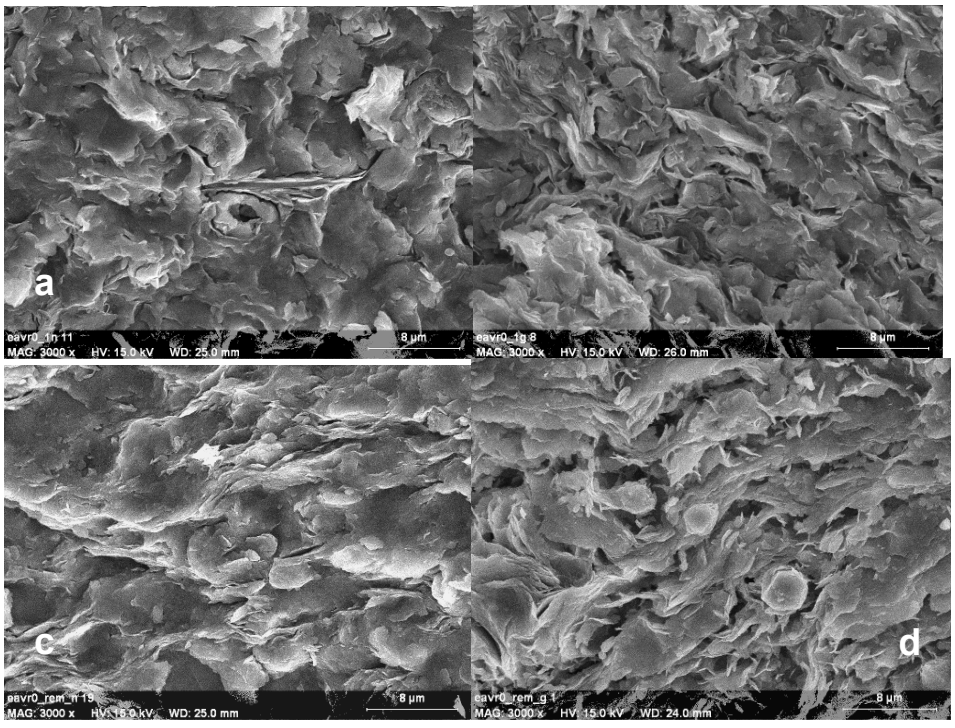

Fig. 6 SEM observations of AVR (Argile verte de Romainville): (a) intact sample before swelling, (b) intact sample after swelling, (c) remoulded sample before swelling, and (d) remoulded sample after swelling.

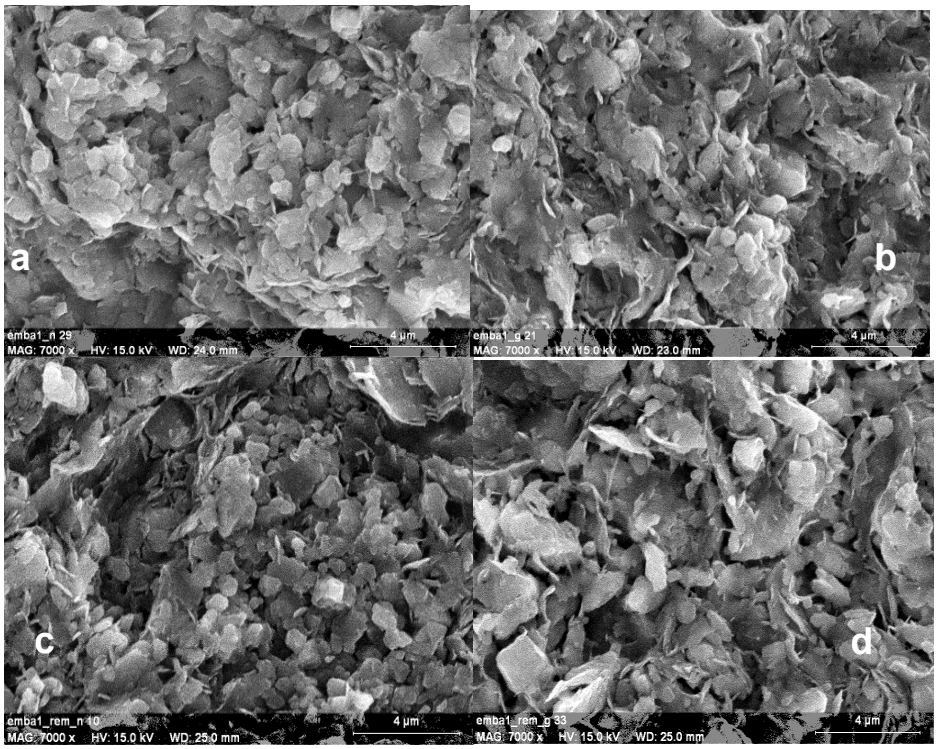

Fig. 7 SEM observations of MBA-1 (Marne bleue d'Argenteuil): (a) intact sample before swelling, (b) intact sample after swelling, (c) remoulded sample before swelling, (d) remoulded sample after swelling.

remoulded MBA-1 sample presents a modified microstructure that is now not clast-supported, but matrix-supported with isolated grains, larger pores and some residual small aggregates made up of grains of micritic calcite linked by clayey particles (Fig. 7(d)). The occurrence of residual small aggregates explains the bimodal porosimetric curve.

CONCLUSION

The analyses and observations carried out on the AVR and MBA samples in an intact or remoulded state lead to the following conclusions:

The mineralogical analysis resulted in the identification of carbonates and smectites in higher percentages for MBA than for AVR.

The geotechnical classifications lead to the conclusion that both types of soils are clayey or marly soils that present a high or very high swelling potential.

The free swelling varies according to the initial water content and the intact or remoulded state. The AVR samples exhibit a swelling ratio of 16% in an intact state and 32% in a remoulded state. The MBA samples exhibit a very low swelling ratio of 1.5 to 4% in an intact state and 15 to 26% in a remoulded state, which corresponds to a relative increase of the swelling ratio of 6.5 to 10%.

At a macroscopic scale, the shrink/swell process of intact samples is highly governed by the diagenetic characteristics of the clayey materials. In a remoulded state these characteristics are more or less obliterated. Only the geotechnical characteristics and the mineralogy play a role in the mechanical behaviour;

At a microscopic scale, the mercury intrusion porosimetry and the observations from the scanning electron microscope confirm the previous analyses.

This research work allowed highlighting of the interdependence of several factors in the shrink/swell process:

The mineralogical content plays a significant role that has to be analysed in a detailed way: smectites are expansive clays at the origin of high swelling potential of soils. However, due to microstructure characteristics and especially the presence of a high content of carbonates, the swelling process can be partly inhibited. In intact states the carbonate content in marly soils appears to be inversely correlated with the swelling ratio (see Table 1);

The initial water content plays a major role in the swelling potential of clayey soils. For a given initial condition (intact or remoulded state), the lower the initial water content, the higher the swelling ratio;

The diagenetic characteristics are at the origin of different behaviours in comparisons between intact or remoulded materials. The resulting microstructures that can exhibit particular characteristics (clast-supported or matrix-supported microstructures, etc.) or slickensides (in the case of AVR samples) can control the characteristics of the shrink/swell behaviour, with sometimes the mineralogy content playing a secondary role. For example, a clayey soil that would be classified as a soil of high to very high swelling potential might exhibit a low swelling ratio as a result of a particular microstructure that is not taken into account in classifications.

From a practical point of view, at the scale of the construction, the shrink/swell behaviour has to be considered by reference to the initial water content and density of soils and also by reference to their mineralogical content and microstructure. In particular, the state of remoulding (natural: colluvium or artificial) has to be analysed for a precise diagnosis of the swelling potential of soils.

Acknowledgements The Centre de Géosciences of Mines-ParisTech is indebted to Fondation MAIF, ANR-ARGIC and R2DS Ile-de-France for making possible the presented results of this paper.

REFERENCES

Al-Mukhtar M., Belanteur N., Tessier D. & Vanapalli S. K. (1996) The fabric of a clay soil under controlled mechanical and hydraulic stress states. *Applied Clay Sciences* **11**, 99–115.

ASTM (1986) Standard test methods for one dimensional swell or settlement potential of cohesive soils. *ASTM D 4546 – 85.*

Audiguier, M. & Delage, P. (1987) Etude microscopique et porosimétrique de sols fins naturels dans une perspective géotechnique. *Actes de la VII*^{ème} *Réunion Internationale de Micromorphologie des sols* (Paris, Juillet 1985) (éd. par N. Fedoroff, L. M. Bresson & M. A. Courty, 493–500, AFES.

Audiguier, M., Geremew, Z., Laribi, S. & Cojean, R. (2007) Caractérisation au laboratoire de la sensibilité au retrait-gonflement des sols argileux. *Revue française de géotechnique* **120-121**, 67–82.

Bauer-Plaindoux, C., Tessier, D. & Ghoreychi, M. (1998) Propriétés mécaniques des roches argileuses carbonatées : importance de la relation calcite-argile. *C. R. Acad. Sci. Paris, Sciences de la terre et des planètes* **326**, 231–237.

Robinet, J. C., Rahbaoui, A., Plas, F. & Lebon, P. (1996) A constitutive thermomechanical model for saturated clays. *Engineering Geology* **41**, 145–149.

Touret, O., Pons, C. H., Tessier, D. & Tardy, Y. (1990) Etude de la répartition de l'eau dans des argiles saturées Mg^{2+} aux fortes teneurs en eau. *Clay Minerals* **25**, 217–233.

(Proceedings of EISOLS 2010, Querétaro, Mexico, 17–22 October 2010). IAHS Publ. 339, 2010.

Evolution of Mexico City clay properties affected by land subsidence

ALBERTO JAIME P. & E. MÉNDES-SÁNCHEZ
Instituto de Ingeniería, Universidad Nacional Autónoma de México, Coyoacán 04510, Mexico D.F.
emendezs@iingen.unam.mx

Abstract The effects of Mexico City aquifer exploitation on the evolution of some index and mechanical properties of Mexico City clays are discussed. The study was carried out at two sites located in the old lake zone of Mexico City. It is based on laboratory and field tests, as well as on piezometric measurements taken at two different times, 25 years apart.

Key words regional subsidence; evolution of clay properties; Mexico City clay

INTRODUCTION

The effects of aquifer exploitation below Mexico City on some index and mechanical properties of Mexico City clays are discussed. Two different sites with reliable information were analysed. At both sites, continuous borings were made in the 1950s and others (next to the older ones) in the 1980s. Piezometric and subsidence information for both sites are also available. The variation with time of water content, volumetric weight, shear strength, compressibility and clay layer thickness are shown.

SUBSIDENCE AND PIEZOMETRIC MEASUREMENTS

Two sites were studied. They are identified as PRJ and CUPJ and are both located in the old lake zone of Mexico City. PRJ site was studied in 1952; piezometric, stratigraphic and laboratory results are available (Marsal & Mazari, 1959). This site was studied again after the earthquakes that shook the city in September 1985. Thus in 1986 new stratigraphic and piezometric information was produced. Similarly, CUPJ site was studied in 1950 and 1986. In addition, at Parque España (a site located nearby PRJ and CUPJ) a piezometric station has been operating since 1952.

In Fig. 1 the evolution with time of measured settlement at PE and PRJ sites are depicted. Figure 1 also shows an inferred curve for settlement at CUPJ. During the 1950s, the aquifer exploitation was very high in that part of the city, thus the pore pressure in the soft clay layers dropped considerably and consequently the rate of settlement was at its peak. For this reason, water pumping was banned in 1953 (Marsal & Mazari, 1959). As a result, the rate of settlement declined, although very slowly in the first few years, as seen in Fig. 1.

The primary and secondary consolidation parameters of Mexico City clay are very high, and both processes start simultaneously as the vertical stresses increase; thus it is impossible to distinguish which one has more effect on the regional subsidence.

EVOLUTION OF INDEX AND MECHANICAL PROPERTIES OF MEXICO CITY CLAYS

The stratigraphic profile of the sites studied consist of a hard crust layer (5-m thick) overlying the so-called Upper Clay Formation (UCF, 30-m thick), followed by a 2-m thick compact layer of silty sand, which rests on the Lower Clay Formation (LCF), Fig. 2(a) and (b). Taking into account the water content and some thin layers of volcanic glass and volcanic ashes, the upper clay formation in turn can be divided into four clay units, Fig. 2(b). In Fig. 2(a) and (b) a comparison is made between water content, volumetric weight, unconfined compression and UU strengths of soil samples taken from continuous borings in 1952 and 1986, respectively. Furthermore, in Fig. 2(b)

Copyright © 2010 IAHS Press

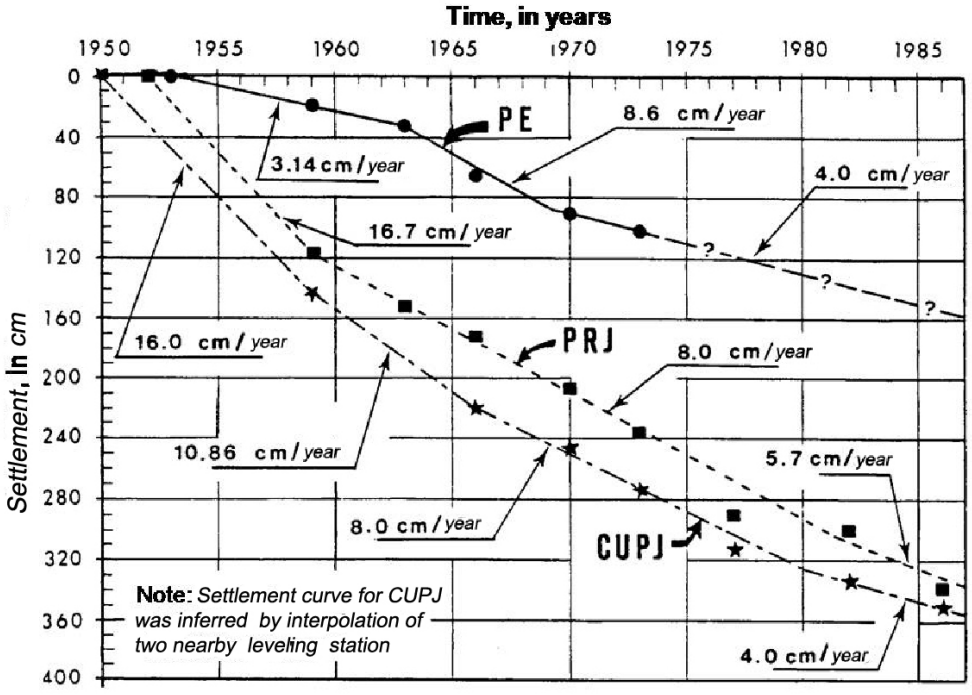

Fig. 1 Mean subsidence evolution in sites PE, PRJ and CUPJ while the period 1950–1986.

the 1952 and 1986 soil profiles are depicted. As can be seen from the figure, the mean water content of the different clay layers changed with time. This variation increases with depth, as expected, since the piezometric pressure drop is greater as the depth increases.

It can be observed from Fig. 3 that the depth to the LCF is 3.47 m less in 1986, which approximately coincides with the regional subsidence from 1952 to 1986, Fig. 1. This settlement is the sum of all the vertical displacements of the strata down to 200 m or so (the water is extracted from the aquifer at depths greater than 180 m).

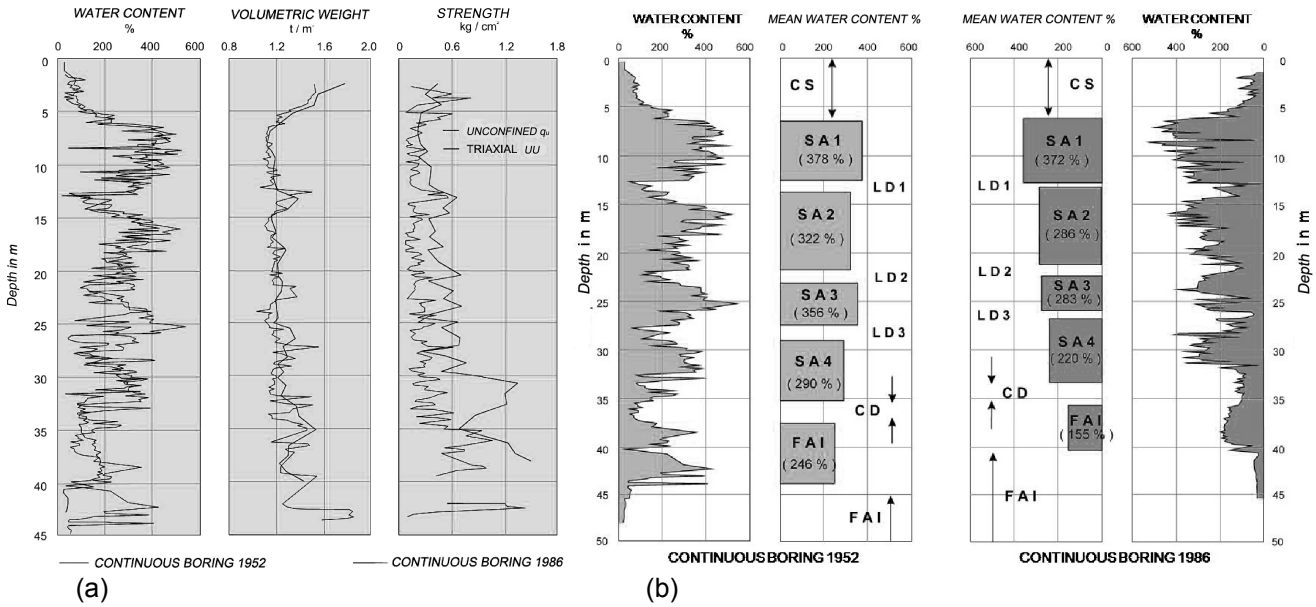

Fig. 2 (a) Water content, volumetric weight, and shear strength variation, at PRJ site from 1952 to 1986. (b) Comparison between stratigraphic units and water content at PRJ site.

In Fig. 3 the compressibility curves *e versus* logσ are shown for soil samples extracted in 1950 and 1986 at the CUPJ site, pertaining to the same stratigraphic unit. From Fig. 3, it can be seen that the 1986 preconsolidation loads are greater than those of 1950 for clay sublayers one, three and four. This indicates that the compressibility of the clays has been affected by the piezometric pressure drop. Given the scarcity of data, a statistical analysis of these changes could not be made.

YEAR	Depth (m)	ω_i (%)	LL (%)	LP (%)	e_i	G_i (%)	$\bar{\sigma}_o$ kg/cm²	σ_c kg/cm²
1950	11.76	244	233	70	5.88	101	0.60	0.70
1986	8.87	220	490	95	4.83	103	0.55	0.72

YEAR	Depth (m)	ω_i (%)	LL (%)	LP (%)	e_i	G_i (%)	$\bar{\sigma}_o$ kg/cm²	σ_c kg/cm²
1950	29.56	299	270	73	7.83	98	1.00	1.60
1986	28.63	273	265	75	6.13	104	1.06	1.92

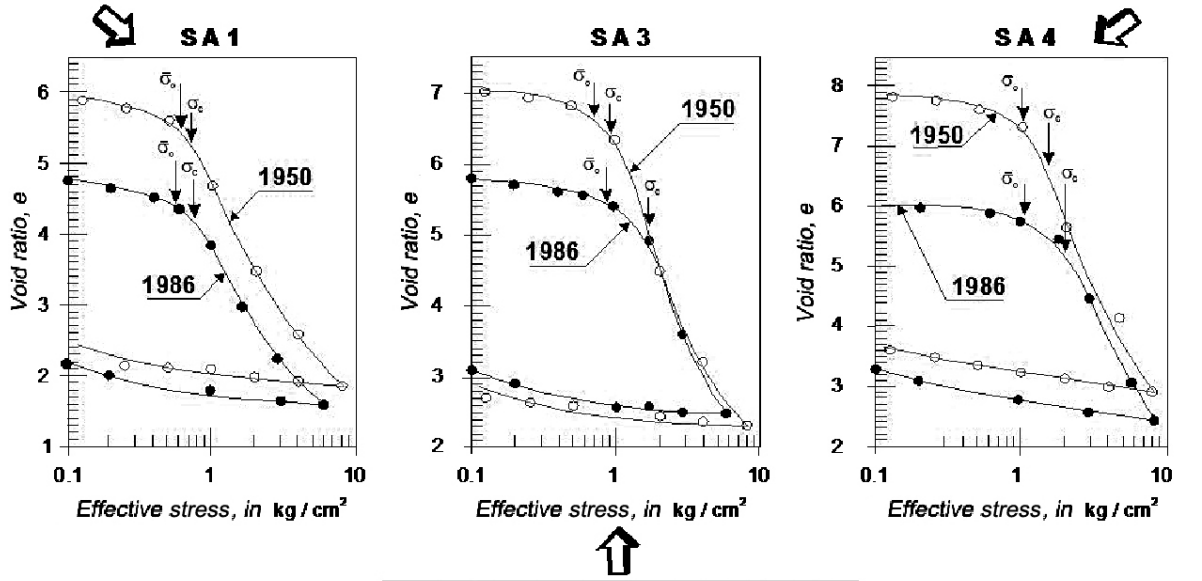

YEAR	Depth (m)	ω_i (%)	LL (%)	LP (%)	e_i	G_i (%)	$\bar{\sigma}_o$ kg/cm²	σ_c kg/cm²
1950	22.76	270	287	80	7.01	98	0.72	0.94
1986	21.87	262	290	85	5.82	102	0.85	1.60

Fig. 3 Comparison of compressibility curves of clay layers SA1, SA3, and SA4 at CUPJ, 1950 and 1986.

CONCLUSIONS

The analysed information from the PRJ and CUPJ sites demonstrates the evolution of water content, volumetric weight, compressibility and shear strength of the clays between 1950 and 1986.

The clay properties were modified by the aquifer exploitation effect on the piezometric pressure. In Mexico City it is impossible to talk about invariable geotechnical conditions. These conditions are modified as water is withdrawn from the aquifer. It was demonstrated that the change in water content, volumetric weight, compressibility and shear strength is lower in the surficial clay layers, and the effect is greater as the depth of the clay layer increases.

Although the dynamic parameters of soil (shear module, Young's dynamic modulus, and damping) are not included in this work, it could be inferred that they have also been modified.

REFERENCES

Marsal, R. & Mazari, M. (1959) The subsoil of Mexico City. Contribution to *First Pan-American Soil Mechanics and Foundation Engineering Conference*, Facultad de Ingeniería, UNAM, México. Re-edited (Spanish–English) in 1969.

Land Subsidence, Associated Hazards and the Role of Natural Resources Development
(Proceedings of EISOLS 2010, Querétaro, Mexico, 17–22 October 2010). IAHS Publ. 339, 2010.

Ground subsidence induced by backfill-mining of a nickel mine and development forecasts

F. S. MA, H. J. ZHAO, Y. M. ZHANG & J. GUO

Key Laboratory of Engineering Geomechanics, Institute of Geology and Geophysics, Chinese Academy of Sciences, PO Box 9825, Beijing 100029, China
zhaohaijun0823@126.com

Abstract Based on geological investigations and GPS monitoring data, this paper presents ground movement phenomena and characteristics for Jinchuan Nickel Mine, China. The results show that ground subsidence occurred with increasing mining depth. The greatest accumulated subsidence reached 1287.5 mm between 2001 and 2008, and 37 considerable fissures were found at the ground surface. By establishing a mining–geological model, and by applying a numerical computation method, a short-term forecast of rockmass movement is proposed. The results show that the rate of ground subsidence and deformation will intensify further, and the distribution of subsidence and degree of damage to the mine roadway and shaft induced by ground subsidence and deformation will also extend in the following several years.

Key words ground subsidence; rockmass movement; backfill mining; metal mine; forecast

INTRODUCTION

Ground movement induced by underground mining has been studied worldwide, including the changes in permeability in the ground movement area, the relation between movement of the earth's surface and mining engineering, the influence of proximate fault morphology, complete subsidence prediction and subsidence models (Holla & Buizen, 1991; Shu & Fleurisson, 1997; Xie *et al*., 1998; Sheorey *et al*., 2000; Cui *et al*., 2001; Dai *et al*., 2002). However, most of these phenomena are induced by long-wall mining or room-and-pillar mining methods, which is distinctly different from the cut-and-fill mining method.

The cemented backfill mining method, a kind of backfill mining method, has developed greatly in the last 30–40 years (Cowling 1998; Fall *et al*., 2005; Benzaazoua *et al*., 2008). It has been generally believed that backfill mining technology effectively controls ground pressure and prevents the occurrence of super-incumbent ground movement and fracture (Whittaker & Reddish, 1989; Singh & Saxena, 1991; Bell *et al*., 2000; Swift & Reddish, 2002). However, significant ground movement problems occurred in the Jinchuan Nickel Mine area described in this paper, which demonstrates that this method can still induce large-scale ground movement and even severe ground fissures.

This paper gives an introduction to the engineering geological characteristics, the phenomena of ground movement and ground fissures, induced by underground mining in Jinchuan nickel mine in China. Using the GPS monitoring data, the characteristics and laws of ground movement were analysed. Based on the mining–geological model and the application of a numerical computation method, a short-term forecast of rockmass movement is proposed.

GEOLOGICAL BACKGROUND AND MINING CONDITIONS

The No. 2 mine, which is the main mine with the largest yield in the Jinchuan Nickel Mine area, is 1.6 km long, 98 m wide on average, 200 m wide at its maximum, at 65–75° angle of inclination, and >1000 m in depth. It is a typical metal deposit with a steep inclination and very thick. The underhand cut-and-fill stoping method was adopted in the mining process. In order to increase mineral production, simultaneous mining downwards in two sublevels was carried out, i.e. sublevels at 1250 and 1150 m were mined at the same time, 50 000 m^2 with continual mining from 1981 to 1996, but no prominent rockmass movement, no filling mass slip or destruction occurred.

Copyright © 2010 IAHS Press

Since 1996, the mining depth varied from 500 to 700 m, the mining areas have been enlarged to about 100 000 m^2 , and the volume of up-filling mass has accumulated to about 8×10^6 m^3. The *in situ* stresses increased with the deepening of the mining depth, and the maximum principal stress tends to reach 45 MPa; *in situ* stress is 3–5 times higher than the rockmass strength.

GROUND MOVEMENT AND DEFORMATION PHENOMENA

After it had been mined using the cementing-backfill mining method for 18 years, evidence of ground movement appeared, and many fissures were apparent on the upper surface of the ore body by the end of 1999. So far, some important engineering facilities, such as shafts and tunnels, have been destroyed by ground deformation or rock mass movement. In 2005, one of the most important ventilating shafts, line no. 14 ventilating shaft in no. 2 mine, was destroyed by the increasing rock movement, which resulted in huge economic loss and serious safety problems.

So far, 37 considerable fissures distributed between exploratory line 6 and 26, are found in Jinchuan no. 2 mine, forming two, almost parallel fissure zones. Their extension directions are approximately the same as the strike of the ore body.

GPS MONITORING SYSTEM FOR GROUND MOVEMENT

GPS is an advanced monitoring technology which can be used to carry out a three-dimensional geodetic survey. At present, the GPS monitoring technology is widely used (Du & Teng, 2007; Psimoulis *et al*., 2007; Mentes, 2008; Samsonov *et al*., 2008).

In order to study the ground movement and deformation, GPS monitoring technology was introduced to Jinchuan Nickel Mine in 2001. Since then, dynamic monitoring has been carried out every 6 months.

The deformation monitoring net includes 100 GPS surveying points on the ground surface. As the GPS monitoring net is used for the deformation monitoring and needs higher precision, the monitoring plan was carried out according to higher level D. According to local specific conditions, the GPS receiver type (GPS receiver of Z-12 type made by Ashtech, USA) and optimization calculation method were used to eliminate or reduce the error. The results showed that the mean square error of the points is ±1.96 mm, which fully meets the monitoring needs.

REGULARITY OF GROUND MOVEMENT AND DEVELOPMENT FORECAST

Through multi-period GPS monitoring data from 2001 to 2008, we gained every monitoring point's horizontal displacement vector, settlement amount and three-dimensional displacement, which quantitatively described these surveying points' movement caused by the impact of underground mining. The general characteristics of ground surface movement were concluded as follows:

(a) Since 2001, almost all coordinates of the points have changed. The settlement is developing continuously with increasing mining depth, its shape approximates an ellipse; the largest accumulated subsidence reached 1287.5 mm between 2001 and 2008.
(b) Almost all the displacement vectors pointed at the underground goaf, which changed with the distance from the monitoring point to the centre of the settlement; the largest accumulated horizontal displacement reached 845.7 mm between 2001 and 2008.
(c) The centres of three-dimensional ground displacement and settlement are in substantial agreement. The largest accumulated displacement reached 1448.9 mm between 2001 and 2008.
(d) Under the long-term effect of underground mining, the long axis of the settlement is basically parallel to the strike of the ore body, it extends about 2.3 km along the exploratory line, and is about 1.5 km long along the strike of the ore body, throughout the whole mine area.

Because the sublevels at 1250 and 1150 m are mined simultaneously, there exists an additive effect of rock mass movement and deformation between the two mining goaf of the two sublevels, which is the main reason that the ground subsidence range and rate keep increasing continuously. By establishing a mining–geological model, and by applying a numerical computation method, a short-term forecast of rock mass movement is proposed. It shows that the rate of ground subsidence will reach a peak when the exploitation works are completed in the 1250 m sublevel (expected in 2012).

CONCLUSIONS

There is significant ground movement in the Jinchan Nickel Mine area; some important engineering facilities have been destroyed by ground deformation or rock mass movements. Thus, it indicates that the large-scale ground deformation could not be avoided absolutely, despite using the cut-and-fill mining method.

Because of the additive effect of rockmass movement and deformation between the two simultaneous mining sublevels, the ground subsidence range and rate keep increasing continuously, and will reach a peak when the exploitation works are complete in the 1250 m sublevel (expected in 2012). Therefore, before the end of 2012, the rate of ground subsidence and deformation will be further intensified, and its distribution and the degree of destruction of the mine roadway and shaft induced by ground subsidence and deformation, will also be extended.

Acknowledgements Grateful appreciation is expressed for funding from the Important Direction Project of Chinese Academy of Sciences Knowledge Innovation Project (KZCX2-YW-113), and NSFC project (40702048, 40972197).

REFERENCES

Bell, F. G., Stacey, T. G & Genske, D. D. (2000) Mining subsidence and its effect on the environment: some differing examples. *Environ. Geol.* **40**(1/2), 135–152.

Benzaazoua, M, Bussière, B, Demers, I, Aubertin, M, Fried, É & Blier, A. (2008) Integrated mine tailings management by combining environmental desulphurization and cemented paste backfill: application to mine Doyon, Quebec, Canada. *Miner. Engng* **21**(4), 330–340.

Cowling, R. (1998) Twenty-five years of mine filling: development and directions. In: *Sixth Int. Symp. on Mining with Backfill* (Brisbane, Australia), 3–10.

Cui, X. M., Wang, J. C & Liu, Y. S. (2001) Prediction of progressive surface subsidence above longwall coal mining using a time function. *Int. J. Rock Mech. Min.* **38**(7), 1057–1063.

Dai, H. Y., Wang, J. Z., Cai, M. F, Wu, L. X & Guo, Z. Z. (2002) Seam dip angel based mining subsidence model and its application. *Int. J. Rock Mech. Min.* **39**(1), 115–123.

Du, J. C. & Teng, H. C. (2007) 3D laser scanning and GPS technology for landslide earthwork volume estimation. *Automa. Constr*. **16**(5), 657–663.

Fall, M., Benzaazoua, M. & Ouellet, S. (2005) Experimental characterization of the influence of tailings fineness and density on the quality of cemented paste backfill. *Miner. Engng* **18**(1), 41–44.

Holla, L. & Buizen, M. (1991) The ground movement, strata fracturing and changes in permeability due to long wall mining. *Int. J. Rock Mech. Min. Sci. Geomech Abstr*. **28**(2/3), 207–217.

Mentes, G. (2008) Observation of recent tectonic movements by extensometers in the Pannonian Basin. *J. Geodyn.* **45**(4/5), 169–177.

Psimoulis, P., Ghilardi, M., Fouache, E. & Stiros, S. (2007) Subsidence and evolution of the Thessaloniki plain, Greece, based on historical leveling and GPS data. *Engng Geol*. **90**(1/2), 55–70.

Samsonov, S. V., Tiampo, K. F & Rundle, J. B. (2008) Application of DInSAR-GPS optimization for derivation of three-dimensional surface motion of the southern California region along the San Andreas Fault. *Comput. Geosci-UK* **34**(5), 503–514.

Shu, J. & Fleurisson, J. A. (1997) Relation between movenment of earth's surface and mining engineering. *China U. Min. Tec.* **26**(4), 30–33 (in Chinese).

Sheorey, P. R, Loui, J. P, Singh, K. B & Sing, S. K. (2000) Ground subsidence observations and a modified influence function method for complete subsidence prediction. *Int. J. Rock Mech. Min.* **37**(5), 801–818.

Singh, B. & Saxena, N. C. (1991). In: *Land Subsidence* (Int. symo. 11–15 December 1989), 51–66. A.A. Balkema, Rotterdam.

Swift, G. M. & Reddish, D. J. (2002) Stability problems associated with an abandoned ironstone mine. *Bull. Engng Geol. Environ.* **61**(3), 227–239.

Whittaker, B. N. & Reddish, D. J. (1989) *Subsidence Occurrence, Prediction and Control*. Elsevier, Amsterdam, 78–86.

Xie, H. P., Yu, G. M., Yang, L. & Zhou, H. W. (1998) The influence of proximate fault morphology on ground subsidence due to extraction. *Int. J. Rock Mech. Min.* **35**(8), 1107–1111.

Land Subsidence, Associated Hazards and the Role of Natural Resources Development
(Proceedings of EISOLS 2010, Querétaro, Mexico, 17–22 October 2010). IAHS Publ. 339, 2010.

Analysis of engineering land subsidence effects caused by shield construction for tunnels

YANG TIANLIANG[1,2], YAN XUEXIN[1], WANG HANMEI[1], ZHAN LONGXI[1], XU ZHUN[1] & ZHUANG YIBIN[1]

1 *Shanghai Institute of Geological Survey, Shanghai 200072 China*
sigs930@163.com
2 *Department of Geotechnical Engineering, Tongji University, Shanghai 200092, China*

Abstract Based on analysis of the mechanism of engineering land subsidence induced by shield construction for tunnels, the regularities and relationships of shield depth, formation loss rate, shield radius, soil properties and the impact scope of land subsidence, the largest settlement amount, were studied individually and thoroughly with the numerical analysis and mathematical fitting method. Moreover, quantitative relations among them were derived. Finally, a case study of shield construction was analysed and verified.

Key words engineering land subsidence; shield depth; shield radius; formation loss rate; soil properties; width coefficient

INTRODUCTION

Shanghai is one of the cities in which land subsidence was first discovered and its impacts are very prominent in China. There are two main reasons: first, the regional groundwater exploitation causes land subsidence, and second, pits, tunnels and other construction projects have resulted in land subsidence. At present, there are 13 subway lines under construction and operation, and their total length reaches more than 500 km. The metro transit network has formed and covered the whole urban region. Under the situation of large-scale subway tunnel construction, land subsidence problems induced by engineering construction would be inevitable. On the one hand, land subsidence would affect the security and stability of all tunnels; on the other hand, it would damage the environment and buildings around tunnels. When the impact scope and subsidence amount is larger, different subsidence problems of a lifeline project such as the metro could damage the urban area and its safety, and result in increasing difficulties for land subsidence control.

The basic cause of engineering land subsidence induced by shield construction was mainly formation loss under undrained conditions and disturbed soil layer consolidation. This paper analyses engineering land subsidence mechanics. It was found that the impact scope of engineering land subsidence and maximum subsidence amount were tightly related to factors such as shield depth, shield radius, formation loss rate and soil properties. The normal influence of land subsidence caused by shield construction can be found by analysis and research of relations between the major impact scope and land subsidence; this will provide technical evidence for impact evaluation and control of engineering land subsidence induced by shield construction.

MECHANICAL ANALYSIS OF ENGINEERING LAND SUBSIDENCE INDUCED BY SHIELD CONSTRUCTION

Shield construction of a tunnel will inevitably disturb the soil layer and result in land subsidence problems. In soft soil areas, formation loss induced by shield construction and manipulation of soil with disturbed or sheared reconsolidation, are essentially the causes of engineering land subsidence.

Formation loss

Formation loss is the value of the difference of the practical soil volume of the shield excavation and the completion tunnel capacity. The soil layer around the shield deforms in order to

compensate for formation loss, thus land subsidence occurs. The formation loss ratio is characterized by the parameters of formation loss. Construction and other reasons for formation loss are mainly as follows: (1) soil displacement at the excavated working face; (2) back-step of shield machine; (3) soil squeezed into the gap of the shield trail; (4) changing orientation of shield advance; (5) moving the obverse barrier of the shield; (6) soil friction and shearing caused by the shield shell moving; and (7) deformation of the tunnel liner.

Consolidation of disturbed soil

After soil around the tunnel is disturbed by shield construction, a pore water pressure area was formed. When the shield machine is driving, as the surface stress of the soil is released the pore water pressure around tunnel drops, due to pore water withdrawal, resulting in soil layer deformation and land subsidence. Moreover, the extrusion action of shield driving and the mudjack action of the shield tail form an overpressure of pore water around the soil layer. Some time after finishing tunnel shield construction, the pore water pressure is gradually released to cause soil water drainage and consolidation, thus land subsidence occurs.

Land subsidence induced by changing pore water pressure is called primary consolidation settlement. When a soil body is disturbed, the soil skeleton will be compressed and keep the continued deformation for a long time, which in land subsidence is called secondary consolidation settlement. Secondary consolidation subsidence of soft plastic and fluid-plastic clay soil with a larger pore ratio and sensitivity will continue for several years, and its proportion of the total settlement could be as high as 35%, or even more.

From the above analysis it is apparent that land subsidence caused by shield construction is closely related to factors such as formation loss rate, shield depth and shield radius through soil layer properties.

NUMERICAL ANALYSIS OF THE MAIN FACTORS OF LAND SUBSIDENCE CAUSED BY SHIELD CONSTRUCTION

The scope of soil displacement and land subsidence caused by shield method construction were derived based on the well-known Peck estimation method, or derivation formulas applied in specific geological conditions on the basis of the Peck formula. Most of those methods use the width coefficient as the characterization of land subsidence.

In order to analyse various factors influencing land subsidence, numerical calculation and mathematical fitting methods are used to analyse the effects of engineering land subsidence caused by the four important factors of shield construction: formation loss rate, shield depth, shield radius and shield through soil layer properties.

Shield depth impact on land subsidence

The depth of the shield has a significant impact on land subsidence caused by shield construction, and is the most critical factor.

It has been analysed by numerical calculation methods for shield construction at five different shield depths: 6 m, 10 m, 14 m, 18 m and 22 m. Moreover, the calculation results have been fitted, giving a correlation coefficient, r^2, of 0.976. Parameters of numerical calculation use common values of shield construction in soft soil areas; other calculation conditions are as follows: soil loss ratio of 2%, crossing the muddy clay layer, shield radius of 3.2m.

From Fig. 1, we can see the regulation of land subsidence impact due to shield depth during shield construction. As the shield depth increases, the width coefficient increases, and the scope of land subsidence also continues to expand. Thus we can obtain a relationship between shield depth and the width coefficient:

$$i = 1.4393H + 3.1025 \tag{1}$$

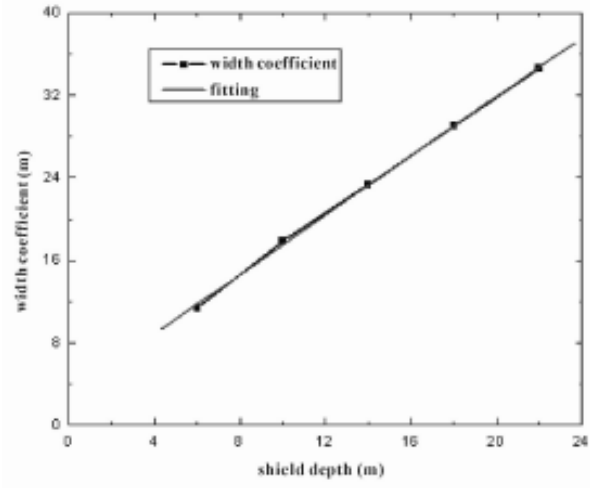

Fig. 1 Relation between shield depth and the width coefficient.

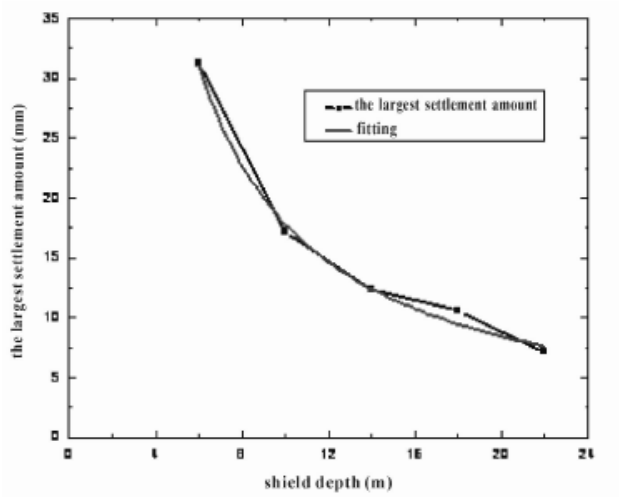

Fig. 2 Relation between shield depth and the largest settlement value.

where the units of i and H are metres, i is the distance of tunnel centre to the subsidence curve inflection point, and H is shield depth.

It is seen from Fig. 2 that different depths of shield impact on the maximum settlement amount. As the shield depth increases, the largest settlement amount is reduced accordingly.

According to the fitting results, the relationship of the maximum settlement amount and shield depth is as follows:

$$S_{\max} = 211.11H^{-1.0722} \tag{2}$$

Formation loss rate to the impact of land subsidence

The impact of formation loss rate on the impact of land subsidence is clear. Liu Jian-hang (1993) considered that the formation loss rate is too large when construction has been beyond the usual conditions and the Peck formula no longer applies. The author worked with the actual situation in the five kinds of soil loss rate: 1%, 2%, 3%, 4% and 5%. Other calculation conditions are as follows: shield centre depth of 10 m, through silt clay layer, shield radius of 3.2 m.

Figure 3 shows how the formation loss rate effects the coefficient of the width. As the formation loss rate increases, the coefficient of the width slightly decreases. This relationship of formation loss rate and the coefficient of the width is as follows:

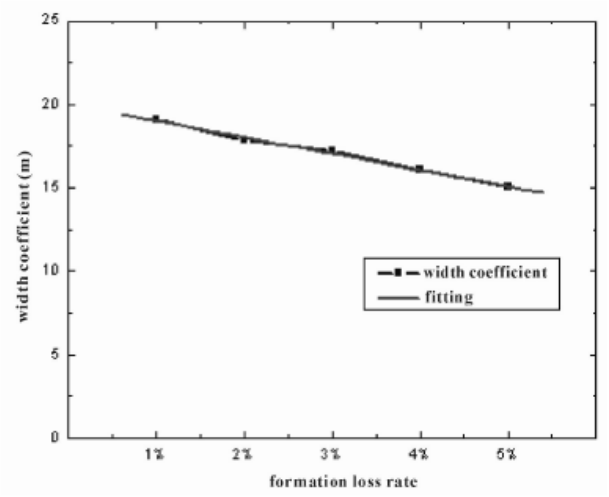

Fig. 3 Relation between soil loss rate and width coefficient.

$$i = -98.7H + 20.023 \tag{3}$$

It is seen from the fitting results of Fig. 4, that the formation loss rate would significantly affect the tunnel maximum settlement amount. As the formation loss rate increases, the maximum settlement grows rapidly. Thus the relationship of different formation loss rate and the maximum settlement amount is as follow:

$$S_{\max} = 5033.5H^{1.4211} \tag{4}$$

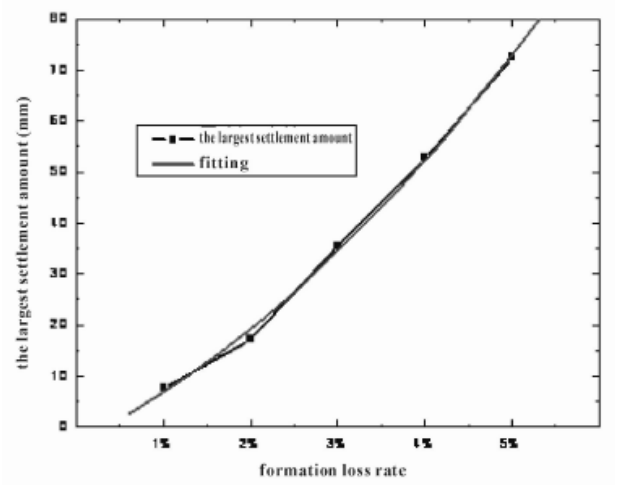

Fig. 4 Relation between soil loss rate and the largest settlement value.

Properties of shield through the soil to the impact of land subsidence

For tunnel excavation in soft soil areas, the shield through the soil layer is mainly responsible for the silty clay, sandy silt, sands. Across different types of soil layer have a significant impact to engineering land subsidence. In general, when other conditions are similar, shielding through the sandy layer will result in a larger settlement amount and width coefficient of the settlement trough than through clay.

Figure 5 shows the effect of land subsidence in the settlement trough when the shield crosses over three different types of soil layer such as the clay, sandy silt and sand. We assume the

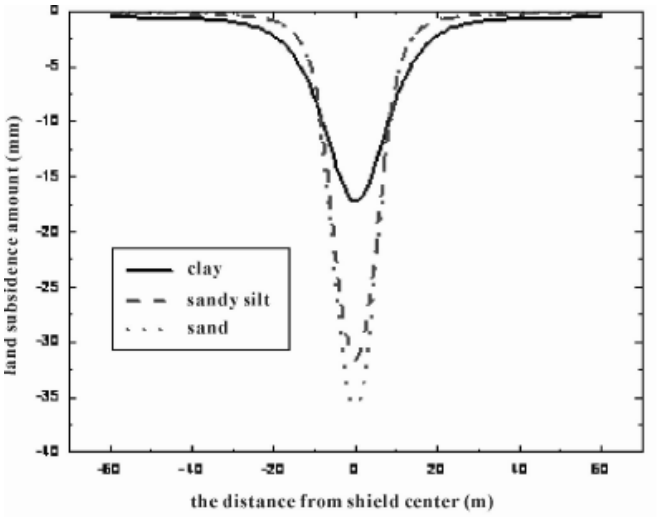

Fig. 5 Settlement trough curve of cross-over different soil layer.

Table 1 Comparison of settlement trough shape of cross-over different soil layer.

Soil property	Silty clay	Sandy silt	Sand
Width coefficient (m)	17.86	11.25	10.94
Maximum settlement value (mm)	17.21	31.65	35.88

calculation conditions are: formation loss rate of 2%, and the same shield depth of 10 m, and shield radius of 3.2 m. The width coefficient and the maximum settlement amount can been seen from Table 1 when shield construction crosses over these soil layers.

From Fig. 5 and Table 1, we can see some obvious different settlement effects due to a shield crossing through clay, sandy silt and sand. In the case of the shield crossing the clay, the width coefficient of the settlement trough is the largest, and the corresponding scope for land subsidence is also the largest, but the maximum settlement amount is the smallest. In the case of shield cross-over sandy silt and sand, the width coefficient of the settlement trough and the scope of land subsidence are smaller, but the maximum settlement amount is almost two times that for clay. It can be also seen that the properties of the shield cross-over soil layer are better, the impact scope of land subsidence is also smaller, yet the amount of the maximum settlement is larger.

Shield radius to the impact of land subsidence

At present, tunnel construction mainly uses the form of a single circular soil-pressure balance shield, a double round soil-pressure balance shield, and a mud-water balance shield crossing under the Yangtze River and Huangpu River. The radius of the soil-pressure balance shield is approximately 6.4 m (with the assumption that the foregoing conditions are basically the same), while the radius of the mud-water balance shield is even greater. For instance, the shield diameter for the ChongMing Yangtze River tunnel created a world record to reach 15.43 m. Four different radii of shield are analysed, as follows: the radius of ordinary single-round shield is 3.17 m, radius of the double round shield is 4.5 m which may be equivalent to a single circle radius, and radius of other shields similar to the ChongMing Yangtze River tunnel are 6 m and 7.5 m. Other calculation conditions are as follows: soil loss rate of 2%, through the silty clay, and shield centre depth of 10 m.

Figure 6 shows that the shield radius is an important impact factor on the width coefficient. With growth of shield radius, the width coefficient of the settlement trough gradually became larger. Moreover, the impact scope of land subsidence due to shield construction will continuously increase and become larger, thus we can obtain the relationship between shield radius and width coefficient as follows:

$$i = -15.62e^{\left(-\frac{H}{1.93}\right)} + 26.80 \tag{5}$$

We can see from Fig. 7, as the shield radius increases, the largest settlement amount of the settlement trough has also grown, thus the relationship of different shield radius and the largest settlement amount is as follows:

$$S_{\max} = 10.326H - 17.794 \tag{6}$$

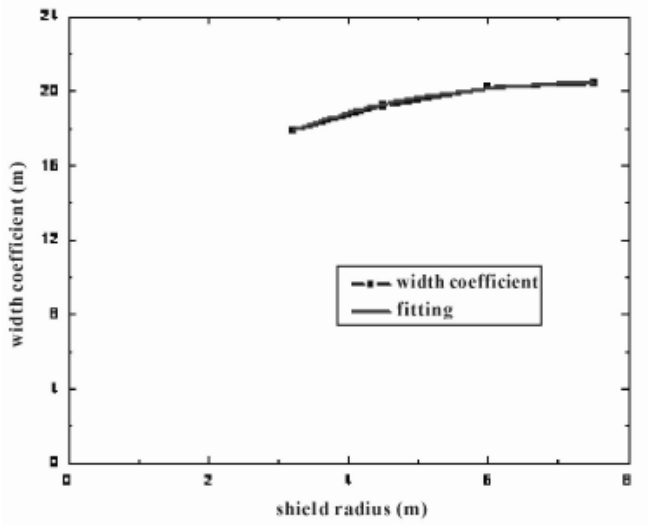

Fig. 6 Relation between shield radius and width coefficient of settlement trough.

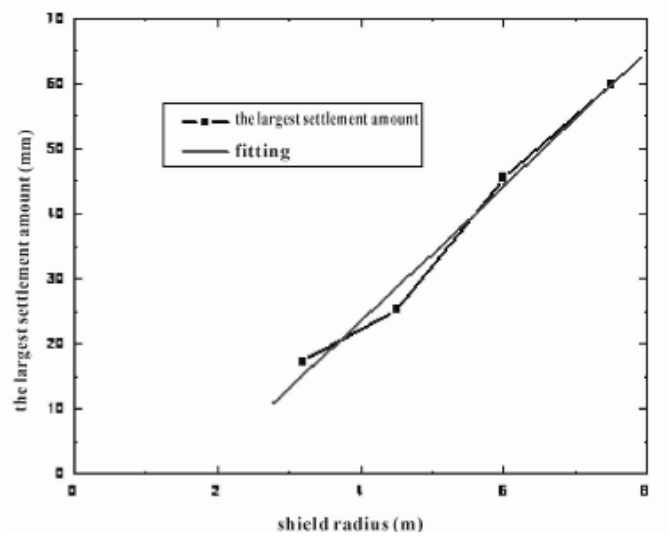

Fig. 7 Relation between shield radius and the largest settlement amount.

By the above analysis, we can draw the conclusion that land subsidence induced by shield construction is mainly derived from four key factors: i.e. formation loss rate, shield radius, shield depth and properties of shield across the soil layer. Moreover, using numerical fitting methods, the impact extent of these four factors on the width coefficient decreases in the order: properties through the soil layer, shield depth, shield radius and formation loss rate. Similarly, the impact extent of these four factors to the largest settlement amount decreases in the order: formation loss rate, properties through the soil layer, shield radius and shield depth.

PROJECTS

As a real case study, the construction of a subway tunnel in Shanghai is used. Land subsidence induced by the shield construction are studied and analysed by land subsidence monitoring and numerical simulation to verify the validity of the above calculation method.

The tunnel uses the method of double circular shield construction with the bottom depth of –12.921 m to –19.815m, and the measured depth of the shield centre section is about 15 m. The main layer the shield crosses is silt clay; the double circle is equivalent to a single round shield for calculation purposes, and the shield radius is 4.5 m. The physical and mechanical properties of various soil layers at the tunnel site are shown in Table 2.

Table 2 Physical and mechanic features parameters of soil layer

Layer code	Layer name	Depth (m)	Thickness (m)	Bulk density (kN/m^3)	Elastic modulus (MPa)	Poisson ratio	Cohesion (kPa)	Angle of internal friction (°)
①	fill	2	2	18				
②1	silty clay	3	1	18.8	5.92	0.35	14	20.5
②3	sandy silt	6	3	18.3	7.40	0.35	5	30.5
③	muddy silty clay	10	4	17.6	2.97	0.40	9	13
④	muddy clay	16	6	16.7	2.18	0.40	11	11
$⑤_{1\text{-}1}$	clay	20	4	17.4	3.02	0.35	13	13
$⑤_{1\text{-}t}$	sandy silt	28	8	18.3	6.89	0.35	7	28.5
$⑤_2$	clayey silt interlayer silty clay	60	32	18.1	6.35	0.35	8	27

To measure the land subsidence caused by shield construction, the two horizontal subsidence monitoring profiles are planned with monitoring point spacing of 5.0 m in the axis on both sides of the tunnel.

Contrasting curves from the experimental monitoring, numerical calculations and fitting can be seen in Fig. 8. The conditions of the numerical calculation are with a formation loss rate of 3%, and give a fitting correlation coefficient of 0.9724. By comparative analysis of the results of monitoring and numerical calculation of land subsidence, this calculation model can be applied in evaluating land subsidence induced by shield construction in soft soil areas such as Shanghai city.

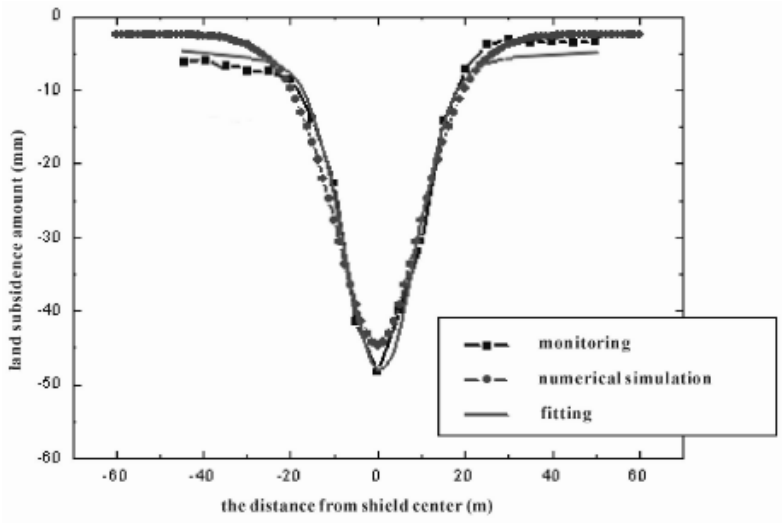

Fig. 8 Comparison curve of actual measurements, numerical calculation and fitting of land subsidence induced by shield construction

CONCLUSION

1 In the soft soil area, formation loss induced by shield construction and reconsolidation of disturbed or sheared soil were the essential reason for engineering land subsidence.
2 Engineering land subsidence caused by shield construction is mainly derived from the four important factors of shield construction: formation loss rate, shield depth, shield radius and properties of shield across soil layer.
3 As the shield depth increases, the width coefficient also increases, and the scope of land subsidence also continues to expand.
4 As the formation rate of loss increases, the coefficient of the width slightly decreases, while the maximum amount of settlement trough will rapidly grow.
5 In case of shield cross-over clay, the width coefficient of the settlement trough is the largest, and the corresponding scope of land subsidence is also the largest, but the maximum settlement amount is the smallest. In case of shield cross-over sandy silt and sand, the width coefficient of the settlement trough and the scope of land subsidence are smaller, yet the maximum settlement amount is almost twice that for shield cross-over clay. It can be seen that as the properties of the shield cross-over soil layer are better, the impact scope of land subsidence is also smaller, yet the amount of the maximum settlement is larger.
6 The shield radius is an important impact factor of width coefficient. With growth of shield radius, the width coefficient of the settlement trough gradually becomes larger. Moreover, the impact scope of land subsidence due to shield construction will continuously increase and become larger.
7 Land subsidence induced by shield construction is mainly derived from four key factors: formation loss rate, shield radius, shield depth and properties of shield across the soil layer. Using a numerical fitting method, the extent of the impact of these four factors on the width coefficient was found to decrease in the order: properties through the soil, shield depth, shield radius, formation loss rate. Similarly, the impact extent of these four factors on the largest settlement value decreases: formation loss rate, properties through the soil, shield radius and shield depth.
8 By a comparative analysis to the results of monitoring and numerical calculation of land subsidence, this calculation model can be applied in evaluating engineering land subsidence induced by shield construction in soft soil areas.

Acknowledgements The study was supported by a cooperative project of the Shanghai Municipal Government and the Ministry of Land and Resources, P.R. China, and funded by the Shanghai Construction and Traffic Commission.

4 Monitoring Techniques of Ground Displacements and Subsurface Deformation

Land Subsidence, Associated Hazards and the Role of Natural Resources Development
(Proceedings of EISOLS 2010, Querétaro, Mexico, 17–22 October 2010). IAHS Publ. 339, 2010.

Advanced monitoring techniques for mapping land displacement on the Venice coastland with satellite SAR data

T. STROZZI[1], L. TOSI[2], P. TEATINI[2,3], U. WEGMÜLLER[1], M. SANTORO[1] & L. CARBOGNIN[2]

1 *Gamma Remote Sensing, Worbstrasse 225, 3073 Gümligen (Bern), Switzerland*
strozzi@gamma-rs.ch

2 *Institute of Marine Sciences, National Research Council, Castello 1364/a, I-30122 Venezia, Italy*

3 *Dept. of Mathematical Methods and Models for Scientific Applications, University of Padova, via Trieste 63, I-35121 Padova, Italy.*

Abstract In this contribution we review the monitoring techniques applied during the last 20 years in the Venice coastland for the control of land subsidence, with particular emphasis on satellite Synthetic Aperture Radar (SAR) interferometry using images acquired by the ERS-1/2, ENVISAT and TerraSAR-X sensors.

Key words monitoring; SAR interferometry; land subsidence; lagoon environment; Venice

INTRODUCTION

The city of Venice and its lagoon represent an extraordinary environment and human heritage which are susceptible to loss in surface elevation relative to the mean sea level. The lagoon covers an area of about 550 km^2 with shallows, tidal flats, salt marshes, islands, in part urbanized, and a network of channels. A complex combination of natural processes and human intervention such as land subsidence, eustacy, river diversions, and inlet and channel dredging contributed to its evolution (Tosi *et al*., 2009). Land subsidence due to groundwater withdrawals, mainly performed during the 1950s and 1960s, has represented one of the most serious environmental problems for Venice and its Lagoon during the last decades. Since the 1970s, the regulation of groundwater withdrawal reduced land subsidence to natural rates of less than 0.5 mm/year (Bortolami *et al*., 1984; Tosi *et al*., 2002; Brambati *et al*., 2003), but the induced process finally caused 10 cm of sinking in the city (Carbognin *et al*., 2004). At the same time, over the 20th century and up to now, the sea level has been rising in the Upper Adriatic by about 1.2 mm/year (Carbognin *et al*., 2009). A 25-cm land elevation loss occurred from the beginning of the last century until today, consisting of about 12 cm of land subsidence and 13 cm of sea level rise, changed the relationship between land and water and contributed to a more than seven-fold increase of flooding events, causing great inconvenience for the population and enormous damage to the cultural heritage.

The past relative sea level rise has required a number of solutions to protect the lagoon urban centres from flooding. Starting at the beginning of the 1990s, the littoral islands were reinforced, the coastal protections stabilized and the sidewalks along the canals elevated by 50 cm in the lowest Venice areas. In addition, rows of mobile gates (the MoSE. protective system) to close the three lagoon inlets of Lido, Malamocco and Chioggia when the Adriatic tide achieves 110 cm above the official Italian datum, are currently in construction. Besides building protection measures against flooding, high importance has been put into the control of land subsidence. Mapping of land displacement in the Venice coastland, traditionally carried out by high precision levelling, has, since the 1990s, taken advantage of differential and continuous GPS surveys and satellite SAR interferometry, which complement well within an integrated monitoring system.

INTERFEROMETRIC PROCESSING OF MULTIPLE SAR ACQUISITIONS

Techniques involving the interferometric processing of multiple satellite SAR acquisitions, i.e. Persistent Scatterer Interferometry (Ferretti *et al*., 2001; Wegmüller *et al*., 2004), were found very effective for the detection of land displacement in the Venice coastal environment. Indeed,

Copyright © 2010 IAHS Press

application of SAR interferometry is limited by temporal decorrelation and inhomogeneities in the tropospheric path delay and only selected pixels that are persistent over an extended observation time period can be analysed. Through the use of multiple SAR scenes errors resulting from atmospheric artefacts are reduced and a higher accuracy can be achieved. Over urban areas or in regions where isolated man made structures (e.g. houses, masts, barriers) are available, it is possible to estimate the progressive deformation of the terrain in the satellite line-of-sight direction.

In our interferometric point target analysis the selection of candidate point targets is based on the temporal mean-to-standard deviation ratio of the co-registered SAR intensity images and the spectral correlation averaged over the single look complex stack. Interferometric processing is performed on an ellipsoidal model without any digital elevation model, because the area is flat. An initial two-dimensional linear regression is applied on the candidate point targets to solve simultaneously for the height and deformation rate of a point relative to another point after solving the 2π phase ambiguity in the temporal domain. Only pairs of points with a high regression standard deviation are first retained. Neighbouring patches of the dimension of a couple of kilometres are considered iteratively. After differential interferometry, phase unwrapping errors are corrected on the spatial domain using a minimum cost–flow algorithm for sparse data. Then, with consideration of the initial height and deformation estimates, the residual phase images containing the atmospheric phase, nonlinear deformation, and error terms, are interpolated to the initial list of point targets and the two-dimensional linear regression with respect to height and deformation rate is performed again with respect to a reference point. This iteration is repeated various times to include as many points as possible, because the quality of potential additional points can be evaluated more reliably if the improved model for the validated points is available. With reliable unwrapped phase images available for all interferometric pairs, the baselines are refined with a least-squares approach based on the unwrapped phases, the corresponding point heights, and measurements from the continuous GPS stations of Chioggia, Venice and Cavallino. Analysis with orbit information and models is not sufficient to prevent observing a phase tilt along the point interferograms. As a final step, the discrimination of atmospheric phase, nonlinear deformation, and error terms is based on their differing spatial and temporal dependencies. The atmospheric path delay is assumed to be correlated on a spatial window of 0.5 km to 1.0 km size, but independent from pass to pass. The nonlinear deformation is assumed in general to be spatially high-pass and temporally low-pass. The phase noise is random in both spatial and temporal dimensions.

ERS-1/2 AND ENVISAT INTERFEROMETRIC POINT TARGET ANALYSIS

Interferometric point target analysis was applied on ERS-1/2 and ENVISAT SAR images for the time periods 1992–2005 and 2003–2009, respectively (Teatini *et al*., 2010). An original integrated monitoring method was designed to infer an accurate and reliable figure of regional land displacements (Teatini *et al*., 2005) by integrating ERS-1/2 and ENVISAT SAR interferometry with spirit levelling and differential and continuous GPS. The integrated monitoring system overcomes the limits characterizing each technique and has been used over the past two decades to provide a new image of the land displacements in the Venice region with a resolution never obtained before. As shown in Fig. 1, the results suggest that the central lagoon, including the city of Venice, is generally stable, while the northern and southern lagoon extremities and their related catchment's sectors sink with rates averaging 3 to 10 mm/year. The observed land displacements have been associated with the regional geological features of the Veneto coastland, i.e. tectonics, seismicity, differential consolidation of the middle–upper Pleistocene and Holocene deposits, and to local anthropogenic activities, such as land reclamation and groundwater withdrawal (Tosi *et al*., 2010).

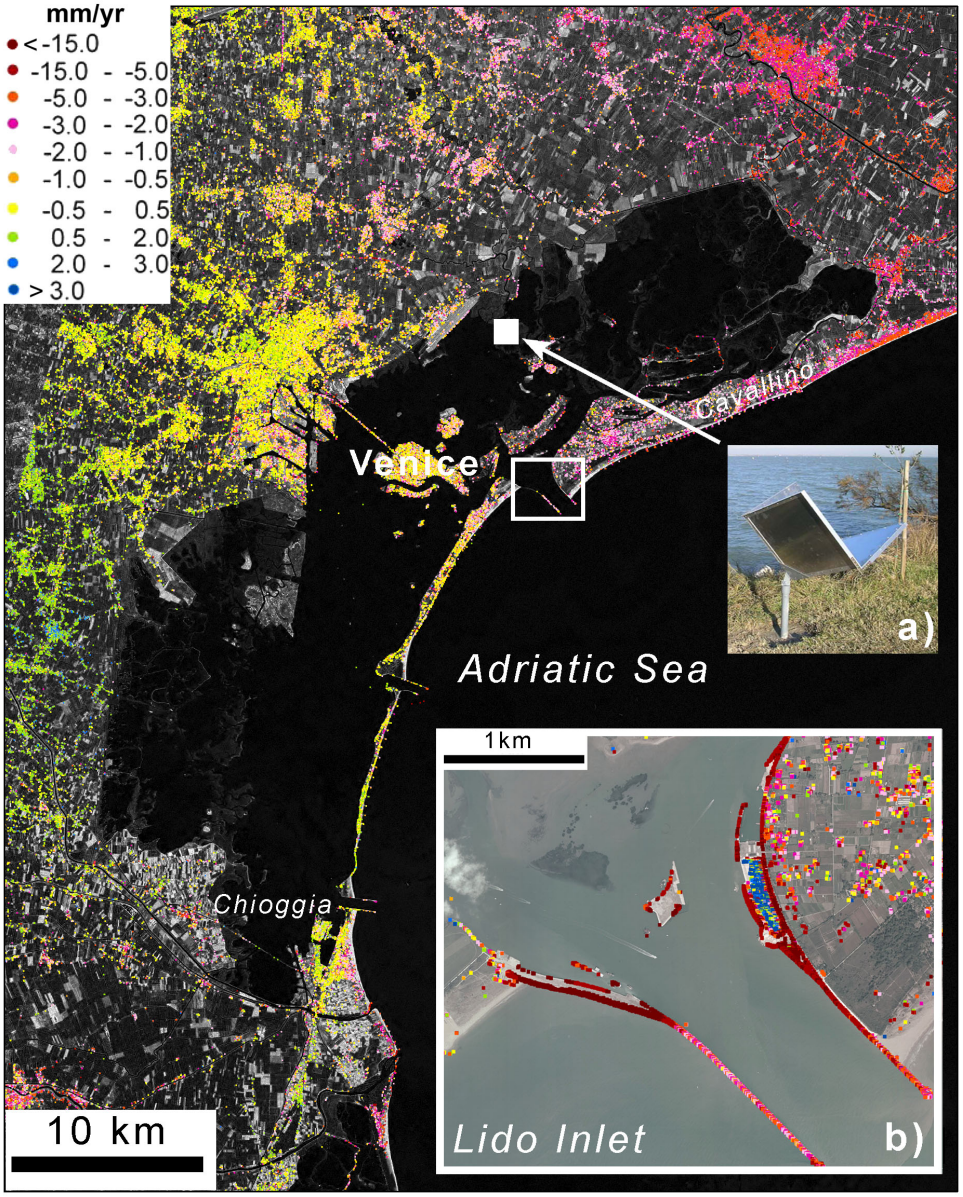

Fig. 1 Mean displacement rates between April 2003 and November 2007 from ENVISAT ASAR interferometry. Inset (a) shows one TCR. Inset (b) presents the mean displacement rates between March 2008 and January 2009 from TerraSAR-X interferometry at the Lido inlet. Movements are in the satellite line-of-sight direction, negative values indicate settlement, positive mean uplift.

In Venice and in the other small urban centres of the lagoon, several thousands of targets with measurable displacement information are detected. The measurements confirm the present general stability of the historical centre but also highlight that small areas of the city (like Sant'Elena to the east and the central part of the Giudecca island) and several single buildings subside at a rate of up to 3 mm/year (Teatini *et al*., 2010). Along parts of the littorals the displacement rates measured for the two periods 1992–2002 and 2003–2007 differ significantly as a consequence of a series of safeguard interventions that have been realized during the 1990s to reduce the beach erosion. The consolidation of the shallow subsoil due to the superficial load of the construction works is responsible for the 2–3 mm/year subsidence rates observed with the ERS-1/2 images. A detailed analysis of the SAR-based time series (Teatini *et al*., 2007) showed in addition that the vertical component of the measured displacements is normally a superposition of a short timescale,

generally seasonal, movement on the order of 1 cm that is likely related to the fluctuation of environmental variables (temperature, piezometric head in the aquifer system underlying the lagoon, sea/lagoon water level) and a long-term ground deformation associated with building construction, the geomorphology of the area, and human development of the natural resources.

TERRASAR-X INTERFEROMETRIC POINT TARGET ANALYSIS

Since 2007, new satellites operate SAR systems with a ground spatial resolution of about 3 m in stripmap mode, a wavelength of 3.11 cm (X-band), and repeat cycles of 10 to 16 days. These characteristics open new perspectives in the mapping of land subsidence from satellite SAR sensors at very high spatial and temporal resolutions. We applied interferometric point target analysis on a stack of 30 TerraSAR-X stripmap images acquired between 5 March 2008 and 29 January 2009 covering a large part of the Venice Lagoon, including the three inlets (Strozzi *et al*., 2009a). TerraSAR-X interferometry on persistent targets permitted, in particular, detection of significant local settlements on the order of a few centimetres at the three inlets connecting the Adriatic Sea to the inner water body induced by the construction works of the series of mobile barriers (see Inset a of Fig. 1). However, the high settlement rates are essentially restricted to the structures under construction or reinforcement and the present effects of the mobile barriers' works on the Venice littoral stability are generally negligible.

In Venice more than 162 000 point targets with valuable displacement information have been detected using TerraSAR-X interferometry. The substantial stability of the city as a whole reflects an average gradient on the order of 0.1×10^{-5} (Gambolati *et al*., 2009). However, detailed investigations reveal that important differential displacements, most likely due to superficial loads and a possible heterogeneity of the upper Holocene deposits the city is founded on, are occurring at the scale of few adjacent buildings, i.e. over a few tens of metres. Settlement rates larger than 10 mm/year over restricted areas cause differential displacements amounting up to as much as 100×10^{-5}.

SAR INTERFEROMETRY ON TRIHEDRAL CORNER REFLECTORS

Because within the inner lagoon anthropogenic structures are completely lacking, or only a few constructions – such as bridges, buildings, fish farm levees, jetties – are scattered at a distance from one to another too large to reliably resolve the radar phase ambiguity, a network of Trihedral Corner Reflectors (TCR) was established. A total of 58 TCR were installed before the summer of 2007 and analysed with ENVISAT and TerraSAR-X data (Strozzi *et al*., 2009b). An optimal TCR network has been established, taking into account the location of "natural" point targets in ERS and ENVISAT SAR interferometric analyses and keeping to a value of about 1 km the maximum distance between the TCR or between an "artificial" and the adjacent "natural" reflectors. The TCR are characterized by a 60-cm long edge, made of aluminium to reduce their weight, placed in areas without any other strong scatterer, and installed with foundations of a range of different depths, but at the same height above ground in order to study possible differences in their relative settlement (see inset (b) of Fig. 1). Salt marshes are constantly visible, except when the tide rises. The TCR, usually installed at a height of 1 m above the mean sea level, are therefore constantly outside the water.

SAR interferometry on the TCR was performed by taking into account their height determined during the installation, and the atmospheric and orbital effects, by the point target analysis on natural targets. By doing this we keep in mind that in the case of strongly varying regional atmospheric conditions – as observed in summer particularly – the interpolation in areas without natural reflectors may be quite inaccurate. This problem is particularly severe in the case of ENVISAT. For TerraSAR-X, on the other hand, the density of natural point targets in the lagoon is remarkable. In addition, because when the acquisition of TerraSAR-X started most of the TCR were already installed, the solution of most of the TCR is already included into the global

interferometric point target analysis. After having applied the atmospheric corrections, the same reference point used for the global interferometric point target analysis can also be considered for the TCR. We found that most of the TCR are stable and only in a few examples – one of those presented in Fig 2(a) – a clear subsidence trend was observed in the time series of displacement. Analysis of these movements on the basis of the local stratigraphic setting and climate conditions is ongoing.

DEM GENERATION USING ERS–ENVISAT INTERFEROMETRY

Space-borne SAR interferometry is also one possible method for the generation of Digital Elevation Models (DEM). ERS2 and ENVISAT operate in identical orbits at slightly different sensor frequencies with ENVISAT preceding ERS2 by 28 minutes. This configuration offers a unique opportunity to apply ERS2-ENVISAT SAR interferometry with a long 1.5–2.5 km baseline for the generation of DEMs in relatively flat rural areas. As shown in Fig. 2(b) ERS2–ENVISAT interferometry was applied to produce a DEM of the farmland bounding the Venice Lagoon (Wegmüller *et al*., 2009). Validation with GPS surveys indicate an accuracy of 0.2–0.3 m. Comparison with DEMs produced in the 1980s by classical methodologies, allowed us, for instance, to map the settlement of the peatlands located in the area.

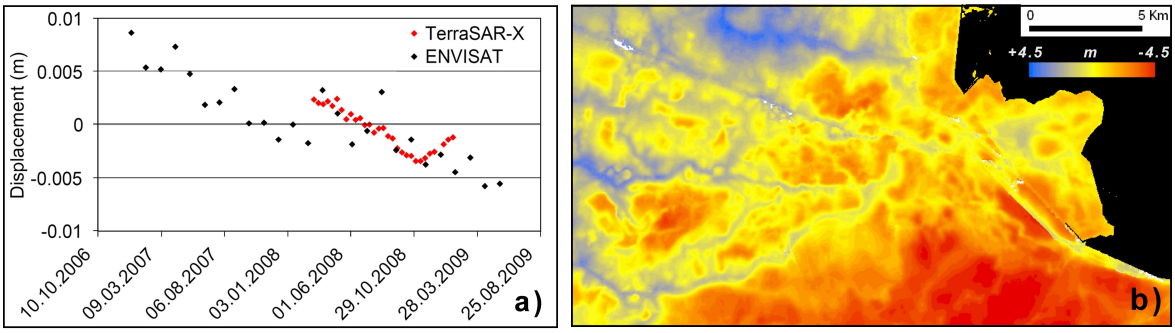

Fig. 2 (a) Example of time series of displacements for on TCR. (b) ERS-ENVISAT cross-interferometry DEM of the farmland bounding the southern Venice Lagoon. The SAR images were acquired on 7 November 2007 with a time interval of 28 minutes, a perpendicular baseline of 2002 m, and a difference of the Doppler Centroids of 817 Hz.

OUTLOOK

Understanding and control of land subsidence in the Venice coastland during the last 20 years has taken full advantage of satellite SAR interferometry. At the end of 2010 the current excellent SAR interferometry capabilities of ENVISAT will terminate, because the satellite on-board hydrazine will be almost completely consumed, and a modification of the orbital parameters will be necessary. Integration of past ERS-1/2 and ENVISAT data into large regional studies is one of our future lines of research. An investigation aimed at mapping the vertical displacements recorded around the year 2000 on the 20–30 km wide, 250-km long coastal area from the Tagliamento River northward of Venice and the Marecchia River to the south of Ravenna is ongoing (Bitelli *et al*., 2010).

The use of SAR interferometry on images acquired by very-high resolution X-band radar satellites, like the German TerraSAR-X and the Italian Cosmo-SkyMed missions, allows for a quasi real-time control of ground movements with an unprecedented observed level of detail. This also opens, in the Venice coastland region, new perspectives to geodynamic research and civil engineering sectors for the monitoring of large infrastructures with potential vulnerability to terrain motion.

Our TCR measurements allowed us for the first time to assess the displacements of salt marshes and tidal flats in a lagoon environment. We plan to continue the analysis and interpretation of these data and to set up additional networks of TCR.

Other attractive satellite SAR data are provided by ALOS PALSAR. L-Band interferometry has the capability to complement the existing applications based on C-band, because of its capacity to penetrate the vegetation canopy, and thus to achieve high coherence interferograms over vegetated areas (Strozzi *et al*., 2003). This raises expectations for more complete results over parts of the Po River delta where subsidence rates of more than 1 cm/year are recorded. Finally, in 2012 ESA is planning to launch its new SAR sensor on board of the Sentinel-1 satellite. With a repeat time interval of 12 days and swath width of 250 km this sensor is ideal for routine subsidence monitoring over large coastland areas.

REFERENCES

Brambati, A., Carbognin, L., Quaia, T., Teatini, P. & Tosi, L. (2003) The lagoon of Venice: geological setting, evolution and land subsidence. *Episodes* **26**(3), 264−268.

Bitelli, G., Bonsignore, F., Carbognin, L., Ferretti, A., Strozzi, T., Teatini, P., Tosi, L., & Vitturi, L. (2010) Radar interferometry-based mapping of the present land subsidence in the lowlying northern Adriatic coastland, Italy. In: *Land Subsidence, Associated Hazards and the Role of Natural Resources Development* (Proceedings of EISOLS 2010, Querétaro, Mexico, 17–22 October 2010). IAHS Publ. 339.(this volume).

Bortolami, G., Carbognin, L. & Gatto, P. (1985) The natural subsidence in the Lagoon of Venice, Italy. In: *Land Subsidence* (ed. by A. I. Johnson, L. Carbognin & L. Ubertini) (Proc. 3rd Int. Symp. on Land Subsidence), 777–785. IAHS Publ. 151, IAHS Press, Wallingford, UK.

Carbognin, L., Teatini, P., & Tosi, L. (2004). Eustacy and land subsidence in the Venice Lagoon at the beginning of the new millennium. *J. Marine Systems* **51**(1-4), 345−353.

Carbognin, L., Teatini, P., Tomasin, A. & Tosi, L. (2009) Global change and relative sea level rise at Venice: What impact in term of flooding. *Climate Dynamics*, doi:10.1007/s00382-009-0617-5.

Ferretti, A., Prati, C. & Rocca, F. (2001) Permanent scatterers in SAR interferometry. *IEEE Trans. Geosci. Remote Sensing* **39**(1), 8–20.

Gambolati, G., Teatini, P., Ferronato, M., Strozzi, T., Tosi, L. & Putti, M. (2009) On the uniformity of anthropogenic Venice uplift. *Terra Nova* **21**(6), 467–473, 10.1111/j.1365-3121.2009.00903.x.

Teatini, P., Tosi, L., Strozzi, T., Carbognin, L., Wegmüller, U. & Rizzetto, F. (2005) Mapping regional land displacements in the Venice Coastland by an integrated monitoring system. *Remote Sensing Environ.* **98**, 403–413, doi:10.1016/j.rse.2005.08.002.

Teatini, P., Strozzi, T., Tosi, L., Wegmüller, U., Werner, C. & Carbognin, L. (2007) Assessing short- and long-time displacements in the Venice coastland by synthetic aperture radar interferometric point target analysis. *J. Geophys. Res.* **112**, F01012, doi:10.1029/2006JF000656.

Teatini, P., Tosi, L., Strozzi, T., Carbognin, L., Cecconi, G., Rosselli, R. & Libardo, S. (2010) Resolving land subsidence within the Venice Lagoon by persistent scatterer SAR interferometry. *J. Phys. Chem. Earth*, doi:10.1016/j.pce.2010.01.002.

Tosi, L., Carbognin, L., Teatini, P., Strozzi, T. & Wegmüller, U. (2002) Evidence of the present relative land stability of Venice, Italy, from land, sea, and space observations. *Geophys. Res. Lett.* **29**(12), 1562, doi:10.1029/2001GL013211.

Tosi, L., Rizzetto, F., Zecchin, M., Brancolini, G. & Baradello, L. (2009) Morphostratigraphic framework of the Venice Lagoon (Italy) by very shallow water VHRS surveys: evidence of radical changes triggered by human-induced river diversion. *Geophys. Res. Lett*. **36**, L09406, doi:10.1029/2008GL037136.

Tosi, L., Teatini, P., Strozzi, T., Carbognin, T., Brancolini, G., & Rizzetto, F. (2010) Ground surface dynamics in the northern Adriatic coastland over the last two decades. *Rend. Fis. Acc. Lincei* doi:10.1007/s12210-010-0084-2.

Strozzi, T., Wegmüller, U., Werner, C., Wiesmann, A. & Spreckels, V. (2003) JERS SAR interferometry for land subsidence monitoring. *IEEE Trans. Geosci. Remote Sensing* **41**(7), 1702–1708.

Strozzi T., Teatini, P. & Tosi, L. (2009a) TerraSAR-X reveals the impact of the mobile barrier works on Venice coastland stability. *Remote Sensing Environ*. **113**, 2682–2688, doi:10.1016/j.rse.2009.08.00.

Strozzi, T., Tosi, L., Teatini, P., Werner, C. & Wegmüller, U. (2009b) Monitoring land subsidence within the Venice Lagoon with SAR interferometry on trihedral corner reflectors. Proceedings of IGARSS 2009, Cape Town, South Africa, 13–17 July 2009.

Wegmüller, U., Werner, C., Strozzi, T. & Wiesmann, A. (2004) Multitemporal interferometric point target analysis. In: *Analysis of Multi-temporal Remote Sensing Images* (ed. by P. Smits & L. Bruzzone), 136−144. Remote Sensing Series, vol. 3. World Science, Hoboken, New Jersey, USA.

Wegmüller, U., Santoro, M., Werner, C., Strozzi, T., Wiesmann, A. & Lengert, W. (2009) DEM generation using ERS-ENVISAT interferometry. *J. Appl. Geophys*. **69**, 51–58, doi:10.1016/j.jappgeo.2009.04.002.

(Proceedings of EISOLS 2010, Querétaro, Mexico, 17–22 October 2010). IAHS Publ. 339, 2010.

Subsidence and fault hazard maps using PSI and permanent GPS networks in central Mexico

E. CABRAL-CANO[1], B. OSMANOGLU[2], T. DIXON[2], S. WDOWINSKI[2], C. DEMETS[3], F. CIGNA[4] & O. DÍAZ-MOLINA[1]

1 *Departamento de Geomagnetismo y Exploración, Instituto de Geofísica, Universidad Nacional Autónoma de México, Ciudad Universitaria, México D.F. 04510, México*
ecabral@geofisica.unam.mx

2 *Rosenstiel School of Marine and Atmospheric Science, University of Miami, 4600 Rickenbacker Cswy, Miami, Florida 33149, USA*

3 *Department of Geoscience, University of Wisconsin-Madison, 1215 Dayton, Madison, Wisconsin 53706, USA*

4 *Earth Sciences Department, University of Firenze, Via La Pira 4, I-50121, Firenze, Italy*

Abstract We present an example of an integrated displacement and horizontal subsidence gradient analysis derived from an ENVISAT-ASAR Persistent Scatterer interferometric analysis. The study area is the southeastern sector of the Mexico City Metropolitan Area that includes Iztapalapa, Ciudad Nezahualcoyotl and Chalco. Correlation of surface faulting gathered from direct field evidence and spatial distribution of subsidence show that the principal factor for constraining hazardous areas is best determined not by solely using the subsidence magnitude rates, but rather by using a horizontal subsidence gradient analysis. This analysis can then be used as the basis for subsidence and fault hazard mapping.

Key words InSAR; subsidence; fault; Chalco, Iztapalapa, Mexico

INTRODUCTION

Mexico City's subsidence has been documented since over a century ago, after the first well battery was drilled to supply water to the rapidly growing city at the end of the 19th century (Cabral-Cano *et al*., 2008 and references therein). The consequences of the subsidence process are costly but the economic impact of subsidence in urban areas is hard to assess due to the fact that their costs are generally factored into yearly maintenance budgets rather than accounting for them as a unique natural disaster. It has thus become increasingly important to assess the extent and magnitude of damage in rapidly subsiding urban environments. This study describes the generation of hazard maps obtained from a horizontal subsidence gradient analysis using Persistent Scatterers InSAR (Synthetic Aperture Radar Interferometry) and continuously operating GPS data sets in the southeastern sector of the Mexico City Metropolitan Area (MCMA), which includes Iztapalapa, Ciudad Nezahualcoyotl and Chalco.

APPROACH

We present an example of a remote sensing approach using available ENVISAT-ASAR (Advanced SAR) archive data to create integrated displacement and horizontal subsidence gradient maps from Persistent Scatterer InSAR (PSI). This analysis can be used as the basis for a high spatial resolution subsidence and fault hazard zonation.

Satellite geodesy

Twenty-three ENVISAT-ASAR scenes acquired between 16 January 2004 and 14 August 2006 were used to generate interferograms with the Delft Object-oriented Radar Interferometry Software (DORIS; Kampes & Usai, 1999). Precise orbits from the Delft Institute were used to minimize orbital errors (Scharroo & Visser, 1998). The 29 July 2005 acquisition was selected as the master scene to minimize the effects of spatial and temporal baselines. The study area was cropped from each SAR scene acquisition and oversampled by a factor of two in range and

Copyright © 2010 IAHS Press

azimuth to avoid under-sampling of the interferogram, especially during resampling of the slave acquisition. Further processing included stacking of interferograms relative to a single master image, a selection of strong scatterers visible in all interferograms and unwrapping of their phase changes through time. These strong scatterers were then filtered to detect and remove the atmospheric phase contribution. Data from three permanent GPS sites (Figs 1 and 4) were used as an aid to improve calibration of InSAR determined subsidence. Finally each scatterer point was georeferenced and its line of sight (LOS) displacement rate was generated and normalized for yearly rates (Fig. 2).

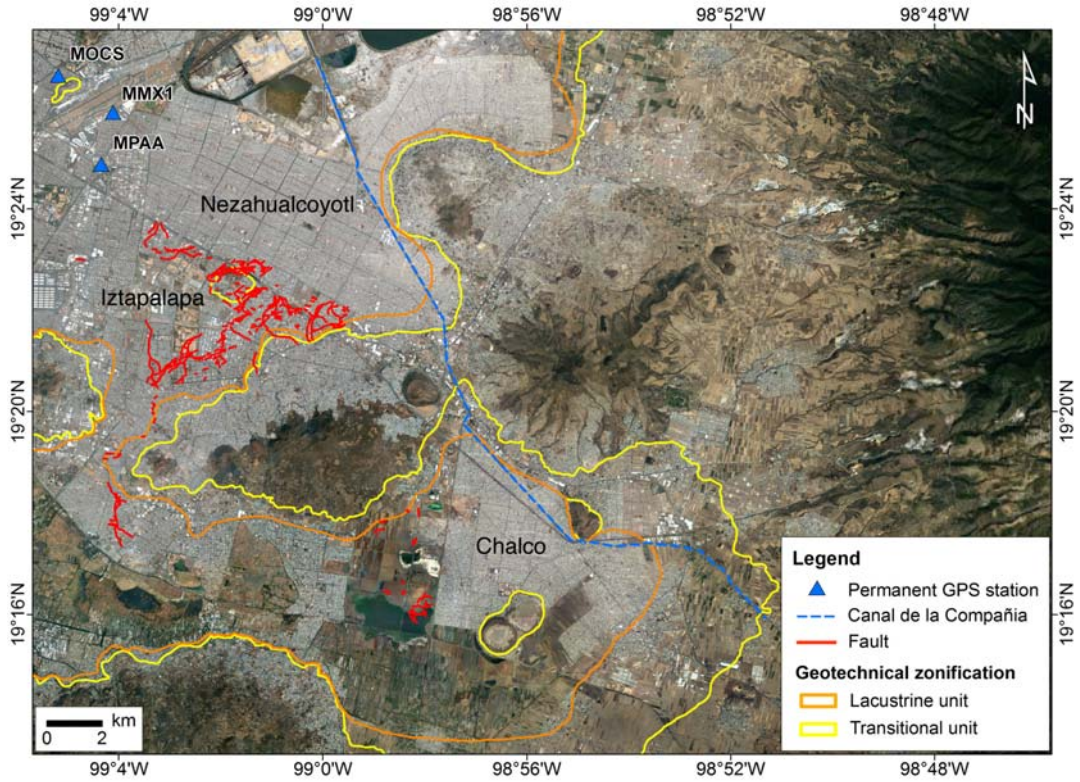

Fig. 1. Satellite image showing the location of study area. Faults in the Iztapalapa and Chalco areas are modified from CMFS (2008) and Ortiz-Zamora (2007) respectively. Geotechnical zonification after GDF (2004).

The resulting PSI data point cloud was interpolated using an Inverse Distance Weighted approach to generate a 100 × 100 m grid resolution in order to obtain a smoother map. The total displacement was then calculated for the whole PSI time interval spanned from SAR acquisitions, assuming that deformation rates are constant over time. Maximum horizontal subsidence gradients (Cabral-Cano *et al*., 2010) were evaluated by computing the difference in subsidence between cells divided by the horizontal distance between adjacent cells (Fig. 3).

Although spatial resolution of ENVISAT-ASAR based InSAR products is very good, its temporal resolution is variable, depending on the frequency of acquisitions. In order to provide better temporal resolution for selected areas and fully validate our results, we also used data from three permanent GPS sites. The coordinate time series for both GPS stations (Fig. 4) were determined using a standard precise point-positioning analysis of the raw code and phase data using GIPSY software from the Jet Propulsion Laboratory (JPL). Daily station coordinates were estimated in a non-fiducial reference frame and then transformed to ITRF2005 using daily seven-parameter Helmert transformations from JPL.

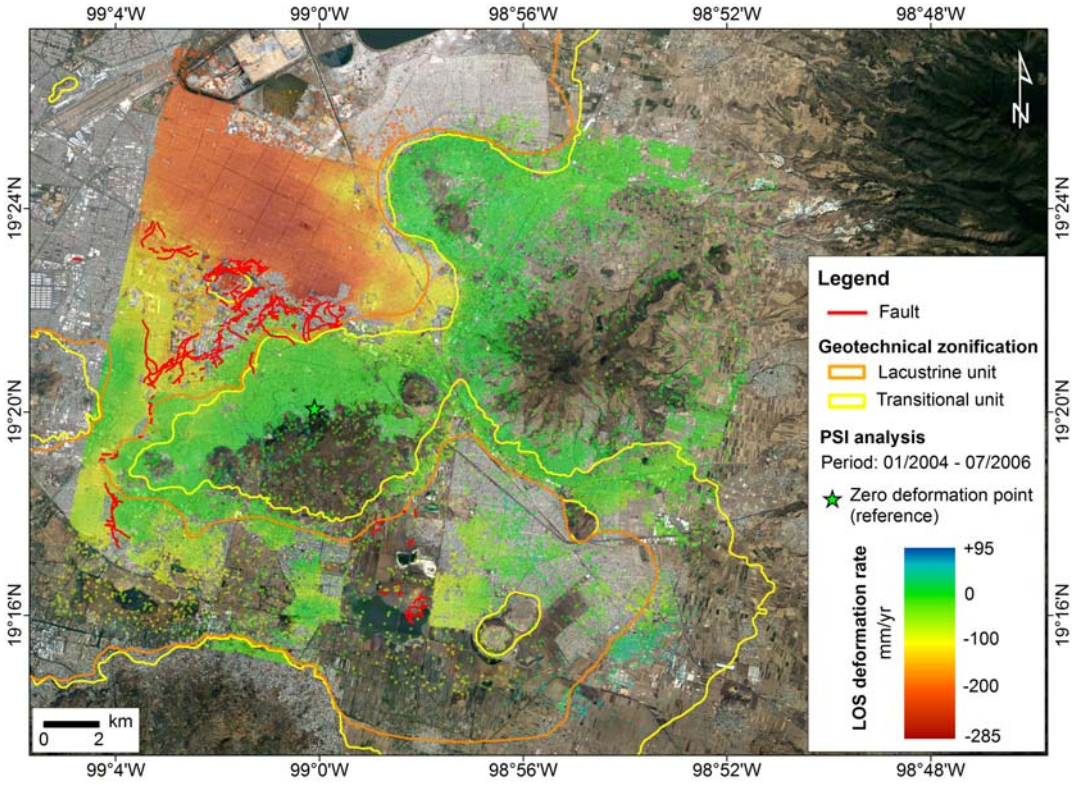

Fig. 2 Persistent Scatterer InSAR (PSI) displacement map of the southeastern sector of the Mexico City Metropolitan area overlapped onto high-resolution satellite imagery. Faults in the Iztapalapa and Chalco areas are modified from CMFS (2008) and Ortiz-Zamora (2007), respectively. Geotechnical zonification after GDF (2004).

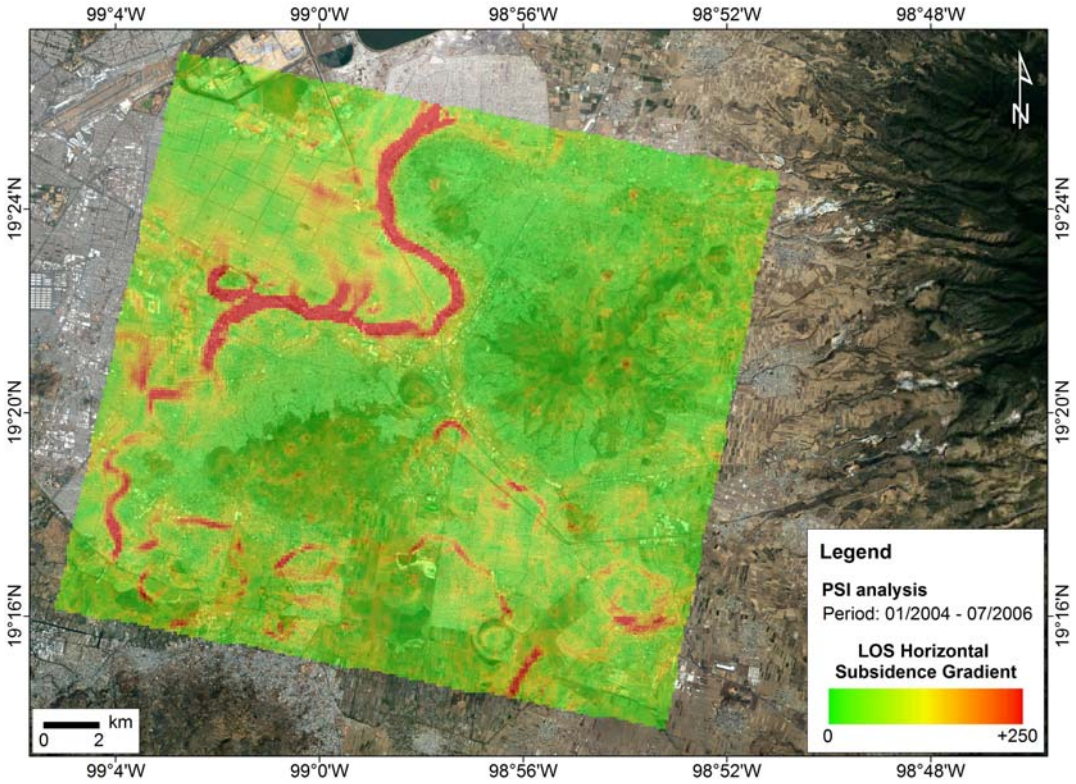

Fig. 3 Line of sight horizontal subsidence gradient map showing the potential for fault development in the study area. Compare to fault location on Figs 1 and 2.

DISCUSSION

The PSI-derived LOS displacement map (Fig. 2) shows that the Ciudad Nezahualcoyotl undergoes LOS deformation rates of more than –280 mm/year, while Chalco and selected areas in Iztapalapa subside at rates of –150 and –100 mm/year, respectively.

Figures 1 and 2 show the location of faults determined after visual reconnaissance and near-surface geophysical exploration in the Iztapalapa area (Ortiz-Zamora, 2007; CMFS, 2008; Ortiz-Zamora & Ortega-Guerrero, 2010). The location of these fault zones is well constrained by the high gradient zones derived from the PSI maps (Fig. 3). This correlation of surface faulting gathered from direct field evidence, urban infrastructure maintenance reports and the spatial distribution of subsidence strongly suggests that the principal factor constraining these hazardous areas is best determined not by solely using the subsidence magnitude rates but rather by using a horizontal subsidence gradient analysis. This product can then be used as the basis for the generation of subsidence-induced surface faulting hazard maps. Selection of high-risk threshold values of the horizontal subsidence gradient can be done empirically from field reconnaissance of fault damage (Cabral-Cano *et al.*, 2010), or alternatively based on the capacity of civil structures to resist shearing from the differential motion of their foundations. Both approaches can be successfully used to correlate the potential for surface faulting in high horizontal subsidence gradient zones. This approach produces high-resolution hazard maps that can be integrated with the decision analysis for land-use regulation, building and zoning codes, and other urban infrastructure maintenance projections.

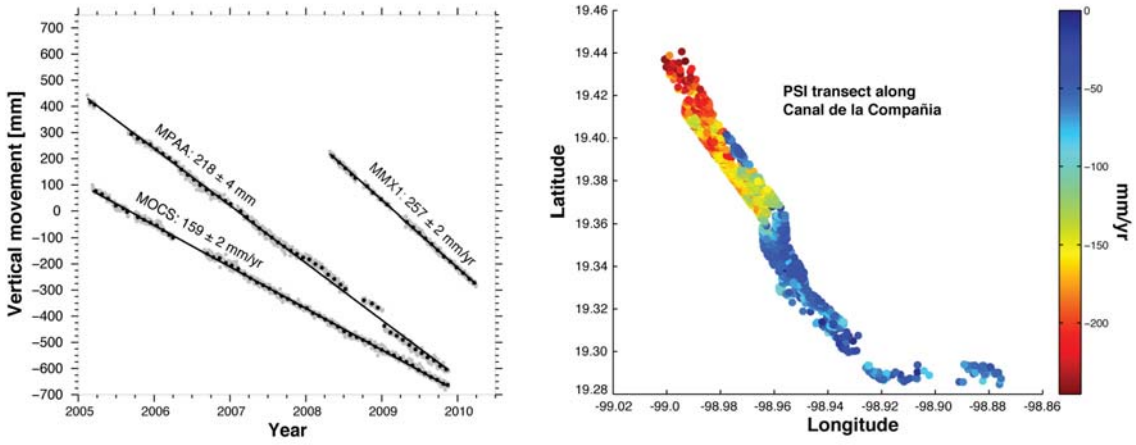

Fig. 4. Left: Vertical time series for MMX1, MRRA and MOCS permanent GPS sites; see Fig. 1 for site location. Grey dots are daily solutions and black dots averaged weekly solutions. Right: Retrieval of PSI points (Fig. 2) along a 250-m wide transect centred on the Canal de la Compañia (see Fig. 1 for location).

The Canal de la Compañia levee failure on January 2010

On January 2010 the Canal de la Compañia (Fig. 1) levee failed, flooding a large portion of the surrounding neighbourhoods near its intersection to Highway Mex-150D Mexico-Puebla. This canal is part of the sewage and drainage system for the MCMA, thus any failure in its integrity poses a serious health hazard for the surrounding communities. Figure 4 shows a 250-m wide transect of the Canal de la Compañia along the PSI map (Fig. 2). This plot illustrates the deformation of its substrate in its northwestern segment and explains the necessity to continuously increase the current height of the levee in order to maintain a proper slope for the canal. However, the height of the levee, several metres above the surrounding housing developments, imposes a high vulnerability to its nearby surrounding areas. This example illustrates the potential of PSI and horizontal gradient analysis for urban infrastructure hazard assessment.

CONCLUSIONS

Displacement and horizontal subsidence gradient analysis derived from Persistent Scatterer Synthetic Aperture Radar Interferometry can be successfully used as the base for subsidence and fault hazard mapping. Our example in the southeastern sector of the Mexico City Metropolitan Area documents an excellent correlation from our mapping products with independently surveyed faults in selected parts of the study area, and validates our approach.

The high density of the PSI point cloud in urban and suburban areas can be further exploited to obtain critical parameters for hazard assessment in a wide range of urban infrastructure elements such as the case of Canal de la Compañia.

Acknowledgements We thank ESA for providing the ENVISAT-ASAR images through CAT-1 Project #1409 to E. Cabral-Cano. This research was funded by UNAM through PAPIIT projects IN-121515, IN-114907, IN117909 and Conacyt projects 61212 and 82868. B. Osmanoglu would like to thank NASA for NESSF Fellowship 09-Earth09R-61. We also thank Freek van Leijen, Mahmut Arikan and Ramon Hanssen and many others from TU-Delft for making the DORIS and PSI Toolbox available.

REFERENCES

Cabral Cano, E., Díaz Molina, O. & Delgado Granados, H. (2010) Subsidencia y sus Mapas de Peligro: Un Ejemplo en el área Nororiental de la Zona Metropolitana de la Ciudad de México. *Boletin de la Sociedad Geológica Mexicana* (in press).

Cabral-Cano, E., Dixon, T. H., Miralles-Wilhelm, F., Sánchez-Zamora, O., Díaz-Molina, O. & Carande, R. E. (2008) Space geodetic imaging of rapid ground subsidence in México City. *Bull Geol. Soc. Am.* **120**(11/12), 1556–1566; doi: 10.1130/B26001.1.

Centro de Monitoreo de Fracturamiento del Subsuelo (CMFS) (2008) Delegacion Iztapalapa. Avance de trabajos de cartograficos a Julio del 2008. http://www.iztapalapa.gob.mx/centrodemonitoreo.

Gobierno del Distrito Federal (2004) Normas técnicas complementarias para diseño y construcción de cimentaciones. *Gaceta Oficial del Distrito Federal II, 103-BIS*, 11–39.

Ortiz-Zamora, D. & Ortega-Guerrero, A. (2010) Evolution of long-term land subsidence near Mexico City: Review, field investigations, and predictive simulations. *Water Resour. Res.* **46**, W01513, 15 p., doi:10.1029/2008WR007398.

Ortiz-Zamora, D. C. (2007) Fracturamiento en el acuitardo lacustre que cubre al acuífero reguional de la Ciudad de México: Orígen, Dinámica e implicaciones. Masters Thesis. Universidad Nacional Autónoma de México, Posgrado en Ciencias de la Tierra. 158 p.

Osmanoglu, B., Dixon, T. H., Wdowinski, S., Cabral-Cano, E. & Jiang, Y. (2010) Mexico City Subsidence Observed with Persistent Scatterer InSAR. *Int. J. Appl. Earth Observation Geoinfo* doi:10.1016/j.jag.2010.05.009 (in press).

(Proceedings of EISOLS 2010, Querétaro, Mexico, 17–22 October 2010). IAHS Publ. 339, 2010.

Measurement of land subsidence using interferometry, Coachella Valley, California

M. SNEED
US Geological Survey, 3020 State University Drive East, Suite 4004, Sacramento, California 95819, USA
micsneed@usgs.gov

Abstract Interferometry of satellite radar data collected from 2003 to 2009 was used to determine the location, extent and magnitude of land subsidence associated with groundwater-level declines in the Coachella Valley, California, USA. Groundwater has been a major source of agricultural, municipal and domestic supply in the valley since the early 1920s, resulting in water-level declines of as much as 30 metres by 2009. Differential subsidence has damaged buildings, roads, water conveyance canals and other infrastructure near La Quinta, in the southwestern part of the valley. Comparison of interferometry data for 2003–2009 to previously reported data for 1996–2000 indicates that subsidence rates have increased by at least a factor of two since 2003 in the urban areas of Palm Desert, Indian Wells and La Quinta. Water levels in most wells in these areas declined to their lowest recorded levels on an annual basis during 2003–2009. The correlation between the deformation time series derived from interferometry and water levels in nearby wells indicates that the preconsolidation stress may have been exceeded and the subsidence likely is mostly permanent. Water-level recoveries during 2009 have reduced the subsidence rates in Indian Wells and La Quinta. The subsidence measured using interferometry is limited to the western margin of the valley although water levels have reached historic lows throughout most of the valley, suggesting that fine-grained compressible sediments have been preferentially deposited in this part of the valley. Subsidence terminates abruptly to the northeast of Palm Desert, suggesting an abrupt change in lithology or differing effective thicknesses of compressible deposits, possibly caused by faulting, that controls the occurrence and extent of subsidence. Co-located continuous-GPS and groundwater-level time series, additional interferograms and detailed geological and water-level information may provide further insight into the physical controls on subsidence processes in the Coachella Valley.

Key words land subsidence; differential aquifer-system compaction; InSAR; geological controls

INTRODUCTION

Groundwater has been a major source of agricultural, municipal and domestic water supply in Coachella Valley, California, USA, since the early 1920s. By 2009, water levels in many wells in the southern Coachella Valley had declined by as much as 30 metres (m) and water levels in some wells were at their lowest recorded values. Declining water levels can contribute to, or induce, land subsidence in alluvial aquifer systems with compressible fine-grained layers such as that of the Coachella Valley. Ikehara *et al.* (1997) determined that as much as 150 millimetres (mm) of subsidence occurred in the southern parts of the Coachella Valley during 1930–1996; Sneed & Brandt (2007) used interferometric synthetic aperture radar (InSAR) to measure as much as 150 mm and 180 mm of subsidence during 1996–2000 and 2003–2005, respectively, along the western margins of Coachella Valley in the urban areas of Palm Desert, Indian Wells and La Quinta. Land subsidence has caused earth fissures and has damaged buildings, roads and water conveyance canals near La Quinta. The objective of this paper is to present the analysis of InSAR results and groundwater levels for 2003–2009.

The Coachella Valley is a 100-km long, northwest-trending valley in southeastern California (Fig. 1) where the 610-m thick aquifer system comprises a complex unconsolidated to partly consolidated assemblage of gravel, sand, silt and clay of alluvial and lacustrine origins (California Department of Water Resources, 1979). Northwest trending faults, including the San Andreas Fault Zone on the eastern side of the valley, affect the movement of groundwater in the valley.

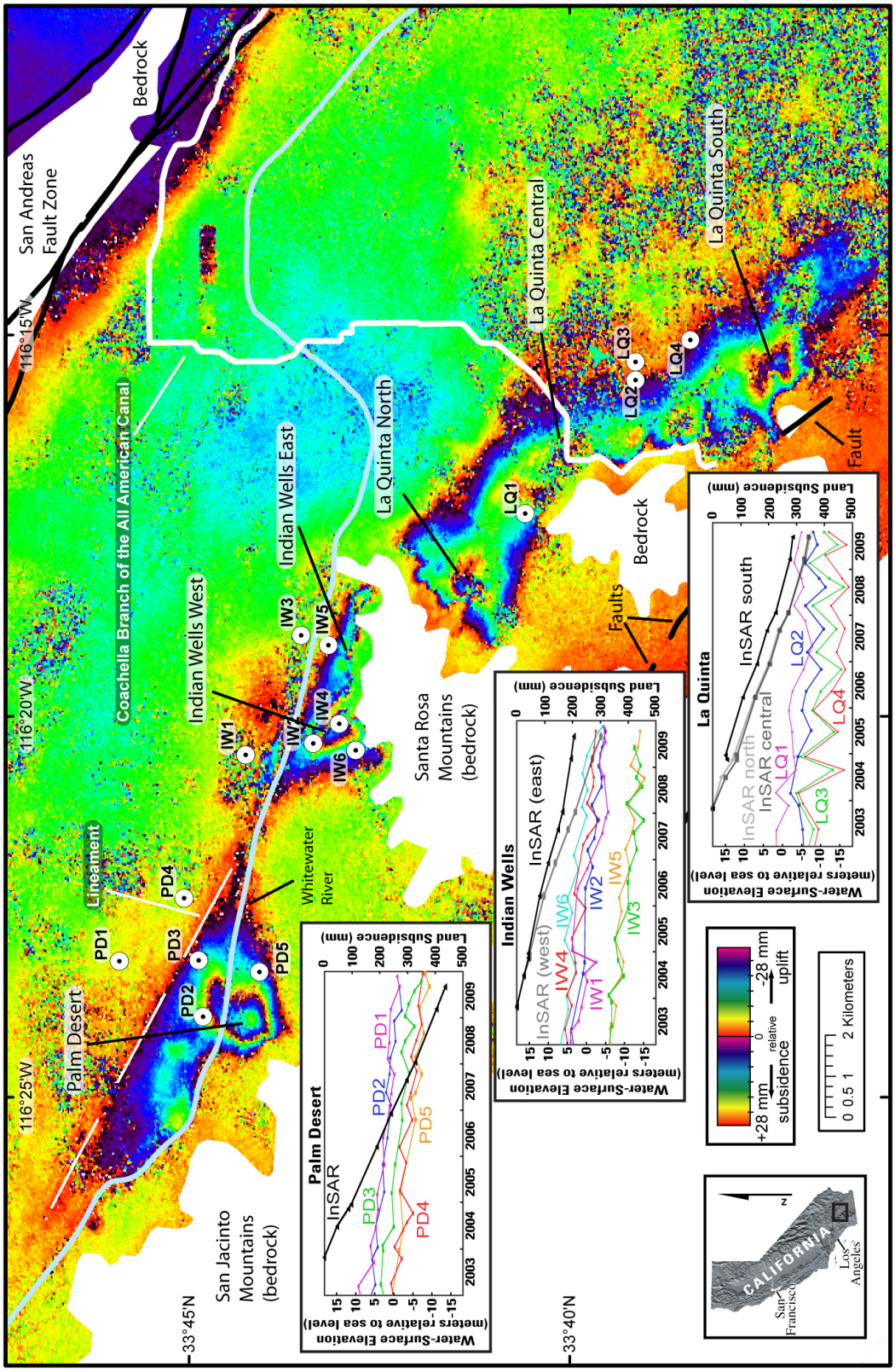

Fig. 1 Interferogram for 1 June 2008–8 March 2009 showing areas of subsidence, geological features and selected wells and hydrographs showing water-surface elevations for selected wells and land subsidence time series for Palm Desert, Indian Wells and La Quinta in the Coachella Valley, California.

LAND SUBSIDENCE AND GROUNDWATER LEVELS

InSAR methods were used to determine the location, extent and magnitude of land subsidence in the Coachella Valley for 2003–2009. Eleven synthetic aperture radar images from the European Space Agency's ENVISAT satellite acquired between 26 October 2003 and 30 August 2009 were used to produce nine interferograms, which indicate subsidence along the western margin of the Coachella Valley in the urban areas of Palm Desert, Indian Wells and La Quinta. The presence of detectable subsidence only along the western margin of the valley suggests that fine-grained compressible sediments have been preferentially deposited in this part of the valley. Fine-grained flood deposits from the Whitewater River may have accumulated in embayments formed by the extension of bedrock from the San Jacinto and Santa Rosa Mountains into the valley. The interferograms were combined to generate deformation time series for each of the three urban areas (Fig. 1), where subsidence has previously been identified using InSAR measurements for 1996–2005 (Sneed & Brandt, 2007). InSAR-computed subsidence for both time periods were compared to water-level measurements provided by the Coachella Valley Water District to help explain the location, extent and magnitude of land subsidence.

Palm Desert

The Palm Desert area had the largest magnitude of subsidence of the three areas during 2003–2009. The deformation time series indicates that about 425 mm of subsidence occurred at a fairly constant rate of 6 mm/month (Fig. 1), which is about double the rate reported by Sneed & Brandt (2007) for 1996–2000. Water levels declined to new lows nearly annually from 2003 through 2009 (Fig. 1), with a greater rate of decline in the 2000s than in the 1990s.

The areal extent of subsidence terminates abruptly to the northeast of Palm Desert, forming a northwest–southeast trending lineament (Fig. 1). Abrupt changes in subsidence can be the result of faults separating compressible from less-compressible deposits or acting as barriers to groundwater flow, creating groundwater-level differences across the faults (Galloway *et al.*, 1999). Groundwater levels are similar on both sides of the lineament (Fig. 1) suggesting that there is difference in the compressibility of the sediments on either side of the lineament. A fault may have displaced compressible sediments on the east side of the lineament above the water table. The lineament has become much sharper in interferograms produced from 2005 data and later, which suggests that groundwater levels declined below the compressible sediments on the east side of the lineament since 2004. Geological and geophysical logs of wells in the area need to be investigated to help determine the cause of the apparent lineament in the interferograms.

Indian Wells

The Indian Wells interferograms delineate subsidence bowls in the west and east part of the area (Fig. 1). The deformation time series for 2003–2009 indicates that about 300 and 200 mm of subsidence occurred at rates of about 4 and 3 mm/month in the western and eastern bowls, respectively. Subsidence occurs at a near-constant rate in the west bowl; whereas, the rate decreases after 2007 in the east bowl (Fig. 1). The 2003–2009 subsidence rates are about double the 1996–2000 rates reported by Sneed & Brandt (2007). Water levels in some wells near the west bowl reached historic lows annually; whereas, water levels near the east bowl reached historic lows annually during 2003–2006, then remained relatively constant during 2007–2009. The reduction in the rate of water-level declines since 2007 in wells near the east bowl explains the reduced subsidence rate (Fig. 1). The Santa Rosa Mountains act as a barrier to groundwater flow to the south, which also controls the extent of subsidence.

La Quinta

The La Quinta subsidence area has the largest geographic extent of the three areas (Fig. 1) and damage to infrastructure, including an important water conveyance canal, has occurred. The deformation time series for 2003–2009 indicates that about 340, 335 and 280 mm of subsidence

occurred in the north, central and southern parts of the La Quinta area, respectively. The subsidence rates are about 5 mm/month for the north and central parts of the area and about 4 mm/month for the southern part of the area. The rates for the northern and southern parts have increased by factors of nearly 2 and 4, respectively, compared to rates reported by Sneed & Brandt (2007) for 1996–2000; a rate for the central part of the area was not previously computed. The subsidence occurs at a near-constant rate for 2003–2008 in all three areas and then decreases slightly during 2008–2009. Water levels in most wells reached historic low levels annually in the La Quinta area from 2003–2008, then remained stable or recovered slightly during 2008–2009 (Fig. 1). The reduction in subsidence rates coincides with recovering water levels and indicates that some of the deposits, probably fairly thin aquitards and the coarser-grained deposits, are responding fairly quickly to the recovering water levels and that pore pressures in the thin aquitards did not exceed the preconsolidation stress in 2009. The Santa Rosa Mountains control the shape of the subsidence on the north and west sides of the La Quinta area.

SUMMARY AND CONCLUSIONS

Groundwater has been a major source of agricultural, municipal and domestic water supply in the Coachella Valley since the early 1920s, resulting in water-level declines of more than 30 m by 2009. Interferometry data collected during 2003–2009 indicate that rates of subsidence in the urban areas of Palm Desert, Indian Wells and La Quinta increased by a factor of 2 or more compared to rates reported for the same areas for 1996–2000. Water levels in most wells in these areas declined to their lowest recorded levels on an annual basis during 2003–2009. The correlation between the deformation time series derived from InSAR and water levels in nearby wells indicates that the preconsolidation stress may have been exceeded; if so, the subsidence likely is mostly permanent. Water-level recoveries during 2009 may have reduced the subsidence rates in Indian Wells and La Quinta.

In the area of investigation in the Coachella Valley, the subsidence measured using interferometry is limited to the western margin of the valley, although water levels have reached historic lows throughout most of the valley, suggesting that fine-grained compressible sediments have been preferentially deposited in this part of the valley. Subsidence terminates abruptly to the northeast of Palm Desert, suggesting an abrupt change in lithology or differing effective thicknesses of compressible deposits, possibly caused by faulting, that controls the occurrence and extent of subsidence.

Continuous-GPS data and groundwater-level data in a nearby well are being collected in the study area to facilitate a stress–strain analysis for computation of storage properties and perhaps determination of preconsolidation stress if water levels fluctuate above and below that threshold. These time series, additional interferograms and detailed geological and water-level information may provide further insight into the physical controls on subsidence processes in the Coachella Valley.

REFERENCES

California Department of Water Resources (1979) Coachella Valley area well standards investigation. Los Angeles, California Department of Water Resources, Southern District, 40 p.

Galloway, D. L., Jones, D. R. & Ingebritsen, S. E. (1999) Land subsidence in the United States. *US Geological Survey Circular 1182.*

Ikehara, M. E., Predmore, S. K. & Swope, D. J. (1997) Geodetic network to evaluate historical elevation changes and to monitor land subsidence in Lower Coachella Valley, California, 1996. *US Geological Survey Water-Resources Investigations Report 97-4237*, scale 1:63,000, 1 sheet [folded in envelope].

Sneed, M. & Brandt, J. T. (2007) Detection and measurement of land subsidence using global positioning system surveying and interferometric synthetic aperture radar, Coachella Valley, California, 1996–2005. *US Geological Survey Scientific Investigations Report 2007-5251.*

(Proceedings of EISOLS 2010, Queretaro, Mexico, 17–22 October 2010). IAHS Publ. 339, 2010.

Monitoring techniques for analysing subsidence: a basis for implementing an Early Warning System

J. MARTURIA[1], J. RIPOLL[1], A. CONCHA[1] & M. BARBERÀ[2]

1 *Institut Geològic de Catalunya, Unitat de Enginyeria Geològica i Riscos, Balmes 209-211, 08006 Barcelona, Spain* jmarturia@igc.cat

2 *GeoCAT Gestió de Projectes. S.A., Av. Josep Tarradelles 34-36, 3a, 08006 Barcelona, Spain*

Abstract The L'Estació neighbourhood located in Sallent (a town near Barcelona, Spain) is affected by large ground subsidence phenomena that extend within the former exploitation limits of an old underground potash mine. In the 1990s, several damages were reported in different buildings. Since then, different monitoring techniques have been implemented. This paper compares and analyses these techniques that identify, measure and monitor subsidence phenomena. On the one hand, high precision topographic surveys are used to investigate the subsidence phenomena extent on the terrain and its effects on buildings. On the other hand, *in situ* extensometers, inclinometers and piezometers are used to investigate the underground conditions and infer the mechanisms that control the subsidence motion in detail. The parameters obtained from the land surface deformation (measured with the automatic total station) and the underground deformation measurements (extensometers network) have been integrated into a real-time monitoring system as a basis for an early warning system developed by the IGC. The use of these techniques, as well as threshold values to activate civil protection alarm and communication procedures, are done on the basis of the experience obtained during the investigation of the phenomena.

Key words mining subsidence; emergency plan; monitoring network; Catalonian potash basin

INTRODUCTION

In the town of Sallent, the L'Estació quarter is located above the exploitation zone of an old underground potash mine, the Enrique Mine. This mine was opened in 1932 and during extraction works a natural great cavity, of about 40 m diameter and 110 m height, was found located under the southeast sector of the present L'Estacio quarter. This cavity had been caused by water circulation and some important groundwater flooding took place during exploitation. The great difficulties of controlling the flooding led to the closure of Enrique Mine in 1973. During the abandonment process the mine was filled up with saturated salty water with the purpose of preventing dissolution processes and the ground subsidence caused by the mining activity. But, in the 1990s damage to several buildings was reported in the L'Estació neighbourhood and so the Catalan ministry for Territorial Planning and Public Works (DPTiOP, its initials in Catalan) started a series of studies through the Geological Institute of Catalonia (IGC) to determine the origin of the damage, monitor the phenomena, and propose solutions to guarantee the population's safety. For this purpose, several techniques have been applied: topographic measurements, DInSAR techniques (satellite and ground-based), geological mapping, geophysical prospecting, extensometric measurements, drilling, etc. The studies concluded that the largest vertical terrain displacements are located at the corners of Barcelona Tarragona and Arquitecte Gaudí streets (critical area), and are related to the existing natural cavity (Fig. 1).

INSTRUMENTATION

Surface monitoring networks

These networks are based on two different techniques: a high precision topographic levelling and a Geodetic Monitoring System for control building status. The topographic levelling was established in 1997, and originally consisted of 34 points, but has grown gradually to nearly 170 measurements in the L'Estacio quarter and surroundings (Fig. 1). The measurement frequency was initially

Copyright © 2010 IAHS Press

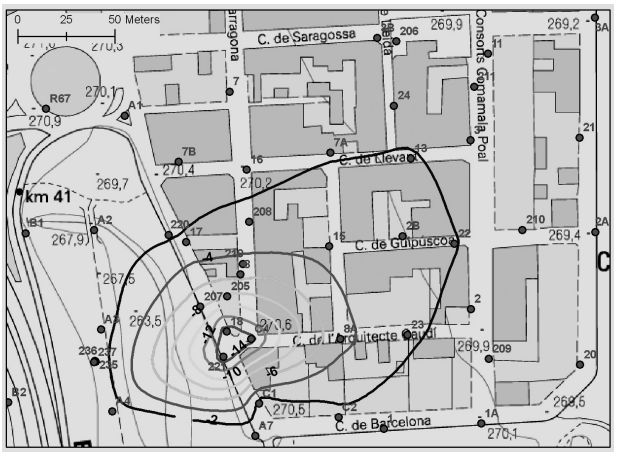

Fig. 1 Location of the maximum subsidence at the L'Estació neighbourhood. Black dots represent the topographic surveying points.

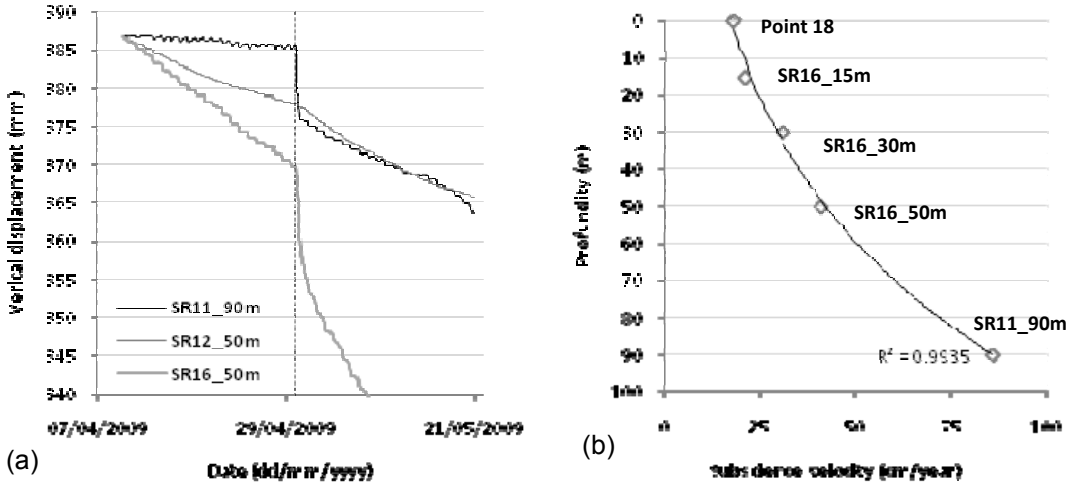

Fig. 2 (a) Simultaneous registered displacements at the SR11 and SR16 extensometers. These extensometers are right above the natural cavity. (b) The deeper the measurement, the larger the descending movement. The plot shows the evolution of vertical movement velocity at the extensometers as function of depth.

monthly, but has varied to weekly during the most active periods (2008 and beginning of 2009). At the critical area, 25 precise prisms are installed on the 8 most vulnerable buildings and monitored by an automatic Leica TCA Total Station in order to control the building response.

Underground monitoring network

This network is located around the critical area, right above the natural cavity, and is composed of extensometers, inclinometers and piezometers. These instruments are installed in 15 boreholes at depths that vary between –140 and –15 m (Fig. 2), and include 25 rod extensometers, four inclinometers (ABS 74, 3 inches, Glötzl Baume β tecnik) and one piezometer. An automatic measurement system was implemented for collecting data from the extensometers and piezometer.

CHARACTERIZATION OF THE SUBSIDENCE PHENOMENA

Topographic surveying shows that the extension of the subsidence phenomena is controlled by the extension of the underground mine, with a maintained subsidence velocity of about 1 cm/year. But the more intense surface vertical displacement is controlled by the existing underground cavity and

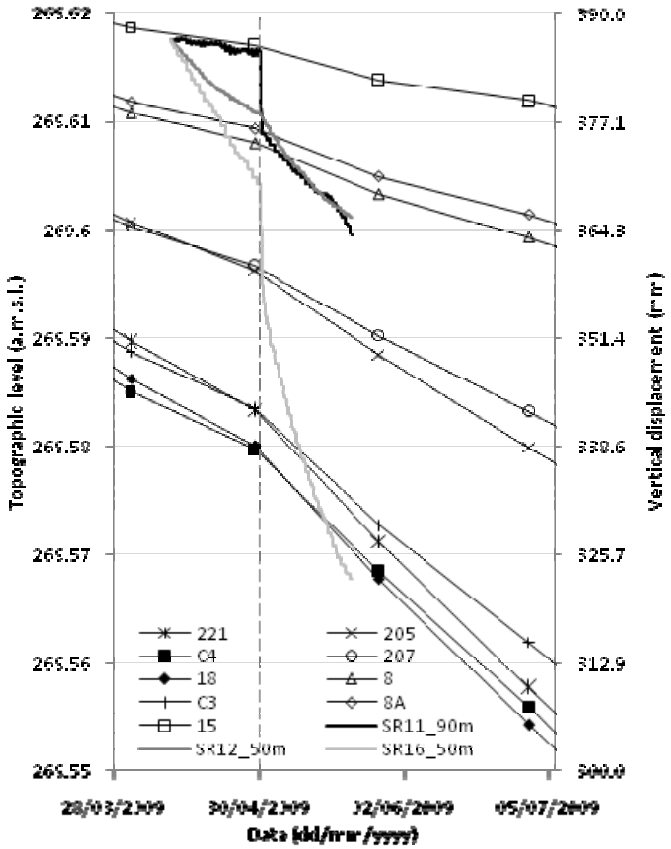

Fig. 3 Diagram showing the orientation and accumulated displacement (during 2009) of points along the extensometers with the largest deformation.

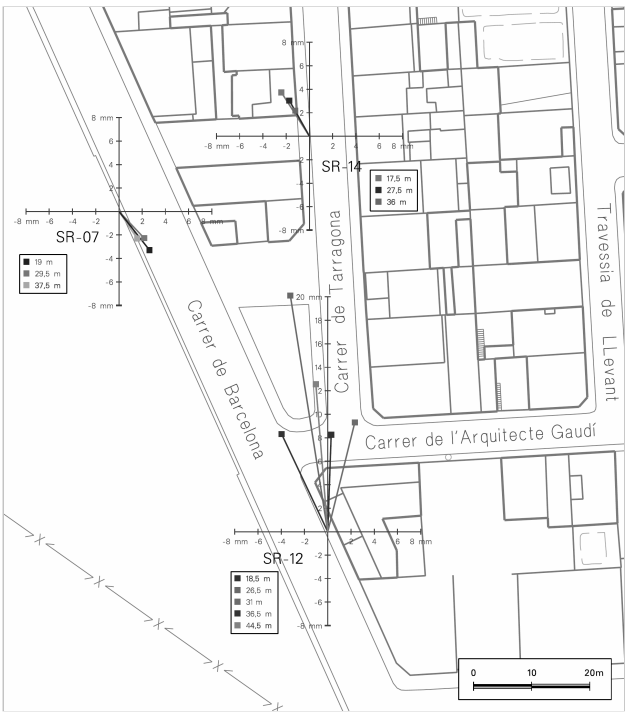

Fig. 4 Main horizontal displacement components from inclinometer registers at different depths. Inclinometer SR14 is further apart and it is less affected by the cavity.

is about 49 cm over the last 13 years, with surface average velocities of about 2.5–4.0 cm/year from the beginning of measurements until July 2008. From this date, the velocity increased to 5.0–8.0 cm/year, and finally in May 2009 there was a significant increase of velocity to between 12–18 cm/year.

Data from the extensometers show that each extensometer progressively registered data which are more or less independent of each other and punctual events (significant jumps on the curves), at the deepest extensometers, are registered (Fig. 2(a)). The evolution of the extensometer measurements have allowed us to establish a velocity gradient as a logarithmic function of depth (Fig. 2(b)) as well as a direct relationship with velocity gradients detected by the topographic surveying (Fig. 3). Also, the direction of the horizontal movements registered by the inclinometers show a convergence to the centre of the cavity, confirming that it induced the most intense subsidence (Fig. 4).

IMPLEMENTATION OF ALERT SYSTEM AND CIVIL PROTECTION PLAN

The maximum subsidence is located immediately above the large natural cavity, and a decrease of land deformation is not expected in the near future and damage to the buildings within the neighbourhood is expected to continue (ICC, 2003; IGC, 2009). An alert (early warning) system and an emergency plan for an organized and efficient response by the civil protection authorities has been elaborated and implemented (Procicat Sallent). The alert triggering levels for the plan are defined on the basis of deformation rates in the critical area. The deformation rates are automatically registered by the monitoring instrument networks: data from the automatic measurements in extensometers and building deformation monitoring systems are sent to the reception centre at the Geological Institute (IGC) that processes the information and evaluates the results. In the case of an alert detection, IGC is in charge of immediately informing the civil defence centre to execute the actions established in an emergency plan.

In December 2008 the control networks showed a significant increase in the speed of subsidence. This situation led to the activation level of alert in the emergency plan and the meeting of different groups in order to assess the activation of the plan. Finally, the preventive evacuation of about 120 residents from 43 homes in the neighbourhood was carried out.

REFERENCES

IGC (Institut Cartogràfic de Catalunya) (2003) Estudi del procés d'esfondrament del terreny que afecta els barris de L'Estació i de la Rampinya de Sallent (Bages). *ICC Internal Report AR-151/03*.

IGC (Institut Cartogràfic de Catalunya) (2009). Resum anual 2009 de les xarxes d'auscultació del Barri de L'Estació (Sallent, Bages). *IGC Internal Report AP-125/09*.

Generalitat de Catalunya (1995) PROCICAT Plà de Protecció Civil de Catalunya. Pla territorial de Protecció Civil. http://www.belt.es/legislacion/vigente/sp_pcivil/pcivil/autonomica/catalu%C3%B1a/procicat%5B1%5D.pdf.

(Proceedings of EISOLS 2010, Queretaro, Mexico, 17–22 October 2010). IAHS Publ. 339, 2010.

DInSAR analysis of land subsidence caused by geothermal fluid exploitation in the Mexicali Valley, B.C., Mexico

O. SARYCHIKHINA[1], E. GLOWACKA[1], F. SUAREZ-VIDAL[1] & R. MELLORS[2]

1 *Earth Sciences Division, CICESE, Carretera Ensenada-Tijuana No. 3918, Zona Playitas, 22860 Ensenada, BC, Mexico* osarytch@cicese.mx

2 *Dept of Geological Sciences, San Diego State University, 5500 Campanile Drive, 92182 San Diego, California, USA*

Abstract The Mexicali Valley is located in the northeastern Baja California, Mexico, in the southern part of Salton Trough and at the tectonic boundary between the Pacific and North American plates. This zone is characterized by high tectonic seismicity, heat flow and surface deformation, related to the tectonic regime of the zone. Besides the tectonic deformation, extraction of fluids in the Cerro Prieto Geothermal Field produces deformation of large magnitude (Glowacka *et al.*, 1999). Significant ground deformation (mainly subsidence) and related ground fissures cause severe damage to infrastructure like roads, irrigation canals and other facilities. In this paper, the technique of Differential Synthetic Aperture Radar Interferometry (DInSAR) is applied to C-band ENVISAR ASAR data acquired between 2003 and 2006 in order to determine the extent and amount of land subsidence information in Mexicali Valley. The DInSAR results are compared with historical precise levelling data (1994–1997 and 1997–2006) and detailed geological information to define the extension, limits and rate of land subsidence in the study area. The analysis of changes in the spatial pattern and in the rate of subsidence was also performed. These changes allow investigation of the relationship between the subsidence dynamics and fluid extraction in the Cerro Prieto Geothermal Field.

Key words DInSAR; land subsidence; Mexicali Valley, Mexico; Cerro Prieto Geothermal Field; geothermal fluid extraction

INTRODUCTION

Surface deformation is an expected consequence of the production of geothermal fluids (Mossop & Segall, 1997; Allis *et al.*, 1998) and it occurs as a consequence of extracting the geothermal fluid at a speed higher than the recharging and/or injection rate. Identification of land subsidence in geothermal fields and monitoring of the spatial and temporal changes of its pattern and magnitude can provide important information about the dynamics of this process and its controlling structures. Identification and monitoring of land subsidence can be accomplished using a number of techniques.

In this paper, the analysis of ground subsidence in the Mexicali Valley was performed. DInSAR data from the conventional two-pass DInSAR method and from stacking was analysed. The stacking results, which span December 2004 and December 2005, were compared with available levelling data from the 1994–1997 and 1997–2006 periods in an attempt to evaluate the changes in the spatial pattern and rate of subsidence. The observed subsidence pattern was also compared to the tectonic framework of the region.

STUDY AREA

The Mexicali Valley is located in the northernmost part of the state of Baja California, Mexico (Fig. 1) and is part of the Salton Trough tectonic province, which lies on the Pacific–North American plate boundary. This zone is characterized by high tectonic seismicity, heat flow and surface deformation, related to the tectonic regime of the zone.

Besides the tectonic deformation, extraction of fluids in the Cerro Prieto Geothermal Field (CPGF) produces deformation of large magnitude (Glowacka *et al.*, 1999).

The subsidence history at the CPGF area has been well documented. Geodetic studies in the Mexicali Valley began in the 1960s. Ground deformation in the studied area has been monitored by repeat ground survey with precise levelling and GPS, and is currently monitored by quasi

Copyright © 2010 IAHS Press

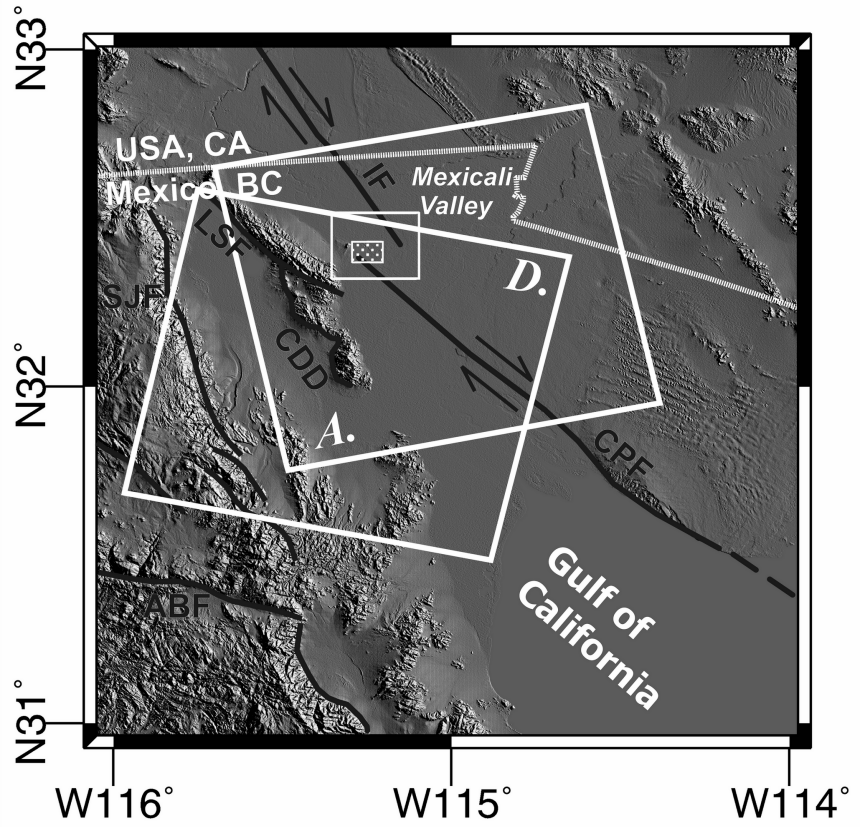

Fig. 1 Regional map of the study area. SRTM DEM is used as the background. Large white rectangles indicate the spatial coverage of Envisat SAR images. D indicates descending track, and A indicates ascending track. The smaller white rectangle represents the study area. The smallest white filled rectangle represents the Cerro Prieto Geothermal Field. The principal tectonic faults are also indicated: Cerro Prieto fault (CPF), Imperial fault (IF), Agua Blanca fault (ABF), Sierra Juarez fault (SJF), Laguna Salada fault (LSF) and Cañada David Detachment (CDD).

continuous records of geotechnical instrument network (tiltmeters and extensometers). Analysis of levelling data and CPGF extraction history (Glowacka *et al.*, 1999), and modelling of the tectonic and anthropogenic components of ground subsidence (Glowacka *et al.*, 2005) suggested that the current deformation rate is mainly related to the fluid extraction. The high deformation rate and spatial correlation between locations of the ground deformation maximum and extraction wells zone was confirmed by DInSAR method (Carnec & Fabriol, 1999; Hanssen, 2001). However the field observation (Gonzalez *et al.*, 1998; Glowacka *et al.*, 1999, 2010; Suárez-Vidal *et al.*, 2008) and geotechnical instruments data (Glowacka *et al.*, 1999, 2007) reveal that the geometry of the subsiding area is controlled by tectonic faults.

DINSAR DATA PROCESSING

DInSAR techniques consist of the combination of two SAR images obtained for the same area at different times from slightly different positions. The result of this combination is a new image known as an interferogram, whose main phase component, after topographic removal, is the ground displacement along the radar Line of Sight (LOS) (Gabriel *et al.*, 1989; Massonnet & Feigl, 1998).

Data from Envisat ASAR systems were used for the analysis presented in this paper. A total of 17 SLC images from descending satellite track 84 and frame 2961, and five SLC images from ascending satellite track 306 and frame 639, were acquired over the study area from October 2003 to May 2006 by the ESA. The spatial coverage of these images is presented in Fig. 1.

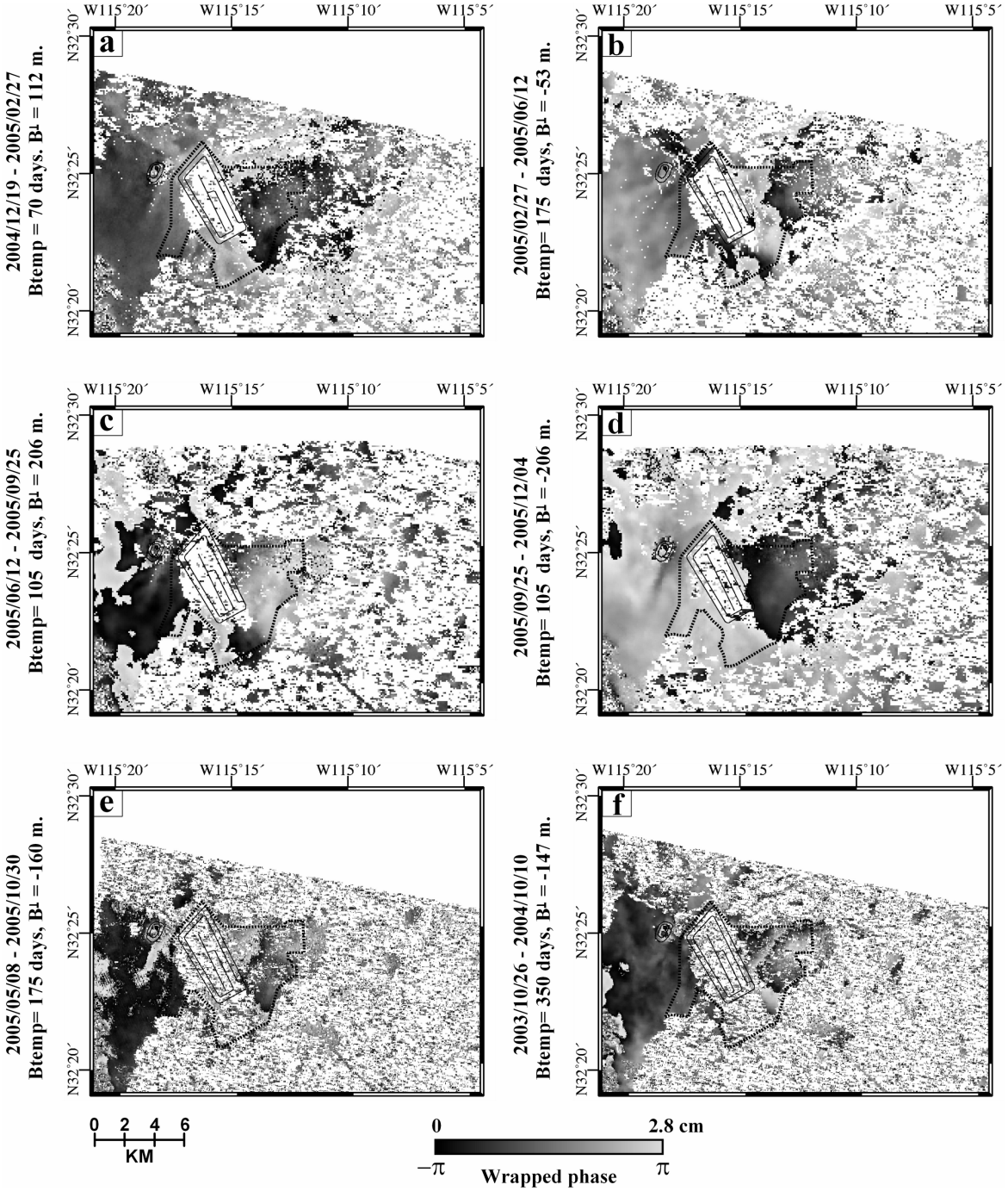

Fig. 2 Six differential (wrapped) interferograms for the study area, showing spatial and temporal distribution of ground deformation in the study area. Areas of low coherence (<0.1) are masked. The black dotted line frames the limits of the CPGF. The borders of the evaporation pond and the Cerro Prieto volcano are superimposed on the images for orientation.

Interferometric processing was done using the public domain DORIS InSAR package (Kampes *et al.*, 2003). Precise satellite orbital information, taken from the Technical Delft University of Technology (Scharoo & Visser, 1998), and a 3-arc second DEM of the study area obtained by the Shuttle Radar Topography Mission (SRTM) were used for the processing. The interferograms were filtered (Goldstein & Werner, 1998) and multi-look processed to improve phase statistics. The interferograms have horizontal resolution at the ground level of about 100 m. Six of the processed differential interferograms are presented in Fig. 2.

The initial review of the resulting deferential interferograms showed strong spatial decorrelation for interferometric pairs with perpendicular baselines longer than 400 m; these interferometric pairs were excluded from the analysis. By limiting the baseline, the most incoherent interferograms were rejected. It also was found that, in spite of having a short perpendicular baseline, several differential interferograms present a high level of phase noise due to temporal decorrelation of the signal. The highly vegetated CPGF surrounding areas cause significant phase decorrelation of SAR couples over periods longer than 3 months (105 days). This suggests that Mexicali Valley conditions are not suitable for long-term interferometry analysis.

In order to calculate the yearly rate of deformation, a simple differential interferogram stacking method was applied. Stacking differential interferograms involves summing multiple differential interferograms into a single interferogram. This is useful for overcoming the two shortcomings of conventional DInSAR: the low coherence over long temporal separations and the atmospheric influence. Four, visually less noisy, differential interferograms of successive periods, with temporal separations between 70 and 105 days (Fig. 2(a)–(d)), were selected for stacking. The phase of each interferogram was first unwrapped using a statistical minimum-cost flow algorithm (Chen & Zebker, 2001), projected into the vertical direction, considering the fact that the main deformation in the area is subsidence, and referenced to a common point in the space, which is the fixed point for the levelling 1997–2006 data. The results from the stacking land subsidence rate map (cm/year) for the December 2004 and December 2005 period is shown in Fig. 3(a) and (b).

RESULTS AND DISSCUTIONS

The DInSAR data reveal that the total area affected by subsidence appears as a roughly NE–SW oriented elliptical-shaped feature with two bowls exhibiting high subsidence rates in the December 2004–December 2005 period: ~11 cm/year below in the east boundary of CPGF production zone, ~17 cm/year in the area between the eastern limits of the CPGF and the Saltillo fault, which was proposed as recharge zone in previous studies (Glowacka *et al.*, 1999; Sarychikhina, 2003). The subsiding area boundaries appear to correlate with faults and/or fissures zones, as can be seen in Fig. 3 where they are superimposed onto the subsidence map.

We compared data from the levelling surveys of 1994–1997 and 1997–2006 (Glowacka *et al.*, 1999, 2006) and DInSAR data from the stacking, to evaluate the changes in the spatial pattern and rate of land subsidence (Fig. 3). This comparison of deformation rates obtained from different techniques and time intervals indicates that the average rate of deformation has increased since 1997. The maximum increase of deformation rate is observed below the recharge zone. The centre of deformation below the CPGF production zone migrates in a northeast direction. The changes in the ground deformation pattern may be caused by production development in the CPGF due to the newest power plant (CP IV) which started its operation in 2000 in the eastern part of field, as was suggested in Sarychikhina *et al.* (2007) and Glowacka *et al.* (2010).

CONCLUSIONS

We have used differential interferometric analysis of space-borne ENVISAT SAR to map land subsidence in the Mexicali Valley, northwest Mexico. The analysis of DInSAR data shows that, despite several limitations in this method application, the radar data could provide a detailed mapping of both the amplitude and spatial extent of land subsidence in the study area. In particular, the DInSAR mapping confirms that the tectonic faults control the spatial extent of the observed subsidence.

The comparison of the radar observations of land subsidence with levelling observations from the 1994–1997 and 1997–2006 periods reveals changes in both the spatial pattern and rate of subsidence. These changes could be related to the production development in the CPGF and suggest that the land subsidence in the study area is a dynamic process.

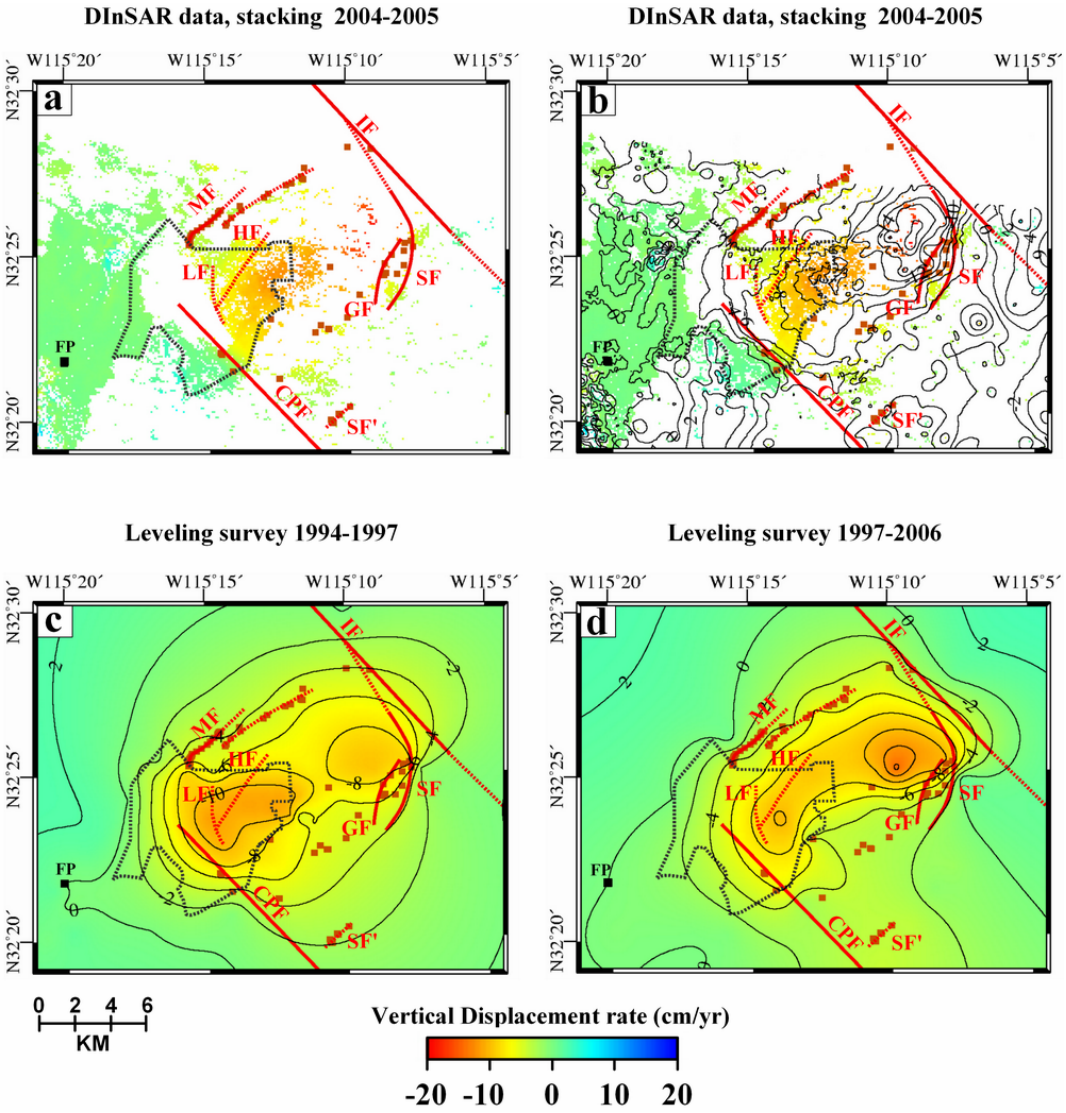

Fig. 3 Vertical displacement rate (cm/year) obtained using data from DInSAR stacking 2004–2005 (a) and (b) and levelling surveys 1994–1997 (c) and 1997–2006 (d). Areas of low coherence (<0.1) are masked in (a) and (b). The contours were obtained by interpolation of the data using Kriging method. FP is the fixed point. The black dotted line frames the limits of the CPGF. Surface traces of tectonic faults (red lines) and mapped fissure zones (brown squares) are shown. CPF = Cerro Prieto fault; IF = Imperial fault; MF=Morelia Fault; SF = Saltillo Fault; SF' = continuation of Saltillo fault as proposed by Suárez-Vidal *et al.* (2008); GF = Guerrero fault; HF = H fault; LF = L fault.

Acknowledgements The European Space Agency's ENVISAT satellite has been used to collect the interferometric data. The data were obtained as part of ESA Cat-1 Project (ID-C1P3508).
This research was sponsored in part by CONACYT, project number 45997-F, CONAGUA, agreement GRPBC-CICESE-01, and CICESE internal funds. The first author was sponsored by the Ministry of Foreign Affairs of Mexico (SRE) PhD scholarship.

REFERENCES

Allis, R. G., Zhan, X. & Clotworthy, A. (1998) Predicting future subsidence at Wairakei Field, New Zealand. *Geothermal Resources Council Trans*. **22**, 43–47.

Carnec, C. & Fabriol, H. (1999) Monitoring and modeling land subsidence at the Cerro Prieto geothermal field, Baja California, Mexico, using SAR interferometry. *Geophys. Res. Lett.* **26**(9), 1211–1214.

Chen, C. W. & Zebker H. A. (2001) Two-dimensional phase unwrapping with use of statistical models for cost functions in nonlinear optimization. *J. Optical Society of America* **18**, 338–351.

Gabriel, A. G., Goldstein, R. M. & Zebker, H. A. (1989) Mapping small elevation changes over large areas: Differential radar interferometry. *J. Geophys. Res.* **94**, 9183–9191.

Glowacka, E., Gonzalez, J. & Fabriol, H. (1999) Recent vertical deformation in Mexicali Valley and its relationship with tectonics, seism city and fluid operation in the Cerro Prieto Geothermal Field. *Pure and Applied Geophysics* **156**, 591–614.

Glowacka, E., Sarychikhina, O. & Nava A. F. (2005) Subsidence and stress change in the Cerro Prieto Geothermal Field, B.C., Mexico. *Pure and Applied Geophysics* **162**, 2095–2110.

Glowacka, E., Sarychikhina, O., Suárez, F., Mendoza, R. & Nava, F. A. (2006) Estudio geológico para definir la zona de hundimiento con el fin de relocalización del canal Nuevo Delta en el Valle de Mexicali. Reporte Técnico. CICESE. México.

Glowacka, E., Sarychikhina, O., Suárez-Vidal, F., Nava, F. A., Farfan, F., Cossio Battani, G. & Guzmán, M. (2007) Aseismic slip observed on the faults in Mexicali Valley, Baja California, Mexico. In: Proceedings of AGU, Spring Meeting.

Glowacka, E., Sarychikhina, O., Suarez-Vidal, F., Nava Pichardo, F. A. & Mellors, R. (2010) Anthropogenic subsidence in the Mexicali Valley, Baja California, Mexico, and slip on the Saltillo fault. *Environ. Earth Sci.* **59**(7), 1515–1524.

Goldstein, R.M. & Werner, C.L. (1998) Radar interferogram filtering for geophysical applications. *Geophys. Res. Lett.* **25**(21), 4035–4038.

González, J. J., Glowacka, E., Suárez, F., Quiñónez, G., Guzmán, M., Castro, J. M., Riviera, F. & Félix, M. G. (1998) Movimiento reciente de la falla Imperial, Mexicali, B. C. *Divulgare, Ciencia para todos, Mexicali, B.C.* **6**(22), 4–15.

Hanssen, R. F. (2001) *Radar Interferometry: Data Interpretation and Error Analysis.* Kluwer Academic Publishers, Dordrecht, The Netherlands.

Kampes, B., Hanssen, R. & Perski, Z. (2003) Radar interferometry with public domain tools, In: Proceedings of FRINGE 2003, 1–5 December, Frascati, Italy (2003).

Massonnet, D. & Feigl, K. L. (1998) Radar interferometry and its application to changes in the Earth's surface. *Rev. Geophysics* **36**(4), 441–500.

Mossop, A. P. & Segall, P. (1997) Subsidence at the Geysers geothermal field, N. California from a comparison of GPS and leveling surveys. *Geophys. Res. Lett.* **24**, 1839–1842.

Sarychikhina, O. (2003) Modelación de subsidencia en el campo geotérmico Cerro Prieto. MSc Thesis, Centro de Investigación Científica y Educación Superior de Ensenada, Ensenada, B.C., Mexico.

Sarychikhina, O., Glowacka, E. & Mellors, R. (2007) Preliminary results of a surface deformation study, using differential InSAR technique at the Cerro Prieto Geothermal Field, B.C., Mexico. *Geothermal Resources Council Trans*. **31**, 581–584.

Scharoo, R. & Visser, P. (1998) Precise orbit determination and gravity field improvement for the ERS satellites. *J. Geophys. Res.* **103** (C4), 8113–8127.

Suarez-Vidal, F, Mendoza-Borunda, R., Naffarrete-Zamarripa, L.M., Ramirez, J. & Glowacka, E. (2008) Shape and dimensions of the Cerro Prieto pull-apart basin, Mexicali, Baja California, México, based on the regional seismic record and surface structures. *Int. Geology Review* **50**(7), 636–649.

(Proceedings of EISOLS 2010, Querétaro, Mexico, 17–22 October 2010). IAHS Publ. 339, 2010.

Long-term Differential InSAR monitoring of the Lampur Sidoarjo mud volcano (Java, Indonesia) using ALOS PALSAR imagery

A. THOMAS[1], R. HOLLEY[1], R. BURREN[1], D. SHILSTON[2], D. WARING[2] & C. MEIKLE[3]

1 *Fugro NPA Limited, Crockham Park, Edenbridge, Kent TN8 6SR, United Kingdom*
a.thomas@fugro-npa.com

2 *Atkins Limited, Woodcote Grove, Ashley Road, Epsom, Surrey KT18 5BW, United Kingdom*

3 *(Formerly of Atkins Limited) Golder Associates Pty Ltd, 124 Pacific Highway, St Leonards, New South Wales 2065, Australia*

Abstract The Lampur Sidoarjo mud volcano (Java, Indonesia), colloquially called LUSI, first appeared in May 2006. Its cause, whether the result of natural or anthropogenic activities (or a combination of both), is still being debated within the academic, engineering and political communities. The mud volcano has expelled up to 150 000 m^3 of mud per day; and over time, this large volume of mud has had a major environmental and economic impact on the region. As of October 2009 the mud flow from LUSI had covered ~6 km^2 to depths of some tens of metres, displacing approximately 30 000 residents; and continues to threaten local communities, businesses and industry. With such a large volume of mud being expelled each day it is inevitable (as with onshore oil and gas production fields) that there will be some ground surface movement and ground surface instability issues at the mud source (the main vent), and in the vicinity of the mud volcano footprint. Due to the dynamic ground surface conditions, engineers and academics alike have found it difficult to reliably monitor ground surface movements within the effected region using conventional surveying techniques. Consequently, the Atkins engineering geologists and geotechnical engineers responsible for the risk assessment of ground surface instabilities within the proximity of LUSI have called upon the use of satellite interferometry to monitor the hazard on a six-month frequency. The Advanced Land Observing Satellite (ALOS), launched 24 January 2006, carries onboard an L-band Synthetic Aperture Radar (SAR) instrument called PALSAR (Phased Array type L-band Synthetic Aperture Radar). In contrast to established C-band (5.6 cm wavelength) SAR instruments onboard ERS-1 and ERS-2, Envisat, Radarsat-1, and the recently launched Radarsat-2 satellite, PALSAR's (L-band/23.8 cm wavelength) instrument presents a number of advantages, including the ability to map larger-scale ground motions, over relatively short timeframes, in tropical environments, without suffering as significantly from signal decorrelation associated with C-band imagery. This paper presents the results of a long-term ALOS PALSAR, differential interferometric (DifSAR) monitoring campaign across the LUSI mud volcano. DifSAR processing was applied to a sequence of single- and dual-polarisation SAR images acquired on a 3- to 6-month basis since May 2006. The results highlight the capability of ALOS PALSAR in detecting decimetres of coherent ground subsidence to assist geologists and engineers in their analysis of the structure, dynamics and overall stability of the mud volcano and its surrounding region.

Key words Differential Interferometry; ALOS PALSAR; Java; mud volcano

INTRODUCTION

The colloquially named "LUSI" mud volcano, Lampur Sidoarjo began erupting on 29 May 2006, during the drilling of an exploratory gas well in the Porong District of Java, Indonesia.

Over the past four years, the continuous flow of hot mud from LUSI has reached estimated rates of between 100 000 and 160 000 m^3 per day and has inundated an area of about 6.4 km^2, which is currently retained by the construction of large earth dams by the local authorities (Fig. 1). Thirteen people have lost their lives and more than 30 000 people have been displaced from their homes by LUSI's eruption. The mud flow has inundated houses, factories, farmland and the Surabaya-Gempol toll road, and caused the rupture of a gas pipeline. It has placed at risk a railway line, the surface water drainage and irrigation network, ecosystems, water pipeline, and fibre-optic cables connecting Surabaya to Eastern Indonesia.

Copyright © 2010 IAHS Press

Fig. 1 The impact of mud inundation. Photograph taken 29 May 2007 © Atkins Ltd, 2007.

The ongoing physical, economic and political effects of LUSI's eruption have been widely documented in newspapers, on the Internet and in academic journals. However, the origin of the LUSI mud volcano is the subject of considerable controversy, with two competing hypotheses. The first proposes that the eruption was the result of an underground blowout caused by the drilling of the Banjarpanji-1 gas exploration well into very deep over-pressured strata (Davies *et al.*, 2007). The second suggests that it was triggered by an earthquake two days earlier, 300 km east of Porong, and this re-activated the local Watukosek fault system which acted as conduit from the over-pressurised strata (Mazzini *et al*., 2007).

In the period shortly after LUSI's initial eruption, there was much political sensitivity regarding its cause, and considerable concern within the local community. People wanted to know what impact the erupting mud was going to have, how long it would last and what mitigating measures would be implemented.

HAZARD MONITORING

In May 2007, Atkins made an initial site visit to reconnoitre the mud volcano and its surrounding area to make an initial assessment of the risks and hazards associated with the mud volcano. LUSI had been erupting for about one year at the time of the visit and best estimates of the longevity were that it would continue to erupt for about 10 to 40 years. Judgements about LUSI's behaviour and the risk posed to local property, industry and businesses in the months and years to come, were necessarily tentative. Atkins suggested that a limited programme of hazard monitoring using remote sensing would be best to meet the requirements for regularly updating the initial risk assessment.

Remote sensing specialists Fugro NPA helped Atkins design and implement a hazard monitoring programme that made use of two types of satellite mapping: VHR (Very High Resolution) optical imagery and satellite InSAR (Interferometric Synthetic Aperture Radar). The imagery was procured and processed by Fugro NPA's InSAR surveying team and analysed by Atkins.

VERY HIGH RESOLUTION IMAGERY

The physical consequences of LUSI have been observed and recorded using regularly acquired VHR optical images from the IKONOS and Quickbird satellites (Fig 2). Comparisons made

between images taken every 1 to 3 months have enabled good assessments to be made. During analysis of the VHR optical imagery, attention was paid to the distribution of mudflows from the vent, the construction and performance of the earth dams, changes in behaviour of the nearby rivers, changes in land use, distribution of surface water flooding, and lateral migration of the mud volcano vent. All observed data were recorded within a GIS (Geographical Information System) geo-database (Fig. 3).

ALOS PALSAR INTERFEROMETRY

In addition to the surface changes due to mud inundation, ground subsidence due to withdrawal of material from subsurface levels was a key concern. Further to the effects of such subsidence on the local environment and infrastructure, the location and magnitude of the subsidence signals also gives valuable information about the subsurface structure and dynamics of the volcano, essential to understanding the ongoing risks. Satellite-based InSAR techniques provide measurements of ground deformation, meeting the requirement for a remote monitoring solution.

The combination of largely agricultural land use and the large amount of ground movement observed and predicted across the area of interest would result in poor interferometric coherence in conventional C-band (5.6 cm wavelength) interferograms. The longer 23.6 cm wavelength of L-band SAR data increases coherence in vegetated areas, and enables measurement of larger magnitude deformation signals.

ALOS PALSAR is an L-band instrument operated by JAXA (Japanese Aerospace Exploration Agency). Fugro NPA acquired a sequence of ten ALOS PALSAR images at approximately 6-month intervals, starting from 19 May 2006 (pre-eruption). Figure 4 shows three wrapped differential interferograms; in each case the mud volcano can be seen as an approximately rectangular area of incoherence surrounded by between 12 cm and 108 cm of line-of-sight subsidence. By comparison with Fig. 2 and Fig. 3, the rectangular patch of incoherence can be seen to correspond to the area inundated by mudflows from the volcano.

From mid-2008 the single-polarisation (FBS) ALOS acquisition plan was reduced to once per year, meaning six-monthly monitoring was no longer possible in this mode. After assessing alternative PALSAR data options, it was identified that dual-polarisation (FBD) data is also acquired on a 12 month basis, offset from the FBS data acquisition by 6 months. Dual polarisation refers to data transmitted in one polarisation and received in both. In this case the radar signal transmitted pulses with horizontal (H) polarisation, but alternated between receiving components of the signal with horizontal or vertical (V) polarisation. This results in two separate SAR data sets, HH and HV, each with half the resolution of single polarisation data. The HH component can then be over-sampled and compared to the single-polarisation HH image to produce an inter-ferogram. This enabled six-monthly monitoring to continue, and the reduced resolution was still more than adequate to record the ongoing subsidence surrounding the mud volcano (Fig. 4).

MODELLING

These interferograms enabled construction of three-dimensional models of the ground surface deformation associated with LUSI. This revealed a primary area of subsidence surrounding the mudflow extent; this is most severe near the vent, where it is difficult to monitor due to loss of coherence over the constantly-changing mudflow. To the west of the mudflow extent there is a zone of secondary subsidence, and there is a zone of lesser magnitude uplift to the northeast. Deformation magnitude was highest in the first interferogram period, spanning the beginning of the eruption; however, noticeable deformation has occurred in each of the subsequent inter-ferograms, indicating ongoing subsidence of the area.

Thus far, the immediate effects of LUSI (specifically the mud flow extent and ground surface deformation) have not had an impact on the client's site.

Fig. 2 Sequence of IKONOS satellite images acquired across the location of the mud volcano (centre of image). Images were acquired on 14 November 2002 (left), 31 October 2006 (middle) and 5 January 2007 (right). Images © GeoEye and Fugro NPA Ltd.

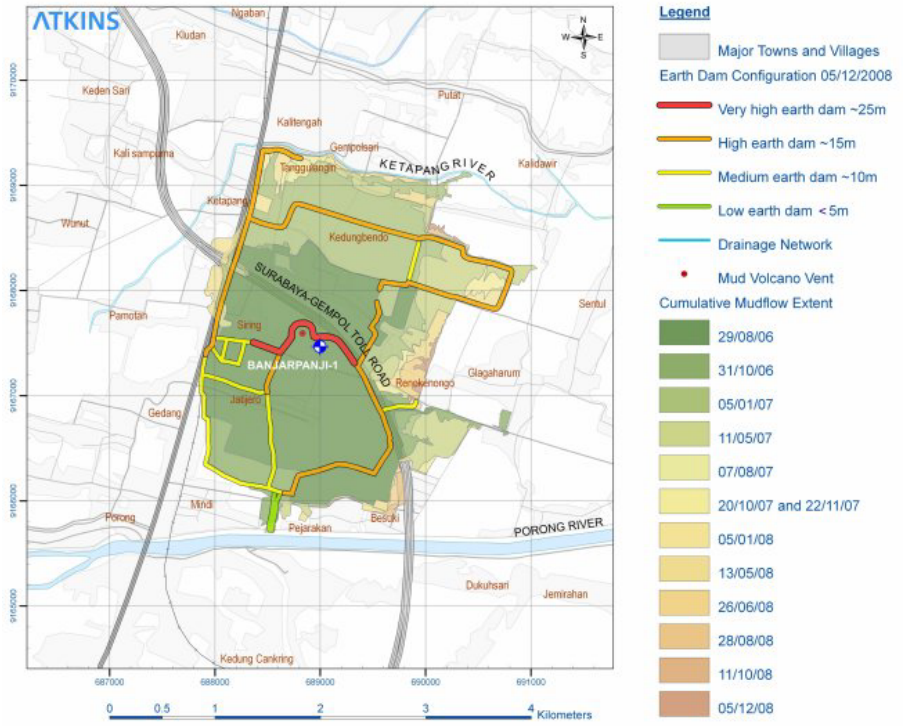

Fig. 3 An extract from the GIS geodatabase (05/12/2008) used to record the physical changes associated with the LUSI mud volcano. Image © Atkins Ltd. 2009.

CONCLUSIONS

Since its initiation on 29 May 2006, LUSI's eruption has had, and continues to have, a devastating effect on the Porong District of Eastern Java (Meikle & Shilston, 2009). The flow of mud and ground surface deformation has caused significant physical, environmental, economical and social damage to the local and regional communities. The remaining lifespan of LUSI's eruption is still not known, but best estimates are that it will continue to erupt for decades and not just a few years.

The sequence of differential interferograms produced so far are an excellent demonstration of the capabilities of the L-band ALOS PALSAR sensor. The results, derived remotely and at a comparatively low cost, have given the team and their client a unique and important insight into

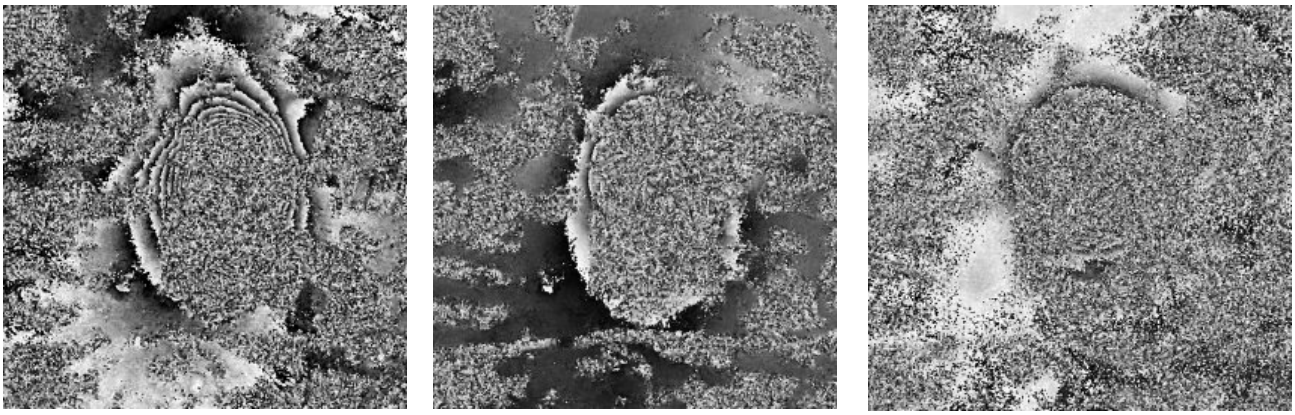

Fig. 4 Sequence of differential interferograms. Left: FBS differential interferogram spanning 19 May–19 November 2006. Middle: FBS differential interferogram spanning 19 February–22 August 2007; Right: FBS-FBD differential interferogram spanning 4 January–7 July 2009. SAR data © JAXA 2007. Image copyright Fugro NPA Ltd. 2010.

the evolution of ground surface deformation across the mud volcano, even with variable levels of coherence across the site. The ability to produce and successfully derive information from FBS-FBD interferograms has enabled monitoring to continue for the foreseeable future.

For now, a continued programme of regular remote monitoring of the mud flow extent and ground surface deformation, such as the one designed and implemented by the team, will provide a valuable resource for updating geohazard and risk assessments, aiding the management of LUSI and its impact into the future.

REFERENCES

Davies, R. J., Swarbrick, R. E., Evans, R. J. & Huuse, M. (2007) Birth of a mud volcano: East Java, 29 May 2006. *GSA Today* **17**(2), 4–9.

Mazzini, A., Svensen, H., Akhmanov, G. G., Alonsi, G., Planke, S., Malthe-Sørens, A. & Istadi, B. (2007) Triggering and dynamic evolution of the LUSI mud volcano, Indonesia. *Earth and Planetary Science Letters* **261**, 375–388.

Meikle, C. D. & Shilston D. T. (2009) Mud wrestling – geohazard monitoring of the erupting LUSI mud volcano, Java. *Ground Engineering* November 2009, 16–18.

Land Subsidence, Associated Hazards and the Role of Natural Resources Development
(Proceedings of EISOLS 2010, Queretaro, Mexico, 17–22 October 2010). IAHS Publ. 339, 2010.

Radar interferometry-based mapping of the present land subsidence along the low-lying northern Adriatic coast of Italy

G. BITELLI[1], F. BONSIGNORE[2], L. CARBOGNIN[3], A. FERRETTI[4], T. STROZZI[5], P. TEATINI[3,6], L. TOSI[3] & L. VITTUARI[1]

1 *Dept of Civil, Environmental and Materials Engineering (DICAM), University of Bologna, Viale del Risorgimento 2, I-40136 Bologna, Italy*
gabriele.bitelli@unibo.it

2 *ARPA Emilia-Romagna, Largo Caduti del Lavoro 6, I-40121 Bologna, Italy*

3 *Institute of Marine Sciences (ISMAR), National Research Council, Castello 1364/a, I-30122 Venezia, Italy*

4 *Tele-Rilevamento Europa S.r.l. (TRE), Via V. Colonna 7, I-20149 Milano, Italy*

5 *Gamma Remote Sensing AG, Worbstrasse 225, CH-3073 Gümligen (Bern), Switzerland*

6 *Dept of Mathematical Methods and Models for Scientific Applications (DMMMSA), University of Padova, via Trieste 63, I-35121 Padova, Italy*

Abstract The northern Adriatic coastal area, Italy (from the Veneto region northward, and to the Romagna region to the south), is characterized by low-lying environments such as lagoons, e.g. those of Venice and of the Valli di Comacchio, wetlands and deltas, such as that of the Po River delta, and reclaimed farmland and beaches subjected to marked anthropogenic pressure. The coastal area is characterized by an elevation generally well below the mean sea level (down to –4 m m.s.l.) and never exceeds 2 m above m.s.l. Man-induced land subsidence has greatly affected the whole coastal area over the 20th century, and especially from the 1950s and the 1970s, when over-exploitation of subsurface fluids was responsible for the occurrence of general lowering. Although the sinking rates have significantly decreased over the last decades, land subsidence is still a process threatening the entire coastal environment. In this study we report a recent investigation aimed at mapping the vertical displacements recorded in the period 1992–2000 on the 20–30 km wide and 250-km long coastal area from the Tagliamento River to the north, to the town of Rimini to the south. Measurements have been carried out by Persistent Scatterer Interferometry (PSI) using levelling and GPS records to reference the interferometric solution. The results identify the variability of the ground movements that are presently occurring along the northern Adriatic coastline. Substantially stable areas, the most important of which are the cities of Venice and Ravenna and their surroundings, contrast with subsidence rates of more than 10 mm/year recorded in some parts of the Po River delta and to the south. The observed land displacements have been associated with the geological features of the study region, i.e. tectonics and differential consolidation of the Middle–Upper Pleistocene and Holocene deposits, and to anthropogenic activities, mainly groundwater withdrawal from the Upper Pleistocene-Holocene alluvial deposits and more locally peatland oxidation in reclaimed areas and gas exploitation from Plio-Pleistocene reservoirs.

Key words land subsidence; PSI; northern Adriatic coastland; geological features; anthropogenic activities

INTRODUCTION

The northern Adriatic coastal area, from the Venice region in the north to the Romagna region to the south (Fig. 1), is underlain by a subsiding sedimentary basin. The Adriatic Sea bed is characterized by shallow water depth and its coastline by the presence of lagoons, deltas, marshes, and reclaimed lands, some of which presently lie below mean sea level, making it a fragile area at great hydrogeological risk.

The area was exposed during the Late Pleistocene period of low sea level, and then was progressively flooded during the Holocene transgression. The coastline reached its maximum landward extent about 6000 years BP, when the climate optimum was achieved, and then prograded during the sea level highstand. Eustacy and land subsidence have been the most important processes inducing geomorphological changes all over the area since its very origin. Throughout recent centuries, human interventions have greatly modified the natural evolution of the coastal setting and hydrodynamics. The contribution of anthropogenic land subsidence to the relative sea/ground elevation change has been predominant.

Copyright © 2010 IAHS Press

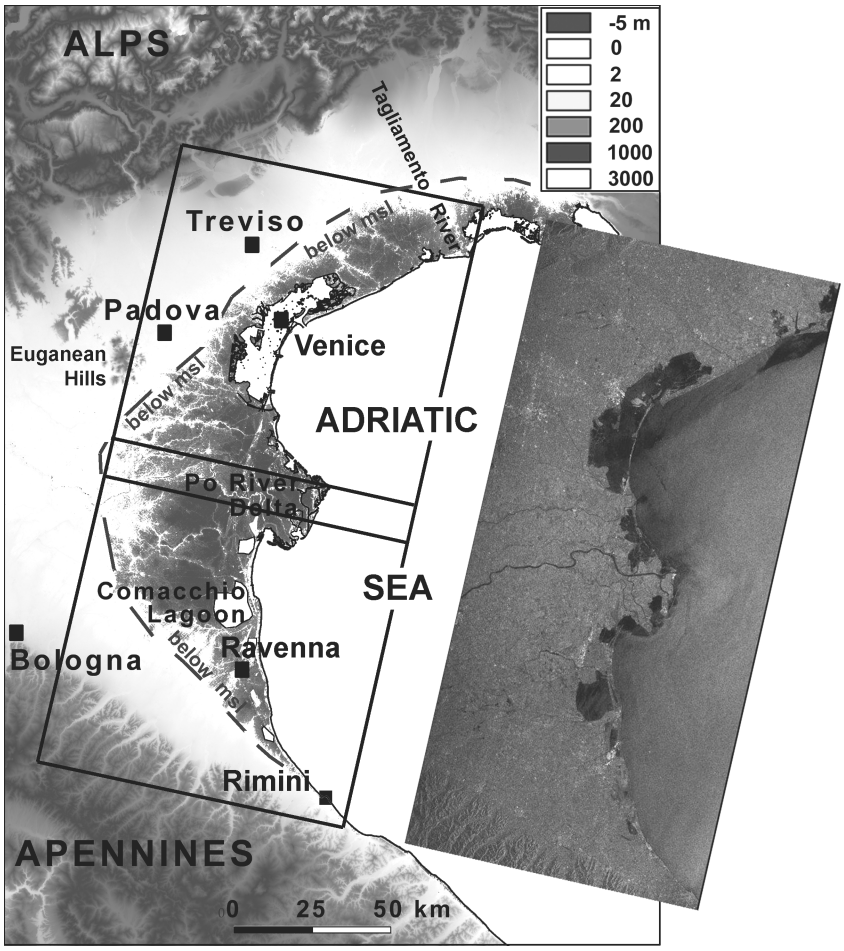

Fig. 1 Digital elevation model (DEM) of the northern Adriatic coastland with the trace of the ERS-1/2 track 122 used by PSI in this study. The 2691 and 2709 frames have been considered in the Venice (northern) and Romagna (southern) regions, respectively. As an example, the ERS-2 image acquired on 4 November 1998, is shown on the right.

Vertical displacements of the northern Adriatic coastal areas are controlled by both natural and anthropogenic factors acting on different timescales (millions to thousands of years, and hundreds to tens of years, respectively), reflecting the geological history and the human development of the territory. The role played by the long-timescale natural causes, i.e. tectonics and glacio-isostasy, became negligible in modern times, while the consolidation of Quaternary sediments has assumed major importance. Short-timescale man-induced causes have become the key factors controlling the changes of land elevation over the 20th century, and especially since World War II. The main cause of land settlement was the exploitation of subsurface fluids. The only difference was the nature of the withdrawn fluids: freshwater in the Venice area, gas-bearing water in the Po Delta, and both groundwater and gas (inshore and offshore) in the Romagna region.

Starting from the 1970s, countermeasures have been taken and levelling surveys have revealed a significant reduction of ground settlement all across the northern Adriatic coastal area. New technologies, in particular Synthetic Aperture Radar (SAR)-based interferometric analyses, have allowed accurate measurement of the movements of the study area over the last two decades. Here, a stack of ERS-1/2 SAR data from 1992 to 2000 is processed by PSI. The Permanent Scatterers – PS (Ferretti *et al.*, 2001) and the Interferometric Point Target Analysis – IPTA (Werner *et al.*, 2003) techniques have been used to the south and to the north of the Po River delta, respectively. The two data sets have been homogenized and integrated to provide a comprehensive picture of the recent movements of the largest flat coastal area in Italy.

GEOLOGICAL SETTING

The northern Adriatic basin is bounded by the Apennine ranges to the south, the Alps to the north, and the Dinaric belts to the east (Fig. 1). The region is a foreland sedimentary basin consisting of a sequence of deposits of Alpine and Apennine origin, accumulated in different environments during the Pliocene and the Quaternary, and mostly made of sandy and silty-clay layers of alluvial and marine deposition, respectively. The geological setting down to about 5000 m consists of pre-Pliocene, Pliocene, and Quaternary deposits. The pre-Quaternary substratum exhibits a complex structure. Southwards it is characterized by folds and faulted overfolds, which are parallel to the main tectonic trend of the Apennines and include several gas-bearing traps at depths ranging between 1000 and 4000 m. In the Venice region, a NW–SE fault system is confined inside the Liassic carbonates and only occasionally crosses the entire carbonate deposits. Neo-tectonics and deep geothermal processes are likely affecting the areas surrounding the Euganean Hills (Doglioni, 1993; Carminati *et al*., 2003; Tosi *et al*., 2009.

The thickness of the Quaternary sediments ranges between 3000 m (southern zone) and hundreds of metres (northern zone). The presence of massive Quaternary deposits confirms that in the past, geological subsidence was quite pronounced in this area and recently was still rather active, it being apparent that the tectonic stresses acting along the SW direction tend to increase the Po basin curvature. In spite of the different thickness, the stratigraphy of the Quaternary soils is quite similar to the well-developed freshwater multi-aquifer systems that are located in the upper 300–450 m (600 m in the Po delta zone). Semi-confined aquifers occur within the Holocene deposits where clayey and sandy layers are discontinuous and heterogeneous. Below 450 m, the salt content becomes very high and the water can no longer be used for human activities (industrial, agricultural, and potable purposes).

PSI AT THE NORTHERN ADRIATIC COASTLAND

Land movements in the northern Adriatic coastal area have been monitored by processing time series of ERS-1/2 satellite radar images through PS and IPTA interferometric techniques. These methodologies are capable of measuring changes in the distance between the satellite sensors and the targets, recording phase differences between the emission of the electromagnetic wave and the reception of back-scattered signal by the targets at two different epochs. Due to their frequency of acquisition (approximately monthly), SAR data provide repeated measurements of deformation of the targets. The PSI techniques aim to exploit all acquisitions available over the same area and to identify those targets for which the electromagnetic characteristics remain unaltered over time.

The analysis of the interferometric radar data involves some technological issues and others related to the specific application, in particular due to the considerable size of the surveyed area. The innovative nature of this technique, especially when applied to areas of great extension, highlights the need to develop shared methodologies and protocols for validation of the results, similar to what has already been done for other more traditional methods of land surveying. One of the most delicate and important tasks is the evaluation of the significance degree of the calculated movements. Two parameters have been first considered regarding the intrinsic data quality, i.e. the coherence and the standard deviation values associated with the velocity determination of each persistent scatterer. Moreover, a second step requires constraining of the PSI solution using levelling and/or GPS records to mitigate the so-called “flattening” problem, i.e. the slight rotation that characterizes the interferometric results over large areas due to the imperfect knowledge of the satellite positions.

This paper highlights the vertical movements derived from a strip of persistent scatterers limited to the 20–40 km wide coastal area (Fig. 2). However, the processed zone covers the whole eastern portion of the Po River plain, in particular the strip corresponding to track 122 (descending orbit) of the ESA ERS-1/2 satellites. We have used all the images acquired between May 1992 and December 2000 and corresponding to the 2691 (Venice region, northward) and 2709 (Romagna region, southward) frames (Fig. 1).

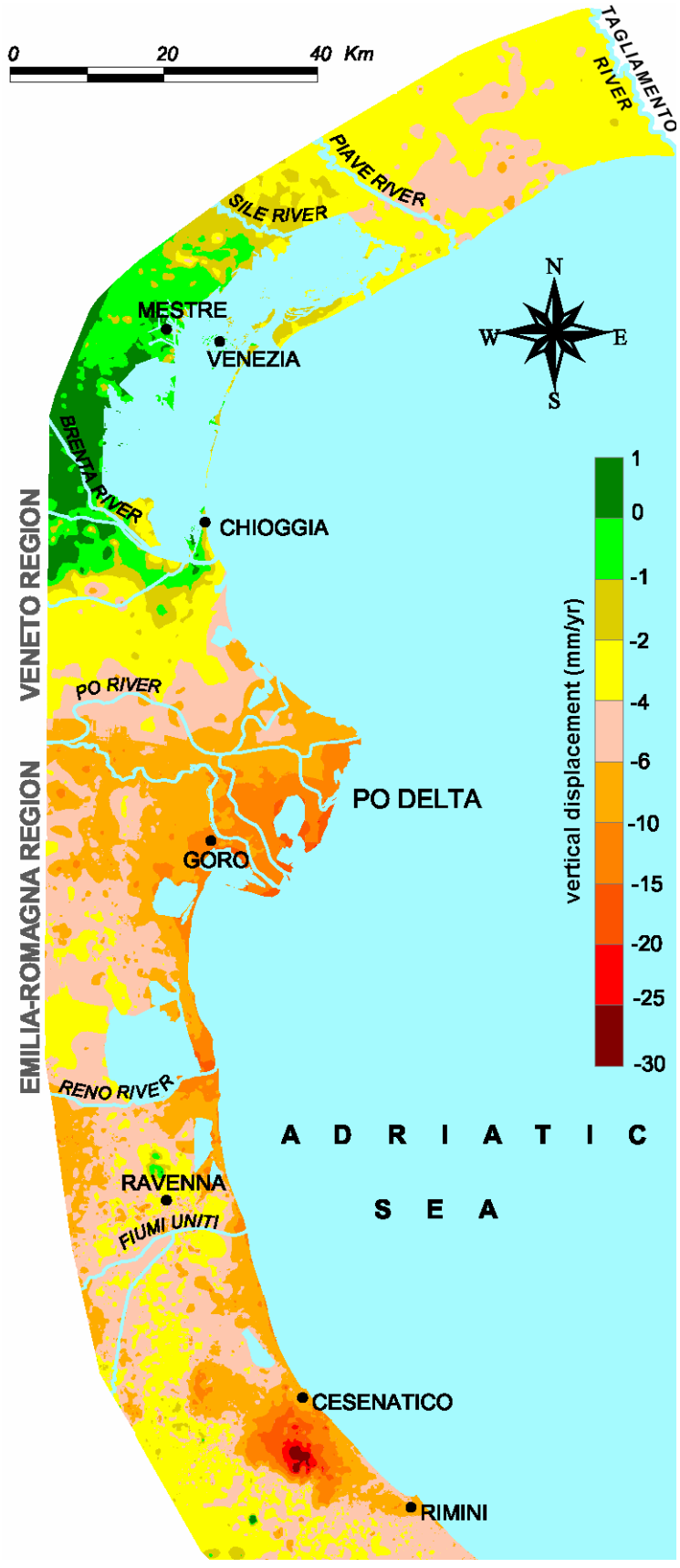

Fig. 2 Map of the displacement rates (mm/year) in the northern Adriatic coastal area obtained by PSI on ERS-1/2 images during the 1992–2000 period. Negative values mean land subsidence.

More than 50 000 persistent scatterers have been detected in the study area. The annual vertical velocity was calculated for each persistent scatterer with respect to two reference points: one in Treviso for the portion to the north of the Po River delta, and the other in Gualtieri (RE) for the southern zone, after verification of its stability with respect to Sasso Marconi (BO) located in the Apennine foothills. The choice of the references was made on the basis of statistical considerations concerning the coherence of the signal and on historical records of land subsidence. In order to validate the interferometric data set, the PSI outcomes have been calibrated using the velocity of movement derived from spirit levelling surveys carried out by ARPA-ER, the regional Emilia-Romagna Environmental Protection Agency (Bitelli *et al*., 2000, 2001, 2008; Bonsignore, 2008), and the Venice Institute of the Italian National Research Council (Carbognin *et al.*, 2000, 2004; Teatini *et al*., 2005a; Tosi *et al*., 2007). Unfortunately, the available levelling data relate to different periods that do not exactly overlap the 1992–2000 interval. In the absence of other information, linear subsidence rates were considered over these periods and a comparison was made between the velocities of levelling benchmarks with respect to the movement rates derived from the interferometric analysis.

RESULTS

The IPTA and PS data described for the Venice and Romagna regions, respectively, have been compared for the few-km wide strip on the Po River delta where the two frames overlap (Fig. 1). A gentle tilt of the two solutions has sufficed to homogenize the data sets. Then, the overall database was interpolated by kriging on a 100 × 100 m grid, assuming that the displacement rate is an isotropic stochastic variable satisfying the intrinsic hypothesis. The result thus obtained is shown in Fig. 2.

Inspection of Fig. 2 reveals a certain difference between the displacement rates observed north- and southward of the Po River, with the Venice area being generally more stable than the Romagna coastland. In particular, moving from the Tagliamento River southward, the following details are worth highlighting: (a) the area north of the Venice Lagoon is characterized by a subsidence rate of between 2 and 6 mm/year; (b) a general land stability is recorded in the central part of the Venice coastland, including the city of Venice, with only a small but significant uplift (~1 mm/year) at the portion of the southern lagoon margin facing the Euganean Hills. A subsidence rate up to 3–4 mm/year is measured along the whole northern littoral of the lagoon and in some parts of the southern lagoon margin; (c) the subsidence rates increase considerably in the Po River delta, with a significant rise moving seaward where values of approximately 15 mm/year are observed; (d) land settlement great than 10 mm/year continues to occur along the coast to the south, at the mouths of the Reno River and Fiumi Uniti, as far as the Ravenna area. Conversely, at Ravenna, the velocities reduce to less than 1 mm/year; (e) from Ravenna to Rimini, land subsidence is characterized by a high variability and with a general trend showing a decrease of the sinking rate moving inland. Within this southernmost sector of the study area, land subsidence ranges between 2 and 10 mm/year, with a zone south of Cesenatico where the settlement increases to up to 30 mm/year.

CONCLUDING DISCUSSION

The northern Adriatic coastal area is a complex system where depositional and tectonic factors, and human interventions contribute to the observed vertical displacements of the land surface. In this paper we focus attention on the 1992–2000 movements as measured by PSI using SAR images acquired from the ERS-1/2 satellites.

The high resolution and accuracy of the measurements show that movements in coastal areas can usually be characterized by significant spatial variability. We briefly analyse in this concluding section the geological information and the anthropogenic activities in order to identify the factors responsible for the observed displacement variability (Fig. 3).

Even if less important than over long timescales, the role played by the natural causes, i.e. tectonics and consolidation of Quaternary sediments, still assumes a certain importance. Land uplift in the coastal plain between the Euganean Hills and the lagoon are most likely related to neo-tectonic activity (Tosi *et al*., 2009). Natural consolidation of the Quaternary sediments has been estimated to range one order of magnitude (from 0.5 to 5 mm/year) along the coastal arc of the northern Adriatic. The higher values occur at the Po River delta and, secondly, at the Ravenna area corresponding to the thicker Quaternary sedimentation (Gambolati & Teatini, 1998; Carbognin *et al.*, 2000). Even larger values are likely to locally occur in recent coastal areas formed over the Holocene (Tosi *et al*., 2009). A value of less than 1 mm/year affects the Venice Lagoon and the northernmost sector. Other natural components such as glacio-isostasy result in practically negligible changes, being characterized by values less than 0.2 mm/year in the northern Adriatic (Spada *et al.*, 2009).

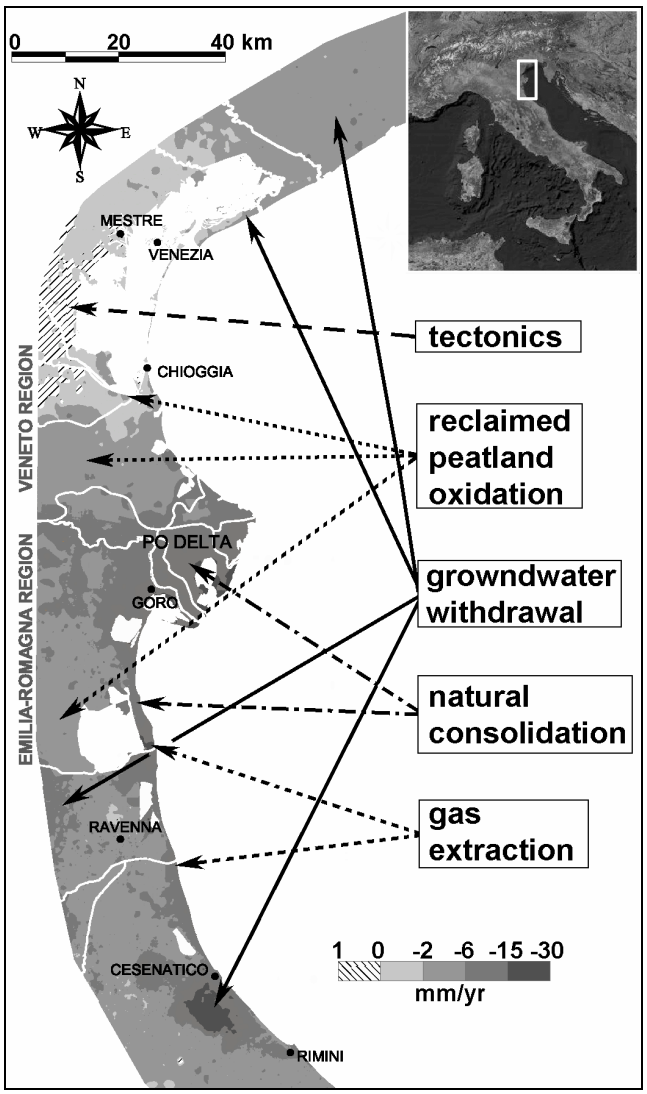

Fig. 3 Distribution of the various factors that likely contribute to the observed land displacements over the 1992–2000 period.

Anthropogenic subsidence due to subsurface fluid withdrawals is recently the cause responsible for the major loss of land elevation, at least in some parts of the study area. These are primarily due to groundwater pumping from a well developed multiaquifer system underlying the coastal zone and, secondly, to gas extraction from deep reservoirs scattered through the area and

still productive nowadays (Teatini *et al*., 2005b; Tosi *et al.*, 2009). Land subsidence due to aquifer exploitation mainly occurs in the northern portion of the Venice coastland, wherein thousands of active wells are primarily used for potable and thermal purposes, and along the northern littoral of the Venice Lagoon for agricultural use. On the basis of the pumping knowledge available to date, land subsidence most recently measured along the strip close to the coastline is likely to be mainly associated with groundwater pumping in the southern part of the Romagna coastland. Over the Ravenna territory and north of the historical city the present coastal settlement does not seem to be strictly related to ongoing water pumping. Some effects are likely to occur westward of Ravenna where groundwater is still used for industrial purposes (Teatini *et al.*, 2006).

Two other factors contribute to the lowering of the coastal zone, although they act at a much smaller scale, i.e. oxidation of recently reclaimed peatlands and gas extraction from deep gas reservoirs. The northern Adriatic coastland, especially the part between the Venice Lagoon and the Valli di Comacchio, is characterized by the presence of outcropping peatlands derived from recent marshland reclamation. Systematic drainage of farmed organic soils is responsible for a lowering of the peatland surface due to the microbial oxidation of the peat carbon (Gambolati *et al*., 2005). An increase of the sinking rate is recorded at the coastland above a couple of gas reservoirs. The data collected from three borehole extensometers located along the coastline, show that the compaction of the upper 350 m sedimentary column is significantly smaller than subsidence, suggesting that the production from these two fields might be a major cause for the settlement measured there (Teatini *et al*., 2005b).

Finally, it is worth remembering that this area is highly sensitive to eustatic sea-level rise (e.g. Carbognin *et al*., 2009) that further contributes to the loss of land elevation with respect to the mean sea level. Concerning this aspect, Carbognin *et al*. (2010) have demonstrated that the contribution of sea level rise to the overall relative land subsidence that occurred over the period 1896–2006 equals 43% at Venice, i.e. in the area that has experienced the smallest ground sinking, 15% in the Ravenna area, and only 5% at the Po Delta where the greatest land subsidence has occurred.

Acknowledgements We are grateful for the financial support to "Servizio Tutela e Risanamento Risorsa Acqua" and "Servizio di Pianificazione di Bacino e della Costa" of the Emilia-Romagna Region. The work was also supported by the VECTOR (Action 3 – Research line 5, CLIVEN), CNR DG.RSTL.156, Co.Ri.La 3.16, MIUR-PRIN2007, and INLET and ISES projects. We thank Monica Branchi (Arpa Emilia-Romagna) for her valuable aid in deriving the land displacement map.

REFERENCES

Bitelli, G., Bonsignore, F. & Unguendoli, M. (2000) Levelling and GPS networks for ground subsidence monitoring in the Southern Po Valley. *J. Geodyn.* **30**(3), 355–369.

Bitelli, G., Bonsignore, F. & Unguendoli, M. (2001) La subsidenza in Emilia-Romagna e le sue conseguenze sulla gestione del territorio. In: *Atti del I° convegno AUTeC, Le tecniche del rilevamento in ambito interdisciplinare*, Napoli, 133–146.

Bitelli, G. & Vittuari, L. (2008) Verifica ed elaborazione dei risultati dell'analisi interferometria. In: *ARPA-ER Rivista - Il Monitoraggio della Subsidenza: Esperienze a Confronto*, 14–15. Suppl. n. 1 gennaio-febbraio.

Bonsignore, F. (2008) Il monitoraggio in Emilia Romagna. In: *ARPA-ER Rivista - Il Monitoraggio della Subsidenza: Esperienze a Confronto*, 12–13. Suppl. n. 1 gennaio-febbraio.

Carbognin, L., Frankenfield Zanin, J. & Marabini, F. (2000) *Po River Delta Region, Italy. An Overview of Environmental Evolution and Land Subsidence*. Published on the occasion of the Sixth International Symposium on Land Subsidence, Ravenna, Italy. La Garangola, Padova, Italy, 42 p.

Carbognin, L., Teatini, P. & Tosi, L. (2004) Relative land subsidence in the lagoon of Venice, Italy, at the beginning of the new millennium. J. *Mar. Sys*. **51**(1-4), 345–353.

Carbognin, L., Teatini, P., Tomasin, A. & Tosi, L. (2009) Global change and relative sea level rise at Venice: What impact in term of flooding. *Climate Dyn.*, doi: 10.1007/ s00382 -009-0617-5.

Carbognin, L., Teatini, P. Tosi, L. & Strozzi, T. (2010) Present relative sea level rise in the northern Adriatic coastal area. In: *Volume Mare: le Rassegna delle attività di ricerca del CNR, Dipartimento Terra e Ambiente*, CNR Roma (in press).

Doglioni, C. (1993) Some remarks on the origin of foredeeps. *Tectonophysics* **228**, 1–20.

Gambolati, G. & Teatini, P. (1998) Numerical analysis of land subsidence due to natural compaction of the Upper Adriatic Sea basin. In: *CENAS, Coastline Evolution of the Upper Adriatic Sea Due to Sea Level Rise and Natural and Anthropogenic Land Subsidence*, (ed. by G. Gambolati), 103–132. Kluwer Academic Publ., Water Science and Technology Library NO. 28.

Gambolati, G., Putti, M., Teatini, P., Camporese, M., Ferraris, S., Gasparetto-Stori, G,. Nicoletti, V., Rizzetto, F., Silvestri, S. & Tosi, L.(2005) Peatland oxidation enhances subsidence in the Venice watershed. *EOS Trans. AGU* **86**(23), 217–224.

Ferretti, A., Prati, C. & Rocca, F. (2001) Permanent scatterers in SAR interferometry. *IEEE Trans. Geosci. Remote* **39**, 8–20.

Spada, G., Stocchi, P. & Colleoni, F. (2009) Glacio-isostatic adjustment in the Po plain and in the northern Adriatic region. *Pure Appl. Geophys.* **166**(8-9), 1303–1318.

Teatini, P., Tosi, L., Strozzi, T., Carbognin, L., Wegmüller, U. & Rizzetto, F. (2005a) Mapping regional land displacements in the Venice coastland by an integrated monitoring system. *Remote Sens. Environ*. **98**(4), 403–413.

Teatini, P., Ferronato, M., Gambolati, G., Bertoni, W. & Gonella, M. (2005b) A century of land subsidence in Ravenna, Italy. *Environ. Geol*. **47**(6), 831–846.

Teatini, P., Ferronato, M., Gambolati, G. & Gonella, M. (2006) Groundwater pumping and land subsidence in the Emilia-Romagna coastland, Italy: Modeling the past occurrence and the future trend. *Water Resour. Res*. **42**, W01406, doi:10.1029/2005WR004242.

Tosi, L., Teatini, P., Carbognin, L. & Frankenfield, J. (2007) A new project to monitor land subsidence in the Northern Venice coastland (Italy). *Environ. Geol*. **52**, 889–898.

Tosi, L., Teatini, P., Carbognin, L. & Brancolini, G. (2009) Using high resolution data to reveal depth-dependent mechanisms that drive land subsidence: The Venice coast, Italy. *Tectonophysics* **474**, 271–284.

Werner, C., Wegmüller, U., Strozzi, T. & Wiesmann, A. (2003) Interferometric point target analysis for deformation mapping. In: *IGARSS 2003*, vol. VII, 4362–4364. Institute of Electrical and Electronics Engineering.

Land Subsidence, Associated Hazards and the Role of Natural Resources Development
(Proceedings of EISOLS 2010, Querétaro, Mexico, 17–22 October 2010). IAHS Publ. 339, 2010.

Monitoring swelling soils through PSI and DinSAR interferometry: applications in eastern Paris Basin, France

H. F. KAVEH[1], B. DEFFONTAINES[1,2,5], B. FRUNEAU[1], R. COJEAN[3], M. AUDIGUIER[3], A. ARNAUD[4] & J. DURO[1,4]

1 *Université Paris-Est, Laboratoire de Géomatériaux et de Géologie de l'Ingénieur (G2I), 5 Bd Descartes, F-77454 Marne-La-Vallée, Cedex 2, France*
frederic.kaveh@univ-mlv.fr, benedicte.fruneau@univ-mlv.fr

2 *Université Pierre et Marie Curie, CNRS-INSU (UMR 7193), Institut des Sciences de la Terre de Paris, 4, Place Jussieu, F-75252 Paris Cedex 05, France*

3 *Centre de Géoscience, Ecole des Mines de Paris. Fontainebleau, France*

4 *Altamira-Information, Parc Technologique du Canal, 10, avenue de l'Europe, F-31520 Ramonville Saint-Agne,France*

5 *Ecole Nationale des Sciences Géographiques, Laboratoire de Géomatique, 6, et 8 avenue Blaise Pascal, Cité Descartes, F-77455 Marne-la-Vallée Cedex 2, France*

Abstract Swelling soils may induce, under various climatic conditions, surface displacements that affect buildings. The aim of this work is to monitor, using new interferometric methods, PSI and DinSAR, those small displacements through time. First, the radar differential interferometry (DinSAR) method, which enables one to map surface displacements from two radar images acquired at different dates, is compared to the results obtained by Persistent Scatterer Interferometry (PSI) as the study area is located in the eastern Paris Basin, France, which has been greatly affected by recent dryness hazards. This new application with interferometric methods presents great potential for better understanding of the geological processes and the natural hazards induced by present climatic modifications.

Key words geotechnical drought; swelling clays; interferometry; DinSAR; PSI; GIS; Villiers-sur-Marne; Gournay-sur-Marne; East Paris Basin

INTRODUCTION

Many individuals' houses in the Paris suburbs are deformed due to differential movement caused by the swelling soil phenomena (max. 15 centimetres revealed by our field analyses). The 2003 drought hazards in France cost more than 3 billions Euros to insurance companies and the French state, and represented a major problem. The French Geological Institute (BRGM) has mapped the clayey soils (www.argiles.fr) using their regional 1/50 000 geological maps. But, the upper superficial formations and soils remain unknown in detail. So the main objective of this work is to locate, characterize and quantify the small displacements due to swelling soil using the new PSI and DinSAR interferometric remote sensing technologies.

RADAR DATA AND METHODS

The PSI method enables the precise analysis of a coherent pixel unit of the radar images. Each geographic element displays an answer, but if only one natural corner mainly reflects the signal, it dominates the wave retrodiffusion and makes it also possible to follow the displacement with time along the radar line of sight (LOS). The radar database used in this study is the ERS 1 & 2 (thanks to the support of the ESA CAT1 project no. 4362). Usually, the linear movements are analysed in interferometry. In this work we use the last chain process from Altamira-Information (Duro, 2009) in order to analyse the nonlinear movement of the ground and houses due to various seasonal climatic conditions.

CONTEXT OF THE GOURNAY-SUR-MARNE AREA

A geological-geographical database has been created using aerial photographs, land use and geological maps, in order to analyse and better interpret the interferometric measurements.

Copyright © 2010 IAHS Press

Figure 1 shows the appropriate thematic data in three-dimensional (3-D) views of the study area. The Gournay-sur-Marne area is located in the alluvial plain of the Marne River.

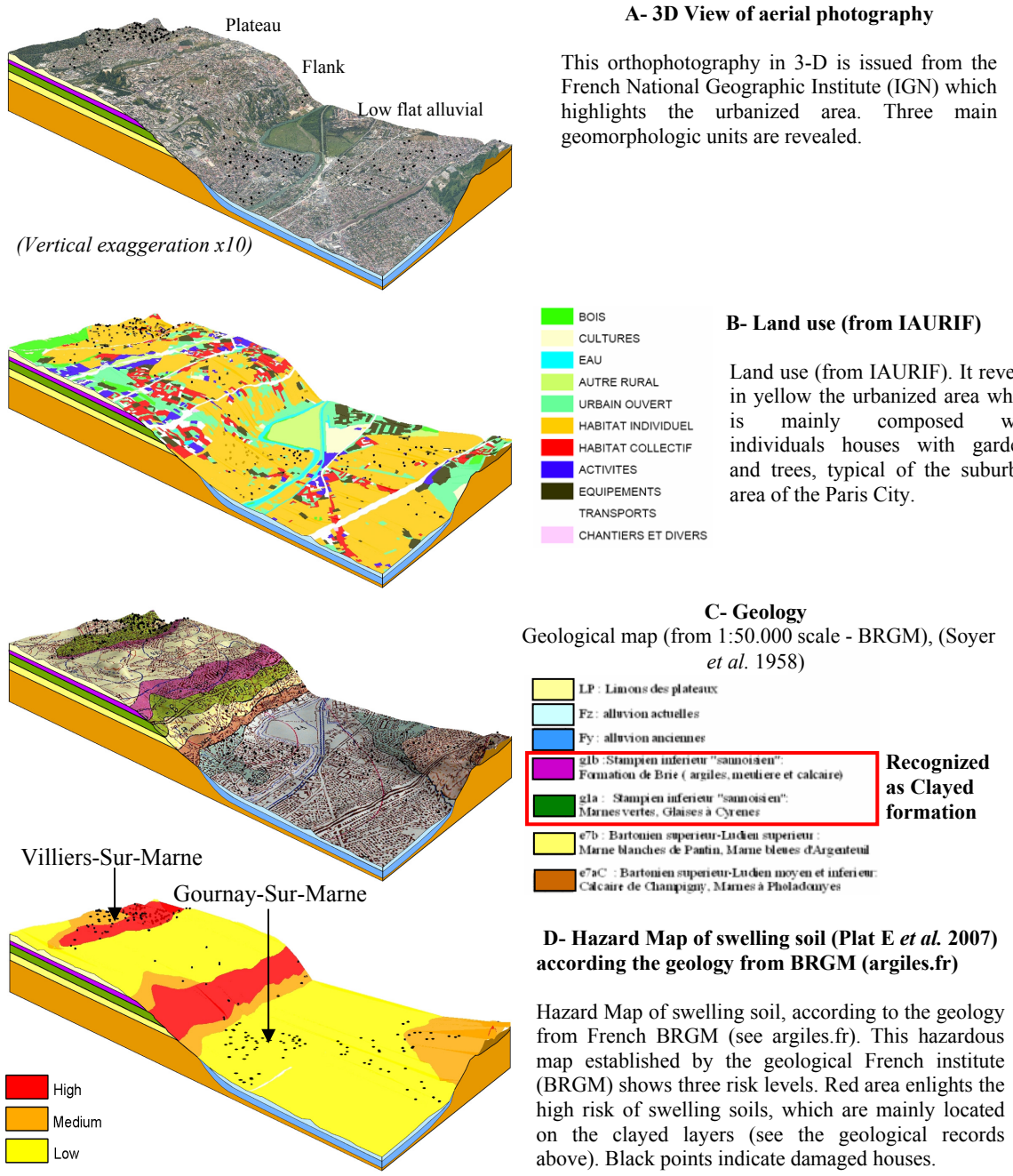

Fig. 1 Geographical Information in 3-D view.

DinSAR RESULTS

The DinSAR method is not precise enough to locate and quantify the movement due to swelling soil phenomena at the scale of a building (1:5000) due to the loss of coherence. However, this differential method allows the detection of others movements such as subsidence due to human activity like water pumping (Fruneau *et al.*, 2005) or natural decrease of a seasonal aquifer

(Thomas, 2005). In the example shown below, the aquifer decreased between 7 April 1995 and 17 January 1998. This dryness phenomenon is confirmed by the aquifer measurement (Fig. 3-C). This subsidence, then, is due to the soil compaction (Fig. 2).

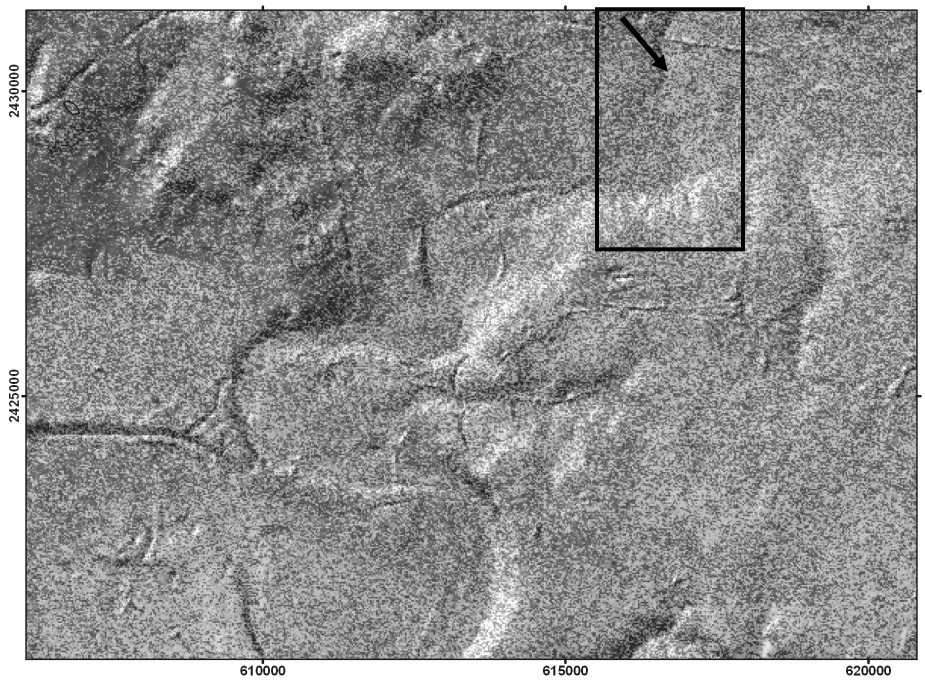

Fig. 2 Filtered interferogram by DinSAR combined with hillshading data. The black arrow shows a subsidence in the Marne River area. This document is not useful to detect up/swelling movements at this scale but there is a good potential to use it as a preliminary observation, which may help identify the location of deformed areas.

PSI RESULTS

At the scale of buildings, the PSI technique offers the possibility of describing the seasonal movement of the ground and the behaviour of houses (Kaveh *et al.*, 2007). Once the local PSI reference (ground behaviour) has been located and described, PS profiles of each house are then compared and analysed. The PS analysis in suburban areas allows understanding of the up/down swelling movements (Fig. 3). The method used to understand if the house is damaged needs several PSI profiles on the same house. Only 55% of the buildings in our study area are not described by PSI due to the lack of reflectors. When they are described by PS reflectors, only 25% of houses have more than two PS. Figures 3A and 3B show preliminary results of the study applied to the Gournay-sur-Marne city, which is then compared to the profiles of Villiers-sur-Marne city (Fig. 3C). PS profiles are compared with piezometric aquifer data (Fig. 3D) of the Marne River alluvium and with the climatic data (Fig. 3E).

Referring to Figure 3

A The PSI profile (a) shows the behaviour of a low damaged building in Gournay-sur-Marne. This behaviour is similar to the PSI soil reference noted (b) and (c). We demonstrate in this case that the ground displacement is homogenous and that the building is rigid enough to support the swelling soil constraint. The house then responds to the ground movement, except in the year of 1998.

B Both (a) and (b) PSI profiles describe the behaviour of the same house in Gournay-sur-Marne, which has been observed to be slightly damaged. They tend to be similar to the ground reference profile noted (c). This reference has been calculated by an average of 134 PSI

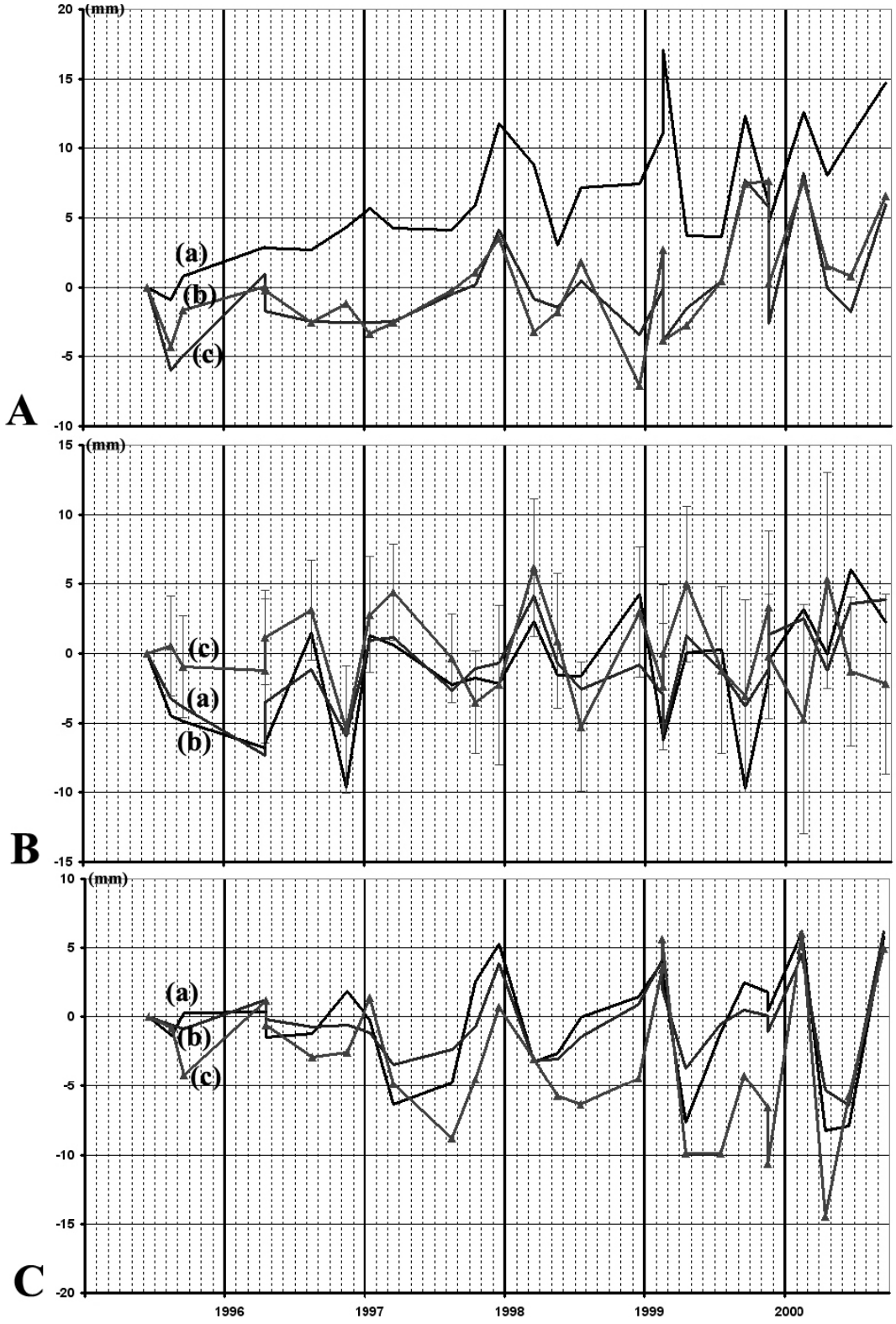

Fig. 3 PSI Results compared with piezometric and climatic data (continued opposite).

profiles which are all influenced by vegetation. The error bar of standard deviation is shown. One can observe the subsidence of the house in September 1999 due to the swelling soils

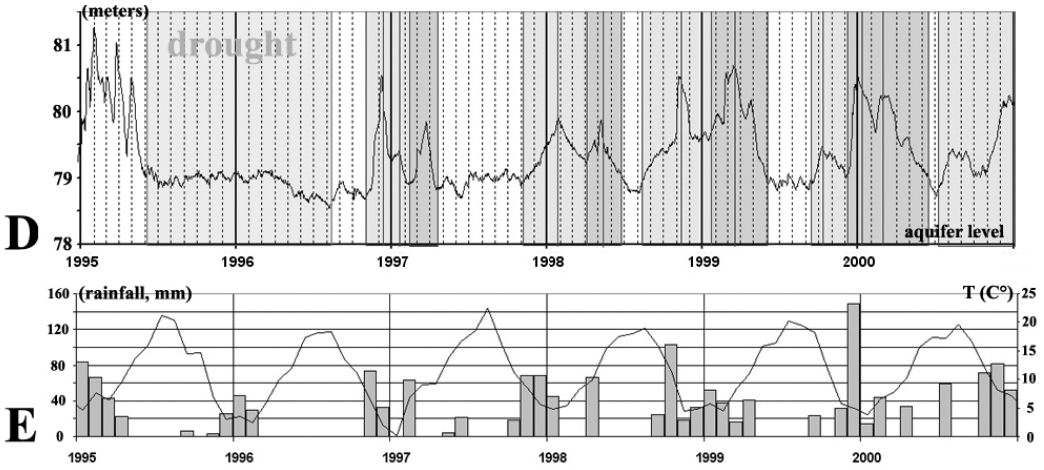

Fig. 3 (continued) PSI Results compared with piezometric and climatic data.

phenomena exacerbated by the vegetation influence. After this event, we notice a misfit between the PS profiles.

C PSI profiles (a) and (b) represent a little-damaged house in Villiers-Sur-Marne. In this case, the two profiles are similar to one another and to the ground reference (c). It is a rather similar case to the example shown in Fig. 3A.

D The superficial aquifer of the Marne alluvium (Fz formation according to BRGM) shown in Fig. 3D, is linked to the seasonal rainfall and temperature data (Fig. 3E). Please note the dryness period in 1996, marked on the graph (low rainfall and no recharge of the aquifer of the Marne River).

E Climatic data constituted by temperature curve (T° in Celsius) and histogram of rainfall (ETP) in millimetres. The time range, 1995–2001, of this graphic corresponds to the PSI profiles shown above.

In both towns we observe the same seasonal nonlinear movement of 0.5 to 1 cm. The movement is caused by cyclical, downswelling in summer or dryness period and upwelling in humid periods, which is in both cases confirmed by geotechnical tests (Geremew *et al.*, 2009). Such movements are correlated with climatic data and the recharge of the aquifer, so it is difficult to determine exactly the mechanism of the observed deformation in the case of Gournay-sur-Marne. Is it the seasonal fluctuation of the Marne piezometric aquifer or is it due to the swelling soil phenomenon only? The future perspective of this work is to prepare maps after analysing all the houses. This cartography may include also the trees and their vicinity in order to better identify their influences and try to better understand the origin of the deformations of the houses.

CONCLUSIONS

The radar differential interferometry (DinSAR) method, which enables one to map surface displacements from two radar images acquired on a specific area, gives rather local results and is not that efficient in the eastern Paris Basin, mainly due to the major temporal decorrelation. It contrasts with the interesting results which are obtained with Persistent Scatterer Interferometry (PSI). The latter shows precisely small seasonal surface displacements monitored continuously through time, compatible with the swelling of soils: uplifting in winter and subsidence in summer. This new application of interferometry to drought hazards presents, therefore, high potential to better locate, characterize and quantify the swelling soil effects and the induced geological processes that affect the eastern Paris Basin.

Acknowledgements The authors thank the MAIF foundation for their financial support and the European Spatial Agency for the radar image (Cat1-AO no. 4362). The meteorological data has been supplied by METEO France. The geological map is the legacy property of the BRGM Institute (see www.argiles.fr). The aerial orthophotography from the BdOrthos© Database is the legacy property of the National Geographic French Institute (IGN). The land use was kindly provided by IAURIF (Île-de-France Region of Urban Management Institute). The Region Île-de-France and the CNRS support the research activities with the proposal R2DS/R2D2.

REFERENCES

Duro, J. (2009) Development of new methodologies for the detection, measurement and on going monitoring of ground deformation using spaceborne SAR data (English version), PhD Thesis, University of Barcelona, Spain.

Fruneau, B., Deffontaines, B., Rudant, J-P. & Le Parmentier, A-M. (2005) Monitoring vertical deformation due to water pumping in the city of Paris (France) with differential interferometry. *Comptes Rendus Geosciences* **337**(13), 1173–1183.

Geremew, Z., Audiguier, M. & Cojean, R. (2009). Analyse du comportement d'un sol argileux sous sollicitations hydriques cycliques. *Bulletin of Engineering Geology and the Environment* **68**(3), 421–436.

Hanssen, R. F., (2001) *Radar Interferometry: Data Interpretation and Error Analysis. Remote Sensing and Digital Image Processing*. Kluwer Academic Publishers, Dordrecht, The Netherlands.

Kariuki, P. C., Woldai, T. & Van der Meer, F. (2004) The role of remote sensing in mapping swelling soils. *Asian J. Geoinformatics* **5**(1). Published by ARSRIN, P.O. Box 4, Klong Luang, Pathumthani 12120, Thailand.

Kaveh, H. F., Deffontaines, B. & Fruneau B. (2007) Apports d'un Système d'Information Géographique et de la télédétection pour l'étude des mouvements de terrain induits par l'aléa sécheresse: Applications à l'Est de l'Île-de-France. *Revue Française Géotechnique* **120–121**, 201–214.

Kaveh, H. F., Fruneau, B., Deffontaines, B., Duro J & Arnaud, A. (2008) Apports de l'interférométrie radar (DINSAR ET PSI) à l'étude du retrait gonflement d'argile dans l'est du bassin Paris. *Symposium SEC* 1,2 et 3 septembre 2008, Marne-la-Vallée, France.

Plat, E., Donsimoni, M. & Vincent, M. (2007) Actualisation de la carte d'aléa retrait-gonflement des sols argileux dans le département de Seine-Saint-Denis. Rapport BRGM/RP-55527-FR, 78 p., 17 ill., 2 ann., 3 cartes h.-t.

Soyer R., Lemoine, M. & Goguel, J. (1958) Carte géol. France (1/50 000), feuille Lagny (type1922), 1e édition – Orléans: Bureau de recherches géologiques et minières.

Tomás, R., Márquez, Y., Lopez-Sanchez, J. M., Delgado, J., Blanco, P., Mallorquí, J., Martínez, M., Herrera, G. & Mulas, J. (2005) Mapping ground subsidence induced by aquifer overexploitation using advanced Differential SAR Interferometry: Vega Media of the Segura River (SE Spain) case study. *Remote Sensing Environ.* **98**(2-3), 269–283.

Land Subsidence, Associated Hazards and the Role of Natural Resources Development
(Proceedings of EISOLS 2010, Querétaro, Mexico, 17–22 October 2010). IAHS Publ. 339, 2010.

Land subsidence at the Kujukuri Plain in Chiba Prefecture, Japan: evaluation and monitoring environmental impacts

H. OBANAWA[1], T. TOKUNAGA[1], S. ROKUGAWA[2], T. DEGUCHI[3] & T. NAKAMURA[2]

1 *Graduate School of Frontier Sciences, The University of Tokyo, 5-1-5 Kashiwanoha, Kashiwa-shi, Chiba, 277-8563, Japan*
obanawa@geoenv.k.u-tokyo.ac.jp

2 *Graduate School of Engineering, The University of Tokyo, 7-3-1 Hongo, Bunkyo-ku, Tokyo, 113-8656, Japan*

3 *Nittetsu Mining Consultants Co., Ltd., 4-2-3 Shiba, Minato-ku, Tokyo, 108-0014, Japan*

Abstract The impacts of land subsidence on surface environmental changes were analysed for the Kujukuri Plain, Japan, where subsurface brine has been abstracted for more than 50 years. Reconstruction of past landforms using airborne laser scanning and existing levelling data showed that the geomorphological setting of the whole region, such as beach ridges and backmarshes, has been retained during the recent 40 years. Apparent and simple relationships between shoreline retreat and land subsidence were not recognized, and the spatio-temporal distribution of shoreline change seems to be mainly controlled by coastal constructions. In addition, a method to measure long-term deformation by combining InSAR and time series analysis was proposed to improve our ability for monitoring land subsidence. The local uplifts and subsidence detected by the proposed method were quite consistent with those obtained from levelling data, suggesting that our method was applicable to the detailed monitoring. By combining and integrating the approaches presented in this paper with numerical modelling of deformation/fluid flow processes, scientifically sound recommendations for the sustainable development of the subsurface resources can be proposed for society.

Key words land subsidence; environmental impact; monitoring; InSAR; GIS; Kujukuri Plain, Japan

INTRODUCTION

Land subsidence causes various types of damage to civil society and it may result in the permanent deterioration of environmental conditions due to the irreducible nature of the subsidence phenomena in general (Deming, 2002). Because of the industrial withdrawals of subsurface fluid resources, such as dissolved methane and groundwater, land subsidence has occurred at many places in Japan (Environmental Management Bureau, Ministry of the Environment, 2009). The Kujukuri Plain, Chiba Prefecture (Fig. 1), is one of the places where heavy subsidence, with a maximum value of accumulated subsidence of 100.7 cm, was observed during the period from 1969 to 2007 (Environmental and Community Affairs Department, Chiba Prefecture, 1970–2007). This coastal plain is composed of alternating beach ridges and backmarshes (Moriwaki, 1979); (Fig. 1). Most of the area is situated below 10 m elevation, therefore it is of concern that continuous land subsidence by abstraction of subsurface brine and possible future sea-level rise due to global warming may increase the risks of flood disaster and coastal erosion. However, our understanding of the surface environmental changes caused by subsidence are not yet sufficient to predict the extent of the environmental impacts and to propose efficient countermeasures against these influences. This paper presents our activities to tackle the problems through two different approaches, i.e. (1) to better understand the surface environmental changes caused by land subsidence, and (2) to further improve the Interferometric Synthetic Aperture Radar (InSAR) method to achieve a high resolution monitoring technique for surface movement. We also present the importance of integrating these approaches to achieve the sustainable development of subsurface resources.

Copyright © 2010 IAHS Press

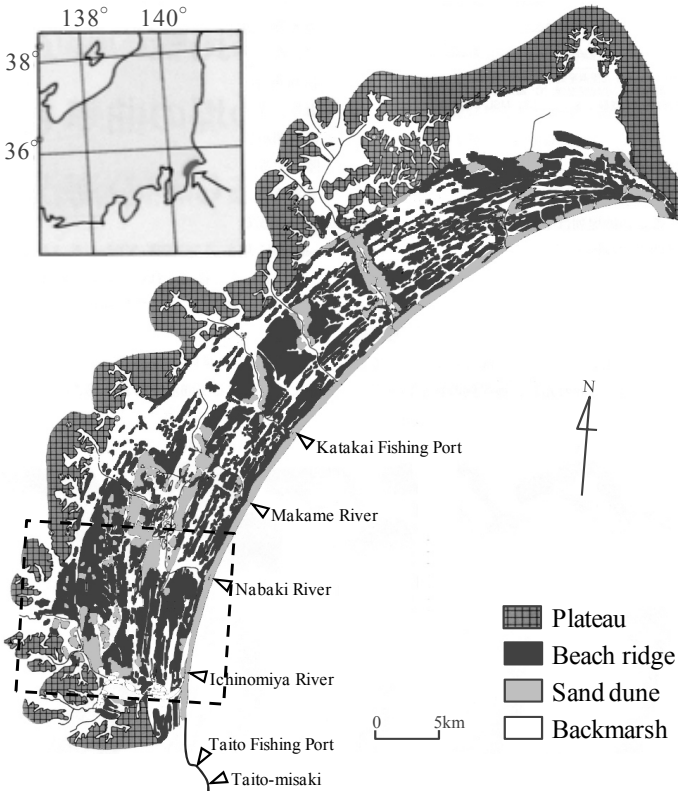

Fig. 1 Geomorphological map of the Kujukuri Plain (modified after Moriwaki, 1979). Square marked by dashed line indicates the area of Fig. 2.

ANALYSING CHANGES OF THE SURFACE ENVIRONMENT

Reconstructing past landforms

We conducted an airborne laser scanning survey in December 2008 to obtain high accuracy and high resolution digital elevation model (DEM) (Fig. 2). The study area includes Mobara City, Shirako Town and Chosei Village on the southern Kujukuri Plain. The DEM has an area of 224 km^2 (14 km × 16 km), 1-m mesh resolution, and 4.0-cm vertical error, which is much higher in accuracy than the existing topographic map and the standard specification for airborne laser scanning, i.e. 25 cm (Ministry of Land, Infrastructure, Transport and Tourism, 2008).

We estimated landform changes by integrating the present DEM-based topographic data and the existing levelling data. We used the "*Precise levelling survey results in Chiba Prefecture*" compiled by Chiba Prefectural Government (Environmental and Community Affairs Department, Chiba Prefecture, 1970–2007) to reconstruct the past ground level. The levelling survey has been carried out every year since 1969. The maximum value of accumulated subsidence was 100.7 cm in the northeastern part of the Mobara City and the minimum value was 39.2 cm in the southern part of Chosei Village during the period from 1969 to 2007. The landform changes were obtained by subtracting the ground-level changes from the present DEM in the study area.

Expansion of lowland

Figure 3(a) shows the expansion of lowland as a function of time. The area below 1 m was 2.4% of the whole study area in 1969, while it has expanded to 5.5% in 2009. Areas below 2 to 6 m have increased more rapidly. For example, the area below 6 m increased by 5.6% during the period 1969–2009. Lowland has expanded along the Nabaki River and partially in the swale behind the beach ridge along the shoreline (Fig. 3(b)). However, overall the spatial pattern of the geomorphological features such as beach ridges and backmarshes has been retained, i.e. regional difference of land subsidence has not caused significant change of the entire landforms during the last 40 years.

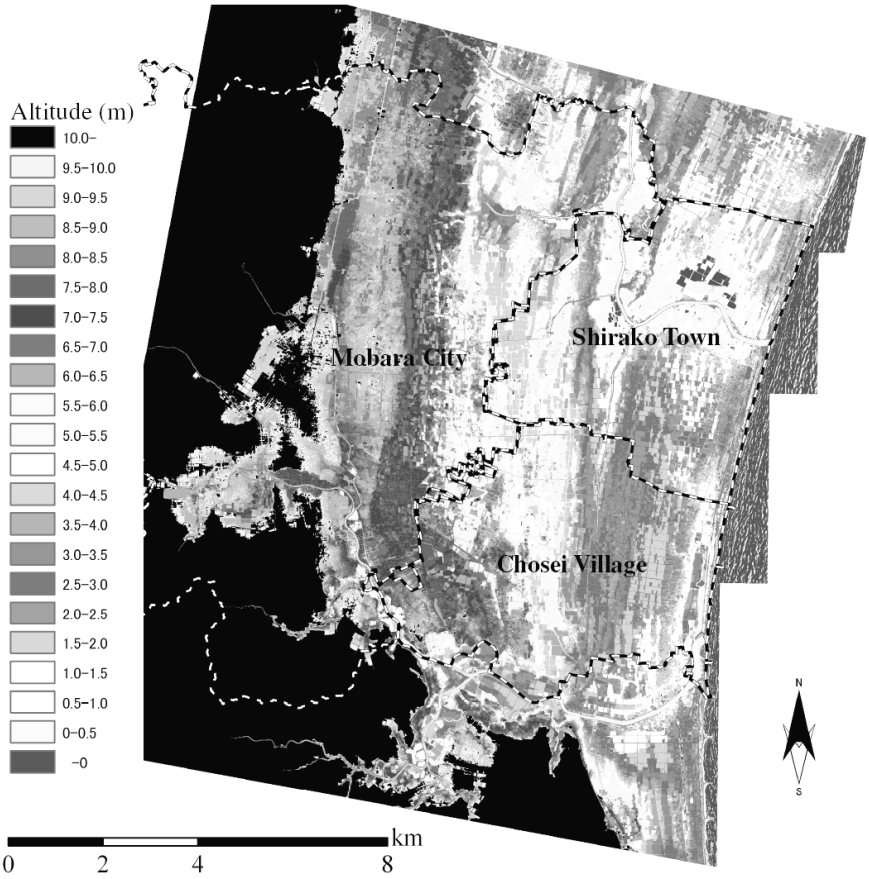

Fig. 2 One metre mesh digital elevation model obtained from the airborne laser scanning survey.

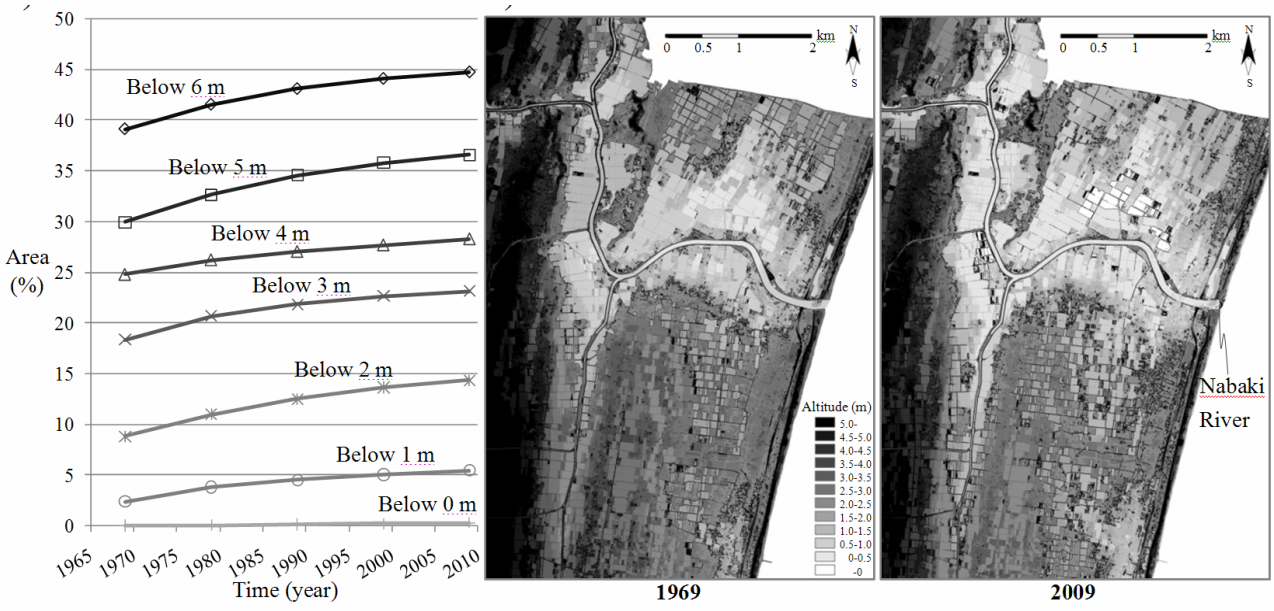

Fig. 3 Temporal change of landform in the past 40 years. (a) Altitude-area relations; and (b) an example of the landform change at the lower reach of the Nabaki River.

Shoreline change

The existing data related to shoreline change were summarized, and we compared the spatio-temporal changes of the shorelines with those of ground levels (Fig. 4). In Fig. 4(a), the sites and the timings of the installation of coastal architectures such as training dikes, jetties and breakwaters were also shown. The apparent and simple relationships between the shoreline retreat and the land subsidence (Fig. 4(b)) were not observed, i.e. the areas with a large amount of accumulated shoreline retreat do not correspond to those with a large amount of land subsidence. Spatio-temporal changes of the shoreline seem to be controlled more by artificial coastal structures. For example, the area of shoreline retreat has expanded after the completion of the construction of the breakwater in front of the sea cliff at Taito-misaki (see Fig. 1 for the location) at 1985, which is considered to be a major source of beach sand at the study area. In addition, the saw-like pattern of alternating high and low erosion areas are observed in between the Ichinomiya River and the Taito Fishing Port. These patterns are interpreted to be caused by the construction of headlands in the area.

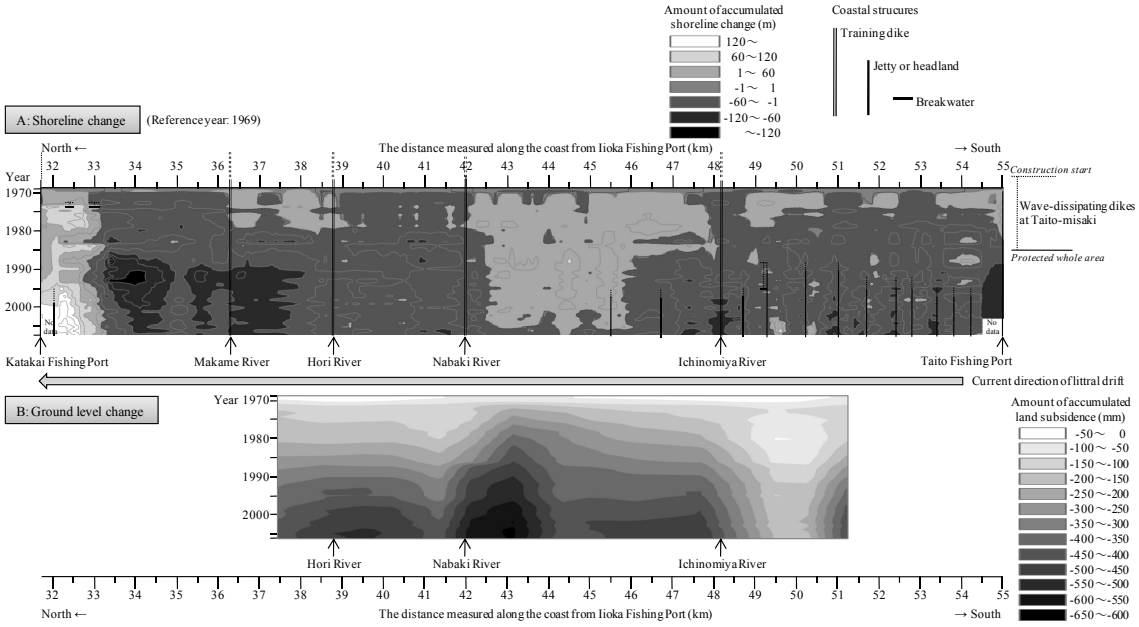

Fig. 4 X-t diagrams showing spatio-temporal changes of shoreline and ground level. The vertical axis indicates time and the horizontal axis distance along the coast. The gradation from white to black indicates the amount of accumulated shoreline change in the upper figure (A) and ground level change in the lower figure (B). The year 1969 was chosen as a reference to construct the diagrams. Solid and dashed lines in the upper figure (A) show the coastal structures.

IMPROVEMENT OF INSAR TECHNIQUE TO MONITOR GROUND DISPLACEMENT

Interferometric Synthetic Aperture Radar (InSAR) is becoming established as a method for monitoring ground displacement that can observe subtle surface movement over a wide area at high resolution (e.g. Ferretti *et al*., 2001; Berardino *et al*., 2002). We recently developed a method to measure long-term deformation by combining InSAR and time series analysis, aiming at establishing the practical and flexible measurement technique (Deguchi *et al.*, 2009). In our measuring method, the value of land deformation is set as an unknown parameter. Then, by applying a smoothness-constrained inversion algorithm, the optimal solution to the amount of land deformation was obtained. We applied our new method at the study area with ENVISAT/ASAR data, and verified its accuracy by comparing our results with levelling data (Fig. 5). It was shown that the local uplifts and subsidence detected by the proposed method were quite consistent with those obtained from levelling data both in spatial distribution and the amount of vertical movement.

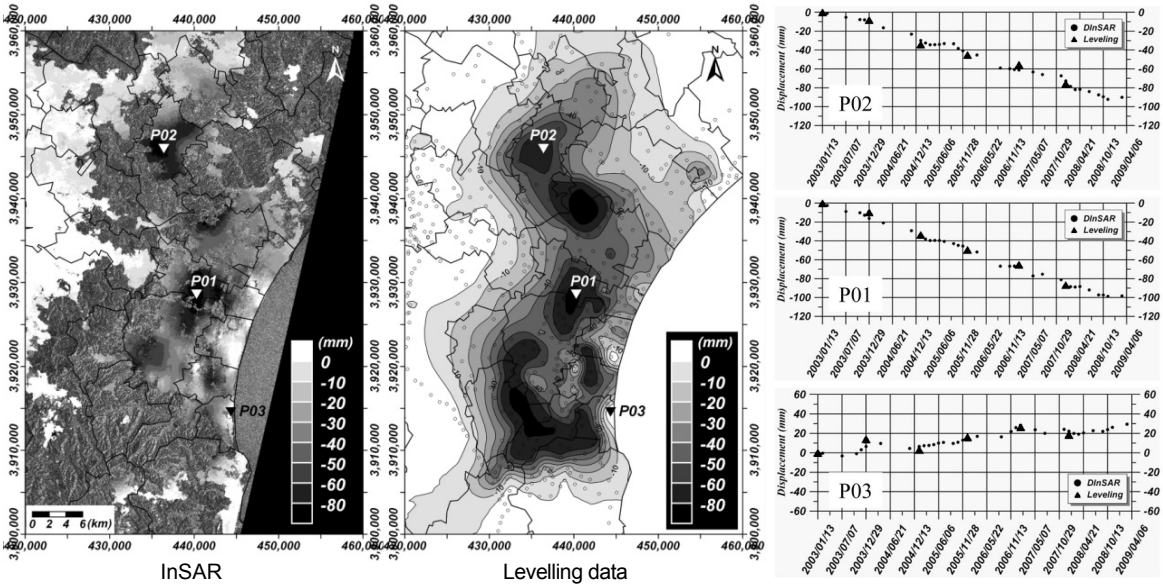

Fig. 5 Comparison among InSAR (left), levelling survey (centre), and the temporal changes of surface deformation obtained from our InSAR analysis (dots) and levelling survey results (triangles) (right).

FUTURE PERSPECTIVES

To evaluate and monitor the environmental impacts by subsurface resources abstraction, integration of the detailed analysis of surface topographic change with GIS platform and the detailed monitoring by InSAR technique is considered to be very effective. Combination of our approaches with numerical modelling of land subsidence by resources abstraction will provide us with reliable and scientifically sound recommendations for the sustainable production scheme, and it will help to build the possible consensus on the sustainable development (Fig. 6). The approach presented here is considered to be universal, and hence it will be used for the areas where similar subsurface development has been conducted and/or planned.

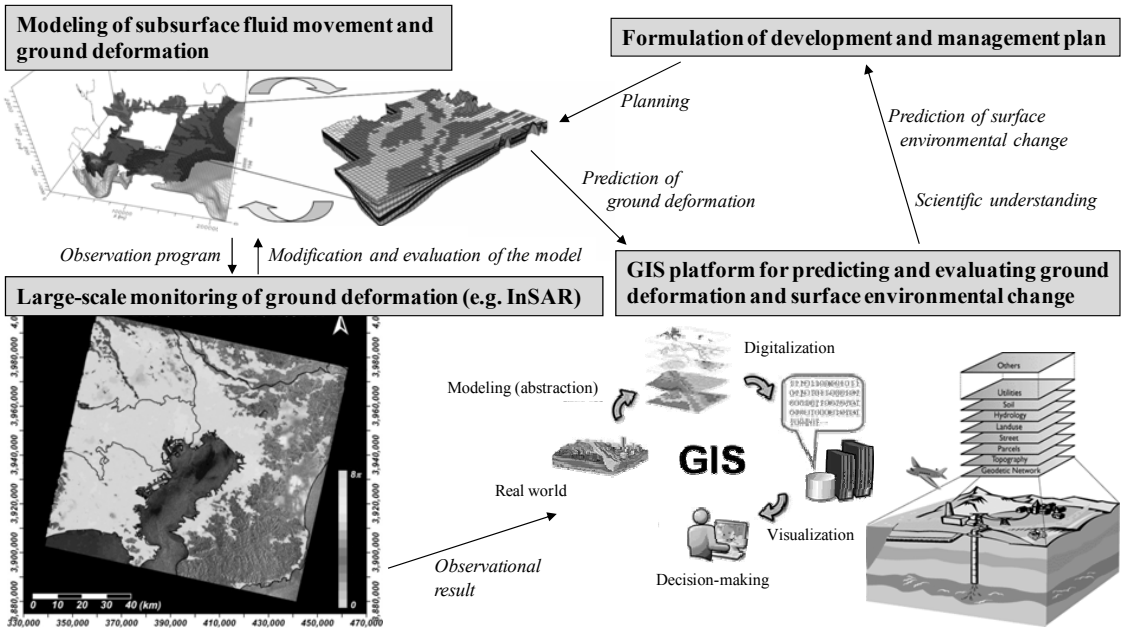

Fig. 6 Conceptual diagram showing the importance of integration of monitoring and modelling for sustainable development of subsurface resources.

Acknowledgements We would like to express our sincere gratitude to the Keiyo Natural Gas Association for supporting this study.

REFERENCES

Berardino, P., Fornaro, G., Lanari, R. & Sansosti, E. (2002) A new algorithm for surface deformation monitoring based on small baseline differential SAR interferograms. *IEEE TG & RS* **40**, 2375–2382.

Deming, D. (2002) *Introduction to Hydrogeology*. McGraw-Hill, New York, USA.

Deguchi, T., Rokugawa, S. & Matsushima, J. (2009) Long-term ground deformation measurement by time series analysis for SAR interferometry. *J. Remote Sensing Soc. Japan* **29**, 418–428 (in Japanese with English abstract).

Environmental and Community Affairs Department, Chiba Prefecture (1970–2007) *Levelling results in Chiba Prefecture [reference date: February 1970–January 1st, 2007]*, (in Japanese).

Environmental and Community Affairs Department, Chiba Prefecture (2007) *State of land subsidence in Chiba Prefecture* (in Japanese).

Environmental Management Bureau, Ministry of the Environment (2009) *Summary of subsidence area in Japan, the year 2008* (in Japanese).

Ferretti, A., Prati, C. & Rocca, F. (2000) Nonlinear subsidence rate estimation using permanent scatterers in differential SAR interferometry. *IEEE TG & RS* **38**, 2202–2212.

Ministry of Land, Infrastructure, Transport and Tourism (2008) *Survey Act, Operation Rules* (in Japanese).

Moriwaki, H. (1979) The landform evolution of the Kujukuri Coastal Plain, Central Japan. *The Quaternary Research* **18**, 1–16 (in Japanese).

(Proceedings of EISOLS 2010, Queretaro, Mexico, 17–22 October 2010). IAHS Publ. 339, 2010.

Subsidence monitoring of an Iranian oil field inferred from SAR interferometry

N. FOULADI MOGHADDAM[1], A. A. MATKAN[1], M. R. SAHEBI[2], M. ROOSTAEI[3] & H. R. BAQTIARI[4]

1 *Dept of Remote Sensing and GIS, University of Shahid Beheshti, Evin 14335-333 Tehran, Iran*
n.f.moghaddam@gmail.com
2 *Dept of Geodesy and Geomatics Eng., Khajeh Nasir University of Technology, Mirdamad, Tehran, Iran*
3 *Remote Sensing Group,Geological Survey of Iran (G.S.I), Azadi, Tehran, Iran*
4 *United Nations Educational, Scientific and Cultural (UNESCO)Office, Saadabad, Tehran, Iran*

Abstract Land subsidence is one of the most hazardous phenomena because its gradual occurrence due to compaction of natural deposits is so excessive. Human activities like hydrocarbon fluid withdrawal can also cause local subsidence and damage industrial structures. Traditional ground surveying can detect the change amount, but the limitations of benchmarks and operational costs necessitate application of modern techniques for change detection. Nowadays, SAR Interferometry (InSAR), an improved geodetic tool, is used for recording reservoir surface changes surveillance at the centimetre scale. The main purpose of this research is to study one of the hydrocarbon extraction sites in Iran which has noticeable subsidence, to determine its main cause. The observed deformation is highly compatible with the production data. This result indicates that the use of InSAR under normal conditions opens up wide applications in both research and industrial contexts.

Key words land subsidence; fluid withdrawal; production rate; InSAR

INTRODUCTION

Differential SAR interferometry is a sensitive new technology with great spatial coverage and high resolution that can detect small-scale deformations for enhanced reservoir management. In this study, radar observations over two years reveal the Iranian oil field surface displacement as subsidence and uplift signals. Detailed inspection of several production wells in the resulting interferograms shows an improvement in the production and subsequent deformation based on geological conditions and production rates. Additionally, due to the unavailability of GPS measurements for the proposed time intervals, production and reservoir pressure drop data are used for results validation. In spite of pressure decline in all parts, further study depicts that both tectonic and non-tectonic factors regarding the wells location and their production are responsible for this subsidence.

AGHAJARI OIL FIELD

Reservoir characteristics

The "Aghajari" oil field, also known as Aghajari anticline, is located in the Dezful embayment of the Zagros mountain ranges, Fig. 1. Since the Neocene period, oil has accumulated in the porous Asmari limestone and dolomite, the main reservoir rock. The Asmari saturated oil reservoir is sealed by the thick Gachsaran formation of salt layers and sandstones. The Aghajari thrust and Hendijan basement fault are proposed as the main source of basement movements in this region, and define the oil field boundaries (Motiei, 1995).

Due to Arabian platform NE–SW compressive stress, axial sag in the anticline creates three parts to the field: eastern, central and western. Three-dimensional seismic data and underground maps illustrate that the eastern part has smoother flexures and deeper fissures and bears higher pressure and metamorphism resulting from the effect of faults and surrounding anticlines.

Copyright © 2010 IAHS Press

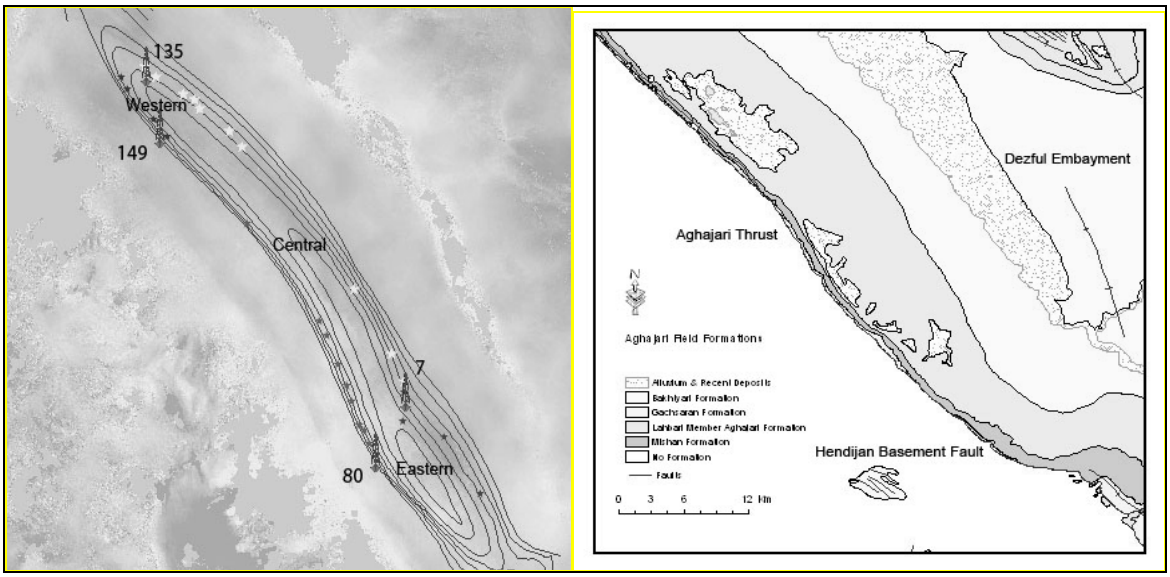

Fig. 1 Surface geology of Aghajari oil field along with two main fault systems in the whole region (right). Three main sections of Aghajari resulting from anticline sag induced by Arabian platform NE–SW stress (left). In this image four well groups in different parts of field are presented regarding to their sample well.

The porous Asmari reservoir is situated at a depth of 1000 m and its thickness varies between 100 and 150 m. Recently, Aghajari production has declined because of oil extraction and a subsequent pressure drop. The initial pressure fell by about 6 p.s.i. in two years in all three parts of the field (NISOC, 2009). Furthermore, the Asmari Reservoir is classified as semi-consolidated so its elastic behaviour is considered.

DINSAR OVER AGHAJARI FIELD

In this study twelve level zero Envisat ASAR images from September 2003 to August 2005 in descending mode are used. The inputs in the Interferometric processing algorithm are the focused SLC (Single-Look Complex) images and the computation of interferograms has been performed using the GAMMA^{TM} Radar Interferometric software (Wegmuller *et al.*, 2006). For Aghajari oil production activities in short time intervals (minimum 2 months, and maximum 7 months) the correlation of the images increases and the results could be interpretable. Thus, based on statistical results of sixteen unwrapped interferograms, only five including 03.09.26–04.02.13 (141 days), 04.02.13–04.08.06 (176 days), 04.08.06–04.10.15 (71 days), 04.10.15–05.05.13 (212 days), and 05.05.13–05.08.26 (108 days) have a lower standard deviation and range, and are the most suitable interferograms for Aghajari deformation interpretation.

CONCLUSIONS

To determine the most leading factors in field subsidence, various tectonic and non-tectonic issues are considered. The subsidence may partially result from tectonic movements; however, oil production operations are the main cause of most subsidence. Regions with high production rates have a correlation with subsidence in which effects of pressure drop, formation thickness and mechanical properties of layers are inevitable.

The results in Fig. 2 indicate that although the production pattern with continuous pressure drop in field regions is the same, abnormal behaviour of the eastern and central part of southern flank in response to production can be observed. Dual thrust in southern flank, Hendijan bed rock

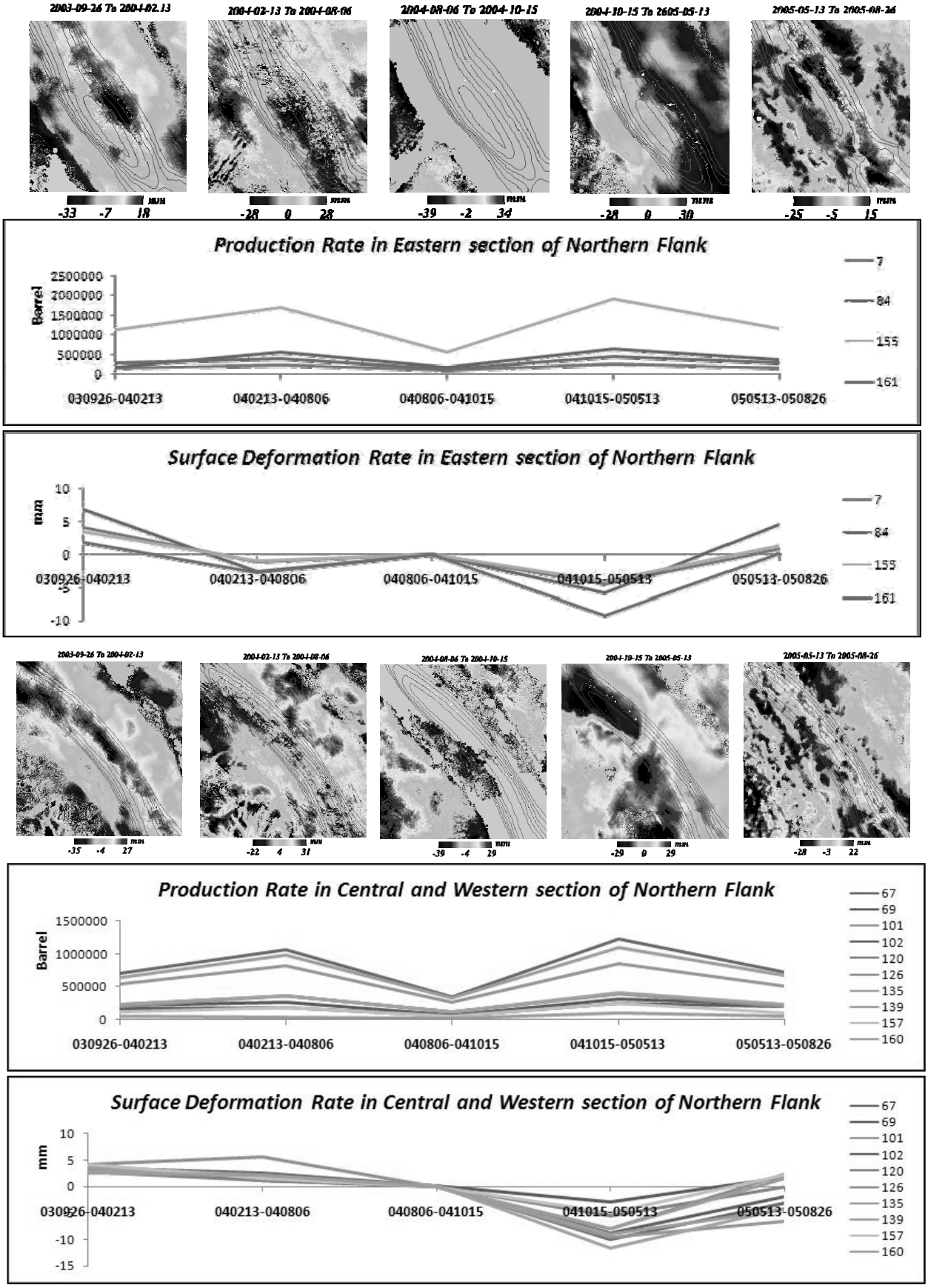

Fig. 2 Deformation rate in four regions of Aghajari compared to oil production in five interferograms.

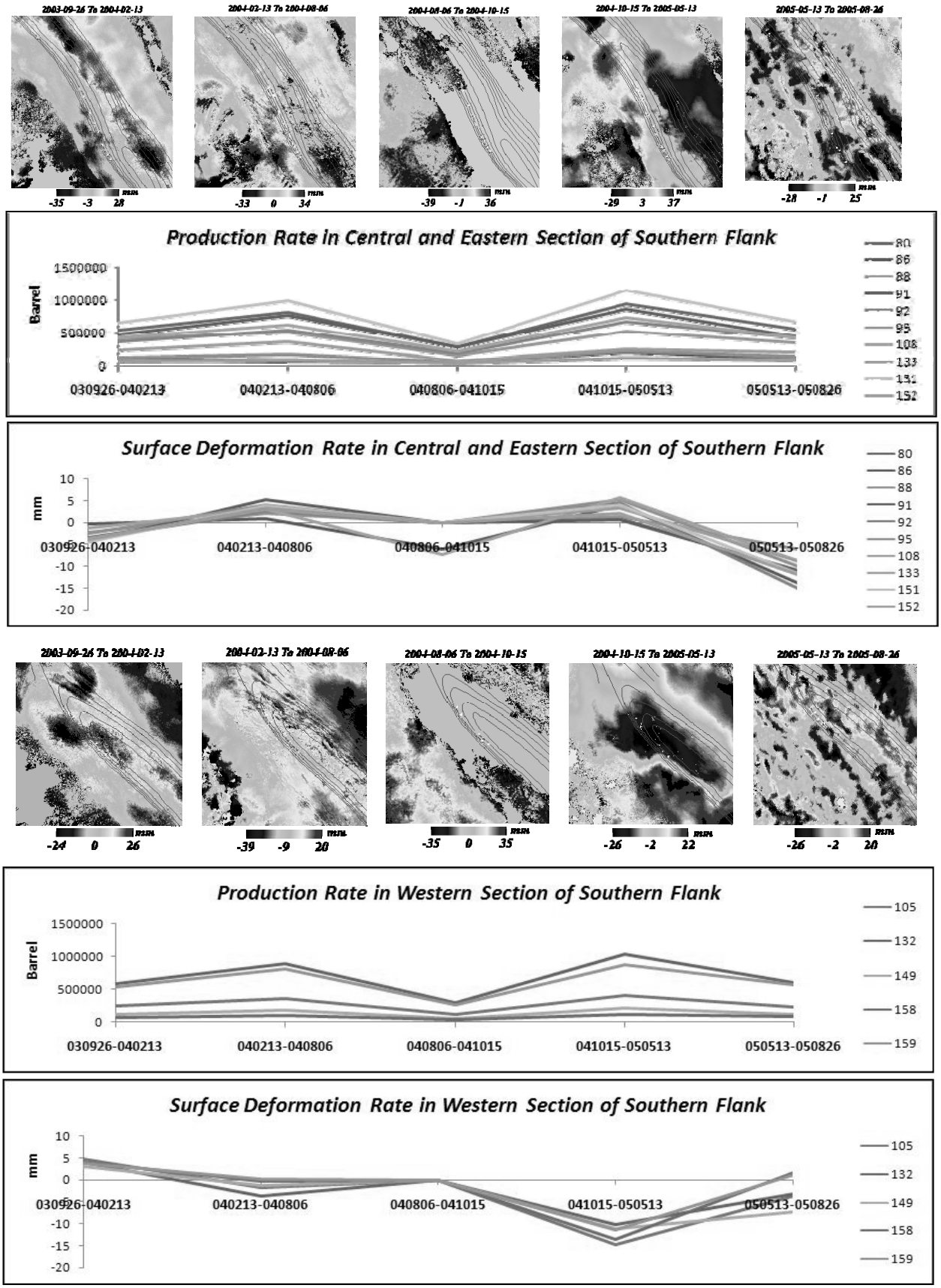

Fig. 2 (continued) Deformation rate in four regions of Aghajari compared to oil production in five interferograms.

fault and its induced geothermal stimulation, thickness and elasticity of Gachsaran, reservoir fractures and oil migration as tectonic factors could be responsible for numerous leakages in this part. Thus, we conclude that tectonic elements in eastern and central part of southern Aghajari forced its wells to have a different behaviour in comparison with other parts since the starting point of production.

Acknowledgements We would like to thank ESA for providing Envisat data as well as NISOC (National Iranian Southern Oil Co.) for permission to use the field data. This research is financially supported by the Geological Survey of Iran (GSI) as an MSc Thesis.

REFERENCES

Chilingarian, G. V., Donaldson, E. C. & Yen, T. F. (1995) *Subsidence Due to Fluid Withdrawal*. School of Engineering, University of Southern California, Los Angeles, California, USA.

Fielding, E. J., Blom, R. G. & Goldstein, R. M.(1998) Rapid subsidence over oil fields measured by SAR interferometry, *Geophys. Res. Lett.* **25**(17), 3215–3218.

Gabriel, A. K., Goldstein, R. M. & Zebker, H. A. (1989) Mapping small elevation changes over large areas: differential radar interferometry. *J. Geophys Res*. **94**(B7), 9183–9191.

Geertsma, J. (1972) Land subsidence above compacting oil and gas reservoir, *SPE* 3730, 17.

Massonnet, D. & Rabaute, T. (1993) Radar interferometry: limits and potential*, IEEE Trans. Geosci.and Remote Sens.* **31**, 455–464.

Motiei, H. (1995) *Geology of Iran, Petroleum Geology of Zagros*, 591–682. Geological Survey of Iran (G.S.I) Publication, Tehran, Iran.

NISOC (2009) Aghajari surface geology technical report. National Iranian South Oil Company.

Wegmuller, U., Werner, C., Strozzi, T., Wiesmann, A. & Santoro, M. D. (2006) User manual to GAMMA SAR and interferometry software. GAMMA Remote Sensing Ltd, Switzerland.

Xu, H., Dvorkin, J. & Nur, A. (2001) Linking oil production to surface subsidence from satellite radar interferometry. *Geophys. Res. Lett.* **28**(7), 1307–1310.

Zebker, H. A. & Villasenor, J. (1992) Decorrelation in interferometric radar echoes. *IEEE Trans. Geosci.and Remote Sens.* **30**, 950–959.

(Proceedings of EISOLS 2010, Querétaro, Mexico, 17–22 October 2010). IAHS Publ. 339, 2010.

Mexico City subsidence analysis assisted by InSAR

P. LÓPEZ-QUIROZ[1], M. P. DOIN[2], F. TUPIN[3], P. BRIOLE[2] & J. M. NICOLAS[3]

1 *Centro de Investigación en Geografía y Geomática "Ing. Jorge L. Tamayo", A.C., Contoy 137, Lomas de Padierna, CP 14240, México DF, Mexico*
penelope@centrogeo.org.mx

2 *Laboratoire de Geologie, École Normale Supérieure, CNRS UMR 8538, Paris, France*

3 *Institut TELECOM, TELECOM ParisTech, LTCI CNRS UMR 5141, F-75013 Paris, France*

Abstract Mexico City is one of the most populated cities of the world. Its aquifer is thus overexploited causing subsidence rates reaching up to 40 cm/year mainly due to the soil compaction. Previous to this work, we mapped the spatio-temporal patterns of the Mexico City subsidence by differential radar interferometry, using 38 ENVISAT images acquired between end of 2002 and beginning of 2007. From the inversion of 71 small baseline unwrapped interferograms we obtained increments of radar propagation delays between the 38 acquisition dates using an algorithm for time series analysis that was best suited to our database. Accurate deformation time series were then derived over the metropolitan area of the city with a spatial resolution of 30 × 30 m. In this work we present some analysis of the nonlinear components present in the time series obtained.

Key words InSAR; time series; land subsidence; Mexico City

INTRODUCTION

In Mexico City subsidence rates reach up to 40 cm/year mainly due to the soil compaction led by the overexploitation of the Mexico Basin aquifer. By means of interferometry, accurate deformation time series were derived over the metropolitan area of the city with a spatial resolution of 30 × 30 m, to monitor the phenomena. We then performed some analyses to investigate the nonlinear components of some of the time series obtained.

ANALYSIS

Details of the interferogram processing and the time series derivation can be found in López-Quiroz *et al.* (2009).

Examples of some of the obtained time series (Fig. 1) show that most of the deformation in Mexico City can be considered as linear. Initially, we adjusted the time series by means of a linear model. However, looking more closely into some of the time series we realized that some of them present a small but significant quadratic behaviour, like those shown in Fig. 2.

We then decided to identify the zones where the linear model was not enough to model the current behaviour (nonlinear behaviour) and constructed Fig. 3 by means of the following formula.

$$res_1 = \sqrt{1/M_l \sum \left(\phi_k - \bar{v}(t_k - t_1) - eB_\perp^k - c\right)^2} \quad (1)$$

where M_l is the number of valid images for pixel l, ϕ_k is the phase delay inverted for every image k, $\bar{v}$ is the annual tax of mean subsidence on each image pixel, t_k is the time and $eB_\perp^k$ is the perpendicular baseline of image k.

Over this map, res_1, we have selected some pixels with a high residual (Fig 4).

We finally decided to adjust the time series with a quadratic model and calculate the corresponding residual (Fig. 5) by means of the following formula,

$$res_2 = \sqrt{1/M_l \sum \left(\phi_k - a(t_k - t_1) - b(t_k - t_1)^2 - eB_\perp^k - c\right)^2} \quad (2)$$

Most of the pixels are well adjusted with the quadratic model; however, some of them show a sinusoidal behaviour lasting several years, like those shown on Fig. 6.

Copyright © 2010 IAHS Press

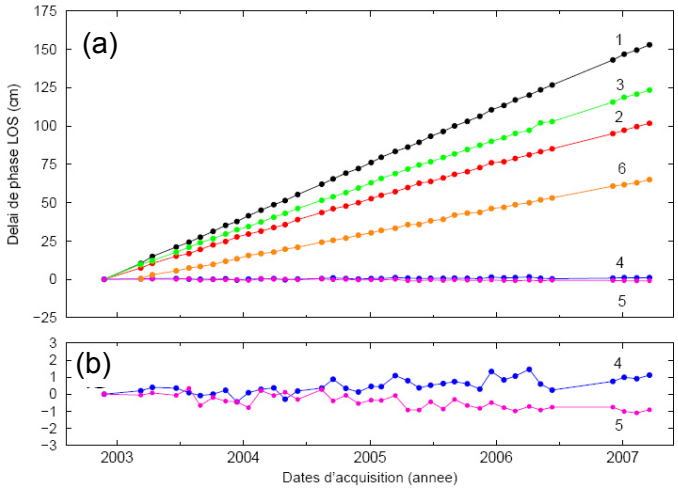

Fig. 1 Time series.

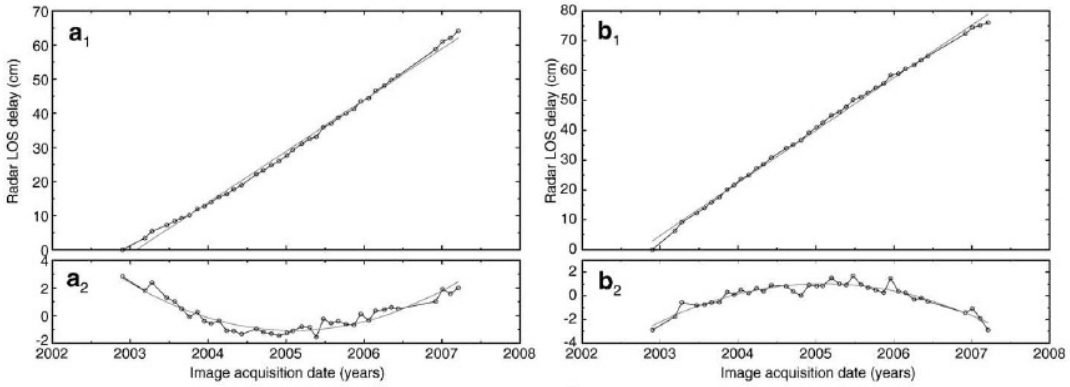

Fig. 2 Time series (a_1,b_1) and residuals (a_2,b_2) with respect to a linear regression, showing the deformation acceleration (a) and deceleration (b) respectively. Residuals are adjusted by a quadratic function.

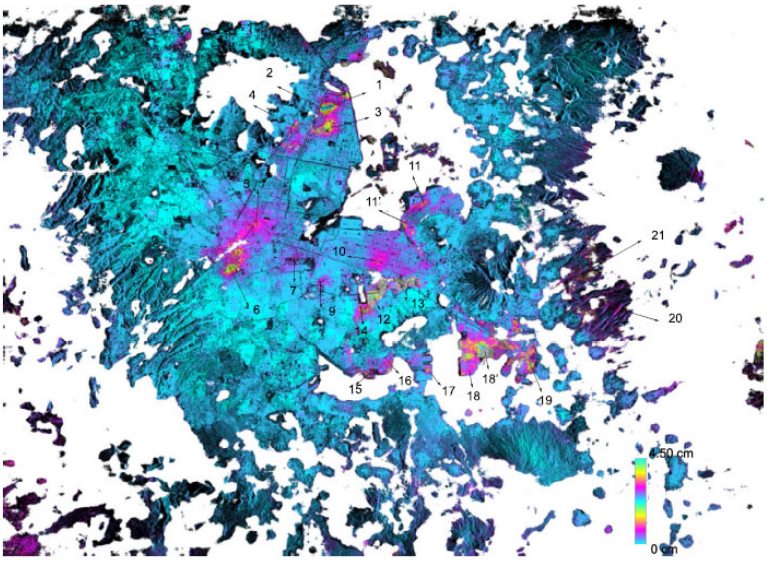

Fig. 3 The res_1 map; the difference between the time series with respect to a linear model in time (equation (1)). This difference is small almost everywhere but in the zones showing a significant non linear deformation. The scale is in LOS cm.

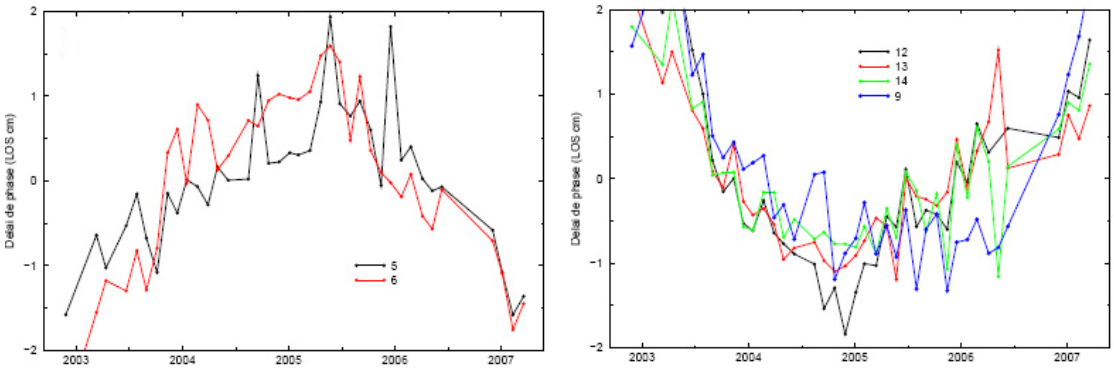

Fig. 4 Residuals with respect to the adjustment of a linear model over the time series. The numbers correspond to the points localized over Fig. 3.

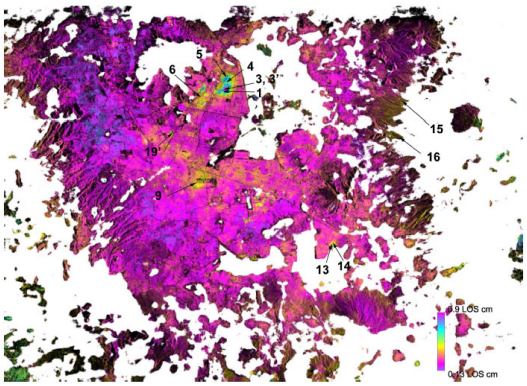

Fig. 5 The res_2 map; the difference between the time series with respect to a quadratic modelling in time.

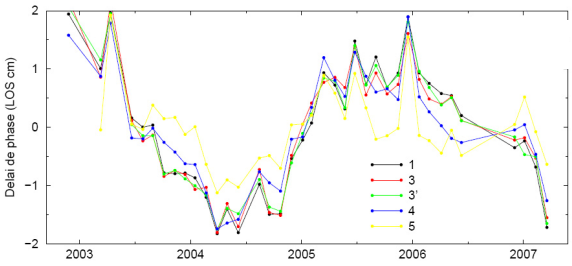

Fig. 6 Residuals with respect to the quadratic adjustment in time over the time series. The numbers correspond to the points localized over Fig. 5.

CONCLUSIONS

Our work analyses deformation time series from the end of 2002 to the beginning of 2007. Although they reflect the almost perfectly linear temporal behaviour of the subsidence in the lacustrine area, we detect areas where the subsidence velocity is gradually increasing, decreasing and even showing a sinusoidal behaviour lasting several years. This should bring constraints on the aquitard compaction phenomenon, the water pore pressure evolution in the clay layer and possible nonlinear clay consolidation properties. In any case, a closer analysis of this kind of phenomena is required in order understand its nature.

Acknowledgements We thank the CONACYT for its financial support.

REFERENCES

López-Quiroz, P., Doin, M. P., Tupin, F., Briole, P. & Nicolas, J. M. (2009) Time series analysis of Mexico City subsidence constrained by radar interferometry. *J. Appl. Geophys*. **69**(1), 1–15.

Land Subsidence, Associated Hazards and the Role of Natural Resources Development
(Proceedings of EISOLS 2010, Querétaro, Mexico, 17–22 October 2010). IAHS Publ. 339, 2010.

Land subsidence in Emilia-Romagna Region, northern Italy: recent results

R. BISSOLI[1], G. BITELLI[2], F. BONSIGNORE[3], A. RAPINO[1] & L. VITTUARI[2]

1 *Regione Emilia-Romagna, Servizio Tutela e Risanamento Risorsa Acqua, 21 via dei Mille, 40121 Bologna, Italy*
rbissoli@regione.emilia-romagna.it

2 *University of Bologna, DICAM - Dept of Civil, Environmental and Materials Engineering, 2 Viale del Risorgimento, 40136 Bologna, Italy*

3 *ARPA-Emilia-Romagna - Regional Agency for Environmental Prevention in Emilia-Romagna, 6 Largo Caduti del Lavoro, 40121 Bologna, Italy*

Abstract In 2005–2007, an update of the geometric knowledge of the subsidence phenomenon in the Emilia-Romagna Region was conducted using the PSInSAR™ satellite radar interferometric analysis technique, supported by high precision levelling. This paper describes a large dimension case study, i.e. the entire portion of the Po River valley contained in Emilia Romagna. A report of the overall activity is presented, together with a summary of the main results achieved.

Key words subsidence; levelling; GPS; SAR

INTRODUCTION

The part of the Po River valley that includes the Emilia-Romagna Region is affected by a natural subsidence phenomenon at a rate of a few mm/year, varying in different areas (Gambolati *et al*., 1998). This phenomenon is due to tectonic causes and to natural sediment compaction, and is accompanied, in most of the area, by higher than natural subsidence due to anthropogenic causes, such as the extraction of fluids. Since the 1950s different agencies have been set up and have managed subsidence monitoring networks, measured by spirit levelling, in the areas in which the phenomenon had become particularly evident. These local monitoring networks highlighted maximum subsidence levels of more than 25 cm/year in 1951–1962 in the Po delta (Caputo *et al*., 1970; Borgia *et al.*, 1985), more than 11 cm/year in 1974–1981 near Bologna (Pieri *et al*., 1984) and more than 4 cm/year in 1972–1977 in Ravenna area (Teatini *et al*., 2005). More recently rates of subsidence have decreased but still remain significant in some places.

In 1999, the ARPA-Emilia-Romagna (Regional Agency for Environmental Prevention in Emilia-Romagna Region) on behalf of the Emilia-Romagna Region and in collaboration with the DISTART Department (now DICAM Dept) of Bologna University, established and measured a levelling network covering the whole regional part of the Po Plain and a GPS network, connected to the levelling one (Bitelli *et al*., 2000). In 2005–2007 a major upgrade of the 1999 survey was made using the interferometric analysis derived from satellite radar data (Ferretti *et al.*, 2001), in particular using the PSInSAR™ technique[1], supported by classic measurements realized by high precision spirit levelling (Bitelli *et al*., 2006; Bonsignore, 2008). Here, a report of the overall activity and a summary of the main results achieved are presented.

GEODETIC INFRASTRUCTURES FOR SUBSIDENCE MONITORING IN EMILIA-ROMAGNA REGION

The current geodetic network consists of two infrastructures: a high precision levelling network composed of over 2300 benchmarks, and a GPS network consisting of about 60 vertices. Both networks were measured for the first time in 1999; the measurement of the GPS network was repeated in 2002. In 2005–2007, the geometric knowledge of the regional subsidence phenomenon

[1] PSInSAR™ algorithm (Permanent Scatterers technique) is patented from Polytechnic University of Milan (POLIMI) and licensed exclusively to TRE Tele-Rilevamento Europa, which realized the interferometric analysis described in the paper.

Copyright © 2010 IAHS Press

was updated through the integration of two techniques (Fig. 1): high precision spirit levelling through the surveying of a subnet of the regional network (about 50% of the whole network, composed of more than 1000 benchmarks), and radar interferometric analysis adopting the PSInSAR™ technique (standard SPSA low resolution method), covering the whole plain territory of the region, i.e. about 11 000 km^2. The last analysis focused, in particular, on two distinct periods: the first time interval 1992–2000 refers to the processing of data from ERS1 and ERS2 ESA satellites, while the second one, concerning the time interval 2002–2006, refers to the processing of data from Envisat (ESA) and Radarsat (Canadian Space Agency) satellites.

Figure 2 shows the distribution of the Permanent Scatterers (PS) used for the analysis of vertical movements for the second period, derived from Envisat-Radarsat data.

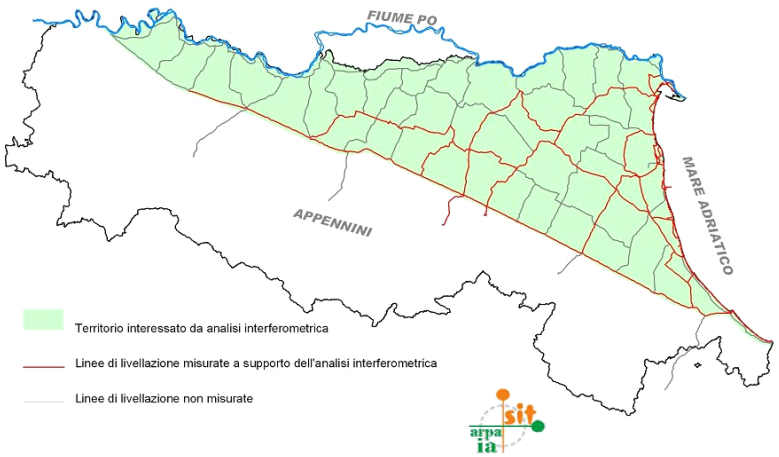

Fig. 1 Area covered by PSInSAR™ interferometric analysis and levelling lines (in red the lines surveyed during the 2005 campaign).

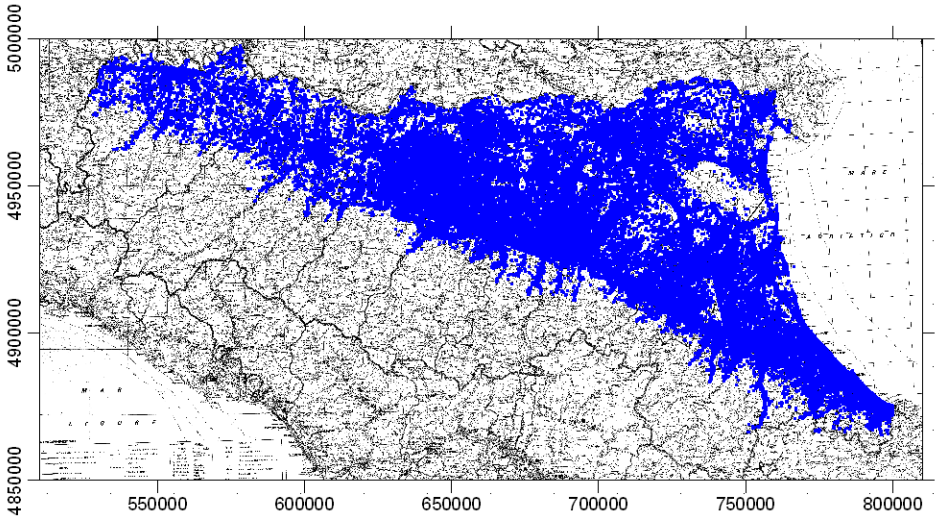

Fig. 2 Distribution of PS derived from ENVISAT+RADARSAT data sets (2002–2006).

One of the critical issues present both in geometric levelling and in interferometric SAR, is the choice of the reference points to be considered fixed in subsequent measurements or processing. These points define the elevation datums and their choice is therefore crucial, because it can introduce systematic effects in absolute heights and so an incorrect evaluation of vertical

motion velocities. Regarding the 1999 and the 2005 levelling campaigns, the origin was fixed in a benchmark situated near Sasso Marconi (Bologna), in the Apennine foothills and located in a position almost barycentric with respect to the network extension. The reference elevation above the geoid was determined in the past by the Italian Istituto Geografico Militare (IGM). Regarding PSInSAR^{TM} data, the processing of each data set was initially conducted separately on selected large areas (sites), and then a single reference point was adopted for each site and sensor type (ERS, Envisat, Radarsat); the final results were then connected together. The choice of the reference point was made through statistical analysis during the radar processing, but was confirmed *a posteriori* on the basis of external considerations related to the geometric levelling evidence. This reference point was fixed in the Reggio Emilia province, near the Po River, after a verification of point's stability with respect to Sasso Marconi.

The period 2002–2006 was characterized by a number of available Envisat images although these were quite limited, in particular in the central part of the region. Therefore the original data set was merged with a multi-temporal stack of Radarsat images. Both data sets (Envisat and Radarasat) were aligned using the subsidence rate measured at several nodal benchmarks of the geometric levelling network.

RADAR INTERFEROMETRIC ANALYSIS

The amount of information derived from the radar interferometry is enormous relative to the traditional spirit levelling surveys, as shown in Fig. 3.

The analysis of the huge amount of data, resulting from radar processing performed by TRE, was realized through a number of testing procedures, carried out at the whole data-set scale or at a more detailed scale. Tests were mainly performed within a GIS. The analysis was related either to the intrinsic reliability of the radar results and to the comparison with outcomes of geometric levelling campaigns, realized in almost the same period (levelling 1999–2005 *vs* PSInSAR^{TM} 2002–2006). The values of standard deviation and coherence derived from the interferometric processing and associated with the velocities of the PS were considered for the three types of sensors; as expected, the estimated velocities for the recent period (2002–2006) show confidence regions higher than the previous one, because of the reduced number of available images.

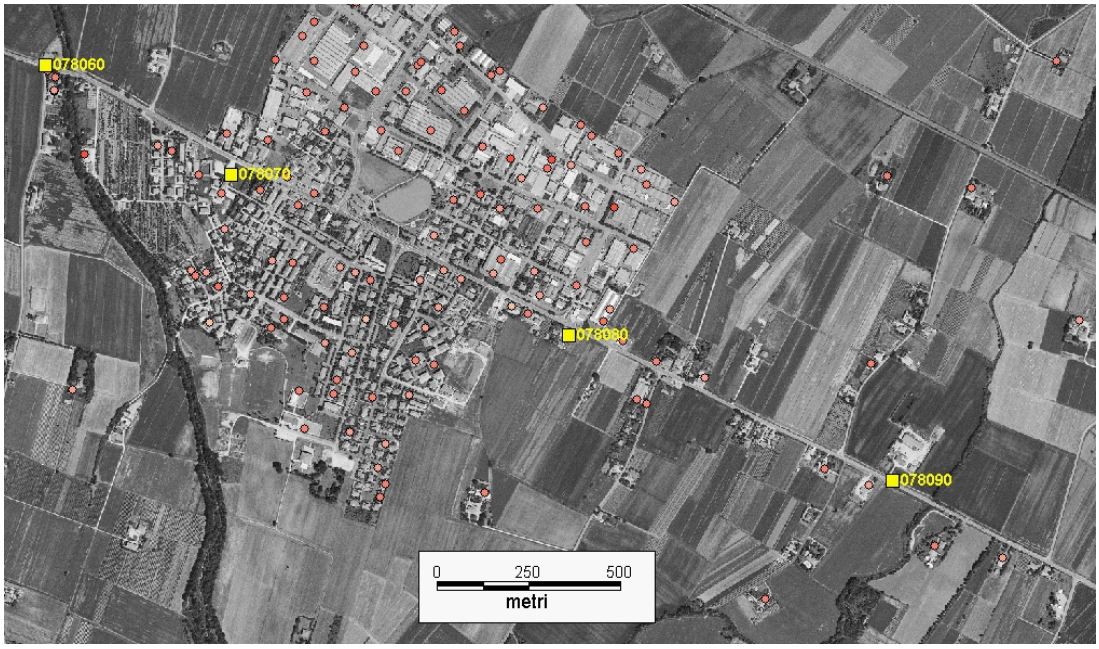

Fig. 3 Image comparing the different density of PS points with respect to levelling benchmarks (square symbol) and showing the spatial distribution of the PS with respect to the buildings distribution.

Using specifically developed GIS tools, some general screening procedures were conducted in order to detect PS related to targets not representative of actual ground movements, in particular for the selection of single isolated points showing displacement velocities significantly different from the surrounding ones (e.g. metallic silos with time-varying load conditions, points in open field areas with no evidence of artefacts, etc.). Through other specific tests, the velocities inferred for nearly coincident PS points derived from Envisat data sets in ascending and descending orbits were also compared. This test was made in order to verify the hypothesis of negligible horizontal movements and to finally reproject along the vertical directions the velocities measured in the line-of-sight directions.

A critical aspect was the identification of procedures in order to compare the velocities derived both from PSInSAR^{TM} and high precision geometric levelling; these data sets in fact do not coincide in terms of horizontal position. Different techniques were experimented with, based on local deterministic methods (e.g. simple proximity, predetermined radius of capture, radius determined according to the local velocity gradient, etc.) or by interpolation through geo-statistical methods (kriging), obtaining a good agreement.

Considering the high spatial density of PS and the required product (a map useful for a general evaluation of subsidence phenomena at the scale of the whole plain area of Emilia-Romagna), an interpolated contours level map of isokinetic curves was finally produced. In fact, based on the availability of satellite data, two different maps were produced (Fig. 4): the first one, covers the time interval 1992–2000 and refers to the processing of ERS1 and ERS2 ESA satellite data, and the second concerns the more recent period, 2002–2006, and refers to Envisat (ESA) and Radarsat (Canadian Space Agency) satellite data processing.

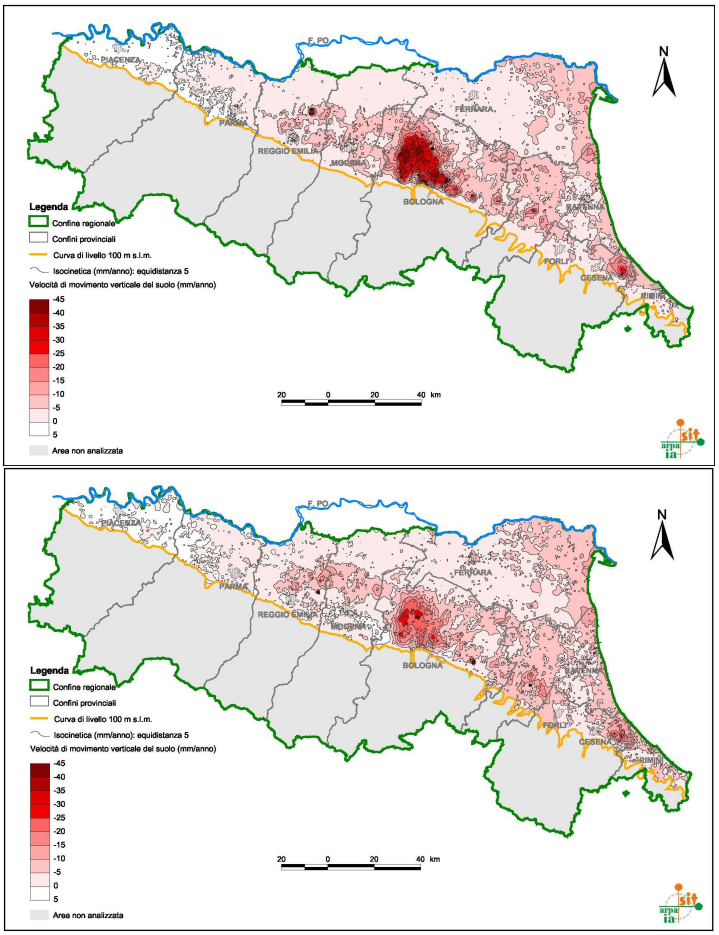

Fig. 4 Subsidence maps (mm/year) for the periods 1992–2000 (top) and 2002–2006 (bottom).

From examination of the results for the two periods, it can be deduced that the rate of subsidence still remains high in the areas historically affected by the phenomenon, though in general we can see a certain reduction, mainly in the central part of the region; for the coastal area, no significant changes are observable.

It should be emphasized that the results of this work have to be considered at a regional scale and they cannot be considered sufficient for an analysis at a very local scale; this is related to the standard SPSA low resolution method adopted and the uneven distribution of the points across the territory.

CONCLUSION

Starting from the experience gained in the study of the subsidence within the Po River plain of the Emilia Romagna, it was possible to identify some key issues in the use of SAR interferometry on a regional scale. In particular, in the lowland areas, where the horizontal movement of terrain can be considered negligible, the interferometric technique has provided measures of vertical relative motions, characterized by a precision of the same order of those obtainable using geometric levelling. However, the distribution of measured points in the case of built environments, was considerably higher than the number of benchmarks usually measured per square kilometre using classical techniques. Excluding particularly unfavourable contexts (lakes, unpopulated areas, lack of manmade infrastructures, etc.) the PSInSAR^{TM} techniques offered a density of measured points that reached values unmatched by traditional monitoring techniques. The maximum rate of velocity detectable through the SAR interferometry techniques is limited in the order of 60–70 mm/year (for ERS and ENVISAT). Within this range of velocity it allows the relative measurements of the movement of the soil, but it has similar requirements with respect to the spirit levelling, in particular regarding the definition of the datum. For these reasons it is important to consider the interferometric techniques within a reference context, defined and validated through the integration and the complementary use of other space geodetic techniques, such as a permanent GNSS network and geometric levelling.

REFERENCES

Bitelli G., Bonsignore F. & Unguendoli M. (2000) Levelling and GPS networks for ground subsidence monitoring in the Southern Po Valley. *J. Geodynamics* **30**(3), 355–369.

Bitelli, G., Bonsignore, F., Bortone, G. & Vittuari, L. (2006) Il monitoraggio della subsidenza a scala regionale in Emilia-Romagna. In: *Atti della giornata di studio Problemi di geoingegneria: estrazione di fluidi e subsidenza* (ed. by P. Macini & E. Mesini) (Geofluid 2006, Piacenza), 57–66.

Bonsignore, F. (2008) Il monitoraggio in Emilia Romagna. *ARPA Rivista* **XI**(1), Supplement: Il monitoraggio della subsidenza. Esperienze a confronto, 12–13.

Borgia, G., Brighenti, C. & Vitali, D. (1985) Estrazione di fluidi dal sottosuolo e subsidenza del delta del Po. *Accademia delle Scienze Ist. di Bologna*, 101–116. Bologna, Italy.

Caputo, M., Pieri, I. & Unguendoli, M. (1970) Geometric investigation of the subsidence in the Po delta. *Boll. Geodesia Teorica e Applicata* **13**(47), 187–207.

Ferretti, A., Prati, C. & Rocca, F. (2001) Permanent scatterers in SAR interferometry. *IEEE Trans. Geoscience & Remote Sensing* **39**, 1.

Gambolati, G., Giunta, G. Putti, M., P. Teatini, P. *et al*. (1998) Coastal evolution of the upper Adriatic Sea due to sea level rise and natural and anthropic land subsidence. In: *CENAS* (ed. by G. Gambolati), 1–34. Kluver Academic Publishers, Dordrecht, The Netherlands.

Pieri, L. & Russo, P. (1984) The survey of soil vertical movements in the region of Bologna. *Proceedings Third International Symposium on Land Subsidence* (Venezia, March 1984).

Teatini, P., Ferronato, M., Gambolati, G., Bertoni, W. & Gonella, M. (2005) A century of land subsidence in Ravenna, Italy. *Environmental Geology* **47**(6), 831–846.

(Proceedings of EISOLS 2010, Queretaro, Mexico, 17–22 October 2010). IAHS Publ. 339, 2010.

Large area observation of land subsidence by PSInSAR and determination of the cause of local land subsidence

K. DAITO[1], S. SAEKI[2], S. KUZUOKA[3] & T. MIZUNO[4]

1 *Dept of Civil Engineering and Environmental Design, Daido University, 457-8532, Nagoya, Japan*
daito@daido-it.ac.jp
2 *Nakanihon Engineering Consultants Co. Ltd, 460-0003, Nagoya, Japan*
3 *NEC Corporation, 183-8501, Tokyo, Japan*
4 *OYO Corporation, 331-8688, Saitama, Japan*

Abstract PSInSAR is a technology that measures the change of ground level by the reflection characteristic of the micro wave irradiated from a space satellite. In this research, the observation of the change of ground level of the Nobi Plain was done by using PSInSAR. Also, the observation accuracy of PSInSAR was confirmed by comparing the observation result of PSInSAR and the levelling results. Moreover, the determination of the cause of the change of ground level was tried. As a result, PSInSAR had the high observation density, and showed almost the same ground deformation tendency as the levelling. It has been understood to be able to presume the factor of the change of ground level by arranging the geological structure, the pumping discharge, the land use, etc. with GIS.

Key words land subsidence; satellite; GIS; PSInSAR

INTRODUCTION

Large-area subsidence progresses continuously over many years. And the progress is a phenomenon that cannot be recognized in the short term. In the Nobi Plain, Japan, large area subsidence was generated by excessive groundwater extraction in the past. Now, due to pumping restrictions and conversion from groundwater to alternative water sources, there is little subsidence in the Nobi Plain. However, there is still a possibility that large area subsidence will be caused if an unusual shortage of water occurs. Therefore, the levelling is still done across the whole area of the Nobi Plain to monitor any subsidence. In the levelling done now, a lot of time is required to complete the measurement work, for arrangement of the measurement data, to identify the subsidence situation, and the specification of the subsidence factor. But the accuracy of observation of the change of ground level has improved with the development of GPS (Global Positioning System) and remote sensing technology in recent years. Therefore, it has become possible to observe the change of ground level in the short term by using these technologies.

In this research, first, the observational results for the change of ground level in the Nobi Plain by PSInSAR (interference synthetic aperture radar that has used a permanent scattered point) were arranged by using GIS. PSInSAR is the remote sensing technology that is able to be observed at the orbital period of the space satellite. Next, the levelling results were compared with the observational result of PSInSAR. The accuracy of observation of PSInSAR was confirmed. And the technique for deriving the factor of the local change of ground level was examined.

OBSERVATION AREA AND OBSERVATION PERIOD

The area of observation is 625 km^2 around the Kanie region that is a typical subsidence region in the Nobi Plain, and includes the Nagoya city area, the estuary area of Kiso-three-rivers, and the right bank area of the Ibi River. The observation period is from 20 October 1992 to 15 September 1998, i.e. the observation period of space satellite JERS-1. The number of observation points (PS points) obtained by this PSInSAR is less in the west part, where there are many fields, than in the east part where the urban area, including Nagoya City, are present, as shown in Fig. 1. The number of PS points observed in the Nobi Plain is about 17 000, and the number of benchmarks

Copyright © 2010 IAHS Press

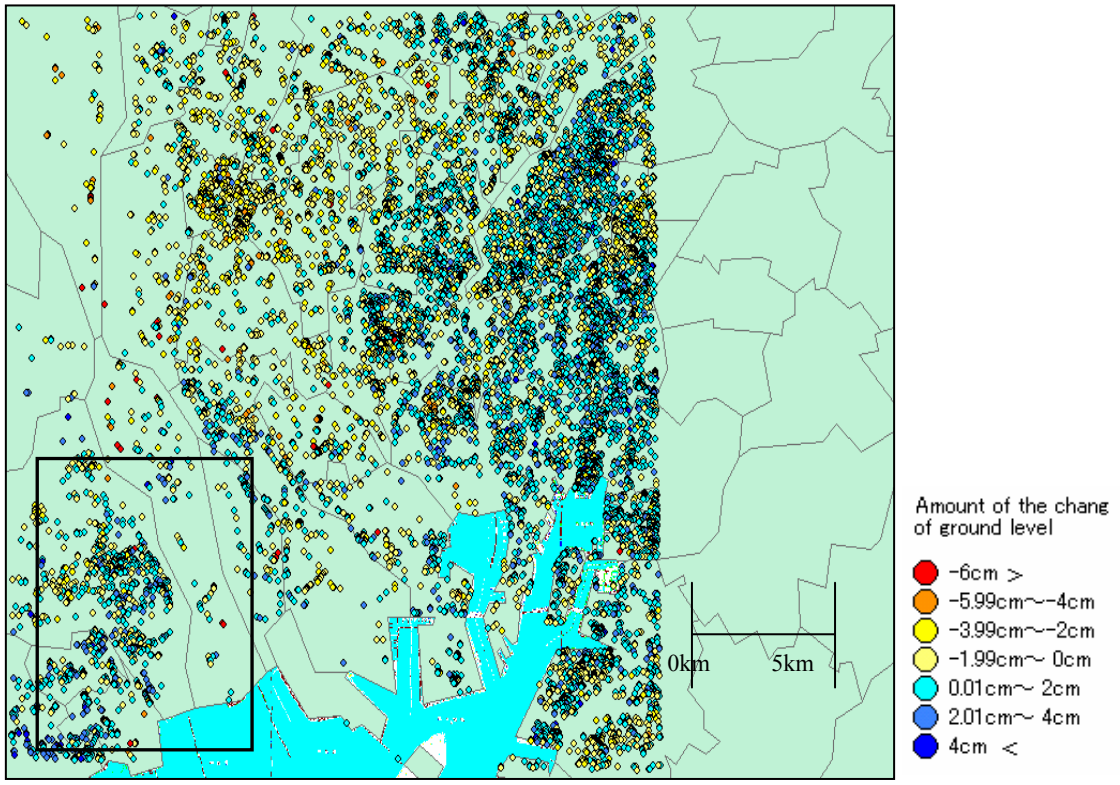

Fig. 1 Observational result of the Nobi Plain by PSInSAR.

observed is about 570. PSInSAR observes the whole area of the Nobi Plain in more detail than the levelling, as apparent from the number of observation points.

TENDENCY OF THE CHANGE OF GROUND LEVEL IN THE SPECIFIC REGION

The tendency of the change of ground level for various places was analysed from the observation results (Daito *et al*., 2003; Saeki, 2006) obtained from PSInSAR, and the factor of the change of ground level was determined for the PS points that experienced a change of ground level greater than that of the local area.

Here, the tendency of the change of ground level around Kuwana City (enclosed in the square in Fig. 1) was analysed. Many PS points were observed for the surroundings of Kuwana City due to the relatively density housing and factory buildings, etc. (Fig. 2). The histogram of the PS points surrounding of Kuwana City was made by using a statistical function of GIS as shown in Fig. 3 when the tendency of the change of ground level was analysed. The mean value of the change of ground level obtained for the observation period was about 0.70 cm, and shows the upheaval tendency from Fig. 3.

EVALUATION OF LOCAL CHANGE OF GROUND LEVEL

Among the PS points in Nagashima-cho, enclosed by the oval in Fig. 2, there were PS points that showed subsidence greater than 10.0 cm for the observation period. The local change of ground level was analysed, and the factor of it was presumed because the change of ground level was obviously very different from the change to the surrounding ground. It was thought that this subsidence occurred due to the load of the fill and the house. Then, the subsidence of Nagashima-cho that the embankment loading had influenced was analysed. The consolidation subsidence

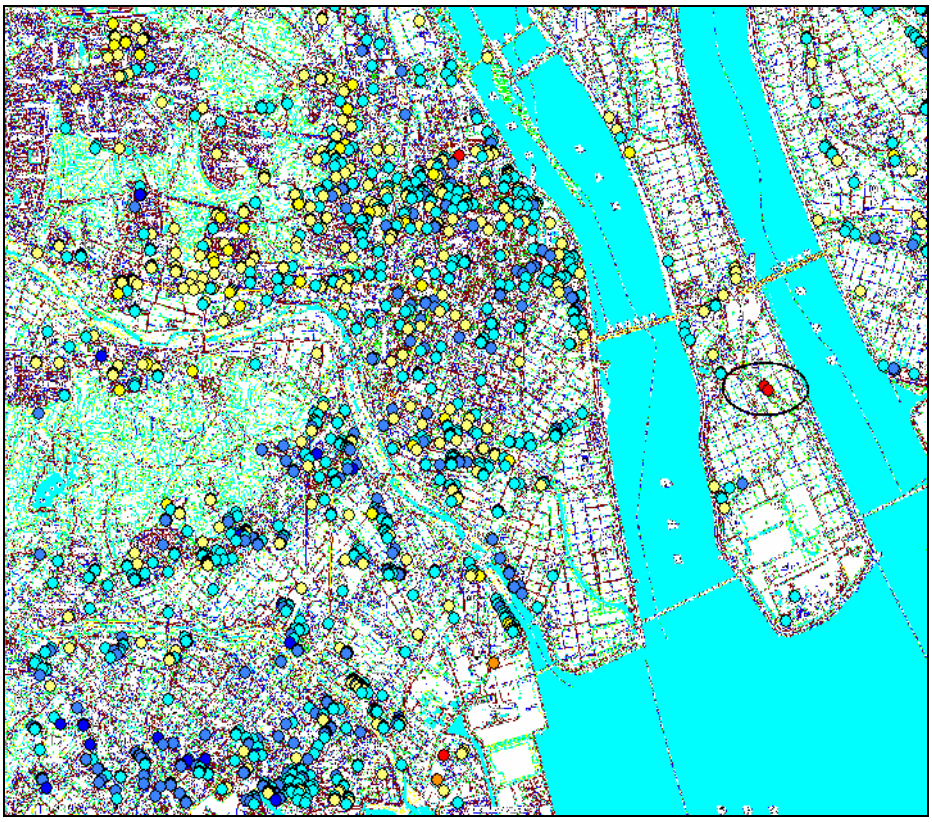

Fig. 2 Distribution chart of PS points around Kuwana City.

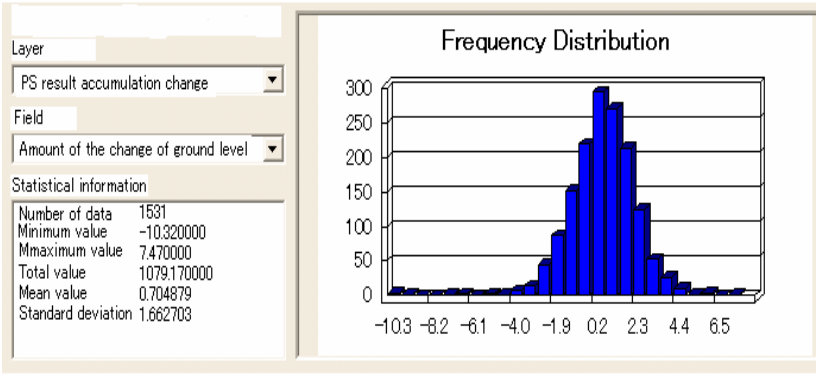

Fig. 3 Statistical information of PS points around Kuwana City.

curve from the embankment loading was made, and was compared with the observational result of PSInSAR. The amount of the consolidation subsidence every month and every year was obtained from the embankment loading and the consolidation subsidence curve. It referred to the investigation report when the numerical value was decided.

The amount of change of ground level determined from the consolidation subsidence curve and the PS points (IG787 and IG822) were compared, as shown in Fig. 4. The subsidence tendencies of the change of ground level from the PS points and the consolidation subsidence curve were almost equal (Fig. 4). Therefore, the factor causing subsidence that has been observed in Nagashima-cho was confirmed to be due to the load of the fill and the house. Moreover, the accuracy of observation by PSInSAR was confirmed by comparing the consolidation subsidence curve with the observed subsidence at PS points.

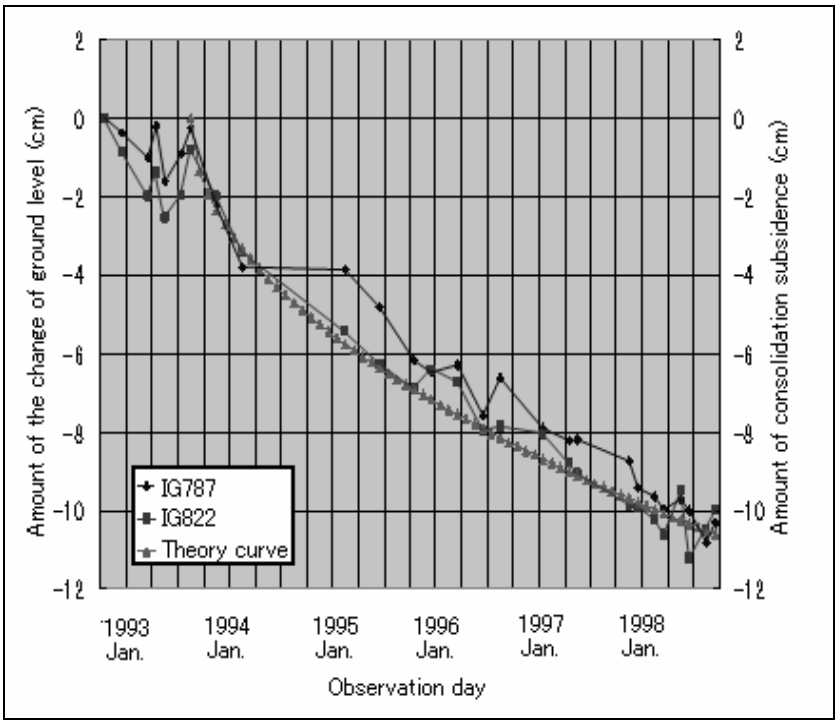

Fig. 4 Amount of change of ground level and consolidation subsidence curve at PS points.

CONCLUSIONS

PSInSAR has the advantage that subsidence over a wide area can be observed very accurately at the same time, and that the tendency of change of ground level in each region can be understood by arranging the observational result with GIS. Moreover, the tendency of change of ground level in the region can be analysed in detail because the number of PS points is more than the number of levelling points. It was apparent that there are many PS points in the urbanized region, and relatively few PS points in the agricultural region from the observational result of PSInSAR in the Nobi Plain. The factor of the change of ground level can be presumed by surveying the local ground conditions. Moreover, the factor of a local change of ground level was able to be presumed by making the consolidation subsidence curve by the embankment loading, and by comparing it with the observational result of PSInSAR.

REFERENCES

Daito, K., Ferretti, A., Kuzuoka, S., Novali, F., Panzeri, P. & Rocca, F. (2003) L-band PS analysis: JERS-1 results and TerraSAR–L predictions. Fringe03, December, 1–5.

Saeki, S., Daito, K., Kuzuoka, S. & Mizuno, S. (2006) The evaluation of characteristics of ground movement in the Nobi Plain by using PSInSAR and GIS. Outline collection of 2006 Space Information Symposium Lectures, 197–201 (in Japanese).

(Proceedings of EISOLS 2010, Querétaro, Mexico, 17–22 October 2010). IAHS Publ. 339, 2010.

Land subsidence monitored by satellite interferometry in Mexican cities

J. A. ÁVILA-OLIVERA[1], P. FARINA[2] & V. H. GARDUÑO-MONROY[3]

1 *Instituto de Investigaciones Sobre los Recursos Naturales (INIRENA), Universidad Michoacana de San Nicolás de Hidalgo (UMSNH), Av. San Juanito Itzicuaro s/n, Col. Nueva Esperanza, CP 58330, Morelia, Michoacán, Mexico*
ja.avilaolivera@gmail.com

2 Formerly at *Dipartimento di Scienze della Terra, Universitá degli Studi di Firenze, Via G. La Pira 4, 50121, Florence, Italy*

3 *Instituto de Investigaciones Metalúrgicas (IIM), Universidad Michoacana de San Nicolás de Hidalgo (UMSNH), Ciudad Universitaria, Morelia, Michoacán, Mexico*

Abstract Land subsidence has been observed in Mexico since the 1980s. The urban centres located in the central part of the Mexican Volcanic Belt (MVB) were the first affected by such a problem. In order to monitor the phenomenon and to retrieve land subsidence rates, a satellite interferometric analysis was carried out for the main cities located within the MVB, namely Morelia, Celaya and Querétaro. Differential interferograms of these cities display phase signals related to ground displacements. Deformations of the ground surface are concentrated along the main surface faults. Through phase unwrapping, maximum land subsidence rates of –35, –100 and –68 mm/year for Morelia, Celaya and Querétaro, respectively, have been recorded.

Key words land subsidence; satellite interferometry; Morelia; Celaya; Querétaro

INTRODUCTION

In Mexico, land subsidence problems have been observed since the 1980s, when they started to cause damage in cities to linear infrastructures and structures, such as roads, pipelines, railways, buildings, etc. At the beginning, the cases were concentrated in the central part of the country, within the geological province known as the Mexican Volcanic Belt (MVB). The cities where the phenomenon was recognized first are Mexico City (Figueroa-Vega, 1984), Celaya (Trujillo-Candelaria, 1985), Aguascalientes, Querétaro (Trejo-Moedano & Martínez-Baini, 1991), Morelia (Garduño-Monroy *et al.*, 1998), and Salamanca.

In order to determine both the spatial extension and the temporal evolution of land subsidence in some cities within the MVB, a satellite geodetic study was carried out. The analysis consists of applying the interferometric technique, which is based on remote sensing, to determine ground deformations along the satellite l.o.s. (line of sight).

METHODOLOGY

The InSAR (Interferometry of Synthetic Aperture Radar) technique consists of comparing two or more SAR scenes of the observed area, to determine the interference pattern (fringes) which is generated by the difference in phase between the scenes. The images are taken by the antennas mounted on an aircraft or on a satellite.

For the study, data acquired by the ENVISAT satellite over the cities of interest (Morelia, Celaya and Querétaro) were used. Scene pairs with short baselines (up to 250 m) were selected, because spatial de-correlation induced by the acquisition geometry limited the technique's applicability. The data span the time interval from July 2003 to May 2006, reaching intervals of from 35 up to 945 days. The method employed to process the coherent scenes pairs, was the "two pass interferometry", and it was carried out by using commercial software.

Copyright © 2010 IAHS Press

RESULTS

The result of an interferometric process is called an interferogram, which in the case of surface deformation in the spanned interval, shows an interference pattern (i.e. fringes). Each fringe corresponds to a cycle phase, and in the cases of radars that work with band C (ERS-1, ERS-2, RADARSAT-1, RADARSAT-2, ENVISAT), it represents a deformation of 28 mm along the satellite l.o.s. (23º from the vertical). Here we present the best interferogram in terms of coherence, for each studied city.

Morelia

Figure 1 shows one of the best interferograms processed for Morelia; it spans a time interval of 490 days. The differential interferogram displays phase signals related to surface deformations: variations of the phase along preferential directions (NE–SW and E–W), and sub-circular bowls with a diameter of a few hundred metres. The interferograms were subjected to a phase unwrapping process and geolocation, and they became ground displacement maps along the satellite l.o.s. With the normalization of these displacements, a land subsidence rate was determined of up to –35 mm/year between 2003 and 2005 (Ávila-Olivera, 2009).

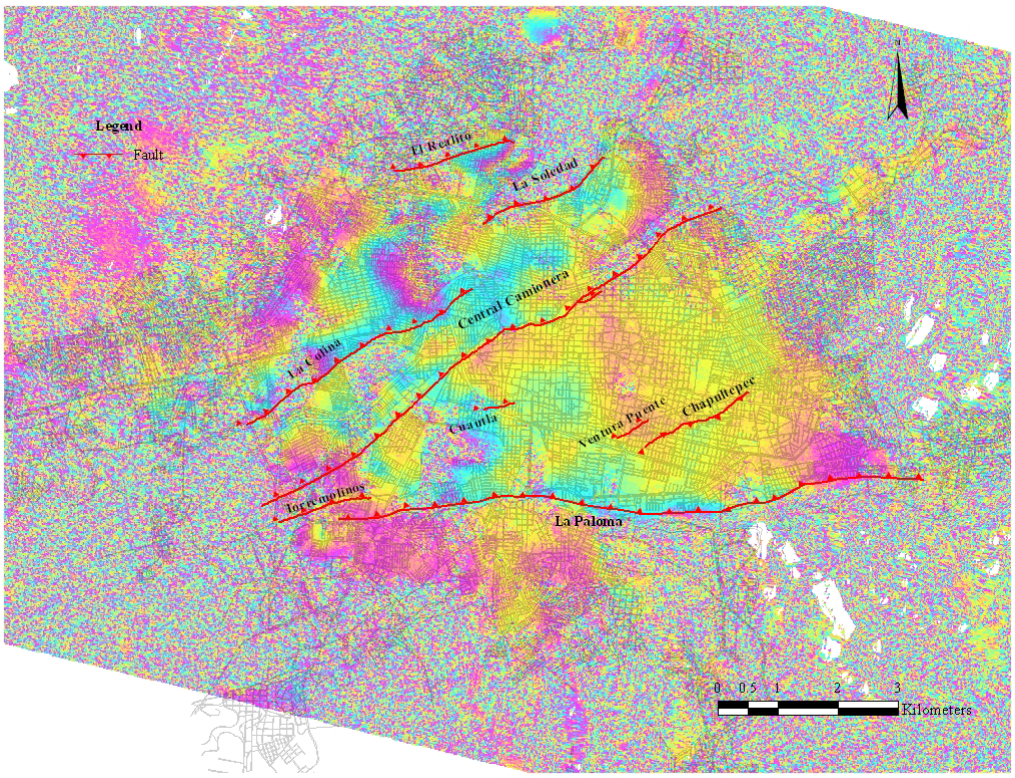

Fig. 1 Interferogram of Morelia spanning a time interval 12/07/2003–13/11/2004.

Celaya

Figure 2 presents one differential interferogram of Celaya, spanning a time interval of 455 days. The interferogram reveals ground displacements along the main faults of the city oriented NNW–SSE. Maximum deformations are concentrated between the "Oriente" and "Universidad Pedagógica" faults, and towards the north where the industrial zone is located, which is probably responsible for sinkings that take place there due to groundwater extraction. The phase unwrapped process carried out on an interferogram realized with data from 2006, reveals the land subsidence rate reached –100 mm/year in the zones mentioned previously (Farina *et al.*, 2008).

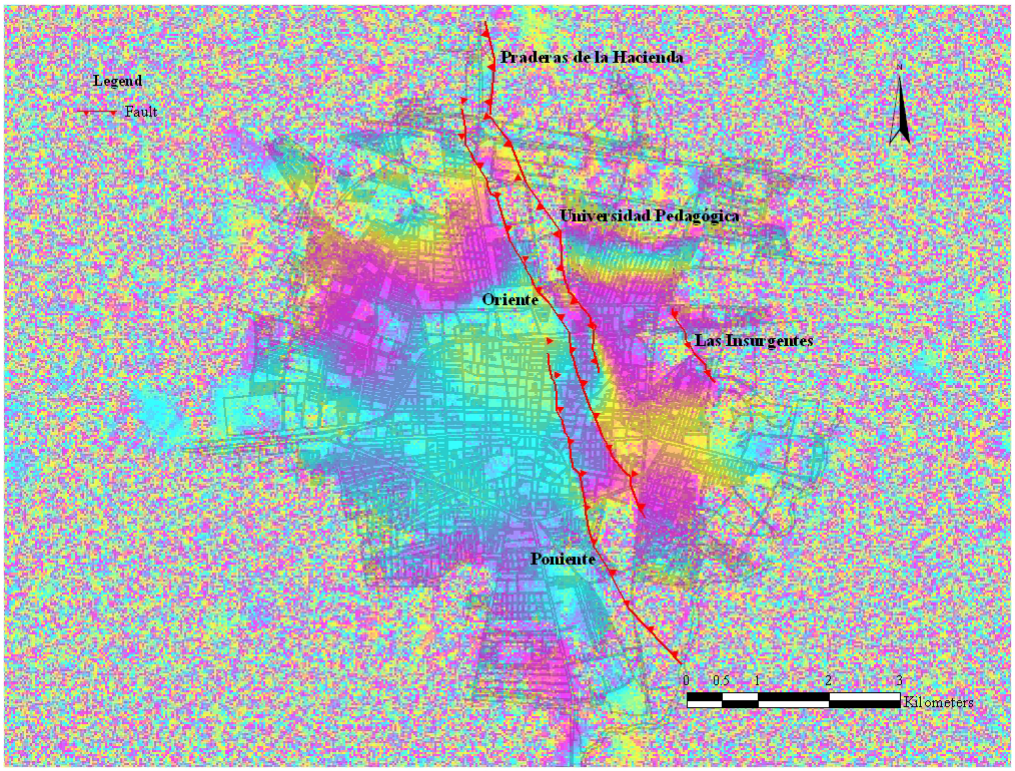

Fig. 2 Interferogram of Celaya spanning a time interval 16/08/2003–13/11/2004.

Querétaro

On the interferograms of Querétaro, two different behaviours in the city clearly separated by the "5 de Febrero" fault with a NNW–SSE direction are observed. The eastern side is stable (signal variations are not visible); while the western portion presents narrow interferometric fringes that represent ground movements. The land subsidence rate reached –68 mm/year between 2003 and 2004.

CONCLUSIONS

The InSAR survey carried out allowed bi-dimensional spatial maps of land subsidence to be obtained for three important cities located within the MVB, measurement of the average annual rate of land subsidence, and identification of a clear correlation between the regional faulting systems of the area and the ground settlements.

REFERENCES

Ávila-Olivera, J. A. (2009) Evolución de los Procesos de Subsidencia-Creep-Falla, casos: Morelia, Mich. y Celaya, Gto. PhD Thesis, Universidad Nacional Autónoma de México, Mexico, D.F.

Farina, P., Ávila-Olivera, J. A., Garduño-Monroy V. H. & Catani, F. (2008) DInSAR analysis of differential ground subsidence affecting urban areas along the Mexican Volcanic Belt (MVB). *Rivista Italiana di Telerilevamento* **40**(2), 103–113.

Figueroa-Vega, G. E. (1984) Case history 9.8 Mexico, D.F. In: *Guidebook to Studies of Land Subsidence Due to Groundwater Withdrawal* (ed. by J. F. Poland), 217–232. International Hydrological Program, Working Group 8.4.

Garduño-Monroy, V. H., Arreygue-Rocha, E, Chiesa, S., Israde-Alcántara, I., Rodríguez-Torres, G. M. & Ayala, G. M. (1998) Las fallas geológicas y sísmicas de la ciudad de Morelia y su influencia en la planificación del territorio. *Ingeniería Civil*, **1**(5), 3–12.

Trejo-Moedano, A. & Martínez-Baini, A. (1991) Agrietamiento de suelo zona Querétaro. In: *Agrietamiento de Suelos* (ed. by SMMS), 67–74.

Trujillo-Candelaria J. A. (1985) Subsidencia de terrenos en la ciudad de Celaya, Gto. *Sociedad Mexicana de Suelos, Asociación Geohidrológica Mexicana* (Reunión sobre Asentamientos Regionales, México, D.F.), 1–2.

(Proceedings of EISOLS 2010, Querétaro, Mexico, 17–22 October 2010). IAHS Publ. 339, 2010.

Using extensometer and Earth tide data to quantify fractured crystalline-rock properties

T. J. BURBEY[1] **& L. C. MURDOCH**[2]

1 *Department of Geosciences Virginia Tech, 4044 Derring Hall, Blacksburg, Virginia 24061, USA*
tjburbey@vt.edu

2 *Clemson University, Department of Environmental Engineering & Earth Sciences, 340 Brackett Hall, Clemson, SC 29634, USA*

Abstract A high-precision borehole extensometer was used during pumping to monitor fracture axial strain at the fractured rock research site in Floyd County, Virginia, USA. Strain data were used with results obtained from Earth tide analyses and borehole logs to quantify a number of hydromechanical properties, including fracture volumetric specific storage, fracture porosity, Poisson's ratio and the drained formation modulus. Tiltmeter data were used to estimate "subsidence" caused by three separate four-hour pumping tests performed in well EX-1. During these three tests the extensometer, located in W-03 and 27.7 m from the pumping well, was anchored over 2.1 metre long sections of: (1) a fracture in hydraulic communication with EX-1, (2) a fracture that is not hydraulically connected with EX-1, and (3) an unfractured portion of bedrock directly below the hydraulically connected fracture. Results from the pumping tests yielded a fracture compression expressed as compliance ranging from 0.1 to 0.16 μm/m. The total vertical strain associated with fractures in W-3 can be evaluated because flowmeter data suggest the extensometer captured both hydraulically active fractures. When coupled with areal strain calculated from Earth tide analyses a volumetric specific storage of 4.52×10^{-7}/m is calculated along with a Poisson's ratio of 0.28. Using this with a calculated barometric efficiency of 0.45 allows for an overall fracture porosity of 0.05 at well W-03.

Key words borehole extensometer; hydromechanics; fractured rocks; land subsidence; field tests

INTRODUCTION

Fractures in crystalline rocks undergo compression during pumping, much like sediments do. One of the main differences in these two settings is that fractures tend to be far stiffer than unconsolidated deposits and therefore the magnitude of compaction being measured during a pumping test is on the order of microns instead of millimetres (Murdoch & Germanovich, 2006). Thus, conventional methods for measuring compaction and land subsidence (at the surface) using InSAR (interferometric synthetic aperture radar) (Galloway *et al*., 1998), GPS (Krijnen & de Heus, 1995), or pipe extensometers (Riley, 1986) fail to provide the necessary resolution in crystalline-rock settings where pumping volumes are very small.

A removable and remotely actuated borehole extensometer is used in this investigation to measure individual fracture compression during short-term aquifer pumping (Schweisinger *et al*., 2007). The extensometer is locked in place with hydraulically-activated mechanical anchors above and below the fracture (2.1 m spacing). An LVDT (linear variable displacement transducer) is used to measure axial displacement between the anchors attached to a pair of 1-m long invar rods, which possess an exceptionally low coefficient of thermal expansion. The LVDT can resolve displacements of about 0.1 micron. However, due to noise and other factors, the accuracy is more likely on the order of 0.3 to 0.5 microns.

When hydraulic head measurements are obtained concurrently with the displacement data during pumping, the relation between stress and strain of an individual fracture can be computed along with an axial strain rate. Vertical strain (displacement/anchor separation distance) can be used with the measured drawdown to compute a uniaxial specific storage. However, if Earth tide data are also used, which provide reasonable estimates of areal strain (Doan *et al*., 2006), these strain estimates can be combined to provide a volumetric specific storage and Poisson's ratio, two valuable parameters in crystalline rock settings.

Copyright © 2010 IAHS Press

FIELD SITE

The field site in Floyd County, Virginia, USA, is located in the complex metamorphic terrain of the Blue Ridge Physiographic Province (Fig. 1). A heterogeneous and usually confined saprolite aquifer overlies variably fractured granulite gneiss. Weathering of the underlying bedrock is variable, but typically is quite shallow, as evidenced by the interflow that occurs on the bedrock surface. Locally, en echelon thrust faults are prevalent in the area and tend to compartmentalize groundwater flow and provide deeper pathways for groundwater to effectively recharge the bedrock system where these faults reach the surface (Seaton & Burbey, 2000).

At the study site, twelve 0.15-m diameter (6-inch) wells have been drilled and used to help characterize the bedrock geology and hydrology (Seaton & Burbey, 2005). Figure 1(a) shows the location of the deep wells that are cased through the saprolite into the topmost portion of the underlying bedrock. The wells are open to depths ranging from 50 m to 350 m. The two named wells in Fig. 1, W-03 (180 m deep) and EX-1 (94 m deep), are the wells used as the pumping well and extensometer, respectively. The natural hydraulic gradient slopes gently to the south. Logging and testing associated with these wells have led to the identification of a fault-zone aquifer that represents the fractured hanging wall adjacent to one of these en echelon thrust faults that reaches the surface at the crest of the hill identified in Fig. 1 (as the arcuate shaded grey region) and ramps downward to the south–southeast, as pictured in Fig. 1(b). The fault appears to become nearly horizontal at a depth of 50–70 m below land surface.

Forty metres north of the extensometer in W-03 and 60 m NW of the pumping well EX-1 a tiltmeter, T1, was employed in a shallow borehole (3.1 m deep) to monitor surface tilt associated with pumping. The measured tilt can be used to approximate any potential subsidence associated with the pumping tests.

Optical televiewer data and heat-pulse flowmeter data from both EX-1 and W-03 (27.7 m apart) indicate that the two wells are connected by what appears to be a single fracture, although the dip angles and depths of each fracture suggest that they may be separate but intersecting fractures. Both fractures appear to have apertures on the order of millimetres. Both wells have at least one other significant hydraulically-open fracture that may be open to other well sites, but is not connected to each other. Figure 2 shows a conceptualization and pumping test design of the fracture system between EX-1 and W-03 with the correct depth locations of fractures intersecting each borehole. When EX-1 is pumped W-03 experiences quantifiable drawdown within about one minute, suggesting properties of high hydraulic diffusivity.

FIELD TESTS

Three separate aquifer tests were performed in which EX-1 was pumped while W-03 was monitored using the borehole extensometer straddling each of the two observed fractures in the well, one connected to EX-1 (fracture at 63 m depth) and one connected to W-7 and W-10 (Fig. 1(a)) and other far-field wells at the site (fracture at 52 m depth). A third test was conducted which positioned the extensometer adjacent to, but not straddling, the fracture connected to EX-1 (63.3–65.4 m depth). Pumping for each aquifer test occurred for four hours followed by a recovery period of up to 18 hours. The rate of pumping was 5.35×10^{-3} m^3/min for the first test and 6.92×10^{-3} m^3/min for the second and third tests. The maximum drawdown in the EX-1 pumping well was approximately 12 m for the first test and 16 m for the subsequent two tests. Meanwhile, the measured drawdown in W-03 located 27.7 m from EX-1 was approximately 10 m during the first test and nearly 12 m for the second and third tests.

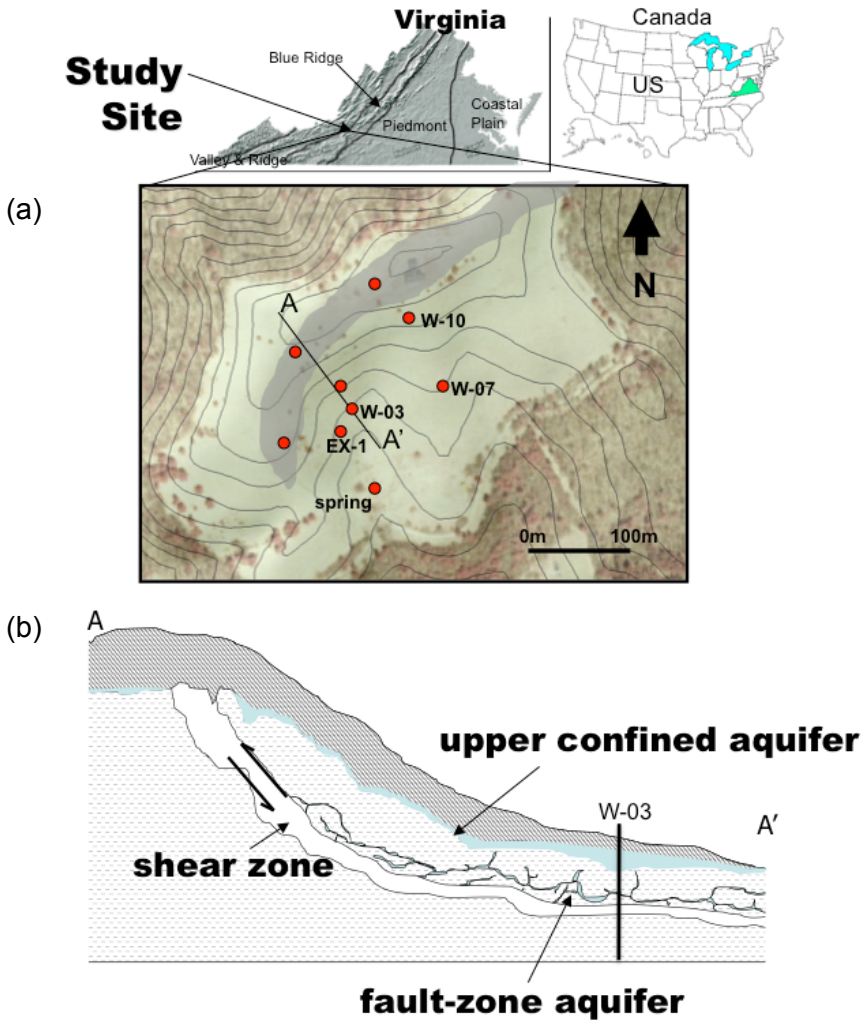

Fig. 1 (a) Location of study site showing well locations. Shaded grey area represents subcrop exposure of thrust fault. Cross section A–A′ is shown in (b) and represents a conceptualization of the fault zone at the site.

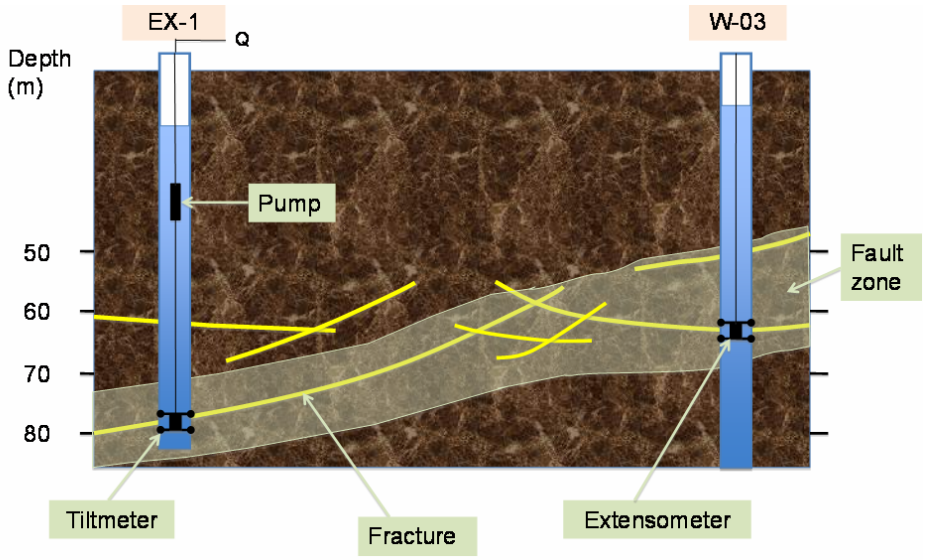

Fig. 2 Conceptualization of fault-zone aquifer and fracture connectivity between EX-1 and W-03. Location of fractures intersecting boreholes is accurate.

Figure 3 shows the displacement-drawdown plots for each of the three tests. The general observations from these three tests reveal that: compression and/or extension occurred within minutes after the start of drawdown; pumping resulting in compression of both hydraulically connected fractures, with a greater compaction occurring in the shallower fracture not connected to EX-1; extension occurred in the first test where the extensometer was anchored just below the fracture connected to EX-1; fracture compression continued to occur during the entire recovery period, even for the third test where recovery was 18 hours long.

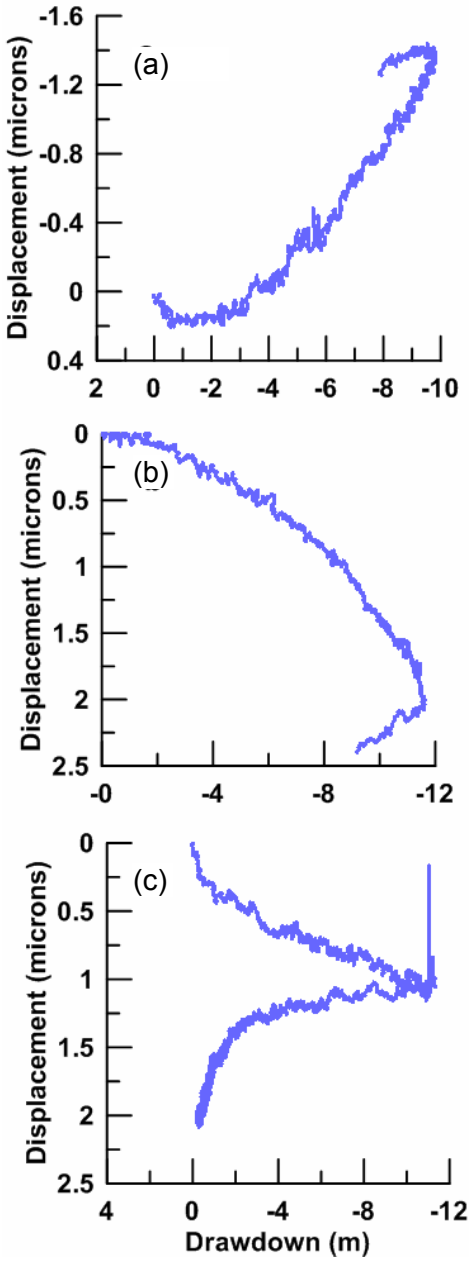

Fig. 3 Displacement-drawdown plots for: (a) test below lower fracture, (b) test straddling lower fracture, and (c) test straddling upper fracture.

ANALYSIS

Uniaxial specific storage (vertical direction) can be calculated from the extensometer data during aquifer testing by dividing the measured displacement by the anchor separation distance of the

extensometer (2.1 m), which yields a vertical strain, ε_v, per unit decline in head. Dividing by the drawdown (stress expressed as a change in head) converts this ratio into specific storage, S_s. The estimated S_s for the open fractures tests (Fig. 3(b), (c)) are 4.76×10^{-8}/m and 7.46×10^{-8}/m, respectively. The extensional compliance of the unfractured rock (Fig. 3(a)) is only slightly greater than the compressional compliance of the overlying fracture (Fig. 3(b)) suggesting that the fracture may have asperities that reflect the bulk modulus of the rock. Moreover, this fracture connecting EX-1 with W-03 was established through hydrofracing only a year earlier, so it possesses no weathering, which would tend to make it more compliant. Thus, the results here are justifiable.

Poisson's ratio represents the contraction of transverse strain to the extension of axial strain and can be represented as:

$$\nu = \frac{1}{\frac{\varepsilon_a}{\varepsilon_v} + 1} \tag{1}$$

where ε_a is the areal strain. Here the areal strain is estimated using Earth tide analysis. The analytical expression for areal strain from the theoretical tidal potential can be expressed (Doan *et al.*, 2006) as:

$$\varepsilon_a = \sum_{l} \frac{2h_l - l(l-1)l_l}{gr} W_l \tag{2}$$

where h_l are the numerically computed Love numbers and l_l are the Shida numbers (Wang, 1997) that are dependent on the structure of the Earth and typically also determined by numerical simulation to a highly precise value. W_l is the theoretical potential and the subscript l is the order that is typically chosen to be 2 because it represents 98% of the total potential (Wenzel, 1997). The constant g is gravity and r is the radius of the Earth. Water-level fluctuations in W-03 show a clear Earth-tide signal that closely mimics the M_2 and O_1 lunar tide-generating strains and is not polluted by periodic barometric tides (Burbey, 2010). The water-level data were reduced to eliminate low-frequency atmospheric tides associated with frontal systems. Figure 4 shows the comparison of water-level changes to the theoretical areal strains (equation (2)) caused by these lunar tidal signals.

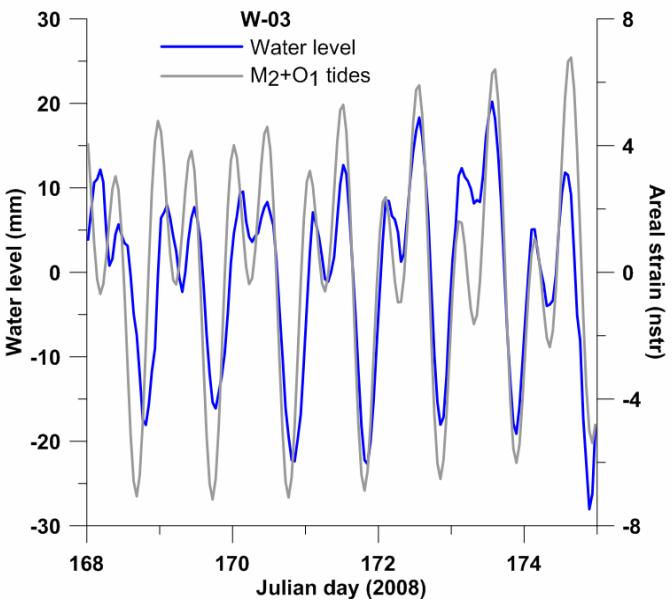

Fig. 4 Reduced water-level changes associated with earth tides compared to the lunar M2 and O1 strains.

Normalizing the hydraulic head changes caused by Earth tides with those caused by pumping, equation (1) allows us to obtain a Poisson's ratio of 0.28 using equation (1). This value seems reasonable because it is within the range typically reported from laboratory measurements of crystalline rock (Jaeger *et al*., 2007). This approach is significant because, to our knowledge, methods for estimating Poisson's ratio at field scales in fractured rocks are unavailable.

From the newly calculated value of Poisson's ratio, the volume strain, ε, can be calculated straightforwardly from either the vertical or areal strain. Here we use the vertical strain to obtain:

$$\varepsilon = \varepsilon_v \left(1 + \frac{1-\nu}{\nu}\right) \tag{3}$$

Now a more realistic volumetric specific storage can be calculated for the two fractures. Because the fractures are dipping, axially calculated specific storage does not adequately describe the storage characteristics of the fractures intersecting W-03. The sum of the areal and vertical specific storage estimates represents the total specific storage for the two fractures intersecting W-03 and is calculated to be $S_s = 4.52 \times 10^{-7}$/m.

The barometric efficiency (BE) is defined by the aquifer pressure head change caused by the atmospheric pressure change and is one of the parameters often used for calculating porosity. Here BE is calculated to be 0.45 using the slope method of Gonthier (2007), which more effectively calculates water-level changes associated with lower frequency barometric-pressure fluctuations associated with frontal systems, while eliminating those responses that are difficult to distinguish from Earth tides.

Jacob (1940) was the first to relate specific storage and barometric efficiency to porosity, θ, for a confined aquifer through the expression:

$$\theta = S_s \cdot BE \cdot \frac{K_f}{\rho_f g} \tag{4}$$

where K_f is the fluid bulk modulus and ρ_f is the fluid density. Using the parameters already calculated in equation (4) results in a porosity of 0.07, a reasonable value for this fractured granulite gneiss. Finally, the drained bulk modulus, K', can now be calculated from the definition of specific storage (Bredehoeft, 1967):

$$S_s = \rho_f g \left(\frac{1}{K'} + \frac{\theta}{K_f}\right) \tag{5}$$

Table 1 summarizes the calculated parameters for well W-03.

Table 1 Calculated parameter values for well W-03.

Parameter	Value
Specific storage, S_s	4.52×10^{-7} /m
Porosity, θ	0.05
Poisson's ratio, ν	0.28
Drained bulk modulus of the formation, K'	6.54×10^{10} Pa^{-1}
Bulk modulus of the fluid, K_f	2.27×10^{9} Pa^{-1}

The tiltmeter data reveal that at the end of the third pumping test T1 had rotated toward the pumping well by approximately 0.2 microrad. Assuming that the surface compression from T1 to EX-1 is linear would result in a "subsidence bowl" with a maximum surface deformation of 11.2 μm at EX-1.

REFERENCES

Bredehoeft, J. D. (1967) Response of well-aquifer systems to earth tides. *J. Geophys. Res*. **72**(12), 3075–3087.

Burbey, T. J. (2010) Fracture characterization using earth tide analysis. *J. Hydrol.* **380**, 237–246.

Doan, M.-L., Brodsky, E. E., Prioul, R. & Signer, C. (2006) Tidal analysis of borehole pressure: A tutorial. University of California, Santa Cruz, USA.

Galloway, D. L. *et al*. (1998) Detection of aquifer system compaction and land subsidence using interferometric synthetic aperture radar, Antelope Valley Mojave Desert, California. *Water Resour. Res*. **34**(10), 2573–2585.

Gonthier, G. J. (2007) A graphical method for estimation of barometric efficiency from continuous data—concepts and application to a site in the Piedmont, Air Force Plant 6, Marietta, Georgia. *US Geological Survey, Sci. Inv. Rept* **2007-5111**, 29 p.

Jacob, C. E. (1940) On the flow of water in elastic artesian aquifers. *Trans. Am. Geophys. Un*. **21**, 574–586.

Jaeger, J., Cook, N. G., & Zimmerman, R. (2007) *Fundamentals of Rock Mechanics*. Wiley-Blackwell, Hoboken, New Jersey, USA.

Krijnen, H. & de Heus, H. (1995) Application of GPS with sub-centimeter accuracy for subsidence monitoring. In: *Land Subsidence* (ed. by F. B. J. Barends, F. J. J. Brouwer & F. H. Schröder) (Fifth International Symposium on Land Subsidence), 333–343. IAHS Publ. 234. IAHS Press, Wallingford, UK.

Murdoch, L. C. & Germanovich, L. N. (2006) Analysis of a deformable fracture in permeable material. *Int. J. Numerical and Analytical Methods in Geomechanics* **30**, 529–561.

Riley, F. S. (1986) Developments in borehole extensometry. In: *Land Subsidence* (ed. by A. I. Johnson, L. Carbognin & L. Ubertini) (3rd International Symposium on Land Subsidence), 169–186. IAHS Publ. 151. IAHS Press, Wallingford, UK.

Schweisinger, T., Murdoch, L.C. and Huey, C., Jr (2007) Removable borehole extensometers for measuring axial displacements during well tests. *Geotechnical Testing J*. **30**(3), 202–211.

Seaton, W. J. & Burbey, T. J. (2000) Aquifer characterization in the Blue Ridge Physiographic Province using resistivity profiling and borehole geophysics: Geologic analysis. *J. Environmental Engineering and Geophysics* **5**(3), 45–58.

Seaton, W. J. & Burbey, T. J. (2005) Influence of ancient thrust faults on the hydrogeology of the Blue Ridge Province. *Ground Water* **43**(3), 301–313.

Wang, R. (1997) Tidal response of the solid Earth. In: *Tidal Phenomena* (ed. by H. Wilhelm, W. Zurn & H.-G. Wenzel), 27–57. Springer, Berlin, Germany.

Wenzel, H.-G. (1997) Tide-generating potential for the Earth. In: *Tidal Phenomena* (ed. by H. Wilhelm, W. Zurn & H.-G. Wenzel), 9–26. Springer, Berlin, Germany.

(Proceedings of EISOLS 2010, Querétaro, Mexico, 17–22 October 2010). IAHS Publ. 339, 2010.

Continuous monitoring techniques of fault displacement caused by geothermal fluid extraction in the Cerro Prieto Geothermal Field (Baja California, Mexico)

EWA GLOWACKA[1], OLGA SARYCHIKHINA[1], F. ALEJANDRO NAVA[1], FRANCISCO SUAREZ[1], JORGE RAMIREZ[2], MIGUEL GUZMAN[2], BRAULIO ROBLES[3], FRANCISCO FARFAN[1] & GUILLERMO DIAZ DE COSSIO BATANI[1]

1 *Centro de Investigación Científica y Educación Superior de Ensenada, Carretera Ensenada-Tijuana 3918, Ensenada, B.C., CP 22860, México*
glowacka@cicese.mx

2 *Universidad Autónoma de Baja California, Mexicali, Mexico*

3 *Instituto Mexicano de Tecnología del Agua, Av. Paseo Cuauhnáhuac, # 8532, CP 62550, Municipio de Juitepec, Estado de Morelos, Mexico*

Abstract Since 1973, fluid extraction, from the depth range of 1500–3000 m, at the Cerro Prieto Geothermal Field (CPGF), has influenced deformation in the Mexicali Valley (northwestern Mexico) area, accelerating the subsidence and causing slip along the traces of tectonic faults. Subsidence and fault rupture are causing damage to infrastructure, such as roads, railroad tracks, irrigation channels, and agricultural fields. The Mexicali valley is an area with high tectonic deformation, recent volcanism, and active seismicity. The subsidence area is bounded by tectonic faults, as evidenced from field mapping along the Cerro Prieto and Morelia faults to the NW and the Imperial and Saltillo faults to the SE, which limit the Cerro Prieto pull-apart basin. Since 1996, geotechnical instruments installed by CICESE have operated in the Mexicali Valley, for continuous recording of deformation phenomena. To date, the network includes three crackmeters and eight tiltmeters; all instruments have sampling intervals in the 1 to 20 minutes range. Data from a 3-D witness, installed by the Cerro Prieto fault in the CPGF area since 2004, show vertical displacement of 3.1 cm/year, in the form of continuous creep, along the 3-m span of the instrument. The crackmeter, installed in a vertical position in 2007, 2 km south from the witness, shows vertical displacement ~1.3 cm/year, and the presence of small episodic slip events. Vertical slip on the Saltillo fault, 5 km outside the CPGF, measured by the crackmeter since 1996, and by 2 tiltmeters, corresponds to about half of the total subsidence, and occurs as continuous creep and episodic slip events, with ~50% of the slip being released during the episodic events. The vertical slip rate on the fault increased from 5.3 cm/year to 7.3 cm/year around the second half of 2003. The distance and time relation between extraction changes in the CPGF and displacement rate changes on the Saltillo fault suggests that extraction affects the fault through diffusive transmission of pore pressure changes with a characteristic hydraulic diffusivity. The paper shows how the fault displacement monitoring techniques applied can be used to monitor subsidence changes and to model subsidence mechanisms.

Key words Cerro Prieto, Mexico; geothermal field; subsidence monitoring; subsidence modelling

INTRODUCTION

Cerro Prieto Geothermal Field (CPGF) is situated in the Mexicali Valley, in the southern part of the Salton Trough tectonic province, which is located at the boundary between the Pacific and the North American plates (Fig. 1). The Salton Trough is the connection between the Gulf of California depression to the south and the transform boundary of the San Andreas fault system to the north; it includes the Brawley, Cerro Prieto, and Heber, step-to-the-right, extensional, basins, and is characterized by being a zone of continuous tectonic deformation, geothermal activity, recent volcanism, and high seismicity. Two main strike-slip faults, Cerro Prieto and Imperial (Fig. 1), limit the Cerro Prieto basin, where geothermal fluid has been extracted since 1973 from depths of between 1500 m and 3000 m for electricity production at the CPGF. The geothermal field is operated by the Mexican Federal Electricity Commission (Comisión Federal de Electricidad, CFE). At present, the CPGF has a 720 MW capacity and is the world's second largest geothermal field. Cerro Prieto is a high-temperature, fluid-dominated field, contained within

Copyright © 2010 IAHS Press

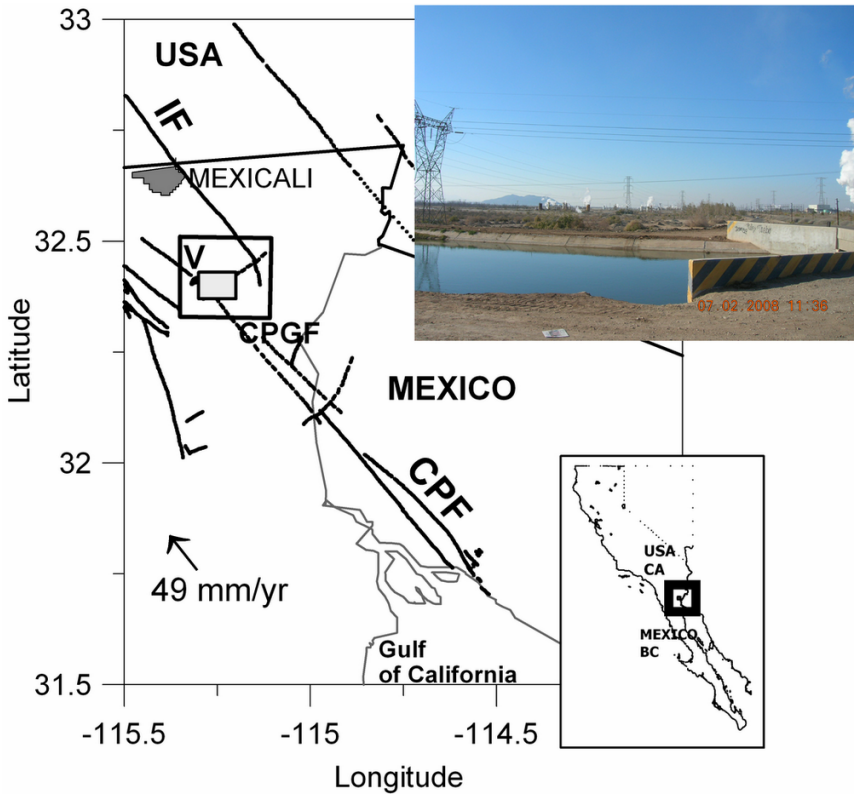

Fig. 1 Study area: CPGF – Cerro Prieto Geothermal Field; IF and CPF – Imperial and Cerro Prieto faults, respectively; V – Cerro Prieto Volcano; inset – view of the CPGF from the south to the field and Cerro Prieto volcano.

sedimentary rocks. The geothermal fluid, with temperatures of 260–350°C, is extracted from grey shales, and is isolated from the unconsolidated rock by layers of mudstone and brown shales which constitute the cap-rock (CFE, 2006). The extracted volume has increased from 14 million tons in 1974 to 72 million tons in 2005.

SUBSIDENCE

From the analysis of the levelling surveys done in the area of CPGF and the Mexicali Valley since 1977, Glowacka *et al.* (1999) noticed that the CPGF area is characterized by subsidence, and that this subsidence is mainly of anthropogenic origin caused by fluid extraction. This observation was confirmed by Carnec & Fabriol (1999) and Hanssen (2001) through analysis of ERS1/2 InSAR images, taken for the 1993–1997 and 1995–1997 periods, respectively. More recent studies by Sarychikhina *et al*. (2007, 2010), using Envisat InSAR data recorded between 2003 and 2006, confirm a similar pattern, with more precision and over a larger area. The ellipsoidal subsidence zone, elongated in the SW–NE direction (Fig. 2), is larger than the area of the production wells, and coincides with the observed geothermal anomaly and with the modelled shape of the pull-apart (stike-slip) basin (Glowacka *et al.*, 1999, 2005).

For the period 1977–2006, the subsidence rate at the centre of the field increased after the steam extraction rate increased significantly in 1979 and 1986. For the period 1994–1997 (Fig. 3) the maximum subsidence rate at the centre of the field was 12 cm/year and diminished to 9.5 cm/year for 1997–2006. From DInSAR observations, for one year, 2004–2005, this subsidence rate was found to be about 11 cm/year (Sarychikhina, 2010).

During this period the subsidence rate in the NE part of the subsidence cone, identified as a recharge area, increased from 8 cm/year for the 1994–1997 period to 17 cm/year during 2004–2005 (Sarychikhina, 2010). The observed subsidence rate decrease at the centre of the field and the

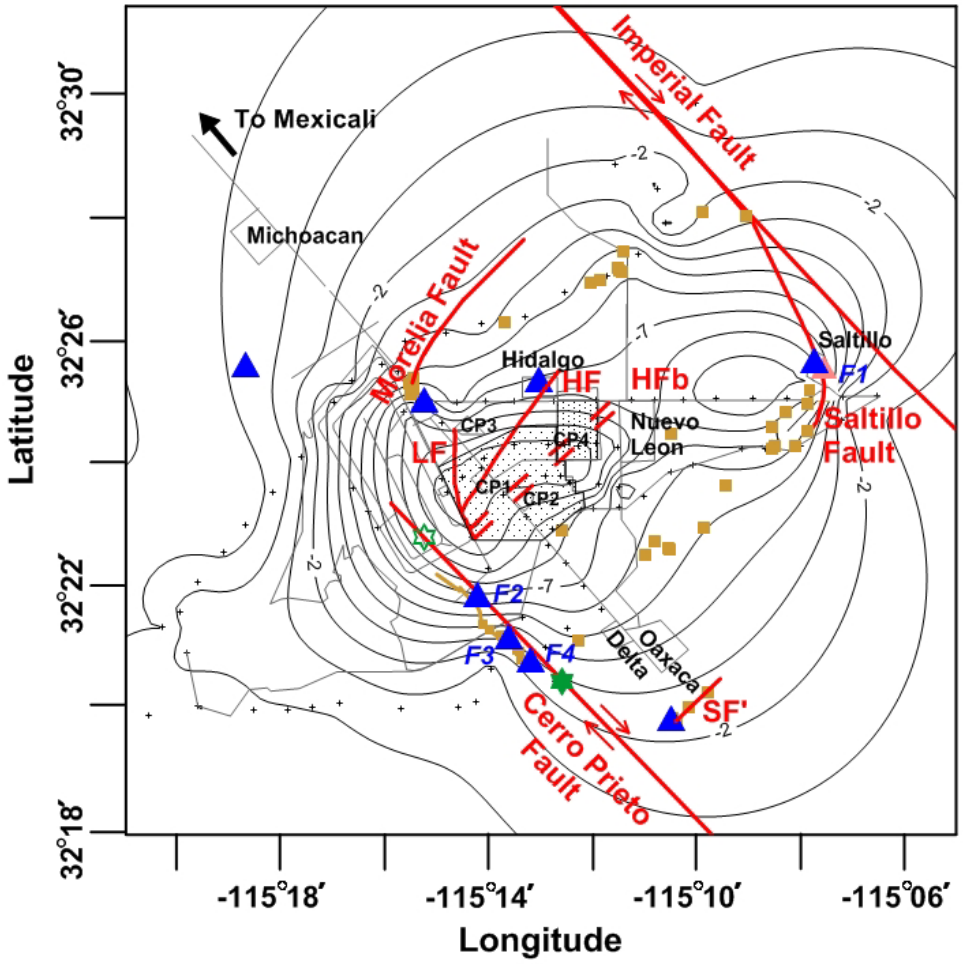

Fig. 2 Subsidence, in cm/year, for 1994–1997 (grey lines), main tectonic faults (thick lines), fissures, fractures and scarps (squares), and geotechnical instruments (triangles). F1 and F3 are crackmeters on the Saltillo and Cerro Prieto faults, F2 indicates the 3-D witness on the Cerro Prieto fault, and F4 is the tiltmeter on the Cerro Prieto fault (modified from Glowacke *et al*., 2010b). Crosses are levelling benchmarks, dotted rectangles are extraction areas. The meaning of the "star" is explained in the text.

increase in the recharge area were interpreted by Glowacka *et al*. (2010a) as an effect of the extraction changing from the reservoir close to Cerro Prieto fault, to the reservoir close to Ejido Nuevo Leon, around the year 2000. Both levelling and DInSAR data show that the subsidence in the Mexicali Valley is a dynamic process probably controlled by production changes in the CPGF.

Detailed field mapping done since 1989 (González *et al.*, 1998; Glowacka *et al.*, 2006, Suárez *et al.*, 2008) in the vicinity of the CPGF shows that many subsidence-induced fractures, fissures, collapse features, small grabens and fresh scarps are related to the known tectonic faults. Some of the observed scarps are presented in Figs 2 and 4.

Analysis of the extension, amplitude, and time behaviour of the slip (relative displacement across the fault) on the Imperial, Saltillo and Cerro Prieto faults, which bound the Cerro Prieto pull-apart basin from the NE, E, and SW (Glowacka *et al.*, 1999, 2005, 2010), suggests that these faults constitute a boundary of the subsiding region, due to differential compaction and/or due to poor permeability in the direction perpendicular to the faults which act as a groundwater barrier. Differential displacement causes tensional and shear stresses on the ground mass, thus producing vertical displacement on the faults which limit the affected aquifer (Sheng & Helm 1998). Thirdly, a diminution of the normal stresses is to be expected at the fault, due to extension at the edge of a subsidence basin, which reduces the friction that locks the fault (Segall, 1989).

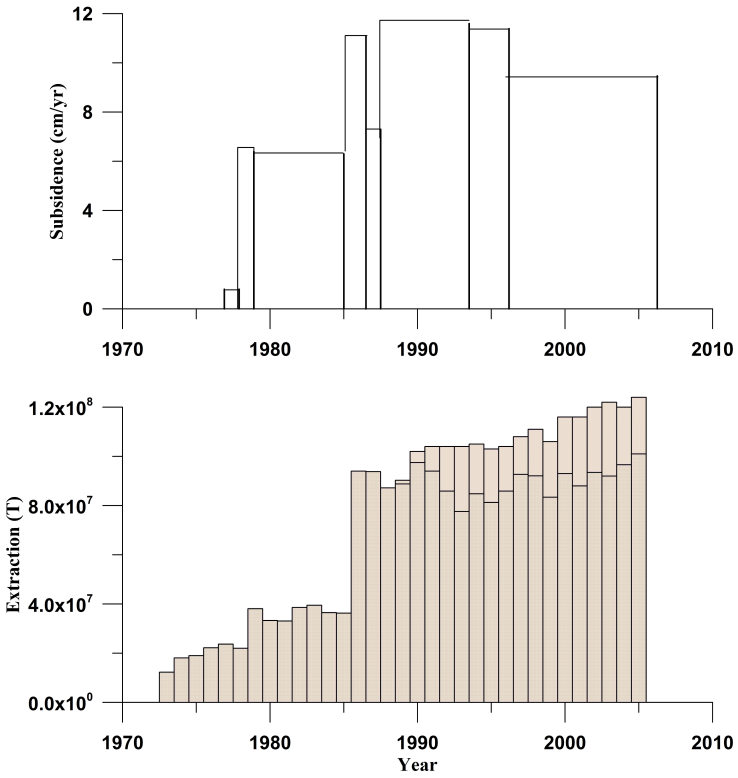

Fig. 3 Subsidence rate (cm/year) for benchmark 10061 (top), and extracted, and extracted minus injected, volumes (bottom) *vs* time for CPGF (modified from Glowacka *et al.*, 1999).

Fig. 4 Photograph of site F1 (Fig. 2) showing the Saltillo fault where the crackmeter is installed, as seen from the south. This place was flat at the beginning of the 1970s.

INSTRUMENTAL DATA

Since 1996, geotechnical instruments installed by CICESE have operated in the Valley for continuous recording of deformation phenomena (Fig. 2). To date, the network includes three crackmeters, eight tiltmeters, and seven piezometers installed in the shallow aquifer; all instruments have sampling intervals in the 1 to 20 minutes range.

In 1996 continuous vertical movement measurements across the Saltillo fault started in Ejido Saltillo (F1 in Figs 2, 4 and 5(a)), using a crackmeter installed in the vertical direction (Nava & Glowacka, 1999; Glowacka *et al.,* 2002). Since then, vertical displacement rates across the fault (along the 3-metre span of extensometer) of from 5.3 (for 1996–2003) to 7.3 cm/year (2003 to the present) have been observed (Fig. 5(a)).

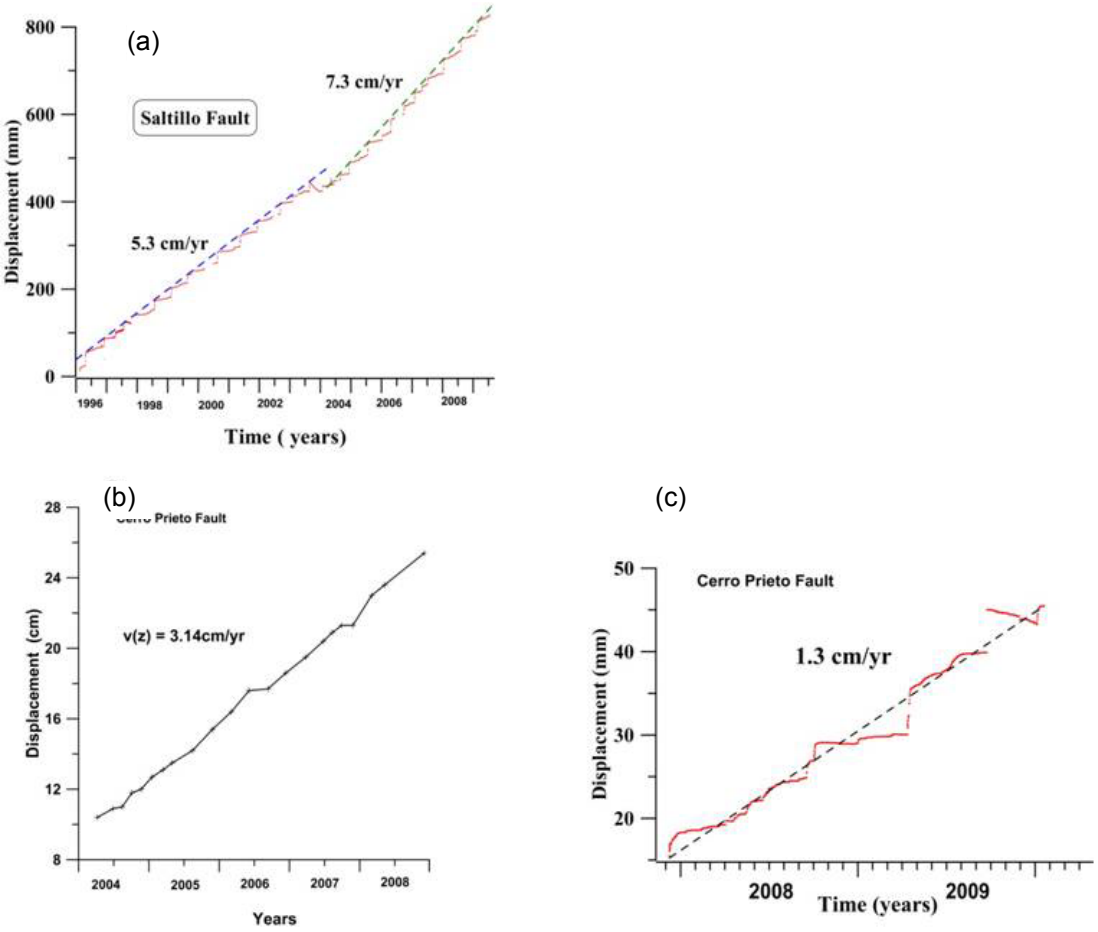

Fig. 5 Vertical displacement and mean displacement rate recorded in F1 (a), F2 (b), and F3 (c) *versus* time.

Deformation is not continuous, but occurs in steps (creep/slip events), separated by months of quiescence; large events account for about 50% of the vertical displacement. Aseismic creep/slip events have amplitudes of 1–3 cm and durations of 1–3 days.

The Cerro Prieto fault, which crosses the CPGF area in a series of small scarps and cracks, has been instrumented since 2004. Data from a 3-D witness (surveyed every 2–3 months), installed at the Cerro Prieto fault in F2 (Figs 2 and 5(b)) since 2004, show vertical displacement of 3.1 cm/year along the 3-metre span of the instrument, while the crackmeter, installed with vertical orientation in F3 in 2007 (Figs 2 and 5(c)), shows the presence of small slip events during 2008–2009 and a vertical displacement rate of 1.3 cm/year.

DISCUSSION

In this section we present an interpretation of the instrumental data in the context of the dynamic changes of subsidence.

Since fault ruptures and scarps produced by the subsidence are causing damage to society infrastructure, it is important to estimate how far from the subsidence centre the fault can be affected by subsidence. Using data from two instruments installed on the Cerro Prieto fault, F2 and F3, we will try to estimate the range of fault rupture. From Fig. 6 one can see that the vertical displacement diminishes with distance from the area of maximum subsidence. The area where the maximum displacement rate should be observed (empty "star" on Fig. 2) is, unfortunately, coincident with the area of the evaporation pond, so that it is (at present) not accessible for geological prospecting, levelling, instrument setting, or DInSAR studies since the water in the pond causes InSAR image decorrelation. However, the place marked in Fig. 2 with an empty star, is located in the zone which had an interpolated subsidence rate of around 5 cm/year during the 1994–1997 levelling survey, so that a value of 5 cm/year for a displacement on the fault appears reasonable. Connecting the values of displacement rates from F3, F2 and Max Rupture we obtain a straight line, which can be interpreted as if the vertical displacement rate observed along the fault is inversely proportional to the distance from the site of maximum displacement. Knowing this, we can calculate the distance at which the displacement rate is negligible (marked as filled star in Fig. 6). The results are shown in Figs 2 and 6.

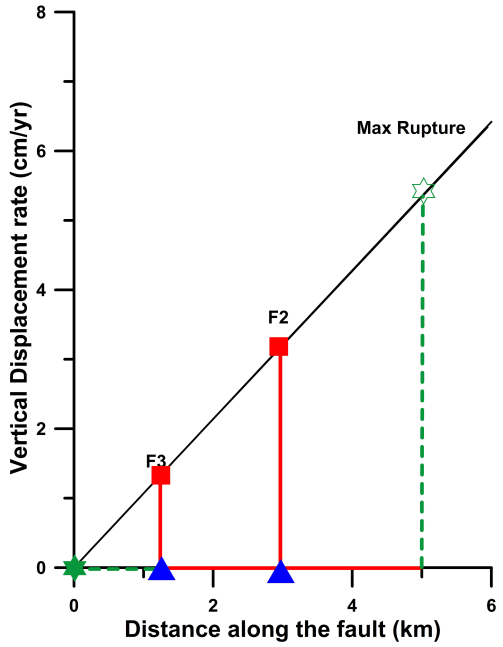

Fig. 6. Vertical displacement rate, along the Cerro Prieto fault. Squares are measured values, stars are calculated values; the empty star indicates the maximum subsidence rate, the filled star indicates the predicted point of zero subsidence rate.

The point with estimated zero vertical displacement, indicated as a filled, green star on Fig. 2, is situated about 1.3 km south from the F3 crackmeter, in an area of intense agricultural activity which makes it impossible to identify the exact trace or measure displacement on the Cerro Prieto fault. However, from geological (Suarez *et al.*, 2009) and DInSAR observations (Sarychikhina, 2010), the subsidence can be traced at least to the a small fault SF′, south of Ejido Delta-Oaxaca (Fig. 2), which suggests that the present analysis underestimates the fault length affected by fluid extraction. A more sophisticated physical model of the fault reactivation should be used in the future.

The vertical slip rate on the Saltillo fault increased from 5.3 cm/year to 7.3 cm/year around the second half of 2003. Extraction changes related to the opening of a new plant, CPIV, took place

around 2000. The distance and time relation between extraction changes in the CPGF and displacement rate changes on the Saltillo fault suggests that extraction affects the fault through diffusive transmission of pore pressure changes, with a characteristic hydraulic diffusivity $\sim 10^4$ cm^2 /sec (Glowacka *et al.*, 2010).

From the analysis of aseismic slip phenomena observed on the crackmeter F1 installed on the Saltillo fault, in the context of observed seismicity and geological structure, and using suggestions presented by Bilham & Behr (1992) for slip events in California faults, Glowacka *et al.* (2010) found that the most probable depth of the origin of slip events is between 1 and 2.5 km. This depth was later found by Sarychikhina (2010) to be closer to 2.5 km. If the slip events result from compaction of the aquifer, because of fluid extraction in the CPGF, as suggested by Glowacka *et al.* (2010), then the presence of asesimic slip suggest that the fluid extraction affects deep parts of the fault, which is a boundary of the subsidence cone in the recharge zone. The depth of the affected reservoir/aquifer (or aquitard) may be estimated by modelling the size of those slip events.

Acknowledgements The results presented in this work are solely the authors and do not express the point of view of CFE. This research was sponsored in part by CONACYT, project 45997-F, CONAGUA, Organismo de Cuenca Penisula de Baja California, Convenio OCPBC-CICESE and CICESE internal funds.

REFERENCES

Bilham, R. & Behr, J. (1992) A two layer model for seismic slip on the Superstition Hills fault, California. *BSSA* **82**(3), 1223–1235.

Carnec, C. & Fabriol, H. (1999) Monitoring and modeling land subsidence at the Cerro Prieto geothermal field, Baja California, Mexico, using SAR interferometry. *Geophys. Res. Lett.* **26**(9), 1211–1214.

CFE (2006) *Campo Geotermíco Cerro Prieto*.

Glowacka, E., Gonzalez, J. J. & Fabriol, H. (1999) Recent vertical deformation in Mexicali Valley and its relationship with tectonics, seismicity and fluid operation in the Cerro Prieto Geothermal field. *Pure and Applied Geophysics* **156**, 591–614.

Glowacka, E., Nava, F. A., Diaz de Cossio, G., Wong, V. & Farfan, F. (2002) Fault slip, seismicity and deformation in the Mexicali Valley (B.C., Mexico) after the 1999 Hector Mine earthquake (M=7.1). *BSSA* **92**(4), 1290–1299.

Glowacka, E., Sarychikhina, O. & Nava, A. F. (2005) Subsidence and stress change in the Cerro Prieto Geothermal Field, B.C., Mexico. *Pure and Applied Geophysics* **162**, 2095–2110.

Glowacka, E., Sarychikhina, O., Suarez Vidal, F., Mendoza Borunda, R. & Nava Pichardo F. A. (2006) Estudio geológico para definir la zona de hundimiento con el fin de relocalización del canal Nuevo Delta en el Valle de Mexicali. Reporte Tecnico, CICESE, Mexico.

Glowacka, E., Sarychikhina, O., Suarez, F., Nava, A. & Mellors, R. (2010a) Anthropogenic subsidence in the Mexicali Valley, B.C., Mexico, and the Saltillo Fault, 2008. *Environmental Earth Sci.* 1515–1524, doi : 10.1007/s12665-009-0137-y.

Glowacka, E., Sarychikhina O., Suárez F., Nava, F. A., Farfan, F., Diaz de Cossio Batani, G. & Garcia Arthur, M. A. (2010b). Anthropogenic subsidence in the Mexicali Valley, B.C., Mexico, caused by the fluid extraction in the Cerro Prieto geothermal field, and the role of faults. *Proc. World Geothermal Congress 2010*, Bali, Indonesia, April 2010.

González, J., Glowacka, E., Suárez, F., Quiñones, J. G., Guzmán, M., Castro, J. M., Rivera, F. & Félix, M. G. (1998) Movimiento reciente de la Falla Imperial, Mexicali, B. C. *Ciencia para todos Divulgare, Universidad Autónoma de Baja California* **6**(22), 4–15.

Hanssen, R. (2001) *Radar Interferometry*. Kluwer Academic Publishers, Dordrecht, The Netherlands.

Nava F. A. & Glowacka, E. (1999) Fault slip triggering, healing, and viscoelastic afterworking in sediments in the Mexicali Imperial Valley. *Pure and Applied Geophysics* **156**, 615–629.

Sarychikhina, O. (2010) The spatial and temporal distribution of the ground deformations in the Mexicali Valley in the context of tectonic, anthropogenic and seismic processes. PhD Thesis, CICESE, Mexico

Sarychikhina, O., Glowacka, E. & Mellors, R. (2007) Preliminary results of a surface deformation study, using differential InSAR technique at the Cerro Prieto Geothermal Field, B.C., Mexico. *Geotherm. Res. Council Trans.* **31**, 581–584.

Segall, P. (1989) Earthquakes triggered by fluid extraction. *Geology* **17**, 942–946.

Sheng, Z. & Helm, D. C. (1998) Multiple steps of earth fissuring caused by ground water withdrawal: tectonic controls of geomorphic processes in land subsidence area. In: *Land Subsidence* (ed. by J. W. Borchers), 149–154. Star Publishing Company.

Land Subsidence, Associated Hazards and the Role of Natural Resources Development
(Proceedings of EISOLS 2010, Querétaro, Mexico, 17–22 October 2010). IAHS Publ. 339, 2010.

Recent extensometric data for the monitoring of subsidence in Bologna (Italy)

F. BONSIGNORE[1], G. BITELLI[2], A. CHAHOUD[1], P. MACINI[2], E. MESINI[2], P. SEVERI[3], B. VILLANI[1] & L. VITTUARI[2]

1 *Regional Agency for Environmental Prevention in Emilia-Romagna, 6 Largo Caduti del Lavoro, I-40121 Bologna, Italy*

2 *University of Bologna, Dept of Civil, Environmental and Materials Engineering, 2 Viale del Risorgimento, I-40131 Bologna, Italy*
paolo.macini@unibo.it

3 *Geological, Seismic and Soil Survey, Regione Emilia-Romagna, 4/3 Viale Silvani, I-40122 Bologna, Italy*

Abstract During the past several decades underground fluid withdrawals induced severe cases of land subsidence in Bologna, Italy. The area features middle Pleistocene to Holocene alluvial deposits more than 400 m thick. Here, levelling measurements revealed a subsidence rate of more than 11 cm/year from 1974 to 1981. Subsidence monitoring was carried out using a levelling network and, recently, an interferometric analysis. In 2005 two pipe extensometers were installed in the northern part of the area, anchored at 100 and 200 m depth, respectively. The regional subsidence rate is now reduced; however, the monitoring performed by means of the two extensometers shows that the subsidence rate is cyclical with seasonal peaks.

Key words subsidence monitoring; vertical extensometer; levelling; interferometric analysis; Italy

GEOLOGICAL OUTLINE

The city of Bologna is located in the southern part of the Po Plain, the biggest alluvial plain in Italy, nestled between the margin of the plain and the Northern Apennines. From the geological point of view, this margin coincides with an important reverse fault, still active, that produces uplift of the Apennines and subsidence of the plain, both with natural displacements of a few millimetres per year (Boccaletti *et al.*, 2004).

The Bologna area is characterized by the presence of the Reno River alluvial fan, a geological body spanning about 220 km^2 with a thickness of 400 m. The internal architecture of this alluvial fan is well known from recent geological surveys and mapping (Carta Geologica, 2009). The proximal fan, near the Apennines, comprises an amalgamated gravel body about 200 m in thickness, that is replaced by alternating sequence of gravels and clays toward the distal fan. The amalgamated gravel body corresponds to a monolayer unconfined aquifer, whereas the intercalation of gravels and clays correspond to a multilayer confined and semi-confined aquifer (Fig. 1).

Since 1970, the Reno River alluvial fan has been subject to intensive groundwater withdrawal, mainly for civil and industrial use, that exceeded the natural groundwater recharge and induced a severe lowering of the piezometric level (more than 60 m in Bologna area). This produced an anthropogenic subsidence of more than one order of magnitude with respect to the local natural subsidence. Recently, in order to understand and manage the subsidence phenomena, the Regione Emilia-Romagna and the Regional Agency for Environmental Prevention in Emilia-Romagna (ARPA) installed two extensometers at 100 m and 200 m deep, and two piezometers monitoring the unconfined (20 m depth) and the first confined (60 m depth) aquifer. Piezometric data interpretation show the strict relationship between unconfined aquifer level and precipitation, and the clear influence of groundwater withdrawal on the confined aquifer level during the summer period.

Copyright © 2010 IAHS Press

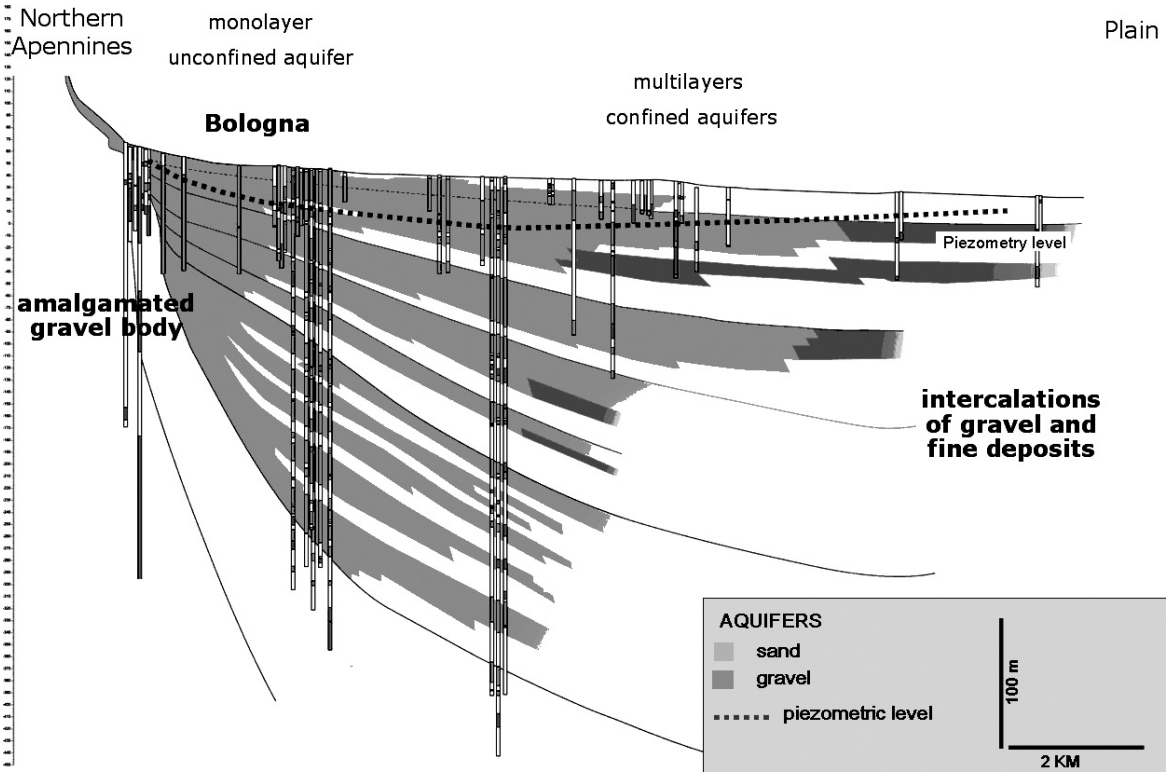

Fig. 1 Geological cross-section of the Bologna area.

SUBSIDENCE MEASUREMENTS

Anthropogenic subsidence in the Bologna area was first identified in the 1970s (Pieri & Russo, 1977; Folloni *et al.*, 1996). Causes were primarily given as the overexploitation of groundwater resources and, in those years, maximum lowering speeds of over 10 cm/year were observed.

Geodetic measurements

Once the phenomenon was identified, a spirit levelling network was established in 1983 and measured by the Municipality of Bologna. It covered a great part of the province and it was aimed at monitoring the geometric components of subsidence. The measurements were repeated in 1987 and 1992. In 1993, a denser network established in 1992 and limited to the historical centre of Bologna, was re-measured. In 1999, the network of Bologna Municipality was surveyed (including Global Positioning System measurements) in the framework of the regional network for subsidence monitoring established by ARPA Emilia-Romagna (Bitelli *et al.*, 2000). The first application of radar satellite imagery for the study of subsidence in Bologna area using Synthetic Aperture Radar (SAR) interferometric analysis was reported in (Strozzi *et al.*, 2000), and an evaluation of the results from radar, levelling and other geodetic techniques for high precision monitoring in the historical centre was presented in Bitelli & Vittuari (2006).

In 2005, ARPA began a new monitoring campaign, applying SAR interferometry at the regional scale, covering the portion of the Po Plain in the Emilia Romagna region. This analysis, made using the PSInSAR^{TM} technique, was supported by the measurement of a levelling network that included a subset of the regional one (Bitelli *et al.*, 2006; Bonsignore, 2008). Radar interferometry allowed a remarkable increase in the number of measurement points, with respect to the spirit leveling, obtaining a distribution of points almost homogeneous throughout the area. In particular, two periods were analysed using SAR interferometry: 1992–2000 and 2002–2006. Figure 2 shows the reported iso-kinetic contour lines with respect to the latest period for an area of

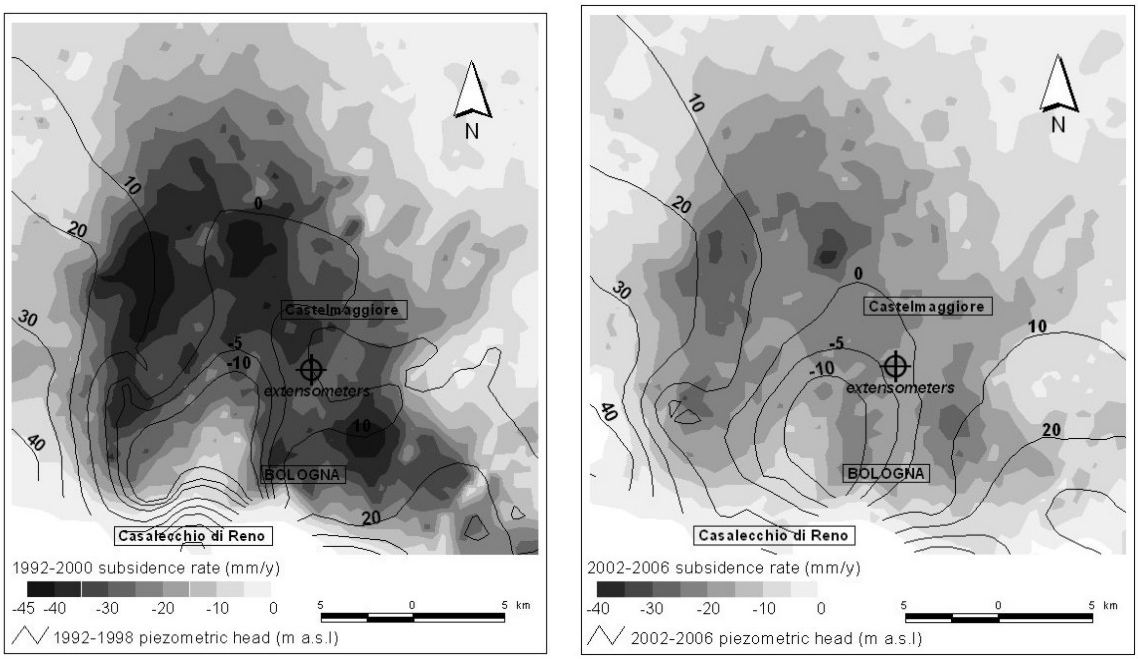

Fig. 2 PSInSAR^{TM} derived subsidence rates in the period 1992–2000 (a) and in the period 2002–2006 (b) for the selected area of Bologna. In black are superimposed the iso-piezometric lines in the same period.

600 km^2 containing Bologna city and the surrounding Northern territory, historically more prone to subsidence. The iso-piezometric contour lines for the same periods are also shown (Fig. 2).

High subsidence rates observed for the Bologna area in the 1970s gradually decreased over time, but they still remain the most significant of the entire Po River valley, both for the absolute values and geographical extent. In the most recent period, 2002–2006, in fact a significant reduction in subsidence rates are observed with respect to the period 1992–2000, however, there remains an average rate of subsidence of 15 mm/year (*vs* 22 mm/year in the previous period) and, in particular, one can easily distinguish some zones of maximum subsidence characterized by peaks of 30 to 40 mm/year.

In April 2009 a spirit levelling line was measured, starting from a relatively stable area (benchmark located in Casalecchio at the Apennine foothills), with the objective of verifying the evolution of the subsidence phenomenon at the benchmark 051110 located near the area of Castel Maggiore, where two new vertical pipe extensometers are installed. The levelling line passed through the urban area of Bologna, with a length of about 16 km. The calculated vertical velocity observed at benchmark 051110 in the period 2005 to 2009 was 21.4 mm /year.

Extensometers

Vertical extensometers are a site-specific method of measuring land subsidence. These instruments consist of a pipe or cable anchored at the bottom of a bored hole. Vertical extensometers (pipe or cable type) extend from the bottom of a cased borehole, through geological layers susceptible to compaction, to the ground surface. The pipe or cable is connected to a recorder that measures the relative distance from the anchoring point to the benchmark at the ground surface. When land subsidence and piezometric monitoring activities are paired together, hydraulic and mechanical properties of the aquifer system can be determined (Brighenti *et al*., 1995). Vertical extensometers provide sufficiently precise measurements of compaction between the land surface and the anchoring point (Brighenti *et al.*, 1995; Macini & Mesini, 2002); normally it is possible to measure vertical strains of the order of one part per million.

In 1955 the US Geological Survey (USGS) conceived a vertical cable extensometer to monitor subsidence in San Joaquin Valley. A steel cable anchored at the bottom of a borehole was held at constant tension by means of a counterweight at the surface. Later, a more sophisticated type of cable extensometer was set up in the Groningen gas field (The Netherlands). In 1966, the USGS introduced the counter-weighted free pipe extensometer, consisting of an external protective pipe (e.g. the casing of an old well) containing the measurement steel pipe secured to the formation a few metres below the casing shoe, with a clearance between the two pipes of about 5 cm, to reduce friction. This instrument was used to depths around 1000 m. In Italy, the first extensometer (cable type) was installed in the 1960s to investigate subsidence in the Po River delta. In recent years, numerous pipe extensometers have been installed in the Bologna and Ravenna areas, and in several locations of the coastal area of the Emilia-Romagna Region. The Public Administration installed three pipe extensometers in Bologna in the late 1980s, all equipped with piezometers. The first two were installed at 147 m and 246 m depth, respectively. The third one was installed at 50 m depth. After a brief but interesting surveying phase, the three sites were dismantled for urban development reasons.

BOLOGNA-CASTEL MAGGIORE EXTENSOMETERS

In 2005 ARPA, under the guidance of the Geological, Seismic and Soil Survey of Regione Emilia-Romagna (Italy) installed a vertical pipe extensometer to a depth of 200 m in the outskirts of Bologna, in the territory of the municipality of Castel Maggiore. Another pipe extensometer (set to a depth of 100 m) was installed at the same time and location in cooperation with the Bologna Province and Reno River Water Management Authority. Data generated by both extensometers are gathered and controlled by a single data processing unit operated by ARPA. The site was chosen in a fully-accessible public property located in an area with a high subsidence rate, close to benchmark 051110 of the subsidence monitoring network. The deepest extensometer was installed inside a geognostic borehole, whose stratigraphy was accurately reconstructed by drill cuttings, cores and monitoring-while-drilling. The first casing pipe (diameter 180 mm) was set at 20 m, and the second casing pipe (diameter 130 mm) was set at the total depth (200 m). The extensometer is a double pipe type, with an external steel casing and an internal centralized steel pipe (measurement pipe) tensioned by a counterweighted tension lever. The casing is centralized every 6 m, and the steel measurement pipe is equipped with antifriction centralizers every 1.5 m. The upper 5 m of pipe inside the borehole is made of Invar™ steel (notable for its uniquely low coefficient of thermal expansion), to mitigate surface temperature effects. The counterweight is designed to generate a vertical force slightly less than the total weight of the string of pipes, with zero horizontal components. The surface measurement device is a “contactless” high-precision inductive transducer, capable of measuring as much as 50 mm of displacement. The calibration curve of the transducer is uploaded in the data processing unit to minimize linearity errors. The overall precision of the transducer and the data processing unit is of the order of 50 μm. A temperature sensor is incorporated in the surface measurement device in order to compensate for the possible thermal drift by means of a dedicated algorithm. The data processing unit is powered by batteries and is equipped with a GSM (Global System for Mobile Communications) modem for remote communication.

EXTENSOMETRIC AND LEVELLING DATA

Table 1 reports the total compaction measured by the Castel Maggiore extensometers from April 2005 to April 2009 and the total vertical displacement of the benchmark 051110. The first 100 m and 200 m of sediments account for 28% and 52% of the total vertical displacement, respectively, and thus the remaining 48% of the total vertical displacement measured at the benchmark 051110 is attributed to the compaction of deep sediments, located below 200 m. Figure 3 shows the compaction recorded by the two extensometers in a continuous time-scale over the same period

Table 1 Total vertical displacement measured at benchmark 051110 and compaction measured by extensometers in the period 2005–2009.

	Vertical displacement (mm)	Vertical displacement (%)
Benchmark 051110	–86	100
Extensometer –100 m	–24	28
Extensometer –200 m	–44	52

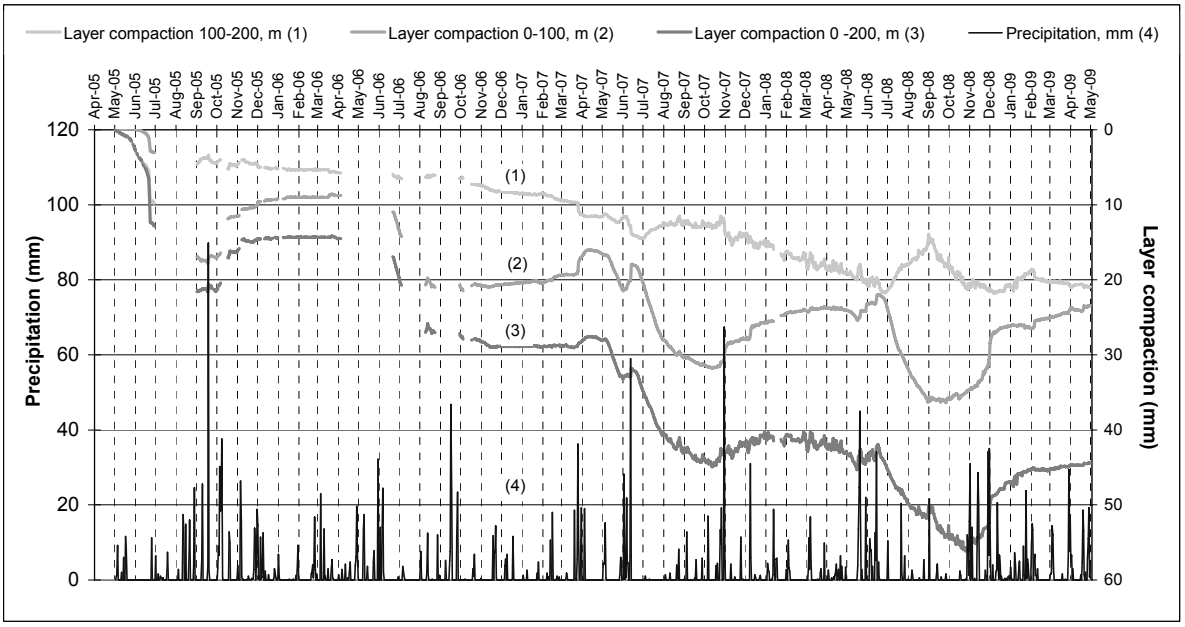

Fig. 3 Extensometric compaction data recorded over the period April 2005–April 2009.

(2005–2009). Here, three curves are reported, the 100 m extensometer (aquifers A0 and A1), the 200 m extensometer (aquifers A0, A1, A2 and A3) and the difference curve (i.e. 100 m value minus the 200 m value) representing the compaction of sediments located between 100 and 200 m. The vertical bars represent the precipitation recorded in the area.

DISCUSSION AND CONCLUSIONS

The overall performances of the Castel Maggiore extensometers during the first 5 years of monitoring are satisfactory and seem quite accurate, compared with the performances observed at similar extensometers installed in Regione Emilia-Romagna. Uncertainties and lack of data are limited to a few months after the installation (May to September 2005), and are probably due to a local settling of the reinforced-concrete foundation. The average subsidence rate recorded by the two extensometers from April 2005 to April 2009 is as follows: 100 m extensometer, 6 mm/year, 200 m extensometer, 11 mm/year. By difference, the average subsidence rate of sediments located between 100 and 200 m is 5 mm/year. The continuous monitoring reveals a cyclic trend of compaction, mainly concentrated during the summer periods (May to September). This behaviour is not reflected in the compaction of sediments in the 100–200 m depth interval, which shows a more linear and continuous compaction.

A more detailed analysis performed to better understand the possible relation between the cyclic trend of compaction and the cyclic underground water withdrawals (with peaks in the summer season) does not reveal a clear correlation between the peak compaction and peak water withdrawals during the dry season (May to September). Obviously, this is not a general rule for the relation between subsidence and water withdrawal, and seems true only locally, where aquifer

extent, depth and complexity may alter surface deformations. Moreover, the cyclic trend of compaction is mainly observed in the first 100 m of sediments, and water withdrawals are located in deepest aquifers.

Extensometric data reveals some time intervals in which compaction is negative (uplift). The phenomenon seems to be confirmed by the analysis of SAR interferometry at the regional scale; in fact, the permanent scatterers located close to the extensometers show a similar behavior. The uplift periods seem to be correlated to the rainy season, or in general to pluviometric data. In fact, the soil in the extensometers foundation mainly comprises clayey layers, which may swell and shrink during wet and dry periods, respectively. This could partially explain the uplift recorded by the 100 m extensometer, and is also confirmed by dedicated soil swelling and shrinking tests performed on samples cored adjacent to the foundation of both extensometers.

The cyclic trend of compaction recorded by the extensometers can be thus interpreted as a sequence of two distinct periods: (1) during the dry season (approximately from May to September) the subsidence rate is higher, because it accounts for both effective sediment compaction (11 mm/year) and surface soil shrinking; (2) during the wet season (approximately from October to April) the subsidence rate is null or negative, because the clayey soil swelling induces uplift larger than (or equal to) the effective sediment compaction. In recent years, the wet season has been longer than the dry one.

Acknowledgements We are grateful to Paola Cavazzi (Bologna Province) for extensometric data availability. We also thank Domenico Preti (Reno River Water Management Authority) for helpful suggestions on surface soil shrinking and swelling, and Luca Gelati (ARPA) for pluviometric and interferometric data comparison.

REFERENCES

Bitelli, G. & Vittuari L. (2006) Integrated methodologies for monitoring of subsidence effects on urban areas and buildings. *Proc. Int. Conf. Heritage Protection: Construction Aspects*, 147–155, SECON HDGK, Dubrovnik, 2006.

Bitelli, G., Bonsignore, F. & Unguendoli, M. (2000) Leveling and GPS networks for ground subsidence monitoring in the Southern Po Valley. *J. Geodynamics* **30**(3), 355–369.

Bitelli, G., Bonsignore, F., Bortone, G. & Vittuari, L. (2006) Il monitoraggio della subsidenza a scala regionale in Emilia-Romagna. *Proc. Problemi di Geoingegneria: estrazione di fluidi e subsidenza*, SEGRATE, Geo-Graph, 57–66.

Boccaletti, M., Bonini, M., Corti, G., Gasperini, P., Martelli, L., Piccardi, L., Severi, P. & Vannucci, G. (2004) *Carta sismotettonica della regione Emilia-Romagna. Scala 1:250.000. Note Illustrative*. Servizio Geologico Sismico e dei Suoli, Regione Emilia Romagna, S.EL.CA., Firenze, Italy.

Bonsignore, F. (2008) Il monitoraggio in Emilia Romagna. *ARPA Rivista* XI(1), Supplemento: Il monitoraggio della subsidenza. Esperienze a confronto, 12–13.

Brighenti, G., Borgia, G.C. & Mesini, E. (1995) Subsidence studies in Italy. In: *Subsidence Due to Fluid Withdrawal* (ed. by G. V. Chilingarian, E. C. Donaldson & T. F. Yen), 215–283. Elsevier, Amsterdam, The Netherlands.

Carta Geologica d'Italia alla scala 1:50.000 (2009) Foglio 220 – Casalecchio di Reno, Foglio 221 – Bologna. APAT, Servizio Geologico d'Italia, Regione Emilia-Romagna. S.EL.CA., Firenze, Italy.

Cibin, U., Severi, P., Chahoud, A., Frassineti, G. & Marcaccio, M. (2006) Water deficit and subsidence in a intensive-exploited alluvial fan (Reno river, Italy): subsurface hydrogeological analysis to support groundwater resource management. *Proc. Fifth European Congress on Regional Geoscientific Cartography and Information System* (Barcelona (Spain), June 2006), 62–64.

Folloni, G., Radicioni, F. & Russo, P. (1996) La subsidenza del territorio bolognese dal 1983 al 1993. *INARCOS* **571**, 400–413.

Macini, P. & Mesini, E. (2002) Measuring reservoir compaction through radioactive marker technique. *J. Energy Resources Technol.* **124**, 269–275.

Pieri, L. & Russo, P. (1977) Studio del fenomeno di abbassamento del suolo in atto nella zona di Bologna. *Bollettino di Geodesia e Scienze Affini* **36**(3), 365–388.

Strozzi, T., Wegmüller, U., Tosi, L., Bitelli, G. & Spreckels, V. (2001) Land subsidence monitoring with differential SAR interferometry. *Photogram. Engng & Remote Sensing* **67**(2), 1261–1270.

(Proceedings of EISOLS 2010, Querétaro, Mexico, 17–22 October 2010). IAHS Publ. 339, 2010.

Land subsidence monitoring system in the southeast part of Kanto groundwater basin, Japan

A. KAGAWA & K. FURUNO
Research Institute of Environmental Geology, Chiba (RIEGC), 3-5-1 Inagekaigan, Mihama, Chiba City, Japan
kagawaa2009@gmail.com

Abstract The Kanto Plain, in Japan, is underlain by the Kanto groundwater basin. The basin is composed of Plio-Pleistocene marine sediments. Chiba Prefecture is located in the southeast part of the Kanto groundwater basin and, as of 2009, land subsidence has been monitored by 148 observation wells and 1159 benchmarks. Based on continuous monitoring, the mechanism of land subsidence is now reasonably well understood. The monitoring system is important for the sustainable use of groundwater.

Key words land subsidence; levelling; monitoring well; groundwater pumpage

INTRODUCTION

The Kanto Plain is underlain by the Kanto groundwater basin. The maximum depth of the basin ranges from about –3000 m to –2500 m. The groundwater basin is composed of Pleistocene marine sediments of the Kazusa group and Shimosa group. Chiba Prefecture is located in the southeastern part of the Kanto groundwater basin, and as of 2009, land subsidence has been monitored by 148 observation wells and 1159 benchmarks. Based on continuous monitoring, the mechanism of land subsidence is now reasonably well understood.

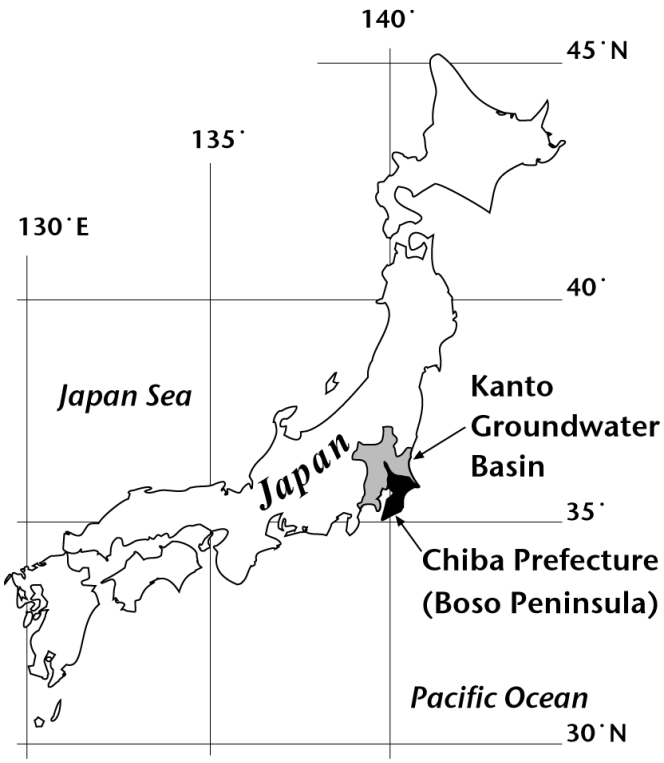

Fig. 1 Location of Kanto groundwater basin and Chiba Prefecture.

Copyright © 2010 IAHS Press

Kanto Groundwater Basin – Kazusa subgroundwater basin

The Kazusa subgroundwater basin contains brine groundwater (fossil sea water), including natural gas and iodine. Maximum land subsidence of 247 mm/year occurred in 1971 and was due to natural gas production. Since that time, groundwater-pumping regulations have been strictly enforced in the Tokyo Bay area. Consequently, groundwater levels have recovered and the surface has been slightly uplifted. Therefore, the pumping is now limited to the area of hills and the Kujukuri Plain in the marginal area of the basin.

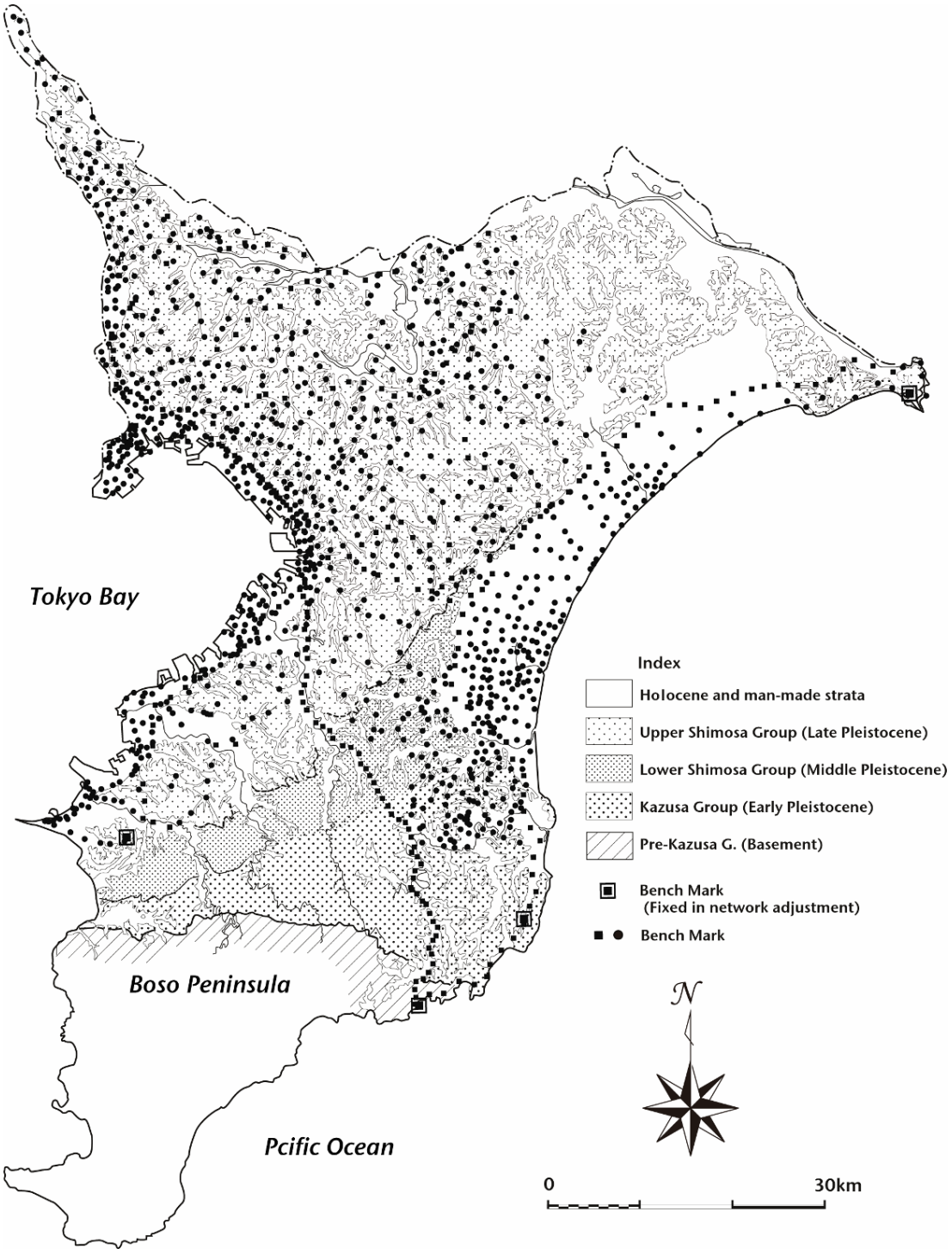

Fig. 2 Distribution of bench marks in Chiba Prefecture.

Shimosa subgroundwater basin

The Shimosa subgroundwater basin has been extensively pumped, mainly for aqueduct, agricultural, industrial, and building use. Groundwater in the aquifer fell to its lowest level in the early 1970s. Many local governments then regulated groundwater pumpage and surface water has since been used in the industrial district. Accordingly, the groundwater level recovered by 20–30 m in the southern Kanto groundwater basin. Water in the lower aquifer has now stabilized to near-historic levels. However, the upper aquifer has not recovered enough yet because the pumping continues.

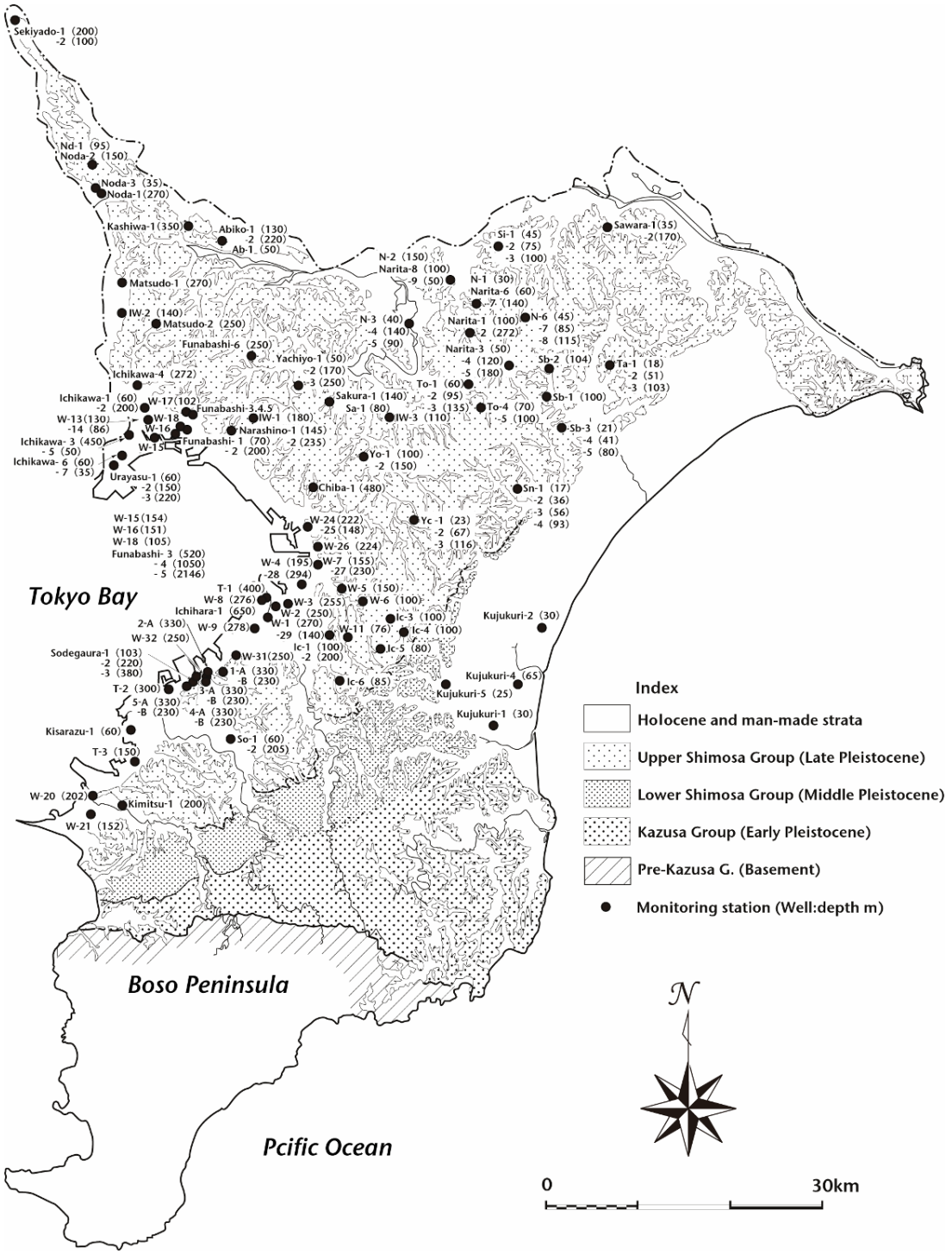

Fig. 3 Distribution of the monitoring wells in Chiba Prefecture.

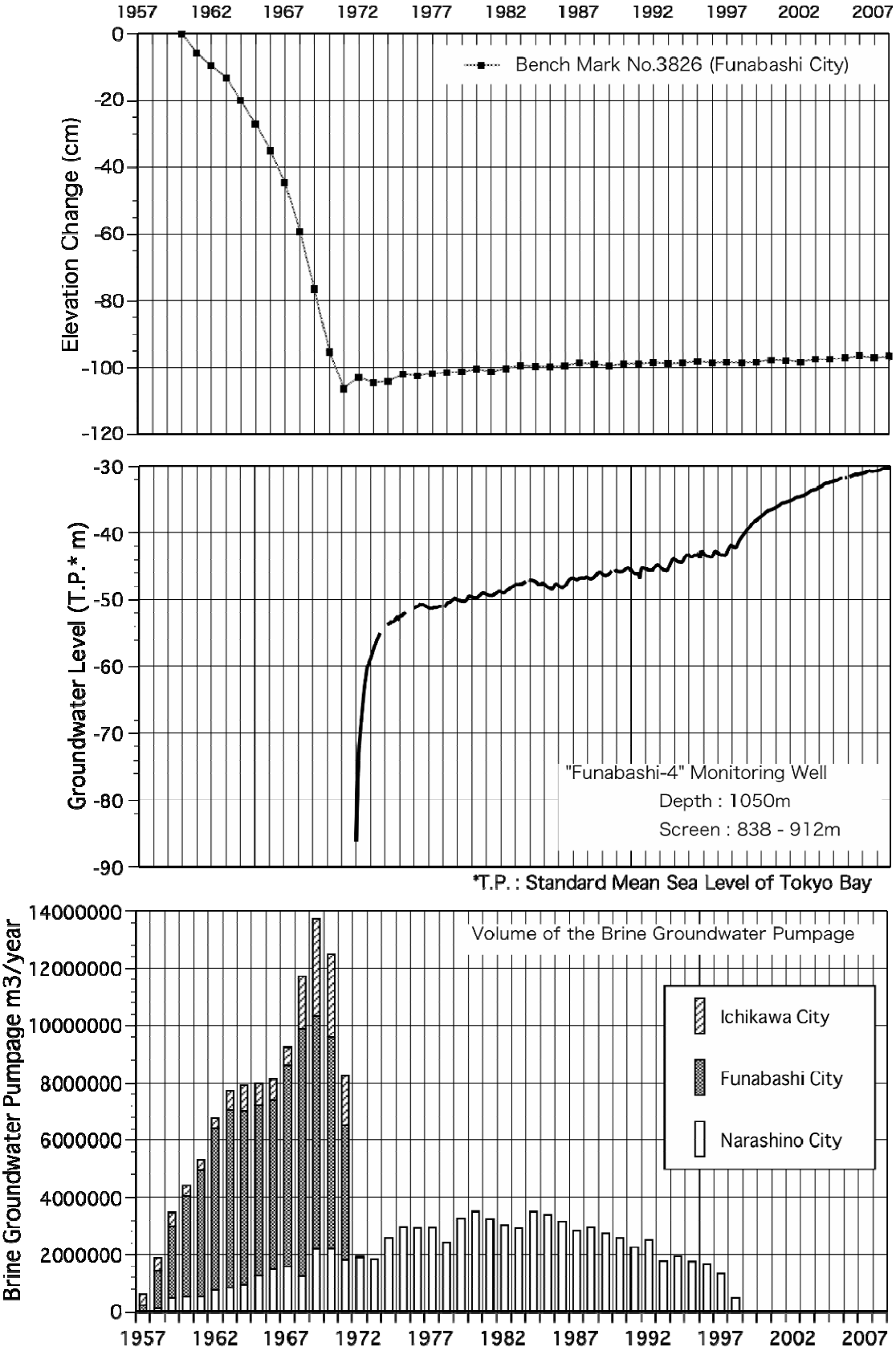

Fig. 4 Historical change of the elevation, groundwater level and volume of the brine groundwater pumpage.

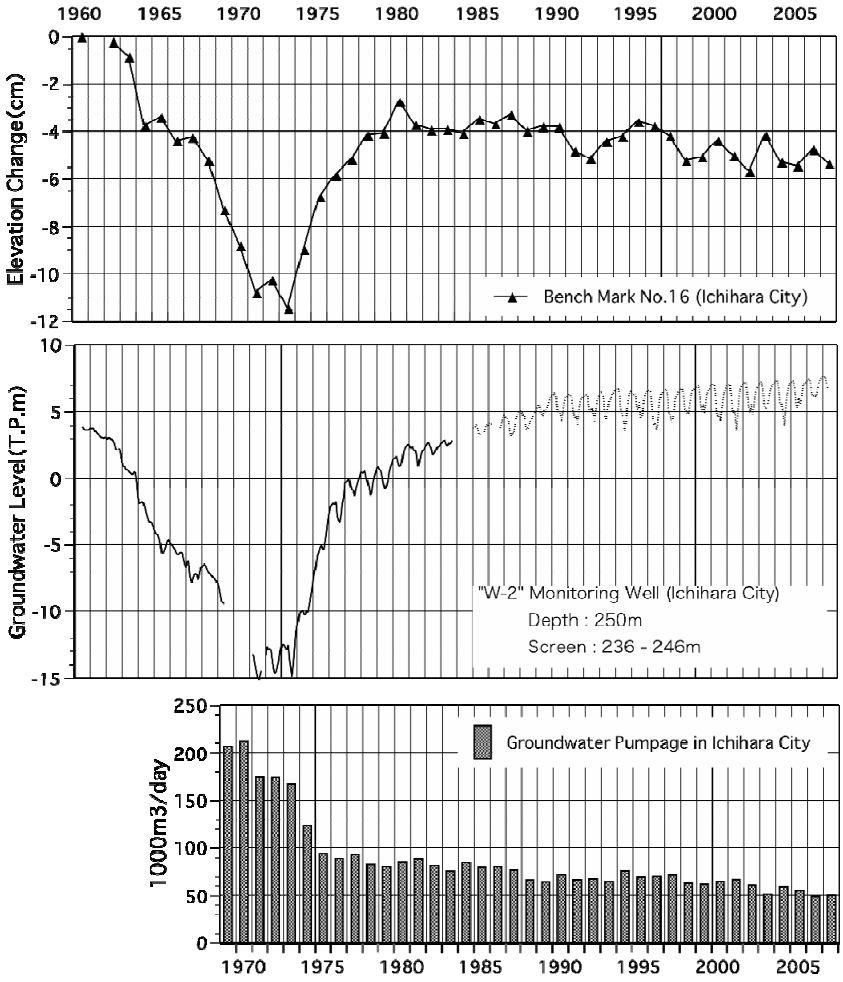

Fig. 5 Historical change of the elevation, groundwater level and volume of groundwater pumpage.

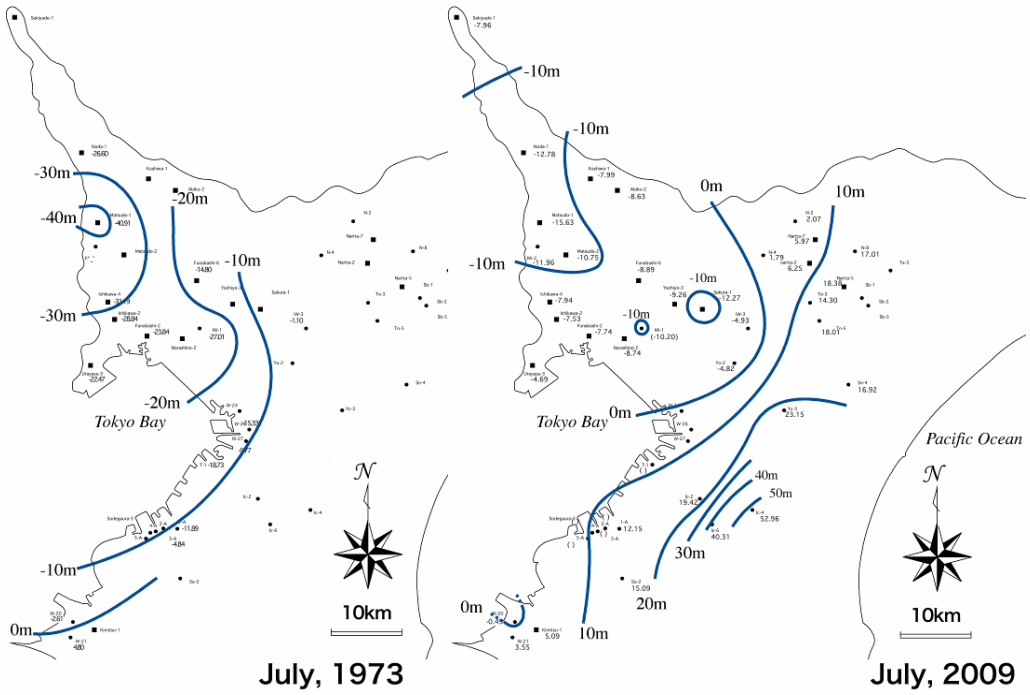

Fig. 6 Groundwater level of the lower aquifer in July 1973 and 2009.

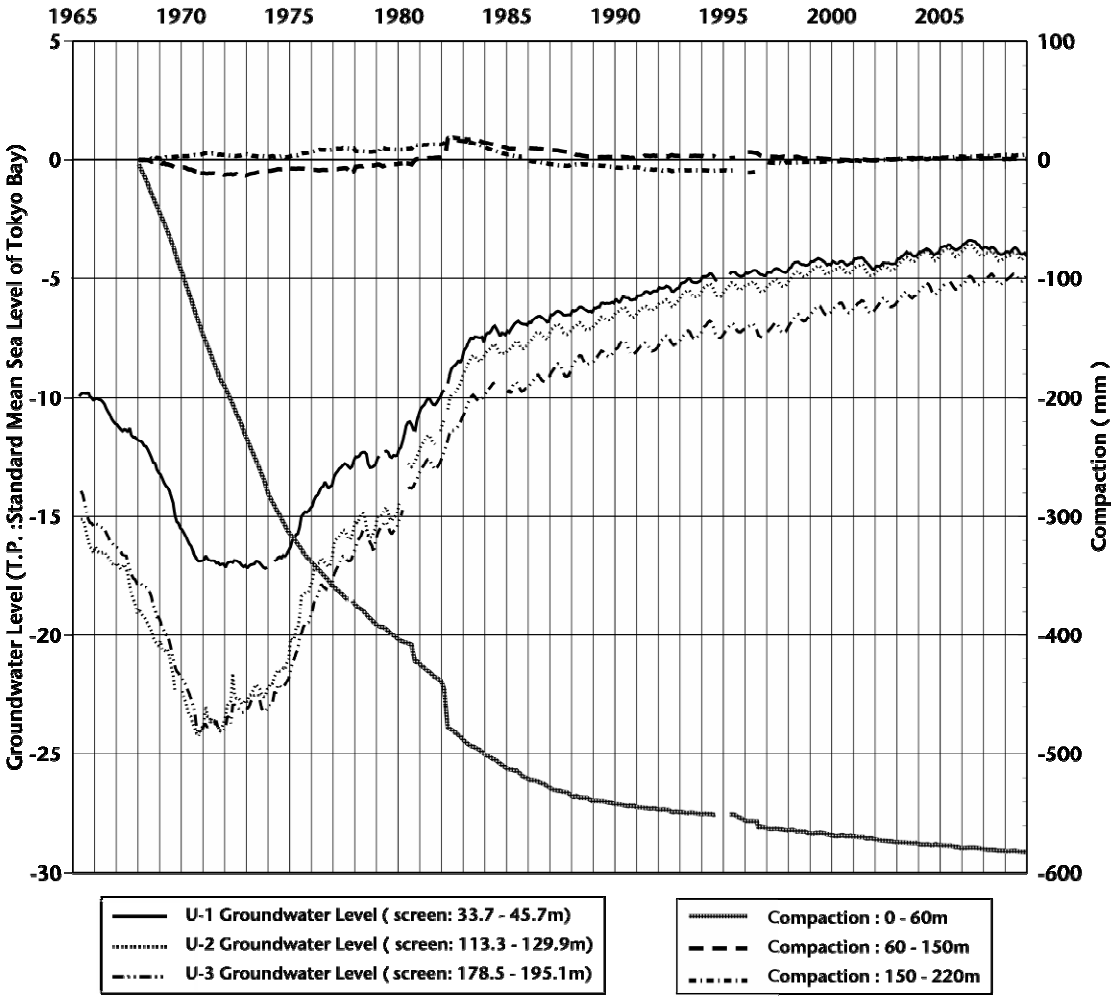

Fig. 7 Historical change of the groundwater level and the strata compaction in Urayasu deltaic plain.

Holocene deposits

The extreme upper part of the basin is subject to compaction of "alluvial" sediments, a phenomenon particularly found in the lower, delta area of the Kanto Plain. It is now widely confirmed that the amount of ground subsidence is affected by the thickness of alluvial deposits.

CONCLUSIONS

Our hydraulic models and general hydrogeological investigations now show that we can reasonably pump groundwater in the Kanto basin without causing undue land subsidence. Nevertheless, groundwater pumping requires constant monitoring for sustained use. In this regard, we now increasingly use GPS and SAR surveys to identify possible groundwater-induced land subsidence.

REFERENCES

Furuno, K., Nemoto, K., Takanashi, Y., Yada, T., Takizawa, H., Oshima, K., Saotome., W. & Nirei, H. (1983) The monitoring of land subsidence and groundwater head in the Kanto groundwater basin. Bull. Chiba Pref. Res. *Inst. Environ. Pollut*. **15**, 99–108.

Land Subsidence, Associated Hazards and the Role of Natural Resources Development
(Proceedings of EISOLS 2010, Queretaro, Mexico, 17–22 October 2010). IAHS Publ. 339, 2010.

Integrated monitoring network for surface deformation in Capo Colonna archaeological area, Crotone, Italy

F. VERDECCHIA, C. ZOCCATELLI, E. NORELLI & R. MIANDRO
ENI E&P Division, GEOD, San Donato Milanese, Italy
federica.verdecchia@eni.com

Abstract A permanent integrated geodetic and geophysics network for surface deformation monitoring was implemented in the Capo Colonna promontory area, where a very important archaeological area of Hellenic inheritance (Hera-Lacinia temple, dating from the fifth century BC) is present, near to a gas producing area. The monitoring network was designed to ensure hydrocarbon extraction sustainability in the promontory area, whose possible effects would increase the evident natural morphological instability. The monitoring network includes: clinometric and accelerometer survey on the Doric column of Hera Lacinia Temple, inclinometer and extensometer surveys of the shallow geological layers; free water table piezometric monitoring; and continuous GPS (Global Position System) surveys. The permanent monitoring station is integrated with geodetic levelling campaigns; satellite SAR (Synthetics Aperture Radar) monitoring; aerophotogrammetric surveys; sea bed bathymetry and altimetry by LADS (Laser Airborne Dual Scanner), and terrestrial interpherometric radar surveys. A micro seismic network is also present to collect and solve any seismo-genetic event occurring in the area. Moreover, to increase the accuracy of satellite and terrestrial surveys a weather station is present to measure parameters including temperature, atmospheric pressure, humidity, precipitation intensity, winds direction and velocity. All the permanent instruments send data to an acquisition switchboard installed in the processing data centre located inside the Capo Colonna Archaeological Museum, for real-time display on demand. The other parameters constantly monitored are the main geological–geomorphological and hydrogeological features, in addition to the coastal dynamics variations. The monitoring network is powered by a photovoltaic panel system (13 kW peak) installed on the Capo Colonna Museum roof. Processing and integration of all the different and complementary data allow us to be continually aware of whatever phenomenon that could modify the morphology and ground stability of the Capo Colonna promontory, by realizing 3-D vector ground displacement deformation maps with millimetric precision of the z-component.

Key words monitoring network; archaeological area; ground displacements

INTRODUCTION

Ten miles south of Crotone, on the promontory overlooking the Ionian coast of Capo Colonna, which the ancient Greeks called Heraion Lakinion, stands the Archaeological Park of Capo Colonna managed by the Archaeological Heritage Superintendence of Calabria.

The park encompasses 30 hectares of land used for archaeological excavation, and another 20 hectares used for forest and Mediterranean maquis-type vegetation. The area of Lakinion Akron, certainly one of the most famous sacred areas across Magna Greece, revolved around the majestic Doric temple of Hera Lacinia, built in the fifth century BC. Until the sixteenth century (AD) many columns of the Hera Lacinia temple were still in place. The temple had the classic floor plan with 6 × 19 columns, and this cape was called the Cape of Columns.

Unfortunately, over the centuries it was used as a building material source for the castle, the port and local palaces, until only one survivor column remained in view of sailors. The column, built on a thick and massive base of sandstone, remains the last sign of the Hera Lacinia Sanctuary (Fig. 1).

The Ionian coast of Calabria, in Southern Italy, and in particular, the coastal area of Crotone province, has been subjected to subsidence over the centuries (Bertoni *et al*., 2000). The causes are very complex due to both natural phenomena (lithology, tectonics and eustatic changes in sea level) and to human activities such as water pumping and natural gas production (Bertoni *et al*. 2000; Guerricchio 2001). To study the complex mechanism of subsidence in the Crotone area and its environmental effects, a "Committee for the Study of Subsidence in the Crotone Area",

Copyright © 2010 IAHS Press

Fig. 1 Aerial view of the Cape of Columns and the surviving column.

operating from 1993 to 1998, was set up. After having carried out a series of geological, geomorphological and hydrogeological surveys in the area, the Committee scheduled and organised annual precision levelling campaigns along 340 km the coastline, as well as static GPS satellite measurements over four offshore platforms for natural gas production. On the basis of the studies and levelling carried out, the Committee deemed that the subsidence (9 mm/year) is mostly correlated with the gravitational tectonics of the zone, as historically ascertained (Bertoni *et al*., 2000).

With the aim of a sustainable development of its activities and to safeguard the integrity of the territory in which the Archaeological Park of Capo Colonna lies, ENI Spa E&P Division in collaboration with the Superintendence for Archaeological Heritage of Calabria, installed in 2005 on the Capo Colonna area a geodetic-geophysical station. The monitoring network has been able to highlight and to quantify, using the most advanced technologies currently available on the market, any phenomenon that could affect the structure and stability of the soil, subsoil and seabed on which the archaeological area of the Calabrian promontory spreads out.

For the design of the monitoring network, the recommendations set out and presented to the *Seventh International Symposium on Land Subsidence* in Shanghai (Gambolati *et al*., 2005b) have been largely followed. The monitoring system has been implemented over the years to ensure an accurate understanding of the altimetric variation of the land surface in every component of the movement with a very high resolution (millimetric resolution in the z-component).

GEOLOGY AND TECTONIC

The Calabrian Arc is one of the most controversial geological issues inside the extremely complex area currently occupied by the Mediterranean Sea. The uplift of the Calabrian Arc with ESE verging thrust is associated with the Adria plate subduction towards the Ionian Sea, together with the development of a correlated accretion wedge (Fig. 2).

The eustatic phenomenon is added to the mountain chain rising, as well as to the local tectonic effects; this, starting in the lower Pleistocene, contributes to producing a series of marine terraces (outlined in places by the presence of pebbly or calcareous sandstone lithologies, and elsewhere by residual flattened morphologies).

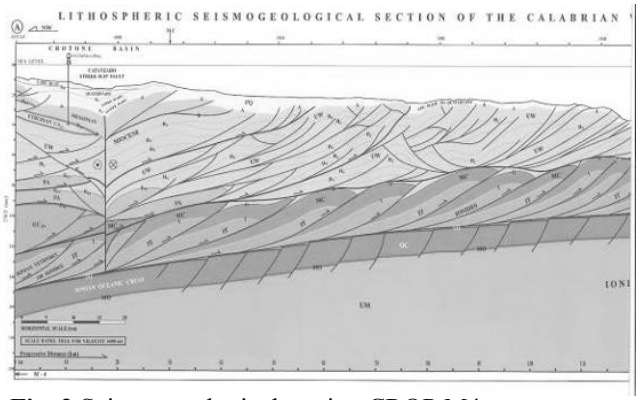

Fig. 2 Seismo-geological section CROP M4.

STRATIGRAPHY

Extensive outcrops of Plio-Pleistocenic blue-grey clays are typical of the study area (Cutro Fms, Actt.) and they form the substratum. Above this, multi-level terraced marine sediments are present, mainly represented by sandstone, pebblestones and conglomerates at different lithification grades, together with bioclastic calcareous sandstone and algal-biostromal limestone.

Stratigraphy of Capo Colonna terrace

The eastern C. Colonna terrace (Tirrenian age) is currently at a height of 15 m above sea level. The terrace internal margin is covered by a colluvial layer deposited from the surrounding heights. The promontory geological structure is made by a composite terrace (Nalin, 2002; Zecchin, 2004) formed by sedimentary bodies that are different from both the depositional and stratigraphic point of view (Fig. 3).

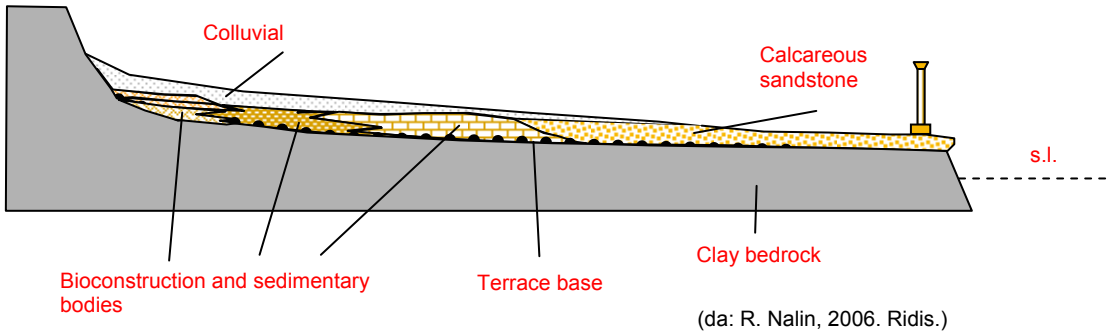

Fig. 3 Schematic C. Colonna terrace morphology.

Such a complex sedimentary body presents a nonhomogeneous behaviour, both hydro-geologically and mechanically. The shoreline bathymetry highlighted the presence of a small submarine canyon by the promontory's north coast; this area shows the greater vertical velocity movements. The promontory's south coast is instead affected by relevant hydrogeological instability phenomena as the Plio-Pleistocenic blue-grey clays are eroded by wave action and consequent undermining of the above ground covering. These portions of the cliff are retreating at a rate of between 0.5 and 1 metre per year. The coastal crumbling occurs along the entire coastline of the promontory, and is also aided by fresh water circulation inside the porous colluvial bodies. The rainfall, together with the agricultural watering, are not properly drained, but flow along the cliff increasing the soil erosion and that of the underlying formations.

GEOMORPHOLOGY

The Plio-Pleistocenic blue-grey clays are affected by extensive gullying due erosion by rainwater; this effect is very evident close to the city of Crotone (Fig. 4). Around the Capo Colonna promontory, the wave-motion mechanically and chemically undermines the clays, generating large cliff collapse and retreat. The frequent winter storms contribute to the coastal erosion. Where the calcareous sandstone covering is missing, the rainfall action causes frequent small landslides.

Fig. 4 The Plio-Pleistocene blue-grey clays and gullying morphology.

THE PERMANENT INTEGRATED GEODETIC AND GEOPHYSICAL NETWORK

In the planning of an effective project to control and predict soil movements in three dimensions it is very important to study both the natural and anthropic components of the phenomenon. The first step is to collect, process and organize all the information relevant to the area examined: geological history, geotechnical data, study and analysis of the environmental processes active in the area. Understanding of the phenomenon will be possible only after thorough integration of the different measurement methodologies used.

The geodetic-geophysical station installed in the Capo Colonna area has been designed to detect and to monitor the Doric column's movements, vertical and/or horizontal deformations of the soil and subsoil, and the free water table changes.

Doric column monitoring

With the aim of detecting any variation in inclination of the column, a clinometer has been installed on the column basement (Fig. 5). Close to the clinometer, a triaxial accelerometer has also been installed to record any kind of vibration occurring in the area, such as those generated by storms, earthquakes, thunder or by human activities.

Subsurface monitoring

For the subsurface monitoring inside three dedicated wells, properly located in the area, have been installed (Fig. 6) with:

- 1 inclinometer to detect deformations mainly occurring on the horizontal plane (creeps or thrusts);
- 1 extensometer to detect deformations along the vertical plane, mainly due to sediment compaction;
- 1 piezometer for the continuous monitoring of the free water table variations.

Fig. 5 Clinometer location in the base of the Doric column.

Fig. 6 The three dedicated wells for surface monitoring.

Local seismic surveys

West of the museum building, a triaxial geophone has been installed and coupled with the ground. The geophone output is integrated with the data coming from five other microseismic stations which form the Crotonian microseismic network. The network has been created to monitor the natural seismicity of the area, allowing detection of the intensity, depth and epicentre location of any earthquake occurring in the area, even if slight.

The permanent monitoring system is also integrated with data and information coming from: annual levelling campaigns; continuous GPS/ satellite surveys; SAR satellite surveys; aerophotogrammetric surveys over the promontory; seabed bathymetric surveys; and periodical hydrogeological monitoring in wells established for civil use (Fig. 7).

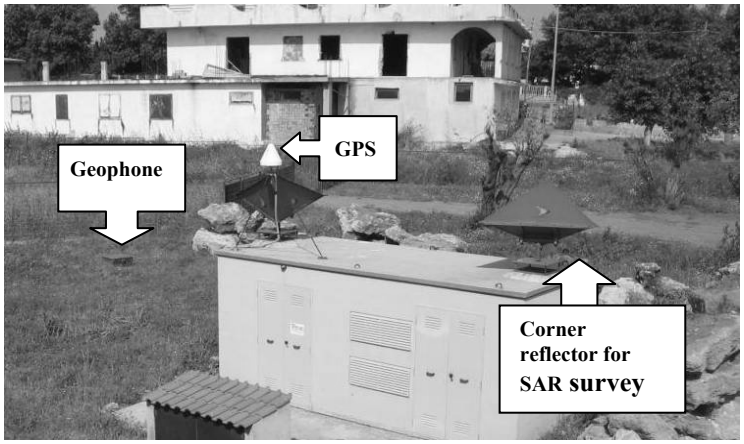

Fig. 7 The satellite survey unit: GPS and SAR satellite surveys.

All the data coming from the permanent monitoring system are collected by a processing centre located inside the museum building. The data, stored in a PC on which the acquisition software is installed, is always locally available but it is also sent in real time to the ENI headquarters through the telephone GSM network (Fig. 8).

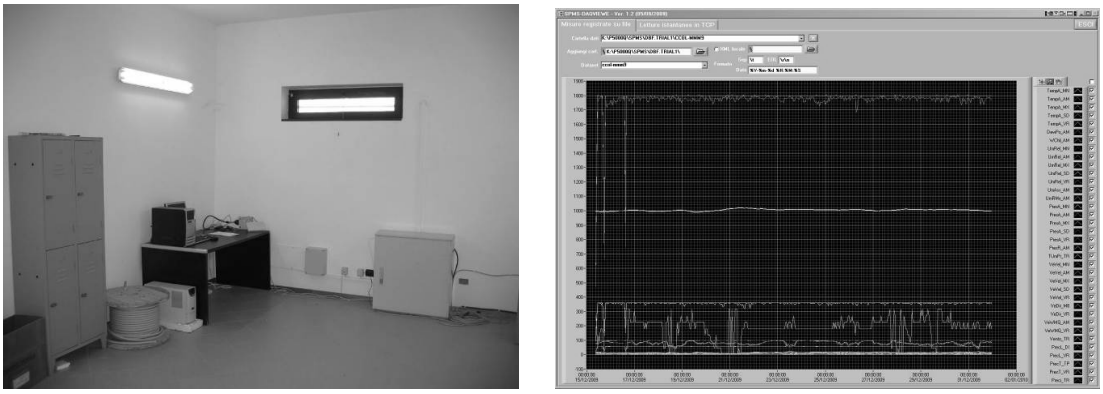

Fig. 8 Processing centre and data acquisition example.

However, the GPS and levelling campaign data are sent to a third-party institute to be certificated and quality controlled before being used. To increase the accuracy of satellite and terrestrial surveys a weather station has been installed on the museum roof (Fig. 9).

Finally, the monitoring network is powered by a photovoltaic panel system installed on the Capo Colonna Museum roof (Fig. 9), that is able to provide, with normal solar radiation, an average electrical power of 8 kW (13 kW peak).

Fig. 9 Weather station and photovoltaic panel system.

CONCLUSIONS

The paper explains the engineering solutions implemented to develop the "Capo Colonna Archaeological Area" geodynamic monitoring system.

The good integration, in such a limited area, of several different detection and monitoring technological systems:

– vibrations and slope on the column (accelerometer and clinometer);
– shallow subsoil layers deformation (extensometer and inclinometer);
– water table variations (piezometer);

– surface elevation changes and patterns of displacements, both vertical and horizontal (CGPS, satellite interpherometry, high precision levelling);
– sea bed, coastline and surface geomorphological variations (aerophotogrammetry and bathymetry);
– regional and local earthquakes and micro earthquakes settlement (seismic network);

will contribute to a better understanding of the driving geodynamic mechanisms of the extremely geologically complex area and makes the "System", at present, a unique high density geodynamic monitoring network.

The short observation period so far does not allow us to draw reliable reports or hypotheses about the "driving mechanism". With a longer period, enabling enough data collection, this singular multidisciplinary approach to geodynamic investigation will enable us not only to finally ascertain if and how much the geomorphological behaviour of the area is affected by anthropic activity (gas production), but also to recognize and make a reliable prediction of possible critical causes compromising the archaeological area stability and integrity.

REFERENCES

Astorri M. & Zoccatelli C. (2001) Rilievi altimetrici nell'area crotonese: sintesi dei risultati , indagini in atto e sviluppi futuri. In: *Atti del Convegno Problemi geo-ambientali nella Costa fra Capo Colonna e Isola di Capo Rizzato* (Le Castella 28/04/2001) (ed. by G. Lena), 61–78. A.M.P. Capo Rizzato, Italy.

Bertoni W. (2001) L'analisi previsionale della subsidenza edell'eustatismo per una corretta gestione delle problematiche geodinamiche delle aree costiere: l'esperienza di Ravenna e proposte per l'area di Crotone. In: *Atti del Convegno Problemi geo-ambientali nella Costa fra Capo Colonna e Isola di Capo Rizzato* (Le Castella 28/04/2001) (ed. by G. Lena), 79–94. A.M.P. Capo Rizzato, Italy.

Bertoni, W., Bratti C., Carbognin, L., Cesi C., Chierici, G. C., Dossena, G., Guerricchio, A., La Monica, U., La Tegola A. & Succetti, A. (2000) Analysis of subsidence in the Crotone Area along the jonian cost of Calabria, Italy. In: *Land Subsidence* (Proc. VIth Int. Symp Land Subsidence, Ravenna, Italiy, September 2000) (ed. by Carbognin *et al*.), vol. I, 155–166.

Bevilacqua, G. (2001) Analisi storica della subsidenza nel crotonese. In: *Atti del Convegno Problemi geo-ambientali nella Costa fra Capo Colonna e Isola di Capo Rizzato* (Le Castella 28/04/2001) (ed. by G. Lena), 103–106. A.M.P. Capo Rizzato, Italy, 103–106.

Bird, E. (2008) *Coastal Geomorphology; An Introduction*, second edn. Wiley, Chichester, UK.

Cosentino D., Gliozzi E. (1988) Considerazioni sulle velocità di sollevamento di depositi eutirreniani dell'Italia meridionale e della Sicilia. *Mem. Soc. Geol. It.* **41**, 653–665.

Finetti, I. R. (ed.) (2005) *Crop Project: Deep Seismic Exploration of the Central Mediterranean and Italy*. Elsevier.

Gabbianelli, G. (2007) Valutazione sintetica inerente l'attività di monitoraggio geodinamico realizzato da ENI E&P nelle zone di Crotone e C.o Colonne nel periodo 2003–2005. University of Bologna, C.I.R.S.A. Interdepartmental Research Centre for Environmental Sciences.

Gambolati, G., Teatini, P. & Ferronato, M. (2007) Linee Guida per lo studio dei fenomeni di Subsidenza nell'ambito dei progetti di sviluppo sostenibile dei campi ad olio e gas. Technical Report /2007. Department of Mathematical Models and Methods for Applied Sciences, University of Padova, Italy.

Gambolati, G., Teatini, P. & Ferronato, M. (2005b) Basic conceptual guidelines for a sustainable gas/oil field development. In: *Land Subsidence* (Proc. Seventh Int. Symp. Land Subsidence Shanghai, Pr China, October 2005) (ed. by A. Zangh *et al*.), vol. II, 919–924. Shanghai Scient. & Tech Publisdhers, Shanghai, China.

Gisotti, G. (2001) Osservazioni sul problema della Subsidenza della Costa fra Crotone e Le Castella e sulla pianificazione del territorio interessato. In: *Atti del Convegno Problemi geo-ambientali nella Costa fra Capo Colonna e Isola di Capo Rizzato* (Le Castella 28/04/2001) (ed. by G. Lena), 15–18. A.M.P. Capo Rizzato, Italy.

Guerricchio A. (2001) Lineamenti geologici e problemi di subsidenza del Bacino Crotonese. In: *Atti del Convegno Problemi geo-ambientali nella Costa fra Capo Colonna e Isola di Capo Rizzato* (Le Castella 28/04/2001) (ed. by G. Lena), 39–59. A.M.P. Capo Rizzato, Italy. 39-59.

Guerricchio, M. & Ponte, M. (2000) Discovery of submerged fixed archaeological structures in the Crotone coastal strip between Strongoli Marina and Le Castella (Calabria Region, Italy). Considerations on coastal erosion and subsidence phenomena. In: *Land Subsidence* (Proc. VIth International Symposium on Land Subsidence, Ravenna, Italia, September 2000) (ed. by Carbognin *et al*.), vol. I, 17–32.

Massari, F., Sgaveti, M., Rio, D., D'alessandro, A. & Prosser G., (1999) Composite sedimentary record of falling stages of Pleistocene glacio-eustatic cycles in a shelf setting (Crotone basin, south Italy). *Sedimentary Geology* **127**, 85–110.

Nalin, R. (2002) Stratigrafia e sedimentologia dei depositi del terrazzo di Cutro, penisola di Crotone (Calabria). Unpublished Thesis. Padova University, Italy.

Strozzi, T., Wegmuller, U., Tosi, L., Bitelli, G. & Spreckels, V. (2001) Land subsidence monitoring with differential SAR interferometry. *Photogramm. Engng & Remote Sensing* **67**(11), 1261–1270.

Van Dijk, J. P. (1990) Sequence stratigraphy, kinematics and dynamic geohistory of the Crotone Basin (Calabrian Arch, Central Mediterranean): an integrated approach. *Mem. Soc.Geol. It.* **44**, 259–285.

Zecchin, M., Nalin, R. & Roda, C. (2004) Raised Pleistocene marine terraces of the Crotone Peninsula (Calabria, southern Italy): facies analysis and organization of their deposits. *Sedimentary Geology* **172**, 165–185.

(Proceedings of EISOLS 2010, Querétaro, Mexico, 17–22 October 2010). IAHS Publ. 339, 2010.

Monitoring land subsidence over a shallow gas reservoir in India using GPS

P. R. PATEL
Senior Associate Professor, Institute of Technology, Nirma University, Ahmedabad-382 481, Gujarat, India
parul.patel@nirmauni.ac.in

Abstract Subsidence is one of the most significant results of reservoir compaction due to extraction of gas/oil. It is difficult to predict the subsidence as it takes place well below the ground surface. Therefore, the prediction of subsidence is a challenging task. Subsidence measuring techniques should be such that they are capable of detecting even 1-mm level change in elevation. With the advancement of space technology, subsidence measurement is being carried out using Global Positioning System (GPS). Subsidence studies have been carried out over the shallow gas reservoir in Gujarat, India. A precise GPS network was established in 2004. Dual-frequency GPS receivers were used to collect the data. A significant amount of subsidence, 86 mm, was observed along with the horizontal displacement. Subsidence is correlated with the parameters responsible for subsidence. The coefficient of compaction is estimated from the subsidence. Subsidence is predicted over this area using empirical methods.

Key words GPS; land subsidence; prediction

INTRODUCTION

Subsidence monitoring techniques should be capable of measuring small change in elevation within a short period. With the development of space technology, now GPS is used to measure land subsidence. GPS is capable of giving millimetre-level accuracy with a geodetic dual-frequency receiver, longer data collection time and data processing with scientific software in post processing mode. Many scientists worldwide have tried to measure subsidence with GPS. Notable are subsidence studies in Jakarta, Indonesia (Abidin *et al.*, 2006), in Ojiya city, Japan (Sato *et al.*, 2003) and in Iran (Mousavi *et al.*, 2001). In this study, subsidence is measured over the shallow gas reservoir in Gujarat, India, by the author along with the IIT Bombay GPS team. Significant subsidence of 86 mm is observed during the period of three years with GPS. Gas extraction is considered as the main cause of subsidence in this region. Pressure depletion is observed in reservoir area, where greater subsidence is measured. Other factors responsible for subsidence, such as the amount of gas extraction and water extraction have been studied rigorously; the study results indicate that there is a definite correlation between gas extraction and pressure depletion with subsidence. An attempt has been made to establish certain empirical methods to predict the subsidence over the study area using the reservoir parameters. Arguably this is the first attempt in India to measure subsidence with GPS.

STUDY AREA, GPS DATA COLLECTION AND PROCEDURE

The subsidence study was carried out over the 14 km^2 shallow gas reservoir, on the north side of the Surat, Gujarat, India. The potential gas-producing zone consists of two unconsolidated sandstone layers, located at between 170 and 240 m below the ground surface. This study has been carried out to understand the subsidence pattern, which may have an adverse effect on the safety of the villages and infrastructure lying above the reservoir.

A precise GPS network of 31 stations (4 Reference and 27 Deformation) has been established. Out of 27 deformation stations, 10 are within the presumed reservoir boundary and the rest are outside. In total, 12 GPS campaigns were carried out between February 2004 and March 2007 at intervals of 3 to 4 months. Dual frequency GPS receivers were used to collect the data. The reference stations were running continuously during the entire field campaign. At each deformation station, at least five to six hours of continuous GPS data were collected during each campaign. Figure 1 shows the details of the deformation stations.

Copyright © 2010 IAHS Press

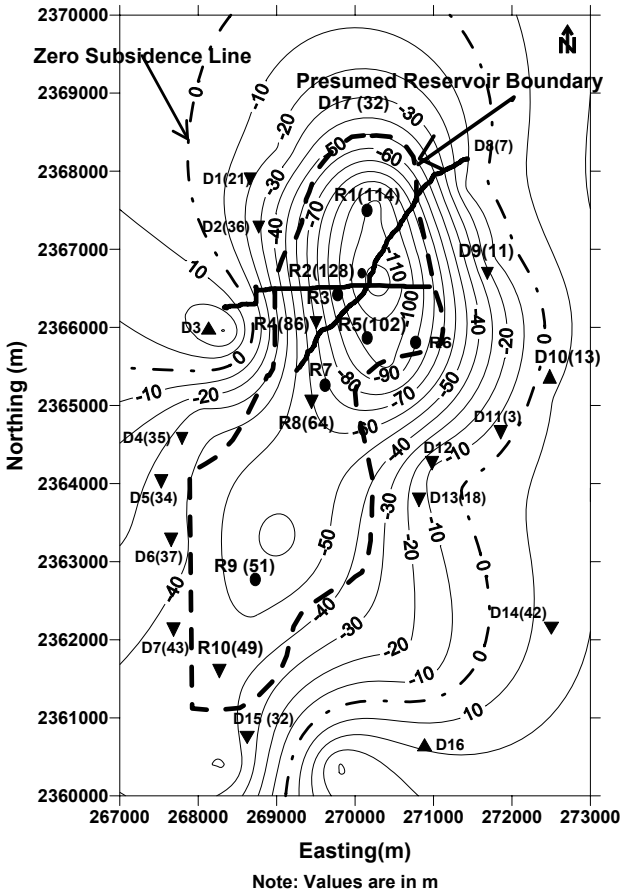

Fig. 1 Contours showing change in elevation (February 2004 to March 2007). (Note: ▼ Subsidence stations, ▲ Uplift stations, ● Stations near gas wells showing subsidence, ——— Contour lines, — — — zero subsidence line, values in parentheses indicate uplift/subsidence. D1 to D17 are deformation stations outside the reservoir boundary and R1 to R10 are deformation stations within the boundary).

The GPS data was processed with BERNESE V4.2 in post processing mode. Three IGS (International GNNS Service) stations (LHAS, BAHR and IISC on three different plates) were selected for constraining the solutions in the ITRF 2000 (International Terrestrial Reference Frame 2000). The precise ephemeris files were also used. Data from a permanent GPS station located at IIT Bombay were also used for this study. The factors that affect the vertical accuracy were taken into account while processing data in post-processing mode, such as satellite geometry, tropospheric and ionospheric correction, and ocean loading effects. During processing, first, precise coordinates for three IGS stations were tightly constrained. Then, the averages of the daily solutions per campaign were determined using the ADDNEQ programme in BERNESE V4.2, and the coordinates of the reference stations thus obtained were used for the second stage. In the second stage, to get the coordinates of all 27 deformation stations, two reference stations and the IITB station were tightly constrained.

ANALYSIS OF SUBSIDENCE

GPS-derived ellipsoidal heights have been used (Abidin *et al.*, 2006) to measure the subsidence. The accuracy of GPS-derived coordinates is quite good, being 3–5 mm for horizontal coordinates and 5–8 mm for heights. This accuracy is adequate to detect and monitor subsidence. In the present GPS network, the lengths of all baselines are less than 25 km, hence the precision estimated for latitude and longitude is 1 to 2 mm and for height, 4 to 5 mm.

To eliminate the effect of swelling/shrinking on elevations due to the top 4–5 m deep layer of expansive black cotton soil, the elevations in the season just prior to monsoon (May 2004, May 2005, May 2006 and March 2007) were compared. To calculate the subsidence, the results of these four campaigns are compared. Average changes in elevation with respect to May 2004 are calculated for the May 2005, May 2006 and March 2007 campaigns using equation (1):.

$$(\Delta h)_{i,j} = h_{i,j} - h_{i,1}[i = 1, n; j = 1, m] \quad \text{I have changed} \tag{1}$$

where, $(\Delta h)_{i,j}$ is change in elevation at station i from (1 May 2004) to the jth campaign, n is the number of deformation stations and m is the number of campaigns. Thus, the average subsidence for any campaign j can be written as:

$$\left[(\Delta h)_{i,j}\right]_{av} = \frac{\sum_{i=1}^{n}(\Delta h)_{i,j}}{n} \tag{2}$$

The effective subsidence is the difference between the average subsidence of the deformation stations of the area and the average subsidence of the reference stations and is calculated as:

$$\left[(\Delta h)_{i,j}\right]_{eff} = \frac{\sum_{i=1}^{n}\Delta h_{i,j}}{n} - \frac{\sum_{k=1}^{r}\Delta h_{k,j}}{n} \tag{3}$$

where $i = 1, n$; $j = 2, m$; $k = 1, r$, and r is the number of the reference stations. The results are shown in Fig. 2. It is seen that, cumulative effective subsidence is 86 mm during May 2004 to March 2007 and the corresponding rate of subsidence is 30 mm per year.

Subsidence contours

To evaluate the subsidence, contours of change in elevation during May 2004 to March 2007 are plotted along with the deformation stations and approximate reservoir boundary superimposed on them (see Fig. 1). It is observed from the contour map that change in elevation is greater on the north side of the study area during May 2004 to March 2007. Two subsidence bowls have been produced, one relatively larger, in the north and a smaller one south of the reservoir. This confirms to the fact that five out of seven gas-producing wells (R1, R2, R3, R5 and R6) were on the north side leading to greater pressure depletion. Only one gas producing well (R9) is located on the south side, and the effect of subsidence is not significant. The local horizontal displacements between two successive campaigns are obtained by subtracting the velocity vector (displacement of Indian plate) during the same time interval from the total displacement observed with GPS. The local displacements of most of the stations are towards the centre of the reservoir. This supports the conclusion that subsidence is taking place in the observation area.

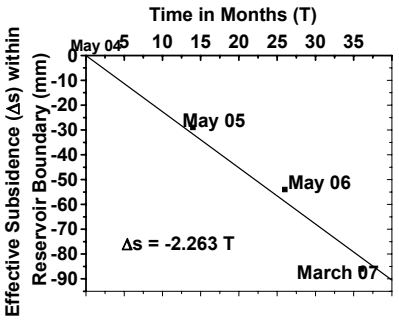

Fig. 2 Cumulative effective subsidence (May 2004 to March 2007).

Relation of subsidence with parameters responsible for subsidence

The volume of gas extraction, the pressure depletion and water level change are the main parameters responsible for subsidence over the present study area. Hence, an attempt has been made to evaluate and model their effects on subsidence.

The relation between the average reservoir pressure and cumulative gas volume extracted from all wells at different points of time from May 2004 to June 2007 is studied to understand the correlation between them. A linear relationship with a correlation coefficient of 0.99 exists between these quantities. Mayuga & Allen (1969) have reported a close correlation between cumulative subsidence and cumulative extraction of gas and oil for California's largest oil field. In the present study, a linear relation with a high correlation of 0.86 was observed between cumulative land subsidence (Δs in mm) and cumulative gas extracted (G in m^3).

To find the relation between subsidence and pressure depletion, the total pressure depletion (Δp) for each campaign with respect to May 2004 and corresponding subsidence values (Δs) for the same wells are plotted. This shows that subsidence is increasing with increase in pressure depletion and linear relationships are observed. In short, pressure depletion is the major cause of subsidence. To determine the relation between subsidence and water level, the average water levels of six different gas wells for campaigns starting from October 2004 were measured along with the corresponding average ellipsoidal heights for the same gas wells. No permanent depletion in water level was observed over the study area. But, there is a consistent reduction in the average ellipsoidal height. Thus, subsidence is not influenced by water level.

Prediction of subsidence over the study area

Experienced from observed data and predicted subsidence values shows that subsidence prediction based on laboratory tests often does not give realistic values. Hence, an attempt has been made to predict the subsidence over the existing gas reservoir based on the actual field measurements. Here, two different methods are suggested to predict subsidence over the study area. Attempt has been made to find out correlation between land subsidence and gas extraction. Figure 3(a) shows cumulative gas extraction and subsidence with respect to May 2004.

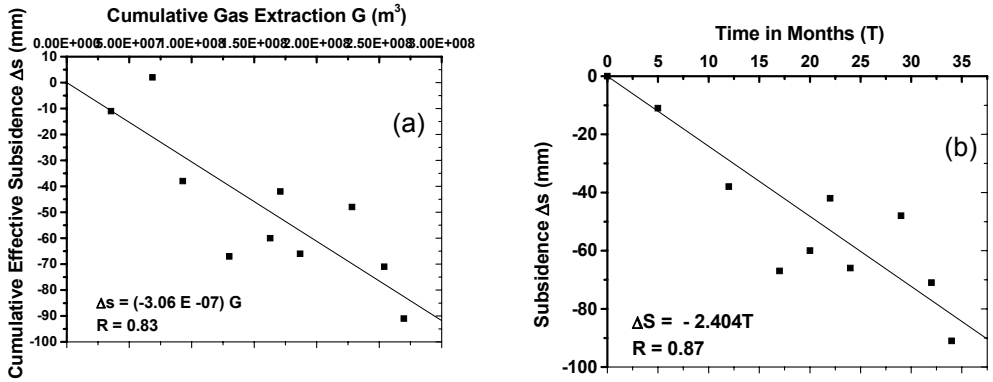

Fig. 3 (a) Relations between cumulative effective. (b) Relation between cumulative subsidence with cumulative gas extraction effective subsidence and time.

Subsidence may be predicted as a function of gas production using equation (4). The correlation coefficient between these parameters was observed to be high (0.83).

$$\Delta s = -(3.06E - 07)G \tag{4}$$

In another method, the available GPS data are extrapolated to derive the future trend. The amount of subsidence is plotted against time expressed in months in Fig. 3(b). Equation (5) can be used to

predict subsidence (Δs) with time T (months) in this study.

$$\Delta s = -(2.40)T \tag{5}$$

Estimation of the uniaxial compaction coefficient

Subsidence is a manifestation of reservoir compaction on the surface of the earth. Three main parameters are responsible for reservoir compaction: uniaxial compaction coefficient (C_m), pressure depletion of reservoir (Δp) and the initial thickness of the reservoir (H). Here an attempt has been made to find the value of C_m, assuming that, for a shallow reservoir, the amount of subsidence is equal to reservoir compaction.

To arrive at an average value of C_m for the entire study area, all values of subsidence and the corresponding values of [(Δp) H] for all wells and for all campaigns were plotted as shown in Fig. 4. Regression analysis was carried out and a linear relationship was observed to be suitable to relate these parameters. Equation (6) is obtained after regression analysis.

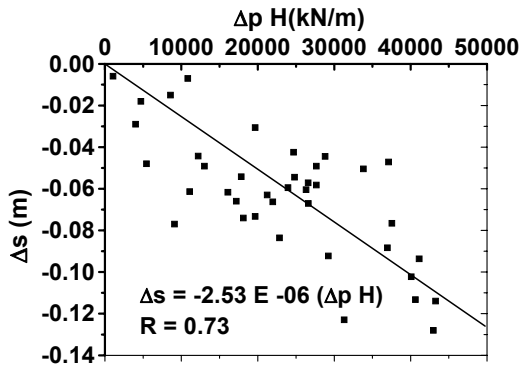

Fig. 4 Average C_m for all wells and all campaigns.

$$\Delta S = -2.53E - 06\left[(\Delta p)H\right] \tag{6}$$

The value of C_m obtained from this graph is 2.53 E-06 m^2/kN. This value is very near to the values suggested by Geertsma (1973) for loose soil. C_m is calculated as 2.7E-05 m^2/kN using the laboratory measured Poisson's ratio (0.33) and modulus of elasticity (2.50E 04 m^2/kN). It is observed that, the theoretical C_m is almost more than ten times the value obtained with GPS. Hence, it is concluded from the study that laboratory measured C_m is always higher than the field value (Cassiani & Zoccatelli, 2000).

CONCLUSIONS

With accurate planning of the GPS survey, a good level of precision can be achieved (1 to 2 mm) for horizontal coordinates. The vertical accuracy of the GPS-derived results is half of the horizontal accuracy, i.e. 4 to 5 mm. this accuracy is enough to measure the subsidence.

Average effective subsidence during May 2004 to March 2007 was 86 mm for stations within the presumed reservoir boundary and 20 mm for stations outside. Hence, the rate of subsidence within reservoir area is 30 mm per year.

A subsidence bowl of approximately 4 km diameter was observed in the north where more gas wells are located, and a small one of approximately 2 km diameter on the south side of the reservoir. In general, local displacements of the stations are towards the centre of the reservoir.

Subsidence is directly related to the amount of gas extracted and resulting pressure depletion. A linear relationship is observed between cumulative gas extraction and average reservoir

pressure. A linear relationship with a correlation coefficient of 0.83 exists between subsidence and cumulative gas extraction. A linear relationship is observed between pressure depletion and subsidence.

Subsidence can be predicted based on actual field measured data as experience shows that subsidence prediction based on laboratory test often does not give realistic values.

Acknowledgements This was a research project undertaken by the Late Prof. Madhav N. Kulkarni. I am grateful to him for his constant guidance for this work. I am indebted to Prof. G. Venkatachalam and Prof. E. P. Rao for their moral support and continuous guidance. Thanks are also due to Mr Shashank Shekar for extending the help during data collection. I am also grateful to the entire IIT Bombay GPS team for field work.

REFERENCES

Abidin, H.Z., Andreas, H., Gamal, M., Djaja, R., Murdohardono, D., Rajiyowiryono, H. & Hendrasto, M. (2006) Studying land subsidence of Bandung Basin (Indonesia) using GPS survey technique. *Survey Review* **38**(299), 397–405.

Cassiani, G. & Zoccatelli, C. (2000) Towards reconciliation between laboratory and in-situ measurements of soil and rock compressibility. In: *Land Subsidence* (ed. by L.Carbognin *et al*.), vol. 2, 3–15. La Garangola Publ., Italy.

Geertsma, J. (1973) Land subsidence above compacting oil and gas reservoirs. *J. Petroleum Technol.* **25**, 733–744.

Mayuga, M. N. & Allen, D. R. (1969) Subsidence in the Wilmington oil field, Long Beach, California, USA. In: *Land Subsidence* (ed. by L. J.Tison), vol. 1, 66–79. IAHS Publ. 88, IAHS Press. Wallingford, UK.

Mousavi, M. S., Shamsai, A., Naggar, H. M. & Khamehchian, A. (2001) A GPS-based monitoring program of land subsidence due to groundwater withdrawal in Iran. *Can J. Civil Engng* **28**, 452–464.

Sato, H. P., Abe, K. & Ootaki, O. (2003) GPS-measured land subsidence in Ojiya city, Niigata Prefecture, Japan. *Engng Geol.* **67**, 379–390.

(Proceedings of EISOLS 2010, Queretaro, Mexico, 17–22 October 2010). IAHS Publ. 339, 2010.

Measuring seabed altimetric variations with a repeat-track SAS interferometry experiment: processing and results

R. DE PAULIS[1], C. PRATI[2], S. SCIRPOLI[2], P. A. SLETNER[3] & A. TESEI[3]

1 *ENI E&P Division GEOLAB Dept 20097 S. Donato Milanese, Italy*

2 *Politecnico di Milano, Dipartimento di Elettronica e Informazione, via Ponzio 34/5, 20133 Milano, Italy*
scirpoli@elet.polimi.it

3 *NURC, viale San Bartolomeo 400, 19126 La Spezia, Italy*

Abstract Synthetic Aperture Sonar (SAS) is an acoustic imaging system that provides high resolution images combining the data collected along a virtual array of receivers. The virtual array is synthesized by the platform motion (an Underwater Autonomous Vehicle). Repeat-track interferometry is a well known technique used in Synthetic Aperture Radar (SAR) to obtain precise measurements of altimetric variations. In principle, the same technique can be exploited with Synthetic Aperture Sonar (SAS) for seabed deformations. This paper presents the results of a two-year study led by ENI gathering data in several sea campaigns in the Tyrrhenian Sea near La Spezia (Italy). The experimental set up is described in the companion paper given by the same authors (De Paulis *et al.*, 2010).

Key words SAS focusing; SAS interferometry

INTRODUCTION

In the framework of sustainable development activities carried out by the ENI Exploration & Production division, the ENI Geological Service in association with the ENI R&D department has promoted and financed the development and the experimentation of an innovative technology for environmental monitoring. This paper describes the experimental activities conducted in the context of a two-year project with the aim to test innovative approaches to better assess the altimetric accuracy and variations of the seabed. Exploiting sonar data to obtain measurement of altimetric variations through interferometry, poses many more problems relative to use of radar. In fact, acoustic waves speed show stronger and faster variations than electromagnetic waves; the actual platform trajectory is not known as precisely and the statistics of a natural target's coherence and its behaviour with time do not exist. Here we present the phase preserving, full-bandwidth SAS focusing technique (including motion compensation and auto-focusing) developed for the 300 KHz SAS system operated by NURC. The results will be shown, obtained on natural and artificial distributed or point targets to be used both as a ground reference for focusing and for interferometry. The quality of the focused images achieved will be analysed taking advantage of particular features of the artificial reflectors specifically designed for this experiment. Then, the achieved repeat-pass SAS interferograms will be shown and analysed showing the potential and limitations of this technique. A comparison with independent measurements carried out at the same location with the presence of an artificial reflector will also be illustrated. Moreover, the time behaviour of the coherence of that particular (sand) seabed will be shown and the utility of artificial reflectors for long term SAS interferometry will be discussed.

DESCRIPTION OF THE ACQUISITION SYSTEM

The real data we are going to present are collected by means of the Muscle AUV system operated by NURC (Fig. 1(a)). The platform moves on a nominal linear trajectory. The acquisition system is formed by a single transmitter and a linear array of 36 receivers as shown in Fig. 1(b) (Bellettini *et al.*, 2007). Some of the system parameters are reported in Table 1.

Copyright © 2010 IAHS Press

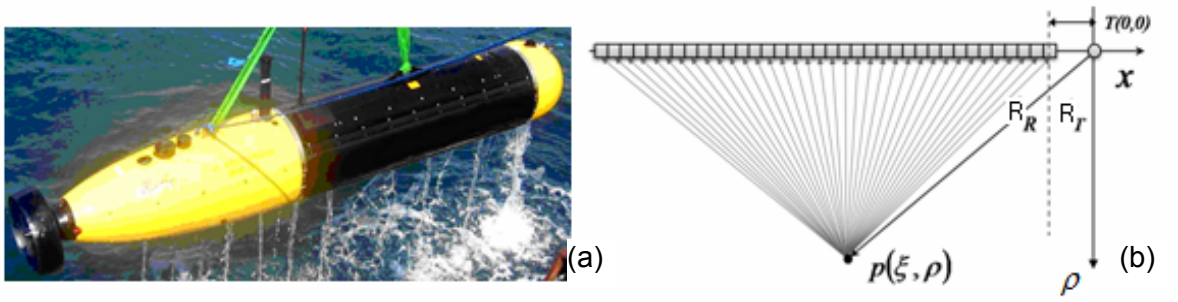

Fig. 1 (a) Muscle AUV system operated by NURC, (b) Geometry acquisition of one ping.

Table 1 System parameters.

Symbol	Value	Parameter
f_0	300 kHz	Central frequency
c	1500 m/s	Sound speed in sea water
λ	5 mm	Wavelength
B	60 kHz	System bandwidth
APD	0.21 m	Average Ping Displacement

SYNTHETIC APERTURE SONAR FOCUSING

A possible approach to image raw SAS data can be summarized in the following two steps: focusing of the echoes of each ping collected by the real array independently, use of a coherent sum of the focused images from different pings.

Single ping data are focused in the wavenumber domain by means of a modification of the standard Omega-K technique in order to cope with the multi-static acquisition system (Cafforio *et al.*, 1991). Exploiting the partial superposition of the real array between consecutive pings, it is possible to estimate the irregular motion of the platform. The sub aperture images are then motion compensated and summed together in order to obtain the full resolution image (De Paulis *et al.*, 2009).

Single ping imaging

Referring to Fig. 1(b) the impulse response of a SAS system for a target at coordinates (ξ, ρ) can be written as:

$$h(t;t_P) = p(t - t_P)\exp(-j\omega_0 t_P) \tag{1}$$

$p(t)$ is the transmitted pulse after range compression. The reception time, t_P, is a function of the target position and of the velocity of the platform v; the motion of the platform between the transmission and the reception time cannot be neglected. In this section we analyse the algorithm developed to image the data of each ping. The block diagram in Fig. 2 summarizes the processing.

First step: integration of INS information and oversampling Data are first pre-processed in order to perform a raw motion compensation based on the Inertial Navigation System information. Then the data are oversampled on the desired output grid.

Second step: Stop and go correction The second step of the focusing algorithm for a single ping is a preprocessing of the data in the time-Doppler domain in order to compensate for the motion of the AUV between the transmission and the reception time. Then, the impulse response of the system can be approximated with the following (stop and go acquisition):

$$h_s(x,t;\xi,\rho) = p\left(t - \frac{R_T(\xi,\rho) + R_R(x;\xi,\rho)}{c}\right)\cdot \exp\left(-j\omega_0 \frac{R_T(\xi,\rho) + R_R(x;\xi,\rho)}{c}\right) \tag{2}$$

$$R_T(\xi,\rho)=\sqrt{\xi^2+\rho^2}, \quad R_R(x;\xi,\rho)=\sqrt{(x-\xi)^2+\rho^2} \tag{3}$$

t is the fast time, $R_R(x;\xi,\rho)$ is the distance of the target in (ξ, ρ) from the receiver in x, $R_T(\xi, \rho)$ is the distance of the target in (ξ, ρ) from the transmitter, and ω_0 is the carrier wavenumber.

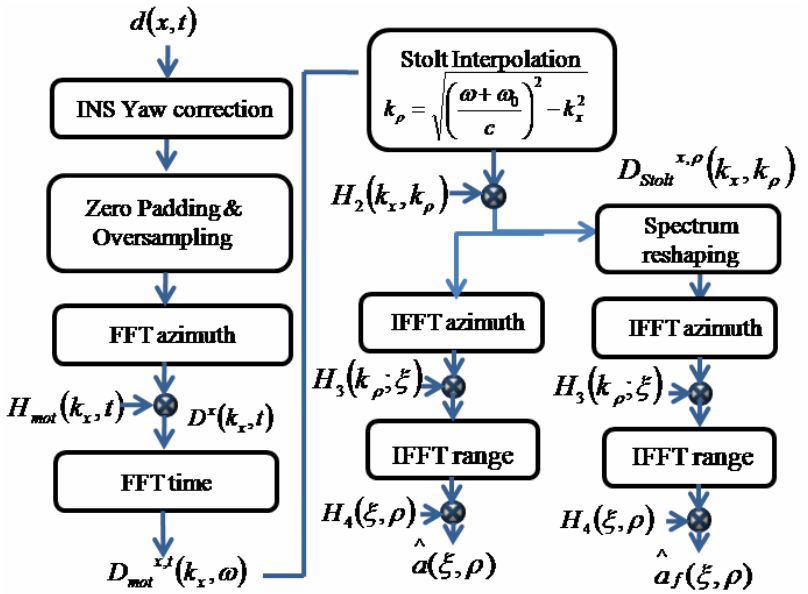

Fig. 2: Block diagram of single ping focusing.

Third step: monostatic approximation We first focus data as if they were acquired from a monostatic geometry ($R_T \approx R_R$).

$$h_m(x-\xi,t;\rho)=p\left(t-\frac{2R_R(x-\xi;\rho)}{c}\right)\cdot\exp\left(-j\omega_0\frac{2R_R(x-\xi;\rho)}{c}\right) \tag{4}$$

The Omega-K algorithm implements the convolution of the data with the matched impulse response in equation (4) in the wavenumber domain through the mapping of the data from the (k_x,ω) space to (k_x,k_ρ), and the multiplication of the focusing kernel in equation (5):

$$k_\rho=\sqrt{\left(\frac{\omega+\omega_0}{c}\right)^2-k_x^2}, \quad H_2(k_x,\omega)=\exp\left(j\rho_P\sqrt{\left(\frac{\omega+\omega_0}{c}\right)^2-k_x^2}\right) \tag{5}$$

Fourth step: multistatic correction The standard Omega-K algorithm is then modified to account for the multi-hydrophone nature of the data collection. The data are first multiplied in the (ω,ξ) domain by the function in $H_3(\xi,\rho)$ and finally corrected by the phase term $H_4(\xi,\rho)$ in the object domain:

$$H_3(\xi,\omega)=\exp\left(j\frac{\omega}{c}\sqrt{\xi^2-\rho_P^2}\right), \quad H_4(\xi,\rho)=\exp\left(j\frac{\omega_0}{c}\sqrt{\xi^2-\rho^2}\right) \tag{6}$$

Multiple ping imaging

In order to sum coherently sub-aperture images we have to take into account the residual perturbations of the AUV trajectory with respect to the information given by the INS. In particular, the platform is affected by shifts (surge, sway, heave) and rotations (yaw, pitch, roll). The system parameters are chosen so that there is superposition of the real array between consecutive pings.

The redundancy of the data is exploited to estimate the motion of the platform. Figure 3(a) shows the processing realized for the MOCOMP of two consecutive pings. We estimate the azimuth and range shifts between the images by means of the amplitude cross-correlation. From the modelling of the "inter-ping" interferometric phase we obtain the phase errors due to the different position and orientation of the platform. Then the shifts and phase corrections are applied to the filtered single-ping images and the coherent sum of the images is performed.

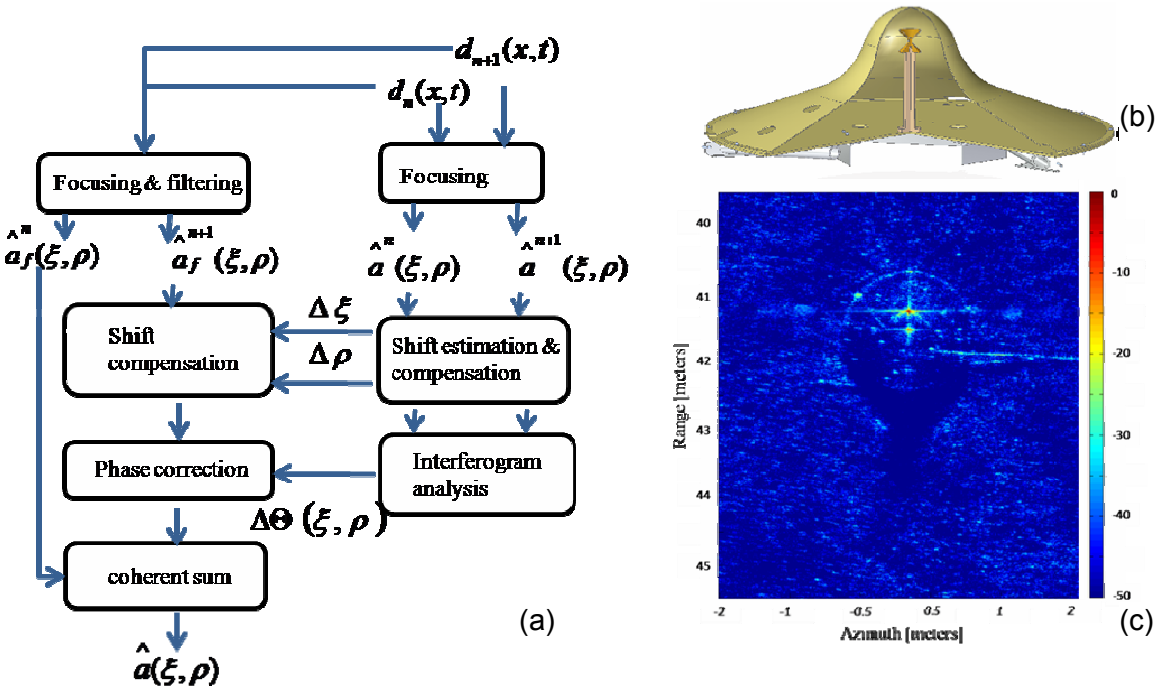

Fig. 3 (a) Block diagram of multiple ping focusing, (b) Design of the artificial targets distributed on the seafloor, (c) Amplitude image of the focused data around an artificial target.

Focusing results

In the context of the project, a number of AUV missions were conducted in an area close to the Cinque Terre coast in Italy. A set of man-made objects were distributed on the area of the seabed to be monitored (see Fig. 3(b)). The details of the experiment are described in the companion paper (De Paulis *et al.*, 2010). In Fig. 3(c) we show the results of focusing an area of the seabed around one artificial target. The colour scale is dB. The shape of the target and the strong scattering due to the bicone are clearly visible.

SYNTHETIC APERTURE SONAR INTERFEROMETRY

The co-registration step is fundamental in interferograms generation. Co-registration should account for orbit crossing, different sensor attitudes, sensor velocity variations, and propagation medium variations. The images are divided in small patches. The range and azimuth offset of each patch is retrieved by means of coherence maximization. In Fig. 4(b) and (d) we show the range and azimuth shifts of the image in Fig. 4(a) with respect to a master image of the same area. The coherence achieved with 20 minutes of interval between the acquisitions is reported in Fig. 4(c). The whole area shows high values of coherence. The block with the highest value of coherence is the one which contains the artificial target. After image co-registration it is possible to obtain the interferograms. Figure 5 shows the amplitude of interferograms coloured with the phases. The

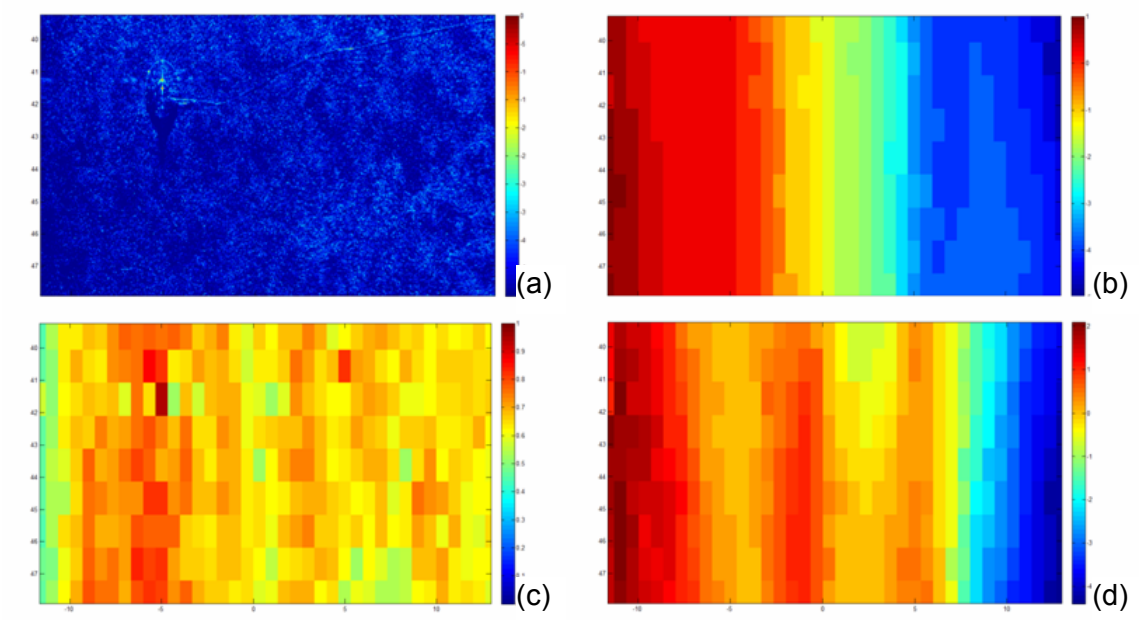

Fig. 4 Example of co-registration. (a) Amplitude of the area to be co-registered (dB scale). (b) Range offset field. (c) Coherence achieved after co-registration. (d) Azimuth offset field

temporal baseline of the interferograms in Fig. 5a and Fig. 5b is 20 and 40 minutes respectively. The interferogram in Fig. 5c has been obtained with a temporal baseline of one day. The statistics of natural target coherence and its behaviour with time were unknown before this experiment. From the interferograms in Fig. 5 it's clearly visible that there is high coherence of the seabed even with one day of time interval between the acquisitions. This is surely a necessary condition to measure altimetric variations. However, the fringes visible in Fig. 5 are mainly due to the relative motion of the platform during the two acquisitions. This suggests that this technique is particularly suitable for measuring altimetric variations of the seafloor that are high pass in space. On the other hand measurements of low pass spatial altimetric variations are more problematic since they require a very precise knowledge of the platform trajectory.

CONCLUSION

We have presented an SAS focusing technique for repeat-track interferometry applications and we have shown the results both of the focusing and the interferometry on a real data set. The data of each ping have been focused by means of a modification of the standard Omega-K algorithm widely used in SAR imaging. The shifts and phase errors due to the irregular motion of the platform have been estimated through the interferometric analysis between the focused images of consecutive pings. The results of focusing have been shown for an area around an artificial target placed for the experiment. Interferograms have been illustrated with a temporal baseline of between 20 minutes and one day. All the interferograms reveal high coherence of the seabed even with a one day time interval between the acquisitions. The high value of coherence obtained shows that it is possible to measure altimetric variations of the seafloor. Nevertheless the presence of many fringes due to the trajectory of the platform suggests that high pass spatial variations of altimetry are easier to detect than smooth altimetric variations.

Acknowledgments The present work has been carried out in the framework of a project lead and supported by ENI S.p.A. The authors wish to thank ENI management for allowing the present publication. They wish also to thank the staff of the NATO Undersea Research Center of La Spezia for their precious collaboration.

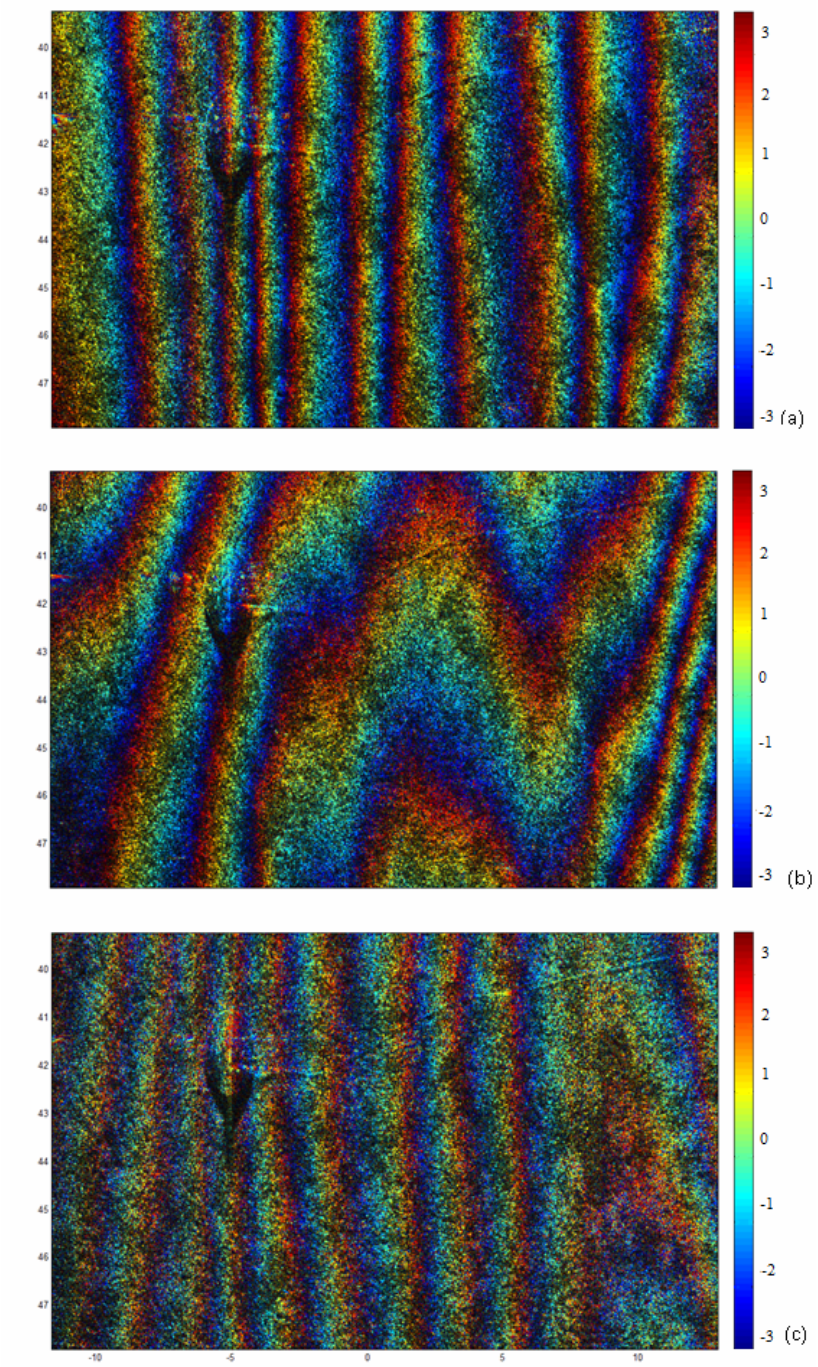

Fig. 5 SAS multipass interferograms: amplitude of the images coloured with phase. (a) The temporal baseline is 20 minutes, (b) The temporal baseline is 40 minutes, (c) The temporal baseline is one day.

REFERENCES

De Paulis, R., Biagini, S.; Carmisciano, C., Gasparoni, F., Guerrini, P., Prati, C., Rocca, F., Scirpoli, S. & Tesei, A. (2010) Acoustic monitoring of seabed altimetric variations by means of an AUV-mounted, high-frequency imaging sonar. In: *Land Subsidence, Associated Hazards and the Role of Natural Resources Development* (EISOLS 2010). IAHS Publ. 339, IAHS Press, Wallingford, UK, this volume.

Bellettini, A., Pinto, M. & Evans, B. (2007) Experimental results of a 300 kHz shallow water synthetic aperture sonar. Proc. Second 2nd Int. Conf. & Exhibition on Underwater Acoustic Measurements: Technologies and Results, June 2007.

Cafforio, C., Prati, C. & Rocca, F. (1991) SAR data focusing using seismic migration techniques. *Aerospace and Electronic Systems, IEEE Trans*. **27**(2), 194–207.

De Paulis, R., Prati, C., Rocca, F., Scirpoli, S. & Tebaldini, S. (2009) Focusing Synthetic Aperture Sonar (SAS) data with the Omega-K technique. In: *IEEE International Geoscience and Remote Sensing Symposium* (IGARSS, July 2009), vol. 1, 1-68–1-71.

(Proceedings of EISOLS 2010, Queretaro, Mexico, 17–22 October 2010). IAHS Publ. 339, 2010.

In situ compaction measurements via radioactive markers in the Northern Adriatic basin: an analysis of data precision over 15 years of monitoring

C. ZOCCATELLI[1], F. VERDECCHIA[1], G. CASSIANI[2], R. DEIANA[2] & N. FRATICELLI[2]

1 *ENI E&P Division, GEOD, San Donato Milanese, Italy*
federica.verdecchia@eni.com

2 *Geoscience Department, Padova University, Padova, Italy*

Abstract Deep compaction of sediments caused by natural gas extraction has been monitored in the Northern Adriatic basin since 1994 using downhole radioactive markers and both Schlumberger and Baker Atlas technologies for acquisition and processing. While laboratory techniques have been proposed to measure deep sediment compressibility (e.g. Hueckel *et al.*, 2001), marker measurements are still the key approach to this end. Currently six wells are equipped with markers and data are acquired on a yearly basis on five wells. In this paper we analyse the accuracy of such data starting from the raw count data. The analysis shows that accuracy of single peak determination depends on the signal/noise ratio, i.e. on the amplitude of the marker count peak with respect to the ambient background. This ratio in turn is an inverse function of marker bullet penetration into the well wall. We also analyse the propagation of this peak determination error into the data processing leading to the estimation of the marker interval length, and ultimately to estimates of compaction. The results show that while in some cases the nominal precision of 1 mm/10.5 m marker interval is achieved, for other wells the actual precision is substantially lower. These results shall be used to derive estimates of *in situ* compressibility having narrower confidence intervals.

Key words deep compaction; radioactive marker; gas extraction

OVERALL STRATEGY

The overall goal of this study is to define the precision relevant to the estimation of marker interval length, that directly feeds into *in situ* estimations of sediment uniaxial compressibility under reservoir depletion. The data available for this study come from five wells equipped with markers in the Adriatic offshore, that will be indicated here as wells A, B, C, D and E. The wells differ in terms of the depths where the markers are located and the time of marker placement, but they all cross loose sandy sediments of the northern Adriatic offshore. The study was performed in two steps: (a) first, we investigated the precision linked to the identification of one single marker location; (b) second, we propagated this uncertainty through the data processing algorithm to derive the precision of the marker interval estimates.

RADIOACTIVE MARKER DATA QUALITY ANALYSIS

The data are provided by the service companies in terms of gamma counts per second as a function of nominal depth TVDSS, for each of the four gamma sensors on the downhole tool. Since the tool velocity is fairly uniform, the shape of the gamma counts as a function of depth resembles the expected theoretical Gaussian distribution caused by a point source coincident with the radioactive marker. Therefore it is possible to fit each stretch of data with a Gaussian function, characterized by the following five parameters (see also Fig. 1):

– peak intensity,
– peak location,
– width of Gaussian curve at half-maximum (equal to 2 times the Gaussian standard deviation),
– mean noise level (computed away from the Gaussian peak itself), and
– standard deviation of the noise level (computed away from the Gaussian peak itself).

Copyright © 2010 IAHS Press

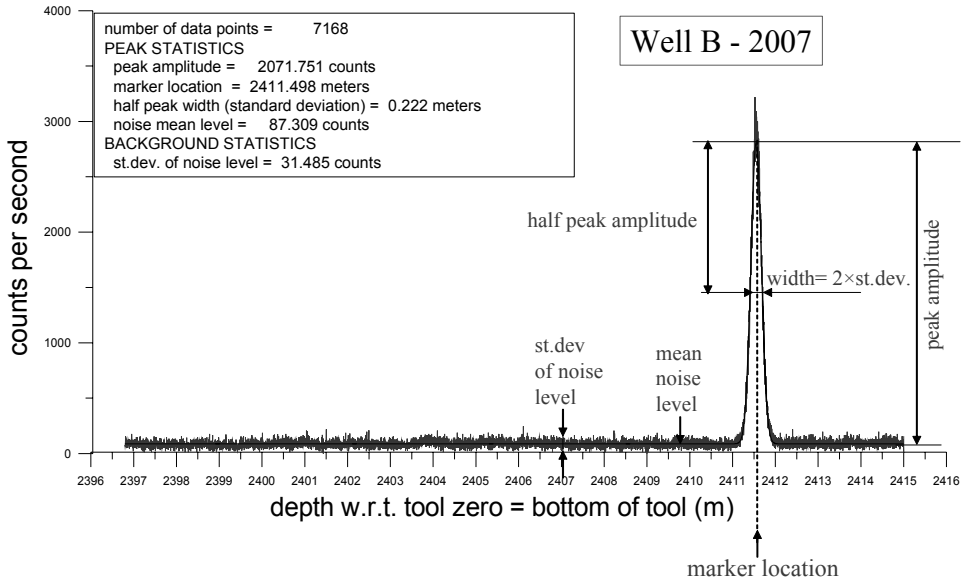

Fig. 1 example of Gaussian fitting of marker raw data: note the five parameters characterizing the data fitting. The example refers to Well B, having a fairly good data quality.

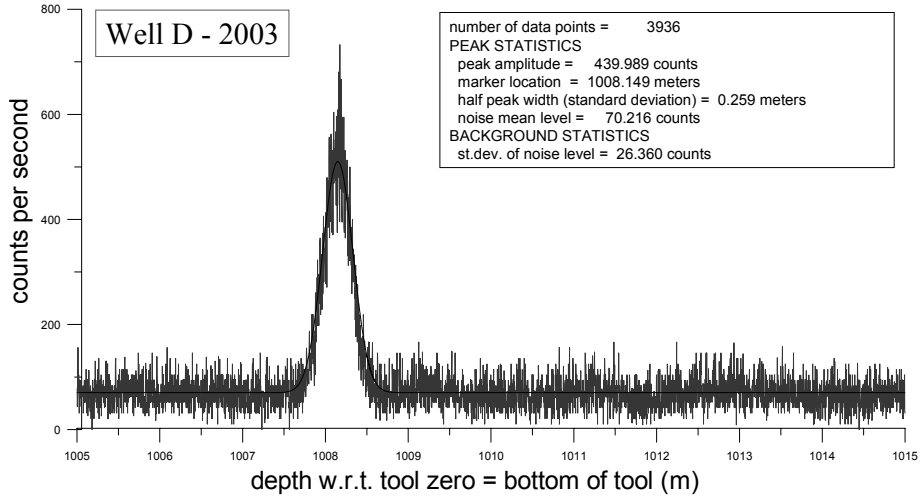

Fig. 2 example of Gaussian fitting of marker raw data. The example refers to Well D, having a bad data quality.

We analysed the entire data set fitting one Gaussian curve to each marker emission peak. Some important conclusions have already been reached at this stage of the study, i.e. peak amplitudes vary substantially from well to well. The maxima are observed in Well A, with more than 13 000 cps, while Well D has minimal peak amplitudes ranging around 400 cps (see Fig. 2).

Peak widths also vary from well to well, and an inverse correlation exists between amplitude and width. We interpreted this phenomenon as a consequence of the larger or smaller penetration of the marker bullets into the formation (a deeper markers has a wider, less pronounced gamma ray peak).

The noise levels, measured as mean value and standard deviation, show some variations from well to well. These variations, however, are orders of magnitude less significant than the corresponding peak amplitude variations.

The statistics of Gaussian fitting to all the marker emission peaks have been grouped well by well and acquisition by acquisition. The corresponding mean values have been used to generate "typical" noiseless emission peaks, one for each well and each acquisition date, and to contaminate each of these peaks with "typical" noise levels. Once a suitable set (10 000 Monte Carlo realizations) of such synthetic peak data has been generated, we applied the same fitting procedure used for real data. As a consequence we can compare the "true" marker location and the fitted marker location for each "typical" peak data set, and draw statistical conclusions about the goodness-of-fit. The corresponding statistics of accuracy in marker location identification are summarized in Table 1.

Table 1 Standard deviation (millimetres) of peak location fitting derived from the Monte Carlo analysis.

Well	1999	2001	2002	2003	2005	2006	2007	2008
A	0.34	-	0.40	0.69	-	3.02	3.08	3.04
B	0.23	-	0.41	0.42	1.87	2.73	2.80	2.10
C	-	-	1.33	-	-	0.29	0.37	0.33
D	-	-	2.87	-	3.19	31.09	4.13	47.72
E	-	1.12	0.74	-	-	-	-	-

UNCERTAINTY PROPAGATION TO MARKER INTERVAL LENGTH

The uncertainty in single peak identification, summarized in Table 1, has subsequently been used to derive the corresponding uncertainty in interval length estimation. To this end we used the description of the data integration procedure given by Pemper (1996). For each well and each acquisition: (a) we defined a reference marker interval to be considered as the "true" interval value between markers A and B; (b) assuming five tool passes, we simulated the detected location of A and B by adding an error derived from sampling Gaussian distributions with standard deviations as in Table 1; (c) on the basis of the synthetic readings above we computed the corresponding interval length; and (d) we repeated the above procedure in a Monte Carlo way with 10 000 realizations. The resulting corresponding standard deviation (our index of uncertainty) of the marker interval was found to be about half of the corresponding single peak standard deviation in Table 1. This is hardly surprising, as the operation of combining all readings of the four gamma detectors over all passes is an average procedure that reduces uncertainty.

CONCLUSIONS

Considering that compaction estimates are derived from *differences* of interval length over time, and using a simple variance combination law (t_1 and t_2 are two acquisition times, $\Delta t = t_2 - t_1$):

$$\sigma_{\Delta t} = \sqrt{\sigma_{t1}^2 + \sigma_{t2}^2} \tag{1}$$

it is possible to estimate the uncertainty associated with each compaction measurement. Table 2 shows the results for Well A.

Table 2 Estimated standard deviation (millimetres) of compaction measurements for Well A.

	Interval st. dev.(mm)	1999	2002	2003	2006	2007	2008
1999	0.15	N/A					
2002	0.18	0.23	N/A				
2003	0.30	0.34	0.35	N/A			
2006	1.32	1.33	1.33	1.36	N/A		
2007	1.35	1.36	1.36	1.38	1.89	N/A	
2008	1.33	1.34	1.34	1.36	1.87	1.89	N/A

This analysis has shown that the nominal precision of 1 mm in marker measurements is achieved under excellent conditions (ideal marker penetration, not too deep), but can be very optimistic in less ideal cases (e.g. Well D in our data set).

REFERENCES

Hueckel, T., Cassiani, G., Tao, F., Pellegrino, A. & Fioravante, V. (2001) Aging of oil/gas bearing sediments, their compressibility and subsidence. *J. Geotechnical & Geoenvironmental Engng* **127**(11), 926–938.

Pemper, R. R. (1996) Compaction Monitoring Instrument (CMI) – Results for AGIP Angela-Angelina Well Angela 14, Western Atlas Logging Services, Nuclear Technology Document NY/96-136.

(Proceedings of EISOLS 2010, Querétaro, Mexico, 17–22 October 2010). IAHS Publ. 339, 2010.

In situ formation compaction monitoring in deep reservoirs by using optical fibres

SHOJI KUNISUE[1] **& TATSUO KOKUBO**[2]

1 *Kanto Natural Gas Development Co. Ltd, 661 Mobara, Mobara City, Chiba Prefecture, 297-8550 Japan*
kunisue@gasukai.co.jp

2 *Kanto Natural 2 Taisei Kiso Sekkei Co. Ltd, 8154-59 Uenohara, Uenohara City, Yamanashi Prefecture, 409-0112 Japan*

Abstract We have devised a new *in situ* monitoring method for the amount of stratified compaction in boreholes drilled several hundred metres underground. Successful monitoring using this method is expected to enable a quantified evaluation of ground compaction associated with natural gas production in the future. This newly developed epoch-making monitoring system differs from conventional monitoring methods for land subsidence in that it is designed to continuously monitor the amounts of displacement in several sections separately, using optical fibres fitted in the sensor assembly.

Key words formation compaction; optical fibres; Southern Kanto natural gas field; natural gas dissolved in water; brine; Kazusa Group

INTRODUCTION

Gas fields distributed in the Southern Kanto region in Japan—collectively known as the Southern Kanto Natural Gas Field—are ranked among the world's largest for natural gas dissolved in water. In particular, the Kujukuri region of Chiba Prefecture not only has abundant reserves of natural gas dissolved in water but also a high concentration of iodine found in brine (in which natural gas is dissolved) that represent precious domestically-produced resources for a resource-poor country like Japan (Fig. 1).

The problems posed by land subsidence in this area were manifested in the late 1960s. Although land subsidence in recent years has been reduced in many areas, some places still experience land subsidence at levels exceeding 10 mm per annum, for which local residents are strongly demanding land subsidence control. The eight private corporations currently engaged in development in this area are making efforts to address environmental problems, including land subsidence, by organizing the Environment Committee of the Japan Natural Gas Association and Keiyo Natural Gas Association (hereinafter referred to as the Environment Committee).

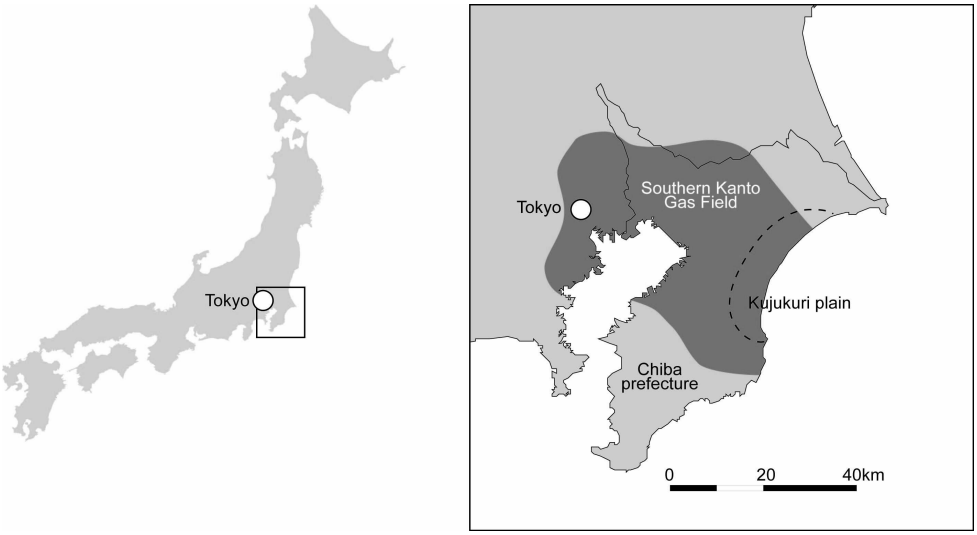

Fig. 1 Southern Kanto gas field in Japan.

Copyright © 2010 IAHS Press

IN SITU FORMATION COMPACTION MONITORING

Land subsidence is generally monitored by levelling and sometimes by a GPS survey or synthetic aperture radar using artificial earth satellites. However, all such methods are intended to monitor relative changes in the ground surface, and not to measure actual amounts of underground stratum compaction or expansion. The observation of *in situ* formation compaction in this study was focused on determining shrinkage or expansion in a certain underground section (Fig. 2). If such a monitoring method is applied to observe the formations from which natural gas dissolved in water and iodine are extracted, we will be able to acquire important data for examining the impact of pumping natural gas and brine on deformation of the ground surface. Moreover, such observational data may help elucidate the mechanism of how formation compaction develops deep underground, a subject not yet well known in the world.

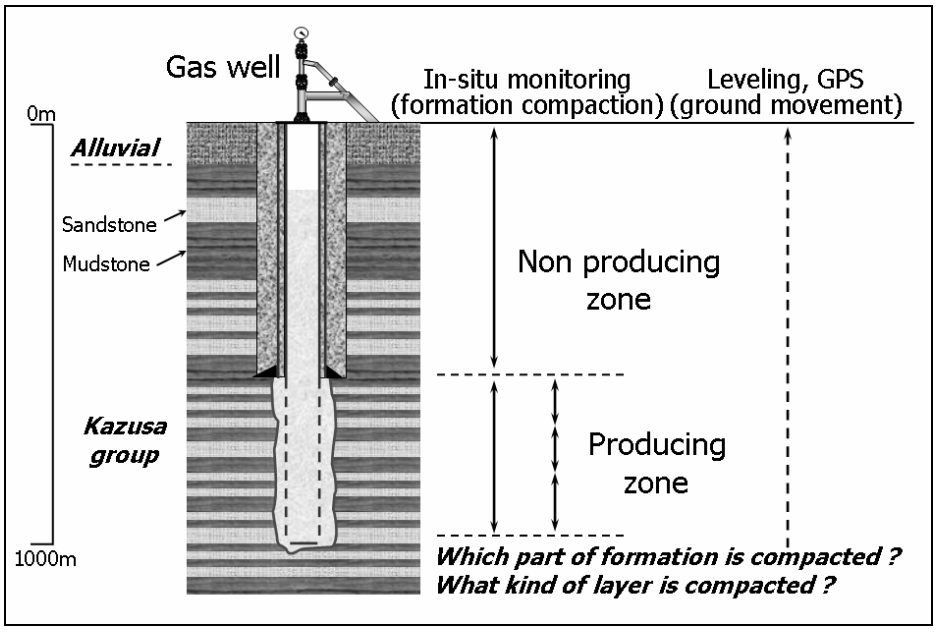

Fig. 2 Concept of *in situ* formation compaction monitoring.

The monitoring sites were selected from regions having an annual ground deformation rate of at least 10 mm as revealed by levelling performed by local governments every year. The monitoring sections were specified based on the lithofacies of formations. In this area, the natural gas dissolved in water is produced by pumping up brine from formations several hundred metres to 2000 m in depth. The gas reservoirs consist of marine sediments that accumulated 2.4 million years to 450 000 years ago, and formed with alternately stacked layers of sand and mudstone ranging from tens of cm to 2 m in thickness.

The monitoring system basically consists of the settlement gauges and rods used in displacement transmission. As a new approach, we introduced a system of using optical fibres as settlement gauges and transmission lines, with an eye on deformation measuring technology through optical fibre. The use of optical fibres is advantageous in terms of high accuracy as settlement gauges, which will most likely enable measurement of minute underground deformations, and of optical fibres communications with settlement gauges installed underground, reducing the number of cables needed.

In the measurement principle of the monitoring system, settlement gauges are installed at several places inside the borehole at a certain interval to monitor changes within the interval length. The settlement gauges are interconnected with rods. Each rod is fixed with an anchor at the

top end; its lower end is directly connected with an optical fibre sensor inside the lower settlement gauge. The optical fibre sensor (made of stainless plate) is designed to bend when pushed down by the rod. The lower part of the settlement gauge is equipped with an anchor mechanism that fixes the gauge directly to borehole. When the settlement gauge drops to the predetermined depth, the metal pad will expand in three directions as a result of the water pressure and be pressed against the side wall to be anchored. The pad is mechanically designed to prevent it from shrinking after being expanded.

CONCLUSIONS

We recently devised a monitoring method using optical fibre sensing technology to enable the observation of *in situ* formation compaction, an engineering subject posing a high level of difficulty, and established the necessary elemental technologies. We also conducted a verification test using a prototype and mostly succeeded in system development. We expect to demonstratively verify the applicability of the system under actual underground conditions by installing it in a shallow test well in the spring of 2010, as a first step.

Acknowledgements The content of this paper is based on the results of a joint study conducted by the Environment Committee of the Japan Natural Gas Association and Keiyo Natural Gas Association. The Environment Committee kindly permitted us to publish their study results in this paper. In addition, our field test and later activities presented in this paper were conducted with the assistance of Japan Oil, Gas and Metals National Corporation. We would also like to express our sincere gratitude to these organizations and their related companies.

REFERENCES

Davis, M. A. & Kersey, A. D. (1997) Fiber Bragg grating sensors for infrastructure sensing. OFC97, Dallas, WL15, 177–178.

Kersey, A. D., Davis, M. A., Patrick, H. J., LeBlanc, M., Koo, K. P., Atkins, C. G., Putnam, M. A. & Friebele, E. J. (1997) Fiber grating sensors. *J. Lightwave Technol.* **15**(8), 1442–1463.

Land Subsidence, Associated Hazards and the Role of Natural Resources Development
(Proceedings of EISOLS 2010, Queretaro, Mexico, 17–22 October 2010). IAHS Publ. 339, 2010.

Comparing several GPS post-processing strategies for a potash basin monitoring network in northeast Spain: first results

J. GILI[1], N. LANTADA[1], A. CONCHA[2], X. SOLER[3], C. PUIG[1] & J. MARTURIA[2]

1 *Technical University of Catalonia, UPC. Dept Geotechnical Engineering and Geosciences. c/ Jordi Girona, 1-3 (D2), 08034 Barcelona, Spain*

2 *Institut Geològic de Catalunya. c/ Balmes, 209-211, 08006 Barcelona, Spain*
aconcha@igc.cat

2 *GPS Global. c/ Àncora, 18, 08800 Vilanova i la Geltrú, Spain*

Abstract In central Catalonia territory (northeast Spain) underground salt mining activities have increased during the 20th century. As a consequence, subsidence has reached the surface in several urban areas underlain by Eocene evaporitic deposits of the Conca Potàssica (CK). The Institut Geològic de Catalunya built a monitoring network covering the western part of the basin with 36 vertexes for precise GPS measurements (2007 and 2008 campaigns) to investigate if general subsidence is occurring regionally within the area. With the objective to define differences in post-processing, five different procedures were tested, ranging from highly specialized and specific geodetic programs to simpler commercial ones. The results show that the different calculations are compatible to each other, and coherent with the final "map of displacements". The standard deviation for the vertical displacements is around one centimetre. This value corresponds fairly well with that expected given the equipment and methods in use.

Key words GPS; GNSS; monitoring; subsidence; potash mining

INTRODUCTION: THE CATALONIAN POTASH BASIN

The Conca Potàssica Catalana (Potash Basin, CK) is located in the so-called Central Catalan Depression, within the Ebre River Depression (Fig. 1). This Eocene sedimentary basin is made of a great saline unit, composed by an alternation of potash salts layers (mainly sylvinita and carnalita) (Marin, 1923). The potash salts have been traditionally exploited since Roman times, and are still the most important mining activity in Catalonia. The underground extraction rate increased in the 20th century at Balsareny, Cardona, Sallent and Súria cities (Marturià *et al*., 2006) where at certain points, total vertical displacements are about one metre in magnitude.

In 2007, the Institut Geològic de Catalunya (IGC, Geological Institute of Catalonia) established a monitoring network covering the eastern portion of the CK. A total of 36 geodesic vertexes from the Spanish geodetic network (ROI) have been selected for precise GPS measurements. In Fig. 1, an outer dark grey area maps the supposedly stable part of the GPS network, whereas the light zone in the centre is likely to be affected by the natural and anthropic subsidence in the near future since very deep the salt layers are located here. Up to the present, two campaigns have been performed (December 2007 and November 2008).

DIFFERENT STRATEGIES OF GPS POST-PROCESSING

The network was established in October 2007, before the measurements of the first campaign. Measurements were performed with six Leica dual frequency GPS receivers forming 6 vertexes, logging simultaneously. After a 10–12 hour session, 3 of the 6 receivers were moved to 3 new stations, and registering continued. With this procedure, the entire network was covered in about two weeks of fieldwork. One year after, the whole procedure was repeated for a second campaign.

For the post-processing, up to five different softwares have been compared. The first two, BERNESE (University of Berna) and the WARTK (Hernández-Pajares *et al*., 2006) are high level, wide area, very powerful software programs. Their use, however, is not straightforward. On the

Copyright © 2010 IAHS Press

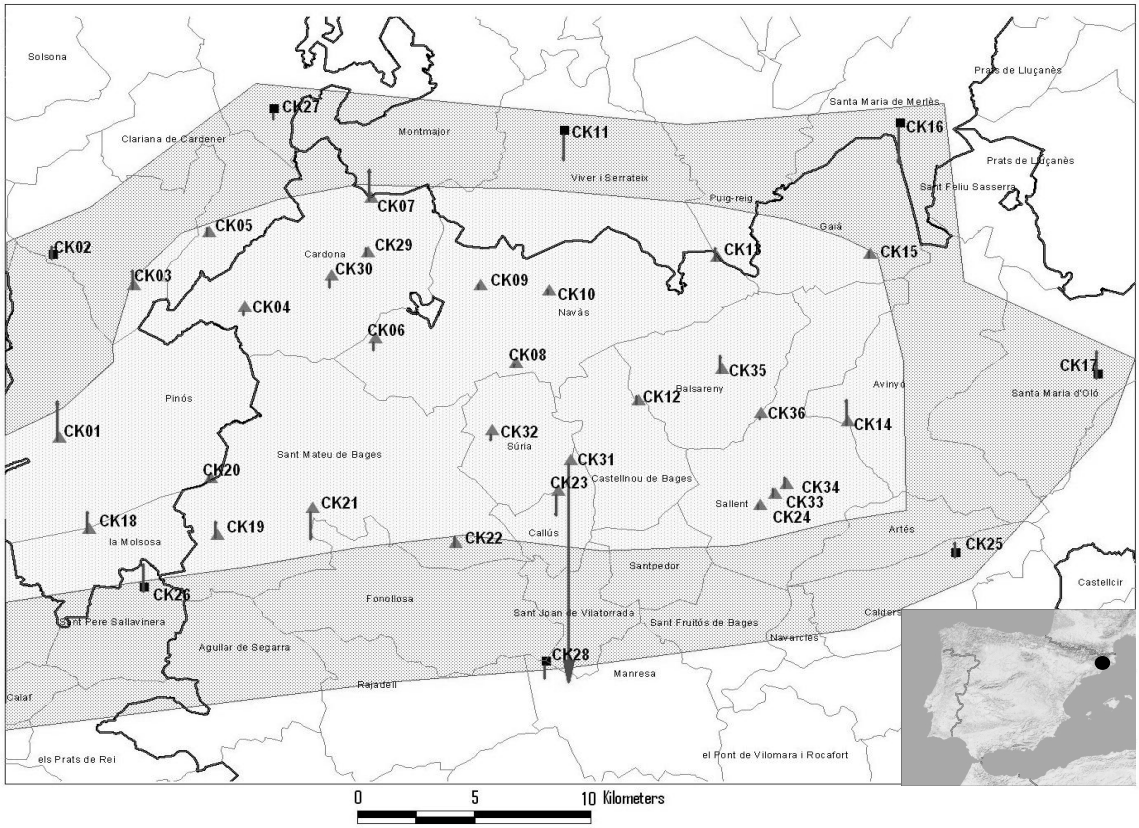

Fig. 1 General view of the east part of the so called Catalonian Potash Basin, Spain (inset). The 36 CK vertexes are highlighted. The elevation differences between 2007 and 2008, enlarged by a factor of 100 000 are shown as vertical arrows.

wide area, very powerful software programs. Their use, however, is not straightforward. On the other hand, the LGO (Leica), the TGO (Trimble) and the Topcon Tools (Topcon) are friendly-use commercial programs, but with some simplified assumptions. Besides the programs, different strategies and assumptions can be used for precise orbits and clocks; troposphere and ionosphere models, etc.

In addition, the reference "fixed" points considered as datum were also a crucial aspect. In this study case, for BERNESE and WARTK-POST computations, EUREF/IGS continuous reference points have been used (>100 km away); for the TGO calculations, points from the regional Catalonian ICC fiducial network (30–40 km apart) were used; finally, for the, LGO and Topcon Tools, no external-to-the-network fixed reference points were used. Although one can select several EUREF/IGS continuous reference points nearby, to monitor the local movements, a belt of stable points (such as the light grey perimeter in Fig. 1) is usually preferred.

RESULTS AND CONCLUSIONS

After the respective campaign post-processing, the differences in position were calculated. Five maps of displacement (similar to the one in the Fig. 1) have been cross-checked. The different sets of results are compatible to each other. Only one point, CK31, has experienced a really significant subsidence, about 9 cm, between the 2007 and the 2008 campaigns; there was no significant movement at the remaining vertexes.

Excluding the CK31 point, the statistics shown in the Table 1 give an estimation of the overall precision for each post-processing procedure.

Table 1 Statistics for the different post-processing approaches used. The apparent vertical displacements (Δh) for 35 stable points have been analysed. Mean and standard deviation (SD), expressed in metres.

WARTK-POST		BERNESE		LGO		TGO		TOPCONTOOLS	
Mean	SD	Mean	SD	Mean	SD	Mean	SD	Mean	SD
0.002	0.010	0.003	0.008	0.001	0.006	0.002	0.007	0.001	0.006

The mean of the 35 displacements is almost zero, which might indicate the stability of the 35 points during the two campaigns. The standard deviation, SD, an estimator of the actual precision of the network for measuring the displacements, is less than 1 cm for all the methods. This value corresponds fairly well with that expected given the equipment and methods used. We can state that the threshold for a significant movement is roughly 2 cm.

The highly specialized and specific geodetic software programs with long baselines (WARTK-POST and BERNESE) enable validation of the results (Δh) of the simpler commercial programs with local baselines (LGO, TGO and Topcon Tools) and the design of the CK network. Furthermore, in the forthcoming campaign of October 2010, a similar field procedure might be used; and the GPS data might be post-processed with commercial software.

REFERENCES

Hernandez-Pajares, M., Juan, J. M. & Sanz, J. (2006) Real time MSTIDs modelling and application to improve the precise GPS and GALILEO navigation. In: *Proc. Institute of Navigation GNSS* (Fort Worth, Texas, USA, September 2006), 1358–1368.

Marín, A. (1923) Investigaciones en la Cuenca Potàsica de Catalunya. *Boletín del Institut Geològic de España*, tomo XLIV, 3a. Serie, 458p.

Marturià, J., Diego, J. de, Martinez, P. & Roca, A. (2006) Implementation of a subsidence risk management system. *Proc. 5th European Congress Geoscientific and Information Systems* (Barcelona 2006), vol. I, S5: 434–436.

University of Bern. BERNESE. http://www.bernese.unibe.ch. BERNESE GPS software. Accessed 10 February 2010.

(Proceedings of EISOLS 2010, Queretaro, Mexico, 17–22 October 2010). IAHS Publ. 339, 2010.

Analysis of landslide monitoring using an e-GPS system and multi-antenna GPS technology

T. K. YEH[1], Y. S. HU[2] & Y. A. LIOU[2]

1 *Institute of Geomatics and Disaster Prevention Technology, Ching Yun University, 229 Jiansing Rd, Jhongli 320, Taiwan* bigsteel@cyu.edu.tw

2 *Center for Space and Remote Sensing Research, National Central University, 300 Jhongda Rd, Jhongli 320, Taiwan*

Abstract Based on GPS technology, this study monitored the movement of the landslide that impacted Taiwan's Formosa Freeway. Two monitoring systems and two data-processing software programs were employed. Auxiliary data were obtained from the GPS, raingauges, inclinometers, and water table meters for landslide analysis. The goal of multi-sensor monitoring was to construct an automatic early warning system for driver safety. Analytical results indicate that the landslide moved on average 1 cm/month in the southeast direction; that is, it moved slowly toward the Formosa Freeway, thereby posing a potential safety hazard for drivers. The positioning precision of the multi-antenna GPS (0.18, 0.25, and 0.57 cm in the north, east and vertical directions, respectively) was better than that of static relative positioning (0.29, 0.44 and 1.01 cm) and that of e-GPS technology (1.69, 1.35 and 2.45 cm).

Key words GPS; multi-antenna GPS; landslide; Taiwan

INTRODUCTION

In Taiwan, landslides on mountains are widespread and over-exploitation has increased the frequency of natural disasters such as landslides, rockslides, and debris flows. For instance, a large landslide occurred on the Kuanhsi section of the Formosa Freeway in the summer of 2004. This landslide ruptured the concrete slope protection, and compressed and deformed the drainage system. At the same time, a large soil and rock landslide damaged the road surface. Although no casualties occurred, it was a serious threat to driver safety.

Although some engineering reinforcement techniques, such as concrete piles, the anchor construction method, and drainage ditches, were applied to prevent further damage, the movement of the landslide warrants attention. This study adopted the landslide area as its study area and used a multi-antenna GPS system to automatically monitor landslide movement in real time under all weather conditions. Other measuring equipment, such as a ground-based LIDAR, raingauges, inclinometers, and water table meters, assisted in the analysis of GPS data. This study also used the e-GPS system (virtual reference station) to measure landslide displacement regularly. The multi-antenna GPS and e-GPS systems were compared to determine the benefits and drawbacks of different GPS techniques and determine the feasibility using GPS for landslide monitoring.

DATA COLLECTION AND ANALYSIS

Eight multi-antenna GPS (labelled P1–P8) were installed in the study area. The monitoring points and GPS antennas were uniformly distributed to monitor landslide movement. Furthermore, this study assessed the efficiency and functionality of the antennas and monitoring points under various topographical restrictions. Other automatic monitoring equipment assisted in GPS data analysis.

Figure 2 shows the average coordinates and standard deviation in the northern (N), eastern (E), and vertical (h) directions at point P3. The slope of the trend in the N direction was −0.0008 and displacement per month was −0.56 cm. Experimental results show that the landslide is moving southward, toward the Formosa Freeway. Conversely, the E direction has a positive trend slope. In this case, the slope value at P3 was 0.0003 and its monthly displacement was 0.21 cm. This analytical result shows that the landslide is sliding eastward, toward a low-lying area. In the h

Copyright © 2010 IAHS Press

Fig. 1 Experimental area and multi-antenna GPS system.

Fig. 2 Trends and standard deviations in the northern, eastern and vertical directions.

direction, the slope value was 0.004 and its monthly displacement was 2.8 cm. According to experimental data, the study area may be receiving pressure from the area at its top, causing the study area to rise in height.

The data collected by the multi-antenna GPS system were processed using MAGMS software version 2.32 and TGO software version 1.5. Table 1 shows the standard deviations measured by different methods, including the e-GPS and multi-antenna GPS systems; the data were processed by MAGMS and TGO. The precision of the multi-antenna GPS processed by MAGMS was the best of the three measurement methods. Conversely, the e-GPS system had poor precision.

Table 1 Standard deviation in centimetre obtained by e-GPS and multi-antenna GPS.

Point	**e-GPS**			**TGO**			**MaGMS**		
	N	E	h	N	E	h	N	E	h
P2	2.03	1.17	3.32	0.10	0.15	0.13	0.05	0.14	0.30
P3	2.05	1.91	2.12	0.36	0.29	0.75	0.28	0.27	0.87
P5	0.99	1.44	2.35	0.20	0.50	1.13	0.19	0.38	0.45
P6	1.69	0.86	2.02	0.16	0.06	0.69	0.19	0.16	0.34
P7	N/A	N/A	N/A	0.64	1.20	2.34	0.22	0.27	0.87
Average	1.69	1.35	2.45	0.29	0.44	1.01	0.18	0.25	0.57

CONCLUSIONS

Experimental results indicate that the landslide is moving in a southeastern direction. The monthly rate of movement was about 1 cm, directly toward the Formosa Freeway. The threat of this landslide hitting the Formosa Freeway must be monitored continuously. Although the e-GPS technology was faster and more economical than the traditional GPS system, it is only suitable for monitoring large movements.

Acknowledgements The authors would like to thank the National Science Council of the Republic of China, Taiwan, for financially supporting this research, under Contract no. NSC 98-2622-E-231-003-CC3.

REFERENCES

Ding, X., Dai, W. J., Yang, W. T., Zhou, X. W., Lam, J., Zhang, Q. & Wang, L. (2007) Application of multi-antenna GPS technology in monitoring stability of slopes. Strategic Integration of Surveying Services, FIG Working Week 2007.

Hu, Y. S. (2008) Monitoring three-dimensional deformation using multi-antenna GPS and virtual reference station. Master Thesis of Ching Yun University, Jhongli, Taiwan.

Luo, N. H. (2007) Application of resistivity image profiling method to monitor landside – A case study. Master Thesis of Ching Yun University, Jhongli, Taiwan.

Yeh, T. K., Hu, Y. S., Ding, X. & Chen, C. S. (2007) Landslide monitoring using multi-antenna GPS deformation monitoring system. AGU Fall Meeting, December 2007, San Francisco, California, USA, G13B-1239.

(Proceedings of EISOLS 2010, Querétaro, Mexico, 17–22 October 2010). IAHS Publ. 339, 2010.

Land subsidence observation using GPS on the Kujukuri Plain

D. MURAI[1], M. NAKAMURA[2], S. IKEDA[1], F. WAKI[3] & N. ISEZAKI[4]

1 *Kanto Natural Gas Development Co., Ltd. 661 Mobara, Mobara City, Chiba Prefecture 297-8550 Japan*
d.murai@gasukai.co.jp

2 *ISE Chemicals Corporation, 10230-15, Ichinomiya, Ichinomiya-machi, Chosei-gun, Chiba Prefecture, 299-4301, Japan*

3 *Nihon Tennen Gas Co., Ltd., Minamihinata, Shirako-machi, Chosei-gun, Chiba Prefecture, 299-4205 Japan*

4 *Earth Science Group, Graduate School of Science, Chiba University, 1-33 Yayoi-cho, Inage-ku, Chiba-shi 263-8522, Japan*

Abstract Land subsidence on the Kujukuri Plain in Chiba Prefecture, Japan, where several companies develop natural gas and iodine is likely caused by the pumping of brine. Therefore, the companies engaged in resource development have been involved in monitoring land subsidence using GPS in collaboration with Chiba University. The monitoring revealed that: (a) relatively significant subsidence is observed at GPS stations located in regions where natural gas and iodine developing activities are carried out, and that (b) GPS monitoring results indicate mostly the same trends as in levelling. We intend to continue monitoring land subsidence as a means to realize the voluntary management of land subsidence.

Key words Chiba Prefecture, Kujukuri Plain, Japan; natural gas dissolved in water; iodine; GPS; Southern Kanto Natural Gas Field, Japan; brine; land subsidence; levelling.

BACKGROUND

One of the world's largest, dissolved-in-water type of natural gas fields, collectively called the Southern Kanto Natural Gas Field, is distributed in the Southern Kanto area of Japan. (Fig. 1). In this area, natural gas and iodine is developed by pumping up brine from formations several hundred to more than a thousand metres in depth.

Levelling has revealed that land subsidence has occurred in this region, and the pumping of brine associated with the production of natural gas is inferred to be the primary cause. The natural gas and iodine developing companies in this area are making efforts to address environmental problems including land subsidence by organizing the Environment Committee.

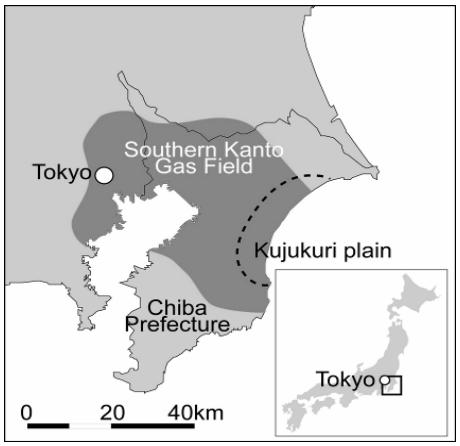

Fig. 1 Southern Kanto Gas Field.

LAND SUBSIDENCE OBSERVATION BY GPS

The Environment Committee has been monitoring land subsidence in Kujukuri Plain (KP) by GPS in collaboration with Chiba University since 2004.

The Environment Committee analyses the GPS data obtained by six monitoring stations established in the KP region together with GEONET (GPS Earth Observation

Copyright © 2010 IAHS Press

Table 1 GPS analysis conditions.

Analytical method	Static relative positioning
Baseline analysis software	Bernese ver 4.2
Base stations	IGS TSKB, USUD, and GENET Chosei
Analysis range	GPS stations in or near Chiba Prefecture
Ephemeris to be used	IGS precise ephemeris

Network system) developed by the Geographical Survey Institute. Table 1 summarizes the analytical method.

The coordinate values obtained from the GPS data are affected by variations of the base station coordinate values, which are set when analysing the data. When the land subsidence is examined by using GPS observation results, the baseline from a certain GPS reference station is thought to be the best method to avoid such effects. We selected Ohara station as the reference station that is regarded as meeting the following requirements:

(a) The reference station shall have been established for many years.
(b) The reference station shall be free from the effect of the pumping of brine.
(c) The reference station shall exhibit similar crustal movement to the KP region.
(d) The reference station shall exhibit similar atmospheric delay and ionospheric delay as in the KP region.
(e) The reference station shall be located near the reference point for levelling and enable easy comparison between GPS and levelling monitoring.

OBSERVATION RESULTS

Vertical movement

Figure 2 shows the results of vertical movement observations in Chiba Prefecture.

The KP region seems to exhibit relatively greater land subsidence than in other regions. Among others, a remarkably large movement was observed at Daida Station which resulted in land subsidence of about 120 mm over the course of six years. This is followed by the Oami, Nitten and Shirako stations each showing land subsidence of about 60 mm over six years. The KA Station and ZH-7 Station indicate large land subsidence velocities of 40 mm and 30 mm per two years, respectively, for their shorter observation periods.

The significant motion observed in August 2007 by some GPS stations around the KP region marked by ⬆ in Fig. 2 may be due to the impact of an earthquake that occurred off Kujukuri around the same time.

Comparison between GPS and levelling

We comparatively analysed the land subsidence data obtained by the GPS and the levelling. For the levelling, we analysed the observation results at the benchmark located in the neighbourhood of the GPS station (at a distance of about 1000 m). Figure 3 shows an example of the validation results.

Although differences are seen between the GPS and levelling in the absolute values of the observation results, partly because some levelling results do not fall within the error range for GPS, both survey methods indicated mostly similar trends in terms of changes in variations.

CONCLUSION

As stated above, the following findings were obtained from GPS monitoring:

GPS monitoring revealed that relatively significant land subsidence is observed at GPS stations located in the area where brine developing activities are carried out.

Comparison of the results of the levelling and GPS methods indicates mostly similar trends, although quantitative differences are seen between the two methods in terms of changes in variations.

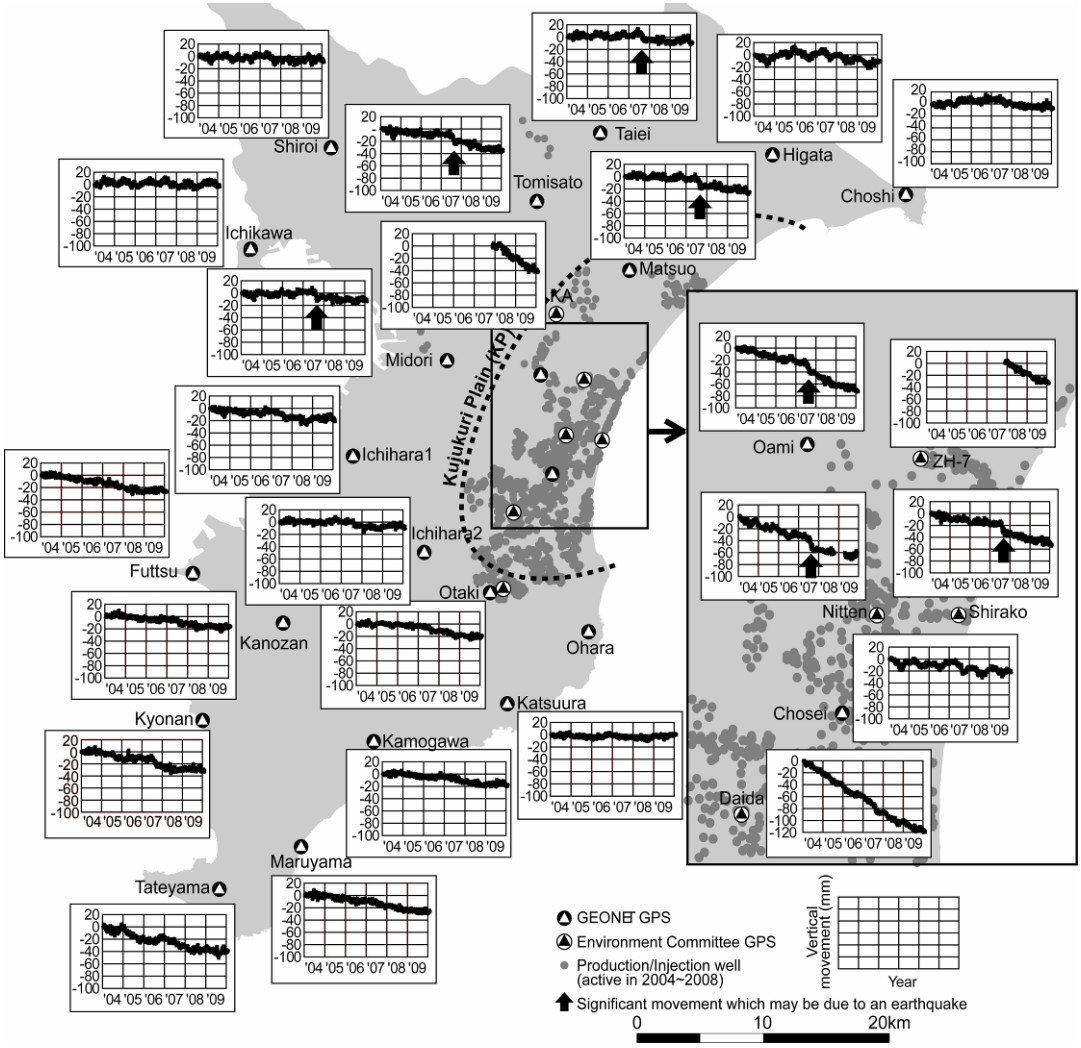

Fig. 2 Vertical movement observed by GPS. (Relative height from Ohara GPS, data on moving average for 10 days).

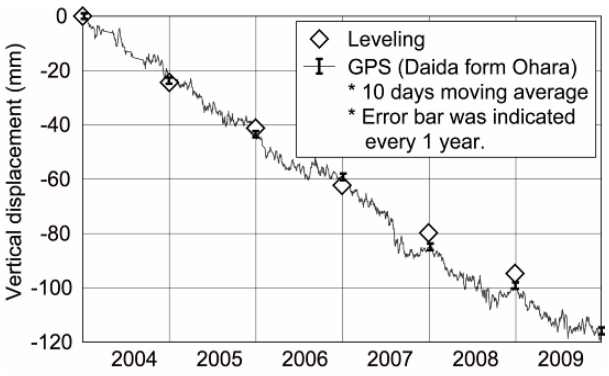

Fig. 3 The examination of comparison between GPS and levelling

SUMMARY

Natural gas and iodine developing companies on the KP in Chiba Prefecture established a GPS monitoring system for land subsidence in collaboration with Chiba University. We intend to continue monitoring land subsidence as a means to realize the voluntary management of land subsidence.

(Proceedings of EISOLS 2010, Querétaro, Mexico, 17–22 October 2010). IAHS Publ. 339, 2010.

Evaluation of Mexico City subsidence

G. AUVINET[1], **E. MÉNDEZ**[1] **& U. MATUS**[2]

1 Geocomputing Laboratory, Instituto de Ingeniería, Universidad Nacional Autónoma de México, Coyoacán 04510, Mexico D.F.

2 Students of the Instituto de Ingeniería, Universidad Nacional Autónoma de México, Coyoacan 04510, Mexico D.F.

Abstract Updated information concerning regional subsidence in Mexico City is presented. The punctual and spatial distribution of the elevations of 2064 benchmarks (SACM, GDF) and other references located in the former Lake of Texcoco are presented. Extensive use was made of new geocomputing tools. Useful geodesic and topographic works made in the middle of the XIXth century for the historic evaluation of the subsidence, are reviewed. Some indirect methods that could be used for a better monitoring of regional subsidence are discussed.

Key words evaluation; subsidence; leveling; Mexico City

INTRODUCTION

Today, the subsidence phenomenon, with over eighty years from Roberto Gayol's discovering, and more than sixty years from its scientific explanation by Nabor Carrillo (1947), persists with cumulative effects through time which causes differential settlements in the colonial and modern structures of Mexico City and lacustrine soil fracturing. Metropolitan installations as important as the metro system, the Gran Canal, and the water system Network suffer their effects too.

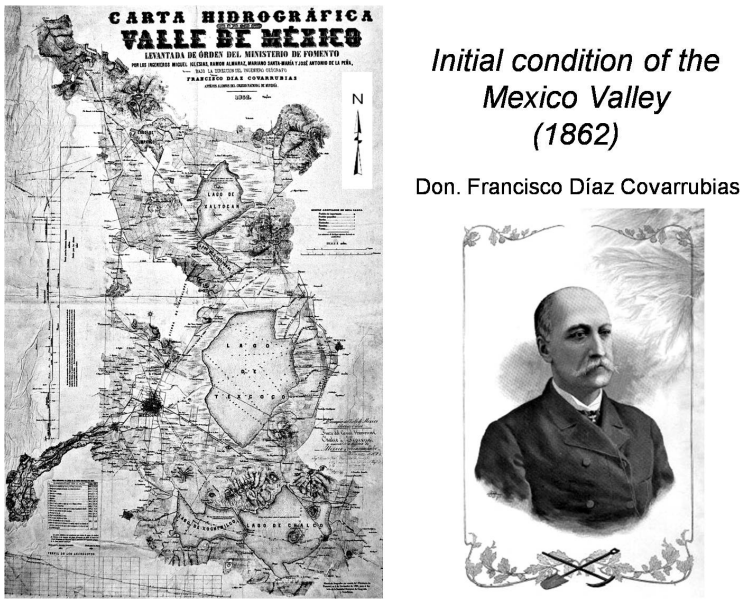

Fig. 1 Geographical positioning of points on the ground.

FRACTURING GEOGRAPHIC INFORMATION SYSTEM (SIG-G)

Thanks to the historic information which has been possible to gather with the support of different institutions among which stands out the Water System of Mexico City (SACM) of the Federal District Government, it has made the reconstruction of the subsidence history in three sites in the Historic Center of Mexico City.

Copyright © 2010 IAHS Press

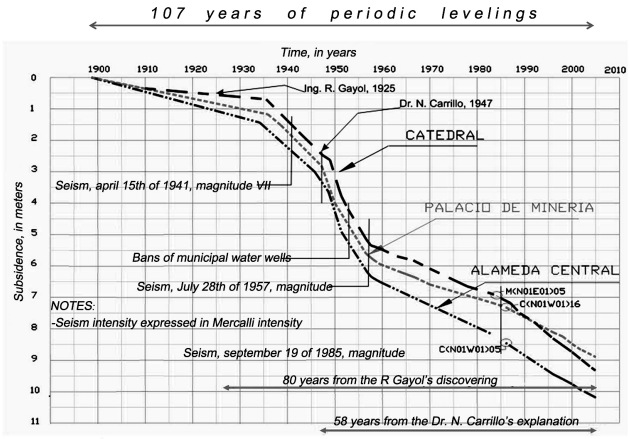

Fig. 2 Punctual evolution of the mean subsidence for the period 1898-2005.

In order to make the estimations of the spatial distribution of the subsidence in the former lacustrine area, it was necessary to build a Geographic Information System for the benchmarks, SIG-BN. From the contour map of same elevation it was constructed the model that gives the cumulative configuration through the time of the surface relief in the bottom of the former lakes.

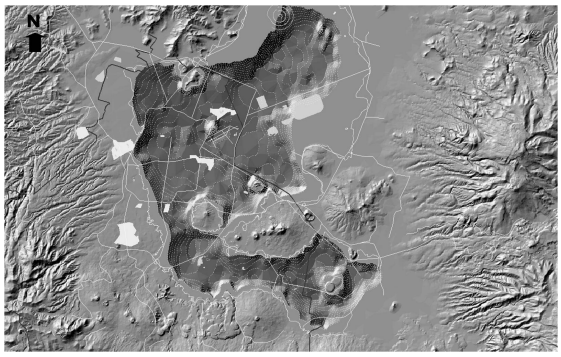

Fig. 3 Relief of the former lakes of the Mexico Valley surface.

Figure 4 shows the subsidence speeds for the period 1998-2002. The sites with more celerity (40 cm/year) are shown at the east side of Tlahuac and Nezahualcoyotl City (in front of the Marquez hill).

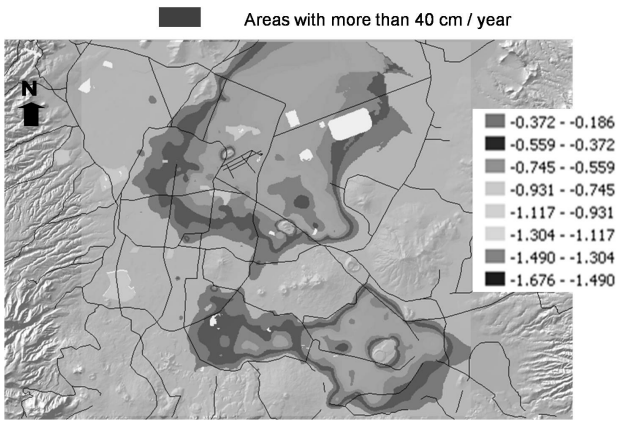

Fig. 4 Relief of the former lakes of the Mexico Valley surface.

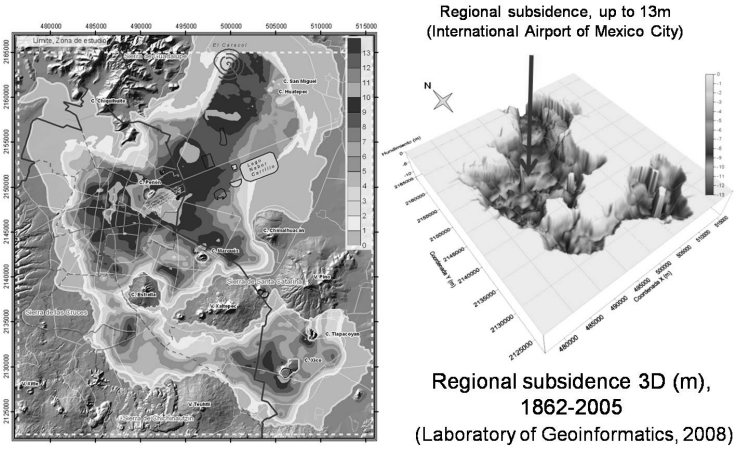

Fig. 5 Subsidence of the lake area.

Figure 5 shows the spatial distribution of the mean estimated subsidence for the period 1862-2005 (143 years) in the areas were damages exist.

Actually, to evaluate the regional subsidence in Mexico City a periodic leveling has to be made to a network of 2050 benchmarks. The subsidence is determined with the elevation differences in a same benchmark at different dates. These leveling tends to leave off practical and to generate some doubts due to the great urban extension to leveling, which transforms in very laboriously and time-consuming works. However, there are currently new technologies which employ direct and indirect methods which take off to evaluate the vertical movements of big surfaces; as well as their monitoring. These new technologies day to day get better, and it is expected in a short time, substitute the traditional techniques.

There exist 3 methods, one direct, the Differential Global Position System (GPS), and two Indirect methods, the Interferometry of synthetic aperture radar (InSAR) and the Light Detection and Ranging system, LIDAR (technique for the detection and measure through the laser light).

CONCLUSIONS

The effort made by different groups, in particular by the Geocomputing Laboratory of II UNAM to achieved a satisfactory evaluation of the subsidence phenomenon, as well as of others aspects of the geotechnical problematic, like the soil fracturing, has allowed to obtain useful and promising results but it just constitutes the first stage of a huge work which should be followed on systematic way in the future.

The will continuity to conduct these studies and the mobility of the required media for its realization is essential to obtain results each time more satisfying.

REFERENCES

Auvinet, G. *et al.* (1995) Sistema de Información Geográfica para Sondeos Geotécnicos. Proc. Xth Pan-American Conference on Soil Mechanics and Foundation Engineering, vol. 1, 312–324. Guadalajara, Mexico.

Auvinet, G. *et al.* (2005) Caractérisation géostatistique du sol de la vallée de Mexico. Revue Française de Géotechnique, N^0 110, Paris, France.

Carrillo, N. (1948) Influence of artesian wells on the sinking of Mexico City. Second Internation Conference on Soil Mechanics and Foundation Engineeering, Netherlands.

Juárez, M. & Auvinet, G. (2000) Caracterización geoestadística del subsuelo del Valle de México. XX Reunión Nacional de Mecánica de Suelos, Oaxaca, Mexico.

Marsal, R. & Mazari, M. (1959) The subsoil of Mexico City. Contribution to Ier Pan-American Soil Mechanics and Foundation Enginering Conference, Facultad de Ingeniería, UNAM, México. Reedited (spanish-english) in 1969.

Méndez, E. (1991) Evolución de las propiedades de la arcilla de la Ciudad de México. Bachelor degree Thesis, ESIA-IPN, México.

5 Social and Economic Impacts and Their Incorporation into Resources Management Strategies

Land Subsidence, Associated Hazards and the Role of Natural Resources Development
(Proceedings of EISOLS 2010, Querétaro, Mexico, 17–22 October 2010). IAHS Publ. 339, 2010.

Review of subsidence management in the Netherlands

F. B. J. BARENDS[1,2]

1 *Deltares, PO Box 177, 2600 MH Delft, The Netherlands*
frans.barends@deltares.nl
2 *TU Delft, CITG, PO Box 5048, 2600 GA Delft, The Netherlands*

Abstract The Dutch Ministry of Economic Affairs, which deals with concessions, directs the supervision of oil- and gas-induced land subsidence and its impact on the environment. The Mining Law dictates that the subsidence process has to be monitored during production and to be compared to the prediction provided in an exploitation plan, the basis of a concession. The accuracy of monitoring and its interpretation is essential for the production stated in the plan. The Dutch Technical Committee on Land Movement (TCBB) is the advisor of the Ministry in matters of concessions and damage claims related to subsidence and induced vibrations. Recently, the Committee has reviewed the different methods of prediction and validation, since various methods may produce different answers, which gives rise to speculation, dispute and suspicion. The outcome of the review is considered to fit the existing law and resulted in an outline for a practitioners guide to be created by the industry. This paper describes the Dutch supervision system and explains the different issues and the chosen way to proceed.

Key words subsidence; monitoring; interpretation; guideline; jurisprudence; policy

INTRODUCTION

It is essential that direct and indirect causes of land subsidence effects can be quantified with sufficient accuracy from a technical and scientific point of view. Laws and jurisprudence provide the legal framework within which claims and mitigations are accepted (Barends, 2000). The discrepancy between the insight of stakeholders, public opinion and legal rules is sometimes so substantial that common sense is lost, which frustrates everybody. Freeze (2000) provides a template for working towards consensus in multiple stakeholder scenarios when negotiating land subsidence strategies. The template is based on concepts of decision analysis to lay out a holistic framework for adversarial conflicts involving technical, social, economic, legal and political aspects. Adversaries are due to the unavoidable presence of uncertainties in land subsidence issues of cost, benefits and risks. Guidelines (e.g. Gambolati, 2005) can provide a basis for appropriate actions to be taken in the planning of underground resource exploitation activities, in order to ensure appropriate measures are taken to safeguard the environment and guarantee a sustainable development of the resource.

This paper adds to the guiding literature by focusing on new development of the process and regulations of subsidence monitoring in the Netherlands, which was initiated after some controversial cases. The Dutch situation is, however, a special case. It is a typical lowland delta, 60% of it surface is below sea level and it is densely populated with high capital land use, where land subsidence of centimetres is critical.

DUTCH LEGAL FRAME FOR LAND SUBSIDENCE

Dealing with uncertainty and risk

In the literature (Staveren, 2006, 2009) risks are categorized according to the certainty of their occurrence and related consequences. They represent a range with at one end completely uncertain risks and at the other end unambiguously well-defined risks. To risks with a well-defined probability, based on sound scientific proof, the concept of own responsibility or solidarity applies. In juridical terms, the principle of prevention prevails. Somewhere in the range, the uncertainty of the probability and consequence of a risk is so large that it is not possible to have sufficient control. To these risks the principle of precaution prevails. This implies that a proactive policy

Copyright © 2010 IAHS Press

should be adopted, which is based on presumptions about possible consequential damage without sound scientific proof. Finally, unknown risks exist for which preparation is not possible.

Three aspects are distinguished in the application of the principle of precaution for human activities in the subsoil: scientific uncertainty, damage threshold and reversal of the burden of proof. From a scientific view, natural processes in the underground are uncertain because of complexity, variability, limited transparency and limited knowledge of long-term effects. Therefore, the type and gravity of related damage is unsure. Before mitigating measures can be or (in a juridical sense) must be taken, the potential damage threshold must be determined. Here, the concept of non-negligible damage with regard to the natural environment prevails, or more precisely, irremediable damage. For the built environment, the criterion is often aesthetic damage, or worse, user damage and structural damage. Because of the lack of knowledge about long-term effects, the determination of an appropriate damage threshold is troublesome. In some cases, a lower boundary can be based on historic evidence, provided the natural system has not changed. This approach has been used for the assessment of the environmental room for gas production in the Wadden Sea (northern Netherlands, Fig. 2).

The principle of precaution is combined with the concept of reversal of the burden of proof. The provoker should demonstrate that his mitigation measures do exclude or sufficiently reduce the uncertainties and related risks, within his capability and according to the state of the art. This applies for induced land subsidence.

Laws and procedures for damage and environmental impact

In the Netherlands, extraction of materials (ores, salt) from a depth below 100 m and gas and oil from a depth below 500 m is regulated in the Mining Law. The first law, the "Code Minier", was settled in 1810 during Napoleon's rule. It dictated the conditions to be satisfied by mining companies in order to obtain a permit for exploration or a concession for exploitation. Since 2003, a new Mining Law has applied in the Netherlands, which also foresees the future use of the underground. This addition was opportune, because the underground becomes more exploited not only for mining, but also for storage and geothermal energy. The law supports and guarantees a safe and sustainable use of the underground.

The Ministry of Economic Affairs grants mining permits and concessions. The State Supervision of Mines (SodM) checks the compliance of the mining regulations from the safety and environment perspectives. The Mining Law states that data collected by the mining companies will be made available with a time delay of a maximum of five years. In the Mining Law, the tasks of the Mining Council and the Technical Committee on Land Movement (TCBB) are defined. The Mining Council advises the Minister on matters of exploration and exploitation of minerals and earth heat, and of their storage. The TCBB has the task to advise the Minister on mining-induced land movements (subsidence and earthquakes). Upon request, this committee also investigates and advises individuals for a fee of €90 and others for €180 on the cause and size of material damage by land movement, when it can reasonably be related to mining. The Dutch Mining Law recognizes the Mining Damage Guarantee Fund, when a mining company does not exist any more; it falls under the auspices of the TCBB.

Some regions in the Netherlands have a special agreement with a mining company for the compensation of damage related to induced land subsidence in their territory. In that case, a specific commission is established that evaluates related claims. This is the case in Groningen (Fig. 1).

Under the wings of the TCBB, two thematic platforms are active, in which the industry plays a strategic role. In the Technical Platform Earthquakes (TPA) mining companies gather with research institutes (TNO, KNMI) and SodM to initiate research on mining-induced earthquakes (Fig. 1) and to define the Seismic Risk Analysis Protocol, which is mentioned in the Law. Recently, an initiative was taken to establish the Technical Platform Surface Motion (TPB) where mining companies gather with research institutes (TNO, Deltares) and SodM to define a protocol for land subsidence monitoring and interpretation, which fits into the Dutch Mining Law.

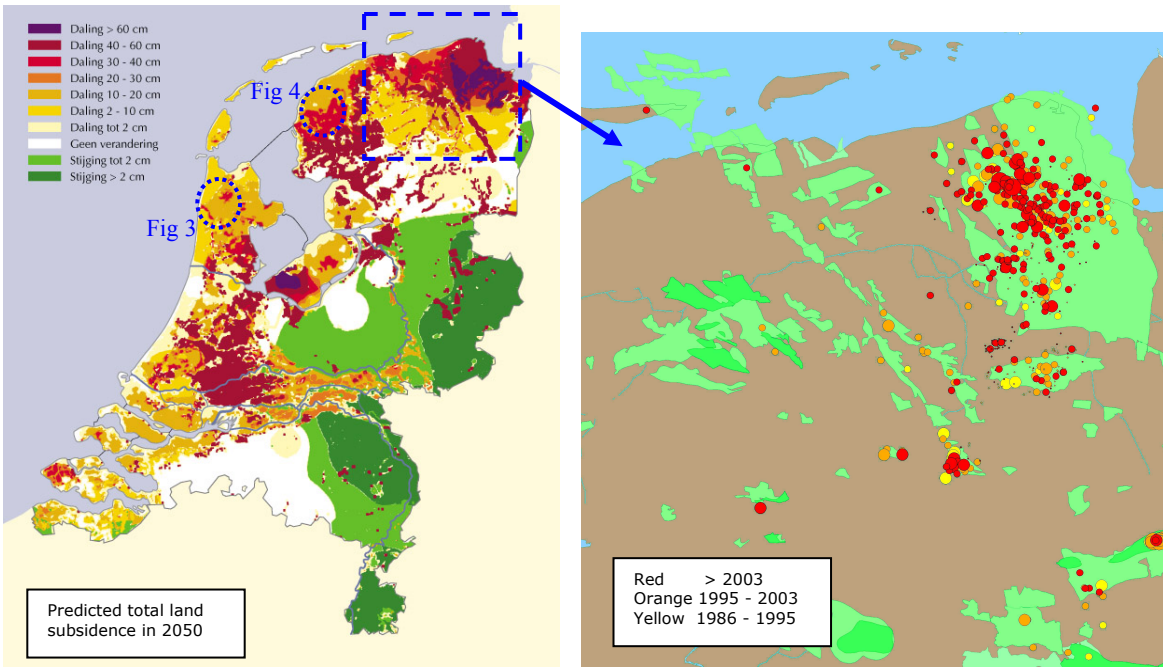

Fig. 1 Predicted subsidence (left) in the Netherlands and induced earthquakes (right) in Groningen.

Since 1961, the Subcommittee on Land Motion and Sea Level Change of The Netherlands Geodetic Commission (NCG) has been active in reviewing and stimulating research and development in the field of land subsidence, and lately in raising public awareness of the processes that cause subsidence and induced soil vibrations, and its consequences.

Since 1974, The Netherlands Oil and Gas Exploration and Production Association (NOGEPA) represents the interests of members, associates and society in general. Following closely the developments in safety, sustainability and climate, NOGEPA constantly seeks an optimal balance between economic viability and responsible operations. In 2007, the Union of Dutch Companies in Geodesy (VNBG) and the Business Platform Geo-informatics merged into Geo-Business Netherlands. NOGEPA and Geo-Business Netherlands represent a powerful voice from the industry and consulting sector, with sound authority and wide support.

On the European level, the Soil Thematic Strategy (COM 2006, 231) and a proposal for a Soil Framework Directive (COM(2006) 232) are adopted with the objective to protect the underground. The strategy and the proposal have been sent to European institutions for further steps in the decision-making process. Important issues are the maintenance and protection of functions, the restoration of polluted zones and biodiversity (subsoil ecology). In future this directive, when ratified, will have an impact on mining activities and their effects.

Since in addition to mining various other human activities and natural processes can cause land subsidence, a similar level of regulations would be effective, but this is not the case. In the Netherlands, all groundwater extraction and infiltration from depths less than 500 m is covered by the Groundwater Law (2006), which is regulated by provincial authorities. It addresses discharge quantities and water quality aspects, but not specifically the induced subsidence. Damage claims can be submitted to a provincial authority that may decide to investigate. There is in fact an imbalance in the legislation concerning land subsidence. Only the subsidence induced by deep mining activities is legally well covered.

Jurisprudence

In August 2007, the Administrative Justice Department of the Dutch Supreme Court dismissed all claims made against the Government decree in 2006 to permit gas production under the Wadden

Fig. 2 Location of gas fields (green) around the Wadden Sea, a natural protectorate.

Sea, a natural protectorate (Fig. 2). Environmental organizations such as Bird Protection Netherlands and the Foundation for Nature and Environment had appealed against this decision. Their claim was that the land subsidence, which might occur because of gas production, would have harmful effects on the natural values of the area. The judgment of the Supreme Court implies that gas production from on and near shore gas fields may continue, under special conditions.

Two workshops (2000, 2005) have been held concerning the environmental impact of gas production on the protected natural area of the lagoon Wadden Sea. Independent experts concluded from extensive monitoring over 15 years that no measurable effects to the natural characteristics have been observed. These findings became the basis of a positive advice with regard to gas production by the Dutch EIA Committee in 2006, which supports the governmental decision in 2005 to permit the gas production. Several objections were filed through the legal system but the Dutch Supreme Court dismissed all claims in 2007.

The Supreme Court concluded in its verdict "*on the basis of the best scientific knowledge it is guaranteed that gas production will not affect the natural characteristics in the area*". Following European guidelines, this is required for such projects. In the last 10 years, the knowledge has increased and for the evaluation of the impact of gas production in the area, the best scientific available knowledge has been used. The Court's opinion is that sufficient research has been carried out on the consequences of gas production. This research has shown that the consequences are limited for these areas; the Court accepted that "*there is no scientific doubt*".

In its judgment, the Supreme Court considered that "*the development and size of the land subsidence can not be predicted with complete certainty*", but that in spite of "*the reality of a certain margin in the expected consequences, the required certainty can be offered that no harmful effects will occur to the natural characteristics of the areas*". It does not imply that uncertainties do not exist. Over a long period of production, there may be consequences. Even if in future it appears that the prognosis is underestimating subsidence, it does not imply, according to the Court, that permanent effects have already arisen. It has been shown to the Court that the rate of land subsidence due to gas production will not increase after stopping of the gas production and that for the situation considered retardation effects are likely to take place within a period of 1.5 to 3 years. For this type of project, the possibility is included to check the potential effects of gas production by the so-called "hand on the tap" principle. This principle is an important control mechanism that,

with regard to the long period of gas production, "*can serve as to continuously guarantee the required certainty*", according to the Supreme Court.

The Supreme Court has accepted the suggestion of the Ministry of Economic Affairs to adopt the 2-cm contour subsidence line as a boundary outside which effects on shore are not noticeable. The Supreme Court accepts the results of the presented hydraulic studies that show that the gas-production induced land subsidence in the area will not cause a noticeable change in the sediment composition offshore and that the induced small changes in water motion and currents will not influence the sedimentation process. Considering the very slow process of land subsidence, the Court finds that proven mitigation measures can be implemented which compensate possible settlements of water defense structures and sluices and hence compensate for land subsidence.

For the first time, the Supreme Court has made a judgment about this type of projects, i.e. of grand-national interest. The Parliament has indicated that the production of gas is of great importance for providing security of supply for the Dutch people, and because of the large contribution, which this gas makes towards the Dutch economy and welfare. Against the verdict of the Supreme Court no higher appeal is possible. This jurisprudence can be used in similar situations elsewhere abroad.

DISCREPANCES IN GEOMETRIC ANALYSIS OF SUBSIDENCE

Frequently, disputes arise, amplified in the media, about the reliability of the results of subsidence monitoring and its environmental effect. The objectivity of the players is often in discredit, fed by differences in the opinions of specialists, leaving society in distrust. Wikipedia states that a fact is objective if it is independent of people's opinion, i.e. when no interpretation is required. For the analysis of subsidence, which naturally has a great deal of uncertainty, pure objectivity is not realistic. Society's confidence can be attained when third parties can reproduce results along alternative lines of reasoning. For issues of land subsidence, instead of objectivity the concept: "credibility = impartiality × professional quality" should be adopted. Indeed, professional experience and individual specific knowledge of the location are indispensable. Two illustrative examples are given: the case along a Dutch sea dike above a gas field and a case where both salt and gas mining take place.

Effect of a large sea dike enforcement

Along the Dutch coast (for the location, see Fig. 1), near the Hondsbossche Sea Dike, gas fields are exploited and the local monitoring network provides information about the subsidence rate. Three of the benchmarks are located on the edge of the massive dike: numbers 14C124, 14C125 and 14C126 (Fig 3(a)).

The gas-production induced subsidence is an important issue, since the dike level is crucial in the flood defense of the lowlands behind. Benchmark data are available from 1981 until the present. A sophisticated analysis of the subsidence, adopting a kinematic model (Fig. 5) has been worked out by Houtenbos (see Barends *et al*., 2008) for the period 1981–2003. The results are shown in Fig. 3(b), pattern 1 (left). The three benchmarks in the dike toe are marked by inverse triangles. The coastal dike seems to be subject to a serious subsidence rate, demanding dike reinforcements much earlier than anticipated, and leading to excessive maintenance cost.

However, history reveals that massive dike reinforcement took place during 1977–1980. The dike crest was raised from 8.50 m to 11.50 m above the average sea level. The added dike "body" caused consolidation in the underlying soil that resulted in attenuating settlement for several years. The subsidence data of the three benchmarks in the dike toe are therefore seriously affected by this temporary settlement.

Accounting for this effect, the subsidence rate pattern becomes significantly different, as depicted in Fig 3(b), pattern 2 (right). The subsidence rate along line A–B shows that proper incorporation of the temporal settlement effect reduces the subsidence rate by a factor 2. The

Fig. 3(a) Benchmarks at the Dutch coast (Hondsbossche Sea Dike).

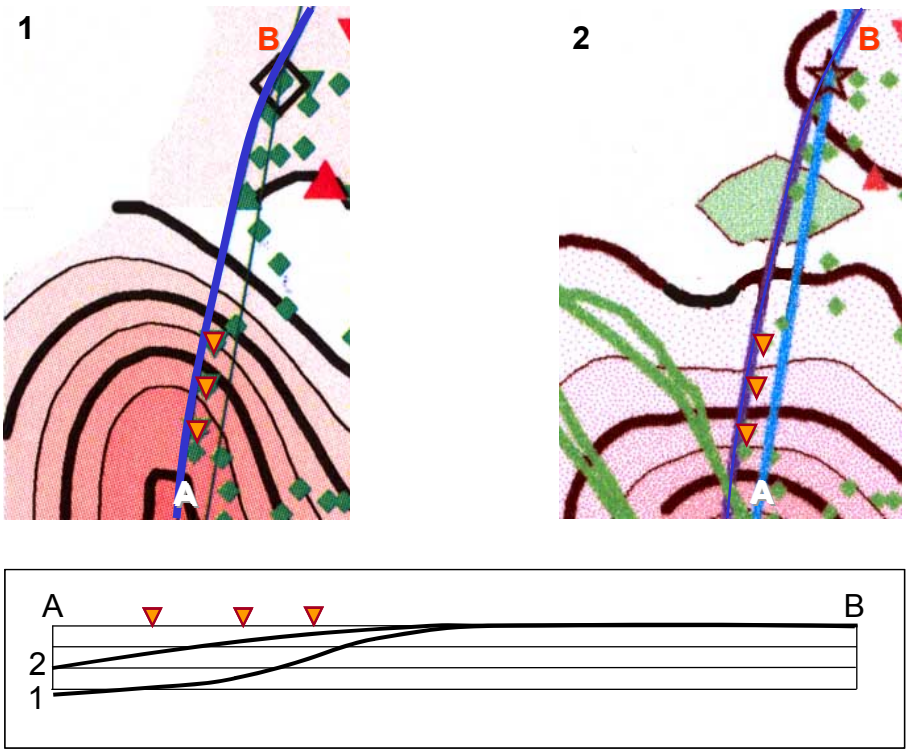

Fig. 3(b) Subsidence rate; different interpretations due to lack of information/experience.

geodetic analysis provides a high accuracy, but when assumptions are not correct or information is incomplete, results may be misleading.

Comparison of different monitoring methods and interpretations

Near the city of Harlingen in the province Friesland, gas production and salt extraction at three different locations (caverns) started in the 1980s. Strict conditions are posed for the induced land subsidence by the authorities and frequent monitoring is performed to track and check the subsidence. Various methods, i.e. spirit levelling and InSAR, and data interpretations caused different results of critical subsidence behaviour and hence a vivid discussion arose amongst experts, and in the press.

In Fig. 4, the total subsidence is shown as obtained from the various sources and interpretations (see also Muntendam, 2009). The two spirit levelling results, 1 and 2 deviate because of a different judgment of the stability of some benchmarks (in the dotted circle). The InSAR, result 3, does not show the sharp bowl (above the salt caverns), because the area there is agricultural land with very poor reflecting capacity.

These differences show that even if each method is correctly applied with care and the correct accuracy, still the outcome depends to some extent on subjective choices or unfortunate conditions. This fact urged the TCBB to review the geodetic analysis procedure and invite experts and industry to improve the code of practice.

GEODETIC ANALYSIS PROCEDURE IN THE NETHERLANDS

Status quo

Dutch Mining Law commands that geodetic monitoring is to be undertaken and interpreted during mining activities according to the granted concession in order to verify the original indications of induced subsidence and vibrations. It is a serious complication that the total land subsidence has more causes, which are not due to be checked in a similarly accurate manner, such as natural subsidence, groundwater level change, peat oxidation and groundwater extraction. Mining companies legally have the task to separate the different causes. Even though the results are checked by the State Supervision of Mines (SodM), NGOs and civilians wonder whether this procedure is really objective.

Focus

In 2008, the Dutch Technical Committee on Land Movement (TCBB) took the initiative to shed new light on the aforementioned problem by reconsidering the state of the art and the practical implementation. The advice, published in November 2009, was composed in a special TCBB Working Group with representatives of major stakeholders, by three interviews with prominent experts and an open workshop with the mining industry, knowledge institutes, NGOs and other stakeholders. This report distinguishes five phases:

1. the mining company predicts the expected subsidence using appropriate (geomechanical) models;
2. a monitoring network is installed for measuring land subsidence;
3. measured (geodetic) observations are analysed;
4. the geodetic result is confronted with the expected subsidence (item 1);
5. if appropriate, the applied models and/or the monitoring network are adjusted so that the prediction of future subsidence remains reliable.

The TCBB Working Group has focused its attention mainly on items 3 and 4, and recommendations are given for item 2. In some cases, e.g. where the hand-on-the-tap approach is due for the eventual environmental impact, intermediate geodetic results may summon adjustment of the production scenario. The outcome is also relevant for the legality of damage claims.

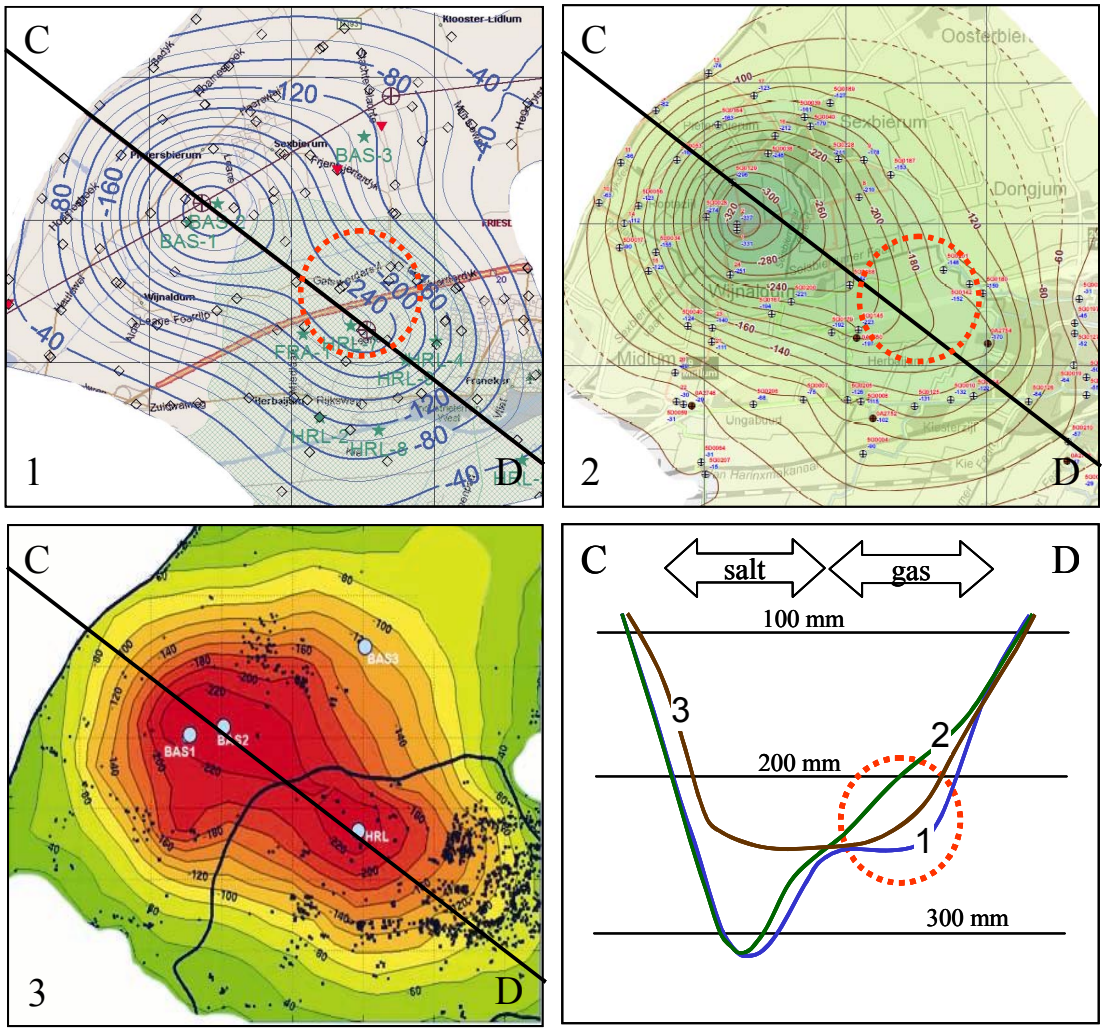

Fig. 4 Results of subsidence due to salt and gas production; 1. Spirit levelling (Houtenbos, 2009); 2. Spirit levelling (Oranjewoud, 2008); InSAR (Hanssen, 2008); (The graphs along C–D represent the subsidence in September 2009).

METHODS

In the literature, two geodetic methodologies are distinguished, descriptive and cause–consequence types (Fig. 5). In the Netherlands, four methods are relevant, two are descriptive and purely geodetic, i.e. the method suggested by SodM and the method by Houtenbos, and two are cause–consequence, i.e. Geertsma's model that involves geodetic data just as a constraint, and the method developed by TNO and Deltares that integrates and balances all data, geomechanical and geodetic (Fig. 5). The descriptive methods principally exclude the use of geomechanical aspects in the analysis for the determination of the geometric land subsidence.

The SodM method elaborates one geodetic monitoring cycle at a time, referred to as a congruent model. It is a simple and orderly method, for which standard software is available. A disadvantage is the required high reliability of the monitoring network, the benchmark quality and the reference benchmark. Error testing is rather limited and (stable) benchmarks should be available from the start.

The method of Houtenbos (2005) is based on an integral analysis of all geodetic measurements in space and time. It is a state-of-the-art kinematic model that can incorporate newly placed benchmarks. It recognizes and eliminates movements that are not correlated in time, i.e. autonomous benchmark motion. Using *a priori* knowledge of spatial and temporal subsidence

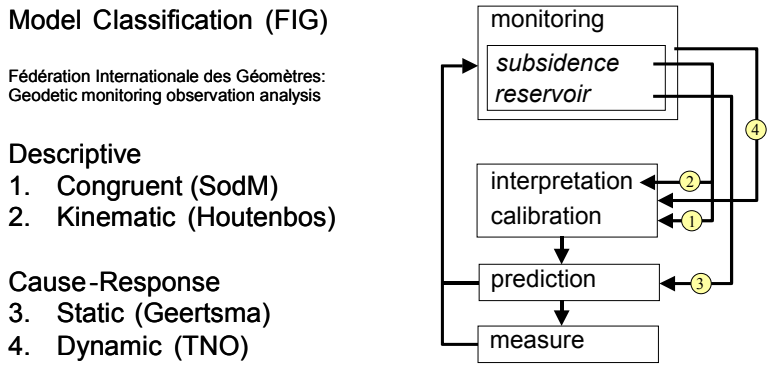

Fig. 5 Model classification and some examples of the analysis protocol.

patterns, different potential causes of subsidence can be identified and quantified by successive iteration. The approach helps to distinguish the various contributions to the subsidence in a rather objective way, i.e. by imposing and rejecting hypotheses. A disadvantage is that high-level geodetic knowledge is required.

For proper monitoring networks, both methods give quite identical results. Houtenbos' model is preferred for scarce or non-uniform monitoring networks.

The method of TNO-Deltares focuses on phase 5, where the geomechanical model of the underground is being improved by reliable geodetic data. It is a cause–consequence approach. Optimum use is made of coupled geodetic and geomechanic information. This is a so-called dynamic model. By the integrated use of all available measurements and physical knowledge of the subsidence process, this method is particularly suited for describing the subsidence behaviour as a consequence of distinct different causes, and future subsidence for various production scenarios.

NUANCING

In general, the surveillance of subsidence due to mining by means of spirit levelling is good practice in the Netherlands. Considering the present gas and oil production from over a hundred large and small fields, the discussion is limited to just a few fields, which attain excessive attention by the media and renders public opinion into a state of worry.

The input of various stakeholders teaches that one-sidedness is common, and fed by different interests. Water boards' investments require predictions beyond decades with an accuracy of a decimetre or so. The agricultural sector has its focus on groundwater level changes of centimetres over a short time span. Geodetic measurements claim millimetre accuracy, while geomechanical simulations hardly reach centimetre precision. In this respect, it is preferable to express land subsidence predictions with a bandwidth, which reflects the accuracy. Authorities and industry should act accordingly, and show sufficient perspective with regard to the inevitable uncertainty and should include not just one interest but all, in a proper balance.

It is advised to give space to different methods. In practice, the same perfection is not always required. Simple methods are often applicable, particularly with proper monitoring networks. Only when autonomous subsidence or other effects are due and a dispute between parties about the different causes remains, is an advance method advised. The integral method with the best prediction capability is then preferred.

RECOMMENDATIONS

– Rules are suggested (see later) for the installation of monitoring networks and the frequency of monitoring campaigns. They should guarantee the relevant quality and quantity in space and time.

- For geodetic analysis, an approach of three stages is advised: (1) determine the height differences in the benchmarks, (2) test the geodetic data and employ a statistical error analysis, (3) confront the obtained land movement and their respective causes with the geomechanical prediction.
- Elimination of malfunctioning benchmarks should occur in an objective way. The advised method is, as a first step, to conduct a geodetic statistical check of the reliability of benchmark behaviour, next, considerations of the physical nature and finally, if necessary a visual inspection of benchmarks.
- The distinction of different causes takes place in the third stage, if relevant. In the Netherlands, according to the mining law, the mining company is responsible for determining the mining-induced land subsidence. The correlation between geodetically analysed and geomechanically predicted subsidence offers an explanation of the deviations, which could be caused by natural processes and human activities other than mining, such as groundwater level adjustment or ground works. The State Supervision of Mines (SodM) has the checking task and is entitled to accept or reject the result of the mining company. If a third party disagrees, an official independent technical review can be obtained from the TCBB, or the matter is solved in a court case.
- Finally, the TCBB Working Group states that a geomechanical model, well calibrated by geodetically determined relative land subsidence, is required to underscore the reliability of land subsidence prediction and its causes.

NEXT STEPS

The TCBB Working Group recommends the following steps:

- A national knowledge centre should be established where knowledge and experience in the field of land subsidence is collected, maintained and disseminated.
- The mining industry should develop a practitioners guide for the installation of monitoring networks, the collection of data and the geodetic analysis (software) and reporting. The guide should obtain formal agreement from the supervising authorities, SodM and TCBB, and be supported in a law amendment.
- Some cases of best practice should be collected for educational purposes and for general acceptance by public and governmental entities. New or adapted models could be subjected to a number of synthetic data sets, of different complexity, in order to prove reliability.

The Dutch mining industry (oil, gas, salt), organized by the TPB, started in March 2010 to develop the practitioner guide.

RULES FOR MONITORING

Monitoring network

- The number and location of benchmarks is adequate to capture expected subsidence shape and rate.
- Place a few benchmark near the subsidence bowl centre.
- Measure benchmark tracks along the subsidence bowl axes.
- Maintain monitoring networks.

Benchmarks

- Benchmarks must be adequate to detect the subsidence described in the concession.
- The stability of buildings carrying benchmarks is to be frequently investigated.
- Benchmarks to be placed in pairs, for checking purposes;
- Autonomous benchmark behaviour is to be checked during monitoring.

Monitoring approach and analysis

- The frequency of monitoring should suit the subsidence rate.
- Before production, two monitoring campaigns are undertaken (zero state).
- In case, intermediate GPS or InSAR monitoring supports the start of a new spirit levelling campaign and may be used to validate the result.

Acknowledgements The writer is indebted to the TCBB for the consent to publish the results of the Working Group. The support and contribution of the members of the Working Group, to wit, Johan Blaauwendraad (chairman), Frans Barends, Frank Kenselaar, Cor Kenter and Roland Klees, its direct supporters Jan van Herk (SodM), Adriaan Houtenbos, Stefan Kampshoff (NAM), Peter Fokker and Annemarie Muntendam (TNO), and the valuable input of Gerard Kruse and the participants from industry and authorities at the workshop "From Monitoring to Subsidence" are greatly acknowledged.

REFERENCES

Barends, F. B. J. (2000) Land subsidence legal affairs against technical know how. SISOLS2000, CNR, 345–352.

Barends, F. B. J., Dillingh, D., Hanssen, R. & Onselen, K. van (2008) *Land Subsidence Along the Dutch Coast: Case Hondbossche and Pettemer Sea Defense* (in Dutch). IOS Press, Amsterdam, The Netherlands.

Freeze, R. A. (2000) Social decision making and land subsidence. SISOLS2000, CNR, 354–384.

Gambolati, G., Teatini, P. & Ferronato, M. (2005) Basic conceptual guidelines for a sustainable gas/oil field development. SISOLS2005, Shanghai Sc&T Pub., 919–924.

Houtenbos, A. P. E. M., Hounjet, M. W. A. & Barends, F. B. J. (2005) Subsidence from geodetic measurements in Ravenna. SISOLS2005, Special Volume: *Multi-Disciplinary Assessment of Subsidence Phenomena in the Ravenna Area*. Millpress, 79–100.

Houtenbos, A. P. E. M. (2009) Land subsidence NW-Friesland 1976–2009, www.waddenzee.nl/fileadmin/content/Dossiers/Energie/pdf/NWFR09.pdf.

Muntendam-Bos, A. G., Hanssen, R. F., Thienen-Visser, K.van & Samiei-Esfahany, S. (2009) Summary of PS-InSAR analysis of land subsidence in North-West Friesland. (Dutch). TNO-034-UT-2009-02294/A.

Staveren, M. Th. van (2006) *Uncertainty and Ground Conditions; A Risk Management Approach*. Elsevier, Amsterdam, The Netherlands.

Staveren, M. Th. van (2009) *Risk, Innovation and Chance*. Ipskamp Drukkers BV Enschede, The Netherlands.

TCBB Report (2009) From Monitoring to Subsidence. (Dutch). www.Tcbb.nl.

Workshop 2000. Summary Monitoring of Land Subsidence on Ameland-East; evaluation of 13 years after start production. Advisory Commission Monitoring Land Subsidence Ameland, 35pp. + 2 CDs (Dutch).

Workshop 2005. Summary Monitoring of Land Subsidence on Ameland-East; evaluation of 18 years after start production. Advisory Commission Monitoring Land Subsidence Ameland (Dutch); English summary: http://www.waddenzee.nl/fileadmin/content/Dossiers/Energie/pdf/Subsidence_and_Sea_level_Rise_in__English_.pdf

(Proceedings of EISOLS 2010, Querétaro, Mexico, 17–22 October 2010). IAHS Publ. 339, 2010.

Land subsidence and environmental law in Mexico: a reflection on civil liability for environmental damage

PEDRO JOAQUÍN GUTIÉRREZ-YURRITA

Centro Interdisciplinario de Investigaciones y Estudios sobre Medio Ambiente y Desarrollo (CIIEMAD) - Instituto Politécnico Nacional (IPN), Calle 30 de Junio de 1520, Barrio La Laguna Ticomán, CP 07340, México DF
pgutierrezy@ipn.mx

Abstract The land subsidence problems in Mexico have been increasing in recent years owing to excessive withdrawal of fluids, especially water and petroleum products. The main problem with the extraction of fluids from below the ground surface is often that the heavily populated cities, like Mexico City, are very much affected; there is an urgent need for new ways to identify and control the land subsidence related processes. Mexico as a whole is dominated by a long chain of mountainous terrain which is dissected by regional and trans-regional faults which run for long distances and along which the major cities are often located. The extraction of large volumes of fluids from the subsoil reduces pore pressure in particular zones, and causes surface subsidence. The combination of human and geological conditions can be related at a smaller scale, as this often happens locally in certain regions, especially in Mexico City. However, despite the importance of such phenomena, so significant as to justify a Federal Regulation and the inclusion in Criminal and Civil Codes of the definition of environmental crime by subsidence and civil damages for the same phenomenon, as well as special rules to repair the damage from this cause, there are none. A review of case law in Mexico (jurisprudence) of either constitutional disputes or any other cause related to subsidence problems did not find any relevant thesis or sentence. In this paper, a review of liability for environmental damage in Mexico and its relationship to the phenomena of subsidence induced by human activities is made.

Key words management of nonrenewable natural resources; mining; water and gas withdrawal; ecology

INTRODUCTION

Land subsidence due to the withdrawal of fluids, underground mining and gas extraction by man has become relatively common in México in the last 50 years and has been described at several other places throughout the world (Gatto & Carbognin, 1981; Holzer, 1981; Fielding *et al*., 1998; Galloway *et al*., 1998; Bell *et al*., 2002; Brambati *et al*., 2003; Dokka, 2006; among others). The overexploitation of underground elements has caused subsidence in rural and urban areas (Poland & Davis, 1969; Bell *et al*., 2001; Teatini *et al*., 2006; Alvin & Zobak, 2007). But, how can we claim compensation for environmental damage from the company responsible for the accident if we do not fully know the ecological, environmental and geological effects of the subsidence? How can we know the effects of subsidence on ecological processes, the resilience of ecosystems and biodiversity if they "have no apparent effects, release date or expiration", or we do not know? How can we prepare a complaint for civil damages if we do not know how to link the causative agent to the company or the alleged perpetrator? Geology and the other Earth sciences have advanced well with recent technological developments, nanotechnology and remote sensing systems, interferometric synthetic aperture radar (InSAR) and new geodetic data (Leake & Prudic, 1991; Hsie *et al*., 1995; Dokka, 2006; Teatini *et al*., 2006; Alvin & Zobak, 2007; Muntendam *et al*., 2009). However, despite some recommendations for mitigating environmental damage produced by subsidence (Barends, 2000; Freeze, 2000), in a phenomenon such as subsidence, because many factors contribute and make it complex, it should be reviewed case by case in order to understand the causes. For instance, the magnitude of land subsidence over of an overexploited confined aquifer system is a function of the compressibility, compaction, particle size and shape, clay mineralogy, geochemistry of pore water in the clayey beds and of the water in contiguous aquifers, and secondary compression (Bouwer, 2006). Thus, subsidence problems are usually alleviated by cessation of withdrawal and increase of reservoir pressure.

Within ecology and its more applied view, natural resource management, the issue of non-renewable resources is of particular interest (Bruges & Smith, 2008) because biotic and

Copyright © 2010 IAHS Press

anthropogenic actions will modulate species' responses to other ecological processes, including climate change (Polokzanska *et al*., 2008), such as mining, gas extraction and excessive withdrawal of fluids, especially water and petroleum products (which are particularly significant because their rates of renewal are thousands of years, even with modern groundwater recharge technologies). Many are the damages to the natural environment (or, in terms of ecology under the ecosystem approach for holistic management, the landscape heritage; Gutiérrez-Yurrita, 2009a), which are caused by overexploitation of so-called non-renewable natural resources, ranging from a simple geo-structural modification of the landscape to its radical transformation through the complete disappearance of natural historical ecosystem by land subsidence.

The geology of the Mexican territory is particularly susceptible to this type of geological phenomena, making it more vulnerable to extractive minerals, gas or water withdrawal. For this reason, it is very important to have a next-generation legal apparatus in the administrative (environmental law), international (agreements signed by México), civil and criminal areas (Rosillo & Gutiérrez-Yurrita, 2010).

MEXICAN ENVIRONMENTAL LAW

The current environmental law, despite its classical formulation of command-control, is preventive not reactive (Real-Ferrer, 2002). And, after an initial period of prevention, this law allowed the incorporation of other United Nations fundamental principles such as the precautionary and sustainability (to name a few that are relevant in this opinion; Sampaio *et al*., 2003). The new law that was created strengthened the initial idea that environmental care should be preventive. And even more, that in the absence of specific information on the effect of human action on ecosystems, we should act with caution (precautionary principle), never overestimate the technical and scientific advance and always with a view of sustainability (Jaquenod, 1989). And this could clearly be justified; nevertheless an environmental accident needs a tougher law than this environmental law, due to their quality of belonging to the body of international administrative law. International environmental law which largely originated many procedures and rules applied in the Mexican Environmental Acts (mainly LGEEPA[1]), is not mandatory. The international treaties and agreements signed by Mexico are not of the strict observance by the signatory parties type. These rules are only suggestions, directives expected to be incorporated in the legal framework of the signatories to the agreement. This kind of law is often referred to as *soft law*.

An environmental accident can be prevented when you know the risks of the activity that may produce it. But when it happens and there is damage to the structural and functional elements of an ecosystem, the accident damages the common values and interests of a society (Curiel, 2007). The damage is not only against an individual, the whole community suffers it. But also there can be a civil direct damage, if the accident damages the private property of individuals, such as their houses or land (Gutiérrez-Yurrita, 2009b). In these cases we do need a different kind of rules, not from environmental law but based in civil code and criminal code (Puig, 1991; Gutiérrez-Yurrita, 2008). And this is precisely where the first major problem appears when applying criminal and civil codes: we do not know, using the scientific principles of statistics, with certainty how to repair environmental damage, nor how much it costs an ecosystem to impose a fine (Christiansen & Walters, 2004; Gutiérrez-Yurrita, 2006; Sanjurgo & Islas, 2007).

Enhancement of preventive measures is needed as the precautionary principle and that should occur before any subsurface exploration studies are presented; it requires strategic assessment of the landscape and zoning according to the values of the potentially affected ecosystems, environmental bonds, studies of risk mitigation and disaster prevention. We must begin a new era in the management and handling of our basement.

[1] Ley General de Equilibrio Ecológico y la Protección al Ambiente (General Act of Ecological Balance and Environmental Protection) new Act since 28 January 1988.

In Mexico, LGEEPA[2], in Art. 5, section XIV mentions that exploitation and beneficiation of minerals or substances, and other subsurface resources belong to the nation, with regard to effects that such activities can produce on the ecological balance and environment, and these activities are regulated by federal laws. Article 11 of the Act provides that the Ministry of Environment and Natural Resources is empowered to sign agreements with states and municipalities for exploration, exploitation and beneficiation of minerals and chemicals reserved for the Federation in terms of the Law of Mining and regulating constitutional Article 27[3]. Similarly, in Mexico, underground exploitation (mining) is an activity that necessarily requires an environmental impact assessment (LGEEPA Art. 28). But the most important item in the regulation of underground mining is Article 99 (LGEEPA), which establishes the ecological criteria for the preservation and the sustainable land use through the use of substances from the underground mining and other activities that alter forest soil cover.

SEMARNAT is the secretariat responsible for issuing the Mexican Official Standards relating to the exploration and exploitation of nonrenewable resources of the subsoil. With regard to the exploitation of groundwater, it is covered by the National Water Act and must be supervised by the Technical Committee on Groundwater and within the guidelines of National Policy and program planning water (Article 15)[4].

Despite this body of laws regulating the extraction of nonrenewable natural resources of the subsoil, there are none that specify who is responsible for environmental damage or that it should contain a specific study of environmental risk caused by mining or fluids withdrawal. And even at the international level there are several theses and rulings on the impact of mining activities in the environment and some related to subsidence phenomena, but there are none in the database of the Institute for Legal Research of UNAM, the body responsible for obtaining all the nation's legal argument for all legal cases in Mexico.

CIVIL LIABILITY FOR ENVIRONMENTAL DAMAGE IN MEXICO

The Mexican Civil Code does not cover damage from underground mining substances. And although the Federal Criminal Code provides a special chapter concerning environmental crimes, there are none related to subsidence cases. Article 414 states that there is the penalty of imprisonment for those who perform illegal activities without taking precautions and safety measures for such activity that would cause harm or damage to the environment. Similarly, Article 420 states that it is a crime for environmental management to work without adequate safety measures to prevent environmental damage. For its part, Article 421 of the same Code provides that in addition to the penalties of the preceding articles on environmental crimes, imposing the repair of damage to the ecosystems or natural elements is needed.

Although Article 20 of the Mexican Constitution provides a guarantee to the victim or the offended party that it is the offender who repairs the damage caused, in Mexico there are no prosecutors or judges with expertise in environmental matters, so one cannot always take note of the complaint and take it to court. What usually happens is that prosecutors dismiss the complaint and it never comes to court.

The LEGEEPA states in Article 203, without prejudice to criminal or administrative sanctions, who will repair damage to the environment in the manner provided by the civil procedure code, and the deadline for a demand for environmental liability is five years from the time when the act occurs. The General Act of Wildlife states in Article 106 something similar to the LEGEEPA, but only applies if damage to wildlife or their habitat is proved. It is worthy of note that only one of the prosecutors of the Federal Attorney for Environmental Protection (PROFEPA) can assess the damage to the environment, and only they can determine its magnitude. And here,

[2] Ley General del Equilibrio Ecológico y la Protección al Ambiente (LGEEPA). Latest amendment *Official Diary of the Federation DOF 06-04-2010.*

[3] Political Constitution of the Mexican United States. Latest amendment *DOF 27-04-2010.*

[4] Act of National Waters. Latest amendment *DOF 18-04-2008.*

to return to the same point, how can the technical committee of the PROFEPA determine the environmental damage by subsidence or a sinkhole when the forces that are acting on such phenomenon are not known precisely, or since when these forces are acting, or when they can stop their influence? A PROFEPA technician cannot estimate environmental damage due to overexploitation of groundwater, gas and mining when the experts cannot decisively express their opinion for lack of sufficient data and evidence.

Article 1915 of the present Federal Civil Code states that repair of environmental damage can be done at the discretion of the victim (in this case of collective interests and the absence of a single victim, society and biodiversity as a whole would be the applicant which established how to repair the damage), but also states that if the offender cannot repair the damage, the offender must pay for damages. We return to the previous point again, what is the cost of losing a biological species and geo-environmental systems? (Mäler *et al.*, 2007, 2009). Maybe the EMERGY computational program could do it, but much is in cash (quantified monetarily); what is the value of the recovery of the resilience of an ecosystem on which depend many ecological processes and thousands of biological species and even ourselves? (Gutiérrez-Yurrita *et al*., 2002).

In addition, the current Federal Criminal Code provides in Article 420Bis to impose a sentence of two to ten years in prison and fines of the equivalent of 3300 days of minimum salary per day on those who illegally damaged mangroves, reefs, lagoons ecosystems in general, but does not mention the term ecosystem damage and rural damage. In the Mexican criminal code it is not considered that there are environmental crimes; ecosystem damage is not listed in the articles. Causing subsidence and related phenomena as a result of overexploitation of groundwater is not considered a crime because exploitation of groundwater is a legitimate activity. Moreover, Article 421 of the Federal Criminal Code states that in addition to a sentence of several years in prison, those guilty of causing the environmental damage must undo the damage caused, by repairing the damaged ecological processes so as to leave the ecosystem in the same condition as it was before the damage. However, it is generally accepted that to repair the damage to an ecosystem that suffers generalized land subsidence is almost impossible:

First, we should have to repair the geologically altered condition; if that were possible we would we need large volumes of material or fluids to return the underground pressure levels to the previous levels of the exploitation.

Secondly, it should restore important ecological functions of the ecosystem to make it resilient again.

And thirdly, it should seek to restore the ecosystem inter-relationships to return to environmentally permeable networked ecosystems at different hierarchical scales of space and time (restore the ecological links among ecosystemic landscapes).

Then, the final question is: how to restore or rehabilitate an ecosystem and the environment damaged by a process of subsidence, if we do not know how to repair the ecological linkages among ecosystems, even if we have the appropriate methods to replace the overexploited underground structure? (Gutiérrez-Yurrita *et al*., 1999; Sanjurjo & Islas, 2007).

CONCLUSION

Environmental law is preventive, not reactive, therefore solutions must be sought for technical service providers to develop more environmentally friendly approaches that are safer in terms of reducing the likelihood of environmental risk, and more friendly with maximum exploitation.

Mexico should be enhanced by thoughtful environmental law, through fiscal stimulus for businesses that exceed the quality and safety standards that are required in the official Mexican standards, by promoting voluntary environmental audits and other instruments of environmental law related to this philosophy

There is need for a training system in the areas of environmental law and ecology for technical environmental attorneys, the prosecutors and judges, so that in a short time our public administration can develop real environmental courts. Environmental courts should only hear

environmental issues; therefore, all the cases will be strictly related to environmental damage, and finally, the judge may determine liability for environmental damage.

An environmental court can operate independently of other courts but does not exclude the possibility that the Supreme Court or a criminal court also conducts a criminal trial for the same environmental crime.

In addition to imprisonment and fines, reparation of environmental damage is needed.

The way in which the guilty must repair the environmental damage must be determined by one expert in the areas of ecology, geology, etc., who must be employed by the court handling the case, to explain how to repair the damage done, and the ecosystem concerned can be left in the best possible condition.

There is a large gap in scientific knowledge in many Earth sciences like geology, geophysics and ecology; therefore, greater support from the authorities, and more involvement by employers and companies is strictly necessary.

We must update our environmental laws and our federal criminal code and civil code, so as to include more environmental crimes such as subsidence, and have better mechanisms to ensure that when civil liability for environmental damage is estimated by fines, the money goes to an environmental fund and is applied in repairing the ecological damage.

Acknowledgements The author wishes to thank Jonathan Muthuswamy Ponniah (CIIEMAD-IPN) for his assistance in the structuring of the abstract and Dora Carreón Freyre (UNAM) for her insightful comments to the manuscript.

REFERENCES

Alvin, W., Mark, Ch. & Zoback, D. (2007) The role of hydrocarbon production on land subsidence and fault reactivation in the Louisiana coastal zone. *J. Coastal Research* **23**(3), 771–786.

Barends, F. B. J. (2000) Land subsidence legal affairs against technical know how. SISOLS2000, CNR, 345–352.

Bell, J., Amelung, F., Ramelli, A. R. & Blewitt, G. (2002) Land subsidence in Las Vegas, Nevada, 1935–2000: New geodetic data show evolution, revised spatial patterns and reduced rates. *Environmental and Engineering Geoscience* **8**(3), 155–174.

Brambati, A., Carbognin, L., Quaia, T. O., Teatini, P. & Tosi, L. (2003) The Lagoon of Venice: geological setting, evolution and land subsidence. *Episodes* **26**(3), 264–268.

Bouwer, H. (2006) Land subsidence and cracking due to ground-water depletion. *Ground Water* **15**(5), 358–364.

Bruges, M. & Smith, W. (2008) Participatory approaches for sustainable agriculture: A contradiction in terms? *Agriculture and Human Values* **25**, 13–23.

Christiansen, V. & Walters, C. (2004) Ecopath with ecosim: methods, capabilities and limitations. *Ecol Model*. **172**, 109–139.

Curiel, A. (2007) El entendimiento de las fuerzas dinamizadoras de la degradación: las aportaciones de Paul Ehrlich. *Gaceta Ecológica, Número especial* **84-85**, 2–5.

Dokka, R. K. (2006) Modern-day tectonic subsidence in coastal Louisiana. *Geology* **34**(4), 281–284.

Fielding, E. J., Blom, R. G. & Goldstein, R. M. (1998) Rapid subsidence over oil fields measured by SAR interferometry. *Geophys. Res. Lett.* **25**(17), 3215–3218.

Freeze, R. A. (2000) Social decision making and land subsidence. SISOLS2000, CNR, 354-384.

Galloway, D. L., Hudnut, K. W., Ingebritsen, S. E., Phillips, S. P., Peltzer, G., Rogez, F., Gatto, P. & Carbognin, L. (1981) The Lagoon of Venice: Natural environmental trend and man-induced modification. *Hydrol. Sci. Bull*. **26**, 379–391.

Gutiérrez-Yurrita, P. J. (2006) Ecocentrismo vs Egocentrismo: IV:. Ecología económica. *Derecho Ambiental y Ecología* **3**(15), 53–60.

Gutiérrez-Yurrita, P. J. (2008) Ecojusticia, o lo que debería entenderse por justicia en las Áreas Naturales Protegidas y Planes de Ordenamiento Ecológico del Territorio. *Derecho Ambiental y Ecología* **5**(26), 63–73.

Gutiérrez-Yurrita, P. J. (2009a) A diseñar el Futuro!. El holismo de la tercera cultura: hacia la integración científica y cultural. Instituto Politécnico nacional-Centro de Estudios Jurídico Ambientales. México. 300 pp.

Gutiérrez-Yurrita, P. J. (2009b) Perspectiva ecológica para mejorar la aplicación de la ley ambiental de cara al cambio climático global. *Revista Aranzadi de Derecho Ambiental* **15**(1), 81–92.

Gutiérrez-Yurrita, P. J., Morales, A., Oviedo, A. & Ramírez, C. (2002) Distribution, spread, habitat characterisation and conservation of the crayfish species (Cambaridae) in Querétaro (Central México). *Freshwater Crayfish* **13**, 288–297.

Gutiérrez-Yurrita, P. J., Martínez, J. M., Ilhéu, M., Bravo, M. A., Bernardo, J. & Montes, C. (1999) The status of crayfish populations in Spain and Portugal. In: *Crayfish in Europe as Alien Species: How to Make the Best of a Bad Situation?* (ed. by F. Gherardi & D. M. Holdich), 161–192. Crustacean Issues. Balkema, Rotterdam/Brookfield.

Holzer, T. L. (1981) Preconsolidation stress of aquifer systems in areas of induced land subsidence. *Water Resour. Res*. **17**(3), 693–704.

Hsieh, P. A. & Cooley, R. L. (1995) Comment on "Horizontal aquifer movement in a Theis-Theim confined system" by Donald C. Helm. *Water Resour. Res*. **31**(12), 3107–3111.

Jaquenod, S. (1989) El derecho Ambiental y sus Principios Rectores. MOPU. p 63.

Mäler, K. G., Aniyar, S. & Jansson, A. (2009) Accounting for ecosystems. *Environ Resource Econ*. **42**, 39–51.

Leake, S. A. & Prudic, D. E. (1991) Documentation of a computer program to simulate aquifer-system compaction using the modular finitedifference ground-water flow mode. Techniques of Water-Resources Investigations of the US Geological Survey, book 6, chap. A2, USGS, Reston, Virginia, USA, 62 pp.

Mäler, K. G., Li, C.-Z. & Destouni, G. (2007) Pricing resilience in a dynamic economy-environment system: a capital theorethical approach. Beijer Discussion Paper Series # 208.

Muntendam-Bos, A. G., Hanssen, R. F., Thienen-Visser, K. van & Samiei-Esfahany, S. (2009) Summary of PS-InSAR analysis of land subsidence in North-West Friesland. TNO-034-UT-2009-02294/A.

Poland, J. F. & Davis, Gh. (1969) Land subsidence due to withdrawal of fluids. *Geol. Soc. Am. Reviews in Engineering Geology* **1**(1), 187–269.

Poloczanska, E., Hawkins, S.J., Southward, A. J. & Burrows, M. T. (2008) Modeling the response of populations of competing species to climate change. *Ecology* **89**(11), 3138–3139.

Puig, M. (1991) Bien jurídico y bien jurídico-penal como límites del jus puniendi. Estudios penales y criminológicos XIV. p205.

Real-Ferrer, G. (2002) La construcción del Derecho Ambiental. *Revista Arazandi de Derecho Ambiental* **1**, 73–93.

Rosen. D. (1998) Detection of aquifer system compaction and land subsidence usinginterferometric synthetic aperture radar, Antelope Valley, Mojave Desert, California. *Water Resour. Res.* **34**(10), 2573–2585.

Rosillo, I. & Gutiérrez-Yurrita, P. J. (2010) Una secretaría de estado con futuro: la Secretaría de Conservación del Patrimonio Paisajístico para la Sustentabilidad. *Derecho Ambiental y Ecología* **7**(38) (in press).

Sampaio, J. A., Wold, Ch. & Nardy, A. (2003) *Princípios de Direito Ambiental*. Del Rey Editora, Brasil.

Sanjurgo, E. & Islas, I. (2007) Las experiencias del Instituto Nacional de Ecología en la valoración económica de los ecosistemas para la toma de decisiones. *Gaceta Ecológica, Número especial* **84-85**, 93–105.

Teatini, P., Ferronato, M., Gambolati, G. & Gonella, M. (2006) Groundwater pumping and land subsidence in the Emilia-Romagna coastland, Italy: modeling the past occurrence and the future trend. *Water Resour. Res.* **42**, 1–19.

(Proceedings of EISOLS 2010, Queretaro, Mexico, 17–22 October 2010). IAHS Publ. 339, 2010.

Considerations on strategies of sustainable management of oil and gas fields in Italy

G. BRIGHENTI, P. MACINI & E. MESINI
University of Bologna, Department of Civil, Environmental and Materials Engineering, 2 Viale del Risorgimento, 40131 Bologna, Italy
paolo.macini@unibo.it

Abstract Many Italian hydrocarbon reservoirs are located in environmentally sensitive areas or close to urban sites, and thus production often poses technical and social problems. In the last decades, hydrocarbon production has induced environmental concerns, so that nowadays the general set of rules point towards enhancing strategies for environmental protection that might foster a sustainable management of these resources. The oil and gas industry is requested to report consistently on its sustainability due to the environmental awareness that has grown in recent years, with particular reference to potential subsidence problems.

Key words energy; environment; hydrocarbons; natural gas; gas storage

INTRODUCTION

World energy use is increasing due to population growth and to the improvement of the well-being of individuals and societies, both calling for larger and larger energy intensity. Today the main energy sources are fossil fuels (83%), and hydrocarbons represent 63% of the total consumption. In Italy about 80% of the energy comes from hydrocarbons. Based on 2007 data, Italian domestic hydrocarbon production covers about 16% of gas and about 7% of oil consumption (ENI, 2008). In dealing with non-renewable resources a sustainable management policy is crucial so as to make energy also available for the future, at least until fossil fuels can be replaced on acceptable conditions in terms of environmental issues and costs.

Italy has a heavy reliance on oil and gas imports, even though it is relatively well endowed with renewable resources, such as hydroelectric, geothermal, solar, biomass and wind. At present, the total amount of energy from renewable sources is about 7%, accounted for by hydroelectric and geothermal power. In this paper, the sustainable management of a hydrocarbon reservoir will be examined (including underground gas storage), by highlighting both potential environmental problems and the effort that industry, national and local authorities, each for their own part, have to make in order to create sustainable conditions for the benefit of all stakeholders, in terms of environmental protection, competitive production costs and favourable fiscal regimes.

ENERGY PRODUCTION AND ENVIRONMENTAL PROTECTION

A large part of the scientific community confirms that the main risk deriving from the use of fossil fuels comes from CO_2 emissions into the atmosphere. In the middle term prospect, the most promising approach to reduce these emissions is the increase of power plants' efficiency and the possibility to develop renewable energy sources, such as hydraulic, geothermal, wind, tide and solar ones, which today account for about 3%. Other strategies to reduce CO_2 emissions could be: (a) Shifting from coal and oil into natural gas for the production of electricity in primary power plants. (b) Implementing carbon capture and CO_2 storage (CCS) in depleted hydrocarbon reservoirs or saline aquifers. To this regard it is worth recalling that in April 2009 the European Parliament and Council approved a directive (Directive, 2009) aimed to propose a regulatory framework on CCS where legal, technological and environmental issues are considered. European state members are required to comply with this Directive by June 2011.

Copyright © 2010 IAHS Press

Sustainable resource management means the rational use of the territory and the conservation of the environment. World population growth is making it more and more difficult to allocate large land areas for the extractive industry (both mining and petroleum), and the safeguarding of health, safety and the environment is a top priority today. As far as environmental protection is concerned, one must distinguish between global issues due to energy production, which might have effects on the entire ecosystem, and localized damage, which only has a marked effect on the site of production and transformation of energy resources. Localized damage is particularly important in urban development areas and in delicate ecosystems.

As for localized environmental damage, one must distinguish between the impact due to the usage of hydrocarbons and the impact of the oil and gas exploration and production (E&P) industry. Damages induced by hydrocarbons utilization can be mainly ascribed to water and soil pollution by liquid spills and to CO_2 (and CH_4) emission and atmospheric pollution (particulate matter, or fine particles). Water and soil management requires careful prevention rules and, in the case of accidents, the rapid remediation of the contaminated site. In the case of oil spills on land, many remediation techniques are already widely used and tested, and being natural products, oils are easily biodegradable. More difficult is the remediation of large oil spills in rivers.

Concerning the impact of the oil and gas industry, both upstream (exploration, drilling and production) and downstream (transport, refining, distribution), one must recall that upstream operations produce only limited environmental concerns. Amongst these, the main impact during exploration is the use of explosives in seismic surveying (a technique now abandoned in offshore exploration and replaced by the use of less invasive methods). During drilling, apart from the temporary occupation of the area enclosing the rig site, environmental damages can be caused by uncontrolled well blow-outs and accidental spills of drilling fluids, with potential danger to people and the surrounding environment (sea or land). Many years of field practice enforced the application of strict safety rules and reliable equipment, and today blow-outs are very rare. As for drilling fluids, for many decades the industry has developed environmentally-friendly formulations and toxic products are banned in almost every country, and drilling fluids and contaminated cuttings are disposed of properly. During production, potential environmental damage can be caused by subsidence due to fluid production, a very sensitive problem in coastal areas, possible spills and the disposal of water produced together with hydrocarbons, which may contain residual crude and high salt content.

The downstream activity poses pollution and noise problems. Possible environmental damages are oil spill out onto the land or into the sea, lakes or rivers, due to the breakage of pipelines or of tanker shipwrecks, and possible accidents inside the refineries. Tanker shipwrecks are relatively frequent accidents, and causes heavy emotional reactions on the part of both local communities and public opinion, amplified by the media (Bilardo & Mureddu, 2004). In this scenario, the oil companies must play a role in finding recommendations and solutions to environmental problems, due to the awareness that has grown in recent years. Environmental preservation is no longer seen as a cost, but as an important investment, included in the budget of all projects.

PECULIARITY OF THE ITALIAN UPSTREAM INDUSTRY

Italy is the fifth European Country in terms of the importance of hydrocarbon reserves. Proven reserves of natural gas and crude oil amount to 94×10^9 m^3 (standard conditions) and to 600×10^6 barrels, respectively (ENI, 2008). In 2007 the domestic production accounted for about 9.5×10^9 m^3 of gas and 45×10^6 barrels of oil. However, strong exploration activity is needed to keep up with the pace of production. At the present rate of production, the reserve-to-production ratio is about 10 years for gas and 13 years for oil. This situation is mainly due to a lack of exploration, and is not positive for the future of the industry. Environmental problems and political or regulatory issues no doubt had a role in diverting the interest of the oil industry from placing investment in this area. In 1995 the domestic production of natural gas amounted to 20×10^9 m^3,

decreased to 14×10^9 m^3 in 2002 and to 9.5×10^9 m^3 in 2007, with a forecast of 5×10^9 m^3 in 2015, if no further exploration and investment are allocated.

As far as natural gas is concerned it is worth noting that Italian legislative Decree 164/00 (*Letta Decree*, May 2000) set the rules for implementing European directives for the internal market. These rules involved the Italian upstream industry by introducing innovations in gas storage systems, allowing the possibility of developing new storage capacity in order to ensure security of supply and to respond to the seasonal nature of the market in terms of both volumes and peaks.

Italy has a long tradition of hydrocarbon production in environmentally sensitive areas. The Italian E&P industry, characterized by the co-existence of highly-valued sites of naturalist, artistic and environmental interest (not to speak of the tourism business), must cope with a careful evaluation of environmental and social issues. In the last two decades these problems have generated many concerns, so that nowadays the general set of rules point towards posing a redundancy of constraints to the industry, not always justified by a mere technical standpoint. The role of technology innovation in E&P industry has been extremely beneficial for the correct environmental management of oil and gas fields. Thanks to the intense use of new technologies and to the strong cooperation with local and central government, it has been possible to also develop sensitive areas (Brighenti *et al.*, 2003). In particular, it is worth recalling two important case histories that mark the application of correct and sustainable management of hydrocarbon reservoirs; they are reported in the Appendix.

The most important concern of the Italian upstream industry is the constant decline of the reserve-to-production ratio, which is more evident in the last decade. The present situation can be partially ascribed to penalizing legislation regulating the E&P of domestic hydrocarbons and to the interplay of bureaucratic powers, making investments more and more uncertain. The complicated bureaucracy can be partly ascribed to the partial devolution of powers from the Central Government to the local authorities (regions, provinces and municipalities, with their own rules and policies). In such a way, delays in both authorization processes and field operations can be imposed by the local authorities. In 2004 a law (Italian law no. 239, 20 August) was issued to solve these conflicts, but delays in the authorization process still contribute to make the management and development of projects problematic, especially in terms of time to market, i.e. the time from the allocation of a budget and the first hydrocarbon production. Investments in developing new prospects decreased drastically in the last decade. This is a lost opportunity in terms of safety of energy supply, benefit for the balance of payments, in entrepreneurship activity and employment.

The problems in evaluating E&P costs are the estimation of the authorization timeframe process and possible uncertainties of the right to produce discovered hydrocarbons. In fact, the license to produce a newly discovered reservoir is an administrative act different from the exploration and drilling permit, and must undergo a new overall evaluation, environmental impact assessment and authorization process, where the local administration can have a strong influence on economic and technical issues. Also, some partially developed fields have suffered delays for the same reasons.

In this regard, it is interesting to analyse the positive case of the Basilicata Region (where environmental concerns of local communities intermingled with social and political issues), and the negative case of the Northern Adriatic Sea (where disputes between the operator and the local government about alleged land subsidence issues were so severe as to put on hold *sine die* the project, which is now apparently abandoned). Finally, to complete the upstream peculiarities, the Italian situation of underground gas storage is reported.

BASILICATA REGION

The recent re-exploration of the Basilicata Region started in the early 1980s, and in 1988 oil was struck. The most recent evaluation of the Val d'Agri and Tempa Rossa oil fields (two complicated

carbonaceous reservoirs at 3500–4500 m depth), have highlighted proven reserves of about 480×10^6 barrels of oil equivalent. The planned 40 development wells should help to reduce the Italian oil bill, and thanks to the royalties and to the direct and induced employment it should be beneficial to the economy of the Region. Output of 11×10^3 barrels per day from the fields began in 2000, but limited transport capacity prevented production reaching its target capacity of over 100×10^3 barrels per day. The construction of a 136-km, 150×10^3 barrels per day capacity pipeline connecting the fields to the Taranto refinery was completed in October 2001. E&P industry in this area must cope with the quality of the natural environment, characterized by an almost intact part of the southern Apennines, with the unique features of the Mediterranean forests and the related tourist trades. Discussions with the institutions led to good returns as they enabled the oil companies to continue productive activities compatible with the environment, contributing towards making the best possible use of the territory. In June 1998 an agreement was reached between ENI (the operator) and the Regional Government, following a model of sustainable development backed by the use of the most innovative technologies. To name a few, one can recall: (a) Reduction of drilling wastes, by adopting lean profile wells that reduced by 50% the drilling wastes and the spent fluids. (b) Multilateral technology to drain more efficiently different pools of the same reservoir. (c) Clustering, allowing considerable savings of territory. And, (d) adoption of compact wellheads that reduced the visual impact of the well system during production.

NORTHERN ADRIATIC SEA

At the end of 1960, a wide exploration campaign started in the Northern Adriatic Sea, between the parallels facing the mouth of the Tagliamento River and the Po di Goro River. The exploration activity resulted in the discovery of 15 gas fields with estimated reserves of 30 to $50 \cdot \times 10^9$ m^3. In 1996 a project was presented with a duration of 25 years, involving investments of about one billion US dollars (1996 value) for the construction of 18 production platforms (plus one platform for water injection and formation compaction monitoring) and the drilling of about 80 wells. Some of these fields are close to the coastline, and correspond to extremely sensitive areas, as far as the altimetry of the mainland is concerned, facing the historical towns of Venice and Chioggia, with their unique features. Soon doubts arose about the opportunity to develop such fields, due to the possible risks of subsidence propagation toward the coast. The project for all exploration and production activities involving hydrocarbon production in the Northern Adriatic Sea generated some disputes and objections from environmentalist associations and local government. To authorize the project, the Ministry of the Environment commissioned studies with the task to predict the effects of the development of the fields located closer to the shoreline. None of the studies were so conclusive as to convince the authorities to authorize the project, and in October 1998 the Advisor Committee to the Ministry for the Environment, considering the priority of the hydraulic control of the region, declared against the development of the gas fields of the Northern Adriatic Sea. At present, the problem is still open to lively debates and discussions, and the Northern Adriatic Sea project is on hold.

UNDERGROUND GAS STORAGE

The *Letta Decree* mentioned above introduced innovations in both gas storage systems and in the domestic E&P industry. The Italian storage system, which in 2008 accounted for about 14×10^9 m^3 capacity (working 9×10^9 m^3 + strategic 5×10^9 m^3), is highly concentrated in both geographic and operational extent (MSE, 2008). It encompasses 10 on-shore fields, most of them located in the Po River valley. These gas fields are depleted at simple expansion or moderate water drive, with good efficiency (working gas to immobilized gas ratio from 65% to 70%) and good permeability of the formation, which concern both sandstone and fractured carbonaceous

formations. Eight of those fields are operated by Stogit S.p.A., a subsidiary of ENI S.p.A. Stogit manages the natural gas storage and modulation activity with an integrated system comprising of reserves, gas treatment plants, compression plants and a dispatching centre. With its approx. 13×10^9 m^3 capacity, which accounts for 97% and 98% of the storage capacity in central and northern Italy, respectively, Stogit remains a dominant player in the Italian storage market. From a technical point of view, the most relevant issue concerns the maximum value of injecting pressure. In the majority of the fields the injecting pressure has not exceeded the initial pressure at reservoir discovery. Only in Settala field was a 7% pressure increment over the initial pressure authorized for a limited time interval. In this regard, a scientific debate is in progress in order to set a technical disciplinary that allows not only the gas storage in the depleted gas field, but also the opportunity to use saline aquifers. The Italian government is devoted to increasing the total gas capacity to reach about 19×10^9 m^3 by 2014 (MSE, 2008). As far as subsidence is concerned, the Italian field experience shows that no particular subsidence problems emerged during injection and production operations.

CONCLUSIONS

Because of Italy's heavy reliance on oil and gas imports, energy security and sources diversification are a top priority in the country's strategic policy and management of energy. In order to help Italy to meet its growing energy demand and reduce its energy bill, the domestic hydrocarbons exploration and production industry should be involved in an increasing development process. Domestic hydrocarbons are an important and a strategic economic resource, but they have to be looked for in a country that is particularly sensitive as far as environmental issues are concerned, especially because Italy holds a significant part of the artistic heritage of the entire world, and many towns are sort of open-air museums.

In the last decade hydrocarbon production has raised many concerns, such that nowadays, the general set of rules point towards strategies for environmental protection that try to allow sustainable management of these energy sources. A very good knowledge of the territory is necessary, with the best efforts of innovation in technology and the use of environmental impact minimizing technologies. The oil and gas industries are requested to report on their environmental performance due to the environmental awareness that has grown in recent years. The "nimby" ("not in my backyard") responses, generally described as extreme opposition to local development projects, must be properly attenuated, so as to diminish parochial and localized attitudes towards problems, which exclude the broader implications. On the other hand, it is claimed that E&P projects are often characterized by limited information about risks and benefits.

In this scenario, the sustainable management of a hydrocarbon reservoir can be performed through both constant dialogue and collaboration among the oil and gas industries, universities, local authorities and the resident population, and through the maximum transparency of environmental impact assessment studies, avoiding highly emotional responses to the conflict and too high concerns about project risks.

APPENDIX

Gas fields – Ravenna area The "Ravenna mare" gas field was the first Italian offshore discovery (1960), and amongst the first offshore developments in Europe. Since then, more than 900 wells have been drilled in the Italian Adriatic offshore north of the 43rd parallel, which nowadays supply about 5×10^9 m^3 of natural gas per year. Here, numerous gas fields are present in the proximity of the coastline. Evidence of soil sinking in this area was recorded during the early 1950s, causing concerns because of the nearby town of Ravenna, 10 km from the seashore but sitting just a few decimetres above the sea level. In this context, the preservation of the wetlands located close to the shoreline by monitoring both natural subsidence of the recent sediments and

the eustatic variation of the mean sea level, is important, and also limiting as much as possible the man-induced subsidence due to underground fluid withdrawal (water and hydrocarbons), in order to avoid possible ingression of the shoreline. Here, the constant collaboration of the E&P industry with the local authorities and residents, the transparency of operations and the accuracy of environmental impact assessment studies is paramount. This is indeed a good example of cooperation and dialogue between the local Government and the industry, resulting in the preservation, and even in the enhancement of the traditional tourist and agricultural vocations of the area.

Oil fields – Ticino Natural Park The Trecate-Villafortuna oilfield is partly located inside the natural park of Ticino River, between Turin and Milan, and sits close to a densely populated and industrialized area. Oil discovery dates back to 1984, and the development of the field demonstrated a good cooperation with the local government and the authority for the preservation of Ticino Natural Park. Production activity is located close to well-wooded areas and/or areas with high naturalist and agricultural interest. The field is characterized by deep wells (more than 5500 m) with high pressures and temperatures up to 200°C; the produced fluids contain CO_2 and H_2S. In 1994, an oil blow-out during the drilling of a well caused a large oil spill above an intensely farmed area; remediation operations were soon planned and correctly managed with the effective cooperation of local authorities. Notwithstanding the accident, oil production continued, and in 1996 it was boosted by the application of multiphase surface ejectors, which increased the production rate by 30% with minimal impact on existing facilities, and by the drilling of horizontal drains from existing wells. In Trecate-Villafortuna field, other innovative technical solutions respectful of the environment have been adopted: surface installations have been kept low; noise sources have been isolated with sound absorbing panels. As for drilling activity, the first use of a mud enriched with paraffin oil with an aromatic content less than 1% (normally, diesel fuel aromatics add up to 30%), was made and drastically reduced its ecological toxicity. Such efforts allowed sustainable hydrocarbon production in this environmentally sensitive area.

REFERENCES

Bilardo, U. & Mureddu, G. (2004) *Crude Oil Traffic and Environmental Sustainability* (in Italian). Unione Petrolifera, Roma, Italy.

Brighenti, G., Macini, P. & Mesini, E. (2003) Environment and sustainable management of oil and gas reservoirs in Italy. *Proc. SPE/EPA/DOE E&P Env. Conf.* (S. Antonio, TX, USA). SPE Paper 80608.

Directive, European Parliament and Council (2009) On the geological storage of carbon dioxide. http://eur-lex.europa.eu/LexUriServ/LexUriServ.do?uri=OJ:L:2009:140:0114:0135:EN:PDF.

ENI (2008) World oil and gas review, .July 2008, 101 pp. Rome, Italy.

MSE (2008) Hydrocarbon exploration and production in Italy. Annual report 2008.

(Proceedings of EISOLS 2010, Querétaro, Mexico, 17–22 October 2010). IAHS Publ. 339, 2010.

Management of the environmental resources of the Kanto groundwater basin in Japan – land subsidence and monitoring system

K. FURUNO[1], A. KAGAWA[1], O. KAZAOKA[1], Y. SAKAI[1], T. KUSUDA[1] & H. NIREI[2]

1 *Research Institute of Environmental Geology, Chiba (RIEGC), 3-5-1, Inagekaigan, Mihama-ku, Chiba 261-0005, Japan* k.hrn50@ma.pref.chiba.lg.jp

2 *(NPO)The Society of Geo-pollution Control, Japan, 5-24-1 Makuharihongoh, Hanamigawa-ku, Chiba 262-0033, Japan*

Abstract Kanto plain in Japan is called Kanto groundwater basin. Groundwater level and land subsidence is monitored by about 500 monitoring wells and almost 5000 benchmarks. The groundwater level fell to its lowest in the early 1970s. Then regulations were strictly adhered to in southern Kanto. Consequently, the recovery of the groundwater level was recognized to be due to the control of the pumping. The groundwater resources can be used while the health condition of the groundwater basin is examined by periodical health checks. The monitoring system is important for the sustainable use of groundwater.

Key words land subsidence; Kanto groundwater basin, Japan; monitoring system; levelling; monitoring well

INTRODUCTION

The Kanto plain, Japan, is also called "the Kanto fore-arc submarine basin" or "the paleo-Kanto-submarine basin", based on surrounding geological and physiographic features such as Nasu Volcanic Zone, Fuji Volcanic Zone, Japan trench and Izu-Ogasawara trench (Nirei *et al*., 1990). Over 40 million people live on the Kanto plain which includes the Tokyo metropolis. The waterfront area around Tokyo Bay mostly includes both alluvium and reclaimed areas and is densely covered with houses and factories. Sediments of the Kanto basin are 2500–3000 m thick and are of Miocene to Holocene age. The basin is also called the Kanto groundwater basin from the standpoint of the production of groundwater, natural gas and iodine. Uncontrolled use of land and resources has caused many environmental problems, such as land subsidence, floods caused by urbanization, slope failure, geo-pollution (sedimentary strata pollution, groundwater pollution and groundair pollution), waste disposal, liquefaction, earthquake disasters, etc.. To ensure effective use of environmental resources without causing environmental problems, a monitoring system for their management and land use has been developed. The system has about 500 self-recording observation wells, almost 5000 benchmarks (levelled every year), a seismic observatory array, and so on. Over-pumping of the groundwater resulted in a serious land subsidence problem in various areas, especially the alluvial plains so that it was inevitably necessary to control the groundwater use to solve the problem (Aihara *et al*., 1969). Consequently, systematic observations of pumping up volumes, groundwater level changes and land subsidence records for the effective groundwater use have been carried out for preventing the land subsidence from a geological point of view (Research Committee on Land subsidence Prevention in Southern Kanto District, 1974).The observations have succeeded in preventing the land subsidence so far in various areas, especially in the Kanto groundwater basin, which is the largest groundwater basin and has the longest records of observations in Japan (Inaba, 1969).

KANTO GROUNDWATER BASIN AND UNDERGROUND FLUID RESOURCES

The Kanto Paleo-submarine basin can be called the Kanto groundwater basin from the standpoint of the distribution and the fluidity of the underground fluid resources (Nirei & Furuno, 1986). The bottom of the groundwater basin corresponds to the base of the Kanto tectonic basin, which is

Copyright © 2010 IAHS Press

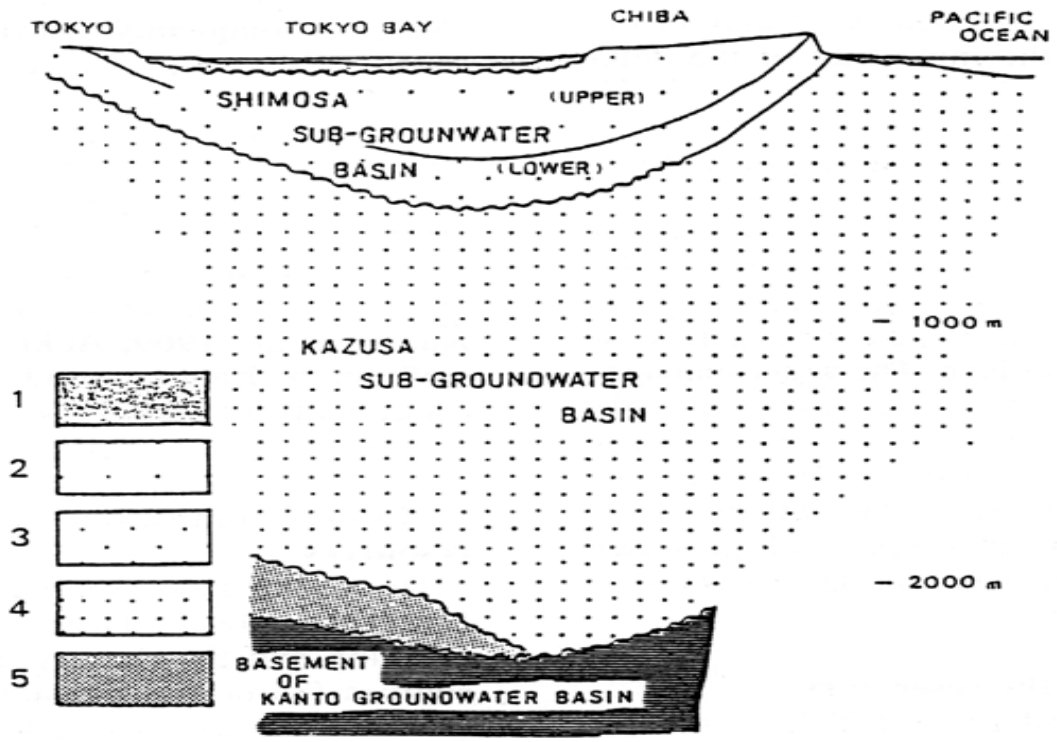

Fig. 1 Schematic section of the Kanto groundwater basin. 1: Alluvial deposits, 2: Upper part of the Shimosa Group, 3: Lower part of the Shimosa Group, 4: Kazusa Group, 5: Miura Group.

situated at 3000–2500 m below the surface. The sediments of the Kazusa sub-groundwater basin in the basin contain brine groundwater including natural gas and iodine (Fig. 1). The equivalent layer of the Kazusa Group that extends to the western and northern part of the Kanto plain, is composed of alternating beds of coarse- to fine-grained deposits and is suitable for groundwater.

The lower part of the Shimosa subgroundwater basin contains groundwater coloured with humic material from the northern to central part of the Boso peninsula, and the coloured groundwater is unsuitable for drinking. In the upper part of the Shimosa sub-groundwater basin, most of the aquifer layers contain freshwater; this basin had the largest pumpage volume of water in the Kanto groundwater basin. However, the more the pumping volume increased, the lower the groundwater level became in the Shimosa upper sub-groundwater basin. This also resulted in lowering of groundwater level even in the alluvial deposits as well as subsidence of the ground surface. It is now widely confirmed that the amount of ground subsidence is affected by the thickness of the alluvial deposits (Nirei *et al*., 1979).

STATUS OF UNDERGROUND FLUID RESOURCE USE

Natural gas and groundwater have been produced as the underground fluid resources in the Kanto groundwater basin. The former is mainly derived from the Kazusa sub-groundwater basin. Annual production of natural gas was 520 million Nm^3 in 1980, and 460 million Nm^3 in 2003. The natural gas produced from the Kazusa sub-groundwater basin was contained in fossil seawater of the Kazusa group. Accordingly, it was inevitable to pump up the fossil seawater when releasing the natural gas, which frequently caused a land subsidence problem. Therefore, the pumping is now limited to the area of hills and the Pacific coast in southern Kanto, a considerable distance from the metropolitan area. Recently, the groundwater has mainly been pumped up at the marginal area of the Shimosa lower sub-groundwater basin and the upper Shimosa sub-groundwater basin. The annual pumped volume was 3.4×10^6 m^3/day in 1978 and 3.1×10^6 m^3/day in 2003 (Prefectural

Governors Committee for Land Subsidence Prevention in Kanto District, 1983, 2008). These data were obtained in the limited area where reporting of pumped volume is required of groundwater users by regulations for preventing land subsidence. This area covers about half of the Kanto groundwater basin. Consequently, the actual pumping volume is estimated to have been twice as much as the values mentioned above. The groundwater has been used for: (1) aqueducts, (2) industries, (3) agriculture, (4) buildings, and (5) other uses. The used volume increases generally as the aqueducts, industries and so on increase in scale. However, the used volume shows a little difference based on each autonomy in the Kanto groundwater basin and the scale of the volume used by the agriculture and building is different in each prefectural government area. The volume of other uses is the smallest amount of the volume, and is of the fifth order. The fact that the aqueducts make up the largest amount of the groundwater use may be a consequence of the concept that it is necessary that groundwater use is for the benefit of inhabitants (Shibasaki, 1976; Research Group for Water Balance, 1976).

CONTROL OF PUMPING VOLUME AND CHANGE OF GROUND LEVEL AND LAND SUBSIDENCE

Each local government has attempted to regulate the pumping volume of the groundwater in order to prevent land subsidence. For example, users are compulsorily required to report the pumping volume. Criteria for the depth and diameter of discharge pipes were set up (Prefectural Governors Committee for Land Subsidence Prevention in Kanto District, 1983). An agreement to control the pumping of fossil seawater containing natural gas was also made between the Chiba prefecture administration and each gas production company. The condition of groundwater levels in the whole Kanto groundwater basin has recently been clarified. The number of observation wells was 375 in total as of 1982 (Furuno *et al*., 1983) and 459 as of 1991. The amount of land subsidence has been measured by precise yearly levelling. The number of benchmarks attained 4880 and the total length of the levelling, 7363.6 km as of 1983, and 4945 benchmarks and 7387.6 km as of 1986. The groundwater management in the Shimosa sub-groundwater basin is described below.

Control of groundwater over-pumping

In the Keihin industrial zone (coastal zone of Tokyo, Yokohama and Kawasaki) located in the southwestern part of the Kanto groundwater basin, the land subsidence phenomena caused by over-pumping of groundwater were recognized in the early 1940s. As a result, industrial aqueducts were established to replace the groundwater pumping from the coastal zone of Kawasaki and Yokohama. In the industrial zone, the pumping was controlled in the 1950s by regulations on the depth of wells and the diameter of discharge pipes. In the industrial zone of Tokyo and its suburbs, the pumping volume was controlled in the 1960s by two laws concerning industrial water and pumping at building sites. However, the countermeasures for land subsidence were often loosely applied by groundwater users, especially the industrial users. In the 1970s, with the rapid growth of the Japanese economy, environmental problems combined with land subsidence were recognized as one of the important problems. In such a social background, not only the national government enacted the strict criteria for the regulation concerning the industrial water and the pumping law for building use, but also the prefectural governments (Tokyo Metropolis, Chiba Prefecture, Kanagawa Prefecture, Saitama Prefecture, Yokohama City and Kawasaki City) in the southern part of the groundwater basin, applied these regulations strictly. As a result, the groundwater level decline and the land subsidence gradually stopped. It was even recognized in certain regions that the groundwater level rose. However, excessive regulations produced another problem in some areas.

Change of groundwater level

It was in the early 1960s that the groundwater level fell to 60 m below sea level in the coastal industrial zone of Tokyo metropolis. After that, the recovery of the water level was monitored

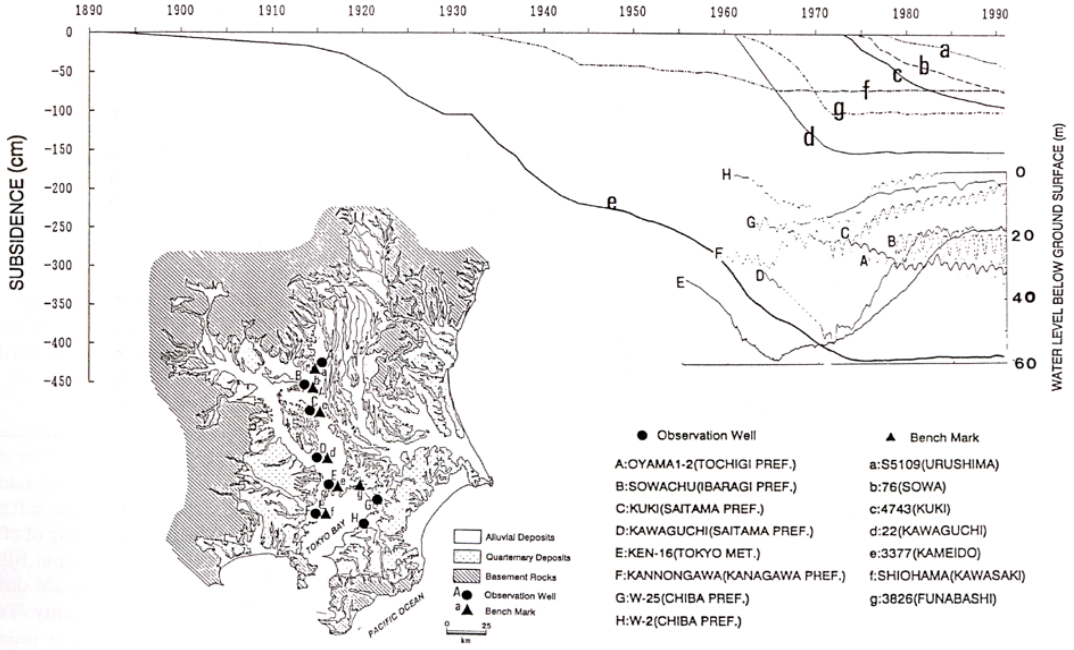

Fig. 2 Historical change of the land subsidence values and groundwater level in the Kanto groundwater basin. (Small letter: land subsidence value, Capital letter: groundwater level).

according to the pumping control. In the 1970s the regulations were strictly adhered to in the southern Kanto groundwater basin. Accordingly, in the years from 1975 to 1980, the water level recovered by 30 to 40 m in the area where groundwater level had lowered. Thus the groundwater level showed a recovering tendency across the whole area (Figs 2 and 3). In recent years, in the central to northern part of the Kanto groundwater basin, the water level has shown a lowering tendency again. The area where groundwater level dropped 20 to 30 m below sea level has expanded. In other words, the centre of the groundwater depression has moved to the northern part because the pumping control in the southern Kanto groundwater basin is applied strictly. The water level is not so low as the former 60 m, but still 20 m below sea level, and the area has spread out.

Change of land subsidence

The land surface has been sinking to below sea level in the downtown Tokyo area of mixed industry and residential use (Shitamachi) since the 1910s. Coincidentally, the areas showing ground level lower than mean sea level and the high water level of ordinary spring tides in Tokyo Bay were widely scattered. Recently, however, these phenomena have been recognized in the alluvial area, not only in Shitamachi of Tokyo, but also in the suburbs of Tokyo such as Kawasaki in Kanagawa Prefecture, Funabashi, Gyotoku and Urayasu on western Chiba Prefecture. This land subsidence has been stabilized by the regulation of the pumping. The land subsidence was stopped in certain areas and the ground surface slightly uplifted by the recovery of the groundwater level (Fig. 3). However, in the area from the central to the northern part of the Kanto groundwater basin, land has begun to subside as a result of over-pumping. That is, the land subsidence area is moving northward.

CONCLUSION

For the purpose of effective use of groundwater and prevention of land subsidence, simulation model analyses based on their relation have been done on several dozen examples (Research

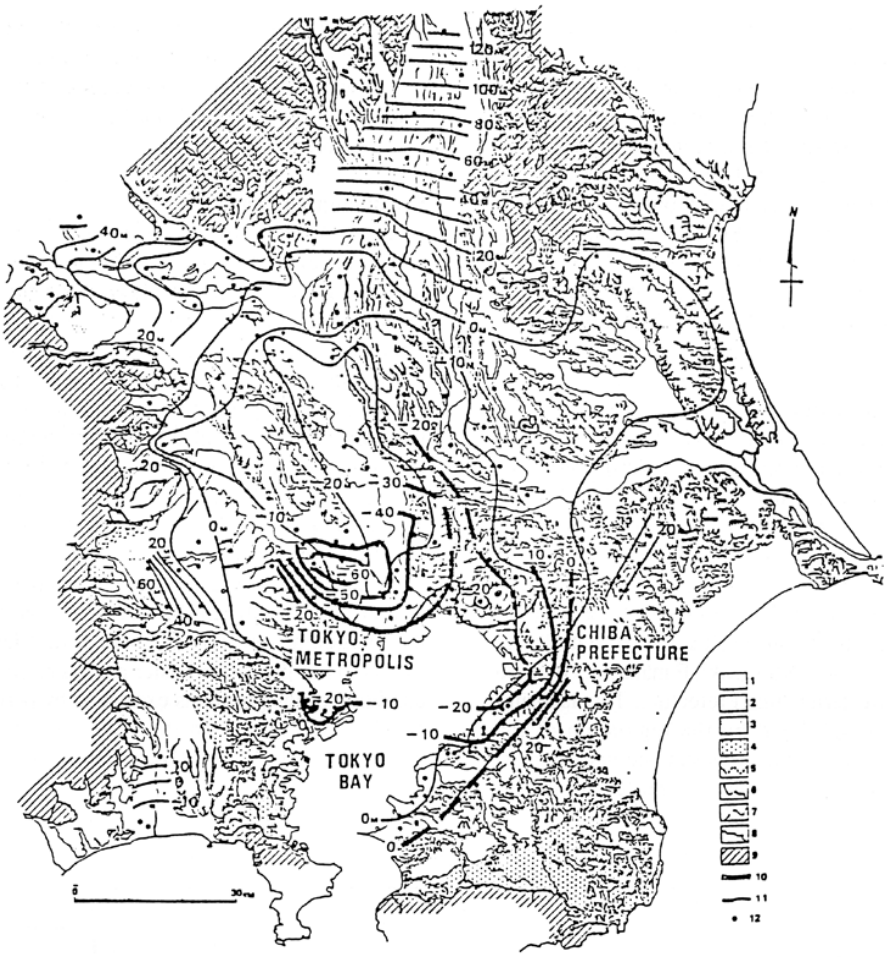

Fig. 3 Confined groundwater level in the Kanto groundwater basin (especially the Shimosa sub-groundwater basin). 1: Alluvial deposits, 2: Upper part of the Shimosa Group, 3: Lower part of the Shimosa Group, 4: Kazusa Group, 5: Boundary between lower part and upper part of the Shimosa Group, 6: Tokyo Bay Unconformity, 7: Naganuma Unconformity, 8: Kurotaki Unconformity, 9: Pre-Kazusa Group, 10: Contour line of confined groundwater level in 1971, 11: Counter line of confined groundwater level in 1984, 12: Monitoring well of groundwater.

Group for Water Balance, 1976; Shibasaki, 1981; Kamata, 1983). These simulation analyses are a prerequisite for calculation of the appropriate pumping volume without causing any land subsidence. It is also necessary to establish a more effective monitoring system for continuous observation of the pumping of groundwater, the changes of groundwater level and land subsidence, and to determine the pumping volume in consideration of the change of groundwater level and the ground movement with the law of dynamic equilibrium between man and nature due to the relation among human groups. In other words, the groundwater resources can be used while the health condition of the groundwater basin is examined by periodical health checks. This idea is in the implementation stage and making a good progress (Nirei *et al*., 1979). The monitoring of the land and groundwater is important for the sustainable use of the groundwater in the groundwater basin.

Acknowledgements We sincerely appreciate help from members of the Research Institute of Environmental Geology, Chiba (RIEGC) and staff of the local governments of Kanto district who developed the monitoring system and kept on recording land subsidence and groundwater level.

REFERENCES

Aihara, S., Ugata, H., Miyazawa, K. & Tanaka, U. (1969) Problems on groundwater control in Japan. In: *Land Subsidence* 2, IAHS-UNESCO, 635–644.

Furuno, K., Nemoto, K., Takanashi, Y., Yada, T., Takizawa, H., Oshima, K., Saotome., W. & Nirei, H. (1983) The monitoring of land subsidence and groundwater head in the Kanto groundwater basin. *Bull. Chiba Pref. Res. Inst. Envir. Pollut***. 15**, 99–108.

Inaba, Y., Abe, I., Iwasaki, S., Endo, T. & Kaido, R. (1969) Reviews of land subsidence researches in Tokyo. In: *Land Subsidence*, 80–86. IAHS Publ. 121. IAHS Press, Wallingford, UK.

Kamata, A. (1983) Development of groundwater simulation models. *Mem. Geol. Soc., Japan* **25**, 463–472.

Nirei. H. & Furuno, K. (1986) Development of Quaternary resources and environmental protection, -status of underground fluid resources use in the Kanto groundwater basin, recent progress of Quaternary research in Japan, National Committee for Quaternary Research in Japan. *Quaternary Research* **11**, 71–80.

Nirei, H., Kusuda., T.,Suzuki, K., Kamura, K., Furuno, K., Hara, Y., Satoh K. & Kazaoka. O. (1990) The 1987 East of Chiba Prefecture earthquake and its hazards. *Mem. Geol. Soc. Japan* **35**, 31–46.

Nirei, H., Yada, T., Hara, Y., Furuno, K., Adachi, I. & Nakamura, M. (1979) Artificial ground movement in the south Kanto district. *Quaternary Research* **17**, 287–298 (in Japanese with English abstract).

Prefectural Governors' Committee for Land Subsidence Prevention Kanto District (1983) Report of groundwater volume pumping up. 228 pp. (in Japanese).

Prefectural Governors' Committee for Land Subsidence Prevention Kanto District (2008) Report of groundwater volume pumping up. 124 pp. (in Japanese).

Research Group for Water Balance (1976) *Groundwater Basin Management* in Japanese). Tokai Univ. Press, Tokyo, Japan.

Research Committee on Land subsidence in Southern Kanto District (1974) Report of research on land subsidence in Southern Kanto District. 297p (in Japanese).

Shibasaki, T. (1976) Carrying capacity of groundwater development and conservation. In: *Groundwater Basin Management*, 47–75. Tokai Univ. Press, Tokyo, Japan (in Japanese).

Shibasaki, T. (1981) Groundwater basin management and land subsidence control. *Recent Proc., Natural Sci. Japan, Science Council of Japan* **6**, 256–267.

(Proceedings of EISOLS 2010, Querétaro, Mexico, 17–22 October 2010). IAHS Publ. 339, 2010.

Environmental and social effects derived from groundwater extraction in Tláhuac and Valle-de-Chalco-Solidaridad, Metropolitan Area of Mexico City

A. TOSCANA[1] **& M. M CAMPOS**[2]

1 *Department of Politics and Culture, Metropolitan Autonomous University, Xochimilco, CP 04960, México, D.F.* atoscana@correo.xoc.uam.mx

2 *Faculty of Geography, Autonomous University of the State of Mexico, Toluca, CP 50110, Estado de México*

Abstract The groundwater extraction in the southeast of the Metropolitan Area of Mexico City has negative consequences for the people who live in Tláhuac and Valle de Chalco Solidaridad, whose houses are exposed to subsidence, salinization and moisture problems that represent economic losses. This area is also exposed to residual water floods due to the lack of maintenance of the La Compañía Channel, the banks of which have broken twice (2000 and 2010) generating great losses too. The governmental response to these problems is limited and usually slow, and governmental authorities have not considered them in urban, rural and civil protection planning. In response, a local community organization (Coordinadora Valle de Chalco) is emerging to accuse three levels of Government for their negligence; this organization is trying to manage the risk and propose alternatives to change the situation for the affected people in the southwest of the Metropolitan Area of Mexico City.

Key words subsidence; flood; Tláhuac; Valle de Chalco Solidaridad; community organization

INTRODUCTION

The high concentration of population in the Metropolitan Area of Mexico City (MAMC) has many negative consequences for the environment. These include significant declines in green areas that impact the recharge of groundwater aquifers; the extraction of water from underground to serve, along with other sources, the growing population of approximately 20 million people; and the difficulties to evacuate the water basin due to the inadequate drainage system. These and other problems are regarded as an environmental crisis that requires in-depth solution. Among the negatives are the subsidence and flooding in some areas of the city. In this case we focus on Tláhuac (delegation of México City) and Valle de Chalco Solidaridad (State of Mexico municipality). In this essay we present only some of the results obtained in our research through bibliographical, statistical analysis and field work. It should be noted that this research has been made using the paradigm that considers that all risks, such as flooding or subsidence, are social constructs.

The study area is located in the basin of Mexico, an endorheic basin with water drainage difficulties. The limits of the basin are: Sierra de Santa Catarina to the southeast; Ajusco Volcano and the Chichinautzin Sierra to the south; to the west, the Sierra de las Cruces; Sierra Nevada and Río Frío to the east; the north is limited by a series of hills and low mountain ranges (Los Pitos, Tepozotlán and Patlachique, among others). The basin was closed approximately 780 000 years ago when the volcanic Chichinautzin Sierra was formed. Then deposition of sediments, fluvio-lacustrine interbedded with volcanic materials, started. The background of the basin formed a system of lakes: Zumpango-Xaltocan, Texcoco and Xochimilco-Chalco (MacGregor Gutierrez *et al.*, 2005). These lakes were fed by the flows that descended from the surrounding mountains and were decisive for the development of human settlements in the region. It is reported that there have been human settlements in the basin since 25 thousand years ago. The most important, in order of flow, are: La Magdalena, La Piedad, Los Remedios and El Cuautitlán, and contribute with springs to the formation of lakes Xochimilco, Chalco, Texcoco, Zumpango and Xaltocan. Lake Chalco basin geomorphically leaves the rest of the watershed by Catarina Sierra (Carreón *et al.*, 2006).

Copyright © 2010 IAHS Press

THE ANTHROPIC TRANSFORMATION TO THE BASIN

Both the subsidence and floods are derived directly from the anthropic changes made to the basin, notably since the Conquest (16th Century), when lakes began to be dried (a process that was not very intensive until 1950), and waterworks were made to drain the water basin. Currently the MAMC occupies 1400 km^2 of the basin, and is located on the ex-lakes that have almost completely dried up; it concentrates almost 20% of the population of the country (Ezcurra, *et al.*, 2006).

Anthropic transformations to the basin have been of different types; we focus on the water-related ones that have been guided by a contradictory logic which is summarized in the following question: How to get water into the basin to serve a growing population and drive economic activities, and at the same time, how to get rid of residual water and rainwater? This logic has been present since the Conquest when the Spaniards, because of the need to extract resources and not understanding the indigenous hydraulic system, began a series of works to transform the environment. The deforestation of the mountains surrounding the basin resulted in sediment accumulation in the lakes and then floods, so the solution was the construction of waterworks in order to control the floods, but they did not function well and the flooding has continued until current time. Some examples of the hydraulic works are: in 1607 the basin was opened to the Gulf of Mexico to drain the waters, then a tunnel was built to the Tula, Montezuma and Pánuco rivers to drain the water; later this became Nochistongo Tajo, that used to drain the water of the Cuatitlán River, main tributary of the Zumpango Lake; in 1974 Canal Guadalupe was built to drain the waters of Lake Xaltocan; in 1867 the works of the Grand Canal drainage began, 47 km long and 100 m deep to evacuate Texcoco waters, this lake was the lowest and it is where the city first was settled; between 1937 and 1942 the basin was drilled for the second time and the Tequixquiac pit was built; deep drainage system (Sistema de Drenaje Profundo) works were initiated in 1975 (Izazola, 2001). However, flooding continued as well as the logic to drain rainwater out of the basin with the wastewater, and bring in water from other basins and the subsoil water, logic that is not only contradictory but also has negative effects.

Coupled with the problem of flooding, in the 17th century the availability of water in the basin began to decline, so, the water extraction from springs far away from the central city started, and in the middle of the 20th century the Lerma River basin and later the Cutzamala River basin water were also incorporated. Groundwater extraction started in the middle of the 19th century by artesian wells, and soon, more and more wells were made in the city centre and its surroundings until it was discovered that the groundwater extraction was causing subsidence. In order to keep the downtown, where the main buildings are located, safe, the extraction moved to peripheral areas of the basin, and the subsidence problems moved from the main city to the edge, gaining a specific configuration in each context.

THE SUBSIDENCE AND FLOODS IN TLÁHUAC AND VALLE DE CHALCO

One of the peripheral areas affected by the removal of groundwater, is southeast of the basin of Mexico, where the Tláhuac delegation and the Valle de Chalco Solidaridad municipality are located. A little subsidence was noted during the 1970s decade, but in the lasts 25 years it has become a great process (almost 40 cm/year). We focus especially on Valle de Chalco Solidaridad because it is the most affected area, not only by the subsidence but also by the floods and the drying out of the former lake. Figure 1 shows a map of the study area.

Valle de Chalco is a settlement that was born irregularly over marshy terrain that corresponds to the old bed of Lake Chalco. It started from the clandestine fractionation of the *ejidos* (collective farmer group properties) in the late 1970s, and grew dramatically during the 1980s, reaching more than 300 thousand inhabitants over 20 years (INEGI, 2001). Growth began on the sides of Highway Mexico-Puebla on ejidal lands of the neighbouring municipality of Chalco de Díaz Covarrubias, and later it grew from a scattered population towards what is now the centre of the municipality, and from Xico, a village in the southern portion of the municipality. It was inhabited

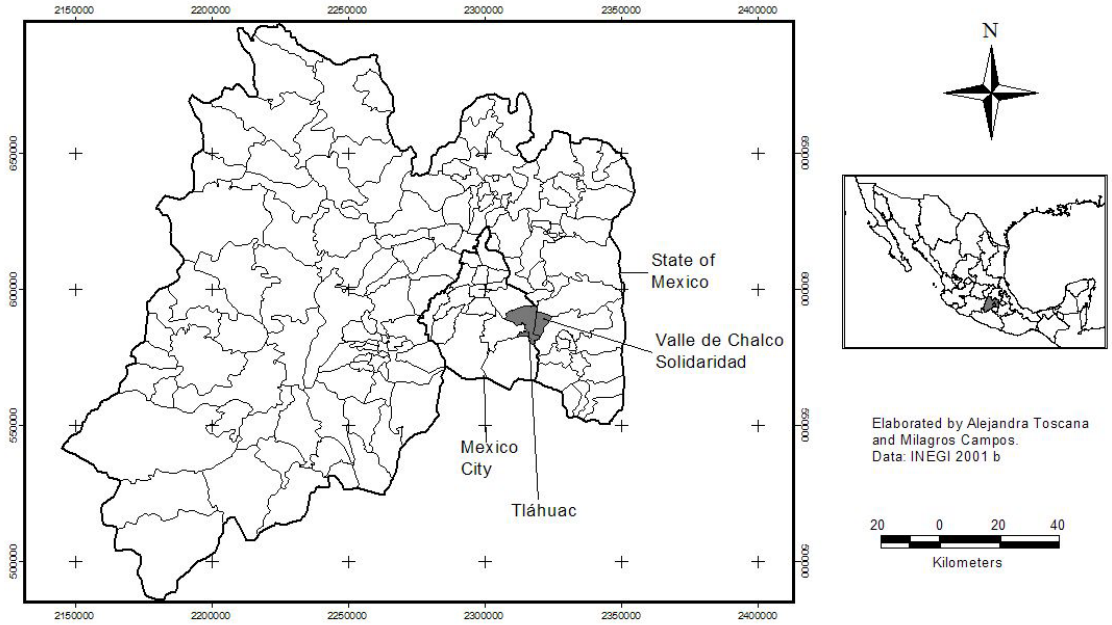

Fig. 1 The study area is located in the central portion of the country, between the southeast of Mexico City and the southwest of the State of Mexico.

by people coming from other peripheral areas of Mexico City (Iztapalapa, Tláhuac and Iztacalco) and metropolitan municipalities (Nezahualcóyotl) when the land/building values in these entities got too expensive and families with limited economic resources had to seek for cheaper housing options. The 1980s put up the price of housing, land and property, and low-income sectors were displaced towards the periphery. It was the first internal migration from edge to edge in the MAMC, in part due to the change from the economic import substitution model to the neoliberal one, which has involved the precarious and uncertain conditions of labour, the low productivity of the soil in Chalco and the lack of territorial reserves for urban growth in the MAMC. Valle de Chalco soon became one of Latin America's largest irregular settlements.

Due to the rough and irregular growth, initially there were no urban services, drainage, tap water, paving of streets, electric light, schools and so on in the area, partly because of the context of the economic crisis across the country during the 1980s, and partly because the population increased at extraordinary speeds. All of these services were got slowly through social struggle. These conditions meant that Valle de Chalco was one of the areas where people most opposed the then official political party, PRI, during the controversial presidential election of 1988, which later motivated Valle de Chalco to be the object of the national programme of "Solidarity" during the six-year term of Carlos Salinas de Gortari (1988–1994) and to become a municipality in 1994 named "Valley of Chalco Solidarity" referring to the social programme (at the beginning, Valle de Chalco was mainly part of the municipality of Chalco de Díaz Covarrubias and other municipalities). In some ways the social programme was successful, since it improved the municipal infrastructure and services; it is worth mentioning that initially the area lacked any services and housing was extremely precarious (Comboni, *et al.*, 1993; Hiernaux, 1995), but the improvements attracted more people to move there and the urban services became insufficient again.

The provision of water was made (and still is) from groundwater extraction, so 14 artesian wells of 400 m depth, called the Mizquic-Santa Catarina system, were built in the plain of Chalco; the groundwater aquifer is fed by the flows from the surrounding mountains, but it is considered to be overexploited by about 36.3% (Lesser *et al.*, 2005); this has caused subsidence at a rate of up to 40 cm/year in the plain of Chalco, where the urban parts of Tláhuac and Valle de Chalco

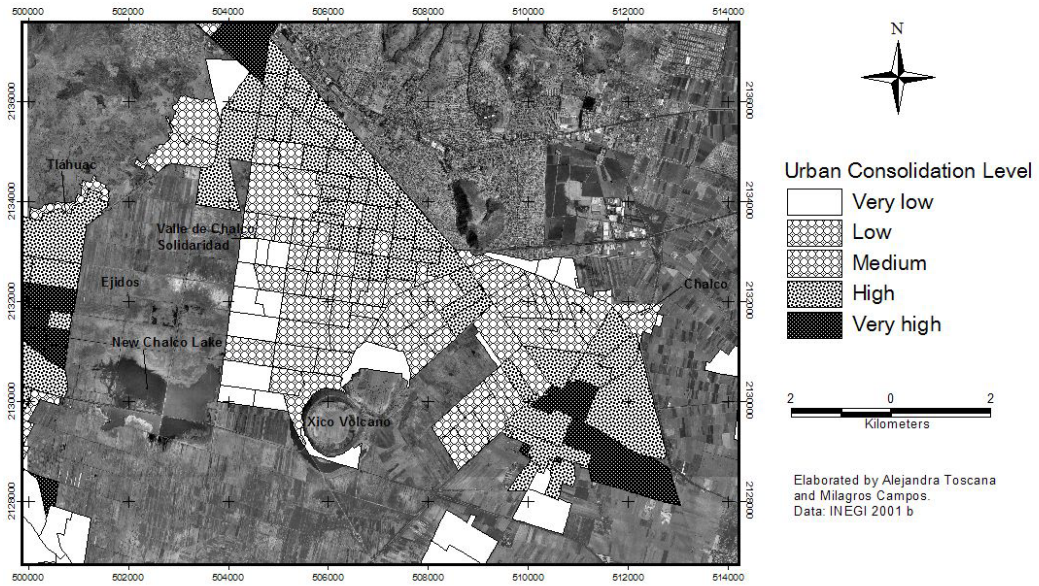

Fig. 2 The New Lake of Chalco growing along the artesian well system Mizquic-Santa Catarina, the urban area on both sides left and right, and remaining *ejidos* at the north and south. Valle de Chalco is at the left of the lake with lower levels of urban consolidation; Tláhuac is at the right side with higher levels. The closest houses to the lake have serious subsidence, salinization and moisture problems, while the houses at the north are the most exposed to the residual waters floods.

Solidaridad have extended. The subsidence is generating a topographic depression where a new lake is being formed by the accumulation of precipitation water that cannot escape by the natural canal system. A study by Ortiz *et al.*, (2007) recognized, by means of aerial photographs, that until the late 1980s, where today there is a lake (New Lake Chalco) of 1000 ha at 12 m below the original ground level, there was only a set of several shallow puddles, that have become a lake that is almost spreading over the densely populated urban areas of Tláhuac and Valle de Chalco Solidaridad. Among the consequences of the new lake formation are urban infrastructure and housing damage (some of them are sinking and are affected by fractures, and have salinization and moisture problems). If the groundwater extraction continues at the same rate, it is possible that in less than ten years, the sinking reaches about 20 m deep, the new lake gets much bigger and deeper and the risk for the population increases considerably.

Through a statistical method (principal components), an urban consolidation index was calculated based on variables about housing (house roof construction materials, quality of the kitchen, availability of running water and drainage inside the house, and number of rooms in the house), income and scholastic level of the family members; the methodology was adapted from Zamorano *et al.* (1999) and the data were provided by INEGI (2001b). These variables have a similar statistical behaviour and allowed us to observe different levels of urban consolidation that were classified into five ranges. The levels obtained for Valle de Chalco Solidaridad are too low to be an urban area; even Tláhuac, which is a peripheral delegation of Mexico City, presents much higher levels of urban consolidation, probably due to the irregular and precarious conditions that have characterized Valle de Chalco since it was originated. The higher levels indicated better housing and urban service availability conditions and they correspond to the oldest neighbourhoods close to the freeway Mexico-Puebla, which have had more time to get consolidated; the lower levels are close to the new lake and correspond to the newest settlements, making these people even more vulnerable (Fig. 2).

Another water-related problem is the lack of maintenance of the La Compañía Channel that passes through the northern part of the study area and moves residual waters from the MAMC out of the basin. This channel overflowed in 2000 and 2010, via fractures in its walls, causing serious

damage to the population. Due to the natural physical conditions of the plain, located in the old bed of the Chalco Valley, it has a tendency to flood; the water remains stuck for days. In the recent floods of February 2010, that affected more than two thousands houses, slow and poor management by the three levels of Government (municipal, state and federal) to the flooding generated major social unrest led by Coordinadora Valle de Chalco, the community organization, and other religious organizations that accused the three levels of Government of generating the flooding problem by not providing any maintenance services, not solving the flooding problem, and not giving the aid promised to the victims (the victims were supposed to receive economic aid to repair the main housing damage). The waters remained for more than nine days inside several houses and on the streets, and the Government did not send any help at all to the affected area when the channel overflowed. Instead they sent soldiers and policemen to watch the neighbourhoods; so Coordinadora Valle de Chalco reproached the authorities for considering them not as victims but as criminals. The civil society, in the absence of Government had to organize hostels, feed the victims, care for the sick and so on – activities that according to current Mexican legislation, belong to the State. Victims protested twice by blocking the Mexico-Puebla Highway to draw attention to the need, but the state of Mexico and federal authorities suppressed the protest (police hit men, women, pregnant women, old people and children), exacerbating the social unrest and creating a social and political conflict that probably is not going to be over soon.

CONCLUSIONS

The Tláhuac–Valle de Chalco Solidaridad area is exposed to a number of dangerous pseudo natural phenomena: the floods, the subsidence and the growth of the New Lake of Chalco, are closely linked processes. These phenomena are not to be seriously taken into account in urban or rural policies or civil protection although representing a danger to the population. There are no attempts to re-investigate these processes, there is no governmental proposal to change the water logic or even to reduce the risk. Obviously the logic that leads the water policies is unsustainable and is going to create more and deeper problems in the short, medium and longer terms. It is important to recall that Valle de Chalco is an urban area with a story of social struggle, in the early 1980s for property rights, then for the provision of urban infrastructure and services, and now for preventing flooding and managing risk; and it is not an isolated struggle, it is linked to La Otra Campaña that has members throughout the country. The problem of floods and subsidence are bringing to light endogenous initiatives that question the established order and, although they are still emerging, comprise alternatives to change the situation “from the bottom and the left”.

REFERENCES

Carreón, D. *et al.* (2006) Mecanismos de fracturamiento de depósitos arcillosos en zonas urbanas. Caso de deformación diferencial en Chalco, Estado de México. *Boletín de la Sociedad Geológica Mexicana* **2**, 237–250.

Comboni , S. *et al.* (1993) La expansión urbana en la periferia de la Ciudad de México: prácticas sociales de los habitantes del Valle de Chalco. *Relaciones* **7**(8), 88–113.

Ezcurra, E. *et al.* (2006) *La Cuenca de México*. FCE, México.

Hiernaux , D. (1995) *Nueva Periferia, Vieja Metrópoli: El Valle de Chalco, Ciudad de México.* UAM-X, México.

INEGI (2001a) XII Censo General de Población y Vivienda, 2000, Estado de México. Aguascalientes, México.

INEGI (2001b) Sistema de Consulta para la información censal, Estado de México. Aguascalientes, México.

Izazola, H. (2001) Agua y sustentabilidad en la Ciudad de México. *Estudios Urbanos y Demográficos* **47**, 285–320.

Gutiérrez de MacGregor, M. T. *et al.* (2005) *La Cuenca de México y sus cambios demográfico- espaciales*. Instituto de Geografia, UNAM, México.

Lesser, J. M. *et al.* (2005) El agua subterránea en la Ciudad de México. V Congreso de Aguas Subterráneas, Hermosillo, México.

Ortiz, D. *et al.* (2007) Origen y evolución de un nuevo lago en la planicie de Chalco: implicaciones de peligro por subsidencia e inundaciones de áreas urbanas en Valle de Chalco (Estado de México) y Tláhuac (Distrito Federal). *Investigaciones Geográficas* **64**, 26–42.

Zamorano, J. J., *et al.* (1999) Geomorphological processes, natural hazards and their socio-spacial differentiation in Mexico City. In *Problems of megacities: social inequalities, environmental risks and urban governance,* (ed. by A. Aguilar) 311–320. Geography Institute and Commission of Urban Development and Urban Life. IGU, México.

(Proceedings of EISOLS 2010, Querétaro, Mexico, 17–22 October 2010). IAHS Publ. 339, 2010.

The centenary of land subsidence monitoring in Shanghai

SHI-LIANG GONG
Center for Land Subsidence of China Geological Survey, Shanghai 200072, China
gong_shiliang@126.com, shanghaigeology@163.com

Abstract Using the one hundred-years of consecutive monitoring data collected since 1910, this paper analyses the characteristic and regular pattern of land subsidence development in Shanghai, China, and advances the direction for more in-depth research of land subsidence and control and countermeasures, given the *status quo* situation and the development trend. Land subsidence in Shanghai is mainly derived from the consolidation compression of the Quaternary strata due largely to the extraction groundwater, but urban engineering construction has more recently become an important factor in land subsidence. Under the impact of periodic groundwater level decline due to long-term extraction of groundwater, the compaction trend of the confined sand aquifers has become obvious day by day. Deformation amounts are over 50% of total land subsidence over the 100-year period. The shallow saturated soft soil layers show the apparent rheological phenomena of water removal due to engineering and building loads, and their deformation amounts are nearly 30% of total land subsidence. The 170–300 m deep aquifers and the 3–75 m deep soft clay layer are the two major layers for land subsidence in Shanghai. Over the last 100 years, the largest accumulated land subsidence amount surpassed 3 m, and the average accumulated land subsidence amount was nearly 2 m. A permanent loss of ground elevation, caused by land subsidence, poses serious threats to the city's flood-control works; the flood-defence walls of the Huangpu River in Shanghai Bund have been increased in height and reconstructed four times. The economic losses due to land subsidence in Shanghai are nearly US$45 billion so far. Land subsidence is not only an important geological disaster affecting sustainable economic and social development, but also an important link to the urban disaster system. It is helpful to restrain the land subsidence development by adopting the implementation of joint scheduling of groundwater resources utilization in the Yangtze River Delta city group, optimizing the groundwater mining pattern, reinforcing the prevention engineering for land subsidence, and strengthening the supervision and management of the construction projects.

Key words land subsidence; geological disasters; groundwater mining; engineering construction; soil deformation; management strategies; systematic control; Shanghai, China

Copyright © 2010 IAHS Press

(Proceedings of EISOLS 2010, Queretaro, Mexico, 17–22 October 2010). IAHS Publ. 339, 2010.

How much subsidence is allowed: the introduction of the "effective subsidence capacity" concept in The Netherlands

JAN VAN HERK[1], HANS ROEST[1], INGRID KROON[2], JAAP BREUNESE[2] & HANS DE WAAL[1]

1 *State Supervision of Mines, PO Box 24037, AA The Hague, The Netherlands*
m.vanherk@minez.nl

2 *TNO Built Environment and Geosciences, Geological Survey of the Netherlands, PO Box 80015, 3508 TA Utrecht, The Netherlands*

Abstract Subsidence caused by the extraction of hydrocarbons or salt mining is a sensitive environmental and socio-economic issue in the Netherlands. Every company involved in such activities has to submit a Production Plan. The Production Plan fully considers potential land subsidence issues for approval to the authorities. The plan provides contour maps of the subsidence to be expected. It also details the measures that will be undertaken to limit the subsidence and the damage from subsidence as much as possible. The Production Plan is made available to the public as part of a legal consultation process. The legal framework makes it possible for the authorities or the judiciary not to approve the plan when the risk of damage from subsidence is considered too large. A key question for the companies involved is therefore: How much subsidence is allowed? The legal framework itself does not provide detailed answers. To address the issue, the concept of "effective subsidence capacity" has been developed together with an operational procedure based on expectation values of subsidence rate. This has enabled extraction of natural gas from the environmentally very sensitive Wadden Sea area. The approach is supported by environmental experts and provides clarity to mining companies. To determine the effective subsidence capacity for an estuary like the Wadden Sea, the maximum volume rate of subsidence (or relative sea level rise) that can be accommodated in the long term, without environmental harm, is established first. The volume of sediment that can be naturally transported and settled into the tidal basin where the subsidence is expected determines this volume rate or "natural subsidence limit". The capability of the tidal basins to "capture" sediment over longer time periods (*c*. 20 years) is the overall rate-determining step. Effective subsidence capacity is the maximum average subsidence rate available for planning human activities. It is obtained by subtracting the subsidence "consumed" by natural subsidence in the area (sea level rise, shallow compaction) from the total long-term natural subsidence limit. In the operational procedure for mining companies, six-year average expectation values of subsidence rates are used to calculate maximum allowed production rates. This is done under the provision that production will be reduced or halted if the expected or actual subsidence rate (natural + man induced) is likely to exceed the natural subsidence limit. Monitoring and management schemes are in place to measure and analyse actual subsidence, to ensure that predicted (6-year average) and actual (19-year average) subsidence stay within the natural subsidence limit and to confirm that no damage is caused to the environment. Regular communication keeps the public and others informed on use of the effective subsidence capacity to demonstrate that the actual average subsidence stays strictly within the defined bounds. The concept of effective-space is generic. It can be customised to manage other subsidence limits if more appropriate.

Key words subsidence management; effective subsidence capacity; natural subsidence limit; Wadden Sea; gas production

INTRODUCTION

Proper management of subsidence – irrespective of its causes – is important for a densely populated country like The Netherlands where most land is near or below sea level. Without the protection of dunes, dikes and pumping, large parts of the country would flood. Subsidence in The Netherlands has many causes: near surface de-watering of peat layers and land regained from the sea can result in 50 cm or more subsidence within a time frame of a few years. Man-induced artesian head changes, water production and extraction of salt, oil or gas are other causes. The predicted sea level rise from global warming will increase the challenge. From a water management perspective, less than five cm subsidence is often considered within the noise of the

Copyright © 2010 IAHS Press

overall system. With more than a hundred producing mining projects in The Netherlands, only a handful show subsidence above a few centimetres. Examples are the Groningen, Ameland and Harlingen gas fields, and a few salt mining locations where present subsidence is of the order of 30 cm. Predicted subsidence at abandonment varies between 35 and 65 cm. In sensitive areas like the Wadden Sea, lower subsidence (rate) numbers can be important. A risk-based approach is taken to distinguish those cases where the expected subsidence, including uncertainties, is at risk of exceeding the robustness limit of the area. Damage can often be prevented provided subsidence is properly managed and measures taken to counter its adverse effects are timely. In The Netherlands an extensive legal, technical and organisational framework is in place.

MANAGEMENT OF SUBSIDENCE

Legal frame

A mining company has to deal with many laws before it can produce natural gas, in particular from underneath an environmentally sensitive area. The most important are: the Dutch Mining Act, the Dutch Nature Protection and Environmental Laws and the Dutch Spatial Planning Law. Under the Mining Act, companies involved in mining activities have to submit a Production Plan which considers potential land subsidence issues. Approval by the Minister of Economic Affairs is required. The Production Plan provides contour maps of the extent of subsidence to be expected. It also details the measures to limit subsidence and damage from subsidence. The Production Plan, other plans and license approvals are made public as part of a legal consultation process. The legal framework makes it possible for the authorities or the judiciary not to approve a Production Plan when the risk of damage from subsidence is considered too large.

Technical frame

Subsidence predictions are the result of integrated multidisciplinary workflows in which static and dynamic reservoir models are developed, calibrated and used to feed geomechanical models. The size and complexity of the effort is driven by the identified exposure and available data; simple where it can be, extensive and complex were it must be. The Netherlands have a long tradition of geodetic and geomechanical expertise. High quality benchmark networks, often preceding the production period, are in place and are regularly monitored. In many of the gas fields compaction and reservoir pressures are effectively de-coupled. This reduces uncertainties and allows modelling simplifications. Still, predictions accurate beyond an order of magnitude can be difficult to make at an early stage, mainly because of the scarcity of data and model uncertainty, e.g. the contribution from aquifers surrounding the reservoir. To manage this, multiple scenarios need to be developed to cover the range of possible outcomes, including a worst case. During the production period the various scenarios are regularly confronted against observations. This triggers scenario probability updates, preferably using a statistical (Bayesian) approach (Nepveu *et al.*, 2010). More and more field data is becoming available indicating nonlinear compaction behaviour (NAM, 2005, 2007; de Waal, 1988). Initial compressibilities are much lower compared to later stages. This is a point of attention when updating predictions based on early observations. A related issue to consider is the large difference in loading rate – typically five orders of magnitude – between laboratory and field. As a result, field compressibilities during later stages of production can become 20–30% higher then expected on the basis of laboratory measurements (de Waal, 1988).

Subsidence measurements are carried out in accordance with a Measurement Plan, which has to cover the period of production and up to 30 years thereafter. It specifies the timing, locations and methods of measurement. It includes at least one reference measurement before the start of production. The Measurement Plan is updated annually by the operator and submitted to the State Supervision of Mines (SSM) for approval. Measurement accuracy to centimetre level is requested

which is a major technical challenge against a background of sea level rise, peat oxidation, noise, benchmark instabilities, etc. Innovations in geodetic measurement and interpretation do help (Houtenbos, 2005; Ketelaar, 2008) but the challenge is growing with increasing and concurrent use of the subsurface for production, storage and geothermal projects.

Organisational frame

Mining companies have responsibility for socially and environmentally acceptable production within the framework of Dutch Law. This includes responsibility for prediction and measurement of subsidence, as well as responsibility for preventing or compensating related damage. Compliance with statutory regulations is verified by SSM. The Ministry of Economic Affairs authorises the Production Plan. Technical advice on soil movements is sought from SSM and from a dedicated technical advisory group at TNO working exclusively for the Ministry. A separate "Technical committee on soil movement" advises the Minister on the treatment of soil movement and the prevention of damage in the Production Plan. It also advises on subsidence claims by citizens. The members are recognised professionals in the field of mining and subsidence. Additional case-specific advisory bodies can be created and/or consulted.

The concept of "effective subsidence capacity"

A key question for companies is: how much subsidence is allowed? The legal framework itself does not provide detailed answers. To address the issue and to constrain production for areas where possible subsidence is of the order of the natural robustness of the area concerned, the concept of *effective subsidence capacity* has been developed. The effective subsidence capacity is the maximum human-induced subsidence that the affected area can robustly sustain. This has been specified more precisely as meaning that a subsidence causing activity is allowed if "from a scientific point of view, there is no reasonable doubt that damage will not occur". Depending on the characteristics of the area concerned, the effective subsidence capacity can be defined in different terms: e.g. a maximum subsidence volume, a maximum subsidence at a given location, a maximum deepest point of subsidence or a maximum subsidence rate (at a deepest point or averaged over an area). Determination of the effective subsidence capacity starts with establishing the *natural subsidence limit*, which is the maximum total subsidence (all causes) that the area can sustainably deal with without damage to its "environmental values". All expected subsidence from natural causes is subtracted from the natural subsidence limit. What remains is the amount of effective subsidence capacity available for human activities, e.g. expected gas production related subsidence. The effective subsidence capacity can depend on location and time, and it can change as a result of new data and/or new insights. To apply the concept the effective subsidence capacity is part of a control loop detailed in a protocol that contains the following elements: (1) natural subsidence limit for the period relevant to the planned activity; (2) scenarios spanning the entire uncertainty range of subsidence expected from natural and human causes (including sea level rise); (3) a measurement plan; (4) an agreed procedure to update expectation values of realised and predicted subsidence; (5) a red flag system to give an early warning in case predicted subsidence threatens to exceed the natural subsidence limit; (6) agreed measures to adjust the man-induced subsidence (rate); and (7) a control system to check that impact on the environment does not occur despite total subsidence remaining within the natural subsidence limit. Lastly there is the need for an independent audit system to ensure compliance and to verify the technical integrity of the underlying work.

Application to the Wadden Sea

The Wadden Sea (Fig. 1) is a large temperate coastal wetland system behind a chain of coastal barrier islands. It is one of the world's important wetlands, featuring a rich diversity of flora and fauna. It is on the UNESCO world heritage list and one of The Netherlands most notable nature

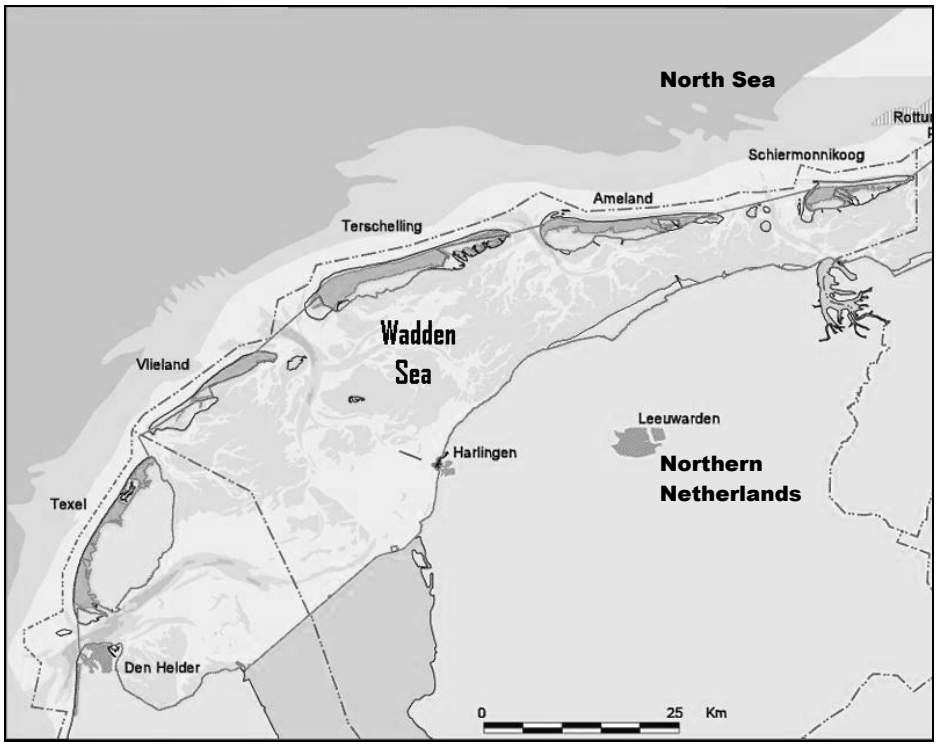

Fig. 1 The Wadden Sea.

conservation areas. Gas production started in the mid-1980s and is only permitted under very strict conditions. For example, all new drilling under the Wadden Sea is done from onshore locations using deviated wells. Damage to the environment from subsidence is prevented by applying the concept of effective subsidence capacity described above as part of an overall subsidence control system. The natural system contains an extensive and coherent system of tidal flats, salt marshes, barriers and ebb tidal deltas. The forces of tides and waves create a complex and highly dynamic pattern of sediment displacement that dominates the morphological system on which the biodiversity thrives. Tide-induced currents transport large volumes of sediment – back and forth – through the tidal inlets. The sand is mainly derived from the coastal region of the islands and the outer deltas, resulting in a net erosion of the coastal region of the barrier islands. Since 1990 this erosion has been compensated by sand supplementation under a dynamic "hold the coast line" preservation policy (Schoeman, 2006). Yearly changes in local sediment height can be tens of cm on the tidal flats and several metres in the vicinity of migrating channels.

The Wadden Sea estuary is characterised by a temporal variability with a characteristic frequency of 18.6 years. For its long-term survival the system depends on a certain level of relative sea level rise. In the case of sea level fall the system will accumulate sediment until it eventually becomes dry. In the case of rapid sea level rise the system will eventually drown, after a period of enhanced barrier erosion and landward migration. This will reduce the effective subsidence capacity to negative. During the decades preceding gas production the rate of relative sea level rise was some 20 cm per century (Schoeman, 2006). The natural subsidence limit, "M", is the maximum rate of relative sea level rise that can be accommodated in the long term without impact on the geomorphological equilibrium and the sedimentation balance. Note that a relative sea level rise may be caused by either absolute sea level rise or subsidence. The sedimentation balance ("the system's hunger for sand") is determined by the capability of the tidal basins to "capture" sediment over longer time periods. It is the overall rate-determining step. Under a conservative approach it is estimated that the tidal basins in the Wadden Sea affected by gas production (Zoutkamperlaag and Pinkegat) can cope with a relative sea level rise of 5–6 mm per year over a period of 18.6 years (as an average over the total tidal basin areas of some 70–140 km^2 each). The

resulting increase in the "sand hunger" of the Wadden Sea is compensated by additional foreshore sand supplementation on the coastal side of the barrier islands.

The effective subsidence capacity available for gas production planning is derived by subtracting the expected average sea level rise – under a conservative cautious scenario – from the natural subsidence limit. The conservative sea level scenario to be used is updated every five years. As sea level rise is predicted to accelerate, effective subsidence capacity shrinks over time. An example for the Pinkegat tidal basin is shown in Fig. 2. Note that for the worst-case sea level rise scenarios the system will eventually start to drown, regardless of whether or not gas is being produced. Gas production profiles are adjusted such that the predicted 6-year average expectation values of subsidence rate (in terms of volume over tidal basin area) – under a range of scenarios and over the full production period – will not exceed the effective subsidence capacity. Expected subsidence rates from production in all relevant gas fields are taken into account. Compliance with the natural subsidence limit is tested in hindcast using the actual subsidence and the actual sea level rise measured for the preceding 19 years. Production is adjusted or halted if the 6-year expectation average indicates a risk of exceeding the effective subsidence capacity now or in the future. The approach is known as "hand on the tap".

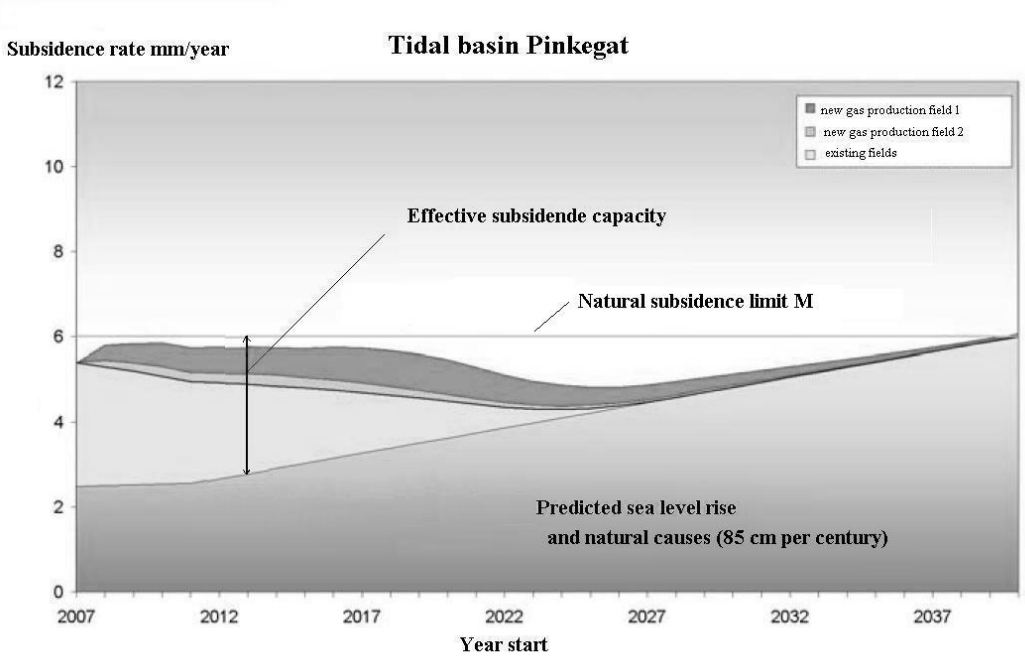

Fig. 2 Application of effective subsidence capacity to the Wadden Sea.

Where possible subsidence is measured using regular benchmarks. In the Wadden Sea special buried benchmarks have been installed on which GPS antennas can be mounted temporarily (five days) during measurement campaigns. Initial results indicate mm-level accuracy. Measurements are repeated once additional subsidence is expected to be greater than noise levels. Onshore, three continuous GPS stations are installed near the subsidence bowl centres, to monitor subsidence rate. They act as an early warning system. In the case of unexpected measurements, there is time to first check the data against additional measurements from other benchmarks and – if the data are confirmed and require action – to timely adjust gas production. Extensive ecological monitoring programmes are carried out to independently confirm that the natural values of the Wadden Sea are not being damaged. Under an agreed measurement and control protocol the operator annually reports latest results and – if needed – updates the models, subsidence predictions, production profiles and production plans. A dedicated Wadden Sea committee of recognised experts has been

installed to evaluate the outcome of the annual measurement and control protocol and the ecological monitoring. To date, measured subsidence has stayed within the natural subsidence limit. No adverse effect from subsidence on the environment has been observed.

FUTURE DEVELOPMENTS

At the moment the effective subsidence capacity concept and the "hand on the tap"` control loop are only applied in the Wadden Sea. The concept could be applied elsewhere, e.g. where available effective subsidence capacity has to be shared between different, competing and possibly concurrent, human activities.

REFERENCES

Ketelaar, V. B. H. (2008) *Satellite Radar Interferometry: Subsidence Monitoring Techniques*. Springer, Berlin, Germany.

NAM (2005) Bodemdaling door Aardgaswinning, NAM velden in Groningen, Friesland en het noorden van Drente. Rapportnummer EP200512202238, 2005.

NAM (2007) Modellering bodemdaling & beheersing bodemdalingssnelheid Waddenzee. Technische bijlage Meet- in Regelprotocol, rapportnummer EP200610217860, NAM B.V., 22 Januari 2007.

Nepveu, M., Kroon, I. C. & Fokker, P. A. (2010) Hoisting a red flag, an early warning system for exceeding subsidence limits. *Mathematical Geosciences* **42**(2), 187–198

Schoeman, P. K. (2006) *Wadden Sea Islands (The Netherlands)*. Eurovision Case Study. Ministry of Transport, Public Works and Water Management, The Netherlands.

Waal, J. A. de & Smits, R. M. M. (1988) Prediction of reservoir compaction and surface subsidence: field application of a new model. *SPE Formation Evaluation* **3**(2), 340–346.

Note An English translation of the Dutch Mining Act, Mining Decree and Mining Regulations can be found on the internet. See: http://www.nlog.nl/en/legal/legislation.html.

(Proceedings of EISOLS 2010, Querétaro, Mexico, 17–22 October 2010). IAHS Publ. 339, 2010.

A warning system for exceeding subsidence limits

M. NEPVEU, I. C. KROON & P. A. FOKKER
TNO Built Environment and Geosciences, Princetonlaan 6, Postbox 80015, 3508 TA Utrecht, The Netherlands
peter.fokker@tno.nl

Abstract In some cases hydrocarbon production is legally restricted to a maximum amount of subsidence that it generates. To support the field management in such circumstances we developed a general framework that enables decision-making when a threshold in a process is about to be exceeded ("an event"). Measurements are combined with prior information to update the probability of such an event. This prior information is derived from the results of an ensemble of model realisations that span the uncertainty present in the model before any measurements are collected; only probability updates need to be calculated, which makes the procedure very fast once the basic ensemble of realisations has been set up. The procedure is demonstrated with an example of a synthetic gas field. Starting with 100 realisations spanning the prior uncertainty of the process, the measurements collected during monitoring bolster some of the realisations while refuting others. In this procedure, more data will mean a sharper determination of the posterior probability. We show the use of two different types of limits: a maximum allowed value of subsidence and a maximum allowed value of subsidence rate for all measurement points at all times. These limits have been applied in real world cases. The framework is general and is able to deal with other types of limits in just the same way. It can also be used to optimise monitoring strategies by assessing the effect of the number, position and timing of the measurement points. Furthermore, in such a synthetic study, the prior realisations do not need to be updated; spanning the range of uncertainty with appropriate prior models is sufficient.

Key words monitoring strategy; decision support; event probability; Bayes; ensemble; subsidence

INTRODUCTION

Gas production in sensitive areas requires close monitoring of the environmental effects and remedial action when limits for these effects are exceeded. Monitoring should enable information to be obtained so that a warning signal can be given whenever the probability that such a limit is exceeded has reached a predefined critical level. The warning, or "red flag", signals the start of an action or a chain of actions. We were confronted with the question of how to devise a monitoring strategy and of how to employ it.

This paper deals with the translation of monitoring data into the probabilities of events occurring at a specified moment in the future. We will refer to the context of subsidence, however the method proposed is applicable to a wide variety of problems within or outside the field of geosciences. Details of the approach followed can be found in Nepveu *et al*. (2010).

METHODOLOGY

Let us assume that gas is produced in an area that has particular heritage or environmental value. A licence is issued to the operating company on the condition that the ground should not subside more than a certain specified limit. This can be expressed as:

$U(t,Y) \equiv$ "Limit will be exceeded Y years from time t"

In this formulation Y will typically stand for a period between two extensive measurement campaigns necessary during the production process, or it is a time span enabling mitigation if critical levels are expected. We are interested in the probability, derived from the monitoring data, that the limit will be exceeded, $P(U(t,Y))$. A completely analogous scheme can be set up for all kinds of probabilities; for example, for a limit not being reached, an aquifer being active, or a fault being sealed.

Before production operations begin, we will make many quantitative models of the sub-surface, using a fixed gas production prognosis so as to take account of alternative geological

Copyright © 2010 IAHS Press

models of the subsurface, as well as of a range of geo-mechanical parameters. Key to our method is that our prior assumptions about $P(U(t,Y))$ are updated with measurements – more accurately, are updated with the probability of each realisation, given the measurements. Suppose the ensemble of subsurface realisations, is $\{M_j;\ j = 1,..., N\}$. Then, following standard probability theory, the posterior probability of "the event" is given as:

$$P\left(U(t,Y)\middle|\text{Data}\right) = \sum_i P\left(U(t,Y)\middle|M_i\right)P\left(M_i\middle|\text{Data}\right) \tag{1}$$

The fact that we write "Data" after the vertical bar in this probability signifies that the probability depends on the data hitherto obtained. It is thus a conditional probability.

The relationship between the subsurface models and the subsidence requires a process, or forward, model. We use a reservoir model in conjunction with a published geomechanical method (Fokker & Orlic, 2006). By running the forward model on the ensemble of subsurface realisations we establish an ensemble of subsidence realisations spanning the uncertainty before any measurements are collected. We know for each member whether it exceeds the subsidence limit or not. In other words, we know what $P(U(t.Y)|M_i)$ is. Although there will inevitably be computational inaccuracies, we assume them to be such that from the models we can infer whether or not $U(t,Y)$ holds: hence $P(U(t.Y)|M_i) = 1$ or 0.

The next question is how to attribute a probability to each realisation in the ensemble. The Bayesian probability of a particular realisation k is:

$$P\left(M_k\middle|\text{Data}\right) = \frac{P\left(M_k\right)\cdot P\left(\text{Data}\middle|M_k\right)}{\sum_j P\left(M_j\right)\cdot P\left(\text{Data}\middle|M_j\right)} \tag{2}$$

In the right-hand side nominator we have the prior probability of the realisation, which is our subjective assessment, and the associated likelihood of the data. The denominator is merely a normalising factor, the sum of all the realisation probabilities considered to be unity.

Since all models are assumed to have a sound geophysical basis before being admitted to our ensemble, all prior probabilities are assumed equal to $1/N$.

The data obtained at a time t ($z(t)$) must be compared with the result calculated for time t for realisation M_k ($z_k(t)$). We should have a general idea about the accuracy of the data and the M_k combined in a standard deviation "σ_k". We propose a Gaussian function for this likelihood, which, for a discrete data set is:

$$P\left(\text{Data}\middle|M_k\right) = \exp\left[-\sum_i \frac{\left(z(t_i) - z_k(t_i)\right)^2}{2\sigma_k^2(t_i)}\right] \tag{3}$$

Using the data acquired, we can now compute the model probability $P(M_k \mid \text{Data})$ with equation (2). This probability is time-dependent, as the longer we monitor, the bigger our data set becomes. Finally, we may compute the required updated probability of "the event", using equation (1).

DEMONSTRATION

We have applied our method to a synthetic case also used in an earlier inversion study (Muntendam-Bos & Fokker, 2009). The case is based on an existing gas field in the northern Netherlands. To be able to apply the method, we used a reservoir model and a geomechanical model to generate synthetic measurements. These we used to update the probabilities of the Monte Carlo realisations created.

The predefined, initial model grid represents a tilted reservoir, cut by three nearly vertical faults (Fig. 1). The field has a surface area of $A = 22.2 \times 10^6$ m^2 and an assumed constant thickness of 91 m, distributed over 6 layers. The gas/water interface has a transmissibility of 0.0337; the

compaction coefficient is a linear function of the pressure. The reservoir is depleted by six wells over a 15-year period, resulting in an average total pressure drop of 90 bar. The model consists of 1036 grid cells for each layer. To be able to calculate subsidence at the surface, we integrate the pressure drop for each surface grid cell at each time step over the 6 layers. Synthetic measurements were created in 89 points every 3 years from the start of production, using the forward model developed by Fokker & Orlic (2006), taking account of the elastic properties of the subsurface. All the measurement points had an associated uncertainty σ_k of 5 mm.

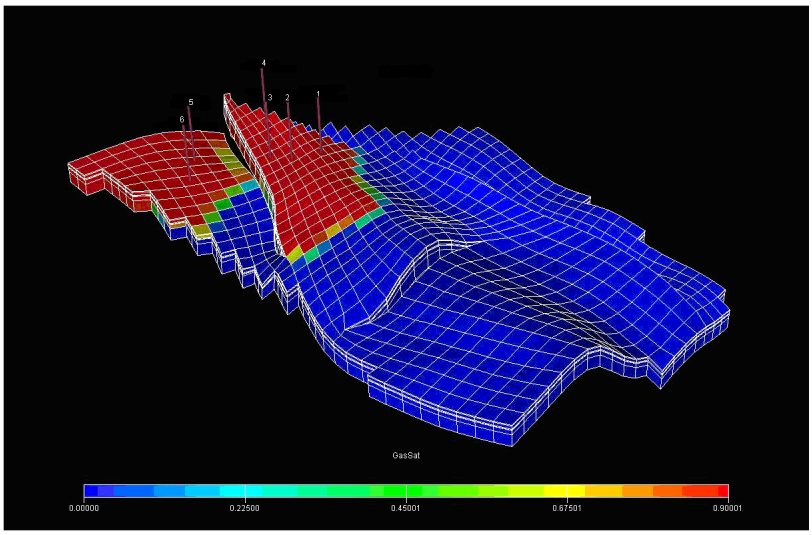

Fig. 1 Synthetic gas field and connected aquifer.

We imposed two different types of limits. The first type is associated with a system that requires remediation measures to be taken if the probability that subsidence exceeding a critical value is imminent meets or exceeds a pre-defined probability. In that case the limit is a maximum permitted value for subsidence for all measurement points at all times: we chose typical values of 3.3 cm and 5.5 cm. Such a limit is often relevant in areas with artificially maintained water management systems. The second type of limit is associated with the subsidence rate. We applied a maximum average rate of 4 mm/year. This can be seen as a simplification of the limit applied in the Dutch Waddenzee area, where gas is produced from below a protected tidal delta sedimentary system.

In our synthetic case we used the same uncertainties as in Muntendam-Bos & Fokker (2009): the transmissibility of the gas/water interface in the reservoir, and the compaction coefficient. For the compaction coefficient, both the absolute value at zero pressure and the dependence on the reservoir pressure were assumed to be uncertain. The prior uncertainties were mapped using Monte Carlo simulations: 100 realisations were created to cover these. The case used to create the synthetic measurements was not part of this ensemble.

For every simulation, the pressure history and the associated compaction were calculated and stored for the complete time sequence. Then we computed the surface subsidence in response to the reservoir compaction on the same network of 89 observation points every 3 years. These subsidence values were compared with the subsidence criterion to assign $P(U(t.Y)|M_i) = 1$ or 0 for each realisation at each time.

The ensemble of the 100 Monte Carlo realisations is represented in Fig. 2 for a location near the centre of the subsidence bowl. As an example, the largest absolute-maximum criterion is exceeded for some of the scenarios after 8 years. The maximum-rate criterion is exceeded for some scenarios right from the beginning; other scenarios follow later, due to the compaction coefficient increasing with pressure.

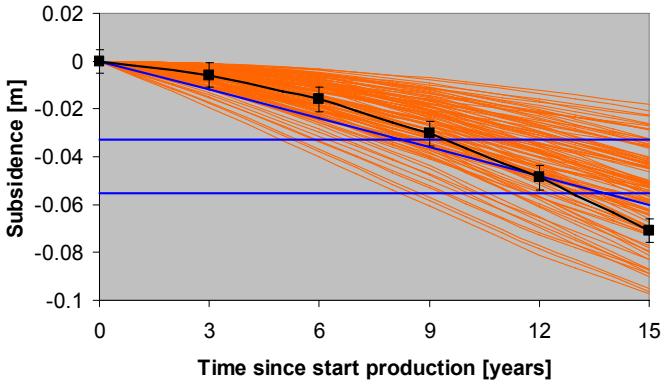

Fig. 2 Ensemble of subsidence realisations in the centre of the subsidence bowl. Orange lines: Monte Carlo results, black symbols/solid line: measurements and their uncertainties obtained with the synthetic truth. The straight blue lines indicate the subsidence criteria: the two absolute values as horizontal lines, the rate criterion as a sloping line.

At the start of the production, all the realisations have the same probability. After the first "measurement campaign", the probabilities of the realisations change. The changing probabilities of realisations with subsequent campaigns result in a higher probability value for realisations showing behaviour close to the truth, while the others decrease in probability. This is indicated in Fig. 3. The distinctive power of the measurements increases with time, along with the increase of the absolute value of the subsidence. After 12 years, only a very limited subset of the original suite of scenarios has a probability that is sizable, e.g. larger than 0.01.

The probability can be determined using all the measurements available, not just the ones in one place. We tested the effect of the number of measurements taken: the development of the probabilities of all the realisations are depicted in Fig. 3. It is clear that with a well-chosen suite of

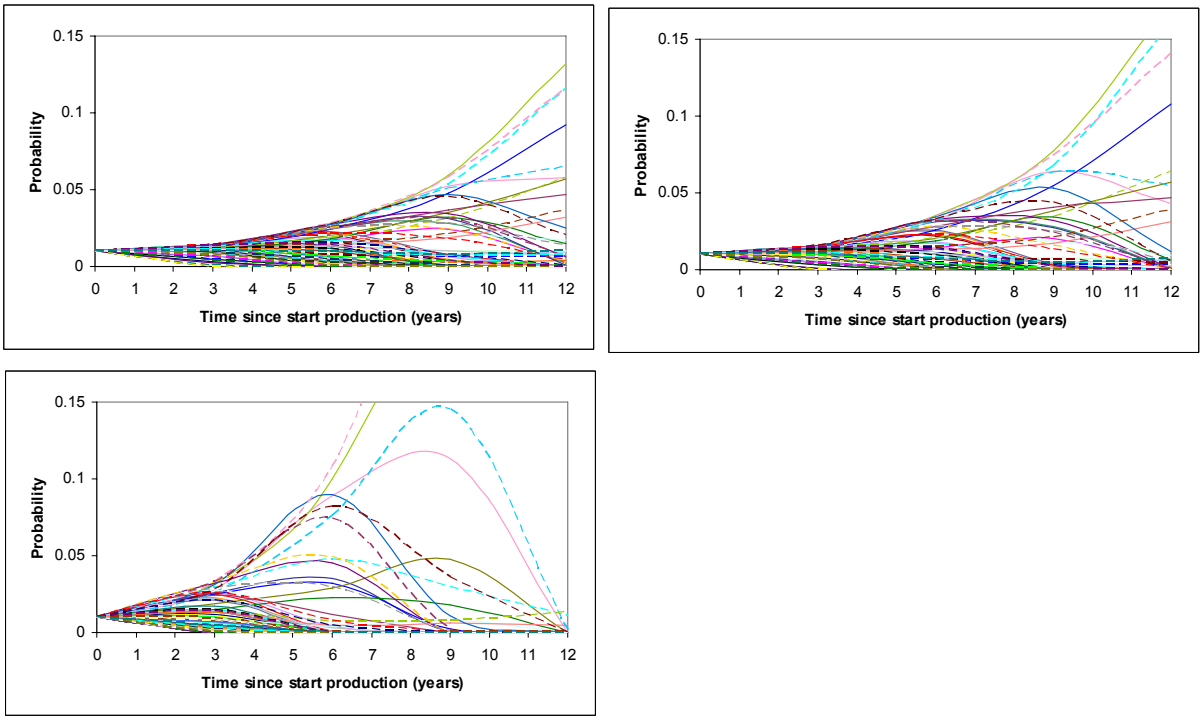

Fig. 3 Competition within the ensemble. With the acquisition of more data with time, the calculated probability of realisations close to the truth increases. When calculating the probabilities, the number of measurement points in each 3-year campaign were: 1 (top left), 7 (top right) and 89 (bottom).

measurements, the quality of the procedure can be much improved. When all the 89 measurements are taken into account, only two of the 100 scenarios retain a reasonable probability; by contrast, in the test with only one measurement in the centre of the subsidence bowl, some 15 scenarios remain probable until the end.

The final step in the procedure is the determination of the probability that the subsidence criterion will be exceeded. The results for the probabilities that the criteria will be exceeded in the next measurement campaign are given in Fig. 4. They are compared with the probabilities determined without any measurements, i.e. assigning equal probability to every single realisation during the complete period. This probability (Fig. 4, Top) slowly increases with time as more and more realisations exceed the subsidence criterion.

When there is only one measurement point, there is already a considerable probability that the limit will be exceeded after 6 years (Fig. 4, bottom left), and already even after the first campaign. This is not the case when all 89 measurement points are included: then the determination of the probability is much sharper. The same is true after 9 years: for a single point, the probability of exceeding the limit in year 12 has only risen to about 0.4. With all the 89 points included, the determination of the probabilities is much sharper. The results for the criterion with the absolute value and 89 points included (Fig. 5, bottom right) also show that the procedure results in a realistic estimate of the probability that the criterion will be exceeded.

The framework that we have developed can be used in a straightforward way to optimise the monitoring strategy. That can be done by assessing the effect of varying the number, position, type and frequency of hypothetical measurements on the probability of exceeding a limit within a certain time window. Note that no actual measurements are needed for such an exercise, which is, in fact, just a sensitivity study.

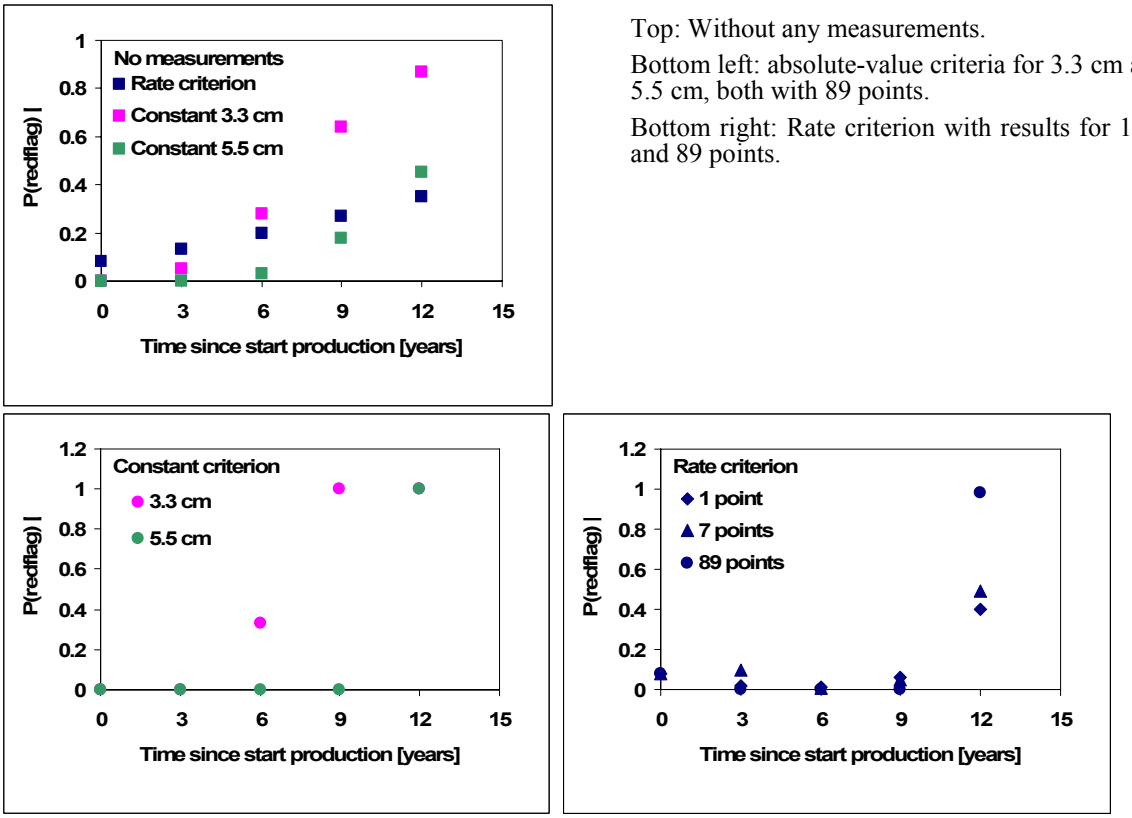

Top: Without any measurements.

Bottom left: absolute-value criteria for 3.3 cm and 5.5 cm, both with 89 points.

Bottom right: Rate criterion with results for 1, 7, and 89 points.

Fig. 4 Probability that in the next campaign the subsidence criterion is exceeded, taking account of the number of measurements.

CONCLUDING REMARKS

We have presented a general framework for translating monitoring results into the probabilities that an event requiring action will happen. The probability of such an event is calculated by combining prior information with the likelihood of the measurements for each subsurface model. The prior probability for all realisations under scrutiny is treated equally, as only sensible realisations are allowed. No updating of the prior models is required. This makes the procedure very fast once the basic ensemble of realisations has been set up.

The procedure has been demonstrated with an example where production of a gas field was limited to a maximum amount of resulting subsidence (or rate of subsidence). Starting with 100 realisations spanning the prior uncertainty of the process, the measurements collected during monitoring bolster some of the realisations while refuting others. Inputting more data in this procedure subjects the realisations to a more severe test.

The monitoring strategy in specific cases can be optimised by assessing the effect of the number, frequency and position of the measurement points. This enables us to find out where truly critical measurements must be gathered. Indeed, in such a synthetic study, it is not necessary to update the prior models, because it is assumed that a number of them are realistic.

REFERENCES

Fokker, P. A. & Orlic, B. (2006) Semi-analytic modelling of subsidence. *Mathematical Geology* **38**, 565–589.

Muntendam-Bos, A. G. & Fokker, P. A. (2009) Unravelling reservoir compaction parameters through the inversion of surface subsidence observations. *Comp. Geosci*. **13**(1), 43–55.

Nepveu, M., Kroon, I. C. & Fokker, P. A. (2010) Hoisting a Red Flag: an early warning system for exceeding subsidence limits. *Math. Geosci*. **42**, 187–198.

(Proceedings of EISOLS 2010, Queretaro, Mexico, 17–22 October 2010). IAHS Publ. 339, 2010.

Need to integrate land subsidence into the legal instruments of Mexico: Morelia, Michoacán case study

L. L. PADILLA-GIL, J. A. ÁVILA-OLIVERA, G. A. HUAPE-PADILLA & M. E. GRANADOS-GARCÍA

Instituto de Investigaciones Sobre los Recursos Naturales (INIRENA), Universidad Michoacana de San Nicolás de Hidalgo (UMSNH), Av. San Juanito Itzicuaro s/n, Col. Nueva Esperanza, CP 58330, Morelia, Michoacán, Mexico
ja.avilaolivera@gmail.com

Abstract The exploitation of an aquifer system causes water table decline when withdrawals exceed the recharge, which in turn activates the process of land subsidence. When sinking is guided by a structural control, the land subsidence is differential and generally is accompanied by earth fissures, fracturing and ground rupturing. All of these effects of the use groundwater generate damage to the infrastructure of cities. In the case of Morelia, Mexico, damages have been observed since 1983, causing economic and social impacts. Reviewing the Mexican legislation, no legal instrument which contemplates the phenomenon of land subsidence and its associate problems was found. Therefore, neither society nor government have legal elements to invoke or claim. However, the proliferation of constructions located in zones identified by scientific studies as risky continues. Accordingly, it is necessary to incorporate land subsidence into legal instruments in order to establish regulation criteria and include them in the urban development plans. These instruments could be the General Law of Ecological Equilibrium and Environmental Protection, the National Water Law, and the Territorial Ecological Zoning.

Key words land subsidence; legislation; environmental planning; Morelia, Mexico

INTRODUCTION

The exploitation of an aquifer system causes water table decline when withdrawals exceed the recharge, which in turn activates the process of land subsidence (Ávila-Olivera & Garduño-Monroy, 2006). This situation occurs generally in urban areas of rapidly growth where the demand for groundwater increases as a result of population explosion; examples in Mexico are Mexico City (Figueroa-Vega, 1984), Morelia (Garduño-Monroy *et al*., 1998), Querétaro (Álvarez-Manilla *et al*., 2004), Celaya (Trujillo-Candelaria, 1991), Aguascalientes (Zermeño-De León, *et al*., 2005), among others.

In Morelia extractions are carried out through 105 pumping wells, generating an annual average water table decline of 3.67 m (Ávila-Olivera & Garduño-Monroy, 2007). The city has been characterized by urban growth beyond measure, with consequent excessive exploitation of groundwater resources. Currently the drinking water service is being provided to 747 136 inhabitants.

One effect of the groundwater overexploitation is land subsidence and its associated problems (earth fissures, fracturing and ground rupturing), which have caused damage to the city since 1983 (Garduño-Monroy *et al*., 2001). Nowadays, Morelia is being affected by differential land subsidence with rates of up to −35 mm/year (Farina *et al*., 2008), and surface faults in a NE–SW direction, with steps of up to 800 mm (the "Central Camionera" fault; Ávila-Olivera & Garduño-Monroy, 2004).

THE PROBLEM

Water supply programmes and projects are not usually planned according to the responsiveness of the geological environment. An extraction greater than recharge, a parameter difficult to estimate, causes lowering of groundwater levels and reduces the water volume available. Overexploitation obligates searching for alternative sources and also consideration of schemes for better resources

Copyright © 2010 IAHS Press

management. However, there are also side effects to inadequate groundwater exploitation (Rodríguez-Castillo & Rodríguez-Velázquez, 2006). One of these effects is land subsidence.

The damage caused by land subsidence and ground rupturing, to buildings and houses, include the cracking of walls, floors, girders and foundations, and ceiling collapse; in some cases a total loss of the construction is reached. The owners make continuous and expensive repairs, not knowing that the process will not stop in the short or medium term. Also the land cost decreases significantly. Naturally, the loss of their heritage affects the quality of their life and creates a social problem.

In Morelia there is a history of complaints to the authorities, submitted by civil society which has been affected by the purchase of houses that in less than three months present cracks in their structural elements. However, neither the owners nor the government have legal instruments to claim. Instead, construction in zones with problems of land subsidence, which has been indentified by scientific studies, continues to proliferate.

LEGAL FRAMEWORK

In 1990 the Organization of American States (OAS) published the document *Disasters, Planning and Development: Managing Natural Hazards to Reduce Loss*, which contains a first effort to integrate development plans with the mitigation of natural disasters. It refers to environmental planning; the document contrasts environmental projects with development projects and concludes that to achieve a lasting development programme, it must incorporate coherent environmental planning.

In Mexican legislation different legal instruments are issued for environment protection, mitigation of environmental impacts, to regulate building construction, for exploitation and use of groundwater and surface water. Some of these instruments are the General Law of Ecological Equilibrium and Environmental Protection, National Water Law, Housing Law, General Law of Human Settlements. Notwithstanding the existence of these laws, none of their paragraphs cover land subsidence risk prevention, the effect on individuals, protective measures against this eventuality, or the application of administrative responsibility to the authorities charged to regulate the establishment and land uses.

While it is true that the National Water Law provides in its article 18 third paragraph that it will issue the regulation for the extraction and use of national water, in relation to groundwater there is no reference to an issue. Maybe a section dealing with the effects of groundwater withdrawal, as a cause of land subsidence, and its associated problems could be inserted in this bylaw.

CONAGUA (the National Water Commission) has issued standards which establish the provisions, specifications and test methods to help ensure that products and services supplied meet with the aim of harnessing and preserving water quality and quantity. However, it has not specified any management for the exploitation and use of groundwater and surface water causing environmental, social and economic risk phenomena related to this activity, such as land subsidence.

DISCUSSION

In the southwestern portion of Morelia, the authorizations to fractionate are unreasonable; they do not take into account the proliferation of pumping wells and the presence of geological faults, despite the fact that there are studies that have established the potential of the area to develop problems of land subsidence, earth fissures, fracturing and ground rupturing; thus, the supply of housing in that zone is irresponsible from both the perspective of the authorities and developers. As a precautionary measure to avoid irreversible economic and social damage, there must be restricted land use in areas with the possibility of natural or anthropogenic risks.

CONCLUSIONS

The Mexican legislation does not consider land subsidence as a natural or an induced disaster, therefore is not included in the National Water Law, nor in the General Law of Ecological Equilibrium and Environmental Protection; also it is not considered in emergency programmes for social assistance. This is due mainly to the fact that the land subsidence effects occur in the long term. Therefore, the affected communities have no legal elements to invoke or claim.

The problems associated with land subsidence should be reflected in the General Law of Ecological Equilibrium and Environmental Protection, and in the Territorial Ecological Zoning, in order to establish the regulation criteria and its inclusion in the urban development plan.

REFERENCES

Álvarez-Manilla, A. A., Fernández-Hernández, F., Poot-Lima, R. M. &Zepeda-Garrido, J. A. (2004) Hundimiento máximo en el Valle de Querétaro en función del potencial acuífero. *XXII Reunión Nacional de Mecánica de Suelos*.

Ávila-Olivera, J. A. & Garduño-Monroy, V. H. (2004) La subsidencia y las fallas geológicas en la Ciudad de Morelia, Michoacán. *XXII Reunión Nacional de Mecánica de Suelos*.

Ávila-Olivera, J. A. & Garduño-Monroy, V. H. (2006) El abatimiento de los niveles freáticos es sólo un elemento de los Procesos de Subsidencia-Creep-Falla, caso: la Ciudad de Morelia, Michoacán. *Geos* **26**(1), 186.

Ávila-Olivera, J. A. & Garduño-Monroy, V. H. (2007) Análisis del abatimiento de los niveles freáticos del sistema acuífero de Morelia. *Revista Ciencia Nicolaita* **46**, 105–122.

Farina, P., Ávila-Olivera, J. A., Garduño-Monroy V. H. & Catani, F. (2008) DInSAR analysis of differential ground subsidence affecting urban areas along the Mexican Volcanic Belt (MVB). *Rivista Italiana di Telerilevamento* **40**(2), 103–113.

Figueroa-Vega, G. E. (1984) Case History 9.8 Mexico, D.F. In: *Guidebook to Studies of land subsidence due to groundwater withdrawal* (ed. by J. F. Poland), 217-232. International Hydrological Program, Working Group 8.4.

Garduño-Monroy, V. H., Arreygue-Rocha, E, Chiesa, S., Israde-Alcántara, I., Rodríguez-Torres, G. M. & Ayala, G. M. (1998) Las fallas geológicas y sísmicas de la ciudad de Morelia y su influencia en la planificación del territorio, *Ingeniería Civil*, **1**(5), 3–12.

Garduño-Monroy, V. H., Arreygue-Rocha, E, Israde-Alcántara, I. & Rodríguez-Torres, G. M. (2001) Efectos de las fallas asociadas a sobreexplotación de acuíferos y la presencia de fallas potencialmente sísmicas en Morelia, Michoacán, México, *Revista Mexicana de Ciencias Geológicas* **18**(1), 37–54.

Ley de Aguas Nacionales (National Water Law).

Ley General de Equilibrio Ecológico y Protección al Ambiente (General Law of Ecological Equilibrium and Environmental Protection).

Rodríguez-Castillo, R. & Rodríguez-Velázquez, I. (2006) Consecuencias sociales de un desastre inducido, subsidencia, *Boletín de la Sociedad Geológica Mexicana,* Número especial de Geología Urbana Tomo LVII(2), 265–269.

Trujillo-Candelaria, J. A. (1991) Fallamiento de terrenos por efecto de la sobreexplotación de acuíferos en Celaya, Guanajuato, México. In: *XXIII Congress of the Association of International Hydrologists*, Sobreexplotación de acuíferos: España, 175–178.

Zermeño-De León, M. E., Esquivel-Ramírez, R., Hernández-Navarro, A., Mendoza-Otero, E. & Arellano-Sánchez, J. (2005) Influencia de la Extracción del Agua en la Subsidencia y Agrietamiento de la Ciudad de Aguascalientes. *Revista Investigación y Ciencia de la Universidad Autónoma de Aguascalientes* **32**(1), 15–22.

Land Subsidence, Associated Hazards and the Role of Natural Resources Development
(Proceedings of EISOLS 2010, Querétaro, Mexico, 17–22 October 2010). IAHS Publ. 339, 2010.

Institutional controls in an area of subsidence induced flooding

SUSAN L. BAIRD
Consulting Geologist, Board Director of the Harris Galveston Subsidence District, NDT Seals Inc., 1333 Sterrett Street, Suite G, Houston, Texas 77002, USA
gr33nbu44alo@gmail.com

Abstract This paper is a summary of the institutional controls enacted after a catastrophic flood in a major metropolitan area. The percentage of property inundated by Tropical Storm Allison (2001) in Harris County, Texas, United Sates of America, was much greater than anticipated. Two thirds of the areas flooded were outside of the 1% (100 year) flood plain. Excessive insurance and property damage claims caused the Federal Emergency Management Agency (FEMA) to underwrite a LiDAR survey of the county to develop a better topographic base for flood plain mapping. New flood plain maps were created and presented at public forums. Areas not thought to be seriously affected by subsidence were better mapped, showing greater areal subsidence and flooding potential. Additional flood insurance, certificates of elevation, and property construction standards were required for lending loan applications. Structures in the areas now realized as prone to flooding were purchased by the government to reduce the economic impact of future floods.

Key words banking; construction; emergency preparedness; FEMA; flooding; flood plain; hurricane; insurance; LiDAR; monitoring; subsidence

INTRODUCTION

The first storm of the hurricane season, Tropical Storm Allison (TSA), made landfall 80 kilometres southeast of Harris County, Texas, USA (metropolitan Houston, Texas) on 5 June 2001. Rainfall amounts of up to 30 centimetres inundated the county as the storm moved inland to the northeast, flooding 1000 residences. Three days later the system reversed its direction and returned to the coast.

Up to 41 centimetres of additional rain fell on soils saturated beyond capacity. Within one week of it leaving the Gulf of Mexico, 73 000 residences and 95 000 automobiles were reported flooded, 30 000 people were in emergency shelters, and US$ 5 billion in direct damages was attributed to the storm.

The storm ranks as the tenth most costly United States tropical cyclone in the interval 1900–2006 (Blake, 2005). Areas of the county which received unprecedented flooding are depicted in Fig. 1 of Harris County flooding, as mapped by TSARP.

Because of the magnitude of the flooding and its impact on the residents of Harris County, the Harris County Commissioners Court and the Harris County Flood Control District (HCFCD) in cooperation with the Federal Emergency Management Agency (FEMA) decided to perform a detailed technical evaluation of the storm and its consequences (TSARP, 2002).

GEOLOGY/SUBSIDENCE SUMMARY

Harris County (4605 km^2) is located in the north portion of the Coastal Lowlands Aquifer system of Texas. The geological sequence consists of Tertiary and Quaternary unconsolidated, interbedded sand, silt, and clay units, which thicken to the gulf basin. Both alluvial and marine deposition features are present in the subsurface. Three aquifers underlying the county provide abundant potable water, the Pleistocene Chicot aquifer, the Pliocene Evangeline aquifer, and the Miocene Jasper aquifer. Pumping from the Chicot and Evangeline has historically supplied the southeastern two thirds of the study area; the deeper Jasper has been drilled recently to supplement the Evangeline in northwest.

The area is covered by impermeable clays which produce high runoff rates; the surface gradient is as low as 0.3 m/km. Drainage problems associated with freshwater flooding have occurred with elevation loss. Tidally influenced bayous sometimes flow landward (Solis, 1981; Garcia, 1991).

Copyright © 2010 IAHS Press

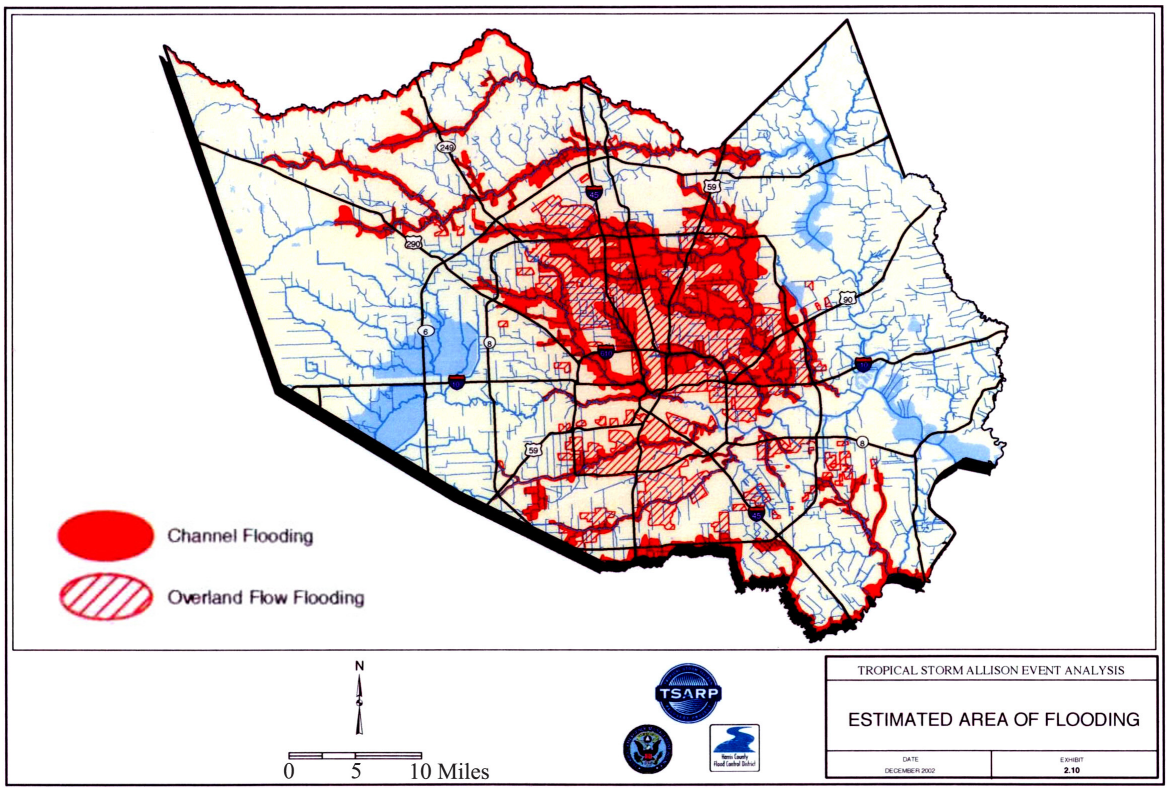

Fig. 1 Harris County flooding as mapped by TSARP.

Surface expression of down-to-the-basin growth faults can be traced within the county. The faults are subparellel to the coastline, with the downthrown side generally coastward. Aerial photographic lineations and stream channels commonly coincide with the surface traces (fault scarps) of active faults extrapolated from the subsurface (Kreitler, 1976; Van Siclen, 1985). The location of several streams and bayous in the Houston area, such as Buffalo Bayou, Clear Creek, Highland Bayou, Brays Bayou, Cedar Bayou, Sims Bayou, and Greens Bayou, appear to be structurally controlled. These streams are either parallel to active faults and fault extrapolations, or exhibit rectilinear drainage patterns indicating fault control.

Differential subsidence associated with subsurface fluid extraction was recognized in 1926 at the Goose Creek Oil Field in eastern Harris County (Minor, 1926). As oil was pumped from the production horizon, the hydraulic pressure declined in the underlying sands. The pressure difference between the clay and sand layers forced the pore fluid within the clay matrix to move into the sands. The internal structure of the clay collapsed and was permanently compacted; the surface expression of this withdrawal is differential subsidence. The surface topography above the small oil and gas fields, Addicks, Goose Creek, Chocolate Bayou, Myakawa, South Houston, Clear Lake, and Webster Fields, shows this type of subsidence.

Progressive or regional land subsidence has only been noted in scientific literature of the last fifty years (Winslow & Wood, 1959; Van Siclen, 1967). Increases in flooding were attributed to subsidence caused by groundwater pumping. The use of surface water for municipal supply began in 1954, but groundwater use remained unregulated until 1976.

The Harris-Galveston Subsidence District (HGSD) was formed in 1975 to monitor and suggest controls of subsidence. Figure 2 is an estimate of regional subsidence before groundwater use was restricted.

The District has developed four regulatory plans to reduce the withdrawal of groundwater within the counties. The plans addressed the geographic areas where the most subsidence had occurred (1976); the goal of changing primary water usage to other available water (1985); and the

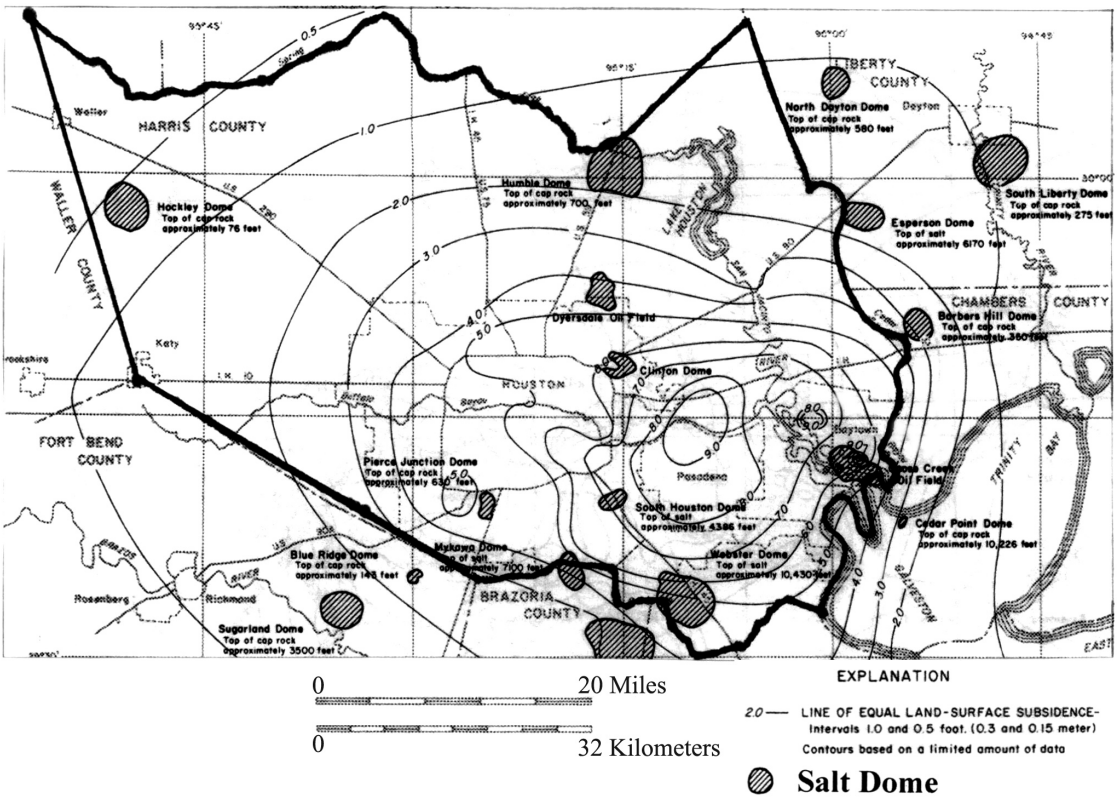

Fig. 2 Pre HGSD subsidence estimate, approximate land-surface subsidence, 1906–1978; from *USGS Open File Report 82-571*, Fig. 13.

assessment of surface water availability, population growth, projected subsidence, and regional water demand (1992, 1999). The ongoing fifth revision of the plan will include the updating of population and water demand projections, the recalibration of regional groundwater models, and the validation and collection of level loop and extensiometer subsidence data (projected completion, 2012).

Reduction of groundwater extraction by volume-limiting permits and an increase in transmission of surface water has slowed additional subsidence in the southeast two thirds of the study area. In 1985, surface water use exceeded groundwater use and potentiometric surfaces have rebounded in the Chicot and Evangeline aquifers.

The US Geological Survey (USGS), in cooperation with the HGSD, prepared USGS Scientific Investigations Map 3097 which documents subsidence in Harris County from 1915–17 to 2001. The map was constructed using geographic information system (GIS) techniques that involved subtraction of digitized 1915–17 topographic map elevations from 2001 land-surface elevations derived from the TSARP Light Detection and Ranging (LiDAR) data. Using this map as a base, a new subsidence isopach, Fig. 3, may be contoured.

Regional land subsidence greater than three metres is found near the industrial facilities utilizing water intensive processes on the Houston Ship Channel. Areas showing two to three metres of subsidence appear above municipal supply well fields, surface fault traces, and oil production. Subsidence attributed to municipal groundwater pumping is greater in the historic population centres of the central county. Faulting and oil production subsidence observed by Minor and Van Siclen are easily located on Fig. 3. Subsidence in the northwestern portion of the study area has increased with increased unzoned residential development heavily dependent on groundwater use and the decrease of areas for groundwater recharge and runoff.

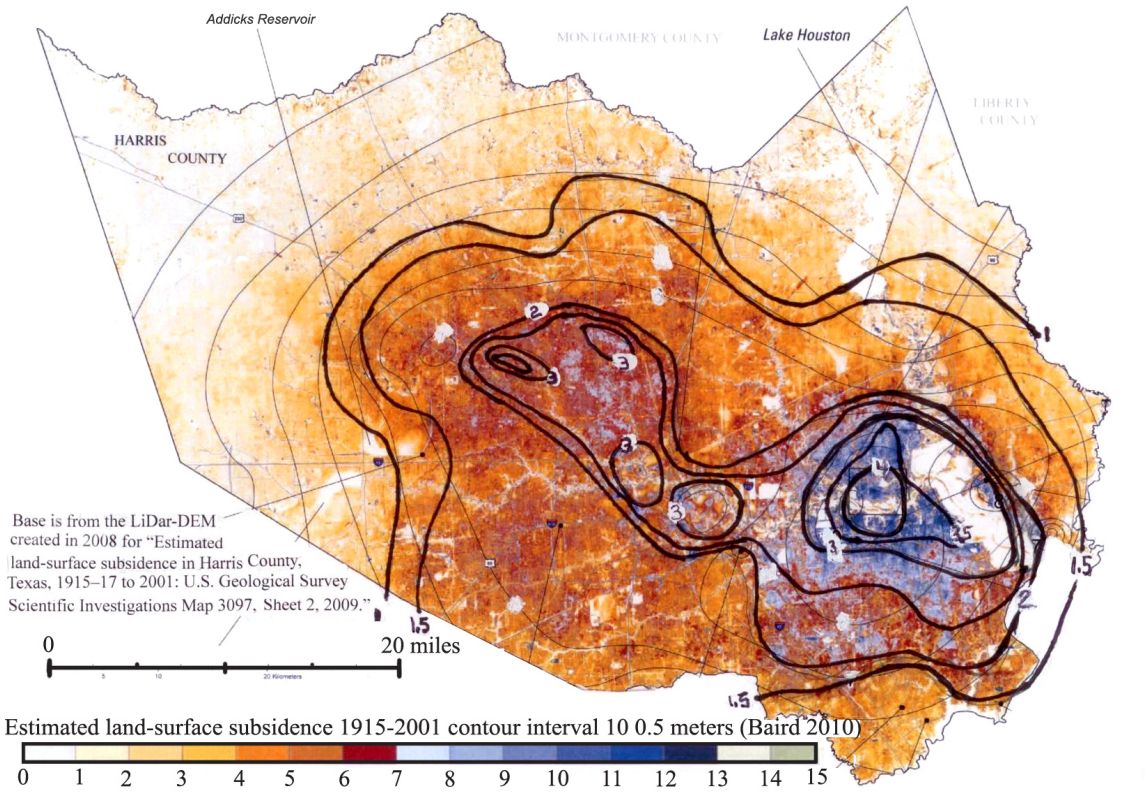

Fig. 3 Subsidence Isopach.

TSARP STUDY AND FINDINGS

The financial impact of TSA flooding caused HCFCD, in cooperation with FEMA, to perform an assessment of flood risks associated with streams, bayous, topography, and drainage pathways (TSARP, 2002). Observed high water marks for TSA exceeded previously recorded highest flood levels at the USGS and HCOEM gauging stations. For the 40 stations in Harris County, 17 exceeded the previous historical peak flood level by amounts ranging from 46% to 126%. The data show that record flooding occurred on most of the streams draining the eastern half of Houston. This area is not as populated as the western portion of the city; had TSA's storm track shifted 26 km to the west, property losses would have been several orders of magnitude higher. Figure 4 shows the number of claims from the flooding reported in Fig. 1.

The majority of flooded residential structures purchased by FEMA are within watersheds which have had two or more metres of subsidence since 1917.

Storm sewers and drainage ditches in Houston necessarily operate on very low gradients. Gradients may be altered by faulting; locally, fault movements and subsidence associated with faults, have decreased or reversed flow within ditches. Properties on the downthrown sides of faults in areas of impaired drainage are increasingly susceptible to flooding. In such areas it is possible to suffer fault-related damage, caused by flooding, hundreds of metres from the nearest fault. Gravity-fed sewer lines may likewise experience reversed flow, backup of storm drains, and ponding of sewage. Altered gradient flooding has been observed along the Eureka Heights and Long Point faults.

TSARP performed a comprehensive remapping of the county's flood plains with a LiDAR topographic survey. The resulting digital elevation model (DEM) is mapped on a scale of 30 cm by 30 cm with a surface elevation accuracy of 15 cm. The DEMs were used to construct 143 new Flood Insurance Rate Maps (FIRMs) to determine insurance requirements and to assist communities with flood damage reduction projects. FIRMs show zones that have 1% and 0.2%

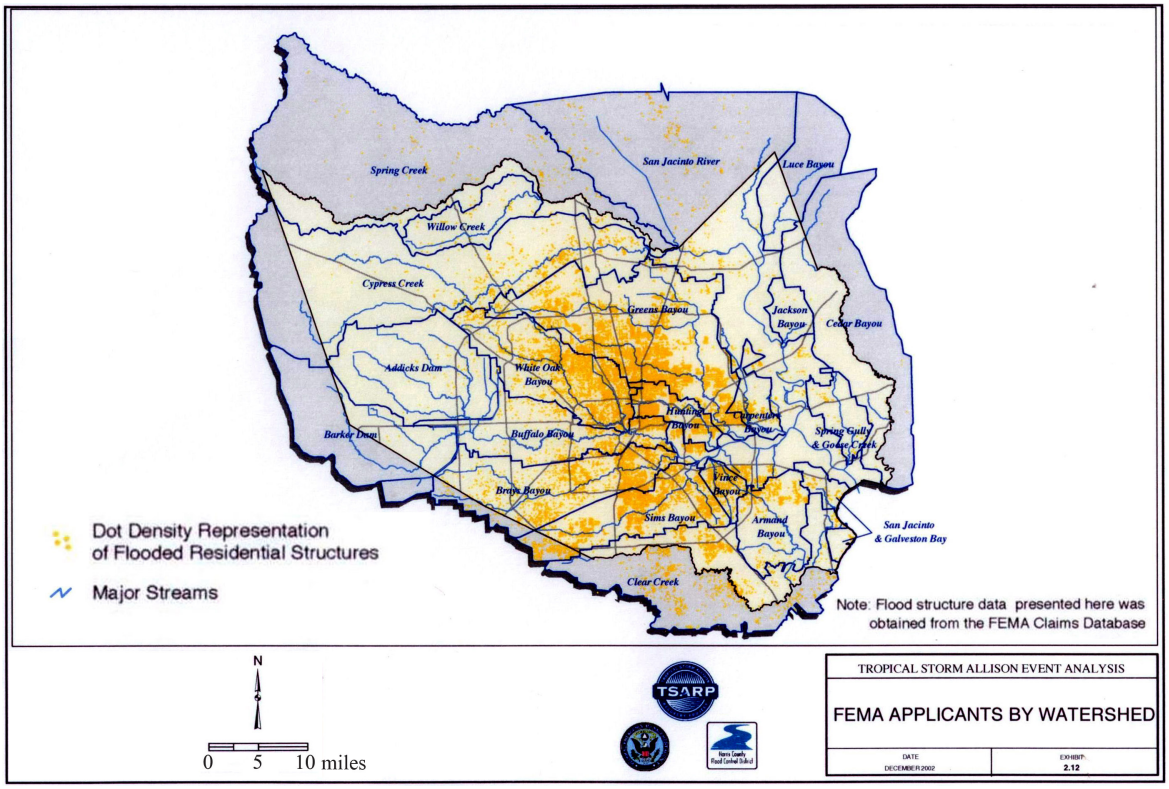

Fig. 4 FEMA claim distribution for TSARP.

chances of flooding in a given year based upon an evenly distributed rainfall of 33 cm in 24 hours. Information on the county's 22 watersheds was distributed to the 35 communities within the county 42 months after TSA for public comment.

The public had the opportunity to contest the validity of the new FIRMS by either appeal or protest. An appeal would be a technical challenge to the computed Base Flood Elevation (BFE) supported by a full engineering analysis. A protest would be a challenge to the flood plains and or map information in general. Extensions of the comment period and filings delayed the new FEMA FIRMs becoming official until 60 months after TSA, in June 2006.

REGIONAL STANDARDS AMENDED

Banking and Insurance

The revision of the FIRMS increased the number of residents who live in a Special Flood Hazard Area (SFHA) or the 1% flood plain, as identified by FEMA. Flood insurance coverage (National Flood Insurance Program, NFIP) for SFHA properties became mandatory for national bank secured mortgages. At a minimum, NFIP coverage must equal the outstanding principal balance of the loan and must be maintained throughout the term of the loan; compliance is a part of the appraisal review and closing requirements. Consulting firms composed of flood status auditors perform reviews similar to the due diligence environmental assessments.

FEMA created the Community Rating System Program (CRS) to recognize communities where flood plain management standards exceed the minimum federal standards. Communities must actively apply for a class rating and are awarded a rating from 10 to 1, with 1 being the highest achievable rating. Flood insurance policyholders located in the SFHA receive discounts on their premiums based on the class rating. In October 2009, the City of Houston improved its CRS from a Class 6 to a Class 5. Premium discounts within the city's SFHAs will range from 10% to

25%. The CRS rating for the remainder of Harris County is Class 8. This rating gives residents a 10% discount on non-preferred risk flood insurance policies.

Construction

FEMA's review of Houston's CRS noted that the city has one of the highest concentrations of repetitive loss structures covered under NFIP. The definition of such a structure is one that has been damaged twice within a ten year period, in which the cost to repair the flood damage exceeds 25% of the market value at the time of each flood loss. The Houston public works department re-drafted the city code, Chapter 19 – *Floodplain*, after the 2006 regional FIRM approval. The purpose of this Chapter is four-fold:

1. public and private losses due to flooding in specific areas are to be minimized;
2. surveyed scaled map and permit issuance will be regulated to reduce the likelihood that development will increase flooding;
3. the degree of regulation required is reasonable and based on FEMA NFIP maps; and
4. these rules and regulations apply throughout the city and take precedence over existing rules.

New construction or substantial property improvement in a SFHA or floodway requires a certificate of elevation stating that the structure is at least 0.5 m above the base flood elevation stated on a FIRM. It is preferred that the foundation system for the structure will be pier and beam construction to allow for overland flow. Determining the correct elevation of the topography in an area of active subsidence allows for the sound use and development of flood prone areas in such a manner to minimize future blight areas. Man-made or natural causes that may cause excessive increases in flood heights or velocities are restricted by careful planning and permitting, (Chapter 19, City of Houston, 2008.) All efforts to maintain control of the alteration of natural flood plains, stream channels, and natural protective barriers, are discussed in the mitigation plan accompanying the permit. Recreational features not requiring a permanent structure may be suggested, such as hiking trails and bikeways. No regulations or permits imply that lands outside the areas of SFHA or uses permitted within such areas will be free from future flooding or flood damage. Protection levees built on subsiding land will suffer loss of freeboard directly proportional to the subsidence experienced and must have their vertical controls re-established on a regular schedule (Carr, 1976).

Emergency preparedness

The City of Houston's Office of Emergency Management maintains an annual registry of citizens who may need special transportation assistance during an emergency evacuation. Areas of southeastern Harris County which have had the most subsidence are also at risk for a hurricane storm surge. If a hurricane's landfall is imminent, elected officials, by way of public service announcements, request residents to leave the coastal zone first, and succeeding inland zones by postal zip codes, Fig. 5.

The intent of the system is to minimize traffic congestion and depopulate low topographic areas while the roadways are still accessible. Elected officials urge citizens outside of the zip zone evacuations to shelter in place. The zip zone evacuation plan was used in the 2008 hurricane season.

Emergency preparedness plans drafted by the Texas legislature, now require water supply facilities to have automatic starting generators able to maintain 240 kPa at all times. Wastewater treatment plants must provide primary clarification at peak design flow. Both the preparedness plans and generator requirement were in place for the 2009 hurricane season.

Acknowledgements The author would like to thank the Mayor's Office of the City of Houston for continued appointment to the Board of Directors of the Harris Galveston Subsidence District.

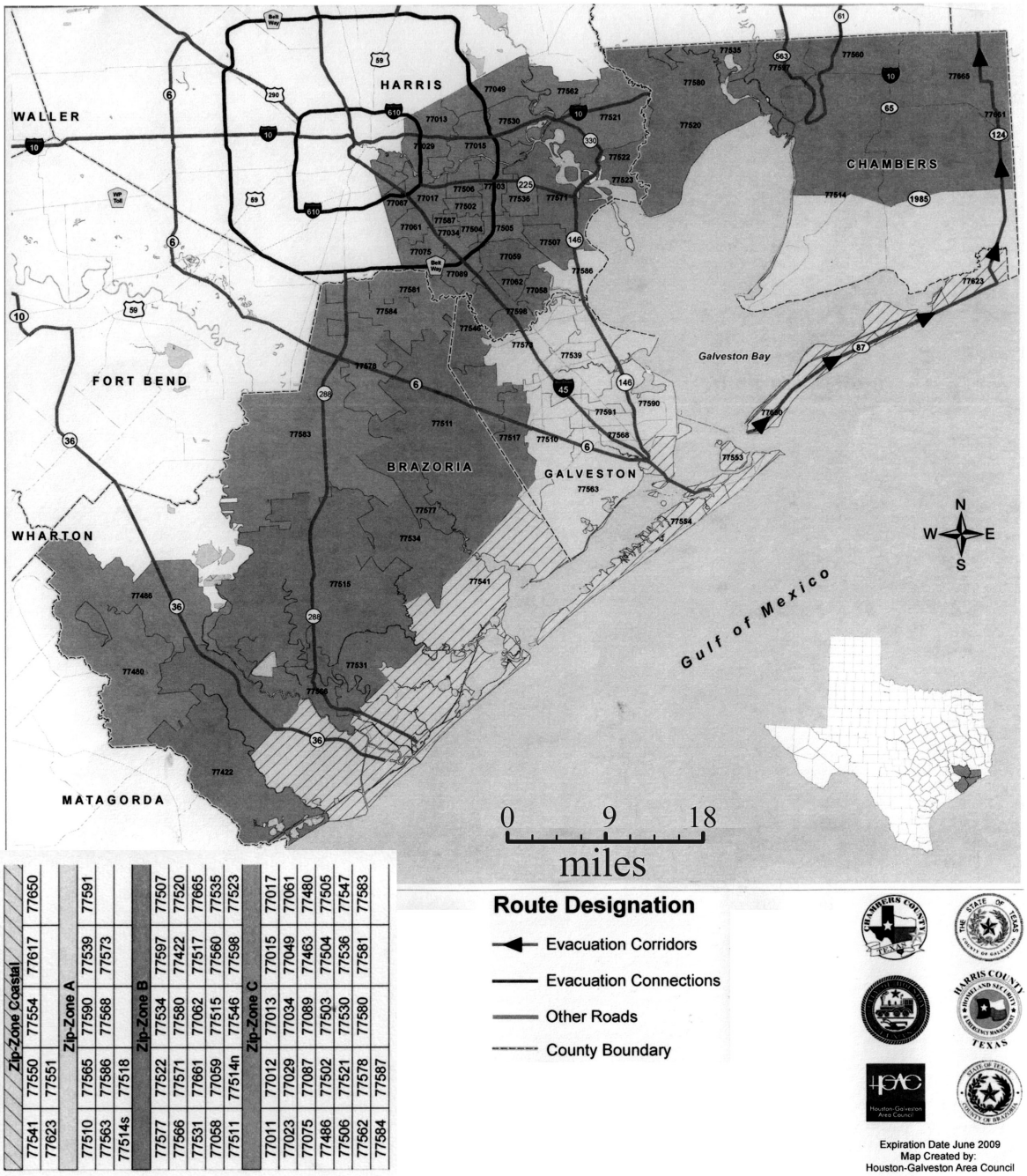

Fig. 5 Zip code evacuation map, from HGAC.

REFERENCES

Blake, E. S., Rappaport, E. N. & Landsea, C. W. (2007) The deadliest, costliest and most intense United States hurricanes from 1851 to 2006 (and other frequently requested hurricane facts). *NOAA Technical Memorandum NWS TPC-5*, 45 pp.

Carr, J. T., Jr (1976) Hurricanes affecting the Texas Gulf Coast. *Texas Water Development Board Report 49*, 58 pp.

City of Houston (2007) The Flood Insurance Study for the City of Houston, 2007, as presented for amendment to the Houston City Council on July 9, 2008.

Garcia, T. D. (1991) Subsidence and Surface Faulting at San Jacinto Monument, Goose Creek Oil Field, and Baytown, Texas, Field Trip Guidebook on Environmental Impact of Clays along the Upper Texas Coast. Clay Minerals Society, National Aeronautics and Space Administration, Lunar and Planetary Institute.

Harris Galveston Subsidence District (1978–2009) Annual Groundwater Reports.

Kasmarek, M. C., Gabrysch, R. K. & Johnson, M. R. (2009) Estimated land-surface subsidence in Harris County, Texas, 1915–17 to 2001. *US Geological Survey Scientific Investigations Map 3097*, 2 sheets.

Kreitler, C. W., (1977) Faulting and land subsidence from ground-water and hydrocarbon production, Houston-Galveston, Texas. In: *Land Subsidence.* IAHS Publ. 121. IAHS Press, Wallingford, UK.

Minor, H. E. (1926) Goose Creek Oil Field, Harris County, Texas. In: *Geology of Salt Dome Oil Fields*, AAPG Special Volume, 546–557.

Solis, R. F. I. (1981) Upper Tertiary and Quaternary depositional systems, central coastal plain, Texas – Regional geology of the coastal aquifer and potential liquid-waste repositories. The University of Texas at Austin, Bureau of Economic Geology Report of investigations, 108, 89 p.

TSARP (2002) Tropical Storm Allison Event Analysis Technical Report, vol. 1, Harris County Flood Control District and the United States Federal Emergency Management Agency, 208 pp.

Van Siclen, D. C. (1967) The Houston fault problem. American Institute of Professional Geologists, Proceedings of the 3rd annual convention, Texas section, 9–31.

Van Siclen, D. C. (l985) Pleistocene meander-belt ridge patterns in the vicinity of Houston, Texas. *Trans. Gulf Coast Association of Geological Societies* **35**, 525–532.

Verbeek, E. R., Ratzlaff, K. W. & Clanton, U. S. (2005) Faults in parts of north-central and western Houston Metropolitan Area, Texas. *US Geological Survey Miscellaneous Field Studies Map 1136*, 14 pp.

Winslow, A. G. & Wood, L. A. (1959) Relation of land subsidence to groundwater withdrawals in the upper Gulf Coast region, Texas. *Mining Eng., Am. Inst. Mining, Metal., and Petroleum Engineers Trans*. **214**, 1030–1034.

Land Subsidence, Associated Hazards and the Role of Natural Resources Development
(Proceedings of EISOLS 2010, Querétaro, Mexico, 17–22 October 2010). IAHS Publ. 339, 2010.

A fuzzy based-approach to building damage risk assessment

AGNIESZKA MALINOWSKA
AGH University of Science and Technology, Faculty of Mine Surveying and Environmental Engineering, al. Mickiewicza 30, 30059 Kraków, Poland
amalin@agh.edu.pl

Abstract Exploitation of mineral deposits or water is often done under intensely built-up areas. Consequently, the need for reliable risk assessment of mining affected areas significantly increases. The aim of this paper is to indicate the most problematic issues concerning proper objective risk assessment of the mining areas. A new method of building damage risk assessment is described. The uncertainty and ambiguous elements in the decision process are accounted for by using a fuzzy inference system in the risk assessment model. This tool, employed together with GIS, enables one to integrate diverse factors affecting damage risk, such as surface deformations and the resistance of building objects, taking into account the data uncertainty and the subjectivity of evaluation of the experts making the assessment.

Key words subsidence; mining exploitation; building damage risk assessment; fuzzy logic; GIS; decision making; Poland

INTRODUCTION

Evaluation of building objects and technical infrastructure in areas of mining impact is becoming a more and more important issue. This situation is caused by the growing number of real estates, development of other non-mining branches of the economy and the necessity to limit the influence of mining on the local population. Exploitation of raw minerals in Poland is partly conducted in strongly urbanized areas and, therefore, a number of objects are subject to their negative impact. As a consequence, it is crucial to correctly assess the mining risk and the potential impact this might have on buildings. The main problem related to risk assessment in mining areas is the complexity of the geological and mining factors that cause the hazard. The other difficulty concerns reliable evaluation of the potential damage that can be brought about in objects (Wittaker, 1989). Due to extensive built-up mining areas, accurate evaluation of building damage risk has become a large-scale issue. Methods which enable only individual evaluation of building damage risk are too costly and time consuming in Polish mining conditions. Therefore, expert methods of object resistance evaluation are used (Przybyła, 1968; Instrukcja GIG, 2000). However, the knowledge thus acquired of object resistance is non-homogeneous and strongly burdened with the subjectivity of construction experts. The magnitude and non-homogeneity of risk factors, uncertainty of information, incompleteness of data and subjectivity of expert assessment make precise evaluation of the risk of building damage impossible (Hejmanowski & Malinowska, 2009; Malinowska & Hejmanowski, 2010). Therefore, attempts were made to approach this problem with a fuzzy inference method. As many objects are involved, GIS was employed as a tool for integrating data and aiding the analyses. Based on the current experience in the field of building damage risk assessment caused by underground mining, a fuzzy inference system of object damaging assessment was developed. The model enables us to take into account directly factors related to continuous surface deformations and the resistance of objects. The final part of the paper is devoted to the advantages of the presented model with an example of objects subject to mining activity hazards.

EVALUATION OF THE FUZZY INFERENCE SYSTEM FOR BUILDING DAMAGE RISK ASSESSMENT

Background

The determination of the damage done to surface objects and underground infrastructure in the mining area can be divided into two stages:

Copyright © 2010 IAHS Press

– evaluation of vulnerability of objects,
– prediction of surface deformation.

The vulnerability of objects to the influence of deformations caused by the mining activity is most frequently determined by the approximated point method. This is an expert method, where the specific properties of a building are ascribed a given number of points. The less resistive the building is, the greater is the number of points (Budryk, 1950; Przybyła, 1968) (Table 1). Then, depending on the summary number of points, a resistance category is attributed to a given object. This category corresponds to the values of horizontal (boundary) deformations, which a given object can carry.

Table 1 Building resistance categories as an output of the expert evaluation method (Przybyła, 1968).

Size of horizontal projection										
Length of building (m)	≤10	≤15	≤20	≤30	≤50	≤100				
Points	2	4	7	15	25	50				
						Points				
Shape of building						0–10				
Foundation of building						0–5				
Subsoil under the building						0–10				
Building condition						2–28				
Existing protection against mining impact						0–15				
Technical state of building						0–17				
Qualification										
Summary points	≤ 20	21–23	24–29	30–33	34–36	37–43	44–46	47–49	50–56	57–59	≥ 60
Strain allowable	7.0–9.0	6.0	5.0	4.0	3.0	2.5	2.0	1.5	1.0	0.5	≤ 0.3
Resistance category	**4**	**3**			**2**			**1**			**0**

The prediction of surface deformations is made on the basis of geological, mining and other data with the use of a calculation model. The model is commonly applied in Poland based on the influence function approach which was developed by S. Knothe in the early 1950s (Knothe, 1953). After certain modifications, this model has been used for predicting deformations in the areas where copper ore and even salt are produced (Hejmanowski & Sroka, 2000). The land subsidence forecast is made for the planned mining exploitation at points on a regular calculation grid. The assessed values of maximal deformation factors are used for interpolating isolines of horizontal strains, curvatures and tilt. For establishing the degree of potential impact of continuous deformations of the existing and planned surface structures, the mining area is divided into six terrain categories labelled from "0" to "V" in view of the values of the "H_s" horizontal strain: 0 cat. $H_s \in (0–0.3\rangle$ mm/m, I cat. $H_s \in (0.3–1.5\rangle$mm/m, II cat. $H_s \in (1.5–3.0\rangle$mm/m, III cat. $H_s \in (3.0–6.0\rangle$mm/m, IV cat. $H_s \in (6.0–9.0\rangle$mm/m, V cat. $H_s > 9$mm/m, where the "0" terrain category is the lowest surface hazard and "V" is the highest surface hazard. At the final stage of evaluation, the buildings having the resistance category lower or equal to the category of the surface are analysed. Exceeding the surface category by one or two categories with respect to the building vulnerability category may denote a potential hazard to the object.

However it should be mentioned that the method presented above is burdened with some uncertainty related with, e.g.:

– generalisation of the real dimension of the predicted surface subsidence by terrain categorisation,
– lack of a direct relationship between the hazard caused by surface deformation and building vulnerability,
– the subjectivity of the expert methods of the building resistance assessment,

– building resistance categorization causes loss of information about the exact building's resistance expressed by points.

Due to these factors building damage risk assessment method is burdened with high uncertainty, ambiguity and imprecision. The low efficiency of the currently-used method and increasing social dissatisfaction with mining damages led to the search for a new solution based on the fuzzy set theory and GIS.

Fuzzy sets inference method for risk assessment of building damage

Fuzzy sets, fuzzy operators and fuzzy reasoning are notions belonging to a mathematical theory, thanks to which complex and vague problems can be approached despite their high uncertainty caused by the lack of information and incompleteness of data (Altrock, 1993; Klir, 1995; Zadeh, 1965; Zimmermann, 1994). Fuzzy sets also enable one to account for uncertainty related with the subjectivity of assessment of persons making the evaluations, their lack of experience or knowledge, deciding factors in the expert's approach. Some imperfection in information given by an expert can neither be avoided nor severed from the final characteristic of the phenomenon. The basic notion of fuzzy logic is a fuzzy set (Zadeh, 1965). Fuzzy set A, in some numerical space X, is defined as a set of ordered pairs:

$$\mathrm{A} = \{(x, \mu_A(x)); x \in \mathbf{X}\} \tag{1}$$

where: $\mu_A : \mathbf{X} \to [0,1]$ is a membership function of fuzzy set A.

The elements can be allotted to a given set on the basis of a fuzzy set. Unlike classical logic, where the only possible result of reasoning is true or false, fuzzy logic enables gradation between true and false. Fuzzy logic enables reasoning in the case of vague and unclear notions and the cause-and-effect uncertainty.

The assumption of the model was to integrate into the inference process two characteristics such as the hazard caused by mining exploitation and the resistance of the buildings, allowing for the ambiguity of surface prognosis and expert assessment methods to be taken into consideration (Malinowska, 2009). The definition of fuzzy rules putting together those two variables and processing with the use of fuzzy inference subjection, enabled us to determine one value that characterizes the risk of building damage.

The model created is based on two linguistic input variables. The first one, describing the surface hazard, was characterized by predicted values of extreme horizontal strains. The other linguistic variable was building vulnerability defined by points obtained from the assessment of resistance with the point method (Table 1). For defining the output variable, a new notion was defined, i.e. the risk of building damage expressed on a point scale from 0 to 100. With this variable it is possible to point define the building hazard degree, a potential source of threat for the user. In the fuzzy inference system creep values of input variables are fuzzified by assessing the grade of their membership to a fuzzy set. Properly defined membership functions enable us to take into consideration the uncertainty and ambiguity of the input data.

Surface hazard was defined by six linguistic values: very low, low, medium, high, very high and extremely high. This can be expressed by the following notation. For everyone of these variables a fuzzy triangle-shape membership function were defined (Fig. 1(a)). The characteristic points of the membership functions were determined based on the borders of terrain categories.

Building vulnerability was described by five linguistic values: very low, low, medium, high and very high. Based on intervals of building resistance categories and points established with the use of an approximated point method, triangle-shape fuzzy membership functions were defined (Fig. 1(b)). The output variable "risk of building damage" was characterized by eight triangle-shape membership functions: lack, very low, low, medium, appreciable, high, very high, extremely high (Fig. 1(c)).

Fuzzy rules which merged input variables (Fig. 1(a) and (b)) with the output variable (Fig. 1(c)) were made on the basis of a legal regulation binding in Poland and the experience of

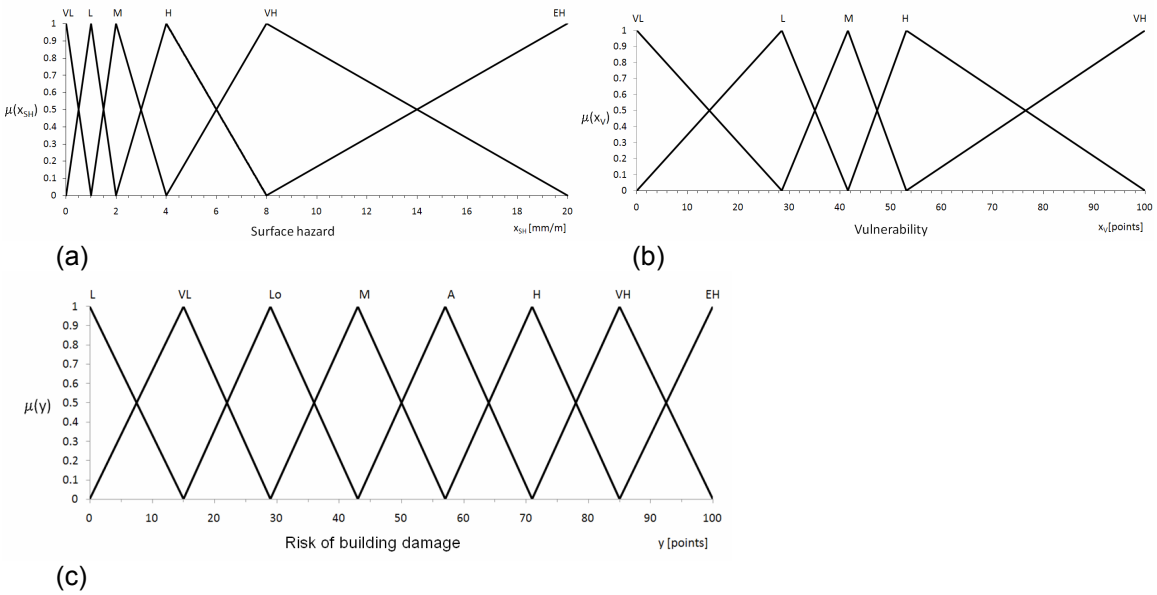

Fig. 1 Membership grade of surface hazard caused by horizontal strain (a), building vulnerability (b), and risk of building damage (c) (Malinowska, 2009).

building engineers. This premise was the foundation for creating a fuzzy rule base (Table 2). Therefore if the surface hazard is "very low" and building vulnerability is "low" there is a "lack" of building damage risk, but if the surface hazard is "very high" and building vulnerability is "high" the risk of building damage is "high".

Table 2 Rule base.

		Surface hazard					
Building vulnerability		VL	L	M	H	VH	EH
	VL	Lack	Lack	Lack	Very Low	Low	Medium
	L	Lack	Lack	Very Low	Low	Medium	Appreciable
	M	Lack	Very Low	Low	Medium	Appreciable	High
	H	Very Low	Low	Medium	Appreciable	High	Very High
	VH	Low	Medium	Appreciable	High	Very High	Extremely High

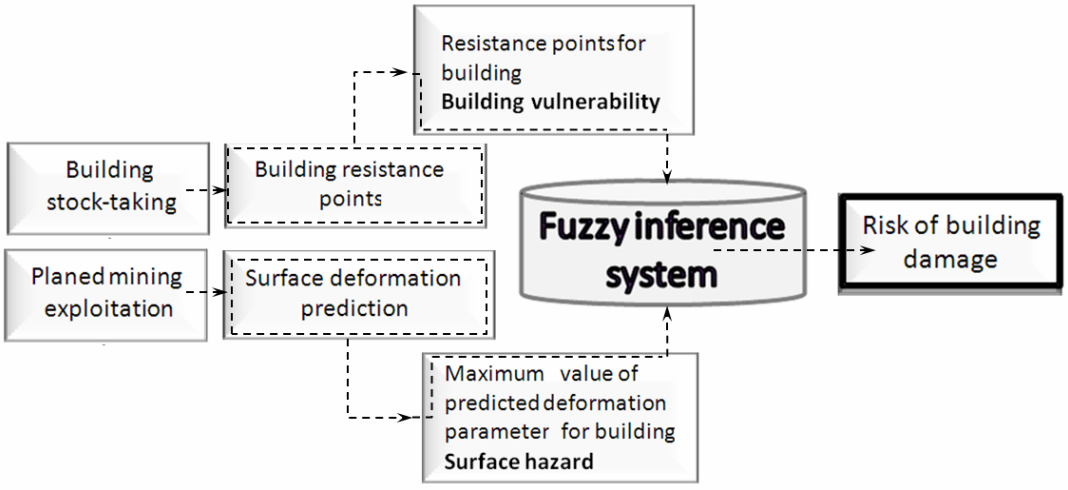

Fig. 2 Building damage risk assessment algorithm.

The final step of the fuzzy model definition was determining parameters of the inference mechanisms: the conjunction premise was assessed with operator PROD; fuzzy implication was done with operator PROD; accumulation was made for operator SUM; and the defuzzification technique was centre of gravity. Those parameters enabled us to obtain an optimal shape of the output surface of the risk of building damage.

The defined model enables us to determine the risk of building damage and to describe it with one value. An algorithm was worked out to help evaluate the risk of building damage with the proposed fuzzy model and tools of GIS type (Fig. 2). With GIS the data, like points of building vulnerability and predicted horizontal strain, can be integrated and the input model data acquired. Based on those data, the risk of building damage is assessed with the fuzzy inference system and using Matlab. The results of inference are then used for the GIS system.

A CASE STUDY

The model presented in this paper is capable of diversifying the risks of building damage. One of the proposed solutions is the use of the algorithm (Fig. 2) to help the mining damage section select objects where the safety of use has not been exceeded and objects which should be investigated individually before they are classified as needing construction prevention measures against potential mining impacts, or not. Moreover, the proposed model enables one to grade the risk both in hazarded and non-hazarded buildings. The elaborated algorithm enables one to automatically assess the building damage risk on a point scale. Risk points are determined for each building, giving more complete information about the potential damage occurrence. Hazarded buildings (resistance category lower than terrain category by 2), where the prevention measures should be used before the exploitation begins are marked by dashed shading in Fig. 3.

Owing to the possibility of an exact risk of building damage assessment, the building engineers receive strict and accurate information about building hazard. Taking into consideration local mining conditions and the type of masonry, they can establish principles to be applied for building protection.

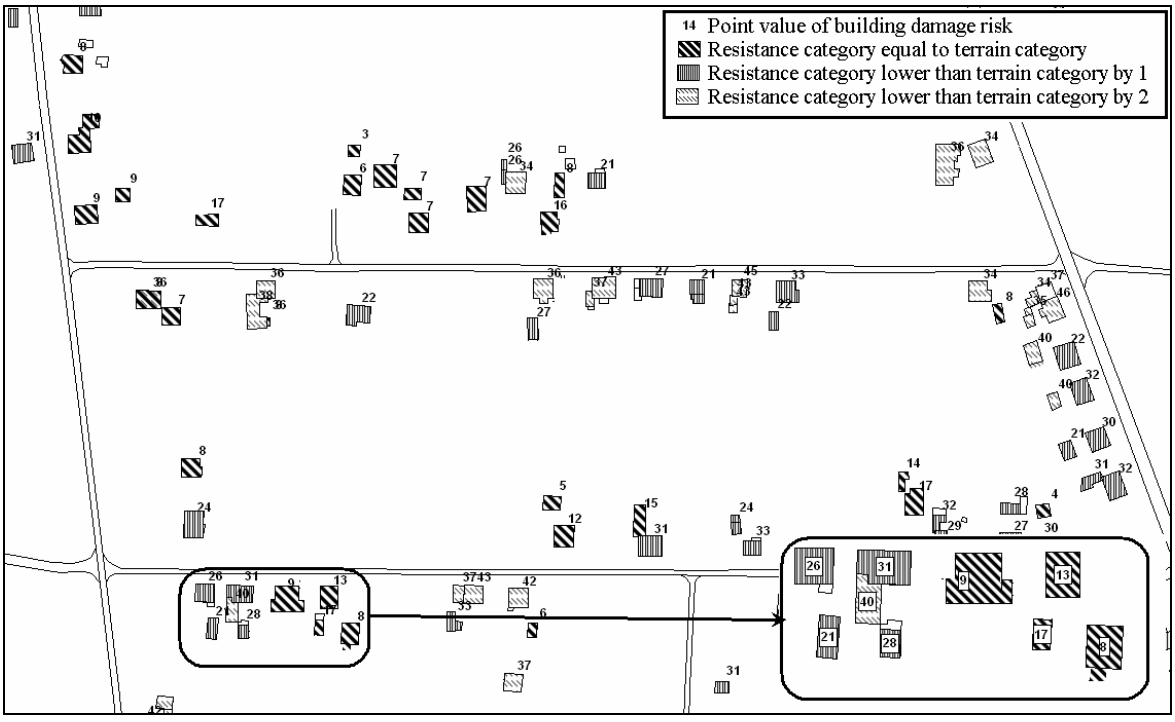

Fig. 3 Evaluation of risk of building damage – proposed grading of risk.

Acknowledgements The research reported in this paper has been supported by the Ministry of Science and Higher Education under grant N N524 373337.

REFERENCES

Altrock, C. (1993) *Fuzzy Logic*, Band 1, *Technologie*. R. Oldenburg Verlag GmbH, München, Germany.

Budryk, W. & Knothe S. (1950) Wpływ eksploatacji podziemnej na powierzchnię z punktu widzenia ochrony obiektów. *Przegląd Górniczy*, no. 11.

Budryk, W. & Knothe, S. (1956) Zasady klasyfikacji terenów Górnośląskiego Okręgu Przemysłowego ze względu na możliwość ich zabudowy (Classification of the mining areas of the Upper Silesian Coal Basin with regards to development). *PAN Komisja Mechaniki Górotworu*, Biuletyn no. 4, Warszawa

Hejmanowski, R.(2001) Prognozowanie deformacji górotworu i powierzchni terenu na bazie uogólnionej teorii Knothego dla złóż surowców stałych, ciekłych i gazowych (Predicting rock mass and surface deformations for solid, liquid and gas deposits on the basis of generalised Knothe theory). *IGSMiE PAN*, 207–214. Kraków, Poland.

Hejmanowski, R. & Malinowska, A. (2009) Evaluation of reliability of subsidence prediction based on spatial statistical analysis. *Int. J. Rock Mechanics & Mining Sci*. **46**(2), 432–438.

Hejmanowski, R. & Sroka, A. (2000) Time-space ground subsidence prediction determined by volume extraction from the rock mass. In: *Land Subsidence* (Proc. Sixth Int. Symp. on Land Subsidence, Ravenna), vol. 2, 367–375.

Instrukcja GIG no. 12 (2000) Zasady oceny możliwości prowadzenia podziemnej eksploatacji. górniczej z uwagi na ochronę obiektów budowlanych (Possibilities of the mining exploitation taking into consideration buildings safety). Katowice, Poland.

Klir, G. J. & Yuan, B. (1995) *Fuzzy Sets and Fuzzy Logic Theory and Applications*. Prentice Hall PTR, New Jersey, USA.

Knothe, S. (1953) Równanie profilu ostatecznie wykształconej niecki osiadania (Equation of the fully-developed subsidence basin). *Archiwum Górnictwa i Hutnictwa* t. 1, z. 1.

Malinowska, A. (2009) Building damage risk assessment method based on fuzzy inference system. Wyd. IGSMiE PAN, Kraków, Poland.

Malinowska, A. & Hejmanowski, R. (2010) Building damage risk assessment on mining terrains in Poland with GIS application. *Int. J. Rock Mechanics & Mining Sci*. **47**(2), 238–245.

Przybyła, H. & Świądrowski, W. (1968) Określenie kategorii odporności istniejących obiektów budownictwa powszechnego na wpływy eksploatacji górniczej (Building resistance assessment to the influence of the mining exploitation). OTG no. 8, Katowice, Poland.

Wittaker, B. N. & Reddish, D. J. (1989) *Subsidence, Occurrence, Prediction and Control*. Elsevier, Amsterdam, The Netherlands.

Zadeh, L.A. (1965) Fuzzy sets. *Information and Control* **38**(1), 1–14.

Zimmermann, H. J. & von Altrock, C. (1994) *Fuzzy Logic*, Band 2, *Anwendungen*. Oldenburg Verlag, München, Germany.

(Proceedings of EISOLS 2010, Querétaro, Mexico, 17–22 October 2010). IAHS Publ. 339, 2010.

Assessment of the state and condition of damaged buildings and structures affected by land subsidence

J. A. ORTIZ[1], F. A. ALONSO[2], J. PACHECO[1], M. E ZERMEÑO[1], G. ARAIZA[1] & E. MENDOZA[1]

1 *Dept. of Construction and Structures, Autonomous University of Aguascalientes, Av. Universidad 940 (module 108), 20100 Aguascalientes, Ags., Mexico*
aortiz@correo.uaa.mx

2 *School of Engineering, Autonomous University of Chiapas, Blvd. Belisario Domínguez Km. 1081, 29000 Tuxtla Gutiérrez, Chis., Mexico*

Abstract Soil fracturing due to land subsidence is a frequent problem in many countries when the water extraction exceeds the natural recharge of aquifers. The effect of soil fracturing due to subsidence may provoke severe damages and compromise the structural stability of buildings. The objective of this paper is to present the development of a methodology of inspection and evaluation, in order to estimate the state of the condition of damaged structures with the purpose of establishing a diagnosis of its structural state. This methodology allows standardizing of the criteria for the inspection and evaluation tasks, which means that the diagnoses issued by inspectors will be more regular. In this way, more reliable and better supported recommendations will be issued regarding the structural safety of houses and the necessary tasks to be done, concerning the reinforcing, rehabilitating, repairing, dislodging or demolition of the structures.

Key words land subsidence; structural pathology; evaluation

INTRODUCTION

The effect of soil fracturing due to subsidence may provoke severe damage and compromise the structural stability of a building. Housing buildings, mainly built based on confined masonry, eventually are unable to bear the stresses (mainly shear and tension) caused by differential settlements due to subsidence (Araiza, 2008).

METHODOLOGY FOR INSPECTION AND EVALUATION

A methodology for inspection and evaluation of housing buildings with damage due to land subsidence is presented. It takes into account mainly two structural parameters which are dependent on each damaged structural element that, eventually, may have impacts on the global performance of the structure. The structural elements to evaluate are the following: slabs, beams, and other elements of the superstructure, columns, foundations, and other elements of the substructure (Alonso, 2006).

The structural parameters used to evaluate the structural elements are: (a) the damage percentage, related to the level of damage in each element, from 0 to 100%; and (b) the importance factor, related to the level of connotation that each element has regarding the global structural stability.

The assessment of the state of condition is obtained by means of the Index of State of Condition (ISC) and is calculated through the following equation:

$$ISC = 5[P_S F_S + P_B F_B + P_{SP} F_{SP} + P_C F_C + P_F F_F + P_{SS} F_{SS}] \quad (1)$$

In equation (1) P refers to the damage percentage, and F is the importance factor, while S refers to slabs, B to beams, SP to other elements of superstructure, C to columns, F to foundation and SS to other elements of substructure.

The criterion used to assign the damage percentage, P, is based in objective measurements such as: beam and slab deflections, the length, width and depth of cracks in bearing walls, beams and slabs, etc.

Copyright © 2010 IAHS Press

The importance factors, F, were obtained from statistical analyses on the basis of the probability of collapse of the whole structure because of the damage level or the deterioration of each structural element (slabs, beams, columns, foundation, etc.).

In this way the importance factors, F, are as follows: slabs (1.88), beams (2.14), other elements of superstructure (1.88), columns (3.75), foundation (2.14) and other elements of substructure (1.88).

The calculated values of ISC are correlated with the State of Condition (SC) of the structure, having finally 5 degrees of SC related to the levels of structural damage; the SC degrees are presented in Table 1.

Table 1 States of Condition (SC).

SC range	State of Condition	Description
0 – 3.75	1 Good	The structure has no damages.
3.75 – 7.50	2 Acceptable	The structure has minor deficiencies and requires only usual maintaining works.
7.50 – 11.25	3 Regular	The structure has several important deficiencies, which if not attended may evolve towards major deficiencies; these problems require mid or short-term corrective measures.
11.25 – 15.00	4 Bad	The structure has one or more major deficiencies which imply an imminent danger for the user's safety; these problems require immediate corrective measures.
> 15.00	5 Damaged	The structure has severe damages that eventually could provoke the collapse of the building; this level requires urgent rehabilitation or reinforcing works, or in any event, demolition.

INVENTORY AND ASSESSMENT SYSTEM OF BUILDINGS

For the purpose of gathering and managing the information derived from the inspections of structures and the assessment of the state of condition, a system called Inventory and Assessment of Housing Building (SIEVA, due to its Spanish initials) was developed.

This system allows determination of statistical parameters related to structural pathologies or damages in the inspected structures, and also calculation of the State of Condition (SC). Figure 1 illustrates the working environment of the SIEVA system, through some windows.

CONCLUSIONS

Using this methodology it is possible to decrease the subjective judgment of inspectors when assessing the structural safety of damaged buildings, especially in land subsidence zones.

With the above-mentioned procedures, the decisions taken related to reinforcing, rehabilitation or demolition would be more reliable and better supported.

Acknowledgements To the Autonomous University of Aguascalientes, Autonomous University of Chiapas, Department of Public Works of the Municipality of Aguascalientes, and the PROMEP Program of the Ministry of Public Education of Mexico (projects 103.5/08/1265 and 103.5/07/2338).

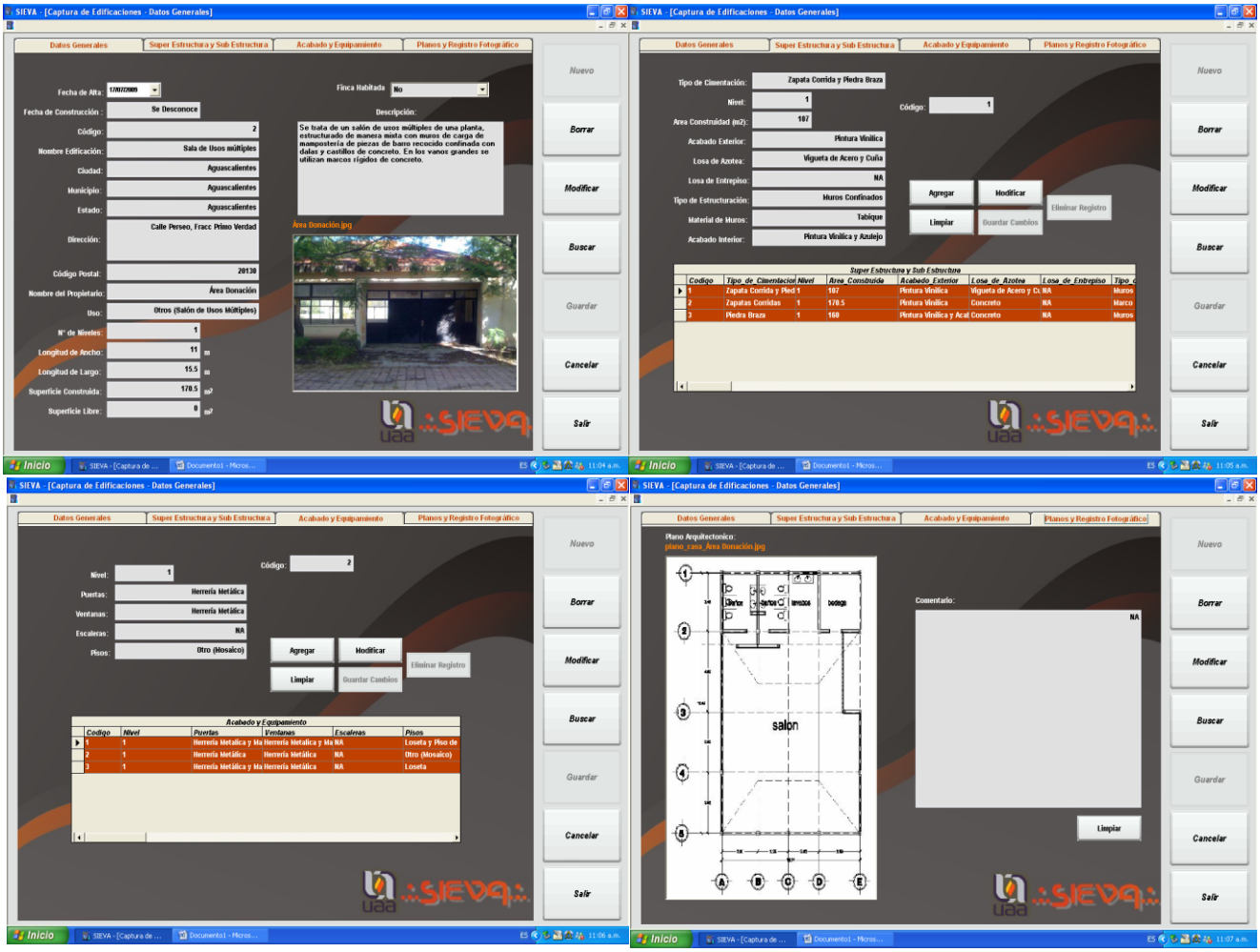

Fig. 1 Working environment of the SIEVA system.

REFERENCES

Alonso, F. (2006) Optimización Conjunta de las Políticas de Mantenimiento y Rehabilitación en Puentes mediante Algoritmos Genéticos. Aplicación al Sistema de Gestión de Puentes del Estado de Chiapas. Tesis Doctoral. España, Departamento de Ingeniería de la Construcción, ETSECCPB, Universidad Politécnica de Cataluña, Barcelona, Spain.

Araiza, G. (2008) Consideraciones en torno a la supresión y control de daño estructural originado por subsidencia del suelo en edificios patrimoniales. In: Memorias del I Congreso Iberoamericano sobre Construcciones Históricas y Estructuras de Mampostería, Universidad Industrial de Santander, Bucaramanga, Colombia. Disco Compacto ISBN 978-958-44-3809-6.

(Proceedings of EISOLS 2010, Querétaro, Mexico, 17–22 October 2010). IAHS Publ. 339, 2010.

Guidelines for the design of a unit of urban risk prevention for subsurface fracturing in the Municipality of Iztapalapa in Mexico City

H. C. CARREÓN-FREYRE & J. C. RODRÍGUEZ-QUIROZ

Instituto Nacional de Investigaciones Forestales, Agrícolas y Pecuarias (INIFAP), Area de Auditoría para Desarrollo y Mejora de la Gestión Pública en el Organo Interno de Control (OIC), Mexico
carreon.hugo@inifap.gob.mx

Abstract The aim of the work is to propose the creation of a unit of prevention of urban risk caused by land subsidence (UPUR-LS) in some areas of Mexico City. The unit of prevention is based on the identification of risks and factors of risk related to the land subsidence phenomenon, the analysis of the probability of occurrence and the quantification of its impact on the urban infrastructure. The applied methodology is a combination of two powerful tools: the systems approach and the risk management model. The former assumes that a system is a group of elements related by a common objective. This approach considers the whole system, its parts (subsystems) and the interactions between them, with the system, and from the system and the environment. The analysis should be addressed so as to improve the system itself. In contrast, the risk management model is a tool used to identify, evaluate and classify a group of risks that can modify the capacity for achievement of specific goals by institutions and organizations. With the integration of both methodologies we have created a conceptual model that permits the evaluation of hazards caused by land subsidence and fracturing and their socio-economic impacts. The analysis of several study cases in the Delegación Iztapalapa of Mexico City permitted the identification of factors of risk and the quantification of their impact on the society. The results obtained led to the design of the UPUR-LS that considers the administrative structure of a governmental agency as a "system" to be improved, and the technical results generated by the Center of Monitoring of the Fracturing of the Subsurface, already created in the Delegación Iztapalapa. Using this method the technical results of monitoring can be managed to optimize the human and economic resources of the governmental agency, to elaborate a guide for procedures, and facilitate the decision making for the creation of mitigation strategies.

Keywords risk management; strategy; social impact

INTRODUCTION

For several years, a populous area of Mexico City, the municipality of Iztapalapa, has presented severe problems of fracturing of the subsoil that has endangered hundreds of homes, various infrastructure works and the physical integrity of thousands of people. In response to this problem, in 2007 the Monitoring Center of the Subsoil Fracturing was created, which led to the Center of Geological Risk Assessment, CGRA (Centro de Evaluacion de Riesgo Geologico; CERG, 2009) in 2010, with the technical support of the Centro de Geociencias de la Universidad Nacional Autónoma de México, Campus Querétaro. Through this Center the subsurface detection of deformation made great progress in identifying the fracturing of the area, the trends and possible impacts on the physical infrastructure of the Delegation.

This paper examines the creation of a Unit of Urban Risk Prevention for Subsurface Fracturing (UURPSF), which identifies the risks associated with this phenomenon, quantifies the potential impacts and evaluates its occurrence. This is achieved by the application of two powerful methodologies of analysis: the systems approach and the model of risk management. By integrating these, the Centre for Geological Risk Assessment (CGRA) will lead to a robust Urban Risk Management System.

METHODOLOGY

The Systemic Approach (SA) model assumes that a "system" is a set of elements related to a common purpose. In this point of view the "system" considers the whole elements (subsystems)

and the interaction between each of them and the "system", and between the "system" and its environment. The model establishes that when several options are displayed, several courses of action should be chosen and by considering all of them should lead to a satisfactory system. Furthermore, the model of Risk Management (MRM) is a tool used to identify, evaluate and categorize a group of risks that could significantly affect the ability to achieve the pre-established objectives in the activities programme of any organization, or of its administrative units. This model can be applied to identify and measure the impact and occurrence of risks within a specific area (i.e. the "Municipality of Iztapalapa" located in Mexico City), a programme, or a specific process (Rosso Ochoa, 1985).

The aim of this work is to integrate the mentioned methodologies to create a consistent conceptual framework that permits structuring and analysis of the information produced by the MRM. Indeed, from the problematical conditions related to land subsidence and the associated fracturing in Iztapalapa, the evaluation of risks to the population has allowed the identification of specific situations that can be classified as "Systemic Risks". This is of utmost importance since both the impact of a risk (a measurement of how the same circumstance affects the achievement of a specific objective), and its probability of occurrence are closely related with the factors that determine them. As a final part of this study, an outline of the operation guidelines of the so-called Unit of Urban Risk Prevention for Subsurface Fracturing (UURPSF) in Iztapalapa is detailed. These guidelines are considered as basic operational recommendations that allow a proper management of available human, technical and economic resources in Iztapalapa and how to take the make greater and best use of the of the Center of Geological Risk Assessment (CGRA) that is already in operation.

THE SYSTEMIC MODEL ASSOCIATED WITH CREATION OF A UNIT OF URBAN RISK PREVENTION FOR SUBSURFACE FRACTURING (UURPSF) IN IZTAPALAPA

The conceptual model

The development of the conceptual model of a complex system should allow the clear identification of its elements: the object of analysis (in this case the system UURPSF-CGRA) and the most significant elements of the environment in which it operates (Fig. 1). It should be noted that for the purpose of this analysis, the UURPSF and CGRA would integrate a system of collaboration to adequately accomplish the objectives planned for the Prevention Unit.

In this model two "environmental levels" that interact with the activities of the UURPFS are represented: the "first-class environment" that represents those elements with a very direct influence on the system, such as the environment that surround the constructions in the municipality, the operational structure, the urban infrastructure, the human resources and, obviously, the elements that integrate the strategic management (fundamental objectives, mission, vision and shared values). Other important elements of the environment are first-order input suppliers of the system such as their funding resources, the existing regulations to apply, the whole administration system of the municipality, and the different levels of government (city, state and country). The "second-order environment" level represents the elements that affect the operation in a general way, for example the civil protection policies, groundwater exploitation policies, land-use local and regional plans, etc. As shown in Fig. 1, some elements are placed in the edge between the first and the second environmental order; this is the case of competitors (i.e. other municipalities), strategic associates, and the rapport of the system with other agencies and units of the Public Federal Administration (PFA).

Before describing the main elements of this model, it is important to underline that a system is a set of interrelated elements that meet for a particular purpose. In this case, that purpose is the accomplishment of the fundamental objectives (Element 4) of the system UURPFS-CGRA presented in Fig. 1 as an integrated system (Element 2) that have five major components: (1) the operational structure outlined by an Organic Statute, (2) the operational and strategic courses of action of the system, that should be defined by its mission, vision, key objectives and shared

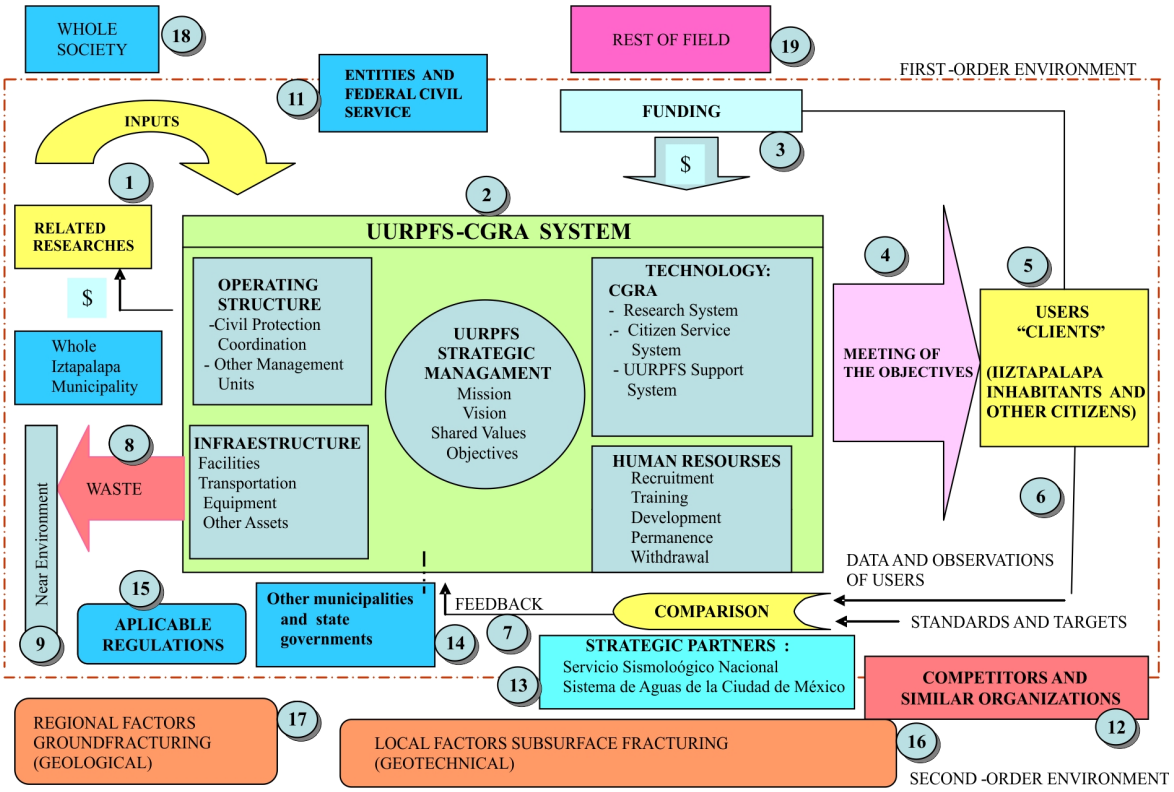

Fig. 1 UURPFS-CGRA conceptual model of the system.

values, (3) the scientific and administrative technology required by the system, (4) the infrastructure and equipment acquired to allow the system to carry out its activities, and (5) the human resources. Through these five major components, the UURPFS-CGRA system transforms its inputs and gives an added value to achieve the fundamental institutional objectives.

Element 1 of Fig. 1 represents suppliers of resources (i.e. electricity, machinery and equipment) required by the system to carry out its operations and for which it must pay a certain amount of money. The source of the funding required by the system to operate is represented by the Element 3 of Fig. 1. Element 4 refers to the previously discussed fundamental objectives. Element 5 represents the users, consumers, or "clients" who benefit from the knowledge and information produced by the system. Element 6 represents the observations made by the users, consumers, or "clients" about the quality of the product and/or knowledge they receive from the system. Element 7 indicates the feedback that comes from comparing the data and previous observations, standards and goals with those fixed by the system for a certain period of time. Element 8 indicates the possible waste discharged by the system to the local environment (Element 9) as a result of its operational activities (i.e. debris left by damaged buildings or produced by land excavations). Element 10 represents the whole administration of the Iztapalapa municipality, that includes all administrative units that do not have a close relationship with the nature of the UURPFS-CGRA operations, but nevertheless can strongly affect its operation; for example: the Chief of Iztapalapa, the Coordinator of Advisors, the Coordination of Social Communication, the General Juridical and Government Direction, the General Direction of Urban Development, the General Direction of Urban Services, the General Direction of Social Development, the General Direction for Development, and the General Direction for Administration. This group does not include the Coordination of Civil Protection (CCP) because of its close relation with the design and prevention operations of the system that are presented in this work. In Element 11 are represented other entities and agencies of the PFA that can have a significant impact on the system activities, such as the Departments of State, and the Federal Company of Electricity (CFE).

Element 12 indicates the potential competitors that can acquire the system. Element 13 indicates the potential strategic associates to the system, i.e. the Agency of Water Management in Mexico City (SACM, *Sistema de Aguas del la Ciudad de Mexico*), which can provide valuable information regarding water resources, their supply and distribution policies, and the nature of the subsoil; or the National Seismological Service (that can also provide very important information); and some national or international universities or government agencies. Element 14 represents other levels of government in Mexico City, other than those of the Iztapalapa Municipality, as well as other municipalities and state governments. Element 15 represents the policies that can be applied to the system related to the Mexico City and Federal government. In Element 16 are represented the local geological and geotechnical factors related to the generation of the fracturing of the subsoil in Iztapalapa (i.e. groundwater exploitation, major urban infrastructure or heavy vehicular circulation). Element 17 illustrates the regional geological factors that determine the generation and propagation of ground fracturing in Iztapalapa. Element 18 illustrates the possible impact of the rest of society in the operations of the system. Finally, Element 19 indicates the influence of the national social and physical environment in the operations of the system (i.e. the national and international pandemic of H1N1 of 2009).

Objectives proposed for UURPSF-CGRA system

The proposed targets are:

1. To support the preservation of the physical integrity and a good quality of life for the Iztapalapa inhabitants and the good condition of existing and projected urban infrastructure.
2. Contribute to the design of effective procedures to prevent ground subsurface fracturing and design appropriate mitigation measures.
3. To provide a reference for the design of similar prevention systems elsewhere in Mexico.

Identification of risks associated with the objectives of the system

To properly define the risks of the system we have conducted an expert dynamic consultation. This dynamic systematic consultation consisted of three people who have worked closely with the implementation of the Center of Geological Risk Assessment of Iztapalapa. Through the brainstorming technique and building on the construction of Ishicawa diagrams, and according to the conceptual model of Fig. 1, the UURPSF-CERG fundamental objectives mentioned in the previous section were defined. After defining these objectives, the role of the experts focused on the determination of the risks associated with the system. An example of the corresponding Ishicawa diagrams are shown in Fig. 2. This diagram represents risk events that can affect the achievement of each UURPSF objective.

Assessment of the risks associated with the system operation

The assessment of the risks associated with the system was defined by the panel of experts by the use of two parameters. The first parameter indicates the level of impact, graded on a scale of 1–10 (1 indicates minimal impact of risk in achieving the objective). If the risk is rated with 10, it indicates that the impact will be such to defeat the purpose to which it is associated. Similarly, the panel assessed the probability of occurrence of each identified risk. If the probability of realization of the risk is evaluated with 1, it indicates that the risk in question is highly unlikely, while a risk whose probability of occurrence is evaluated by 10, indicates that the associated risk will occur with certainty.

Construction of the risk map associated with the operation of the system

Once the panel of experts evaluated all the risks identified, a numerical analysis allowed definition of the risk map (Fig. 3). The risk map shows clearly that 85% of the identified risks are included in the so-called Quadrant I or Quadrant Risk that requires immediate attention (risks that have both a high level of impact and a high probability of occurrence). Note that in the risk map of Fig. 3, four risks were clearly identified: the risk 1.8, related to the existence of ineffectiveness of financial

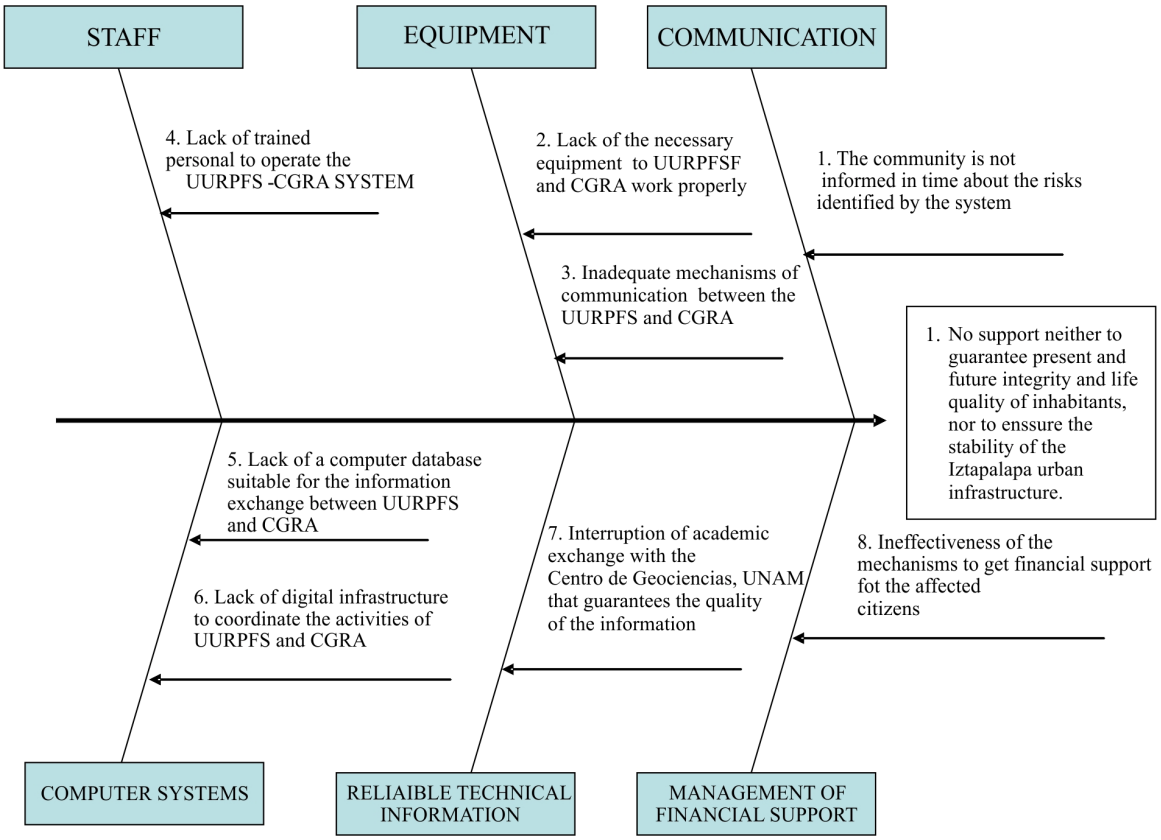

Fig. 2 Events that can affect the achievement of each UURPS objective.

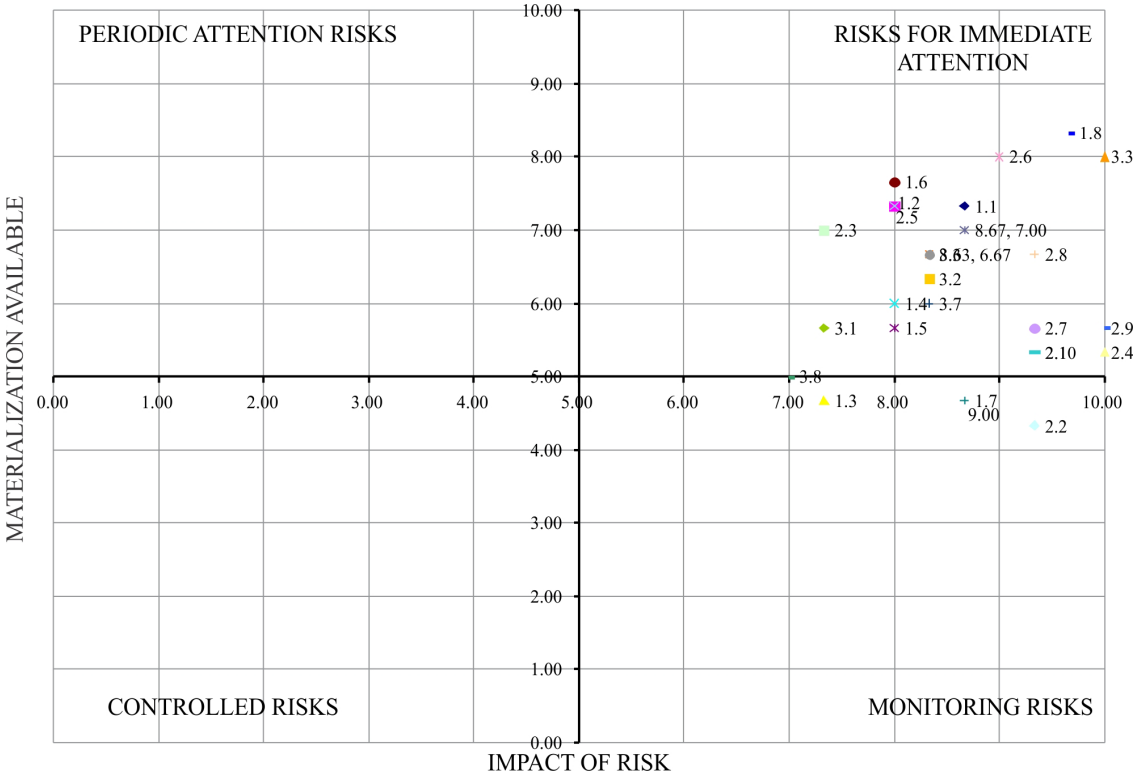

Fig. 3 Risk map associated with the operation of the system.

support mechanisms to assist the affected population; the risk 3.3: related with a lack of enough trained personnel to perform an adequate job of spreading the benefits and achievements of the system; the risk 2.9 related to the UURPSF-CGRA not being able to develop effective solutions to the required interdisciplinary approach. Finally, it also highlights the importance of risk 2.4 related to there not being enough qualified personnel (geological engineers, civil engineers, architects, etc.) to develop accurate solutions in the appropriate time.

Recommendations for management of risks associated with the UURPFSF-CGRA operation

1. The operational success of the system depends largely on the establishment of effective communication between this UURPFS, the CGRA, the potential users of the system and potential strategic associates.
2. The system's ability to have the human talent needed to operate both the Unit of Prevention and the CGRA, as well as experts who are required to generate effective solutions. This is very important, since the deformation of the subsoil of the Iztapalapa is a challenge whose management necessarily requires a multidisciplinary approach.
3. The authorities' commitment to support the system in the medium and long term. It is very important to seek mechanisms in order to maintain the operation at a high technological and operational level.
4. It is important to note that the Risk Map shown in Fig. 3 represents only a stage in a very dynamic environment in which the risks can "move" on the map over time. Therefore, the steps proposed in this work leading to the construction of the Risk Map, should be carried out in cycles. As a consequence the system should be improved continuously, providing elements for better decision making and to improve the management system UURPSF – CGRA.

CONCLUSIONS

This study identified the advantages of the integration of two sources of modern scientific knowledge. The first one studies the behaviour of a very complex physical phenomenon, such as the process of fracturing of the subsoil in the Iztapalapa Municipality, through the application of advanced methods of geophysics and soil mechanics performed by the Center of Geological Risk Assessment (CGRA). This was complemented with the methodologies provided by engineering production systems, such as the Systemic Method and Model Risk Management (performed by the UURPFS). The result was a robust system for monitoring the deformation of the subsoil in the Iztapalapa area, supplemented with an adequate system of risk management, that allows more effective, relevant and timely decision-making to properly manage the risks that land subsidence bring to the population and to the existing urban infrastructure.

Acknowledgements The authors wish to acknowledge the support received by the staff responsible for operating the Centro de Evaluacion de Riesgo Geologico, and the academic group of the Centro de Geociencias, Universidad Nacional Autónoma de México, Campus Querétaro who participated in this project since 2007, for the information provided and their valuable participation in exercises identifying risks and for their patience in reviewing this work.

REFERENCES

CERG (Centro de Evaluación de Riesgo Geológico) (2009) Reporte de Actividades. Delegación Iztapalapa del Gobierno del Distrito Federal. 31 p.

Churchman, C. (1993) *El Enfoque de Sistemas* (The Systems Approach). Diana, West México DF, Mexico.

Rosso Ochoa, F. (1985) *Systems Approach*. Division of Graduate Studies, Faculty of Engineering, Universidad Nacional Autónoma de México, Mexico.

Segundo Informe Parcial (2009) Mayo-Agosto, del Convenio de Colaboración entre el Centro de Geociencias (CGEO) de la Universidad Nacional Autónoma de México y la Delegación Iztapalapa del Distrito Federal.

6 Land Subsidence Caused by Subsurface Fluids Withdrawal

(Proceedings of EISOLS 2010, Querétaro, Mexico, 17–22 October 2010). IAHS Publ. 339, 2010.

Pumping effects on land subsidence in the Toluca Valley, Mexico

A. I. CALDERHEAD[1,5], R. MARTEL[1], J. GARFIAS[2], A. RIVERA[3] & R. THERRIEN[4]

1 *Institut National de la Recherche Scientifique, University of Quebec, Québec, Québec, Canada*
aicalderhead@gmail.com

2 *Centro Interamericano de Recursos del Agua – Universidad Autónoma del Estado de México, Toluca, State of Mexico, México*

3 *Geological Survey of Canada, Natural Resources Canada, 490 de la Couronne, Quebec, Canada*

4 *Département de géologie et de génie géologique, Université Laval, Québec, QC G1K 7P4, Canada*

5 *Jet Propulsion Laboratory, California Institute of Technology, 4800 Oak Grove, Pasadena, California 91106, USA*

Abstract The Toluca Valley, Mexico, experiences heavy groundwater pumping and significant land subsidence. This study examines pumping induced regional land subsidence of the Toluca Valley. The study is divided as follows: (1) obtaining InSAR data, field data, and all available literature for the Toluca Valley; (2) coupling compaction to the groundwater flow equation with the HGS model; and (3) constraining the model with available data to eventually examine several pumping scenarios for minimizing future land subsidence. It is apparent that continuing at the current rates of the water consumption will lead to more subsidence. Average estimates predict a maximum subsidence in the valley that will reach 1.2 m in the next 40 years.

Key words land subsidence; 1-D geomechanical model; InSAR; Toluca, Mexico

INTRODUCTION

InSAR, field data, and a newly coupled finite element 1-D instantaneous compaction and 3-D groundwater flow model, Hydrogeosphere (HGS) (Therrien *et al*., 2009) are used for the analysis of land subsidence in the Toluca Valley, Mexico. The Toluca Valley presently exports 38% (6 m^3/s) of its groundwater resources to Mexico City (CNA, 2007). The Toluca Valley's water resource and land subsidence problems are of interest because the basin was formally seen as an important source of water to the Mexico City basin, yet today the Toluca Valley can no longer support its own growth, let alone provide for that of Mexico City. In contrast to Mexico City's well documented subsidence, very little compaction information has been documented in the Toluca Valley, even though subsidence occurrences have been noticed since the early 1970s. Remote sensing information (Synthetic Aperture Radar (SAR) images) in the last 10 years has added to the overall understanding of the subsidence occurrences.

BACKGROUND AND METHODOLOGY

The Toluca Valley background

The Toluca Valley basin (Fig. 1) covers an area of approximately 2100 km^2. The basin is adjacent to the Mexico City Valley, with the Sierra Las Cruces forming a natural border between the two basins. The Toluca Valley's geographic position in the centre of the country, and its proximity to Mexico City, as well as its rapidly developing infrastructure, have allowed the city to grow into a major industrial zone for the country.

Heavy groundwater pumping for local use and for export to Mexico City have caused a significant groundwater deficit over the last 45 years. Calderhead (2010) shows that the deficit will continue to increase.

Copyright © 2010 IAHS Press

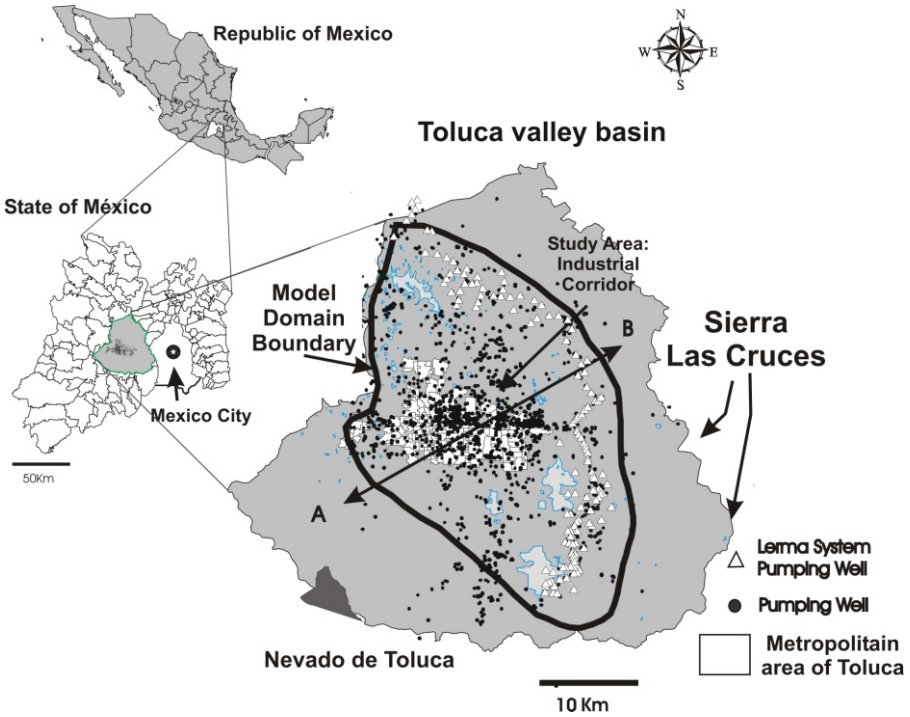

Fig. 1 Location map of the Toluca Valley and model domain boundary within the Republic of Mexico and the State of Mexico. Over 935 pumping wells are in operation in the Valley, including the 230 Lerma system wells that are located along the Lerma River on the eastern edge of the valley.

Clay compaction in the Toluca Valley

Terzhagi's (1925) principle is applicable in the Toluca Valley. For some sediment, inelastic compaction is proportional to the logarithm of the effective stress (Jorgensen, 1980). However, in many cases applicable to aquifer-system compaction where incremental changes in effective stress are typically small (e.g. the Toluca Valley), the relationship can be linearized as:

$$\Delta b = S'_k \, \Delta h \tag{1}$$

where Δb is the change in thickness of the sediment layer, S'_k is the skeletal storage coefficient, and Δh is the change in hydraulic head. To account for the marked change of the skeletal specific storage when the effective stress exceeds the preconsolidation stress, two separate values are often used:

$$S'_k = \begin{cases} S'_{ske} & for \ \sigma'_{zz} < \sigma'_{zz\,(pre)} \\ S'_{skv} & for \ \sigma'_{zz} \geq \sigma'_{zz\,(pre)} \end{cases} \tag{2}$$

where S'_{ske} is the elastic skeletal specific storage, S'_{skv} is the inelastic, or virgin, skeletal specific storage, and $\sigma'_{zz\,(pre)}$ is the preconsolidation effective stress.

Very little compaction data was available from the literature, thus efforts were made to obtain subsidence data from two bore holes equipped with one extensometer each, and from D-InSAR subsidence maps.

Extensometers

The objective of installing the extensometers was to obtain accurate field measurements at point locations. Two R-4 magnetic reed switch probe extensometer systems (Fig. 2) were installed in the Industrial Corridor (Fig. 3(a)). Boreholes with a 15 cm diameter were bored by a rotary drill and reach 115 and 78 m depth, respectively, for Extensometer-1 and Exsensometer-2. For this study, reading frequencies from the extensometers varied from 1 to 6 months and spanned two years beginning in July of 2006 and ending in July of 2008.

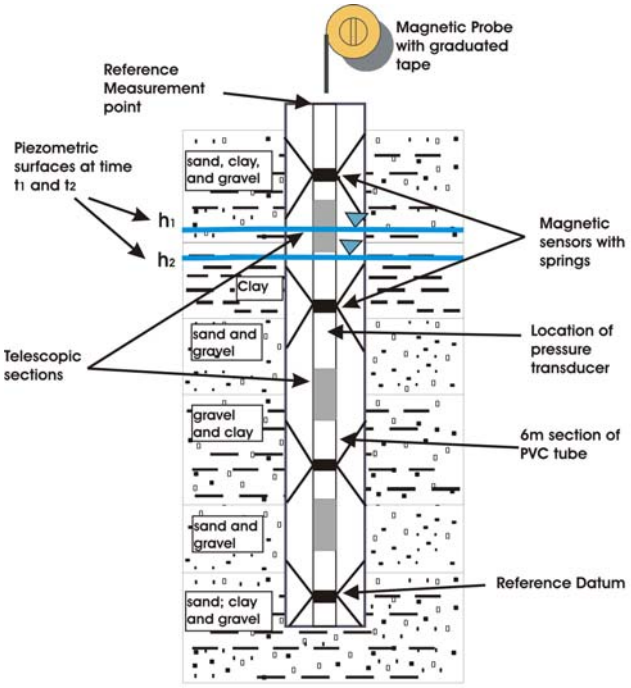

Fig. 2 Schematic drawing of the magnetic probe extensometer. Piezometric surface variations with time and location of pressure transducer are also represented. Drawing is not to scale.

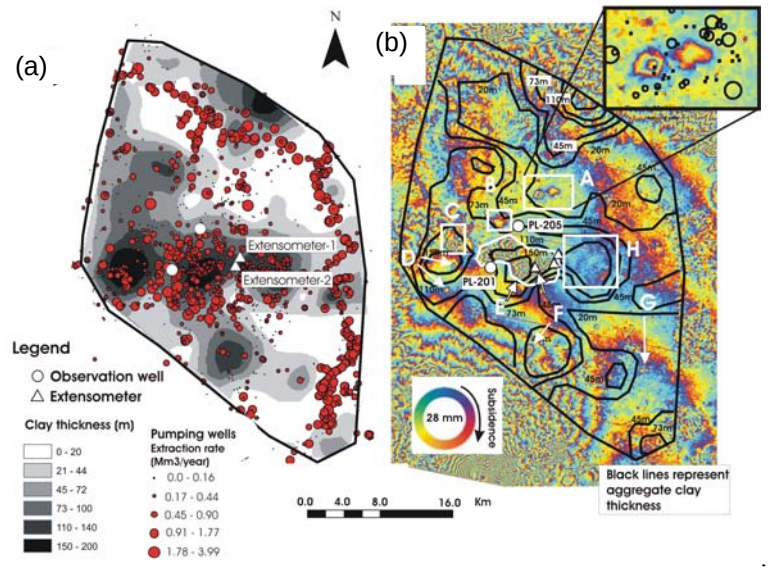

Fig. 3 (a) Aggregate clay thickness and pumping occurrences. (b) Differential interferogram of the Toluca Valley with a time interval of 70 days. ENVISAT ASAR images were acquired on 5 December 2007 and 13 February 2008. Lines of equal aggregate thickness are overlain and shown on the map.

InSAR

InSAR derived subsidence maps are used to constrain the compaction model. The interferograms and deformation maps are useful for locating compacting regions and quantifying subsidence magnitudes. SAR images were obtained from ERS-1, ENVISAT ASAR, and RADARSAT-1 between 1996 and 2008. Calderhead *et al.* (2009) presents the complete InSAR results for the Toluca Valley. Figure 3(a) shows pumping occurrences overlaying the aggregate clay thickness;

and Fig. 3(b) is a representative D-InSAR interferogram of the entire valley showing localized subsidence zones over a 70-day period. From Fig. 3(b), usable results are obtained throughout the central part of the valley. For the 70 days between 5 December and 13 February, zones A through G are "hotspots" with very clear subsidence patterns observed. If one observes the zoom on zone A (Fig. 3(b)), two colour cycles (clockwise: yellow-blue-red; see legend of Fig. 3(b)) are observed and represent a total subsidence of 56 mm for the given period. This translates to subsidence rates of 29 cm/year. However, as noted by Calderhead *et al.*'s (2009) D-InSAR study of the Toluca Valley, depending on the geological context and the pumping rates, the maximum subsidence rates are often variable in space, time, and magnitude.

Coupling compaction to groundwater flow

Several numerical models have been developed for simulating subsidence (e.g. Gambolati, 1972; Helm, 1975; Leake & Galloway *et al.*, 2007). With the objective of representing land subsidence in the Toluca Valley, Mexico, a compaction module was added to the multipurpose 3-D finite element groundwater flow model HGS. The following equation is used to describe HGS's modified version of 3-D transient subsurface flow for a fully saturated porous medium (Therrien *et al.*, 2009):

$$-\nabla q + \sum \Gamma_{ex} \pm Q = S_s \frac{\partial h}{\partial t} \tag{2}$$

with the fluid flux q given by $q = -K \nabla h$ and the hydraulic head h. The hydraulic conductivity, K, is given by: $K = \frac{\rho_w g}{\mu} k$ where g is the gravitational acceleration constant, μ is the viscosity of water, k is the permeability tensor of the porous medium and ρ is the density of water. If the aquifer system includes compressible sediments, this term can be multiplied by $(1 - \gamma^*)$, where γ^* is the fraction, by volume, of compressible interbeds in the aquifer system.

Combining the compaction term to the governing equation yields:

$$-\nabla \cdot q + \sum \Gamma_{ex} \pm Q = \left[(1-\gamma^*) * S_s + \gamma * S'_{sk}\right] \frac{\partial h}{\partial t} \tag{3}$$

where S_{sk} is as defined in equation (1).

RESULTS

At the Extensometer-1 location, similar subsidence patterns are observed from ENVISAT ASAR, RADARSAT-1, Extensometer-1, and the HGS compaction simulation (Fig. 4).

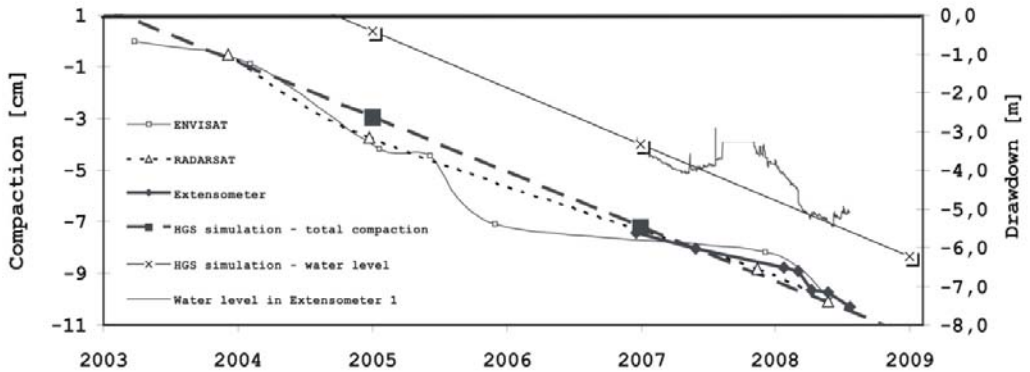

Fig. 4 Simulated and measured total compaction at Extensometer 1 by ENVISAT ASAR, RADARSAT-1, Extensometer-1, and HGS simulation. Simulated and measured hydraulic head at Extensometer-1 are also included.

Figure 5 presents the total compaction results between 2010 and 2050 for eight scenarios. Maximum total subsidence reaches 2.2 m for the worst case scenario (scenario 1), 1.4 m for the best case scenario (scenario 2), and 1.6 m for the average expected subsidence (scenario 3). Comparing scenarios 3, 4 and 5 is of interest. There are only subtle differences between stopping water exports (scenario 4) and cutting exports in half (scenario 5). However, there are noticeable differences between constant exports (scenario 3) and cutting exports in half (scenario 5).

The most marked change in subsidence occurs when moving the pumping centres (scenarios 7 and 8) away from compressible clays. Total compaction can be drastically reduced by simply moving the pumping centres to different locations within the valley. The most desirable results (scenario 8) show a localized maximum subsidence of <0.3 m in 2050, otherwise there is only limited subsidence throughout the valley.

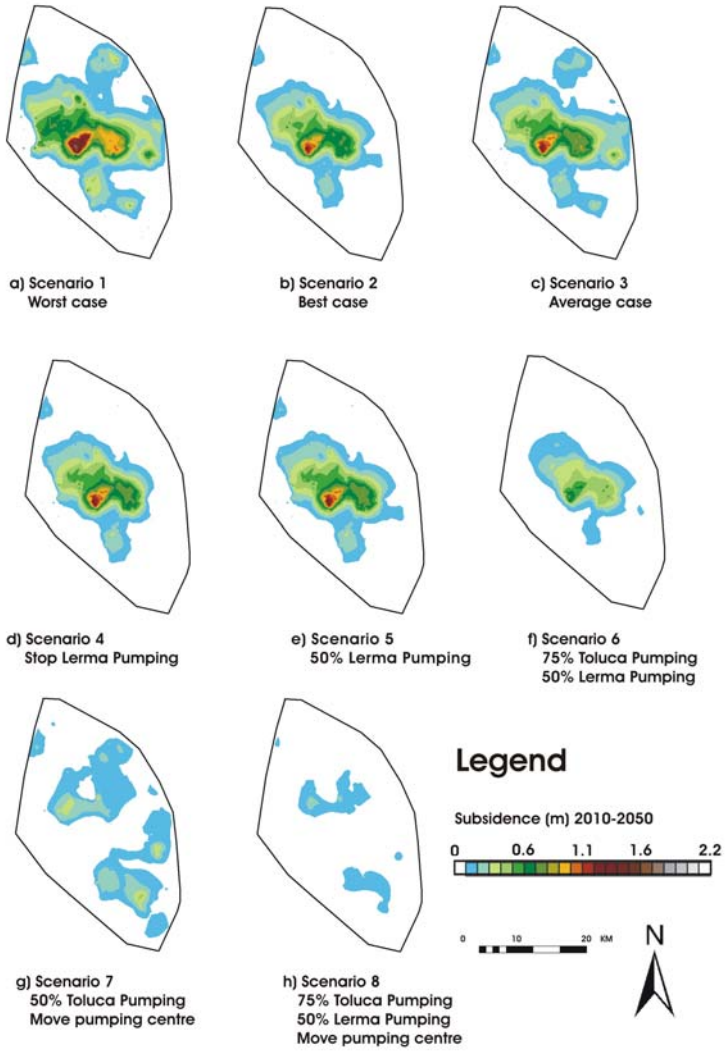

Fig. 5 Subsidence scenarios 2010–2050 (see Fig. 1 for location of the simulated domain).

DISCUSSION AND CONCLUSION

Limitations exist for the new HGS-compaction numerical model in representing subsidence. Hoffman *et al.* (2003) estimates that if the effective stress increases by 10%, compaction would be overestimated by about 5%. For sediments relatively deep below the land surface, a given decline in head will result in a smaller percentage increase in effective stress than for shallower sediments.

The new HGS-compaction code gives very reasonable estimates for instantaneous subsidence in confined aquifers; however, there is room for improving the estimates by including aspects such as dependence on hydraulic conductivity, nonlinear deformation, time delays, effects of moving water tables, and extending to a 3-D representation of deformation. The D-InSAR data was very useful in calibrating the subsidence model. InSAR has a large potential for mapping subsidence.

It is apparent that continuing at the current rates of water consumption will lead to more subsidence. Even in the best case scenario (scenario 2), maximum subsidence occurrences over a 40-year period will reach 1.4 m. Considering that the Lerma pumping system is mostly located in regions with low clay content, and little difference is observed between scenarios 4 and 5, completely stopping exports to Mexico City (scenario 4) is not necessary for controlling the subsidence. However, decreasing exports by half (scenarios 2, 5, 6, and 8) does have a positive effect on the overall water budget and subsidence. It can be argued that all scenarios will require inter-basin water transfer at a later date because the water budget deficit is not sustainable.

Acknowledgements We are thankful to the Ministère des Relations Internationales du Quebec, CONACyT, the Autonomous University of the State of México (UAEM), INRS-ETE, NSERC (a discovery grant held by Richard Martel), AUCC/IDRC, and the Ministère d'Éducation du Québec for their financial support. We are appreciative of Sergio Murillo from the Comision National del Agua for logistical support on the field. We are grateful to the Canadian Space Agency and the Geological Survey of Canada for providing the RADARSAT-1 data and finally, we acknowledge the European Space Agency's contribution for providing ERS and ENVISAT ASAR data at cost of reproduction under project C1P 3821.

REFERENCES

Calderhead, A. I. (2010) An increasing groundwater budget deficit induced by urbanization, industrialization, and climate change in the Toluca Valley, Mexico. *J. Hydrol.* (submitted).

Calderhead, A. I., Martel, R., Allasset, P.-J., Rivera, A. & Garfias, J. (2009) Land subsidence induced by groundwater pumping, monitored by C-band D-InSAR and field data in the Toluca Valley, Mexico. *Can. J. Remote Sensing* (accepted).

CNA (2007) Base Aquiferos Nacional y Regional. Comisión Nacional del Agua database. CNA, Mexico.

Galloway, D. L. & Hoffmann J. (2007) The application of satellite differential SAR interferometry-derived ground displacements in hydrogeology. *Hydrogeol. J.* **15**, 133–154.

Gambolati, G. (1972) A three-dimensional model to compute land subsidence. *Bull. Int. Assoc. Hydrolog. Sci*. **17**, 219–226.

Helm, D. C. (1975) One-dimensional simulation of aquifer system compaction near Pixley, California, 1, Constant parameters. *Water Resour. Res.* **11**, 465–478.

Hoffmann, J., Leake, S. A., Galloway, D. L. & Wilson, A. M. (2003) MODFLOW-2000 ground-water model-user guide to the subsidence and aquifer-system compaction (SUB) package. *USGS Open-File Rep 03-233*.

INEGI (2009) Instituto Nacional de Estadística, Geografía e Informática, Synthesis of geographic information for the state of Mexico. Aportación al Producto Interno Bruto (PIB) nacional/ Contribution to Gross Domestic Product (GDP) http://cuentame.inegi.org.mx.

Johnson, A. I., Moston, R. P.& Morris, D. A. (1968) Physical and hydrologic properties of water-bearing deposits in subsiding areas in California. *US Geological Survey Professional Paper 497-A*.

Jorgensen, D. G., (1980) Relationships between basic soils-engineering equations and basic ground-water flow equations. *US Geological Survey Water-Supply Paper 2064*.

Leake, S. A. & Galloway, D. L. (2007) MODFLOW ground-water model—User guide to the Subsidence and Aquifer-System Compaction Package (SUB-WT) for water-table aquifers. *US Geological Survey, Techniques and Methods 6–A23*.

Leake, S. A. & Prudic, D. E. (1991) Documentation of a computer program to simulate aquifer-system compaction using the modular finite-difference ground-water flow model. *US Geological Survey Techniques of Water-Resources Investigations, book 6, chap. A2*.

Legorrreta, J. (1997) Rainfall, the key to the future of the Valley of Mexico. *La Jornada Ecologica* **5**(58), 1–12.

Liu, Y. & Helm, D. C. (2008) Inverse procedure for calibrating parameters that control land subsidence caused by subsurface fluid withdrawal: 1. Methods, *Water Resour. Res.*, 44, W07423, doi:10.1029/2007WR006605.

Terzaghi, K. (1925) *Erdbaumechanik auf bodenphysikalisher Grundlage* (Earthworks Mechanics Based on Soil Physics). Franz Deuticke, Vienna, Austria.

Therrien, R., McLaren, .G. Sudicky, E. A. & Panday, S. M. (2009) User Guide: HydroGeoSphere – A three-dimensional numerical model describing fully-integrated subsurface and surface flow and solute transport. The University of Waterloo, Canada.

Land Subsidence, Associated Hazards and the Role of Natural Resources Development
(Proceedings of EISOLS 2010, Querétaro, Mexico, 17–22 October 2010). IAHS Publ. 339, 2010.

Integrated simulation of consumptive use and land subsidence in the Central Valley, California, for the past and for a future subject to urbanization and climate change

R. T. HANSON[1], A. L. FLINT[2], L. E. FLINT[2], C. C. FAUNT[1], WOLFGANG SCHMID[3], M. D. DETTINGER[4], S. A. LEAKE[5] & D. R. CAYAN[4]

1 *USGS, 4165 Spruance Rd., Suite 200, San Diego, California 92101, USA*
rthanson@usgs.gov
2 *USGS, 6000 J St, Placer Hall, Bldg 56, Sacramento California 95619A, USA*
3 *Dept Hydrology and Water Resources, University of Arizona, 1133 E James E. Rogers Way, Tucson, Arizona 85721, USA*
4 *USGS/SIO, 201 Nierenberg Hall, La Jolla, California 92093, USA*
5 *USGS, 520 North Park Avenue, Tucson, Arizona 85719, USA*

Abstract Competition for water resources is growing throughout California, particularly in the Central Valley where about 20% of all groundwater used in the United States of America is consumed for agriculture and urban water supply. Continued agricultural use coupled with urban growth and potential climate change would result in continued depletion of groundwater storage and associated land subsidence throughout the Central Valley. For 1962–2003, an estimated 1230 hectametres (hm^3) of water was withdrawn from fine-grained beds, resulting in more than three metres (m) of additional land subsidence locally. Linked physically-based, supply-constrained and demand-driven hydrological models were used to simulate future hydrological conditions under the A2 climate projection scenario that assumes continued "business as usual" greenhouse gas emissions. Results indicate an increased subsidence in the second half of the twenty-first century. Potential simulated land subsidence extends into urban areas and the eastern side of the valley where future surface-water deliveries may be depleted.

Key words groundwater; climate change; hydrological model; land subsidence

INTRODUCTION

Competition for water resources is growing throughout California (USA), particularly in the Central Valley, where about 20% of all groundwater used in the United States is consumed for agriculture and urban water supply (Faunt *et al.*, 2009). Groundwater pumpage from 1926–1970 resulted in as much as 8.5 m of land subsidence in the Los Banos-Kettleman City area of the San Joaquin Valley (Poland *et al.*, 1975). Between 1980 and 2003, the Central Valley's population nearly doubled to 3.8 million people; projections suggest continued urban growth of 1.2% (Johnson, 2009) to 4% (Faunt *et al*., 2009a–d) per year. Continued agricultural use coupled with urban growth can be expected to result in further depletion of groundwater storage throughout the Central Valley and associated land subsidence in susceptible areas. Climate change is expected to reduce the quantity of water available for surface-water deliveries and groundwater recharge, which will exacerbate the problem. Linked physically-based, supply-constrained and demand-driven hydrological models were used to simulate future hydrological conditions, including land subsidence. Of the historical water withdrawn, depletion of interbed storage was a significant source of water locally in the Tulare basin. Simulation of conjunctive use, its related effects, and potential alternative scenarios of water use can be quantified through a series of linked physically-based hydrological models; it can assess secondary effects such as land subsidence that are driven by the disparity between supply and demand. Linkage of these models to Global Climate Models (GCMs) allows for analysis of potential future conjunctive use.

SIMULATION OF SUBSIDENCE WITHIN A CONJUNCTIVE USE FRAMEWORK

The Central Valley Hydrologic Model (CVHM) (Faunt *et al*., 2009a–d) simulates subsidence within a conjunctive use framework using MODFLOW (Harbaugh, 2005) with the Farm Process

(FMP) (Schmid & Hanson, 2009) that includes the subsidence package (SUB) (Hoffman *et al*., 2003). The SUB package was additionally modified to explicitly track elastic and inelastic compaction (Hanson *et al*., 2009). Properties used for elastic and inelastic storage were based upon the estimates derived by Ireland *et al.* (1984) combined with critical head values that were derived from the calibration of the original Central Valley hydrological model (Williamson *et al*., 1989). The hydraulic properties, including subsidence properties, were distributed on the basis of a new and detailed textural model of the alluvial deposits within the Central Valley (Faunt *et al*., 2009e). This included explicitly simulating the major confining unit, known as the Corcoran Clay, using two separate model layers.

The subsidence is driven by the climate and supply-and-demand forcings of conjunctive use through the simulation of monthly agricultural demand that is estimated implicitly with FMP and is linked to the additional forcings from seasonal to interannual climate variability. These demands are combined with urban demands that collectively drive the groundwater withdrawals within the Central Valley. Unlike previous models of the Central Valley, the CVHM explicitly simulates multi-aquifer wellbore flow across the Corcoran Clay from municipal pumpage and from agricultural pumpage that is implicitly linked to irrigation demands estimated by FMP.

The supply and demand components are a combination of inflows and outflows simulated as the use and movement of water across the landscape, as well as from streamflow and groundwater flow. Flows on the landscape are based on historical crop and land-use attributes combined with monthly climate data (precipitation and potential evapotranspiration) for the period water years 1962–2003 for each 259 hectare model cell (Faunt *et al*., 2009b,c). Streamflow from 41 rivers and 66 agricultural diversions were simulated from reported inflows and diversions. Groundwater inflows as recharge and outflows owing to evapotranspiration, stream leakage, and pumpage are largely driven by the simulation of landscape processes by FMP and simulated streamflow.

Future hydrological conditions were simulated by linking the results of the GCM GFDL-A2 (Delworth *et al.*, 2006) to a regional water-balance model and CVHM. The GCM GFDL-A2 climate projection scenario represents continued "business as usual" greenhouse gas emissions. The GCM climate data was downscaled to simulate recharge and runoff from the surrounding Coast Ranges and Sierra Nevada mountains using the Basin Characteristics Model (BCM) (Flint & Flint, 2007), a regional water-balance model (Fig. 1). The BCM simulated from 25% to more than

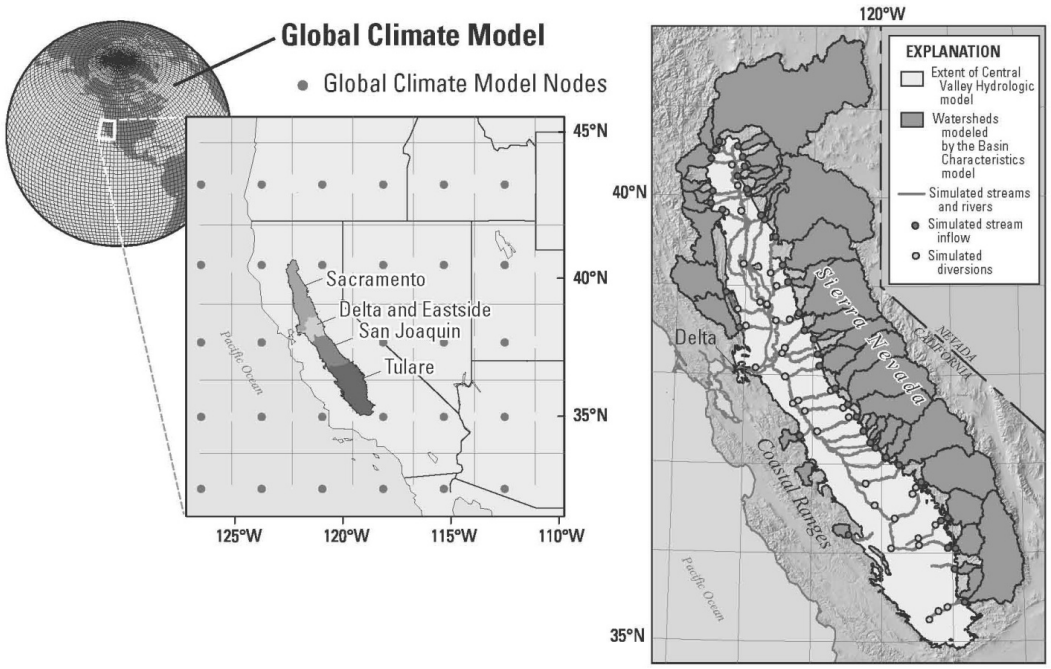

Fig. 1 Map showing linkage and downscaling from GCM to regional hydrological models of the Central Valley, California, USA.

60% reductions in runoff using the GCM future climate, which reduces the surface water available for diversions and results in increased groundwater pumpage. The CVHM uses the downscaled climate data (Fig. 1), runoff and recharge of the surrounding mountains as stream inflows simulated from the BCM, climate-driven diversions, and groundwater outflow at the Sacramento Delta controlled, in part, by GCM driven monthly sea-level changes of about 0.9 m. (Cayan *et al*., 2009). CVHM simulates a 30% increase in total farm delivery requirements as a result of increased ET from elevated minimum temperatures and reduced precipitation from climate change, which, in turn increases groundwater pumpage. This projection assumes no changes in land use and a 1.2% increase in urbanization through at least 2029 (Johnson, 2009) for urban groundwater demand.

SIMULATION OF SUBSIDENCE AND REGIONAL FLOW

During water years 1962–2003, agricultural water use in the Central Valley was supplied by surface-water deliveries and groundwater pumpage, with surface-water deliveries dominating during wet periods and groundwater pumpage dominating during dry periods (Fig. 2). Model simulations for 1962–2003 indicate that an additional 1230 hm^3 of water was withdrawn from fine-grained beds during this period, resulting in more than 3 m of additional land subsidence locally (Fig. 3). The projection of water use in the 21st century indicates a declining contribution of surface water and a potential increase in groundwater use in the second half of the century (Fig. 2). Model simulations indicate that as much as 70 800 hm^3 of water could be withdrawn from fine-grained beds from 2000–2099; this occurs predominantly during the second half of the 21st century, resulting in 5 m to more than 30 m of additional subsidence throughout the valley (Fig. 3). The severity and distribution of the simulated land subsidence is also affected by the assumed sustained increases in urban demand for water. Simulated groundwater storage depletion largely occurs in the Tulare Basin in the southern portion of the Central Valley, but is also present in the eastern parts of the San Joaquin Basin and the northern regions that include the Delta, east-side streams, and the Sacramento Valley. These areas were more reliant on surface-water deliveries and show the largest impact in transition to more groundwater pumpage. While the areas with historical subsidence sustain additional subsidence, the majority of the simulated future subsidence occurs along the Sierra Nevada on the eastern side of the valley (Fig. 3). The projected storage

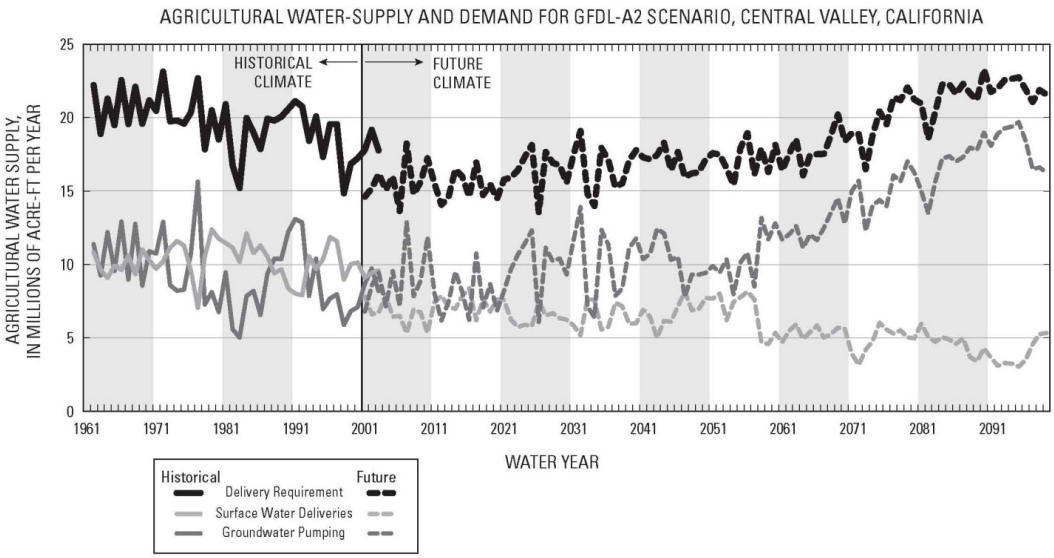

Fig. 2 Graphs showing the historical (1962–2003) and projected (2000–2099) water use for agriculture for the Central Valley (modified from Faunt *et al.*, 2009c).

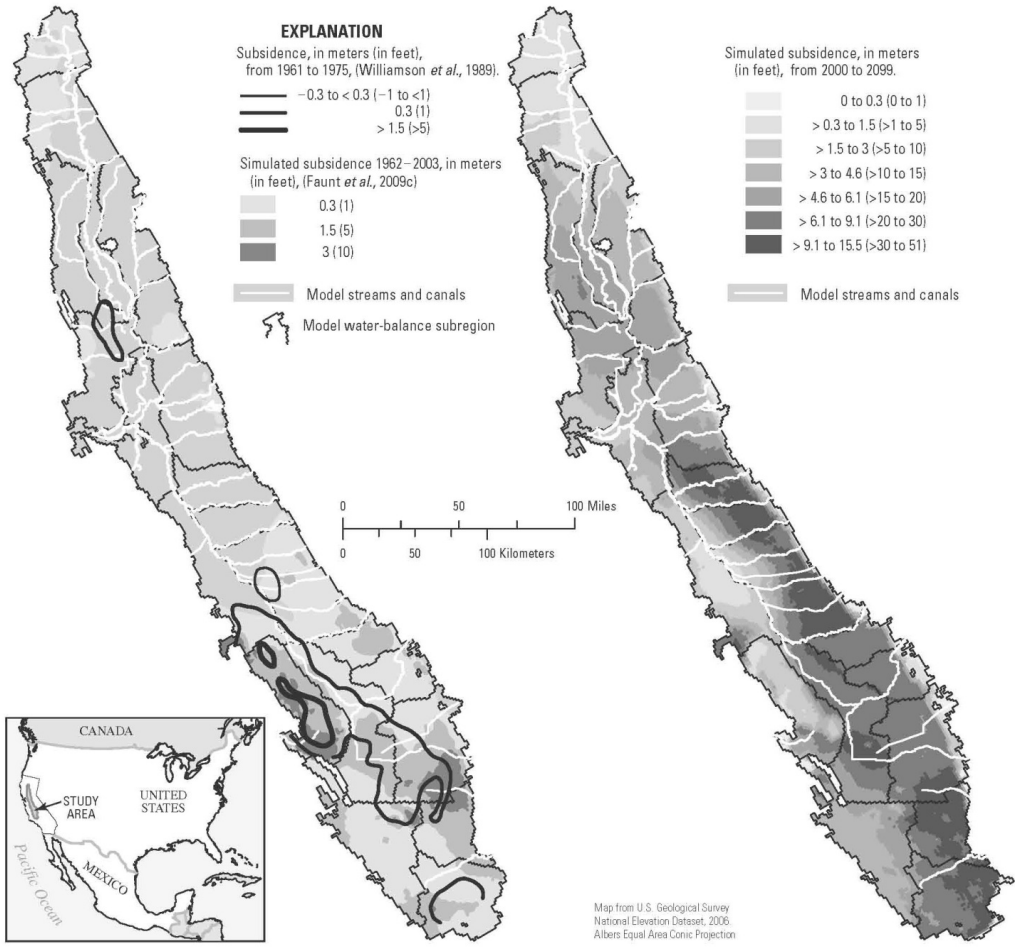

Fig. 3 Map showing the historical and projected future land subsidence for the Central Valley, California, USA.

depletion is accompanied by differential land subsidence that may affect local and regional canals, agricultural drainage, flood hazard zones, urban infrastructure, and conveyance through these canals (Fig. 3).

With projections of increased urban demand, the potential storage depletion and land subsidence may extend into urban areas. Greater urban demand for water may also contribute to reduced groundwater outflow and increased streamflow infiltration in the Delta outflow region to San Francisco Bay, which may further restrict water transfers and deliveries through the Delta.

CONCLUSIONS

Overall, the model results indicate that additional groundwater storage depletion may occur in the Central Valley under the A2 scenario, assuming 2003 agricultural demand and a 1.2% increase in urban water demand per year. The greatest amount of groundwater storage depletion is simulated to occur during intermittent droughts in the first half of the 21st century, followed by sustained drought in the second-half of the 21st century. During the droughts the models simulate a transition from surface-water to groundwater dominated irrigation supplies. Model simulations indicate that continued agricultural demand, increased urban-water demand, and climate change all impact conjunctive use and contribute to adverse effects on water sustainability in the Central Valley, including land subsidence and reduced outflow at the Delta. Increased land subsidence and

differential subsidence are simulated to occur throughout the Central Valley and especially in the Tulare Basin (southern Central Valley) and along the southeastern San Joaquin Valley where surface-water deliveries are depleted with decreased runoff from the southern Sierra Nevada. Because there are so many uncertainties in climate projections and the related hydrological assumptions of future conditions made in this projection, only the general trends may be considered reliable relative to the assumptions made.

Acknowledgements The authors would like to thank the USGS Climate Change program and the NOAA's RISA – California Application Program for funding this research.

REFERENCES

Cayan, D. R., M. Tyree, M., Dettinger, M. D., Hidalgo, H. & Das, T. (2009) California climate change scenarios and sea level rise estimates. California 2008 Climate Change Scenarios Assessment.

Delworth, T. L., *et al.* (2006) GFDL's CM2 global coupled climate models – Part 1: formulation and simulation characteristics. *J. Climate* **19**(5), 643–674.

Faunt, C. C., Hanson, R. T. & Belitz, K. (2009a,b) Introduction and conceptual model of the Central Valley, California: *US Geol. Survey Professional Paper 1766, Chapters A,B*. In: *Ground-Water Availability of California's Central Valley* (ed. by Claudia Faunt), 1–120.

Faunt, C. C., Hanson R. T., Schmid, W., Belitz, K. & Predmore, S. (2009c) Documentation of the ground-water flow model. *US Geol. Survey Professional Paper 1766, Chapter C*. In: *Ground-Water Availability of California's Central Valley* (ed. by Claudia Faunt) 121–212.

Faunt, C. C., Hanson, R. T., Belitz, K. & Rogers, L. (2009d) California's Central Valley Groundwater Study: A Powerful New Tool to Assess Water Resources in California's Central Valley. *US Geol. Survey Fact Sheet 2009-3057*.

Faunt, C. C., Belitz, K., & Hanson, R. T. (2009e) Texture model of the valley fill deposits of the Central Valley, California. *Hydrogeol. J*., doi:10.1007/s10040-009-0539-7.

Flint, A. L., & Flint, L. E. (2007) Application of the basin characterization model to estimate in-place recharge and runoff potential in the Basin and Range carbonate-rock aquifer system, White Pine County, Nevada, and adjacent areas in Nevada and Utah. *US Geol. Survey Scientific Investigations Report 2007-5099*.

Hanson, R. T., Leake, S. A. & Schmid, W. (2009) Appendix B, Summary of other enhancements to MODFLOW-2005. In: The Farm Process Version 2 (FMP2) for MODFLOW-2005 – Modifications and Upgrades to FMP1 (by W. Schmid & R. T. Hanson). *US Geol. Survey Techniques and Methods 6–A32*, 93–101.

Harbaugh, A. W. (2005) MODFLOW-2005, the U.S. Geological Survey modular ground-water model—the Ground-Water Flow Process. *US Geol. Survey Techniques and Methods 6–A16*.

Hoffmann, J., Leake, S. A., Galloway, D. L. & Wilson, A. M. (2003) MODFLOW-2000 ground-water model—User guide to the subsidence and aquifer-system compaction (SUB) package. *US Geol. Survey Open-File Report 03–233*.

Ireland R. L., Poland, J. F. & Riley, F. S. (1984) Land Subsidence in the San Joaquin Valley, California, as of 1980. *US Geol. Survey Professional Paper 437–I*.

Johnson, H. (2009) California population: planning for a better future. Public Policy Institute of California. (http://www.ppic.org/main/publication.asp?i=900).

Poland J. F., Lofgren, B. E., Ireland, R. L. & Pugh, A. G. (1975) Land subsidence in the San Joaquin Valley, California, as of 1972. *US Geol. Survey Professional Paper 437-H*.

Schmid, W. & Hanson R. T. (2009) The Farm Process Version 2 (FMP2) for MODFLOW-2005 – Modifications and Upgrades to FMP1. *US Geol. Survey Techniques and Methods 6–A32*.

Williamson, A. K., Prudic, D. E. & Swain, L. A. (1989) Ground-water flow in the Central Valley, California. *US Geol. Survey Professional Paper 1401–D*.

(Proceedings of EISOLS 2010, Queretaro, Mexico, 17–22 October 2010). IAHS Publ. 339, 2010.

1-D infiltration, analysis of unsaturated flow and increase in land subsidence

S. A. MASOUDZADE, M. M. TOUFIGH, H. YAZDANI & R. RAHGOZAR
Civil Engineering Department, University of Kerman, 22 Bahman Blvd, PO Box 133, 76175 Kerman, Iran
omid.masoudzade@gmail.com

Abstract Artificial groundwater recharge has several applications, including preventing the subsidence that takes place due to pumping. The investigations show that whenever the average of recharge in a year is more than pumping, we do not have any lowering of the groundwater level. But if recharge is less than the pumping and if the characteristics of the soil are suitable, land subsidence can occur. Investigations in the central regions of Kerman, a city in southern Iran, show that although we observe the groundwater level is rising, we unexpectedly have settlement. Ordinarily, the rise of groundwater level will increase the pore water pressure and decrease the effective stress, so subsidence will not occur. A possible explanation for the subsidence that occurs when groundwater levels are rising is the seepage forces generated by downward flowing water in the unsaturated zone. As we demonstrate, the vertical movement of water and the infiltration of water through unsaturated soil imparts forces to the soil, and when the flow direction is downward, the forces should add to effective stresses. Inclusion of unsaturated zone processes makes the problem more complicated, and taking them into account involves a coupled problem that is not amenable to analytical solutions. In this paper, with some simplifications, we show that the coupled problem should be considered in evaluating the effect of recharge on subsidence and that for artificial recharge, the rate of recharge should be considered. The resulting effective stresses can sometimes be greater than expected.

Key words unsaturated flow; effective stress; infiltration; groundwater level

INTRODUCTION

Land subsidence is settling of the surface of the ground because of deformations in the subsurface layers. This phenomenon is one of the several kinds of settlement that may occur and cause subsidence.

Investigations in the central regions of Kerman, a city in southern Iran, show that although we observe the groundwater level is rising, we unexpectedly have settlement. Most studies on soils suggest that the rise of groundwater level will increase the pore water pressure and, as a result, there will be a decrease in effective stress. So, subsidence should not occur.

The problem may occur for various reasons but the one we mention in this paper is the seepage forces caused by water flowing in a downward direction through the surface or wells. As we will show, the vertical movement of water inserts forces to the soil when it moves and when the direction is downward the forces increase the effective stresses.

As shown in Fig. 1, the soil in Region 1 becomes saturated due to water infiltrated through the soil. But it does not reach the groundwater and so Region 2 becomes saturated too and also

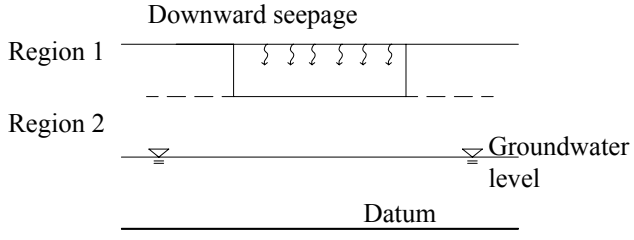

Fig. 1 Schematic of infiltration through unsaturated soil.

Copyright © 2010 IAHS Press

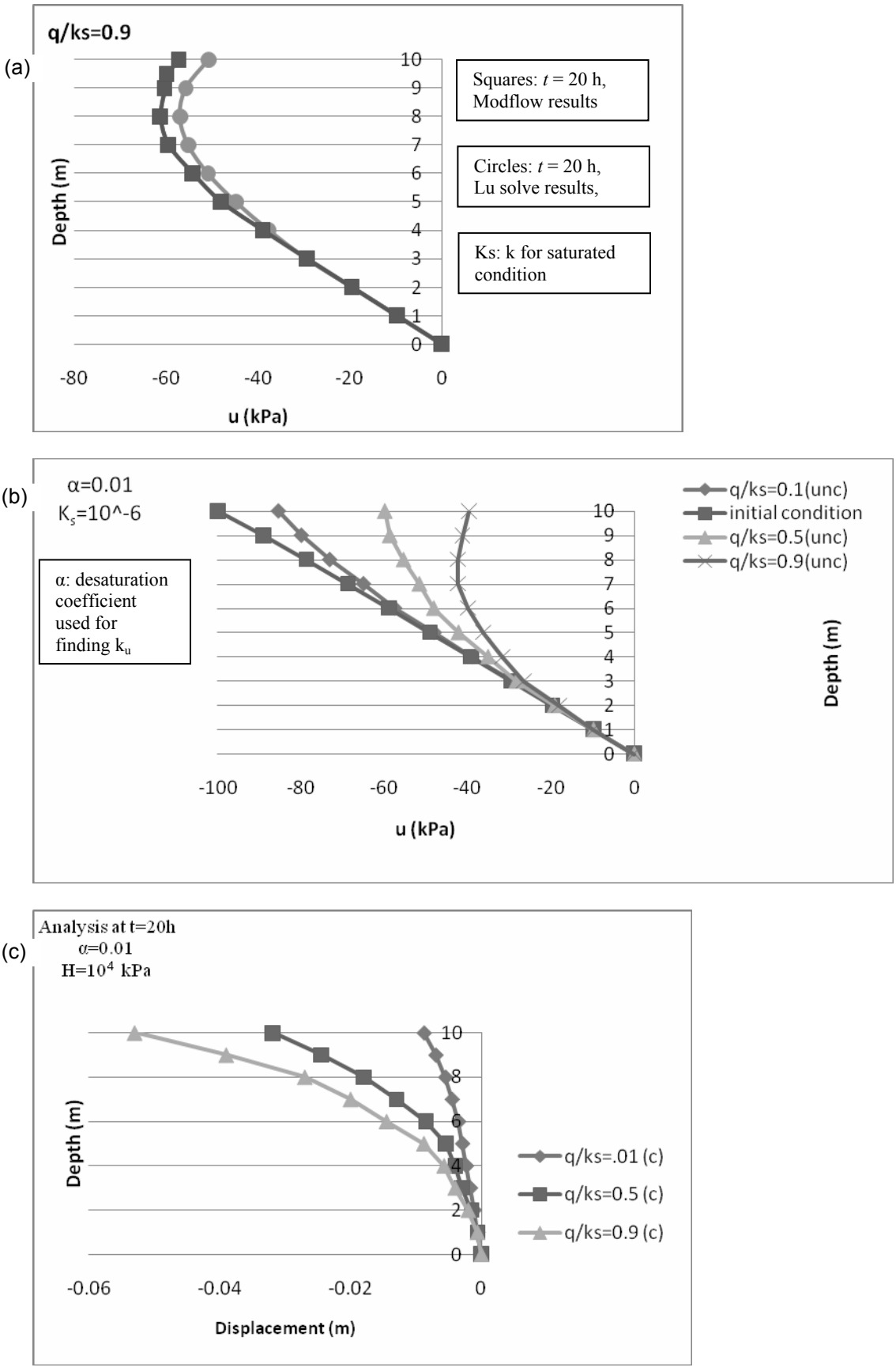

Fig. 2 The series (a), (b) and (c) demonstrates the results of different analytical models for change in pore pressure with increasing in flow rate.

causes a rise in groundwater level. So we observe that before reaching the groundwater and groundwater level rise, the injection of water creates forces when it gets into the soil and the type of infiltration is unsaturated flow.

In this paper we analyse the unsaturated flow to explain the theory and obtain the stresses in the unsaturated zone and show the relation between stresses and deformation.

THE FLOW THEORY TO OBTAIN SUCTION PROFILE

Based on Darcy's law, the Gardner model for hydraulic conductivity and flow rules, we can find the hydraulic gradient changes for the flow:

$$\frac{\partial}{\partial z}\left(k(u)\frac{\partial}{\partial z}\left(\frac{u_w}{\gamma_w}+z\right)\right)=\left(e\frac{\partial S_w}{\partial u}+S_w\eta\frac{(1+\mu)}{H(1-\mu)}\right)\frac{\partial u}{\partial t} \tag{1}$$

where k is the hydraulic conductivity for saturated soil, u is pore pressure, S_w is the degree of saturation, $\eta = (1 - n)^2/(1 - n_0)$, n is the porosity, e is the void ratio, and H is the elastic modulus of the soil.

MODEL AND FIGURES

some provided analytical solve for equation, with which we can solve for the stresses caused by changing the hydraulic gradients between two points, and consequently we have settlement in land. And we also used a model with the software MODFLOW for downward infiltration. The results were similar. In both of them with increasing flow rate, we had a change in pore pressure, as shown in Fig. 2(a), (b) and (c):

CONCLUSIONS

As shown in Fig. 2, changes in pore pressures can cause settlement. These changes are because of infiltration that inserts forces through downward flows. If the flow rate is much greater than the hydraulic conductivity, we will have much bigger settlement. Some other parameters have effects on the result, α and H, which show the properties of the soil. We also compare the results of MODFLOW with an analytical solution. They were similar. In these cases, we can say that if we have downward flows, because of the forces these exert on the soil, subsidence may occur, although the level of groundwater is rising.

REFERENCES

Fredlund, D. G. & Rahardjo, H. (1993) *Soil Mechanics for Unsaturated Soil*, 152–158. John Wiley & Sons, New York, USA.

Masoudzade, S. A. & Toufigh, M. M. (2010) 1-D infiltration and influence on the effective stress calculation. Proceedings of 17th IAHR Congress, APD2010, Auckland University, New Zealand.

Ouria, A. (2004) Modeling the surface settlement with groundwater level fluctuation with finite element methods. Ms Thesis, Bahonar University of Kerman, Kerman, Iran.

Wu, L. Z. & Zhang, L. M.(1998) Analytical solution to 1D coupled water infiltration and deformation in unsaturated soils. *Int. J. Numerical & Analytical Methods in Geomechanics*, doi: 10.1002/nag.742.

(Proceedings of EISOLS 2010, Queretaro, Mexico, 17–22 October 2010). IAHS Publ. 339, 2010.

A theory of three-dimensional land motion in terms of its velocity field

J. LI & D. C. HELM
Dept of Civil Engineering, Morgan State University, 5200 Perring Parkway, Baltimore, Maryland 21251, USA
jiang.li@morgan.edu

Abstract The present paper develops a new theory for the velocity field of land movement that may be driven by various forces, including hydraulic, seismic and gravitational forces caused, respectively, by depressurizing aquifers, earthquakes, and loading the overburden perhaps by accumulation of sedimentary deposits or by adding man-made structures. The new theory is derived from the first principles of physics (conservation of mass and linear momentum), secondary laws of physics (the viscous and drag force relation for relative flow, the constitutive law of poroelasticity and an equation of state of constituent materials), and two relations of bulk flux. Similar to Biot's theory, the new theory can model three-dimensional deformation of saturated sedimentary material, including both volume and shear deformation. However, unlike Biot's theory, the new model expresses itself entirely in terms of the velocity field of the skeletal frame and does not require as part of its solution scheme the coupling of motion with another physical field, such as pore-water pressure (or hydraulic head).

Key words land movement; displacement field; velocity field; land subsidence; groundwater; aquifer

INTRODUCTION

Land movement is a common occurrence worldwide. It includes vertical and horizontal components (e.g. land subsidence and earth fissures) caused by hydraulic forces (Helm, 1994a) associated with the withdrawal of ground fluids (water, oil or gas) and with other types of forces (e.g. seismic forces from earthquakes or imposed gravitational forces such as the added weight of new structures or buildings). Traditional analyses of the movement of aquifer systems in response to pumping groundwater have been based largely on Biot's three-dimensional consolidation model (Biot, 1941). Biot's theory requires coupling two physical fields: the field of excess pore-water pressure (or hydraulic head) and the displacement field of the skeletal frame of an aquifer of interest. Because such a requirement results in significant complexity of analysis, modelling and computation, previous investigators have tried to simplify Biot's theory by introducing various completely uncoupled or semi-decoupled computational schemes (Lewis & Schrefler, 1978; Lewis *et al.*, 1991; Gambolati *et al.*, 1992; Gambolati, 2000). Consequently, the accuracy of the final results is compromised. In contrast, the present investigation focuses on developing a new theory that is expressed in terms of the aquifer velocity field, while remaining faithful to the physical laws invoked by Biot. The new theory is completely coupled during its derivation phase. Hence, there is no longer a need to couple one physical field to another physical field during the solution phase in order to model accurately the land movement impelled by hydraulic or other forces (gravitational or seismic). To derive such a theory, the following fundamental principles and laws of physics are introduced.

FUNDAMENTAL PRINCIPLES AND LAWS

In the present investigation, the following laws and principals are presented. When combined, they establish the governing equation for the three-dimensional movement of saturated sediments:

Principle of effective stress (Terzaghi, 1925):

$$\boldsymbol{\sigma} = \boldsymbol{\sigma}' + \boldsymbol{I}p \tag{1}$$

Copyright © 2010 IAHS Press

where the second-order tensors $\boldsymbol{\sigma}$ and $\boldsymbol{\sigma}'$ are, respectively, the total and effective stresses on the sediment's skeletal framework; p is pore-water pressure; $\boldsymbol{I}$ is a 3 × 3 identity (or unit) matrix. The total stress is composed of spherical (volume) and deviatoric (shear) components, i.e. $\boldsymbol{\sigma} = \boldsymbol{I}\mathrm{tr}\boldsymbol{\sigma}/3 + \boldsymbol{\sigma}_D$ where $\mathrm{tr}\boldsymbol{\sigma}/3$ (or σ_v) and $\boldsymbol{\sigma}_D$ denote the total volume and shear stress, respectively, and tr stands for the trace of a stress tensor and the subscript D denotes the deviatoric (or shear) component. This is similarly for effective stress, $\boldsymbol{\sigma}' = \boldsymbol{I}\mathrm{tr}\boldsymbol{\sigma}'/3 + \boldsymbol{\sigma}_D'$.

Constitutive law of poroelasticity (Biot, 1941):

$$\boldsymbol{\sigma}' = \boldsymbol{E} : \boldsymbol{\varepsilon} \tag{2}$$

where $\boldsymbol{\varepsilon}$ is the strain on the porous structure of the sediment's skeletal frame, a second-order tensor that is composed of volume and shear strain tensors (i.e. $\mathrm{tr}\boldsymbol{\varepsilon}$ and $\boldsymbol{\varepsilon}_D$); $\boldsymbol{E}$ is the poroelastic modulus of elasticity for the porous structure, a fourth-order tensor that is assumed to be isotropic within an elemental volume; the mathematical operator ":" stands for a double-dot product between $\boldsymbol{E}$ and $\boldsymbol{\varepsilon}$, which results in a second-order stress tensor. Similarly, constitutive relation, equation (2) is composed of two physical relations. One is the bulk stress-strain relation: $\mathrm{tr}\boldsymbol{\sigma}'/3 = (\lambda + 2\mu/3)\mathrm{tr}\boldsymbol{\varepsilon}$, and the other is the shear stress-strain relation: $\boldsymbol{\sigma}_D' = 2\mu\boldsymbol{\varepsilon}_D$, where λ and μ are elastic constants. In fact, the parameters $(\lambda + 2\mu/3)$ and μ are the bulk and shear moduli of three-dimensional poro-elasticity, respectively.

Conservation of linear momentum (Malvern, 1969):

$$\nabla \cdot \boldsymbol{\sigma} + \rho_b \boldsymbol{b} = \rho_b \boldsymbol{a}_b \tag{3}$$

where the vector $\boldsymbol{b}$ denotes the body force; the differential operator ∇ is a vector and is defined by $\nabla \equiv \{\partial/\partial x, \partial/\partial y, \partial/\partial z\}$ in a Cartesian coordinate system, where "≡" stands for equals by definition; the operator "·" indicates the single-dot product between the vector ∇ and the tensor $\boldsymbol{\sigma}$; ρ_b is the average bulk density defined by $\rho_b \equiv (V_w\rho_w + V_s\rho_s)/V_b$, where ρ_w and ρ_s are the average densities of pore water and individual solid grains, respectively, within a carefully defined volume element V_b composed of two sub-volumes, V_w and V_s, respectively occupied by water and solids for saturated sediments; $\boldsymbol{a}_b$ is the average bulk acceleration defined by $\boldsymbol{a}_b \equiv (m_w\boldsymbol{a}_w + m_s\boldsymbol{a}_s)/m_b$, where the vectors $\boldsymbol{a}_w$ and $\boldsymbol{a}_s$ are the average accelerations of pore fluid and solid grains, respectively, within the V_b, m_b ($\equiv m_w + m_s$) is the bulk mass where m_w and m_s denote the total mass of the two constituent materials (water and solids, respectively) within the V_b. The terms $\rho_b\boldsymbol{b}$ and $\rho_b\boldsymbol{a}_b$ in equation (3) represent the bulk body force and the bulk inertial force per unit bulk volume contributed by the sum of both constituent materials (water and solid within the V_b); the subscripts, b, w and s represent bulk, water and solid phases, respectively. Note that in this paper the terms porous structure and the skeletal frame are used interchangeably.

General relation between the drag and driving forces (Li & Helm, 1998):

$$\boldsymbol{q} + \boldsymbol{f}(\boldsymbol{a}_r) = -\boldsymbol{K} \cdot \nabla h_t \tag{4}$$

in which the specific discharge $\boldsymbol{q}$ is defined by $\boldsymbol{q} \equiv n(\boldsymbol{v}_w - \boldsymbol{v}_s)$, where n is the porosity and $\boldsymbol{v}_w$ and $\boldsymbol{v}_s$ are the average velocities of pore water and solid grains within a specified V_b, respectively; $\boldsymbol{f}(\boldsymbol{a}_r)$ is a function of the relative acceleration, $\boldsymbol{a}_r$ ($\equiv \boldsymbol{a}_w - \boldsymbol{a}_s$) which is the acceleration of water relative to that of the skeletal frame; $\boldsymbol{K}$ is the hydraulic conductivity of water flowing relative to the skeletal frame, a second-order tensor; the term $\boldsymbol{K}\cdot\nabla$ on the right-hand side stands for the single-dot product of $\boldsymbol{K}$ and ∇; ∇h_t ($\nabla h + \boldsymbol{a}_w/g$) is defined by Li & Helm (1998), where h_t and h are the total and hydraulic head, respectively, and are given by equation (5).

The left-hand side of equation (4) is related to the viscous drag force. This force is associated with the relative velocity and acceleration (i.e. $\boldsymbol{v}_r$ and $\boldsymbol{a}_r$). In contrast, the right-hand side of (4) represents the driving force inside a gravitational field. The term $\boldsymbol{f}(\boldsymbol{a}_r)$ in (4) can be dropped if this

term is negligibly small when compared to specific discharge $\boldsymbol{q}$ ($\equiv n\boldsymbol{v}_r$), which is a function of the relative velocity, $\boldsymbol{v}_r$. For this special case, equation (4) reduces to $\boldsymbol{q} = -\boldsymbol{K}\cdot(\nabla h + \boldsymbol{a}_w/g)$. This formulation is adopted in the present paper and is used to derive the final governing equation. This relation requires neither $\boldsymbol{a}_w$ nor $\boldsymbol{a}_s$ individually to be negligibly small so long as their acceleration relative to one another is sufficiently small compared to their relative speed. If the term $\boldsymbol{a}_w/g$ is also assumed to be negligibly small when compared to the first term ∇h, (4) simplifies to the Darcy-Gersevanov law: $\boldsymbol{q} = -\boldsymbol{K}\cdot\nabla h$ that can be further reduced to geohydrologists' standard use of Darcy's law: $n\boldsymbol{v}_w = -\boldsymbol{K}\cdot\nabla h$ for the special case $\boldsymbol{q} = n\boldsymbol{v}_w$ when $\boldsymbol{v}_s$ itself becomes negligible. The relation of drag and driving forces (4) is accordingly a generalization of the Darcy-Gersevanov law (Gersevanov, 1934; DeWiest, 1965). The total head or potential h_t is defined in the next section.

Potential function (Li & Helm, 1998):

$$h_t = \int_{p_0}^{p} \frac{dp}{g\rho_w(p)} + \int_{z_0}^{z} d\xi + \frac{\dot{\Phi}}{g} = h + \frac{\dot{\Phi}}{g} \tag{5}$$

where p_0 is the value of pore-water pressure on an unstrained system (hydrostatic); g is the gravitational acceleration; ξ is an integral dummy variable; the hydraulic head, h, is defined as $h = \int_{p_0}^{p} dp / g\rho_w + \int_{z_0}^{z} d\xi$ (Hubbert, 1969; Verruijt, 1969); Φ is the velocity potential of the pore-water continuum; the upper and lower integral limits in the second term on the right-hand side of (5), z and z_0, are elevations of the point interest P and a specified fixed datum, respectively.

Mass conservation (Helm, 1987):

$$\nabla\cdot\boldsymbol{q}_b = -[\frac{n}{\rho_w}(\frac{\partial\rho_w}{\partial t} + \boldsymbol{v}_w\cdot\nabla\rho_w) + \frac{(1-n)}{\rho_s}(\frac{\partial\rho_s}{\partial t} + \boldsymbol{v}_s\cdot\nabla\rho_s)] \tag{6}$$

where the operator $\partial/\partial t$, as mentioned earlier, denotes the local or partial derivative with respect to time, and $\boldsymbol{q}_b$ is the volume bulk velocity that is defined and discussed in the next section. It is important to point out that equation (6) does not include any sinks or sources of mass that may occur within an arbitrarily selected bulk volume V_b of interest. Sinks and sources are discussed in the following section.

Volume and mass bulk velocities:

$$\boldsymbol{q}_b \equiv \left(V_w / V_b\right)\boldsymbol{v}_w + \left(V_s / V_b\right)\boldsymbol{v}_s \tag{7}$$

where $\boldsymbol{q}_b$, the volume bulk velocity as mentioned earlier, is a resultant of the constituent velocities that are weighted by the ratio of the constituent volume to the bulk volume. For computational convenience, the volume bulk velocity of (7) can be expressed by either of two alternative forms, $\boldsymbol{q}_b = n\boldsymbol{v}_w + (1-n)\boldsymbol{v}_s$ or $\boldsymbol{q}_b = \boldsymbol{v}_s + \boldsymbol{q}$ (Helm, 1987) where specific discharge $\boldsymbol{q}$ is defined as after equation (4). V_b ($\equiv V_w + V_s$) is the bulk volume of saturated sedimentary materials, where V_w and V_s are the volumes of water and solid, respectively.

DERIVATION OF THE GOVERNING EQUATION

The governing equation for aquifer movement in terms of the displacement field of the skeletal frame, $\boldsymbol{u} \equiv \int_0^t \boldsymbol{v}_s \mathrm{d}t$, can be developed by taking the following three steps. First, invoke the principle of effective stress in equation (1), the constitutive law of poroelasticity in (2) and the conservation of linear momentum in (3). This gives a general form of the Navier equation in terms of the displacement field (Malvern, 1969):

$$(\lambda+\mu)\nabla(\nabla\cdot\boldsymbol{u})+\mu\nabla^2\boldsymbol{u}+\nabla\cdot\boldsymbol{I}p+\rho_b\boldsymbol{b}=\rho_b\boldsymbol{a}_b \tag{8}$$

where $\boldsymbol{u}$ is the displacement of the skeletal frame. In (8), the terms of pore water pressure and body force (i.e. the last two terms on the left–hand side) are included. Second, substituting the relation between drag and driving force in (4) with a negligibly small value for $\boldsymbol{f}(\boldsymbol{a}_r)$ into the definition of the bulk volume flux $\boldsymbol{q}_b$ (= $\boldsymbol{v}_s + \boldsymbol{q}$) in (7) while recalling the Hubbert potential function in (5) gives:

$$\boldsymbol{q}_b=\frac{\partial\boldsymbol{u}}{\partial t}-\boldsymbol{K}\cdot\left(\frac{\nabla p}{\gamma_w}+\frac{\boldsymbol{a}_w}{g}+\boldsymbol{k}\right) \tag{9}$$

in which γ_w ($\equiv g\boldsymbol{\rho}_w$) is the unit weight of water; $\boldsymbol{k}$ is a unit vector in the vertical direction and the relation $\nabla\dot{\Phi}=\boldsymbol{a}_w/g$ is applied. The hydraulic conductivity, $\boldsymbol{K}$ reduces to that for pore-water flow in the principal direction. As mentioned above, the term $\boldsymbol{f}(\boldsymbol{a}_r)$ in (4) can be dropped when its value is negligibly small compared to $\boldsymbol{q}$.

Finally, combining equations (8) and (9) by eliminating the term ∇p leads to the following governing equation for the aquifer displacement field:

$$\frac{\partial\boldsymbol{u}}{\partial t}+\frac{1}{\gamma_w}\boldsymbol{K}\cdot[(\lambda+\mu)\nabla(\nabla\cdot\boldsymbol{u})+\mu\nabla^2\boldsymbol{u}]=\boldsymbol{R} \tag{10}$$

where the vector $\boldsymbol{R}$ equals:

$$\boldsymbol{R}=\boldsymbol{q}_b-\left(\frac{\rho_b}{\rho_w}-1\right)\boldsymbol{K}\cdot\boldsymbol{k}+\frac{\boldsymbol{K}}{g}\cdot\left(\frac{\rho_b}{\rho_w}\boldsymbol{a}_s+\boldsymbol{a}_w\right) \tag{11}$$

It should be noted that assuming $\boldsymbol{a}_r \approx 0$ and applying this assumption to drag-driving force relation (4) require that the bulk inertial term $\boldsymbol{\rho}_b\boldsymbol{a}_b$ in (3) reduces to $\boldsymbol{\rho}_b\boldsymbol{a}_b \approx \boldsymbol{\rho}_b\boldsymbol{a}_s$. This approximation is included in the third term of equation (11).

Taking the derivative of (10) with respect to time leads to a governing equation in terms of the velocity field of saturated sedimentary material:

$$\frac{\partial\boldsymbol{v}}{\partial t}+\frac{1}{\gamma_w}\boldsymbol{K}\cdot[(\lambda+\mu)\nabla(\nabla\cdot\boldsymbol{v})+\mu\nabla^2\boldsymbol{v}]=\dot{\boldsymbol{R}} \tag{12}$$

where $\boldsymbol{v}$ ($\equiv \boldsymbol{v}_s \equiv \dot{\boldsymbol{u}}$) denotes the velocity field of the skeletal frame and $\dot{\boldsymbol{R}}$ denotes the time derivative of the vector $\boldsymbol{R}$ in (11). The latter is given by:

$$\dot{\boldsymbol{R}}=\dot{\boldsymbol{q}}_b+\dot{n}(G-1)\boldsymbol{K}\cdot\boldsymbol{k} \tag{13}$$

where G ($\equiv\boldsymbol{\rho}_s/\boldsymbol{\rho}_w$) is the specific gravity of solid particles and the dot product of $\boldsymbol{K}\cdot\boldsymbol{k}$ gives K_z, the vertical component of $\boldsymbol{K}$. The porosity relation of $\boldsymbol{\rho}_b/\boldsymbol{\rho}_w$ [= $n + (1 - n)G$] in (11) is used to reach the second term in (13). It should be mentioned that after applying the derivative with respect to time to (11), the last two terms related to accelerations are ignored in (13) as any change in inertial force with respect to time are assumed to be negligibly small when compared to the terms that remain in (12) and (13). Other assumptions are also contained in (12), namely, that the parameters hydraulic conductivity, elastic constants and water density do not change significantly with time.

If the right-hand side vector $\dot{\boldsymbol{R}}$ can be determined, the velocity field becomes solvable and equation (12) emerges as a powerful governing equation. Transient and dynamic volumetric and shear deformations of an aquifer system can be modelled in three dimensions. Unlike Biot's theory, there is no requirement for equation (12) to be coupled with other physical fields such as pore-water pressure or hydraulic head within the solution scheme. The next section discusses and evaluates the terms included in the vector $\dot{\boldsymbol{R}}$.

DISCUSSION OF THE VECTOR $\dot{\boldsymbol{R}}$

Without a known $\dot{\boldsymbol{R}}$, equation (12) stays unsolvable because it represents three equations with a

total of six unknowns, namely, three components for each vector, $\boldsymbol{v}$ and $\dot{\boldsymbol{R}}$. Thus, it is necessary to reduce the number of unknowns by independently evaluating the two terms $\dot{\boldsymbol{q}}_b$ and $\dot{n}$ in (13).

Evaluation of the term $\dot{\boldsymbol{q}}_b$

Assuming the incompressibility condition for each constituent (water and individual solids where ρ_w = constant and ρ_s = constant) as Biot has done and applying Gauss' divergence theorem to (6) yields:

$$\oint_{A_b} \boldsymbol{q}_b \cdot d\boldsymbol{A} = \int_{V_b} \nabla \cdot \boldsymbol{q}_b dV = 0 \tag{14}$$

where $\boldsymbol{A}_b$ is the bounding surface of an arbitrary bulk volume V_b whose interior is devoid of sinks or sources. When interior sinks or sources, or both, occur within $\boldsymbol{A}_b$, a more general form of (14) for any mixture of incompressible constituents can be expressed by:

$$\oint_{A_b} \boldsymbol{q}_b \cdot d\boldsymbol{A} = Q \tag{15}$$

where Q is the cumulative (or net) volume rate of production at a specified time t within the closed surface $\boldsymbol{A}_b$ of interest. Equation (15) states that the volume rate of incompressible material that crosses orthogonally an arbitrarily specified closed surface $\boldsymbol{A}_b$ equals the net volume rate of incompressible material that is being withdrawn through the various interior sinks and being added through the various interior sources that all lie within A_b. The bounding surface A_b can be specified at a convenient scale in order to solve either equation (14) or (15) based on a real world problem. Zone ABC in Fig. 1(a), for instance, represents a saturated idealization of an $\boldsymbol{A}_b$ that is specified at a regional scale such that the base of the V_b of interest rests on rigid and impermeable basement rock and the sides are truncated by rigid impermeable bedrock. In Zone ABC (i.e. subsiding saturated material near the land surface (AB) and impermeable bedrock), V_b includes n wells (for illustration, here we let n = 3) so that the cumulative rate of production from discharge and/or recharge wells is $Q = \sum_{i=1}^{n} \pm Q_i$ where $\pm Q_i$ (i = 1, 2,… n) is the individual well flow rate, which is positive for recharge (a source) and negative for discharge (a sink).

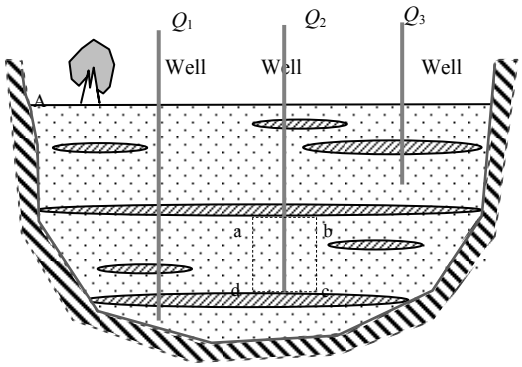

Fig. 1 (a) A subsiding sedimentary basin at a regional scale (zone ABC).

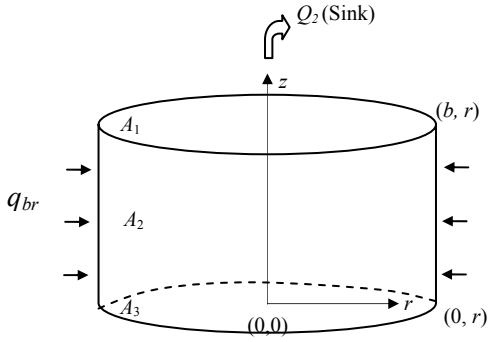

Fig. 1 (b) Radial bulk flux toward a sink at the scale of a single aquifer (zone abcd in Fig. 1(a)) with axial symmetry.

In contrast, the closed surface $\boldsymbol{A}_b$ in Fig. 1(b) illustrates a pumping event at a smaller scale. It corresponds roughly to Zone abcd in Fig. 1(a). It has a cylindrical shape within a single aquifer. This bounding surface is composed of three sub-areas ($\boldsymbol{A}_b = \sum_{i=1}^{3} \boldsymbol{A}_i$) as marked in Fig. 1(b). In this case, Well 2 of Fig. 1(a) is expressed as a sink, namely, $Q = Q_2$. If an average value of the orthogonal component of $\boldsymbol{q}_b$ in (15) is taken over $\mathbf{A}_b$, (15) becomes $\langle q_b \rangle = Q/\boldsymbol{A}_b$, namely $\langle q_b \rangle$ =

$(\iint_{A_b} \boldsymbol{q}_b \cdot d\boldsymbol{A}) / A_b$ where the symbol < > denotes an average value. When $\boldsymbol{A}_b$ is selected to be fixed in space (and hence is constant with respect to time), the derivative of the average bulk velocity with respect to time equals zero (i.e. $<\dot{q}_b> = 0$) if the well flow rate Q is constant.

For the special case of impermeable and rigid surfaces along $\boldsymbol{A}_1$ and $\boldsymbol{A}_3$ in Fig. 1(b) (Theis' (1935) condition) one-dimensional radial bulk flow occurs within the $\boldsymbol{A}_b$ of Fig. 1(b) (Helm, 1994b). The following relation can be found from (15):

$$\iint_{A_b} \boldsymbol{q}_b \cdot d\boldsymbol{A} = 0 - \int_{A_1} q_{br} dA + 0 = -2\pi br < q_{br} >= -Q_2 \tag{16}$$

which further leads to $<q_{br}> = Q_2/2\pi br$ where b is the thickness of the aquifer and $<q_{br}>$ is the average radial bulk flow. The conclusion $\dot{q}_{br} = 0$ can be drawn for a constant discharge or recharge rate Q_2. Similar discussion regarding (15) was given by Li (2007a,b) when the same relation $<q_{br}> = Q_2/2\pi br$ was found by applying $\boldsymbol{v}_b$ to mass balance within a confined aquifer without leakance through a fixed overlying surface $\boldsymbol{A}_1$.

Instead of using integral form (14) one can also find the same one-dimensional radial bulk flow solution $q_{br} = Q_2/2\pi br$ from the differential form (6) when similarly assuming the incompressibility condition for constituent material. In a cylindrical coordinate system, (6) becomes:

$$\nabla \cdot \boldsymbol{q}_b = \frac{\partial q_{br}}{\partial r} + \frac{\partial q_{b\theta}}{\partial \theta} + \frac{\partial q_{bz}}{\partial z} = \frac{\partial q_{br}}{\partial r} + \frac{q_{br}}{r} + 0 = 0 \tag{17}$$

where axially symmetric lateral bulk flux $\partial q_{b\theta} / \partial \theta = q_{br} / r$ is assumed along with the special case of a negligibly small vertical gradient of vertical bulk flow (i.e. $\partial q_{bz} / \partial z = 0$). This special case can be called a "Theis-like case" because of its differential equivalence to Theis' classic boundary condition long surfaces $\boldsymbol{A}_1$ and $\boldsymbol{A}_3$ in Fig. 1(b). Requiring $\partial q_{bz} / \partial z = 0$ in turn requires $\partial v_{sz} / \partial z = -\partial q_z / \partial z \,(= K_z \partial^2 h / \partial z^2)$ which is also found to equal to zero when the Dupuit condition ($\partial h / \partial z = 0$) is assumed within a confined aquifer. Hence, if v_{sz} is set equal to zero at the base of an aquifer, it is also zero at its top when the Dupuit condition is invoked along with equation (20).

In brief, based on (15), one can assume $\dot{\boldsymbol{q}}_b = 0$ when the well flow rate Q is constant. Groundwater models usually jump stepwise from one set of constant flow rates at sinks and sources to another, namely from a well flow rate Q_a to another rate Q_b. Similarly, bulk flux $\boldsymbol{q}_b$ would jump everywhere mathematically, from one constant rate to another, within the traditional numeric solution used by groundwater modellers. Accordingly, the condition $\dot{\boldsymbol{q}}_b = 0$ can be reasonably applied to each and every time step during which Q is modelled as a constant.

Evaluation of the term $\dot{n}$

Recalling the bulk volume ($V_b \equiv V_w + V_s$) as defined after equation (7) and taking the derivative with respect to time ($\dot{V}_b = \dot{V}_w + \dot{V}_s$) gives:

$$0 = \dot{n} + (1-n)\dot{\varepsilon}_V = \dot{n} + (1-n)\nabla \cdot \boldsymbol{v} \tag{18}$$

when the following four relations are introduced: $\dot{V}_b = 0$ for a control volume (V_b fixed in space) and correspondingly $\boldsymbol{v}_P = 0$; $\dot{V}_w / V_b = \dot{n}$; $\dot{V}_s / V_b = (1-n)\dot{\varepsilon}_V$ and $\dot{\varepsilon}_v = \nabla \cdot \boldsymbol{v}$ for infinitesimal strain. Consequently, expression (13) reduces to:

$$\dot{\boldsymbol{R}} \approx -(\gamma' / \gamma_w)(\nabla \cdot \boldsymbol{v})\boldsymbol{K} \cdot \boldsymbol{k} \tag{19}$$

for $\dot{Q} = 0$ and where $\gamma' \equiv (1-n)(G-1)\gamma_w$ expresses the submerged (buoyant) unit weight of solid

grains within a saturated medium. Using Terzaghi's (1925) terminology, it can also be called the "effective" unit weight of solid grains. Although incompressible constituents (pore water and solid grains) are assumed here (as done so by Biot (1941)), the porous structure of the skeletal frame is compressible. Hence, in Biot's theory and in the present theory, any change in porosity Δn is caused completely by change in the structure of the saturated skeletal frame, namely in the rearrangement of the submerged incompressible grains into a tighter or a looser configuration. A tighter configuration indicates a decrease in porosity and a looser configuration corresponds to an increase in porosity.

Inserting (19) into (12) results in governing equation (12) being expressed in a solvable form:

$$\frac{\partial \boldsymbol{v}}{\partial t}+\frac{1}{\gamma_w}\boldsymbol{K}\cdot\{[(\lambda+\mu)\nabla(\nabla\cdot\boldsymbol{v})+\mu\nabla^2\boldsymbol{v}]+\gamma'(\nabla\cdot\boldsymbol{v})\boldsymbol{k}\}=0 \tag{20}$$

where the effective (submerged) unit weight γ' is defined in (19) and for practical purposes can be treated as a constant.

Equation (20) is valid for a region (or element) V_b that contains no sinks or sources. Even if this region (or element) of interest contains an active sink or source of volume flow rate Q, equation (20) remains rigorously valid when Q = constant. When a step-wise approximation of change in Q cannot be made, appropriate function $\dot{Q}$ must be added to the right-hand side of equation (20).

For such problems of variable Q, $\dot{Q}$ can alternatively be specified as a "boundary condition" at a boundary of a new V_b (say at $r = r_w$). In this way, equation (20) remains rigorously valid within the new V_b. For example, the cylindrical V_b of Fig. 1(b) can be replaced by a new cylindrical V_b that is doughnut-shaped and where the variable Q (a specified $\dot{Q}$) occurs along the new doughnut-hole boundary at r_w rather than being specified as a variable rate sink or source within the old V_b as portrayed by Fig.1(b). Solving (17) results in $q_{br}r = q_{brw}r_w$ where q_{brw} is the measurable average radial bulk flow at a well screen of radius r_w. This can alternatively be written as $q_{br} = Q_2/2\pi br$ after introducing the classic relation $q_{brw} = Q_2/2\pi br_w$.

Equation (20) can alternatively be written as an extended expression within a Cartesian coordinate system:

$$\begin{aligned}
&\frac{\partial v_x}{\partial t}+\frac{K_x}{\gamma_w}[(\lambda+\mu)\frac{\partial}{\partial x}(\frac{\partial v_x}{\partial x}+\frac{\partial v_y}{\partial y}+\frac{\partial v_z}{\partial z})+\mu(\frac{\partial^2}{\partial x^2}+\frac{\partial^2}{\partial y^2}+\frac{\partial^2}{\partial z^2})v_x]=0\\
&\frac{\partial v_y}{\partial t}+\frac{K_y}{\gamma_w}[(\lambda+\mu)\frac{\partial}{\partial y}(\frac{\partial v_x}{\partial x}+\frac{\partial v_y}{\partial y}+\frac{\partial v_z}{\partial z})+\mu(\frac{\partial^2}{\partial x^2}+\frac{\partial^2}{\partial y^2}+\frac{\partial^2}{\partial z^2})v_y]=0\\
&\frac{\partial v_z}{\partial t}+\frac{K_z}{\gamma_w}\{[(\lambda+\mu)\frac{\partial}{\partial z}-\gamma'](\frac{\partial v_x}{\partial x}+\frac{\partial v_y}{\partial y}+\frac{\partial v_z}{\partial z})+\mu(\frac{\partial^2}{\partial x^2}+\frac{\partial^2}{\partial y^2}+\frac{\partial^2}{\partial z^2})v_z\}=0
\end{aligned} \tag{21}$$

where K_i ($i = x$, y and z) is the hydraulic conductivity in a principal direction; x, y and z are the three principal directions of a Cartesian coordinate system.

In contrast to (10) which is expressed in terms of the displacement field, (21) is solvable because it represents a set of three equations with three unknowns (v_x, v_y and v_z). The analytic or numerical solution of (21) can be found when appropriate boundary and initial conditions are expressed in terms of the velocity field. Cumulative land movement expressed in terms of the displacement field can then be determined by integrating the velocity field over the time domain, namely:

$$\boldsymbol{u}(x,y,z,t)=\int_{t_0}^{t}\boldsymbol{v}(x,y,z,t)dt \tag{22}$$

It is worth comparing the present theory to more traditional theories. The next section discusses the differences between the present model and Biot's classic model. The latter is widely applied to land movement by hydrogeologists and to the consolidation of soils by geotechnical engineers.

COMPARISON OF THE PRESENT THEORY TO BIOT'S THEORY

To compare the present theory to Biot's complete three-dimensional theory (Biot, 1941), it is necessary to outline Biot's development.

Brief review of Biot's theory

Based on the previous discussion, Biot's theory can be conveniently derived by taking two steps. First, simplifying equation (8) in the absence of both body and inertial forces produces equation (23); then, introducing the Darcy-Gersevanov law simplified from (4) and the Hubbert potential reduced from (5) into the incompressibility condition $\nabla \cdot \boldsymbol{q}_b = \nabla \cdot (\boldsymbol{v}_s + \boldsymbol{q}) = 0$ from the mass balance (6) yields (24). Equations (23) and (24) are given below in the following forms:

$$(\lambda + \mu)\nabla(\nabla \cdot \boldsymbol{u}) + \mu\nabla^2 \boldsymbol{u} + \nabla \cdot \boldsymbol{I}p = 0 \tag{23}$$

$$\frac{\partial(\nabla \cdot \boldsymbol{u})}{\partial t} = \frac{1}{\gamma_w} K \nabla^2 p \tag{24}$$

where the basic assumptions $\partial(\nabla \cdot \boldsymbol{u}) / \partial t = \nabla \cdot \boldsymbol{v}$ and $\partial \boldsymbol{u} / \partial t = \dot{\boldsymbol{u}} = \boldsymbol{v}$ for $\boldsymbol{v}_p = 0$ have been made. The aquifer system is assumed to be isotropic and homogeneous (Biot, 1941). The two expressions above comprise Biot's widely-used consolidation theory. The terms of water pressure in (23) and (24) are sometimes expressed in terms of hydraulic head by applying the Hubbert potential:

$$h = \int_{p_0}^{p} dp / \gamma_w + \int_{z_0}^{z} d\xi \tag{25}$$

Comparison of the present theory to Biot's theory

Comparing the theory developed in the present paper to Biot's leads to the following conclusions:

1. The present theory is based on the same principles and physical laws as were invoked by Biot. Therefore, both are inherently complete three-dimensional models and are capable of simulating both three-dimensional volumetric and shear deformations in response to hydraulic forces as well to other forces (e.g. gravitational forces induced in part by man-made structures upon or beneath the land surface and seismic forces induced by earthquakes and sometimes by man-induced shock waves).
2. The present model is at least as solvable as Biot's equations in simulating three-dimensional land movement. Biot's equations (23) and (24) are actually four equations with four variables, including three for the directional components of skeletal displacement and one for water pressure (or hydraulic head). In contrast, equation (20), or (21), based on the present theory, represents three equations where the three unknowns are the directional components of the velocity field.
3. The present theory is significantly simpler than Biot's theory for finding the directional components of motion in three dimensions. Equation (20) or (21), indicates that the solution can be found in the velocity field. The cumulative displacement $\boldsymbol{u}$ can be determined at any specified point of interest simply by integrating the velocity over time. In contrast, Biot's theory is developed in two different physical fields $\boldsymbol{u}$ and p (or h). Biot's four equations have to be solved simultaneously in the two coupled fields though some previous investigators have tried an ad-hoc approximation with the so-call two-step technique.

In brief, the present theory offer a simpler solution scheme than Biot's consolidation model without sacrificing any accuracy in simulating actual land movement driven by various physical forces (e.g. gravitational, seismic, hydraulic forces).

SUMMARY AND CONCLUSIONS

A theory of three-dimensional land movement in response to hydraulic and other forces (such as loads from structures and seismic forces) has been developed in terms of the velocity field of the skeletal frame. A solution for the displacement field can be found by integrating the velocity over the time domain. The development of this theory is based on the first principles of physics (conservation of mass and linear momentum), secondary laws of physics (the constitutive law of poroelasticity, the relation of drag forces to driving forces, the equations of state for the constituent materials and the potential function) and bulk flow relations.

The present theory has been compared to Biot's classic theory of three-dimensional deformation of saturated poroelastic material. Unlike Biot's theory, the present theory can address the problems related to the skeletal velocity field without coupling it to another physical field during the solution phase. As a consequence, the innovative derivation and methodology introduced in the present paper is substantially different from those employed by previous investigators. The present theory includes the effect that the self-weight of solids and water has on the movement of the skeletal frame. Biot's does not. In brief, the present theory is mathematically simpler than Biot's theory and thereby gains in flexibility. The present theory includes even more physical processes without losing generality and thereby gains in physical power.

Acknowledgements Reviews of the original manuscript by the anonymous reviewers are acknowledged. Conducting the investigation and writing this paper are supported by the grant of the US Department of Energy (DE-FG02-94EW11424).

REFERENCES

Biot, M. A. (1941) General theory of three-dimensional consolidation. *J. Appl. Physics* **12**, 55–64.

Carslaw, H. S. & Jaeger, J. C. (1959) *Conduction of Heat in Solids*, second edn. Oxford University Press, London, UK.

De Wiest, R. J. M. (1965) *Geohydrology.* John Wiley, New York, USA.

Gambolati, G. (1992) Comment on coupling *versus* uncoupling in soil consolidation. *Int. J. Numerical & Analytical Methods* in *Geomechanics* **16**, 833–837.

Gambolati, G., Teatini, P., Bau, D. & Ferronato, M. (2000) Importance of poroelastic coupling in dynamically active aquifers of the Po river basin, Italy. *Water Resour. Res.* **36**(9), 2443–2450.

Gersevanov, N.M. (1937) *The Foundations of Dynamics of Soils* (in Russian), third edn. Stroiizdat, Leningrad.

Helm, D. C. (1987) Three-dimensional consolidation theory in terms of the velocity of solid. *Geotechnique* **37**, 369–392.

Helm, D. C. (1994a) Hydraulic forces that play a role in generating fissures at depth. *Bull. Assoc. Engng Geologists* **16**(3), 293–304.

Helm, D. C. (1994b) Horizontal aquifer movement in a Theis-Thiem confined aquifer system. *Water Resour. Res.* **30**, 953–964.

Hubbert, M. K. (1969) *The Theory of Ground-Water Motion and Related Papers*. Hafner, New York, USA.

Lewis, R. W. & Schrefler, B. A. (1978) A fully coupled consolidation model of the subsidence of Venice. *Water Resour. Res.* **14**(2), 223–230.

Lewis, W. R., Schreffer, B. A. & Simoni, L. (1991) Coupling *versus* uncoupling in soil consolidation. *Int. J. Numerical & Analytical Methods* in *Geomechanics* **15**, 533–548.

Li, J. (2007a) Transient radial movement of a confined leaky aquifer due to variable well flow rates. *J. Hydrol.* **333**(2-4), 542–553.

Li, J. (2007b) Analysis of radial movement of a confined aquifer due to well pumping and injection. *Hydrogeology J.* **15**(3), 442–458.

Li, J. & Helm, D. C. (1998) Viscous drag, driving forces, and their reduction to Darcy's law. *Water Resour. Res.* **34**, 1675–1684.

Malvern, L. E. (1969) *Introduction to the Mechanics of a Continuous Medium*. Prentice-Hall, Englewood Cliffs, New Jersey, USA.

Terzaghi, K. (1925) Principles of soil mechanics: IV, Settlement and consolidation of clay. *Engineering New-Records* **95**, 874–878.

Theis, C. V. (1935) The relation between the lowering of piezometric surface and the rate and duration of discharge of a well using ground-water storage. *Trans. Am. Geophys. Un.* **16**, 519–524.

Verruijt, A. (1969) Elastic storage of aquifers. In: *Flow through Porous Media* (ed. by R. L. M. DeWeist), 331–376. Academic Press, San Diego, California, USA.

(Proceedings of EISOLS 2010, Querétaro, Mexico, 17–22 October 2010). IAHS Publ. 339, 2010.

Deformation characteristics of aquifer sands due to groundwater pumping in the Southern Yangtze Delta, China

Y. ZHANG, Y. Q. XUE, J. C. WU & X. Q. SHI
School of Earth Sciences and Engineering, Nanjing University, Nanjing 210093, China
yunzhang.nj@gmail.com

Abstract Excessive groundwater withdrawal has caused severe land subsidence in many areas in the world. Previous studies attribute land subsidence primarily to the compaction of aquitard units, which consist mainly of clay and silty clay. However, the field data in recent decades in the Southern Yangtze Delta, China, a typical land subsidence area caused by groundwater pumping, and from elsewhere, have proven that the main compaction may occur in aquifer units that consist of sands. The purpose of this paper is to investigate the deformation characteristics of the aquifer units under changing groundwater level. By collecting long-term field data, the deformation characteristics of sands were recognized and the relationship of deformation, effective stress and time was specified. It was found that, besides elastic deformation, sands exhibit plastic and creep deformation. It is the creep behaviour of sands that make the compaction of aquifer units lag behind the change in groundwater level in the unit. Consequently, both aquifer and aquitard units should be taken into account when modelling land subsidence. Based on analysing the field data, a new mechanical model of deforming aquifer units was constructed to simulate land subsidence in the Southern Yangtze Delta.

Key words land subsidence; deformation characteristics; groundwater pumping; lagging deformation; visco-elasto-plasticity

INTRODUCTION

Land subsidence due to excessive groundwater withdrawal has occurred for a very long time in the world. Many countries and areas, such as Italy, Thailand, the USA, Mexico, and China, have encountered this problem. Land subsidence results in loss of ground surface elevation, cracking of buildings, and causes considerable economic loss. Therefore, many researchers have been dedicated to studying land subsidence due to groundwater withdrawal. Groundwater extraction causes the pore water pressure in soil units to change, causing corresponding changes in the effective stress. The change in effective stress causes the soil units to compact, and land then subsides. In such cases, solving the deformation characteristic of individual hydrostratigraphic units is an essential problem in studying land subsidence.

In the previous work, many researchers have concentrated on the deformation of aquitard units, which consist primarily of clay and silty clay. Li *et al*. (2000) assumed the aquitard unit to be an elasto-plastic material and applied this assumption to the calculation of land subsidence in Shanghai. Gu *et al*. (2000) proposed that the aquitard units in Shanghai compacted visco-elastically. In contrast, little research has addressed the deformation characteristics of aquifer units, which consist mainly of sands. In fact, the deformation of aquifer units has often been thought to be elastic, which means that the aquifer units compact immediately when groundwater level in them declines, and expand when the groundwater level rises. It is also thought that the contribution of aquifer units to the total land subsidence is so small that it can be ignored in some cases. However, long-term field data reveal that both aquitard and aquifer units compact when groundwater level changes, and aquifer units may be the primary subsidence unit in certain conditions (Zhang *et al*., 2003). Therefore, the deformation of aquifer sands is more complex than previously realized. It has not only unrecoverable plastic deformation but also time-dependent creep deformation (Liu *et al.*, 2004; Zhang *et al.*, 2007). More attention has to be paid to the deformation characteristics of aquifer units. This paper aims to investigate the deformation characteristics of aquifer units under the condition of changing groundwater level and to construct a corresponding mechanical model on the basis of the long-term field data from extensometer groups and observation wells in the Southern Yangtze Delta, China.

Copyright © 2010 IAHS Press

BASIC SITUATION

The Southern Yangtze Delta is located in the lower reach of the Yangtze River, in eastern China, and includes Shanghai, SXC (Shouzhou, Wuxi, Changzhou cities) of Jiangsu Province, and HJH (Hangzhou, Jiaxin, Huzhou cities) of Zhejiang Province, with a total area of 30 340 km^2. It is one of the developed areas in China. With the rapid economic development and rise in population, the requirement for water has increased greatly and a large amount of groundwater is extracted. The distribution of the Quaternary deposits in the Southern Yangtze Delta is affected by the base tectonics and ancient landforms. The thickness of the deposits increases from west to east. The Quaternary deposits are alluvial, lacustrine, marine, and palustrine, including clay, silty clay, silt, sand, and gravel. Clay and silty clay units and sand units are interbedded vertically. The deposits in the Southern Yangtze Delta can be considered to be composed of five aquifer units (Zhang & Wei, 2005): an unconfined aquifer and four confined aquifers. The confining aquitards interbedded between the aquifer units are denoted as aquitards 1–5 from top to bottom, respectively.

Groundwater has been extracted for over 100 years in the Southern Yangtze Delta. Groundwater withdrawal in Shanghai dates back to 1860, and extensive exploitation occurred in the 1950s when 80.5% of the total pumpage was obtained from the first and second confined aquifers. Consequently, land subsidence developed rapidly during the period 1957 to 1960, with an average annual rate of 110 mm/year. Groundwater pumpage was then limited strictly in order to mitigate land subsidence. After 1966, a small rebound even occurred at some sites. The demand for groundwater increased once again in the late 1980s, and the groundwater was mainly extracted from the third and fourth confined aquifers to control the development of land subsidence. The pumpage from the third and fourth confined aquifers accounted for, respectively, 70% and 15% of the total in 2000, causing the groundwater levels in the two units to decline continuously.

Groundwater exploitation began in 1927 in the SXC area, and extensive extraction occurred after 1983. In SXC, groundwater was mainly pumped from the first and second confined aquifers and land subsidence was first reported in around 1970. The most severe land subsidence occurred in the period 1985–1990 when the annual rate of land subsidence was 91, 74, and 109 mm/year in Suzhou, Wuxi, and Changzhou, respectively. Groundwater extraction in HJH began in 1914 and occurred primarily in the second and third confined aquifers. The extensive exploitation occurred after 1980, and the centre of the subsidence bowl was located in the city of Jiaxing.

DEFORMATION CHARACTERISTICS OF AQUIFER UNITS

In order to investigate and study land subsidence due to groundwater pumpage, many observation wells and more than 20 extensometer groups have been constructed in the Southern Yangtze Delta to measure the changes of groundwater levels in individual aquifers and the compaction of individual hydrostratigraphic units. The field data actually reveal the deformation characteristics of aquifers under changing groundwater level. Consequently, curves of compaction of an aquifer unit measured by extensometer groups, and groundwater level in the same unit obtained from observation wells, can represent the stress–strain characteristics of this deforming aquifer unit.

The first and second confined aquifers

The first confined aquifer consists of silt to fine sand, fine to medium sand, and medium to coarse sand. It is subdivided into two sub-units: the upper and lower first confined aquifer. The upper first confined aquifer distributes discontinuously. The lower first confined aquifer occurs continuously, and its thickness and the depth of its top become greater from west to east. The second confined aquifer, consisting of silt sand, fine sand, fine to medium sand, and medium to coarse sand with gravel, distributes continuously in the study area, and the depth of its top deepens from west to east. These two confined aquifers present similar deformation characteristics because they have similar compositions and have experienced similar changing groundwater level.

Groundwater was mainly extracted from the lower first confined aquifer and the second confined aquifer in Shanghai before the 1960s, when the groundwater level in these two aquifers decreased rapidly and reached the lowest value of –30 m in the early 1960s. As a result of adjustment of primarily pumped units and limitation of pumpage, the groundwater level in those two units recovered greatly. It rose to levels higher than –5 m in the early 1970s and its average nearly remained constant. In the late 1980s, these two aquifers declined again because of increasing pumpage, but the groundwater levels were still much higher than their previous low level in the 1960s. Figure 1 indicates the history of the groundwater level and cumulative compaction of the second confined aquifer at extensometer group F004 in Shanghai during the period 1965–2002. These data are replotted into a curve of groundwater level *vs* cumulative compaction, as shown in Fig. 2. These two figures illustrate that the cumulative compaction closely follows the change in groundwater level: the aquifer unit compacts when groundwater level decreases, and *vice versa*. The groundwater level in the second confined aquifer at extensometer group F004 reached its lowest value of –22 m in 1965 as a consequence of previous heavy exploitation. Then the groundwater level rose rapidly and reached about –0.07 m in 1973 because of the limitation of pumpage after 1965. During the period 1973–1988, the groundwater level fluctuated within a certain range, with the average being approximately –1 m and the amplitude being about 2 m. After 1988, groundwater level declined slowly and fell to –8 m in 2002. The curve of groundwater level and cumulative compaction (Fig. 2) shows that the second confined aquifer behaves as an elastic material during the period 1965–1988 when the yearly average groundwater level rose continuously or almost remained constant, and that the aquifer unit exhibited primarily elasto-plastic deformation during the period 1989–2002 when the groundwater level fell but was still higher than the historically lowest value the aquifer had ever experienced. During the latter period, there was remarkable plastic deformation in each yearly cycle of rising and falling groundwater level.

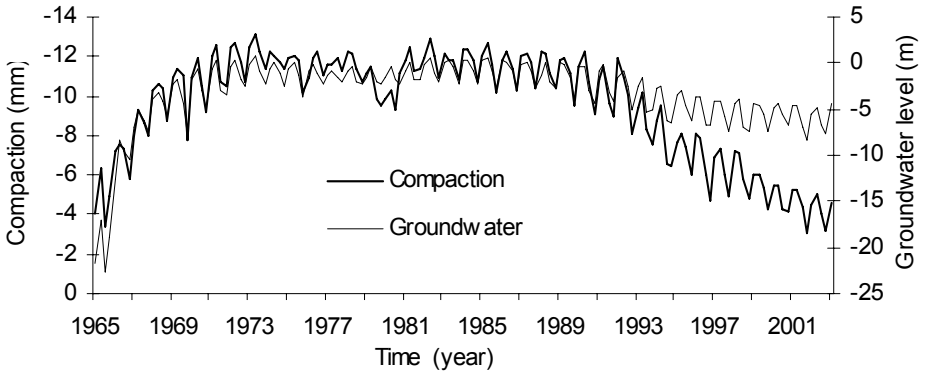

Fig. 1 Histories of groundwater level and cumulative compaction of the second confined aquifer at extensometer group F004.

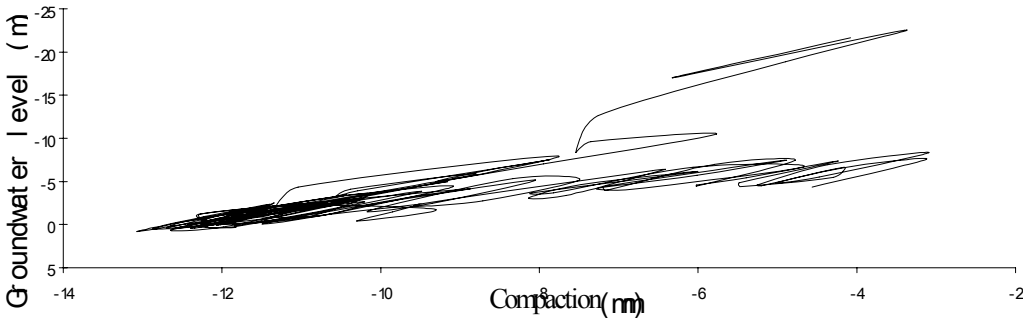

Fig. 2 Curve of groundwater level and cumulative compaction of the second confined aquifer at extensometer group F004.

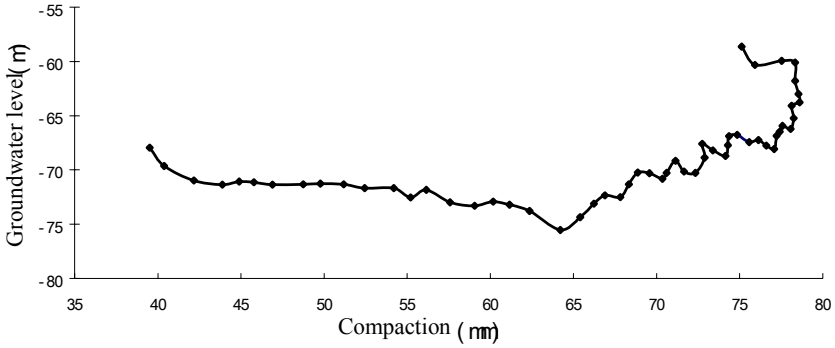

Fig. 3 Curve of groundwater level and cumulative compaction of the second confined aquifer at extensometer group FQL.

The second confined aquifer was also the main exploited aquifer in SXC and HJH. Figure 3 indicates the curve of groundwater level and cumulative compaction of the second confined aquifer at the extensometer group FQL that is located at Qingliang Primary School, Changzhou, from 1990 to 2003. Groundwater level in the second confined aquifer at Changzhou decreased continuously before 1994 and reached the historically lowest level of –75.53 m in 1994. Then the groundwater level in the unit rose continuously and reached –58.63 m in 2003. However, the aquifer unit still compacted continuously after 1994, and the compaction did not stop until 2001. After 2002, the curve moved to the left, indicating that net expansion occurred. This reveals that the deformation of the second confined aquifer at FQL lags behind the change in groundwater level for eight years.

The third confined aquifer unit

The third confined aquifer, consisting of silt to fine sand, fine sand, medium to coarse sand, and medium to coarse sand with gravel. Figure 4 shows the historical groundwater level and cumulative compaction of the third confined aquifer at extensometer group F004 in Shanghai. Before 1986, the groundwater level fluctuated within a certain range and the aquifer unit compacted, closely following the change in groundwater level. The aquifer sand behaved as an elastic material. During the period 1986–1992, the yearly average groundwater level declined continuously but was still higher than the previous lowest value, and there was significant unrecoverable deformation in each yearly cycling of groundwater level. After 1992, the groundwater level declined below the previous lowest value and the compaction of the aquifer unit obviously lagged behind the change in groundwater level. After 1998, the compaction continued

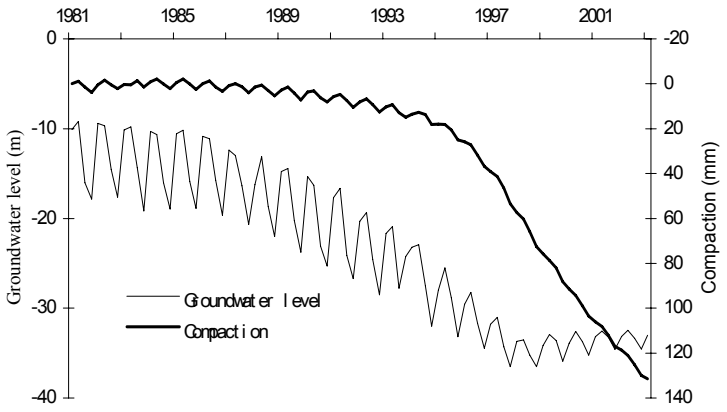

Fig. 4 History of groundwater level and compaction of the third confined aquifer at extensometer F004 in Shanghai.

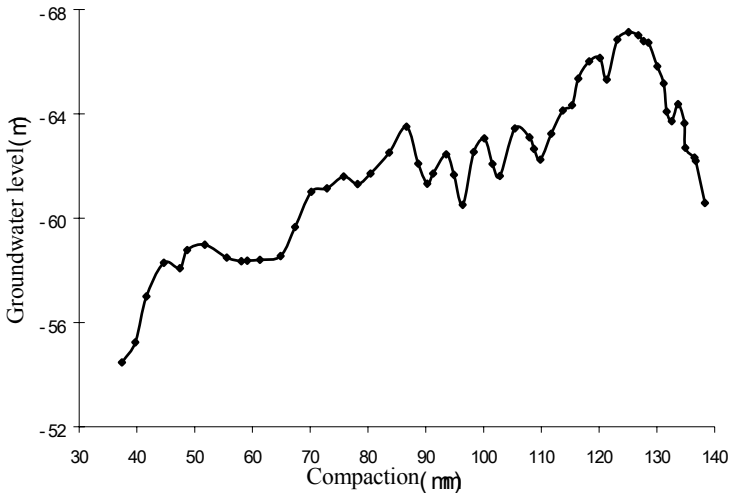

Fig. 5 Curve of groundwater level and compaction of the third confined aquifer at extensometer FQL in Changzhou.

although the average groundwater level increased. The curve of compaction of the third confined aquifer and the groundwater level in it from 1990 to 2003 at extensometer group FQL is plotted in Fig. 5. It shows that the aquifer unit still compacted in the period when groundwater level increased continuously, and that the compaction obviously lagged behind.

As described above, the deformation characteristics of aquifer units are not always elastic, but depend on the changing patterns of groundwater level the units have experienced. When the groundwater level is higher than the previous lowest value, the aquifer unit deforms elastically or elasto-plastically. When the groundwater level is lower than the previous lowest value, the aquifer obviously presents lagging.

RELATIONSHIP OF STRESS–STRAIN–TIME OF AQUIFER UNITS

From the field investigation, the deformation of the aquifer unit can be illustrated through the mechanical model in Fig. 6. The model includes four types of deformation: elastic, visco-elastic, plastic, and visco-plastic deformation. In the model, the elements s1 and s2 are springs and their elastic moduli are E1 and E2, respectively. The plastic elements p1 and p2 are of plastic moduli of H1 and H2, respectively. The elements c1 and c2 are dashpots, with viscosity factors of η_1 and η_2, respectively. σ_{01} represents the first yielding stress, meaning that the aquifer deforms plastically when the effective stress exceeds this limit stress. σ_{02} represents the second yielding stress, meaning that the aquifer deforms visco-plastically when the effective exceeds the stressσ_{02}. σ_{01} is no greater than σ_{02}. On the condition of changing groundwater level, σ_{02} is equivalent to the effective stress corresponding to the lowest groundwater level in each yearly cycle. With various effective stresses, different equations describing the relationship of stress–strain–time can be obtained.

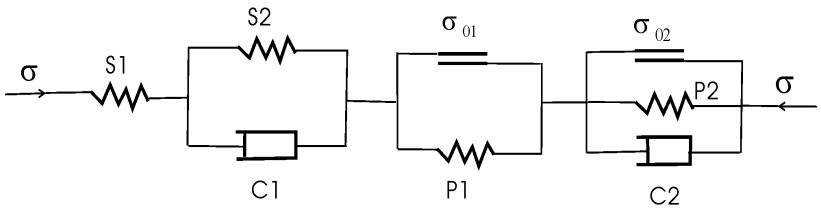

Fig. 6 Mechanical model for the deformation of aquifer sand.

If $\sigma \le \sigma_{01}$, the relationship is:

$$E_2\varepsilon + \eta_2\dot{\varepsilon} = \sigma + \frac{E_2}{E_1}\sigma + \frac{\eta_2}{E_1}\dot{\sigma} \tag{1}$$

If $\sigma_{01} < \sigma \le \sigma_{02}$, the relationship is:

$$E_2\varepsilon + \eta_1\dot{\varepsilon} = \sigma + \frac{E_2}{E_1}\sigma + \frac{E_2}{H_1}(\sigma - \sigma_{01}) + \frac{\eta_1}{E_1}\dot{\sigma} + \frac{\eta_1}{H_1}\dot{\sigma} \tag{2}$$

If $\sigma > \sigma_{02}\varepsilon$, the total deformation includes three components: elasto-plastic deformation ε_1, visco-elastic deformation ε_2, and visco-plastic deformation ε_3. The relationship is:

$$\begin{cases} \varepsilon = \varepsilon_1 + \varepsilon_2 + \varepsilon_3 \\ \varepsilon_1 = \dfrac{\sigma}{E_1} + \dfrac{\sigma - \sigma_{01}}{H_1} \\ E_2\varepsilon_2 + \eta_1\dot{\varepsilon}_2 = \sigma \\ H_2\varepsilon_3 + \eta_2\dot{\varepsilon}_3 = \sigma - \sigma_{02} \end{cases} \tag{3}$$

In this case, if the visco-elastic deformation is ignored, the stress–strain–time relationship in equation set (3) becomes:

$$H_2\varepsilon + \eta_2\dot{\varepsilon} = \sigma - \sigma_{02} + \frac{H_2}{E_1}\sigma + \frac{H_2}{H_1}(\sigma - \sigma_{01}) + \frac{\eta_2}{E_1}\dot{\sigma} + \frac{\eta_2}{H_1}\dot{\sigma} \tag{4}$$

In the previous equations, σ is effective stress, kPa; ε is strain. Six parameters are involved in this mechanical model, which can be acquired from the field data of groundwater level and corresponding compaction for an identical aquifer unit. The methods of determining the parameters will be discussed in another paper.

CONCLUSION

Based on the field data, the deformation characteristics of aquifer units are investigated in this paper. It has been found that the aquifer units may deform as elastic, elasto-plastic, or visco-elasto-plastic materials, depending on the changing patterns of groundwater level the units have experienced. When the groundwater level increases continuously, or fluctuates within a certain range, the aquifer unit mainly deforms elastically. When the groundwater level decreases continuously and is higher than the previous lowest value the unit has experienced, the aquifer unit deforms primarily as an elasto-plastic material. When the groundwater level declines continuously and is below the previous lowest value, the aquifer unit behaves as a visco-elasto-plastic material. On the basis of this analysis, a mechanical model was constructed to represent the deformation characteristics of aquifer units under groundwater level changing.

Acknowledgements This paper was financially supported by the National Nature Science Foundation of China grant 40772168 and the National Science Foundation of China grant for Distinguished Youth Scholar 40725010.

REFERENCES

Gu, X. Y. & Ran, Q. Q. (2000) A 3-D coupled model with consideration of rheological properties. In: Proceedings of the 6th International Symposium on Land Subsidence (ed. by L. Carbognin, G. Gambolati & A. I. Johnson) (September, Ravenna, Italy), 355–365.

Li, Q. F., Fang, Z. & Wang, H. M. (2000) Calculation and prediction of exploitable groundwater in Shanghai (in Chinese). *Shanghai Geology* **2**, 36–43.

Liu, C. H., Pan, Y. W., Liao, J. J., Huang, C. T. & Ouyang, S. (2004) Characterization of land subsidence in the Chaoshui River alluvial fan. *Taiwan. Environmental Geology* **45**, 1154–1166.

Zhang, A. G. & Wei, Z. X. (2005) *Land Subsidence in China*. Shanghai Science and Technology Press, Shanghai (in Chinese)

Zhang, Y., Xue, Y. Q. & Li, Q. F. (2003) Current prominent subsidence layer and its deformation properties in Shanghai (in Chinese). *Hydrogeology and Engineering Geology* **30**(5), 6–11.

Zhang, Y., Xue, Y. Q., Wu, J. C., Ye, S. J., Wei, Z. X., Li, Q. F. & Yu, J. (2007) Characteristics of aquifer system deformation in the Southern Yangtze Delta, China. *Engineering Geology* **90**(3-4), 160–173.

Land Subsidence, Associated Hazards and the Role of Natural Resources Development
(Proceedings of EISOLS 2010, Querétaro, Mexico, 17–22 October 2010). IAHS Publ. 339, 2010.

Post-audit of land subsidence modelling of Saga-Shiroishi plain, Japan — lessons and improvements toward useful modelling

K. FUJISAKI
Geo-environmental Consultant, 7-60-2-517, Rokkodai, Matsudo, Chiba 270-2203, Japan
fujisakika@u01.gate01.com

Abstract In Japan, land subsidence caused by excess groundwater withdrawal was a serious problem in the 1960s to 1980s. Groundwater modelling was applied to prevent land subsidence and for groundwater resources management. It is important to investigate the accuracy of the modelling by comparing the prediction results with observation data. This process is referred to as a post-audit. The modelling of land subsidence on the Saga-Shiroishi Plain was examined with regard to its prediction results. A quasi three-dimensional model was adopted to calculate piezometric heads and a one-dimensional consolidation model was used to calculate the land subsidence rate at observation wells. The predicted piezometric heads agreed well with the observation data. However, some prediction results for land subsidence differed considerably from the observation data. The difference between the predicted results for piezometric head and land subsidence is attributed to the difference between the calibration accuracies of the piezometric head and subsidence rate. Post-audits show that accuracies of predictions are not always high. In the case of one-time prediction, accurate prediction cannot always be guaranteed. To improve the accuracy of prediction, it is necessary to revise the model by assimilating observation data and to iterate the prediction for groundwater resources management.

Key words groundwater modelling; land subsidence; post-audit; prediction

INTRODUCTION

Post-audits are essential for examining the accuracy of long-term predictions in groundwater modelling (Konikow, 1986). In Japan, there have been hundreds of modelling studies for groundwater basin management in the past three decades. Among these, only a few predictions have been post-audited and the results published. The author has experience of tens of modelling studies, and has followed up prediction results in terms of the accuracy and efficiency of the groundwater modelling and published post-audit results (Fujisaki, 2000, 2003; Fujisaki *et al*., 2005). This paper presents the post-audit results of land subsidence modelling of the Saga-Shiroishi Plain, Japan. Post-audits have shown that predictions are not always accurate, as mentioned by Konikow (1995). In addition, Bredehoeft (2003) pointed out that a conceptual model is incorrect in many cases. Therefore, in this paper, a method for improving model accuracy is presented.

LAND SUBSIDENCE MODELLING OF THE SAGA-SHIROISHI PLAIN

Modelling results

The research area is one of the major land subsidence areas in Japan in which the rate of subsidence increased in the 1960s and intensified suddenly in drought years. The plain is underlain by the Ariake clay formation, Shimabarakaiwan formation, Aso pyroclastic flow, and Pleistocene series in descending order. Groundwater is withdrawn from the Pleistocene series. Annual extraction in 1981 was about 6.8×10^6 m^3, mainly for industrial use in the Saga area, and about 8.6×10^6 m^3 for agricultural and municipal use in the Shiroishi area. In the Shiroishi area, the Ariake clay formation has a thickness of 20–30 m, and compaction of this layer has been the main cause of land subsidence (Fig. 1).

Groundwater flow was calculated using a quasi three-dimensional model in which the Pleistocene series was the main confined aquifer and the Ariake clay formation was the confining layer. Land subsidence at observation wells was calculated using a one-dimensional consolidation

Copyright © 2010 IAHS Press

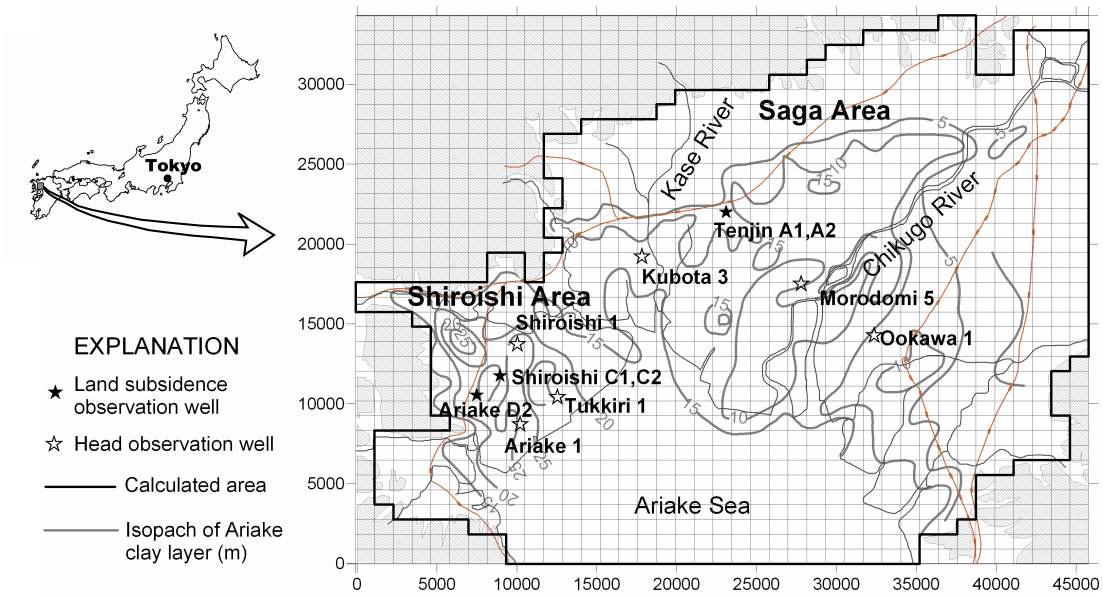

Fig. 1 Modelling area and isopach of the Ariake clay layer (from Fujisaki, 1983).

model (Fujisaki, 1983). The period of the model calibration spanned 5 years (1976–1980). The prediction period was 10 years (1981–1990). Piezometric head changes were predicted. From the head changes, land subsidence was predicted at the observation well sites. The prediction results of five scenarios showed that the annual extraction rate should be reduced to 4.1×10^6 m^3 in the Shiroishi area and 7.4×10^6 m^3 in the Saga area in order to halt land subsidence.

Evaluation of prediction results

Figure 2 compares the extraction rates of prediction scenarios 1 to 5 with the measured rates in the Saga and Shiroishi areas. Predicted piezometric heads and land subsidence changes at representative observation wells are compared with measurement data (Figs 3 and 4). The annual extraction rate in the Shiroishi area has been maintained almost at the rate of scenario 1, which assumed the extraction rate to be that of 1980. In 1994, the extraction rate increased suddenly to 20×10^6 m^3. Afterward, extraction gradually decreased to a rate lower than that of scenario 1. The observed piezometric head at the Shiroishi C1 observation well agreed well with the predicted

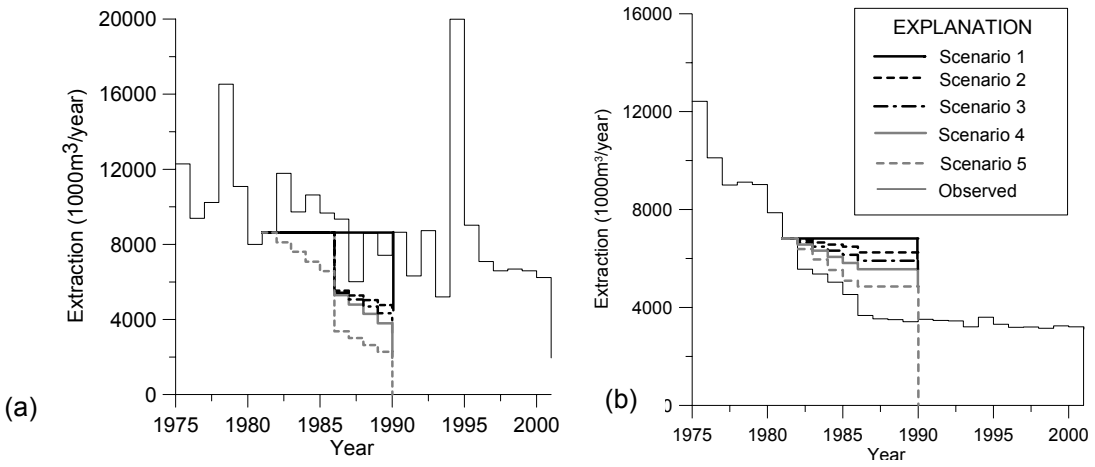

Fig. 2 Annual extraction in prediction scenarios for 1981–1990 (Fujiaki, 1983) and observed extraction for 1975–2001 (Saga Prefecture, 1981–2001). (a) Shiroishi area, (b) Saga area.

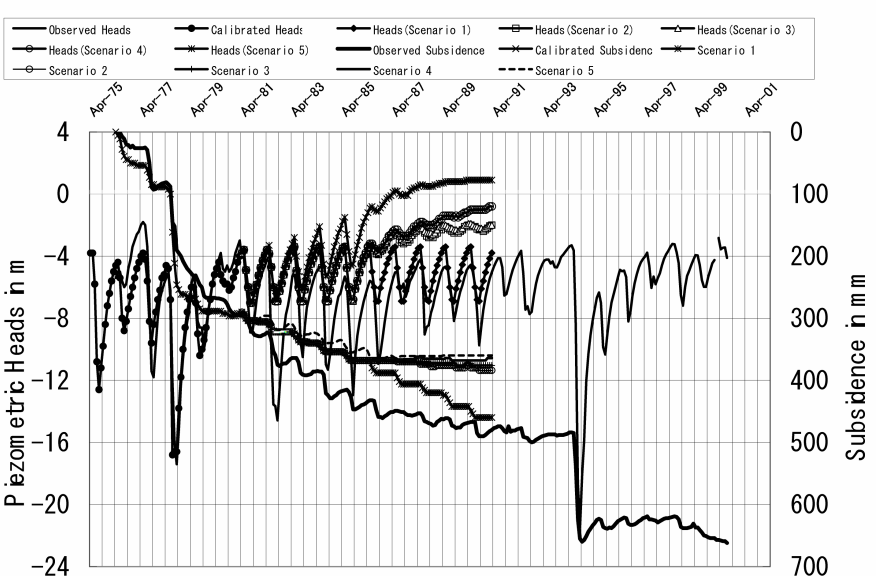

Fig. 3 Comparison of predicted heads and land subsidence with observation results at Shiroishi C1 observation well. Predicted results are from Fujisaki (1983) and observation results from Saga Prefecture (1981–2001).

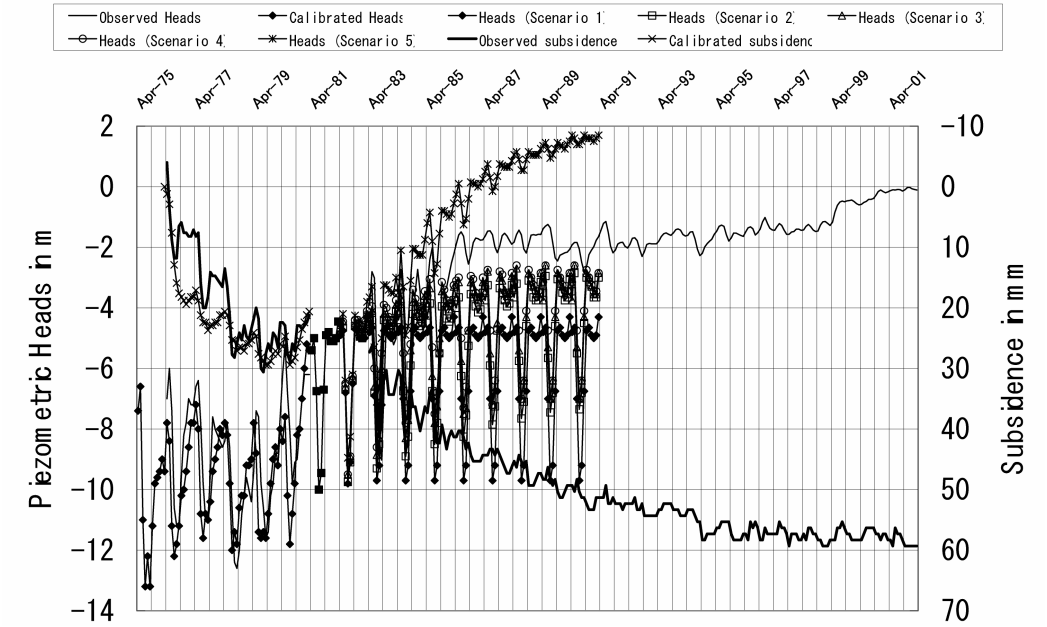

Fig. 4 Comparison of predicted heads with observation results at Tenjin A2 observation well. Predicted results are from Fujisaki (1983) and observation results from Saga Prefecture (1981–2001).

head in scenario 1. It was predicted that linear subsidence would have continued; however, the measured subsidence gradually decreased and nearly stopped. Therefore, the predicted and observed results did not agree.

Annual extraction in the Saga area reduced by nearly half from 1981 to 1986, and was steady afterward. The decrease in the extraction rate was greater than that in scenario 5. The piezometric head at the Tenjin A2 observation well recovered until 1985 to be similar to the head predicted in scenario 5. Afterwards, it remained at a level lower than the head predicted in scenario 5. In scenario 5, extraction was assumed to reduce in both the Shiroishi and Saga areas. However,

because the actual extraction rate in the Shiroishi area did not change, it is understandable that the observed head recovery remained small. In the Saga area, observed land subsidence was less than 1 cm per year and may not have caused serious problems; therefore, land subsidence was not predicted.

Examination of calibration accuracy

The flow model was calibrated visually to compare observed and calculated head contour maps and historical head changes at the observation wells. The average difference between observed and calculated heads is commonly used to express calibration accuracy. Three ways of expressing the average difference were used: mean error (ME), mean absolute error (MAE), and root mean squared error (RMS). The average errors of heads at observation wells are presented in Table 1. Seasonal fluctuations of heads were relatively large in the Shiroishi area. Therefore, the average errors are generally large in the Shiroishi area, while they are small in the Sage area.

Table 1 Mean errors and correlation coefficients in the head calibration. ME: Mean error, MAE: Mean absolute error, RMS: Root-mean-square error, R: Correlation coefficient, K: Kendal's coefficient of rank correlation.

Area	Obs. Well	ME (m)	MAE (m)	RMS (m)	R	K
Shiroishi	Shiroishi C1	0.60	1.26	1.56	0.905	0.941
	Shiroishi 1	1.53	1.72	1.96	0.853	0.672
	Ariake D2	1.20	1.42	1.70	0.929	0.705
	Ariake 1	0.22	0.80	1.03	0.953	0.780
	Tukkiri 1	–1.36	1.43	1.68	0.950	0.810
Saga	Tenjin A2	0.63	1.11	1.47	0.712	0.535
	Takagise 2	–1.44	1.44	1.52	0.869	0.689
	Kubota 3	0.18	0.41	0.51	0.809	0.668
	Morodomi 5	-0.62	0.62	0.72	0.897	0.735

Another expression of model accuracy is the correlation of the observed head with the calculated head. The correlation coefficients for observation wells are also presented in Table 1. Correlation coefficients in the Shiroishi area were higher than those in the Saga area. Accuracy as represented by the coefficients has a trend opposite to that of average errors. In addition, Kendal's coefficients of rank correlation, which express a trend, are given in Table 1. These values are higher in the Shiroishi area, where they have the same trend as the correlation coefficients. Observation wells with a high correlation coefficient do not necessarily have a high coefficient of rank correlation.

The one-dimensional land-subsidence model was calibrated visually to compare observed and calculated cumulative land subsidence at the observation wells. The average errors and correlation coefficients are shown in the top tier of the same cell in Table 2. The difference in errors in the Shiroishi and Saga areas may reflect the amount of land subsidence. The correlation coefficients and rank correlation coefficients are higher in the Shiroishi area. The correlation with accumulated data is generally high. Correlations with monthly land subsidence data were calculated and the results are given in the bottom rows of Table 2. The average errors are smaller for monthly data; however, correlation coefficients and rank correlation coefficients for monthly data are less than those for accumulated data.

The accuracy of model calibration seems to be well represented by the correlation coefficient. For piezometric head with a high correlation coefficient, the prediction result agreed well with observation data. However, prediction results of land subsidence with a low correlation coefficient did not agree with the observed trend and the accuracy of calibration was low. In the case of the land subsidence model for the Shiroishi area, the calibration period was too short at 5 years and it included large subsidence in 1983. The low calibration accuracy may be related to this.

Table 2 Mean errors and correlation coefficients in the land subsidence calibration. Top: cumulative subsidence, bottom (highlighted row): monthly subsidence.

Area	Obs. Well		Depth (m)	ME (mm)	MAE (mm)	RMS (mm)	R	K
Shiroishi	Shiroishi	C1	260	–22.4	23.1	28.1	0.988	0.941
				0.1	4.1	7.3	0.381	0.428
		C2	24	–12.3	14.6	18.0	0.988	0.976
				0.1	3.0	5.1	0.445	0.362
	Ariake	D1	150	1.3	12.7	16.4	0.983	0.954
				0.0	2.7	5.7	0.747	0.407
Saga	Tenjin	A1	187	–1.3	4.5	5.6	0.886	0.787
				0.1	2.1	2.8	0.687	0.426
		A2	58	–3.8	4.2	5.5	0.874	0.741
				0.0	2.0	2.6	0.458	0.287

Influence of agricultural use

In the Shiroishi area, agriculture is responsible for a large portion of extraction. In drought years such as 1983 and 1994, extraction suddenly increased. Land subsidence at the Shiroishi C1 observation well slowed in 1991 and 1992, despite there being no reduction in the extraction rate. However, there was much subsidence in 1994. Municipal-use extraction in the Shiroishi area was abandoned in 2002, after which the extraction rate sharply reduced. However, agricultural use, which changes with the amount of precipitation, remained at the same level. Therefore, it should be examined whether land subsidence occurs in a drought year.

IMPROVEMENT OF MODEL ACCURACY

There may be sources of prediction error in each stage of conceptual model construction, numerical model construction, and calibration. The post-audit results indicate that prediction errors are partly due to errors in parameter estimation and partly due to an incorrect conceptual model. Even in the case of an incorrect conceptual model, calibration can be completed and a prediction executed (Bredehoeft, 2003). In the case of a one-time prediction, the accuracy of prediction is difficult to guarantee. To improve the accuracy of prediction, revision of the model according to the observation data and iteration of prediction are necessary (Fig. 5). The iterative modelling may be effective in managing groundwater resources continuously.

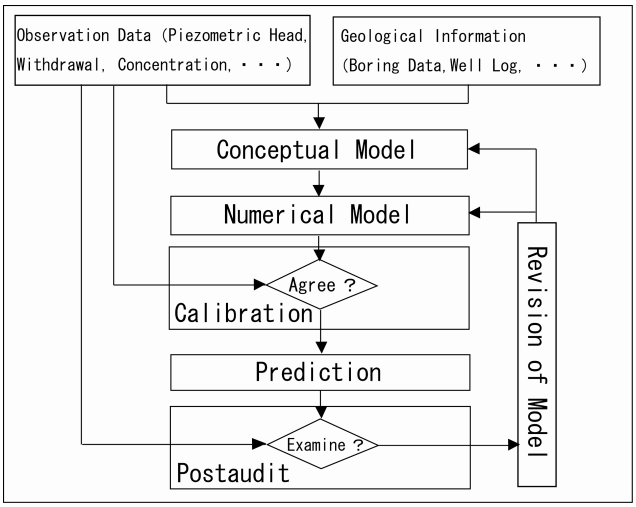

Fig. 5 Iterative groundwater modelling (modified from Fujisaki, 2008).

SUMMARY

Predictions of land subsidence on the Saga-Shiroishi Plain according to five scenarios were compared with observation data for 10 years. The annual extraction rate in the Shiroishi area was nearly maintained at the same value as that of scenario 1, in which the extraction rate was set equal to that of 1980. The predicted piezometric heads agreed fairly well with observation data. It was predicted that linear land subsidence would continue. However, the observed land subsidence gradually decreased and tended to cease. The trends of calculated subsidence were entirely different from the observation data. To determine the cause of the differences in the trends, average errors, correlation coefficients, and Kendal's coefficients of rank correlation were calculated and the accuracy of model calibration analysed. It is difficult to explain the difference between the prediction results of piezometric head and land subsidence on the basis of average errors. However, correlation coefficients can explain the difference. The accuracy of land subsidence calibration was poor because the calibration period was too short at 5 years and included the drought year of 1983, during which there was much land subsidence. The post-audit result shows that the prediction accuracy was not high. Prediction errors originated from calibration errors and an incorrect conceptual model in some cases. It is difficult to guarantee the accuracy of a one-time prediction. It is necessary to revise the model according to observation results and to iterate predictions to improve the accuracy of prediction. The iterative modelling would be a useful management tool of groundwater resources.

REFERENCES

Bredehoeft, J. (2003) From models to performance assessment—the conceptualization problem. *Ground Water* **40**(4), 340–345.

Fujisaki, K. (1983) Report on countermeasures against land subsidence in the Chikugo-Saga Plain. Environment Agency (in Japanese).

Fujisaki, K. (2000) Groundwater simulation in the Kanto Groundwater Basin and evaluation of its results. Abstracts, the 107th Annual Meeting of the Geological Society Japan, 192 (in Japanese).

Fujisaki, K. (2003) Post-audit of groundwater simulation 3 – Groundwater flow and land subsidence modelling in Nirayama Town. Proc. of the 13th symposium on Geo-environments and Geo-technics, Kobe, 321–326 (in Japanese with English abstract).

Fujisaki, K. (2008) Uncertainty of groundwater prediction models. Proc. of the 17th Symposium on Geo-environments and Geo-technics, Tokyo, 51–54 (in Japanese with English abstract).

Fujisaki, K., Furuno, K., Takanaka, F. & Nirei, H. (2005) A post audit of numerical modelling of VOC contamination sites. *J. PMUG* **1**(1), 1–18 (in Japanese with English abstract).

Konikow, L. F. (1986) Predictive accuracy of a ground-water model—Lessons from a post-audit. *Ground Water* **24**(2), 173–184.

Konikow, L. F. (1995) The value of postaudits in groundwater model applications. In: *Groundwater Models for Resources Analysis and Management* (ed. by A. I. El-Kadi), 59–78. CRC Press, Inc., Boca Raton, Florida, USA.

Saga Prefecture (1981–2001) Overview of land subsidence (in Japanese).

(Proceedings of EISOLS 2010, Querétaro, Mexico, 17–22 October 2010). IAHS Publ. 339, 2010.

Hazards of gases migrating over oilfields due to subsidence

J. O. ROBERTSON, Jr[1] **& G. V. CHILINGAR**[2]

1 *Earth Engineering, Inc. and ITT, ITT – Tech, Vista, California, USA*

2 *Department of Civil and Environmental Engineering, University of Southern California, Los Angeles, California, USA*
gchiling@usc.edu

Abstract Subsidence due to fluid(s) withdrawal from oil/gas reservoirs can give rise to faults and fractures in the overlying strata above the reservoir, through which gas and fluids can migrate from the reservoir to the surface. Prevention/mitigation of this hazard is also discussed.

Key words fracturing; hazard; oil fields; Los Angeles basin, USA; sediment compaction

INTRODUCTION

Subsidence due to fluid withdrawal occurs when: (1) reservoir fluid pressures are lowered, (2) reservoir rocks are compactable and/or are unable to effectively resist deformation upon the transfer of load from the fluid phase to the grain-to-grain contacts, and (3) the overburden lacks internal self-support and the formations can easily deform downward (see Donaldson & Chilingarian, 1997, p. 253).

The principal lithological and structural characteristics of the subsiding areas include the following:

(1) Sediments are unconsolidated and lack appreciable cementation.
(2) Porosity of the sands is high (20 to 40%).
(3) The sediments are of Miocene age or younger.
(4) Producing formations are located at a shallow depth (300 to 1000 m).
(5) The aquifer is thick (more than 30 m).
(6) The overburden is composed of structurally weak sediments and rocks.

Subsidence over formations producing oil, gas and/or water, is caused by the reduction of pore (fluid) pressure within the producing formation through the removal of fluids in the pores:

P_e (effective, grain-to-grain stress) = P_t (total overburden stress) – nP_p (pore or fluid pressure)

In 1974, Rieke & Chilingarian, however, proved experimentally that coefficient n is equal to one. Dobrynin & Serebryakov (1989) and Serebryakov & Chilingar (2000) presented a simple method of predicting subsidence due to fluid withdrawal.

In addition to the grain response to increased stress, the subsurface reservoir as a whole undergoes several types of changes adjusting to the imbalance of forces caused by fluid withdrawal. Loosely-cemented rocks undergo permanent rearrangement of grains and pore spaces resulting in the loss of porosity and permeability. This type of compaction, induced by the mobility of grains, is only partially reversible if the fluid pressure is increased by water injection or natural recharge. Thus, indiscriminate fluid production can lead to permanent loss of the capacity of an aquifer or a reservoir to contain (and to conduct) fluids.

Information published on total and annual rates of subsidence is relatively abundant but quite incomplete. It allows us to get an idea of an approximate maximum amount of subsidence. It is impossible, however, to obtain some definite dependence of the subsidence rates on pressure decline rates and on thicknesses, depths, and characteristics of reservoir and overlying rocks.

The total subsidence can reach up to 10 m. The largest subsidence in the San Joaquin Valley, California, USA, had reached 8.5 m by the year 1970. In Wilmington Oilfield, total subsidence was 8.8 m. Lesser values of subsidence of the order of 0.9 to 1.5 m are commonplace. The annual rate of subsidence depends on the rate of pore pressure decline and may be as high as 0.6 m per year. In San Joaquin Valley, the average annual rate of subsidence was up to 2.4 m for 10 years

Copyright © 2010 IAHS Press

(from 1959 to 1969), i.e. 24 cm per year. In Wilmington Oilfield, the annual subsidence rate reached 70 cm, the total for a three-year period (from 1951 to 1954) being 2.1 m. Rates of about 0.3 m per year are encountered often: 25 cm per year in Taipei Basin, Taiwan, and 32 cm per year (in 1960) in Tokyo, Japan. Rates of the order of several cm per year are quite common.

SUBSIDENCE HAZARDS IN THE LOS ANGELES BASIN, CALIFORNIA, USA

Serious environmental problems due to subsidence have been caused by oilfield operations within the Los Angeles Basin (e.g. Chilingarian *et al.*, 1995). Subsidence exists over virtually every oilfield and producing horizon (Wentworth *et al.*, 1969). Initially subsidence was noted over shallow water aquifers. Subsidence typically causes a bowl-shaped depression at the surface, centred over the oilfield. Commonly, the area of subsidence is approximately twice the size of the area from which the fluid is withdrawn.

BALDWIN HILLS DAM FAILURE (LOS ANGELES BASIN)

The Baldwin Hills Dam formed a large water reservoir that held water in a highly-developed residential portion of Los Angeles and was located over a large oilfield and two active faults. Although an ongoing surveillance for leaks within spillways had been carried out, no monitoring for oilfield subsidence had been undertaken. On 14 December 1963, the dam broke and a very large volume of water suddenly poured out into urban Los Angeles.

The Inglewood Oilfield, discovered in September 1924, lies under the western half of the Baldwin Hills area. It covers about 4.9 km^2 and in 1963 there were more than 600 producing wells. The field lies under the water reservoir site on the south and west. The nearest reported production at the time of the reservoir failure was from three wells within 213 m of the south rim of the dam.

Analysis of dam failure revealed that it was due to ground differential subsidence that correlated directly with the Inglewood Oilfield fluids production. The total area of subsidence resembled an elliptical bowl with its centre about 805 m west of the reservoir and centred over the oilfield. Subsidence at the reservoir site was about 0.9 m, compared to nearly 3.4 m at the subsidence bowl. Noteworthy was the fact that the southwest corner (viz. direction of maximum subsidence) had dropped more than the northeast corner, resulting in differential settlement across the dam of approximately 0.15 m. Furthermore, a review of survey data from 1934 to 1961 and 1963 showed lateral movement in the direction of subsidence depression.

The Inglewood-Newport Beach Fault (an active major strike-slip fault) bisects this area with numerous tension relief faults branching off from the main fault. There was enormous potential for differential movement along individual fault blocks. Indeed, a post-accident investigation revealed that differential fault block movement had caused rupturing of the asphaltic membrane used as a water seal over the floor of the dam.

Although fluid extraction and the resultant subsidence were the prime contributors to the rupture of the reservoir, there is substantial evidence to indicate that water injection to stimulate oil production was also a contributing factor to fault movement (Hamilton & Meehan, 1971). The main lesson to be learned is that differential subsidence was responsible for this disaster and property loss, and could have been diminished if proper monitoring for subsidence had been undertaken. Virtually every oilfield in the Los Angeles Basin has experienced subsidence as a result of fluid production (Chilingar & Endres, 2005). Accordingly, an appropriate standard of care for all oilfield operators should be to undertake monitoring from the onset of production.

PLAYA DEL REY FIELD, MARINA DEL REY (LOS ANGELES BASIN)

Historical measurement data regarding subsidence in the Playa del Rey Venice oilfield, California, areas reveal almost 0.6 m of subsidence from the time that oil production began in the 1920s and up to 1970. However, no subsidence monitoring has been made since 1970, despite the fact that

the field still produces fluids. The Marina del Rey breakwater is vulnerable to subsidence, as is the coastal area, thus exposing the coastline to more potential damage during storms.

The sources of gas migration in this area are the faults and the older wells that were drilled and completed in the 1930s. Any damage to the oilwells (including cement seals) due to movement along faults, results in the potential for increased gas migration to the surface. This is especially critical because the oilfields underlying this area are also being used to store high-pressure gas which is imported from out of the State of California. Figure 1 illustrates the interrelationships among the production of fluids, compaction, subsidence, gas migration and seismic activity (Chilingarian *et al.*, 1996; Gurevich *et al.*, 1993).

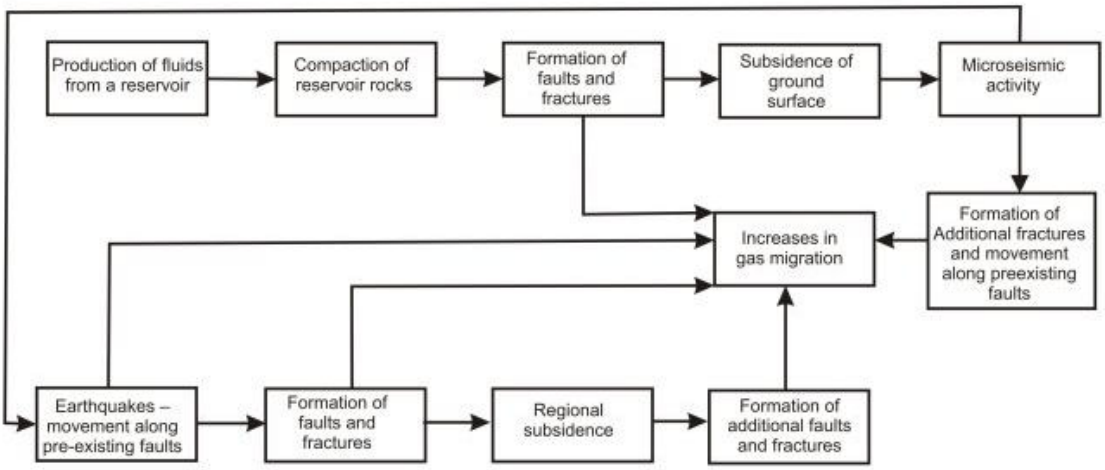

Fig. 1 Schematic diagram of system relationships among the production of fluids, compaction, subsidence, and seismic activity (modified after Chilingarian *et al.*, 1996, Fig. 1, p. 41).

Oilfield operations require the utmost degree of vigilance in order to protect the high-density urban development in the area. Monitoring for subsidence and gas migration is essential in order to meet this standard of care.

Distribution of stresses and strain within the rock mass above the compacting reservoir is an important feature of subsidence from a viewpoint of fracturing of rocks and increase in vertical permeability (Fig. 2). Mostly, large surface fissures form as a result of withdrawal of water from shallow aquifers, which are, as a rule, alluvial. Withdrawal of oil, with substantial formation pressure decline, also causes surface deformation, which mostly consists of horizontal displacements and fractures (Pratt & Johnson, 1926; Strehle, 1989). Surface cracking due to oil and gas withdrawal is usually not investigated. Thus, fissures due to water withdrawal also give useful indirect information on phenomena above oil and gas fields, which were observed by the authors.

The issue of the full depth range of fissures to the producing formation, which is very important from the gas migration or leakage viewpoint, stays unexplored. It is suggested that surface cracks extend much deeper than measured. This problem needs extensive field exploration.

A fractured zone may arise from, or be seriously aggravated by, non-uniform compaction of sediments and subsidence. Deformation can also take place as a result of difference in the compaction rates of clays and sands. Differential movements occur in many oilfields, in adjoining fault blocks, because of preferential production or injection of fluids within the various fault blocks. Subsidence as a direct result of oilfield production in the Wilmington Field, California, has been estimated to have been as great as 6 m (20 feet). Even subsidence of a few feet can result in the fracturing of the subsurface layers (creation of new fractures), cause enlargement of existing faults, and facilitate gas migration to the surface.

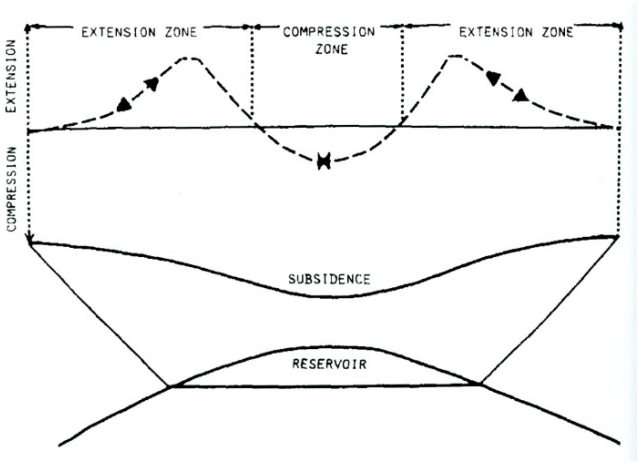

Fig. 2 Schematic diagram of compressive and tensile stress distribution in subsiding formations (modified after Gurevich & Chiligarian, 1993).

In order to exercise a high degree of vigilance regarding the environmental hazards posed by oilfield production, it is necessary to undertake soil and groundwater monitoring (Chilingar & Endres, 2005). Soil and groundwater must be carefully evaluated for contamination in order to take steps necessary for remediation. This requires an evaluation of the underlying aquifers, which become a ready target to the migrating oil and gas.

Lastly, water-flooding operations must be started upon initiation of oil and gas production in subsidence-prone areas.

BIBLIOGRAPHY AND REFERENCES

Chilingar, G. V., Serebryakov, V. A. & Robertson, J. O. Jr (2002) *Origin and Prediction of Abnormal Formation Pressures*. Dev. Petrol. Sci. 50. Elsevier, Amsterdam, The Netherlands, 373 pp.

Chilingar, G. V. & Endres. B. (2005) Environmental Hazards posed by the Los Angeles Basin urban oilfields: an historical perspective of lessons learned. *Environmental Geology* **47**, 302–317.

Chilingarian, G.V., Khilyuk, L. F.& Katz, S. A. (1996) Pronounced changes of upward gas migration as precursors of major seismic events. *J. Petrol. Sci. Engr*. **14**, 133–136.

Chilingarian, G. V. & Wolf, K. H. (1975) *Compaction of Coarse-Grained Sediments, 1*. Developments in Sedimentology, 18A. Elsevier, Amsterdam, The Netherlands, 552 pp.

Chilingarian, G. V., Donaldson, E. C. & Yen, T. F. (1995) *Subsidence Due to Fluid Withdrawal.* Dev. Petrol. Sci. 41, Elsevier, Amsterdam, The Netherlands, 498 pp.

Chilingarian, G. V., Robertson, Jr, J. O. & Kumar. S. (1987) *Surface Operations in Petroleum Production, I,* Dev. Petrol. Sci. 19A, Elsevier, Amsterdam, The Netherlands, 821 pp.

Contaldo, G. J. & Mueller, J. E. (1991) Earth fissures and land subsidence of the Mimbres Basin, Southwestern New Mexico, U.S.A. In: *Land Subsidence* (ed. by A. I. Johnson), 301–310. IAHS Publ. 200. IAHS Press, Wallingford, UK.

Dobrynin. V. M. & Serebryakov, V. A. (1989) *Geologic-Geophysical Methods of Predicting Abnormal Formation Pressures*. Nedra, Moscow, 285 pp.

Donaldson, E. C. & Chilingarian, G. V. (1997) Review of subsidence due to groundwater withdrawal. Second Ann. Symp. Groundwater Resources and Groundwater Quality Protection, Jan 9-10, National Cheng Kung Univ., Tainan, Taiwan, 247–264.

Endres, B. L., Chilingar, G. V. & Yen, T.F. (1991) Environmental hazards of urban oilfield operations, *J. Petrol. Sci. Engng* **6**, 95–106.

Guacci, G. (1979) The Pixley fissure, San Joaquin Valley, California. In: *Evaluation and Prediction of Subsidence* (ed. by S. K. Saxena), 303–319. ASCE Publ., New York, USA.

Gurevich, A. E., Endres, B. L., Robertson, Jr, J. O. & Chilingarian, G. V. (1993) Gas migration from oil and gas fields and associated hazards. *J. Pet. Sci. Eng*. **9**, 223–238.

Gurevich, A. E. & Chilingarian, G. V., (1993). Subsidence over producing oil and gas fields, and gas leakage to the surface. *J. Petrol. Sci. Engng* **9**, 239–250.

Hamilton, D. H. & Meehan, R. l. (1971) Ground rupture in the Baldwin Hills. *Science* **172**, 333–344.

Haneberg, W. C., Reynolds, C. B. & Reynolds, I. E. (1991) Geophysical characterization of soil deformation associated with earth fissures near San Marcial and Deming, New Mexico. In: *Land Subsidence* (ed. by A. I. Johnson), 371–280. IAHS Publ. 200. IAHS Press, Wallingford, UK.

Holzer, T. L. (1984) Ground failure induced by ground water withdrawal from unconsolidated sediments. In: *Man-induced Land Subsidence* (ed. by T. L. Holzer), *Geol. Soc. Am. Rev. Eng. Geol.* **7**. 67–105.

Keaton, J. R. & Shlemon, R. J. (1991) The Fort Hancock earth fissure system, Hudspeth County, Texas: Uncertainties and implications. In: *Land Subsidence* (ed. by A. I. Johnson), 281–290. IAHS Publ. 200. IAHS Press, Wallingford, UK.

Khilyuk, L. F., Chilingar. G. V., Robertson, J. O. & Endres. B. L. (2000) *Gas Migration – Events Preceding Earthquakes.* Gulf Publ. Co., 389 pp.

Kovach, R. L. (1974) Source mechanism for Wilmington Oilfield, California, subsidence earthquakes. *Bull. Seismol. Soc. Am.*, **64**, 699–711.

Lee, K. L. (1979) Subsidence earthquakes at a California oil field. In: *Evaluation and Prediction of Subsidence* (ed. by S. K. Saxena) (Eng. Found. Conf. ASCE), 549–564.

Lister, L. A. & Secrest, C. D. (1985) Giant desiccation cracks and differential surface subsidence, Red Lake Playa, Mojave County, Arizona. *Am. Assoc. Eng. Geol. Bull*. **22**, 299–314.

Love, D. W., Reimers, R. F., Hawley, J. W., Johnpeer, G. D. & Bobrow, D. J. (1987) Summary of geotechnical investigations near Espanola, New Mexico. In: *Quaternary Tectonics, Landform Evolution, Soil Chronologies, and Glacial Deposits* (ed. by C. Menges), 133–157. New Mexico Dep. Geol., Albuquerque, New Mexico, USA.

Pampeyan, E. H., Holzer, T. L. & Clarke, M. M. (1988) Modern ground failure in the Garlock fault zone, Fremont Valley, California. *Geol. Soc. Am. Bull*. **100**, 677–691.

Pewe, T. L., Raymond, R. H. & Schumann, H. H. (1987) Land subsidence and earth-fissure formation in eastern Phoenix metropolitan area, Arizona. In: *Geologic Diversity of Arizona and Its Margins. Excursions to Choice Areas* (ed by G. H. Davis & E. M. Vanden Dolder). Ariz. Bur. Geol. Min. Tech. Geol. Surv. Branch, Spec. Pap., 5, 199–211.

Pratt, W. E. & Johnson, D. W. (1926) Local subsidence of the Goose Creek Oil Field. *Geology* **34**(7, Part I), 577–590.

Ratigan, J. L., (1990) Scale effects in the hydraulic fracture test associated with the estimation of tensile strength. In: *Scale Effects in Rock Masses* (ed. by A. Pinta da Cunha), 297–306. Balkema. Rotterdam, The Netherlands.

Rieke, H. H., III & Chilingarian, G. V. (1974) *Compaction of Argillaceous Sediments.* Developments in Sedimentology, 16. Elsevier, Amsterdam, The Netherlands, 424 pp.

Serebryakov, V. A. & Chilingar, G. V. (2000) Prediction of subsidence: relationship between lowering of formation pressure and subsidence due to fluid withdrawal. *Energy Sources* **22**(5), 49–41.

Strehle, R. W. (1989) Subsidence hazards – A history. In: *Environmental Concerns in the Petroleum Industry* (ed. by S. M. Testa), 107–116. AAPG Publications.

(Proceedings of EISOLS 2010, Querétaro, Mexico, 17–22 October 2010). IAHS Publ. 339, 2010.

Subsidence faulting and aquifer vulnerability – their relation in Irapuato, Mexico

A. SCHROEDER[1] **& R. RODRÍGUEZ**[2]

1 *Programa de posgrado en Ciencias de la Tierra Universidad Nacional Autónoma de México, Cd. Universitaria, Del. Coyoacán, 04510 Mexico*
schroeder.aaa@gmail.com

2 *Instituto de Geofísica, Universidad Nacional Autónoma de México, Cd. Universitaria, Del. Coyoacán, 04510 Mexico*

Abstract In areas affected by subsidence the occurrence of fractures and faults alter aquifer vulnerability. Faults act as preferential channels for infiltration, fluid flow and solute transport. In urban areas faults break water-supply and wastewater pipelines. Chlorination transformation by-products can be found in the groundwater. Methods like SINTACS allow the incorporation of faults in aquifer vulnerability assessment through permeability values. The vulnerability assessment method, SINTACS was applied in Irapuato, Guanajuato state, central Mexico. Faults were mapped in Irapuato; 15 systems were detected. The intense groundwater abstraction of more than 1600 wells has induced subsidence. Hydrocarbons were detected in groundwater in wells near faults and gas stations. Aquifer pollution affected water supply.

Key words subsidence; abstraction; groundwater

INTRODUCTION

Subsidence and the associated faulting and fractures, provoked by the intense groundwater abstraction of local and regional aquifer systems is a worldwide problem mainly in urban areas surrounded by agriculture lands (Poland, 1984). Subsidence is also occurring in several Mexican regions located in the Highlands, such as Querétaro in Querétaro State, Salamanca, Celaya, Silao and Irapuato in Guanajuato State, and Morelia in Michoacán. Geological, climatic and hydrogeological conditions mean that groundwater has became the main water supply for urban, industrial and agriculture sectors. There are no alternative water sources in the Mexican Highlands. Cities like Salamanca and Irapuato used only groundwater for urban supply. Subsidence is not considered a natural or induced disaster. There are no federal founds for the affected population. The estimated cost of damages up to 2006 was more than $US 20 million.

THE STUDY AREA

Irapuato is located in the central part of Guanajuato State, with an area of 225 km^2. In late 2008, in the urban area, more than 450 000 inhabitants were reported. Agriculture is the main economic activity. There are more than 1600 active wells. More than 90 urban wells supply the city's requirements. Extraction across the whole region is greater than 650×10^6 m^3 per year (Lesser, 2000). Of this volume, 77% is used for irrigation. The first mapping of subsidence faults was done in 2001 (FOSEG, 2001). Subsidence was associated with abstraction until early 2000 (Rodriguez *et al.*, 2006).

LOCAL GEOLOGICAL FRAMEWORK

Irapuato is located in the Transmexican Volcanic Belt. The area is characterized as a tectonic basin. Mesozoic rocks underlie Tertiary volcanic rocks and the El Capulín and Las Capillas Quaternary formations composed of alluvial and lacustrine material. These sediments are represented by sands, clayey units and conglomerates. There are also lutites, limestones and intercalations of tuffs and pyroclastic material.

Copyright © 2010 IAHS Press

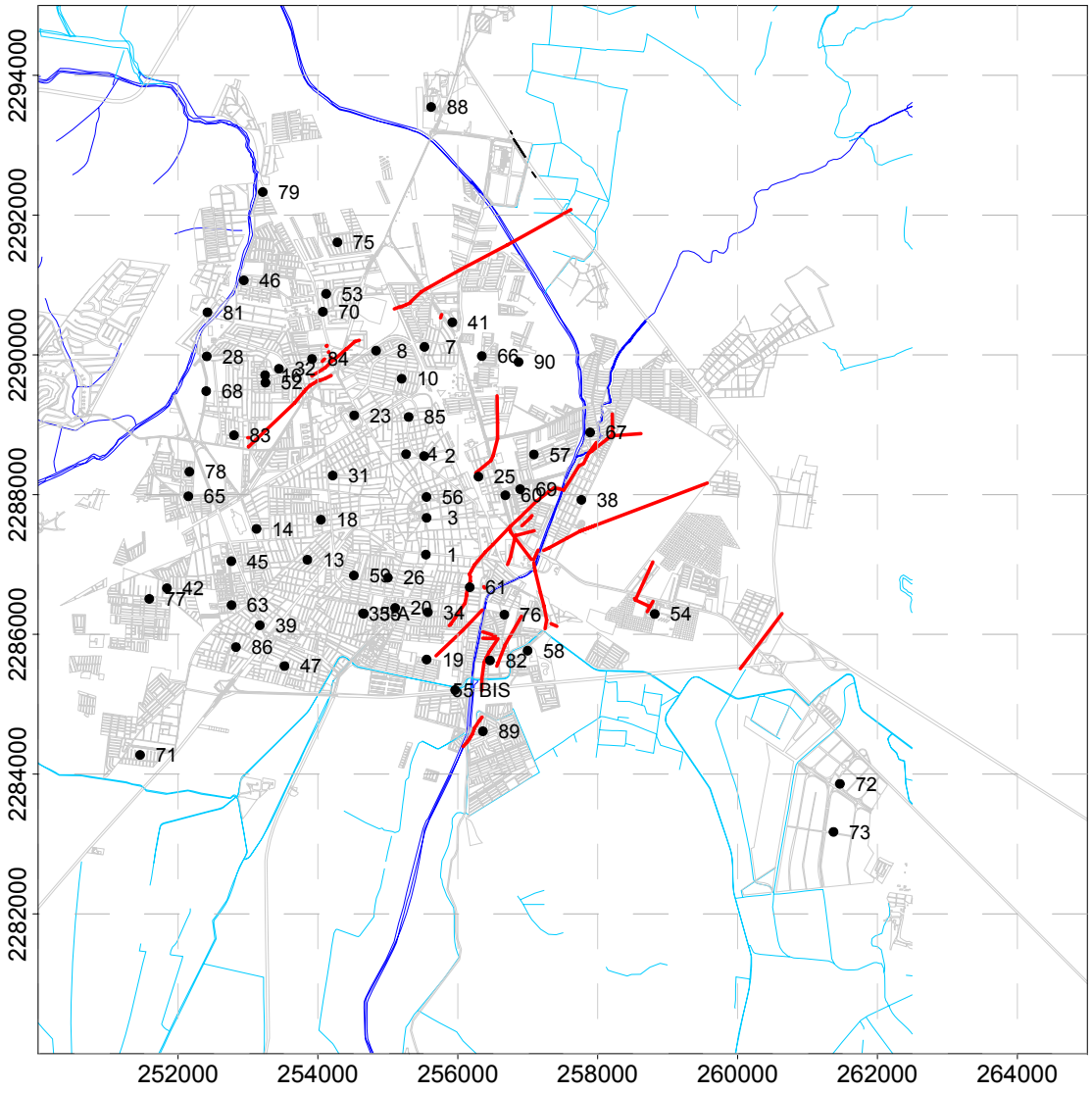

Fig. 1 Subsidence fault systems in Irapuato city.

Irapuato valley is filled with alluvial sediments of variable grain size that overlie older igneous rocks. The aquifer system is composed of four permeable units: clastic sedimentary rocks; acid igneous rocks; basic and intermediate igneous rocks, and lacustrine and fluvial deposits. The exploited aquifer is unconfined.

METHODOLOGY

Faults and fractures were identified and geopositioned. Total station measurements were done along the main faults. A groundwater quality monitoring was carried out. Chemical analyses included organic compounds. Faults were incorporated into the SINTACS method as high permeability areas. The method incorporated seven parameters (geology, water-table depth, infiltration, vadose zone, hydraulic conductivity, soil type and topography). The study area has medium to high vulnerability degrees (Fig. 2). Data were incorporated into a geographic information system, GIS.

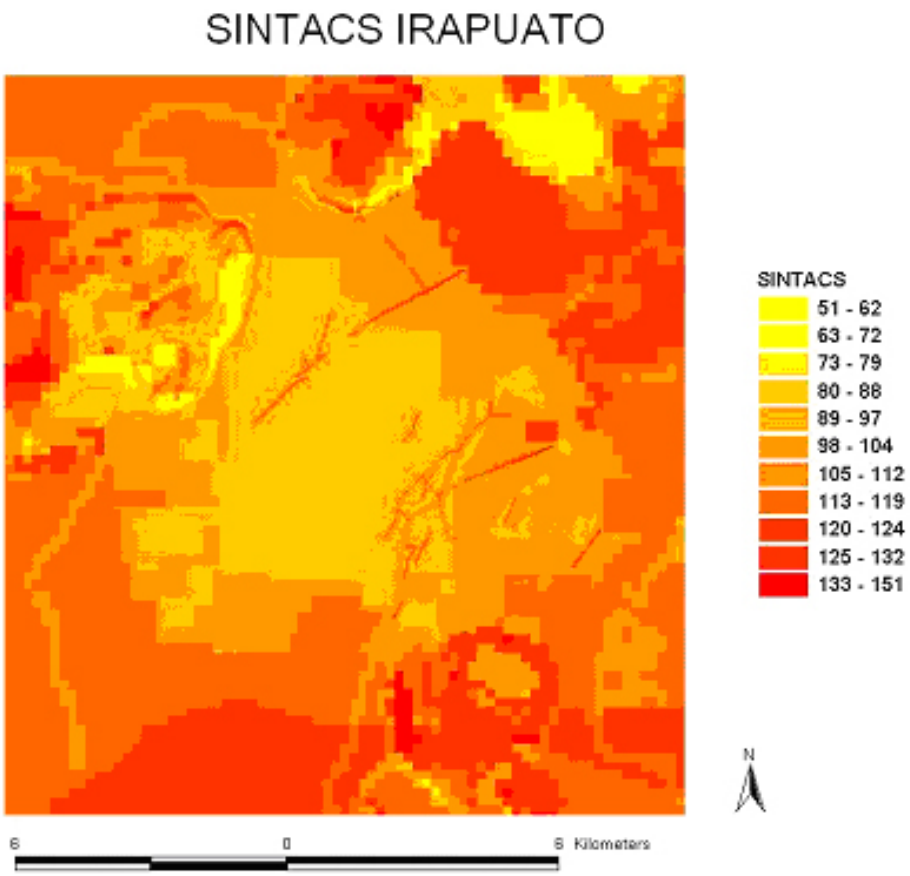

Fig. 2 SINTACS vulnerability mapping of Irapuato urban area.

CONCLUSIONS

Fifteen fault systems were found in late 2006 (Fig. 1). The subsidence rate during 2006 was 6–7 cm per year. The accumulated vertical displacement over 10 years varies from 0.60 to 2.2 m. There are agriculture wells and urban wells inside the urban area. There are 80 active urban wells. The agriculture well operation is one of the main causes of subsidence. Active tectonic faults were not detected. There is no seismic activity in the area. Aquifer vulnerability increases along the fault traces. In wells located near two of the fault systems and gas stations, hydrocarbons were detected in the groundwater (Rodríguez *et al.*, 2006). Groundwater is the main water source for the Irapuato inhabitants. The contamination of the aquifer affected potable water distribution.

Acknowledgements This project was supported by the DGAPA UNAM grant IN1160102.

REFERENCES

FOSEG (2001) *Atlas de Riesgos del Estado de Guanajuato*. Coordinación Estatal de Protección Civil. Fondo de Seguridad. Secretaría de Gobierno, Estado de Guanajuato, Mexico.

Lesser y Asociados (2000) Seguimiento del estudio hidrogeológico y modelo matemático del Acuífero de Irapuato-Valle de Santiago-Huanímaro Gto. Technical Report, Comisión Estatal de Aguas del Estado de Guanajuato CEAG. CEAG Library, Guanajuato, México, 230 pp.

Poland, J. F. (1984) *Guidebook to Studies of Land Subsidence Due to Groundwater Withdrawal*. UNESCO Studies and Reports in Hydrology no. 40. Unipublications, New York, USA.

Rodriguez, R., Armienta, A., Morales, P., Silva, T. & Hernández, H. (2006) Evaluación de Vulnerabilidad Acuífera del valle de Irapuato Gto. JAPAMI, CONCyTEG, IGF UNAM. ReporteTécnico il. 90 pp.

Land Subsidence, Associated Hazards and the Role of Natural Resources Development
(Proceedings of EISOLS 2010, Queretaro, Mexico, 17–22 October 2010). IAHS Publ. 339, 2010.

Axisymmetric motion of a confined leaky aquifer due to pumping groundwater from a partially penetrating well

J. LI
Department of Civil Engineering, Morgan State University, 5200 Perring Parkway, Baltimore, Maryland 21251, USA
jiang.li@morgan.edu

Abstract This paper presents a new analytic solution for aquifer axisymmetric movement driven by the hydraulic force that is induced by groundwater withdrawal from a partially-penetrating well installed in an infinite confined-leaky aquifer. In contrast to the traditional approach, the present investigation emphasizes velocity and displacement fields through the flow relation rather than stress and strain fields. Development of a new governing equation is based on bulk linear momentum and conservation of bulk mass, the Darcy-Gersevanov law, and the Hantush hydraulic drawdown for large times. The solution indicates that aquifer movement is significantly affected by various factors including leaky flow, well penetrating depth, aquifer depth and radial distance from the centre of a pumping well. Analysis results also indicate that aquifer movement in the radial direction behaves similarly to the one-dimensional radial movement researched previously. Particularly when the pumping well fully penetrates the confined aquifer, the analytic solution for aquifer axisymmetric movement reduces to that for aquifer radial transient movement.

Key words transient flow; aquifer transient movement; leaky flow; aquifer axisymmetric movement

INTRODUCTION

Groundwater withdrawal causes land subsidence, earth fissures, or both, because the induced hydraulic forces impel the aquifer matrix to move axisymmetrically (i.e. radially and vertically) in an area surrounding a pumping well. Traditionally, land movement due to groundwater withdrawal was investigated in stress and strain fields (Biot, 1941; Terzaghi, 1943; Mikasa, 1965; Helm, 1987; Li & Helm, 2000, 2001; Li, 2003). In contrast, the present paper emphasizes the flow relation and hydraulic driving forces in velocity and displacement fields. Aquifer radial movement in response to constant and variable pumping rates in a discharging well was investigated previously by Helm and Li (Helm, 1994; Li, 2007a,b,c) using an analytic approach that incorporates various analytic solutions of drawdown for unsteady flow. In contrast, the present investigation emphasizes the three-dimensional (axisymmetric) movement of a confined leaky aquifer in response to groundwater withdrawal from a partially penetrating well.

MASS CONSERVATION

Mass conservation for a mixed bulk flow flowing through a control volume V indicated in Fig. 1 can be given below:

$$\int_{A_i} \rho_b \mathbf{v}_{bi} \cdot d\mathbf{A}_i + \int_V \frac{\partial \rho_b}{\partial t} dV = \frac{dm_b}{dt} \tag{1}$$

where m_b is bulk mass; ρ_b is the bulk density defined by $\rho_b \equiv n\rho_w + (1-n)\rho_s$ in which ρ_w and ρ_s are densities of water and individual solid grains, respectively; i (= 1, 2, 3) is an integer for summation when repeated; the term $\rho_b \boldsymbol{v}_{bi}$ [$\equiv \rho_w n \boldsymbol{v}_w + \rho_s(1-n)\boldsymbol{v}_s$] is the linear momentum per volume, where $\boldsymbol{v}_{bi}$ is the gravitational bulk velocity; $\boldsymbol{A}_i$ (i = 1, 2, 3) represents the closed surface comprising three areas that cover the specified cylindrical zone with a depth z and radius r from the centre of the pumping well. In particular, as indicated in Fig. 1, A_1 (= $2\pi rz$) is the circumferential vertical surface of the cylinder; A_2 and A_3 ($A_2 = A_3 = \pi r^2$) are the areas on the top and bottom of the cylinder at $z = 0$ and z, respectively, where z and r are coordinates in the vertical and radial directions in Fig. 1.

Copyright © 2010 IAHS Press

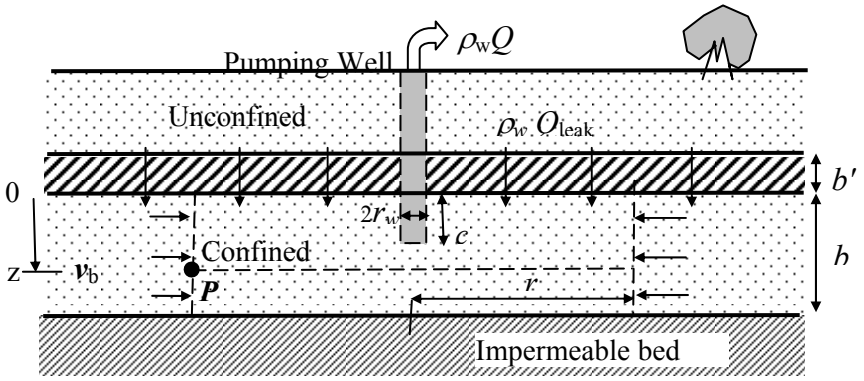

Fig. 1 Groundwater withdrawal from a partially penetrating well in a confined leaky aquifer.

On the left side of equation (1), the first term represents the bulk mass flux into or out of the control volume V by crossing the closed surface A, and the second term is for cumulative changes in mass within V. The term on the right side of equation (1) stands for changes in mass with time because of drains (sinks) or springs (sources) within the cylindrical zone. If the following assumptions are applied: (i) the well pumpage Q is constant; (ii) the leaky flow is assumed to be vertical; (iii) the Darcy-Gersevanov law is applicable to the leaky flow crossing the top confining bed; (iv) the vertical component of the bulk flux decouples the radial component; and (v) the pore water and individual grains are incompressible, equation (1) can take the form:

$$2\pi r z q_{br} + \pi r^2 q_{bz} = Q - Q_{leak} \tag{2}$$

where q_{br} and q_{bz} are the radial and vertical components of the volumetric bulk velocity $\boldsymbol{q}_b$ [$\equiv n\boldsymbol{v}_w + (1-n)\boldsymbol{v}_s$]; Q_{leak} is the leakance into the aquifer from the top confining bed and is defined as $Q_{leak} = (K'/b')\int_0^r \Delta h' \pi\, dr^2$ (Bear, 1972) where b' and K' are thickness and vertical conductivity of the confining bed, respectively; $\Delta h'(r, t)$ is hydraulic drawdown crossing the confining bed. The further evaluation of Q_{leak} will be discussed in a later section. Li (2007a) proposed that equation (2) has the same form no matter where the velocity $\boldsymbol{v}_p$ at a point P of interest in V is chosen to fix on (i.e. $\boldsymbol{v}_p = 0$, $\boldsymbol{v}_p = \boldsymbol{v}_w$ or $\boldsymbol{v}_p = \boldsymbol{v}_s$).

DARCY-GERSEVANOV LAW FOR AXISYMMETRIC FLOW

For saturated and porous sedimentary materials, if inertial forces are assumed to be negligibly small when compared to viscous drag forces that relate to flow velocity, the general relation of viscous drag *versus* hydraulic driving force reduces to the Darcy-Gersevanov law (Li & Helm, 1998). For the axisymmetric flow, the Darcy-Gersevanov law can be written in the form of a matrix:

$$\begin{bmatrix} q_r \\ q_z \end{bmatrix} = -\begin{bmatrix} K_{rr} & K_{rz} \\ K_{zr} & K_{zz} \end{bmatrix} \begin{bmatrix} \dfrac{\partial h}{\partial r} \\ \dfrac{\partial h}{\partial z} \end{bmatrix} \tag{3}$$

in which q_i ($i = r$ and z) is the specific discharge in the radial or vertical direction, K_{ij} ($i = r, z$ and $j = r, z$) is a component of the matrix of hydraulic conductivity. The tangential component of the specific discharge is not introduced in equation (3).

SOLUTION OF AQUIFER AXISYMMETRIC TRANSIENT MOTION

If a single well partially penetrates a homogenous and isotropic confined aquifer with leakance (Fig. 1), the following analytic solution in terms of hydraulic drawdown was solved by Hantush (1957, 1961, 1964) for large times:

$$s(r,z,t)=\frac{Q}{4\pi T}\{w(\xi,r/B)+\frac{2b}{\pi c}\sum_{i=1}^{\infty}\frac{1}{i}\cos(\frac{i\pi z}{b})\sin(\frac{i\pi c}{b})w_i(\xi,r/B,ir/b\} \tag{4}$$

where $s = h - h_0$ is drawdown; Q is the constant pumpage; ξ (= $r^2S/4Tt$) is a dimensionless variable; c is the depth of well penetration (Fig. 1); i is an integer for summation; B [=$(Tb'/K')^{1/2}$] is the leaky parameter where T is the transmissivity of the confined aquifer in Fig. 1; w and w_i are the Hantush and Jacob well functions for a confined leaky aquifer (Hantush & Jacob, 1955) and are given below:

$$w=\int_{\xi}^{\infty}\frac{e^{-(k+\frac{(r/2B)^2}{k})}}{k}dk \quad \text{and} \quad w_i=\int_{\xi}^{\infty}\frac{e^{-(k+\frac{(r/2B)^2+(i\pi r/2b)^2}{k})}}{k}dk$$

where k is a dummy variable of integration, i is an integer for summation. Substituting equation (4) in to (3) and recalling (2) and $\boldsymbol{q}_b$ result in axisymmetric movement of an isotropic and homogenous aquifer in a velocity field:

$$\begin{bmatrix}v_{sr}\\ v_{sz}\end{bmatrix}=Q\begin{bmatrix}\frac{e^{-[\xi+\frac{(r/2B)^2}{\xi}]}}{2\pi rb}[1+2\sum_{i=1}^{\infty}\frac{\sin(\frac{i\pi c}{b})}{\frac{i\pi c}{b}}\cos(\frac{i\pi z}{b})\,e^{-\frac{(i\pi r/2b)^2}{\xi}}]+\frac{(1-R)}{C_1}\\ \frac{-1}{2b^2}[\sum_{i=1}^{\infty}i\frac{\sin(\frac{i\pi c}{b})}{\frac{i\pi c}{b}}\sin(\frac{i\pi z}{b})w_i(\xi,r/B,ir/b)]+\frac{(1-R)\beta}{C_1}\end{bmatrix} \tag{5}$$

where C_1= ($2\pi zr + \beta\pi r^2$) and $\beta = q_{bz}/q_{br}$; R (= Q_{leak}/Q) is the ratio of the leaky flow rate over the pumpage and will be evaluated in a later section. Equation (5) is the analytic description in the velocity field for the aquifer transient movement impelled by hydraulic forces that are induced by axisymmetric unsteady groundwater flow due to well discharge from a partial penetrating well. Aquifer cumulative displacement can be found by integrating the aquifer velocity over time (i.e. $\mathbf{u}_s=\int_0^t\mathbf{v}_s dt$):

$$\begin{bmatrix}u_{sr}\\ u_{sz}\end{bmatrix}=QC_2\int_{\xi}^{\infty}\begin{bmatrix}\frac{e^{-[k+\frac{(r/2B)^2}{k}]}}{2\pi rb}[1+\frac{2b}{\pi c}\sum_{i=1}^{\infty}\frac{1}{i}\cos(\frac{i\pi z}{b})\sin(\frac{i\pi c}{b})e^{-\frac{(i\pi r/2b)^2}{k}}]+\frac{(1-R)}{C_1}\\ \frac{-1}{2\pi cb}[\sum_{i=1}^{\infty}\sin(\frac{i\pi z}{b})\sin(\frac{i\pi c}{b})w_i(k,r/B,ir/b)]+\frac{(1-R)\beta}{C_1}\end{bmatrix}\frac{dk}{k^2} \tag{6}$$

where $C_2 = r^2S/4T$ in which S is the storage coefficient and k is an integral dummy variable. An initial condition of zero displacement, $\boldsymbol{u}_s(r, z, 0) = 0$, is applied to (6). To appreciate the generality of the solutions (5) and (6), several special cases of (5) and (6) will be discussed in a later section.

EVALUATION OF THE RATIO *R*

It is necessary to evaluate the ratio R ($\equiv Q_{leak}/Q$). From the earlier discussion, the leaky flow along the upper interface between the aquitard and aquifer can be given in terms of drawdown in the following form (Li, 2007a):

$$Q_{leak} = \int_0^r \frac{K'}{b'} s(r,0,t) d(\pi r^2) \tag{7}$$

where $s(r, 0, t)$ is the drawdown along the confining bed and can be determined from (4) as below:

$$s(r,0,t) = \frac{Q}{4\pi T}\{w(\xi, r/B) + \frac{2b}{\pi c}\sum_{i=1}^{\infty}\frac{1}{i}\sin(\frac{i\pi c}{b}) w_i(\xi, r/B, ir/b\} \tag{8}$$

Inserting equation (8) into (7) yields the form of the ratio R as:

$$R = Q_{leak}/Q = \int_u^{\infty} e^{-u}(1 - e^{-\frac{(r/B)^2}{u}})du + \frac{8b}{\pi c}\sum_{i=1}^{\infty}\frac{1}{i}\sin(\frac{i\pi c}{b})\int_{\xi}^{\infty}\frac{e^{-k}}{1+(i\pi B/b)^2}[e^{-(\frac{[(1/2B)^2+(i\pi/2b)^2]r^2}{k})} - 1]dk \tag{9}$$

For no well penetration ($c = 0$), (9) reduces to:

$$R = \int_u^{\infty} e^{-u}(1 - e^{-\frac{(r/B)^2}{u}})du + 8\sum_{i=1}^{\infty}\{\int_{\xi}^{\infty}\frac{e^{-k}}{1+(i\pi B/b)^2}[e^{-(\frac{[(1/2B)^2+(i\pi/2b)^2]r^2}{k})} - 1]\}dk \tag{10}$$

For full well penetration ($c = b$), (10) further reduces to:

$$R = \int_u^{\infty} e^{-u}(1 - e^{-\frac{(r/B)^2}{u}})du \tag{11}$$

which was derived by Li (2007a,b) for radial movement of a confined aquifer. For a confined aquifer without leakance, R becomes zero.

DISCUSSION OF SPECIAL CASES OF ANALYTIC SOLUTIONS

It is worth discussing special cases of solutions (5) and (6) so that aquifer axisymmetric movement with simplified conditions can be investigated. The following special cases are discussed:

Aquifer transient movement in response to pumping from a well without penetration in a confined leaky aquifer

By noticing the limit $\sin(x)/x \to 1$ when $x \to 0$ and $c = 0$ (, (5) and (6) reduce to:

$$\begin{bmatrix} v_{sr} \\ v_{sz} \end{bmatrix} = \begin{bmatrix} Q\{\frac{-e^{-[\xi+\frac{(r/2B)^2}{\xi}]}}{2\pi br}[1 + 2\sum_{i=1}^{\infty}\cos(\frac{i\pi z}{b})e^{-\frac{(i\pi r/2b)^2}{\xi}}] + \frac{(1-R)}{C_1}\} \\ Q\{\frac{1}{2b^2}[\sum_{i=1}^{\infty} i\sin(\frac{i\pi z}{b}) w_i(\xi, r/B, ir/b)] + \frac{(1-R)\beta}{C_1}\} \end{bmatrix} \tag{12a}$$

$$\begin{bmatrix} u_{sr} \\ u_{sz} \end{bmatrix} = \begin{bmatrix} C_2 Q\int_{\xi}^{\infty}\frac{\frac{-e^{-[k+\frac{(r/2B)^2}{k}]}}{2\pi br}[1 + 2\sum_{i=1}^{\infty}\cos(\frac{i\pi z}{b})e^{-\frac{(i\pi r/2b)^2}{k}}] + \frac{(1-R)}{C_1}}{k^2}dk \\ C_2 Q\int_{\xi}^{\infty}\frac{\frac{Q}{2b^2}\sum_{i=1}^{\infty} i\sin(\frac{i\pi z}{b}) w_i(k, r/B, ir/b) + \frac{(1-R)\beta}{C_1}}{k^2}dk \end{bmatrix} \tag{12b}$$

where R reduces to equation (10) for the special case $c = 0$.

Aquifer transient movement in response to pumping from a partial penetrating well with an insignificant ratio *R* when compared to a unit in a confined leaky aquifer

For $R << 1$, the leaky flow is significantly smaller than the well pumpage (i.e. $Q_{\text{leak}} << Q$), (12a) and (12b) become:

$$\begin{bmatrix} v_{\text{sr}} \\ v_{\text{sz}} \end{bmatrix} = \begin{bmatrix} Q\{\dfrac{-e^{-[\xi+\frac{(r/2B)^2}{\xi}]}}{2\pi br}[1+\dfrac{2b}{\pi c}\sum_{i=1}^{\infty}\dfrac{1}{i}\cos(\dfrac{i\pi z}{b})\sin(\dfrac{i\pi c}{b})e^{-\frac{(i\pi r/2b)^2}{\xi}}]+\dfrac{1}{C_1}\} \\ Q\{\dfrac{1}{2\pi bc}[\sum_{i=1}^{\infty}\sin(\dfrac{i\pi z}{b})\sin(\dfrac{i\pi c}{b})w_i(\xi,r/B,ir/b)]+\dfrac{\beta}{C_1}\} \end{bmatrix} \tag{13a}$$

$$\begin{bmatrix} u_{\text{sr}} \\ u_{\text{sz}} \end{bmatrix} = \begin{bmatrix} QC_2\int_{\xi}^{\infty}\dfrac{\dfrac{-e^{-[k+\frac{(r/2B)^2}{k}]}}{2\pi br}[1+\dfrac{2b}{\pi c}\sum_{i=1}^{\infty}\dfrac{1}{i}\cos(\dfrac{i\pi z}{b})\sin(\dfrac{i\pi c}{b})e^{-\frac{(i\pi r/2b)^2}{k}}]+\dfrac{1}{C_1}}{k^2}dk \\ QC_2\int_{\xi}^{\infty}\dfrac{\dfrac{1}{2\pi bc}\sum_{i=1}^{\infty}\sin(\dfrac{i\pi z}{b})\sin(\dfrac{i\pi c}{b})w_i(k,r/B,ir/b)+\dfrac{\beta}{C_1}}{k^2}dk \end{bmatrix} \tag{13b}$$

Aquifer transient movement in response to discharge without well penetration in a confined unleaky aquifer

For neither leakage nor well penetration (i.e. $c = 0$ and $B \to \infty$), the Hantush drawdown in (4) is simplified, and (13a) and (13b) accordingly reduce to:

$$\begin{bmatrix} v_{\text{sr}} \\ v_{\text{sz}} \end{bmatrix} = \begin{bmatrix} Q\{\dfrac{-e^{-\xi}}{2\pi br}[1+2\sum_{i=1}^{\infty}\cos(\dfrac{i\pi z}{b})e^{-\frac{(i\pi r/2b)^2}{\xi}}]+\dfrac{1}{C_1}\} \\ Q\{\dfrac{1}{2b^2}[\sum_{i=1}^{\infty}i\sin(\dfrac{i\pi z}{b})w_i(\xi,r/B,ir/b)]+\dfrac{\beta}{C_1}\} \end{bmatrix} \tag{14a}$$

$$\begin{bmatrix} u_{\text{sr}} \\ u_{\text{sz}} \end{bmatrix} = \begin{bmatrix} QC_2\int_{\xi}^{\infty}\dfrac{\dfrac{-e^{-k}}{2\pi br}[1+2\sum_{i=1}^{\infty}\cos(\dfrac{i\pi z}{b})e^{-\frac{(i\pi r/2b)^2}{k}}]+\dfrac{1}{C_1}}{k^2}dk \\ QC_2\int_{\xi}^{\infty}\dfrac{\dfrac{1}{2b^2}[\sum_{i=1}^{\infty}i\sin(\dfrac{i\pi z}{b})w_i(k,r/B,ir/b)]+\dfrac{\beta}{C_1}}{k^2}dk \end{bmatrix} \tag{14b}$$

Aquifer movement in response to discharge from a fully penetrating well in a confined leaky aquifer

When $c = b$ for full well penetration in the confined leaky aquifer, the Hantush drawdown in (4) consequently simplifies to the Hantush-Jacob drawdown for large times $s(r,0,t) = Qw(\xi,r/B)4\pi T$ (Hantush & Jacob, 1955), and the volumetric bulk velocity only has a radial term: $q_{\text{br}} = (Q - Q_{\text{leak}})/2\pi br$. Thus, (14a) and (14b) are simplified to:

$$v_{\text{sr}} = \frac{Q}{2\pi br}[(1-e^{-[\xi+\frac{(r/2B)^2}{\xi}]})-R] \tag{15a}$$

$$u_{sr} = \frac{C_2 Q}{2\pi br}\int_{\xi}^{\infty} \frac{(1-e^{-[k+\frac{(r/2B)^2}{k}]}) - R}{k^2} dk \tag{15b}$$

where R reduces to equation (11) for the special case $c = b$.

As the vertical components of aquifer velocity and displacement disappear, (15a) and (15b) represent the Hantush-Jacob radial transient movement for constant pumpage that is a special case of the solution developed by Li (2007a) for a confined leaky aquifer in response to variable well flow rates.

Aquifer movement in response to discharge from a fully penetrating well in a confined unleaky aquifer

For a confined unleaky aquifer ($B \to \infty$ or $R = 0$) and full well penetration ($c = b$), (15a) and (15b) eventually reduce to the solution for the Theis transient radial movement developed by Helm (1994): $v_{sr} = Q(1-e^{-\xi})/2\pi br$ and $u_{sr} = (C_2 Q/2\pi br)\int_{\xi}^{\infty}[(1-e^{-k})/k^2]dk$, respectively.

GOVERNING EQUATION IN TERMS OF DIMENSIONLESS VARIABLES

This section presents how aquifer movement in terms of the velocity and displacement fields responds to various parameters in dimensionless forms.

Dimensionless aquifer velocity

The dimensionless velocity of the aquifer in response to well discharge can be written in the following two forms:

$$\begin{bmatrix} v^*_{sr}(Z,t^*) \\ v^*_{sz}(Z,t^*) \end{bmatrix} = \begin{bmatrix} -e^{-[\frac{1}{4t^*}+4B_1{}^2 t^*]}[1+2\sum_{i=1}^{\infty}\frac{\sin(i\pi c^*)}{i\pi c^*}\cos(i\pi z^*)e^{-4(i\pi B_2)^2 t^2}] + \frac{(1-R)}{z^*+B_2\beta} \\ \sum_{i=1}^{\infty} i\frac{\sin(i\pi c^*)}{i\pi c^*}\sin(i\pi z^*)\int_{\frac{1}{4t^*}}^{\infty} e^{-[k+\frac{B_1{}^2+(i\pi B_2)^2}{k}]}\frac{dk}{k} + \frac{(1-R)\beta}{2\pi B_2(z^*+B_2\beta)} \end{bmatrix} \tag{16a}$$

$$\begin{bmatrix} v^*_{sr}(Z,r^*) \\ v^*_{sz}(Z,r^*) \end{bmatrix} = \begin{bmatrix} -e^{-[\frac{r^{*2}}{4}+\frac{4B_1^2}{r^{*2}}]}[1+2\sum_{i=1}^{\infty}\frac{\sin(i\pi c^*)}{i\pi c^*}\cos(i\pi z^*)e^{-4(i\pi B_2)^2 t^2}] + \frac{(1-R)}{z^*+B_2\beta} \\ \{\sum_{i=1}^{\infty} i\frac{\sin(i\pi c^*)}{i\pi c^*}\sin(i\pi z^*)\int_{\frac{r^{*2}}{4}}^{\infty} e^{-[k+\frac{B_1^2+(i\pi B_2)^2}{k}]}\frac{dk}{k}\} + \frac{(1-R)\beta}{2\pi B_2(z^*+B_2\beta)} \end{bmatrix} \tag{16b}$$

where the dimensionless velocities, respectively expressed as a function of dimensionless time in (16a) and radius in (16b), are defined by $v^*_{sr} = 2\pi br v_{sr}/Q$ and $v^*_{sz} = 2b^2 v_{sz}/Q$; the dimensionless variables of the radius, vertical coordinate and time are defined by $r^* = r(S/Tt)^{1/2}$, $z^* = z/b$ and $t^* = tT/r^2 S$, respectively; superscript * denotes dimensionless variables; dimensionless parameters are defined by $B_1 = r/2B$, $B_2 = r/2b$.

Analysis of dimensionless aquifer displacement

Similarly, the dimensionless forms of the aquifer displacement as:

$$\begin{bmatrix} u^*_{sr}(Z,t^*) \\ u^*_{sz}(Z,t^*) \end{bmatrix} = \begin{bmatrix} \int_{\frac{1}{4t^*}}^{\infty} \frac{-e^{-(k+\frac{B_1^2}{k})}[1+2\sum_{i=1}^{\infty}\cos(i\pi Z)e^{\frac{(i\pi B_2)^2}{k}}]+\frac{(1-R)}{Z+B_2\beta}}{k^2}dk \\ \int_{\frac{1}{4t^*}}^{\infty} \frac{\sum_{i=1}^{\infty} i\sin(i\pi Z)\int_k^{\infty} e^{-[k+\frac{B_1^2+(i\pi B_2)^2}{k}]}\frac{dk}{k}]+\frac{\beta(1-R)}{2(ZB_2+B_2^2\beta)}}{k^2}dk \end{bmatrix} \quad (17a)$$

$$\begin{bmatrix} u^*_{sr}(Z,r^*) \\ u^*_{sz}(Z,r^*) \end{bmatrix} = \begin{bmatrix} \frac{r^*}{2}\int_{\frac{r^{*2}}{4}}^{\infty} \frac{-e^{-(k+\frac{B_1^2}{k})}[1+2\sum_{i=1}^{\infty}\cos(i\pi Z)e^{\frac{(i\pi B_2)^2}{k}}]+\frac{(1-R)}{Z+B_2\beta}}{k^2}dk \\ \int_{\frac{r^{*2}}{4}}^{\infty} \frac{\sum_{i=1}^{\infty} i\sin(i\pi Z)\int_k^{\infty} e^{-[k+\frac{B_1^2+(i\pi B_2)^2}{k}]}\frac{dk}{k}]+\frac{\beta(1-R)}{2\pi B_2(Z+B_2\beta)}}{k^2}dk \end{bmatrix} \quad (17b)$$

where the dimensionless components of the aquifer displacement are defined as: $u^*_{sr} = 8\pi bTu_{sr}/(rSQ)$ and $u^*_{sz} = 8b^2Tu_{sz}/(r^2SQ)$ in (17a); $u^*_{sr} = 4\pi b(T/St)^{0.5}u_{sr}/Q$ and $u^*_{sz} = 8b^2Tu_{sr}/(r^2SQ)$ (17b), respectively.

Vector diagrammatic presentation in velocity and displacement fields

Finally, vector diagrams for aquifer transient movement in the velocity and displacement fields are presented in Figs 2 and 3 using dimensionless formats of velocity, as given in equation (16b) and cumulative displacement as given in equation (17b). As the aquifer movement is axisymmetric, the velocity and displacement fields are illustrated within the zone of $r^* > 0$ and $0 \le Z \le 1$. The parameters applied to the vector diagrams in Figs 2 and 3 are $B_2 = 0.5$ and $B_1 = 0.01$, and $\beta = 0.2$. Figure 2 illustrates that the aquifer moves faster horizontally than vertically near the pumping well. When both the aquifer depth and radial distance increases, aquifer movement becomes opposite, namely, the aquifer moves faster in the vertical direction than in the horizontal direction. Figure 3 demonstrates that the cumulative displacement is significantly contributed to by the vertical component near the pumping well and dominated by the horizontal component when radial distance increases.

SUMMARY AND CONCLUSIONS

The findings and conclusions from the present investigation are summarized below:

1. New analytic solutions for axisymmetric transient movement in a confined leaky aquifer have been found in the velocity and displacement fields that are substantially different from those found using traditional approaches that emphasize stress and strain fields. The development of these solutions for aquifer velocity and cumulative displacement are based on the linear momentum of bulk mass, conservation of bulk mass, the Darcy-Gersevanov law, and the Hantush-Jacob analytic drawdown solution due to groundwater withdrawal from a pumping well that partially penetrates through a confined leaky aquifer.
2. Several special cases related to the simplified analytic solutions of hydraulic drawdown, leaky flow and well penetration depth have been discussed. It was found that when the simplified Hantush well function and the Theis well function are applied, aquifer axisymmetric movement becomes a special case of the new solutions. For a fully penetrating well, the solutions for aquifer axisymmetric movement further reduce the one for aquifer radial movement found by Li and Helm.

3. Dimensionless aquifer velocity and cumulative displacement *versus* time and aquifer depth, have been analysed. The velocity vector diagram indicates that the aquifer moves faster horizontally than vertically near the pumping well, and reverses this behaviour for points farther from the well. The displacement vector diagrams show that aquifer displacement exhibits a significant vertical component near the pumping well and becomes dominated by the radial component when the radial distance increases.

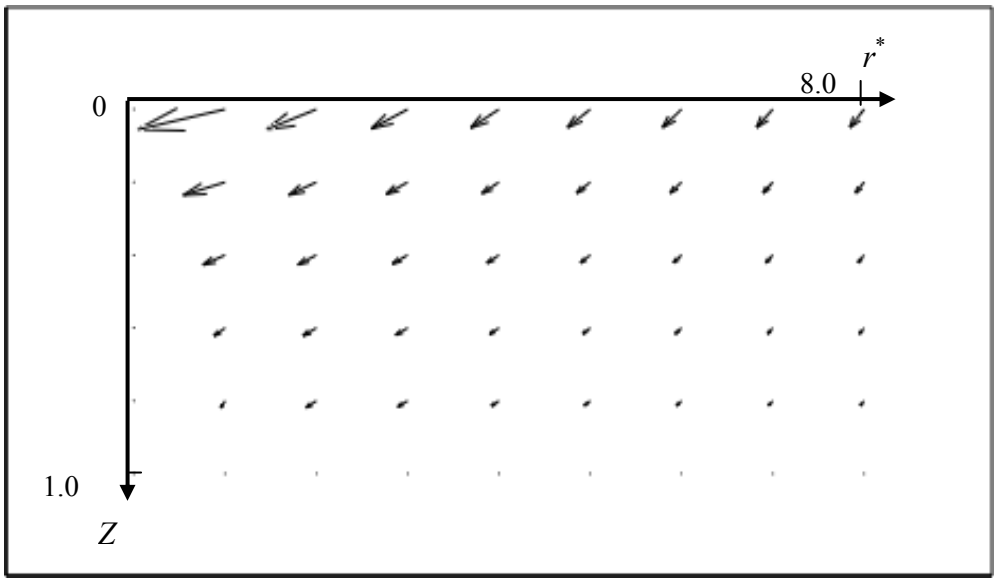

Fig. 2 The aquifer motion in a dimensionless velocity field.

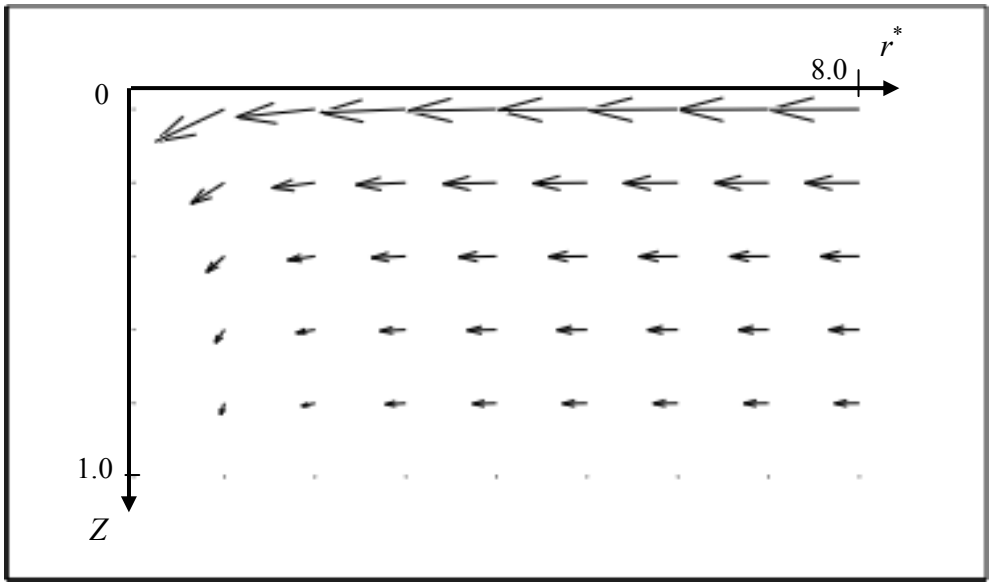

Fig. 3 The aquifer motion in a dimensionless displacement field.

Acknowledgements Reviews of the original manuscript by the anonymous reviewers are acknowledged. Conducting the investigation and writing of this paper were supported by the grant of the US Department of Energy (DE-FG02-94EW11424).

REFERENCES

Bear, J. (1972) *Dynamics of Fluid in Porous Media*. Elsevier, New York, USA.

Biot, M. A. (1941) General theory of three-dimensional consolidation. *J. Appl. Physics* **12**, 55–64.

Hantush, M. S. (1957) Non-steady flow to a well partially penetrating an infinite leaky aquifer. *Proc. Iraqi Scientific Society* **1**, 10–19.

Hantush, M. S. (1961) Drawdown around a partially penetrating well. *J. Am. Soc. Engnrs* **87**, 83–98.

Hantush, M. S. & Jacob, C. E. (1955) Non-steady radial flow in an infinite leaky aquifer. *Trans. Am. Geophys. Un.* **37**, 95–100.

Helm, D. C. (1987) Three-dimensional consolidation theory in terms of the velocity of solid. *Geotechnique* **37**, 369–392.

Helm, D. C. (1994) Horizontal aquifer movement in a Theis-Thiem confined aquifer system. *Water Resour. Res.* **30**, 953–964.

Li, J. (2003) A nonlinear elastic solution of one-dimensional subsidence due to aquifer storage and recovery applications. *Hydrogeology J.* **11**(6), 710–720.

Li, J. (2007a) Transient radial movement of a confined leaky aquifer due to variable well flow rates. *J. Hydrol.* **333**(2-4), 542–553.

Li, J. (2007b) Analysis of radial movement of a confined aquifer due to well pumping and injection. *Hydrogeology J.* **15**(3), 442–458.

Li, J. (2007c) Analysis of radial movement of an unconfined leaky aquifer due to well pumping and Injection. *J. Hydrol.* **15**(4), 1063–1076.

Li, J. & Helm, D. C. (1998) Viscous drag, driving forces, and their reduction to Darcy's law. *Water Resour. Res.* **34**, 1675–1684.

Li, J. & Helm, D. C. (2000) A nonlinear viscous model for aquifer compression associated with ASR applications. In: *Land Subsidence* (ed. by L. Carbognin *et. al*.) (Proc 6th Int. Symp. on Land Subsidence, Ravenna, Italy), vol.2, 319–330.

Li, J. & Helm, D. C. (2001) Using an analytical solution to estimate the subsidence risk caused by ASR applications. *J. Environ. & Engng Geosciences* **7**(1), 67–79.

Mikasa, M. (1965) The consolidation of clay – a new consolidation theory and its application. In: *Civil Engineering in Japan*, 21–26. JSCE, Tokyo, Japan.

Sheng, Z., Helm, D. C. & Li, J. (2003) Mechanisms of earth fissuring caused by groundwater withdrawal. *J. Environ. & Engng Geosciences* **9**, 313–324.

Terzaghi, K. (1943) *Theoretical Soil Mechanics*. John Wiley and Sons Inc., New York, USA.

Theis, C. V. (1935) The relation between the lowering of piezometric surface and the rate and duration of discharge of a well using ground-water storage. *Trans. Am. Geophys. Un.* **16**, 519–524.

(Proceedings of EISOLS 2010, Querétaro, Mexico, 17–22 October 2010). IAHS Publ. 339, 2010.

Climate change impact and anthropogenic effects in land subsidence of Querétaro valley, Mexico

E. GONZÁLEZ-SOSA[1], N. R. RAMOS-SALINAS[2] & C. A. MASTACHI-LOZA[1]

1 *Universidad Autonoma de Querétaro, School of Engineering, Graduate Program in Environmental and Water Resources Engineering, C. U. Cerro de las Campanas, 76010 Querétaro, Mexico*
egs@uaq.mx

2 *Tecnológico regional de Querétaro, Av. Tecnológico S/N. Esq. M. Escobedo. Co. Centro, CP 76000, Querétaro, Mexico*

Abstract Recently, long drought periods and the requirements of large water amounts for urban and agricultural uses have occasioned a high groundwater overexploitation, that is closely related to land subsidence in the Querétaro Metropolitan Zone (QMZ). The urbanized areas around QMZ have experienced a rapid growing period. In this paper we present the results of the spatial precipitation distribution in the QMZ and its potential influence on the processes of land subsidence. Some possible areas were identified where large rainfalls are concentrated. The spatial distribution analysis of precipitation showed that the highest rainfall is localized in the northwest zone of QMZ. The results shows the importance that climate changes can play and the role of anthropogenic conditions in highly urbanized zones for a better understanding of the land subsidence phenomena at the scale of hydrological basins and micro-basins.

Key words climate change; precipitation; water withdrawal

INTRODUCTION

The subsidence problem in Queretaro City, as well as in other large cities in Mexico, is often investigated in terms of aquifer overexploitation. This vision seems consistent with the geological point of view. However, the subsidence problem has more importance in greatly urbanized areas due to its interaction with the environment and the collateral effects of climate change which generate greatly concentrated runoff pollutant loads and heavy metals from "cleaning" the streets and avenues; both are negative to health. That is, the fractures caused by subsidence are common aquifer contamination pathways; they are preferential flow paths that can increase a point-source contamination in a very short time, even hours, depending on the network connectivity over aquifer free surface. In other words, it is important to point out that recharge wells are part of the efforts to mitigate soil crack formation caused by subsidence, but nevertheless become adverse because they also are sources of aquifer contamination due to injecting contaminants through the internal flows. These are generated through connections between soil cracks and because the deep recharge takes place over very short periods compared to natural recharge times. In some cases, natural recharges occur over hundreds of years, depending on the depth of the unsaturated zone and hydrodynamic properties of soil. Since the 1970s the Querétaro Metropolitan Zone (QMZ) has grown enormously, producing a significant increase in impermeable surface and consequently an increase in urban runoff. Queretaro aquifer overexploitation favours the subsidence phenomenon and the formation of cracks in various directions and with diverse geometric properties. The cracks affect the urban system of water evacuation; depending on where it is placed and where it crosses over the cracks, it represents a high aquifer contamination risk. The contamination levels and volume are closely related to the spatial distribution of precipitation, since it depends on contaminant loads injected indirectly into the aquifer. This paper determines and analyses the potential contamination impact in the Queretaro aquifer through its indirect interaction with subsidence and the spatial distribution of precipitation in the QMZ. Finally, the impact of the main cause of climatic change on precipitations is illustrated.

Copyright © 2010 IAHS Press

CASE STUDY

The QMZ, including the Queretaro peri-urban zone (QSZ), located in the central part of Mexico. The QMZ has an area of 15 544.2 ha which extends through Huimilpan, El Marques, Corregidora and Querétaro municipalities, this last representing 80% of the urbanized area. The annual recharge of the aquifer, in the QMZ is estimated at 70×10^6 m^3. The average annual precipitation is about 550 mm and the temperature ranges between 16°C and 18°C. The Water Quality Index (WQI) (ICA, SEMARNAT 2002a, 2003) observed in three sites of the urban water evacuation system are composed as follows: to the west at the discharge point the WQI is 20–30 (Las Adjuntas), to the south 20–40 (El Cimatario) and in the north 20–30 (El Arenal). Those values also including the washing and loading of contaminants as a result of sewage discharge. The classification levels of contamination are corresponding: highly contaminated and contaminated. With the objective of evaluating the potential contamination and its relation with the subsidence in the QMZ, this work to investigate the precipitation rate and potential contaminant loads was carried out. This analysis was realized during June to September of 2006. The spatial distribution of precipitation was analysed using the kriging interpolation technique, which has been widely applied to spatial analysis of climatic variables (Hartkam *et al.*, 2001; Mardikis *et al.*, 2005). The analysis was: maximum, average and total precipitation, also maximum intensity (Table 1). Figure 1 shows that the northwest zone of QMZ concentrates high precipitation levels and in consequence high water runoff levels. In addition, the individual events were studied separately to analyse their behaviour and estimate the potential contamination discharge into the faults and fractures that cross the evacuation system of QMZ urban water.

Table 1 Distribution and intensity of precipitation registered during June to September.

Station	Number of events	Total precipitation (mm)	I max (mm h^{-1})	P max per event (mm)	P mean per event (mm)
La constelación	51	306.09	86.88	50.25	2.68
Peñuelas	61	937.51	289.56	144.02	15.89
Lomas de Peñuelas	50	279.70	59.40	36.80	5.28
San José el Alto	46	341.68	76.20	53.85	5.89
CFE Cimatario	72	882.91	S/D	120.14	10.90
L. Cárdenas	69	997.97	S/D	123.19	12.32
Ecuestre	69	879.60	S/D	131.06	11.73
Parcelas UAQ	54	440.66	310.90	64.52	6.68
La Alameda	49	300.33	74.40	51.70	6.53
La Loma	47	307.51	S/D	48.47	5.31

RESULTS AND DISCUSSION.

The precipitation was recorded at 10 stations; 57 events were observed at at least half of the stations and 38 at 7 stations. The month with highest precipitation was August (606.30 mm) and the lowest June (66.60 mm). The maximum instant intensity was observed in July (310.90 mm h^{-1}) and the minimum in June (91.44 mm h^{-1}). This means July and August are potentially better for the load of contaminants. Table 1 shows the cumulative precipitation and the instant maximum intensities. The potential contamination is exemplified with the Ignacio Zaragoza Avenue, being one of the main arteries and highly transited, and which produces runoff to the fault that runs north to south on 5 de Febrero Avenue. Zaragoza Avenue has a total length of 2.9 km from the "water tank" to the intersection with 5 de Febrero Avenue, Fig. 2. The potential sources of contamination (Baudin, 2006) that were identified for the study are: panels, posts, traffic lights, buildings, city lights, traffic and trees. Total Suspended Solids (TSS) were evaluated as well as metals (Cd, Cr, Cu, Ni, Pb, and Zn). Also, pollutants associated with emissions of metals, such as tyres, brakes,

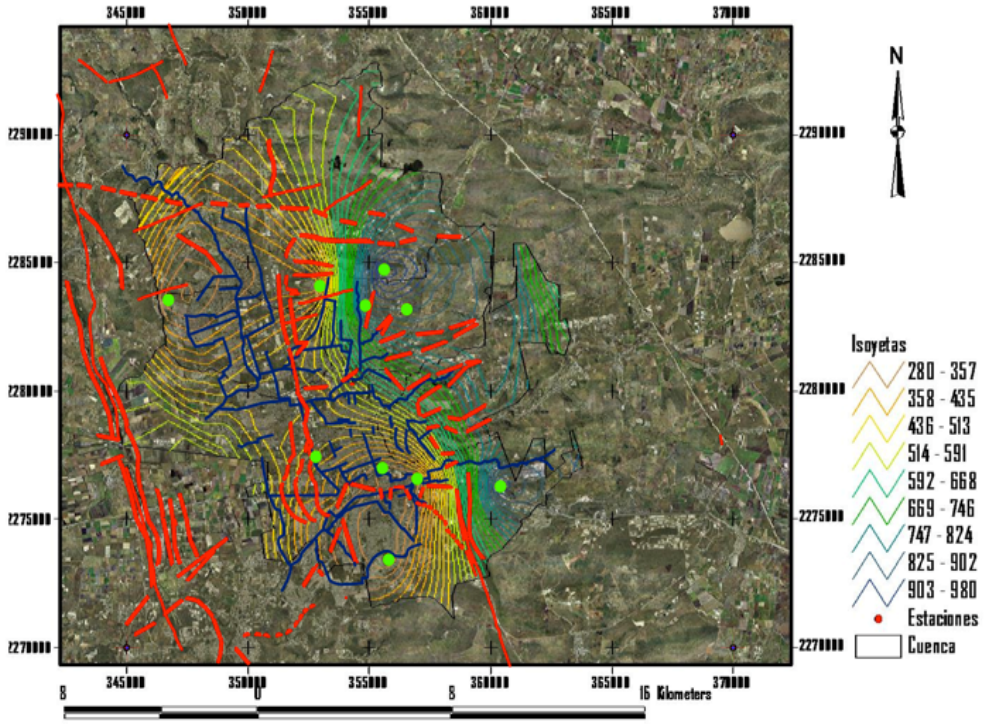

Fig. 1 Subsidence, faults and fracture distribution in the QMZ (red lines), urban water evacuation system (blue lines) and mean precipitation of June–September 2006 (yellow).

Fig. 2 Zaragoza Avenue.

fuel and vehicle additives, and paint for buildings were noted. To determine the potential concentrations of each one of the parameters mentioned, the equation developed by Roesner (1982) and modified by Huber & Dickinson (1988) was used (Akan *et al.*, 2003):

$$\Delta P_T = P_0\left(1 - e^{-kR}\right) \tag{1}$$

where ΔP_T is the total of washed solids during the event (kg), P_0 is the initial load of contamination (kg), k the wash coefficient and R the runoff volume divided by the study area (m). For practical purposes the equation can be rewritten as follows:

$$P_2 = P_1 e^{-kr_a \Delta t} \tag{2}$$

where P_2 is the weight (kg) of the solids washed at t_1 time, P_2 weight (kg) of the solids washed at t_2 time r_a mean of runoff rate in Δt (m h^{-1}), Δt time increment ($t_2 - t_1$) (h) where t_2 final time (h), and t_1 initial time (h). The parameter k_r, according to Sonnen (1980), may vary from 2.5 m^{-1} to 260 m^{-1} depending on the particle characteristics, rain intensity, and watershed area. In this case the value 181.10 m^{-1} was used because it is recommended for a 90% removal of suspended solids.

As shown in Tables 2 and 3, the concentration levels depend on the duration and intensity of events; also the increase of concentration levels when the rain is of lower intensity is notorious. This can be associated with the exponential law of equations (1) and (2) given that washing is greater when the intensities are higher.

Table 2 Estimated load of contaminants on 25 August 2006 event.

Event		Contamination elements (μg L^{-1})						
Time (h)	Intensity (mm h^{-1})	Solids	Cd	Cr	Cu	Ni	Pb	Zn
0.17	109.20	1.964	0.005	0.2450	64.637	0.654	177.473	26.349
0.50	88.80	0.038	0.0001	0.005	1.277	0.012	3.506	0.520
1.00	3.60	0.006	1.76E-05	7.49E-04	0.197	0.002	0.542	0.080
1.50	3.60	0.005	1.36E-05	5.76E-04	0.152	0.001	0.417	0.062
2.00	3.60	0.004	1.03E-05	4.37E-04	0.115	0.001	0.316	0.047

Table 3 Results comparison with NOM-002-ECOL-1996.

Parameters	SS	Cd	Cr	Cu	Ni	Pb	Zn
Units	(ml L^{-1})	(μg L^{-1})	(μg L^{-1})	(μg L^{-1})	(μg L^{-1})	(μg L^{-1})	(μg L^{-1})
NOM-002-ECOL-1996	10	1000	1000	20000	8000	2000	12000
Event 08-25	1.964	0.006	0.245	64.637	0.654	177.473	26.349
Event 08-27	8.364	0.024	1.043	275.261	2.785	755.772	112.211

CONCLUSIONS

Due to the different techniques used, sampling type and data collection, it is difficult to compare between each study; however, it is possible to make a comparison of the results found with the Official Mexican Standard NOM-002-ECOL-1996, which establishes the maximum permissible limits of contaminants in wastewater discharges from the municipal sewage system. The contaminant load was below that of the NOM. It is noticeable that the results obtained are much lower in most cases compared with permissible values established in the NOM-002-ECOL-1996, but these are only for one event and in particular for the runoff that can be generated. It should be noted that the quantity of water which runs through the streets depends on the spatial distribution of precipitation, and potential levels of aquifer contamination depend on the magnitude of the active flow and the size of fractures, and also the connections between them. In other words, the severity of contamination depends on the dynamic interaction of the distribution of subsidence and precipitation intensity and the sources of environmental and urban contamination.

REFERENCES

Akan O. & Houghtalen, R. (2003) In: *Urban Hydrology, Hydraulics, and Stormwater Quality*, 268–271. Wiley & Sons Inc, ISBN 0-471-43158-3.

Baudin, J. (2006) Caractérisation des polluants des eaux pluviales urbaines: donnes bibliographiques et études d'une avenue à Santiago de Querétaro, Qro., Mexique.

Hartkamp, D., *et al*. (2001). Interpolations techniques for climate variables. CIMMYT National Resources Group, Wageningen Agricultural University, The Netherlands.

Huber, W. C. & Dickinson, R. E. (1988) Stormwater management model (SWMM), version 4, User's manual (no. EPA/600/3-88/001a). US Environmental Protection Agency, Athens, Georgia, USA.

Mardikis, M. G., Kalivas, D. P. & Kollias, V. J. (2005) Comparison of interpolation methods for the prediction of reference evapotranspiration : An application in Greece. *Water Resour. Manage.* **19**(3), 251–278.

Rosner, L. A. (1982) Quality urban runoff. In: *Urban Storm Water Hydrology*, 161–188. American Geophysical Union. Washington DC, USA.

Key word index

1-D geomechanical model, 461
3-D geomechanical model, 68
ABAQUS, 27
abstraction, 502
Aguascalientes, Mexico, 191, 207
ALOS PALSAR, 274
analytical solution, 102
Antelope Valley, California, USA, 61
anthropogenic
    activities, 279
    uplift, 96
aquifer, 475
aquifer
    axisymmetric movement, 505
    mechanics, 3
    transient movement, 505
aquifer-system compaction, 61
archaeological area, 345
artificial neural network, 173

backfill mining, 235
banking, 435
basaltic flows, 213
Bayes, 126, 426
borehole extensometer, 319
brine, 368, 377
building damage risk assessment, 443

Catalonian potash basin, 264
cavity collapse, 216
Celaya, 319
Cerro Prieto Geothermal Field, 268
Cerro Prieto, Mexico, 326
Chalco, Iztapalapa, Mexico, 255
Chiba Prefecture, China, 377
China
    Chiba Prefecture, 377
    Shanghai, 238, 419
    Suzhou-Wuxi-Changzhou area, 108
climate change, 467, 514
community organization, 414
complex deformation, 76
conceptualization, 185
construction, 435
cracks, 51
creep, 9
cyclic loading, 90

database management, 44
decision
    making, 443
    support, 426
deep compaction, 364
deformation characteristics, 484
differential
    aquifer-system compaction, 260
    deformation, 149
Differential Interferometry, 274
DinSAR, 268, 287
displacement field, 475

earth fissure, 3, 9, 27, 179
earthquakes, 33
ecology, 396
EDM, 39
effective stress, 472
effective subsidence capacity, 420
Eglington fault, 27
emergency
    plan, 264
    preparedness, 435
energy, 402
engineering
    construction, 419
    land subsidence, 238
ensemble, 426
environment, 402
environmental
    impact, 293
    planning, 432
erosion zones, 210
evaluation, 380, 449
event probability, 426
evolution of clay properties, 232
expansive soils, 224
extensometer, 170

faults, 3, 149, 164, 198, 255
FEMA, 435
field tests, 319
finite
    2-D poroelastic media, 102
    difference method, 90
    element Aster Code, 114
    elements, 133
    sine and cosine transforms, 102

fissures, 39, 51
FLAC-2D, 136
flood, 414
flood
  plain, 435
flooding, 435
fluid withdrawal, 299
forecast, 235
formation
  compaction, 368
  loss rate, 238
fracture, 82
fracture
  mechanics, 20
fractured rocks, 319
fracturing, 20, 33, 149, 219, 497
France, Villiers-sur-Marne, Gournay-sur-Marne, East Paris basin, 287
fuzzy logic, 443

gas, 144
gas
  extraction, 364
  production, 420
  storage, 402
genetic algorithm, 120
geodesy, 9
geodetic levelling, 39
geological
  controls, 260
  disasters, 419
  features, 279
  hazards, 44
  structure, 108
geomorphology, 210
geophysical and geotechnical studies, 216
geotechnical
  characterization, 33
  drought, 287
geothermal
  field, 326
  fluid extraction, 268
GIS, 287, 293, 312, 443
GNSS, 371
GPS, 307, 352, 371, 374, 377
ground
  deformation, 9
  displacements, 345
  fissures, 133
  fracturing, 44, 201
  Penetrating Radar, 54, 219
  subsidence, 235
groundwater, 9, 467, 475, 502
groundwater
  drawdown, 191
  level, 472
  management, 149
  mining, 419
  model, 61
  modelling., 491
  pumpage, 133, 339, 484
guideline, 385

hazard, 497
highway embankment, 120
Holocene subsidence, 158
hurricane, 435
hydrocarbons, 402
hydrologic model, 467
hydromechanics, 319
hydro-thermo-mechanical modelling, 96

implemented actions, 207
infiltration, 472
InSAR, 164, 255, 260, 293, 299, 304, 461
insurance, 435
integrated study, 185
interface elements, 133
interferometric analysis, 287, 333
interpretation, 385
inversion, 126
iodine, 377
Italy, 96, 249, 333
Iztapalapa, Mexico, 44

Japan
  Kanto groundwater basin, 408
  Kujukuri Plain, 293, 377
  Southern Kanto Natural Gas Field, 368, 377
Java mud volcano, 274
jurisprudence, 385

Kanto groundwater basin, Japan, 408
Kazusa Group, 368
Kujukuri Plain, Japan, 293, 377
lagging deformation, 484
lagoon environment, 249
land
  movement, 475
  subsidence PSI, 279
  subsidence zonation, 173
  subsidence, 3, 90, 108, 185, 195, 201, 219, 249, 260, 268, 293 299, 304, 312, 316, 319, 339, 352, 377, 408, 419, 432, 449, 461, 467, 475, 484, 491

landslide, 374
land-surface deformation, 39
Las Vegas valley, USA, 27
leaky flow, 505
legislation, 432
levelling, 307, 333, 339, 377, 380, 408
LiDAR, 39, 435
longwall mining, 120
Los Angeles basin, USA, 497
Lower Llobregat River, Spain, 136

macropolygons, 39
management of nonrenewable natural
    resources, 396
management strategies, 419
metal mine, 235
Mexicali Valley, 268
Mexico City clay, 232,
Mexico, 149, 213
Mexico
    Aguascalientes 191, 207
    Cerro Prieto, 326
    Chalco, Iztapalapa, 255
    Iztapalapa, 44
    Mexico City, 33, 304, 380
    Morelia, 164, 185, 316, 432
    Queretaro, 114, 191, 316
    San Luís Potosí, Mexico, 179, 201
    Tláhuac, 414
    Toluca, 461
    Valle de Chalco Solidaridad, 414
    Zacatecas and Guadalupe, 210
microcracking, 224
microstructures, 224
Midas GTS, 170
mine subsidence, 120
mineralogy, 224
mining, 396
mining
    exploitation, 443
    subsidence, 264
Mobara-type production performance, 140
modelling, 144
modified Merchant model, 76
monitoring, 9, 44, 170, 249, 293, 371, 385, 435
monitoring
    network, 264, 345
    strategy, 426
    system, 408
    well, 339, 408
Morelia, Mexico, 164, 185, 316, 432
multi-antenna GPS, 374

Nakamura's method, 51
natural gas deposit of dissolved-in-water type,
    140
natural gas, 402
natural gas
    dissolved in water, 368, 377
natural subsidence limit, 420
near surface sequences, 201
nonlinear consolidation, 90
northern Adriatic coastland, 279
numerical
    modelling, 20, 82, 114
    simulation, 27

oil, 144
oil
    fields, 497
optical fibres, 368

parameters estimation, 144
peat oxidation, 158
plane strain consolidation, 102
Poland, 443
policy, 385
post-audit, 491
potash mining, 371
precipitation, 514
prediction, 352, 491
production rate, 299
PSI, 279, 287
PSInSAR, 68, 312

Queretaro, Mexico, 114, 191, 316

radioactive marker, 364
rainwater infiltration, 82
refraction method, 213
regeneration, 216
regional
    faults, 201
    land subsidence model, 76
    subsidence, 232
reservoir compartmentalization, 126
risk management, 452
rockmass movement, 235

San Luís Potosí, Mexico, 179, 201
SAR Differential Interferometry, 136, 249
SAR, 307
SAS
    focusing, 358
    interferometry, 358
satellite, 312
satellite
    interferometry, 316

sedimentary basins, 3
sediments compaction, 497
seismic modelling, 213
Shanghai, China, 238, 419
shield
    depth, 238
    radius, 238
signal processing, 54
simulator, 140
social impact, 452
soil, 33
soil
    deformation, 419
    land subsidence, 20
    properties, 238
Southern Kanto Natural Gas Field, Japan, 368, 377
Spain, Lower Llobregat River, 136
strategy, 452
structural
    control, 195
    pathology, 449
subsidence, 9, 39, 51, 61, 82, 114, 126, 136, 164, 170, 179, 198 255, 307, 371, 380, 385, 414, 426, 435, 443, 502
subsidence
    and active faulting, 191
    management, 420
    modelling, 326
    monitoring, 326, 333
    subsidence monitoring
    prediction, 144, 173
    subsidence prediction
subsurface
    composition, 158
    water withdrawal, 173
surface fault, 179
Suzhou-Wuxi-Changzhou area, China, 108
swelling clays, 287
synsedimentary fault, 195
systematic control, 419

Taiwan, 374
tape extensometer, 39
tectonics, 164
time series, 304
time-frequency analysis, 54
Tláhuac, Mexico, 414
Toluca, Mexico, 461
transient flow, 505,
triggering factors, 207

underground
    coal mining, 120
    gas storage, 68
unsaturated
    flow, 472
    zone, 82
USA, 9
USA
    Antelope Valley, California, 61
    Las Vegas valley, 27
    Los Angeles basin, 497

Valle de Chalco Solidaridad, Mexico, 414
variable
    compressibility, 90
    permeability, 90
velocity field, 475
Venice, Italy, 96, 249
vertical
    extensometer, 333
    reflection, 213
Villiers-sur-Marne, Gournay-sur-Marne, East Paris basin, France, 287
virtual reality, 108
visco-elasto-plasticity, 484
volcanic edifice, 219
vulnerability, 44, 149

Wadden Sea, 420
water
    and gas withdrawal, 396
    drainage, 144
    flow and strain-stress coupled models, 136
    withdrawal, 514, 519
width coefficient, 238

Wigner-Ville distribution, 54

Zacatecas and Guadalupe, Mexico, 210
zoning risk, 179

EISOLS

Eighth International Symposium On Land Subsidence

Querétaro - México - 2010

International Association of Hydrological Sciences

Association Internationale des Sciences Hydrologiques

IAHS AISH

www.iahs.info

IAHS Publication 339 ISBN 978-1-907161-12-4 ISSN 0144-7815